

# Talanta

The International Journal of Pure and Applied Analytical Chemistry

---

## Editors-in-Chief

**Professor G.D. Christian**, University of Washington, Department of Chemistry, 36 Bagely Hall, P.O. Box 351700, Seattle, WA 98195-1700, U.S.A.

**Professor J.-M. Kauffmann**, Université Libre de Bruxelles, Institut de Pharmacie, Campus de la Plaine, C.P. 205/6, Boulevard du Triomphe, B-1050 Bruxelles, Belgium

## Associate Editors

**Professor J.-H. Wang**, Research Center for Analytical Sciences, Northeastern University, Box 332, Shenyang 110004, China

**Professor J.L. Burguera**, Los Andes University, IVAQUIM, Faculty of Sciences, P.O. Box 542, 5101-A Mérida, Venezuela.

## Assistant Editors

**Dr R.E. Synovec**, Department of Chemistry, University of Washington, Box 351700, Seattle, WA 98195-1700, U.S.A.

**Professor J.-C. Vire**, Université Libre de Bruxelles, Institut de Pharmacie, Campus de la Plaine, C.P. 205/6, Boulevard du Triomphe, B-1050 Bruxelles, Belgium

## Talanta

R. Apak (Istanbul, Turkey)  
E. Bakker (Auburn, AL, U.S.A.)  
D. Barceló (Barcelona, Spain)  
B. Birch (Luton, UK)  
K. S. Booksh (Tempe, AZ, U.S.A.)  
J.-L. Capelo-Martinez (Caparica, Portugal)  
Z. Cai (Kowloon, Hong Kong)  
O. Chailapakul (Thailand)  
S. Cosnier (Grenoble, France)  
D. Diamond (Dublin, Ireland)  
W. Frenzel (Berlin, Germany)  
A.G. Gonzales (Seville, Spain)  
E.H. Hansen (Lyngby, Denmark)  
P. de B. Harrington (OH, U.S.A.)

A. Ho (Hsin-chu, Taiwan)  
P. Hubert (Liège, Belgium)  
J. Kalivas (Pocatella, ID, U.S.A.)  
B. Karlberg (Stockholm, Sweden)  
J.-M. Lin (Beijing, China)  
Y. Lin (Richland, WA, U.S.A.)  
M.D. Luque de Caastro (Cordoba, Spain)  
I.D. McKelvie (Victoria, Australia)  
S. Motomizu (Okayama, Japan)  
D. Nacapricha (Bangkok, Thailand)  
J.-M. Pingarron (Madrid, Spain)  
E. Pretsch (Zürich, Switzerland)  
W. Schuhmann (Bochum, Germany)  
M. Shamsipur (Kermanshah, Iran)

M. Silva (Porto Alegre, Brazil)  
P. Solich (Hradec Králové, Czech Republic)  
K. Suzuki (Yokohama, Japan)  
D.G. Themelis (Thessaloniki, Greece)  
D.L. Tsalev (Sofia, Bulgaria)  
Y. van der Heyden (Belgium)  
B. Walczak (Katowice, Poland)  
J. Wang (Tempe, AZ, U.S.A.)  
J.D. Winefordner (Gainesville, U.S.A.)  
Xiu-Ping Yan (Tianjin, China)  
E.A.G. Zagatto (Piracicaba, SP, Brazil)  
X. Zhang (China)

---

Copyright © 2008 Elsevier B.V. All rights reserved

**Publication information:** *Talanta* (ISSN 0039-9140). For 2008, volumes 74–76 are scheduled for publication. Subscription prices are available upon request from the Publisher or from the Regional Sales Office nearest you or from this journal's website (<http://www.elsevier.com/locate/talanta>). Further information is available on this journal and other Elsevier products through Elsevier's website: (<http://www.elsevier.com>). Subscriptions are accepted on a prepaid basis only and are entered on a calendar year basis. Issues are sent by standard mail (surface within Europe, air delivery outside Europe). Priority rates are available upon request. Claims for missing issues should be made within six months of the date of dispatch.

**Orders, claims, and journal enquiries:** please contact the Customer Service Department at the Regional Sales Office nearest you:

**Orlando:** Elsevier, Customer Service Department, 6277 Sea Harbor Drive, Orlando, FL 32887-480 USA; phone: (+1) (877) 8397126 [toll free number for US customers], or (+1) (407) 3454020 [customers outside US]; fax: (+1) (407) 3631354; e-mail: [usjcs@elsevier.com](mailto:usjcs@elsevier.com)

**Amsterdam:** Elsevier, Customer Service Department, PO Box 211, 1000 AE Amsterdam, The Netherlands; phone: (+31) (20) 4853757; fax: (+31) (20) 4853432; e-mail: [nlinfo-f@elsevier.com](mailto:nlinfo-f@elsevier.com)

**Tokyo:** Elsevier, Customer Service Department, 4F Higashi-Azabu, 1-Chome Bldg, 1-9-15 Higashi-Azabu, Minato-ku, Tokyo 106-0044, Japan; phone: (+81) (3) 5561 5037; fax: (+81) (3) 5561 5047; e-mail: [jp.info@elsevier.com](mailto:jp.info@elsevier.com)

**Singapore:** Elsevier, Customer Service Department, 3 Killiney Road, #08-01 Winsland House I, Singapore 239519; phone: (+65) 63490222; fax: (+65) 67331510; e-mail: [asiainfo@elsevier.com](mailto:asiainfo@elsevier.com)

**USA mailing notice:** *Talanta* (ISSN 0039-9140) is published monthly by Elsevier B.V. (P.O. Box 211, 1000 AE Amsterdam, The Netherlands). Annual subscription price in the USA US\$ 4,085 (valid in North, Central and South America), including air speed delivery. Application to mail at periodical postage rate is paid at Rutherford, NJ and additional mailing offices.

**USA POSTMASTER:** Send address changes to *Talanta*, Publications Expediting Inc., 200 Meacham Avenue, Elmont, NY 11003.

**AIRFREIGHT AND MAILING** in the USA by Publications Expediting Inc., 200 Meacham Avenue, Elmont, NY 11003.



## Short communication

## Determination of OH groups in humic acids using methylation with dimethylsulfate

Pavel Kuráň<sup>a,b,\*</sup>, Pavel Janoš<sup>b</sup>, Libuše Madronová<sup>a</sup>, Jaromír Novák<sup>a</sup>, Josef Kozler<sup>a</sup>

<sup>a</sup> Research Institute of Inorganic Chemistry, a.s., Revoluční 84, 400 01 Ústí nad Labem, Czech Republic

<sup>b</sup> University of Jan Evangelista Purkyně, Faculty of the Environment, Králova Výchina 3132/7, 400 96 Ústí nad Labem, Czech Republic

## ARTICLE INFO

## Article history:

Received 5 December 2007

Received in revised form 11 April 2008

Accepted 16 April 2008

Available online 24 April 2008

## Keywords:

Humic acids

OH groups content

Carboxylic groups content

Methylation

## ABSTRACT

The methylation of humic acids (HA) with dimethylsulfate in acetone and methanol followed by the iodometric determination of the methoxy groups (Zeisel reaction) were applied to determine the contents of –OH groups in solid samples of HA of different origins. For the coal- and peat-derived HA samples, the contents of –OH groups determined after methylation in acetone ranged from 6.6 to 8.7 mmol/g, whereas the contents of –OH groups determined after methylation in methanol ranged from 4.0 to 5.0 mmol/g. These differences may be related to the content of carboxylic groups in the HA molecule that were not methylated in methanol, as confirmed by a comparison with results of conventional titrimetric determinations. Observed differences were interpreted as results of different polarity of both solvents and alkalinity of the reaction mixture during the methylation. The contents of alcoholic groups as well as some other minor –OH groups can be estimated using the –OH group contents obtained after methylation in both solvents together with the results of the conventional determinations of acidic functional groups. A repeatability of the –OH groups determination as estimated from a series of triplicate analyses of different HA samples ( $n = 7$ ) was in range of 0.15–0.73 mmol/g and 0.08–1.06 mmol/g (standard deviations) for methylation in acetone and methanol, respectively. Thus, the average repeatability of the –OH groups determination was estimated to be 0.38 and 0.50 mmol/g for methylation in acetone and methanol, respectively.

© 2008 Elsevier B.V. All rights reserved.

### 1. Introduction

The diversity of functional groups and a complex structural skeleton of humic substances (HS) make their fractionation and structural characterization by common approaches rather difficult. Therefore, the development of new analytical approaches or combination of different known techniques is still desirable. One of important tools in the characterization of HS represents derivatization. The aim of derivatization is a modification of certain properties of HS in a desired way, e.g. for easier detection, elimination of hydrogen bonds or reduction of HS polarity [1]. The most frequent functional groups occurring in the structure of HS are –OH groups either alone standing (phenolic, alcoholic, enolic –OH) or as a part of other functional groups (carboxylic –COOH, hydroperoxidic –O–OH). The derivatization of –OH groups in HS is mainly done using methylation as a relatively common way of acidic hydro-

gen substitution in –OH groups [2,3]. Ricca et al. [4] reported on the methylation of –OH groups in humic acids (HA) obtained from Leonardite using the mixture  $\text{CH}_3\text{I}/\text{Ag}_2\text{O}$  in methanol and dimethylformamide. The main goal of methylation was the removal of strong hydrogen bonds in HA leading to the formation of intra- and intermolecular aggregates disabling their dissolution in organic solvents and thereby the determination of their molecular mass. The methylated products were well soluble in organic solvents, which enabled their analysis by spectral techniques (IR,  $^1\text{H}$  and  $^{13}\text{C}$  NMR). The IR spectra of the methanolic product showed that all –COOH groups were derivatized to methyl esters (absorption band at  $1730\text{ cm}^{-1}$ ). Other –OH groups were methylated only partly (absorption at  $3450\text{ cm}^{-1}$ ). When dimethylformamide was used as a solvent both carboxylic –OH as well as other –OH groups were methylated (no absorption at  $3450\text{ cm}^{-1}$ , strong absorption at  $1730\text{ cm}^{-1}$ ). The analysis of HA by  $^{13}\text{C}$  NMR after methylation by diazomethane and alkali hydrolysis of methylated products was the subject of the paper published by Sachs et al. [5]. In the first step, the –COOH groups were blocked by methylation in the form of methylesters, whereas the phenolic –OH groups were blocked as methylethers, as confirmed by NMR. In the second step, the selective hydrolysis of methylesters in alkali solution was carried out. Thereby the –COOH

\* Corresponding author at: Research Institute of Inorganic Chemistry, a. s., Revoluční 84, 400 01, Ústí nad Labem, Czech Republic. Tel.: +420 475 309 269; fax: +420 475 212 079.

E-mail address: [pavel.kuran@vuanch.cz](mailto:pavel.kuran@vuanch.cz) (P. Kuráň).

groups were again unblocked. The methylethers did not hydrolyzed under given conditions. This procedure enabled to study the influence of phenolic OH groups on the complexation behaviour of HA. The methylation of HA in situ with tetramethylammonium hydroxide (TMAH) was applied to study the HA structure by conventional flash pyrolysis [6]. It was stated that the methylation protected –COOH groups and aliphatic chains during the pyrolysis against the cleavage and chemical reactions even with an excess of sulphur. The similar technique was used for the study of distribution of HS and lipids in two different sewage sludges [7]. HA were investigated by elemental analysis, IR and thermally assisted hydrolysis and methylation coupled to GC–MS (THM–GC–MS). The influence of methylation with diazomethane on molecular mass distribution in aqueous fulvic acids was investigated by electrospray mass spectrometry [8]. The aim of methylation was to suppress the influence of acidic hydrogens in the formation of aggregates of fulvic acids and to eliminate the formation of higher charged ions during the MS analysis. The successfulness of methylation was monitored by IR.

The methylation with dimethylsulfate [1–3] or acetylation with acetic anhydride [1,3] have been applied often for the determination of –OH groups (or “total –OH”) contents in HA. When dimethylsulfate is used as methylating agent the sample is repeatedly let to react with it in alkali solution. The formed precipitate is analyzed after acidification on the presence of methoxy groups by Zeisel reaction. It is supposed usually that only phenolic and enolic –OH groups react with dimethylsulfate. The possible problems with side reactions of formed sulfate in aqueous alkali solution can be eliminated by using acetone [2] or methanol [1] as solvent instead of water.

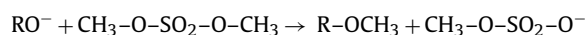
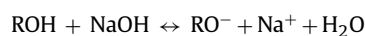
In this work, the methylation with dimethylsulfate was employed for the determination of the –OH groups contents in HA. Significant differences were observed when acetone and methanol were used as solvents during the methylation—a possible explanation of this phenomenon is given in the paper. It was also shown that some useful additional parameters, such as amounts of alcoholic or some minor –OH groups, can be estimated from the –OH groups content determined by the proposed method and other parameters determined by conventional titrimetric procedures.

## 2. General principle of the determination

The procedure for the determination of –OH groups consists of two steps:

1. The substitution of hydrogen in –OH groups by methyl groups (–CH<sub>3</sub>).
2. The cleavage of the methoxy groups (–OCH<sub>3</sub>) by hydroiodic acid under formation of gaseous methyl iodide, which is trapped in bromine water and determined by iodometric titration as released iodine (Zeisel reaction).

The substitution of hydrogen in –OH group is realized by reaction between HA and dimethylsulfate (CH<sub>3</sub>)<sub>2</sub>SO<sub>4</sub>, which can be described by the following equations [2]:



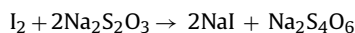
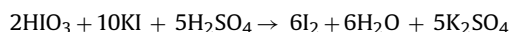
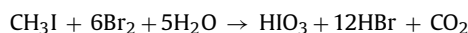
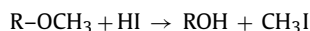
The methylation reaction can be carried out in the system of acetone with K<sub>2</sub>CO<sub>3</sub> or methanol with K<sub>2</sub>CO<sub>3</sub>. Because none of these solvents is preferred in literature, the methylation was done in both solvents in this work in order to investigate their influence on the determination of the –OH groups in HA.

**Table 1**  
Solid HA used in this work

Sample	Origin and basic characteristics
HA1	HA from oxihumolite <sup>a</sup> from North-Bohemian coal basin, mining site Václav (1), content of H <sub>2</sub> O 7.1%, ash content 2.8%
HA2	Refined HA from HA1, content of H <sub>2</sub> O 7.5%, ash content 1.8%
HA3	HA from oxihumolite <sup>a</sup> from North-Bohemian coal basin, mining site Václav (2), content of H <sub>2</sub> O 5.7%, ash content 7.7%
HA4	HA from oxihumolite <sup>a</sup> from North-Bohemian coal basin, mining site Vršany, content of H <sub>2</sub> O 7.3%, ash content 11.2%
HA5	HA from peat from South-Bohemian basin Třeboň, locality Braná, content of H <sub>2</sub> O 7.0%, ash content 7.1%
HA6	HA from peat from Bohemian Forest, locality Světlík, content of H <sub>2</sub> O 6.6%, ash content 5.1%
HA7	HA from young brown coal oxidized by HNO <sub>3</sub> , mining site Družba, Sokolov Basin, content of H <sub>2</sub> O 6.2%, ash content 2.0%

<sup>a</sup> Weathered, naturally oxidized young brown coal.

The determination of –OCH<sub>3</sub> groups by the Zeisel reaction can be described by the following equations [3]:



The content of methoxy groups in HA samples found by the Zeisel reaction should be recalculated on the –OH content (in mmol/g of the dried- and ash-free sample).

## 3. Experimental

### 3.1. Materials and reagents

Various kinds of solid HA were prepared from young brown coals and other materials (peats) by alkaline extraction and acid precipitation, as described in details elsewhere [9]. The solid samples were used without an additional pre-treatment except of grinding. A list of the HA samples used in this work is given in Table 1 together with their basic characterization. Stock solution of Na<sub>2</sub>S<sub>2</sub>O<sub>3</sub> (0.1 mol/l) was prepared from reagent-grade product (Lach-Ner, Neratovice, Czech Republic) and standardised by a conventional titrimetric procedure. The solutions were prepared in deionised water from the system Demi Ultra 20 (Goro, Prague, Czech Republic) utilising reverse osmosis and mixed-bed ion-exchange for the water purification. Bromine water for the Zeisel reaction was prepared as follows: Dissolve 100 g of potassium acetate (Lach-Ner) in 1000 ml of solution containing 900 ml of glacial acetic acid (Penta, Chrudim, Czech Republic) and 100 ml of acetic acid anhydride (Aldrich, Steinheim, Germany). Then dissolve 5 ml of bromine (Aldrich) in 145 ml of the potassium acetate solution. This solution must be prepared daily fresh. Water-free K<sub>2</sub>CO<sub>3</sub> was prepared by ignition of the reagent-grade product (Lach-Ner) over the Bunsen burner in a Pt vessel for 15 min and stored in a desiccator over silica gel. Sodium acetate buffer was prepared by dissolving 220 g sodium acetate (Lach-Ner) in 1 l of deionized water. Organic solvents (acetone, methanol) were of reagent-grade quality, obtained from Penta, Chrudim, Czech Republic, dimethylsulfate (99%) was obtained from Aldrich.

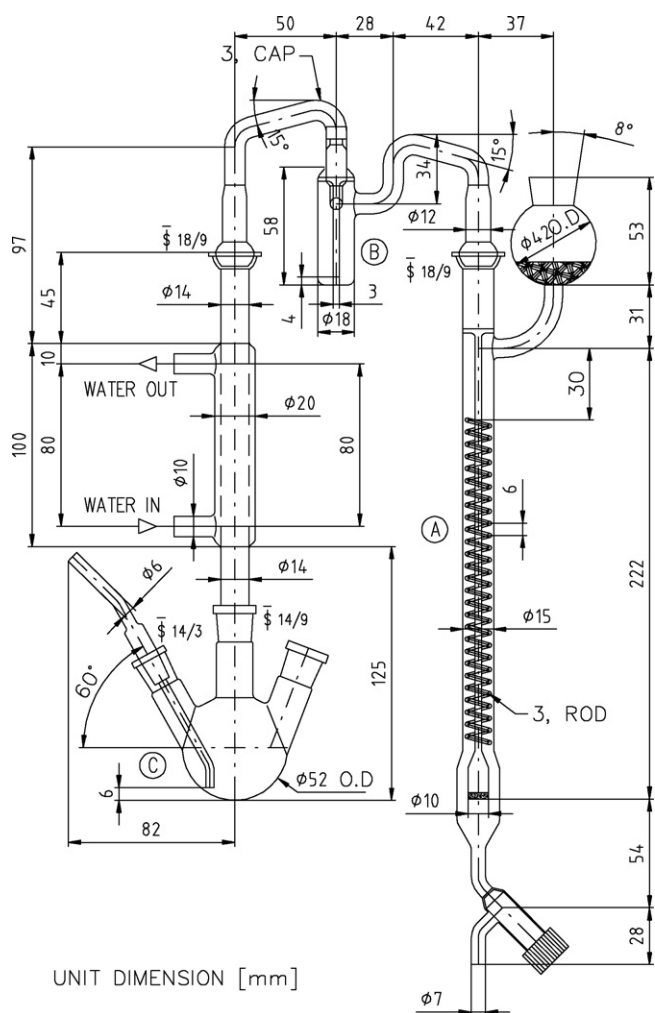


Fig. 1. Apparatus for the Zeisel reaction. (A) Absorber filled with bromine water; (B) iodine vapour trap; (C) reaction flask with water cooler.

### 3.2. Apparatus and procedures

Procedure for methylation with dimethylsulfate: 1 g of HA was refluxed for 24 h with 14 ml of dimethylsulfate and 24 g of water-free  $K_2CO_3$  in 40 ml acetone or methanol in 100 ml rounded flask under water cooler. The reaction mixture was continuously stirred by magnetic stirrer to avoid a secret boiling. Then the organic solvent was removed from the reaction mixture by distillation under normal pressure using a water bath. The reaction mixture was acidified to pH 2 with HCl (ca. 2 mol/l) to precipitate solid HA. The precipitated HA was dried overnight at 40 °C in an oven. Dry HA was re-methylated three times with 8 ml of dimethylsulfate and 16 g of water-free  $K_2CO_3$  in 40 ml acetone or methanol.

Procedure for the Zeisel reaction: the apparatus for the Zeisel reaction was constructed as described in the literature [10,11] with slight modifications only (Fig. 1). In principle, the apparatus consists of an absorber (A) filled with bromine water and of a distillation part containing an iodine vapour trap (B), water cooler and a reaction flask (C) with the arm for nitrogen supply. The Zeisel reaction was carried out as follows: add 3 ml of deionized water to the iodine vapour trap and 10 ml of bromine water to the absorber. Attach the absorber to distillation part. Weigh 50 mg of HA sample into the reaction flask, add 6 ml of hydroiodic acid (57%, Aldrich) and attach the reaction flask to the apparatus. Connect the side arm of the reaction flask to nitrogen source and adjust the flow rate of nitrogen

Table 2

Determination of the OH groups content using methylation in acetone ( $(OH)_{ac}$ ) and in methanol ( $(OH)_{meth}$ ) with corresponding standard deviations (S.D.) calculated from triplicate analyses

Sample	$(OH)_{ac}$ (mmol/g)	S.D. (mmol/g)	$(OH)_{meth}$ (mmol/g)	S.D. (mmol/g)
HA1	8.4	0.26	4.9	0.20
HA2	8.4	0.15	4.0	1.06
HA3	8.7	0.64	5.0	0.35
HA4	8.7	0.73	4.4	0.65
HA5	6.9	0.25	4.1	0.50
HA6	6.6	0.37	4.7	0.68
HA7	7.1	0.29	4.6	0.08

Values were re-calculated on the water- and ash-free samples.

through iodine vapour trap to 2 bubbles/s. Heat the reaction flask for 3 h at 150 °C. Then transfer the content of the absorber to the vial containing 15 ml of sodium acetate buffer. Eliminate the excess of bromine by adding a few drops of formic acid (check with the methyl red indicator [12]). When the solution is free of bromine add 5 ml of sulphuric acid (ca. 2 mol/l) and titrate the released iodine with 0.1 mol/l sodium thiosulfate. Simultaneously, the blank experiments with all reagents were carried out.

It should be taken into account that the methylation reaction increases the weight of the sample. Therefore, the conversion of percentage of methoxy groups in methylated product to percentage of –OH groups in the original sample must be done as follows:

$$\text{percentage of –OH in original sample} = \frac{1700(Y_2 - Y_1)}{3100 - 14Y_2}$$

where  $Y_1$  is the percentage of –OCH<sub>3</sub> in the original sample and  $Y_2$  is the percentage of –OCH<sub>3</sub> in the methylated product.

Conventional titrimetric procedures were used for the determination of acidic functional groups in HA, namely the barium hydroxide method for the determination of total acidity and the calcium acetate exchange method for the determination of carboxylic groups, respectively [13]. For comparison, the content of carboxylic groups was determined also from the acid–base titration curves [14] using the method of Ritchie and Perdue [15].

## 4. Results and discussion

The –OH groups contents and corresponding standard deviations from triplicate analyses obtained by methylation with dimethylsulfate in acetone ( $(OH)_{ac}$ ) and in methanol ( $(OH)_{meth}$ ) followed by the Zeisel reaction are given in Table 2. It is distinct that the values of  $(OH)_{ac}$  are almost two times higher in comparison with  $(OH)_{meth}$ . As already mentioned, the difference in using acetone or methanol for determination of the –OH groups is not emphasized in literature [2,3]. The possible explanation of this difference consists in a different reaction environment, especially regarding the alkalinity of the reaction mixture and polarity of the used solvents.

Table 3

Determination of carboxylic functional groups—a comparison of various methods

Sample	Ca acetate method (mmol/g)	From titration curve <sup>a</sup> (mmol/g)	From the difference between $(OH)_{ac}$ and $(OH)_{meth}$ (mmol/g)
HA1	4.9	4.5	3.6
HA2	4.1	5.0	4.4
HA3	4.0	4.1	3.7
HA4	3.7	4.4	4.3
HA5	2.7	3.4	2.8
HA6	2.5	3.2	1.9
HA7	3.0	3.3	2.5

<sup>a</sup> Calculated according to the procedure of Ritchie and Perdue [15] from the base consumption up to pH 8.

**Table 4**  
Contents of various functional groups in HA

Sample	Total acidity <sup>a</sup> (mmol/g)	Phenolic groups <sup>b</sup> (mmol/g)	TAB groups <sup>c</sup> (mmol/g)	Alcoholic groups <sup>d</sup> (mmol/g)
HA1	9.4	4.5	1.0	0.3
HA2	9.3	5.2	1.0	<0.1
HA3	9.6	5.6	1.0	<0.1
HA4	10.0	6.3	1.3	<0.1
HA5	8.1	5.4	1.2	<0.1
HA6	7.4	5.0	0.9	<0.1
HA7	7.6	4.6	0.5	<0.1

<sup>a</sup> Barium hydroxide method.

<sup>b</sup> Determined by the conventional procedures as a difference between the total acidity and the content of carboxylic groups.

<sup>c</sup> Sum of tertiary allyl and benzyl OH groups determined as a difference between the total acidity and (OH)<sub>ac</sub>.

<sup>d</sup> Calculated from the difference between (OH)<sub>meth</sub> and the phenolic group content.

Due to higher polarity of methanol in comparison to acetone the solubility of K<sub>2</sub>CO<sub>3</sub> in the reaction mixture was higher, and consequently the alkalinity of the reaction mixture was higher, too. Increased alkalinity of the reaction mixture led to the methylation of phenolic, alcoholic and hydroperoxidic –OH groups (–O–OH) only in methanol. When acetone was used as solvent, on the other hand, the methylation of carboxylic groups (–COOH) together with the previously mentioned –OH groups took place. It was found in early studies on the methylation of HA with dimethylsulfate that the carboxylic groups are not methylated in strongly alkaline solutions [16,17], but they are methylated under mildly alkaline conditions [18], which supports the above explanation. Thus, the difference between (OH)<sub>ac</sub> and (OH)<sub>met</sub> could give the content of –COOH groups in the HA molecule. The comparison of the contents of carboxylic groups as determined by three different procedures is given in Table 3. As can be seen, the obtained results for the three different procedures are in a reasonable agreement, taking into account quite different principles of the determinations. The values of –COOH content calculated as the difference between (OH)<sub>ac</sub> and (OH)<sub>met</sub> are mostly in the interval allocated by two remaining techniques.

As can be deduced from literature [1], some minor –OH groups (tertiary, allyl and benzyl) are not methylated with dimethylsulfate. Hence, the content of these groups can be estimated from the difference between the total content of –OH groups (total acidity) and the (OH)<sub>ac</sub> value—see Table 4. Moreover, the content of alcoholic groups can be calculated as a difference between (OH)<sub>meth</sub> and the content of phenolic groups, as determined by the titrimetric procedure (Table 4).

## 5. Conclusions

The methylation of HA with dimethylsulfate in acetone and methanol was applied to various solid samples of HA of different origins. It was found that the content of –OH groups determined after methylation in acetone is higher than the content of –OH groups determined after methylation in methanol. This difference may be related to the content of carboxylic groups in the HA molecule, as confirmed by a comparison with results of conventional titrimetric determinations. Observed differences were interpreted as results of different polarity of both solvents and alkalinity of the reaction mixture. The contents of alcoholic groups as well as some other minor –OH groups can be estimated using

the –OH group contents obtained after methylation in both solvents together with the results of the conventional determinations of acidic functional groups. A repeatability of the –OH groups determination as estimated from a series of triplicate analyses of different HA samples ( $n = 7$ ) was in range of 0.15–0.73 mmol/g and 0.08–1.06 mmol/g (standard deviations) for methylation in acetone and methanol, respectively. Thus, the average repeatability of the –OH groups determination was estimated to be 0.38 and 0.50 mmol/g for methylation in acetone and methanol, respectively.

## Acknowledgments

The paper was prepared in the research centre “Advanced remediation technologies and processes”, which is supported from the Ministry of Education, Youth and Sports of the Czech Republic, grant no. 1M0554. The financial support from the Ministry of Industry and Trade of the Czech Republic, project no. FT-TA/038, is also acknowledged.

## References

- [1] J.A. Leenheer, T.I. Noyes, in: M.H.B. Hayes, P. MacCarthy, R.L. Malcolm, R.S. Swift (Eds.), *Humic Substances II: In Search of Structure*, John Wiley, New York, 1989, pp. 257–280.
- [2] M. Schnitzer, *Soil Sci.* 117 (1974) 94.
- [3] F.J. Stevenson, *Humus Chemistry. Genesis, Composition, Reactions*, 2nd edition, Wiley, New York, 1994, pp. 212–235.
- [4] G. Ricca, F. Severini, G. Di Silvestro, C.M. Yuan, F. Adani, *Geoderma* 98 (2000) 115.
- [5] S. Sachs, M. Bubner, K. Schiede, G.R. Choppin, K.H. Heise, G. Bernhard, *Talanta* 57 (2002) 999.
- [6] C. Saiz-Jimenez, *Org. Geochem.* 23 (1995) 955.
- [7] V. Réveillé, L. Mansuy, E. Jardé, E. Garnier-Sillam, *Org. Geochem.* 34 (2003) 615.
- [8] C.E. Rostad, J.A. Leenheer, *Anal. Chim. Acta* 523 (2004) 269.
- [9] J. Novák, J. Kozler, P. Janoš, J. Čežíková, V. Tokarová, L. Madronová, *React. Funct. Polym.* 47 (2001) 101.
- [10] D. Miller, E.P. Samsel, J.G. Cobler, *Anal. Chem.* 33 (1961) 677.
- [11] D.G. Anderson, K.E. Isakson, D.L. Snow, D.J. Tesari, J.T. Vandenberg, *Anal. Chem.* 43 (1971) 894.
- [12] R.F. Milton, W.A. Waters (Eds.), *Methods of Quantitative Microanalysis*, 2nd edition, Edward Arnold Ltd., London, 1955.
- [13] E.M. Perdue, in: G.R. Aiken, D.M. McKnight, R.L. Wershaw (Eds.), *Humic Substances in Soil, Sediment and Water. Geochemistry, Isolation, and Characterization*, John Wiley&Sons, New York, 1985, pp. 493–526.
- [14] P. Janoš, S. Kříženecká, L. Madronová, *React. Funct. Polym.* 68 (2008) 242.
- [15] J.D. Ritchie, E.M. Perdue, *Geochim. Cosmochim. Acta* 67 (2003) 85.
- [16] W.S. Gilliam, *Soil Sci.* 49 (1940) 433.
- [17] W.G.C. Forsyth, *J. Agric. Sci.* 37 (1947) 132.
- [18] G.C. Briggs, G.J. Lawson, *Fuel* 49 (1970) 39.



## Enhanced sensitivity for Cu(II) by a salicylidine-functionalized polysiloxane carbon paste electrode

Hazem M. Abu-Shawish<sup>a,\*</sup>, Salman M. Saadeh<sup>b</sup>, Ahmad R. Hussien<sup>a</sup>

<sup>a</sup> Faculty of Science, Al-Aqsa University, Gaza, Palestine

<sup>b</sup> Chemistry Department, College of Sciences, The Islamic University of Gaza, P.O. Box 108, Gaza, Palestine

### ARTICLE INFO

#### Article history:

Received 10 January 2008

Received in revised form 24 April 2008

Accepted 25 April 2008

Available online 13 May 2008

#### Keywords:

Carbon paste electrodes

Potentiometry

Sol-gel

Copper(II) selective

Functionalized polysiloxane

### ABSTRACT

A new approach for decreasing the detection limit for a copper(II) ion-selective electrode (ISE) is presented. The ISE is designed using salicylidine-functionalized polysiloxane in carbon paste. This work describes the attempts to develop the electrode and measurements of its characteristics. The new type of renewable three-dimensional chemically modified electrode could be used in a pH range of 2.3–5.4, and its detection limit is  $2.7 \times 10^{-8} \text{ mol L}^{-1}$  ( $1.2 \mu\text{g L}^{-1}$ ). This sensor exhibits a good Nernstian slope of  $29.4 \pm 0.5 \text{ mV/decade}$  in a wide linear concentration range of  $2.3 \times 10^{-7}$  to  $1.0 \times 10^{-3} \text{ mol L}^{-1}$  of Cu(II). It has a short response time ( $\sim 8 \text{ s}$ ) and noticeably high selectivity over other Cu(II) selective electrodes. Finally, it was satisfactorily used as an indicator electrode in complexometric titration with EDTA and determination of copper(II) in miscellaneous samples such as urine and various water samples.

© 2008 Elsevier B.V. All rights reserved.

### 1. Introduction

Solid electrodes based on carbon materials are commonly used in electroanalysis due to their broad potential window, low background current, rich surface chemistry, low cost, chemical inertness and suitability for various sensing and detection applications [1,2]. Among them, carbon paste electrodes (CPEs) combine a carbon powder with a pasting liquid (an organic binder). The advantages of carbon paste electrodes drew the attention of researchers in recent years where these advantages were exploited for various measurements including potentiometric [3–7]. However the exact behaviour of carbon paste electrodes is not fully understood.

Silica-based organic–inorganic hybrids, most often dispersed in carbon paste electrodes, have been used for determination of metal ions [8].

Chemical modification of electrode surfaces is a strategy for improving the analytical performance of conventional electrode materials for specific applications in various fields, especially electroanalysis and sensors [9].

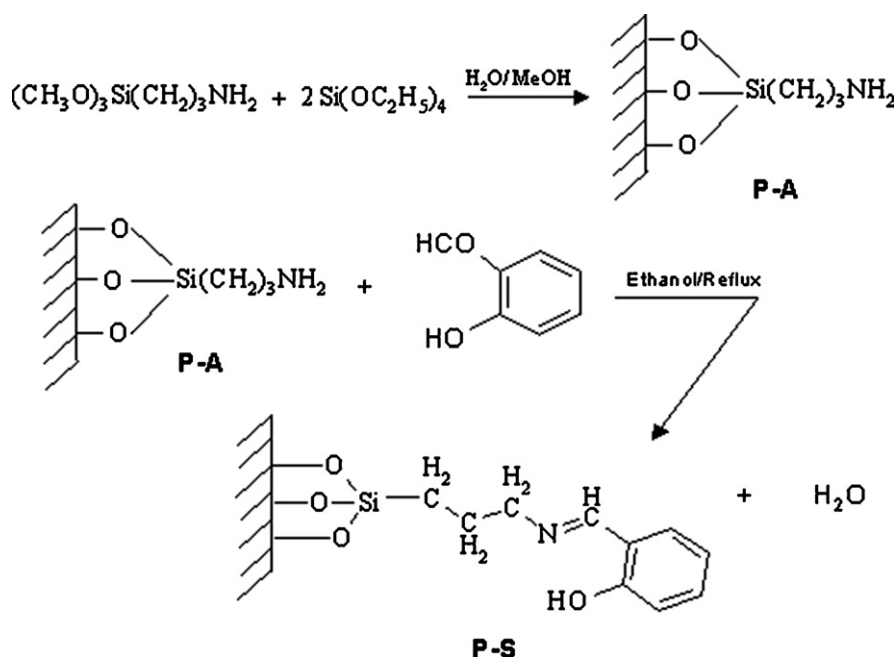
Silica-based organic–inorganic hybrids combine in a single solid both the properties of a rigid three-dimensional silica network with particular reactivity of the organic components [9,10]. These multifunctional materials are robust inorganic solids displaying both

high specific surface area and open surfaces interconnected to each other. They have been reported to be particularly suitable to design integrated electrochemical systems that likely offer attractive features in the field of electroanalytical chemistry [11,12]. These materials can be manufactured quite easily at room temperature by the sol-gel process and the resultant material will have properties of the tailor-based materials incorporated in the polymer. Therefore, these polymers were applied in various fields including chemical and biological sensors, separation processes and catalysis [13–17]. In particular, it is noted that organic and inorganic components are usually linked through strong chemical bonds and can coordinate metal ions efficiently. The complex-impregnated polymer has properties that can be utilized for specific targets. Use of silica gel in a sensor is likely to improve the detection limit because of its strong polar bonds, between silicon and oxygen, that can improve conductivity of the electrode and enhance its response.

Potentiometric determination of copper using carbon paste electrodes assumes importance in view of its widespread occurrence in various samples [3,18–20]. Copper deficiency results in anemia while its accumulation results in Wilson disease (WD) [21]. Therefore, devising proper methods for its determination in various samples is of utmost importance. In this work, a silica gel surface chemically modified with salicylaldehyde was prepared, characterized and found as a sensing material for Cu(II); it was employed in construction of an electrode that has competitive properties over many other electrodes.

\* Corresponding author.

E-mail address: [hazemona1@yahoo.co.uk](mailto:hazemona1@yahoo.co.uk) (H.M. Abu-Shawish).



**Scheme 1.** Preparation of 3-aminopropylpolysiloxane (P-A) and salicylic dinepropylimine polysiloxane ligand system (P-S).

## 2. Experimental

### 2.1. Reagents and materials

All chemicals used were of analytical grade. Tetraethylorthosilicate, 3-aminopropyltrimethoxysilane, and salicylaldehyde were purchased from Merk. Salicylaldehyde was obtained from Riedel-de Haen. Reagent grade pure graphite powder, bis(2-ethylhexyl) adipate (DOA), dioctyl phthalate (DOP), dibutyl phthalate (DBP), tris(2-ethylhexyl) phosphate (DOPh), dioctyl sebacate (DOS), paraffin oils (P.O.), as well as all metal salts such as chlorides, nitrates and sulphates were purchased from Aldrich. Diethyl ether and methanol (pectroscopic grade) were commercially available. All reagents and solvents were used as received.

### 2.2. Apparatus

All EMF measurements were carried out with the following assembly:

$\text{Hg}, \text{Hg}_2\text{Cl}_2(\text{s}), \text{KCl}(\text{sat.}) \parallel \text{sample solution} \mid \text{carbon paste electrode.}$

The potential measurements were carried out at  $25 \pm 0.1$  with a digital millivoltmeter (SR-MUL-3800). pH measurements were made on a digital pH meter (HANNA pH 211). A saturated calomel electrode (SCE) was used as a reference electrode. Analysis for carbon, hydrogen, and nitrogen were carried out, using an Elemental Analyzer EA 1110-CHNS CE Instrument. The infrared spectra for the materials were recorded on a PerkinElmer FTIR spectrophotometer using KBr disk in the range  $4000\text{--}400 \text{ cm}^{-1}$ .

### 2.3. Preparations

#### 2.3.1. Preparation of modified carbon paste electrode

A modified carbon paste electrode was prepared according to a previously reported method [22]. The paste was prepared by thoroughly mixing weighed amounts of the ionophore, high purity graphite and plasticizers as shown in Table 2 in plastic Petri dishes until a uniformly wet paste was obtained which was used for sensor

construction. Electrode bodies were made from 1 mL polypropylene syringes (3 mm i.d.), the tip of which had been cut off with a cutter. The mixture was packed in the end of the syringe. Electrical contact to the carbon paste was made by a copper wire. A fresh electrode surface was obtained by squeezing out a small amount of paste and scraping off the excess against a conventional paper then polishing the electrode on a smooth paper to obtain a shiny appearance. The electrode was used directly for potentiometric measurements without pre-conditioning.

#### 2.3.2. Synthesis of 3-aminopropylpolysiloxane (P-A)

Aminopropylpolysiloxane was prepared by adding 3-aminopropyltrimethoxysilane (9.86 g, 50 mmol) to a stirred solution of tetraethylorthosilicate (20.83 g, 100 mmol) in 15 mL methanol and HCl (9.95 mL,  $0.42 \text{ mol L}^{-1}$ ). Gelation occurred within a few seconds. The product was left to stand for 12 h then dried in a vacuum oven at  $90^\circ\text{C}$ . The material was crushed, sieved, washed successively with 50 mL portions of  $0.025 \text{ mol L}^{-1}$  NaOH, water, methanol and diethyl ether and then dried in vacuum oven at  $90^\circ\text{C}$  at 0.1 torr for 10 h. The elemental analysis for the aminopropylpolysiloxane is given in Table 1.

#### 2.3.3. Synthesis of salicylidinepropylimine polysiloxane ligand system (P-S)

3-Aminopropylpolysiloxane (P-A) (5.0 g, 17.5 mmol) was refluxed for 12 h with an excess (5 g, 41 mmol) of salicylaldehyde in 50 mL ethanol. The solid product was filtered off, washed successively with 50 mL portions of  $0.025 \text{ mol L}^{-1}$  NaOH, methanol

**Table 1**  
Elemental analysis data for P-A and P-G

Polysiloxane	%C	%H	%N	C/N
P-A				
Expected	15.7	3.9	6.1	3.0
Found	13.1	4.6	4.9	3.1
P-S				
Expected	30.9	3.1	3.6	10.0
Found	24.68	3.8	4.3	6.69

and diethyl ether and then dried in a vacuum oven at 90 °C for 12 h. The elemental analysis for salicylidinepropylimine polysiloxane (P-S) is given in Table 1 and Scheme 1.

#### 2.3.4. Metal uptake measurements

Metal uptake measurements were performed as described elsewhere [23]. To 50 mg samples of the functionalized polysiloxane-immobilized ligand system, P-S, was added a 25 mL 0.01 mol L<sup>-1</sup> solution of the appropriate metal ion (Cr<sup>3+</sup>, Co<sup>2+</sup>, Ni<sup>2+</sup>, Cu<sup>2+</sup>, Zn<sup>2+</sup>, Ag<sup>+</sup> and Cd<sup>2+</sup>) in the buffer using 50 mL polyethylene bottles. The mixture was shaken and allowed to stand for a week. Out of the supernatant solution, 250 μL was taken and diluted to 25 mL with water. The concentration of each metal ion in its aqueous solutions was measured versus an analogously made reference solution using a PerkinElmer AAnalyst-100 to estimate the metal uptake. Replicate solutions were used in the analyses.

### 2.4. Characterization

#### 2.4.1. Elemental analysis

From elemental analysis, given in Table 1, it is obvious that the reaction between 3-aminopropylpolysiloxane and salicylaldehyde occurred. The percentage of carbon increased and the percentage of nitrogen decreased in the product (P-S) as compared with the starting material (P-A). The lower carbon and higher nitrogen values are probably due to incomplete reaction of the amino groups with salicylaldehyde and that the surface amino groups only were involved in the reaction.

#### 2.4.2. The FTIR spectra

The FTIR spectra of the immobilized 3-aminopropylpolysiloxane (P-A) and the salicylidine-modified form (P-S) ligand systems are given in Fig. 1a and b. The spectrum in Fig. 1a shows three characteristic absorption bands: at 3500–3000 cm<sup>-1</sup> due to ν (OH) and/or ν (NH<sub>2</sub>), 1645–1560 cm<sup>-1</sup> due to δ(OH) and/or δ (NH<sub>2</sub>) and 1200–900 cm<sup>-1</sup> due to ν (Si–O). The spectrum of the immobilized ligand (P-S) in Fig. 1b shows a strong band at 1647 cm<sup>-1</sup> due to ν (C=N) stretching vibration. This confirms that the salicylidine-functionalized group is chemically bonded to the surface of the polysiloxane.

### 2.5. Selectivity of the electrode

Potentiometric selectivity of the sensor towards different inorganic cations in the chloride form and several anions were evaluated by applying the matched potential method (MPM) [24]. According to this method, the activity of Cu(II) was increased from  $a_A = 1.0 \times 10^{-5}$  mol L<sup>-1</sup> (reference solution) to  $\hat{a}_A = 2.0 \times 10^{-5}$  mol L<sup>-1</sup>, and the corresponding changes in potential (ΔE) were measured. Next, a solution of an interfering ion of concentration  $a_B$ , in the range  $1.0 \times 10^{-1}$  to  $1.0 \times 10^{-3}$  mol L<sup>-1</sup>, was added to a new  $1.0 \times 10^{-5}$  mol L<sup>-1</sup> (reference solution) until the same potential change (ΔE) was recorded. The selectivity factor,  $K_{A,B}^{MPM}$ , for each interferent was calculated using the following equation:

$$\frac{\Delta a_A}{a_B} = \frac{(\hat{a}_A - a_A)}{a_B} \quad (1)$$

In addition, the selectivity coefficients of interfering species were evaluated by the modified separate solution method, as described by Radu et al. and Bakker et al. [25,26]. According to this method, the potentiometric calibration curves are obtained for primary (I) and interfering ions (J), and the values of  $E_I^0$  and  $E_J^0$  are determined by extrapolating the response function to 1.0 mol L<sup>-1</sup>

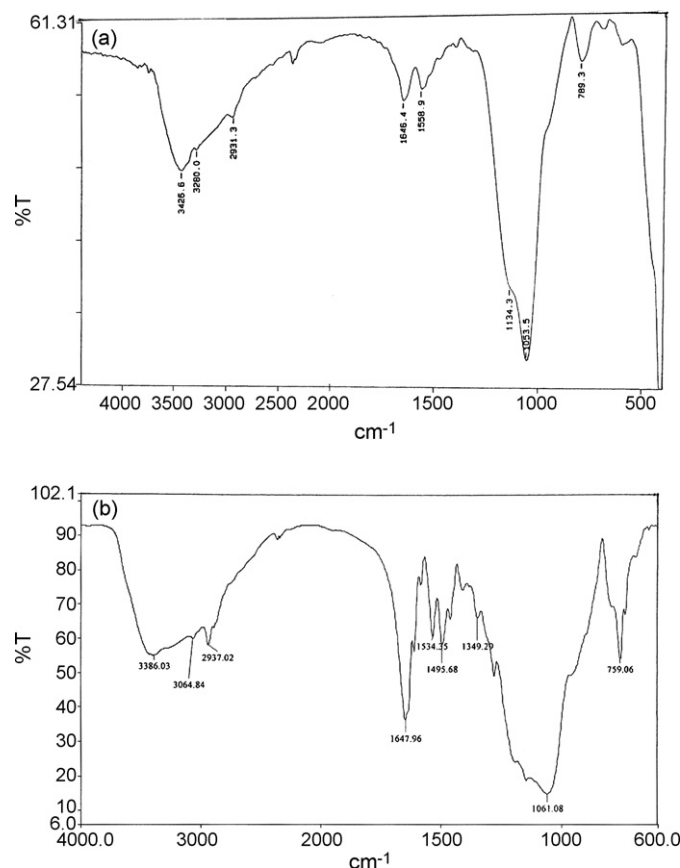


Fig. 1. FTIR spectra of (a) 3-aminopropylpolysiloxane (P-A), (b) salicylidinepropylimine polysiloxane.

activities. Eq. (1) can be used to determine the selectivity coefficients by this method.

$$K_{IJ}^{pot} = \frac{a_I}{a_J^{z_I/z_J}} \exp \left\{ \frac{E_J - E_I}{RT} z_I F \right\} = \exp \left\{ \frac{E_J^0 - E_I^0}{RT} z_I F \right\} \quad (2)$$

### 2.6. Sample preparation

The analysis of water samples does not require pretreatment before potentiometric determination using the present sensor. Analyses were performed using the standard addition method on 80 mL of water samples followed by spiking with either  $1.0 \times 10^{-3}$  or  $1.0 \times 10^{-2}$  mol L<sup>-1</sup> CuCl<sub>2</sub>. Different quantities of CuCl<sub>2</sub> and 4 mL urine were transferred to 25 mL measuring flasks and were filled completely to the mark with doubly distilled water to give solutions of concentrations ranging from  $1.0 \times 10^{-7}$  to  $1.0 \times 10^{-5}$  mol L<sup>-1</sup> CuCl<sub>2</sub> and measured as indicated above.

## 3. Results and discussion

Silica are promising candidates as sensing layers of mass sensitive devices because of their advantages and known applications in different areas of analytical chemistry. Organic modification of silica enables incorporation of different functional groups in order to improve the selectivity as these materials possess many advantages like molecular recognition and selective properties on the matrix. Walcarius et al. [14] presented reviews about the preparation and application of silica-modified electrodes showing their importance as electroanalytical sensors.



Salicylaldehyde reacts with 3-aminopropylpolysiloxane, (P-A), to produce the salicylidine derivative, (P-S), which is a bidentate ligand. It is known that this ligand produces a much more stable complex due to the well-known chelate effect in coordination chemistry [27]. Measurements indicate that metal uptake of the ligand, P-S, has this order: Cu(II) > Co(II) > Ni(II) > Zn(II) > Cr(III) > Ag(I) > Cd(II).

Copper(II) uptake was the highest among the metal ions due to the higher stability of copper(II) complex with this ligand system. Therefore, it was considered a candidate for construction of a Cu(II) selective electrode.

### 3.1. Characteristics of the electrode

The general characteristics of sensor are outlined by determining its sensitivity, detection limit, linear range and selectivity coefficients. Some important features of carbon paste electrode, such as the properties of the plasticizer, the graphite(G)/plasticizer(P) ratio, the nature and amount of the ionophore, are reported to significantly influence the sensitivity and selectivity of the sensor.

#### 3.1.1. Effect of functionalized polysiloxane concentration on electrode potential

The influence of the amount of functionalized polysiloxane as an ionophore on the potential response of the electrode was studied and the corresponding results are summarized in Table 2. The electrode without the ionophore shows poor sensitivity to copper cations, sensor no. 1, whereas the sensitivity of the electrode response increased with increasing ionophore content until the value of 3.5 wt% was reached. It is interesting to note that the graphite/plasticizer ratio of ca. 1.12 showed the optimum physical properties and ensured high enough mobilities of their constituents [28]. Further addition of the ionophore (sensor nos. 10 and 11), however, resulted in a little decrease in the response of the electrode, most probably due to some inhomogenities and possible saturation of the paste [29].

#### 3.1.2. Plasticizer selection

Two parameters are of importance when manufacturing a carbon paste: (1) its mechanical stability and (2) its active surface area. Mechanical stability can be interpreted as the ability of the carbon paste to avoid erosion in solution. The use of plasticizers will give some permeable properties to the paste and will improve its mechanical stability by promoting binding between grains [30]. A range of G/P ratios can be used. In this study, the highest useful ratio of G/P considered was 1.25 which produced a “crumbly” paste. The lowest ratio of 1.01 had a consistency resembling that of “peanut butter”. It was found that G/P ratio of 1.12 showed the best results.

In addition, the solvent mediator, in particular, has a dual function: it acts as a liquifying agent, enabling homogenous solubilization and modifying the distribution constant of the ionophore used. The proportion of solvent mediator must be optimized in order to minimize the electrical asymmetry of the paste, to keep the sensor as clean as possible, and to stop leaching to the aqueous phase [31]. For a plasticizer to be adequate for use in sensors, it should gather certain properties and characteristics such as having high lipophilicity, high molecular weight, low tendency for exudation from the paste matrix, low vapor pressure and high capacity to dissolve the substrate and other additives present in the paste [32]. In exploration for a suitable plasticizer for constructing this electrode, we used six plasticizers, with the values of dielectric constants, lipophilicity and molecular weight respectively listed in parantheses, namely, DOA ( $\epsilon_r = 3.9$ ,  $P_{TLC} = 6.1$ , M.wt. = 370), DOP ( $\epsilon_r = 5.1$ ,  $P_{TLC} = 7.0$ , M.wt. = 391), DBP ( $\epsilon_r = 6.4$ , M.wt. = 278), DOS ( $\epsilon_r = 3.9$ ,  $P_{TLC} = 10.1$ , M.wt. = 427), DOPh ( $\epsilon_r = 4.8$ ,  $P_{TLC} = 10.2$ ,

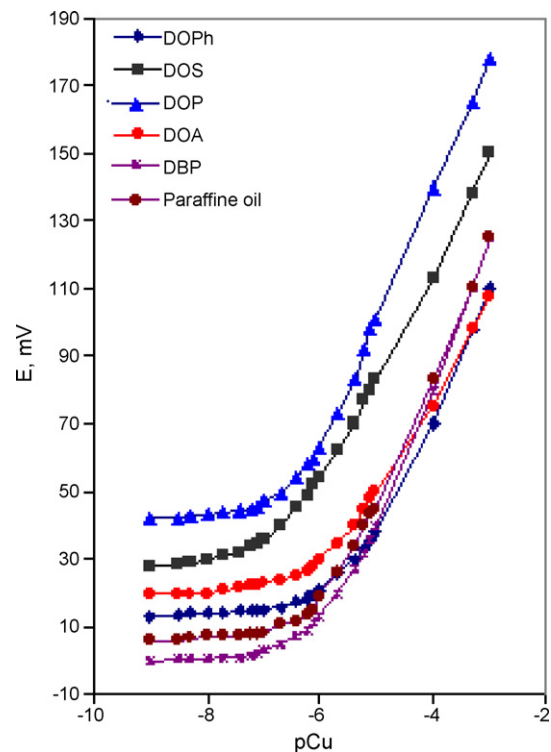


Fig. 2. Effect of different plasticizers on the response of Cu-CMCE.

M.wt. = 434) and paraffin oil, in sample electrodes to figure out the plasticizer with the best response. The CPE with DOS as a solvent mediator produced the best response, as shown in Fig. 2, likely due to high lipophilicity, relatively high molecular weight and low dielectric constant as well as two ester groups that, in principle, are capable of interacting with cationic species; this plasticizer may solvate and adjust the mobility of ionophore.

The results, given in Table 2, indicate that sensor no. 5, composed of 44.5% DOS, 52.0% graphite and 3.5% ionophore, gives the best sensitivity, with a Nernstian slope of  $29.4 \pm 0.5$  mV/decade and detection limit of  $2.7 \times 10^{-8}$  mol L<sup>-1</sup> over a relatively wide dynamic range ( $2.3 \times 10^{-7}$  to  $1.0 \times 10^{-3}$  mol L<sup>-1</sup>) of Cu<sup>2+</sup> ions. Therefore, this composition was used to study various operation parameters of the electrode. The electrochemical performance characteristics of this electrode were systematically evaluated according to the IUPAC recommendations [33].

#### 3.1.3. Homogeneity, surface-renewal and reproducibility of the electrode

The main attraction of using the modified electrode is that the electrode surface can be renewed after every use. The bulk-modified electrode can be renewed by squeezing a little carbon paste out of the tube and a fresh surface is smoothed on a piece of weighing paper whenever needed [34]. Accordingly, a paste of optimum composition and suitable weight (~2.0 g) can be used for several months without any deterioration or change in the response of the electrode.

To test paste homogeneity, the proposed electrode was applied for copper measurement in a  $5.0 \times 10^{-5}$  mol L<sup>-1</sup> copper(II) solution. The measurement was repeated ten times and after each measurement the electrode surface was renewed as explained above. The average potential was 105 mV and relative standard deviation (R.S.D.) 0.41, which are reasonable values.

The slope of the calibration graph was found to decrease slightly from  $29.4 \pm 0.5$  to  $21.6 \pm 1.8$  mV/decade after three times of use. This

**Table 2**  
Composition and response characteristics of Cu-CMCPE

Composition (wt%)				Electrode characteristics					
No.	I.P.	G	P	S (mV)	R.S.D.	C.R. (M)	$r^2$	LOD (M)	$t_{\text{resp}}$ (s)
1	–	51.0	49.0 (DOS)	$9.5 \pm 0.5$	0.85	$9.5 \times 10^{-7}$ to $1.0 \times 10^{-3}$	0.89	$6.3 \times 10^{-7}$	$\leq 36$
2	3.5	51.0	45.5 (DOA)	$18.5 \pm 0.7$	1.02	$8.5 \times 10^{-7}$ to $1.0 \times 10^{-3}$	0.98	$5.3 \times 10^{-7}$	$\leq 25$
3	3.5	51.0	45.5 (DOP)	$22.8 \pm 0.3$	1.32	$1.5 \times 10^{-7}$ to $1.0 \times 10^{-3}$	0.99	$4.8 \times 10^{-8}$	$\leq 15$
4	3.5	51.0	45.5 (DBP)	$26.1 \pm 0.9$	1.00	$2.9 \times 10^{-7}$ to $1.0 \times 10^{-3}$	0.98	$1.4 \times 10^{-7}$	$\leq 15$
5	3.5	51.0	45.5 (DOS)	$29.4 \pm 0.5$	0.54	$2.3 \times 10^{-7}$ to $1.0 \times 10^{-3}$	0.99	$2.7 \times 10^{-8}$	$\leq 8$
6	3.5	51.0	45.5 (DOPh)	$23.1 \pm 0.6$	0.89	$8.9 \times 10^{-7}$ to $1.0 \times 10^{-3}$	0.98	$2.1 \times 10^{-7}$	$\leq 25$
7	3.5	51.0	45.5 (P.O.)	$23.1 \pm 0.6$	2.36	$1.2 \times 10^{-6}$ to $1.0 \times 10^{-3}$	0.97	$7.4 \times 10^{-7}$	$\leq 43$
8	0.3	52.2	47.5 (DOS)	$19.1 \pm 1.2$	1.56	$8.2 \times 10^{-7}$ to $1.0 \times 10^{-3}$	0.98	$1.4 \times 10^{-7}$	$\leq 20$
9	2.0	52.5	45.5 (DOS)	$27.5 \pm 1.1$	1.85	$4.4 \times 10^{-7}$ to $1.0 \times 10^{-3}$	0.99	$5.4 \times 10^{-8}$	$\leq 12$
10	6.0	50.0	44.0 (DOS)	$20.8 \pm 1.3$	0.77	$9.0 \times 10^{-7}$ to $1.0 \times 10^{-3}$	0.97	$2.3 \times 10^{-7}$	$\leq 23$
11	10.0	50.0	40.0 (DOS)	$11.2 \pm 0.7$	2.95	$9.0 \times 10^{-7}$ to $1.0 \times 10^{-3}$	0.97	$2.3 \times 10^{-7}$	$\leq 20$

I.P.: ionophore, G: graphite, P: plasticizer, S: slope (mV/decade), C.R.: concentration range, LOD: low of detection,  $r^2$ : correlation coefficient,  $t_{\text{resp}}$ : response time (s).

decrease may be attributed to surface contamination and memory effect. Every use of the electrode results in coordination of copper ions to some of the functional groups on the surface. Repeated use of the electrode results in a drop of the measured potential as the number of coordination sites at the surface is limited. Precision in potential measurements of a certain solution requires removal of the coordinated sites. Therefore, the electrode surface should be polished to expose a fresh layer for use.

The sensor reproducibility was evaluated on the same surface by three successive measurements and resulted in a relative standard deviation of 4.1% and 1.9% for  $1.0 \times 10^{-3}$  and  $1.0 \times 10^{-4}$  mol L<sup>-1</sup> of Cu(II), respectively.

### 3.1.4. Response time and reversibility of the electrode

Generally, dynamic response time is a significant parameter for any ion-selective electrode (ISE). According to IUPAC recommendations, the response time may be defined as the time between addition of the analyte to the sample solution and the time when a limiting potential has been reached [33].

In this study, the response time of the electrode was measured by varying the copper concentration over the range  $1 \times 10^{-8}$  to  $1 \times 10^{-3}$  mol L<sup>-1</sup>. The electrode reaches equilibrium in about 5–10 s. As shown in Fig. 3, the response time increased to 15 s when the concentration was lowered to  $1 \times 10^{-8}$  mol L<sup>-1</sup>, where the error bars indicate the standard deviation obtained from three independent determinations. This apparently short response time is due to fast exchange kinetics of the metal–ligand complexation–decomplexation at the surface of the paste at concentrations  $\geq 1 \times 10^{-6}$  mol L<sup>-1</sup> [35].

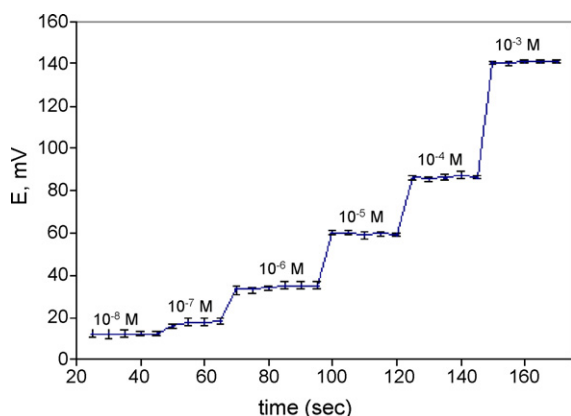


**Fig. 3.** Dynamic responses of the Cu-CMCPE obtained by successive increase of copper ion.

To evaluate the reversibility of the electrode [36], the potential measurements were performed in the sequence high-to-low (from  $1.0 \times 10^{-3}$  to  $1.0 \times 10^{-4}$  M) sample concentrations. The results showed that the response of the electrode was reversible; although the time needed to reach equilibrium values (37 s) was longer than that for low-to-high sample concentrations.

### 3.2. pH dependence

The influence of pH on the electrode potential of the Cu-CMCPE was studied for  $2.0 \times 10^{-5}$  and  $2.0 \times 10^{-4}$  mol L<sup>-1</sup> CuCl<sub>2</sub> solutions. The acidity was adjusted by adding small volumes of (1 mol L<sup>-1</sup>) HCl or NaOH to the test solutions and the variation in potential was followed. The results, shown in Fig. 4, indicate that the variation in potential due to pH change is considered acceptable in the pH range 2.3–5.4. However, there is a slight deviation at pH values lower than 2.3 which may be due to H<sup>+</sup> interference. On the other hand, the potential decreases gradually at pH values higher than 5.4. This drop may be attributed to formation of free copper hydroxide in the test solution.

### 3.3. Interference studies

Selectivity is an important characteristic of a sensor that delineates the extent to which the device may be used in estimation of the analyte ion in presence of other ions and the extent of utility of any sensor in real sample measurement [36]. The selectivity coefficients of the modified carbon paste electrode towards many inorganic cations, carbohydrates and amino acids were evaluated by the matched potential method [24] and the modified separate solution method, MSSM [25,26]. The values of the selectivity coefficients are listed in Table 3. It is noteworthy that the results obtained

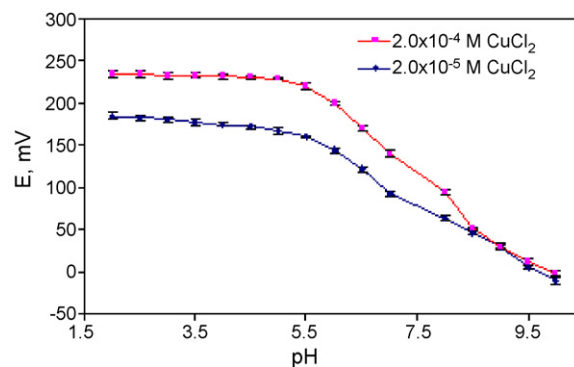


**Fig. 4.** Effect of pH of the test solution on the potential response of Cu-CMCPE.

**Table 3**  
Selectivity coefficients using MPM and MSSM for Cu-CMCPE

Interfering species, B	$K_{MPM}$	$K_{MSSM}$
Na <sup>+</sup>	$3.52 \times 10^{-5}$	$1.88 \times 10^{-6}$
K <sup>+</sup>	$4.18 \times 10^{-5}$	$1.18 \times 10^{-6}$
NH <sub>4</sub> <sup>+</sup>	$9.22 \times 10^{-3}$	$5.41 \times 10^{-5}$
Li <sup>+</sup>	$3.96 \times 10^{-5}$	$2.13 \times 10^{-7}$
Ag <sup>+</sup>	–	$1.97 \times 10^{-3}$
Ca <sup>2+</sup>	$3.13 \times 10^{-3}$	$4.43 \times 10^{-6}$
Cd <sup>2+</sup>	$1.08 \times 10^{-3}$	$2.52 \times 10^{-5}$
Zn <sup>2+</sup>	$2.19 \times 10^{-4}$	$8.42 \times 10^{-7}$
Co <sup>2+</sup>	$3.12 \times 10^{-3}$	$3.32 \times 10^{-5}$
Pb <sup>2+</sup>	$5.92 \times 10^{-3}$	$8.83 \times 10^{-5}$
Ni <sup>2+</sup>	$1.52 \times 10^{-5}$	$2.07 \times 10^{-6}$
Ba <sup>2+</sup>	$2.29 \times 10^{-3}$	$7.63 \times 10^{-5}$
Mg <sup>2+</sup>	$7.52 \times 10^{-5}$	$5.09 \times 10^{-7}$
Cr <sup>3+</sup>	$7.68 \times 10^{-2}$	$3.12 \times 10^{-3}$
Al <sup>3+</sup>	$3.52 \times 10^{-2}$	$1.39 \times 10^{-4}$
Ce <sup>3+</sup>	$1.12 \times 10^{-2}$	$2.54 \times 10^{-5}$
Fructose	No response	$1.19 \times 10^{-8}$
L-Histidine	No response	$6.39 \times 10^{-6}$
L-Cysteine	No response	$2.21 \times 10^{-6}$
Maltose	No response	$8.02 \times 10^{-8}$
D-Galactose	No response	$1.51 \times 10^{-8}$
L-Tyrosine	No response	$4.39 \times 10^{-6}$
Glycine	No response	$6.39 \times 10^{-8}$

from the two methods are different. The MSSM produced much better values than those obtained by the MPM. This is in accordance with expectations that the MSSM produces unbiased, thermodynamic selectivity coefficients [25]. The values in Table 3 reflect a very high selectivity of this electrode for copper cation over most of the tested species. This result is in accordance with our findings that this ligand has the highest uptake of Cu(II) over other metal ions.

#### 4. Analytical performance

In order to test the analytical applicability of the proposed sensor, it has been applied for determination of copper ions in biological and environmental samples using the standard additions method [37].

##### 4.1. Titration of copper solution with a standard EDTA solution

The proposed electrode was successfully applied as an indicator in titration of 5.0 mL Cu<sup>2+</sup> ( $1.0 \times 10^{-3}$  mol L<sup>-1</sup>) with a standard EDTA solution ( $1.0 \times 10^{-2}$  mol L<sup>-1</sup>). The resulting titration curve is shown in Fig. 5. The amount of Cu<sup>2+</sup> ions in solution could be accurately determined with the electrode.

**Table 4**  
Practical application of Cu-CMCPE

Sample	M		X ± S.E.	R.S.D.%
	Taken	Found		
Mineral water	$1.00 \times 10^{-7}$	$(9.91 \pm 0.01) \times 10^{-8}$	$99.1 \pm 0.028$	0.74
	$1.00 \times 10^{-6}$	$(9.74 \pm 0.01) \times 10^{-7}$	$97.4 \pm 0.055$	0.88
	$1.00 \times 10^{-5}$	$(1.02 \pm 0.01) \times 10^{-5}$	$102.0 \pm 0.014$	0.95
Tap water	$1.00 \times 10^{-6}$	$(9.71 \pm 0.08) \times 10^{-7}$	$97.1 \pm 0.031$	1.14
	$1.00 \times 10^{-5}$	$(1.02 \pm 0.01) \times 10^{-5}$	$102.0 \pm 0.075$	0.96
Well water	$1.00 \times 10^{-6}$	$(1.01 \pm 0.03) \times 10^{-6}$	$101.1 \pm 0.042$	0.48
	$1.00 \times 10^{-5}$	$(9.72 \pm 0.06) \times 10^{-6}$	$97.2 \pm 0.035$	1.06
Urine	$1.00 \times 10^{-7}$	$(1.02 \pm 0.01) \times 10^{-7}$	$102.0 \pm 0.030$	1.74
	$4.00 \times 10^{-7}$	$(3.93 \pm 0.01) \times 10^{-7}$	$98.3 \pm 0.028$	0.59
	$1.00 \times 10^{-5}$	$(1.01 \pm 0.01) \times 10^{-5}$	$101.0 \pm 0.034$	0.75

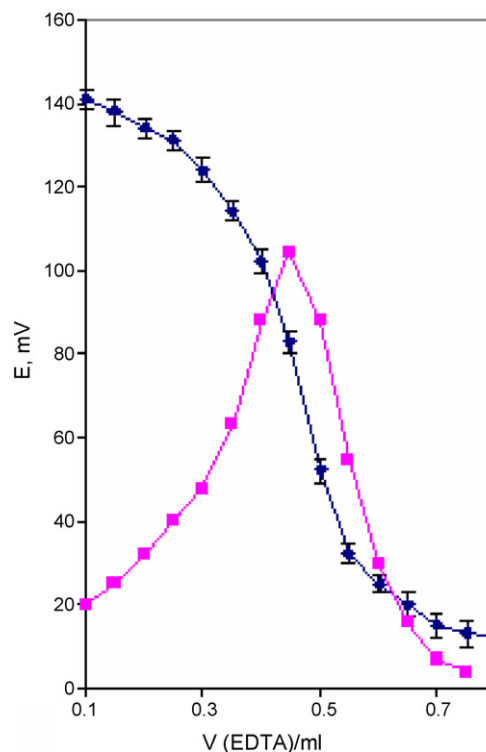


**Fig. 5.** Potential titration curves of 5.0 mL  $1.0 \times 10^{-3}$  M CuCl<sub>2</sub> solution with  $1.0 \times 10^{-2}$  M of EDTA and its first order derivative.

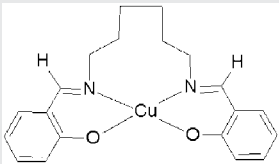
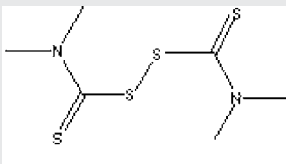
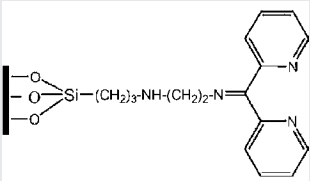
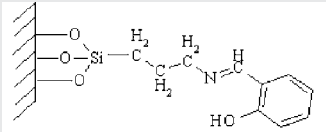
##### 4.2. Recovery and determination of copper ions in urine

The basal 24-h urinary excretion should be measured as an aid to the diagnosis of Wilson disease. Basal 24-h urinary excretion of copper in WD is typically greater than 100 μg (1.6 μmol) in symptomatic patients, but a finding greater than 40 μg (>0.6 μmol or 600 nmol) may indicate WD and requires further investigation (II) [38]. Recovery experiments were conducted by spiking urine samples with appropriate amounts of copper(II), and determined by this electrode. The results obtained using the standard addition method are presented in Table 4. Recoveries and R.S.D. values range between 98.3% and 102.0% of Cu(II), and 0.59 to 1.74, respectively. Thus the sensor can be employed for quantification of Cu(II) in urine samples.

##### 4.3. Determination of copper ions in various water samples

In an analogous way, copper(II) was determined in tap water, mineral water and well water using this electrode and the results,

**Table 5**  
Comparison of the proposed Cu-CMCPE with reported electrodes

Electrode type	Concentration range (mol L <sup>-1</sup> )	Low of detection (mol L <sup>-1</sup> )	Slope (mV/decade)	Response time (s)	Refs.
 N,N'-Disalicylidenehexamethylenediamine Copper(II)	$1.3 \times 10^{-7}$ to $1.0 \times 10^{-2}$	$6.3 \times 10^{-8}$	31.2	8–12	[3]
 Tetraethyl thiuram disulfide	$6.6 \times 10^{-8}$ to $6.0 \times 10^{-4}$	$4.0 \times 10^{-8}$	43.1	3–4	[16]
 Functionalized nanoporous silica gel with dipyriddy group	$1.0 \times 10^{-7}$ to $1.0 \times 10^{-2}$	$8.0 \times 10^{-8}$	28.4	50	[17]
3,4-Dihydro-4,4,6-trimethyl-2(1H)-pyrimidine thione	$9.7 \times 10^{-7}$ to $7 \times 10^{-2}$	$7.0 \times 10^{-7}$	30.0	45	[18]
 Salicylidine-functionalized polysiloxane in carbon paste (present work)	$2.3 \times 10^{-7}$ to $1.0 \times 10^{-3}$	$2.7 \times 10^{-8}$	29.4	8	Present work

presented in Table 4, are reasonable as the recovery ranges are 97.4–102% and R.S.D. ranges are 0.48–1.74.

## 5. Comparison with other electrodes

The performance characteristics of the proposed electrode and those of some reported carbon paste electrodes are presented in Table 5 for comparison. It is clear that its detection limit is lower than found for the other electrodes and its working range is wider than the others except those of Refs. [3,17]. Overall evaluation indicates this electrode is more useful in such applications.

## 6. Conclusions

In the field of silica-modified electrodes applied for electroanalytical purposes, the aforementioned results have clearly demonstrated the significant advantage in using derivatized polysiloxane materials where this electrode is found to be an efficient Cu<sup>2+</sup> selective sensor and can be used for determination of this ion in the presence of considerable concentrations of common interfering ions. Notably the low detection limit, and the concentration range of the proposed sensor are attractive properties to be the sensor of choice for this purpose.

## References

- [1] J. Wang, Analytical Electrochemistry, Wiley-VCH, New York, 2000.
- [2] P. Fanjul-Bolado, D. Hernández-Santos, P.J. Lamas-Ardisana, A. Martín-Pernía, A. Costa-García, Electrochim. Acta 53 (2008) 3635–3642.
- [3] H.M. Abu-Shawish, M.S. Saadeh, Sens. Lett. 5 (2007) 565.
- [4] G.A. Mostafa, A.M. Homoda, Bull. Chem. Soc. Jpn. 81 (2008) 257–261.
- [5] H.M. Abu-Shawish, Electroanalysis 20 (2008) 491.
- [6] M.H. Mashhadizadeh, M. Talakesh, M. Peste, A. Momeni, H. Hamidian, M. Mazlum, Electroanalysis 18 (2006) 2174.
- [7] M.J. Gismera, M.T. Sevilla, J.R. Procopio, Talanta 74 (2007) 190.
- [8] M. Javanbakht, M.R. Ganjali, P. Norouzi, A. Badii, A. Hasheminasab, M. Abdoussa, Electroanalysis 19 (2007) 1307.
- [9] M. Etienne, J. Cortot, A. Walcarius, Electroanalysis 19 (2007) 129.
- [10] G. Kickelbick, Angew. Chem. Int. Ed. 43 (2004) 3102.
- [11] A. Walcarius, D. Mandler, J. Cox, M.M. Collinson, O. Lev, J. Mater. Chem. 15 (2005) 3716.
- [12] M.M. Collinson, Mikrochim. Acta 129 (1998) 149.
- [13] J. Wang, Anal. Chim. Acta 399 (1999) 21.
- [14] A. Walcarius, D. Mandler, J.A. Cox, M. Collinson, O. Lev, J. Mater. Chem. 15 (2005) 3663.
- [15] Z. Navratilova, P. Kula, Electroanalysis 15 (2003) 837.
- [16] J. Lin, C.W. Brown, Trends Anal. Chem. 16 (1997) 200.
- [17] M.M. Collinson, Trends Anal. Chem. 21 (2002) 30.
- [18] M.J. Gismera, D. Hueso, J.R. Procopio, M.T. Sevilla, Anal. Chim. Acta 524 (2004) 347.
- [19] M. Javanbakht, A. Badii, M.R. Ganjali, P. Norouzi, A. Hasheminasab, M. Abdoussa, Anal. Chim. Acta 601 (2007) 172.
- [20] A. Abbaspour, S.M.M. Moosavi, Talanta 56 (2002) 91.
- [21] M.B. Gholivand, M. Rahimi-Nasrabadi, M.R. Ganjali, M. Salavati-Niasari, Talanta 73 (2007) 553.
- [22] H.M. Abu-Shawish, M.S. Saadeh, Can. J. Anal. Sci. Spectrosc. 53 (2007) 225.
- [23] S.M. Saadeh, N.M. El-Ashgar, I.M. El-Nahhal, M.M. Chehimi, J. Maquet, F. Babonneau, Appl. Organomet. Chem. 19 (2005) 759.

- [24] Y. Umezawa, P. Buhlmann, K. Umezawa, K. Tohda, S. Amemiya, *Pure Appl. Chem.* 72 (2000) 1851.
- [25] A. Radu, S. Peper, E. Bakker, D. Diamond, *Electroanalysis* 19 (2007) 144.
- [26] E. Bakker, E. Pretsch, P. Buhlmann, *Anal. Chem.* 72 (2000) 1127.
- [27] N.M. Ashgar, S.M. Saadeh, *AlAqsa Univ. J.* 10 (2006) 153–161.
- [28] M. Shamsipur, M. Yousefi, M. Hosseini, M.R. Ganjali, *Anal. Chem.* 74 (2002) 5538.
- [29] M. Arvand, S.A. Asadollahzadeh, *Talanta* 75 (2008) 1046–1054.
- [30] E.A. Cummings, P. Mailley, S. Linquette-Mailley, B.R. Eggins, E.T. McAdams, S. McFadden, *Analyst* 123 (1998) 1975.
- [31] J. Sánchez, M. Valle, *Crit. Rev. Anal. Chem.* 35 (2005) 15.
- [32] M.A.A. Perez, L.P. Marin, J.C. Quintana, M.Y. Pedram, *Sens. Actuators B* 89 (2003) 262.
- [33] P.R. Buck, E. Lindner, *Pure Appl. Chem.* 66 (1994) 2527.
- [34] H. Hamidi, E. Shamsb, B. Yadollahi, F.K. Esfahani, *Talanta* 74 (2008) 909.
- [35] S.K. Mittal, A.K.S.K.N. Gupta, S. Kaur, S. Kumar, *Anal. Chim. Acta* 585 (2007) 161.
- [36] A.K. Singh, S. Mehtab, *Talanta* 74 (2008) 806.
- [37] G. Li, B.J. Polk, L.A. Meazell, D.W. Hatchett, *J. Chem. Educ.* 77 (2000) 1049.
- [38] M.L. Schilsky, *J. Hepatol.* 47 (2007) 172.



# Indirect voltammetric determination of caffeine content in coffee using 1,4-benzoquinone modified carbon paste electrode

Muluken Aklilu, Merid Tessema, Mesfin Redi-Abshiro\*

Chemistry Department, Addis Ababa University, PO Box 1176, Addis Ababa, Ethiopia

## ARTICLE INFO

### Article history:

Received 12 February 2008

Received in revised form 8 April 2008

Accepted 11 April 2008

Available online 24 April 2008

### Keywords:

1,4-Benzoquinone

Modified carbon paste electrode

Caffeine

Voltammetry

## ABSTRACT

In this paper a simple and highly sensitive electroanalytical method for the determination of caffeine content using 1,4-benzoquinone modified carbon paste electrode is presented. The method is based on suppression of 1,4-benzoquinone peak current on addition of caffeine. Square-wave and cyclic voltammetric techniques were utilised for the investigation. The 1,4-benzoquinone modified electrode exhibited a well-defined peak with reproducible peak current values for repetitive measurements; and showed a decrease in peak current value with an increase in caffeine content. The result revealed two linear range regions between 0 mmol L<sup>-1</sup> and 0.5 mmol L<sup>-1</sup> and 0.5 mmol L<sup>-1</sup> and 8.0 mmol L<sup>-1</sup>, with detection limits of 0.3 μmol L<sup>-1</sup> and 5.1 μmol L<sup>-1</sup>, respectively. The method was then successfully applied to the determination of caffeine content in coffee samples. The effects of pH, electrode composition, step potential, pulse amplitude and square-wave frequency on the voltammetric responses were also investigated.

© 2008 Elsevier B.V. All rights reserved.

## 1. Introduction

Caffeine is an alkaloid; a class of naturally occurring compounds containing nitrogen and having the basic properties of an organic amine. It belongs to a class of organic compounds called xanthines. Other common members of this class include theophylline and theobromine [1–14]. It is found naturally in foods such as coffee, tea, cola nuts, yerbamate, guarana berries, and (in small amounts) cacao beans. For the plant, caffeine acts as a natural pesticide since it paralyzes and kills some of the insects that attempt to feed on the plant [15–18]. Caffeine ingestion causes many physiological effects such as gastric acid secretion, diuresis and stimulation of the central nervous and the cardiovascular systems. It is considered to be a risk factor for cardiovascular diseases and may also cause depression and hyperactivity [12,13].

The main and active ingredient of coffee is caffeine. Because of its important role in determining the quality of coffee beverages, the development of a sensitive, fast and cost-effective method for monitoring caffeine is highly needed [13]. Normally, high performance liquid chromatographic separation and UV-spectrophotometric detection methods are applied to both regular decaffeinated green and roasted coffee for caffeine content determination. Also, other methods such as capillary electrophoresis, thin layer chromatography and gas chromatography are used for separation of caffeine

in the analysis of mixtures, combined with several other detection methods such as mass spectroscopy and FTIR spectrophotometric measurements [14,16,19,20]. However, very expensive instrumentation, highly skilled technicians, complicated and time-consuming procedures are required for such methods. Thus, the development and application of new caffeine detection methods remain an active area of investigation, in particular in food and clinical chemistry.

Chemically modified electrodes, with improved sensitivity and selectivity, have also been used for the determination of caffeine in beverages [21]. However, the sensitivity reported was relatively low due to the high oxidation potential used for caffeine oxidation.

In this study, 1,4-benzoquinone chemically modified carbon paste electrode is applied for the indirect voltammetric determination of caffeine in coffee with the aim of raising the selectivity and sensitivity of the carbon paste electrode.

## 2. Experimental

### 2.1. Reagents and apparatus

Graphite powder and paraffin oil (Fluka, Switzerland), caffeine (Evans, UK), NaH<sub>2</sub>PO<sub>4</sub>, Na<sub>2</sub>HPO<sub>4</sub> and H<sub>3</sub>PO<sub>4</sub> (Wagtech International Ltd., UK), and Sodium hydroxide (Lammark Chemicals Pvt., India) were used in the experiments. Caffeine stock solution was prepared using deionised water. Working standard solutions of lower concentrations were freshly prepared by using dilution method. Electrochemical experiments were carried out in a conventional three-electrode cell, and platinum wire was used as an

\* Corresponding author. Fax: +251 11 1239470.

E-mail address: [mesfinr@chem.aau.edu.et](mailto:mesfinr@chem.aau.edu.et) (M. Redi-Abshiro).

auxiliary electrode. All potentials are given versus Ag/AgCl reference electrode. The working electrode used was a 1,4-benzoquinone modified carbon paste electrode, and the surface area of the electrode was  $0.39 \text{ cm}^2$ . The experiment and processing of data were made using a BAS 50 W electrochemical analyzer (Bioanalytical System Inc., US) connected to a personal computer.

## 2.2. Procedure

### 2.2.1. Preparation of unmodified electrodes

Unmodified carbon paste electrodes were prepared by mixing graphite powder with paraffin oil. The composition of the paste was 75% (w/w) graphite powder and 25% (w/w) paraffin oil. The mixture was homogenized by grinding for 20 min, and allowed to rest for at least 24 h [22]. The homogenized paste was packed into the tip of a plastic syringe (7 mm diameter, 3 mm deep). A copper wire was inserted from the backside to provide electrical contact. The surface was then smoothed with a smooth white paper while a light manual pressure was applied to the syringe tip until a shiny surface was emerged.

### 2.2.2. Preparation of 1,4-benzoquinone modified electrodes (BQMCPPE)

To the mixture of 0.2 g of 1,4-benzoquinone and 1.4 g of graphite powder, 0.4 g of paraffin oil was added and thoroughly mortared together for 20 min to form 1,4-benzoquinone modified carbon paste. The paste was packed into the tip of the syringe by extruding a small amount of paste from the tip of the previously prepared electrode.

## 2.3. Application of the method to real samples

The coffee bean was milled and ground with an analytical grinder. The ground bean was sieved with a mesh size of  $500 \mu\text{m}$ . One hundred milligrams of ground coffee was added into a 125 mL Erlenmeyer flask fitted with a stopper then 25 mL of distilled water was added to the flask and boiled for 1 h in a hot plate while stirring. After allowing the residue to settle, the hot solution was filtered. For removal of interferences liquid–liquid extraction using dichloromethane was performed using separatory funnel. The extraction was performed with 100 mL of dichloromethane three times as described earlier [26]. The extracts were mixed and passed through 0.25 g anhydrous  $\text{Na}_2\text{SO}_4$  for drying. Dichloromethane was removed to dryness in the hood. The residue was dissolved in 5 mL hot supporting electrolyte buffer solution and transferred to a volumetric flask. Dissolving was repeated three times and diluted with the buffer solution up to the mark. The concentration of caffeine was determined using standard addition method.

## 3. Results and discussion

### 3.1. Voltammetric behaviour of caffeine at 1,4-benzoquinone modified carbon paste electrode

#### 3.1.1. Cyclic voltammetric investigation

Cyclic voltammogram for the redox behaviour of caffeine at the unmodified carbon paste electrode at pH 6 is shown in Fig. 1. As can be observed in Fig. 1, caffeine is an electroactive compound and undergoes oxidation at around 1.45 V. In the absence of caffeine no peak was observed. A further increase in peak current was also observed when the concentration of caffeine was increased from  $2 \text{ mmol L}^{-1}$  to  $8 \text{ mmol L}^{-1}$ .

However, the anodic determination of caffeine at relatively large positive potential ( $>1.4 \text{ V}$  versus SCE) is limited to a high concen-

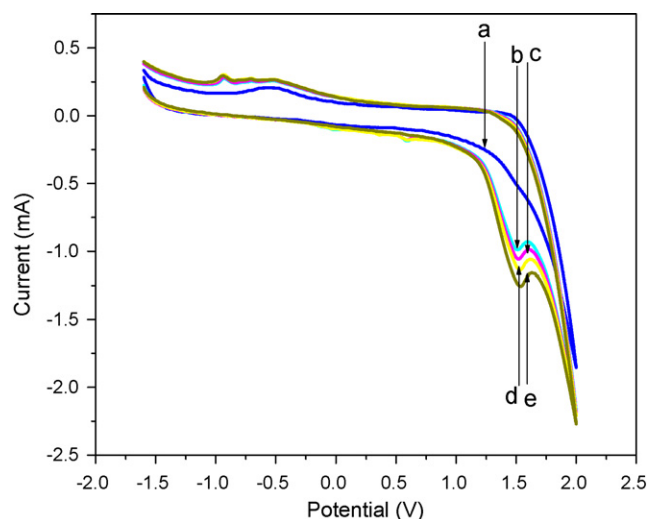


Fig. 1. Cyclic voltammogram of (a) 0 mM caffeine, (b) 2 mM caffeine, (c) 4 mM caffeine, (d) 6 mM caffeine and (e) 8 mM caffeine at unmodified electrode.

tration range due to the background currents from the oxidation of oxygen in water.

The electrochemical redox behaviour of 1,4-benzoquinone in the absence of caffeine was also investigated. Cyclic voltammograms recorded with 1,4-benzoquinone modified and unmodified carbon paste electrodes in the absence of caffeine is shown in Fig. 2. The unmodified electrode showed no current responses in buffer solution, whereas 1,4-benzoquinone modified electrode gave a well-defined and reversible redox peak (Fig. 2). The 1,4-benzoquinone peak current was found to decrease when caffeine was added to the solution. This enables the determination of caffeine by analysing the magnitude of the decrease in peak current at a potential of 0.4 V, far away from the oxidation potential of oxygen.

#### 3.1.2. Square-wave investigation

The square-wave voltammogram for 1,4-benzoquinone showed a well-defined peak at about the same potential as observed in the cyclic voltammograms, and in the presence of caffeine it displayed a distinct reduction of the peak current (Fig. 3). Further

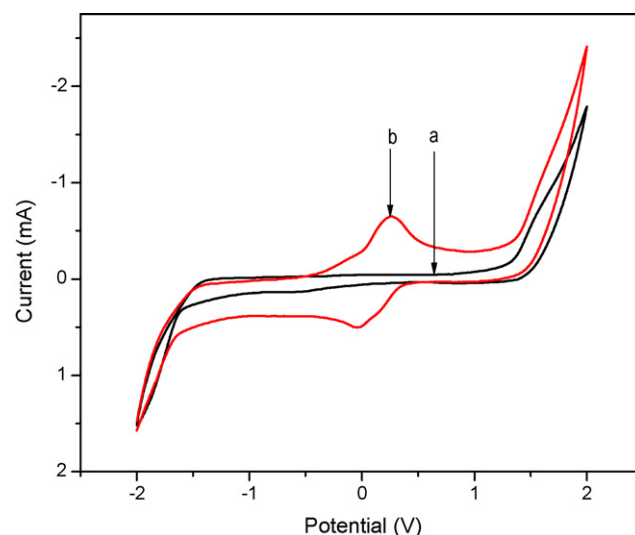


Fig. 2. Cyclic voltammogram for the redox behaviour of 1,4-benzoquinone in the absence of caffeine: (a) unmodified electrode and (b) 1,4-benzoquinone modified electrode.

increase in the concentration of caffeine resulted in a successive decrease of 1,4-benzoquinone (BQ) redox peak current, as observed in cyclic voltammetry. The decrease in peak current was found to be directly related with the concentration of caffeine. Based on the observation, the following expression was derived:

$$i_p(\text{BQ}) = K_{\text{BQ}}c_{\text{BQ}}, \quad -\Delta i_p(\text{BQ}) = K_{\text{ca}}c_{\text{ca}}$$

where  $c_{\text{BQ}}$  is the initial concentration of 1,4-benzoquinone and  $c_{\text{ca}}$  is the concentration of caffeine. The reason for the reduction of the peak current with increase in caffeine concentration is not well-known. A reasonable explanation could be given by investigating the redox mechanism proposed in literature [23].

Presumably, two reasons may be considered to be responsible for the observed decrease of the voltammetric peak current of 1,4-benzoquinone in the presence of caffeine. The first reason could be the formation of an electroactive complex at the surface of the electrode (adsorption), which may result in the change of electrochemical parameters such as the electron transfer coefficient and the surface reaction rate constant.

In order to verify whether there is a competitive surface adsorption as a possible explanation for the observed decrease in current as a function of caffeine; concentration measurements were conducted using 1,4-benzoquinone in solution at different caffeine concentrations with unmodified carbon paste electrode. The result showed that the peak current decreased in the same manner as with the BQMCPPE. From this, it is concluded that competitive surface adsorption cannot be considered to be a significant factor for the decrease of 1,4-benzoquinone peak current.

The second could be the formation of an electrochemical non-active complex of 1,4-benzoquinone with caffeine. The results obtained from UV–vis and IR measurements, however, gave no evidence for any complex formation between caffeine and 1,4-benzoquinone.

The exclusion of the two possible phenomena for the observed peak current decrease may be considered as enough proof for the absence of dipolar neutral state interaction between BQ and caffeine, and eventually raises the possibility of the involvement of oxidised form of 1,4-benzoquinone in  $\pi$ -complex formation with caffeine. If this may be the case, similar effect should be observed in the presence of any nucleophilic compound instead of caffeine.

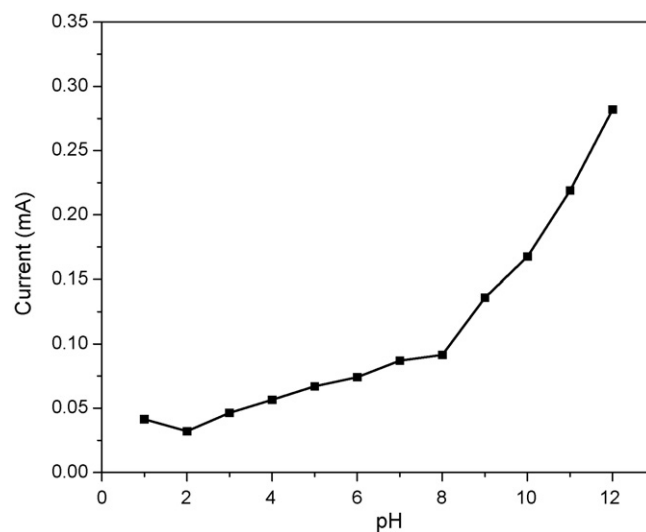


Fig. 4. Dependence of the peak current of 1,4-benzoquinone on pH for 2 mM caffeine.

Of course this is what was observed when the experiments were conducted with *p*-nitroaniline. This may indicate complex formation between the oxidized form of BQ with caffeine. However, for detailed description of the mechanism further investigations, including in-situ spectroelectrochemical studies, are necessary.

### 3.2. Optimization of experimental conditions

#### 3.2.1. Effect of pH of supporting electrolyte

Since the electrochemical reaction of 1,4-benzoquinone involves protons, the effect of pH on the kinetics of the reduction of 1,4-benzoquinone was investigated. The reduction generally becomes more irreversible at higher pH values [3]. On the basis of this, it has been proposed that the reduction pathway of 1,4-benzoquinone is HeHe (proton–electron–proton–electron) at lower pH and eHeH at higher pH. This important variable was studied for the redox behaviour of 1,4-benzoquinone by square-wave voltammetry in the pH range of 1–12. The pH of the solution was adjusted using NaOH and HCl. Above pH 12 the electrode became very unstable, and the peak current decreased significantly in repetitive measurements.

The dependence of the peak current and the peak potential of 1,4-benzoquinone on various pH ranges are shown in Figs. 4 and 5, respectively. In the pH range 2 to 8, the peak current of 1,4-benzoquinone increases linearly, with a slope  $(\partial i/\partial \text{pH})_{c,T}$  equal to  $8.72 \times 10^{-6}$ . Further, the current increases sharply, in the pH range 9–12 with a slope  $(\partial i/\partial \text{pH})_{c,T}$  equal to  $4.895 \times 10^{-5}$ . Since current is proportional to the rate of the electrochemical reaction, one could say that the rate of the electrochemical reaction of 1,4-benzoquinone increases with increasing pH. Furthermore, the change in the slope of current versus pH implies that the mechanism for the electrochemical reaction of 1,4-benzoquinone changes at about pH 8.

For the reduction of 1,4-benzoquinone, the position of 1,4-benzoquinone/hydroquinone peak potential is proportional to the square of the hydrogen-ion concentration. This implies that the electrode potential is sensitive to pH; a change of one unit of pH in water solution changes the potential of the electrode by 0.059 V [24]. The shift in the square-wave peak potential as a function of pH was studied and linear dependence was observed, with the peak potential of 1,4-benzoquinone shifting towards negative potential as the pH increases. This indicates that hydrogen-ion takes part

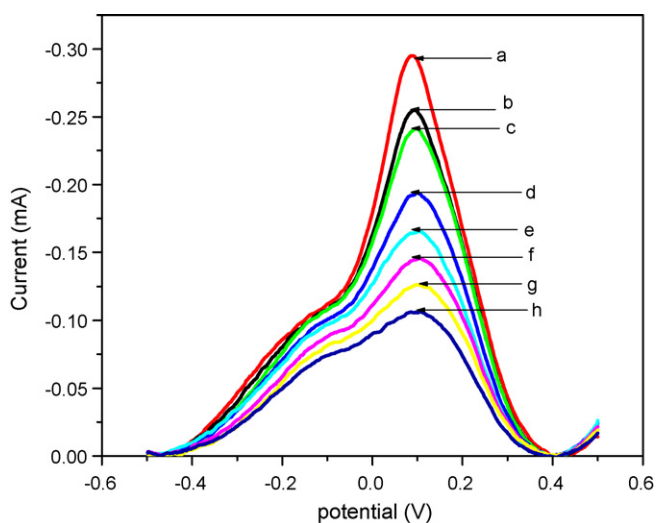
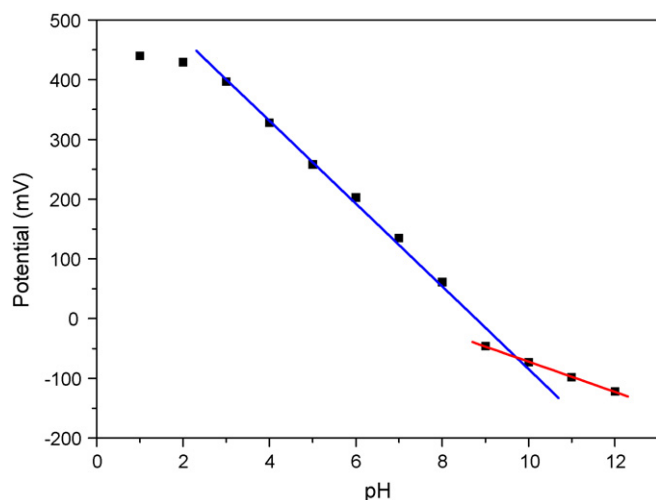


Fig. 3. Square-wave voltammogram for the redox behaviour of 1,4-benzoquinone at different caffeine concentrations: (a) 0, (b) 0.01, (c) 0.05, (d) 0.2, (e) 0.5, (f) 2, (g) 4 and (h) 6 mM caffeine.





**Fig. 5.** Dependence of the peak potential of 1,4-benzoquinone on pH for 2 mM caffeine.

in the electrode reaction. According to the literature [25], for a reversible reaction  $E_p = K_a - (0.059y/n)pH$ , where  $y$  is the number of hydrogen-ions that take part in the electrode reaction and  $n$  is the number of electrons. The two linear plots in Fig. 5 may be described by the following expressions:

$$E_p(\text{mV}) = -66.1 \text{ pH} + 595; \quad R = -0.9993 \text{ for pH 3 to pH 8}$$

$$E_p(\text{mV}) = -25.3 \text{ pH} + 181; \quad R = -0.9996 \text{ for pH 9 to pH 12}$$

The linear fit of the dependence of the peak potential on pH resulted in two slopes with values 66 mV and 25 mV per pH unit, implying the number of protons involved in the redox process changes from two to one as the pH increases (for  $n=2$ ). Electrode process involving a weak acid or weak base have potential-pH variations, which shows a change in slope at  $\text{pH} = \text{p}K_a$ . From the intersection of the linear parts of the plots, the  $\text{p}K_a$  value of 1,4-benzoquinone was calculated to be 10.0, which is in a very good agreement with the literature value of 10.16 [25].

In our experiments, the reproducibility of the magnitude of the peak current decreased for pH values above 6. The decrease became even more pronounced as the pH was increased further. This may be due to the irreversible reaction of 1,4-benzoquinone with alkali [24]. Therefore, a constant pH of 6, where the peak current value in repetitive measurements was reproducible with great certainty, was used throughout the experiments.

The effect of square-wave frequency, square-wave pulse amplitude, step potential and electrode composition were also studied. The optimum values for these parameters are: frequency 25 Hz, amplitude 30 mV, step potential 2 mV and electrode composition of 10% (w/w) 1,4-benzoquinone.

### 3.3. Linear range and detection limit

The analytical utility of a given procedure derives validity through obtaining well-defined dependence of (current) response on concentration. The dependence of the voltammetric signal of 1,4-benzoquinone on the concentration of caffeine and the inherent sensitivity of this method is illustrated by square-wave voltammetry for different concentration of caffeine based on the optimum experimental conditions. The relationship between the square-wave voltammetric peak current of 1,4-benzoquinone and caffeine concentration was examined. A calibration curve was constructed

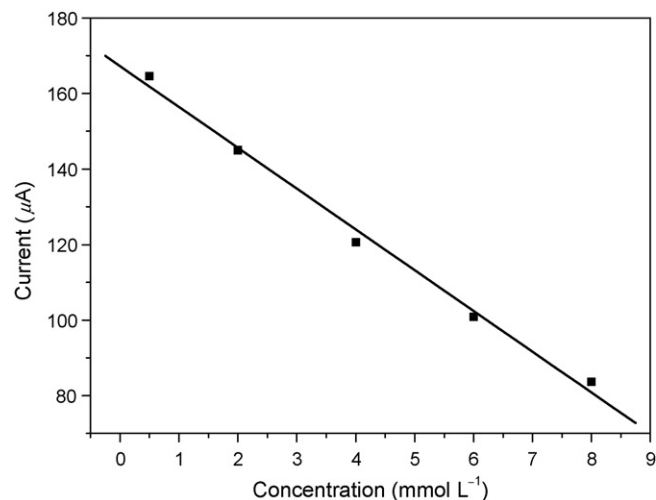


**Fig. 6.** Calibration curve for the effect of caffeine (concentration range 0.5–8 mM) on the redox behaviour of 1,4-benzoquinone. Slope:  $-10.8 \pm 1.712 \mu\text{A}/\text{mM}$ ; regression coefficient:  $-0.9982$ .

by measuring the peak currents of 1,4-benzoquinone for each calibration standard.

Figs. 6 and 7 show calibration curves for the dependence of the square-wave peak current of 1,4-benzoquinone on the concentration of caffeine. After repeated measurements two linear ranges could be obtained; one from  $0 \text{ mmol L}^{-1}$  to  $0.5 \text{ mmol L}^{-1}$  with a detection limit of  $0.3 \mu\text{mol L}^{-1}$ , and the second from  $0.5 \text{ mmol L}^{-1}$  to  $8.0 \text{ mmol L}^{-1}$  with detection limit equals to  $5.1 \mu\text{mol L}^{-1}$ .

Table 1 shows the comparison of linear range and detection limit between 1,4-benzoquinone modified carbon paste electrode (BQMCPPE) and the other methods. The detection limit of BQMCPPE in the lower concentration range is much better than the Nefion CMC method. Although the detection limit of the HPLC method is comparable with the BQMCPPE method, the less amount and the low cost reagents necessary and also the simplicity of the experimental procedure makes the BQMCPPE method advantageous over the HPLC method.

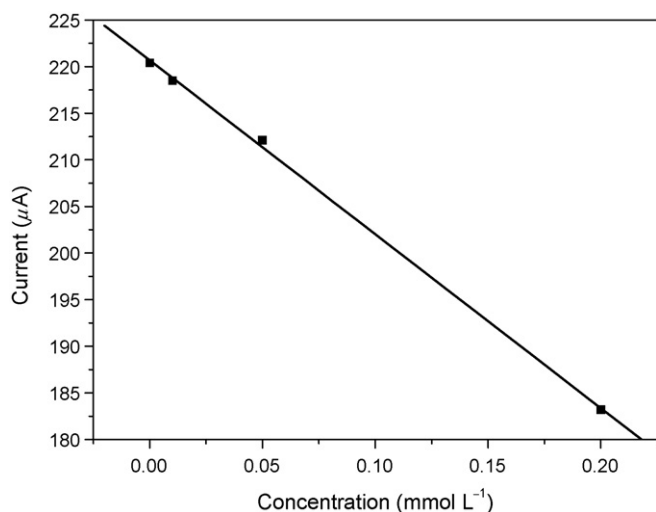


**Fig. 7.** Calibration curve for the effect of caffeine (concentration range 0–0.5 mM) on the redox behaviour of 1,4-benzoquinone. Slope:  $-77.8 \pm 0.11 \mu\text{A}/\text{mM}$ ; regression coefficient:  $-0.9997$ .

**Table 1**  
Comparison between BQMCPPE and other methods<sup>a</sup>

Method	Detection limit ( $\mu\text{mol L}^{-1}$ )	Linear range
BQMCPPE	0.3	0–0.5 $\text{mmol L}^{-1}$ (0–97 $\text{mg L}^{-1}$ )
	5.1	0.5–8 $\text{mmol L}^{-1}$ (97–1552 $\text{mg L}^{-1}$ )
HPLC method [3]	0.3	0–300 $\text{mg L}^{-1}$
Nafion CME method [13]	2	0–100 $\text{mg L}^{-1}$
Anodic stripping voltammetry <sup>a</sup>	47.4	0–0.5 $\text{mg L}^{-1}$

<sup>a</sup> Ref. [27].

### 3.4. Real sample analysis

To obtain the calibration curve, a series of standard solutions of caffeine were used. The unknown sample solutions were prepared using the same procedure as the standard solutions. The peak current of the unknown sample solutions was within the linear range covered by the standards. With that the validity of the calibration was established and the quantity of caffeine in the unknown samples were determined. The quantity of caffeine obtained using this method were  $3.73 \pm 0.02 \text{ mmol L}^{-1}$  and  $4.28 \pm 0.00 \text{ mmol L}^{-1}$ . The results are in good agreement with the value  $3.6 \pm 0.2 \text{ mmol L}^{-1}$  and  $4.1 \pm 0.2 \text{ mmol L}^{-1}$ , obtained employing UV–vis spectroscopic method [26].

### 4. Conclusion

In summary, in this paper the application of 1,4-benzoquinone modified carbon paste electrode peak current reduction for the indirect determination of caffeine content in coffee is demonstrated. The method presented is fast, simple, sensitive and cost-effective. Moreover, it does not require sophisticated equipment and produces significantly less organic waste compared to the HPLC technique. It can thus be concluded that the BQMCPPE method is comparable with well-established techniques for the quantitative analysis of caffeine in coffee sample with regard to sensitivity and expense of analysis. Thus, the method suggested here may be applied for the determination of the caffeine in coffee.

### 5. Novelty statement

In this work a novel electroanalytical procedure, which showed a better sensitivity than those reported in the literature using electroanalytical technique, is presented. The method is based on the investigation of suppression of the peak current of the modifier (1,4-benzoquinone) due to the analyte (caffeine) in a modified carbon paste electrode.

### Acknowledgement

The authors are thankful to the Department of Chemistry, Addis Ababa University, for the financial support.

### References

- [1] M.N. Clifford, K.C. Wilson, *Coffee: Botany, Biochemistry and Production of Beans and Beverages*, Croom Helm, USA, 1985.
- [2] F.L. Wellman, *Coffee: Botany, Cultivation and Utilization*, Interscience Inc., UK, 1961.
- [3] Y. Getnet, MSc Thesis, AAU, Department of Chemistry, Addis Ababa, 2005.
- [4] A.S. Franca, J.C.F. Mendonca, S.D. Oliveria, *Food Sci. Technol.* 38 (2005) 709.
- [5] W.M.N. Ratnayake, R. Hollywood, B.G. Stavric, *Food Chem. Toxicol.* 31 (1993) 263.
- [6] M.J. Martin, F. Pablos, A.G. Gonzalez, *Anal. Chim. Acta* 358 (1998) 177.
- [7] M.J. Martin, F. Pablos, A.G. Gonzalez, *Food Chem.* 66 (1999) 365.
- [8] E.J. Dos Santos, E. De Oliveria, *J. Food Comp. Anal.* 14 (2001) 523.
- [9] R. Coste, *Coffee: The Plant and the Product*, MacMillan, London, 1992.
- [10] M. Ravikumar, M. Adinarayana, *Proc. Indian Acad. Sci.* 112 (2000) 551.
- [11] Y.-L. Wei, C. Dong, S.-M. Shuang, D.-S. Liu, *Spectrochim. Acta Part A* 61 (2005) 2584.
- [12] N. Spataru, B.V. Sarada, D. Tryk, A. Fujishima, *Electroanalysis* 11 (2002) 721.
- [13] S. Kerrigan, T. Lindsey, *Forensic Sci. Int.* 153 (2005) 67.
- [14] S. Emara, *Biomed. Chromatogr.* 18 (2004) 479.
- [15] A. Pizzariello, J. Svorc, M. Sted'ansky, S. Miertus, *J. Sci. Food Agric.* 79 (1999) 1136.
- [16] R. Fiammengio, M. Crego-Calama, P. Timmerman, D.N. Reinholdt, *Chem. Eur. J.* 9 (2003) 784.
- [17] I. Pavel, A. Szeghalmi, D. moigno, S. Cinta, W. Kiefer, *Biopolym. Biospectrosc.* 72 (2003) 25.
- [18] R.J. Clark, R. Marceal, *Coffee Chemistry*, Elsevier, Amsterdam, 1985.
- [19] K.R.C. Matos, M.H. Taboens, M. Bertotti, *Electroanalysis* 15 (2003) 733.
- [20] I. Svancara, K. Vytras, J. Barek, J. Zima, *Crit. Rev. Anal. Chem.* 31 (2001) 311.
- [21] M. Tessema, T. Ruzgas, L. Gorton, T. Ikeda, *Anal. Chim. Acta* 310 (1995) 161.
- [22] H. Alemu, P. Wagana, P. Tseki, *The Analyst* 127 (2002) 129.
- [23] K. Schachl, H. Alemu, K. Kalcher, J. Jezkova, I. Svancara, K. Vytras, *The Analyst* 122 (1997) 985.
- [24] X. Hu, K. Jiao, W. Sun, J.Y. You, *Electroanalysis* 18 (2006) 613.
- [25] J.D. Roberts, M.C. Caserio, *Basic Principles of Organic Chemistry*, 2nd ed., W.A. Benjamin, Inc., New York, 1977.
- [26] A. Belay, K. Ture, M. Redi-Abshiro, A. Asfaw, *Food Chem.* 108 (2008) 310.
- [27] S.Y. Ly, Y.S. Jung, M.H. Kim, I.K. Han, W.W. Jung, H.S. Kim, *Microchim. Acta* 146 (2004) 207.



# Sequential and simultaneous determination of bromate and chlorite (DBPs) by flow techniques Kinetic differentiation

A. Alonso-Mateos, M.J. Almendral-Parra\*, M.S. Fuentes-Prieto

Departamento de Química Analítica, Nutrición y Bromatología, Faculty of Chemistry, University of Salamanca, Plaza de la Merced s/n, E-37008 Salamanca, Spain

## ARTICLE INFO

### Article history:

Received 17 December 2007  
Received in revised form 21 April 2008  
Accepted 23 April 2008  
Available online 8 May 2008

### Keywords:

Bromate  
Chlorite  
Disinfection by-products  
Water analysis  
Flow injection analysis  
Spectrophotometry  
Dianisidine

## ABSTRACT

3-3'-Dimethoxybenzidine (*o*-dianisidine, ODA) is oxidised by Br<sub>2</sub>, among other oxidants, generating a compound that absorbs at 450 nm, while the non-oxidised reagent absorbs in the UV region. This reaction has been used previously as the basis of a continuous-flow method for the determination of bromate in ozonised water, with a detection limit lower than the maximum permitted for drinking water (10 µg L<sup>-1</sup>). The only interference observed in the method was that due to the chlorite ion (ClO<sub>2</sub><sup>-</sup>), which generated the same ODA bromation product. Thus, in systems in which O<sub>3</sub> is employed as a disinfectant and disinfection is later enhanced with ClO<sup>-</sup> and ClO<sub>2</sub>, there exists the possibility of finding BrO<sub>3</sub><sup>-</sup> and ClO<sub>2</sub><sup>-</sup>, oxoanions generated as subproducts. The kinetic behaviour of the reaction between bromate and chlorite with bromine in acidic medium is different, allowing the proposal of a continuous-flow method for the simultaneous or sequential determination of both subproducts in water purification systems. None of the other subproducts interfered in the reaction. Kinetic differentiation was achieved by combining the temperature of the reaction and the length of the coils, after which it was possible to determine both analytes sequentially within a concentration range of 6–160 µg L<sup>-1</sup>.

© 2008 Elsevier B.V. All rights reserved.

## 1. Introduction

As a result of the processes used to disinfect drinking water, important inorganic oxyhalide disinfection by-products (DBPs) have been reported. Chlorite (ClO<sub>2</sub><sup>-</sup>) and chlorate (ClO<sub>3</sub><sup>-</sup>) are formed when chlorine dioxide (ClO<sub>2</sub>) is used as a disinfectant [1–3], and the presence of chlorate in waters treated with hypochlorite has also been described [4,5]. Additionally, the ozonation of water containing bromide induces the formation of several by-products [6], among which bromate is of paramount importance since it has been shown to be a carcinogenic substance at concentrations above 0.05 µg L<sup>-1</sup> [7]. Accordingly, bromate has been considered for regulation by the US Environmental protection Agency (EPA) and European Directive 98/83/CEE, which establishes that the maximum contaminant level (MCL) of bromate in drinking water should not exceed 10 µg L<sup>-1</sup> [8,9].

The literature contains many references to methods for the determination of bromate in drinking water. Among them, ion chromatography with conductivity detection has been chosen as

an official model by the EPA and ISO [10–15]. However, these methods require long analysis times and the use of costly instrumentation, which in turn demands expensive upkeep, such that they are not suited for routine on-site monitoring. To achieve this aim, several methods employing flow injection (FI) techniques with colorimetric and chemiluminescent detection have been reported [16–20].

In preliminary studies a procedure for the on-line determination of bromate was reported. The method is based on the reaction of bromate with *o*-dianisidine (ODA) [21] by flow techniques. The chemical reaction is based on the formation of Br<sub>2</sub> in the presence of excess Br<sup>-</sup> and the bromation of ODA, generating a compound that absorbs at 450 nm. The method, which is rapid and allows the determination of the anion for concentrations of up to 6 µg L<sup>-1</sup>, only shows interference by the chlorite ion (ClO<sub>2</sub><sup>-</sup>), which generates the same ODA bromation product, which absorbs at 450 nm. In systems that employ O<sub>3</sub> as disinfectant, followed by enhancement with ClO<sup>-</sup>, and although usually with ClO<sub>2</sub>, there exists the possibility of finding BrO<sub>3</sub><sup>-</sup> and ClO<sub>2</sub><sup>-</sup>; i.e., oxoanions generated as by-products in the disinfection process. Here we report a procedure for the simultaneous and sequential determination of both analytes in drinking water. The method is based on the reaction described above and employs kinetic differentiation processes.

\* Corresponding author. Tel.: +34 923294483; fax: +34 923294483.  
E-mail address: [almendral@usal.es](mailto:almendral@usal.es) (M.J. Almendral-Parra).

## 2. Experimental

### 2.1. Apparatus and materials

Minipuls HP4 (Gilson, France) peristaltic pumps with silicone or vinyl pump tubes; L-100-1 PTFE rotary injection valve (Rheodine) and two-way valves (Scharlau) were used. Detection was performed with a UV-160 spectrophotometer (Shimadzu, Japan) fitted with a 30- $\mu\text{L}$  flow-cell (Hellma, model 178.011, Germany) with an optical pathway of 1.0 cm. For kinetic studies in discontinuous mode, a double beam Shimadzu UV-2101 spectrophotometer with CSP-260 cuvette holder with six cells thermostatted with a Peltier system, controlled by a computer, were used. PTFE tubing of 0.5 mm internal diameter with standard tube fittings and connectors (Upchurch Scientific, Inc.) was employed. A Crison 501 potentiometer and a Digitherm 3000542 (Selecta) water bath were also used.

### 2.2. Reagents and solutions

All Chemicals used in this work were of analytical grade and were prepared with ultra-high quality deionized water. Solutions of *o*-dianisidine (Sigma–Aldrich) between  $0.20 \times 10^{-3}$  and  $1.95 \times 10^{-3}$  M prepared by weighing the reagent and dissolution in distilled water. Solutions of potassium bromide, KBr (Carlo Erba) between  $5.0 \times 10^{-3}$  and  $3.9 \times 10^{-2}$  M in distilled water. Solutions of  $\text{HNO}_3$  (Prolabo) at concentrations in the 0–10 to 1.22 M range. Standard concentrated solutions of  $1.0017 \text{ g L}^{-1}$  of potassium bromate,  $\text{KBrO}_3$  (Panreac) and of  $0.4200 \text{ g L}^{-1}$  of sodium chlorite,  $\text{NaClO}_2$  (Acros organics). Working standard solutions were prepared after suitable dilutions of the stock solution with distilled water.

### 2.3. Flow systems

To study the chemical, geometric and hydrodynamic variables affecting the ODA bromation reaction, the flow scheme shown in Fig. 1 was designed. Channel  $C_1$  carries the reagent solution,  $R$ , formed by *o*-dianisidine, ODA at a concentration of  $1.95 \times 10^{-3}$  M in 1.22 M  $\text{HNO}_3$  medium and KBr in excess:  $3.9 \times 10^{-2}$ . Channel  $C_2$  transports the carrier,  $P$  - bidistilled water, into which a volume,  $V_i = 288 \mu\text{L}$ , of standard solution or sample containing  $\text{BrO}_3^-$  or  $\text{ClO}_2^-$  at different concentrations is injected. The flow rates of both solutions,  $F_R = 0.124 \text{ mL min}^{-1}$  and  $F_P = 0.288 \text{ mL min}^{-1}$ , are controlled by the peristaltic pump and the diameter of the silicone tubes. Both solutions merge at a T junction, where they mix and become diluted. Then, when  $\text{BrO}_3^-$  or  $\text{ClO}_2^-$  are injected, the reactions with  $\text{Br}^-$  to generate  $\text{Br}_2$  and the bromation of ODA begin. The time and kinetics of the reaction are controlled, together with total flow,  $F_R + F_P$ , with a reactor,  $R$ , of 200 cm length placed in a bath thermostatted at  $60^\circ\text{C}$ . The reaction product is monitored by measuring absorbance at 450 nm.

For sequential determination, the flow scheme depicted in Fig. 2 was used. The set-up comprises two reactors— $R_1 = 200$  cm and  $R_2 = 500$  cm (reaction times of 68 and 154 s, respectively), ther-

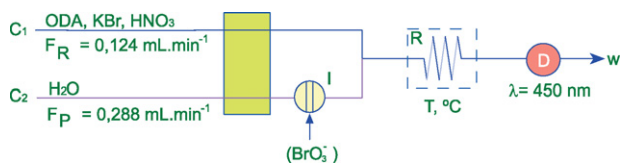


**Fig. 1.** Flow scheme for continuous mode determination of  $\text{BrO}_3^-$  by means of the ODA bromation reaction.  $C_1$  and  $C_2$ : channels; I: injection valve;  $V_i$ : injection volume:  $288 \mu\text{L}$ ;  $R$ : coiled reactor: 100 cm, temperature:  $60^\circ\text{C}$ ; D: spectrophotometric detector. [ODA]:  $1.95 \times 10^{-3}$  M; [KBr]:  $3.9 \times 10^{-2}$  M; [ $\text{HNO}_3$ ]: 1.22 M;  $F_R = 0.124 \text{ mL min}^{-1}$ ;  $F_P = 0.288 \text{ mL min}^{-1}$ .

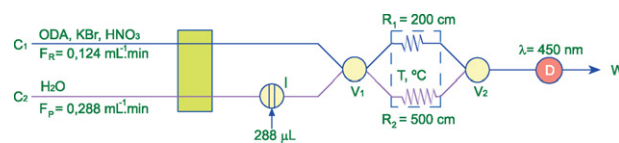


**Fig. 2.** Flow scheme for sequential determination of  $\text{BrO}_3^-$  and  $\text{ClO}_2^-$ , under continuous flow by means of kinetic differentiation.  $C_1$  and  $C_2$ : channels; I: injection valve;  $V_i$ : injection volume:  $288 \mu\text{L}$ ;  $V_1$  and  $V_2$ : two-way valves;  $R_1$ : coiled reactor: 200 cm;  $R_2$ : coiled reactor: 500 cm (sequential determination) or 700 cm (simultaneous determination); D: spectrophotometric detector. [ODA]:  $1.95 \times 10^{-3}$  M; [KBr]:  $3.9 \times 10^{-2}$  M; [ $\text{HNO}_3$ ]: 1.22 M;  $F_R = 0.124 \text{ mL min}^{-1}$ ;  $F_P = 0.288 \text{ mL min}^{-1}$ , temperature:  $60^\circ\text{C}$ .

mostatted at  $60^\circ\text{C}$ . Two two-way valves were also used to allow choice (by means of a turn) of the direction of flow: towards  $R_1$  or towards  $R_2$ . The chemical and hydrodynamic variables used were those considered optimum in Fig. 1.

## 3. Results and discussion

### 3.1. Optimization of experimental conditions

#### 3.1.1. Preliminary experiments

The ODA bromation reaction was not instantaneous. It initially evolved positively with time, and as from 6 min (at room temperature) absorbance at 450 nm began to decrease owing to the decomposition of the bromated product. To optimise this reaction for the determination of  $\text{BrO}_3^-$  in flow regime with the system proposed in Fig. 1,  $288 \mu\text{L}$  of solutions containing the anion at an elevated concentration in comparison with the normal values found in water samples  $-3 \text{ mg L}^{-1}$  was injected, and keeping a concentration of  $3.9 \times 10^{-2}$  M KBr and 1.22 M  $\text{HNO}_3$  in channel 2, the concentration of ODA was modified between  $0.20 \times 10^{-3}$  and  $1.95 \times 10^{-3}$  M. The best results were obtained for concentrations higher than  $1.59 \times 10^{-3}$  M, above which the signal remained constant. The same way was used to deduce the optimum concentrations of KBr (maximum signal as from  $20 \times 10^{-3}$  M for the same concentration of  $\text{BrO}_3^-$ ) and  $\text{HNO}_3$  (a constant signal between 0.60 and 1.22 M), together with the optimum length of the reactor (100 cm) and thermostating temperature:  $60^\circ\text{C}$ . In preliminary studies performed in discontinuous mode, the interference by chlorite in this determination was checked. These studies involved the preparation of solutions containing [ODA]:  $1.95 \times 10^{-3}$  M, [KBr]:  $3.2 \times 10^{-2}$  M, and [ $\text{HNO}_3$ ]: 1.22 M, and amounts of  $\text{BrO}_3^-$  and  $\text{ClO}_2^-$  varying between 60 and  $900 \mu\text{g L}^{-1}$ , recording the kinetic development at room temperature. Fig. 3 shows the kinetics for similar amounts of both analytes. It was observed that in the presence of KBr, in acid medium,  $\text{ClO}_2^-$  generated the same ODA bromation product as  $\text{BrO}_3^-$ , absorbing at 450 nm.

From the kinetic curves it may be deduced that the kinetics of the  $\text{ClO}_2^-$ - $\text{Br}^-$  reaction is less rapid than that of  $\text{BrO}_3^-$ - $\text{Br}^-$  and hence the ODA bromation reaction is slower in the first case. Whereas the bromation product in the case of  $\text{BrO}_3^-$  began to decompose at room temperature at around 500 s, in the case of  $\text{ClO}_2^-$  in no case was the decomposition of the bromation product observed up to 3500 s after the reaction had started. During this time, the maximum rate of product formation was reached again for most  $\text{ClO}_2^-$  concentrations, thereafter remaining stable until at least 3500 s.

As an example, Fig. 4 shows the kinetic development of the solutions containing  $\text{ClO}_2^-$  and  $\text{BrO}_3^-$  for similar analyte concentrations. It may be seen that in all cases the solutions containing  $\text{BrO}_3^-$  initially evolve with time at a greater rate than those containing  $\text{ClO}_2^-$ , generating more bromated product and hence the higher absorbance value at 450.

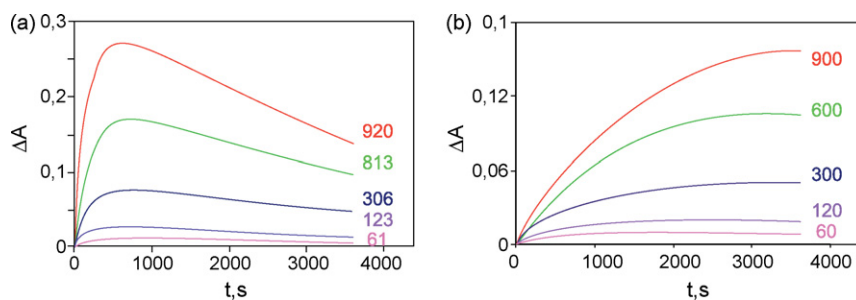


**Fig. 3.** Influence of the oxoanion concentration in the ODA bromation reaction. Discontinuous mode kinetic study at room temperature of solutions containing  $\text{BrO}_3^-$  (a) between 61 and 920  $\mu\text{g L}^{-1}$  and  $\text{ClO}_2^-$  (b) between 60 and 900  $\mu\text{g L}^{-1}$ . [ODA]:  $1.95 \times 10^{-3}$  M; [KBr]:  $3.2 \times 10^{-2}$  M; [ $\text{HNO}_3$ ]: 1.22 M.

For intermediate times, the signal corresponding to the solution of  $\text{BrO}_3^-$  began to decrease owing to the decomposition of the bromated product. As from a certain time, the signal generated in the  $\text{BrO}_3^-$  solutions reached even lower values than that generated by the  $\text{ClO}_2^-$  solutions.

It may also be observed that for each concentration studied there was a reaction time in which both solutions afforded the same signal (cross-over point) or values very similar to the neighbourhood of this point. These observations suggest that the interference of  $\text{ClO}_2^-$ , as regards its levels, will depend not only on its concentration but also on the time at which the measurement is made.

### 3.2. Behaviour of $\text{ClO}_2^-$ in continuous-flow mode in the bromation reaction of ODA

#### 3.2.1. Influence of reactor length and thermostating time

The above results explain the kinetic differences between  $\text{BrO}_3^-$  and  $\text{ClO}_2^-$  in the bromation reaction of ODA in acid medium at room temperature. To explore the behaviour of  $\text{ClO}_2^-$  in continuous-flow mode in this reaction, the two main variables – reactor length and thermostating temperature – were studied. To accomplish this,

under the conditions described for the flow system a standard solution of  $\text{ClO}_2^-$  at 300  $\mu\text{g L}^{-1}$  was injected, modifying reactor length from 100 to 900 cm, such that the reaction time varied between 39 and 268 s. For each reactor length considered, a study was made of the thermostating temperature from 23 to 65 °C.

The mean values of  $\Delta A$  obtained upon triplicate injection of the standard solution of  $\text{ClO}_2^-$  at 300  $\mu\text{g L}^{-1}$  under the different experimental conditions are plotted against reaction time and reactor length in Fig. 5. In that figure, it may be seen that the analytical signal clearly increases with the thermostating temperature and with the reactor length. For the same reaction time, the signal increases with the increase in temperature.

Decomposition of the bromated product was only seen for reaction times longer than 154 s (reactor length 500 cm) and a thermostating temperature of 65 °C.

Since there were clear differences between the behaviour of  $\text{BrO}_3^-$  and of  $\text{ClO}_2^-$  in the ODA bromation reaction as a function of the reaction time and the thermostating temperature, the  $\Delta A$  values obtained for 300  $\mu\text{g L}^{-1}$  of  $\text{BrO}_3^-$  and of  $\text{ClO}_2^-$  under the same experimental conditions were plotted (Fig. 6). In that figure, it may be seen that in all cases  $\text{BrO}_3^-$  generated a higher analytical signal,

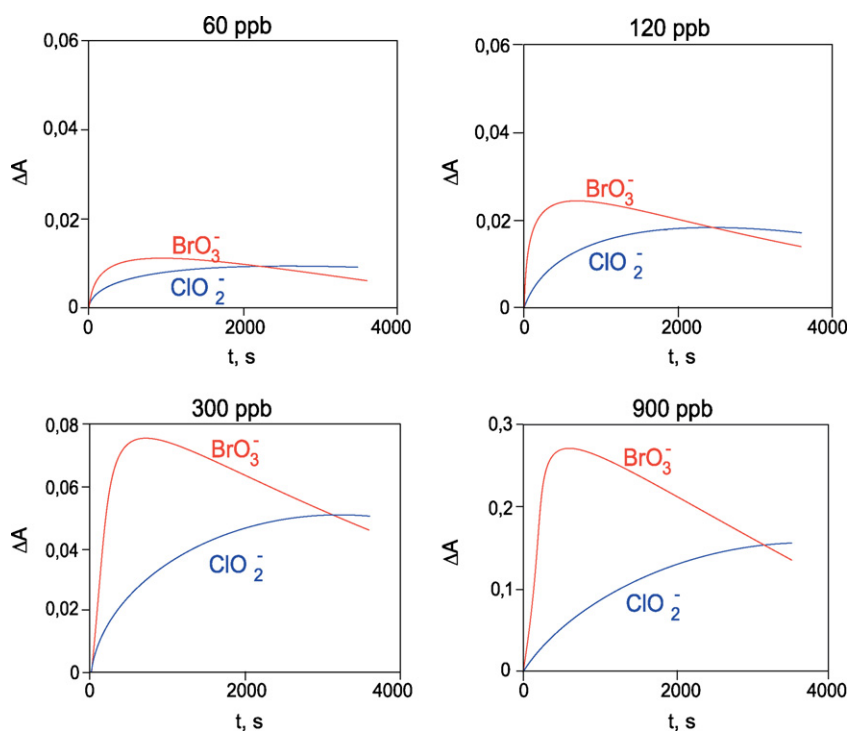


**Fig. 4.** The ODA bromation reaction. Kinetic development of solutions containing  $\text{ClO}_2^-$  and  $\text{BrO}_3^-$  grouped by similar concentrations. [ODA]:  $1.95 \times 10^{-3}$  M; [KBr]:  $3.2 \times 10^{-2}$  M; [ $\text{HNO}_3$ ]: 1.22 M, temperature, 22 °C.

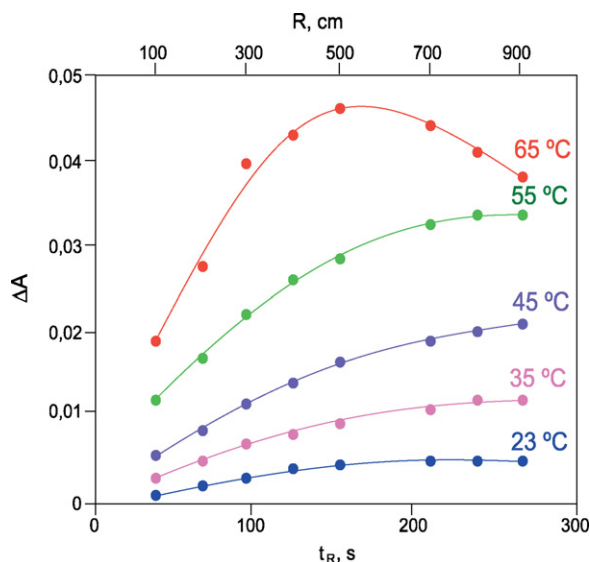


**Fig. 5.** Study of interference of  $\text{ClO}_2^-$  in the determination of  $\text{BrO}_3^-$  in continuous-flow mode by means of the ODA bromation reaction. Effect of reactor length and of thermostating temperature on the analytical signal generated by  $\text{ClO}_2^-$ . [ODA]:  $1.95 \times 10^{-3}$  M; [KBr]:  $3.9 \times 10^{-2}$  M; [ $\text{HNO}_3$ ]: 1.22 M;  $F_R = 0.124$  mL  $\text{min}^{-1}$ ;  $V_i = 288$   $\mu\text{L}$ ;  $F_P = 0.288$  mL  $\text{min}^{-1}$ ; [ $\text{ClO}_2^-$ ]:  $300$   $\mu\text{g L}^{-1}$ .

its bromation reaction evolving kinetically at a greater rate than that corresponding to  $\text{ClO}_2^-$ .

For high temperatures ( $55^\circ\text{C}$  and  $65^\circ\text{C}$ ) the reaction generated by  $\text{BrO}_3^-$  afforded maximum compound formation for reaction times of 96 and 39 s, respectively; at longer times, the compound began to be destroyed. The reaction in the presence of  $\text{ClO}_2^-$  at only  $65^\circ\text{C}$  reached maximum product generation for reaction times of the order of 154 s, the product decomposing for longer reaction times.

From this comparative kinetic study it is possible to obtain sufficient information to study the effect of  $\text{ClO}_2^-$  on the method of  $\text{BrO}_3^-$  determination in continuous-flow mode. This allows us to propose continuous methods for the joint but non-specific determination of  $\text{BrO}_3^-$  and  $\text{ClO}_2^-$ , and even the individual determination of these analytes, one in the presence of the other, by means of kinetic differentiation.

### 3.3. Interference of $\text{ClO}_2^-$ in the determination of $\text{BrO}_3^-$ in continuous-flow mode

In the method set-up for the determination of  $\text{BrO}_3^-$  in drinking water using  $\text{O}_3$  as a disinfectant, a short 100-cm coiled reactor thermostatted at  $60^\circ\text{C}$  was used; this allowed analytical signals to be obtained at 38 s after the start of the reaction. It was decided to use a thermostating temperature of  $60^\circ\text{C}$  instead of  $65^\circ\text{C}$ , where the analytical signal generated was slightly higher, in order to avoid the formation of small bubbles of steam that could have affected (that affected) the reproducibility of the method.

As may be seen in Fig. 6, at high temperatures – in this case at  $65^\circ\text{C}$  – and for short reaction times the differences between the analytical signals generated by  $\text{BrO}_3^-$  and by  $\text{ClO}_2^-$  in the ODA bromation reaction were greater. Under these conditions,  $\text{ClO}_2^-$  interfered less in the determination of  $\text{BrO}_3^-$ .

In the flow scheme depicted in Fig. 1, and under the conditions considered to be optimum for the determination of  $\text{BrO}_3^-$  in continuous-flow mode ( $R = 100$  cm;  $T = 60^\circ\text{C}$ ), triplicate  $288$   $\mu\text{L}$  injections were made of  $\text{BrO}_3^-$  solutions at concentrations of 10

**Table 1**

Interference of  $\text{ClO}_2^-$  on the determination of  $\text{BrO}_3^-$  in continuous-flow mode by the ODA bromation reaction

$\text{ClO}_2^-$ ( $\mu\text{g L}^{-1}$ )	$\Delta A$ (450 nm)
$\text{BrO}_3^-$ , 10 $\mu\text{g L}^{-1}$	
–	0.0020
5.0	0.0021
10.0	0.0024
20.0	0.0029
50.0	0.0042
$\text{BrO}_3^-$ , 25 $\mu\text{g L}^{-1}$	
–	0.0051
5.0	0.0053
10.0	0.0055
20.0	0.0060
50.0	0.0075

$R = 100$  cm,  $T = 60^\circ\text{C}$ ,  $V_i = 288$   $\mu\text{L}$ , [ODA]:  $1.95 \times 10^{-3}$  M, [KBr]:  $3.9 \times 10^{-2}$  M, [ $\text{HNO}_3$ ]: 1.22 M,  $F_R = 0.124$  mL  $\text{min}^{-1}$ ,  $F_P = 0.288$  mL  $\text{min}^{-1}$ .

and  $25$   $\mu\text{g L}^{-1}$  with and without  $\text{ClO}_2^-$  in the range  $5$ – $50$   $\mu\text{g L}^{-1}$ . The results are shown in Table 1.

It may be seen that the presence of  $5$   $\mu\text{g L}^{-1}$  of  $\text{ClO}_2^-$  in the  $10$   $\mu\text{g L}^{-1}$  and  $25$   $\mu\text{g L}^{-1}$  solutions of  $\text{BrO}_3^-$  generated fluctuations in the absorbance value. These can be attributed to the imprecision of the measuring method. However, when the concentration of  $\text{ClO}_2^-$  reached  $10$   $\mu\text{g L}^{-1}$ , the variations generated in the absorbance value represent 72% for  $25$   $\mu\text{g L}^{-1}$  of  $\text{BrO}_3^-$  and 15% for  $10$   $\mu\text{g L}^{-1}$  of  $\text{BrO}_3^-$ . Accordingly, in continuous-flow mode  $\text{ClO}_2^-$  can be said to exert an interference in the determination of  $\text{BrO}_3^-$  by means of the ODA bromation reaction, under the high-sensitivity conditions for  $\text{BrO}_3^-$ , as from concentrations as low as  $8$ – $10$   $\mu\text{g L}^{-1}$ .

The ODA bromation method for the determination of  $\text{BrO}_3^-$  in continuous-flow mode (Fig. 1) would only be useful in water purification systems that use  $\text{O}_3$ . If, apart from ozonation,  $\text{ClO}^-$  and  $\text{ClO}_2$  are used for supplementary disinfection, above  $8$ – $10$   $\mu\text{g L}^{-1}$  the  $\text{ClO}_2^-$  will generate interference.

### 3.4. Simultaneous determination of $\text{BrO}_3^-$ and $\text{ClO}_2^-$ as disinfection by-products

As mentioned, in systems that use  $\text{O}_3$  as a disinfectant and disinfection is enhanced with  $\text{ClO}_2^-$ , and mainly  $\text{ClO}_2$ , it is possible to detect  $\text{BrO}_3^-$  and  $\text{ClO}_2^-$ , oxoanions generated as by-products in the disinfection processes.

In the comparative kinetic study between  $\text{BrO}_3^-$  and  $\text{ClO}_2^-$  in the ODA bromation reaction in acid medium (Fig. 6), it was observed that at a high temperature ( $65^\circ\text{C}$ ) and for reaction times of the order of 211 s ( $R = 700$  cm) the analytical signals generated by both oxoanions were almost identical.

This kinetic observation allows us to propose a continuous-flow method based on the aforementioned reaction in acid medium for the joint but not differentiated determination of  $\text{BrO}_3^-$  and  $\text{ClO}_2^-$ . This would provide a method for the simultaneous determination of oxyhalides as disinfection by-products.

The crossing of the  $\text{BrO}_3^-$  and  $\text{ClO}_2^-$  kinetic curves at high temperatures depends not only on the thermostating temperature but also on the concentration of oxoanion. To study the effect of  $\text{BrO}_3^-$  and  $\text{ClO}_2^-$  concentrations on the cut-off time of the kinetic curves (the time of reaction at which they generate the same analytical signal), a study similar to that carried out for  $\text{BrO}_3^-$  and  $\text{ClO}_2^-$  at concentrations of  $300$   $\mu\text{g L}^{-1}$  was performed, but for equal concentrations of both analytes and with values of 180, 90 and  $50$   $\mu\text{g L}^{-1}$ .

The values of  $\Delta A$  obtained upon triplicate injection of  $288$   $\mu\text{L}$  of the solutions of  $\text{BrO}_3^-$  and  $\text{ClO}_2^-$  are plotted against time in Fig. 7.

It may be seen that for a reaction time between 211 and 240 s the analytical signals generated, regardless of whether the oxidant

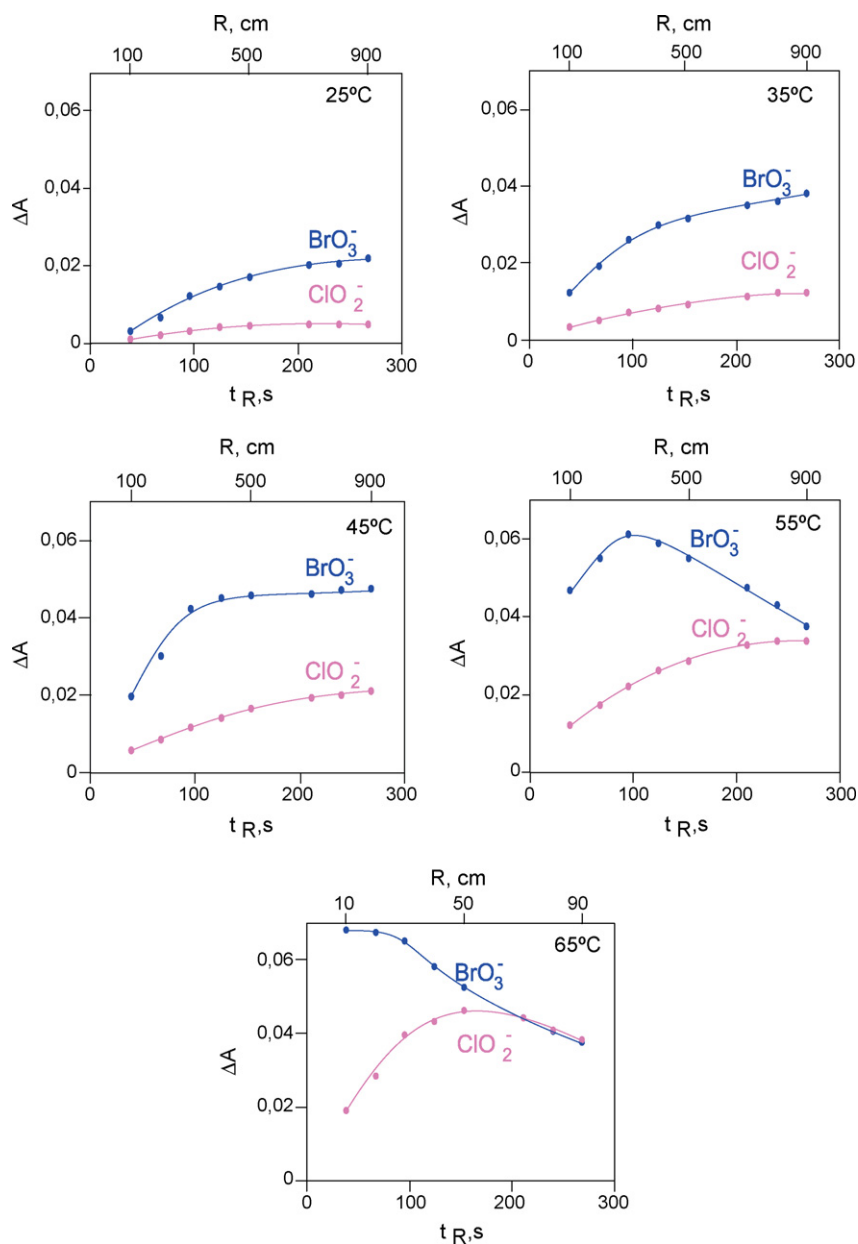


**Fig. 6.** ODA bromation reaction in continuous mode. Comparative analytical signals generated by the same concentration of  $\text{ClO}_2^-$  and  $\text{BrO}_3^-$  ( $300 \mu\text{g L}^{-1}$ ) for different reactor lengths and different temperatures. [ODA]:  $1.95 \times 10^{-3} \text{ M}$ ; [KBr]:  $3.9 \times 10^{-2} \text{ M}$ ; [ $\text{HNO}_3$ ]:  $1.22 \text{ M}$ .  $F_R = 0.124 \text{ mL min}^{-1}$ ;  $V_i = 288 \mu\text{L}$ ;  $F_p = 0.288 \text{ mL min}^{-1}$ .

is  $\text{BrO}_3^-$  or  $\text{ClO}_2^-$ , are very similar, with differences of less than 3%. Accordingly, a reaction time of 211 s was chosen, corresponding to a reactor coil with a length of 700 cm.

To check the concentration range at reaction times of 211 s in which the behaviour of  $\text{BrO}_3^-$  and  $\text{ClO}_2^-$  was similar, a study was made of the variation in the analytical signal of both analytes as a function of concentration up to a value of  $336 \mu\text{g L}^{-1}$  under the conditions described for the flow system shown in Fig. 2, but using a reactor of 700 cm and thermostating at  $60^\circ\text{C}$ . The values obtained fit straight lines, with equations of

$$\Delta A = 6.31 \times 10^{-5} + 1.53 \times 10^{-4}[\text{BrO}_3^-]; \quad R^2 = 1. \quad (1)$$

$$\Delta A = -2.71 \times 10^{-4} + 1.51 \times 10^{-4}[\text{ClO}_2^-]; \quad R^2 = 0.998. \quad (2)$$

It may be seen that up to a concentration of  $340 \mu\text{g L}^{-1}$  both  $\text{BrO}_3^-$  and  $\text{ClO}_2^-$  generate identical analytical signals for each concentration value. The slopes of the calibration lines

( $1.53 \pm 0.08$ ) and ( $1.51 \pm 0.02$ ) do not differ for a confidence level of 95%.

To check that solutions containing both oxoanions at the same time afforded the same calibration – i.e., that there was no chemical interaction between them – triplicate injections were made of standard solutions containing concentrations of freshly prepared oxoanion between 14 and  $300 \mu\text{g L}^{-1}$ .

The mean  $\Delta A$  values obtained are shown in Table 2 and it may be seen that the plot of  $\Delta A$  at 450 nm against oxoanion concentration in  $\mu\text{g L}^{-1}$  follows a straight line, with an equation of:

$$\Delta A = (1 \pm 1) \times 10^{-4} + (1.53 \pm 0.01) \times 10^{-4}[\text{oxoanion}], \mu\text{g L}^{-1}; \quad R^2 = 0.999. \quad (3)$$

The slope of the calibration line for the oxoanions does not differ significantly from the slopes of the individual calibration lines for a confidence level of 95%.

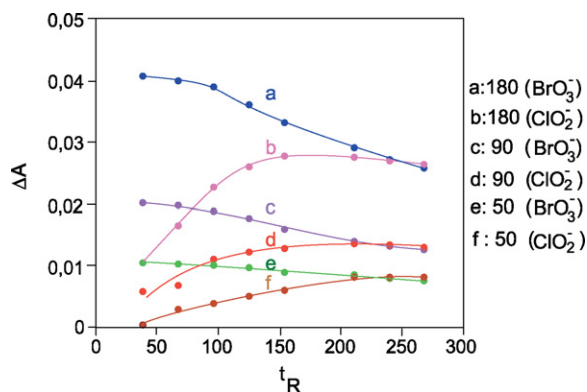


**Fig. 7.** Simultaneous determination of  $\text{ClO}_2^-$  and  $\text{BrO}_3^-$  in continuous-flow mode by means of the ODA bromation reaction. Effect of concentration of  $\text{ClO}_2^-$  and  $\text{BrO}_3^-$  lower than  $300 \mu\text{g L}^{-1}$  on the analytical signal.  $[\text{ClO}_2^-] = [\text{BrO}_3^-]$ : 180, 90 and  $50 \mu\text{g L}^{-1}$ . [ODA]:  $1.95 \times 10^{-3} \text{ M}$ ; [KBr]:  $3.9 \times 10^{-2} \text{ M}$ ;  $[\text{HNO}_3]$ :  $1.22 \text{ M}$ .  $F_R = 0.124 \text{ mL min}^{-1}$ ;  $V_i = 288 \mu\text{L}$ ;  $F_P = 0.288 \text{ mL min}^{-1}$ ,  $T = 60^\circ\text{C}$ .

During the time elapsed between the preparation of the standard solution until the more diluted solutions were determined in continuous-flow mode, no chemical reaction between  $\text{BrO}_3^-$  and  $\text{ClO}_2^-$  was observed.

At 72 h, the same standard solutions, kept under refrigeration, generating a calibration equation thus:

$$\Delta A_{450 \text{ nm}} = (-0.003 \pm 0.005) + (1.2 \pm 0.1) \times 10^{-4} [\text{oxoanion}], \mu\text{g L}^{-1}; \quad R^2 = 0.992, \quad (4)$$

indicating, for a confidence level of 95%, that at the end of this time a chemical reaction between  $\text{BrO}_3^-$  and  $\text{ClO}_2^-$  does occur. The standards were prepared fresh before each session.

The limit of detection calculated from the expression  $C_L = 3X_B^{\text{max}}/b$ , afforded a value of  $9.8 \mu\text{g L}^{-1}$ , taking into account the slope of the calibration line ( $b$ ) and the maximum fluctuation of the baseline  $X_B^{\text{max}} = 0.0005$  ( $X_B^{\text{max}} > S_B$ : absolute standard deviation of the baseline) [22].

The precision of the method was studied using  $n = 12$  standard solutions at an oxoanion concentration of  $14 \mu\text{g L}^{-1}$  ( $6 \mu\text{g L}^{-1}$  of  $\text{BrO}_3^-$  and  $8 \mu\text{g L}^{-1}$  of  $\text{ClO}_2^-$ ), injecting them into the flow system ( $V_i = 288 \mu\text{L}$ ) under the calibration conditions and obtaining a value of  $S_R = 8.5\%$ . A similar study with a more concentrated solution –  $75 \mu\text{g L}^{-1}$  of oxoanion,  $n = 12$  ( $50 \mu\text{g L}^{-1}$  of  $\text{BrO}_3^-$  and  $25 \mu\text{g L}^{-1}$  of  $\text{ClO}_2^-$ ) – afforded a value of  $S_R = 6.2\%$ . Under the optimum geometric and hydrodynamic conditions it is possible to achieve a determination rate of 8 samples per hour.

**Table 2**

Simultaneous determination of  $\text{ClO}_2^-$  and  $\text{BrO}_3^-$ , as oxoanions, in continuous-flow mode by means of the ODA bromation reaction

$\text{BrO}_3^-$ ( $\mu\text{g L}^{-1}$ )	$\text{ClO}_2^-$ ( $\mu\text{g L}^{-1}$ )	[Oxoanion] ( $\mu\text{g L}^{-1}$ )	$\Delta A$ (450 nm)
6	8	14	0.0022
15	10	25	0.0039
20	25	45	0.0067
25	25	50	0.0079
50	25	75	0.0118
50	50	100	0.0151
100	25	125	0.0194
75	100	175	0.0265
100	100	200	0.0314
100	200	300	0.0460

Effect of the concentration of the oxoanions on the value of  $\Delta A$  at 450 nm. [ODA]:  $1.95 \times 10^{-3} \text{ M}$ , [KBr]:  $3.9 \times 10^{-2} \text{ M}$ ,  $[\text{HNO}_3]$ :  $1.22 \text{ M}$ ;  $F_R = 0.124 \text{ mL min}^{-1}$ ;  $V_i = 288 \mu\text{L}$ ;  $F_P = 0.288 \text{ mL min}^{-1}$ ,  $R = 700 \text{ cm}$ ;  $T = 60^\circ\text{C}$ .

**Table 3**

Simultaneous determination of  $\text{BrO}_3^-$  and  $\text{ClO}_2^-$  in continuous-flow mode by means of the ODA bromation reaction

[Oxoanion], added ( $\mu\text{g L}^{-1}$ )	[Oxoanion], found <sup>a</sup> ( $\mu\text{g L}^{-1}$ )
10	$11 \pm 3$
22	$19 \pm 3$
35	$36 \pm 2$
40	$38 \pm 2$
50	$52 \pm 2$

Validation of the determination method. [ODA]:  $1.95 \times 10^{-3} \text{ M}$ , [KBr]:  $3.9 \times 10^{-2} \text{ M}$ ,  $[\text{HNO}_3]$ :  $1.22 \text{ M}$ ;  $F_R = 0.124 \text{ mL min}^{-1}$ ;  $V_i = 288 \mu\text{L}$ ;  $F_P = 0.288 \text{ mL min}^{-1}$ ,  $R = 700 \text{ cm}$ ;  $T = 60^\circ\text{C}$ .

<sup>a</sup> With 95% confidence limit. Average of three determinations.

With a view to checking the applicability of the method, 25 mL of Aquabona<sup>®</sup> water was spiked with  $\text{BrO}_3^-$  or  $\text{ClO}_2^-$ , diluting up to 50 mL. The amounts of standard added ranged between  $10 \mu\text{g L}^{-1}$  of oxoanion ( $5 \mu\text{g L}^{-1}$  of  $\text{BrO}_3^-$  and  $5 \mu\text{g L}^{-1}$  of  $\text{ClO}_2^-$ ) and  $50 \mu\text{g L}^{-1}$  of oxoanion ( $25 \mu\text{g L}^{-1}$  of  $\text{BrO}_3^-$  and  $25 \mu\text{g L}^{-1}$  of  $\text{ClO}_2^-$ ).

Under the above optimum experimental conditions, and after repeating the analytical calibrations with  $n = 6$  standards between 8 and  $60 \mu\text{g L}^{-1}$  of oxoanion, the spiked solutions were determined following triplicate injection. The results are shown in Table 3. It may be seen from the results obtained that the found values do not differ significantly from those initially added for a confidence level of 95%.

It should be noted that in systems that use  $\text{ClO}_2$  as a disinfectant  $\text{BrO}_3^-$  is not normally found, in which case the method would only be of use for the determination of  $\text{ClO}_2^-$ . Current legislation demands that this parameter be evaluated (Official State Bulletin. no. 45, 21-02-2003, note (3) p. 7240) when  $\text{ClO}_2$  is used as a disinfectant, although the parametric level has not been set. The American EPA has established a value of  $25 \mu\text{g L}^{-1}$  for this parameter.

### 3.5. Sequential determination of $\text{BrO}_3^-$ and $\text{ClO}_2^-$ by kinetic differentiation in continuous-flow mode

The different kinetic behaviour of the ODA bromation reaction generated by  $\text{BrO}_3^-$  and by  $\text{ClO}_2^-$  suggests that it would be possible to determine both analytes in continuous-flow mode by means of kinetic differentiation. The optimum temperature to achieve this with the greatest sensitivity possible for both analytes is  $60^\circ\text{C}$ .

A flow set-up similar to that shown in Fig. 2 was used, with the difference that two reactors –  $R_1$  and  $R_2$ , thermostatted at  $60^\circ\text{C}$  – were necessary. The chemical and hydrodynamic variables were those considered optimum, choosing lengths for  $R_1$  and  $R_2$  that would afford reaction times that generated sufficiently different but sufficiently sensitive analytical signals for  $\text{BrO}_3^-$  and  $\text{ClO}_2^-$  to be determined at values below the parametric levels:  $R_1 = 200 \text{ cm}$  and  $R_2 = 500 \text{ cm}$ , corresponding to reaction times of 68 and 154 s, respectively.

For practical application of the sequential method it was necessary to use two two-way valves, which allowed the direction of flow to be selected towards reactor  $R_1$  or reactor  $R_2$ . For the analysis of each sample, the injection of two volumes of  $288 \mu\text{L}$  was required; one flowing through reactor  $R_1$  (position 1 of the valves) and the other through  $R_2$  (position 2 of the valves) (Fig. 2).

#### 3.5.1. Influence of the concentration of $\text{BrO}_3^-$ and $\text{ClO}_2^-$ using each of the reactors

(A)  $R_1 = 200 \text{ cm}$ .

Under the above chemical and hydrodynamic conditions,  $288 \mu\text{L}$  of standards of  $\text{BrO}_3^-$  and  $\text{ClO}_2^-$  were injected sep-



arately at concentrations ranging from 6 to 160  $\mu\text{g L}^{-1}$ . The mean  $\Delta A$  values observed upon injecting each solution in triplicate, plotted against the concentration of each of the analytes, afforded straight lines with equations of:

$$\text{BrO}_3^- : \Delta A = (8 \pm 16) \times 10^{-5} + (2.07 \pm 0.02) \times 10^{-4} [\text{BrO}_3^-], \mu\text{g L}^{-1}; R^2 = 0.999. \quad (5)$$

$$\text{ClO}_2^- : \Delta A = (7 \pm 8) \times 10^{-5} + (9.3 \pm 0.1) \times 10^{-5} [\text{ClO}_2^-], \mu\text{g L}^{-1}; R^2 = 0.999. \quad (6)$$

(B)  $R_1 = 500$  cm.

Under the same chemical and hydrodynamic conditions, and for the same concentration range, the analytical calibrations for  $\text{BrO}_3^-$  and  $\text{ClO}_2^-$  were obtained using the longer reactor  $R_2$  (500 cm). The mean  $\Delta A$  values obtained upon injecting each standard solution in triplicate also provided straight lines, with equations of:

$$\text{BrO}_3^- : \Delta A = (-6 \pm 8) \times 10^{-5} + (1.78 \pm 0.01) \times 10^{-4} [\text{BrO}_3^-], \mu\text{g L}^{-1}; R^2 = 1.0. \quad (7)$$

$$\text{ClO}_2^- : \Delta A = (1 \pm 1) \times 10^{-4} + (1.4 \pm 0.2) \times 10^{-4} [\text{ClO}_2^-], \mu\text{g L}^{-1}; R^2 = 0.999. \quad (8)$$

In light of the equations of the calibration straight lines obtained for the 200-cm and 500-cm reactors, and taking into account that the ordinates at the origin with their fluctuation encompass the origin of the coordinates, the following set of equations is proposed for solving problem samples containing  $\text{BrO}_3^-$  and  $\text{ClO}_2^-$ :

$$\Delta A_{200\text{cm}} = 2.07 \times 10^{-4} [\text{BrO}_3^-] + 0.93 \times 10^{-4} [\text{ClO}_2^-] \quad (9)$$

$$\Delta A_{500\text{cm}} = 1.78 \times 10^{-4} [\text{BrO}_3^-] + 1.38 \times 10^{-4} [\text{ClO}_2^-], \quad (10)$$

expressing the concentrations of  $\text{BrO}_3^-$  and  $\text{ClO}_2^-$  in  $\mu\text{g L}^{-1}$ .

The precision of the method was determined using 12 standard solutions containing  $[\text{BrO}_3^-] = 10 \mu\text{g L}^{-1}$  and  $[\text{ClO}_2^-] = 20 \mu\text{g L}^{-1}$ . These were injected into the flow system under the above experimental conditions, obtaining standard deviations of 8.5% for  $\text{BrO}_3^-$  and 8.8% for  $\text{ClO}_2^-$ . The determination rate was 5 samples per hour.

### 3.5.2. Validation of the method

Using Aquabon<sup>®</sup> mineral water as matrix, solutions spiked with standards of  $\text{BrO}_3^-$  and  $\text{ClO}_2^-$  was prepared and the proposed method was implemented after collecting the analytical signals obtained with the 200-cm and 500-cm reactors and solving the set of equations mathematically.

Table 4 shows the results obtained, expressing the values at a confidence of 95% and taking into account the  $S_x$  value of the two individual calibrations, for each reactor length, conforming each of the equations and the fact that the values were obtained by difference.

The values found do not differ from the amounts added for a confidence level of 95%, although the imprecision of each value is relatively high because the values were obtained by difference.

**Table 4**

Sequential determination of  $\text{BrO}_3^-$  and  $\text{ClO}_3^-$  in continuous-flow mode by means of the ODA bromation reaction

BrO <sub>3</sub> <sup>-</sup> + ClO <sub>3</sub> <sup>-</sup> (μg L <sup>-1</sup> )		
Added	Found <sup>a</sup>	
10+20	8 ± 5	17 ± 6
25+25	26 ± 5	21 ± 5
25+40	23 ± 5	40 ± 4
40+25	43 ± 4	28 ± 5
40+40	38 ± 4	42 ± 4
50+50	54 ± 4	47 ± 4

Validation of method. [ODA]:  $1.95 \times 10^{-3}$  M, [KBr]:  $3.9 \times 10^{-2}$  M, [HNO<sub>3</sub>]: 1.22;  $V_i = 288 \mu\text{L}$ ;  $T = 60^\circ\text{C}$ ;  $R = 200 \text{ cm} \times 500 \text{ cm}$ .

<sup>a</sup> With 95% confidence limit. Average of three determinations.

## 4. Conclusions

The proposed method is efficient for the simultaneous and sequential determination of  $\text{BrO}_3^-$  and  $\text{ClO}_2^-$ , generated as by-products of disinfection in systems in which  $\text{O}_3$  is used as a disinfectant and the disinfection is then enhanced with  $\text{ClO}^-$  and  $\text{ClO}_2$ . The behaviour of the ODA bromation reaction, which for both analytes differs with time and temperature, allows a flow scheme to be proposed that will enable the kinetic differentiation of both. The method can be readily adapted for routine use and does not require preconcentration steps or the elimination of interferences.

## References

- [1] G. Gordon, R. Keiffer, D.H. Rosenblatt, Progress in Inorganic Chemistry, Wiley-Interscience, New York, 1972.
- [2] E.M. Aieta, J.D. Berg, J. Am. Water Works Assoc. 78 (1986) 62–72.
- [3] H.P. Wagner, B.V. Pepich, D.P. Hautman, D.J. Munich, J. Chromatogr. A 850 (1999) 119–129.
- [4] M. Bolyard, P.S. Fair, D.P. Hautman, Environ. Sci. Technol. 26 (1992) 1663–1667.
- [5] G. Gordon, L. Adam, B. Bubnis, Report of the American Water Works Association Research Foundation, Denver, CO, 1995.
- [6] Y. Kurokawa, A. Maekawa, M. Takahashi, Y. Hayashi, Environ. Health Perspect 87 (1990) 309–335.
- [7] K.M. Crofton, Toxicology 221 (2006) 212–216.
- [8] Council Directive 98/83/EC (November 3rd 1998), Official Journal of the European Communities Legislation, p. 32, 1998.
- [9] U.S. Environmental Protection Agency; National Primary Drinking Water Regulations: Disinfectants and Disinfection Byproducts; Final Rule, Fed. Reg., 63, No. 241: 69390, 1998.
- [10] V. Ingrand, J.L. Guinamant, A. Bruchet, C. Brosse, Th.H.M. Noij, A. Brandt, F. Sacher, C. McLeod, A.R. Elwaer, J.P. Croué, Ph. Quevauviller, Trends Anal. Chem. 21 (2002) 1–12.
- [11] EPA method 300.0; EPA/600/R93/100, 1991.
- [12] EPA method 300.1; EPA/600/R98/188, 1997.
- [13] ISO/DIS 15061, 1998.
- [14] H.P. Wagner, B.V. Pepich, D.P. Hautman, D.J. Munich, J. Chromatogr. A 884 (2000) 201–210.
- [15] H.P. Wagner, B.V. Pepich, D.P. Hautman, D.J. Munich, J. Chromatogr. A 956 (2002) 93–101.
- [16] W. Ketai, L. Huitao, C. Xingguo, H. Zhide, Food Chem. 70 (2000) 509–515.
- [17] G. Gordon, B. Bubnis, D. Sweetin, C. Kuo, Ozone Sci. Eng. 16 (1994) 79–83.
- [18] K. Urasin, T. Takayanagi, D. Nacapricha, S. Motomizu, Anal. Chim. Acta 580 (2006) 68–74.
- [19] A.B. Syropoulos, E.G. Sarantonis, A.C. Calorkerinos, Anal. Chim. Acta 239 (1990) 195–202.
- [20] J.C.G. Esteves da Silva, J.R.M. Dias, J.M.C.S. Magalhaes, Anal. Chim. Acta 450 (2001) 175–184.
- [21] M. Catalá Icardo, J.V. García Mateo, J. Martínez Calatayud, Anal. Chim. Acta 443 (2001) 153–163.
- [22] L.A. Currie, Pure Appl. Chem. 67 (1995) 1699–1723.



## Development of a sensitive thermal desorption method for the determination of trihalomethanes in humid ambient and alveolar air

J. Caro, M. Gallego\*

Department of Analytical Chemistry, Campus of Rabanales, University of Córdoba, E-14071 Córdoba, Spain

### ARTICLE INFO

#### Article history:

Received 22 January 2008

Received in revised form 14 April 2008

Accepted 16 April 2008

Available online 26 April 2008

#### Keywords:

Thermal desorption

Sorbent tubes

Trihalomethanes (THMs)

Swimming pools

Ambient and alveolar air

### ABSTRACT

A sensitive and reliable method has been developed for the determination of trihalomethanes (THMs) in air samples through adsorption in sorbent tubes and thermal desorption (TD) of the compounds, followed by gas chromatography (GC)–mass spectrometry (MS) analysis. Three commercial sorbent materials were compared in terms of adsorption efficiency and breakthrough volume, finding Chromosorb 102 to be the most appropriate adsorbent for air sampling. The method allows us to reach detection limits of 0.03 ng (0.01  $\mu\text{g m}^{-3}$  for 3 l of air), linear ranges from 0.1 to 2000 ng and specific uncertainties of ca.  $5.0 \pm 0.2$  ng for all THMs. Several salts were tested to reduce water retention (from the humid air of an indoor swimming pool) at the sampling stage,  $\text{Na}_2\text{SO}_4$  being the one that provides optimum efficiency. The method was validated by a new recovery study in which several tubes with and without adsorbent were spiked with THMs and analyzed by TD-GC/MS, recoveries ranging from 92% to 97% for all the compounds. Finally, the performance of the method was evaluated through the analysis of ambient air samples from an indoor swimming pool and alveolar air samples from swimmers to assess their THM uptake. THMs were found to be stable in the sorbent tubes for at least 1 month when stored at 4 °C.

© 2008 Elsevier B.V. All rights reserved.

### 1. Introduction

Trihalomethanes (THMs), including chloroform, bromodichloromethane, dibromochloromethane and bromoform, are one of two major groups of organic disinfection by-products (DBPs) identified in chlorinated water in the 1970s [1]. Because of their carcinogenic risks, THMs were first regulated by the US Environmental Protection Agency (EPA) under the THM regulation in 1979 with a maximum contaminant level at 100  $\mu\text{g l}^{-1}$ , which was lowered to 80  $\mu\text{g l}^{-1}$  in 1998 [2,3]. Public pools are usually disinfected by gaseous chlorine or sodium hypochlorite and cartridge filters in the United States and Europe [4,5]. These methods produce a variety of DBPs such as THMs, as reported since 1980 [6]. Human exposure studies have shown that THMs can be found in the blood, plasma and exhaled breath [7–9] and urine [10] of swimmers and even of non-swimmers within an indoor pool setting. Inhalation and dermal exposure are likely to be important routes of human exposure to THMs in swimming pools, with ingestion from accidental swallowing of water being a minor route.

Volatile halogenated compounds are usually extracted from air onto sorbent columns, and after carrying out a solvent or thermal

desorption (TD) step, the target compounds are transferred into a gas chromatograph (GC) [11]. Along with GC separation, electron capture detection (ECD) and electron impact mass spectrometry (MS) are the most frequent detectors used; recent integration of other detectors has been reviewed [11,12]. Infrared spectroscopic methods have also been proposed due to their simplicity and rapidity in detecting gas samples containing volatile organic compounds (VOCs) [13]. The performance of a short-path TD method for 77 VOCs using a dual sorbent system (Tenax GR and Carbosieve SIII) provided excellent performance except for very low concentrations or large samples of highly humid air [14]. Automated monitoring of volatile halogenated compounds is currently an issue in ambient air analysis; the combination of adsorbent traps with Peltier cooling and with selective MS allowed good analyte recovery and rapid desorption without the need for post-desorption cryofocussing [15]. A type of multi-walled carbon nanotubes (MWCNTs) has been evaluated as an adsorbent for trapping VOCs (chloroform included). The breakthrough volume of chloroform (using gas injection into a GC/FID) is two orders larger with MWCNTs than on Carbo-pack B [16]. Novel trends in sample preparation have recently been summarized for the determination of VOCs in air [17].

THM concentrations in the air of swimming pools have been determined by collecting 10 l of air on activated carbon adsorbents, desorption with 3-phenoxybenzylalcohol at 110 °C for 30 min in a vial, and manual injection of the extract into a GC/ECD [18]. Air and breath samples from people exposed to household water-use

\* Corresponding author. Tel.: +34 957 218 614; fax: +34 957 218 614.

E-mail address: [qa1gafem@uco.es](mailto:qa1gafem@uco.es) (M. Gallego).

activities have been collected directly into canisters to determine THMs by automated GC/MS using a modified version of US EPA Method TO-14 [19]. Aggazzotti et al. have published several articles about the determination of THMs in water, blood and air as indicators of exposure in indoor swimming pools. Ambient air and breath samples were analyzed by direct injection of samples into a gas chromatograph with ECD using a gas-tight syringe [7]. More recently, air samples were collected in tedlar bags and breath on glass tubes with two valves (at the end of expiration the valves were closed) [9]. Both air samples were analyzed as described above [7]. Water interference is a special issue in order to avoid chromatographic problems and detector damage. Several options to reduce the amount of water that is brought into the GC system via the sorbent materials are found in the literature [20]. Therefore, water removal remains an important issue in the analysis of volatile halogenated compounds [11].

This paper describes the development and evaluation of a TD-GC/MS method for the determination of THMs in the ambient air of a swimming pool and in the alveolar air of people exposed (swimmers). In this sense multisorbent tubes (usually employed to date for mixtures of VOCs) are not necessary and only tubes filled with the best adsorbent for these compounds (low water retention, high breakthrough volumes, no generation of artefacts, etc.) were used. Furthermore, the present work is the first of its kind to include a rigorous study of several salts packed into a tube placed in front of the sorbent tube in order to eliminate the water present in the ambient air of the indoor swimming pool. The inclusion of a drying tube is mandatory, taking into account the high levels of humidity in the swimming pool (60–80% relative humidity), as the water can reach the chromatographic column as well as the mass spectrometer in addition to a decrease in the retention of analytes in the sorbent material. On the other hand, the methods proposed for the sampling of breath are neither robust nor reliable [7–9]; in this method a Bio-VOC sampler for alveolar air was used. Finally, a new recovery experiment was proposed using TD-GC/MS in all instances, since it is normally carried out in the VOC literature by comparing the analysis of a spiked tube by TD-GC/MS versus the response obtained by direct injection of the same amount by GC/MS [14,21].

## 2. Experimental

### 2.1. Chemicals and materials

Chloroform ( $\text{CHCl}_3$ ), bromodichloromethane ( $\text{CHBrCl}_2$ ), dibromochloromethane ( $\text{CHBr}_2\text{Cl}$ ) and bromoform ( $\text{CHBr}_3$ ), all of them with a purity  $\geq 99\%$ , were purchased from Sigma-Aldrich (Madrid, Spain). Methanol, calcium chloride, potassium carbonate and sodium sulphate were supplied by Panreac (Barcelona, Spain). Three commercial sorbent materials, including two porous polymers (Tenax TA and Chromosorb 102 with a surface area of 35 and  $350 \text{ m}^2 \text{ g}^{-1}$ , respectively) and a graphitized carbon black (Carbopack B, surface area  $100 \text{ m}^2 \text{ g}^{-1}$ ), all of them with 60/80 mesh, and unsilanized glass wool were supplied by Supelco (Madrid, Spain).

### 2.2. Sorbent tubes

Stainless steel thermal desorption tubes (6 mm O.D.  $\times$  90 mm long, 5 mm I.D., Markes International Limited, Pontyclun, UK) were used in this study. The tubes were cleaned in ultrasonic shaker with methanol for 2 h and dried in an oven at  $100^\circ\text{C}$  for 1 h. Clean tubes were then packed with 200 mg of Tenax TA, Chromosorb 102 or Carbopack B and plugged at both ends with a sorbent retain-

ing gauze. A TC-20 tube conditioning system (Markes International Limited) was used to clean up to 20 tubes simultaneously. According to the commercial conditions recommended for each sorbent material, tubes were conditioned at variable temperatures heating at 220, 250 and  $300^\circ\text{C}$  for 120 min and then at 230, 300 and  $400^\circ\text{C}$  for 30 min, for Chromosorb 102, Tenax TA and Carbopack B, respectively; in all cases a flow rate of nitrogen (5.0 grade, Air Liquid, Seville, Spain) at  $100 \text{ ml min}^{-1}$  was applied. After conditioning, background chromatograms of the sorbent tubes were investigated and these conditioning parameters were found to be effective for cleaning the tubes. Moreover, in blank experiments, the tubes were found to be stable for at least 30 days since no background levels of the target compounds were found. Therefore, after conditioning, the sorbent tubes were immediately capped with brass long-term storage caps and stored in sealed glass jars at  $4^\circ\text{C}$  for up to 1 month.

Calibration solutions containing the four THMs at concentrations between  $10 \mu\text{g l}^{-1}$  and  $200 \text{ mg l}^{-1}$  were prepared fortnightly in methanol by serial dilution of the stock standard solutions of each THM in methanol ( $1 \text{ mg ml}^{-1}$ ), which were stored in amber glass bottles at  $4^\circ\text{C}$ . A calibration solution loading rig (CSLR) system was used for the introduction of liquid calibration standards into the sorbent tubes. The CSLR system consisted of an unheated injector with a controlled carrier gas supply (nitrogen) and a sorbent tube connection point. The sampling end of the sorbent tube was connected to the CSLR system and the carrier gas flow rate was set at  $90 \text{ ml min}^{-1}$ , which was swept via the injector through the sorbent tube to vent.  $10 \mu\text{l}$  aliquots of the calibration solutions were introduced through the injector septum using a standard GC syringe. A tube loading time of 10 min was used to ensure that methanol was eliminated being the target analytes quantitatively retained. Then the sorbent tubes containing known amounts of THMs (from 0.1 ng to  $2 \mu\text{g}$ ) were analyzed immediately by TD-GC/MS.

### 2.3. Air samples

The study was carried out in an indoor swimming pool located in the Rabanales University Campus in Córdoba (Spain). Ambient air samples were taken in the sorbent tubes using a SKC Sidekick pump (Markes International Limited), with a pump flow calibrated by a rotameter at  $200 \text{ ml min}^{-1}$ , passing through the tubes an air stream during 15 min to obtain air volumes of 3 l. The relative standard deviation of the flow rate was less than 2%. The samples were collected at a height of 50 cm at the edge of the pool, being the tubes immediately capped after collection with the storage caps to avoid losses. During each sampling session (1 h), three spot samples of ambient air were collected. To reduce/avoid the water (that is brought into the GC system via the sorbent materials) retention at the sampling stage from the ambient air of the swimming pool installation, a drying tube was placed in front of the sampling tube. For this purpose, a glass tube (6 mm O.D.  $\times$  90 mm long, 4 mm I.D., Markes International Limited) was filled with 400 mg of  $\text{Na}_2\text{SO}_4$ , fixed with unsilanized glass wool plugs, and then capped with the storage caps. The drying and the sorbent tubes were connected by using specific stainless steel unions fitted with PTFE ferrules (Markes International Limited) before the sampling stage. To check that the pump flow does not undergo changes after sampling due to the retention of water in the drying tube, the flow rate passing through both tubes was again measured. No significant difference between the flow rates before and after sampling was obtained.

Alveolar air samples were kindly supplied by swimmers at the indoor swimming pool. During the time in which the study was carried out, all subjects consumed only mineral water, free from THMs. These samples were collected approximately 5 min before and after the bath activity in the sorbent tubes using Bio-VOC sam-

plers (Markes International Limited) for exhaled air. Alveolar air samples were collected in an area separated from the site of exposure in order to avoid the risk of contamination. Subjects were asked to breathe normally into the Bio-VOC sampler and only the last 100 ml of the exhaled air, all from the alveolar portion of the lungs, were left in the Bio-VOC sampler. Once the alveolar air was collected, a screw-in plunger was used to steadily discharge the air sample into the sorbent tube, which was immediately capped. Therefore, the sampler collected a representative sample of end-tidal air, without contamination or dilution due to breath from the bronchial tubes or mouth, which was then completely transferred to a sorbent tube for its later thermal desorption and GC analysis. Sorbent tubes containing ambient and alveolar air samples were transported to the laboratory in a portable freezer and immediately analyzed or stored in sealed glass jars at 4 °C for up to 1 month.

#### 2.4. Analysis by TD-GC/MS

Determination of THMs in air was performed by using an Unity thermal desorber (Markes International Limited) coupled with an HP 6890 gas chromatograph (Agilent Technologies, Palo Alto, CA), equipped with an HP 5973 mass selective detector. Thermal desorption of the sampling tubes was carried out for 10 min at 200 °C for Chromosorb 102, at 250 °C for Tenax TA and at 300 °C for Carboxpack B with a flow rate of 30 ml min<sup>-1</sup> (primary desorption) of ultra-pure helium (6.0 grade, Air Liquid); during this time, the eluted THMs were swept from the tube to a preconcentration cold trap (-10 °C), made of quartz (60 mm length, 2 mm I.D.) and packed with 80 mg of Tenax TA. After the focusing step, the analytes were rapidly desorbed with a flow rate of 20 ml min<sup>-1</sup> of the carrier gas from the trap by heating to 300 °C (approximately within 5 s, secondary desorption); the analytes were introduced on-column through an uncoated/de-activated fused silica transfer

line (1 m length, 0.25 mm I.D.) that was part of the TD instrument. The cold trap was maintained at 300 °C during 3 min and then cooled down to -10 °C. The THMs were submitted to a 1:14 flow split ratio. The cold trap consisted of a Peltier device which allowed the cooling and the rapid heating of the trap, being refrigerated with a continuous stream of nitrogen (5.0 grade, Air Liquid). The flow path temperature into the thermal desorption unit was 120 °C. Other instrumental parameters such as the prepurge time and flow rate were 1 min and 20 ml min<sup>-1</sup>, respectively. The separation of THMs was performed on a crosslinked HP-5MS [(5%)-phenyl-(95%) methylpolysiloxane] capillary column (60 m × 0.25 mm I.D., 0.25 μm film thickness, J & W Scientific, Cromlab, Barcelona, Spain). Mass spectra were obtained at 70 eV in the electron impact ionization mode. The source and quadrupole temperatures were maintained at 230 and 150 °C, respectively. Total ion current chromatograms were acquired and processed using G1701DA (rev. D.01.02) MSD Productivity ChemStation software (Agilent Technologies).

A constant pressure of 23 psi was maintained into the GC column during the analysis and an helium flow rate of 1.5 ml min<sup>-1</sup> was selected at the beginning of the GC run. The oven temperature was kept at 40 °C during the first 4 min, then the temperature was increased to 125 °C at 10 °C/min and finally late-eluting compounds were removed by increasing the temperature to 200 °C at 25 °C/min, for 2 min. The chromatographic run was complete in 17.5 min. Identification and quantification of THMs was performed in selected ion monitoring (SIM) mode. From 3 to 8 min the mass spectrometer was focused at *m/z* 83 (ion chosen for quantification of chloroform and bromodichloromethane), and 85, 47 and 129 for identification purposes; from 8 to 10 min at *m/z* 129 (for quantification of dibromochloromethane), and at 127 and 208; from 10 to 17.5 min at *m/z* 173 (for quantification of bromoform), and at 171 and 175. All the scans were performed in high-resolution mode and with a dwell time of 100 ms. The analytical procedure followed in this work for

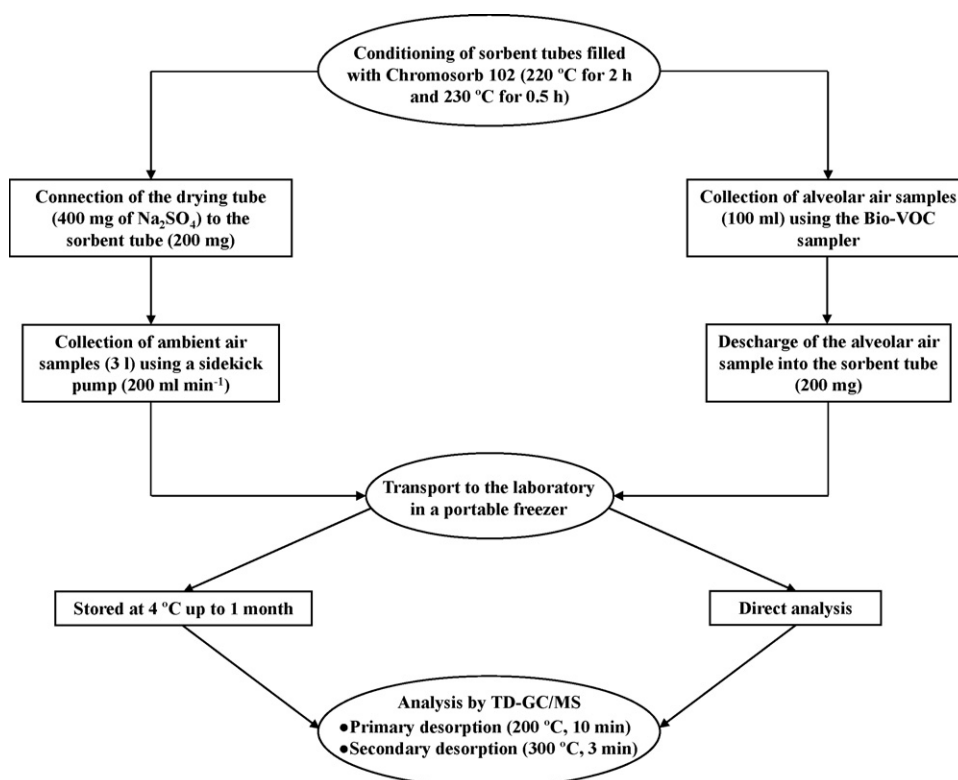


Fig. 1. Flow diagram representing the whole analytical protocol.

the determination of THMs in air samples is schematically depicted in Fig. 1.

### 3. Results and discussion

#### 3.1. Optimization of the TD parameters

In the literature, chloroform and occasionally other THMs were normally determined in mixtures with other VOCs by using multi-sorbent tubes filled with Tenax TA and Carboxen B [22] or Carbotrap, Carboxen X and Carboxen 569 [21], at desorption parameters of 200 °C for 5 min and 300 °C for 10 min, respectively. The sorbent materials used, as well as the thermal desorption instrumental conditions, were those most appropriate for the determination of the group of VOCs as a whole. However, there is no rigorous study on the specific determination of THMs employing different individual adsorbents. Thus, the most adequate instrumental conditions for thermal desorption were studied for three adsorbents, namely Chromosorb 102, Tenax TA and Carboxen B, in order to select the lowest desorption temperatures and times that would ensure complete THM desorption from the sorbent tubes, avoiding carryover and overcoming excessive levels of artefacts. Sorbent tubes were injected with 10 µl of a methanolic solution containing 25 ng of each THM by using the CSLR system, and then thermally desorbed and analyzed by GC/MS. The maximum desorption temperature permissible with the desorption unit was 400 °C. The abundance signal increased for all THMs when the desorption temperature increased to 180 °C for Chromosorb 102, up to 230 °C for Tenax TA and up to 280 °C for Carboxen B, above which it remained constant. The desorption time showed a similar influence on THM recoveries for all materials selected for 10 min. The focusing step of the analytes using the cold trap and secondary desorption provided rapid injection and thus narrow bands. As can be expected at lower temperatures, the THM recoveries increased, –10 °C being selected (minimum temperature permissible for the cold trap with the desorption unit used). Other instrumental parameters were also studied and those that provided the highest sensitivity were selected, all parameters being cited in Section 2.4. To evaluate the good performance of THM desorption from sorbent tubes, several samples containing 1 ng or 0.5 µg of each THM were prepared for the three adsorbents, and analyzed. A subsequent re-analysis of the already desorbed tube was carried out at the same instrumental conditions and no remaining analytes were found.

#### 3.2. Selection of the sorbent materials

An ideal sorbent for preconcentrating VOCs from an air matrix needs to have four main properties, namely: infinite breakthrough volume, complete desorption of the target compounds at moderate temperatures, no generation of artefacts and no retention of water vapour. No single available sorbent material meets all of these criteria for a wide range of VOCs; thus there is a tendency to use multiple adsorbents. A comprehensive review of this aspect has been gone into extensively [20]. However, the use of multi-sorbent tubes for preconcentrating only four compounds (THMs) is not justified, and therefore in this experiment only tubes filled with one sorbent material were used. Adsorption efficiency and the breakthrough volume were evaluated for three adsorbents: Tenax TA, Chromosorb 102 and Carboxen B. For this purpose, 0.5 µg of each THM (10 µl solution) were injected directly into 6 tubes filled with each sorbent material (200 mg). Volumes between 1 and 6 l of uncontaminated ambient air (from the open air free of THMs sampled outside the laboratory) were passed through the tubes using the SKC Sidekick pump at a flow rate of 200 ml min<sup>-1</sup>. The

experiment was made in triplicate at ambient conditions of 40 ± 5% relative humidity and at 24 ± 1 °C. Fig. 2 shows, as an example, the peak areas of chloroform for the three adsorbents at different air volumes. Tenax TA and Chromosorb 102 had similar peak areas for chloroform at low air volumes, being almost two times higher than that obtained for Carboxen B (similar results were obtained for the other THMs). On the other hand, the optimum air volume range was different in each case; the breakthrough volumes (maximum air volumes that can be sampled before a compound exits the trap) of THMs on Chromosorb 102 were the highest of the three adsorbents studied. Chloroform was the limiting compound since it tolerated the lowest breakthrough volume of all THMs, being at its lowest at 6 l for Chromosorb 102 while for Tenax TA and Carboxen B it was only 3 and 2 l, respectively (see Fig. 2). The other THMs permitted air volumes over 6 l using Chromosorb 102 or Tenax TA and between 4 and 6 l for Carboxen B. The higher breakthrough volume obtained for Chromosorb 102 can be ascribed to its large surface area (350 m<sup>2</sup> g<sup>-1</sup>). For practical purposes, a sampling time of 15 min at a flow rate of 200 ml min<sup>-1</sup> was used (air volume of 3 l), and therefore it was Chromosorb 102 (the only adsorbent that ensured a safe sampling volume) that was selected as the best adsorbent for THMs. Determination of adsorption efficiency for Chromosorb 102 was assessed by combining two sorbent tubes in series. A liquid mixture of THMs was injected (10 µl, 0.5 µg) into the first tube and a clean air stream of 3 l was passed through the tubes which were individually analyzed afterwards. No carryover was found in the second tube (THMs were undetected) and so an adsorption efficiency close to 100% was obtained. In order to confirm that the data obtained in the laboratory are representative of those obtained in the field, two sorbent tubes connected in series were used to sample an air volume of 3 l from the indoor swimming pool. No THM was found in the second tube, so the method was totally confirmed.

In addition, the stability of the compounds on the adsorbent selected, Chromosorb 102, was studied. For this purpose, 21 sorbent tubes were injected with 10 µl of a methanolic solution containing 25 ng of each THM by using the CSLR system, capped and stored at 4 °C. Individual analysis of each tube was carried out at different times. Three of them were analyzed immediately and the remaining tubes were stored in sealed glass jars at 4 °C and analyzed after 1, 2, 4, 8, 15 and 30 days in triplicate. The results showed that no significant changes in the chromatographic signals were obtained for any THM after 1 month of storage.

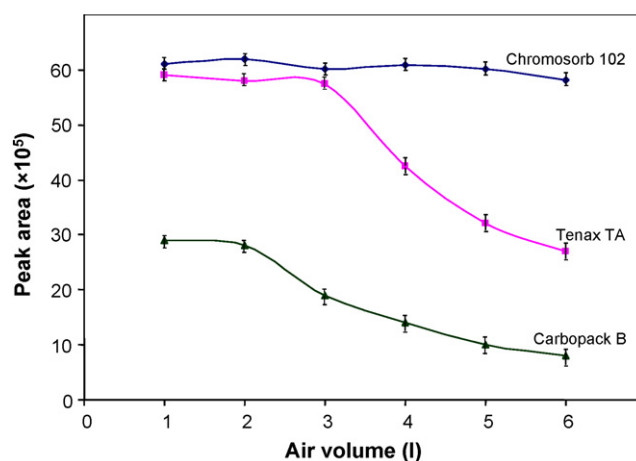


Fig. 2. Influence of the air volume on the adsorption efficiency for chloroform (0.5 µg/tube) using different sorbent tubes.

### 3.3. Selection of the drying tube

Due to the high relative humidity found in the atmosphere of the indoor swimming pool (60–80%), water interference was a special issue in order to avoid chromatographic problems and detector damage. In addition, the adsorbents can retain water at the sampling stage, decreasing the retention of the analytes. In spite of the hydrophobicity of the sorbent materials used, all sorbents are affected by water in high humidity atmospheres. Thus, McCaffrey et al. [23] have pointed the significant water retention of hydrophobic carbon based materials like Carboxen 102 used for the preconcentration of VOCs (THMs are not included) in air. Moreover, Helmig and Vierling [24] have investigated the water trapping capacity of several solid sorbents (Tenax, Carbotrap, Carbosieve, etc.) by collecting temperature- and humidity-controlled air samples onto cartridges and measuring gravimetrically the water gain to determine sorbent water saturation points; possible alternatives for minimizing the amount of water trapped are: decreasing the amount of sorbent, moderate heating of the sorbent tube during sampling, etc. Several authors have proposed the use of a water-sorbing polymer (nafion) or a tube with hygroscopic salts in front of the sampling tube to eliminate the water [12,20]. The third option was based on dry purge stages in order to remove water from the sorbent tube; however, loss of VOCs could occur in this way [12]. In the present work we select a drying tube packed with a hygroscopic salt to reduce water retention at the sampling stage. Several salts have been proposed in the literature, such as  $MgCO_3$ ,  $Mg(ClO_4)_2$  and  $K_2CO_3$ , but no systematic study has been carried out with them; furthermore the salt selected,  $Mg(ClO_4)_2$ , can be used only once [25]. From the foregoing it follows that a rigorous study of the behaviour of several salts was mandatory. For this purpose, a glass tube was filled with 400 mg of each salt ( $Na_2SO_4$ ,  $CaCl_2$  or  $K_2CO_3$ ) and connected in series with the sorbent tube. As can be expected, the drying tubes were more effective with increasing the amount of salt; 400 mg was finally selected since above this value the pump flow rate changes due to the increase of the impedance in the flow path. The experiment was carried out as follows: both tubes were connected to the SKC Sidekick pump, which operated at a flow rate of  $200\text{ ml min}^{-1}$ , and a humid air stream from the swimming pool installation was passed through the tubes (74% relative humidity). The process was checked visually while the salt absorbed the water, controlling the pumping time and thus the air volume that passed through the tubes. The drying tube has a salt bed from 4 to 6 cm long depending on the salt, and is labeled on its surface in cm. Thus the water can be observed advancing the whole way down the tube as the humid air stream passes through it. In these conditions there is a parallel relationship between the length of the salt bed that is liquated and the percentage of water absorbed. Therefore, when the percentage of liquated salt bed reaches 50%, half of the tube is liquated and the other half tube remains dry, so the drying tube can be reused. As can be seen in Fig. 3,  $Na_2SO_4$  salt proved to be the most effective, since it was the most resistant to the humid air stream path. In fact, only 25% of the salt bed was liquated after the passing of 6 l of humid air.  $K_2CO_3$  as well as  $CaCl_2$  tubes were completely liquated at air volumes lower than  $Na_2SO_4$ . Otherwise, the retention of THMs on the salts assayed was negligible (less than 2%) and no artefacts were found. Finally, for an air sample volume of 3 l, the drying tube packed with  $Na_2SO_4$  could be reused at least six times before being dried at room temperature with a stream of nitrogen.

As well as being necessary to avoid the damage of the instrumentation, water elimination is mandatory due to the retention of the analytes in the adsorbent decreases, which was confirmed by collecting humid ambient air samples in the sorbent tubes with and without drying tube and analyzing them. When the water was not removed, the competition for the sorption sites between ana-

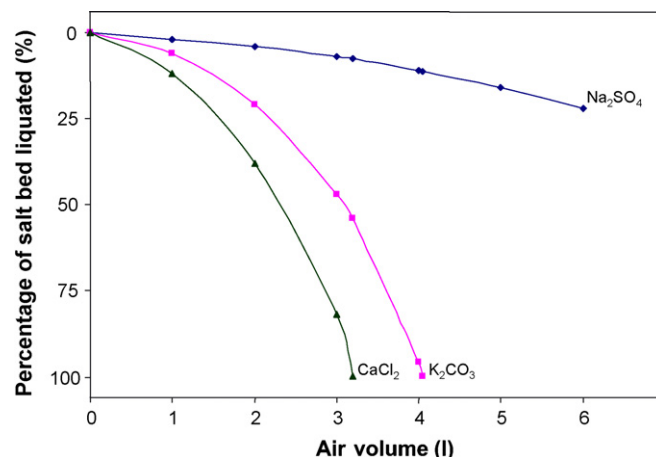


Fig. 3. Effect of the humid air volume (74% relative humidity) on the liquation of the drying tubes packed with different salts.

lytes and water molecules on the sorbent material resulted in a decrease of ca. 30% in the analytical signal for all THMs. In addition, a prepurge step in the TD instrument to eliminate a large quantity of water needs high flow rate, time and temperature, arising important evaporative losses of THMs therefore these operation conditions cannot be used in this study.

### 3.4. Validation of the method

The analytical methodology proposed was validated extensively. For this purpose, liquid calibration standards containing all THMs at different concentrations in methanol were injected into the sorbent tubes filled with 200 mg of Chromosorb 102 by using the CSLR system, as explained in Section 2.2. A calibration curve for each THM, at amounts ranging between 0.1 ng and 2  $\mu\text{g}$  using 13 points per triplicate ( $n = 39$ ), was constructed by plotting the analyte peak area against the amount of analyte; good regression coefficients ( $r \geq 0.995$ ) were obtained in all instances. Table 1 lists the limit of detection (LOD, expressed as three times the regression standard deviation divided by the slope of the calibration graph), the limit of quantification (LOQ) and the linear range of the proposed method for each THM. As can be seen, a wide linear range is needed due to the great differences of concentration that are found between ambient air (3 l) and alveolar air (100 ml) samples. Therefore, a linear range from 0.1 to 2000 ng is obtained for all analytes; the LODs are very similar for all THMs, being approximately 0.03 ng (0.01  $\mu\text{g m}^{-3}$  for an air sample volume of 3 l). Table 1 also summarizes the specific uncertainty of each THM for the whole procedure. In order to calculate it, 12 samples containing 5 ng of each THM were subjected to all the process: preparation of the standards, injection into a sorbent tube, storage at 4 °C for 2 days and analysis (by using the TD-GC/MS). The specific uncertainty of a result is a symmetric interval around the result ( $R \pm U$ ) and is calculated from the standard deviation ( $S$ ) for a set of results:  $U = tS/\sqrt{n}$  (where  $U$  is the uncertainty,  $t$  is a statistical parameter and  $n$  is the number of measures). The specific

Table 1  
Analytical figures of merit of the determination of THMs

Compound	LOD (ng)	LOQ (ng)	Linear range (ng)	Uncertainty <sup>a</sup> (ng)
Chloroform	0.02	0.07	0.1–2000	$5.0 \pm 0.2$
Bromodichloromethane	0.02	0.07	0.1–2000	$4.9 \pm 0.2$
Dibromochloromethane	0.03	0.10	0.1–2000	$4.9 \pm 0.3$
Bromoform	0.03	0.10	0.1–2000	$5.1 \pm 0.3$

<sup>a</sup> Uncertainty of the whole procedure expressed as  $R \pm U$  ( $n = 12$ ,  $K = 2$ ).

uncertainty can be easily calculated from:  $U = KS$ , where  $K = 2$  for a probability imposed at the 95% confidence levels [26].

Otherwise, the methods described in the literature for the determination of VOCs in air carry out recovery studies in two ways, namely: by comparing the responses obtained for each compound by sampling spiked clean air with the responses obtained when compounds were spiked directly on the sorbent material [27], or by comparing the fraction of the mass recovered for each compound from the adsorbent to that injected directly (by removing the desorber system from the GC) [14,21]. The first one has the shortcoming of needing a clean room with a laminar flow system and the preparation of standards in a clean and homogeneous atmosphere; the second one has the limitation of including the efficiency of the desorption unit (for the amount found) and later eliminating it (for the amount added). Therefore, we have considered a new validation method that is simple, and does not require either the preparation of standards in clean and homogeneous air or the obviating of errors in the desorption step. Apparent recoveries were calculated for each THM, comparing the response obtained by spiking the analytes into a sorbent tube to that obtained injecting the compounds directly into a tube without adsorbent, all tubes being analyzed by TD-GC/MS. For this purpose, five sorbent tubes containing 1 ng or 0.5  $\mu\text{g}$  of each THM were prepared by using the CSLR system (see Section 2.2). In parallel, 10 empty tubes were filled with 500 mg of unsilanized glass wool, instead of the sorbent material, and prepared by directly injecting the THM calibration standards (1 ng or 0.5  $\mu\text{g}$  of each THM). THMs were not adsorbed on the unsilanized glass wool, so the analyte recoveries were quantitatively reliable enough to assign them a recovery of 100%. The analysis of the tubes was made omitting the prepurge step in the TD unit to avoid losses of the analytes, because they were only deposited in the glass wool tubes; therefore, the carrier gas only passed through the tubes to drive the content to the cold trap (primary desorption), in which the analytes were retained but not the methanol. After the secondary desorption, the analytes were introduced into the GC column, as explained in Section 2.4. The recoveries ranged from 92% to 95% for the low amount level (1 ng) and from 94% to 97% for the high amount level (0.5  $\mu\text{g}$ ). These results indicate that the sorbent air sampling system established in this study was well suited for quantitative analysis of the target compounds, since the degree of irreversible adsorption of THMs on the adsorbent used was insignificant at the desorption temperature.

### 3.5. Analysis of air samples

In order to evaluate the performance of the analytical method in field samples, the exposure to THMs in indoor swimming pools and the THM uptake of swimmers were studied. Ambient air samples from the swimming pool water installation and alveolar air samples from 12 swimmers were collected simultaneously and analyzed by the proposed TD-GC/MS. Ambient air samples (36) were collected at 200  $\text{ml min}^{-1}$  up to 3 l, through a drying tube filled with  $\text{Na}_2\text{SO}_4$  in front of the sorbent tube, as described in Section 2.3. Three samples were collected during each sampling session and the mean value was considered to be representative of the THM concentration in the session. The four THMs were present in all the ambient air samples analyzed,  $\text{CHCl}_3$  being the one that reached the highest values, while  $\text{CHBr}_3$  was only detected at unquantifiable concentrations.  $\text{CHCl}_3$  levels varied, according to the sampling sessions (12), from 80 to 320  $\mu\text{g m}^{-3}$ , with a mean concentration in all sessions of 210  $\mu\text{g m}^{-3}$ ;  $\text{CHBrCl}_2$  levels ranged from 4 to 15  $\mu\text{g m}^{-3}$ , with a mean value of 10  $\mu\text{g m}^{-3}$ ; and  $\text{CHBr}_2\text{Cl}$  levels varied from 0.25 to 1.85  $\mu\text{g m}^{-3}$  (mean value, 1.05  $\mu\text{g m}^{-3}$ ). The bromated THMs appeared in ambient air samples at insignificant values, since the surface water which supplied the pool contained a low concen-

**Table 2**

Determination of THMs in alveolar air samples by TD-GC/MS

Subject	Concentration found ( $\mu\text{g m}^{-3}$ ) <sup>a</sup>			
	$\text{CHCl}_3$		$\text{CHBrCl}_2$	
	Before the bath	After the bath	Before the bath <sup>b</sup>	After the bath
Swimmer 1	2.5 ± 0.2	48 ± 5	n.d.	2.0 ± 0.2
Swimmer 2	3.1 ± 0.3	98 ± 8	n.d.	2.3 ± 0.2
Swimmer 3	4.9 ± 0.4	85 ± 8	n.d.	2.4 ± 0.2
Swimmer 4	2.6 ± 0.2	107 ± 11	n.d.	3.0 ± 0.3
Swimmer 5	4.0 ± 0.4	89 ± 8	n.d.	2.2 ± 0.2
Swimmer 6	2.2 ± 0.2	57 ± 5	n.d.	2.1 ± 0.2
Swimmer 7	5.6 ± 0.4	75 ± 7	n.d.	2.0 ± 0.2
Swimmer 8	2.6 ± 0.2	94 ± 9	n.d.	2.3 ± 0.2
Swimmer 9	2.1 ± 0.2	105 ± 10	n.d.	2.9 ± 0.2
Swimmer 10	5.9 ± 0.5	110 ± 11	n.d.	2.8 ± 0.3
Swimmer 11	2.0 ± 0.2	59 ± 6	n.d.	2.1 ± 0.2
Swimmer 12	3.5 ± 0.3	92 ± 8	n.d.	2.7 ± 0.2
Non-swimmer 1	5.1 ± 0.4		n.d.	
Non-swimmer 2	3.8 ± 0.4		n.d.	
Non-swimmer 3	2.4 ± 0.2		n.d.	

<sup>a</sup> ± Standard deviation,  $n = 3$ .

<sup>b</sup> n.d., not detected.

tration of bromides [28]. Thus, in the above experiments on the water in this swimming pool, we found average concentrations of 120 and 2.2  $\mu\text{g l}^{-1}$  for  $\text{CHCl}_3$  and  $\text{CHBrCl}_2$ , respectively, and  $\text{CHBr}_2\text{Cl}$  and  $\text{CHBr}_3$  remained undetected [29]. The ambient concentration interval for all THMs is in agreement with other ambient air samples from swimming pools [7,18].

Alveolar air samples from people exposed (swimmers) were collected simultaneously to the ambient air sampling in order to assess their THM uptake. Twelve swimmers who spent 1 h swimming 2 days a week as well as nine non-swimmers participated voluntarily in this study. Samples (100 ml of alveolar air) were collected approximately 5 min before and after the bathing activities as described in Section 2.3. Subjects were asked to breathe three times into the sampler for each collection, in order to analyze the samples in triplicate. As can be expected, only  $\text{CHCl}_3$  and  $\text{CHBrCl}_2$  were found in all the alveolar air samples, while  $\text{CHBr}_2\text{Cl}$  and  $\text{CHBr}_3$  remained undetected. Table 2 shows the average concentrations for both THMs;  $\text{CHCl}_3$  levels for the swimmers before bathing varied between 2 and 6  $\mu\text{g m}^{-3}$ , while  $\text{CHBrCl}_2$  was not detected. Similar levels were found in the alveolar air of non-swimmers. These  $\text{CHCl}_3$  concentrations found in alveolar air before exposure suggest either that there was a recent exposure before participating in the study associated with household water use activities (including ingestion of beverages, showering, cooking, etc.) and indirect exposure [19], or that these compounds have bioaccumulated over time from repeated exposure to heavily chlorinated water [30]. A high increase in  $\text{CHCl}_3$  levels from 50 to 110  $\mu\text{g m}^{-3}$  was found after swimming;  $\text{CHBrCl}_2$  was also found at values between 2 and 3  $\mu\text{g m}^{-3}$ , as shown in Table 2. These results agreed with the high chlorinated THM concentrations found (mainly  $\text{CHCl}_3$ ) in the ambient air at the indoor swimming pool and showed an elevated exposure of swimmers to THMs, since their uptake was not only due to inhalation but also to dermal absorption and occasionally ingestion [29]. On the other hand, the average values for alveolar air were taken from three sequential samples, providing high standard deviations (8–10%) since THM levels in alveolar air decrease rapidly after the exposure ends.

## 4. Conclusions

A fast and straightforward TD-GC/MS method for the determination of THMs in ambient and alveolar air has been developed to evaluate the exposure in indoor swimming pools and the uptake

of swimmers. The method has several advantages when compared to other alternatives, namely: for the first time, a rigorous study was carried out that avoided the retention of water from the ambient air at a swimming pool (60–80% relative humidity) into the sorbent tube, employing a drying tube; second, only one sorbent material was packed into the sorbent tube, and Chromosorb 102 was found to be the adsorbent providing the best adsorption efficiency and no breakthrough for any THM up to at least 6 l of air; third, the method is more simple and sensitive (LODs  $0.01 \mu\text{g m}^{-3}$ , recovery over 92%) than those described in the literature for air samples which included any THM. So, by using multisorbent tubes, the LODs for  $\text{CHCl}_3$  (included in mixtures of several VOCs) were  $0.1 \mu\text{g m}^{-3}$  (93% recovery) [14],  $0.01 \text{ ng/tube}$  (47% recovery) [21] and  $0.2 \mu\text{g m}^{-3}$  (84% recovery) [22], but none of these methods had been applied either to highly humid ambient air (normally only lower than 30% relative humidity) or to personal exposure. Furthermore, the methods developed to determine THMs in breath do not use thermal desorption and the sampling methods are not very reliable, as noted in Section 1 [7–9]. This study carried out on swimmers has revealed the relationship between the THM concentrations found in ambient and alveolar air.

### Acknowledgments

The authors would like to thank to the DGI of the Spanish Ministry of Science and Technology for financial support awarded in the form of Grant CTQ2007-63962. The authors also thank to the Consejería de Empleo, Junta de Andalucía (Grant SC/UNI/00013/2007), as well as to the volunteers for their collaboration.

### References

- [1] J.J. Rook, *Treat. Exam.* 23 (1974) 234.
- [2] R. Zhao, W. Lao, X. Xu, *Talanta* 62 (2004) 751.
- [3] C. Zwiener, S.D. Richardson, *Trends Anal. Chem.* 24 (2005) 613.
- [4] Guidelines for Safe Recreational Water Environments, volume 2: Swimming Pools and Similar Recreational Water-Environments, 2006. World Health Organization. [http://www.who.int/water\\_sanitation\\_health/bathing/srwe2full.pdf](http://www.who.int/water_sanitation_health/bathing/srwe2full.pdf).
- [5] National Swimming Pool Foundation home page. <http://www.nspf.org>.
- [6] J.A. Beech, R. Diaz, C. Ordaz, B. Palomeque, *Am. J. Public Health* 70 (1980) 79.
- [7] G. Aggazzotti, G. Fantuzzi, E. Righi, G. Predieri, *Sci. Total Environ.* 217 (1998) 155.
- [8] B. Levesque, P. Ayotte, R. Tardif, G. Charest-Tardif, E. Dewailly, D. Prud'Homme, G. Gingras, S. Allaire, R.J. Lavoie, *J. Toxicol. Environ. Health Pt. A* 61 (2000) 225.
- [9] G. Fantuzzi, E. Righi, G. Predieri, G. Ceppelli, F. Gobba, G. Aggazzotti, *Sci. Total Environ.* 264 (2001) 257.
- [10] J. Caro, A. Serrano, M. Gallego, *J. Chromatogr. B* 848 (2007) 277.
- [11] J. Dewulf, T. Huybrechts, H. Van Langenhove, *Trends Anal. Chem.* 25 (2006) 300.
- [12] J. Dewulf, H. Van Langenhove, *Trends Anal. Chem.* 21 (2002) 637.
- [13] G.G. Huang, C. Wang, H. Tang, Y. Huang, J. Yang, *Anal. Chem.* 78 (2006) 2397.
- [14] C. Peng, S. Batterman, *J. Environ. Monit.* 2 (2000) 313.
- [15] D.J. Wevill, L.J. Carpenter, *Analyst* 129 (2004) 634.
- [16] Q. Li, D. Yuan, Q. Lin, *J. Chromatogr. A* 1026 (2004) 283.
- [17] K. Demeestere, J. Dewulf, B. De Witte, H. Van Langenhove, *J. Chromatogr. A* 1153 (2007) 130.
- [18] L. Erdinger, K.P. Kühn, F. Kirsch, R. Feldhues, T. Fröbel, B. Nohynek, T. Gabrio, *Int. J. Hyg. Environ. Health* 207 (2004) 571.
- [19] J.R. Nuckols, D.L. Ashley, C. Lyu, S.M. Gordon, A.F. Hinckley, P. Singer, *Environ. Health Perspect.* 113 (2005) 863.
- [20] J. Dewulf, H. Van Langenhove, *J. Chromatogr. A* 843 (1999) 163.
- [21] A. Ribes, G. Carrera, E. Gallego, X. Roca, M.J. Berenguer, X. Guardino, *J. Chromatogr. A* 1140 (2007) 44.
- [22] O.O. Kuntasal, D. Karman, D. Wang, S.G. Tuncel, G. Tuncel, *J. Chromatogr. A* 1099 (2005) 43.
- [23] C.A. McCaffrey, J. MacLachlan, B.I. Brookes, *Analyst* 119 (1994) 897.
- [24] D. Helmig, L. Vierling, *Anal. Chem.* 67 (1995) 4380.
- [25] E. Kivi-Etelälä, O. Kostianen, M. Kokko, *J. Chromatogr. A* 787 (1997) 205.
- [26] R. Kellner, J.-M. Mermet, M. Otto, M. Valcárcel, H.M. Widmer (Eds.), *Analytical Chemistry*, Second edition, Wiley-VCH, Weinheim, 2004.
- [27] R. Barro, S. Ares, C. García-Jares, M. Llompart, R. Cela, *J. Chromatogr. A* 1045 (2004) 189.
- [28] A. Serrano, M. Gallego, *J. Chromatogr. A* 1154 (2007) 26.
- [29] J. Caro, M. Gallego, *Environ. Sci. Technol.* 41 (2007) 4793.
- [30] D.L. Ashley, J.D. Prah, *Arch. Environ. Health* 52 (1997) 26.





# Amperometric glucose biosensor based on boron-doped carbon nanotubes modified electrode

Xiaoli Chen, Jinhua Chen\*, Chunyan Deng, Chunhui Xiao, Yanmin Yang, Zhou Nie\*, Shouzhao Yao

State Key Laboratory of Chemo/Biosensing and Chemometrics, College of Chemistry and Chemical Engineering, Hunan University, Changsha 410082, PR China

## ARTICLE INFO

### Article history:

Received 15 December 2007  
Received in revised form 7 April 2008  
Accepted 12 April 2008  
Available online 20 April 2008

### Keywords:

Boron-doped carbon nanotubes (BCNTs)  
Poly(*o*-aminophenol) (POAP)  
Amperometric glucose biosensor  
Glucose oxidase

## ABSTRACT

Doped carbon nanotubes are now extremely attractive and important nanomaterials in bioanalytical applications due to their unique physicochemical properties. In this paper, the boron-doped carbon nanotubes (BCNTs) were used in amperometric biosensors. It has been found that the electrocatalytic activity of the BCNTs modified glassy carbon (GC) electrode toward the oxidation of hydrogen peroxide is much higher than that of the un-doped CNTs modified electrode due to the large amount of edge sites and oxygen-rich groups located at the defective sites induced by boron doping. Glucose oxidase (GOD) was selected as the model enzyme and immobilized on the BCNTs modified glassy carbon electrode by entrapping GOD into poly(*o*-aminophenol) film. The performance of the sensor was investigated by electrochemical methods. At an optimum potential of +0.60 V and pH 7.0, the biosensor exhibits good characteristics, such as high sensitivity ( $171.2 \text{ nA mM}^{-1}$ ), low detection limit ( $3.6 \mu\text{M}$ ), short response time (within 6 s), satisfactory anti-interference ability and good stability. The apparent Michaelis–Menten constant ( $K_m^{\text{app}}$ ) is 15.19 mM. The applicability to the whole blood analysis of the enzyme electrode was also evaluated.

© 2008 Elsevier B.V. All rights reserved.

## 1. Introduction

Electrocatalytic oxidation of glucose has potential medical application in blood glucose sensing [1] and bio-fuel cells [2]. The development of glucose biosensors utilizing glucose oxidase (GOD) is an active research area [3]. A majority of glucose sensors, especially those used in in-vivo application are based on the electrochemical oxidation of hydrogen peroxide, which is formed in the course of the enzyme-catalyzed oxidation of glucose by dissolved oxygen. Sensitivity, selectivity, stability and reproducibility are major characteristics of amperometric glucose biosensor. On the other hand, carbon nanotubes (CNTs) have been of great interest since their discovery in 1991 [4]. CNTs modified electrodes have been widely utilized in electrocatalytic and sensing applications [5–7]. These great interests are the consequence of some unique properties of CNTs: firstly, their length/diameter aspect ratio provides a high surface/volume ratio. Secondly, CNTs have a unique ability to promote fast electron transfer for a wide range of electroactive species.

Additionally, it has been reported that the physicochemical properties of CNTs could be tailored by doping CNTs with for-

eign atoms (B or N atom) [8–11]. Boron- or nitrogen-doped carbon nanotubes have their potential application in many fields, such as nanosized photonic [12] and electronic devices [13,14], superhard materials [15], electron field emitters [16] and even sensitive chemical sensors [17–19]. On the other hand, doping CNTs with foreign atoms would make large amount of defective sites onto the nanotube surfaces [20–22]. This would produce large amount of edge sites and oxygen-rich functional groups located on the defective sites. As proved by several groups, the edge sites and oxygen-rich groups presented on the carbon nanotubes are indeed responsible for their good electrocatalytic properties [23,24]. The higher proportion of edge sites may lead to more facile electron transfer [25]. Nitrogen-doped carbon nanotubes (NCNTs) have been successfully used on the direct electrochemistry of hemoglobin and glucose oxidase, and the obtained NCNT electrode showed excellent performances [20,26]. Our previous work has also demonstrated that the boron-doped carbon nanotubes (BCNTs) are good candidates for the direct electrochemistry of glucose oxidase [27]. However, to our best knowledge, there are no amperometric biosensors based on the BCNTs.

Here, based on the good electrocatalytic properties of BCNTs shown in our previous paper [27], BCNTs were firstly employed for fabricating amperometric enzyme biosensor and the benefits of BCNTs in the amperometric biosensor were demonstrated. GOD

\* Corresponding authors. Tel.: +86 731 8821961; fax: +86 731 8821848.  
E-mail address: [chenjinhua@hnu.cn](mailto:chenjinhua@hnu.cn) (J. Chen).

was selected as the model enzyme. Poly(*o*-aminophenol) (POAP) film, as a typical non-conducting film and effective barrier to protect the electrode from fouling in hydrogen peroxide, glucose and uric acid biosensors [28–31], was employed in this study to immobilize GOD. The performance of the glucose biosensor based on the glassy carbon (GC)/BCNTs/POAP-GOD electrode was investigated in detail.

## 2. Experimental

### 2.1. Chemicals and apparatus

The un-doped CNTs with multi-walls and diameter of about 20–30 nm were obtained from Shenzhen Nanotech Port Company. Before use, the un-doped CNTs were pretreated by sonicating CNTs in a mixture of concentrated sulfuric acid–nitric acid (3:1, v/v) for about 3 h, and then filtered and washed with double-distilled water thoroughly. After that, the treated CNTs were dried in a vacuum at 60 °C. The resulting black powder was sonicated in double-distilled water for about 1 h to obtain CNT aqueous solution with a concentration of 0.5 mg mL<sup>-1</sup>. Glucose oxidase (E.C. 1.1.3.4, 300 U mg<sup>-1</sup>) was purchased from Amresco (USA), and used without further purification. *o*-Aminophenol (*o*-AP) (99%), ascorbic acid (AA), uric acid (UA) and acetaminophen (AP) were used as received (Chemical Reagent Co. of Shanghai, China). All other chemicals were analytical grade. Double-distilled water was used throughout.

All electrochemical experiments were carried out in a conventional three-electrode cell controlled by CHI 660A Electrochemical Work Station (Chenhua Instrument Co., Shanghai, China). A glassy carbon electrode (GC, with diameter of 3 mm) was used as the working electrode. A platinum foil was applied as the counter electrode and a saturated calomel electrode (SCE) served as the reference electrode. All potential values given below refer to SCE. Amperometric measurements were carried out under stirred condition and the response current was marked with the change value between the steady-state current and background current. All electrochemical experiments were performed at room temperature.

### 2.2. Procedures

BCNTs were synthesized through a substitution reaction between CNTs and B<sub>2</sub>O<sub>3</sub> powder [27,32]. The detailed information about the synthesis and pretreatment of BCNTs were described in our previous paper [27]. Prior to the preparation of the modified electrode, the GC electrode was polished with 1.0 and 0.3 μm alumina slurries, washed with double-distilled water under sonication to get a slippery and clean surface. Then, the bare GC electrode was activated by potential cycling in 0.5 M H<sub>2</sub>SO<sub>4</sub> from -0.15 V to +1.0 V for 15 cycles. 5 μL of BCNTs (or CNTs) solution (0.5 mg mL<sup>-1</sup>) was dropped onto the surface of the activated GC electrode, and dried under infrared lamp. This is marked as the GC/BCNTs (or GC/CNTs) electrode.

The immobilization of GOD on the GC/BCNTs electrode was performed by co-electropolymerization of GOD and *o*-AP in 0.2 M acetate buffer solution (pH 5.0) containing 2.5 mg mL<sup>-1</sup> GOD and 5.0 mM *o*-AP monomer. The electrochemical co-polymerization of POAP-GOD film was carried out by cyclic voltammetry in the potential range from 0.0 to 0.8 V at a scan rate of 50 mV s<sup>-1</sup> for 15 cycles. The resulting enzyme electrode (marked as GC/BCNTs/POAP-GOD electrode) was thoroughly washed by double-distilled water and stored in phosphate buffer solution (pH 7.0) at 4 °C for future use.

## 3. Results and discussion

### 3.1. Electrocatalytic properties of the BCNTs modified electrode toward hydrogen peroxide

The electrochemical behavior of the GC/BCNTs, GC/CNTs and bare GC electrodes in 1/15 M phosphate buffer solution (PBS, pH 7.0) with or without 1 mM H<sub>2</sub>O<sub>2</sub> is shown in Fig. 1. From Fig. 1, it is noted that the background current of the electrode increases after the CNTs modification due to the high specific area of CNTs. Also, the background current of the GC/BCNTs electrode in PBS is about two times higher than that of the GC/CNTs electrode. This is ascribed to the more defective sites of BCNTs introduced by B-doping [9]. After the addition of H<sub>2</sub>O<sub>2</sub>, no obvious change of the related cyclic voltammogram can be observed at the bare GC electrode. However, the oxidation current of H<sub>2</sub>O<sub>2</sub>, which starts at around +0.42 V, can be found obviously at both GC/CNTs and GC/BCNTs electrodes. Also, the oxidation current of H<sub>2</sub>O<sub>2</sub> at GC/BCNTs electrode is much higher than that at the GC/CNTs electrode. This indicates that the BCNTs modified electrode has higher electrocatalytic activity than the un-doped CNTs modified electrode. This result is in accordant with that observed in our previous work [27]. The main reason may be that BCNTs have higher proportion of edge sites than the

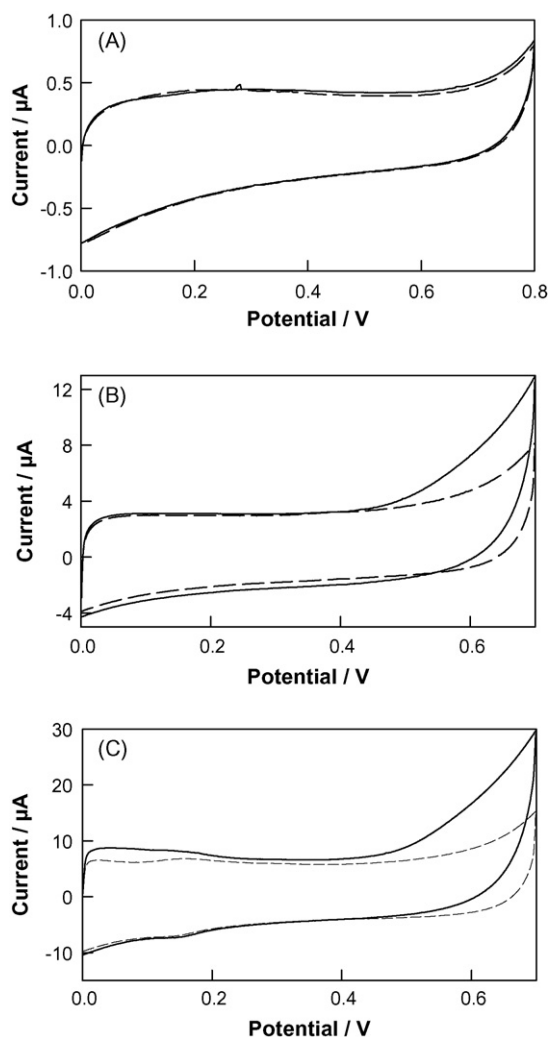
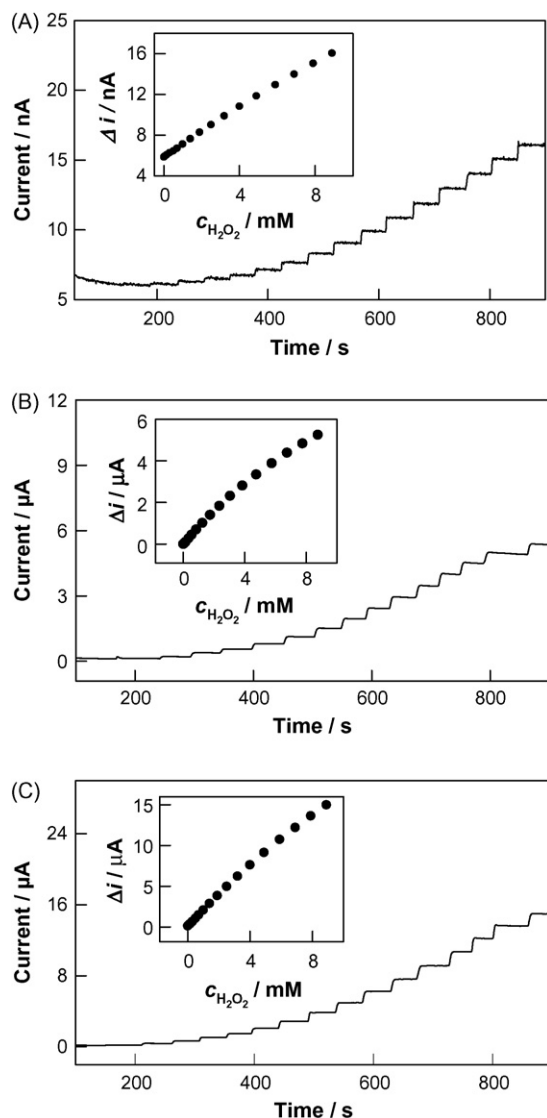


Fig. 1. Cyclic voltammograms obtained at the bare GC (A), GC/CNTs (B) and GC/BCNTs (C) electrodes in a 1/15 M phosphate buffer solution (pH 7.0) with (solid line) and without (dashed line) 1.0 mM hydrogen peroxide. Scan rate, 50 mV s<sup>-1</sup>.



**Fig. 2.** Current responses to the addition of hydrogen peroxide in stirred 1/15 M phosphate buffer solution (pH 7.0) at the bare GC (A), GC/CNTs (B) and GC/BCNTs (C) electrodes. Inset plots are the calibration curves derived from the related  $i-t$  curves. Applied potential: +0.60 V.

un-doped CNTs due to the much more defective sites of BCNTs introduced by B-doping [9]. A large amount of oxygen-rich functional groups were produced at the defective sites of BCNTs during the chemical/electrochemical activation process [23]. The edge sites and oxygen-rich groups presented on the BCNT surface could be responsible for its good electrocatalytic behavior [23–25].

In order to further confirm the electrocatalytic behavior of the BCNTs for the oxidation of  $H_2O_2$ , the response currents at an applied potential of +0.60 V were obtained at the bare GC (A), GC/CNTs (B) and GC/BCNTs (C) electrodes. It can be seen from Fig. 2 that the response current at the bare GC electrode is much smaller than that at the GC/CNTs and GC/BCNTs electrodes and the following order can be observed: bare GC  $\ll$  GC/CNTs < GC/BCNTs. The calibration curves between current response and  $H_2O_2$  concentration for the bare GC, GC/CNTs and GC/BCNTs electrodes are also obtained and shown in the inset plots of Fig. 2(A)–(C), respectively. The characteristics of these three electrodes for  $H_2O_2$  detection are listed in Table 1. For bare GC electrode, the linear relationship for  $H_2O_2$  detection is up to 5 mM with a sensitivity of  $1.24 \text{ nA mM}^{-1}$  and a

correlation coefficient ( $R$ ) of 0.9995. The GC/CNTs electrode shows a linear relationship up to 4 mM with a sensitivity of  $0.75 \text{ } \mu\text{A mM}^{-1}$  ( $R = 0.9974$ ). However, it is surprising to find that the linear relationship obtained from GC/BCNTs electrode is up to 4.0 mM with the sensitivity of  $1.93 \text{ } \mu\text{A mM}^{-1}$  ( $R = 0.9996$ ) which is 2.5 times higher than that obtained from the GC/CNTs electrode. On the other hand, the detection limit of the GC/BCNTs, GC/CNTs and bare GC electrodes is 17, 112 and  $287 \text{ } \mu\text{M}$  (signal-to-noise = 3), respectively. The detection limit obtained from the BCNTs electrode is much lower than that obtained from the other two electrodes. This indicates that the BCNTs modified electrode is more efficient for catalyzing the oxidation of  $H_2O_2$ . These excellent performances make the possibility of utilizing BCNTs to improve the performance of the carbon nanotube based glucose biosensors.

### 3.2. Electrochemical co-polymerization of *o*-AP and GOD on BCNTs modified GC electrode

In order to improve the stability and the anti-interference ability, the GOD was immobilized on the GC/BCNTs electrode by electrochemical co-polymerization of GOD and *o*-AP. Fig. 3 shows the electrochemical impedance spectra of the GC/BCNTs, GC/BCNTs/POAP and GC/BCNTs/POAP-GOD electrodes recorded in equimolar 5.0 mM  $\text{Fe}(\text{CN})_6^{3-}/\text{K}_4\text{Fe}(\text{CN})_6^{4-} + 0.1 \text{ M KCl}$  aqueous solution. A semicircle with a small diameter along with a straight line can be seen at the GC/BCNTs electrode (curve a). However, a semicircle with much larger diameter can be observed at both GC/BCNTs/POAP (curve b) and GC/BCNTs/POAP-GOD (curve c) electrodes due to the formation of POAP film. On the other hand, the diameter of the semicircle at the GC/BCNTs/POAP-GOD electrode is much larger than that at the GC/BCNTs/POAP electrode. This implies that the electron-transfer resistance of the electrode increases with the entrapment of GOD in POAP film because GOD is the non-conductive macromolecule. These results indicate that the GOD has been immobilized on the GC/BCNTs electrode by electrochemical co-polymerization of *o*-AP and GOD.

### 3.3. Effects of the pH value and the applied potential on the response of the GC/BCNTs/POAP-GOD electrode

The effect of the pH value of the solution on the response of the GC/BCNTs/POAP-GOD electrode (operated at +0.60 V) has been investigated and the corresponding results are shown in Fig. 4. From Fig. 4, the response current of the GC/BCNTs/POAP-GOD electrode increases with the increase of the pH value and the maximum

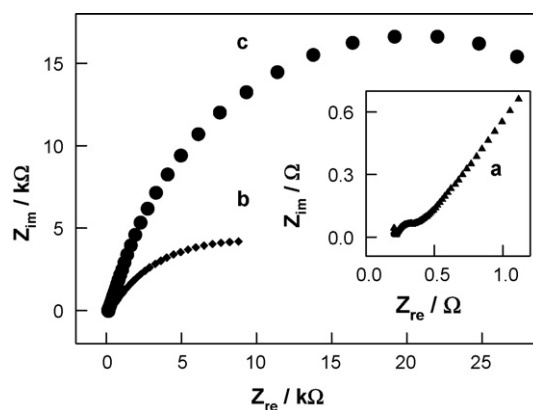


**Fig. 3.** The Nyquist plots for the electrochemical impedance measurements at the GC/BCNTs (a), GC/BCNTs/POAP (b) and GC/BCNTs/POAP-GOD (c) electrodes in 5 mM  $\text{Fe}(\text{CN})_6^{3-}/4- + 0.1 \text{ M KCl}$  aqueous solution. The applied potential, +0.22 V; ac amplitude, 5 mV; frequency range, 0.1 Hz to 100 kHz.

**Table 1**  
Comparison of the performance of the different electrodes toward the oxidation of hydrogen peroxide

Electrodes	Linear range up to (mM)	Correlation coefficient, <i>R</i>	Sensitivity (mM <sup>-1</sup> )	Detection limit (mM)
Bare GC	5	0.9995	1.24 nA	0.287
GC/CNTs	4	0.9974	0.75 μA	0.112
GC/BCNTs	4	0.9996	1.93 μA	0.017

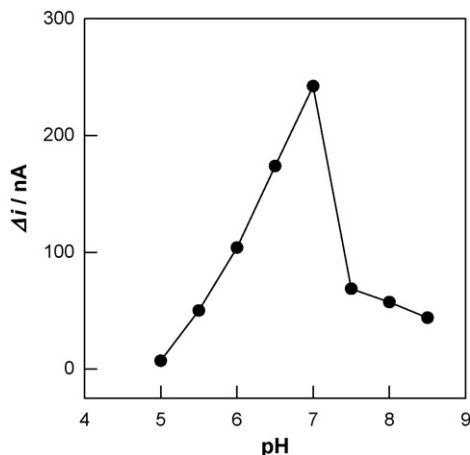


**Fig. 4.** Effect of the pH value of the 1/15 M phosphate buffer solution on the response current to 1 mM glucose at the GC/BCNTs/POAP-GOD electrode. The applied potential, +0.60 V.

response current is observed at pH 7.0. This is in agreement with that reported in literatures [33,34]. Therefore, pH 7.0 was selected in the glucose detection.

Fig. 5 shows the effect of the applied potential on the response current of the GC/BCNTs/POAP-GOD electrode in 1/15 M PBS (pH 7.0) containing 1 mM glucose. It is noted that the response current increases with the increase of the applied potential. This means that the response of the enzyme electrode in this potential range may be controlled by the electrochemical oxidation of hydrogen peroxide [35]. However, it is well known that the response current to the electroactive interferents also increases with the increase of the applied potential. In order to obtain relatively large response current, short response time and good anti-interference ability, +0.60 V is selected as the applied potential for the amperometric determination of glucose [33].

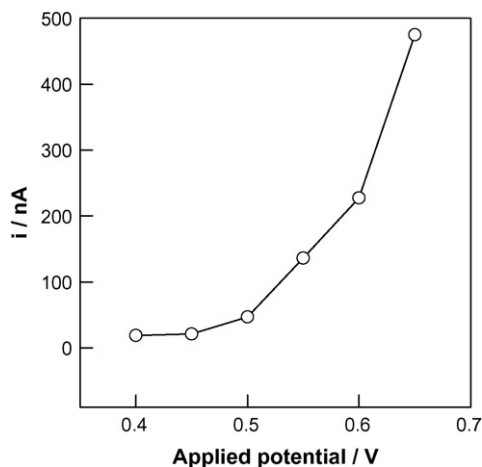


**Fig. 5.** Effect of the applied potential on the response current to 1 mM glucose at the GC/BCNTs/POAP-GOD electrode in 1/15 M phosphate buffer solution (pH 7.0).

#### 3.4. Amperometric determination of glucose at the GC/BCNTs/POAP-GOD electrode

The amperometric determination of glucose at the GC/BCNTs/POAP-GOD electrode has been investigated and the calibration curve of the response current of the GC/BCNTs/POAP-GOD electrode to glucose concentration is shown in Fig. 6. The inset plot shows the response current of the electrode to the successive addition of 1 mM glucose. From Fig. 6, it can be observed that the linear range is up to 8 mM with a correlation coefficient (*R*) of 0.9940 and then a plateau is reached gradually at higher glucose concentration. The biosensor has a good detection limit of 3.6 μM (signal-to-noise = 3), a high sensitivity of 2.43 μA mM<sup>-1</sup> cm<sup>-2</sup> (171.2 nA mM<sup>-1</sup>) and a short response time (within 6 s).

The apparent Michaelis–Menten constant  $K_m^{app}$  is an indicator of the enzyme–substrate reaction kinetics and used to evaluate the biological activity of the immobilized enzyme. According to the Lineweaver–Burk form of the Michaelis–Menten equation, the relationship between the response current and the glucose concentration is obtained:

$$\frac{1}{I_{ss}} = \frac{1}{I_{max}} + \frac{K_m^{app}}{I_{max}} C_{glucose} \quad (1)$$

where  $I_{ss}$  is the steady-state response current after the addition of substrate,  $I_{max}$  is the maximum response current under saturated substrate conditions and  $C_{glucose}$  is the bulk concentration of glucose. The apparent Michaelis–Menten constant  $K_m^{app}$  in the present study is calculated to be 15.19 mM, lower than that reported in literature [34], which indicates that the enzyme immobilized on the electrode keeps its bioactivity.

#### 3.5. The anti-interference ability of the GC/BCNTs/POAP-GOD electrode

Selectivity is one of the major characteristics of an amperometric glucose biosensor. The oxidizable compounds such as AA, UA and AP are usually co-existed with glucose in real samples. The

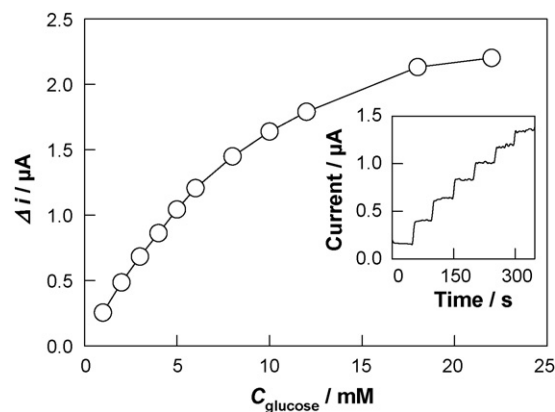


**Fig. 6.** Calibration curve of the response current at the GC/BCNTs/POAP-GOD electrode to glucose concentration in 1/15 M phosphate buffer solution (pH 7.0). Inset plot shows the current response of the enzyme electrode to successive addition of 1 mM glucose. The applied potential, +0.60 V.

**Table 2**  
Glucose content in human blood samples

Sample number	Provided by the local hospital (mM)	Determined by the current method (average of three times) (mM)	Relative error (%)
1	5.66	5.92 ± 0.05	+4.6
2	5.85	6.03 ± 0.09	+3.1
3	6.10	6.19 ± 0.06	+1.5
4	6.28	6.22 ± 0.08	−1.0

interference of electroactive compounds (AA, UA and AP) to the glucose response was examined in the presence of their physiological normal level (0.1 mM AA, 0.5 mM UA and 0.1 mM AP) [33] with a glucose concentration of 5.6 mM. The influence of AA, UA and AP to the glucose response is little under the testing conditions. The ratio of  $I_{G+I}$  to  $I_G$  is 1.05 for AA, 1.02 for UA and 1.06 for AP, respectively. These mean that the GC/BCNTs/POAP-GOD electrode has satisfactory anti-interference ability, which may result from the good properties of the POAP film [28–31].

### 3.6. The long-term stability and real sample analysis

The storage stability of the GC/BCNTs/POAP-GOD electrode in 1/15 M PBS (pH 7.0) at 4 °C was evaluated. 8% loss of the response signal of the GC/BCNTs/POAP-GOD electrode was observed after first 7 days by every day use. However, 80% response current is still retained after 20 days. This implies that the GC/BCNTs/POAP-GOD electrode is considerably stable.

Human plasma samples were assayed to demonstrate the practical use of the GC/BCNTs/POAP-GOD electrode. Fresh plasma samples were first analyzed in the local hospital with ASCA AG-II Chemistry System (Landmark, USA). The samples were then re-assayed with the GC/BCNTs/POAP-GOD electrode. A plasma sample (0.5 mL) was added into 5 mL PBS (pH 7.0), and the response was obtained at +0.60 V. The contents of glucose in blood can then be calculated from the calibration curve. The results, which are shown in Table 2, are satisfactory and agree closely with those measured by the biochemical analyzer in the hospital.

## 4. Conclusions

The glassy carbon electrode modified with B-doped carbon nanotubes shows high electrocatalytic activity for the oxidation of  $H_2O_2$  due to the large amount of edge sites and oxygen-rich groups located at the defective sites induced by boron doping. A glucose biosensor based on the GC/BCNTs/POAP-GOD electrode exhibits the good characteristics for the glucose determination: such as high sensitivity ( $171.2 \text{ nA mM}^{-1}$ ), low detection limit ( $3.6 \mu\text{M}$ ), wide linear range (up to 8 mM), short response time (within 6 s), satisfactory anti-interference ability and good stability. The apparent Michaelis–Menten constant ( $K_m^{\text{app}}$ ) of the immobilized GOD is 15.19 mM. These imply that the BCNTs have potential application in constructing enzyme-based amperometric biosensors.

## Acknowledgments

This work was financially supported by the National Natural Science Foundation of China (20675027, 20575019, 20335020) and the National Basic Research Program of China (No. 2006CB600903).

## References

- [1] G. Reach, G.S. Wilson, *Anal. Chem.* 64 (1992) 381A.
- [2] X. Zhang, K.Y. Chan, J.K. You, Z.G. Lin, A.C.C. Tseung, *J. Electroanal. Chem.* 430 (1997) 147.
- [3] X.H. Chen, Y.B. Hu, G.S. Wilson, *Biosens. Bioelectron.* 17 (2002) 1005.
- [4] S. Iijima, *Nature* 354 (1991) 96.
- [5] J.X. Wang, M.X. Li, Z.J. Shi, N.Q. Li, Z.N. Gu, *Anal. Chem.* 74 (2002) 1993.
- [6] Y.H. Lin, F. Lu, Y. Tu, Z.F. Ren, *Nano Lett.* 4 (2004) 191.
- [7] K.P. Gong, M.N. Zhang, Y.M. Yan, L. Su, L.Q. Mao, S.X. Xiong, Y. Chen, *Anal. Chem.* 76 (2004) 6500.
- [8] A. Rubio, J.L. Corkill, M.L. Cohen, *J. Phys. Rev. B* 49 (1994) 5081.
- [9] Z. Wang, C.H. Yu, D.C. Ba, J. Liang, *Vacuum* 81 (2007) 579.
- [10] Q.H. Yang, W.H. Xu, A. Tomita, T. Kyotani, *J. Am. Chem. Soc.* 127 (2005) 8956.
- [11] C. Zhang, R.F. Li, D.J. Zhang, Z.F. Shang, G.C. Wang, *J. Mol. Struct.: Theochem.* 765 (2006) 1.
- [12] X.B. Wang, Y.Q. Liu, D.B. Zhu, *J. Phys. Chem. B* 106 (2002) 2186.
- [13] W. Mickelson, S. Aloni, W.Q. Han, J. Cumings, A. Zettl, *Science* 300 (2003) 467.
- [14] J. Zhao, R.H. Xie, *J. Nanosci. Nanotechnol.* 3 (2003) 459.
- [15] A.Y. Liu, M.L. Cohen, *Science* 245 (1989) 841.
- [16] D.M. Teter, R.J. Hemley, *Science* 271 (1996) 53.
- [17] P. Shu, C. Kyeongiaem, *Nano Lett.* 3 (2003) 513.
- [18] R.X. Wang, D.J. Zhang, Y.M. Zhang, C.B. Liu, *J. Phys. Chem. B* 110 (2006) 18267.
- [19] Y.M. Zhang, D.J. Zhang, C.B. Liu, *J. Phys. Chem. B* 110 (2006) 4671.
- [20] N.Q. Jia, L. Liu, Q. Zhou, L.J. Wang, M.M. Yan, Z.Y. Jiang, *Electrochim. Acta* 51 (2005) 611.
- [21] E. Katz, I. Williner, *Chemphyschem* 5 (2004) 1084.
- [22] J.W. Wang, C.E. Lee, S.C. Lyu, T.J. Lee, *Appl. Phys. Lett.* 84 (2004) 2877.
- [23] A. Chou, T. Boecking, N.K. Singh, J.J. Gooding, *Chem. Commun.* (2005) 842.
- [24] L. Wu, X.J. Zhang, H.X. Ju, *Anal. Chem.* 79 (2007) 453.
- [25] C.E. Banks, R.G. Compton, *Analyst* 130 (2005) 1232.
- [26] N.Q. Jia, L.J. Wang, L. Liu, Q. Zhou, Z.Y. Jiang, *Electrochim. Commun.* 7 (2005) 349.
- [27] C.Y. Deng, J.H. Chen, X.L. Chen, C.H. Xiao, L.H. Nie, S.Z. Yao, *Biosens. Bioelectron.* 23 (2008) 1272.
- [28] M.A.V. Garcia, P. Tunon Blanco, A. Ivaska, *Electrochim. Acta* 43 (1998) 3533.
- [29] Z.N. Zhang, H.Y. Liu, J.Q. Deng, *Anal. Chem.* 68 (1996) 1632.
- [30] E. Miland, A.J. Miranda Oridieres, P. Tunon Blanco, M.R. Smyth, C.O. Fagein, *Talanta* 43 (1996) 785.
- [31] D.W. Pan, J.H. Chen, L.H. Nie, W.Y. Tao, S.Z. Yao, *Anal. Biochem.* 324 (2004) 115.
- [32] W.Q. Han, Y. Bando, K.J. Kurashima, T. Sato, *Chem. Phys. Lett.* 299 (1999) 368.
- [33] D.W. Pan, J.H. Chen, L.H. Nie, W.Y. Tao, S.Z. Yao, *Electrochim. Acta* 49 (2004) 795.
- [34] J. Li, X.Q. Lin, *Biosens. Bioelectron.* 22 (2007) 2898.
- [35] F. Ricci, A. Amine, G. Palleschi, D. Moscone, *Biosens. Bioelectron.* 18 (2003) 165.



## Enzyme immobilisation on electroactive nanostructured membranes (ENM): Optimised architectures for biosensing

Frank N. Crespilho<sup>a</sup>, M. Emilia Ghica<sup>b</sup>, Carla Gouveia-Caridade<sup>b</sup>,  
Osvaldo N. Oliveira Jr.<sup>a</sup>, Christopher M.A. Brett<sup>b,\*</sup>

<sup>a</sup> Instituto de Física de São Carlos, Universidade de São Paulo, 13560-970 São Carlos-SP, Brazil

<sup>b</sup> Departamento de Química, Faculdade de Ciências e Tecnologia, Universidade de Coimbra, 3004-535 Coimbra, Portugal

### ARTICLE INFO

#### Article history:

Received 9 January 2008

Received in revised form 17 April 2008

Accepted 23 April 2008

Available online 2 May 2008

#### Keywords:

Layer-by-layer

Glucose oxidase

Gold nanoparticles

PAMAM dendrimer

Cobalt hexacyanoferrate redox mediator

### ABSTRACT

Electroactive nanostructured membranes have been produced by the layer-by-layer (LbL) technique, and used to make electrochemical enzyme biosensors for glucose by modification with cobalt hexacyanoferrate redox mediator and immobilisation of glucose oxidase enzyme. Indium tin oxide (ITO) glass electrodes were modified with up to three bilayers of polyamidoamine (PAMAM) dendrimers containing gold nanoparticles and poly(vinylsulfonate) (PVS). The gold nanoparticles were covered with cobalt hexacyanoferrate that functioned as a redox mediator, allowing the modified electrode to be used to detect H<sub>2</sub>O<sub>2</sub>, the product of the oxidase enzymatic reaction, at 0.0 V vs. SCE. Enzyme was then immobilised by cross-linking with glutaraldehyde. Several parameters for optimisation of the glucose biosensor were investigated, including the number of deposited bilayers, the enzyme immobilisation protocol and the concentrations of immobilised enzyme and of the protein that was crosslinked with PAMAM. The latter was used to provide glucose oxidase with a friendly environment, in order to preserve its bioactivity. The optimised biosensor, with three bilayers, has high sensitivity and operational stability, with a detection limit of 6.1 μM and an apparent Michaelis–Menten constant of 0.20 mM. It showed good selectivity against interferences and is suitable for glucose measurements in natural samples.

© 2008 Elsevier B.V. All rights reserved.

### 1. Introduction

Monolayers prepared by direct adsorption of dendrimers onto solid substrates have been proven to be highly stable and amenable to functionalisation without loss of dendrimers into solution [1]. The large surface area of dendrimers allows various functional units to be immobilised, which is important in applications such as sensors. Biosensors based on enzymes have been built which exploit the properties of dendrimers.

Dendrimer-encapsulated platinum nanoparticles have been used for layer-by-layer (LbL) glucose biosensor development on platinum electrodes [2] and on carbon nanotubes [3], and for a glutamate biosensor on carbon nanotubes [4], without redox mediator.

Yoon and Kim [5] prepared layer-by-layer films with polyamidoamine (PAMAM) dendrimer alternated with periodate oxidized glucose oxidase, on a gold substrate, and detected glucose using ferrocenemethanol in solution as diffusional electron-transfer mediator. A similar method, with the same redox mediator, was used by Yang et al. [6] but with gold nanoparticles in combina-

tion with the covalently attached cross-linker cysteamine instead of PAMAM. The main disadvantage of these methods is the addition of a mediator to the reaction medium.

A new method for enzymatic immobilisation was recently demonstrated by us, which uses a combination of LbL self-assembly, redox mediator electrodeposition and cross-linking [7]. It was shown how one can benefit from combining the biocatalytic properties of the enzyme with the conductivity and electrocatalytic properties of gold nanoparticles. The strategy used consists in applying a new concept in nanoarchitecture: electroactive nanostructured membranes (ENM) with ITO-PVS/PAMAM-Au LbL electrodes [8], where indium tin oxide (ITO) is the electrode substrate and PVS is poly(vinylsulfonate), which alternates with PAMAM-Au (PAMAM containing gold nanoparticles) in the bilayer structure. A redox mediator (Me) is then electrodeposited around the Au nanoparticles to form an ITO-PVS/PAMAM-Au@Me system. The redox mediators used were Co, Fe, Ni and Cu hexacyanoferrates. These hexacyanoferrate modified electrodes showed electrocatalytic activity towards hydrogen peroxide, demonstrating that this new approach can be used in biosensors and nanodevices, where a redox mediator is required.

The LbL assembly of oppositely charged species is a simple and powerful method to provide a suitable nanoenvironment to

\* Corresponding author. Tel.: +351 239835295; fax: +351 239835295.  
E-mail address: [brett@ci.uc.pt](mailto:brett@ci.uc.pt) (C.M.A. Brett).

retain the biomolecular activity. Methods to build ordered enzymatic monolayer or multilayers include Langmuir–Blodgett [9], self-assembly [10], layer-by-layer electrostatic adsorption [6,11], antigen–antibody interaction [12] and surfactant films [13].

The present paper concerns several new developments with respect to the report in [7], focusing on optimising enzymatic devices and further characterising the biosensor architectures obtained with the LbL approach. Glucose oxidase (GOx) was the enzyme of choice because the catalytic properties of this enzyme are well known in the literature and because the determination of glucose concentration is important in clinical, biological and chemical samples, as well as in food processing and fermentation [14]. The preparation and characterisation of bilayer nanostructured membranes, containing gold nanoparticles, is presented. Strategies for covering the gold nanoparticles with the redox mediator cobalt hexacyanoferrate (CoHCF), and methodologies for coating by the enzyme-containing layer are investigated. Optimisation of the biosensor construction involved testing different numbers of bilayers and different ways of immobilising glucose oxidase. Sensor performance and operational stability were evaluated.

## 2. Experimental

### 2.1. Reagents and buffers

Glucose oxidase (E.C. 1.1.3.4, from *Aspergillus Niger*, 24 U/mg) was acquired from Fluka.  $\alpha$ -D(+)-glucose, glutaraldehyde (GA) (25%, v/v in water) and bovine serum albumin (BSA) were purchased from Sigma. Potassium hexacyanoferrate (III) ( $K_3Fe(CN)_6$ ) and cobalt chloride ( $CoCl_2 \cdot 6H_2O$ ) were obtained from Merck. The supporting electrolyte solution for electrochemical measurements was sodium phosphate buffer saline (NaPBS) (0.1 M  $NaH_2PO_4/Na_2HPO_4 + 0.05$  M NaCl, pH 7.0), prepared with ultrapure water supplied by a Millipore Milli-Q nanopure system (resistivity >18 M $\Omega$  cm). Experiments were performed at room temperature,  $25 \pm 1$  °C. Polyamidoamine (PAMAM) and poly(vinylsulfonate) (PVS) were purchased from Aldrich, Germany.

### 2.2. Methods and instruments

Measurements were performed in a 15 mL, one-compartment cell containing the ITO (indium tin oxide) modified electrode (geometric area 1.0 cm<sup>2</sup>) as working electrode, a platinum auxiliary electrode and a saturated calomel electrode (SCE) as reference. Voltammetric and amperometric experiments were carried out using a CV-50 W Voltammetric Analyser from Bioanalytical Systems, West Lafayette, IN, USA, controlled by BAS CV-2.1 software or a  $\mu$ -Autolab Type II potentiostat/galvanostat running with GPES 4.9 software (Eco Chemie, Netherlands). Electrochemical impedance measurements were carried out with a PC-controlled Solartron 1250 Frequency Response Analyser coupled to a Solartron 1286

electrochemical interface using ZPlot 2.4 software (Solartron Analytical, UK). A sinusoidal voltage perturbation of amplitude 10 mV rms was applied in the frequency range between 65 kHz and 0.1 Hz with a 10 frequency steps per decade. The pH measurements were performed with a CRISON 2001 micro pH-meter.

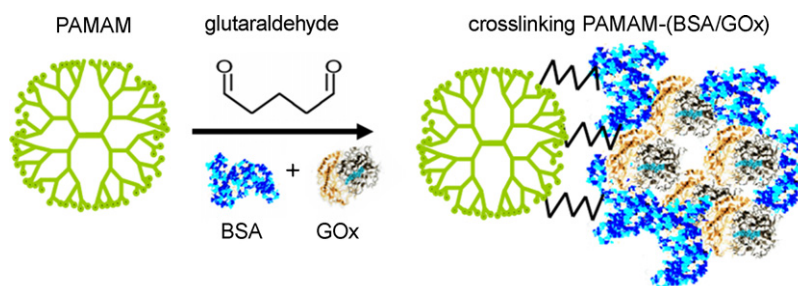
Atomic force microscopy (AFM) images were obtained with a Multimode™ Atomic Force Microscope controlled by a Digital Instruments Nanoscope E controller (Veeco Instruments, USA). The cantilevers were silicon nitride NanoProbes™ V-shaped, 100  $\mu$ m long, and with a spring constant of 0.58 N m<sup>-1</sup>. All AFM images were taken in the contact mode in air at room temperature. The contrast and brightness of the images were adjusted.

### 2.3. Electrode preparation

The working electrode was prepared from an ITO-covered glass electrode by electrostatic deposition of up to three bilayers of (PVS/PAMAM-Au) as described in detail in [7,15]. Briefly, gold metallic nanoparticles of diameter  $\sim$ 3 nm stabilised by PAMAM dendrimer molecules were synthesized in aqueous solution, which was then used as cationic polyelectrolyte to build multilayers containing nanoparticles together with poly(vinylsulfonate). The sequential deposition was performed by immersing the ITO substrate alternately into the PAMAM-Au and PVS solutions for 5 min; it was found by cyclic voltammetry and UV–vis spectroscopy that 5 min is sufficient for complete surface coverage by PAMAM-Au.

Following this, cobalt hexacyanoferrate was electrochemically deposited on the ITO-(PVS/PAMAM-Au)<sub>n</sub> ( $n = 1, 2$  or 3) electrode and finally glucose oxidase was immobilised using the cross-linking method. Cobalt hexacyanoferrate was deposited, as described in [16], by cycling the ITO-(PVS/PAMAM-Au)<sub>n</sub> electrode 30 times between  $-0.2$  and  $0.9$  V vs. SCE at a scan rate of 50 mV s<sup>-1</sup> in a freshly prepared solution containing 0.5 mmol L<sup>-1</sup>  $CoCl_2$ , 0.25 mmol L<sup>-1</sup>  $K_3Fe(CN)_6$  and 0.05 mol L<sup>-1</sup> NaCl at pH 3.0 (pH adjusted with HCl).

Enzyme immobilisation was performed using the cross-linking reaction with glutaraldehyde, depicted in Scheme 1. Two enzyme immobilisation procedures were compared: dip-coating and drop-coating. GOx immobilisation by dip-coating was performed using a mixture of the enzyme with glutaraldehyde and bovine serum albumin. In the optimised procedure, the mixture contained 100  $\mu$ L of GA (2.5%, v/v in water) and 240  $\mu$ L of enzyme solution. The latter was prepared by dissolving 20 mg BSA and 50 mg GOx in 1 mL of 0.1 M NaPBS (pH 7.0). Electrodes previously modified with the mediator were immersed in the mixture for 2 h, and then allowed to dry for another 2 h at room temperature. For drop-coating, 10  $\mu$ L of enzyme solution (GOx and BSA in the same proportion as used above) were placed onto the electrodes modified with the mediator. After 1 h, 10  $\mu$ L of GA (2.5%, v/v in water) were placed on top of the electrodes and allowed to dry for 2 h. The biosensors were first used on the day after preparation when the response was bet-



**Scheme 1.** Cross-linking between PAMAM and BSA/GOx system using glutaraldehyde.

ter. When not in use, the electrodes were kept at 4 °C in phosphate buffer electrolyte, pH 7.0.

### 3. Results and discussion

#### 3.1. Preparation of an electroactive nanostructured membrane (ENM) modified electrode: ITO-(PVS/PAMAM-Au)<sub>3</sub>@CoHCF

Using PAMAM dendrimers as matrix, metallic gold nanoparticles of ~3 nm diameter were deposited from an aqueous solution

onto an ITO substrate using the LbL technique, as described in Section 2. In previous work, three bilayers of PVS/PAMAM-Au was found to be the best configuration to prepare an ITO modified electrode, since 3-bilayer PVS/PAMAM-Au LbL films were found to possess high organisation and outstanding uniformity [8].

To verify the influence of PVS/PAMAM-Au multilayers on the ITO surface morphology, a bare ITO and ITO-(PVS/PAMAM-Au)<sub>n</sub> (n=1, 2 or 3 bilayers) systems were examined by AFM, Fig. 1. The images of ITO-(PVS/PAMAM-Au)<sub>n</sub> revealed a globular morphology, analogous to other LbL films [17]. Profile and roughness

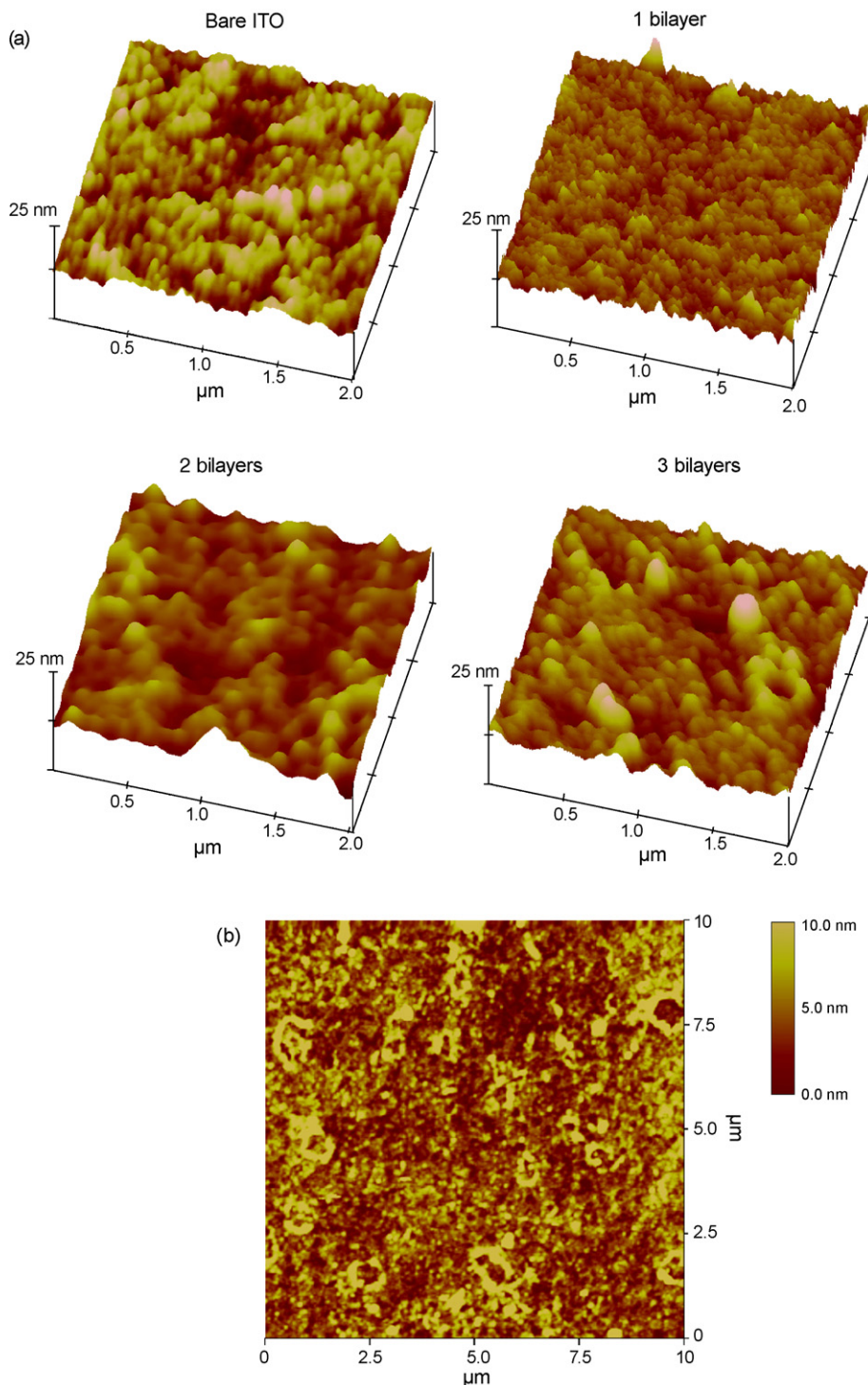


Fig. 1. (a) 3D AFM topographical images of ITO and ITO-(PVS/PAMAM-Au)<sub>n</sub> (n=1, 2, and 3). (b) AFM topographical image of ITO-(PVS/PAMAM-Au)<sub>2</sub>.



analysis, carried out on images of  $10\ \mu\text{m} \times 10\ \mu\text{m}$ , revealed some differences in morphological parameters with the number of bilayers. The root mean square roughness, representing the standard deviation of the distribution of surface heights [18], and typically used to quantify variations in surface elevation, increases with the number of bilayers. The values were  $\sim 1.93\ \text{nm}$  for ITO and  $\sim 2.88$ ,  $\sim 3.31$  and  $\sim 4.35\ \text{nm}$  for ITO-(PVS/PAMAM-Au) $_n$  with  $n = 1, 2$  or 3 bilayers, respectively. Cross-section plots of surface morphology (not shown) reveal a uniform particle distribution with maximum height of ca. 6 nm for ITO, and ca. 9, 11 and 13 nm for the first, second and third bilayer respectively. The difference in the maximum height between the first bilayer and ITO corresponds to the diameter of one gold nanoparticle ( $\sim 3\ \text{nm}$ ). The second and third bilayers showed a uniform distribution of PAMAM nano-rings containing Au nanoparticles inside their cavities, which can be seen in the AFM 2D image for the second bilayer in Fig. 1b.

The last step for ITO-(PVS/PAMAM-Au) $_3$ @CoHCF build-up was to use the system ITO-(PVS/PAMAM-Au) $_3$  as working electrode to electrochemically modify the PAMAM-Au surface. We previously showed that ITO-(PVS/PAMAM-Au) $_3$  structures are suitable for biosensors and electrocatalysis owing to their low capacitive and high Faradaic currents associated with low ohmic drop [8]. Electrodeposition by potential cycling of cobalt hexacyanoferrate onto ITO-(PVS/PAMAM-Au) $_3$  electrodes was carried out according to the optimised conditions in previous work [7,16]. As shown in Fig. 2a, CoHCF was successfully deposited onto ITO-(PVS/PAMAM-Au) $_3$  electrodes by potential cycling, with the cathodic and anodic peak currents increasing linearly with the number of cycles. The deposited mediator was characterised by cyclic voltammetry in 0.1 M NaPBS (pH 7.0) supporting electrolyte, the anodic and cathodic peak currents being a linear function of the square root of the scan rate, as shown in Fig. 2b. Therefore, the electrochemical process is controlled by diffusion of the counter ion.

In [8] and by comparing electrochemical impedance spectra of different electrodeposited metal hexacyanoferrate mediators, it was demonstrated that the charge-transfer at ITO-(PVS/PAMAM-Au) $_3$ @Me electrodes is faster than at ITO-(PVS/PAMAM-Au) $_3$ , and the charge-transfer resistance using CoHCF is lower than for other hexacyanoferrates (e.g. CuHCF, FeHCF and NiHCF). In general terms, the spectra collected after mediator deposition differ from those of ITO-(PVS/PAMAM-Au) $_3$  electrodes with the mediator in solution. The strategy used here to study diffusion and charge-transport mechanisms was to analyse the impedance at high frequencies for ITO-(PVS/PAMAM-Au) $_3$  electrodes before and after immobilisation of CoHCF redox mediator. After cycling to immobilise the redox mediator, the spectra of the new system containing Au@CoHCF were recorded. The results obtained at the open circuit potential are shown in the complex plane plots of Fig. 3a, with a semi-circle at high frequencies in the complex plane plot after redox mediator immobilisation. The relatively small diameter is evidence of fast charge-transport, and the value of the charge-transfer resistance can also be related to the degree of coverage of the gold nanoparticles by CoHCF, assuming that electron-transfer reactions occur at CoHCF sites inside the LbL film. The spectra for the ITO-(PVS/PAMAM-Au) $_3$  system both with and without CoHCF also exhibit very reproducible near-vertical parallel lines at low frequencies, a typical finite-diffusion behaviour observed for electrodes covered by conducting films.

The ITO-(PVS/PAMAM-Au) $_3$ @CoHCF electrode was used as working electrode for amperometric measurements of  $\text{H}_2\text{O}_2$  in 0.1 M NaPBS (pH 7.0), at an applied potential of 0.0 V vs. SCE. The current changed cathodically with the injection of fifteen aliquots of  $\text{H}_2\text{O}_2$  stock solution to the buffer, with a good linearity between 20 and 100  $\mu\text{M}$  (data not shown); the total analysis time was half

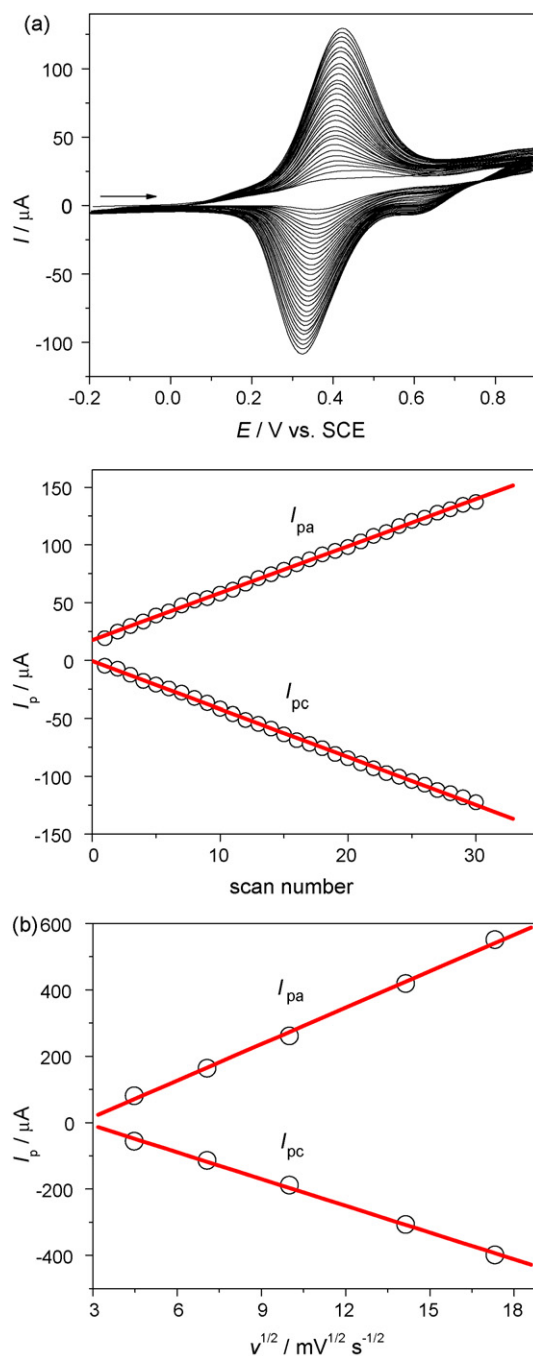


**Fig. 2.** (a) Cyclic voltammograms showing continuous growth of CoHCF on ITO-(PVS/PAMAM-Au) $_3$  electrodes and dependence of anodic and cathodic peak currents on the number of cycles. (b) Dependence of anodic and cathodic peak currents on the square root of scan rate for the ITO-(PVS/PAMAM-Au) $_3$ @CoHCF electrode in 0.1 M NaPBS (pH 7.0).

an hour. The detection limit (three times the signal-to-noise ratio) was 5.7  $\mu\text{M}$ . The corresponding regression equation of the linear plot was  $I/nA = 3.44 - 237.55c$ , where  $c$  is the  $\text{H}_2\text{O}_2$  concentration in  $\mu\text{M}$ , with a correlation coefficient  $R = 0.9989$ . The stability of the CoHCF mediator on the ITO-(PVS/PAMAM-Au) $_3$  electrode was studied by performing successive calibration curves at the same electrode leading to a decrease of up to 50%, probably due either to some damage of the mediator film caused by the peroxide or by leaching of the mediator. However, this loss of sensitivity should not affect the operation of the enzyme biosensor since the media-

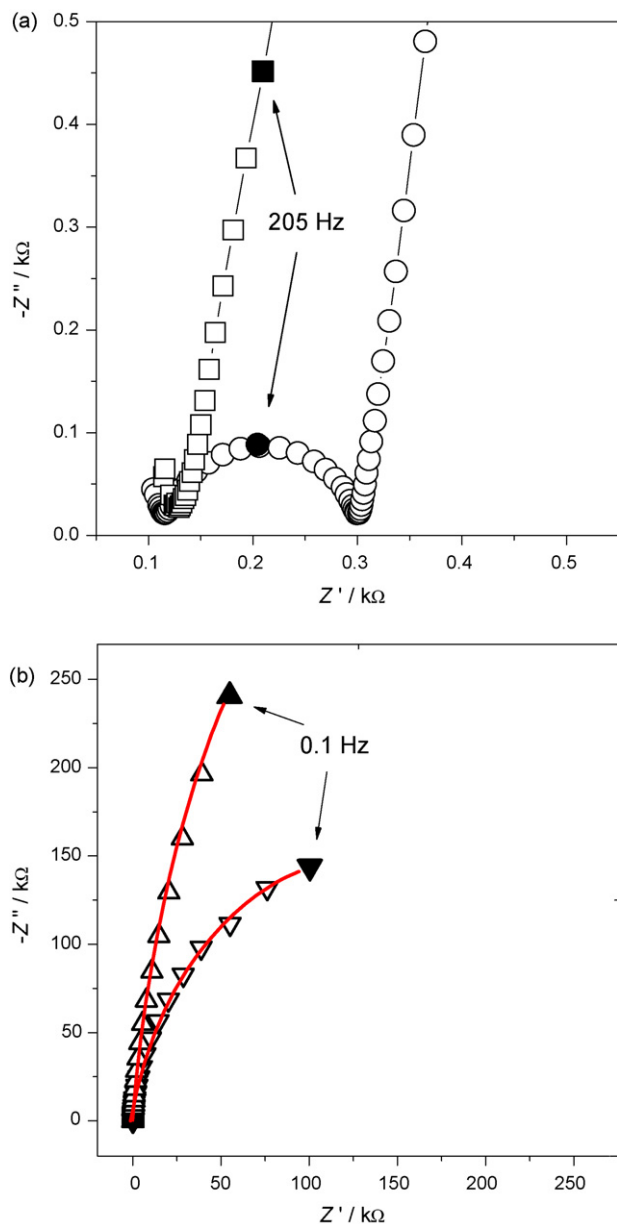


**Fig. 3.** Complex plane impedance spectra for electrode at 0.0 V vs. SCE in 0.1 M NaPBS, pH 7.0 of (a) ITO-(PVS/PAMAM-Au)<sub>3</sub> electrode before (□) and after (○) CoHCF electrodeposition; (b) ITO-(PVS/PAMAM-Au)<sub>3</sub>@CoHCF-GOx in the absence (△) and presence (▽) of glucose. Frequency range: 65 kHz to 0.1 Hz.

tor is trapped under the enzyme layer and the amount of peroxide is less, as will be demonstrated below.

### 3.2. Enzyme immobilisation onto ITO-(PVS/PAMAM-Au)<sub>3</sub>@CoHCF electrode using dip-coating and drop-coating procedure

Enzyme immobilisation onto ITO-(PVS/PAMAM-Au)<sub>3</sub>@CoHCF was carried out by assembling GOx using dip-coating or drop-coating, as described Section 2. The resulting architecture is ITO-(PVS/PAMAM-Au)<sub>3</sub>@CoHCF-GOx electrode. The response to glucose was evaluated in amperometric mode at 0.0 V vs. SCE. Detection at this low potential represents a significant improvement for the determination of glucose with respect to previous glucose enzymatic devices using dendrimers, in which the potentials (vs. SCE) used were 0.67 V [19], 0.55 V [20] and 0.25 V [6].

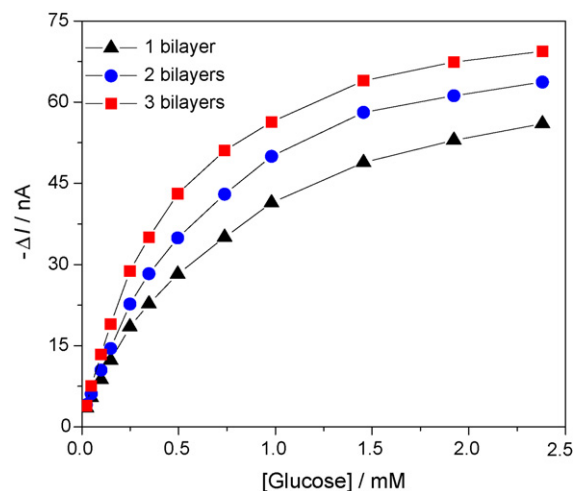


**Fig. 4.** Glucose response curves at ITO-(PVS/PAMAM-Au)<sub>3</sub>@CoHCF-GOx electrode prepared with 20 mg mL<sup>-1</sup> BSA, 50 mg mL<sup>-1</sup> GOx and 2.5% GA by drop-coating using (▲) 1 bilayer; (●) 2 bilayers and (■) 3 bilayers of (PVS/PAMAM-Au) in 0.1 M NaPBS (pH 7.0). Applied potential 0.0 V vs. SCE.

Several parameters were studied to optimise the biosensor response. It was first investigated whether the number of bilayers, up to three, deposited on the ITO electrode influenced the results. In previous papers [15,21], it was found that the electrodes with best performance were prepared with up to 3 bilayers, and additional bilayers led to no improvement in response. Therefore, electrodes with one and three bilayers of (PVS/PAMAM-Au) were prepared, CoHCF mediator was electrodeposited and then the enzyme was immobilised by dip-coating or drop-coating of the enzyme solution (see Section 2 for enzyme solution preparation). Fig. 4 shows a better glucose response curve for a drop-coated electrode with three bilayers of (PVS/PAMAM-Au), in comparison to that with one or two bilayers. Similar results were obtained with the electrode prepared by dip-coating of enzyme solution (not shown).

Secondly, the response to glucose following enzyme immobilisation by dip-coating or by drop-coating was compared, see Fig. 5. The drop-coating method proved more suitable than dip-coating for enzyme immobilisation, leading to a higher response by about 30% and a detection limit up to three times lower comparing with that obtained by the dip-coating technique. The reason for this

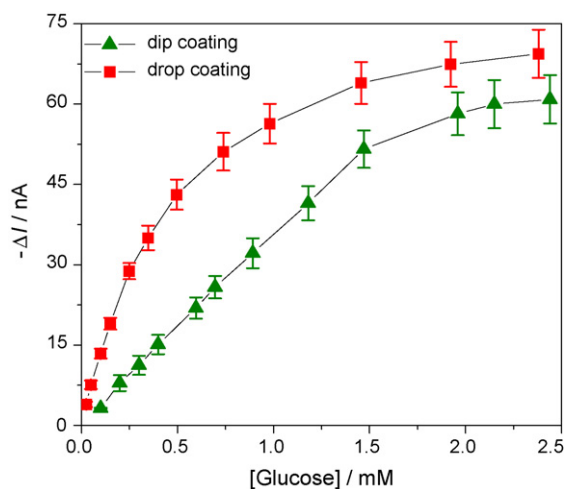


**Fig. 5.** Glucose response curves at ITO-(PVS/PAMAM-Au)<sub>3</sub>@CoHCF-GOx electrode obtained by (▲) dip-coating and (■) drop-coating in 0.1 M NaPBS (pH 7.0). Applied potential 0.0 V vs. SCE.

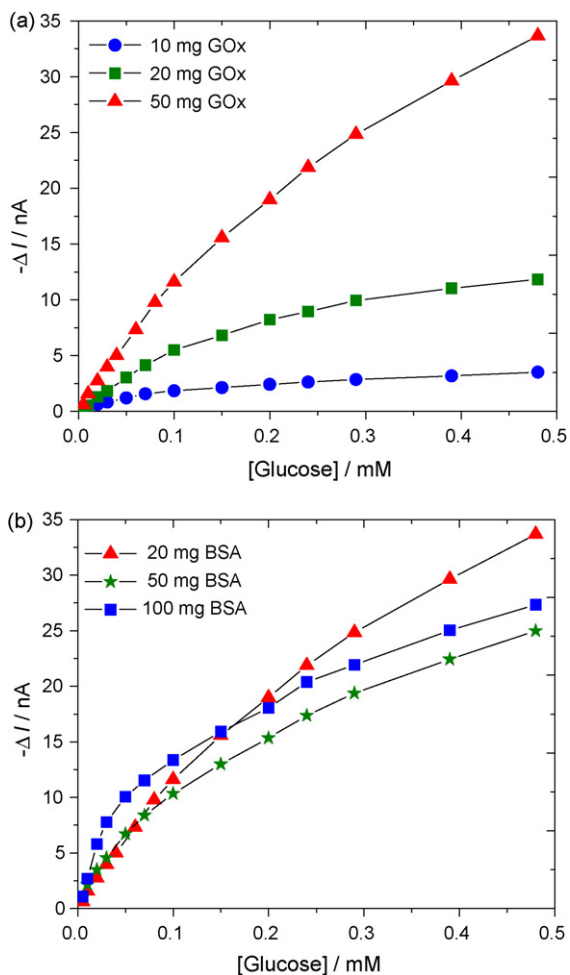


**Fig. 6.** Glucose response curves at ITO-(PVS/PAMAM-Au)<sub>3</sub>@CoHCF-GOx electrode in 0.1 M NaPBS (pH 7.0) at 0.0V vs. SCE using drop-coating with 2.5% GA and (a) 20 mg mL<sup>-1</sup> BSA and different GOx concentrations: (●) 10; (■) 20; (▲) 50 mg mL<sup>-1</sup>. (b) 50 mg mL<sup>-1</sup> GOx and different BSA concentrations: (▲) 20; (★) 50; (■) 100 mg mL<sup>-1</sup>.

difference may be due to the preparation method. In the case of drop-coating, an aliquot of the enzyme solution with BSA was placed on the mediator-modified electrode and left to dry for 1 h, the time required for the enzyme to bind to the dendrimer amino group. Then, glutaraldehyde was placed on top of the enzyme to perform cross-linking. It is likely that a more robust biosensor is achieved when using this technique by permitting stronger binding between enzyme and dendrimer, before cross-linking by glutaraldehyde, leading to better stability and sensitivity. Moreover, the amount of immobilised enzyme is better controlled by drop-coating.

Finally, the influence of the concentration of the enzyme and BSA on the electrode response was studied by keeping the concentration of BSA constant and varying the concentration of GOx, and vice versa. Fig. 6a shows a higher glucose response for increasing enzyme concentrations in the range from 10 to 50 mg mL<sup>-1</sup>; it is likely that the response could be further increased with larger amounts of enzyme, but this would increase the cost of the biosensor. With the GOx concentration fixed at 50 mg mL<sup>-1</sup>, an increase of sensitivity was observed for increasing BSA concentrations, but this was accompanied by a decrease of the linear range of the biosensor, as shown in Fig. 6b. Therefore, to study the effect of the concentration of glutaraldehyde, 50 mg mL<sup>-1</sup> of GOx and 20 mg mL<sup>-1</sup> of BSA were employed. The response with 25% GA was a factor of five lower

than that for 2.5% GA, which might be due to enzyme deactivation during cross-linking.

### 3.3. Analytical characteristics of the ITO-(PVS/PAMAM-Au)<sub>3</sub>@CoHCF-GOx electrode

The optimised electrode system, i.e. ITO-(PVS/PAMAM-Au)<sub>3</sub>@CoHCF-GOx with GOx immobilised by the drop-coating method using a solution of 50 mg mL<sup>-1</sup> of GOx, 20 mg mL<sup>-1</sup> of BSA and 2.5% GA, was used to obtain the full analytical characteristics of the biosensor.

The response to glucose measured in 0.1 M NaPBS (pH 7.0) at 0.0V vs. SCE was found to be linear up to 250 μM glucose with a sensitivity of 111 nA mM<sup>-1</sup>, correlation coefficient  $R = 0.9998$  and a detection limit (three times signal-to-noise ratio) of 6.1 μM. The glucose sensor described in [16], which used a CoHCF mediator layer on a carbon film substrate covered by the enzyme layer, had a detection limit of 1.9 μM, lower by a factor of three, and a smaller linear range up to 30 μM. The sensor described here shows a larger linear range, which may be advantageous in the analysis of some natural samples such as sweet wines, in that less sample dilution is required.

Another important characteristic of this electrode, which can be obtained from electrochemical impedance data, see Fig. 3b, is the lower charge-transfer resistance for hydrogen peroxide reduction when glucose is present in the electrolyte solution. This supports the hypothesis that the ITO-(PVS/PAMAM-Au)<sub>3</sub>@CoHCF-GOx electrode promotes easier electron-transfer reaction, as mentioned above. The apparent Michaelis–Menten constant ( $K_M^{\text{app}}$ ) was determined from the Lineweaver–Burk plot. The value of  $K_M^{\text{app}}$  obtained was 0.20 mM, which is similar to other values reported in the literature [20] and lower than the value for the enzyme in solution. This might be explained by the fact that in the case of immobilised enzymes the overall reaction rate is not controlled just by the diffusion of the substrate, some other processes occurring in the same time leading to a slower kinetic rate.

The operational stability was tested by measuring the response to a glucose concentration of 0.74 mM during 20 measurements, after which the current response dropped by 30%. This loss of stability after consecutive measurements can be due to the interaction of the hydrogen peroxide produced in the enzymatic reaction with the mediator, which can damage the CoHCF film. The storage stability was good when the electrodes were kept at 4 °C in phosphate buffer solution. After 1 month of storage the biosensor still maintained 65% of its initial response.

The selectivity of the biosensor was assessed by checking the influence of interferents such as chemical species normally present in wines. In these experiments, a concentration of 0.30 mM glucose and 0.60 mM interferent was used. From the interferents studied, viz. fructose, ethanol, acetic acid, ascorbic acid, citric acid, lactic acid, malic acid, oxalic acid and tartaric acid, only ascorbic acid was detected at 0.0V vs. SCE. In order to reduce the ascorbic acid interference, experiments were performed in which glucose was measured at two other potentials, -0.050 and -0.180V vs. SCE (not shown). The response to ascorbic acid then decreased, and at -0.180V vs. SCE the signal was only 8.6% of that at 0.0V. The response to glucose also showed some decrease, but by much less, to 78.3%. Since the response to glucose normally increases when applying more negative potentials (verified in independent measurements, data not shown) this decrease in the glucose response might be due to some loss of stability during consecutive measurements, as stated before. However, at -0.180V vs. SCE it is possible to measure glucose without interferences from the above-mentioned compounds, and the response to ascorbic acid, present in the form of ascorbate, at the value of pH used in the experiments, is reduced

much more. Taking into account the fact that the concentration of ascorbic acid in natural samples, such as wine, is much lower than that of glucose, it should therefore not represent any interference in the determination of glucose. If necessary, an outer layer of a cation exchange polymer, such as Nafion, can be added to the biosensor assembly in order to exclude anions, such as ascorbate, for measurements in complex natural samples.

#### 4. Conclusions

A novel glucose biosensor has been developed using ITO-covered glass electrodes modified with three bilayers of (PVS/PAMAM-Au) self-assembly as supporting electrode with cobalt hexacyanoferrate mediator and glucose oxidase enzyme. Electrodeposition of cobalt hexacyanoferrate on the gold nanoparticles led to successful determination of hydrogen peroxide at lower potentials where other compounds had less electroactivity. After optimising the immobilisation of glucose oxidase on the modified electrode assembly, glucose was measured amperometrically at 0.0V vs. SCE; the biosensor showed a linear response up to 250  $\mu$ M glucose with a detection limit ( $3\sigma$ ) of 6.1  $\mu$ M. The biosensor had a good operational and storage stability, and was tested successfully against interferences normally present in wines. This work opens up excellent future perspectives for the development of electrochemical biosensors constructed using such a layer-by-layer modification strategy.

#### Acknowledgements

Financial support from FAPESP, CAPES, CNPq, IMMP/MCT (Brazil), from European Project HPRN-CT-2002-00186, and from Fundação para a Ciência e Tecnologia (FCT) Portugal, project

PTDC/QUI/65255/2006, POCI 2010 (co-financed by the European Community Fund FEDER), PhD grants SFRH/BD/14014/2003 – MEG and SFRH/BD/18659/2004 – CGC, and ICEMS (Research Unit 103), is gratefully acknowledged.

#### References

- [1] W.M. Lackowski, J.K. Campbell, G. Edwards, V. Chechik, R.M. Crooks, *Langmuir* 15 (1999) 7632.
- [2] Y. Zhu, H. Zhu, X. Yang, L. Xu, C. Li, *Electroanalysis* 19 (2007) 698.
- [3] L. Xu, Y. Zhu, L. Tang, X. Yang, C. Li, *Electroanalysis* 19 (2007) 717.
- [4] L. Tang, Y. Zhu, L. Xu, X. Yang, C. Li, *Talanta* 73 (2007) 438.
- [5] H.C. Yoon, H.S. Kim, *Anal. Chem.* 72 (2000) 922.
- [6] W. Yang, J. Wang, S. Zhao, Y. Sun, C. Sun, *Electrochem. Commun.* 8 (2006) 665.
- [7] F.N. Crespilho, M.E. Ghica, M. Florescu, F.C. Nart, O.N. Oliveira Jr., C.M.A. Brett, *Electrochem. Commun.* 8 (2006) 1665.
- [8] F.N. Crespilho, M.E. Ghica, V. Zucolotto, F.C. Nart, O.N. Oliveira Jr., C.M.A. Brett, *Electroanalysis* 19 (2007) 805.
- [9] S.K. Sharma, R. Singhal, B.D. Malhotra, N. Sehgal, A. Kumar, *Biotechnol. Lett.* 26 (2004) 645.
- [10] S. Campuzano, R. Galvez, M. Pedrero, F.J.M. de Villena, J.M. Pingarron, *Anal. Bioanal. Chem.* 377 (2003) 600.
- [11] G. Liu, Y. Lin, *Electrochem. Commun.* 8 (2006) 251.
- [12] R. Blonder, E. Katz, Y. Cohen, N. Itzhak, A. Riklin, I. Willner, *Anal. Chem.* 68 (1996) 3151.
- [13] J.F. Rusling, *Acc. Chem. Res.* 31 (1998) 363.
- [14] S. Liu, H. Ju, *Biosens. Bioelectron.* 19 (2003) 177.
- [15] F.N. Crespilho, V. Zucolotto, C.M.A. Brett, O.N. Oliveira Jr., F.C. Nart, *J. Phys. Chem. B* 110 (2006) 17478.
- [16] M. Florescu, C.M.A. Brett, *Anal. Lett.* 37 (2004) 871.
- [17] Z.-M. Liu, Y. Yang, H. Wang, Y.-L. Liu, G.-L. Shen, R.-Q. Yu, *Sens. Actuators B* 106 (2005) 394.
- [18] E.S. Gadelmawla, M.M. Koura, T.M.A. Maksoud, I.M. Elewa, H.H. Soliman, *J. Mater. Process. Technol.* 123 (2002) 133.
- [19] M. Snejdarkova, L. Svoboda, V. Gajdos, T. Hianik, *J. Mater. Sci. Mater. Med.* 12 (2001) 1079.
- [20] B. Alonso, P.G. Armada, J. Losada, I. Cuadrado, B. Gonzalez, C.M. Casado, *Biosens. Bioelectron.* 19 (2004) 1617.
- [21] F.N. Crespilho, F. Huguenin, V. Zucolotto, P. Olivi, F.C. Nart, O.N. Oliveira Jr., *Electrochem. Commun.* 8 (2006) 348.



## Application of PLE for the determination of essential oil components from *Thymus vulgaris* L.

Andrzej L. Dawidowicz\*, Ewelina Rado, Dorota Wianowska, Marek Mardarowicz, Jan Gawdzik

Faculty of Chemistry, Maria Curie Skłodowska University, 20-031 Lublin, Pl. Marii Curie Skłodowskiej 3, Poland

### ARTICLE INFO

#### Article history:

Received 11 September 2007  
Received in revised form 22 April 2008  
Accepted 23 April 2008  
Available online 2 May 2008

#### Keywords:

*Thymus vulgaris* L.  
Essential oil  
Sample preparation methods

### ABSTRACT

Essential plants, due to their long presence in human history, their status in culinary arts, their use in medicine and perfume manufacture, belong to frequently examined stock materials in scientific and industrial laboratories. Because of a large number of freshly cut, dried or frozen plant samples requiring the determination of essential oil amount and composition, a fast, safe, simple, efficient and highly automatic sample preparation method is needed.

Five sample preparation methods (steam distillation, extraction in the Soxhlet apparatus, supercritical fluid extraction, solid phase microextraction and pressurized liquid extraction) used for the isolation of aroma-active components from *Thymus vulgaris* L. are compared in the paper. The methods are mainly discussed with regard to the recovery of components which typically exist in essential oil isolated by steam distillation.

According to the obtained data, PLE is the most efficient sample preparation method in determining the essential oil from the thyme herb. Although co-extraction of non-volatile ingredients is the main drawback of this method, it is characterized by the highest yield of essential oil components and the shortest extraction time required. Moreover, the relative peak amounts of essential components revealed by PLE are comparable with those obtained by steam distillation, which is recognized as standard sample preparation method for the analysis of essential oils in aromatic plants.

© 2008 Elsevier B.V. All rights reserved.

### 1. Introduction

Wide interest in essential oils as stock for pharmaceutical, agricultural, cosmetic, perfume and food industries requires the determination of essential oil amounts both in freshly cut, dried or frozen plants and in the analysis of essential oil components [1].

In the situation when a large number of plant samples require analysis of their aromatic composition, an efficient, very fast, simple, safe and a highly automatic sample preparation method is needed [2,3].

Steam distillation is the routine method recommended by pharmacopoeias for controlling the quality of plant materials as essential oil sources [4]. However, this standard method in essential oil analysis is very time consuming and therefore not efficient enough for screening numerous plant samples for their aroma composition [5,6].

Solid phase microextraction (SPME) is a relatively new method recommended for the analysis of aroma compounds [7–9]. This

simple and cheap solvent-free sample preparation method is more and more frequently applied in routine laboratory analyses of organic volatile compounds; however, it is less effective in the case of substances existing in trace amounts. Moreover, for aromatic compounds with higher boiling points, longer equilibrium time is needed between a sample and headspace, which lengthens total analysis time.

Supercritical fluid extraction (SFE) is another solvent-free method, very effective for determining essential oil components [10–13]. In SFE, extraction conditions can be regulated by variation of temperature and pressure, which improves the effectiveness of the method. Yet because in most applications carbon dioxide acts as a supercritical fluid (due to its low costs, lack of toxicity and easiness of obtaining supercritical conditions), the usage of SFE is limited mainly to non-polar and medium polar substances of high volatility [14].

Solvent extraction is the most frequently applied sample preparation procedure in plant material analysis. The method is limited by the compound solubility in the specific solvent used, and hence the quality and quantity of the extracted mixture are determined by the type of extractant applied [3]. Although, the method is relatively simple and quite efficient, it suffers from such disadvantages as a long extraction time, relatively high solvent consumption and

\* Corresponding author. Tel.: +48 81 537 55 45; fax: +48 81 533 33 48.  
E-mail address: [dawid@hermes.umcs.lublin.pl](mailto:dawid@hermes.umcs.lublin.pl) (A.L. Dawidowicz).

often unsatisfactory reproducibility. Moreover, the extraction process, classically carried out in the Soxhlet apparatus, is not fully exploited as the temperature of the condensed solvent flowing into the thimble is lower than its boiling point [2].

Pressurized liquid extraction (PLE), a recently developed solvent extraction technique, could, in principle, eliminate some of the drawbacks of the Soxhlet and other classical solvent extraction methods [15]. Variations of temperature and pressure during the PLE process have an influence on the solubility behavior of the compounds. Furthermore, PLE, due to high pressure of the extraction process, allows using an extractant at a temperature above its normal boiling point and in consequence, to remove the analytes efficiently and quickly from various matrices [16].

*Thymus vulgaris* L. belongs to a wide range of herbs frequently examined for their essential oil amount and composition. It is because its specific antimicrobial, antioxidant and antifungal activity and flavor properties, aroma-active constituents have been widely applied, for instance as agreeable components in throat lozenges, dental hygiene products, mouthwashes, in topical skin creams and salves. The main aroma constituents of thyme essential oil are: thymol (20–80%), carvacrol (0.5–6%), *p*-cymene (9–43%), limonene (0.2–24%) and  $\gamma$ -terpinene (0–13%) [6,13,16–18].

The aim of this research was to determine the most efficient and low time consuming method for the extraction of the essential oil components from thyme herb. The five methods characterized above were compared in the present study with regard to the recovery of components which typically exist in essential oil obtained by steam distillation and with respect to relative composition of the aroma compounds. The fastest method revealing the greatest total amount of essential oil components was assumed as the most efficient one. Another aim was to find how some experimental variables of the least time consuming and the most efficient sample preparation method affect the yield of chosen essential oil components extracted from the thyme herb.

## 2. Experimental

### 2.1. Plant material

The thyme herb used for the experiments was cultivated in the eastern part of Poland. The whole plant was cut and air-dried before the leaves were separated from the branches. Immediately before each extraction, plant material was grounded and its exactly weighed portions were subjected to the sample preparation procedure.

In the presented experiments it was assumed that at least 0.5 g of plant material constitutes a representative sample.

### 2.2. Steam distillation

A sample of the thyme herb (10 g) was submitted to steam distillation process with 500 mL distilled water for 3 h using a Deryng-type apparatus. The measurements of the distillation time started after the falling of the first drop of distillate. The separated essential oil distillate was dried by freezing and, after filtration, stored at +8 °C until further experiments. The procedure was repeated three times, each time on a fresh portion of the thyme herb.

### 2.3. Soxhlet extraction

A 3 g sample of the thyme herb was extracted with 70 mL of *n*-hexane (POCH S.A., Gliwice, Poland) for 3 h in a Soxhlet apparatus. The extracts were stored at +8 °C until their analysis. Soxhlet

extractions were repeated three times on fresh portions of the material.

### 2.4. Supercritical fluid extraction (SFE)

The SFE extractions were performed using the equipment described in [19]. The extracts were collected in dichloromethane (2 mL) (Merck, Germany) placed in 4 mL vials. 0.5 g samples of thyme leaves were extracted. In all extractions CO<sub>2</sub> (SFE grade) was used with a flow rate of ca. 1.5 mL/min measured as a liquid. The influence of extraction pressure (at 60 or 80 °C) and extraction time on the extraction yield of all essential oil components was examined. Extraction time, pressure and temperature equal 20 min, 500 bar and 80 °C, respectively, were assumed as optimal SFE parameters for further experiments. All extractions were performed in triplicate.

### 2.5. Headspace solid-phase microextraction (SPME) procedure

A 30  $\mu$ m Carboxen-PDMS fibre (Supelco, Bellefonte, PA, USA) placed into a SPME holder for manual sampling was applied in the investigations. The fibre was conditioned according to the supplier's prescription. During the SPME extraction procedure the SPME fibre was introduced for 30 min into the thermostated vial (25 °C) containing 2.0 g of the dried foliage. The plant sample was closed tightly with a rubber seal in the vial for 24 h before extraction. After the SPME extraction process the fibre was immediately transferred into a GC injector port and the 2-min thermo-desorption process was carried out. The SPME procedure was repeated three times.

### 2.6. Pressurized liquid extraction (PLE)

PLE was performed with a Dionex ASE 200 instrument (Dionex, Sunnyvale, CA, USA). An exactly weighed portion of the plant material (0.5 g) was mixed with neutral glass, to reduce the volume of the solvent used for the extraction [20], and placed into a 22 mL stainless steel extraction cell. The influence of the following factors on extraction recovery was examined:

- extracting solvent type: *n*-hexane (POCH S.A., Gliwice, Poland), dichloromethane (Merck, Germany), ethyl acetate (POCH S.A., Gliwice, Poland) and distilled water;
- extraction temperature (in the range 20–175 °C) estimated for hexane and the extractant giving the best yield;
- extraction time (in the range 5–30 min) for hexane, the best extractant and temperature;
- extraction pressure (in the range 40–100 bar) for hexane, the best extractant, temperature and time.

After the extraction process, the extraction cell content was flushed using the same solvent in the amount equal to 100% of the extraction cell volume, and purged for 60 s applying pressurized nitrogen (150 psi). All extraction procedures were repeated three times.

### 2.7. SPE procedure for water extracts

All extracts, except water extracts, were directly analyzed by GC/MS. In the case of PLE water extracts, the essential oil components were re-extracted to hexane–ethyl acetate mixture (9:1) using SPE procedure described in [21].

**Table 1**  
Peak areas (in %) and total amounts (mg/g) of components estimated in thyme herb using Soxhlet extraction, PLE, SFE, steam distillation and SPME methods

No.	Compound	RI	Peak area (%)					Section
			Isolation method					
			Soxhlet	PLE	SFE	Steam distillation	SPME	
1	$\alpha$ -Thujene	924	0.3	0.1	0.2	0.4	0.5	
2	$\alpha$ -Pinene	931	0.2	0.1	0.1	0.2	0.5	
3	1-Octen-3-ol	979	0.4	0.4	0.4	0.2	0.2	
4	$\beta$ -Myrcene	990	0.7	0.4	0.3	0.6	0.9	
5	$\alpha$ -Terpinene	1015	0.8	0.5	0.4	0.5	0.7	
6	<i>p</i> -Cymene	1024	11.4	6.0	4.8	3.9	14.7	
7	Limonene	1027	0.2	0.2	0.1	0.2	2.2	
8	1,8-Cineole	1030	0.2	0.2	0.2	0.2	2.9	
9	$\gamma$ -Terpinene	1058	8.0	6.5	5.5	4.0	10.5	
10	<i>cis</i> -Sabinene hydrate	1066	0.8	1.0	1.2	0.8	2.2	
11	Linalool	1100	1.7	1.9	1.9	1.9	3.2	
12	Borneol	1167	0.4	0.5	0.6	0.6	1.5	
13	Terpineol-4	1178	0.2	0.2	0.2	0.5	1.2	
14	$\alpha$ -Terpineol	1193	–	–	0.1	–	–	
15	Thymol methyl ether	1235	0.3	0.4	0.5	0.4	1.1	A
16	Carvacrol methyl ether	1244	0.4	0.5	0.5	0.4	1.3	
17	Thymoquinone	1256	–	–	0.2	–	–	
18	Thymol	1302	68.2	72.1	75.3	77.8	48.5	
19	Carvacrol	1308	2.9	3.1	3.4	3.3	1.7	
20	Iso-ascaridol	1313	0.1	0.2	0.1	–	–	
21	$\beta$ -Caryophyllene	1420	1.9	2.4	2.7	2.8	6.2	
22	Geranyl <i>N</i> -propanoate	1475	–	2.1	0.1	–	–	
23	$\gamma$ -Muuroolene	1478	–	0.1	0.1	0.2	–	
24	$\gamma$ -Cadinene	1515	0.2	0.2	0.2	0.3	–	
25	$\delta$ -Cadinene	1525	–	0.2	0.3	0.4	–	
26	Caryophyllene oxide	1586	0.3	0.2	0.2	0.2	–	
27	$\tau$ -Cadinol	1644	0.1	0.2	0.2	0.2	–	
28	Phytol	2113	0.3	0.3	0.2	–	–	
	$\Sigma_A$ ( $\mu$ g/g)		9700 $\pm$ 26	14107 $\pm$ 4	13360 $\pm$ 28	10575 $\pm$ 22	–	
31	Unknown 1449	1449	1.4	0.1	2.9	–	–	
32	Unknown 1841	1841	–	–	–	–	–	
33	(2 <i>E</i> )-3,7,11,15-Tetramethyl-2-hexadecen-1-ol NIST	1884	–	0.2	–	–	–	
34	Heptakozane	2700	–	0.1	0.2	–	–	B
35	Nonakozane	2900	1.0	0.9	0.9	–	–	
36	Hentriakontane	3100	0.2	1.4	1.3	–	–	
37	Tritriakontane	3300	–	0.4	0.3	–	–	
	$\Sigma_B$ ( $\mu$ g/g)		254 $\pm$ 26	450 $\pm$ 10	788 $\pm$ 38	–	–	

## 2.8. Quantity standard solution

The amounts of essential oil components were expressed in two forms: as peak area percentage and/or in milligrams relating the peak area of a given component to the peak area of hexadecane, a known amount of which was added to the examined extracts before GC/MS measurements. For this purpose hexadecane (1 g) (Aldrich, Gillingham, UK) dissolved in *n*-heptane (50 ml) (Merck, Germany) was applied. Due to different extraction ability of the examined methods and due to different amount of plant materials used in examined procedures, the amount of added hexadecane solution was various. In each case the hexadecane solution was added in the amount giving hexadecane peak of height similar to the thymol peak.

## 2.9. GC/MS measurements

Soxhlet, SFE, SPME and PLE extracts and essential oil samples from Deryng apparatus were analyzed by the GC/MS system GCQ (Thermo-Finnigan, USA). The chromatograph injector was equipped with a Merlin Microseal Septum (Supelco, USA). RTx-5 fused-silica capillary column (20 m  $\times$  0.18 mm, 0.2  $\mu$ m) (Restek, USA) was used. Helium (grade 5.0) was used as carrier gas. A split-splitless injector was operated in the split mode 1:20 for all chromatographic runs. The injector's temperature was 280 °C. The

following temperature programmes were applied: 1 min at 50 °C and then a linear temperature increase up to 320 °C at the rate 10 °C/min for the Soxhlet, SFE, PLE and steam distillation extracts, and 8 °C/min for SPME extracts. The mass spectrometer was operated in EI mode at 70 eV; manifold temperature was 220 °C. The mass spectra were measured in the range 35–500 amu.

Qualitative analysis was carried out comparing the obtained MS spectra with the spectra from the libraries [NIST library and own library]. The presence of a given component was additionally confirmed by published and own temperature retention indexes.

## 3. Results and discussion

Table 1 lists peak area percentage for compounds contained in the thyme herb extracts obtained using the five examined sample preparation methods. As mentioned before, steam distillation is recommended by European Pharmacopoeia [4] as the isolation method for essential oils analysis with respect of their quality and quantity. In contrast to the liquid extraction process, which always depends on the solubility behavior of the components, only the steam-volatile ingredients of aromatic plants can be isolated during steam distillation. For this reason, Table 1 is divided into two sections. The components typically existing in essential oil from steam distillation are contained in section A. The other, non-volatile ones are grouped in section B. Table 1 contains also the total amounts

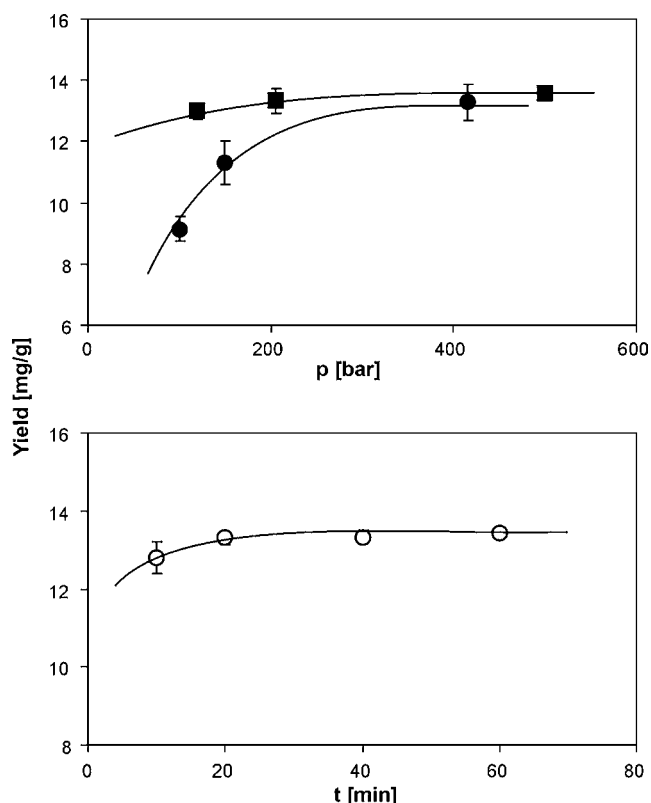


**Fig. 1.** The influence of extraction pressure [at 60 °C (●) or at 80 °C (■) and at time 40 min] and extraction time [at 80 °C (○) and at pressure 500 bar] on the yield of all essential oil components from thyme herb in SFE.

of constituents for part A ( $\Sigma_A$ ) and part B ( $\Sigma_B$ ). Their values were calculated in relation to the known amount of hexadecane added to extracts as a quantity standard. The table presents only the compounds for which the peak area exceeds 0.1% in chromatograms of the analyzed extracts. The PLE and SFE results were obtained in optimal extraction conditions established in preliminary studies – see Figs. 1 and 2, respectively. As appears from Fig. 1, the SFE process performed at 80 °C, at pressure above 200 bar and over time longer than 20 min yields maximal total amount of essential oil components from thyme herb. According to Fig. 2, extraction time 10 min, extraction temperature 100 °C and extraction pressure above 30 bar are the most optimal for the PLE process of essential oil components extracted by hexane. The SPME procedure was not optimized because its application for quantitative estimation of the total amount of essential oil components in plant matrices is complex and controversial.

As results from section A of Table 1, the relative composition (expressed by peak area percentage) of essential oil components from the thyme herb revealed by the applied methods varies. The observed discrepancies are connected with different extraction ability of the examined methods towards individual aroma compounds. The relative aroma composition estimated using the SPME procedure differs most from that gained by steam distillation. It is easily seen for the main components of thyme oil (see: thymol, carvacrol, *p*-cymene,  $\gamma$ -terpinene,  $\beta$ -caryophyllene), for which SPME reveals their significantly greater or significantly lower amounts in comparison to the data obtained from steam distillation. Moreover, low volatile components with retention indices above 1420, which exist in small amounts, are not detectable by SPME in the applied conditions. The observed distinction of the SPME data results both from the difference in the boiling point (vapor pressure) of essential oil compounds and from different sorption ability of the SPME

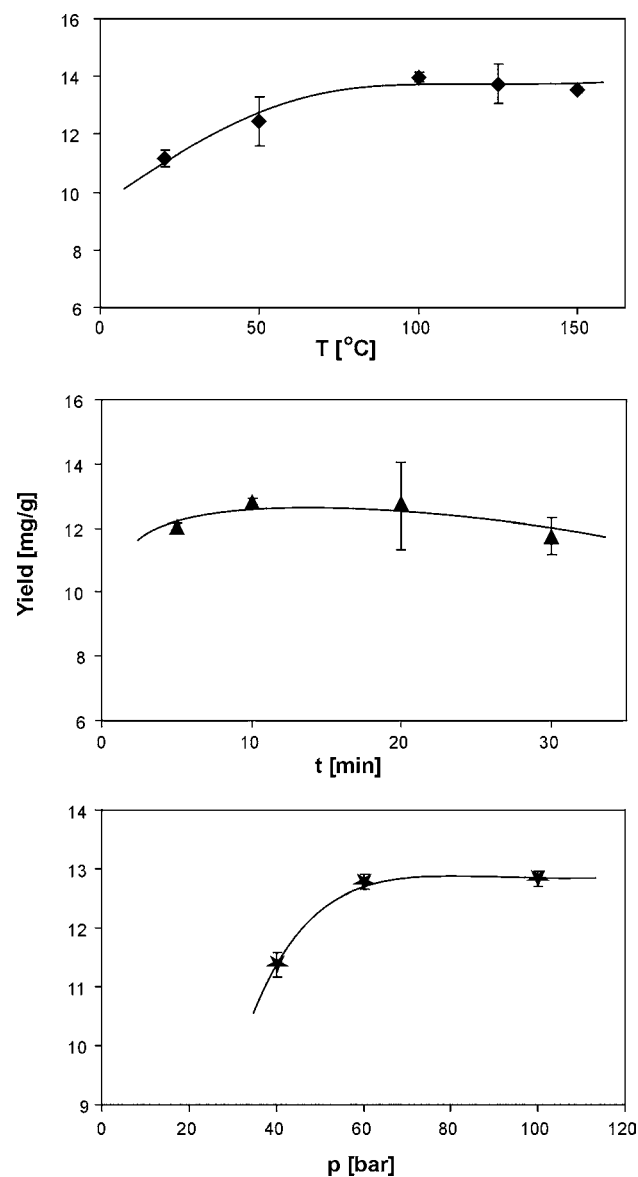


**Fig. 2.** The influence of extraction temperature (◆) (at pressure 60 bar and at time 10 min), extraction time (▲) (at temperature 100 °C and at pressure 60 bar) and extraction pressure (★) (at temperature 100 °C and at time 10 min) on the yield of all essential oil components from thyme herb in PLE. Extracting agent—hexane.

fibre towards individual components. It is obvious that the application of other SPME fibre (i.e. PDMS) would give relative aroma composition more similar to that obtained by steam distillation; however, the application of optimized SPME procedure was not the aim of these experiments. Considering the results for other extraction methods (in Soxhlet apparatus, PLE, SFE) there is no significant variation in the relative composition of the essential oil components from the thyme herb, except for *p*-cymene and  $\gamma$ -terpinene. The greatest peak area percentages of those two compounds are revealed by means of extraction in the Soxhlet apparatus. As results from Table 1 (section A), the quantitative aroma-active composition most similar to standard oil composition (from steam distillation) is demonstrated by SFE, whereas slightly lesser similarity is observed in the case of PLE. Greater variations among the examined methods are seen for the data presented in section B of Table 1, which shows not only the quantitative but also qualitative differences in the composition of non-essential oil compounds.



**Table 2**  
Comparison of extraction time, sample mass and solvent volume applied in Soxhlet, PLE, SFE, steam distillation, SPME processes

Parameter	Sample preparation method				
	Steam distillation	Soxhlet	PLE	SFE	SPME
Amount of sample (g)	10.0	3.0	0.5	0.5	2.0
Time of procedure (min)	180	180	10	20	30
Volume of solvent used (mL)	500	70	38	40	–
Extraction temperature (°C)	100	70	100	80	25
Extraction pressure (bar)	Atmospheric	Atmospheric	60	200	Atmospheric
Yield (µg/g)	10575 ± 22	9700 ± 26	14107 ± 4	13360 ± 28	–

As mentioned in Section 1, the aim of the experiments was to establish the most suitable, efficient and the least time consuming sample preparation method for the estimation of the essential oil composition from the thyme herb.

According to [8], SPME is the shortest and the most useful sample preparation method for the estimation of essential oil components in aroma herbs, including thyme. Yet the diagrams presented in [8] confirm the significant differences in the peak area percentage for aroma components observed in the present study, when SPME and steam distillation methods were compared. In addition, for less volatile components more time is required for reaching equilibrium between the phases in the SPME procedure. In consequence, the total analysis time increases. The tempera-

ture growth of the SPME process shortens the time required for reaching equilibrium but usually it leads to a loss of highly volatile compounds. Moreover, the SPME method is not recommended for direct quantification of individual aroma components and it does not allow for estimation of total amount of essential oil components (expressed as a sum of particular compound amounts). Taking into account these factors and the values comparing some practical extraction parameters (see Table 2), PLE seems to be a more appropriate the thyme herb sample preparation procedure than SPME for the analysis of essential oil components. The relative composition of essential oil components revealed by PLE is close to that estimated by steam distillation. Furthermore, PLE is characterized by a very short extraction time and shows the highest extrac-

**Table 3**  
Peak areas (in %) and total amounts (mg/g) of components estimated in thyme herb employing hexane, ethyl acetate, dichloromethane and water in PLE

No.	Compound	RI	Peak area (mg/g)				Section
			Extrahent type				
			Hexane	Ethyl acetate	Dichloromethane	Water	
1	α-Thujene	924	0.1	0.2	0.2	–	
2	α-Pinene	931	0.1	0.1	0.2	–	
3	1-Octen-3-ol	979	0.4	0.3	0.3	1.0	
4	β-Myrcene	990	0.4	0.5	0.4	–	
5	α-Terpinene	1015	0.5	0.5	0.5	0.1	
6	p-Cymene	1024	6.0	6.5	6.5	1.1	
7	Limonene	1027	0.2	1.0	0.2	–	
8	1,8-Cineole	1030	0.2	0.2	0.2	0.4	
9	γ-Terpinene	1058	6.5	6.6	6.4	0.3	
10	cis-Sabinene hydrate	1066	1.0	1.0	1.0	0.6	
11	Linalool	1100	1.9	1.8	1.8	2.8	
12	Borneol	1167	0.5	0.5	0.6	0.7	
13	Terpineol-4	1178	0.2	0.2	0.2	0.7	
14	α-Terpineol	1193	–	0.1	0.1	0.3	
15	Thymol methyl ether	1235	0.4	0.5	0.4	0.1	A
16	Carvacrol methyl ether	1244	0.5	0.4	0.4	–	
17	Thymoquinone	1256	–	0.2	0.3	0.2	
18	Thymol	1302	72.1	72.5	72.8	88.0	
19	Carvacrol	1308	3.1	3.1	3.2	3.6	
20	Iso-ascaridol	1313	0.2	0.1	0.2	–	
21	β-Caryophyllene	1420	2.4	2.4	2.5	–	
22	Geranyl N-propanoate	1475	2.1	0.1	0.1	–	
23	γ-Murolene	1478	0.1	0.1	0.1	–	
24	γ-Cadinene	1515	0.2	0.1	0.2	–	
25	δ-Cadinene	1525	0.2	0.2	0.3	–	
26	Caryophyllene oxide	1586	0.2	0.3	0.3	0.1	
27	τ-Cadinol	1644	0.2	0.2	0.2	–	
28	Phytol	2113	0.3	0.3	0.4	–	
	Σ <sub>A</sub> (µg/g)		14107 ± 4	16066 ± 4	14242 ± 9	7607 ± 21	
29	Unknown 1449	1449	2.0	2.0	3.2	0.2	
30	Unknown 1841	1841	0.2	1.2	0.4	–	
31	(2E)-3,7,11,15-Tetramethyl-2-hexadecen-1-ol NIST	1884	0.1	0.3	0.1	–	
32	Heptakozane	2700	0.1	0.2	0.2	0.2	B
33	Nonakozane	2900	0.9	1.7	1.5	0.1	
34	Hentriakontane	3100	1.4	2.9	1.9	–	
35	Tritriakontane	3300	0.4	0.8	0.3	–	
	Σ <sub>B</sub> (µg/g)		738 ± 10	1585 ± 8	1168 ± 28	9 ± 14	

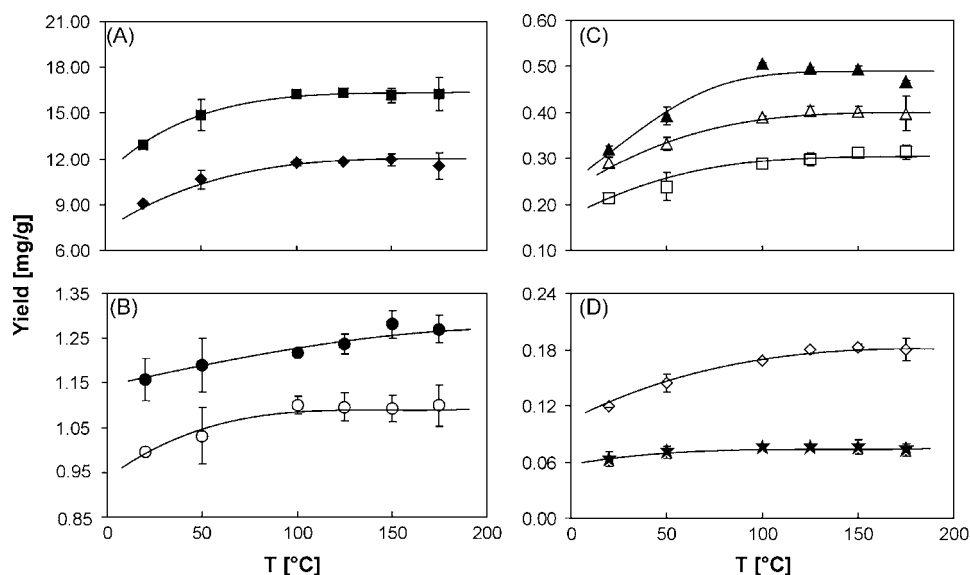


**Fig. 3.** The influence of extraction temperature on the extraction yield of all (■) and of the most representative essential oil components from the thyme herb (◆: thymol, ●: *p*-cymene, ○:  $\gamma$ -terpinene, ◇: *cis*-sabinene hydrate, ▲: carvacrol, □:  $\beta$ -linalol, △:  $\alpha$ -caryophyllene, ★: limonene) in PLE. Extracting agent—ethyl acetate.

tion efficiency towards essential oil components (see section A of Table 1).

SFE, in comparison to PLE, demonstrates a similar amount of essential oil components from the thyme herb, however, its optimal extraction time is longer and the result is characterized by greater standard deviation.

The PLE data presented in Table 1 were obtained using *n*-hexane, which is most often employed as extracting solvent in liquid extraction processes of essential oil components from herbs [2,21]. Hexane, due to its physicochemical character, exhibits the highest extraction power towards non-polar compounds. As results from Table 1, essential oil components from the thyme herb consists not only of non-polar but also of semi-polar components. For this reason it is advisable to estimate the extraction ability of both semi-polar and polar solvents in the PLE process of the herb.

Table 3 lists data for PLE extracts obtained from thyme herbs using ethyl acetate, dichloromethane and water. For convenience and better comparison of the results the PLE data for hexane are repeated. Analyzing the results from section A of Table 3, one observes no significant differences in the relative composition of extracts obtained using non-polar (hexane) and semi-polar (ethyl acetate, dichloromethane) solvents. The lack of difference is especially evident for the main components of thyme oil (thymol, *p*-cymene,  $\gamma$ -terpinene and carvacrol). Quite a different picture is observed for water extract. The number of essential oil components extracted by this solvent is lower. Moreover, in comparison to other extrahents applied, the total amount of essential oil components extracted by water is extremely low (see  $\Sigma_A$ ) and the relative composition of the extracted components is quite different. According to the data from Table 3 (section A), ethyl acetate exhibits the high-

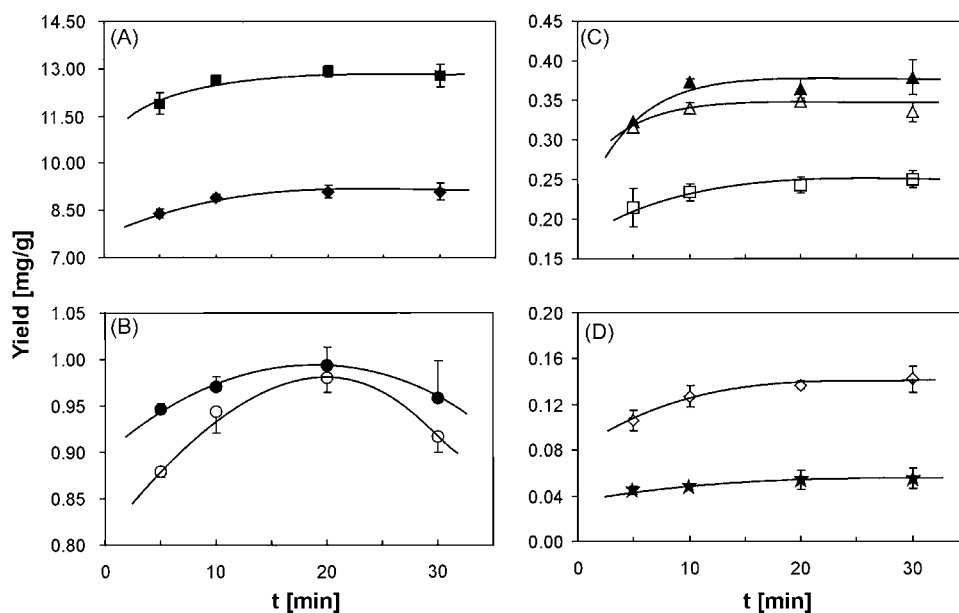


**Fig. 4.** The influence of static extraction time on the extraction yield of all (■) and of the most representative essential oil components from thyme herb (◆: thymol, ●: *p*-cymene, ○:  $\gamma$ -terpinene, ◇: *cis*-sabinene hydrate, ▲: carvacrol, □:  $\beta$ -linalol, △:  $\alpha$ -caryophyllene, ★: limonene) in PLE. Extracting agent—ethyl acetate.

est extraction power towards essential oil components from the thyme herb.

As to non-essential oil components (see section B of Table 3), the difference in the extraction ability of individual extrahents used is not very pronounced. Like in volatile components, the greatest extraction power towards non-volatile ingredients is exhibited by ethyl acetate (see total amount of extracted components in section B).

The PLE results presented in Tables 1 and 3 were obtained in conditions optimal for extraction of essential oil components using hexane. These conditions prove to be in agreement with default PLE extraction conditions (i.e. extraction time – 10 min; extraction temperature – 100 °C; extraction pressure – 60 bar) and can be inappropriate in the case of ethyl acetate which shows greater extraction ability towards essential oil components from thyme herb. Figs. 3 and 4 show the influence of extraction temperature and time, respectively, on the total amounts of essential oil components and on the yield of some individual components from the thyme herb extracted by ethyl acetate. As seen in Fig. 3, the temperature increase causes a similar change of the extraction efficiency for all the considered components. At the temperature range up to 100 °C the growth of the extraction efficiency with the temperature increase is observed. Above this temperature the extraction yields are almost constant, although small variations can be seen. Only for *p*-cymene the yield vs. temperature dependence increases in wider temperature range.

The shape of the dependences in Fig. 4 is similar to that in Fig. 3. The plots show, however, that the change in the extraction time is accompanied by a small increase in extraction efficiency. For almost all components the equilibrium is reached after 10 min. A different run of this dependence is seen for  $\gamma$ -terpinene and *p*-cymene because longer extraction time results in the decrease of their yield.

The results showing the influence of extraction pressure on the yield of chosen essential oil components are not presented due to negligible influence of this parameter on the PLE process in the range above 60 bar.

As appears from the presented relationships, in the case of the thyme herb, the optimization procedure of the PLE process is not required. The highest extraction yields of essential oil components are gained in the default conditions.

#### 4. Conclusions

Considering all the presented results, PLE seems to be the most efficient and the most appropriate sample preparation method

in determining essential oil compounds from the thyme herb. Although co-extraction of non-volatile components is the main drawback of this method, it is characterized by the highest yield of essential oil components and the shortest extraction time required. As results from the presented data, the default PLE conditions are optimal for the thyme herb. Thus, the PLE optimization procedure can be avoided, which is an extra advantage of the method application in the case of the examined herb. Recently headspace SPME has been recommended for estimation of essential oil components in aroma herbs, including thyme, due to its short extraction time and no need for solvent in the SPME process, which warrants the absence of non-aroma compounds in SPME fibre [8,9]. It should be stressed, however, that the essential oil composition estimated by means of SPME is very different from that for steam distillation and the application of SPME for quantitative estimation of the total amount of essential oil components in plant matrices is complex. Hence, from among the examined methods, PLE is the best alternative technique to the standard method of steam distillation.

#### References

- [1] M.D. Luque de Castro, M.M. Jiménez-Carmona, V. Fernández-Pérez, Trends Food Sci. Technol. 18 (1999) 708–716.
- [2] L. Wang, C.L. Weller, Trends Food Sci. Technol. 17 (2006) 300–312.
- [3] G. Romanik, E. Gilgenast, A. Przyjazny, M. Kamiński, J. Biochem. Biophys. Methods 70 (2007) 253–261.
- [4] European Pharmacopoeia, 3rd ed., 1997 (Ph. Eur. 1997).
- [5] M.M. Jimenez-Carmona, J.L. Uebera, M.D. Luque de Castro, J. Chromatogr. A 855 (1999) 625–632.
- [6] B. Nickavar, F. Mojab, R. Dolat-Abadi, Food Chem. 90 (2005) 609–611.
- [7] P. López, M.A. Huerga, R. Batlle, C. Nerin, Anal. Chim. Acta 559 (2006) 97–104.
- [8] J. Richter, I. Schellenberg, Anal. Bioanal. Chem. 387 (2007) 2207–2217.
- [9] E.E. Stashenko, J.R. Martínez, J. Biochem. Biophys. Methods 70 (2007) 235–242.
- [10] S.M. Pourmortazavi, S.S. Hajimirsadeghi, J. Chromatogr. A 1163 (2007) 2–24.
- [11] M. Moldao-Martins, A. Palavra, M.L. Beirao da Costa, M.G. Bernardo-Gil, J. Supercrit. Fluids 18 (2000) 25–34.
- [12] Q. Lang, C.M. Wai, Talanta 53 (2001) 771–782.
- [13] R.M. Smith, J. Chromatogr. A 856 (1999) 83–115.
- [14] E. Reverchon, I. De Marco, J. Supercrit. Fluids 38 (2006) 146–166.
- [15] B. Benthin, H. Danz, M. Hamburger, J. Chromatogr. A 837 (1999) 211–219.
- [16] R. Carabias-Martínez, E. Rodríguez-Gonzalo, P. Revilla-Ruiz, J. Hernández-Méndez, J. Chromatogr. A 1089 (2005) 1–17.
- [17] C. Blum, K. Kubeczka, K. Becker, J. Chromatogr. A 773 (1997) 377–380.
- [18] S.-J. Lee, K. Umano, T. Shibamoto, K.-G. Lee, Food Chem. 91 (2005) 131–137.
- [19] J. Gawdzik, M. Mardarowicz, Z. Suprynowicz, J. High Resol. Chromatogr. 19 (1996) 237–240.
- [20] ASE 200 Accelerated Solvent Extractor Operator's Manual, Document No. 031149, Revision 01, Dionex, Sunnyvale, CA, 1995, Sect. 3–5.
- [21] M.Z. Ozel, H. Kaymaz, Anal. Bioanal. Chem. 379 (2004) 1127–1133.



## Variable incidence angle X-ray absorption fine structure spectroscopy: A zirconia film study

Claude Degueldre<sup>a,\*</sup>, Michael Kastoryano<sup>a</sup>,  
Kathy Dardenne<sup>b</sup>

<sup>a</sup> LWV, Paul Scherrer Institut, 5232 Villigen-PSI, Switzerland

<sup>b</sup> INE, Karlsruhe Forschungszentrum, PoB 3640, 76021 Karlsruhe, Germany

### ARTICLE INFO

#### Article history:

Received 5 September 2007

Received in revised form 1 April 2008

Accepted 7 April 2008

Available online 26 April 2008

#### Keywords:

X-ray absorption  
Zirconium monoxide  
Zirconium dioxide  
Film  
Variable incidence

### ABSTRACT

Variable incidence angle X-ray absorption fine structure (VIAXAFS) spectroscopy offers a non-destructive ability to investigate film nano-structures. This technique was applied, spanning sample-beam angles from a grazing to normal incidence on a film obtained by zirconia sputtering on flat sample of stainless steel. X-ray absorption fine structure analysis on the Zr K edge identified chemical, defects and fractal structures through the film depth. VIAXAFS revealed occurrence of zirconium monoxide fractions at the surface a reduced state of zirconium oxide vs. the zirconium dioxide bulk. The discussion underlines that the technique may quantify the profile of various sub-layers, nano-pores, dislocations, vacancies or defect features.

© 2008 Elsevier B.V. All rights reserved.

### 1. Introduction

There is a need to study depth profile at the atomic level of films in a non-destructive way. For this purpose X-ray absorption spectroscopy has a potential that can be exploited. One promising technique is to apply variable incidence angle X-ray absorption fine structure (VIAXAFS) methodology. This requires, however, to apply the methodology for photon self-absorption in the film as well as use the VIAXAFS approach. The mathematical analysis developed earlier by the author [1] was inspired from previous work on self-absorption correction by Booth and Bridges [2] and Tröger et al. [3], it was, however, completed for quantitative calculation of the absorption features. The film depth profile may be evaluated for nano-structures, and atom environment.

Thin films are widely used in today's technology, among them zirconia stabilized, monoclinic or amorphous are applied as coating in semiconductor sciences [4,5], thermal coating barriers [6,7], inert layers or protective layers [8], membranes [9] for ultrafiltration [10] electrophoresis [11] and fuel membrane [12]. The thermal conductivity that makes the attractiveness of zirconia coating films is driven by phonon transport, which is primarily a function of varying pore and distortion densities in the film [13]. These underlined

applications render the study of zirconia layers of great interest particularly with regard to its behaviour at the atomic level.

The zirconia films may include distortions, dislocations and/or nano-pores as well as zirconia reduction which modify the Zr environment. Their structural analysis to extract statistically representative microstructure information (e.g., void volume fraction size distributions, internal surface areas, pore morphologies) and chemical phases features includes X-ray diffraction, e.g. [14], X-ray tomography [15], small angle X-ray and neutron scattering [16]. The later complements the information obtained from diffraction methods, X-ray microtomography, or electron microscopy and small angle neutron scattering, however, being limited at 1.0–0.5 nm size.

It has been shown that X-ray absorption studies provide insights, not obtainable by other means, on the processing–microstructure–property relationships that frequently govern technological performance, e.g. [17]. The influence of oxygen deficiency on the electronic and local structure of monoclinic zirconia has recently been examined and compared to the cubic stabilized sample in X-ray absorption fine structure (XAFS) studies, e.g. [18,19]. In this study the VIAXAFS analysis has been tested on a zirconia film obtained by sputtering, thereby complementing a recent study of the films by grazing incidence–XAFS [20]. In this study the VIAXAS technique was applied, shifting angles from a grazing to normal incidence on films obtained by zirconia sputtering on stainless steel.

\* Corresponding author. Tel.: +41 56 3104176; fax: +41 56 3102203.  
E-mail address: [claude.degueldre@psi.ch](mailto:claude.degueldre@psi.ch) (C. Degueldre).

## 2. Theoretical background

The bases underlying the VIAXAFS method are summarised below. The author revisited recently the theory applied to VIAXAFS [1]. A general expression was obtained for the fluorescence yield intensity reaching the detector for a given incidence angle (with  $\varphi$  the incident angle and  $\theta$  the detection angle). The penetration depth of the incoming beam follows an inverse exponential law known as Lambert's law defining  $\mu_T$  the energy ( $E$ ) dependant coefficient of absorption. The absorption edge energy is evaluated from the maximum of the first derivative of the absorption:  $(\delta\mu(E)/\delta E)=0$  for  $E=E_0$ .

The spectra are normalized, and, the normalized absorption data ( $\chi$ ) are given by  $\chi=(\mu-\mu_0)/\mu_0$  where  $\mu_0$  is the so-called spline function corresponding to the absorption without the fine structures. The  $\chi$ -spectrum is a normalized extended X-ray-absorption fine structure (EXAFS) spectrum whose energy dependence is expressed in the transformed  $k$  scale ( $k=\sqrt{2m_e/h^2(E-E_0)}$ ), with  $m_e$  the electron mass,  $h$  the Boltzmann constant and  $E_0$  the edge energy. The  $\chi$ -spectra are further  $k^3$  weighted in order to develop relevant features at higher  $k$  values.

The experimental normalized absorption factor ( $\chi$ ) for the target depth ( $x$ ) region ( $x; x+\Delta$ ) was then derived as a function of the  $\chi$ -data from the spectra at of the two successive angles ( $\varphi; \varphi+\delta\varphi$ ) spanning the target region, and additionally the self-absorption was accounted for in a quasi-exact formulation of the  $\chi$ -factor the experimental data as reported by [2]. The incoming X-ray beam being of constant intensity, its penetration depth is always the same on a given sample [3].

The goal of the VIAXAFS method is to express the absorption spectrum as a function of the sample depth. The procedure consists of "subtracting" from the spectrum of penetration depth  $x+\Delta x$  the information from the spectrum of penetration depth  $x$ .

## 3. Experimental

The studied samples consisted of one pure Zr film (reference) as well as zirconia samples. As a reference, a ZrO<sub>2</sub> monoclinic powder (Fluka Proanalysis, monoclinic) was mixed with polyethylene (PE) and pressed into a pellet. A zirconium monoxide (ZrO 99.3% with 1% Hf, 550 ppm Ti from Umicore) was also used as reference. A zirconia film of 1  $\mu$ m thickness was obtained by sputtering on a 1.0 cm  $\times$  4.2 cm flat stainless steel (SS) piece (1  $\mu$ m ZrO<sub>2</sub>/SS) as described by Scardi et al. [8]. The 1  $\mu$ m ZrO<sub>2</sub>/SS sample shows sub-micrometer grains on top of a rather flat surface as observed with the optical microscope. The SEM pictures reveal similar features

(Fig. 1a and b). The larger grains reach the  $\mu$ m in size while a large proportion forming the film surface ranges apparently from 0.1 to 0.5  $\mu$ m. Some holes ( $\mu$ m in size) are locally observed.

The Zr K X-ray absorption spectra were recorded at the ANKA-INE beam line at the Forschungszentrum Karlsruhe, Germany. The ANKA storage ring was operated at 2.5 GeV electron energy with a mean electron current of 120 mA. The design of the beamline is multi-purposed, allowing for a number of different X-ray spectroscopic methods and their associated  $\mu$ -techniques. VIAXAFS was applied on this facility because it completes the Grazing incidence XAFS methodology applied on this line.

The line uses a Lemonnier-type double crystal X-ray monochromator. The photon energies spanned by the monochromator range from 2475 to 23,220 eV, and the beam focus has roughly a 1 mm<sup>2</sup> cross-section with sealed media feed-through chicanes and separate ventilation/filter system for the experimental hut. The detector is a 5-pixel low energy fluorescence germanium solid-state detector (Canberra-Packard Ultra-LEGe) capable as well of studying dilute samples and GI-XAFS. All measurements were recorded at room temperature. The reference sample spectrum was recorded in transmission mode while film samples spectra were taken in a grazing and variable incidence angle (GI-VIA) geometry with fluorescence detection mode. The two setups include a high precision goniometre ( $\pm 0.01^\circ$ ) for the angles 0–3° and a goniometre with  $\pm 0.2^\circ$  precision for the large angles (0–90°). The ZrO<sub>2</sub> film was measured without further preparation at angles of 0.25, 0.50, 1.5, 5, 30, 45 and 60°.

Three Ar-filled ionization chambers at ambient pressure were used for simultaneous detection of the transmission signals of the ZrO<sub>2</sub> (monoclinic) sample and a Zr metal reference foil for energy calibration. The 1st ionization energy of Zr<sup>0</sup> (17,998 eV) [21] was taken at the first inflection point in the spectrum of Zr metal. Spectra were recorded at a 4 eV step-width in the pre-edge region (17,850–17,980 eV), 1 eV at the rising edge (17,981–18,100 eV), 2 eV above the edge (18,101–18,250 eV) and equidistant  $k$ -steps (0.04  $\text{\AA}^{-1}$ ) in the EXAFS region (18,250–19,000 eV). The intensity of the monitor ionization chamber was held constant during each scan by means of a piezo-driven feedback to the second crystal (MOSTAB). The parallel alignment of the reflecting crystal faces was detuned to  $\sim 70\%$  of the maximum beam intensity. The beam-detector geometry was set up with fixed angles and  $\varphi+\theta=90^\circ$ .

FEFF8 calculates extended X-ray-absorption fine structure, X-ray-absorption near edge structure (XANES), using an ab initio self-consistent real space multiple scattering approach for clusters of atoms ( $Z<99$ ), including polarization dependence, e.g. see Ankudinov and Rehr [22,23]. Calculations are based on an all-electron, real space relativistic Green's function formalism with no symmetry requirements. The method combines both full multiple

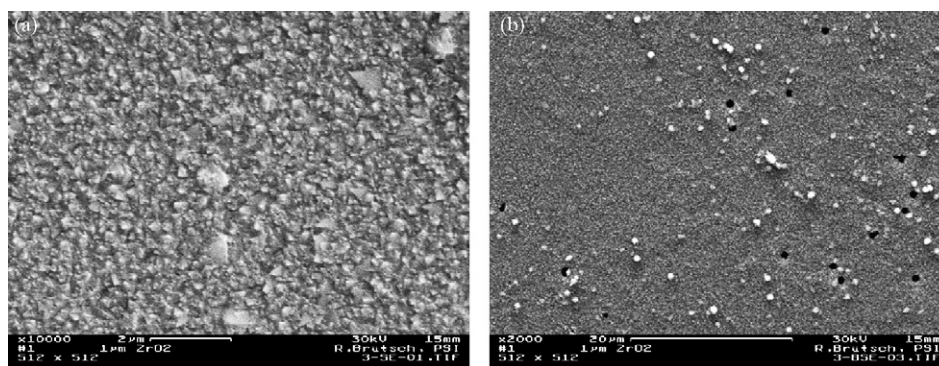


Fig. 1. (a) 1  $\mu$ m ZrO<sub>2</sub>/SS sample, 10,000 $\times$  SEM zoom, 2  $\mu$ m scale; (b) 1  $\mu$ m ZrO<sub>2</sub>/SS sample, 2000 $\times$  SEM zoom, 20  $\mu$ m scale.

scattering based on LU or Lanczos algorithms and a high-order path expansion based on the Rehr–Albers multiple scattering formalism. Calculation of the X-ray elastic scattering amplitude ( $f$ ) is performed using the ATOMS program to provide the crystallographic functionality for the X-ray absorption spectroscopy. Its primary function is to generate input files for the FEFF8 from crystallographic data (e.g. Tables 1a and 1b).

#### 4. Results and discussion

First the theoretical spectrum of monoclinic zirconia was generated by FEFF8, using input from ATOMS and data from Tables 1a and 1b. The  $1\ \mu\text{m}$   $\text{ZrO}_2/\text{SS}$  sample is presumed to be composed of only monoclinic zirconium. Both XANES and EXAFS results are discussed in a comparative way in this section using current methodology of Gualtieri et al. [24]. At the zirconium K-edge energy, the X-ray beam passes straight through the stainless steel bed of the sample. The GI-XAFS result confirms what has been observed earlier by the author, see Degueldre and Dardenne [20]. The spectra as well as the first derivative of the spectra recorded for increasing incident angles compared with the spectra of the reference materials, i.e. Zr, ZrO and  $\text{ZrO}_2$ , are presented in Fig. 2.

Clearly the spectra show a shift towards higher energy when increasing the incident angle. Analysis of this shift using the derived data reveals that this shift may be due to the existence of another zirconium oxide species located at the very surface of the film. The apparent  $E_0$  was calculated using the two polynomial fits (1st degree, 2nd degree), and the apparent  $E_0$  values were determined by derivative tests. The apparent values of  $E_0$  gained for increasing incident angles and for Zr, ZrO and  $\text{ZrO}_2$ , are given in Tables 2a and 2b.

The normalized absorption spectra are derived for the sample at various angles. Comparison between the spectra at grazing

**Table 1a**  
Crystal structure data for  $m\text{-ZrO}_2$

Space gr.	$P2_1/c$
$a$ [pm]	514.6
$b$ [pm]	521.3
$c$ [pm]	531.1
$\alpha^\circ$	90.00
$\beta^\circ$	99.23
$\gamma^\circ$	90.00

**Table 1b**  
Atomic coordinates for  $m\text{-ZrO}_2$

Atom sites	Fractional coordinate
$x_{\text{Zr}}$	0.276
$y_{\text{Zr}}$	0.041
$z_{\text{Zr}}$	0.208
$x_{\text{O}1}$	0.070
$y_{\text{O}1}$	0.336
$z_{\text{O}1}$	0.341
$x_{\text{O}2}$	0.442
$y_{\text{O}2}$	0.755
$z_{\text{O}2}$	0.479

**Table 2a**  
Apparent  $E_0$  values measured for Zr, ZrO and  $\text{ZrO}_2$

Phase	$E_0$ (keV)	
Zr	17.9984	18.0085
ZrO	18.0016	18.0096
$\text{ZrO}_2$	(18.0036)	18.0145

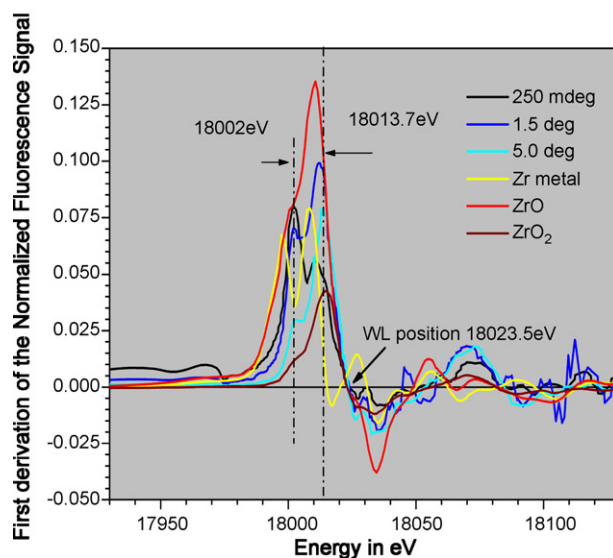
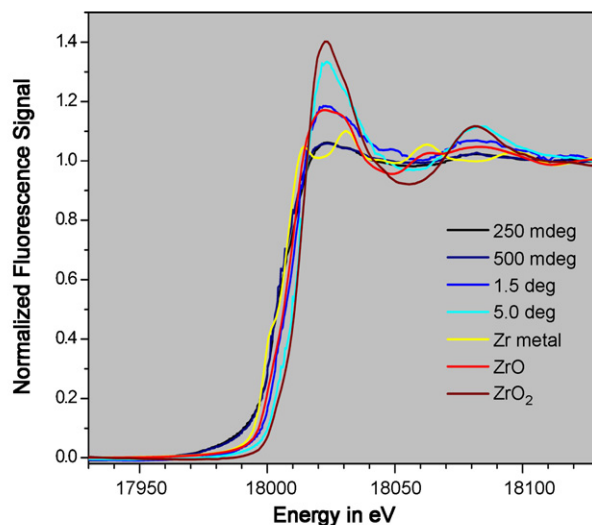


**Fig. 2.**  $1\ \mu\text{m}$   $\text{ZrO}_2/\text{SS}$  normalized XAFS spectra and the derivative for shallow incident angles and for Zr, ZrO and  $\text{ZrO}_2$  as reference materials; WL stands for white line.

incidence and those at higher incidence angles on the three samples indicates a clear evolution of the “white” line, which is much stronger at larger angles. As can be seen in the SEM images (Fig. 1a and b), the sample shows imperfections on the surface. Due to the surface heterogeneities, some of the absorbing atoms will not have the same number of next neighbours as the atoms within the sample. Thus, for very small incidence angles, the XAFS spectra resemble more the spline absorption spectrum of the surface material.

**Table 2b**  
Apparent  $E_0$  values measured for incident angles  $\varphi$

$\varphi$ ( $^\circ$ )	$E_0$ (keV)	
0.25	18.002	18.007
0.50	18.002	18.007
1.5	18.002	18.012
5.0	(18.002)	18.013
30	–	18.015
45	–	18.015
60	–	18.014

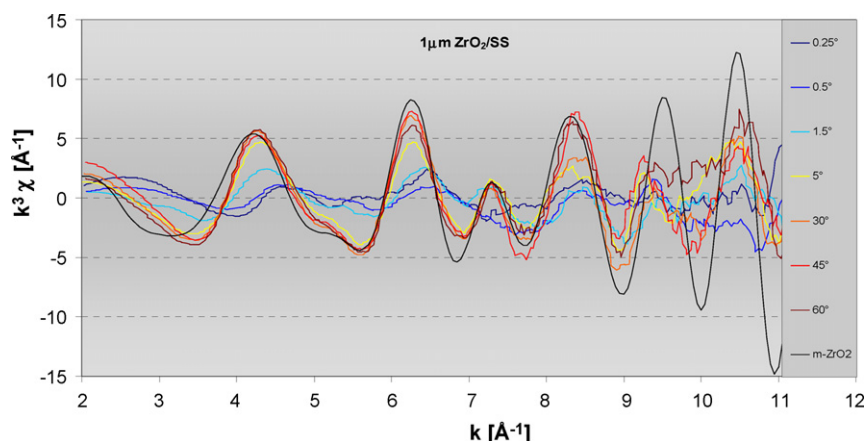


Fig. 3.  $1\ \mu\text{m}\ \text{ZrO}_2/\text{SS}$  normalized EXAFS spectra recorded for the incident angles and compared to the theoretical monoclinic zirconia spectrum.

Information about many different material properties of a given sample can be extracted from the  $\chi$ -spectra by comparing it with theoretical spectra of known materials generated by FEFF simulation. In order to emphasize the fluctuations occurring at large  $k$  ( $k > 5\ \text{\AA}^{-1}$ ), the normalized spectra was weighted by a factor of  $k^3$ . The  $1\ \mu\text{m}\ \text{ZrO}_2/\text{SS}$  sample is presumed to contain only marginal traces of materials other than pure monoclinic zirconia, thus their spectra should resemble quite closely the black curve in Fig. 3. The extrapolated values of apparent  $E_0$  summarized in Table 2b for the various measured angles were used to calculate the spectra. Fig. 3 depicts the  $\chi$ -spectra at various angles for the zirconia sample.

The  $1\ \mu\text{m}\ \text{ZrO}_2/\text{SS}$  sample exhibits quite clearly the effects of GI measurement. At incidence angles greater than  $\sim 1.5^\circ$  – where the absorption in the sample is less than 90% – the spectra look very much like the theoretical monoclinic zirconia, although there is a very slight shift at the first maximum. At lower incidence angle, the spectra are increasingly dampened and noisy, while their extrema are shifted to the right. In other words, for small incidence angles, the apparent  $E_0$  decreases, as can be seen in Table 2b. The data for this sample shows a rather good signal to noise ratio up to fairly high  $k$  ( $\sim 10\ \text{\AA}^{-1}$ ).

The major work of this study consisted of modeling the spline functions for the different values of the spline absorption coefficients and intensities used when handling the data. For a uniform ideal sample of a given material, the absorption coefficient is assumed to remain constant regardless of

the incidence angle of the X-ray beam. With some materials for which absorption coefficients have similar magnitudes, the self-absorption correction has to be operated in order to compensate for the damping of the signal amplitude. However, the samples being studied in VIAXAFS will generally not have a uniform absorption coefficient throughout, so the depth evolution of the spline absorption functions has to be accounted for.

For the  $1\ \mu\text{m}\ \text{ZrO}_2/\text{SS}$  sample, the depth evolution is only dependant on the density of the material, so the absorption coefficients can be written as:  $\mu(x) = \rho(x)\mu$ . The purpose of the VIAXAFS method is also to model the  $\rho$  factor for the sample under investigation. The constant  $\rho$  that was used was a weighted average of  $\rho(x)$  for the target depth  $x$ . This approximation is adequate as long as the density/depth evolution is not too irregular and sharp. With the  $1\ \mu\text{m}\ \text{ZrO}_2/\text{SS}$ , for example, as can be seen in Figs. 3 and 4 (blue spectra), the surface shows shifts, weaker waves and random irregularities, and a regular increase in sample density as the sample depth  $x$  increases is observed. The values for the spline absorption coefficients were extrapolated from virtual tables of material X-ray properties [21].

The spectra in Fig. 4 resemble those in Fig. 3. However, there are a few minor differences that are worth pointing out. First of all, the extrapolated spectrum between  $0.14$  and  $0.26\ \mu\text{m}$  is inconclusive. The traditional fluorescence spectrum ( $0.00$ – $1.00\ \mu\text{m}$ ) has a first peak that is unaligned with the theoretical monoclinic zir-

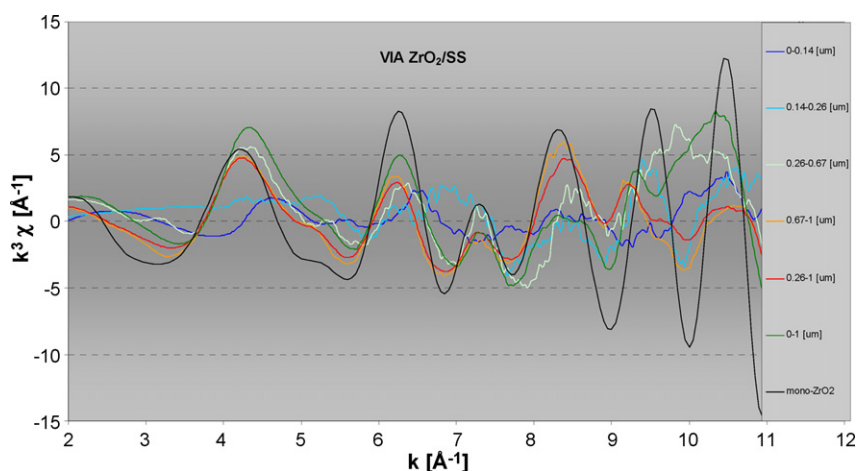


Fig. 4. Trend of the EXAFS spectra of the  $1\ \mu\text{m}\ \text{ZrO}_2/\text{SS}$  sample evaluated for various depths and compared with the theoretical monoclinic zirconia spectrum.

conia spectrum, and goes astray from the theoretical spectrum as of  $k = 8 \text{ \AA}^{-1}$ . Both of these effects are due to the influence on the spectrum of the zirconia fragments at the sample surface causing a reduction in density.

Layer subtraction by VIAXAFS data treatment was however successful for describing the film regions and the following may be noted.

For the depths 0–0.14  $\mu\text{m}$  the surface species are not identified to be pure zirconium dioxide, the surface species which corresponds to an  $E_0$  10 eV lower than zirconium dioxide is suggested to be made of zirconium monoxide, corresponding to the  $E_0$  shift. This material implies also a lower white line and a lower coordination number with oxygen decreasing the amplitude of the EXAFS signal.

For the depths 0.14–0.26  $\mu\text{m}$ , VIAXAFS explores mixed phases of mono- and di-oxides of zirconium which enrich in  $\text{ZrO}_2$ .

For depths 0.26–0.67  $\mu\text{m}$  and 0.67–1.00  $\mu\text{m}$  the first four maxima are perfectly aligned with the calculated spectrum of zirconium dioxide.

The  $\rho(x)$  function that was used for the modeling of these VIAXAFS spectra is an inverse exponential:

$$\rho(x) = \rho(0)[1 - A \exp(-\kappa x)] \quad (1)$$

starting at  $\rho = 0.50$  for  $x = 0.00 \mu\text{m}$  and reaching  $\rho = 0.99$  at  $x = 0.65 \mu\text{m}$  with  $A = 0.50$  and  $\kappa = 6.06 \times 10^6 \text{ m}^{-1}$ . This result is clearly supported by the features observed in Fig. 1a and b on which pores are observed limiting the density below 100% and on which a relief of 100–200 nm grains at the average are identified justifying the drop of the density and the increase of fractal features nearby the surface.

The results obtained are satisfying in that they clearly indicated that the method of VIAXAFS for deep layer is feasible and reliable for a wide range of samples. The VIAXAFS analysis on the 1  $\mu\text{m}$   $\text{ZrO}_2/\text{SS}$  sample was successful because it was possible to adequately subtract the features from the surface in order to get a clear spectrum of the film material structure. It clearly corrects the spectra from a nanoscopic layer of zirconium monoxide (see Xiali Zhe et al. [25], for details on formation and characterization by XRD) that must be present onto the bulk of the sputtered layer as described by Aita [26]. It also describes the occurrence specific attenuations in the XAFS signal due to decrease of next neighbour number for the shallow features (relief and local defects due to surface and film structure) and as observed for nano-zirconia phases [27]. The presence of a tetragonal zirconia sub-layer that yields a different signal [28] compared to the monoclinic material is not detected.

The results obtained do show that the method has a lot of potential even with complex samples.

## 5. Conclusions

Variable incidence angle X-ray absorption fine structure spectroscopy has been examined and successfully tested for investigating films. The VIAXAFS theory was developed and adapted to the variable incidence angles of the light beam. The derived expressions allow translation of spectral features gained for variable incident angle to be translated in depth profile data for nano-structures and atom environment examination. This technique was

applied, from a grazing to normal incidence on a thin layer sample obtained by zirconia sputtering on a flat stainless steel sample. XAFS analysis on the Zr K edge identifies spectra distortions due to occurrence of mono- and di-oxide with the lower Zr redox state of the oxide around the surface vs. the bulk of the layer. This reflects also the high density of dislocations and defects at the surface of this film. This feasibility study has shown that VIAXAFS is a promising method because of its non-destructive probing nature delivering data on macro-properties such as density and at the sub-nanoscopic level information as provided by XAFS.

## Acknowledgments

We would like to thank Melissa Denecke and Jörg Rothe from the INE-ANKA beamline for their precious help in operating the line for the sample investigations. We are grateful to Roland Brüttsch at the PSI-LWV for his SEM work. We also thank Johannes Bertsch, Goutam Kuri (PSI-LWV) and Rainer Dähn (PSI-LES) for the useful discussions we had. Umicore Material AG from Balzers, Lichtenstein is thanked for providing the zirconium monoxide reference material. An anonymous reviewer is acknowledged for his constructive remarks. The VIA-XAFS study was partially supported by Swissnuclear.

## References

- [1] C. Degueldre, M. Kastoryano, K. Dardenne, J. Nucl. Mater. 362 (2007) 316.
- [2] C.H. Booth, F. Bridges, Phys. Scr. T115 (2005) 202.
- [3] L. Tröger, D. Arvanitis, K. Baberschke, H. Michaelis, U. Grimm, E. Zschech, Phys. Rev. B 46 (1992) 3283.
- [4] S.J. Wang, C.K. Ong, P.L. You, S.Y. Xu, Semiconduct. Sci. Technol. 15 (2000) 836.
- [5] C.S. Hwang, H.J. Kim, J. Mater. Res. 8 (1993) 1361.
- [6] R. Di Maggio, P. Scardi, A. Tomasi, Mater. Eng. 5 (1994) 13.
- [7] M.J. Lance, J.A. Haynes, M.K. Ferber, W.R. Cannon, J. Therm. Spray Technol. 9 (2000) 68.
- [8] P. Scardi, M. Leoni, M. Loch, G. Barbezat, Mater. Sci. Forum 443/444 (2004) 77.
- [9] F. Shojai, T. Mäntylä, J. Eur. Ceram. Soc. 21 (2001) 45.
- [10] F. Shojai, T. Mäntylä, J. Porous Mater. 8 (2001) 137.
- [11] M. Crosnier de Bellaistre, L. Renaud, P. Kleimann, P. Morin, J. Randon, J.-L. Rocca, Electrophoresis 25 (2000) 3086.
- [12] M. Hartmanová, M. Jergel, I. Thurzo, F. Kudracik, K. Gmucova, S. Chromik, L. Ortega, Rus. J. Electrochem. 39 (2003) 479.
- [13] C. Degueldre, T. Arima, Y.W. Lee, J. Nucl. Mater. 319 (2003) 6.
- [14] L. Combemale, G. Caboche, D. Stuerger, D. Chaumont, Mater. Res. Bull. 40 (2005) 529.
- [15] C. Degueldre, M. Pouchon, M. Streit, O. Zaharko, M. Di Michel, Prog. Nucl. Energy 38 (2001) 241.
- [16] A.J. Allen, J. Am. Ceram. Soc. 88 (2005) 1367.
- [17] B.K. Teo, EXAFS: Basic Principles and Data Analysis, Springer-Verlag, Berlin, 1986.
- [18] P. Villela, S. Conradson, F. Espinosa-Faller, S.R. Foltyn, K.E. Sickafus, J.A. Valdez, C. Degueldre, Phys. Rev. B 64 (2001) 104101 1.
- [19] S. Conradson, C. Degueldre, F.J. Espinosa-Faller, S.R. Foltyn, K.E. Sickafus, J.A. Valdez, P. Villela, Prog. Nucl. Energy 38 (2001) 221.
- [20] C. Degueldre, K. Dardenne, Nucl. Instrum. Meth. B 238 (2005) 323.
- [21] W.H. McMaster, N. Kerr Del Grande, J.H. Mallett, J.H. Hubbell, Compilation of X-Ray Cross Sections, Lawrence Livermore National Laboratory, 1969.
- [22] A.L. Ankudinov, B. Ravel, J.J. Rehr, S.D. Conradson, Phys. Rev. B 58 (1998) 7565.
- [23] A.L. Ankudinov, J.J. Rehr, Phys. Rev. B 62 (2000) 2437.
- [24] A. Gualtieri, P. Norby, J. Hanson, J. Hrilpac, J. Appl. Cryst. 29 (1996) 707.
- [25] C.A. Xiali Zhe, A. Dioka, Hendry, J. Eur. Ceram. Soc. 25 (2005) 695.
- [26] C.R. Aita, Nanostruct. Mater. 4 (1994) 257.
- [27] S.L.P. Savin, A.V. Chadwick, L.A. O'Dell, M.E. Smith, Solid State Ionics 177 (2006) 2519.
- [28] G.G. Long, D.R. Black, A. Feldman, E.N. Farabaugh, R.D. Spal, R.D. Tanaka, Z. Zhang, Thin Solid Films 217 (1992) 113.





## Reagentless amperometric formaldehyde-selective biosensors based on the recombinant yeast formaldehyde dehydrogenase

Olha Demkiv<sup>a</sup>, Oleh Smutok<sup>a</sup>, Solomiya Paryzhak<sup>a</sup>, Galyna Gayda<sup>a</sup>, Yusif Sultanov<sup>b</sup>, Dmitrii Guschin<sup>c</sup>, Halyna Shkil<sup>c</sup>, Wolfgang Schuhmann<sup>c</sup>, Mykhailo Gonchar<sup>a,\*</sup>

<sup>a</sup> Department of Analytical Biotechnology, Institute of Cell Biology, Drahomanov Street 14/16, 79005 Lviv, Ukraine

<sup>b</sup> Institute of Chemical Problems, National Academy of Sciences of Azerbaijan, H. Javid avenue 29, AZ1143 Baku, Azerbaijan

<sup>c</sup> Anal. Chem. – Elektroanalytik & Sensorik, Ruhr-Universität Bochum, Universitätsstr. 150, D-44780 Bochum, Germany

### ARTICLE INFO

#### Article history:

Received 4 January 2008

Received in revised form 9 April 2008

Accepted 16 April 2008

Available online 24 April 2008

#### Keywords:

Formaldehyde

Recombinant formaldehyde dehydrogenase

Glutathione

NAD<sup>+</sup>

Redox polymer

Amperometric biosensor

### ABSTRACT

Novel formaldehyde-selective amperometric biosensors were developed based on NAD<sup>+</sup>- and glutathione-dependent formaldehyde dehydrogenase isolated from a gene-engineered strain of the methylotrophic yeast *Hansenula polymorpha*. Electron transfer between the immobilized enzyme and a platinized graphite electrode was established using a number of different low-molecular free-diffusing redox mediators or positively charged cathodic electrodeposition paints modified with Os-bis-*N,N*-(2,2'-bipyridil)-chloride ([Os(bpy)<sub>2</sub>Cl]) complexes. Among five tested Os-containing redox polymers of different chemical structure and properties, complexes of osmium-modified poly(4-vinylpyridine) with molecular mass of about 60 kDa containing diaminopropyl groups were selected. The positively charged cathodic paint exhibited the best electron-transfer characteristics. Moreover, the polymer layers simultaneously served as a matrix for keeping the negatively charged low-molecular cofactors, glutathione and NAD<sup>+</sup>, in the bioactive layer. Additionally, covering the enzyme/polymer layer with a negatively charged Nafion membrane significantly decreased cofactors leakage and simultaneously enhanced the sensor's stability. The developed sensors revealed a high selectivity to formaldehyde (FA) and a low cross-sensitivity to other substances (such as, e.g. butyraldehyde, propionaldehyde, acetaldehyde, methylglyoxal). The maximum current value was  $34.2 \pm 0.72 \mu\text{A}/\text{mm}^2$  (3.05 mm diameter electrode) and the apparent Michaelis–Menten constant ( $K_M^{\text{app}}$ ) derived from the FA calibration curves was  $120 \pm 5 \text{ mM}$  with a linear detection range for FA up to 20 mM. The best observed sensitivity for reagentless sensor was  $1.8 \text{ nA } \mu\text{M}^{-1}$  ( $358 \text{ A m}^{-2} \text{ M}^{-1}$ ). The developed sensors had a good operational and storage stability. The laboratory prototype of the sensor was applied for FA testing in some real samples of pharmaceutical (formidron), disinfectant (descoton forte) and industrial product (formalin). A good correlation was revealed between the concentration values measured using the developed FdDH-based sensor, an enzymatic method and standard chemical methods of FA determination.

© 2008 Elsevier B.V. All rights reserved.

### 1. Introduction

Formaldehyde (FA) has found broad application in chemical synthesis of phenol-, urea-, and melamine–formaldehyde resins which are used in the manufacturing of building plates, plywood and lacquer materials. FA is additionally necessary for the production of different consumer goods such as detergents, soaps, and shampoos, as well as in pharmacology and medicine as a sterilising agent [1]. Advanced technologies of water pre-treatment which include ozonization lead to FA formation by the reaction of ozone with natural humus traces [2,3] or with contaminations of chlorinated

benzene derivatives [3]. It was reported that FA is found in more than 2000 commercial products to which many industrial workers are exposed on a daily basis. This calls for a continuous control of possible contamination processes [4]. The permissible level of FA in industrial areas was set to 0.5–2.0 ppm. FA is produced also in the atmosphere as a product of photo-chemical oxidation of automobile exhaust and combustion processes.

FA has a negative influence on human's health, especially on the central nervous, blood and immune systems. It is a potent nasal irritant, causes stunted growth, blindness and respiratory diseases. FA is one of the chemical mediators of apoptosis and is considered as a mutagenic and a possibly human carcinogenic compound [5]. However, FA is not only of artificial origin. It is a natural metabolite found in tissues, cells, and body fluids. It is present in fruits, vegetables, meat, and fish. In extreme cases, some frozen fishes,

\* Corresponding author. Tel.: +380 32 2612144; fax: +380 32 2611648.  
E-mail address: [gonchar@cellbiol.lviv.ua](mailto:gonchar@cellbiol.lviv.ua) (M. Gonchar).

especially of the gadoid species, can accumulate up to 200–780 mg of FA per kg of moist weight due to the enzymatic degradation of trimethylamine oxide which is a natural fish component [6,7].

All these facts convincingly demonstrate the requirement of reliable analytical devices for an accurate FA determination in testing consumer goods, the environment, as well as biological samples. A number of attempts to develop biosensors for the detection of FA were reported [8–13] including amperometric sensors [14–16], potentiometric detection schemes [10,17–21] and optical sensors [12,22]. However, some serious problems remain unsolved such as a low sensitivity of the potentiometric sensors, insufficient stability, and poor selectivity. These limitations provoke the development of new biosensors based on novel enzymes including recombinant proteins isolated from genetically modified microbial cells.

We have described the fabrication and properties of a reagentless bienzyme amperometric biosensor based on alcohol oxidase/oxidase in combination with Os-complex modified electrodeposition paint [23]. Although the developed alcohol biosensor showed a good co-sensitivity for the detection of FA, the poor selectivity of alcohol oxidase used as biological recognition element limited the application of this sensor for FA determination.

As new approach to development of highly selective FA assays, formaldehyde dehydrogenase (FdDH), a key enzyme of FA metabolism in microorganisms, was proposed to be used as biorecognition element in biosensors [10,16,24–30]. However, the broad application of FdDH in analytical practice is hampered by its insufficient activity, as well as by relatively high costs of the commercially available enzymes' preparations. Recently, we have reported about the construction of a recombinant yeast clone originated from the recipient strain of thermotolerant methylotrophic yeast *Hansenula polymorpha* which is a NAD<sup>+</sup>- and glutathione-dependent FdDH over-producer [31]. A simple scheme for the isolation and chromatographic purification of the target enzyme from the over-producing yeast cells was proposed and highly purified FdDH preparations were obtained [32].

Recently, we have described the construction of highly selective biosensors [28–30] using, on the one hand, commercial bacterial FdDH [28] and, on the other hand, the yeast FdDH from the recombinant over-producer [29–30]. Although in the case of the amperometric biosensor [30] a good sensitivity was achieved ( $22 \text{ A m}^{-2} \text{ M}^{-1}$ ), the procedure of FA measuring was complicated by the need for addition of the yeast FdDH cofactors to the analyte solution.

In this communication, we propose an improved sensor architecture for the development of yeast FdDH-based amperometric biosensors providing the secure fixation of all sensor components in a bioactive layer on the transducer surface. Specifically, the sensor architecture was designed to prevent any leakage of the low-molecular and free-diffusing cofactors (NAD<sup>+</sup> and glutathione), thus avoiding the need for any addition of these cofactors to the analyte solution. For the design of the electron-transfer pathway between electrode surface and enzyme, besides standard free-diffusing and low-molecular weight redox mediators, different positively charged cathodic electrodeposition polymers, synthesized on the basis of 4-vinylpyridine and butylmethacrylate as monomers and modified with Os-bis-*N,N*-(2,2'-bipyridil)-chloride ( $[\text{Os}(\text{bpy})_2\text{Cl}]$ ) were used as mediators and supporting carriers for enzyme and its cofactors.

The obtained biosensors were successfully applied for FA determination in real samples of commercial chemical product (formalin), pharmaceutical (formidron) and disinfectant (descoton forte).

## 2. Experimental

### 2.1. Materials

DEAE-Toyopearl 650 M was from Toyo Soda (Tokyo, Japan); EDTA and nitrotetrazolium blue (NTB) were from Merck (Darmstadt, Germany); hexachloroplatinum(IV)-acid-hexahydrate, ferrocene, formalin and methanol were from Merck-Schuchardt (Hohenbrunn, Germany). Methylene blue was obtained from Riedel-de Haën (Seelze, Germany); dithiothreitol (DTT), *para*-formaldehyde, phenylmethylsulfonyl fluoride (PMSF), potassium hexacyanoferrate(III), potassium hexacyanoferrate(II), triton X-100, 3-methyl-2-benzothiazolinone hydrazone hydrochloride (MBTH), phenazine ethosulfate and methylglyoxal were from Sigma (Deisenhofen, Germany). Glutathione (reduced) and phenazine methosulfate (PMS) were from Fluka (Buchs, Switzerland), NAD<sup>+</sup> and NADH were obtained from Gerbu Biotechnik (Gailberg, Germany). Nafion, butyraldehyde, propionaldehyde and acetaldehyde were from Aldrich (Deisenhofen, Germany).

Poly(4-vinylpyridines) (P4PV), poly(4-vinylpyridine-co-butyl methacrylate) (CP4VPBMA), epichlorhydrin (99%), and 4(5)-imidazol-carboxaldehyde (ICA) (98%) were obtained from Aldrich (Taufkirchen, Germany). Potassium hexachloroosmate ( $\text{K}_2\text{OsCl}_6$ ), 2,2'-bipyridine (99%; bpy), 1,3-diaminopropane (DAP) (99%), 1,8-diaminooctane (DAO) (98%) were from Acros (Geel, Belgium), osmium-bis-*N,N*-(2,2'-bipyridil)-chloride was synthesized according to Ref. [33]. Descoton forte was from Desomark (Novovorivsk, Ukraine), formidron was obtained from Ternofarm (Ternopil, Ukraine).

All chemicals were of analytical reagent grade and all solutions were prepared using HPLC-grade water. FA solution (1 M) was prepared by hydrolysis of the corresponding amount of *para*-formaldehyde in water (300 mg; 10 ml water) by heating the suspension in a sealed ampoule at 105 °C for 6 h.

### 2.2. Synthesis of Os-containing redox polymers

As a polymer base for mediators, poly(4-vinylpyridines) with a molecular mass 60 kDa (P4VP60) and 160 kDa (P4VP160) and copolymers of 4-vinylpyridine with butylmethacrylate (poly(4-vinylpyridine-co-butyl) methacrylate; CP4VPBMA) have been chosen. P4VP60, P4VP160 and CP4VPBMA were alkylated with epichlorhydrin and the resulting products were treated with DAP or DAO. After this, ICA was added to the reaction mixture. The obtained polymers [34] were modified by coordinating osmium-complexes by means of a ligand exchange reaction of osmium-bis-*N,N*-(2,2'-bipyridil)-chloride with suitable ligands at the polymer chains. Molecular structures of the synthesized Os-containing redox polymers are shown in Fig. 1.

The redox properties of the synthesized Os-modified polymers were studied using differential pulse voltammetry.

### 2.3. Formaldehyde dehydrogenase (FdDH)

As a microbial source of NAD- and glutathione-dependent FdDH, the gene-engineered yeast strain Tf 11-6, derivative of the recipient *H. polymorpha* strain NCYC 495, was chosen [31]. Cells of recombinant strain Tf 11-6, over-producing thermostable FdDH, were cultivated and a cell-free extract was prepared according to Ref. [31].

FdDH was isolated from the cell-free extract by a two-step ion-exchange chromatography on DEAE-Toyopearl 650 M [32]. FdDH activity was determined by the rate of NADH formation [35]. One

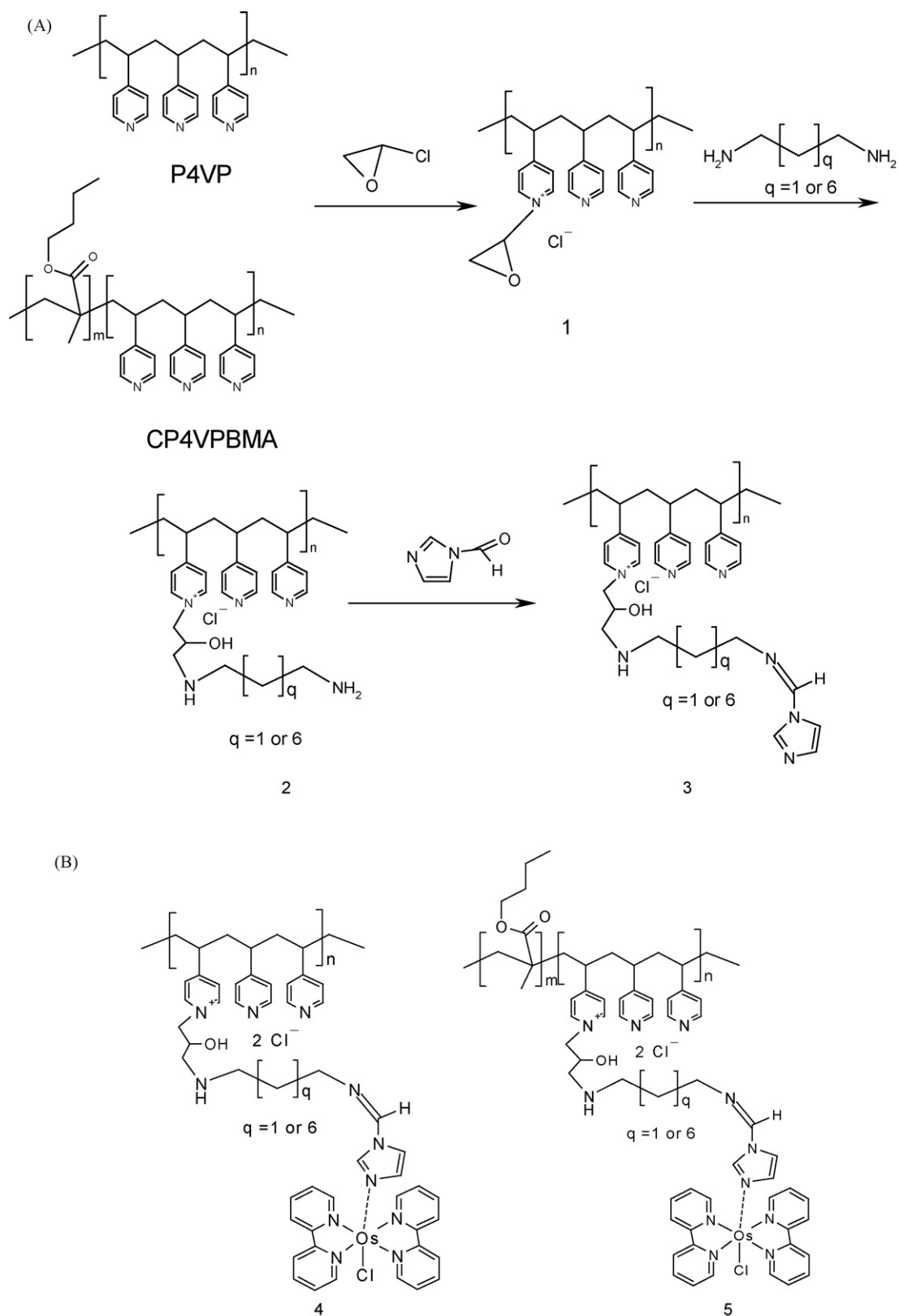


**Fig. 1.** Schematic representation of the synthesis of the Os-complex modified polymers (A) and of the molecular structures of the synthesized Os-complex containing redox polymers (B): P4VP – poly(4-vinylpyridines); CP4VPBMA – poly(4-vinylpyridine-co-butyl methacrylate).

unit of the FdDH activity is defined as that amount of the enzyme which forms 1  $\mu\text{mol}$  NADH per minute under standard conditions of the assay (25 °C, 30 mM phosphate buffer, pH 8.0; 1 mM FA, 1 mM NAD<sup>+</sup> and 2 mM glutathione). Protein concentration was determined by the Lowry method. The enzyme preparation with a specific activity 12 U mg<sup>-1</sup> protein was stored as a suspension in 80%-saturated ammonium sulphate in 50 mM Tris–HCl buffer, pH 8.0, with 2 mM DTT, at –10 °C.

#### 2.4. FA assay

Chemical assays of FA were performed following three methods using either chromotropic acid [36], MBTH [37], or Purpald [38]. For enzymatic assays of FA, the previously developed kit Format-est, was used [32]: 0.5 ml of model and real samples (water for the blank sample) were treated at room temperature with 0.5 ml FdDH-containing reagent (23 mU ml<sup>-1</sup> FdDH, 0.63 mM glutathione, 0.31 mM NAD<sup>+</sup>, 1.0 mM NTB, 0.024 mM PMS, and 0.01% triton X-100 in 60 mM PB, pH 8.0) during 30 min. To terminate the reaction, 3 ml 0.3 M HCl was added. The optical density of the sample at 570 nm was measured and the FA content was calculated from a calibration curve.

#### 2.5. FdDH-based amperometric biosensor

##### 2.5.1. Electrodes

Graphite rods (type RW001, 3.05 mm diameter) from Ringsdorff Werke (Bonn, Germany), sealed in glass tubes by means of epoxy glue and used as working electrodes, were polished with emery paper of decreasing size. Platinization of the graphite electrodes was carried out in a 6 mg ml<sup>-1</sup> solution of hexachloroplatinum(IV)-acid hexahydrate in HPLC-grade water by cyclic voltammetry (–0.6 to 0.4 V vs. Ag/AgCl/KCl at a scan rate of 50 mV s<sup>-1</sup>, 3–4 potential cycles). After platinization, the electrodes were rinsed with 20 mM phosphate buffer, pH 8.2.

The properties of FdDH-based amperometric biosensors were evaluated by means of constant-potential amperometry in a three-electrode configuration with an Ag/AgCl/KCl (3 M) reference electrode and a Pt-wire counter electrode.

##### 2.5.2. Biosensor construction

In order to form the biorecognition layer, immobilization of FdDH together with its cofactor (NAD<sup>+</sup>) was performed using an electrodeposition method. As polymer matrix, cathodic paints (CP) were used which contained covalently bound Os-complex (1CPOs–5CPOs) or were devoid of this mediator (CP6) [39] in the case of exploiting alternative free-diffusing or precipitated redox compounds. For this, 2  $\mu\text{l}$  25 mM NAD<sup>+</sup>, 2  $\mu\text{l}$  FdDH suspension (15 U ml<sup>-1</sup>) and 2  $\mu\text{l}$  of the corresponding CP solution were mixed and dropped onto the surface of a platinized graphite electrode. Electrodeposition was induced by a potentiostatic pulse sequence (–1200 mV for 0.2 s and a resting phase at a potential of 0 mV for 5 s) [40]. At the applied cathodic potential, water is reduced at the electrode surface leading to an increase of the pH-value in a diffusion zone in front of the working electrode surface. By this, the CP was deprotonated causing a significant change in its solubility which leads to the precipitation of the polymer on the electrode surface simultaneously entrapping the enzyme with NAD<sup>+</sup> within the polymer film. After the immobilization procedure, the electrodes were rinsed with 20 mM phosphate buffer, pH 8.2.

For co-entrapment of glutathione and covering of the sensing layer by means of a Nafion membrane, 3  $\mu\text{l}$  50 mM solution of reduced glutathione (GSH) neutralized to pH 8.0, were dropped on the top of a CP–NAD<sup>+</sup>–FdDH-modified electrode. After drying (2–4 min), 5  $\mu\text{l}$  1% Nafion solution in ethanol were placed on

the sensor surface. The Nafion membrane was allowed to dry for 20–25 min at +4 °C.

##### 2.5.3. Redox mediators

Potassium hexacyanoferrate(III), methylene blue and phenazine ethosulfate were used as free-diffusing redox mediators in experiments with FdDH–CP6-based electrodes. 10 ml of a 1 mM solution (0.5 mM for methylene blue) of the selected redox mediator in 20 mM phosphate buffer, pH 8.2, was added to the electrolyte solutions. In case of experiments involving the light sensitive phenazine ethosulfate the glass cell was wrapped with aluminium foil.

Ferrocene was initially dissolved in acetone. For the preparation of the mediator-containing sensing layer, 4  $\mu\text{l}$  of a 10 mM ferrocene solution was dropped on the surface of the electrode at room temperature prior to FdDH immobilization (see Section 2.5.2). Electrodeposition of prussian blue on the electrode prior to FdDH immobilization was performed by means of cyclic voltammetry (10 cycles from 0.4 to 1.3 V vs. Ag/AgCl/KCl with a scan rate of 50 mV s<sup>-1</sup> in 5 mM solution of K<sub>3</sub>[Fe(CN)<sub>6</sub>], containing 5 mM FeCl<sub>3</sub> and 10 mM HCl) [41]. After the electrodeposition of the prussian blue film the modified electrode was rinsed with 20 mM phosphate buffer, pH 8.2.

#### 2.6. Amperometric measurements

Amperometric measurements were carried out using a Autolab PGstat12 potentiostat (Eco Chemie, Utrecht, Holland) controlled by the GPES4.9 software. Amperometric experiments were performed in steady-state mode using a standard cell with 10 ml volume at 25 °C under continuous stirring. After 20 min of stabilizing the background current, the experiments were started by addition of sample aliquots. As working potentials (vs. Ag/AgCl) either 0 mV was chosen for the free-diffusing mediator phenazine ethosulfate or +200 mV for Os-complex modified cathodic electrodeposition paints (1CPOs–5CPOs), potassium hexacyanoferrate(III), prussian blue, methylene blue and ferrocene.

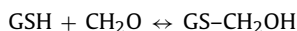
Between experiments, the modified electrodes were stored in 20 mM phosphate buffer, pH 8.2, at 4 °C. The operational stability of the developed FdDH-based amperometric biosensors was tested in flow injection analyses (FIA) mode using an in-house developed sequential-injection analyser “OLGA” [42] with a flow-rate of 5 ml min<sup>-1</sup> and a sample injection every 4 min. All measurements were repeated at least 3 times. Statistic data evaluations were calculated using Origin 6.0 and Microsoft Excel.

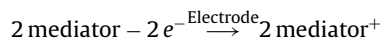
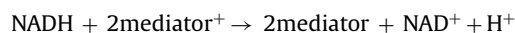
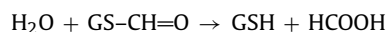
### 3. Results and discussion

#### 3.1. Design and optimization of FdDH-based biosensor

In methylotrophic yeasts, NAD<sup>+</sup>- and glutathione-dependent FdDH catalyzes the oxidation of FA to formic acid. In the physiological electron-transfer pathway, the electrons are transferred from FA via intermediate hydroxymethylglutathione to the active centre of FdDH under simultaneous reduction of NAD<sup>+</sup> to NADH. For the design of an electron-transfer pathway from an immobilized FdDH to the electrode surface, enzymatically generated NADH has to be re-oxidized additionally at the electrode surface using a suitable redox mediator.

Chemical, enzymatic and electrochemical reactions involved in amperometric FA assay are the following:





For design of the electron-transfer pathway between electrode surface and enzyme, several low-molecular weight redox mediators and positively charged cathodic electrodeposition paints (CP), modified by Os-bis-*N,N*-(2,2'-bipyridil)-chloride ([Os(bpy)<sub>2</sub>Cl]) [34] were investigated. The chemical structure of these polymers is shown in Fig. 1. To choose the optimal composition for the electrode construction, the redox properties of the Os-containing polymers were studied. Table 1 summarizes their preparation mode (see Section 2.2), as well as their electrochemical features [34].

The redox properties of a polymer layer formed by electrochemically induced pH-modulation in the diffusion layer in front of the platinumized graphite electrode, were evaluated using differential pulse voltammetry (Fig. 2A). The peak potential for the Os<sup>2+</sup>/Os<sup>3+</sup> redox reaction for 1CPOs was observed at +200 mV vs. Ag/AgCl/KCl. The other four polymers had two redox waves for the Os<sup>2+</sup>/Os<sup>3+</sup> reaction: 2CPOs and 4CPOs at +200 and +365 mV; 3CPOs at +196 and +360 mV; 5CPOs at +195 and +361 mV (see the last column

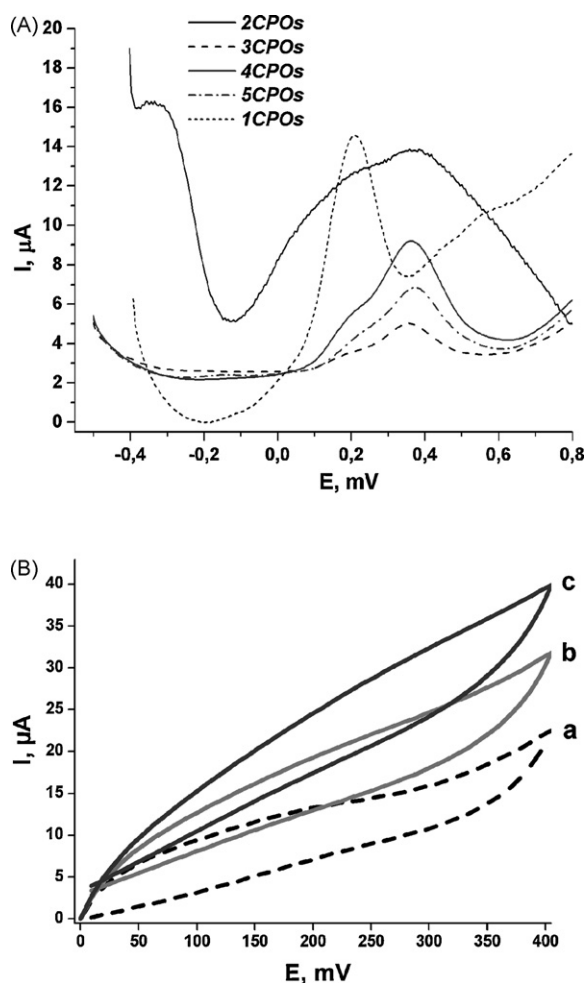


**Fig. 2.** (A) Differential pulse voltammograms (DPV) of CPOs-modified electrodes (scan rate 25 mV s<sup>-1</sup>, modulation amplitude 49.5 mV). (B) Cyclic voltammogram of a 1CPOs-NAD<sup>+</sup>-FdDH-GSH-Nafion-modified platinumized graphite electrode in the absence (a) and in the presence of 16 mM (b) and 32 mM (c) FA (potential sweep from 0.0 to 0.4 V at a scan rate of 5 mV s<sup>-1</sup> in 20 mM phosphate buffer, pH 8.2).

of Table 1). Cyclic voltammetry in the absence and presence of FA showed a biocatalytic increase in the anodic current (Fig. 2B shows as example only the case of 1CPOs under CV). Since higher potentials may induce direct oxidation of glutathione, a potential of +200 mV was chosen as working potential for constant-potential amperometry for all subsequent experiments using Os-containing CP-polymers.

A variety of redox mediators in combination with FdDH were investigated. Amperometric responses to different FA concentrations are presented in Fig. 3. The most promising results were obtained with the cathodic paints 1CPOs and 2CPOs (for their molecular structure and concerning maximal current values, see Fig. 3A). The cathodic paint 1CPOs was shown to be the most effective electron-transfer catalyst when compared to the different free-diffusing and co-immobilized redox mediators (Fig. 3B).

Relative signals to 80 mM FA, obtained for biosensors with different mediators at optimal potential value, were as following: 1CPOs – 100%; phenazine ethosulphate – 94%; potassium ferricyanide – 66%; ferrocene – 30%; prussian blue – 13% and methylene blue – 10%. Due to the properties of the Os-complex modified electrodeposition paints which allow the formation of a sensing layer with tightly bound electron-transfer mediator, the best ones (1CPOs and

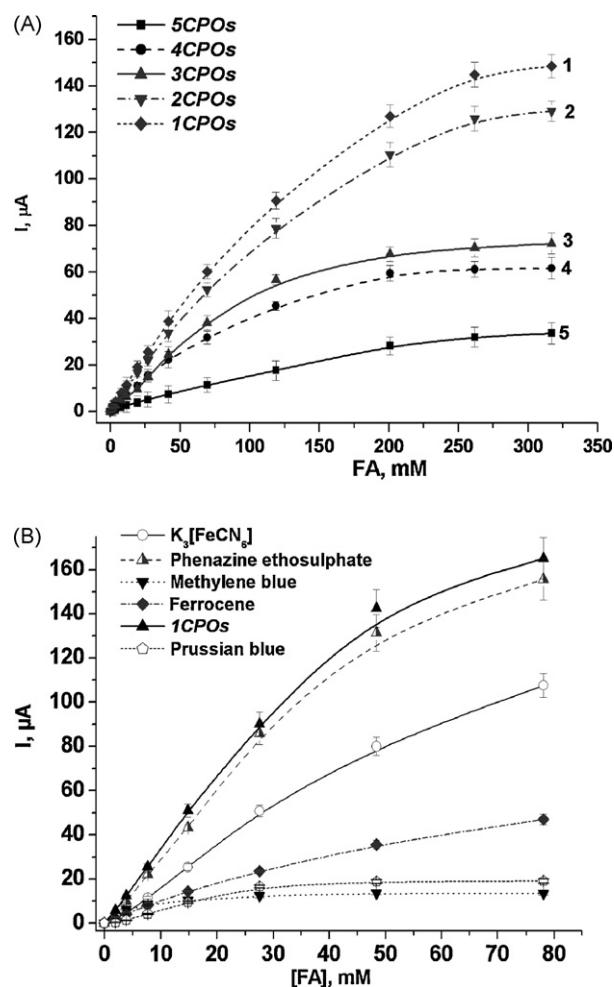


**Fig. 3.** FA calibration curves for the CP-NAD<sup>+</sup>-FdDH-GSH-Nafion-modified platinumized graphite electrodes. (A) Os-complex modified cathodic electrodeposition paints (1CPOs, 2CPOs, 3CPOs, 4CPOs, 5CPOs); (B) 1CPOs and low-molecular redox mediators in combination with CP6 (potassium ferricyanide, phenazine ethosulphate, methylene blue, ferrocene, prussian blue).

**Table 1**  
Electrochemical properties of Os-containing redox polymers

No.	Symbol	Polymers	Aminoderivatives	Aldehyde	Redox potential (mV), vs. Ag/AgCl
1	1CPOs	P4VP60	DAP	ICA	200
2	2CPOs	CP4VPBMA	DAP	ICA	200; 365
3	3CPOs	P4VP60	DAO	ICA	200; 365
4	4CPOs	P4VP160	DAO	ICA	196; 360
5	5CPOs	CP4VPBMA	DAO	ICA	195; 361

2CPOs) were chosen for the design of the optimized FdDH biosensor.

A major concern which is related to the application of FdDH as biorecognition element in the presented biosensor design, is the need of the simultaneous presence of two low-molecular cofactors. Thus, a major emphasis was put in the prevention of their leakage from the sensing layer. For this, a sophisticated sensor architecture is proposed consisting of an electrochemically deposited Os-complex-modified cathodic polymer (1CPOs or 2CPOs) co-entrapping FdDH and NAD<sup>+</sup>, covered by glutathione-containing layer and a negatively charged Nafion membrane, additionally preventing leakage of the cofactors due to charge interactions.

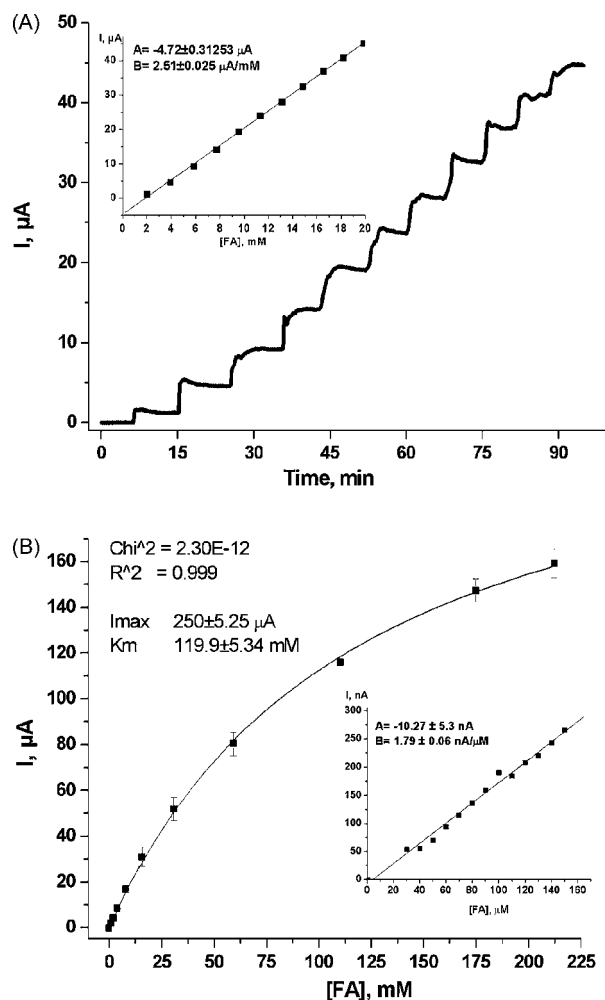


**Fig. 4.** Chronoamperometric determination of FA using 1CPOs–NAD<sup>+</sup>–FdDH–GSH–Nafion modified platinumized graphite electrode (A) and derived FA calibration curves (B). 25  $\mu$ l aliquots of a 0.8 M FA solution were added stepwise to 10 ml electrolyte solution. Statistical data: A and B – parameters of the linear regression (coefficients of the equation  $Y = A + B \cdot X$ , where Y – current,  $\mu$ A; X – FA concentration).

### 3.2. Properties and analytical performances of the FdDH-based biosensor

A typical response of the developed 1CPOs–NAD<sup>+</sup>–FdDH-modified electrode towards FA and the linear range is shown in Fig. 4. The maximum current was  $250 \pm 5 \mu$ A for a 3.05 mm diameter electrode which corresponds to a current density of  $34.2 \pm 0.7 \mu$ A/mm<sup>2</sup>. The apparent Michaelis–Menten constant ( $K_M^{\text{app}}$ ) derived from the FA calibration curves for the immobilized enzyme was  $120 \pm 5$  mM with a linear detection range for FA up to 20 mM. The observed  $K_M^{\text{app}}$  value differs significantly from the  $K_M$  value of the used FdDH in solution (0.18 mM) and reported for homologous enzymes from the wild strains of the methylotrophic yeasts, *Candida boidinii* (0.25–0.29 mM [35]), *H. polymorpha* (0.21 mM [43]) and *Pichia pastoris* (0.43 mM [44]). Possibly, this difference is associated with an influence of the rather complicated composition of the biorecognition membrane on the diffusional availability of the substrate to the immobilized enzyme.

The detection limit of the developed biosensor was derived using 10 measurements of the sensor response to a stepwise addition of FA in the range of 10–100  $\mu$ M (see inset in Fig. 4).

The current value was  $17.9 \pm 3.5$  nA for each 10  $\mu$ M addition. The noise level was about 2 nA. Hence, a detection limit could be calculated about 3  $\mu$ M FA (90 ng ml<sup>-1</sup>) which is of a similar order as reported for FdDH-based flow-cell amperometric sensor using bacterial FdDH [24,25]. The sensitivity of the biosensor was  $1.8 \text{ nA} \cdot \mu\text{M}^{-1}$  ( $358 \text{ A} \cdot \text{m}^{-2} \cdot \text{M}^{-1}$ ) a value which is 16-fold higher as compared to the previously described amperometric biosensor [30]. The observed sensitivity for reagentless sensors is much higher than required for detection of the permissible level of 0.5–2 ppm (or 18–70  $\mu$ M) FA in different environmental media and FA containing products.

The optimal pH-value for the developed FdDH-based biosensor is in the range of 7.6–8.3 with an optimal temperature between 45 and 50  $^{\circ}$ C (data not shown); values of pH and temperature optima are similar to the estimated ones for the free enzyme in solution [32].

The FA-dependent current output of the FdDH-based sensor is significantly altered with the buffer concentration decreasing with higher electrolyte concentrations of the used phosphate buffer. Besides changes in properties of the Nafion membrane at higher electrolyte concentrations [45], this effect may be explained by an influence in the interaction between glutathione and FA in the first step of the reaction sequence and the charge interaction between the negatively charged enzymatically generated NADH and the positively charged Os-complex at the redox polymer backbone.

The selectivity of the 1CPOs–NAD<sup>+</sup>–FdDH–GSH–Nafion-biosensor for the determination of FA was evaluated using different substances which show structural similarities to FA. The developed biosensor exhibited only a minor co-sensitivity to other aldehydes: quantitatively, the ratio of the sensor output to different potentially interfering analytes to the formaldehyde response are as following: FA (100%), butyraldehyde (0.9%), propionaldehyde

**Table 2**  
FA content in real samples determined by different methods: chemical and FdDH-based approaches

Sample/method	FA molar concentration, $M \pm m$					
	Chemical methods			FdDH-based methods		
	MBTH	Purpald	Chromotropic acid	Formatest	Biosensor	Biosensor, integrated in "OLGA"
Formalin	$12.6 \pm 0.7$	$12.9 \pm 0.7$	$14.0 \pm 0.8$	$13.5 \pm 0.8$	$13.6 \pm 0.6$	$13.6 \pm 0.6$
Descoton	$3.6 \pm 0.3$	$3.3 \pm 0.3$	$3.6 \pm 0.4$	$3.3 \pm 0.8$	$3.6 \pm 0.1$	$3.5 \pm 0.3$
Formidron	$1.6 \pm 0.6$	$1.2 \pm 0.2$	$1.5 \pm 0.3$	$1.5 \pm 0.3$	$1.6 \pm 0.1$	$1.5 \pm 0.6$

(1.9%), acetaldehyde (5.1%), methylglyoxal (9.1%). Due to the observed significant differences in sensitivity between FA and the tested aldehydes, it can be assumed that the cross-sensitivity will be insignificant for the determination of FA in real samples. In addition, the sensor exhibited a small sensitivity towards methanol (0.9%).

The operational and storage stabilities of the developed FA sensors (1CPOs–NAD<sup>+</sup>–FdDH–GSH–Nafion and 2CPOs–NAD<sup>+</sup>–FdDH–GSH–Nafion) were studied. It is pertinent to note that the prevention of potential leakage of both NAD<sup>+</sup> and glutathione from the sensing layer is of crucial importance for the long-term stability of the developed FA biosensors. All subsequent tests were

performed at a constant temperature of 24 °C with 2 and 7 mM FA solutions for 1CPOs based biosensor and with 1 mM solution for 2CPOs based biosensor in 20 mM phosphate buffer, pH 8.2, for the investigation of the operational stability, and a 7.7 mM FA solution for the evaluation of the storage stability. The operational stability was tested using the automatic sequential injection analyser "OLGA" [42]. The sensors were integrated into an electrochemical flow-through cell, and 12 injections of the FA standard solution per hour were performed automatically. Fig. 5A and B shows the current response of the sensors upon sample injection along about 14 h using three different concentrations of FA.

The developed sensors demonstrated a good operational stability at comparatively low FA concentrations: 2 mM during 14 h (Fig. 5A) and 1 mM during 22 h (Fig. 5B) of continuous operation in a sequential injection analyser (about 210 individual measurements). At higher concentrations (7 mM) the peak current continuously decreased with the operation time which may be attributed to a deterioration of the components forming multi-layer sensing chemistry by the highly reactive FA. Nevertheless, the developed biosensor exhibited satisfactory operation stability especially when integrated into the sequential injection analyser which allows for a repetitive recalibration.

The storage stability of the developed biosensors was found to be longer than 18 days at 4 °C (data not shown). After 4 days of storage in buffer solution, the detected signal exceeded the initial one by about 30%. This effect is often seen with amperometric biosensors and is indicative of an equilibration of the sensor architecture potentially leading to an improved permeability of the immobilization matrix for the substrate.

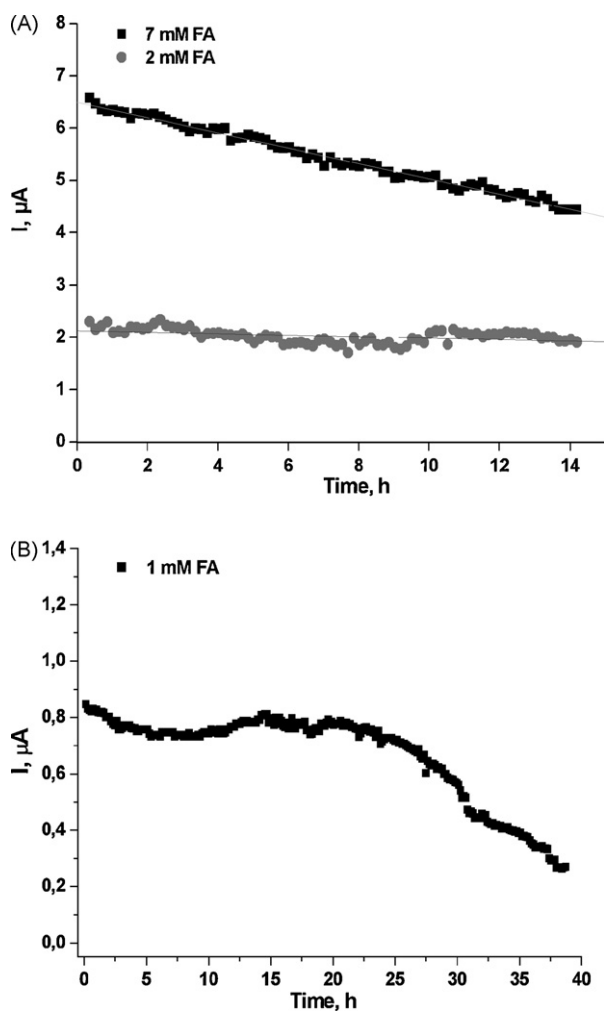


**Fig. 5.** Operational stability of the optimized FA biosensors: 1CPOs–NAD<sup>+</sup>–FdDH–GSH–Nafion (A) and 2CPOs–NAD<sup>+</sup>–FdDH–GSH–Nafion (B) tested in an automatic sequential injection analyser (flow-rate 5 ml min<sup>-1</sup>; sample injection every 4 min).

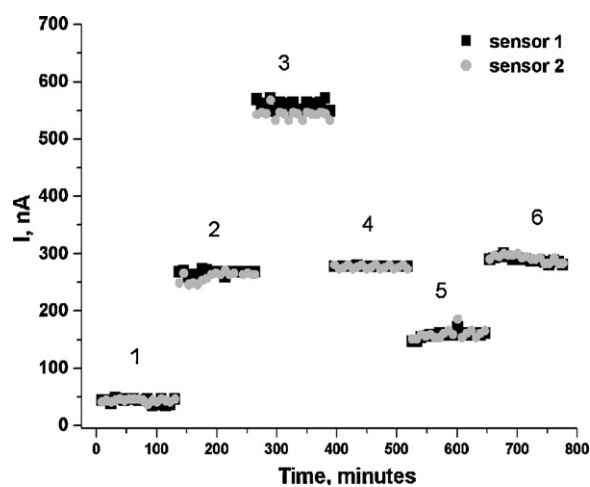


**Fig. 6.** Reproducibility of the analytical data for FA assay in model and real samples using an automatic sequential injection analyser "OLGA": (1) 1 mM FA; (2) 5 mM FA; (3) 10 mM FA (model samples of FA in water); (4) formalin: 5.04 mM, dilution factor 2700,  $C_0 = 13.6 \pm 0.6$  M; (5) formidron: 2.54 mM, dilution factor 570,  $C_0 = 1.45 \pm 0.06$  M; and (6) descoton: 5.31 mM, dilution factor 650,  $C_0 = 3.45 \pm 0.25$  M.

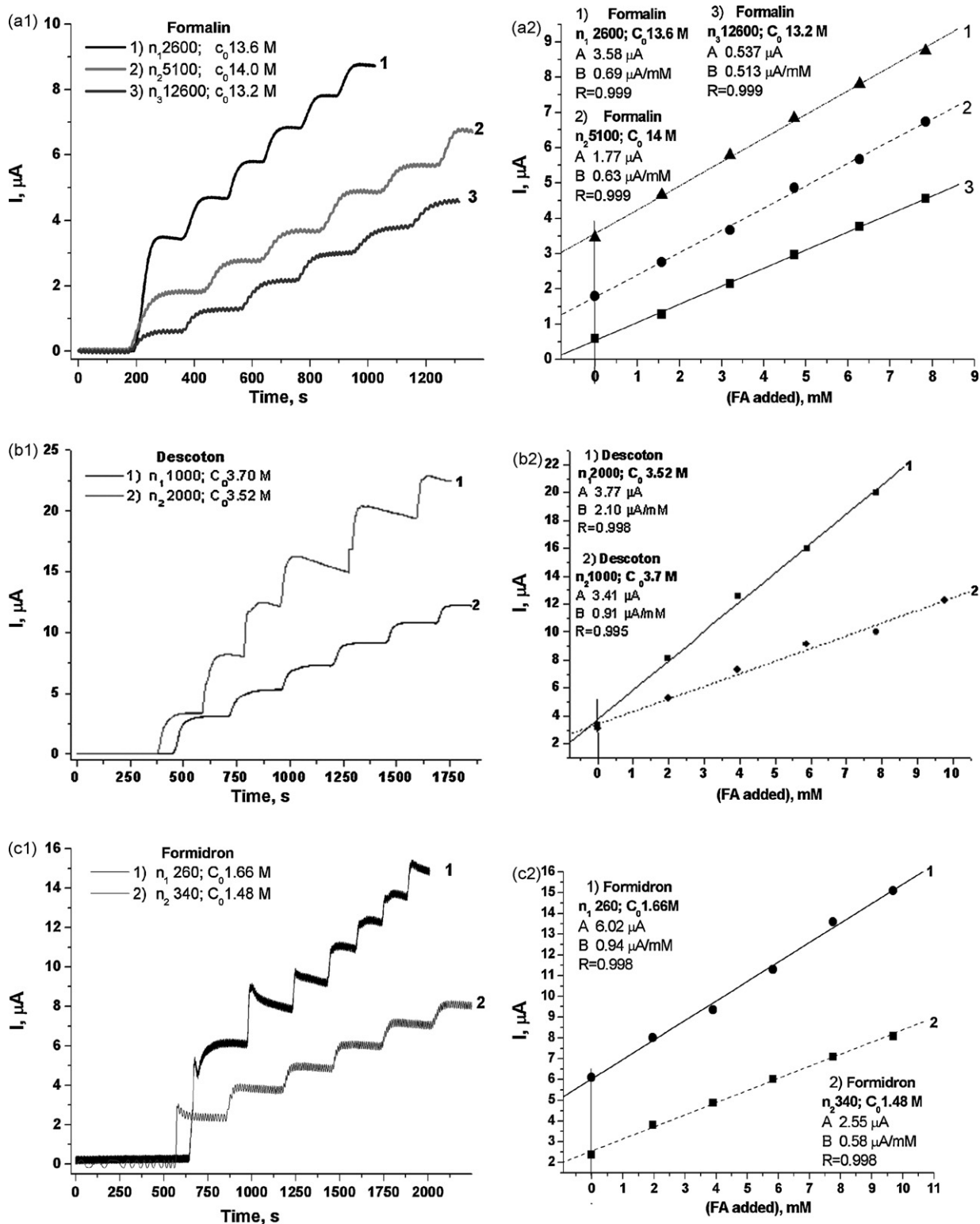


**Fig. 7.** Chronoamperograms of FA assay (a<sub>1</sub>, b<sub>1</sub>, c<sub>1</sub>) and calibration curves for standard addition tests (a<sub>2</sub>, b<sub>2</sub>, c<sub>2</sub>) using FdDH-based sensors (2CPOs–NAD<sup>+</sup>–FdDH–GSH–Nafion) for the analysis of real samples: a – formalin; b – disinfectant descoton; and c – antiperspirant formidron. The dilution factors ( $n$ ), the calculated initial concentration ( $C_0$ ) and statistical data such as parameters of linear regression (coefficients of the equation  $Y=A+B \cdot X$ , where  $Y$  – current,  $\mu$ A;  $X$  – FA concentration, mM;  $A$  – current corresponding to the variant without addition of exogenous FA;  $B$  – slope value; and  $R$  – linear regression coefficient) are indicated.



### 3.3. Real sample analysis with the FdDH-based biosensor

The constructed amperometric FdDH-based biosensor (2CPOs–NAD<sup>+</sup>–FdDH–GSH–Nafion) was evaluated in determining the FA content in real samples of the industrial product formalin and two pharmaceuticals, namely the antimicrobial agent descoton forte and antiperspirant formidron, using both the steady-state and FIA mode. The obtained biosensor was integrated into the automatic sequential injection analyser using a specifically adapted flow-through electrochemical cell. It was shown that the developed system can be used in automatic analyser systems for FA assays in formalin and pharmaceuticals. The conformity of the data obtained with the developed biosensor integrated into the automated analyser and routine industrial analytical methods for real samples of descoton forte, formalin and formidron was approved (Table 2 and Fig. 6).

It is worth to emphasize that the standard chemical approaches to FA analyses are not free from possible mistakes due to interfering effects of the co-impurities, usually represented in the real samples, for example, phenol which is an attendant pollutant of FA-containing wastes [36]. Recently we have tested FA in real samples of wastes by the developed photometric FdDH-based assay “Formatest” in comparison with standard chemical methods [32]. We have demonstrated that in order to evaluate the possible interfering effect of real samples’ components on FA assay, it was necessary to perform a standard addition test in both approaches (chemical and enzymatic) and that analytical data obtained by enzymatic method are more reliable than chemical ones.

The amperometric FdDH-based biosensor (2CPOs–NAD<sup>+</sup>–FdDH–GSH–Nafion) was evaluated to determine FA content in real samples (in steady-state mode) using the multiple standard addition method. Results are presented in Fig. 7 and summarized in Table 2. It is obvious from Fig. 7, that interfering effects of real sample components were observed for all samples, but at a different extent. The maximal interfering effect is observed for descoton, less for formidron, and the smallest for formalin, derived from the slopes of the calibration curves obtained on the background of the real samples in different dilutions: for descoton the difference is +56.6% (2.10 and 0.91 for dilution factors 2000 and 1000, respectively), for formidron the difference is +38.3% (0.94 and 0.58 for dilution factors 260 and 340, respectively), and for formalin the difference is +25.6% and 8.69% (0.69, 0.63 and 0.51 for dilution factors 12,600, 5100 and 2600, respectively). For all samples, good correlation was observed between the sensor values and enzymatic or chemical methods.

The collected analytical data confirm the possibility to exploit the developed FdDH-based biosensors for FA assay in real samples using a standard addition test.

## 4. Conclusion

Reagentless amperometric FA biosensors based on NAD<sup>+</sup>- and glutathione-dependent FdDH isolated from the gene-engineered methylothrophic yeast *H. polymorpha* have been developed. Screening of different mediators revealed that an Os-complex containing cathodic electrodeposition paints exhibited the best catalytic activity. Among five tested polymers for biosensors with CPOs–NAD<sup>+</sup>–FdDH–GSH–Nafion architecture the best two were chosen as optimal for entrapping FdDH and NAD<sup>+</sup>. The first layer was impregnated with reduced glutathione before it was covered with a Nafion membrane. This multi-layer sensor architecture prevented leakage of low-molecular cofactors from the bioselective layer thus avoiding the need for addition of the cofactors to the analyte solution and provided the observed good operational and

storage stability. The developed sensors revealed a high selectivity to FA and a low cross-sensitivity to other aldehydes and methanol. The observed sensitivity for developed reagentless sensors is 16-fold higher compared to the previously described biosensor [30] and is much higher than required for detection of the permissible level FA in different environmental media and FA containing products. The sensors were successfully applied for FA determination in some real samples of commercial preparations of formalin and pharmaceuticals. A good correlation was observed between the data of FA testing by the FdDH-based biosensor’s approaches and enzymatic or standard chemical methods.

## Acknowledgements

This work was supported by the EU (INTAS 03-51-6278), NATO (linkage grants LST.NUKR.CLG 980621 and PDD (CP)-(CPP.NUKR.CLG 982955)), and the project of NAS of Ukraine in the framework of the Program “Sensors’ Systems for Medico-Ecological, Industrial and Technological Purposes”.

## References

- [1] H.R. Gerberich, G.C. Seaman, Encyclopedia of Chemical Technology, vol. 11, fourth ed., John Wiley & Sons, New York, USA, 1994, p. 929.
- [2] D.S. Schechter, P.C. Singer, Ozone Sci. Eng. 17 (1995) 53.
- [3] B. Kasprzyk-Hordern, M. Ziólek, J. Nawrocki, Appl. Catal. B: Environ. 46 (2003) 639.
- [4] M.A. Flyvholm, P. Andersen, Am. J. Ind. Med. 24 (1993) 533.
- [5] V.J. Feron, H.P. Til, F. deVrijer, R.A. Woutersen, F.R. Cassee, P.J. van Bladeren, Mutat. Res. 259 (1991) 363.
- [6] H. Rehbein, Arch. Lebensmittelhyg 46 (1995) 122.
- [7] H.M. Pavlishko, T.M. Honchar, M.V. Gonchar, Exp. Clin. Physiol. Biochem. 4 (2003) 56 (in Ukrainian).
- [8] M.J. Dennison, J.M. Hall, A.P.F. Turner, Analyst 12 (1996) 1769.
- [9] M. Hämmerle, E.A.H. Hall, N. Cade, D. Hodgins, Biosens. Bioelectron. 11 (1996) 239.
- [10] F. Vianello, A. Stefani, M.L. Di Paolo, A. Rigo, A. Lui, B. Margesin, M. Zen, M. Scarpa, G. Soncini, Sens. Actuators B 37 (1996) 49.
- [11] L. Feng, Y. Liu, X. Zhou, J. Hu, J. Colloid, Interface Sci. 284 (2005) 378.
- [12] K. Kawamura, K. Kerman, M. Fujihara, N. Nagatani, T. Hashiba, E. Tamiya, Sens. Actuators B. Chem. 105 (2005) 495.
- [13] R. Knake, P. Jacquinet, A.W.E. Hodgson, P.C. Hauser, Anal. Chim. Acta 549 (2005) 1.
- [14] B. Winter, K. Cammann, Anal. Chem. 334 (1989) 720.
- [15] E.A.H. Hall, M. Preuss, J.J. Gooding, M. Hämmerle, NATO ASI Ser. 2: Environ. 38 (1997) 227.
- [16] W. Vastarella, R. Nicastri, Talanta 66 (2005) 627.
- [17] Y.I. Korpan, M.V. Gonchar, N.F. Starodub, A.A. Shul’ga, A.A. Sibirny, A.V. El’skaya, Anal. Biochem. 215 (1993) 216.
- [18] Y.I. Korpan, M.V. Gonchar, A.A. Sibirny, A.V. El’skaya, J. Chem. Technol. Biotechnol. 68 (1997) 209.
- [19] Y.I. Korpan, M.V. Gonchar, A.A. Sibirny, C. Martelet, A.V. El’skaya, T.D. Gibson, A.P. Soldatkin, Biosens. Bioelectron. 15 (2000) 77.
- [20] Y.I. Korpan, S.V. Dzyadevich, V.N. Arkhipova, A.V. El’skaya, M.V. Gonchar, T.D. Gibson, N. Jaffrezic-Renault, C. Martelet, A.P. Soldatkin, Sens. Mater. 12 (2000) 79.
- [21] M. Gonchar, M. Maidan, Y. Korpan, V. Sibirny, Z. Kotylak, A. Sibirny, FEMS Yeast Res. 2 (2002) 307.
- [22] K.-P. Rindt, S. Scholtissek, GBF Monogr. 13 (1989) 405.
- [23] O. Smutok, B. Ngounou, H. Pavlishko, G. Gayda, M. Gonchar, W. Schuhmann, Sens. Actuators B 113 (2006) 590.
- [24] Y. Herschkovitz, I. Eshkenazi, C.E. Campbell, J. Rishpon, J. Electroanal. Chem. 491 (2000) 182.
- [25] N. Kiba, L. Sun, S. Yokose, M. Tachibana, K. Tani, T. Suzuki, Anal. Chim. Acta 378 (1999) 169.
- [26] C.E. Campbell, J. Rishpon, J. Electroanal. 13 (2001) 17.
- [27] T. Yao, S. Handa, Anal. Sci. 19 (2003) 767.
- [28] M. Ben Ali, Y. Korpan, M. Gonchar, A. El’skaya, M.A. Maaref, N. Jaffrezic-Renault, C. Martelet, Biosens. Bioelectron. 22 (2006) 575.
- [29] M. Ben Ali, M. Gonchar, G. Gayda, S. Paryzhak, M.A. Maaref, N. Jaffrezic-Renault, Y. Korpan, Biosens. Bioelectron. 22 (12) (2007) 2790.
- [30] O. Nikitina, S. Shleev, G. Gayda, O. Demkiv, M. Gonchar, L. Gorton, E. Csöregi, M. Nistor, Sens. Actuators B 125 (2007) 1.
- [31] O.M. Demkiv, S.Ya. Paryzhak, E.S. Krasovs’ka, O.V. Stasyk, G.Z. Gayda, A.A. Sibirny, M.V. Gonchar, Biopolymers Cell 21 (6) (2005) 525 (in Ukrainian).
- [32] O.M. Demkiv, S.Ya. Paryzhak, G.Z. Gayda, V.A. Sibirny, M.V. Gonchar, FEMS Yeast Res. 7 (2007) 1153.

- [33] K. Habermüller, A. Ramanavicius, V. Laurinavicius, W. Schuhmann, *Electroanalysis* 12 (2000) 1383.
- [34] D.A. Guschin, Yu.M. Sultanov, N.F. Sharif-zade, E.H. Aliyev, A.A. Efendiev, W. Schuhmann, *Electrochim. Acta* 51 (2006) 5137.
- [35] H. Schutte, J. Flossorf, H. Sahm, M.-R. Kula, *Eur. J. Biochem.* 62 (1976) 151.
- [36] Polish Com. Standard. (Eds.), *Polska Norma PN-71 C-04568*, fifth ed., Warsaw, 1988.
- [37] E. Sawicki, T.R. Hauser, T.W. Stanley, W. Elbert, *Anal. Chem.* 33 (1961) 93.
- [38] G. Avgard, *Anal. Biochem.* 134 (1983) 499.
- [39] S. Reiter, D. Ruhlig, B. Ngounou, S. Neugebauer, S. Janiak, A. Vilkanauskyste, T. Erichsen, W. Schuhmann, *Macromol. Rapid Commun.* 25 (2004) 348.
- [40] B. Ngounou, S. Neugebauer, A. Frodl, S. Reiter, W. Schuhmann, *Electrochim. Acta* 49 (2004) 3855.
- [41] E.A. Paganova, A.A. Karyakin, *Sens. Actuators B* 109 (2005) 167.
- [42] W. Schuhmann, H. Wohlschläger, J. Huber, H.-L. Schmidt, H. Stadler, *Anal. Chim. Acta* 315 (1995) 113.
- [43] J.J. Allais, A. Louktibi, J. Baratti, *Agric. Biol. Chem.* 47 (1983) 1509.
- [44] R.J.S. Baerends, G.J. Sulter, T.W. Jeffries, J.M. Cregg, M. Veenhuis, *Yeast* 19 (2002) 37.
- [45] I.A. Stenina, Ph. Sizat, A.I. Rebrov, G. Pourcelly, A.B. Yaroslavtsev, *Desalination* 170 (2004) 49.



## Electrochemical determination of chromium(VI) using metallic nanoparticle-modified carbon screen-printed electrodes

Olga Domínguez-Renedo, Laura Ruiz-Espelt, Natalia García-Astorgano, M. Julia Arcos-Martínez\*

Departamento de Química, Área de Química Analítica, Facultad de Ciencias, Universidad de Burgos, Plaza Misael Bañuelos s/n, E-09001 Burgos, Spain

### ARTICLE INFO

#### Article history:

Received 30 January 2008

Received in revised form 9 April 2008

Accepted 16 April 2008

Available online 24 April 2008

#### Keywords:

Silver nanoparticles

Gold nanoparticles

Screen-printed electrodes

Chromium

Voltammetry

### ABSTRACT

Carbon screen-printed electrodes (CSPEs) modified with metal nanoparticles present an interesting alternative in the determination of chromium(VI) by differential pulse voltammetry (DPV).

Metallic silver and gold nanoparticle deposits have been obtained by electrochemical deposition. Scanning electron microscopy measurements show that the electrochemically synthesized silver and gold nanoparticles are deposited in aggregated form.

The detection limit for the analytical procedures developed in this work were  $8.5 \times 10^{-7}$  and  $4.0 \times 10^{-7}$  M for silver and gold nanoparticle-modified CSPE, respectively.

In terms of reproducibility, the precision of the above-mentioned method was calculated at 6.7% in %R.S.D. values for silver and 3.21% for gold nanoparticle CSPE.

© 2008 Elsevier B.V. All rights reserved.

### 1. Introduction

The transition metal chromium exists in a number of oxidation states, all of which are not of equal stability. The most common valences are 0, +II, +III and +VI. Both Cr(III) and Cr(VI) are found in nature. Cr(III) is proved to be biologically essential and related to human glucose tolerance [1]. However, Cr(VI) species are carcinogenic and toxic. The major toxic effects of Cr(VI) are chronic ulcers, dermatitis, corrosive reaction in nasal septum and local effects in the lung [2].

Chromium is commonly used in metallurgical, refractory and chemical industries, such as in pigment and paint production, galvanizing, plating, tanning as well as timber. It may be released in a considerable amount into the environment. Therefore, an accurate determination of each species rather than a total concentration level is required to evaluate the physiological and toxicological effects.

Various techniques for the determination of Cr(III) and Cr(VI) have been developed in recent years. The common method was the separation of chromium ions by high-performance liquid chromatography (HPLC) often coupled with sophisticated detection systems such as inductively coupled plasma (ICP) atomic emission

or mass spectrometry [3–6]. However, these procedures do not satisfy all requirements for routine analysis, mainly because of their complicated process design, time consumption or the high cost of instrumentation.

Electrochemical methods, in particular, adsorptive stripping voltammetry [7–11], have important advantages such as high sensitivity, low detection limit, relative simplicity and low cost of equipment and automatic on-line and portable options, for the determination of metals at trace levels.

Screen-printed electrodes are planar devices with plastic substrates that are coated with layers of electroconductive and insulating inks at controlled thickness. The advent of screen-printed (thick-film) technology has made it possible to mass-produce inexpensive disposable electrodes for use with electrochemical instruments [12–16]. Their use in potentiometric, amperometric and voltammetric devices have been reported for the detection of different heavy metals [17–24] although the bibliography shows very few examples of determination of chromium with this kind of electrodes [11].

The great versatility of screen-printed electrodes resides in their wide range of possible modifications. In fact, the composition of the inks used in the printing process can be modified by the addition of substances of a very different nature, such as metals, enzymes, polymers, complexing agents, etc. Moreover, the possibility also exists of modifying the electrodes once they have been printed through the deposition of films containing those substances.

\* Corresponding author. Tel: +34 947258818; fax: +34 947258831.

E-mail addresses: [olgado@ubu.es](mailto:olgado@ubu.es) (O. Domínguez-Renedo), [jarcos@ubu.es](mailto:jarcos@ubu.es) (M.J. Arcos-Martínez).

The design of new nanoscale materials has acquired ever-greater importance in recent years due to their wide-ranging applications in various fields. Among these materials, metallic nanoparticles are of great interest due to their important properties and their numerous possible applications [25,26]. The bibliography lists numerous methods describing the synthesis of metallic nanoparticles in solution as well as by deposition on solid surfaces. These methods include chemical synthesis by means of reduction with different reagents [27], UV light or electron-beam irradiation [28] and electrochemical methods [29–34]. The latter provides an easy and rapid alternative for the preparation of metallic nanoparticle electrodes in a short period of time. In spite of their possibilities these nanoparticle-modified carbon screen-printed electrodes have not been highly used in the analysis of toxic elements. To the best author's knowledge only four works are described about the determination of arsenic [35,36] and antimony [37,38] using nanoparticle-modified screen-printed electrodes.

Silver and gold nanoparticle-modified carbon screen-printed electrodes show important advantages when they are used as working electrodes in electrochemical techniques. However, only a few works are described in the reference literature on the fabrication and analytical applications of such electrodes in the analysis of different metals including chromium [37–39].

The aim of this work is the voltammetric determination of Cr(VI) using screen-printed electrodes modified with silver and gold nanoparticles.

## 2. Experimental

### 2.1. Reagents

All solutions were prepared with deionized water obtained with a Barnstead NANO Pure II system.

Hydrogen tetrachloroaurate (III) trihydrate ( $\text{HAuCl}_4$ ) was purchased from Sigma–Aldrich (analytical-reagent grade, Sigma–Aldrich, Steinheim, Germany) and silver perchlorate hydrate from Fluka (Buchs, Switzerland).

Stock standard solutions of Cr(VI) were prepared by dissolving the adequate amount of  $\text{K}_2\text{Cr}_2\text{O}_7$  (analytical-reagent grade, Merck, Darmstadt, Germany) in water.

Electrodag PF-407 A (carbon ink), Electrodag 418 SS (silver ink), Electrodag 6037 SS (silver/silverchloride ink) and Electrodag 452 SS (dielectric ink) were supplied by Achenson Colloiden (Scheemda, The Netherlands).

The Britton–Robinson buffer solution consisted in a 0.04 M *o*-boric acid, 0.04 M *o*-phosphoric acid and 0.04 M acetic acid solution prepared using Merck analytical grade reagents. Solutions of dif-

ferent pH values ranging from 2 to 12 were prepared from this solution by the addition of 0.2 M sodium hydroxide (analytical-reagent grade, Merck, Darmstadt, Germany).

Sulphuric acid was purchased from Merck (analytical-reagent grade, Merck, Darmstadt, Germany).

### 2.2. Apparatus

Screen-printed electrodes were produced on a DEK 248 printing machine (DEK, Weymouth, UK) using polyester screens with appropriate stencil designs, mounted at  $45^\circ$  to the printer stroke.

Voltammetric measurements were taken using a  $\mu$ Autolab Type III electrochemical system with GPES 4.9. software (Eco Chemie, Utrecht, The Netherlands).

Scanning electron microscopy (SEM) images were obtained using a JEOL JSM-6460LV with an INCA elemental X-ray analysis system.

### 2.3. Screen-printed electrodes preparation

Hand-made screen-printed electrodes were used in the determination of Cr(VI). For the construction of the screen-printed electrodes, successive layers of different inks were printed onto a PVC strip substrate (30 mm  $\times$  15 mm, 0.5-mm thick). Four different screens with appropriate stencils were used to transfer the required design. The printing procedure has already been described in previous works [38,40].

### 2.4. Preparation of nanoparticle-modified electrodes

#### 2.4.1. Silver nanoparticle-modified carbon screen-printed electrodes

In comparison to other electrochemical methods described for the generation of silver nanoparticles [32–34], this work describes an easier procedure to obtain silver nanoparticle-modified CSPE. The method consists in the electrochemical deposition of silver on the working electrode surface, using a 0.10 mM  $\text{AgClO}_4$  solution in Britton–Robinson pH 2. The deposition was performed by applying a potential of  $-0.80$  V during 400 s under stirring. These conditions were found to be the more adequate for silver nanoparticle generation on the CSPE surface [37].

SEM analysis shows the formation of silver nanoparticles on the CSPE surface which are deposited in aggregated form (Fig. 1a). Moreover, energy-dispersive X-ray (EDX) analysis of CSPE confirmed the presence of deposited silver.

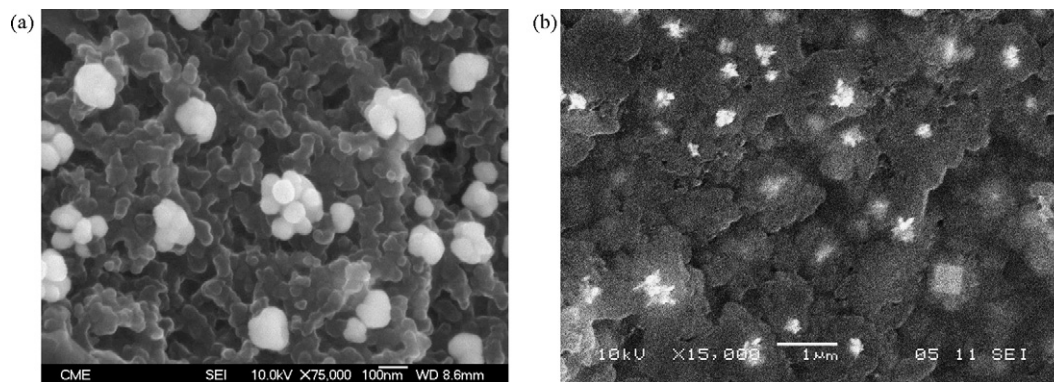


**Fig. 1.** SEM images of: (a) silver nanoparticle-modified CSPE formed by electrodeposition from a 0.10 mM  $\text{AgClO}_4$  solution during 400 s at  $-0.80$  V and (b) gold nanoparticle-modified CSPE formed by electrodeposition from a 0.10 mM  $\text{HAuCl}_4$  solution during 600 s at 0.18 V.

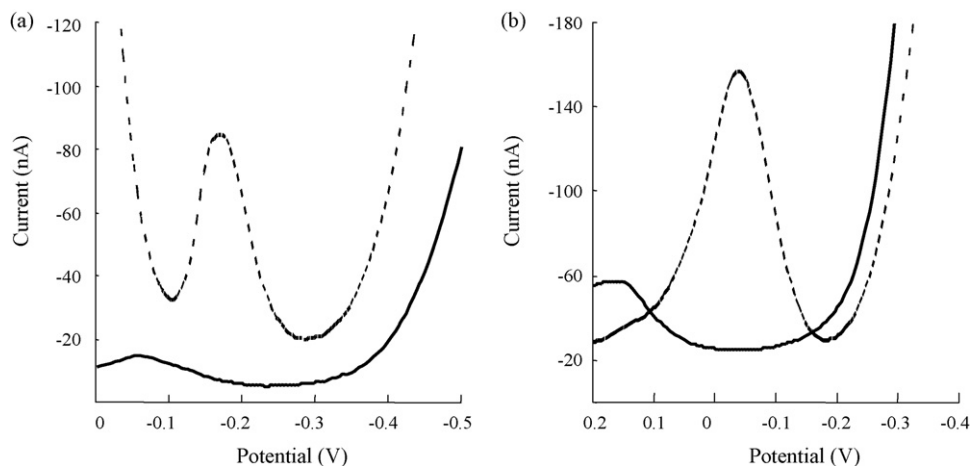


**Fig. 2.** Differential pulse voltammograms for Cr(VI) using: (a) silver nanoparticle-modified CSPE (pH 4): (—) blank; (---) [Cr(VI)] = 1 μM and (b) gold nanoparticle-modified CSPE (pH 6): (—) blank; (---) [Cr(VI)] = 1 μM. Potentials given versus an Ag/AgCl reference electrode.

#### 2.4.2. Gold nanoparticle-modified carbon screen-printed electrodes

In a similar manner, gold nanoparticles were deposited over the CSPE surface, using a 0.5 M H<sub>2</sub>SO<sub>4</sub> solution containing 0.10 mM of HAuClO<sub>4</sub>. The time and potential of deposition applied were 200 s and 0.18 V, respectively [38].

SEM analysis shows the formation of gold nanoparticles on the CSPE surface which have been deposited in aggregated form (Fig. 1b). Moreover, EDX analysis of CSPE confirmed the presence of deposited gold.

### 3. Results and discussion

#### 3.1. Determination of chromium using silver nanoparticle-modified CSPEs

No analytical signal for chromium(VI) was observed by differential pulse voltammetry (DPV) when neither Ag nor carbon solid electrodes were used. However, modification of a graphite electrode by the deposition of silver nanoparticles produced signals of a sufficiently high quality for analytical purposes, as may be observed from Fig. 2a. Since Cr(III) did not give any response under these conditions, the observed peak in Fig. 2a at a potential about -0.19 V can be attributed to the reduction of Cr(VI) to Cr(III).

The electrochemical study of chromium in this kind of modified electrodes was carried out using different supporting electrolytes. The best results were obtained in acetic–acetate medium. The experiments performed in this medium at different pH values showed that the best response for Cr(VI) reduction was obtained for a value of 6 (Fig. 3a).

#### 3.2. Determination of chromium using gold nanoparticle-modified CSPEs

The DPV measurements of Cr(VI) using gold solid electrodes shown that this kind of electrodes are not very sensitive for the electrochemical determination of Cr(VI). In fact, no response was obtained for concentrations lower than 5 μM. However, the electrochemical reduction of Cr(VI) to Cr(III) by DPV can be observed when using gold nanoparticle-modified CSPE even at very low Cr(VI) concentrations. In fact, a well-defined reduction peak may be observed in Fig. 2b at about -0.05 V, which is strongly affected by pH. In Fig. 3b it can be observed that the best conditions were obtained when a pH 4 acetic–acetate solution was used as the supporting electrolyte.

#### 3.3. Calibration and detection limit

Once the optimal experimental conditions were found for the analysis of chromium by means of silver and gold nanoparticle-

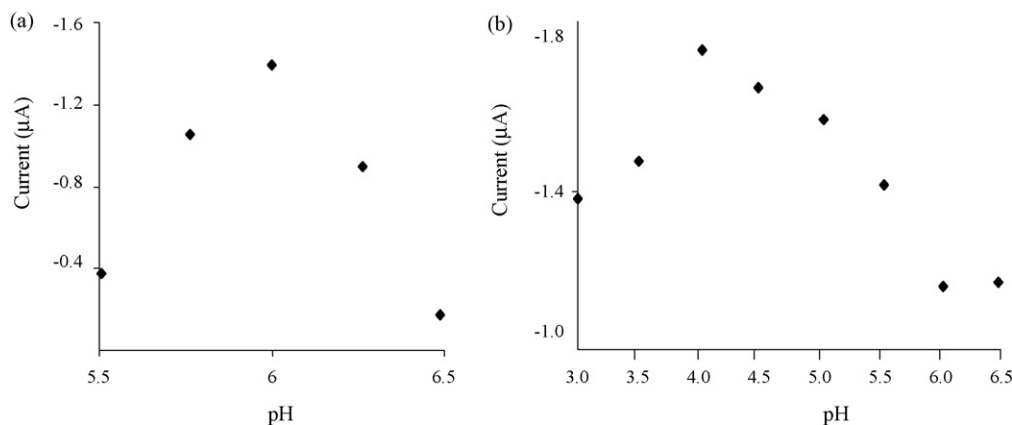


**Fig. 3.** Effect of pH in the DPV determination of Cr(VI) using: (a) a silver nanoparticle-modified CSPE ([Cr(VI)] = 10 μM) and (b) a gold nanoparticle-modified CSPE ([Cr(VI)] = 10 μM). Potentials given versus an Ag/AgCl reference electrode.

modified CSPE, a calibration was performed using a least-median-squares (LMS) regression to detect the existence of anomalous points [41], which might have led to incorrect adjustments altering the sensitivity and the detection limit.

The calibration equation obtained by DPV for standard solutions containing Cr(VI) in the range of concentrations between  $5.0 \times 10^{-7}$  and  $3.8 \times 10^{-5}$  M was  $I = 2.66 \times 10^{-9} + 1.83 \times 10^{-2} C$  ( $R^2 = 0.99$ ) for silver nanoparticle-modified electrodes. For gold nanoparticle electrodes, the calibration was made using standard solutions containing concentrations of Cr(VI) ranging between  $4.0 \times 10^{-7}$  and  $3.0 \times 10^{-5}$  M, obtaining the following calibration equation:  $I = 1.72 \times 10^{-9} + 2.01 \times 10^{-2} C$  ( $R^2 = 0.99$ ).

Calculation of the detection limit, based on the variability of 10 samples with a very low analyte concentration ( $2.0 \times 10^{-7}$  M), was calculated according to [42] and ISO 11843-2 [43]. At the chosen probability level of 5% ( $\alpha = \beta = 0.05$ ), the detection limits for silver- and gold-modified electrodes were  $8.5 \times 10^{-7}$  and  $4.0 \times 10^{-7}$  M, respectively.

### 3.4. Precision

This parameter was calculated in terms of reproducibility. A series of five measurements of samples containing  $10^{-7}$  M of Cr(VI) were carried out obtaining a %R.S.D. value of 6.7% and 3.21% for silver and gold, respectively.

### 3.5. Accuracy

As the best results, in terms of sensibility and reproducibility, were obtained for the gold nanomodified electrodes, the accuracy of the method was evaluated only for this kind of electrodes. The analysis of a certified sample in comparison to the corresponding National Institute of Standards and Technology was analyzed. The Cr(VI) concentration quantified ( $1002 \pm 12 \text{ mg L}^{-1}$ ;  $n = 5$ ;  $\alpha = 0.05$ ) matches the certified value of the sample ( $1000 \pm 2 \text{ mg L}^{-1}$ ) considering the associated uncertainties. Therefore, the proposed method is both accurate and suitable for the analysis of Cr(VI) in water samples.

### 3.6. Recovery

Recovery studies were carried out in different spiked water samples with Cr(VI). The results obtained are shown in Table 1. On the basis of these results, it may be affirmed that no influence of the matrix composition of the water sample was observed.

### 3.7. Interferences

An analysis of any possible effects caused by the presence of foreign ions in the electrochemical response of Cr(VI) at silver and gold nanoparticles-modified electrodes was carried out. No one of the metallic ions analyzed – Cd(II), Cu(II), Ni(II), Pb(II), Zn(II), Sn(II) and Cr(III) – produced an interfering electrochemical signal in the determination of Cr(VI) with silver nanoparticle CSPEs in the range of concentrations between  $10^{-7}$  and  $10^{-4}$  M. In the case of gold nanomodified CSPEs, only Cu(II) concentrations higher than  $10^{-5}$  M gave rise to peaks in the same zone of potentials as Cr(VI).

**Table 1**

Recovery studies in spiked water samples by means of DPV with a gold nanoparticle-modified CSPE ( $n = 5$ ;  $\alpha = 0.05$ , Britton–Robinson pH 4)

Sample	Cr(VI) added (M)	Cr(VI) found (M)
Tap water	$1.00 \times 10^{-6}$	$1.01 \times 10^{-6} \pm 1.67 \times 10^{-8}$
Seawater	$1.00 \times 10^{-6}$	$9.99 \times 10^{-7} \pm 1.20 \times 10^{-8}$

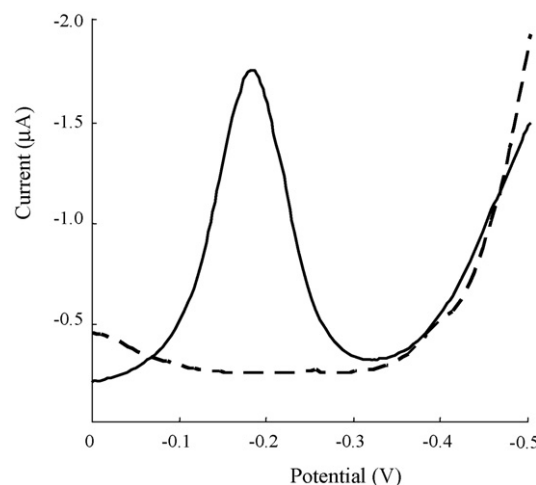


**Fig. 4.** DPV voltammograms in a silver nanoparticle-modified CSPE: (---) [Cr(III)] = 10 µM, (—) [Cr(III)] = 10 µM and [Cr(VI)] = 10 µM. Potentials given versus an Ag/AgCl reference electrode.

From these results, it can be affirmed that the nanoparticle-modified CSPE constructed according to the method described in this paper is an excellent electrochemical sensor for sensitive and highly selective analysis of Cr(VI), even in the presence of high concentrations of foreign ions. In this respect, the analysis of Cr(VI) in the presence of Cr(III) is of special interest. The described method allows the analysis of Cr(VI) even in the presence of high concentrations of Cr(III), as it can be seen in Fig. 4.

## 4. Conclusions

The silver and gold nanoparticle-modified carbon screen-printed electrodes developed in this work present an environmentally friendly method for the analysis of chromium. They offer an important advantage from other electrodes in the analysis of chromium. The developed electrodes allow the selective analysis of Cr(VI) in the presence of even high concentrations of Cr(III) offering a method for the speciation analysis of this specie.

## Acknowledgements

The financial support made available by the Junta de Castilla y León (BU022A07) and the Ministerio de Educación y Ciencia (MAT 2005-01767) is gratefully acknowledged.

## References

- [1] V. Volkovic, Trace Elements Analysis, Taylor and Francis Ltd., London, 1975.
- [2] R. Cornelis, Trace Element Analysis in Biological Specimens, Elsevier, The Netherlands, 1994.
- [3] J.F. Jen, G.L. Ouyang, C.S. Chen, S.M. Yang, Analyst 118 (1993) 1281.
- [4] C.M. Andrie, J.A.C. Broekaert, Fresenius J. Anal. Chem. 346 (1993) 653.
- [5] C.M. Andrie, N. Jakubowski, J.A.C. Broekaert, Spectrochim. Acta B 52 (1997) 189.
- [6] M. Pansarkallio, P.K.G. Manninen, Fresenius J. Anal. Chem. 355 (1996) 716.
- [7] O. Domínguez, S. Sanlloriente, M.A. Alonso, M.J. Arcos, Electroanalysis 13 (2001) 1505.
- [8] O. Domínguez, M.A. Alonso, M.J. Arcos, Electroanalysis 14 (2002) 1083.
- [9] C.M.A. Brett, O.M.S. Filipe, C.S. Neves, Anal. Lett. 36 (2003) 955.
- [10] M. Grabarczyk, L. Kaczmarek, M. Korolczuk, Electroanalysis 16 (2004) 1503.
- [11] M.F. Bergamini, D.P. dos Santos, M.V.B. Zanoni, Sens. Actuator B: Chem. 123 (2007) 902.
- [12] J. Wang, J.M. Lu, B.M. Tian, C. Yarnitzky, J. Electroanal. Chem. 361 (1993) 77.
- [13] C. Yarnitzky, J. Wang, B.M. Tian, Talanta 51 (2000) 333.
- [14] P. Ugo, L.M. Moretto, P. Bertocello, J. Wang, Electroanalysis 10 (1998) 1017.
- [15] D. Desmond, B. Lane, J. Alderman, M. Hill, D.W.M. Arrigan, J.D. Glennon, Sens. Actuator B: Chem. 48 (1998) 409.
- [16] M. Jasinski, P. Grundler, G.U. Flechsig, J. Wang, Electroanalysis 13 (2001) 34.

- [17] V. Beni, V.I. Ogurtsov, N.V. Bakunin, D.W.M. Arrigan, M. Hill, *Anal. Chim. Acta* 552 (2005) 190.
- [18] H. Palchetti, S. Laschi, M. Mascini, *Anal. Chim. Acta* 530 (2005) 61.
- [19] B.B. Rodriguez, J.A. Bolbot, I.E. Tothill, *Anal. Bioanal. Chem.* 380 (2004) 284.
- [20] K.C. Honeychurch, D.M. Hawkins, J.P. Hart, D.C. Cowell, *Talanta* 57 (2002) 565.
- [21] R.O. Kadara, L.E. Tothill, *Talanta* 66 (2005) 1089.
- [22] I. Palchetti, S. Majid, A. Kicela, G. Marrazza, M. Mascini, *Int. J. Environ. Anal. Chem.* 83 (2003) 701.
- [23] J.M. Zen, C.C. Yang, A.S. Kumar, *Anal. Chim. Acta* 464 (2002) 229.
- [24] J.Y. Choi, K. Seo, S.R. Cho, J.R. Oh, S.H. Kahng, J. Park, *Anal. Chim. Acta* 443 (2001) 241.
- [25] M. Starowicz, B. Stypula, J. Banas, *Electrochem. Commun.* 8 (2006) 227.
- [26] C.W. Welch, R.G. Compton, *Anal. Bioanal. Chem.* 384 (2006) 601.
- [27] L. Sun, Z.J. Zhang, H.X. Dang, *Mater. Lett.* 57 (2003) 3874.
- [28] M. Fukushima, H. Yanagi, S. Hayashi, N. Sugauma, Y. Taniguchi, *Thin Solid Films* 438 (2003) 39.
- [29] E. Majid, S. Hrapovic, Y.L. Liu, K.B. Male, J.H.T. Luong, *Anal. Chem.* 78 (2006) 762.
- [30] X. Dai, O. Nekrassova, M.E. Hyde, R.G. Compton, *Anal. Chem.* 76 (2004) 5924.
- [31] M.S. El-Deab, T. Okajima, T. Ohsaka, *J. Electrochem. Soc.* 150 (2003) A851.
- [32] C.M. Welch, C.E. Banks, A.O. Simm, R.G. Compton, *Anal. Bioanal. Chem.* 382 (2005) 12.
- [33] B.S. Yin, H.Y. Ma, S.Y. Wang, S.H. Chen, *J. Phys. Chem. B* 107 (2003) 8898.
- [34] Z.Y. Tang, S.Q. Liu, S.J. Dong, E.K. Wang, *J. Electroanal. Chem.* 502 (2001) 146.
- [35] Y.S. Song, G. Muthuraman, J.M. Zen, *Electrochem. Commun.* 8 (2006) 1369.
- [36] Y.S. Song, G. Muthuraman, Y.Z. Chen, C.C. Lin, J.M. Zen, *Electroanalysis* 18 (2006) 1763.
- [37] O.D. Renedo, M.J.A. Martinez, *Electrochem. Commun.* 9 (2007) 820.
- [38] O.D. Renedo, M.J.A. Martinez, *Anal. Chim. Acta* 589 (2007) 255.
- [39] G.D. Liu, Y.Y. Lin, H. Wu, Y. Lin, *Environ. Sci. Technol.* 41 (2007) 8129.
- [40] M.E.B. Calvo, O.D. Renedo, M.J.A. Martinez, *Talanta* 74 (2007) 59.
- [41] P.J. Rousseuw, A.M. Leroy, *Robust Regression and Outlier Detection*, Wiley, New York, 1989.
- [42] D.L. Massart, B.G.M. Vandeginste, L.M.C. Buydens, S. De Jong, P.J. Lewi, J. Smeyers-Verbeke, *Handbook of Chemometrics and Qualimetrics. Part A*, Elsevier, Amsterdam, 1997.
- [43] ISO 11843-2, *Capability of Detection*, Geneva, Switzerland, 2000.



## Fluorometric determination of heparin based on self-quenching of fluorescein-labeled protamine

Yuya Egawa<sup>a,b,\*</sup>, Ryosuke Hayashida<sup>a</sup>, Toshinobu Seki<sup>b</sup>, Jun-ichi Anzai<sup>a</sup>

<sup>a</sup> Graduate School of Pharmaceutical Sciences, Tohoku University, Aramaki, Aoba-ku, Sendai, Miyagi 980-8578, Japan

<sup>b</sup> Faculty of Pharmaceutical Sciences, Josai University, 1-1 Keyaki-dai, Sakado, Saitama 350-0295, Japan

### ARTICLE INFO

#### Article history:

Received 17 January 2008

Received in revised form 11 April 2008

Accepted 11 April 2008

Available online 20 April 2008

#### Keywords:

Fluorescein

Fluorescence

Heparin

Protamine

Self-quenching

### ABSTRACT

A new signaling technique for a fluorometric heparin assay has been developed using the self-quenching of fluoresceinisothiocyanate-labeled protamine (F-protamine). The binding between F-protamine and heparin led to a significant fluorescence quenching due to enhancing the proximity of the F-protamine molecules. The fluorescence of F-protamine (5.9  $\mu\text{g/mL}$ ) decreased to 13% in the presence of 2.0  $\mu\text{g/mL}$  heparin. An advantage of this self-quenching system is that the detection can be carried out without using other indicators. With the present system, we could monitor the therapeutic level of heparin in bovine plasma, and the response was quick. These properties of the self-quenching system are suitable for practical use.

© 2008 Elsevier B.V. All rights reserved.

### 1. Introduction

Heparin is a highly sulfated glycosaminoglycan [1]. It is a widely used anticoagulant drug for surgical procedures and extracorporeal therapies. Because of its short biologic half-life and the potential bleeding risk, the accurate monitoring of heparin is critical [2–4]. The most commonly used clinical assays are the activated clotting time measurement and antifactor Xa assay [4]. Despite wide clinical use for many years, these methods are not specific for heparin and lack speed.

In the past few years, there has been an extensive effort to develop the direct monitoring of heparin based on a spectrophotometric analysis [5–9]. In general, a heparin sensor compound is composed of heparin recognition elements and signaling molecules. A signaling technique for heparin binding is one of the most important issues for the heparin sensor. For example, a halide-sensitive fluorophore 6-methoxyquinolium has been attached to a heparin-specific peptide sequence [8]. The fluorescence of the heparin sensor was quenched in a NaCl aqueous solution because  $\text{Cl}^-$  ion acted as a quencher of quinolium. Heparin binding induced displacement of the  $\text{Cl}^-$  ion around the quinolium, and the fluorescence of the quinolium then recovered. This approach is an excellent achievement in supramolecular chem-

istry. However, there is the possibility that the use of a quencher or indicator causes unexpected errors. It is recognized that sensor compounds, which do not require other indicators, are desirable for practical use [7,9].

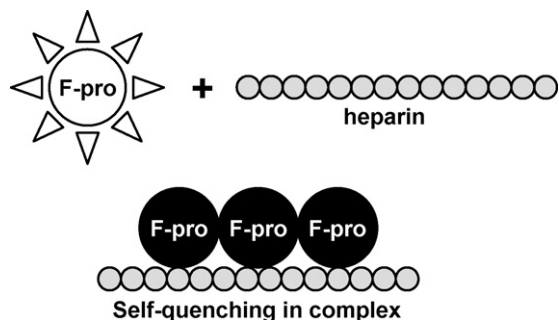
We have utilized the self-quenching phenomenon of fluorescein as a new signaling technique for heparin detection. The self-quenching of FITC-derivatives is attributed to the resonance energy transfer between the fluorescein molecules [10–14]. Fluorescein has a high potential for self-quenching because the emission spectrum sufficiently overlaps with the absorption spectrum. During self-quenching, fluorescein molecules must be within a critical distance of each other. It has been reported that the Forster distance for the self-quenching of fluorescein is about 42 Å [10]. Since this distance is comparable to or greater than the size of many proteins, the self-quenching phenomenon has been used to study protein folding and macromolecule association reactions [11–13]. Recently, our group also reported that the fluorescence of FITC-labeled concanavalin A was quenched by forming complexes with glycogen by enhancing the proximity of the FITC-labeled concanavalin A molecules [15].

These studies of self-quenching prompted us to use FITC-derivatives for the fluorometric determination of heparin. To get a strong binding ability for heparin, we selected protamine as a heparin recognition element and prepared FITC-labeled protamine (F-protamine). Protamine is a highly basic peptide that forms a stable complex with heparin through electrostatic interactions [16–18]. The average molecular weight of protamine (about

\* Corresponding author. Tel.: +81 49 286 2233.

E-mail address: [yegawa@josai.ac.jp](mailto:yegawa@josai.ac.jp) (Y. Egawa).





**Scheme 1.** Schematic representation of self-quenching of F-protamine upon complexation with heparin.

5000 Da) is relatively small compared to that of heparin (about 15,000 Da) [18]. In addition, heparin is a linear polysaccharide [1]. Thereby, one heparin molecule may bind more than one protamine molecule [19]. The complexation of F-protamine/heparin may induce self-quenching by enhancing the proximity of the F-protamine molecules (Scheme 1). It should be noted that this assay system does not require the use of other indicators, which will be advantage for practical use.

In this study, we demonstrate that heparin can be quantitatively detected in a therapeutic concentration by utilizing the self-quenching phenomenon of F-protamine. The self-quenching system was investigated with respect to its measurement range, selectivity, and response time.

## 2. Experimental

### 2.1. Materials

Protamine sulfate (from salmon), heparin sodium salt, chondroitin sulfate A sodium salt, hyaluronic acid sodium salt, and bovine serum albumin (BSA) were purchased from Wako Pure Chemical Industries, Ltd. (Osaka, Japan). Fluorescein-4-isothiocyanate (FITC) was obtained from Dojindo Laboratories (Kumamoto, Japan). Low molecular weight heparin sodium salt (average molecular weight ~3000) and bovine plasma were from Sigma–Aldrich. All other chemicals used in this study were of the highest grade available and were used without further purification. F-protamine was prepared according to a previous procedure [20]. FITC (19  $\mu\text{mol}$ ) dissolved in pyridine (1.0 mL) was added to a solution containing 10  $\mu\text{mol}$  protamine, 1.0 M NaCl and 0.10 M  $\text{NaHCO}_3$  (20 mL, pH 9.1) The resulting solution was stirred for 2 h at room temperature and dialyzed against water using a dialysis tube (molecular mass cutoff 3000 Da) to remove unreacted FITC.

### 2.2. Apparatus

The fluorescence emission spectrum was measured using a Shimadzu RF-5300PC spectrofluorophotometer (Kyoto, Japan). The UV–vis absorption spectrum was recorded by a Shimadzu 3100PC spectrophotometer (Kyoto, Japan).

### 2.3. General procedure for heparin detection with F-protamine

A stock solution (0.3 mL) containing various concentrations of heparin was mixed with an F-protamine solution (6.5  $\mu\text{g mL}^{-1}$ , 2.7 mL) in a cuvette for the fluorescence measurements. The resulting concentration of F-protamine was 5.9  $\mu\text{g mL}^{-1}$ . The pH of the solutions was adjusted to 7.4 (10 mM phosphate) or 3.0 (10 mM acetate). The fluorescence emission spectra of the pH 7.4 solution were measured with excitation light at 493 nm because the

UV–vis absorption maximum of F-protamine was observed at this wavelength. For the pH 3.0 solution, 439 nm light was used for the excitation.

### 2.4. Stoichiometric analysis of F-protamine/heparin complex

The stoichiometry of F-protamine/heparin was determined by the Job's plot [21]. The heparin and F-protamine concentrations were calculated by assuming an average molecular mass of 15,000 and 5000 Da, respectively [18]. A 1.3  $\mu\text{M}$  solution of F-protamine and the same concentration of heparin solution were separately prepared. They were mixed at varying volume ratios, but the total volume was constant at 3 mL.  $\Delta I$  is the fluorescence change due to the observed complexation; from the fluorescence intensity of the solution containing F-protamine was subtracted that of the solution containing F-protamine and heparin. The observed  $\Delta I$  values were plotted versus the volume ratio of the heparin solutions. All experiments were carried out at room temperature ( $\sim 20^\circ\text{C}$ ).

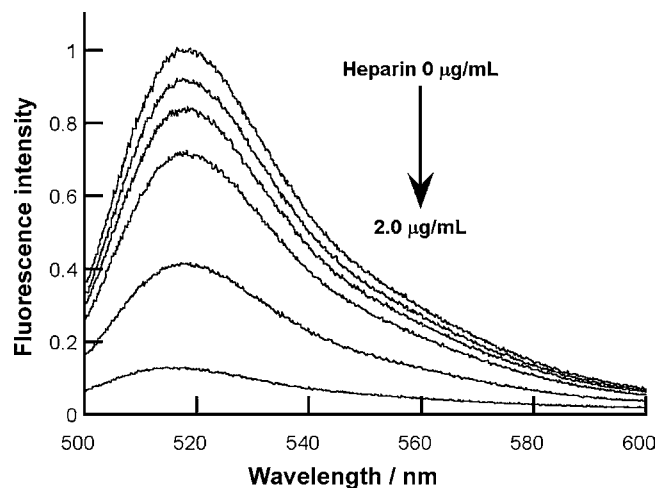
## 3. Results and discussion

### 3.1. Heparin detection with F-protamine

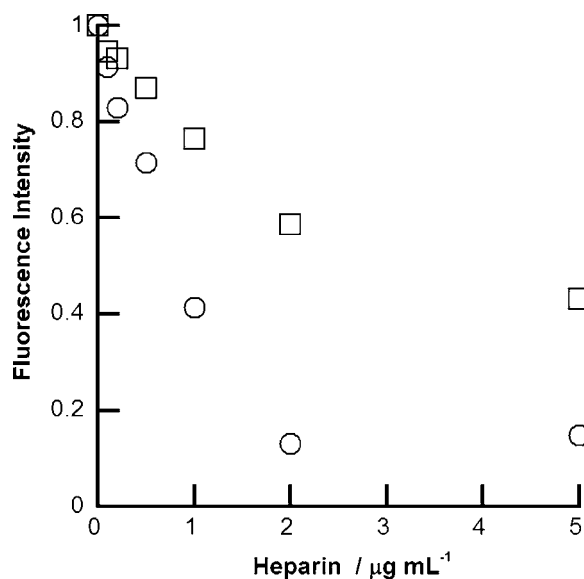
For the preparation of F-protamine, the ratio of FITC/protamine is important because fluorescence of a highly FITC labeled molecule is quenched by self-quenching without complexation to heparin [14]. The ratio of FITC/protamine was determined by comparing the UV–vis spectra of the F-protamine and fluorescein solution at pH 7.4. The ratio of FITC/protamine was calculated to be 0.8, which was used for the present system.

Fig. 1 shows the fluorescence emission spectra of 5.9  $\mu\text{g mL}^{-1}$  F-protamine with various concentrations of heparin. The spectra exhibited an emission maximum at 518 nm which was derived from the FITC moiety [22]. The fluorescence intensity at 518 nm linearly decreased with the increasing heparin concentration. When the concentration of heparin was 2.0  $\mu\text{g mL}^{-1}$ , the fluorescence intensity decreased to 13% (Figs. 1 and 2). This result indicates that the self-quenching of F-protamine is successfully achieved upon complexation with heparin, and we can monitor the heparin concentration by the fluorescence intensity of F-protamine.

We also used pH 3.0 solutions instead of pH 7.4 solutions. At pH 3.0, the fluorescent intensity at the emission maximum (517 nm) decreased to 43% in the presence of 5.0  $\mu\text{g mL}^{-1}$  heparin (Fig. 2).



**Fig. 1.** Fluorescence emission spectra of F-protamine solution (5.9  $\mu\text{g mL}^{-1}$ ) in the absence and presence of heparin (0, 0.1, 0.2, 0.5, 1.0, 2.0  $\mu\text{g mL}^{-1}$ ) at pH 7.4. F-protamine was excited by 493 nm light.



**Fig. 2.** Fluorescence intensity change of F-protamine solution ( $5.9 \mu\text{g mL}^{-1}$ ) as a function of concentration of heparin at pH 7.4 ( $\circ$ ,  $\lambda_{\text{ex}} = 493 \text{ nm}$ ,  $\lambda_{\text{em}} = 518 \text{ nm}$ ) and 3.0 ( $\square$ ,  $\lambda_{\text{ex}} = 439 \text{ nm}$ ,  $\lambda_{\text{em}} = 517 \text{ nm}$ ).

This result indicates that the pH 3.0 solution can also be used in the present system.

The quenching of F-protamine is lower at pH 3.0 than at pH 7.4. The difference in the self-quenching behavior is probably due to the pH sensitivity of fluorescein. The absorption and emission spectra of fluorescein change depend upon the pH value of the solution. The F-protamine solution at pH 7.4 exhibited an absorption maximum at 493 nm and an emission maximum at 518 nm. The difference between the positions of the band maxima of the absorption and emission spectra (Stokes shift) was 25 nm at pH 7.4. At pH 3.0, the Stokes shift increased to 78 nm. A small Stokes shift means a large overlap of the absorption and emission spectra, which is indispensable for the self-quenching. The small Stokes shift at pH 7.4 probably causes a significant quenching of F-protamine.

### 3.2. Stoichiometric analysis of F-protamine/heparin complex

To determine the stoichiometry of the F-protamine/heparin in the complex, we used Job's method (Fig. 3) [21]. According to Sec-

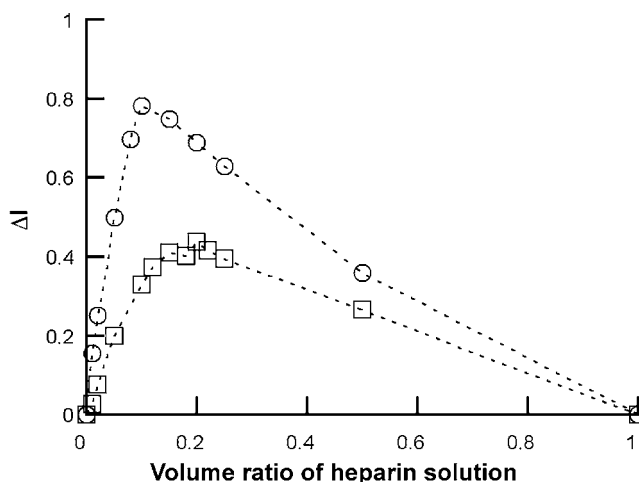


**Fig. 3.** Job's plot of F-protamine and heparin at pH 7.4 ( $\circ$ ,  $\lambda_{\text{ex}} = 493 \text{ nm}$ ,  $\lambda_{\text{em}} = 518 \text{ nm}$ ) and pH 3.0 ( $\square$ ,  $\lambda_{\text{ex}} = 439 \text{ nm}$ ,  $\lambda_{\text{em}} = 517 \text{ nm}$ ).

tion 2.4, a  $1.3 \mu\text{M}$  F-protamine solution and the same concentration of heparin solution were mixed at varying volume ratios. At pH 7.4, the maximum value of  $\Delta I$  was observed when the volume ratio of heparin was about 0.1. This result means that the stoichiometry of the F-protamine/heparin in the complex was about a 9/1 molar ratio. The stoichiometry of the F-protamine/heparin by mass was about 3/1, which was higher than that of the native protamine (1.1/1 to 1.5/1 in mass) [19]. At pH 3.0, the maximum value of  $\Delta I$  was found around a 0.20 volume ratio of heparin, and the stoichiometry of the F-protamine/heparin was about a 4/1 molar ratio (1.3/1 by mass). These results indicate that multiple F-protamine molecules were assembled on a heparin molecule in the complex at pH 7.4 and 3.0, which supports the proposed mechanism for self-quenching of F-protamine. The difference in stoichiometry is probably due to the pH-induced structural change in fluorescein. At pH 7.4, fluorescein has two negative charges [22]. It is likely that the anionic charges reduce the electrostatic repulsion between the F-protamine molecules, which results in a high F-protamine/heparin ratio. The closely-packed F-protamines at pH 7.4 may cause a significant quenching of F-protamine because the quenching of the FITC-derivatives depends on their proximity. In contrast, the major conformation of fluorescein at pH 3.0 is the neutral form [22]. As in the case of the native protamine, there is a strong repulsion between the F-protamine molecules at pH 3.0.

### 3.3. The selectivity and sensitivity of F-protamine

Fig. 4(a) shows the fluorescence responses of F-protamine to heparin, low molecular weight heparin (average molecular weight  $\sim 3000$ ), chondroitin sulfate, and hyaluronic acid. Hyaluronic acid was monitored in the range of  $0.10\text{--}1.0 \text{ mg mL}^{-1}$  since its solubility was low. These results show that the selectivity of F-protamine is related to the anionic charge of the analytes, that is heparin > chondroitin sulfate > hyaluronic acid.

The addition of 150 mM NaCl improved the selectivity for heparin (Fig. 4(b)). High concentrations of  $\text{Na}^+$  and  $\text{Cl}^-$  screen the charges of polyelectrolytes and decrease the affinity between F-protamine and glycosaminoglycan. It is likely that only highly anionic heparin can bind to F-protamine in the high ionic strength condition. This result shows the possibility of using this sensor directly in biological media.

The response to low molecular weight heparin (average molecular weight  $\sim 3000 \text{ Da}$ ) is similar to that of native heparin (average molecular weight  $\sim 15,000 \text{ Da}$ ). This result can be explained with the self-quenching mechanism of F-protamine. The fluorescence intensity of F-protamine is closely relevant to the distance between F-protamine molecules. This distance depends on the charge density of glycosaminoglycan. Because native heparin and low molecular weight heparin have virtually the same charge density, they induce the similar fluorescence change of F-protamine. This result indicates that the present system can be applied to low molecular weight heparin that is recently being very often used due to fewer side-effects [23].

We carried out the binding study with  $0.59 \text{ mg/mL}$  F-protamine in the presence of 150 mM NaCl (Fig. 4(b)). In this condition, the fluorescence intensity changed depending on the heparin concentration in the range of  $0.010\text{--}0.20 \mu\text{g/mL}$ . This result indicates that the measurement range can be changed by selecting a proper concentration of F-protamine.

### 3.4. The effect of albumin

For clinical use, albumin is not negligible even if its binding affinity to a sensor compound is low since the concentration of albumin in serum is very high ( $\sim 40 \text{ mg mL}^{-1}$ ) [24]. To investigate the effect

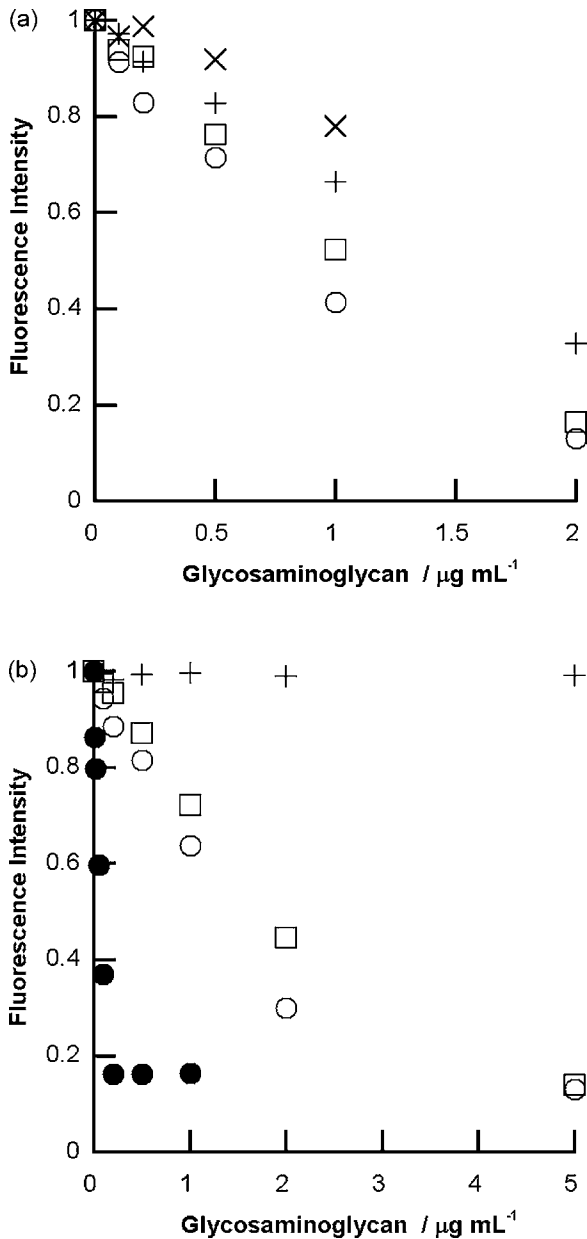


**Fig. 4.** (a) Fluorescence intensity change of F-protamine solution ( $5.9 \mu\text{g mL}^{-1}$ ) as a function of the glycosaminoglycan concentration (○: heparin; □: low molecular weight heparin; +: chondroitin sulfate; ×: hyaluronic acid, pH 7.4,  $\lambda_{\text{ex}} = 493 \text{ nm}$ ,  $\lambda_{\text{em}} = 518 \text{ nm}$ ). The effect of hyaluronic acid was investigated in the range of  $0.10\text{--}1.0 \mu\text{g mL}^{-1}$  due to its low solubility. (b) In the presence of  $150 \text{ mM NaCl}$ , fluorescence intensity change of  $5.9 \mu\text{g/mL}$  F-protamine solution (○: heparin; □: low molecular weight heparin; +: chondroitin sulfate) and  $0.59 \mu\text{g/mL}$  F-protamine solution (●: heparin) at pH 7.4 ( $\lambda_{\text{ex}} = 493 \text{ nm}$ ,  $\lambda_{\text{em}} = 518 \text{ nm}$ ).

of albumin on the present system, we measured the fluorescence of F-protamine in the presence and absence of BSA.

Addition of BSA induced a decrease of the fluorescence intensity of F-protamine. This result suggests the electrostatic interaction between BSA and F-protamine. Because BSA has negative charges at pH 7.4 [25], some F-protamine molecules may bind to one BSA molecule, which results in the decrease of the fluorescence intensity of F-protamine. However, about 70% of the fluorescence intensity remained when the BSA concentration was in the range of  $0.20\text{--}4.0 \text{ mg mL}^{-1}$ . The most likely cause for the incomplete quenching is the low charge density of BSA. An important finding here is that the fluorescence intensity of F-protamine does not

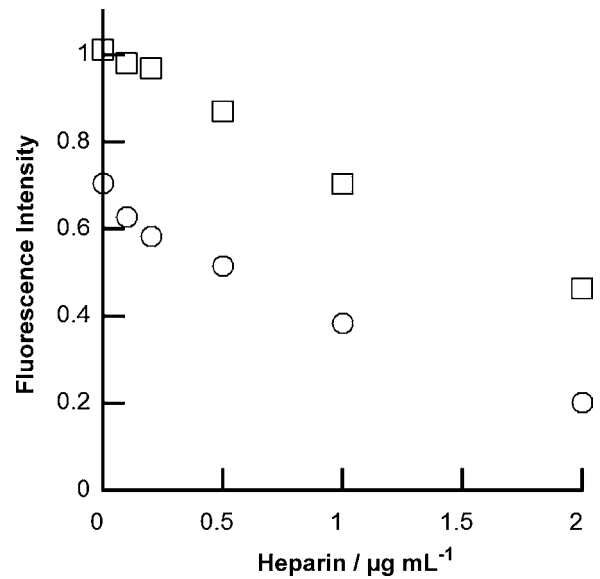


**Fig. 5.** Fluorescence intensity change in F-protamine solution ( $5.9 \mu\text{g mL}^{-1}$ ) in the presence of  $4.0 \text{ mg BSA}$  as a function of the heparin concentration at pH 7.4 (○,  $\lambda_{\text{ex}} = 493 \text{ nm}$ ,  $\lambda_{\text{em}} = 518 \text{ nm}$ ) and pH 3.0 (□,  $\lambda_{\text{ex}} = 439 \text{ nm}$ ,  $\lambda_{\text{em}} = 517 \text{ nm}$ ).

change even though the concentration of albumin slightly changes. Taking advantage of this property, we monitored the heparin concentrations in the presence of albumin.

We prepared heparin stock solutions in the presence of  $40 \text{ mg mL}^{-1}$  BSA which corresponds to the concentration of albumin in serum [24]. It is known that a therapeutic concentration of heparin is in the range of  $0.2\text{--}1.2 \text{ U mL}^{-1}$ , which is calculated to be  $1.5\text{--}9.2 \mu\text{g mL}^{-1}$  based on the activity of heparin used in this study ( $\sim 130 \text{ U/mg}$ ) [2–4]. Thereby, the concentration of heparin was set in the range of  $1.0\text{--}20 \mu\text{g mL}^{-1}$ . A  $0.3 \text{ mL}$  aliquot of the stock solution was added to  $2.7 \text{ mL}$  of the F-protamine solution ( $6.5 \mu\text{g mL}^{-1}$ ).

The fluorescence intensity decreased depending on the concentration of heparin even in the presence of  $4.0 \text{ mg mL}^{-1}$  BSA (Fig. 5). This result indicates that the present system can be used with a therapeutic level of heparin in the presence of a high concentration of albumin.

We also investigated the effect of BSA in a pH 3.0 solution. The fluorescence intensity of F-protamine at pH 3.0 remains virtually unchanged upon BSA addition. It is likely that BSA does not interact with F-protamine because both of them have positive charges at pH 3.0 [25]. We tried to prepare pH 3.0 stock solutions containing heparin and BSA. However, a large amount of precipitate was formed, which was due to the electrostatic interaction between heparin and BSA at pH 3.0. To avoid precipitation, we used the pH 7.4 stock solution containing heparin and BSA. The stock solution ( $0.3 \text{ mL}$ , pH 7.4) was added to the F-protamine solution ( $2.7 \text{ mL}$ , pH 3.0). We confirmed that the resulting solution pH was 3.0. The titration result is shown in Fig. 5. The fluorescence intensity decreased depending on the heparin concentration. These results suggest that using the acidic pH is a good way to avoid the effect of BSA, although the fluorescence intensity and self-quenching were lower at pH 3.0 than at pH 7.4.

### 3.5. The response for heparin in plasma

A  $0.3 \text{ mL}$  aliquot of the bovine plasma was added to  $2.7 \text{ mL}$  of the F-protamine solution ( $6.5 \mu\text{g mL}^{-1}$  F-protamine,  $150 \text{ mM NaCl}$ ). At pH 7.4, the fluorescence intensity of F-protamine at  $518 \text{ nm}$  decreased to 52% upon addition of plasma without heparin (Fig. 6(a)). This decrease of fluorescence intensity is due to nonspe-

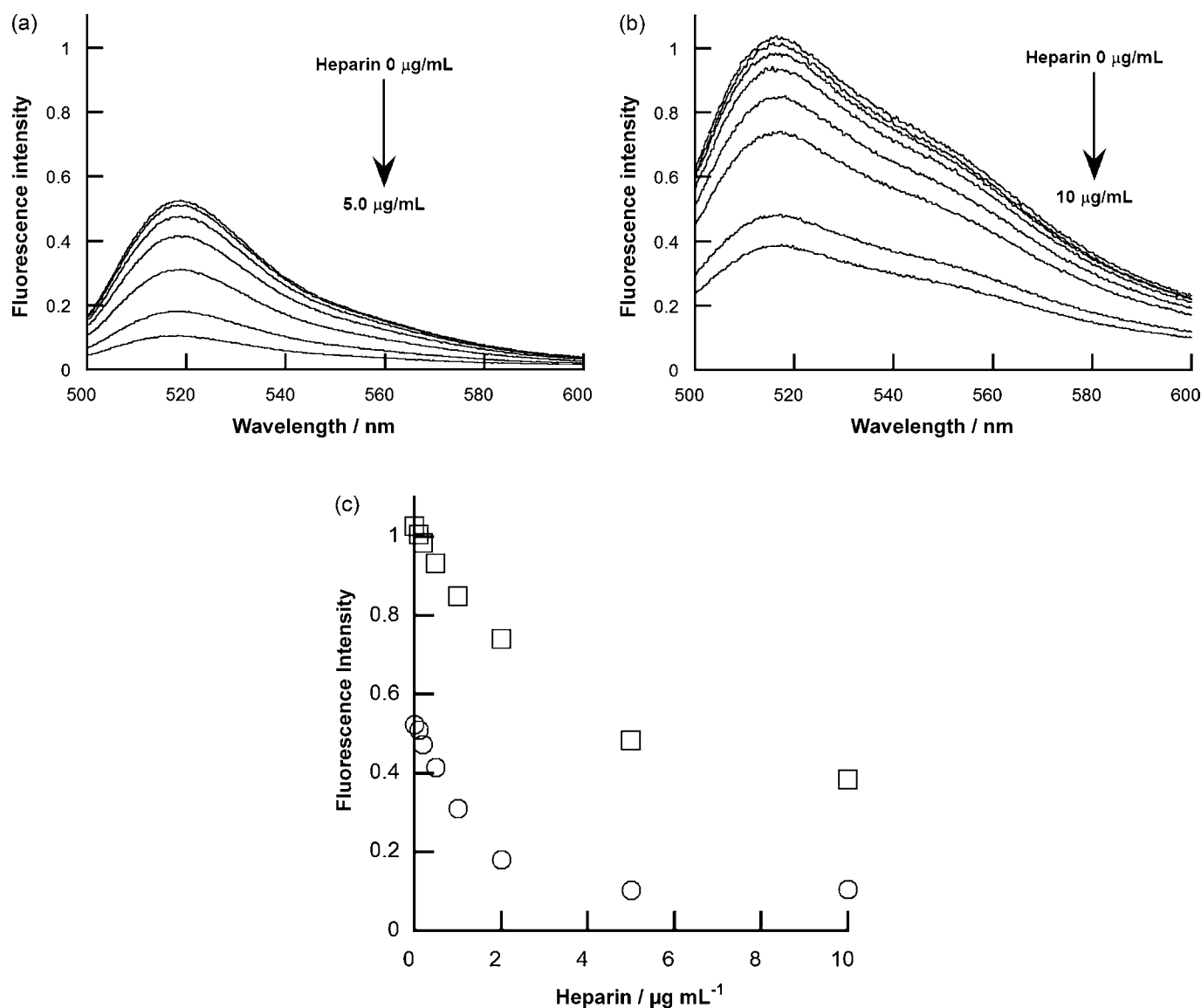


**Fig. 6.** The response for heparin in bovine plasma. (a) Fluorescence emission spectra of F-protamine solution ( $5.9 \mu\text{g mL}^{-1}$ ) varying the concentration of heparin at pH 7.4 ( $\lambda_{\text{ex}} = 493 \text{ nm}$ ), (b) at pH 3.0 ( $\lambda_{\text{ex}} = 439 \text{ nm}$ ). (c) Fluorescence intensity change at pH 7.4 ( $\circ$ ,  $\lambda_{\text{ex}} = 493 \text{ nm}$ ,  $\lambda_{\text{em}} = 518 \text{ nm}$ ) and pH 3.0 ( $\square$ ,  $\lambda_{\text{ex}} = 439 \text{ nm}$ ,  $\lambda_{\text{em}} = 517 \text{ nm}$ ).

cific bindings. Increase of the heparin concentration induced the further decrease of fluorescence intensity (Fig. 6(a) and (c)).

At pH 3.0, a 0.3 mL aliquot of the bovine plasma was added to 2.7 mL of the F-protamine solution ( $6.5 \mu\text{g mL}^{-1}$  F-protamine, 150 mM NaCl). The fluorescence intensity of F-protamine at pH 3.0 remains virtually unchanged upon plasma addition (Fig. 6(b)). The fluorescence intensity decreased depending on the concentration of added heparin (Fig. 6(b) and (c)).

We confirmed that the responses at pH 7.4 and 3.0 were quick (within 1 min). These results indicated that this self-quenching system of F-protamine can be used for plasma sample. In particular, using acidic pH is suitable for avoiding nonspecific binding.

#### 4. Conclusion

We have demonstrated a new signaling technique for heparin detection utilizing the self-quenching phenomenon of FITC-derivatives. The fluorescence intensity of F-protamine decreased depending on the heparin concentrations. Based on the stoichiometry analysis, it was confirmed that multiple F-protamine

molecules were assembled on a heparin molecule in the complex. The proximity of the F-protamine molecules in the complex is probably responsible for the self-quenching. An advantage of the self-quenching system is that the optical signal can be produced without using other indicators. With the present system, we can monitor the therapeutic level of heparin even in plasma. In addition, the response is quick. These properties of the self-quenching system are suitable for practical use.

#### References

- [1] R.J. Linhardt, *J. Med. Chem.* 46 (2003) 2551.
- [2] G.J. Despotis, G. Gravlee, K. Filos, J. Levy, *Anesthesiology* 91 (1999) 1122.
- [3] R. Jelinek, S. Kolusheva, *Chem. Rev.* 104 (2004) 5987.
- [4] S. Kitchen, *Br. J. Haematol.* 111 (2000) 397.
- [5] S.P. Liu, H.Q. Luo, N.B. Li, Z.F. Liu, W.X. Zheng, *Anal. Chem.* 73 (2001) 3907.
- [6] Z. Zhong, E.V. Anslyn, *J. Am. Chem. Soc.* 124 (2002) 9014.
- [7] A.T. Wright, Z. Zhong, E.V. Anslyn, *Angew. Chem.-Int. Ed.* 44 (2005) 5679.
- [8] J.C. Saucedo, R.M. Duke, M. Nitz, *ChemBioChem* 8 (2007) 391.
- [9] W. Sun, H. Bandmann, T. Schrader, *Chem.-Eur. J.* 13 (2007) 7701.
- [10] A. Kowski, *Photochem. Photobiol.* 38 (1983) 487.

- [11] X. Zhuang, T. Ha, H.D. Kim, T. Centner, S. Labeit, S. Chu, *Proc. Natl. Acad. Sci. U.S.A.* 97 (2000) 14241.
- [12] L.W. Runnels, S.F. Scarlata, *Biophys. J.* 69 (1995) 1569.
- [13] J. Karolin, M. Fa, M. Wilczynska, T. Ny, B.-A. Johansson, *Biophys. J.* 74 (1998) 11.
- [14] J.R. Lakowicz, J. Malicka, S. D'Auria, I. Gryczynski, *Anal. Biochem.* 320 (2003) 13.
- [15] K. Satoh, J. Anzai, *Anal. Bioanal. Chem.* 384 (2006) 1297.
- [16] J.C. Van Kerkhof, P. Bergveld, R.B.M. Schasfoort, *Biosens. Bioelectron.* 10 (1995) 269.
- [17] N. Ramamurthy, N. Baliga, J.A. Wahr, U. Schaller, V.C. Yang, M.E. Meyerhoff, *Clin. Chem.* 44 (1998) 606.
- [18] A. Shvarev, E. Bakker, *Anal. Chem.* 77 (2005) 5221.
- [19] S.A. Buchanan, T.P. Kennedy, R.B. MacArthur, M.E. Meyerhoff, *Anal. Biochem.* 346 (2005) 241.
- [20] K. Wehling, S. Krauss, K.G. Wagner, *Nucleic Acids Res.* 3 (1976) 149.
- [21] K.A. Connors, *Binding Constants: The Measurement of Molecular Complex Stability*, Wiley-Interscience, New York, 1987, p. 24.
- [22] N. Klonis, W.H. Sawyer, *J. Fluoresc.* 6 (1996) 147.
- [23] J. Hirsh, *Circulation* 98 (1998) 1575.
- [24] S. Curry, H. Mandelkow, P. Brick, N. Franks, *Nat. Struct. Biol.* 5 (1998) 827.
- [25] S.H. Brewer, W.R. Glomm, M.C. Johnson, M.K. Knag, S. Franzen, *Langmuir* 21 (2005) 9303.



## Screening method for phthalate esters in water using liquid-phase microextraction based on the solidification of a floating organic microdrop combined with gas chromatography–mass spectrometry

Hadi Farahani<sup>a</sup>, Mohammad Reza Ganjali<sup>a,b</sup>, Rassoul Dinarvand<sup>c</sup>, Parviz Norouzi<sup>a,b,\*</sup>

<sup>a</sup> Center of Excellence in Electrochemistry, Faculty of Chemistry, University of Tehran, P.O. Box 14155-6455, Tehran, Iran

<sup>b</sup> Endocrinology & Metabolism Research center, Medical Science/University of Tehran, Tehran, Iran

<sup>c</sup> Medical Nanotechnology Research Center, Medical Sciences/University of Tehran, P.O. Box 14155-6451, Tehran, Iran

### ARTICLE INFO

#### Article history:

Received 8 December 2007

Received in revised form 2 March 2008

Accepted 4 March 2008

Available online 13 March 2008

#### Keywords:

Liquid-phase microextraction (LPME)

Phthalate esters

Gas chromatography–mass spectrometry (GC–MS)

Water samples

### ABSTRACT

A simple and efficient liquid-phase microextraction (LPME) technique was developed using directly suspended organic microdrop coupled with gas chromatography–mass spectrometry (GC–MS), for the extraction and the determination of phthalate esters (dimethyl phthalate, diethyl phthalate, diallyl phthalate, di-*n*-butyl phthalate (DnBP), benzyl butyl phthalate (BBP), dicyclohexyl phthalate and di-2-ethylhexyl phthalate (DEHP)) in water samples. Microextraction efficiency factors, such as nature and volume of the organic solvent, temperature, salt effect, stirring rate and the extraction time were investigated and optimized. Under the optimized extraction conditions (extraction solvent: 1-dodecanol; extraction temperature: 60 °C; microdrop volume: 7 µL; stirring rate: 750 rpm, without salt addition and extraction time: 25 min), figures of merit of the proposed method were evaluated. The values of the detection limit were in the range of 0.02–0.05 µg L<sup>-1</sup>, while the R.S.D.% value for the analysis of 5.0 µg L<sup>-1</sup> of the analytes was below 7.7% (*n* = 4). A good linearity (*r*<sup>2</sup> ≥ 0.9940) and a broad linear range (0.05–100 µg L<sup>-1</sup>) were obtained. The method exhibited enrichment factor values ranging from 307 to 412. Finally, the designed method was successfully applied for the preconcentration and determination of the studied phthalate esters in different real water samples and satisfactory results were attained.

© 2008 Published by Elsevier B.V.

### 1. Introduction

Phthalate esters (PEs) are well-known polymer additives that are used in formulations of pesticides, paints, poly (vinyl chloride) plastics, and etc. However, their most important use by far is as plasticizers, improving the flexibility and workability of polymeric materials. Having the mentioned properties, the phthalate esters production and their use have increased significantly in the recent years. The main drawback of PEs is that they can migrate from the material to the environment and, consequently, pollute water, soil, air, food products [1–5]. Furthermore, certain phthalate esters and/or their metabolites are suspected to be human cancer-causing agents and endocrine disruptors [6,7] which makes their trace determination of special importance.

The most commonly used phthalates include bis-2-ethylhexyl phthalate (DEHP), di-*n*-butyl phthalate (DnBP) and butyl benzyl

phthalate (BBP). DEHP is the most widely used PE in the world and it represents a quarter of the total plasticizers production [8]. These phthalates are on the first three priority lists for the risk assessment, in accordance with the European Union's Regulation 793/93 on the existing substances [9,10]. The US Environmental Protection Agency (EPA) has set the maximum contamination level (MCL) for DEHP in water systems at 6 µg L<sup>-1</sup> and recommended that concentrations above 0.6 µg L<sup>-1</sup> should be closely monitored [11].

Gas chromatography (GC) [12–15] and high performance liquid chromatography (HPLC) [16–18] have been used commonly for the detection of these compounds in water samples. Nevertheless, when the concentration levels are low, a previous enrichment step is usually needed. The preconcentration techniques, which are commonly applied to monitor phthalates in water, are liquid–liquid extraction (LLE) with dichloromethane or hexane [2,15] and solid-phase extraction (SPE) [2,16,18]. However, these sample pretreatment methods are considered expensive, time-consuming and labor-intensive methods, which often result in high blank values [19].

Solid-phase microextraction (SPME), now a commercial product, was developed by Pawliszyn's group [20]. It is an innovative solvent-free procedure that has gained tremendous popularity. It

\* Corresponding author at: Center of Excellence in Electrochemistry, Faculty of Chemistry, University of Tehran, P.O. Box 14155-6455, Tehran, Iran.

Tel.: +98 21 61112294; fax: +98 21 66405141.

E-mail address: [norouzi@khayam.ut.ac.ir](mailto:norouzi@khayam.ut.ac.ir) (P. Norouzi).

satisfies most of the desired characteristics of a sample preparation technique mentioned above, having been used for numerous applications particularly in environmental, biological and pharmaceutical analyses [21–27], including some PEs [4,5,17,27]. In addition, it is portable, relatively fast and it can be automated and coupled online with analytical instrumentation. Nevertheless, the coated fibers may be considered to be expensive and, for some applications, they have limited lifetimes [28,29].

Liquid-phase microextraction (LPME) is a fairly new method of sample preparation [30]. It is a miniaturized implementation of the conventional LLE, where only microliters of the solvents are used. LPME has been used to preconcentrate compounds from aqueous samples [31–38]. In 2003, Psillakis and Kalogerakis developed the hollow-fiber LPME (HFLPME), combined with GC for the PEs determination in water samples [39]. This technique is simple, inexpensive and providing minimal exposure to toxic organic solvents.

Recently, Yamini and co-workers have reported a simple and efficient preconcentration and microextraction method, based on LPME, which was initially applied for the determination of polycyclic aromatic hydrocarbons (PAHs) in water samples [40]. In this technique, a free microdrop of the organic solvent is delivered to the surface of an aqueous sample, while being agitated by a stirring bar in the bulk of the solution. Under the proper stirring conditions, the suspended microdrop can remain in the top-center position of the aqueous sample. After the completion of the extraction, the sample vial is cooled by placing it into an ice bath for 4 min. The solidified microdrop is then transferred into a conical vial, where it melts immediately. Finally, the analytes determination in the extractant can be performed by GC. This quantitative LPME method is a green and satisfactory analytical procedure, for which excellent accuracy and precision are demonstrated, being simpler and more convenient, compared with the conventional sample preparation methods.

The goal of this study was to assess the technique suitability for the detection of a group of the PEs compounds in water samples. The analytes were monitored by gas chromatography combined with mass spectrometry (GC–MS). The influence of different experimental parameters on the yield of the sample preparation step is described and discussed. In the end, this recommended method was employed to investigate the levels of the target species in several water samples.

## 2. Experimental

### 2.1. Reagents

The studied compounds were dimethyl- (DMP), diethyl- (DEP), diallyl- (DAP), di-*n*-butyl- (DnBP), benzyl butyl- (BBP), dicyclohexyl- (DCHP) and di-2-ethylhexyl- (DEHP) phthalate

esters. All PEs were purchased from Merck (Darmstadt, Germany). The stock standard solutions of 2000.0 mg L<sup>-1</sup> of each compound were prepared in methanol. The working standard solution of 100 mg L<sup>-1</sup> was prepared weekly in methanol. The stock and working standard solutions were stored at 4 °C at the refrigerator. The aqueous solutions were prepared daily by diluting the working solution with water. The used reagent water was purified with a Milli-Q water purification system (Millipore, Bedford, MA, USA). 1-Undecanol, 1-dodecanol, 2-dodecanol and *n*-hexadecane as the extraction solvents, benzyl benzoate as the internal standard as well as sodium chloride were purchased from Merck (Darmstadt, Germany). A solution of the internal standard with the concentration of 2.0 mg L<sup>-1</sup> in 1-dodecanol was used as the extracting solvent.

### 2.2. Instrumentation

The analysis was performed on a Hewlett-Packard (Agilent Technologies, Palo Alto, CA, USA) HP 6890 series GC, equipped with a split/splitless injector and a HP 5973 mass selective detector system. The MS was operated at the electron impact (EI) mode (70 eV). The chromatographic data were recorded using a HP Chemstation, which was controlled by Windows NT (Microsoft). Helium (99.999%) was employed as carrier gas at the flow rate of 0.8 mL min<sup>-1</sup>. The analytes were separated on a 30 m × 0.25 mm i.d. × 0.25 μm film thickness DB-5MS gas chromatographic column (J&W Scientific, Folsom, CA, USA) with the following oven temperature program: initial 60 °C, from 60 °C (held 3 min) to 180 °C at 20 °C min<sup>-1</sup>, increased at 10 °C min<sup>-1</sup> to 285 °C and held for 5 min. The injection port was operated at 350 °C and was used at the split mode with a split ratio of 1:10. The EI ion source, quadrupole mass analyzer and the interface temperature were maintained at 230, 150 and 280 °C, respectively. The MS was tuned to *m/z* 69, 219 and 502 for the EI corresponding to perfluorotetrabutylamine (PFTBA). It was equipped with the mass spectral library Wiley 275, which was used to compare the obtained experimental spectra. The MS was operated on the total ion current (TIC) mode, scanning from *m/z* 50 to 550 for identification purposes. To gain the highest possible sensitivity, the acquisition was performed at the selected ion monitoring (SIM) mode, based on the selection of some mass peaks of the highest intensity for each compound. Table 1 lists the retention times, selected masses and the start scan times for each compound studied by GC–MS.

A magnetic heater-stirrer (IKA-Werke, Staufen, Germany) and an 8 mm × 1.5 mm PTFE coated stirring bar were used to stir the solutions. A simple water bath placed on the heater-stirrer was used for control the temperature of the sample solutions. All injections were carried out using a 1.00 μL microsyringe (zero dead volume, cone tip needle, SGE, Australia).

**Table 1**  
Retention times, selected ions, scan start time and some quantitative data of the PEs studied by the LPME–GC–MS

Compound	Retention time (min)	Selected ions ( <i>m/z</i> )	Scan start time (min)	LOD <sup>a,b</sup> (μg L <sup>-1</sup> )	<i>r</i> <sup>2</sup>	LR <sup>b,c</sup> (μg L <sup>-1</sup> )	EF <sup>d</sup>	R.S.D.% <sup>e</sup> ( <i>n</i> = 4)
DMP	10.5	163, 194	10.0 <sup>f</sup>	0.03	0.9947	0.05–100	391	5.8
DEP	11.4	149, 177	11.0	0.02	0.9959	0.05–100	358	6.4
DAP	13.8	149, 189	13.3	0.02	0.9953	0.05–50	412	7.7
DnBP	15.5	149, 223	15.0	0.03	0.9960	0.05–50	376	5.5
BBP	18.8	149, 206	18.3	0.03	0.9940	0.05–100	389	7.3
DCHP	20.2	149, 167	19.8	0.05	0.9971	0.1–50	307	6.9
DEHP	20.4	149, 279	20.3	0.02	0.9955	0.05–100	409	6.1

<sup>a</sup> Limit of detection for S/N = 3.

<sup>b</sup> Concentration unit is μg L<sup>-1</sup>.

<sup>c</sup> Linear range.

<sup>d</sup> Enrichment factor.

<sup>e</sup> Relative standard deviation at the concentration of 5.0 μg L<sup>-1</sup> of each PE.

<sup>f</sup> The MS detector was OFF before the time point of 10.0 min.

### 2.3. Analytical procedure

A total of 10.0 mL of the aqueous PEs solution (containing  $5.0 \mu\text{g L}^{-1}$  of each PE) was transferred into an 11.0 mL vial.  $10.0 \mu\text{L}$  of 1-dodecanol were delivered to the solution surface using a  $10.0 \mu\text{L}$  model 701 N microsyringe (Reno, NV, USA). The vial was sealed and then the magnetic stirrer was turned on. Under the proper stirring conditions, the suspended microdrop could remain in the top-center position of the aqueous sample. In an immiscible liquid–liquid system with the proper interface tension, the microdrop would not break up even in the absence of any support from the microsyringe needle, polymer rod or other supporting material like hollow fibers. On the other hand, the microdrop movement was affected by the flow field, which favored the promotion of the mass transfer inside the microdrop [40]. After the desired extraction time, the sample vial was transferred into an ice beaker and the organic solvent was solidified after 4 min. Then, the solidified solvent was transferred into a conical vial and it melted immediately. Finally,  $1.00 \mu\text{L}$  of the extractant was injected into the gas chromatograph.

A univariate approach was employed to optimize the influential factors in this method. All quantifications, made in this study, were based on the relative peak area of the analyte to the internal standard (benzyl benzoate) from the average of three replicate measurements.

## 3. Results and discussion

### 3.1. Selection of the extracting solvent

The selection of an appropriate extraction solvent is of great importance for the optimization of the LPME process. To choose a suitable organic solvent, the following points should be considered. Firstly, the chosen solvent should illustrate a high boiling point and a low vapor pressure in order to reduce the risk of evaporation [41]. Secondly, it should exhibit a good chromatographic behavior [42] and, thirdly, the partitioning coefficient of the analyte should be high. Furthermore, the solvent must have a good affinity for the target compounds [43] and, finally, it should demonstrate a melting point near the room temperature (in the range of  $10\text{--}30^\circ\text{C}$ ) [40]. According to these considerations, several extracting solvents, including 1-undecanol, 1-dodecanol, 2-dodecanol and *n*-hexadecane were considered. Among the tested extracting solvents, 1-dodecanol presented the best extraction efficiency (Fig. 1). Thus, 1-dodecanol was chosen as the extracting solvent in this investigation. In order to improve the precision and accuracy of the method, benzyl benzoate was used as the internal standard and was added into the extracting solvent.

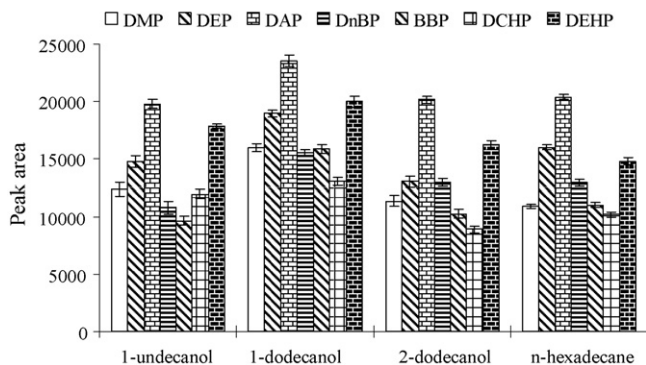


**Fig. 1.** The effect of the organic solvent type on the extraction efficiency. Conditions: sample volume, 10.0 mL; extraction temperature,  $60^\circ\text{C}$ ; extraction solvent volume,  $10.0 \mu\text{L}$ ; stirring rate, 600 rpm; extraction time, 30 min, and without salt addition.

### 3.2. Sample solution temperature

Solution temperature affects extraction kinetics. At higher temperatures, diffusion coefficients of analytes increase, therefore, this process facilitated the mass transfer of the analyte from the sample to the organic solvent and the time required to reach equilibrium decrease [44]. The effect of the sample solution temperature on the extraction efficiency was studied in the temperature range of  $30\text{--}70^\circ\text{C}$  by floating a 1-dodecanol microdrop for 30 min on the surface of the water samples. The experimental results clearly exhibited that by increasing the temperature, the extraction efficiency increased for all the analytes. However, high temperatures ( $>60^\circ\text{C}$ ) can alter the microdrop size dramatically and cause over-pressurization in the sample vial, making the extraction system unstable. For this reason, the solution temperature was held at  $60^\circ\text{C}$  for the subsequent experiments.

### 3.3. Effect of the ionic strength

The effect of salt concentration on the extraction efficiency was studied with different NaCl concentrations in the range of  $0\text{--}4 \text{ mol L}^{-1}$  (Fig. 2). The results revealed that in this method the salt addition restricted the extraction of the target analytes, except for that of DMP. A possible explanation for this observation may be that apart from the salting-out effect, NaCl dissolved in the aqueous solution may have changed the physical properties of the Nernst diffusion film and reduced the rate of diffusion of the target analytes into the drop [44]. This means that by increasing salt concentration, the diffusion of analytes towards the organic drop becomes more and more difficult and thus limits extraction [34,45]. Hence, we decided not to alter the salt content of the sample solutions in the following extractions as the sensitivity of the procedure was not poor.

### 3.4. Organic solvent volume

Based on LLE equations, the rate of the analytes transport into the microdrop is directly related to the interfacial area between the two liquid phases and inversely related to the organic-phase volume [46–48]. Therefore, by increasing the drop volume, the effect of the interfacial area predominates and the analytical signals increase. By further increasing of the microdrop volume, the effect of the solvent volume is predominated and the analytical signals are decreased [49,50]. The influence of the organic solvent volume on the analytical signal was studied in the range of  $6.0\text{--}12.0 \mu\text{L}$ . Fig. 3 depicts that the PEs analytical signals increase by increasing

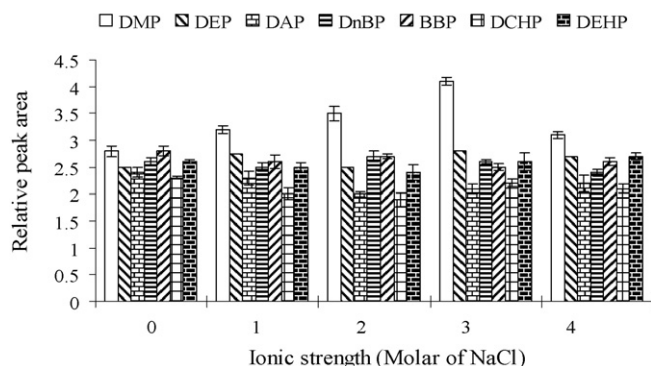


**Fig. 2.** The effect of the salt addition on the relative peak area. Extraction conditions as with Fig. 1, extraction solvent: 1-dodecanol.



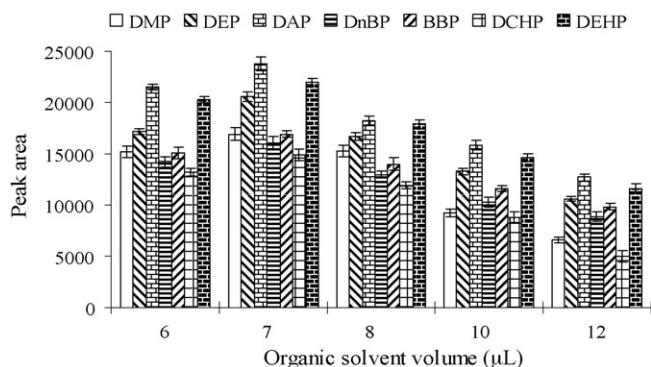


**Fig. 3.** The effect of the organic solvent volume on the extraction efficiency. Extraction conditions as with Fig. 2.

the solvent volume to 7  $\mu\text{L}$ , but it diminished when the solvent volume was increased to 12.0  $\mu\text{L}$ . So, volume of 7  $\mu\text{L}$  was selected as the optimum.

### 3.5. Stirring rate

Magnetic stirring enhances extraction and reduces the time required to reach thermodynamic equilibrium, and facilitate the mass transfer process and thus improves the extraction efficiency [51,32,33]. In this work, samples with the volume of 10.0 mL were agitated at different stirring rates (0, 150, 300, 450, 600 and 750 rpm). According to obtained results, the relative peak area of all analytes increases with the stirring rate up to 750 rpm. Higher stirring rates (>750 rpm) were not used, because, in this case the microdrop was spattered and damaged. Hence, for the following studies, the stirring rate of 750 rpm was chosen.

### 3.6. Extraction time

Like SPME, LPME is not an exhaustive extraction method under real conditions [52–54]. To increase repeatability of the extraction, it is necessary to choose an extraction time during which the equilibrium between the aqueous and the organic phase is reached. The time for reaching equilibrium determines the maximum amount of analyte that can be extracted by the microdrop [31,55]. The extraction time was investigated in the range of 5–35 min at the optimized experimental conditions. The relative peak areas increased with the extraction time up to 25 min (Fig. 4). After 25 min, the extraction system basically reached a steady state and no dramatic increase in the relative peak areas was observed with an additional extraction time. Therefore, a 25 min extraction time was selected for subsequent experiments.

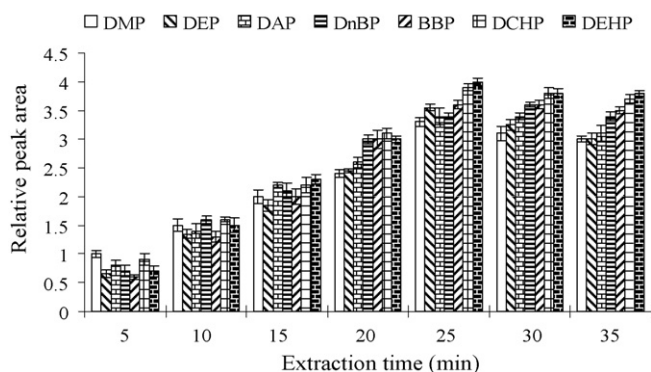


**Fig. 4.** The effect of the extraction time on the extraction efficiency. Extraction conditions as with Fig. 2, organic solvent volume: 7.0  $\mu\text{L}$  and stirring rate: 750 rpm.

### 3.7. Evaluation of the method performance

Under the selected optimum experimental conditions, the suggested methodology was applied to a series of standard solutions containing various analytes concentrations, in order to develop the respective calibration curves. For each level, three replicate extractions were conducted. The limit of detections (LODs), based on the signal-to-noise ratio (S/N) of three, the correlation coefficients ( $r^2$ ), the linear ranges (LRs), the relative standard deviations (R.S.D.s) and the enrichment factors (EFs) were calculated and summarized in Table 1.

For the EF calculation of each analyte, three replicate extractions were performed at the optimal conditions from the aqueous solution, containing 5.0  $\mu\text{g L}^{-1}$  of the analytes. The EF was calculated as the ratio of the final analyte concentration in the microdrop and its concentration in the original solution. The PEs standard solutions were prepared in 1-dodecanol as solvent and the calibration curves were drawn in the concentration range of 0.25–2.5  $\text{mg L}^{-1}$  with three replicate direct injections. The actual concentration of each extracted analyte in 1-dodecanol was calculated from the calibration curves and the EFs were determined.

As it is illustrated in Table 1, LODs for the tested PEs were found to be 0.02 up to 0.05  $\mu\text{g L}^{-1}$ . The linearity values varied from 0.05 to 100  $\mu\text{g L}^{-1}$  with a correlation coefficient of 0.9940–0.9971. The precision of the method was investigated with a 5.0  $\mu\text{g L}^{-1}$  PEs mixed standard solution. Regarding the R.S.D.s for four replicates, they varied from 5.5 to 7.7%, while the EF values ranged from 307 to 412.

### 3.8. Comparison of this technique with other methods

Table 2 indicates the LOD, LR and R.S.D. values, the extraction time and the sample volumes of other methods together with LPME (present method) for the PEs extraction and determination from water samples. In comparison with other microextraction methods, LPME provided a comparable LOD value and a wider linear range. Moreover, the precision of the recommended method was better than those of SPME and HFLPME and also comparable with that of single drop microextraction (SDME). The required volume of the sample solution for this procedure was small, same as SPME and HFLPME. Also, the extraction time was relatively short and was comparable with the other methods. All these results revealed that this technique is sensitive, rapid and reproducible that can be used for the PEs preconcentration in water samples and be extended to other applications.

### 3.9. Real water analysis

The performance of this system was tested by analyzing the PEs in four different water samples – tap water from our chemical laboratory (University of Tehran), two drinking mineral water samples available at the supermarket packed in polymeric containers (Cheshmeh and Koohrang) and Jajrood river water (Tehran, Iran). The tap and river water samples were collected in glass bottles. The river water sample was filtered before the analysis using a 0.45  $\mu\text{m}$  nylon membrane filter (Whatman, Maid-stone, UK) to eliminate the particles. All water samples were transported and stored at the refrigerator at 4  $^{\circ}\text{C}$  until their analysis time. The results showed that the analyzed samples had not been contaminated by PEs. All the real water samples were spiked with the PEs standard solutions at different concentration levels to assess the matrix effects. The relative recoveries of the analytes are given in Table 3. The obtained relative recoveries were between 84–115%, exhibiting that the real water matrices in our present context had little effect on LPME. After performing LPME, the chromatograms obtained by GC–MS of the mineral water (Koohrang) are displayed in Fig. 5, prior to (a)

**Table 2**  
The results obtained from the analysis of the real water samples

Sample	DMP	DEP	DAP	DnBP	BBP	DCHP	DEHP
Tap water (0.20 $\mu\text{g L}^{-1}$ added)							
Concentration ( $\mu\text{g L}^{-1}$ )	ND <sup>a</sup>	ND	ND	ND	ND	ND	ND
Found ( $\mu\text{g L}^{-1}$ )	0.181	0.188	0.214	0.219	0.192	0.167	0.228
Relative recovery (%)	91	94	107	110	96	84	114
R.S.D.% ( $n=4$ )	7.1	7.9	8.1	6.5	6.8	8.4	8.8
Mineral water, Cheshmeh (0.80 $\mu\text{g L}^{-1}$ added)							
Concentration ( $\mu\text{g L}^{-1}$ )	ND	ND	ND	ND	ND	ND	ND
Found ( $\mu\text{g L}^{-1}$ )	0.705	0.735	0.876	0.762	0.905	0.914	0.898
Relative recovery (%)	88	92	110	95	113	114	112
R.S.D.% ( $n=4$ )	6.9	8.5	5.7	6.8	8.2	9.0	7.2
Mineral water, Koohrang (5.0 $\mu\text{g L}^{-1}$ added)							
Concentration ( $\mu\text{g L}^{-1}$ )	ND	ND	ND	ND	ND	ND	ND
Found ( $\mu\text{g L}^{-1}$ )	4.59	5.35	5.29	5.68	5.77	4.81	4.44
Relative recovery (%)	92	107	106	114	115	97	89
R.S.D.% ( $n=4$ )	7.5	7.4	6.1	8.2	5.9	9.40	7.8
Jajrood river water (20.0 $\mu\text{g L}^{-1}$ added)							
Concentration ( $\mu\text{g L}^{-1}$ )	ND	ND	ND	ND	ND	ND	ND
Found ( $\mu\text{g L}^{-1}$ )	21.71	19.05	220.91	22.26	19.31	18.12	21.97
Relative recovery (%)	109	95	105	111	97	91	110
R.S.D.% ( $n=4$ )	7.4	9.1	6.4	8.1	9.8	8.7	8.4

<sup>a</sup> Not detected.

**Table 3**  
Comparison of the LPME with the other methods performing PEs determination

Method	LOD <sup>a</sup> ( $\mu\text{g L}^{-1}$ )	LR <sup>b</sup> ( $\mu\text{g L}^{-1}$ )	R.S.D. <sup>c</sup> (%)	Extraction time (min)	Sample volume (mL)	References
SDME-GC-FID	0.02–0.1	0.1–50	3.5–8	25	20	[55]
SPME-GC-MS	0.003–0.01	0.1–10	4–11	20	5	[39]
HFLPME-GC-MS	0.005–0.1	0.5–10	4–19	20	5	[39]
LPME-GC-MS	0.02–0.05	0.05–100	5.5–7.7	25	10	Present method

<sup>a</sup> Limit of detection.

<sup>b</sup> Linear range.

<sup>c</sup> Relative standard deviation.

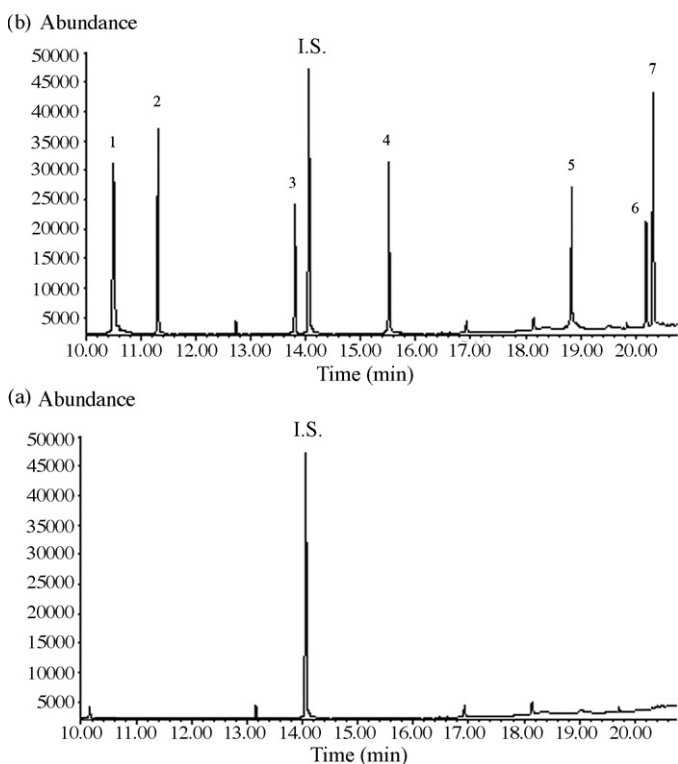


**Fig. 5.** The chromatograms obtained by GC-MS of the mineral water (Cheshmeh) after performing LPME, without spiking PEs (a) and spiked with PEs (b) at the concentration level of 5.0  $\mu\text{g L}^{-1}$  of each analyte. Peak numbers correspond to (1) DMP; (2) DEP; I.S.: benzyl benzoate; (3) DAP; (4) DnBP; (5) BBP; (6) DCHP; (7) DEHP.

and after spiking the plasticizers (b) at the concentration level of 5.0  $\mu\text{g L}^{-1}$  of each analyte.

#### 4. Conclusion

This paper outlines a successful development and application of a method based on the LPME technique, combined with the capillary GC-MS, for the qualitative and quantitative analysis of the PEs group in water samples. The designed method is concluded to be precise, reproducible and linear over a broad range with sufficient selectivity (using the MS detector at the SIM mode) and high sensitivity. Compared with other conventional sample preparation methods, the analytical technique offered numerous advantages such as simplicity, low cost, ease of operation, no possibility of sample carry-over and high enrichment factors. In addition, the technique requires only a small volume of organic extractants, being therefore an environmentally friendly approach. The performance of this procedure in the PEs extraction from different water samples with various matrices was excellent. Subsequently, this method can be used routinely for screening purposes.

#### Acknowledgement

This work has been supported by grants from the University of Tehran Research Council which is hereby gratefully acknowledged.

#### References

- [1] M. Castillo, D. Barceló, A.S. Pereira, F.R. Aquino Neto, Trends Anal. Chem. 18 (1999) 26.
- [2] K. Holadová, J. Hajslová, Int. J. Environ. Anal. Chem. 59 (1995) 43.

- [3] M. Castillo, D. Barceló, *Trends Anal. Chem.* 16 (1997) 574.
- [4] A. Peñalver, E. Pocurull, F. Borrull, R.M. Marcé, *J. Chromatogr. A* 872 (2000) 191.
- [5] A. Peñalver, E. Pocurull, F. Borrull, R.M. Marceí, *J. Chromatogr. A* 922 (2001) 377.
- [6] J. Xu, P. Liang, T. Zhang, *Anal. Chim. Acta* 597 (2007) 1.
- [7] C.R. Tyler, S. Jobling, J.P. Sumpter, *Crit. Rev. Toxicol.* 28 (1998) 319.
- [8] P.M. Lorz, F.K. Towae, W. Enke, R. Jäckh, N. Bhargava, *Phthalic acid and derivatives*. Ullmann's encyclopedia of industrial chemistry, Wiley VCH, Weinheim 7, 2002.
- [9] Council Directive 88/378/EEC of 3 May 1988 on the Approximation of The Laws of the Member State Concerning The Safety of Toys, European Union, Brussels, 1988.
- [10] Council Regulation (EEC) No. 793/93 of 23 March 1993 on the evaluation and control of the Risks of Existing Substances (OJ L 84, 5 April 1993), European Union, Brussels, 1993.
- [11] National Primary Drinking Water Regulations, Federal register; Part 12, 40 CFR Part 141, US Environmental Protection Agency, Washington, DC, July 1991, p. 395.
- [12] M. Castillo, M.F. Alpendurada, D. Barceló, *J. Mass Spec trom.* 32 (1997) 1100.
- [13] B. Tienpont, F. David, P. Sandra, F. Vanwallegem, *J. Microcol. Sep.* 4 (2000) 194.
- [14] J. Bartulewicz, E. Bartulewicz, J. Gawlowski, J. Niedzielski, *Chem. Anal. (Warsaw)* 41 (1996) 753.
- [15] A. Yasuhara, H. Shiraishi, M. Nishikawa, T. Yamamoto, T. Uehiro, O. Nakasugi, T. Okumura, K. Kenmotsu, H. Fukui, M. Nagase, Y. Ono, Y. Kawagoshi, K. Baba, Y. Noma, *J. Chromatogr. A* 774 (1997) 321.
- [16] M. Castillo, A. Oubiña, D. Barceló, *Environ. Sci. Technol.* 32 (1998) 2180.
- [17] M.T. Kelly, M. Larroque, *J. Chromatogr. A* 841 (1999) 177.
- [18] S. Jara, C. Lysebo, T. Greinbrokk, E. Lundanes, *Anal. Chim. Acta* 407 (2000) 165.
- [19] G. Prokupkova, K. Holadova, J. Poustka, J. Hajslova, *Anal. Chim. Acta* 457 (2002) 211.
- [20] C.L. Arthur, J. Pawliszyn, *Anal. Chem.* 62 (1990) 2145.
- [21] A. Peñalver, E. Pocurull, F. Borrull, R.M. Marcé, *Chromatographia* 50 (1999) 685.
- [22] X. Yu, J. Pawliszyn, *Anal. Chem.* 72 (2000) 1788–1792.
- [23] A. Peñalver, E. Pocurull, F. Borrull, R.M. Marceí, *J. Chromatogr. A* 839 (1999) 253.
- [24] H. Daimon, J. Pawliszyn, *Anal. Comm.* 34 (1997) 365.
- [25] K. Jinno, M. Kawazoe, Y. Saito, T. Takeichi, M. Hayashida, *Electrophoresis* 22 (2001) 3785–3790.
- [26] R.T. Marsili, *J. Agric. Food Chem.* 48 (2000) 3470–3475.
- [27] E.U. Ramos, S.N. Meijer, W.H.J. Vaes, H.J.M. Verhaar, J.L.M. Hermens, *Environ. Sci. Technol.* 32 (1998) 3430–3435.
- [28] P. Helena, I.K. Iocita, *Trends Anal. Chem.* 18 (1999) 272.
- [29] L. Xu, C. Basheer, H.K. Lee, *J. Chromatogr. A* 1152 (2007) 184.
- [30] L. Hou, H.K. Lee, *J. Chromatogr. A* 1038 (2004) 37.
- [31] Y. Wang, Y.C. Kwok, Y. He, H.K. Lee, *Anal. Chem.* 70 (1998) 4610.
- [32] R. Zhao, W. Lao, X. Xu, *Talanta* 62 (2004) 751.
- [33] L.S. de Jager, A.R.J. Andrews, *J. Chromatogr. A* 911 (2001) 97.
- [34] E. Psillakis, N. Kalogerakis, *J. Chromatogr. A* 907 (2001) 211.
- [35] K. Carlsson, B. Karlberg, *Anal. Chim. Acta* 415 (2000) 1.
- [36] A.L. Theis, A.J. Waldack, S.M. Hansen, *Anal. Chem.* 73 (2001) 5651.
- [37] M.B. Melwanki, W.H. Hsu, S.D. Huang, *Anal. Chim. Acta* 552 (2005) 67.
- [38] G. Shen, H.K. Lee, *Anal. Chem.* 74 (2002) 648.
- [39] E. Psillakis, N. Kalogerakis, *J. Chromatogr. A* 999 (2003) 145.
- [40] M.R. Khalili Zanjani, Y. Yamini, S. Shariati, J.A. Jönsson, *Anal. Chim. Acta* 585 (2007) 286.
- [41] A. Tankeviciute, R. Kazlauskas, V. Vickackaite, *Analyst* 126 (2001) 1674–1677.
- [42] H. Ebrahimzadeh, Y. Yamini, F. Kamarei, M.R. Khalili-Zanjani, *Talanta* 72 (2007) 193.
- [43] A. Tor, M.E. Aydin, *Anal. Chim. Acta* 575 (2006) 138.
- [44] H. Bagheri, A. Saber, S.R. Mousavi, *J. Chromatogr. A* 1046 (2004) 27.
- [45] D.A. Lambropoulou, T.A. Albanis, *J. Chromatogr. A* 1049 (2004) 17.
- [46] L. Zhao, H.K. Lee, *J. Chromatogr. A* 919 (2001) 381.
- [47] T. Heberer, H.J. Stan, *Anal. Chim. Acta* 341 (1997) 21.
- [48] L. Rodriguez, M.I. Turnes, M.C. Mejuto, R. Cela, *J. Chromatogr. A* 721 (1996) 297.
- [49] Y. Lu, Q. Lin, G. Luo, Y. Dai, *Anal. Chim. Acta* 566 (2006) 259.
- [50] H. Bagheri, F. Khalilian, *Anal. Chim. Acta* 537 (2005) 81.
- [51] A. Columé, S. Cárdenas, M. Gallego, M. Valcárcel, *Talanta* 54 (2001) 943.
- [52] M.A. Jeannot, F.F. Cantwell, *Anal. Chem.* 68 (1996) 2236.
- [53] M.A. Jeannot, F.F. Cantwell, *Anal. Chem.* 69 (1997) 235.
- [54] Y. He, H.K. Lee, *Anal. Chem.* 69 (1997) 4634.
- [55] R. Battle, C. Neřin, *J. Chromatogr. A* 1045 (2004) 29.



# Fabrication of polymer microsphere particle standards containing trace explosives using an oil/water emulsion solvent extraction piezoelectric printing process

Robert A. Fletcher<sup>a,\*</sup>, Jacquelyn A. Brazin<sup>b</sup>, Matthew E. Staymates<sup>a</sup>, Bruce A. Benner Jr.<sup>a</sup>, J. Greg Gillen<sup>a</sup>

<sup>a</sup> National Institute of Standard and Technology, Gaithersburg, MD 20899, United States

<sup>b</sup> Massachusetts Institute of Technology, Cambridge, MA 02139, United States

## ARTICLE INFO

### Article history:

Received 6 February 2008  
Received in revised form 24 April 2008  
Accepted 25 April 2008  
Available online 17 May 2008

### Keywords:

Inkjet printing  
Polymer particles  
Encapsulation  
Standards  
Explosives  
Ion mobility spectrometry

## ABSTRACT

We present a methodology for fabricating polymer microspheres using inkjet printing of a biodegradable polymer containing either high explosives or high explosive simulant. Poly(DL-lactide/glycolide) 85:15 (PLGA) microsphere production is based on an oil/water emulsion solvent extraction process. The inkjet printing process allows for precise control of the microsphere diameter and the chemical composition. The microspheres can be used as calibrants or verification standards for explosives trace detection instruments. Gas chromatography/mass spectrometry analysis demonstrated that the composition of the microspheres was consistent with predicted concentrations based on the amount of analyte incorporated into the polymer solution and the inkjet operating parameters. We have demonstrated that the microspheres can be fabricated with a mass fraction of 70% of an analyte compound.

© 2008 Elsevier B.V. All rights reserved.

## 1. Introduction

Current national priorities in homeland security have led to the widespread deployment of explosives trace detection systems throughout the United States. In a typical implementation of such a detection system, an ion mobility spectrometer (IMS) is used to identify micrometer sized explosive particles on people and their belongings [1]. Samples are typically collected by physical swiping of a suspect surface with a hand wand or small piece of cloth (called a trap). After sampling, the trap is inserted into the IMS instrument where the particles of interest on the trap are thermally vaporized and analyzed. This method is effective for screening objects like a briefcase or a laptop computer, but it is not optimal for screening people or their clothing and is also slow and limited in sample throughput. To address these issues, another approach currently being deployed is the walk-through portal detection system. In this system, a person enters a chamber similar to a metal detector, and is interrogated with multiple air jets that dislodge particles from the person and/or their clothing. An air shower stream carries the

dislodged particles to a collector, which in turn admits this material to a detector (generally an IMS) [2].

In order to characterize and validate the performance of these systems, well-characterized test materials are required. Explosives residues are typically found as small particulates with size distributions ranging from sub-micrometer to several 100  $\mu\text{m}$  in diameter [3]. In order to make realistic standards to serve as effective test materials for trace detection instruments, particulate test standards should have several desirable properties: appropriate size and aerodynamic behavior; known chemical composition; known surface adhesive properties; a distinguishable IMS detector response. Particle size is particularly important because particle release from surfaces by air jets and aerodynamic transport are particle diameter-dependant [4,5]. Some additional considerations include useful lifetime of the standard in the local ambient environment, contamination control at the test site that results from standard testing, and the safety (non-toxicity) of the materials in the event of accidental human exposure.

One novel and promising method for generation of these trace particle standards is the production of uniform polymer microspheres containing the explosive compound (or simulant) of interest by inkjet printing. The use of polymer microspheres is advantageous because they are monodisperse, the sphere diameters can be tailored for specific tests, and the microspheres may contain high levels of test compound.

\* Corresponding author at: National Institute of Standard and Technology, Chemical Science and Technology, 100 Bureau Drive Stop 8371, Gaithersburg, MD 20899, United States. Tel.: +1 301 975 3912.

E-mail address: [robert.fletcher@nist.gov](mailto:robert.fletcher@nist.gov) (R.A. Fletcher).

In this paper, we present a methodology for fabricating uniform polymer microspheres by using inkjet printing of a biodegradable polymer containing the compound of interest. This approach was originally developed for drug delivery applications using inkjet printing of a polymer solution containing poly(DL-lactide/glycolide) (PLGA) and paclitaxol [6,7]. Here we use a similar approach for preparing PLGA spheres containing high explosives or a simulant. Uniform microspheres have been made by piezoelectric fluid flow disruption over 35 years ago [8]. Production is based on an oil/water emulsion solvent extraction process that produces polymer microspheres [9]. Others have presented methods for making drug delivery microspheres, using a co-flow polymer/water system [10]. One reason to incorporate drugs into polymer microspheres (PLGA and polylactide, PLA) is that the polymer slowly degrades or dissolves by hydrolysis in the body to provide a slow release drug delivery platform [11–13].

We have demonstrated the incorporation of two high explosives, 1,3,5,7-tetranitroperhydro-1,3,5,7-tetrazocine (HMX) and 2,4,6 trinitrotoluene (TNT), and one simulant, 2,6-bis(1,1-dimethylethyl)-4-methylphenol (BHT, CAS number 128-37-0), into PLGA microspheres. We are using the simulant BHT because it is a food additive, considered safe for human consumption and gives a good IMS response in the negative ion mode where explosives are detected. A safe simulant is desirable to prevent contamination of the security check points and to prevent potential health risk from accidental human exposure. The above analytes contained in the PLGA microspheres have been correctly identified for the respective compound by a table-top IMS.

## 2. Experimental

### 2.1. Materials

The polymer solution was made by dissolving either 0.3 g or 0.6 g of poly(DL-lactide/glycolide) 85:15 (PLGA, Polysciences Inc., Warrington, PA)<sup>1</sup> into 10 mL dichloroethane (DCE) (Sigma–Aldrich, St. Louis, MO). Low and high concentration solutions of BHT (Sigma–Aldrich, St. Louis, MO) were made by dissolving either 0.07 g or 5 g BHT into 10 mL DCE. HMX was first dissolved in acetone (J.T. Baker) and then the acetone solution was added to the DCE to make a  $2.73 \times 10^{-4}$  g/mL HMX solution in DCE–acetone. For a low concentration solution of TNT, 0.025 g of TNT was dissolved in 10 mL DCE. A final solution of polymer and analyte was made by mixing a known volume of analyte solution into the PLGA–DCE solution. Approximately 200  $\mu$ L of rhodamine B (Eastman Kodak Co., Rochester, NY) was also added to the final polymer–analyte solution as a fluorescent dye marker.

### 2.2. Microsphere fabrication

Microspheres were prepared by an oil/water emulsion process using a piezoelectric inkjet printer (sphere jet) to deliver precisely controlled microdrops of the polymer solution. The sphere jet is a drop-on-demand piezoelectric inkjet printer (MicroFab Technologies Inc., Plano, TX) with a 50- $\mu$ m orifice diameter jet, operated in a pressure assisted mode to prepare PLGA microspheres containing analytes of varying concentrations. A magnified image of the inkjet printer producing a stream of monodisperse droplets

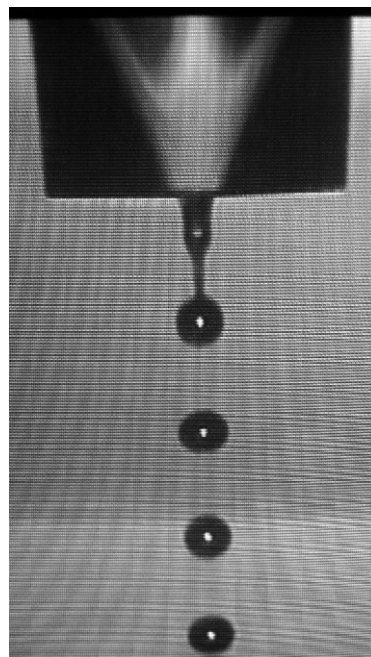
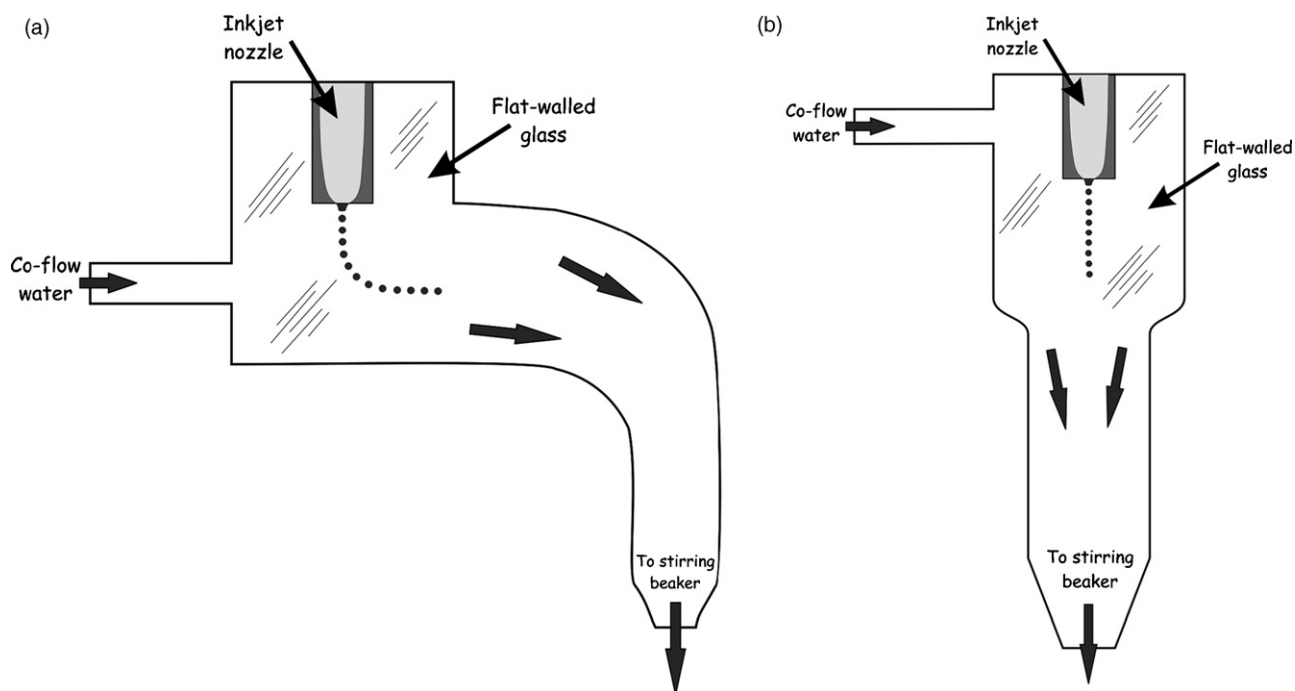


Fig. 1. Inkjet printer operating in a continuous mode producing uniform droplets.

is shown in Fig. 1. The waveform and frequency were controlled using the instrument's software (JetLab2) and pressure regulation was maintained using a pressure regulator (Druck DPI 530, Druck Inc., Fairfield, CT). Operating parameters were varied to allow for controlled production of microspheres, but typical parameters include a frequency of 10 kHz, rise time 1  $\mu$ s, dwell time 30 ms, and dwell voltage of 30 V. A video camera with strobe illumination (Advanced Illuminations, Signatech, Rochester, VT) was used to monitor the shape and relative size of the jetted droplets. The pressure-controller driven stream of the polymer solution flowed through the inkjet tip forming microspheres as a result of uniformly disrupting (or chopping) the stream by the capillary piezoelectric tip. The jetting process takes place under water where the microspheres are captured and cured in a 500-mL beaker (containing filtered, deionized water) continuously stirred for several minutes to several hours. Any DCE that remained after sphere formation was allowed to evaporate. Using vacuum filtration, a small volume (approximately 25 mL) of the microsphere suspension was filtered through a 25- $\mu$ m diameter polycarbonate filter with a 1.0- $\mu$ m pore size and the remaining solution was filtered through a 47- $\mu$ m polycarbonate filter with a 1.0- $\mu$ m pore size. Optical microscopy was used to image the microspheres collected on the 25 mm filter and the microspheres collected on the 47 mm filter were dried and carefully removed from the filter using a spatula and stored in 5 mL closed vials.

Three different jetting experimental configurations were examined as a way to reduce the variability of the microsphere size distribution. The first configuration is considered a "pure-shear" mode because the piezoelectric nozzle is directly submerged in the 500 mL beaker filled with rotationally stirred water. The droplets are immediately sheared from the nozzle by the rotating body of water. The limitation of this method is that it makes it difficult to focus the camera on the nozzle and droplets because of the curved walls of the beaker. Configurations 2 and 3 were designed to overcome this visualization issue by using a co-flow tube with flat glass walls (see Fig. 2a and b). Results of these three arrangements will be discussed later.

<sup>1</sup> Commercial equipment, instruments, and materials, or software are identified in this report to specify adequately the experimental procedure. Such identification does not imply recommendation or endorsement of these items by the NIST, nor does it imply that they are the best available for the purpose.



**Fig. 2.** Arrangement 1, not shown, was directly submerging the nozzle in a rotating beaker of water. Curved co-flow nozzle (a) is arrangement 2 and straight co-flow nozzle (b) is arrangement 3. Particles are generated by the submerged inkjet printer and are carried by a continuous stream of water into a collection beaker where they are left to cure.

### 2.3. Experimental design: fabrication parameters

An experimental design was followed that included a wide range of operating conditions for microsphere production by the sphere jet. The relevant parameters related to producing spherical particles of a given diameter from the sphere jet are the solute concentration, the liquid flow rate and the operating frequency of the jet. We varied the solute concentration for PLGA in DCE (0.06 g/mL and 0.12 g/mL), the BHT (0.014 g/mL and 1 g/mL), the frequency (5 kHz, 10 kHz and 20 kHz), and the flow rate through the jet from 0.0022 mL/s to 0.0069 mL/s. The experimental parameters allow us to predict the resultant sphere diameter and compare this value to the measured diameter.

### 2.4. Characterization of the microspheres

#### 2.4.1. Optical microscopy

The microspheres were imaged using a fluorescence optical microscope (Zeiss Stemi SV 11) for analyses of the microsphere diameter and degree of monodispersity. Samples which showed obvious polydispersity were not included for further study. The mean diameter of selected spheres in monodisperse samples was calculated using image analysis (ImagePro Software [Media Cybernetics Inc.]). Individual spheres were sized while the sizes of clusters or agglomerations of spheres were rejected due to the inability of the program to differentiate individual spheres. However, visual inspection indicated that the size of microspheres in clusters matched the microsphere sizes of the individual spheres.

#### 2.4.2. Microsphere size distribution

A known volume of microspheres in aqueous suspension was sized by an optical particle counter that utilizes single particle optical extinction (model HR LD 150, HACH ULTRA, Grants Pass, OR). The instrument was calibrated with polystyrene latex spheres (Duke Scientific), over the size range from 1  $\mu\text{m}$  to 100  $\mu\text{m}$ . It is important to note that the micrograph images of the microspheres are of

filtered and dried microspheres, which were observed to agglomerate while the optical particle counter performed the measurement in suspension, where the particles did not appreciably aggregate. A Coulter Multisizer 3 (Beckman Coulter Inc.) with a 100- $\mu\text{m}$  orifice was used to measure the size distribution of certain cured PLGA spheres.

#### 2.4.3. Scanning electron microscopy

Microspheres were sputter coated with a thin layer of gold. Spheres were viewed using a field emission scanning electron microscope. Some of the samples were imaged at an acute angle to examine contact angle of the sphere attachment to the surface.

#### 2.4.4. Gas chromatography–mass spectrometry analysis

A known mass (1.30 mg) of the HMX in PLGA sample was transferred to a 2-mL amber vial to which was added a known mass of a solution of deuterium labeled HMX (Cambridge Isotope Laboratories, Andover, MA) and approximately 1 mL of acetone (J.T. Baker, Baker's Analyzed HPLC solvent). A known mass of a standard HMX solution was fortified with the same labeled-HMX solution as the sample. This solution was used as a calibrant to determine a response factor for the HMX relative to the labeled compound (see below).

For the BHT in PLGA sample, 2.43 mg was deposited into a 2-mL amber vial and the material was dissolved in approximately 1 mL of acetone (described above). For the BHT calibration, a solution at a similar concentration to that predicted from the sample composition was prepared from pure BHT (Sigma, St. Louis, MO). The calibrant was used to generate a response factor relating the amount of BHT injected to the area of the resulting BHT chromatographic peak.

The HMX and BHT concentrations were determined by gas chromatography/negative ion chemical ionization mass spectrometry (GC/NICI-MS) using an Agilent 6890 GC system interfaced with an Agilent 5973 MS. Aliquots of the extracts (1  $\mu\text{L}$ ) were injected by an autosampler onto a 1 m  $\times$  0.25 mm uncoated/deactivated fused sil-

ica capillary (retention gap) connected to a 6 m × 0.22 mm (0.1 μm phase, SGE, Austin, TX, serial number 9835C15) HT-5 column. The retention gap-column combinations were operated at a constant flow rate of 14 mL/min helium, and temperature programmed from 80 °C (1 min hold) to 100 °C at 45 °C/min, then to 170 °C at 5 °C/min (10 min hold). The mass spectrometer was operated in the NICI mode with methane as the reagent gas (40 mL/min), scanning from 40 to 350 mass/charge ( $m/z$ ) for the BHT measurements and monitoring for ions 176  $m/z$  (HMX) and 181  $m/z$  (labeled-HMX) for the HMX measurements. The source and analyzer temperatures were set at 150 °C and 200 °C, respectively, and the MS was tuned prior to the sample runs. Peak areas of reconstructed ion chromatograms for 176  $m/z$ , 181  $m/z$  and 219  $m/z$  (BHT) were used to determine relative response factors from calibrant runs that were then used to quantify the concentrations of BHT and HMX in the prepared solutions. The precision of the methods suggests a run-to-run uncertainty of approximately 5%. The uncertainty due to heterogeneity in the materials was not addressed in this work due to limitations in the amount of sample available.

#### 2.4.5. Ion mobility spectrometry (IMS)

Weighed amounts of microspheres incorporated with BHT and TNT were analyzed using a commercial IMS (Itemiser 3, GE Security) operated with a 220 °C desorber temperature. For microspheres incorporated with HMX, an IonScan 400B (Smiths Detection) was used with a 280 °C desorber temperature. IMS plasmagrams of the microspheres were obtained for analysis.

### 3. Results and discussion

One of the primary advantages of using the piezo inkjet approach compared to conventional methods of emulsion polymerization methods is that monodisperse microspheres can be made that contain the same amount of analyte per sphere, which is critical if it is to be used as a test material. In the current implementation, the inkjet is used in a continuous mode. The polymer solution is pushed continuously through the nozzle by a constant applied back pressure. We produce a uniform stream of polymer solution and apply a waveform to drive the piezoelectric crystal in the frequency range of 5–20 kHz. Uniform liquid stream break-up behavior is described [10,14]. There is similarity between our particle generation device and a well-known aerosol particle generator, the vibrating orifice aerosol generator. The aerosol generator sends a chopped stream into air or gas and the present device streams into water. The droplet diameter,  $d_d$ , can be predicted by the following expression:

$$d_d = \left( \frac{6Q}{\pi f} \right)^{1/3}, \quad (1)$$

where  $Q$  (mL/s) is the liquid flow rate and  $f$  is the disruption or chopping frequency. The final particle diameter,  $d_p$  is controlled by the volumetric concentration of solute present,  $C$ , in the solution and expressed as

$$\frac{d_p}{d_d} = C^{1/3}. \quad (2)$$

We designed a fabrication experiment that included high and low concentrations for PLGA, BHT and various applied chopping frequencies. Using Eqs. (1) and (2) and measuring the solute concentration and the liquid flow rate, we are able to calculate the expected particle diameter. Fig. 3 shows a scatter plot of calculated particle diameters versus those measured by optical microscopy. This data is for both BHT and HMX containing PLGA spheres and excludes any samples not deemed monodisperse. The plot shows that although the predictability is not ideal, we do have control of

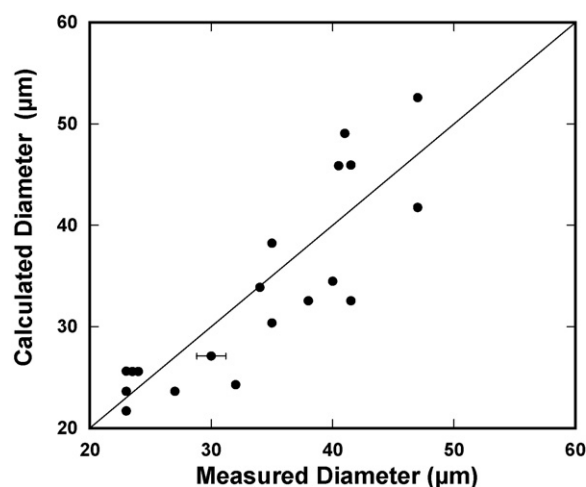


Fig. 3. Scatter plot of calculated sphere diameter versus measured sphere diameter. The line is a 1:1 relation drawn for comparison. The uncertainty bar corresponds to standard deviation in the measured diameter.

particle and composition by varying the operation parameters for the fabrication.

A typical fluorescence micrograph of nominal 30 μm diameter PLGA spheres containing BHT and rhodamine B are shown in Fig. 4. The spherical shape and uniformity are evident. The particles appear to be agglomerated due to filtering from the suspension. A scanning electron micrograph of the microspheres is shown in Fig. 5. The particles are mounted on a silicon wafer, coated with a thin gold coat and imaged at an acute angle. The particles appear to be rigid, well defined spheres. This imaging technique allows verification of the shape to a much finer degree and also visualization of any defects or residues that could be on the sphere's surface or at the sphere–substrate interface.

The particles were characterized in suspension using an optical particle sensor based on light extinction described above. The extinction sensor was calibrated using monodisperse polystyrene spheres. The extinction sensor provides a quick diagnostic tool to obtain the relative size of the microspheres and the breadth of the size distribution while the spheres are in suspension. An example of a measurement is presented in Fig. 6 that shows a single peak at a sphere diameter of approximately 20 μm. Over 64,000 particles were characterized to make this plot. The sample was made

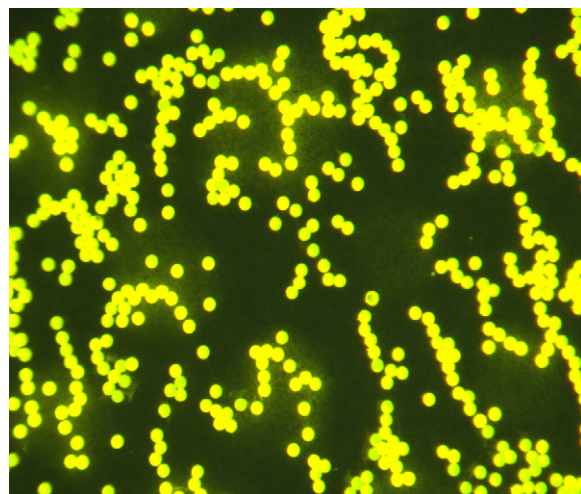
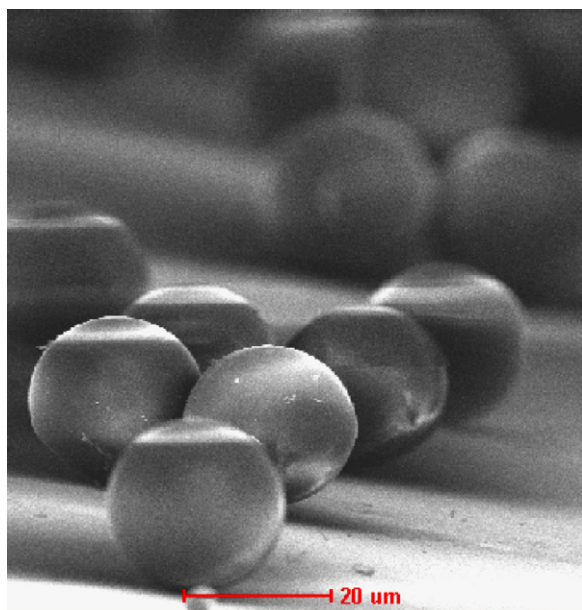


Fig. 4. Fluorescence micrograph of PLGA spheres containing BHT and rhodamine B.



**Fig. 5.** SEM micrograph of PLGA–BHT spheres viewed at an acute angle with respect to the substrate.

from a 0.03-g/mL PLGA solution containing 0.007 g/mL BHT with the inkjet operating at a frequency of 20 kHz. The full-width half-max of the peak is approximately 2  $\mu\text{m}$ , indicating approximately 10% dispersion in the particle diameter using this method.

In order to optimize the fabrication process, polymer microspheres produced from the three jetting arrangements (see Fig. 2) were analyzed by the Coulter counter to determine the size distribution of the sphere population. In the arrangements shown in Fig. 2a and b, the polymer droplets would travel with the co-flow fluid through the tube. However, the fluid flow rate was not high enough to keep the droplets separate and a fraction of the droplets began to coalesce into larger droplets before curing and hardening. Coalescence occurred as a repeating process of two droplets forming a larger droplet all along the transport tube until finally settling into the beaker. The results of droplet coalescence is shown in Fig. 7. Multiple peaks are in fact derived from coalescence of droplets as evidenced by the fact that the peaks scale as multiples of the cube root of the number of droplets coalescing ( $n$ ) times the initial diameter ( $n^{(1/3)} \times \text{diameter}$ ; for  $n = 1, 2, 3, \dots$ ).

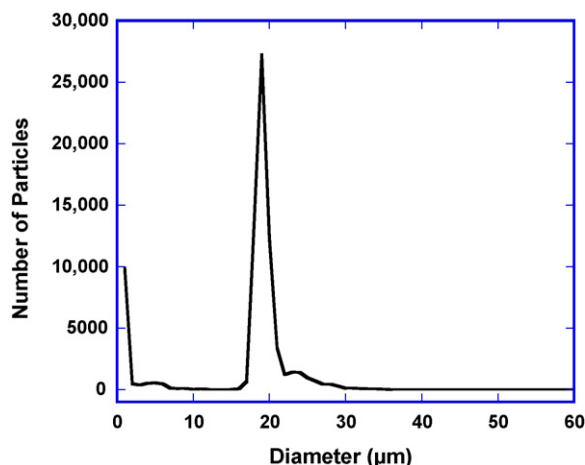


**Fig. 6.** Relative particle diameter obtained for suspended PLGA spheres containing BHT. Measurements were made using the optical extinction particle sensor.

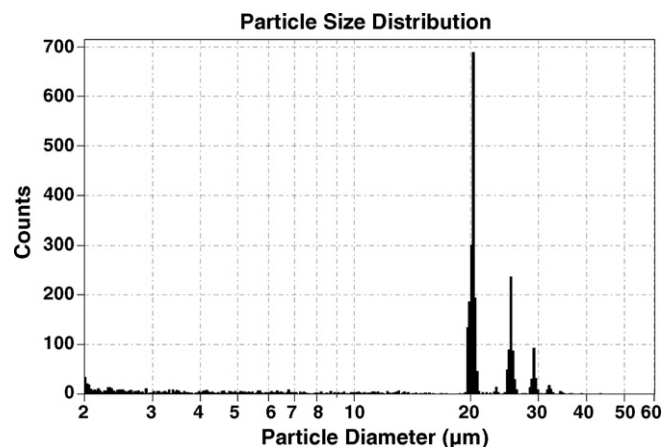


**Fig. 7.** Particle size distribution of PLGA spheres for co-flow nozzle shown Fig. 2a and b, arrangements 2 and 3. Multiple peaks indicates coalesce of the microspheres prior to curing while the droplets are still the liquid phase.

Submerging the nozzle directly into the stirring water (arrangement 1) was the only way to eliminate the coalescence problem. Fig. 8 shows a typical size distribution plot for arrangement 1 (jetting directly into the beaker). The mean is 19.43  $\mu\text{m}$  with a standard deviation of 0.29  $\mu\text{m}$  (number of spheres is 1260). The coefficient of variation is 1.5%, which is comparable to commercially available materials, such as NIST standard reference material polystyrene latex microspheres.

Another set of spheres was made from solution concentrations of 0.06 g/mL PLGA with 0.007 g/mL BHT and an operating frequency of 20 kHz was analyzed using fluorescence light microscopy and image analysis. The particles were collected on a polycarbonate filter and were agglomerated due to the filtration process. Using a deagglomeration feature of the image analysis software, 175 spheres were selected at random and sized. The results of image analysis are shown in Fig. 9. The mean of this population was 29.32  $\mu\text{m}$  with a standard deviation of 1.15  $\mu\text{m}$ .

The polymer's capacity to degrade thermally is very important for the proposed application. The PLGA spheres should release the high explosive or simulant when heated during the trace analysis technique. Also, the ions formed from the polymer degradation could become potential interference peaks for the IMS. Fortunately, it was observed that PLGA does not produce any interfering peaks in the negative or positive ion mode for IMS. Measurements at

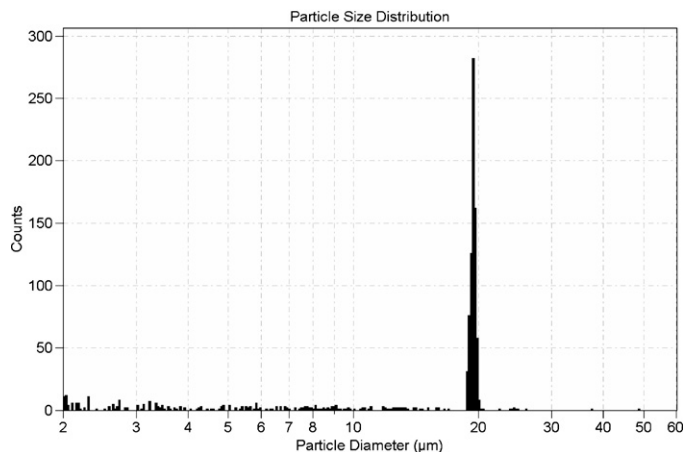


**Fig. 8.** Particle size distribution of PLGA sphere obtained for jetting arrangement 1 where the droplets are deposited directly in a rotating water bath. No coalescence is observed.



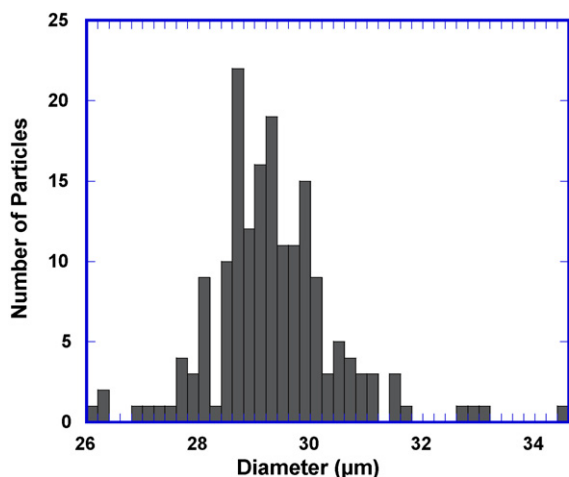


Fig. 9. Histogram representation of PLGA-BHT spheres sized by fluorescence microscopy and image analysis.

NIST and in the literature indicate that PLGA does not thermally degrade before 300 °C [15]. All three analytes TNT, HMX and BHT incorporated in PLGA have been detected by IMS without further preparation other than heating the spheres in the IMS desorber. Desorber temperatures were either 220 °C or 280 °C depending upon the analyte analyzed. Although elevated temperatures were used to desorb HMX, they are not necessary to melt the PLGA spheres. Experiments on a controlled hot stage indicate that the PLGA microspheres melt between 100 °C and 130 °C leaving a visible residue. Using Eq. (2), we can calculate the amount of explosive or simulant in each sphere. Given a final sphere diameter of 30 μm fabricated from the dilute HMX solution specified above with the 0.03 g/mL PLGA solution, we arrive at an inkjet ejected drop diameter of approximately 111 μm. With the solution containing  $4.5 \times 10^{-5}$  g/mL, we obtain approximately 32 pg of HMX in each sphere. The mass of HMX per sphere is so small (trace) that we needed multiple spheres with this concentration to detect HMX by IMS.

The temporal variation of characteristic ions observed in IMS provides information of both the compound desorption rate and detection. A plot of  $(\text{HMX} - \text{Cl})^-$  peak height as a function of time for pure HMX and for HMX desorbed PLGA-HMX is shown in Fig. 10.

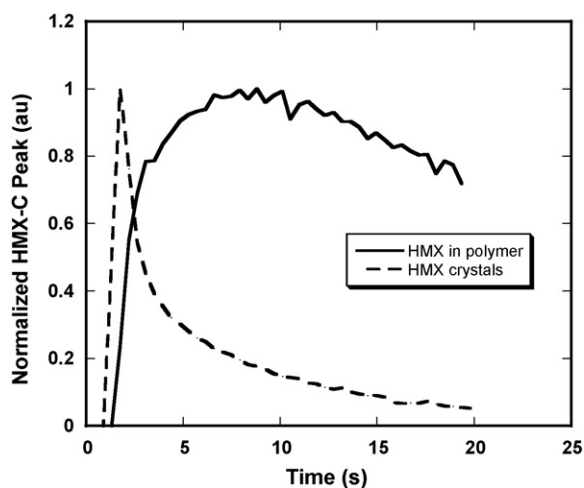


Fig. 10. IMS response for approximately 20 ng of pure HMX and HMX incorporated in PLGA spheres. The peak height  $(\text{HMX} + \text{Cl}^-)$  is normalized to the maximum in the scan and plotted as a function of desorption time.

The pure HMX was deposited and dried from DCE solution onto a sample trap. In both cases the IMS operating conditions and sample trap were the same. The pure HMX compound (approximately 20 ng) desorbs nearly completely in the first few seconds, peaks at approximately 3 s and then decays. The HMX signal derived from the HMX-PLGA spheres takes about 8 s to reach maximum and stays fairly constant out to 20 s, the duration of the analysis scan. The fact that the polymer appears to retain some of the explosive compound is not surprising and does not negate the applicability of this technique. In fact for some volatile compounds the slow thermal release may be beneficial for molecular preservation and stability of the compound. Further testing will be needed to quantify the thermal release rate from the polymer.

Preliminary results for the final concentrations of HMX and BHT in two PLGA sphere samples as determined by GC/NICI-MS suggest that the observed levels are close to those predicted by the formulations. Duplicate injections of the HMX in PLGA dissolved in acetone yielded concentrations of 1204 μg/g and 1213 μg/g HMX, in good agreement with the range of predicted levels of 1820 μg/g. The result for the BHT in PLGA sample was somewhat lower than predicted, with the GC/NICI-MS measurement yielding a concentration of about 0.71 g/g, or mass fraction of 71% BHT compared with the predicted mass fraction of 76% BHT. We estimate that there is approximately 10% uncertainty in the results. As indicated above, sample limitations prevented a thorough determination of the homogeneity of the analytes in the PLGA polymer, but these preliminary results do suggest the proof-of-concept of generating known levels of HMX and BHT in the PLGA material by the method described above.

#### 4. Summary

There is a need for test particles of high explosives and their simulants for testing IMS based trace portal systems. We have developed a potential method to produce particle-based standard test materials at the trace levels for IMS portal systems. Two high explosives and one high explosive simulant were incorporated into PLGA biodegradable polymer microspheres using inkjet printing. The design parameters, i.e., the solution concentrations, feed rate and inkjet operating frequency largely control the outcome regarding microsphere size. We have demonstrated that 70% (by mass) of the microsphere can contain the BHT simulant. When incorporated into PLGA, explosive compounds can be detected by an IMS and there is compatibility of PLGA with the IMS in the negative ion mode. The concentrations determined for HMX and BHT analytes residing in the PLGA spheres are close to the predicted values based on dilution ratios. To our knowledge, this is the first time high explosive compounds have been incorporated into PLGA microspheres. Additional testing will be necessary to quantify the polymer retention rate of various compounds during heating. Further studies have been initiated to compositionally map the PLGA microspheres to understand the degree of spatial uniformity present in the polymer material. There are ongoing tests to determine the stability of the microspheres and other materials will be examined to determine their feasibility for trace explosives test standards application.

#### Acknowledgements

The Department of Homeland Security sponsored the production of this work under an interagency agreement with the National Institute of Standards and Technology. The authors would like to acknowledge helpful discussions with Dr. Cory Berkland.

## References

- [1] R.G. Ewing, D.A. Atkinson, G.A. Eiceman, G.J. Ewing, *Talanta* 54 (3) (2001) 515–529.
- [2] S. Hallowell, *Talanta* 54 (2001) 447–458.
- [3] J.R. Verkouteren, *J. Forensic Sci.* 52 (2) (2007) 335–340.
- [4] M.B. Ranada, *Aerosol Sci. Technol.* 7 (1987) 161–176.
- [5] A.D. Zimon, *Adhesion of Dust and Powder*, Consultants Bureau, New York, A Division of Plenum Publishing Corporation, New York, NY, 1982.
- [6] D. Radulescu, N. Schwade, D. Wawro, *Proceedings of the 11th International Symposium on Recent Advances in Drug Delivery Systems*, Salt Lake City, UT, 2003.
- [7] D. Radulescu, H.J. Trost, D. Taylor, B. Antohe, N. Schwade, P. Tarcha, D. Silva, S. Dhar, G. Evans, *Proceedings of the Image Science and Technology DF05, the International Conference on Digital Fabrication Technologies*, Baltimore, MD, 2005.
- [8] M.J. Fuwyler, J.D. Perrings, L.S. Cram, *Rev. Sci. Instrum.* 44 (2) (1973) 204–206.
- [9] P.B. O'Donnel, J.W. MacGinity, *Adv. Drug Deliv. Rev.* 28 (1997) 25–42.
- [10] C. Berklund, K. Kim, D. Pack, *J. Control. Release* 73 (2001) 59–74.
- [11] D.T. Birnbaum, L. Brannon-Peppas, in: D.M. Brown (Ed.), *Microparticle Drug Delivery Systems in Drug Delivery Systems in Cancer Therapy*, Humana Press, Inc., Totowa, NJ, 2003.
- [12] C. Berklund, K. Kim, D. Pack, *Pharm. Res.* 20 (7) (2003) 1055–1062.
- [13] C. Raman, C. Berklund, K. Kim, et al., *J. Control. Release* 103 (2005) 149–158.
- [14] R. Berglund, B.Y.H. Liu, *Environ. Sci. Technol.* 7 (1973) 147–153.
- [15] A.A. Silva-Junior, M.V. Scarpa, K.C. Pestana, L.P. Mercuri, J.R. de Matos, A.G. de Oliveira, *Thermochim. Acta* 467 (1/2) (2008) 91–98.



## Determination of fenthion and fenthion-sulfoxide, in olive oil and in river water, by square-wave adsorptive-stripping voltammetry

T. Galeano Díaz\*, A. Guiberteau Cabanillas, M.D. López Soto, J.M. Ortiz

Department of Analytical Chemistry, University of Extremadura, Avd. Elvas s/n 06071, Badajoz, Spain

### ARTICLE INFO

#### Article history:

Received 19 October 2007

Received in revised form 14 April 2008

Accepted 16 April 2008

Available online 24 April 2008

#### Keywords:

Fenthion

Fenthion-sulfoxide

Square-wave

Adsorptive-stripping voltammetry (AdSV)

Olive oil

Water

### ABSTRACT

Square-wave adsorptive-stripping voltammetry technique has been used to develop a method for the determination of fenthion in olive oil. Due to the fact that fenthion does not give any electrochemical signal at mercury electrode, the method has been based on a previous oxidation of fenthion to its metabolite, fenthion-sulfoxide, by using  $\text{KMnO}_4$ . The metabolite gives rise to a peak due to an adsorptive-reductive process at  $-0.786\text{ V}$ . Fenthion is isolated from olive oil by carrying out a solid-liquid extraction procedure using silica cartridge, followed by a liquid-liquid partitioning with acetonitrile. The detection limit in olive oil is  $78.8\text{ ng g}^{-1}$  and recoveries for four levels of fortification are ranged from 85% to 109%. On the other hand, it has been developed a method for the simultaneous determination of fenthion and its metabolite fenthion-sulfoxide, in river water. Pesticides are isolated from water by carrying out a liquid-liquid partitioning with trichloromethane. The detection limits are  $0.41\text{ ng g}^{-1}$  and  $0.44\text{ ng g}^{-1}$ , for fenthion and fenthion-sulfoxide, respectively. Recoveries for three levels of fortification are ranged from 96% to 103% for fenthion and 94% to 104% for fenthion-sulfoxide.

© 2008 Elsevier B.V. All rights reserved.

### 1. Introduction

Fenthion is a contact and stomach organophosphorous pesticide widely used in the control of many sucking, biting pests, especially fruit flies, stem borers and mosquitoes on crops such as alfalfa, rice, sugar cane, cereal, vegetables and forests. It is also used for the control of insects affecting public health, especially mosquitoes and flies, and for animals health. More concretely, fenthion is frequently applied to olive crops to combat olive fly (*Bactocera (Dacus) oleae*) and olive moth (*Prays oleae*) [1].

Fenthion is moderately toxic to mammals and highly toxic to birds. The toxicological effect of fenthion, as organophosphorous pesticides, is almost entirely due to the inhibition of acetylcholinesterase in the nervous system, resulting in respiratory, myocardial and neuromuscular transmission impairment.

Fenthion is of moderate persistence in soil, with an average field half-life of 34 days under most conditions. In soil, residues of fenthion may persist for approximately 4–6 weeks. In one study of its persistence in water, 50% of applied fenthion remained in river water 2 weeks later, while 10% remained after 4 weeks. It is more rapidly degraded under alkaline conditions. The persistence half-life of fenthion in water under field conditions is reported to range from 3 to 21 days for various oceans, rivers and swamps. However,

it may be more persistent in some environments, such as salt marsh sediments, where light and oxygen are limited [2].

Fenthion is slowly degraded in olives with a half-life of about 35 days. The main route of fenthion metabolism in plants is by oxidation to fenthion-sulfoxide, which has a higher biological activity than the parent compound. Subsequent oxidation of sulfoxide to sulfone, a compound with lower biological activity, is slow in plants. An additional route of bioactivation is through oxidative enzymatic desulfuration to form fenthion-*O*-analogue. These metabolites tend to partition into the olive oil [3]. Fenthion is most probably to be found in olive oil because of its lipophilic properties ( $\log K_{o/w}$  4.8), while other metabolites are not detectable. In the olive fruit pulp the main compounds founded are fenthion and fenthion-sulfoxide and small amounts of fenthion-sulfone and fenthion-*O*-analogue [4]. However, taking into account that fenthion-sulfoxide polarity is greater,  $\log K_{o/w}$  1.9, it is highly probable to be present in environmental waters near to olive crops [1].

FAO, WHO and Codex Alimentarius Commission have established  $1\text{ }\mu\text{g g}^{-1}$  as maximum residue limits (MRLs) for fenthion and its major metabolites, determined separately or together and expressed as fenthion [5].

Gas chromatography is the technique most commonly used to analyse fenthion and its metabolites in olive oil samples [3,6–13]. As olive oil is a complex matrix, normally different clean-up procedures have to be performed to avoid interferences owing to the presence of different olives oil compounds such as pigments, polyphenols and mostly lipid material. Liquid-liquid partitioning

\* Corresponding author. Tel.: +34 924289375; fax: +34 924289375.  
E-mail address: [tgaleano@unex.es](mailto:tgaleano@unex.es) (T. Galeano Díaz).

with different solvents are used in many cases [3,6,8], being acetonitrile the most common one [3,6]. In other cases a clean-up step by solid–liquid extraction is included [9,10], or sometimes olive oil samples are just diluted in cyclohexane [11]. Other isolation methods are headspace solid–phase microextraction [7] and on-line coupling reversed-phase liquid chromatography/gas chromatography by means of an automated through-oven transfer adsorption–desorption (TOTAD) interface [12].

Referring to electrochemical methods for the determination of fenthion, they are quite scarce. Fenthion is determined together with other pesticides by GC with N–P detector and HPLC using an electrochemical detector [14]. In other case, an amperometric biosensor with acetylcholinesterase is used to determine fenthion [15]. Other authors analyse fenthion and fenitrothion by a flow injection system with amperometric detection, using a glassy carbon electrode [16]. In the revised bibliography, it has not been found any method in which fenthion was determined by using mercury electrode.

In this paper we propose a method to determine fenthion in olive oil samples and fenthion and fenthion-sulfoxide in river water samples. Both methods are developed by using adsorptive-stripping voltammetry (AdSV).

## 2. Experimental

### 2.1. Apparatus

The Crison basic 20 pH-meter has a combined SCE-glass electrode.

An Autolab AUT 12.v PSTAT10 (Ecochemie, The Netherlands) was used in combination with a Metrohm VA-663 polarographic stand, with a three electrode system with hanging mercury drop electrode as working electrode, a Ag/AgCl saturated KCl reference electrode and a Pt wire auxiliary electrode. The system is monitored by the General Purpose Electrochemical System (GPES4) version 4.0, software package (Ecochemie, Utrecht, The Netherlands). Golden Software (Grapher, v. 1.32) (Golden, CO) was used for the transformation of initial signals.

### 2.2. Reagents and materials

All chemical employed were analytical-reagent grade or better. NaOH and hexane were from Merck (Darmstadt, Germany), ethanol, acetonitrile, perchloric acid and potassium permanganate were from Panreac (Barcelona, Spain). Ultrapure water was obtained from a Millipore Milli-Q system. SEP-PAK Plus silica cartridge (Waters Corporation, Milford).

Fenthion, fenthion-sulfoxide and fenthion-sulfone from Dr. Ehrenstorfer (Augsburg, Germany). Standard solutions of compounds in ethanol were prepared by weight and direct dilution.

### 2.3. Recommended procedure for determination of fenthion in olive oil

A 1-g sample of olive oil is mixed with 5 mL of hexane. The solution is passed through a silica cartridge and the pesticide is eluted with 20 mL of hexane. The hexane solution is transferred into a 100-mL beaker with 15 mL of acetonitrile. The mixture is stirred during 15 min by using a magnetic stirrer. The acetonitrile phase is then run into a 100-mL separating funnel and the lipid material, co-extracted in the acetonitrile phase, is removed by carrying out a liquid–liquid extraction with 10 mL of hexane. The mixture is shaken and left until phases are separated. The acetonitrile phase is run into a 250-mL round-bottomed flask and it is rotary evaporated to dryness. Then the residue is rinsed with 2.5 mL of acetonitrile

and collected into a 25-mL volumetric flask. 0.1 M HClO<sub>4</sub> and 4 mM KMnO<sub>4</sub> are added to the volumetric flask. The solution is diluted to the mark with deionized water and placed into the polarographic cell. The solution is deoxygenated with N<sub>2</sub> for 120 s and the AdSV voltammogram of the sample is recorded at the following instrumental conditions:  $t_{acc} = 15$  s,  $E_{acc} = -0.200$  V, frequency = 200 Hz, step potential = 10 mV, amplitude = 50 mV, stirring rate = 500 rpm. From the analytical signal, peak intensity or  $I_p$ , the concentration is calculated by using standard addition method.

### 2.4. Recommended procedure for determination of fenthion and fenthion-sulfoxide in river water

A liquid–liquid partitioning between 100-mL of river water sample and 10 mL of trichloromethane is carried out to isolate fenthion and fenthion-sulfoxide from river water samples. Once phases are separated, the lower trichloromethane phase is run into a 250-mL round-bottomed flask and it is rotary evaporated. The residue is rinsed with 2.5 mL of acetonitrile and collected into a 25-mL volumetric flask. 0.1 M HClO<sub>4</sub> is also added to the volumetric flask, the solution diluted to the mark with deionized water is placed into the polarographic cell. The AdSV voltammogram is recorded at the following instrumental conditions:  $t_{acc} = 15$  s,  $E_{acc} = -0.200$  V, frequency = 200 Hz, step potential = 10 mV, amplitude = 50 mV, stirring rate = 500 rpm. The peak corresponding to fenthion-sulfoxide is obtained. From this analytical signal, peak intensity or  $I_p$ , the concentration of fenthion-sulfoxide is calculated by using a suitable prepared calibration graph. Afterwards, 4 mM KMnO<sub>4</sub> is added to the solution placed in the polarographic cell, and the AdSV voltammogram of the sample is recorded at the instrumental conditions described above. The resulting peak is the sum of fenthion oxidized to fenthion-sulfoxide and fenthion-sulfoxide initially present. The peak intensity of fenthion is calculated by subtracting  $I_p$  (fenthion-sulfoxide) from  $I_p$  (sum of fenthion and fenthion-sulfoxide). The concentration of fenthion is calculated by a suitable prepared calibration graph.

## 3. Results and discussion

The electrochemical response of fenthion was studied at mercury electrode (HMDE) in 0.4 M Britton–Robinson buffer at different pH values and containing 4.0  $\mu\text{g mL}^{-1}$  of fenthion. Fenthion produced an insignificant cathodic electrochemical signal at  $-1.1$  V and both  $E_{1/2}$  (half-wave potential) and limiting current ( $I_{lim}$ ) of the signal, remained constant over the studied pH range (Fig. 1a). However, an important point to be considered, it was that fenthion molecule contains a thiophosphate (P=S) and thioether (–S–) group. The –S– group may be oxidized to a sulfoxide or sulfone and the P=S group to P=O group, giving a total of six compounds. According to bibliographic antecedents, KMnO<sub>4</sub> oxidizes fenthion to fenthion-sulfoxide and fenthion-sulfone because, unlike peroxide, KMnO<sub>4</sub> leaves the P=S group intact and therefore the formation of oxon compounds does not take place [6]. The possibility of determining fenthion as one of these two metabolites was examined. Firstly the electrochemical behaviour of the metabolites was studied.

Fenthion-sulfone, at mercury electrode, behaved quite similar to fenthion. Fenthion-sulfone produced a cathodic signal close to  $-1.1$  V. Both  $E_{1/2}$  and  $I_{lim}$  did not depend on the pH of the solution and the signal disappeared at the voltammogram as of pH around 3, probably because the signal was overlapped by the background discharge signal (Fig. 1b).

On the other hand fenthion-sulfoxide, produced a cathodic signal which  $E_{1/2}$  shifted to more negative values as the pH was increasing up to pH 6, from which  $E_{1/2}$  did not change and also

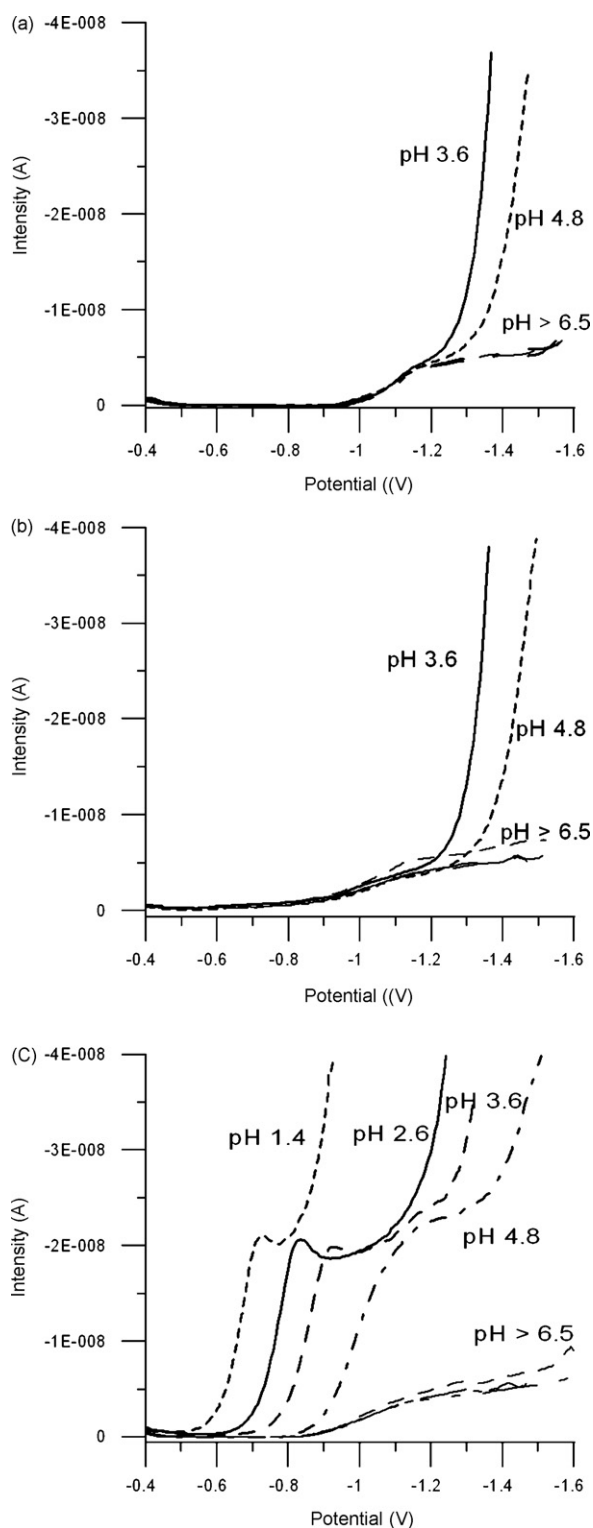


**Fig. 1.** Sampled DC voltammograms of  $4 \mu\text{g mL}^{-1}$  of (a) fenthion, (b) fenthion-sulfone (c) fenthion-sulfoxide, in 0.4 M Britton-Robinson buffer at different pH values.

$I_{\text{lim}}$  fell sharply as of pH around 6 (Fig. 1c). The voltammogram of fenthion-sulfoxide registered by CV technique showed that there was no peak at the reverse scan, indicating that the reductive process was irreversible (Fig. 2).

Looking at the voltammograms of the three compounds (Fig. 1), it is observed that as of pH around 7, the three analytes behaved in

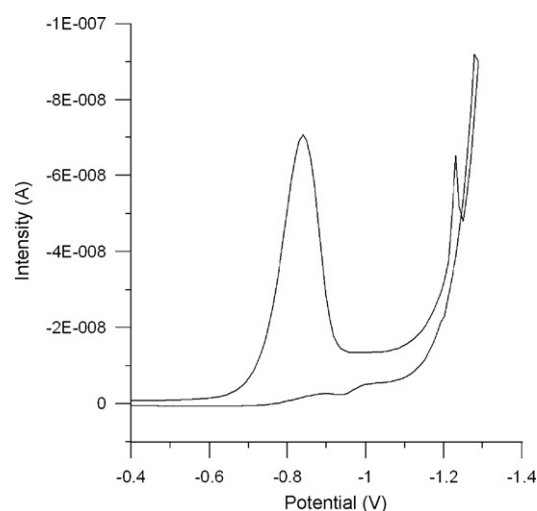


**Fig. 2.** CV voltammogram of  $4 \mu\text{g mL}^{-1}$  fenthion-sulfoxide at pH 2.6.

a similar way, while in acidic media fenthion-sulfoxide produced a signal with much higher intensity than that for fenthion and fenthion-sulfone. Best results were obtained for fenthion-sulfoxide in acidic media.

The study of scan rate of fenthion-sulfoxide by CV technique demonstrated the adsorption nature of the reductive process, since linearity between  $I_p$  and scan rate it was observed but not between  $I_p$  and the square root of the scan rate.

With the aim of determining fenthion indirectly and knowing the possibility of analysing fenthion-sulfoxide by stripping techniques, the oxidation of fenthion to fenthion-sulfoxide was examined in depth. With this purpose UV-spectra of the three compounds were registered in 0.1 M  $\text{HClO}_4$  (Fig. 3a). Different concentrations of  $\text{KMnO}_4$  were added over a sample of fenthion in 0.1 M  $\text{HClO}_4$  and both spectra (Fig. 3b) and voltammograms (Fig. 3c) were recorded. It was observed that the absorbance maximum of fenthion ( $\lambda = 250 \text{ nm}$ ) disappeared when  $\text{KMnO}_4$  concentration was greater than 10 mM. However, not only fenthion-sulfoxide was produced (maximum  $\lambda = 237 \text{ nm}$ ) but also a mixture of fenthion-sulfoxide and fenthion-sulfone (Fig. 3b). In Fig. 3b, it can be appreciated the similarity between the absorption spectra of a standard of fenthion-sulfoxide + fenthion-sulfone and the absorption spectra of the resulting solution after adding  $\text{KMnO}_4$  to fenthion. For concentrations above 25 mM, the electrochemical signal of fenthion-sulfoxide decreased, and therefore less amount of this metabolite was produced (Fig. 3c).

In addition, it was proven that the presence of  $\text{KMnO}_4$  did not affect to the voltammetric determination.

The study of the influence of chemical and instrumental variables over peak intensity ( $I_p$ ) of fenthion-sulfoxide was carried out by square-wave adsorptive-stripping voltammetry.

For  $100 \text{ ng mL}^{-1}$  of fenthion-sulfoxide, it was observed that peak intensity of the pesticides remained constant when  $\text{HClO}_4$  concentration was varied from 0.02 M to 2.0 M. Therefore 0.10 M  $\text{HClO}_4$  was selected as the most suitable concentration for the determination by AdSV.

The influence of ionic strength was studied by varying  $\text{NaClO}_4$  concentration from 0.00 M to 0.15 M. Also in this case, peak intensity did not suffer variations so that no  $\text{NaClO}_4$  was used for the determination.

Considering acetonitrile to be the solvent used for the pesticide extraction procedure from olive oil, it was studied how the presence of this solvent affected peak intensity. In this case peak intensity decreased as acetonitrile percentage was increasing from

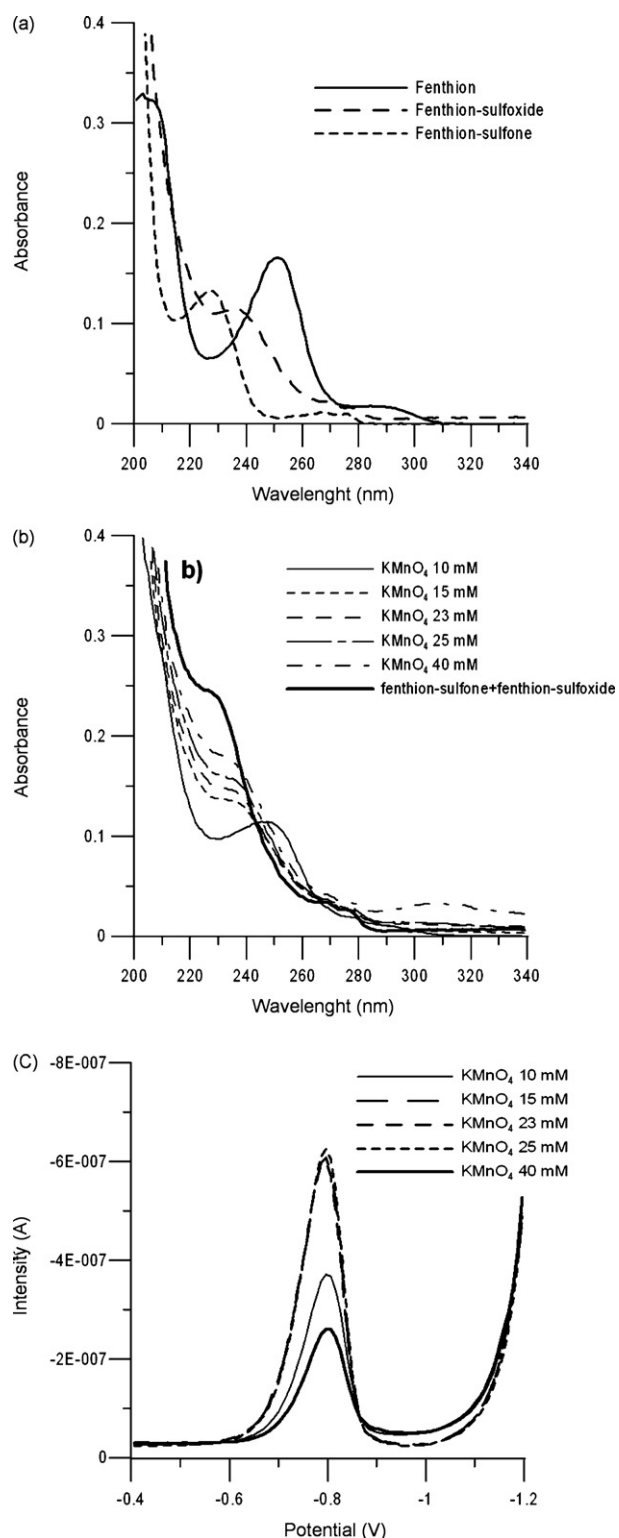


**Fig. 3.** (a) UV-spectra of fenthion, fenthion-sulfoxide and fenthion-sulfone ( $1.44 \times 10^{-5}$  M, HClO<sub>4</sub> 0.10 M); (b) UV-spectra of fenthion with different concentrations of KMnO<sub>4</sub> and — UV-spectra sum of fenthion-sulfoxide + fenthion-sulfone, both  $1.44 \times 10^{-5}$  M, HClO<sub>4</sub> 0.10 M; (c) SW voltammograms of fenthion with different concentrations of KMnO<sub>4</sub>.

2% to 18%. It was selected 10% acetonitrile although this percentage would vary depending on extraction procedure.

KMnO<sub>4</sub> concentration was ranged from 0.5 mM to 15 mM. It was found that the highest peak intensity values were obtained between

1.2 mM and 6 mM. 4 mM was selected as the most suitable KMnO<sub>4</sub> concentration to oxidize fenthion to fenthion-sulfoxide.

It was also observed that the oxidation of fenthion to fenthion-sulfoxide with KMnO<sub>4</sub> was immediate and the obtained solution of fenthion-sulfoxide was stable for at least 1 h.

It was proven that deoxygenating time did not influence over  $I_p$  and 120 s was selected as purge time.

The accumulation time ( $t_{acc}$ ) was evaluated by varying it from 0 s to 30 s and for  $50 \text{ ng mL}^{-1}$  and  $100 \text{ ng mL}^{-1}$  of fenthion-sulfoxide. The relationship between peak intensity and  $t_{acc}$  was linear up to 20 s, for  $100 \text{ ng mL}^{-1}$ , while for  $50 \text{ ng mL}^{-1}$  the linearity was up to 50 s. 15 s as  $t_{acc}$  was selected for later studies. The accumulation potential ( $E_{acc}$ ) was varied from +0.100 V to -0.500 V, founding the maximum peak intensity from 0.000 V to -0.300 V. Therefore -0.200 V was chosen for subsequent studies.

With regard to frequency, step potential and amplitude, they were also optimised taking into account to get maximum values for peak intensity, but always considering peak width and peak definition. The values selected were 200 Hz, 10 mV and 50 mV, respectively.

### 3.1. Calibration and precision in aqueous solution

Calibration plot was constructed by varying fenthion-sulfoxide concentration from  $5 \text{ ng mL}^{-1}$  to  $100 \text{ ng mL}^{-1}$  and measuring peak intensity in the square-wave voltammograms of the obtained solutions. It was obtained the following calibration plot:  $I_p = 2.45 C + 0.19$  ( $C = \text{fenthion-sulfoxide concentration, ng mL}^{-1}$ ) (Fig. 4a). Correlation coefficient = 0.9993, and detection limit =  $1.75 \text{ ng mL}^{-1}$  [16] were found.

On the other hand, other calibration plot was constructed for fenthion oxidized to fenthion-sulfoxide (Fig. 4b). In this case it was obtained:  $I_p = 1.98 C + 1.54$  ( $C = \text{fenthion-sulfoxide concentration, ng mL}^{-1}$ ), being correlation coefficient = 0.9991, and detection limit =  $1.63 \text{ ng mL}^{-1}$  [17]. Both calibration plot were statistically compared, resulting in there were significant differences.

It was examined the possibility that the differences in the slopes of the calibration plots were due to the presence of KMnO<sub>4</sub> in the case of fenthion. However a comparison between two calibration plots of fenthion-sulfoxide, with and without KMnO<sub>4</sub>, showed there were not significant differences between both graphs. This meant that the oxidation of fenthion to fenthion-sulfoxide is not a quantitative process. An estimation of the conversion fraction of fenthion to fenthion-sulfoxide could be deduced by the ratio between the slopes of both calibration, being this value equal to  $\approx 81\%$ .

To calculate the concentration of each compound it was necessary to use their corresponding calibration plot. The relative error of the method was estimated for two levels of concentrations of fenthion:  $5 \text{ ng mL}^{-1}$  and  $50 \text{ ng mL}^{-1}$ , from 11 samples for each concentration level. For  $5 \text{ ng mL}^{-1}$  the mean value for peak intensity was 11.9 nA and the relative standard deviation was 6.3%. For  $50 \text{ ng mL}^{-1}$  the mean value for peak intensity was 128.4 nA and the relative standard deviation was 1.9%. The reproducibility of the method was calculated by registering voltammograms during 2 months period and for  $100 \text{ ng mL}^{-1}$  of fenthion. The mean value for peak intensity was 219.8 nA and the relative standard deviation was 4.6%.

### 3.2. Determination of fenthion in olive oil

A procedure to isolate fenthion from olive oil was optimised. Initially several experiments testing liquid-liquid extraction procedures with different solvents, acetonitrile and ethanol, were performed. Solid-liquid extraction was also tested. With Envi-Carb cartridges and different eluents as acetonitrile and hexane

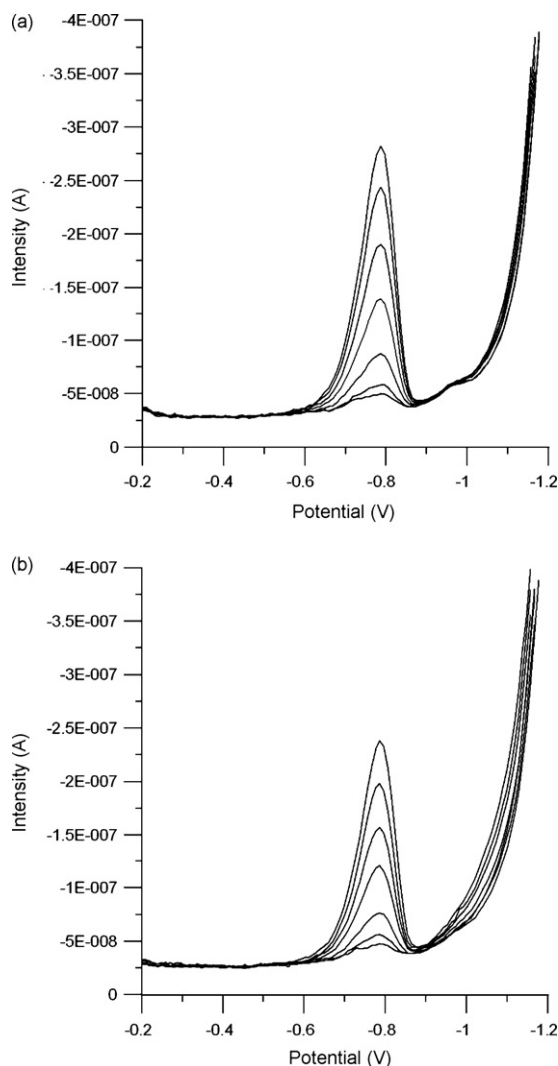


**Fig. 4.** AdSV voltammograms of (a) fenthion-sulfoxide for concentrations between  $5 \text{ ng mL}^{-1}$  and  $100 \text{ ng mL}^{-1}$  at the following conditions:  $0.10 \text{ M HClO}_4$ ,  $10\% \text{ ACN}$ , purge time =  $120 \text{ s}$ ,  $E_{\text{acc}} = -0.280 \text{ V}$ ,  $t_{\text{acc}} = 15 \text{ s}$ , frequency =  $200 \text{ Hz}$ , amplitude =  $50 \text{ mV}$  and step potential =  $10 \text{ mV}$ . (b) Fenthion at the same chemical and instrumental conditions +  $4 \text{ mM KMnO}_4$ .

many peaks appeared at the voltammogram, but fenthion was not distinguished. With C18 and silica cartridges, lipid material or polyphenols caused interferences. It was considered the possibility of using liquid–liquid extraction together with solid–liquid extraction to remove olive oil material that was caused interferences. Best results were achieved when an olive oil hexane solution was passed through a silica cartridge, the pesticide was eluted with hexane, and extracted into acetonitrile. To remove lipid material that affected the voltammetric determination, the acetonitrile extract was cleaned up by performing a liquid–liquid partitioning with hexane. The variables that could affect to the extraction procedure of fenthion from olive oil were optimised, and the procedure described in the section: recommended procedure for the determination of fenthion in olive oil, was deduced.

### 3.3. Calibration in olive oil

A new calibration plot was constructed following the proposed olive oil extraction procedure for fenthion, and adding different fenthion concentrations to the extract (Fig. 5). Their voltammograms were registered under the optimised AdSV conditions. It was

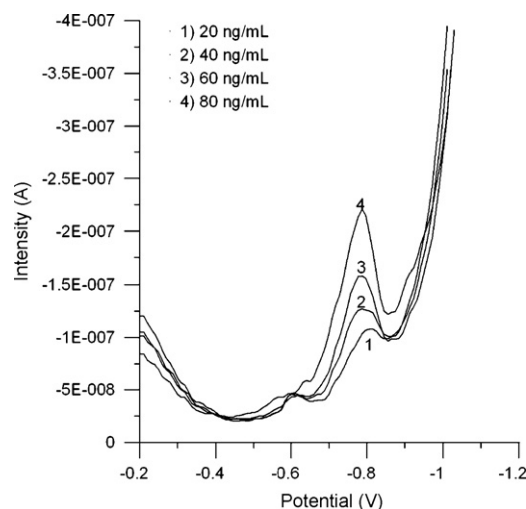


**Fig. 5.** AdSV voltammograms of fenthion in the olive oil extract, for concentrations between  $20 \text{ ng mL}^{-1}$  and  $80 \text{ ng mL}^{-1}$  (chemical and instrumental variables as in Fig. 4).

obtained the calibration plot:  $I_p = 1.47C + 2.37$  ( $C$  = fenthion concentration  $\text{ng mL}^{-1}$ ), correlation coefficient =  $0.9984$  and detection limit =  $3.15 \text{ ng mL}^{-1}$  [17]. This calibration graph was compared to that obtained in aqueous solution and significant differences of the slopes were found, indicating matrix effects. Therefore it was necessary to apply standard addition method to determine fenthion in olive oil by means of this procedure.

The proposed method was applied to the determination of fenthion in olive oil samples. Samples of olive oil were fortified with fenthion at four different levels and the results of recovery are in Table 1.

### 3.4. Simultaneous determination of fenthion and fenthion-sulfoxide in river water

The extraction procedure of the compounds was carried out by an optimised procedure consisted in liquid–liquid extraction with trichloromethane as it has been described at section: recommended procedure for the determination of fenthion and fenthion-sulfoxide in river water. For each compound, a calibration plot was constructed in river water extract following the described procedure. The resulting calibration plots were statistically compared to those obtained in aqueous solution. In this case, no significant differences were found for both analytes. Consequently the simultaneous determination of fenthion and fenthion-sulfoxide in river water was performed by applying external standard method.

The proposed method was applied to determine fenthion and fenthion-sulfoxide in river water samples. Samples of river water were fortified with these compounds at three concentration levels and the results of recovery are in Table 2.

**Table 1**  
Recovery values for the determination of fenthion in olive oil

Sample	Added ( $\text{ng g}^{-1}$ )	Found ( $\text{ng g}^{-1}$ ) $\pm$ S.D. <sup>a</sup>	Recovery (%) $\pm$ S.D. <sup>a</sup>
1	500	$543.8 \pm 47.0$	$109 \pm 9$
	1000	$894.3 \pm 146.2$	$89 \pm 15$
2	750	$640.8 \pm 63.5$	$85 \pm 9$
	1250	$1110.3 \pm 74.4$	$89 \pm 6$

<sup>a</sup> Three determinations.

**Table 2**  
Recovery values for the determination of fenthion and fenthion-sulfoxide in river water

Compound	Added (ng mL <sup>-1</sup> )	Found (ng mL <sup>-1</sup> ) ± S.D. <sup>a</sup>	Recovery (%) ± S.D. <sup>a</sup>
Fenthion	2.5	2.35 ± 0.06	94 ± 2
	5	5.20 ± 0.38	104 ± 8
	10	9.43 ± 1.15	94 ± 12
Fenthion-sulfoxide	2.5	2.39 ± 0.18	96 ± 8
	5	4.77 ± 0.10	95 ± 2
	10	10.3 ± 0.45	103 ± 5

<sup>a</sup> Three determinations.

### 3.5. Interferences from other pesticides

Other common organophosphorous pesticides used to control olive pests, are dimethoate and fenitrothion. It was examined if the presence of these compounds and also of the two metabolites of fenitrothion (fenitroxon and 3-methyl-4-nitrophenol) would affect to the determination of fenthion. Dimethoate does not give any electrochemical signal in acidic media and therefore it could not interfere in the determination of fenthion. On the other hand, it was observed that fenitrothion and its metabolites, although they produce electrochemical signals in acidic media, the potentials of these peaks are below  $-0.200$  V and consequently they did not interfere in the determination of fenthion.

## 4. Conclusions

The proposed electrochemical method for the determination of fenthion in olive oil allows acceptable recovery values for it. Also, with the proposed extraction procedure it is obtained an olive oil

extract free of polyphenols and pigments and very low presence of lipid material, which it is quite difficult when working with olive oil samples. The determined detection limit for fenthion in olive is below the MRL regulated by FAO.

In the case of the determination of fenthion and its metabolite fenthion-sulfoxide in river water samples, the method allows the simultaneous analysis of the compounds by a simple liquid–liquid extraction with trichloromethane. Moreover, the obtained detection limits show the possibility of analysing low quantities of those analytes and the recovery values show good results for both compounds.

## References

- [1] The joint FAO/WHO meetings on pesticide residues, Toxicological Monographs [www.inchem.org/pages/jmpr.html](http://www.inchem.org/pages/jmpr.html).
- [2] <http://www.inchem.org/documents/pims/chemical/pimg001.htm>.
- [3] E. Botitsi, P. Kormali, S. Kontou, A. Mourkojanni, E. Stavrakaki, D. Tsiipi, Int. J. Environ. Anal. Chem. 84 (2004) 231.
- [4] <http://www.fao.org/docrep/005/x2570s/X2570S10.htm>.
- [5] Codex Alimentarius Commission. Codex Alimentarius Pesticide Residues in Food-maximum Residues Limits, 2nd ed., vol. 2B, FAO/WHO Press, 1996.
- [6] C. Lentza-Rizos, E.J. Avramides, Analyst 115 (1990) 1037.
- [7] C. Tsoutsis, I. Konstantinou, D. Hela, T. Albanis, Anal. Chim. Acta 573 (2006) 216.
- [8] G. Dugo, G. Di Bella, L. La Torre, M. Saitta, Food Control 16 (2005) 435.
- [9] A. Di Muccio, A. Ausili, L. Vergori, I. Carmona, R. Dommarco, L. Gambetti, A. Santillo, F. Vergori, Analyst 115 (1990) 1167.
- [10] L. Rastrelli, K. Totaro, F. De Simona, Food Chem. 79 (2002) 303.
- [11] B. Jongenotter, H.G. Janssen, LC-GC-Europe 15 (2002) 338.
- [12] R. Sánchez, J.M. Cortés, J. Villén, A. Vázquez, J. AOAC Int. 88 (2005) 1255.
- [13] S. Barrek, O. Paise, M.F. Grenier-Loustalot, Anal. Bioanal. Chem. 376 (2003) 355.
- [14] R. García-Repetto, M. Paz-Giménez, M. Repetto, J. AOAC Int. 84 (2001) 342.
- [15] E. Wilkins, M. Carter, J. Voss, D. Ivnitski, Electrochem. Commun. 2 (2000) 786.
- [16] J. Hernández-Méndez, R. Carabias-Martínez, F. Becerro-Domínguez, J.I. Jiménez-Jiménez, Anal. Chim. Acta 209 (1988) 205.
- [17] G.L. Long, J.D. Winefordner, Anal. Chem. 55 (1983) 713A.





## Determination of photoirradiated high polar benzoylureas in tomato by HPLC with luminol chemiluminescence detection

M. Martínez Galera, M.D. Gil García\*, R. Santiago Valverde

Department of Analytical Chemistry, Faculty of Experimental Sciences, University of Almeria, 04061 Almeria, Spain

### ARTICLE INFO

#### Article history:

Received 19 November 2007

Received in revised form 8 April 2008

Accepted 16 April 2008

Available online 2 May 2008

#### Keywords:

Chemiluminescence detection

Photochemical derivatization

HPLC

Luminol

Vegetables

Benzoylureas

Tomato

### ABSTRACT

This study reports the first analytical application of luminol chemiluminescence reaction for the sensitive detection of two benzoylurea insecticides (diflubenzuron and triflumuron). Off-line experiments demonstrated that previously irradiated traces of these benzoylurea insecticides largely enhanced the chemiluminescence emission yielded from the oxidation of luminol in methanol: water mixtures, by potassium permanganate in alkaline medium, the enhancement being proportional to the concentration of both pesticides. The two benzoylureas were determined in tomato samples by coupling liquid chromatography with post-column photoderivatization and detection based on this chemiluminescence reaction. Tomato samples were extracted using the QuEChERS method based on extraction with acetonitrile and dispersive solid-phase clean-up using primary and secondary amine (PSA). Interferences due to matrix effect were overcome by using matrix-matched standards. The optimised method was validated with respect to linearity, limits of detection and quantification, precision and accuracy. Under the optimised conditions, calibrations graphs were linear between 0.05 and 0.50  $\mu\text{g mL}^{-1}$  for diflubenzuron and between 0.10 and 1.00  $\mu\text{g mL}^{-1}$  for triflumuron. Method detection limits were 0.0025 and 0.0131  $\mu\text{g mL}^{-1}$  (equivalent to 0.0005 and 0.0026  $\text{mg kg}^{-1}$ ) and quantification limits were 0.05 and 0.10  $\mu\text{g mL}^{-1}$  (equivalent to 0.01 and 0.02  $\text{mg kg}^{-1}$ ) for diflubenzuron and triflumuron, respectively. In both cases, quantification limits were lower than the maximum residue levels (MRLs) established by the European legislation. The relative standard deviation of intra-day precision was below 10% and recoveries were between 79.7% and 94.2% for both pesticides.

© 2008 Elsevier B.V. All rights reserved.

### 1. Introduction

Substituted ureas are an important group of pesticides that are used as herbicides (phenylureas and sulfonylureas) and insecticides (benzoylureas). Benzoylureas are promising insecticides, widely used because their ability to act as powerful insect growth regulators which interfere with chitin synthesis in target pests and cause death. These insecticides show some attractive properties such as high selectivity, high biological activity, rapid degradation in both soil and water and acute low toxicity for animals, which make them suitable for inclusion in integrated pest management programs for crops [1]. Nevertheless, due to the high interest in the safety of products, the maximum residue levels (MRLs) established for these pesticides [2] are in the same order that those established for another ones considered with high toxicity.

Even though some papers reported the determination of benzoylureas by gas chromatography (GC) with different detec-

tors [3–6], due to their thermostability, the technique of choice for analysing these pesticides has been high-performance liquid chromatography (HPLC) with UV [7–10], fluorescence [11–13] or mass spectrometry (MS) [14–19] detection. Thus, diflubenzuron, triflumuron, teflubenzuron, lufenuron and flufenoxuron were determined in grapes and wine [20] and diflumuron, flufenoxuron and hexaflumuron in citrus [21] by HPLC-UV; diflubenzuron, triflumuron, hexaflumuron, lufenuron and flufenoxuron were determined in vegetables by HPLC with post-column photochemically induced fluorescence (PIF) derivatization and fluorescence detection [13] and finally some of this benzoylurea compounds were determined by HPLC-MS in fruits [16], apples [22] and vegetables [23] and by HPLC-MS/MS in processed fruit and vegetables [24] and citrus [19].

Nowadays, multiresidue methods by HPLC-MS or HPLC-MS/MS are becoming the most powerful techniques for the analysis of highly polar, less volatile and thermally labile compounds [25], but alternative low cost methods may be of high interest, mainly when a reduced number of pesticides must be determined.

Analytical interest in liquid-phase chemiluminescence (CL) has been continuously growing over the last 20 years, the best

\* Corresponding author.

E-mail address: [mdgil@ual.es](mailto:mdgil@ual.es) (M.D.G. García).

demonstration of this interest being the large number of recent manuscripts dealing with analytical applications for pesticides [26–30], drugs [31–33], antioxidants [34,35] and others [36–38] in a variety of industrial, clinical and environmental matrices.

CL is becoming an attractive technique to be used as detection system in LC due to its high sensitivity, wide linear range and simple instrumentation. Furthermore, CL detection is very sensitive because the absence of a light source reduces noise and eliminates Rayleigh and Raman scattering, allowing photon detectors to be operated at high gains to improve the signal-to-noise ratio (S/N). In addition, the elimination of the excitation source in CL can reduce stray light and background emissions and removes the possibility of light-source instability. Despite these advantages, CL has been used less than fluorescence and absorbance for pesticide residue analysis.

The coupling of luminol CL with HPLC provides high efficiency in separation and low limits of detection (LODs) inherent to CL, although its application in pesticide residue analysis has been limited [27].

The yield of strong CL emission by the oxidation of luminol in alkaline medium is one of the best known and most efficient CL reactions. Different oxidants can be used, such as hydrogen peroxide, molecular oxygen, hypochlorite or permanganate, mainly in the presence of some type of initiator or catalyst such as peroxidase, hexacyanoferrate(III), and compounds or metal ions ( $\text{Co}^{2+}$ ,  $\text{Cu}^{2+}$ ,  $\text{Cr}^{3+}$ ,  $\text{Ni}^{2+}$ , etc.). The luminol– $\text{KMnO}_4$  CL system has been used for the selective detection of carbaryl [39] and carbofuran [40], both determinations being based on a FIA configuration. In both methods, luminol carrier was mixed with permanganate carrier before CL detector, and then, this oxidant solution was mixed with the analytes without any catalyst. The CL mechanism proposed for carbofuran consists in the oxidation of this compound with permanganate yielding an intermediate which could subsequently to oxidize luminol upto the excited state 3-aminophthalate anion; finally this excited anion decay to the ground state and produce CL [40].

On the other hand, it has been established that the irradiation of photoreactive analytes leads to the formation of species that can be detected by CL providing very sensitive procedures [41], but only some few papers dealing with photodegradation and CL have been published for pesticides determination [28–30,42–44].

For analytical purposes, photochemical derivatization is extremely useful because of their selectivity and sensitivity and many of these reactions have been adapted as post-column detection systems in HPLC [45–50]. The main advantages of the post-column derivatization are that the analytes are separated in their original form, without the need for a complete derivatization reaction (assuming reproducibility) and the photoproducts need no stability for a long time [51].

The purpose of our study was to check the usefulness of the CL reaction of luminol for the determination of benzoylurea residues in vegetables. We found that after irradiation of both benzoylureas with UV light, the corresponding photoproducts produced a great enhancement on the CL emission from the luminol– $\text{KMnO}_4$  system in alkaline medium without any catalyst. This enhancement in the CL emission is proportional to the concentration of the selected compounds, which can be determined by measuring the increase in the CL intensity. Based on these findings, a new HPLC-CL method has been developed for the sensitive determination of diflubenzuron and triflumuron, which has been satisfactorily applied in tomato samples.

## 2. Experimental

### 2.1. Chemical and solvents

Analytical standards (pestanal quality) of diflubenzuron (99.5%) and triflumuron (99.9%) were obtained from Riedel-de Haën (Seelze, Germany).

Acetonitrile (ACN) and methanol (MeOH) of HPLC grade were obtained from Merck (Darmstadt, Germany); sodium acetate ( $\text{NaAc}\cdot 3\text{H}_2\text{O}$ ), magnesium sulphate anhydrous ( $\text{MgSO}_4$ ) and acetic acid glacial (HAc) for pesticide residue analysis were obtained from Panreac (Barcelona, Spain). Luminol (5-amino-2,3-dihydro-1,4-phthalazine dione,  $\text{C}_8\text{H}_7\text{N}_3\text{O}_2$ ), potassium permanganate ( $\text{KMnO}_4$ ) and sodium hydroxide ( $\text{NaOH}$ ) for analysis were obtained from Panreac (Barcelona, Spain). Primary and secondary amine (PSA)-bonded silica was supplied by Supelco (USA).

Ultrapure water, obtained from a Milli-Q water purification system from Millipore (Bedford, MA, USA), was used. Mobile phases were filtered through a  $0.45\text{-}\mu\text{m}$  cellulose acetate (water) or polytetrafluoroethylene (PTFE) (organic solvents) and degassed with helium prior and during use.

The luminol solution  $0.1\text{ mmol L}^{-1}$ , prepared in  $\text{NaOH}$   $0.1\text{ mol L}^{-1}$  aqueous solution, and permanganate solution  $0.001\text{ mmol L}^{-1}$  were filtered through a Millipore membrane of cellulose acetate ( $0.45\text{ }\mu\text{m}$  particle size) before pumping into the chromatographic system.

### 2.2. Instrumentation

The HPLC-CL system consisted of a Waters (Milford, MA, USA) HPLC equipment, composed of a Model 600E multisolvent delivery system and a Rheodyne 7725i manual injector valve with a  $200\text{ }\mu\text{L}$  sample loop. The photochemical step was carried out on a photochemical reactor Model PHRED-8 (Aura Industries, USA) fitted with a knitted open tube reactor coil ( $7\text{ m} \times 0.6\text{ mm o.d.}$  and  $0.3\text{ mm i.d.}$ ) of PTFE and an 8 W Mercury lamp. CL detection was conducted on a CL detector from Jasco CL-2027 (Tokyo, Japan), which incorporated a modification consisting of placing the mixing chamber as near as possible to the detection cell.

The CL detector was connected to the HPLC equipment through an interface (Waters busSAT/IN Module). The reagent solutions (luminol– $\text{NaOH}$  and  $\text{KMnO}_4$ ) were pumped with two systems Waters Model 510. The luminol solution was firstly mixed with the column effluent and  $\text{KMnO}_4$  solution was after mixed with the resulting effluent inside the box containing the reaction cell and the CL detector. HPLC separations were performed with a Gemini C18  $150\text{ mm} \times 4.6\text{ mm}$  ( $5\text{ }\mu\text{m}$  particle size) column from Phenomenex (USA).

A digital venturis FP 575 pentium personal computer using a Millennium 32 software (Chromatography Manager, Waters) was used for acquisition and treatment of data. A Model BV-401C blender (Fagor Guipuzcoa, Spain) was used for blending the vegetable samples.

### 2.3. Preparation of standards and spiked samples

Individual analytical standard solutions of pesticides ( $400\text{ }\mu\text{g mL}^{-1}$ ) were prepared by exactly weighing and dissolving the corresponding compounds in MeOH. Furthermore, the standard solutions were protected against light and stored at  $4^\circ\text{C}$ . In these conditions, they were stable for at least 3 months.

Working standard solutions were prepared in  $\text{MeOH:H}_2\text{O}$  (50:50, v/v) as solvent. Calibration standard solutions of the analytes and extract of vegetable samples were prepared in  $\text{MeOH:H}_2\text{O}$  (50:50, v/v) and were filtered through Millipore membrane PTFE

filters (0.2  $\mu\text{m}$  particle size) before injection into the chromatographic system.

For recovery determinations, samples (15 g) of finely chopped vegetable were spiked, by addition of a standard stock solution (20  $\mu\text{g mL}^{-1}$  of each pesticide) at two levels of concentration: the limits of quantification (LOQs) (0.01 and 0.02  $\text{mg kg}^{-1}$ , according with the pesticide, equivalent to 0.05 and 0.10  $\mu\text{g mL}^{-1}$  in the final extract) and two times the LOQ (0.02 and 0.04  $\text{mg kg}^{-1}$ , equivalent to 0.10 and 0.20  $\mu\text{g mL}^{-1}$  in the final extract).

The spiked samples were allowed to stand for a few minutes before extraction, to permit the spiking solution to penetrate the test material.

#### 2.4. Extraction procedure

A sample (15 g) of chopped tomato was placed in a 50 mL PTFE vessel, 15 mL of ACN (1% HAC) were added to the sample and the mixture was hand-shaken for 1 min. Then, 6 g of anhydrous  $\text{MgSO}_4$  and 2.5 g of  $\text{NaAc}\cdot 3\text{H}_2\text{O}$  were added, and the mixture was hand-shaken for another minute in such a way that a well-defined phase separation was obtained after 5 min of centrifugation at 3500 rpm. An aliquot (8 mL) was cleaned-up with 400 mg PSA and then dried with 1200 mg  $\text{MgSO}_4$  by mixing them in a Vortex. After centrifugation, 5 mL extract was evaporated to dryness under a gentle  $\text{N}_2$  stream. The obtained residue was redissolved in 1 mL  $\text{MeOH:H}_2\text{O}$  (50:50, v/v) and then filtered through a 0.2  $\mu\text{m}$  PTFE filter before injection in the chromatographic system. In order to avoid interferences, the PTFE filter were cleaned with 1 mL  $\text{MeOH:H}_2\text{O}$  (50:50, v/v) before its use.

#### 2.5. HPLC procedure

200  $\mu\text{L}$  of  $\text{MeOH:water}$  (50:50, v/v) sample solutions were analyzed by HPLC-CL. The mobile phase was  $\text{MeOH:water}$  (75:25, v/v) isocratic at a flow rate of 1  $\text{mL min}^{-1}$ . After separation of pesticides into the analytical column and photochemical derivatization with a Mercury lamp (254 nm low pressure mercury lamp), the resulting photoproducts were mixed with luminol (0.1  $\text{mmol L}^{-1}$ )- $\text{NaOH}$  (0.1  $\text{mol L}^{-1}$ ) solution pumped at a flow rate of 0.8  $\text{mL min}^{-1}$ . Before CL detection, the eluent was mixed with permanganate solution (0.001  $\text{mmol L}^{-1}$ ), which was pumped at a flow rate of 0.6  $\text{mL min}^{-1}$ , inside the box containing the reaction cell and the CL detector.

### 3. Results and discussion

When we tried to enhance the CL yield from the system luminol/ $\text{KMnO}_4/\text{OH}^-$ , by adding benzoylureas, through some experiments in batch using a luminometer and microplates, none reaction was positive. Therefore, we attempted to take advantage of the possibility of changing their molecular structure by irradiation with UV light, and then, to try the CL reaction [41,52,53].

In some previous works, we studied the effect of pH, nature and percentage of organic solvent and irradiation time on the fluorescent behaviour of the benzoylurea insecticides diflubenzuron, triflumuron, lufenuron, hexaflumuron, and flufenoxuron, after irradiation with UV light. We found that these compounds were successfully transformed to fluorescent photoproducts and the strongest fluorescence signal occurred in binary aqueous mixtures with organic solvent such as MeOH and ACN [11,54].

After irradiation, in presence of the photoproducts, a fast CL reaction occurs between luminol and  $\text{KMnO}_4$  in alkaline medium which depends on the nature and percentage of organic solvent in the reaction medium. This increase on the CL signal was observed for the five above-mentioned benzoylurea insecticides. Fig. 1A,

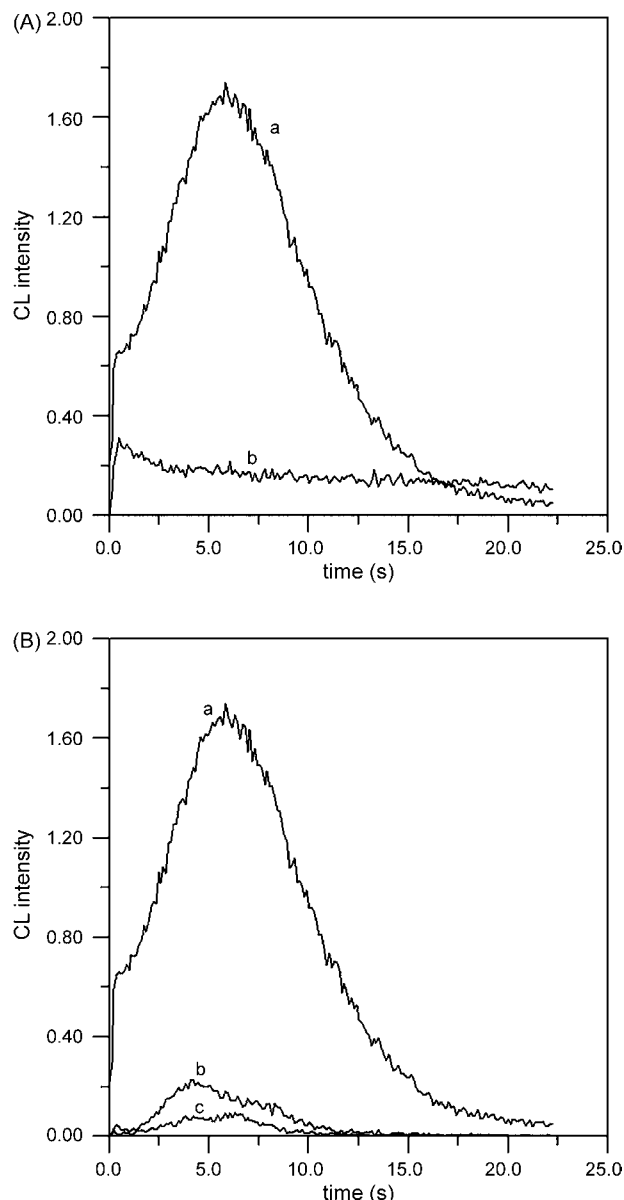


**Fig. 1.** (A) Kinetic profile corresponding to the CL reaction of diflubenzuron in  $\text{MeOH:H}_2\text{O}$  (60:40, v/v) (a) and in  $\text{ACN:H}_2\text{O}$  (60:40, v/v) (b). (B) Kinetic profile of CL reaction of diflubenzuron in 60% MeOH (a), 80% MeOH (b) and 90% MeOH (c) in the reaction medium.

corresponding to the kinetic curve for the CL reaction of diflubenzuron in ACN and MeOH, shows that the CL yield increased when using MeOH. Therefore, this organic solvent was selected for further experiments. Fig. 1B shows that the yield for the CL reaction improved when decreasing the percentage of MeOH in the CL reaction medium; the same effect was found when the percentage of this solvent was decreased in the photoderivatization step.

As the CL reaction is produced by the resulting photo-fragments, which are different for different irradiation intervals, the influence of the photoreaction was studied versus CL yield. Fig. 2 shows that the CL intensity increases with the irradiation time upto 10 min and then, the increase is not significant.

The order of addition of reactives is sometimes a key factor, the CL intensity depending to a great extent on it. Batch experiments demonstrated that the CL signal was higher for both analytes when  $\text{KMnO}_4$  was the last reagent added (Fig. 3). Therefore, the

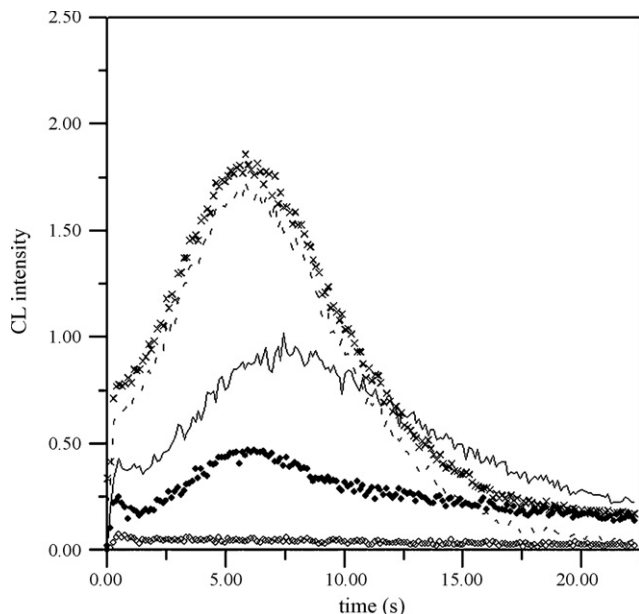


**Fig. 2.** Influence of time of irradiation with UV light on CL intensity for a standard solution containing  $10 \text{ mg mL}^{-1}$  of diflubenzuron prepared in MeOH:H<sub>2</sub>O (60:40): (○) 0 min, (●) 2 min, (—) 5 min, (---) 10 min, and (×) 15 min.

photolyzed benzoylureas were firstly mixed with luminol–NaOH at the outlet of the photoreactor and then,  $\text{KMnO}_4$  was added at the mixing point, the latter located as described below. In fact, when luminol–NaOH and  $\text{KMnO}_4$  were firstly mixed and then were added to the eluate, CL signal was 10 times lower and its intensity was also decreased if the last reagent added was luminol or when both reagents were simultaneously mixed with the eluate at the mixing point.

### 3.1. Modification of the CL detector

Previous studies showed that the rate of the CL reaction was fast (from the reagent mixing to the peak maximum in the kinetic curve, only 5 s were elapsed and it took about 20 s for the signal decay to nearly the baseline). Initially, the commercial CL detector was equipped with an external mixing chamber placed upstream and just outside the dark box containing the detection cell, in such a way

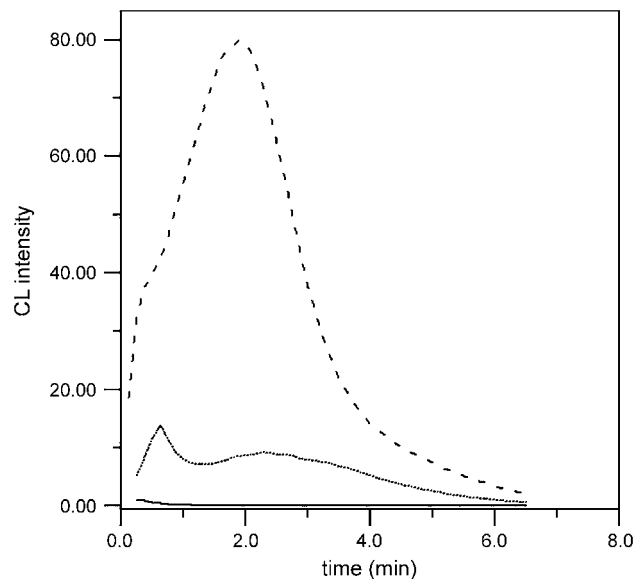


**Fig. 3.** Kinetic profile to CL reaction when the last reagent was  $\text{KMnO}_4$  (---), luminol/NaOH solution (—) or the three reagents mixed together (.....).

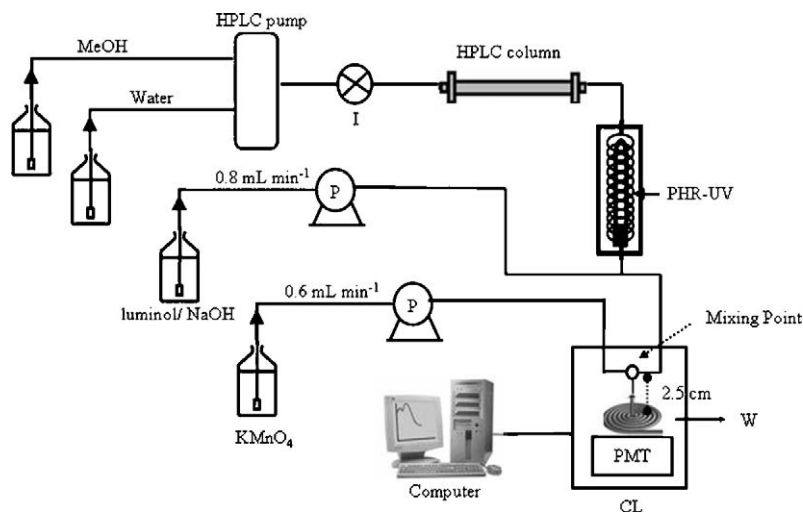
that in this reaction, the light intensity was emitted in this mixer rather than in the cell. Therefore, a modification, which consists of placing the mixing chamber as near as possible to the cell, inside the dark box, was carried out (Fig. 4).

Fig. 5 shows that CL intensity increases exponentially when decreasing the distance from the point of mixture to the detector, according to the above considerations. Therefore,  $\text{KMnO}_4$  solution was mixed with the eluent inside the dark box containing the measure cell.

### 3.2. Optimization of HPLC-CL conditions

To obtain the maximum CL intensity in the determination of benzoylureas by HPLC-CL, the effects of NaOH, luminol and  $\text{KMnO}_4$  concentrations were investigated (Table 1).

The concentration of NaOH versus signal intensity was studied at concentrations ranging from 0.001 to  $0.1 \text{ mol L}^{-1}$ , as shown in Table 1. It can be seen that CL intensities increased with



**Fig. 4.** Schematic diagram of the HPLC-CL system used in the determination of benzoylureas. P, HPLC pump; I, injector; PHR-UV, photochemical UV reactor; CL, chemiluminescence detector; PMT, photomultiplier tube; W, waste.

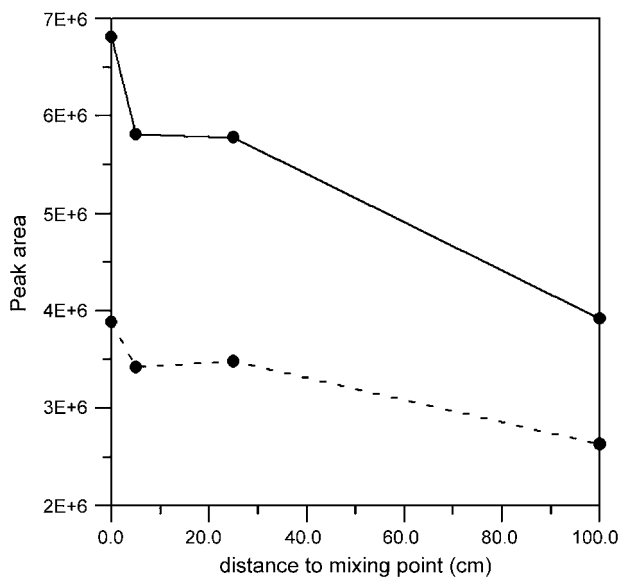


Fig. 5. Effect of distance from the mixer chamber to the detector on the CL intensity of (.....) DFB, (—) TFB, ( $1 \mu\text{g mL}^{-1}$  of each pesticide).

the concentration of NaOH, up to  $0.1 \text{ mol L}^{-1}$ . Higher concentrations were not studied because they could cause precipitation in the flow tubes and  $0.1 \text{ mol L}^{-1}$  was chosen for further experiments.

The effect of luminol concentration on the CL intensities of benzoylureas was investigated in the range of  $0.001$ – $0.5 \text{ mmol L}^{-1}$  (Table 1). Even though the CL intensity increased with the luminol concentration through the range studied,  $0.1 \text{ mmol L}^{-1}$  was chosen because higher concentrations could cause problems due to its precipitation in the tubes of flow devices, given the low solubility of luminol in presence of organic solvents.

The concentration of  $\text{KMnO}_4$  versus CL intensity was studied from  $10^{-4}$  to  $10^{-2} \text{ mmol L}^{-1}$ , as shown in Table 1. CL intensities increased with the permanganate concentration, up to  $10^{-3} \text{ mmol L}^{-1}$ , whereas higher concentrations decreased the CL yield. Thus,  $\text{KMnO}_4$   $10^{-3} \text{ mmol L}^{-1}$  was used in the last flowing solution.

Table 1

Effect of NaOH, luminol and  $\text{KMnO}_4$  concentrations on the CL intensity of benzoylureas

Reactive	Concentration <sup>a</sup>	Peak area	
		Diflubenzuron	Triflumuron
NaOH	0.001	115,730	37,670
	0.005	444,554	184,531
	0.010	723,158	522,880
	0.050	3,792,549	2,900,052
	0.100 <sup>b</sup>	4,538,594 <sup>b</sup>	2,961,725 <sup>b</sup>
Luminol	0.005	371,622	350,276
	0.010	702,343	666,823
	0.050	2,831,695	2,887,925
	0.100 <sup>b</sup>	5,144,618 <sup>b</sup>	4,433,272 <sup>b</sup>
	0.250	7,872,262	6,676,660
$\text{KMnO}_4$	0.0001	800,366	644,306
	0.0010 <sup>b</sup>	1,163,514 <sup>b</sup>	764,783 <sup>b</sup>
	0.0050	1,012,984	736,613
	0.0100	864,869	658,543

<sup>a</sup>  $\text{mol L}^{-1}$  (NaOH),  $\text{mmol L}^{-1}$  (luminol and  $\text{KMnO}_4$ ).

<sup>b</sup> Optimum conditions.

Table 2

Effect of flow rates of luminol–NaOH y  $\text{KMnO}_4$  on the CL intensity of benzoylureas

Reactive	Flow rate ( $\text{mL min}^{-1}$ )	Peak area	
		Diflubenzuron	Triflumuron
Luminol/NaOH	0.4	8525	5867
	0.6	12,728	8207
	0.8 <sup>a</sup>	27,739 <sup>a</sup>	19,807 <sup>a</sup>
	1	28,512	21,112
	1.2	30,327	21,751
$\text{KMnO}_4$	0.2	63,467	43,092
	0.4	46,851	42,665
	0.6 <sup>a</sup>	60,019 <sup>a</sup>	50,981 <sup>a</sup>
	0.8	–54,538	–23,567

<sup>a</sup> Optimum conditions.

On the other hand, the flow rates of reagent solutions are crucial for the CL reaction and should be regulated as when too slow or too high flow rates are used, CL may not be emitted in the flow cell and hence, the emitter could not be detected. The effect of flow rate of luminol–NaOH solution on the CL intensities of benzoylureas was studied over the range  $0.2$ – $1.2 \text{ mL min}^{-1}$ . The results obtained showed that the CL intensities increased for both benzoylureas when the flow rates increased up to  $0.8$ – $1.0 \text{ mL min}^{-1}$ , the CL intensity being then constant for triflumuron and subsequent increases, being no significant for diflubenzuron (Table 2). A flow rate of  $0.8 \text{ mL min}^{-1}$  was chosen with the aim of avoiding excessive pressure in the PTFE flow tubing devices.

The effect of flow rate of  $\text{KMnO}_4$  was studied from  $0.2$  to  $0.8 \text{ mL min}^{-1}$ . CL intensities were slightly increased up to  $0.6 \text{ mL min}^{-1}$ , whereas at  $0.8 \text{ mL min}^{-1}$  the signal decreased dramatically and negative peaks were obtained. Therefore, a flow rate of  $0.6 \text{ mL min}^{-1}$  was selected.

After optimization of the HPLC variables and the HPLC–CL conditions, we found that only diflubenzuron and triflumuron could be detected with the adequate sensitivity. This fact would be explained because as the percentage of MeOH in the mobile phase increases with the run time to elute the less polar analytes, the yield of the CL reaction decreases, according to the behaviour observed in the previous studies (Fig. 1B).

### 3.3. Extraction and clean-up

Although the traditional liquid–liquid extraction (LLE) requires handling large volume of solvents, some methods have been proposed to extract these pesticides from vegetables using dichloromethane [13] and ethyl acetate [11], the extracts being cleaned up with aminopropyl [11] or silica [42] cartridges.

In our case, both reported LLE methods were assayed, but the chromatograms obtained showed interferent peaks, as shown in Fig. 6. Therefore, besides these classic extraction methods, the method QuEChERS [55,56] was also utilized. This extraction and clean-up approach was proposed in 2003 for the analysis of pesticide residues in fruits and vegetables and since then it has been used for the determination of pesticides in fruits and vegetables samples [57], honey [58] and oil [59], among other matrices, being favourably compared versus another extraction methods [56]. The QuEChERS method is a promising option which is being increasingly used in multiresidue methods due to its considerable advantages. Thus, this extraction method uses minimal amount of solvents, requires no special equipment and provides high quality results for a wide range of pesticides [55], in addition, avoiding the use of halogenated solvents. Furthermore, the chromatogram obtained with this method shows the baseline free of the interfer-

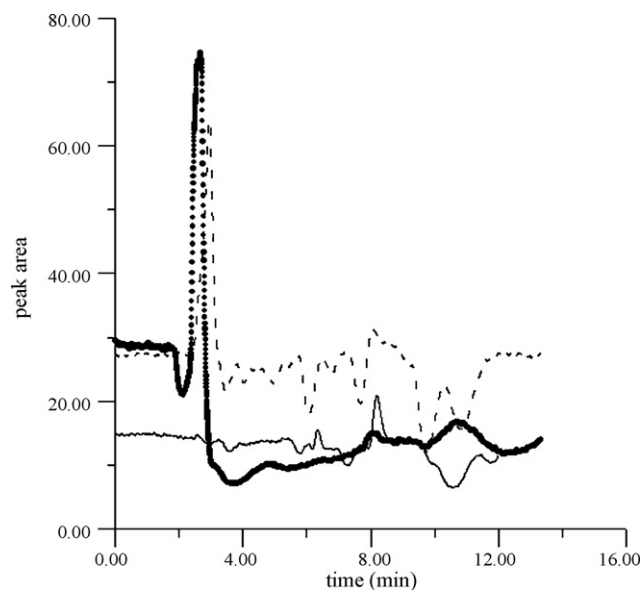


**Fig. 6.** Different extraction methods for diflubenzuron and triflumuron in tomato samples using extraction with  $\text{CH}_2\text{Cl}_2$  and clean up with aminopropyl cartridge (—), extraction with  $\text{CH}_2\text{Cl}_2$  and clean up with silica cartridge (---) and extraction with QuEChERS method (●).

ent peaks which appeared in the extracts obtained by LLE extraction methods (Fig. 6).

### 3.4. Optimization of the HPLC system

Firstly, two different short analytical columns were checked in order to achieve the shorter run time with the lower percentage of MeOH in the mobile phase, thus, optimizing the CL signal according to the behaviour found in the batch experiments. With this purpose, an Aquasil C18 (50 mm  $\times$  4.6 mm, 5  $\mu\text{m}$  particle size) column from Thermo and a Gemini C18 (50 mm  $\times$  4.6 mm, 3  $\mu\text{m}$  particle size) column from Phenomenex were used. As expected, in both cases, peak resolution was achieved with a mobile phase containing a high percentage of water, but peak broadening and asymmetry were also obtained. The best resolution and peaks shape were, finally, obtained with a Gemini C18 (150 mm  $\times$  4.6 mm 5  $\mu\text{m}$  particle size) column from Phenomenex, using MeOH:H<sub>2</sub>O (75:25, v/v), with a run time in the same order than those obtained with the short columns.

The volume of sample analyzed was optimised by injecting 0.5  $\mu\text{g}$  of each pesticide dissolved in different volumes of MeOH:H<sub>2</sub>O (50:50, v/v) in the above-mentioned isocratic conditions. The injection volume tested ranged from 20 to 1000  $\mu\text{L}$ , showing the possibility of performing large volume injection (LVI) with good peak shape (width and symmetry) even for 200  $\mu\text{L}$ . Thus, a sample volume of 200  $\mu\text{L}$  was selected to provide sufficient sensitivity.

**Table 3**  
Analytical figures of merit obtained using solvent-based standards

Compound	Linear range ( $\mu\text{g mL}^{-1}$ )	$R^2$	LOD <sup>a</sup> ( $\mu\text{g mL}^{-1}$ )	LOQ <sup>a</sup> ( $\mu\text{g mL}^{-1}$ )	LOQ <sup>b</sup> ( $\mu\text{g mL}^{-1}$ )	Repeatability R.S.D. (%) <sup>c</sup>	
						0.10 $\mu\text{g mL}^{-1}$	0.25 $\mu\text{g mL}^{-1}$
Diflubenzuron	0.05–0.50	0.996	0.002	0.01	0.05	7.2	1.4
Triflumuron	0.10–1.00	0.992	0.017	0.06	0.10	6.0	4.6

<sup>a</sup> IUPAC criterion.

<sup>b</sup> EURACHEM criterion (R.S.D. 10%).

<sup>c</sup>  $n = 10$ .

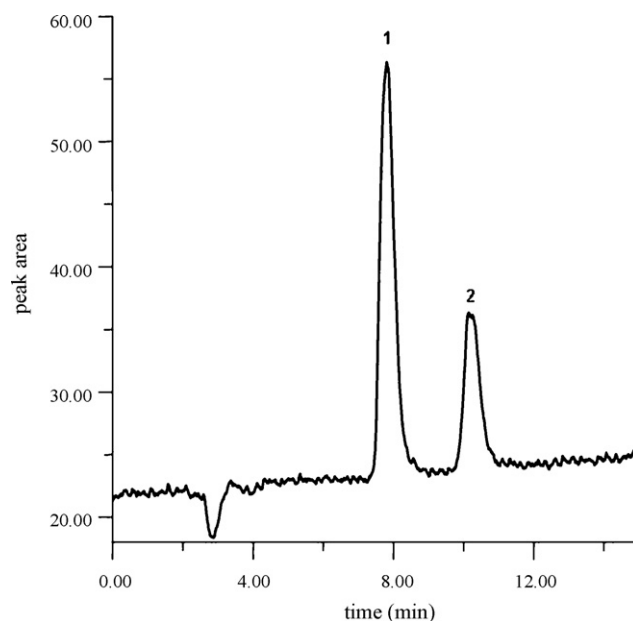


**Fig. 7.** HPLC-CL chromatogram of a standard solution containing 1  $\mu\text{g mL}^{-1}$  of (1) diflubenzuron and (2) triflumuron.

Fig. 7 shows a chromatogram of the two benzoylureas in the optimised conditions. In all cases, the peak area was used as analytical signal for quantification because of its higher repeatability.

### 3.5. Validation in solvent

The analytical figures of merit in pure solvent, obtained under the optimum conditions described above, are summarized in Table 3. LODs and LOQs were calculated statistically [60] as 3.84 and 10 times, respectively, the standard deviation of the signals corresponding to 10 blank solutions divided by the slope of the calibration curve. The LOQs were also calculated, according to the EURACHEM Guidance [61], as the lowest concentration of the analyte for which the relative standard deviation (R.S.D.) of the signal is equal to a fixed percentage (10% in our case).

Linear range was established for each pesticide, the lower limit being the LOQ calculated according to the last criterion and the upper limit being the concentration for which the signal deviates from the linearity by 3–5% [62].

Calibration curves (eight standards covering the whole range) showed linear relationship ( $R^2 > 0.992$ ) between 0.05 and 0.50  $\mu\text{g mL}^{-1}$  for the diflubenzuron and between 0.10 and 1.00  $\mu\text{g mL}^{-1}$  for triflumuron.

The intra-day precision was tested with 10 repeated injections of two sample solutions containing the analytes at two concentration levels (0.10 and 0.25  $\mu\text{g mL}^{-1}$ ) for each pesticide, the R.S.D.s being lower than 7.2% in all cases (Table 3).

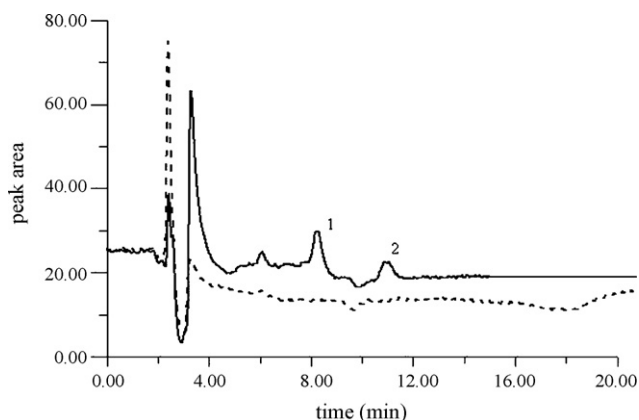


**Fig. 8.** HPLC-CL chromatograms of: a tomato blank extract (.....) and tomato sample extract (—) spiked at LOQs concentration levels: (1) diflubenzuron and (2) triflumuron.

### 3.6. Validation in tomato matrix

With the aim of determining the two benzoylureas in tomato samples, the optimised method was validated in matrix. Fig. 8 shows the HPLC-CL chromatograms of a tomato blank extract and of a tomato blank extract spiked with the two insecticides at concentration levels corresponding to the LOQs. Peaks of benzoylureas were well resolved and showed no interferences with the vegetable matrix. However, when calibration graphs obtained using solvent-based and matrix-matched standards were compared, a decrease effect on the analytical signal, which was due to the matrix, was observed for both compounds in the vegetable matrix. With the aim of confirming the presence of matrix effect, the slopes of calibration graphs obtained in both ways were compared for each pesticide by means of a *t*-test [63]. The results of the *t*-test showed significant differences between the slopes of the two calibration curves for the two pesticides in this matrix. Therefore, analytical figures of merit were calculated using standards prepared spiking blank extracts of tomato.

Method detection limits (MDLs) were calculated according to the procedure proposed by de U.S. EPA [64]. The MDL is defined by this organism as “the minimum concentration of a substance that can be measured and reported with 99% confidence that the analyte concentration is greater than zero and it is determined from analysis of a sample in a given matrix containing the analyte. It is essential that all sample processing steps of the analytical method be included in the determination of method detection limit”. In this way, the MDL takes into account, not only matrix effect, but also the variability introduced by all the sample processing steps.

With this aim, seven aliquots of tomato samples were spiked at 0.016 and 0.040 mg kg<sup>-1</sup> (equivalent to 0.08 and 0.20 μg mL<sup>-1</sup> in the final extract) of diflubenzuron and triflumuron, respectively and the procedure described by the U.S. EPA was carried out. Each replicate was processed through the entire analytical method and an initial estimate of the MDL was then calculated by multiplying

the standard deviation of the results by the appropriate *t*-statistic.

$$MDL = t_{(n-1, \alpha=0.01)} S_A$$

where *n* is the number of replicate analyses, *S<sub>A</sub>* is the standard deviation of the replicate analyses, and *t* is the Student's *t*-value for *n* – 1 degrees of freedom at 99% confidence level.

Thus, the estimated MDLs were 0.00166 and 0.000798 mg kg<sup>-1</sup> (equivalent to 0.0083 and 0.00399 μg mL<sup>-1</sup> in the final extract) for diflubenzuron and triflumuron, respectively.

Next, seven aliquots of tomato samples, spiked at 0.01 and 0.02 mg kg<sup>-1</sup> (corresponding to 0.05 and 0.1 μg mL<sup>-1</sup>) were analyzed through the entire method and *S<sub>B</sub>* was also calculated for each pesticide. After to verify that *S<sub>A</sub>* and *S<sub>B</sub>* were not statistically significant (based on the *F*-statistic of their ratio), these two variances were pooled to obtain a single estimated *S<sup>2</sup>* as follows:

$$S_{\text{pooled}}^2 = \frac{(n_A - 1)s_A^2 + (n_B - 1)s_B^2}{n_A + n_B - 2}$$

where *n<sub>A</sub>* and *n<sub>B</sub>* are the number of samples analyzed in each set.

The MDLs were then calculated using the pooled standard deviation as:

$$MDL = t_{(n_A+n_B-2, \alpha=0.01)} \times S_{\text{pooled}}$$

The values of MDL obtained in this way for diflubenzuron and triflumuron were 0.0005 and 0.0026 mg kg<sup>-1</sup>, respectively (equivalent to 0.0025 and 0.0131 μg mL<sup>-1</sup> in the final extract), being in the same order than the LODs obtained in pure solvent.

The LOQs were also calculated, according to the EURACHEM Guidance [61], as described above. Each replicate was processed through the entire analytical method and the results obtained are summarized in Table 4.

The proposed method provided LOQs which are 8–16 times the values obtained by another previously developed CL method using photochemical derivatization and K<sub>3</sub>Fe(CN)<sub>6</sub> in basic medium [30] and they are comparable with those obtained by a PIF-based method [11]. Anyway, they are lower than the MRLs established by the Spanish and European legislation [2,65].

The intra-day precision was calculated using standards prepared in blank tomato extract as described above (0.02 and 0.05 mg kg<sup>-1</sup>, equivalent to 0.10 and 0.25 μg mL<sup>-1</sup> in the final extract), the R.S.D.s values being lower than 10.0% for all pesticides (Table 4). These values were similar to the ones obtained by CL with K<sub>3</sub>Fe(CN)<sub>6</sub> in basic medium [30].

### 3.7. Recovery studies

In order to establish the accuracy and precision of the total method, six replicates of vegetable samples were spiked at two concentration levels of each benzoylurea: corresponding to the LOQs in blank matrix extract (0.01 and 0.02 mg kg<sup>-1</sup> for diflubenzuron and triflumuron, respectively) and two times the LOQs (0.02 mg kg<sup>-1</sup> for diflubenzuron and 0.04 mg kg<sup>-1</sup> for triflumuron), extracted and analyzed by using the described method. The mean recovery per-

**Table 4**  
Analytical figures of merit obtained using matrix-matched standards

Compound	Linear range (μg mL <sup>-1</sup> )	<i>R</i> <sup>2</sup>	LOD <sup>a</sup> (μg mL <sup>-1</sup> )	LOQ <sup>b</sup> (μg mL <sup>-1</sup> )	Repeatability R.S.D. (%) <sup>c</sup>	
					0.10 μg mL <sup>-1</sup>	0.25 μg mL <sup>-1</sup>
Diflubenzuron	0.05–0.50	0.995	0.0025	0.05	5.2	9.5
Triflumuron	0.10–1.00	0.997	0.0131	0.10	6.6	7.6

<sup>a</sup> Method detection limit.

<sup>b</sup> EURACHEM criterion (R.S.D. 10%).

<sup>c</sup> *n* = 10.

**Table 5**  
Recovery percentages and R.S.D. (%) for the determination of diflufenuron and triflumuron in tomato spiked at two concentration levels, using calibration graphs built with matrix-based standards for quantification

Compound	LOQ (mg kg <sup>-1</sup> )		2 × LOQ (mg kg <sup>-1</sup> )	
	Mean recovery (%) <sup>a</sup>	R.S.D. (%) <sup>a</sup>	Mean recovery (%) <sup>a</sup>	R.S.D. (%) <sup>a</sup>
Diflufenuron	85.5	7.8	94.2	2.6
Triflumuron	86.5	6.5	79.7	3.4

<sup>a</sup> n = 6.

centages and the R.S.D.s of the six replicate samples are shown in Table 5.

In general, it can be observed that recoveries were satisfactory for both insecticides (between 94.2% and 79.7%), being in the range expected for residue analysis [66].

#### 4. Conclusions

HPLC combining CL detection represents an interface between the selectivity of an elegant separation method and the sensitivity of an ultrasensitive detection method. However, although numerous compounds are detectable by some CL reactions in flow injection systems, the mobile phases of HPLC are sometimes incompatible with the CL reactions, leading to that some compounds are undetectable in HPLC-CL detection.

An efficient and sensitive HPLC-CL method has been developed in order to determine diflufenuron and triflumuron in vegetable samples. It is based on the CL which appears when the target analytes react with luminol–NaOH in presence of KMnO<sub>4</sub>, previous post-column photolysis. The proposed method is simple, rapid, fairly sensitive, selective and sufficiently accurate and precise. In addition, it requires no sophisticated instruments.

The tandem photodegradation-CL detection offers an interesting strategy for improving sensitivity and permits to increase the number of compounds to be determined by direct CL (compounds even without or with very weak CL behaviour).

#### Acknowledgement

The authors are grateful to INIA (Project CAL-03-099) for financial support.

#### References

- [1] British Crop Protection Council and the Royal Society of Chemistry, The Pesticide Manual, 10th ed., British Crop Protection Council and the Royal Society of Chemistry, London, UK, 1997.
- [2] European Council Directives 76/895/EEC, 83/362/ECC, 86/363/EEC and 90/642/EEC, updated on 04/11/2004, European Union: Brussels, Available: [http://ec.europa.eu/comm/food/plant/protection/pesticides/index\\_en.htm](http://ec.europa.eu/comm/food/plant/protection/pesticides/index_en.htm).
- [3] S. Koning, G. Lach, M. Linkerhägner, R. Löscher, P.H. Tablack, U. Brinkman, J. Chromatogr. A 1008 (2003) 247.
- [4] J.K. Mensah, E. Lundanes, T. Greibrokk, B. Holen, J. Chromatogr. A 765 (1997) 85.
- [5] N.M. Brito, S. Navickiene, L. Polese, E.F.G. Jardim, R.B. Abakerli, M.L. Ribeiro, J. Chromatogr. A 957 (2002) 201.
- [6] G. Huang, J. Ouyang, W.R.G. Baeyens, Y. Yang, Ch. Tau, Anal. Chim. Acta 474 (2002) 21.
- [7] M. Gamón, R. Pelegrí, I. Peris, J.G. de la Cuadra, R. Coscolla, J. AOAC Int. 81 (1998) 1037.
- [8] A. Balinova, J. Chromatogr. A 823 (1998) 11.
- [9] C. Bicchi, C. Balbo, A. D'Amato, O. Panero, Chromatographia 43 (1996) 439.
- [10] C. Bicchi, C. Balbo, A. Binello, A. D'Amato, J. High Resolut. Chromatogr. 19 (1996) 105.
- [11] M. Martínez-Galera, T. López-López, M.D. Gil-García, J.L. Martínez-Vidal, P. Parrilla-Vázquez, J. Chromatogr. A 918 (2001) 79.
- [12] M.D. Gil García, M. Martínez Galera, D. Barranco Martínez, J. Gisbert Gallego, J. Chromatogr. A 1103 (2006) 271.
- [13] M.D. Gil García, D. Barranco Martínez, M. Martínez Galera, P. Parrilla Vázquez, J. Sep. Sci. 27 14 (2004) 1173.
- [14] K.A. Barnes, R.J. Fussell, J.R. Startin, S.A. Thorpe, S.L. Reynold, Rapid Commun. Mass Spectrom. 9 (1995) 1441.
- [15] K.A. Barnes, R.J. Fussell, J.R. Startin, M.K. Pegg, S.A. Thorpe, S.L. Reynolds, Rapid Commun. Mass Spectrom. 11 (1997) 117.
- [16] A. Garrido-Frenich, M.D. Gil-García, F.J. Arrebola, J.L. Martínez-Vidal, M. Martínez-Galera, T. López-López, Chromatographia 52 (2000) 569–574.
- [17] X. Yang, Y. Xia, X. Liao, Y. Zuo, Y. Liao, H. Liu, Talanta 60 (2006) 75.
- [18] H.J. Stan, P. Klaffenbach, Fresen. J. Anal. Chem. 339 (1991) 40.
- [19] A.I. Valenzuela, Y. Picó, G. Font, Rapid Commun. Mass Spectrom. 14 (2000) 572.
- [20] G.E. Miliadis, G. Nicholas, Tsiropoulos, G. Pipina, Aplada-Sarlis, J. Chromatogr. A 835 (1999) 113.
- [21] A.I. Valenzuela, R. Lorenzini, M.J. Redondo, G. Font, J. Chromatogr. A 839 (1999) 101.
- [22] J. Zrostlíková, J. Hajslová, T. Kovalczuk, R. Stépán, J. Poustka, J. AOAC Int. 86 (2003) 612.
- [23] J.L. Martínez Vidal, A. Garrido Frenich, T. López López, I. Martínez Salvador, L.H. Asan, M.H. Benajiba, Chromatographia 61 (2005) 127.
- [24] A. Sannino, M. Bandini, Rapid Commun. Mass Spectrom. 19 (2005) 2729.
- [25] A.C. Hogenboom, W.M.A. Niessen, U.A.Th. Brinkman, J. Sep. Sci. 24 (2001) 331.
- [26] E. Orejuela, M. Silva, J. Chromatogr. A 1007 (2003) 197.
- [27] L. Gámiz-Gracia, A.M. García-Campaña, J.J. Soto-Chinchilla, J.F. Huertas-Pérez, A. González-Casado, Trends Anal. Chem. 24 (2005) 927.
- [28] M. Palomeque, J.A. Garía Bautista, M. Catalá Icardo, J.V. García Mateo, J. Martínez Calatayud, Anal. Chim. Acta 512 (2004) 149.
- [29] M. Martínez Galera, M.D. Gil García, R. Santiago Valverde, J. Chromatogr. A 1113 (2006) 191.
- [30] M.D. Gil García, M. Martínez Galera, R. Santiago Valverde, Anal. Bioanal. Chem. 387 (2007) 1973.
- [31] M.D. Green, D.L. Mount, G.D. Todd, A.C. Capomacchia, J. Chromatogr. A 695 (1995) 237.
- [32] C. Molins-Legua, P. Campís-Falcó, A. Sevillano Cabeza, Anal. Chim. Acta 378 (1999) 83.
- [33] J.M. Ramos Fernández, J.M. Bosque-Sendra, A.M. García-Campaña, F. Alés Barro, J. Pharm. Biomed. Anal. 36 (2005) 969.
- [34] H. Ciu, C. He, G. Zhao, J. Chromatogr. A 855 (1999) 171.
- [35] T. Toyooka, T. Kashiwazaki, M. Kato, Talanta 60 (2003) 467.
- [36] M. Cobo, M. Silva, J. Chromatogr. A 848 (1999) 105.
- [37] S. Meseguer Lloret, C. Molins-Legua, J. Verdú Andrés, P. Campís-Falcó, J. Chromatogr. A 1035 (2004) 75.
- [38] T. Pérez Ruiz, C. Martínez-Lozano, V. Tomás, J. Martín, J. Chromatogr. A 1077 (2005) 49.
- [39] L. García-Gámiz, L. Cuadros-Rodríguez, J.J. Soto-Chinchilla, J.F. Huertas Perez, A. Gonzalez-Casado, A.M. García Campaña, Anal. Bional. Chem. 384 (2006) 295.
- [40] J.F. Huertas Pérez, L. Gámiz-García, A.M. García Campaña, A. Gonzalez Casado, J.L. Martínez Vidal, Talanta 65 (2005) 980.
- [41] I. Sahuquillo Ricart, G.M. Antón-Fos, M.J. Duart, J.V. García Mateo, L. Lahuerta Zamora, J. Martínez Calatayud, Talanta 72 (2007) 378.
- [42] A. Chivulescu, M. Catalá Icardo, J.V. García Mateo, J. Martínez Calatayud, Anal. Chim. Acta 519 (2004) 113.
- [43] T. Pérez Ruiz, C.M. Lozano, V. Tomás, J. Martín, Anal. Chim. Acta 476 (2003) 141.
- [44] T. Pérez Ruiz, C.M. Lozano, V. Tomás, J. Martín, Analyst 111 (2002) 1526.
- [45] B.M. Patel, H.A. Moye, R. Weinberg, Talanta 38 (1991) 913.
- [46] I.S. Lurie, D.A. Cooper, I.S. Krull, J. Chromatogr. A 629 (1993) 143.
- [47] K.M.S. Sundaram, J. Curry, J. Chromatogr. A 672 (1994) 117.
- [48] H. Liu, Ch.T. Duda, T.H. Huang, W.O. Aruda, P.T. Kissinger, J. Chromatogr. A 818 (1998) 69.
- [49] T. López López, M.D. Gil García, J.L. Martínez Vidal, M. Martínez Galera, Anal. Chim. Acta 447 (2001) 101.
- [50] A. Muñoz de la Peña, M.C. Mahedero, A. Bautista Sánchez, J. Chromatogr. A 950 (2002) 287.
- [51] T. Pérez-Ruiz, C. Martínez-Lozano, V. Tomás, J. Martín, J. Chromatogr. A 1026 (2004) 57.
- [52] M. Catalá Icardo, J.V. García Mateo, M. Fernández Lozano, J. Martínez Calatayud, Anal. Chim. Acta 499 (2003) 57.
- [53] V. David, J.V. García Mateo, J. Martínez Calatayud, Analyst 125 (2000) 1313.
- [54] M.D. Gil García, M. Martínez Galera, T. López López, J.L. Martínez Vidal, M.C. Mahedero, F. Salinas, Talanta 53 (2001) 915.
- [55] M. Anastasiades, S.J. Lehotay, J. AOAC Int. 86 (2003) 412.
- [56] C. Díez, W.A. Traag, P. Zommer, P. Mariner, J. Aienza, J. Chromatogr. A 1131 (2006) 11.



- [57] S.J. Lehotay, A. De Kok, M. Hiemstra, P. Van Bodegraven, J. AOAC Int. 88 (2005) 595.
- [58] C. Pan, H. Zhang, S. Chen, Y. Xu, S. Jiang, Acta Chromatogr. 17 (2006) 320.
- [59] J.F. García-Reyes, C. Ferrer, M.J. Gómez-Ramos, A.R. Fernández-Alba, J.F. García-Reyes, A. Molina-Díaz, TrAC Trends Anal. Chem. 26 (2007) 239.
- [60] L.A. Currie, Anal. Chim. Acta 391 (1999) 105.
- [61] EURACHEM Guidance Document No. 1/WELAC Guidance Document No. WGD 2, Accreditation for Chemical Laboratories, Guidance on the interpretation of the EN 45000 series of Standard and ISO/IEC Guide 25, 1993, Available from the EURACHEM Secretariat, P.O. Box 46, Teddington, Middlesex TW11 0NH, UK.
- [62] D.L. Massart, B.G.M. Vandeginste, S.N. Deming, Y. Michotte, L. Kaufman, Chemometrics: A Textbook, Part 2, Elsevier, Amsterdam, 1988.
- [63] D.L. Massart, B.G.M. Vandeginste, L.M.C. Buydens, S. De Jong, P.J. Lewi, J. Smeyers-Verbeke, Handbook of Chemometrics and Qualimetrics Part A, Elsevier, Amsterdam, 1997, pp. 190, 209, 436.
- [64] Definition and Procedure for the Determination of the Method Detection Limit, Appendix B to Part 136, Title 40, Revision 1.11, Statistics for Environmental Engineers, Paul Mac Berthovex, Linfield C. Brown, Lewis Publishers, United States of America 1994.
- [65] Legislación Internacional de Residuos de Plaguicidas en Productos Vegetales, Secretaria General de Comercio Exterior de España, <http://www.mapa.es/es/agricultura/pags/fitos/registro/menu.asp>.
- [66] Guidance document on Residue Analytical Methods SANCO/825/00 Rev. 6, European Union, Brussels, 2000.



# Anion recognition using newly synthesized hydrogen bonding disubstituted phenylhydrazone-based receptors: Poly(vinyl chloride)-based sensor for acetate

Vinod K. Gupta\*, Rajendra N. Goyal, Ram A. Sharma

Department of Chemistry, Indian Institute of Technology Roorkee, Roorkee 247 667, India

## ARTICLE INFO

### Article history:

Received 4 March 2008

Received in revised form 15 April 2008

Accepted 16 April 2008

Available online 30 April 2008

### Keywords:

Ion-selective electrode

Acetate ion

butane-2,3-dione,bis[(2,4-

dinitrophenyl)hydrazone]

Poly(vinyl chloride)

## ABSTRACT

A potentiometric acetate-selective sensor, based on the use of butane-2,3-dione,bis[(2,4-dinitrophenyl)hydrazone] (BDH) as a neutral carrier in poly(vinyl chloride) (PVC) matrix, is reported. Effect of various plasticizers and cation excluder, cetyltrimethylammonium bromide (CTAB) was studied. The best performance was obtained with a membrane composition of PVC:BDH:CTAB ratio (w/w; mg) of 160:8:8. The sensor exhibits significantly enhanced selectivity toward acetate ions over a wide concentration range  $5.0 \times 10^{-6}$  to  $1.0 \times 10^{-1}$  M with a lower detection limit of  $1.2 \times 10^{-6}$  M within pH range 6.5–7.5 with a response time of <15 s and a Nernstian slope of  $60.3 \pm 0.3$  mV decade<sup>-1</sup> of activity. Influences of the membrane composition, and possible interfering anions were investigated on the response properties of the electrode. Fast and stable response, good reproducibility and long-term stability are demonstrated. The sensor has a response time of 15 s and can be used for at least 65 days without any considerable divergence in their potential response. Selectivity coefficients determined with the separate solution method (SSM) and fixed interference method (FIM) indicate that high selectivity for acetate ion. The proposed electrode shows fairly good discrimination of acetate from several inorganic and organic anions. It was successfully applied to direct determination of acetate within food preservatives. Total concentration of acetic acid in vinegar samples were determined by direct potentiometry and the values agreed with those mentioned by the manufacturers.

© 2008 Elsevier B.V. All rights reserved.

## 1. Introduction

Ion-selective sensors have been used for analytical determination of a wide variety of ions since the 1970s. Ion-selective sensor's utility and simplicity have replaced other wet analytical methods that were often far slower and more cumbersome to perform. Ionophore plays a key role in the sensitivity of an ion-selective electrode (ISE). The creation of cavities and cleft in the ionophore that are complementary to the size and charge of a particular ion can lead to very selective interactions. One of the most important figures of merit for ISEs is the selectivity towards a specific analyte, which is generally limited by the interaction of ionophore within the membrane with other ions in solution. Recently, there has been much focus on the construction of anion-selective electrodes that function on the basis of chemical recognition principle [1]. The demand for ionophores with either new or improved selectivities in the field of ion-selective electrodes (ISEs) is high particularly in the area of anion-selective electrodes. For a truly anion-selective electrode, a

strong interaction between the ionophore and the anion is required in order to complex anion in a selective fashion. Potentiometric response of the membranes doped with these complexes believed to be based on the coordination of analyte anion with carrier molecule.

The Acetate ion has significant role in biological, medical and environmental fields. Acetate ion can be determined in aqueous, environmental, biological and food samples by different methods like colorimetric [2], liquid membrane sensor [3], flow injection analysis systems [4,5]. These methods are time consuming, involve multiple sample manipulations, require large infrastructure backup, expertise and not very appropriate for analysis of large number of samples. Ion-sensors provide analytical procedures that overcome the above drawbacks since they are fast convenient and require no sample pretreatment and are also suitable for online analysis.

Few sensors have been reported for acetate based on porphyrin [6] and trimethylcetyl ammonium acetate [3]. The electrode sensors reported for acetate exhibit narrow working concentration ranges and show interferences to various anions such as  $\text{Cl}^-$ ,  $\text{HSO}_3^-$ ,  $\text{HCO}_3^-$ ,  $\text{NO}_3^-$ ,  $\text{SCN}^-$ ,  $\text{I}^-$  and  $\text{Br}^-$ . Thus there is still a need for having a good sensor for acetate and further efforts are required to develop it.

\* Corresponding author. Fax: +91 1332273560.

E-mail address: [vinodfcy@iitr.ernet.in](mailto:vinodfcy@iitr.ernet.in) (V.K. Gupta).

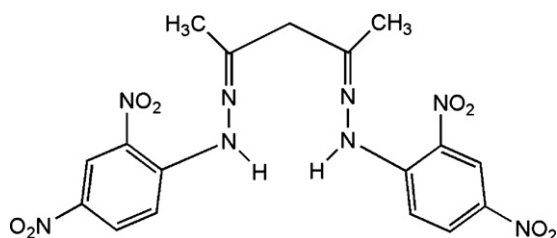


Fig. 1. Structural formulae of butane 2,3-dione, bis[(2,4-dinitrophenyl)hydrazone] ionophore.

In recent times intensive research has been directed towards the preparation of a variety of selective receptors for anions [7–10]. These have included Lewis acids, guanidium and amidinium, pyrroles, metallo receptors and amides. Such receptors are now used for anion binding due to their flexibility, which allows for adjustment in the size of the cavity as well as the formation of strong hydrogen bonds [11–13]. Keeping this in mind, we synthesized a new disubstituted phenylhydrazone (BDH)-based derivative (Fig. 1). From spectroscopic studies it was found that it showed receptivity for the anion in general and for acetate ion in particular, to which the affinity is maximum. Thus newly synthesized receptors are likely to act as potential material for preparing membranes, which may show selective potential response to acetate ion. Therefore their PVC-based membranes have been prepared and investigated as acetate selective sensor.

## 2. Experimental

### 2.1. Reagents

All reagents were of analytical grade and used without further purification. Acetylacetone from CDH (Mumbai, MH, India). High molecular weight poly(vinylchloride) (PVC), Aldrich, (St. Louis, USA). Di-*n*-butyl phthalate (DBP), dioctylphthalate (DOP) from SD Fine-Chem Limited (Mumbai, MH, India). Analytical reagent grade tetrahydrofuran (THF), acetonitrile (MECN) were obtained from Ranbaxy (Okhla, New Delhi, India). 2,4-Diaminophenylhydrazine, sodium acetate, sodium sulphate, sodium chloride and sodium dihydrogen phosphate were obtained from Merck (Darmstadt, Germany). 2-[4-(2-Hydroxyethyl)-piperazinyl]ethanesulfonic acid (HEPES) was obtained from Dojindo Laboratories (Kumamoto, Japan). *N,N,N,N*-Cetyl trimethyl ammonium bromide (CTAB), chloronaphthalene (CN) and tri-*n*-butyl phosphate were obtained from Highmedia laboratories (Mumbai, MH, India).

### 2.2. Synthesis of butane-2,3-dione, bis[(2,4-dinitrophenyl)hydrazone]

The ionophore BDH (Fig. 1) was synthesized as previously described method [14]. 2,4-Dinitrophenyl hydrazine was dissolved in methanol (600 ml) and acetylacetone was added drop wise to a solution of 2,4-dinitrophenylhydrazine was added dropwise with stirring. A catalytic amount of acetic acid was added in the solution. This mixture was refluxed for 1 h and yellow precipitates were formed. The precipitate was filtered off, washed with cold diethyl ether/water and dried in vacuo. The residue was purified by recrystallization from ethanol/acetonitrile (1:1). It had an mp-179 °C, Anal. Calc. for [C<sub>17</sub>H<sub>16</sub>N<sub>8</sub>O<sub>8</sub>]: C, 44.35, H, 3.50, N, 24.34%. Found: C, 44.28, H, 3.65, N, 23.97. The <sup>1</sup>H NMR (CDCl<sub>3</sub>) exhibited signals at: δ<sub>H</sub> 2.17 (s, 6H, CH<sub>3</sub>), 3.57 (s, 2H, CH<sub>2</sub>), 7.93 (d, J=9.5 Hz, 2H, Ar), 8.34 (dd, J=9.5, 2.0 Hz, 2H, Ar), 11.14 (s, 2H, NH). The <sup>13</sup>C NMR (CDCl<sub>3</sub>) showed signals at δ 16.27, 48.54, 116.58, 123.71, 129.86, 130.44, 138.25, 145.22, 153.07. The IR (KBr) spectrum showed bands

at  $\nu(\text{cm}^{-1})$  3313s (–N–H), 3102m (–C–H, Ar), 2985m (–C–H, CH<sub>3</sub>), 1615vs. (>C=N–).

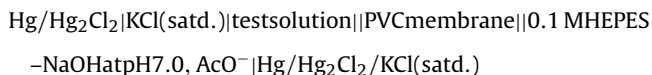
### 2.3. Preparation of normal PVC-membrane and sandwich PVC membranes

The PVC-based membranes were prepared by dissolving appropriate amounts of ionophore, cation excluder (CTAB), solvent mediators (DOP, TBP, CN and DBP) and PVC in THF (10 ml). After complete dissolution of all the components, the homogeneous mixture was concentrated by evaporating THF and it was then poured into polyacrylate rings placed on a smooth glass plate. After 24 h of evaporation, transparent membranes of 0.4 mm thickness were removed carefully from the glass plate. A 5-mm diameter piece was cut out and glued to one end of a “Pyrex” glass tube. A 0.1 M HEPES–NaOH buffer solution of pH 7.0 containing 10 mM sodium acetate and 1 mM NaCl was used as the internal filling solution. The membranes were equilibrated for 2 days in 0.1 M solution of anions in the same buffer solution and were further used for potential measurement studies. Sample solutions were buffered to pH 7.0 with 0.1 M HEPES–NaOH because no emf response to HEPES buffer in a concentration range of 0.001–0.1 M was observed.

The sandwich membrane was made by pressing two individual membranes (ordinarily one without ionophore and one with the same components and an additional ionophore) together immediately after blotting them individually dry with tissue paper. The obtained sandwich membrane was visibly checked for air bubbles before mounting on electrode body with the ionophore-containing segment facing the sample solution. The combined segmented membrane was then rapidly mounted on to the electrode body and potentials were measured.

### 2.4. Apparatus and potential measurements

IR spectra were recorded with a PerkinElmer FT-IR 1000 spectrometer using KBr pellets. <sup>1</sup>H NMR spectra were recorded on a Bruker AC 500 MHz spectrophotometer. The melting point was determined on JSGW apparatus. Elemental analysis was performed with Vario ELIII instrument. The potential measurements were carried out at 25 ± 0.1 °C with a digital potentiometer (modal 5652 A, ECIL, India) by setting the following cell assembly, employing saturated calomel electrodes (SCE) as a reference electrode.



## 3. Result and discussion

### 3.1. Anion-binding studies

The affinity of ionophore for various anions was determined by UV–vis spectroscopic method [15,16]. Fig. 2 shows the changes in absorption spectrum of ionophore ( $5.0 \times 10^{-5}$  M) in acetonitrile upon addition of equal volume of anions ( $2.0 \times 10^{-5}$  M). It is seen from Fig. 2 that among all anions, acetate showed highest interaction with ligands and the affinity and sensing capability of ligands for anions in aqueous solution is in the order of  $\text{CH}_3\text{COO}^- \gg \text{H}_2\text{PO}_4^{2-} > \text{SO}_4^{2-} > \text{Cl}^-$  ions.

### 3.2. Potential responses of the sensor

In order to know the ion to which membrane of BDH respond ideally, preliminary experiments involving measurement of potential as a function of concentration of different anions (taken as test

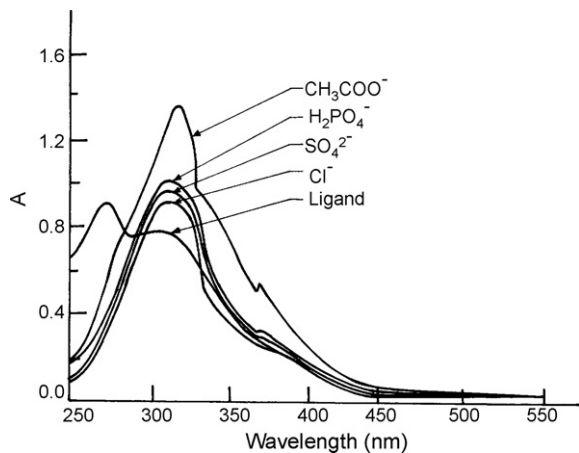


Fig. 2. Observed changes in UV-vis spectrum of ligand ( $5.0 \times 10^{-5}$  M) in acetonitrile after the addition of aqueous anions ( $2.0 \times 10^{-5}$  M).

solution) were determined. The potential responses of these electrodes are shown in Fig. 3. It is seen that except for acetate ion, the slope of corresponding potential vs. pM plots are not Nernstian and concentration ranges are also narrow. This indicates that the membrane is not responding to these anions probably due to low affinity for them and slow exchange kinetics of the anion with ionophore complex in the membrane phase. However, membranes of both the BDH respond to acetate over a wide concentration range with a near Nernstian slope. Thus, they can be used as acetate sensors. Following these experiments, membranes were further studied as acetate sensor only.

### 3.3. The effect of membrane composition on potential response of the acetate sensor

The above studies have shown that phenylhydrazone-based receptor exhibit high affinity for acetate ion as compared to other ions and therefore, can act as a selective ionophore for its potentiometric determination. The sensitivity and performance of an ionophore (BDH) significantly depends on the membrane composition and the nature of solvent mediator and additive used. Thus to optimize potentiometric performance of acetate-selective electrode various PVC membrane based on BDH were prepared and investigated. The influence of plasticizer type and concentration on the characteristics of acetate ion-selective electrode was investigated.

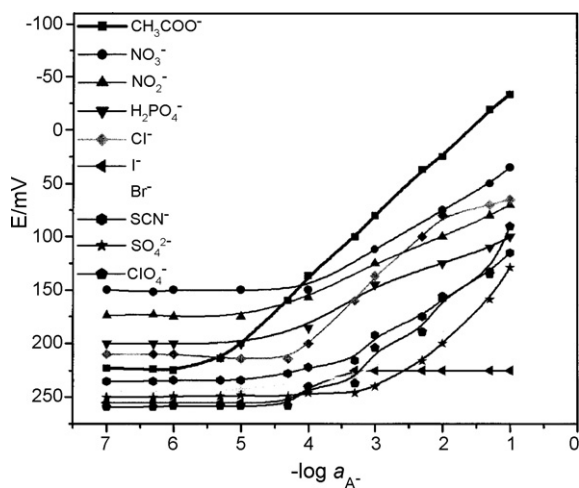


Fig. 3. Potential responses of ion-selective membrane sensor for various anions.

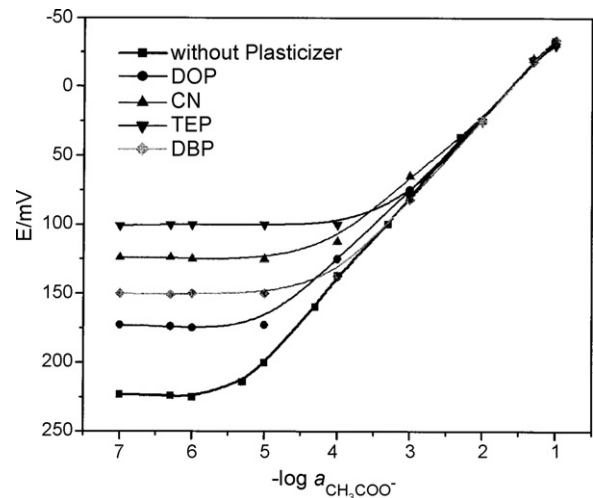


Fig. 4. Variation of membrane potential with activity of acetate ions of PVC-based membranes of without plasticizers (1); with plasticizers, DOP (2); CN (3); TEP (4) and DBP (5).

igated by using four plasticizers with different polarities including DBP, CN, DOP, TBP (Fig. 4; Table 1). It seems that without plasticizer membrane produced maximum sensitivity.

It has also been demonstrated that the presence of ionic additives improves potentiometric behavior by reducing the ohmic resistance [17] and catalyzing exchange kinetics at the sample-membrane interface [18]. Better response characteristics, *i.e.* Nernstian response and improved selectivity were observed with an optimum CTAB amount of 8 mg in membrane. Several membrane were prepared and tested with different compositions, and best results obtained on the optimization of the membrane composition, are reported in Table 1.

### 3.4. Potentiometric calibration characteristics of the proposed sensor

It was found that for selected membrane with composition PVC:BDH:CTAB as (w/w; mg) of 160:8:8, potential response was linear for acetate ions (Fig. 5). The emf response of the membrane sensor of varying  $\text{Ac}^-$  concentration depicts a rectilinear range from  $5.0 \times 10^{-6}$  to  $1.0 \times 10^{-1}$  M with a slope of  $60.3 \pm 0.3$  mV decade $^{-1}$  of

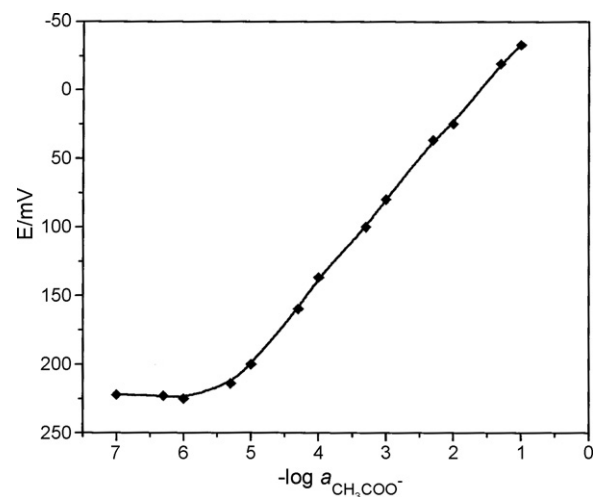


Fig. 5. Calibration plot of acetate-selective sensors based on butane 2,3-dione, bis[(2,4-dinitrophenyl)hydrazone] ionophore.

**Table 1**  
Composition of PVC membranes of ligands and performance characteristics of  $\text{CH}_3\text{COO}^-$  selective sensors

Sensor no.	Composition (w/w; mg)				Slope $\pm 0.3$ (mV decade <sup>-1</sup> of activity)	Linear range (M)	Detection limit (M)
	Ionophore (BDH)	CTAB	Plasticizer	PVC			
1	8	8	DBP, 153.6	77	32.1	$1.0 \times 10^{-4}$ to $1.0 \times 10^{-2}$	$3.1 \times 10^{-4}$
2	8	8	CN, 142	71	55.2	$1.0 \times 10^{-4}$ to $1.0 \times 10^{-2}$	$1.0 \times 10^{-4}$
3	8	8	TBP, 150	75	40.1	$1.0 \times 10^{-4}$ to $1.0 \times 10^{-2}$	$3.9 \times 10^{-5}$
4	8	8	DOP, 150	75	50.3	$5.0 \times 10^{-4}$ to $1.0 \times 10^{-2}$	$1.5 \times 10^{-5}$
5	8	8	0.00	160	60.0	$5.0 \times 10^{-6}$ to $1.0 \times 10^{-1}$	$1.2 \times 10^{-6}$

$\text{Ac}^-$  activity for sensor no. 5. The limit of detection defines as the concentration of acetate obtained when extrapolating the linear range of calibration curve to the base line potential is  $1.2 \times 10^{-6}$  M. Repeated monitoring of potentials and calibration, using the same electrode, over several days gave good slope reproducibility, as given in Table 1.

### 3.5. Response and life time

Response time of the sensors has been determined by measuring the time required to achieve a stable potential for  $1.0 \times 10^{-4}$  M solution, when acetate ion concentration was increased 10-fold from  $1.0 \times 10^{-5}$  to  $1.0 \times 10^{-4}$  M. Sensor having membrane without plasticizer gave a stable response in 15–25 s were smaller than 3 min. The addition of plasticizer to membrane did not increase the response time. The sensing behavior of the membrane electrode remains unchanged when the potential was recorded either from low to high concentration or vice versa. It is seen from Table 2 that the sensor continued to generate reproducible potential for the period of 65 days and standard deviation of 20 measurement made on a solution ( $1.0 \times 10^{-4}$  M) was found to be  $\pm 0.1$  mV.

The ionophore (BDH) is insoluble in aqueous solution; hence, it is difficult to measure the concentration of ionophore in water. To determine the partition coefficient water–octanol mixture was used. It was found that the initial amount of ionophore dissolved in octanol quickly and thus the value partition coefficient is almost 0.1–99.9 in water–octanol. This indicates that the ionophore (BDH) is highly lipophilic in nature. After life time period membrane became mechanically weak. Therefore, deviation in potential occurs and slight gradual decrease in slope is observed.

### 3.6. Potentiometric selectivity

Selectivity is an important characteristic of a sensor that delineates the extent to which the device may be used in the estimation of analyte ion in the presence of other ions and extent of utility of any sensor in real sample measurement. In this work, the selectivity coefficients of the sensors toward different cationic species ( $\text{A}^{n+}$ ) were evaluated by using both the matched potential method (MPM) [19] and the fixed interference method (FIM) [20].

**Table 2**  
Conditioning time of optimized  $\text{CH}_3\text{COO}^-$  ion-selective sensor

Time (days)	Slope $\pm 1.0$ (mV decade <sup>-1</sup> of activity)	Linear range (M)
1	60.0	$5.0 \times 10^{-6}$ to $1.0 \times 10^{-1}$
5	60.0	$5.0 \times 10^{-6}$ to $1.0 \times 10^{-1}$
11	60.0	$5.0 \times 10^{-6}$ to $1.0 \times 10^{-1}$
17	60.0	$5.0 \times 10^{-6}$ to $1.0 \times 10^{-1}$
25	60.0	$5.0 \times 10^{-6}$ to $1.0 \times 10^{-1}$
36	60.0	$5.0 \times 10^{-6}$ to $1.0 \times 10^{-1}$
49	59.9	$5.0 \times 10^{-6}$ to $1.0 \times 10^{-1}$
65	59.9	$5.0 \times 10^{-6}$ to $1.0 \times 10^{-1}$
75	59.9	$1.0 \times 10^{-5}$ to $1.0 \times 10^{-1}$

In the MPM, the selectivity coefficient ( $K_{\text{Ac,B}}^{\text{pot}}$ ) was determined by measuring the change in potential upon increasing the primary ion ( $\text{Ac}^-$ ) activity from an initial value of  $a_{\text{Ac}}$  to  $a'_{\text{Ac}}$  and  $a_{\text{B}}$  represents the activity of interfering ion added to the reference solution of primary ion of activity  $a_{\text{Ac}}$  which also brings about same potential change. It is given by expression:

$$K_{\text{Ac,B}}^{\text{pot}} = \frac{\Delta a_{\text{Ac}}}{a_{\text{B}}} = \frac{a'_{\text{Ac}} - a_{\text{Ac}}}{a_{\text{B}}} \quad (1)$$

In the present studies  $a_{\text{Ac}}$  and  $a'_{\text{Ac}}$  were kept at  $1.0 \times 10^{-6}$  and  $5.0 \times 10^{-6}$  M  $\text{Ac}^-$  and  $a_{\text{B}}$  was experimentally determined. FIM is the most widely used procedure as per IUPAC recommendation for determining selectivity coefficients [21]. In the FIM, the selectivity coefficient was evaluated from potential measurement on solutions containing a fixed concentration of interfering ion ( $1.0 \times 10^{-2}$  M) and varying amount of  $\text{Ac}^-$  ions. The values of selectivity coefficient so determined are compiled in Table 3. A value of selectivity coefficient equal to 1.0 indicates equal response to both primary ion and interfering ions. The value <1.0 shows that the sensor is selective to the primary ion over the interfering ion. It is seen from Table 3 that the selectivity coefficients determined by both the methods are sufficiently <1.0, indicating that the present sensors are significantly selective to acetate ion over all the interfering ions.

It is seen that the selectivity of the proposed sensor toward acetate is better for most of the anions as compared to all reported sensors. The electrode based on BDH shows better selectivity and detection limit. The presence of strong electron withdrawing nitro groups of ionophore increases its hydrogen bond donor capacity and thus bonding with acetate ion. In view of its good selectivity, the proposed sensor could be used to determine acetate in solutions containing appreciable concentrations of  $\text{Cl}^-$ ,  $\text{H}_2\text{PO}_4^-$  and  $\text{SO}_4^{2-}$  ions.

### 3.7. Determination of formation constant

The formation constant of the ion–ionophore complex within the membrane phase is a very important parameter that dictates the practical selectivity of the sensor. To determine the formation constant, two membrane segments are fused together, with only

**Table 3**  
Selectivity coefficient of various interfering anions

Interfering ions	Selectivity coefficients ( $-\log K_{\text{Ac,B}}^{\text{pot}}$ )	
	MPM	FIM
$\text{Cl}^-$	0.04	0.07
$\text{H}_2\text{PO}_4^-$	0.16	0.14
$\text{SO}_4^{2-}$	0.11	0.08
$\text{Br}^-$	0.13	0.10
$\text{ClO}_4^-$	0.12	0.15
$\text{I}^-$	0.05	0.07
$\text{NO}_3^-$	0.68	0.65
$\text{NO}_2^-$	0.22	0.19
$\text{SCN}^-$	0.15	0.17
$\text{OH}^-$	0.17	0.19

**Table 4**

Complex-formation constants of ionophore (BDH) in segmented sandwich-PVC membrane with different anions

Anions	Formation constant ( $\log \beta_{ILn}$ ) <sup>a</sup>
CH <sub>3</sub> COO <sup>-</sup>	5.5
Cl <sup>-</sup>	3.8
H <sub>2</sub> PO <sub>4</sub> <sup>-</sup>	3.0
SO <sub>4</sub> <sup>2-</sup>	3.3
Br <sup>-</sup>	3.1
ClO <sub>4</sub> <sup>-</sup>	3.3
I <sup>-</sup>	3.8
NO <sub>3</sub> <sup>-</sup>	2.0
NO <sub>2</sub> <sup>-</sup>	2.2
SCN <sup>-</sup>	2.9

<sup>a</sup> RSD was < 2.5% for n = 3.**Table 5**

Determination of total acetate ion flowing samples

Samples	Total acetate ion determined (g/100 mL)	
	Determined by proposed sensor	Labeled
Vinegar (brand-1)	4.56 ± 0.01	4–5
Vinegar (brand-2)	4.85 ± 0.03	5
Food preservative	1.98 ± 0.04	2

one containing the ionophore, to give a concentration-polarized sandwich membrane. A membrane potential measurement of this transient condition reveals the ion activity ratio at both interfaces, which translates into the apparent binding constant of the ion-ionophore complex [22]. In this method complex formation constants are obtained by neglecting ion pairing. As reported, the membrane potential  $E_M$  is determined by subtracting the cell potential for a membrane without ionophore from that for the sandwich membrane. The formation constant is then calculated using the equation:

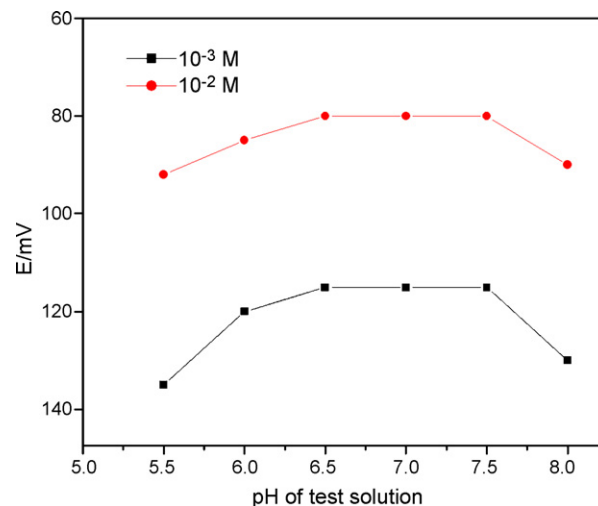
$$\beta_{ILn} = \left( L_T - \frac{nR_T}{Z_I} \right)^{-n} \exp \left( \frac{E_M Z_I F}{RT} \right) \quad (2)$$

where  $L_T$  is the total concentration of ionophore in the membrane segment,  $R_T$  is the concentration of lipophilic ionic site additives,  $n$  is the ion-ionophore complex stoichiometry, and  $R$ ,  $T$  and  $F$  are the gas constant, the absolute temperature, and the Faraday constant respectively. The ion  $I$  carries a charge of  $Z_I$ . The determined formation constants ( $\log \beta_{ILn}$ ) for the examined different complexes were recorded in Table 4. The elapsed time between sandwich fusion and exposure to electrolyte was typically <1 min. The potential was recorded as the mean of the last minute of a 5-min measurement period in the appropriate salt solution. The potential of such sandwich membranes remains free of diffusion-induced potential drifts for about 20 min. Standard deviations were obtained based on the measurements of sets of at least three replicate membrane disks that were made from the same parent membrane. A careful anal-

**Table 6**

Comparison of some of the characteristics of the proposed electrode with of previous acetate ISEs

References	Ionophore name	Linear range (M)	Slope (mV decade <sup>-1</sup> of activity)	Selectivity coefficients ( $-\log K_{Ac,B}^{pot}$ )	Response time (s)
Proposed sensor	Butane-2,3-dione,bis[(2,4-dinitrophenyl)hydrazone]	$5.0 \times 10^{-6}$ to $1.0 \times 10^{-1}$	$60.0 \pm 1.0$	Cl <sup>-</sup> (0.04), NO <sub>2</sub> <sup>-</sup> (0.22), NO <sub>3</sub> <sup>-</sup> (0.68), Sal <sup>-</sup> (1.58), SCN <sup>-</sup> (-0.15), ClO <sub>4</sub> <sup>-</sup> (0.02), Br <sup>-</sup> (0.13)	<15
[6]	( $\alpha,\alpha,\alpha,\alpha$ )-5,10,15,20-tetrakis[2-(4-Fluorophenylureylene)phenyl]-porphyrin	$1.0 \times 10^{-5}$ to $1.0 \times 10^{-2}$	$54.8 \pm 0.8$	Cl <sup>-</sup> (0.57), NO <sub>2</sub> <sup>-</sup> (0.22), NO <sub>3</sub> <sup>-</sup> (0.76), Sal <sup>-</sup> (1.58), SCN <sup>-</sup> (-0.65), ClO <sub>4</sub> <sup>-</sup> (0.00), Br <sup>-</sup> (-0.15)	<30
[3]	Liquid membrane (trimethylcetylammmonium acetate)	$3.0 \times 10^{-5}$ to $5.0 \times 10^{-2}$	Not reported	NO <sub>3</sub> <sup>-</sup> (7.6), ClO <sub>4</sub> <sup>-</sup> (2.42), NO <sub>2</sub> <sup>-</sup> (4.1), Br <sup>-</sup> (5.9), Cl <sup>-</sup> (2.3), F <sup>-</sup> (0.346), OH <sup>-</sup> (2.7), Benzoate (0.50), I <sup>-</sup> (0.50), HCOO <sup>-</sup> (1.8), SO <sub>4</sub> <sup>2-</sup> (0.85)	2–3

**Fig. 6.** Effect of pH on potential response of the acetate ion-selective sensor.

ysis of the data in Table 4 reveals that acetate ion has maximum value of formation constant for acetate ion than other ions. Hence, it shows significant anion-binding characteristics with ionophore as compared to other ion.

### 3.8. Effect of pH

The pH dependence of the electrode potential was investigated in the pH range 5–8 for  $10^{-3}$  and  $10^{-4}$  M of acetate solutions. The pH of the solution was adjusted by the addition of 0.1 M HEPES-NaOH/H<sub>2</sub>SO<sub>4</sub> buffer solution. As shown in Fig. 6, the potential was independent of pH in the range of 6.5–7.5. The increase in electrode potential of electrode at pH < 6.5 could be due to the presence of H<sup>+</sup> ion which will convert acetate into acetic acid. This will decrease the hydrogen bonding between acetate ion and ionophore. Similarly the deviation in potential at pH > 7.5 may be due to the interference of OH<sup>-</sup> ion. The electrode then starts responding to OH<sup>-</sup> ions in addition to acetate ions.

### 3.9. Effect of non-aqueous content

As the samples may possess some non-aqueous content in them, hence the performance of the proposed electrode is also assessed in non-aqueous media using methanol-water, ethanol-water and acetonitrile-water mixtures. The non-aqueous content was varied between 10 and 35% (v/v). The sensor does not show appreciable change in working concentration range ( $5.0 \times 10^{-6}$  to  $1.0 \times 10^{-1}$  M) or slope ( $60.0 \pm 1.0$  mV decade<sup>-1</sup> activity) in mixture up to 20% (v/v) non-aqueous content. However, in mixtures having higher percentage of non-aqueous content the working range was decreased

( $4.2 \times 10^{-5}$  to  $1.0 \times 10^{-1}$  M) and the slope decreased from 60 to  $\sim 50$  mV decade<sup>-1</sup> of activity. Such an observed behavior can be explained on the basis of leaching of the ionophore in organic phase.

#### 4. Analytical application

The proposed sensor was used for the determination of acetate in two commercially available brands of vinegar containing 4–4.5 g/100 mL acetic acid. The sample solution was prepared by dilution of 50  $\mu$ L of vinegar to 50 mL with 0.1 M HEPES–NaOH buffer, pH 7.0. The analysis was carried out by direct potentiometry using a calibration curve obtained with standard solution of sodium acetate prepared in the same buffer. It is seen from Table 5 that there is a satisfactory agreement between the determined values and the labeled acetate content.

#### 5. Conclusions

An acetate selective electrode has been developed using diphenylhydrazone-based neutral ionophore with hydrogen bond donors. This electrode has a greater sensitivity and selectivity for acetate; it exhibits wider working concentration range ( $5.0 \times 10^{-6}$  to  $1.0 \times 10^{-1}$  M). Nernstian compliance ( $60 \pm 0.3$  mV decade<sup>-1</sup> activity), fast response time (15 s), and showed high selectivity for acetate. The proposed sensor is superior to the reported sensors (Table 6) as it possesses high selectivity for acetate even over interfering anions such as Cl<sup>-</sup>, HSO<sub>3</sub><sup>-</sup>, HCO<sub>3</sub><sup>-</sup>, NO<sub>3</sub><sup>-</sup>, SCN<sup>-</sup>, I<sup>-</sup> and Br<sup>-</sup> which causes considerable interference in the functioning of other reported sensors. Thus, the sensor can be used for selective determination of acetate ion. Acetic acid in

vinegar was successfully determined using the proposed electrode.

#### Acknowledgement

One of the authors Ram Avatar Sharma is grateful to Ministry of Human Resource Development (MHRD), New Delhi, India, for financial support.

#### References

- [1] E. Bakker, E. Malinowska, R.D. Schiller, M.E. Meyerhoff, *Talanta* 41 (1994) 881.
- [2] Y.H. Qiao, H. Lin, H.K. Lin, *J. Incl Phenom Macrocycl Chem. U.S. Patent* 6689272.
- [3] L. Campanella, T. Ferri, *Fresen. Z. Anal. Chem.* 302 (1980) 304.
- [4] H. Beutler, in: H.U. Bergmeyer (Ed.), *Method of Enzymatic Analysis*, vol. 6, 3rd ed., VCH, Weinheim, 1984, p. 639.
- [5] G. Wagner, G.G. Guilbault (Eds.), *Method of Enzymatic Analysis*, vol. 6, Marcel Dekker, New York, 1994.
- [6] S. Amemiya, P. Buhlmann, Y. Umezawa, *Anal. Chem.* 71 (1991) 1049.
- [7] P.D. Beer, P.A. Gale, *Angew. Chem. Int. Ed.* 40 (2001) 486.
- [8] M.D. Best, S.L. Tobey, E.V. Anslyn, *Coord. Chem. Rev.* 240 (2003) 3.
- [9] P.D. Beer, E.J. Hayes, *Coord. Chem. Rev.* 240 (2003) 167.
- [10] L. Sessler, S. Camilo, P.A. Gale, *Coord. Chem. Rev.* 240 (2003) 17.
- [11] R.C. Bondy, J.S. Loeb, *Coord. Chem. Rev.* 240 (2003) 77.
- [12] S. Camilo, P.A. Gale, M.B. Hursthouse, M.E. Light, *Tetrahedron Lett.* 43 (2003) 6995.
- [13] K. Kavallieratos, M.C. Bertaio, R.H. Crabtree, *J. Org. Chem.* 64 (1999) 1675.
- [14] Z.X. Wang, H.L. Qin, *J. Green Chem.* 6 (2004) 90.
- [15] S. Nishizawa, R. Kato, T. Hayashita, N. Teramae, *Anal. Sci.* 14 (1998) 595.
- [16] D.H. Lee, H.Y. Lee, K.H. Lee, J. Hong, *Chem. Commun.* (2001) 1188.
- [17] T. Rosatzin, E. Bakker, K. Suzuki, W. Simon, *Anal. Chim. Acta* 280 (1993) 197.
- [18] U. Schaller, E. Bakker, U.E. Spichiger, E. Pretsch, *Anal. Chem.* 66 (1994) 391.
- [19] V.P.Y. Gadzekpo, G.D. Christian, *Anal. Chim. Acta* 164 (1984) 279.
- [20] E. Bakker, E. Pretsch, P. Buhlmann, *Anal. Chem.* 72 (2000) 1127.
- [21] Y. Umezawa, K. Umezawa, H. Sato, *Pure Appl. Chem* 67 (1995) 507.
- [22] Y. Mi, E. Bakker, *Anal. Chem.* 71 (1999) 5279.



# Using near-infrared spectroscopy and differential adsorption bed method to study adsorption kinetics of orthoxylene on silica gel

Qing-Juan Han, Hai-Long Wu\*, Chen-Bo Cai, Li-Juan Tang, Ru-Qin Yu

State Key Laboratory of Chemo/Biosensing and Chemometrics, College of Chemistry and Chemical Engineering, Hunan University, Changsha 410082, China

## ARTICLE INFO

### Article history:

Received 3 December 2007  
Received in revised form 3 April 2008  
Accepted 12 April 2008  
Available online 20 April 2008

### Keywords:

Near-infrared spectroscopy  
Local partial least squares  
PLS  
Differential adsorption bed  
Orthoxylene  
Silica gel

## ABSTRACT

This paper has demonstrated the study on the adsorption kinetics of orthoxylene on silica gel with a novel experimental methodology. In the method, there was a differential adsorption bed (DAB) where the solid adsorbent always contacted with the same bulk concentration of the adsorbate vapor, and the DAB was monitored with near-infrared diffuse reflectance spectroscopy (NIRDRS) continuously as well as non-invasively. Local partial least squares (PLS) algorithm was suggested to replace normal global PLS method in multivariate calibration models for processing NIRDRS data, because the concentration of the adsorbate on the adsorbent varied greatly as the adsorption process was going on. In this way, we, conveniently as well as promptly, obtained instantaneous adsorption rates of several orthoxylene/silica gel adsorption processes under different conditions like partial pressure of orthoxylene vapor and velocity of gas, and discovered that the adsorption process was physical adsorption, and mainly controlled by external diffusion.

© 2008 Elsevier B.V. All rights reserved.

## 1. Introduction

In most cases, studying kinetics of vapor adsorbate on solid adsorbent with experimental methods is necessary for optimal design and operation of any adsorption unit in engineering, or for completely understanding the adsorption process in science, because the complicated mass and heat transfer in the system often make results predicted by various adsorption theories unreliable. Until recently there are a variety of experimental methods for this purpose, mainly including pulse chromatography, fixed-bed breakthrough, diffusion cell and gravimetric measurement. But they all have their own difficulties. Pulse chromatography and fixed-bed breakthrough methods suffer from the drawback that the “bed processes” must be accounted for in the analysis of the results. These significantly increase the complexity of the mathematical analysis or even may lead to erroneous results. Diffusion cell method can avoid the complications of the fixed-bed breakthrough, but requires a specially formed and representative pellet of the adsorbent that is usually very difficult to be obtained. Gravimetric measurement, including intelligent gravimetric analyze technology developed nowadays, is based on continuously recording the increase of the adsorbent in weight

during the adsorption process. Accordingly, this method can avoid the mathematical complications. However, according to this method, the adsorption process must be carried out in a “static” environment in order not to affect the high-sensitivity balance (usually  $10^{-6}$  g). When the adsorption process is implemented in a flow of gas (common situation in practical adsorption process), obviously it is no longer appropriate. In addition, all methods mentioned above share one deficiency: the adsorption heat may lead a non-isothermal environment, and makes kinetic data treatment based on isothermal hypothesis unavailable [1,2].

In 1985, Carlson and Dranoff reported a new method called “differential adsorption bed (DAB)” [3], which was then developed by Do et al., and has become popular recently [4,5]. DAB consisted of three main sections: gas mixing, collection and analysis. The principle of operation was to pass adsorbate gas over an adsorbent for a known duration of time, then to desorb, collect and analyze the quantity of adsorbed phase. Adsorbate gas flows at high rates to have an isothermal adsorbent, remove stagnant layers in time and ensure a constant bulk concentration (the differential condition) making subsequent analysis easier [6]. Of course, there are some deficiencies in DAB. Firstly, the equipment of DAB is somewhat complex and inconvenient to operate; secondly, the operation, including desorbing, collecting and analyze, is time-consuming because it usually takes tens of minutes to obtain merely one kinetic datum; and finally, the record of DAB is accumulated changes dur-

\* Corresponding author. Fax: +86 731 8821818.  
E-mail address: [hlwu@hunu.edu.cn](mailto:hlwu@hunu.edu.cn) (H.-L. Wu).



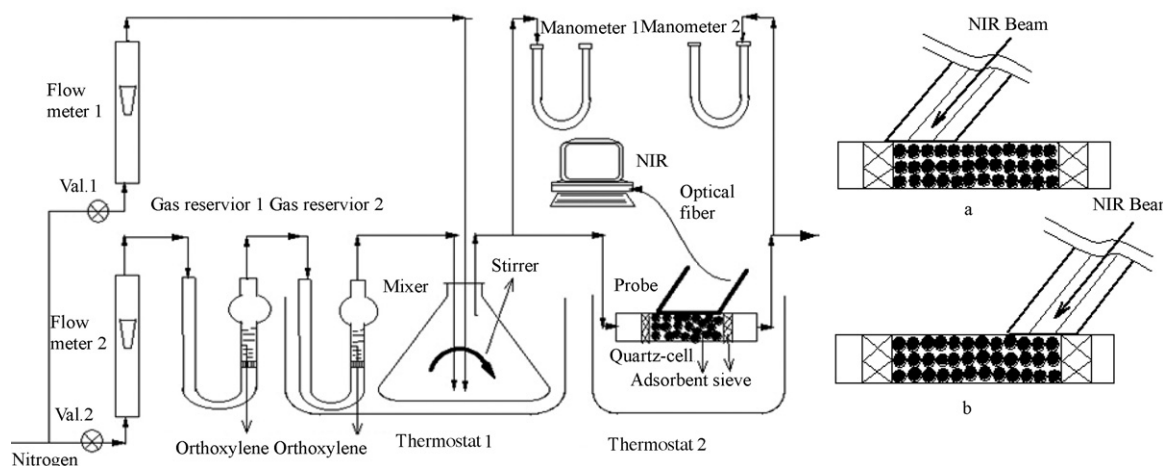


Fig. 1. Experimental setup.

ing a long period rather than the instantaneous adsorption rate at a certain time.

Since the 1980s, in chemistry as well as chemical engineering, process analytical chemistry (PAC) or process analytical technique (PAT) has attracted more and more attention. However, gas–solid adsorption process includes at least two phases, namely, the solid adsorbent and the gas adsorbate, making most common PAC techniques, such as chromatography, flow injection analysis or mass spectroscopy, impossible for in-line monitoring. As for spectroscopic methods, “near-infrared spectroscopy (NIR) continues to dominate spectroscopic work for real-time and process analysis,” [7], because: (1) it is a non-invasive, non-destructive technique; (2) solid sample can be directly measured without pretreatment if an appropriate device is used; (3) the optical fiber makes remote monitoring or control possible; (4) rapid response (usually less than 10 s); (5) quantitatively measuring all components simultaneously; (6) less analytical cost [8]. In fact, just owing to the advantages above, NIR has been already widely used in PAC for some years, for example, chemical reaction [9–12], petrochemical industry [13–15], and polymer industry [16–18].

Two strategies could be chosen to in-line monitor the gas–solid adsorption process with NIR. One is to detect the effluent gas through NIR diffuse transmission spectroscopy as the adsorption process is going on, and the other is to monitor the solid adsorbent with NIR diffuse reflectance spectroscopy (NIRDRS) when it is adsorbing the gas adsorbates. The former method has been used in monitoring the uptake of butane isomers by zeolite [19], while to our knowledge nobody has quantitatively studied thermodynamics or kinetics of gas–solid adsorption with the latter one. But the latter is probably more advantageous than the former in some aspects since (1) the adsorbate vapor could be concentrated by the adsorbent so that it is possible to detect the adsorbate vapor with relatively low concentration by NIRDRS; (2) with the NIRDRS we could directly measure the concentration of the adsorbate adsorbed by the adsorbent, and consequently avoid influence of error from measuring gas volume and pressure; (3) NIRDRS might shed light on some information about the interaction between the adsorbate molecules and adsorbent surface simultaneously in some cases.

## 2. Experimental

### 2.1. Reagents and materials

Silica gel (average pore diameter: 8.0–10.0 nm, pore volume: 0.8–1.0 ml/g, BET area: 300–400 m<sup>2</sup>/g), produced by Qingdao

Haiyang, Qingdao, China, was selected as the adsorbent. Orthoxylylene was analytical-reagent grade and made by Sinopharm Chemical Reagent, Shanghai, China. High-purity N<sub>2</sub> was supplied by Jingxiang Chemical Factory, Changsha, China.

All the chemometrics algorithms were written and performed in MATLAB environment on a personal computer.

### 2.2. Near-infrared apparatus

All the NIR spectra were collected from a FT-IR/NIR spectrometer (Nexus 870, Nicolet, Thermo Electron Company, Madison, USA) equipped with smart near-IR FiberPort accessory and an indium gallium arsenide (InGaAs) detector. The diameter of the optical fiber probe was about 3 mm. NIR spectra were all recorded over the spectral range of 4000–10,000 cm<sup>-1</sup> at a resolution of 4 cm<sup>-1</sup>. A total of 15 scans were accumulated per measurement. The spectra of reference (i.e., the silica gel) were collected at the beginning of each experiment. Then all other spectra in the adsorption process were recorded as difference spectra, namely, subtracting reference spectra away from sample spectra to obtain the “pure” spectral effect just out of orthoxylylene.

### 2.3. Experimental setup and procedure for adsorption monitoring

The experimental setup is shown in Fig. 1. High-purity N<sub>2</sub> was brought in as inert carrier through valve 1 and 2. A part of N<sub>2</sub> flew through gas reservoir 1 and 2 holding liquid orthoxylylene. After coming out of the gas reservoir 2, the N<sub>2</sub> was already saturated by orthoxylylene vapor, and then mixed with the other part of N<sub>2</sub> in the mixer with a stirrer to improve blending. Lastly, the gas mixture was ushered into a rectangular quartz-cell, in which the gas passed through silica gel and was adsorbed by it. At the same time, the NIRDRS of silica gel containing orthoxylylene were continuously recorded by a NIR spectrometer via the optical fiber probe.

A special custom-made quartz-cell (length × width × thickness: 50 mm × 10 mm × 2 mm) that was 50 mm in length, 10 mm in width and 2 mm in thickness was chosen in order that a differential adsorption bed (DAB) was possible. For further simplifying the treatment of kinetic data afterward, the probe must be placed appropriately so that the foremost part of silica gel in the quartz-cell was covered with the NIR FiberPort probe (see ‘a’ in Fig. 1). When the volume flow rate of influent gas ( $F_0$ ) was not too small, the concentration of orthoxylylene in the gas was not too low, and the sieve (made of stainless steel) before the silica gel did

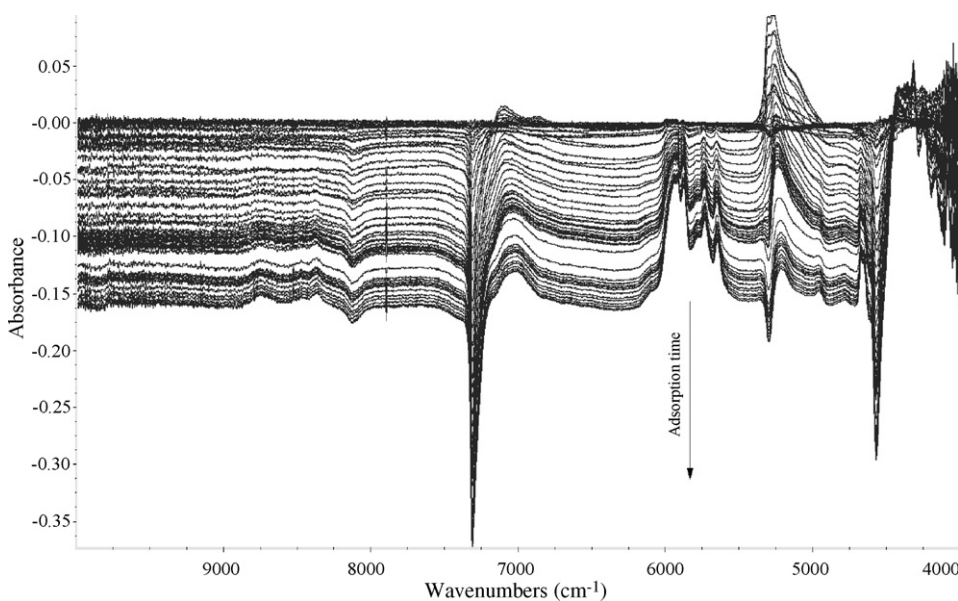


**Fig. 2.** Raw NIRDRS during ortho-xylene–silica gel adsorption process. Temperature: 293.15 K;  $P/P_0$  of ortho-xylene: 1.00;  $F_0$ : 100 ml/min; intervals of recording time: about 30 s.

not adsorb ortho-xylene, the tiny space (i.e., the foremost part of the silica gel in the quartz-cell: 3 mm × 10 mm × 2 mm) can be reasonably regarded as a DAB where each part of silica gel contacted with not only a constant bulk concentration of ortho-xylene, but the concentration of the ortho-xylene in the influent gas. At the same time, the adsorption heat was removed quickly by the gas flow for keeping an isothermal environment. In addition, due to the rapid response of NIR, NIRDRS could be recorded frequently (in fact, it needed less than 10 s to record a spectrum with our NIR spectrometer). This made our experimental setup possible to record concentration change within a relatively short time.

Clearly, the experimental setup was capable to alter and measure flow rate of influent gas ( $F_0$ ), concentrations of adsorbate in gas phase, and temperature, which all worked on adsorption kinetics. Besides temperature and concentration of ortho-xylene on the silica gel, the NIRDRS of the silica gel were influenced by three other factors, i.e., the granularity, thickness and packing density of silica gel, which should be eliminated or at least reduced in order to more accurately predict the concentration of ortho-xylene on the silica gel. We solved these problems with the following strategies respectively: granularity was 80–100 meshes for all experiments; NIRDRS were recorded in the same quartz-cell; and the same amount of silica gel was compressed into the same length in the same rectangular quartz-cell in each experiment. It is worth noting that the silica gel could neither be compressed so tightly that the gas penetrated it difficultly, nor so loosely that part of the silica gel could not contact the gas well or the influent gas may affect NIRDRS (as a result of the movement of silica gel granules). In all experiments of the paper, 0.0900 g of silica gel was compressed into 10 mm in the quartz-cell.

Fig. 2 has shown an example of monitoring an adsorption process from the beginning of adsorption up to the equilibrium of adsorption with our experimental setup and procedure. Here, the concentration of ortho-xylene in the gas phase was represented as the ratio of its partial pressure ( $P$ ) to its saturated vapor pressure ( $P_0$ ) at the same temperature, i.e.,  $P/P_0$ . From Fig. 2, one could clearly observe that the ortho-xylene was adsorbed on the silica gel gradually.

#### 2.4. Chemometrics of data analysis

In order to quantitatively determine the amount of ortho-xylene adsorbed by the silica gel, a calibration set and a validation set were required to build chemometrics models. Since the ortho-xylene was pure chemical and the influence of ortho-xylene vapor upon NIRDRS could be neglected, the actual samples during the adsorption process could be simply simulated as the following means. Each sample in calibration and validation sets was prepared by well blending the given amount of ortho-xylene and the known amount of the silica gel together. If just a small amount of ortho-xylene was demanded,  $\text{CCl}_4$  solution was used. The reason was that  $\text{CCl}_4$  was NIR-transparent, non-polar, and able to rapidly evaporate after blending. The NIRDRS of 108 mixture samples were recorded in the same quartz-cell under the same conditions but without gas flow.

From Fig. 2, one could also see some spectral characteristics of the adsorption process. For example, the problem of baseline drift was obvious, while the problem of baseline rotation was relatively insignificant. Therefore, the first-derivative was chosen to preprocess raw spectra, for it could equally eliminate the effect of baseline drift as the second derivative, but was more stable and less enlarges the noise than the latter (when the concentration of adsorbed ortho-xylene was very low, the second-derivative of NIRDRS was much smaller and varied more greatly with noise than its first-derivative). Because ortho-xylene was pure chemical, and the silica gel, as inorganic materials, hardly influence NIRDRS in certain spectral ranges, the selection of wavelength ranges for building chemometrics models became simplified. The wavenumber ranges of 5600–6200  $\text{cm}^{-1}$  (the first overtone of C–H stretching vibration), and 8300–8900  $\text{cm}^{-1}$  (the second overtone of C–H stretching vibration) were selected at the beginning of chemometrics model building.

Because partial least squares (PLS) was able to choose the most relative wavenumbers out of the spectral ranges mentioned above automatically, it, as a popular algorithm in NIR [20,21], was also introduced in our study. Our process of building PLS calibration model was carried out by cross-validation method. However, in the study on kinetics, one characteristic – the great variety of concentration during the adsorption process – should not be neglected.

This might make a linear model covering the whole concentration range unsatisfactory. In chemometrics, several methods have been developed to cope with the problem such as non-linear PLS (NLPLS) [22], and artificial neural network (ANN) [23,24]. Considering there was only one component (i.e., orthoxylene) needed to be predicted, a more simple strategy was developed as follows. 108 samples prepared by blending method were divided into three groups: 40 samples – called “low concentration group” – ranged in concentration from 0.0000 to 0.0039 g/g; 36 samples – called “middle concentration group” – ranged from 0.0040 to 0.0390 g/g; and 32 samples – called “high concentration group” – ranged from 0.0450 to 0.2000 g/g. Here, the concentration of orthoxylene on silica gel was represented as the ratio of the orthoxylene to the silica gel by weight (w/w). Within each groups the concentration range was less than 10 times, and the non-linear problem might be largely overcome. The samples in the “low concentration group” is divided into calibration set and validation set. The validation set contained one-fourth of 40 samples (i.e., 10 samples), while other 30 samples were assigned to calibration set for building the first local PLS calibration model (local-PLS). The samples in the middle and high concentration group were also treated in the same way to build the second and third local PLS calibration model, respectively. The selection of the correct calibration model to obtain predicted value is straightforward for most unknown samples. For some rare borderline samples, for example, the samples within 0.0039–0.0040 or 0.0390–0.0450, the mean of two concentrations predicted by two nearest models respectively was regarded as the final estimated concentration. The three local models based on their own validation set were described by squared correlation coefficient ( $R^2$ ), also called coefficient of determination, and the root mean standard error of predication (RMSEP), both of which can be interpreted as the average modeling/prediction error. Here, RMSEP could be calculated as follows:  $RMSEP = [\sum(C_p - C_A)^2/n]^{1/2}$ , where  $C_p$  represented the predicted concentrations of the samples from the validation set,  $C_A$  was the actual concentrations of the samples in the validation set, and  $n$  stood for the number of the predicted samples. Their results were shown in Fig. 3(a)–(c). For comparison, we also built a global PLS model (global-PLS) that was based on all samples of three calibration sets. The performance of the global PLS model was judged in the same way and shown in Fig. 3, too. In order to indicate the relative error more exactly, the relative standard deviation (R.S.D.) was introduced as:  $R.S.D. = RMSEP/C_M$ , where  $C_M$  was the mean of the actual concentrations.

Fig. 3 shows that for samples with high concentrations, satisfactory concentrations predicted by global PLS were obtained, while for samples with middle concentrations, particularly those with low concentrations, the results were almost unacceptable. It is comprehensible: the wide range of concentration made linear model unreasonable; the global-PLS model based on samples of all calibration sets was more greatly determined by samples with higher concentrations than by those with lower concentrations, and accordingly was more effective for high concentrations. The strategy of local-PLS obviously improved the situation in the middle, and especially in the low concentration groups. Although for the samples with low concentrations the R.S.D. was still somewhat high, the accuracy was enough for our research on the adsorption process. In fact, it was beyond the capability of NIR to accurately measure samples with very low concentrations (the LoD of NIR is commonly about  $10^{-4}$ ). As for those with high concentrations, the global-PLS was just slightly better than local-PLS, and the reason was probably that the former had more data to build calibration model than the latter.

In order to further evaluate the performance of our method, spectra of 12 adsorption equilibrium states were also recorded and treated with the local PLS strategy to obtain predicted con-

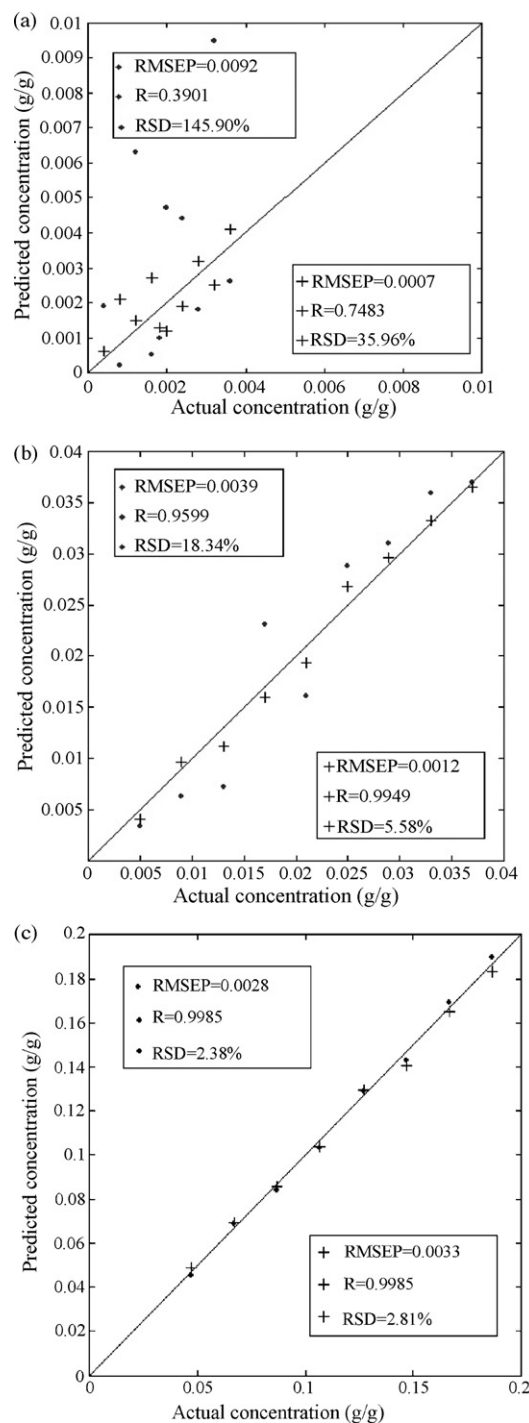


**Fig. 3.** Predicted concentrations of the validation samples with global-PLS (•) and local-PLS (+) respectively. Samples in (a) the low concentration group, (b) the middle concentration group and (c) the high concentration group.

centrations, while these same samples were later desorbed with thermogravimetry promptly to obtain actual concentrations. These results are shown in Fig. 4, and one could assume that the predicted results were acceptable. Unlike the study of adsorption kinetics, the NIR probe should be placed over the rearmost part of the silica gel in the quartz-cell to decide whether the adsorption equilibrium was achieved (see ‘b’ in Fig. 1), since the front part of silica gel always achieved equilibrium earlier.

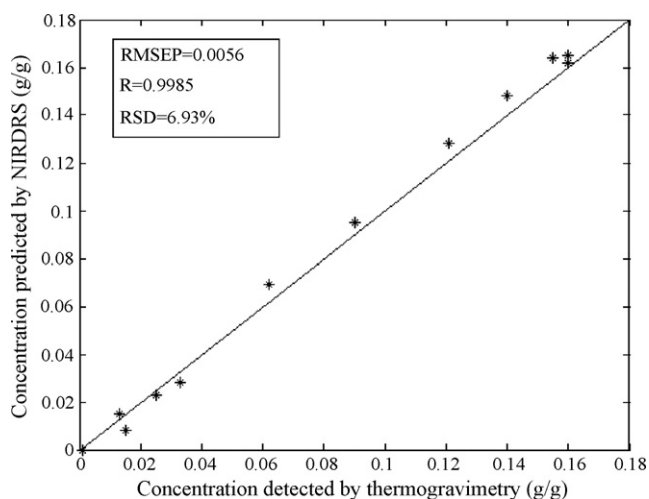


**Fig. 4.** Concentrations predicted by NIRDRS and measured by thermogravimetry for 12 adsorption equilibrium states. Temperature: 293.15 K;  $P/P_0$  of orthoxylyene: 1.00;  $F_0$ : 100 ml/min.

### 3. Result and discussion

Fig. 5 presented the results of four adsorption processes under different adsorption conditions. For every case, the whole adsorption process was monitored and its spectra were recorded at intervals of about 30 s. Then all NIR spectra have been treated with the local-PLS calibration method described before. In Fig. 5, changes in the concentration were indicated as the adsorption process was taking place. Through process 1 and 4, one could find out that the adsorption process was obviously affected by the bulk concentration of orthoxylyene vapor in the gas flow, and the higher the bulk concentration was, the more rapidly the adsorption process went on. Comparing process 1 with 2, 3 with 4, respectively, the influence of velocity of gas flow upon the adsorption rate was revealed: higher velocity resulted in larger adsorption rate. These conclusions strongly suggested that the process of silica gel adsorbing orthoxylyene was mainly controlled by external diffusion. By the way, the observation that the concentrations in process 3 and 4 fluctuated more largely, especially near equilibrium states, than those in pro-

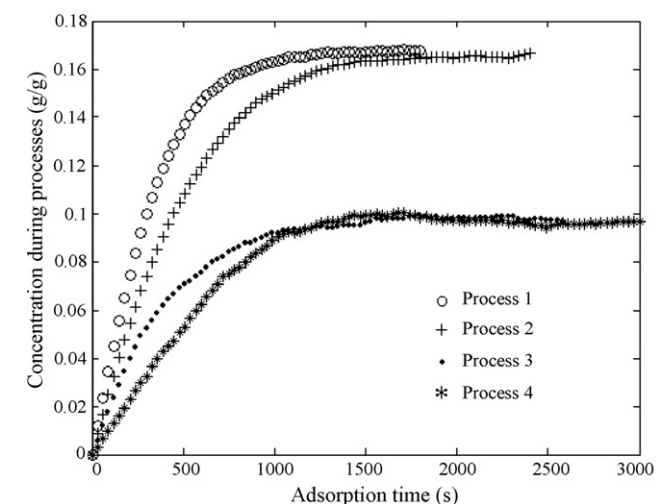


**Fig. 5.** The concentration of orthoxylyene on silica gel during different adsorption processes. Process 1:  $F_0 = 200$  ml/min,  $P/P_0 = 1.00$ ,  $T = 293.15$  K; process 2:  $F_0 = 100$  ml/min,  $P/P_0 = 1.00$ ,  $T = 293.15$  K; process 3:  $F_0 = 400$  ml/min,  $P/P_0 = 0.30$ ,  $T = 293.15$  K; process 4:  $F_0 = 200$  ml/min,  $P/P_0 = 0.30$ ,  $T = 293.15$  K.

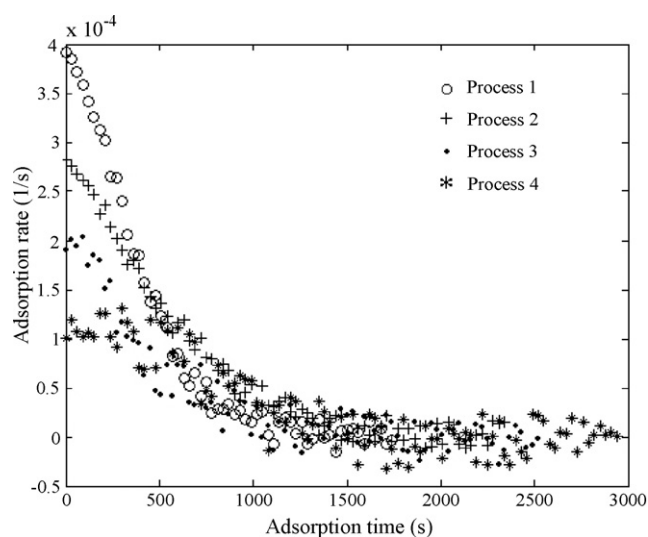


**Fig. 6.** Correlation between instantaneous adsorption rate and adsorption time during different adsorption processes (experimental conditions are the same as Fig. 4).

cess 1 or 2, was caused mainly by the change of  $P/P_0$  in process 3 and 4. The change resulted from the incapability of the two valves controlling the gas flow stably in our experimental setup, whereas in process 1 and 2, this instability did not affect the value of  $P/P_0$ .

Since the interval of recording time was not too long (roughly 30 s), instantaneous adsorption rate can be calculated approximately as follows:  $R_n = (C_{n+1} - C_n)/t$ , where  $C_n$  was the concentration at one recording time,  $C_{n+1}$  was the concentration at the next recording time, and  $t$  meant the time passed. Fig. 6 shows the correlation between instantaneous adsorption rate and adsorption time, and Fig. 7 demonstrated the relationship between instantaneous adsorption rate and the concentration of orthoxylyene in silica gel during different adsorption processes.

Fig. 6 and 7 could also confirm the conclusion demonstrated in Fig. 5. Furthermore, it clearly told us that the adsorption rate decreased with adsorption time and concentration of the adsorbate on the adsorbent monotonously. This was common in physical adsorption. What is more important, the adsorption rates obtained

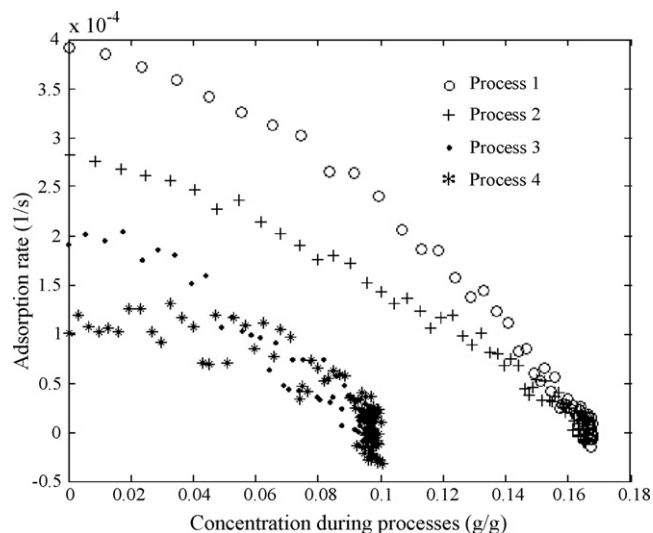


**Fig. 7.** Correlation between instantaneous adsorption rate and concentration of orthoxylyene adsorbed by silica gel during different adsorption processes (experimental conditions are the same as Fig. 4).

from the method demanded no hypothetical mass transfer theory. Therefore, the correlation revealed by the two figures made it reliable and straightforward to construct quantitative mass transfer models for engineering purpose in future. Finally, with Fig. 6 or Fig. 7 we could make certain that the foremost part of the silica gel in the quartz-cell could be regarded as a DAB. The concentration of orthoxylene in saturated vapor at 293.15 K was about 0.0270 g/l. In process 1 ( $F_0=200$  ml/min) the gas flow carried 0.0054 g orthoxylene into the quartz-cell in a minute. However, during the same time, the foremost part of the silica gel in the quartz-cell (0.027 g) could only adsorb 0.000648 g of orthoxylene even estimated according to the largest instantaneous adsorption rate ( $0.0004\text{ s}^{-1}$ ). Consequently, we could reasonably assume that the bulk concentration of gas flow did not change roughly, and all silica gels in the foremost quartz-cell contacted with the same concentration during the process. Other processes could be also calculated in the same way, and the results were similar.

#### 4. Conclusion

Through non-invasive monitoring a DAB with NIRDRS, we have modified the DAB method for studying kinetics of gas–solid adsorption. Compared with all other techniques until now, this innovative methodology can provide more information about the adsorption process in a more convenient (the adsorbent needed hardly any pretreatment), rapid (all kinetic data were obtained as soon as the adsorption process was completed), economical (NIR spectrometer was less expensive than most analytical instrument such as infrared or mass spectrometer), as well as straightforward (not requiring any hypothetical mass transfer model for kinetic data treatment) way. Moreover, not only was it feasible to study the adsorption process under different experimental conditions like temperature, partial pressure of adsorbate or flow rate of gas, but it was useful to non-invasively monitor an industrial adsorption process, where the quartz-cell containing adsorbent would be replaced by the industrial adsorption bed. Considering another advantage of NIR—quantitatively measuring all components simultaneously, the

method should be adapted to multicomponent adsorption system where there was over one kind of gas adsorbates after necessary improvements. This was one of subjects that we would further study in future.

#### Acknowledgments

This research was financially supported by National Natural Science Foundation of China (Grants no. 20775025 and Grants no. 20435010).

#### References

- [1] P.L.J. Mayfield, D.D. Do, *Ind. Eng. Chem. Res.* 30 (1991) 1262.
- [2] S. Sircar, *Adsorption* 12 (2006) 167.
- [3] N.W. Carlson, J.S. Dranoff, *Ind. Eng. Chem. Proc. Des. Dev.* 24 (1985) 1300.
- [4] X.J. Hu, D.D. Do, *Langmuir* 9 (1993) 2530.
- [5] D.D. Do, K. Wang, *AIChE J.* 44 (1998) 68.
- [6] D.D. Do, H.D. Do, *Adsorption* 7 (2001) 189.
- [7] J.J. Workman, M. Koch, D.J. Veltkamp, *Anal. Chem.* 75 (2003) 2859.
- [8] M. Blanco, I. Villaroya, *Trends Anal. Chem.* 21 (2002) 240.
- [9] C. Coffey, B.E. Cooley Jr., D.S. Walker, *Anal. Chem. Acta* 395 (1999) 335.
- [10] J. Helminen, M. Leppamaki, E. Paatero, P. Minkkinen, *Chemometr. Intell. Lab. Syst.* 44 (1998) 341.
- [11] W. Joseph, T.H. Paul, *Appl. Spectrosc.* 57 (2003) 293.
- [12] M. Blanco, D. Serrano, *Analyst* 125 (2000) 2059.
- [13] J. Bürck, G. Wiegand, S. Roth, H. Mathieu, K. Krämer, *Talanta* 68 (2006) 1497.
- [14] E.D. Yalvac, M.B. Seasholtz, M.A. Beach, S.R. Crouch, *Appl. Spectrosc.* 51 (1997) 1565.
- [15] R. Guchardi, A. da Costa, P. Filho, R.J. Poppi, C. Pasquini, *J. Near Infrared Spectrosc.* 6 (1998) 333.
- [16] Y. Hu, J. Zhang, H. Sato, Y. Futami, I. Noda, Y. Ozaki, *Macromolecules* 39 (2006) 3841.
- [17] T. Rohe, W. Becker, S. Kölle, N. Eisenreich, P. Eyerer, *Talanta* 50 (1999) 283.
- [18] K. Sakei, K. Funatsu, K. Tanabe, *Anal. Sci.* 19 (2003) 309.
- [19] A.F.P. Ferreira, H.F.M. Boelens, J.A. Westerhuis, *Langmuir* 21 (2005) 6830.
- [20] Y. Roggo, P. Chaluz, L. Maurer, C. Lema-Martinez, A. Edmond, N. Jent, *J. Pharm. Biomed. Anal.* 44 (2007) 683.
- [21] B. Lavine, J. Workman, *Anal. Chem.* 78 (2006) 4137.
- [22] M. Blanco, J. Coello, H. Iturriaga, S. MasPOCH, J. Pages, *Chemometr. Intell. Lab. Syst.* 50 (2000) 75.
- [23] Y. Dou, Y. Sun, Y.Q. Ren, Y.L. Ren, *Anal. Chim. Acta* 528 (2005) 55.
- [24] B.B. Li, P.A. Hassel, A.J. Morris, E.B. Martin, *Comput. Stat. Data Anal.* 48 (2005) 87.



## Comparison of the effectiveness of solid-phase and ultrasound-mediated liquid–liquid extractions to determine the volatile compounds of wine

Dolores Hernanz<sup>a</sup>, Valeria Gallo<sup>a</sup>, Ángeles F. Recamales<sup>a</sup>,  
Antonio J. Meléndez-Martínez<sup>b</sup>, Francisco J. Heredia<sup>b,\*</sup>

<sup>a</sup> Department of Analytical Chemistry, Faculty of Experimental Science, University of Huelva, Spain

<sup>b</sup> Laboratory of Food Color and Quality, Department of Nutrition and Food Science, Faculty of Pharmacy, University of Seville, Spain

### ARTICLE INFO

#### Article history:

Received 13 February 2008

Received in revised form 18 April 2008

Accepted 23 April 2008

Available online 2 May 2008

#### Keywords:

Liquid–liquid extraction

Solid-phase extraction (SPE)

Ultrasound-assisted

Volatile compounds

Wine

### ABSTRACT

Two ultrasound-assisted liquid–liquid extraction (LLE-I, LLE-II) methods were compared to a solid-phase extraction (SPE) protocol to assess their effectiveness for the analysis of up to 44 volatile compounds in a synthetic and several commercial white, red and “cream” wines produced in the southwest of Spain. Regardless of the extraction protocol used the highest recoveries corresponded to acids and terpene alcohols and the lowest to lactones and alcohols. In any case, it was concluded that one of the liquid–liquid extraction protocols evaluated led to higher recoveries for a greater number of odorants that could be implicated in the aroma of the wines than the solid-phase extraction. However, the SPE method also presented some advantages that should not be overlooked, like higher repeatability and throughput and lower solvent consumption.

© 2008 Elsevier B.V. All rights reserved.

### 1. Introduction

Volatiles, a term that refers to hundreds of compounds encompassing alcohols, esters, organic acids, aldehydes, ketones, and monoterpenes, play a prominent role in the organoleptic characteristic of wines in general and in their varietal character in particular. The flavor of a wine is therefore extremely complex, not only due to the great number of compounds present, but also to the fact that they have different polarities, volatilities and, moreover, are found in a wide range of concentrations. In this sense it is not surprising that the extraction and concentration of the volatile compounds is a key step in aroma analysis and continues attracting the scientific community's interest. Thus, several methods in this regard have been developed to date, which present advantages and disadvantages regarding each other [1].

Liquid–liquid extraction (LLE) has been widely used in the sample preparation for the determination of wine aromas [2–7], since all the volatiles (exhibiting low, medium or high volatility) have a high partition coefficient to the organic phases commonly used, such as dichloromethane [8–10], freon-11 [11], *n*-pentane [12], diethyl ether [13], hexane–ethyl ether [14] and diethyl ether–*n*-pentane [15], among others. A downside of this methodology is,

however, that it requires solvent evaporation, which, in some cases, results in the loss or degradation of some of the compounds of interests. Other methodologies, like continuous liquid–liquid extraction [16], supercritical fluid extraction [17] and microwave extraction [18] protocols have also been developed, as well as ultrasound-assisted extractions, which are also being accepted currently in the analytical laboratory for sample preparation as an alternative to microwaves, superheated liquids or supercritical fluids [19]. The usefulness of the ultrasound-assisted extractions is unquestionable as it facilitates the mass transfer between two immiscible phases, hence the fact that it has been used to extract aroma compounds in wine [10,15,20], polyphenols in extra virgin olive [21], isoflavones in soybeans [22], mycotoxins in foods and drinks [23], metals from environmental matrixes [24], etc.

Aside from this array of LLE approaches, solid-phase extractions (SPE) [25,26] and solid-phase microextractions (SPME) [27–31] are also commonly used for the extraction of wine volatiles. These techniques diminish the extraction time and, in addition, are more environmentally friendly as they also reduce the sample manipulation and solvent consumption. Other methods, such as the stir bar sportive extraction (SBSE), have been successfully applied in wine [32].

In the present work we have compared two LLE and a SPE protocols through the analysis of five commercial wines with markedly different aromatic characteristics and a synthetic wine, which was used to compare their sensitivity and repeatability.

\* Corresponding author. Tel.: +34 954556761; fax: +34 954557017.  
E-mail address: [heredia@us.es](mailto:heredia@us.es) (F.J. Heredia).

## 2. Experimental procedures

### 2.1. Samples, reagents and standards

Five commercially available wines, produced from distinct grape varieties in wineries based in Huelva (Spain), were used due to the great difference in their volatile composition. Specifically, three young white wines (obtained from Zalema, Colombar and Palomino Fino grapes in 2006), one young red wine (made from Syrah grapes in 2005) and one “cream” wine (liquor wine produced by fermentation of musts from sun-dried Pedro Ximenez grapes) were considered. All the wines were bottled in 750-mL bottles.

The reagents used were of HPLC grade (99.9% purity). The solvents ethanol, *n*-pentane, dichloromethane, diethyl ether and *n*-pentane were purchased from Romil (Cambridge, U.K.), BHA (3-*tert*-butyl-4-hydroxyanisole) was procured from Panreac (Barcelona, Spain) and the Lichrolut EN resins, prepacked in 200 mg cartridges (3 mL total volume), from Merck (Darmstadt, Germany). The ultrapure water was obtained from a Milli-Q purification system (Millipore, USA). The standards of aroma compounds, whose purities ranged from 98% to 99%, were obtained from Chemservice (West Chester, PA) and Aldrich (Gillingham, UK). 4-Methyl-2-pentanol (750 µg/mL in ethanol) and 2-octanol (650 µg/mL in ethanol) were used as internal standards.

A model wine solution was prepared with 1.15 g/L potassium bitartrate and at 0.7 g/L tartaric acid (pH 3.02) in 10.5% (v/v) aqueous ethanol solution [5]. To obtain the synthetic wine, model wine solution (250 mL) was spiked with a 1% (w/v) ethanol solution of the aroma mix, such that the concentration of the 44 aroma compounds studied in the synthetic wine was 50 µg/mL. All the standard solutions were stored at 4 °C.

### 2.2. Methods

Three different methodologies were used for the extraction of the volatile components from the synthetic wine and the wine samples:

#### 2.2.1. Liquid–liquid extraction with diethyl ether–*n*-pentane (2:1) mixture as extractant (LLE-I)

The volatile compounds were extracted by the methodology described by Hernanz et al. [15]. In brief, 100-mL samples containing 4 g of MgSO<sub>4</sub> were poured into a 200 mL flask and subsequently extracted twice with 50 mL of diethyl ether–*n*-pentane mixture (2:1). The solutions so obtained were sonicated for 30 min at 25 °C under a nitrogen atmosphere to prevent oxidative reactions and then the pooled extracts were dried on anhydrous sodium sulphate and concentrated to 5 mL in a vacuum rotatory evaporator. 25 µL of an internal standard solution was added (final concentration of 3.7 µg/mL of 4-methyl-2-pentanol and 3.2 µg/mL of 2-octanol) and 1.0 µL of the solution was injected into the gas chromatography system.

#### 2.2.2. Liquid–liquid extraction with dichloromethane as extractant (LLE-II)

Volatile compounds were extracted according to the method described by Cabredo–Pinillos et al. [10]. Briefly, 25-mL samples were placed in a 100 mL beaker with 10 mL of dichloromethane and 4 g of NaCl and sonicated for 15 min at 25 °C. 5-mL volumes of the organic phase were mixed with 25 µL of the internal standards solutions (final concentration of 3.7 µg/mL of 4-methyl-2-pentanol and 3.2 µg/mL of 2-octanol) and 1-µL aliquots eventually injected into the GC system.

#### 2.2.3. Solid-phase extraction (SPE)

The solid-phase extractions were performed according to the methodology proposed by López et al. [26]. The cartridges with the sorbent were placed in the extraction system and activated with 4 mL of dichloromethane, 4 mL of methanol, and 4 mL of a water–ethanol mixture (12%, v/v). 50-mL volumes of the samples (containing 25 µL of BHA solution) were passed through the SPE cartridges at around 2 mL/min, after which the sorbent was dried by letting air pass through it. The analytes were recovered by eluting with 1.3 mL of dichloromethane, and after adding 25 µL of the internal standards solutions (final concentration of 14.4 µg/mL of 4-methyl-2-pentanol and 12.5 µg/mL of 2-octanol in ethanol) 1-µL aliquots were injected in the GC system.

Regardless of the procedure followed, the extractions were carried out in triplicate, and each sample was injected into the GC system three times. Prior to their analysis, the extracts were stored in a freezer (–25 °C). Gas chromatography with flame-ionization detector (GC-FID) was used for quantitative analysis and gas chromatography with mass spectrometer (GC-MS) for identification purposes.

### 2.3. Equipment

A 7-l Selecta ultrasound bath (Barcelona, Spain) was used for the LLE.

#### 2.3.1. Chromatography

The volatile compounds were separated on a capillary column CP-Wax 52 CB (60 m × 0.25 mm × 0.25 µm) from Varian (Walnut Creek, CA, USA) using an Agilent Technologies 6890N GC-FID system (Palo Alto, CA, USA). The following conditions were used: injector temperature, 250 °C; detector temperature, 250 °C; carrier gas flow (He), 1 mL/min. The injections were made in split mode (split ratio 1:20) and the oven temperature was maintained at 40 °C for 5 min, then increased from 40 to 200 °C at 1.5 °C/min and eventually held for 20 min.

The identification of volatiles was carried out by CG coupled to ion-trap MS, for which a 3800 CG system fitted with a Saturn 2200 mass detector from Varian was employed. The compounds were separated on a CP24-MS column (30 m × 0.25 mm × 0.5 µm) from Varian (Walnut Creek, CA, USA). The temperature was held at 45 °C for 3.5 min, then raised to 230 °C at 2 °C/min and finally held for 5 min. The extracts were injected in splitless mode and helium at 1 mL/min was used as carrier. The mass spectra were obtained by electron impact at 70 eV and the 40–220 *m/z* region was scanned. The volatile compounds were identified by comparing the retention times and mass spectra to those of standards and to the library of mass spectra NIST 98 (Gaithersburg, MD, USA).

### 2.4. Analytical quality control

The quantification of the analytes was carried out by the internal standard method. The stock solutions of standards were made up in ethanol to a concentration of 1000 µg/mL and calibrations were made for each compound and by the three methods (LLE-I, LLE-II and SPE). For linearity studies, dose–response calibration curves were obtained with six standard solutions, considering the usual concentration ranges of the analytes in wines (0.5–50 mg/L for acids and carbonyl compounds; 0.5–150 mg/L for esters and alcohols; and 0.5–25 mg/L for volatile phenols, lactones and terpene alcohols). In this sense, it was noticed that the volatiles studied showed a good linearity in the range of concentrations studied, the regression coefficients (*r*) varying between 0.9917 (β-ionone) for LLE-I and 0.9999 (δ-decalactone) for LLE-I. The limits of detection, calculated as three times the relative standard deviation of the analytical blank

values obtained from the calibration curve, ranged from 0.010 mg/L (for ethyl lactate in LLE-I) to 0.44 mg/L (for diethyl succinate in LLE-II).

The repeatability (precision) was evaluated by the relative standard deviation of six independent assays performed under the same analytical conditions in the shortest period of time (UNE 82009-1:1998). To determine recoveries a series of six consecutive extractions were performed on the synthetic wine using the three extraction methods surveyed. For each volatile compound, the recovery rate was calculated by the ratio  $(C_1/C_2) \times 100$ , where  $C_1$  is the means of measured concentrations in sample, and  $C_2$  is the amount of the analyte added to model wine solution.

## 2.5. Statistics

All the statistical analyses were performed using the Statistica® v.6.0 [33] software.

## 3. Results and discussion

Up to 44 volatile compounds were studied, which were classified into seven different groups: (a) acids (phenylacetic acid, hexanoic acid, octanoic acid, and decanoic acid); (b) alcohols (2-butanol, isobutanol, isoamyl alcohol, Z-3-hexenol, furfuryl alcohol, benzyl alcohol, and 2-phenylethanol); (c) carbonyl compounds ( $\beta$ -ionone, acetaldehyde, 5-methylfurfural, and 5-hidroxyethylfurfural); (d)

**Table 1**  
Recovery (%R) and repeatability (%R.S.D.) of the extraction methods surveyed in the synthetic wine ( $n=6$ )

	LLE-I		LLE-II		SPE	
	R (%)	R.S.D. (%)	R (%)	R.S.D. (%)	R (%)	R.S.D. (%)
<b>Acids</b>						
Phenylacetic acid	107.8	1.6	54.3	>15	94.5	5.7
Hexanoic acid	90.8	12.4	86.7	8.9	57.7	5.2
Octanoic acid	100.3	9.6	27.6	>15	107.9	6.1
Decanoic acid	85.8	9.2	20.8	7.9	110.4	7.4
<b>Alcohols</b>						
2-Butanol	10.7	4.7	2.1	0.1	0.7	0.1
Isobutanol	62.9	3.0	13.7	13.9	3.1	>15
Isoamyl alcohol	97.6	5.0	47.2	14.0	61.1	10.4
Z-3-Hexenol	93.7	6.4	15.2	13.6	59.2	11.3
Furfuryl alcohol	53.3	6.7	16.7	>15	5.9	>15
Benzyl alcohol	83.5	8.4	17.7	13.9	38.8	10.7
2-Phenylethanol	92.6	8.7	18.6	13.2	96.5	9.2
<b>Carbonyl compounds</b>						
$\beta$ -Ionone	104.3	4.4	26.4	>15	100.9	4.6
Acetaldehyde	2.9	>15	12.9	9.0	4.6	6.8
5-Methylfurfural	81.5	6.8	19.9	13.2	47.0	10.8
5-Hidroxyethylfurfural	107.4	9.2	98.8	0.8	106.4	5.6
<b>Esters</b>						
Ethyl acetate	37.9	4.8	13.9	>15	3.5	3.0
Isobutyl acetate	87.9	1.7	15.0	11.7	78.1	6.6
Ethyl butyrate	94.2	2.3	24.1	13.5	69.5	6.7
Ethyl 2-methylbutyrate	91.0	3.4	16.5	13.4	88.4	5.8
Ethyl isovalerate	96.1	3.5	16.2	13.3	85.3	5.5
Butyl acetate	99.9	2.8	15.9	13.2	83.5	5.7
Isoamyl acetate	94.2	4.1	31.6	7.9	92.7	5.3
Ethyl hexanoate	99.7	6.8	25.1	12.9	95.3	4.6
Ethyl lactate	35.2	7.5	15.7	14.6	7.2	11.3
Ethyl octanoate	98.4	11.4	31.0	>15	90.9	4.1
Ethyl decanoate	51.1	1.6	10.2	>15	27.8	5.7
Diethyl succinate	94.3	5.0	42.5	13.5	95.4	7.0
Ethyl vanillate	76.1	9.1	20.6	13.1	113.7	6.8
<b>Volatile phenols</b>						
Guaiacol	25.2	8.9	5.1	12.6	33.6	5.4
<i>m</i> -Cresol	98.3	8.7	30.2	13.1	96.3	5.7
Isoeugenol	105.9	11.0	28.2	11.3	109.3	4.5
4-Vinylguaiacol	76.7	9.9	26.3	11.7	28.4	2.1
4-Vinyl-phenol	4.7	2.7	2.7	12.5	3.5	5.80
Vainillin	98.3	>15	27.4	12.0	91.7	4.8
4-Allyl-2,6-dimethoxy	103.1	11.4	10.1	>15	100.0	>15
Acetovanillone	96.4	9.8	18.2	12.8	94.0	4.8
<b>Lactones</b>						
$\gamma$ -Nonalactone	44.4	9.0	7.3	12.7	36.5	5.1
$\gamma$ -Decalactone	41.7	9.6	6.7	12.5	32.9	5.2
$\delta$ -Decalactone	98.9	10.2	14.1	>15	55.3	1.5
<b>Terpene alcohols</b>						
Linalol	109.6	8.3	19.7	13.5	98.7	4.9
Citronellol	97.2	9.5	19.4	14.2	88.9	5.0
Nerol	97.0	9.1	19.3	13.4	88.2	5.1
Geraniol	99.3	9.3	20.7	13.4	97.4	5.0
$\alpha$ -Terpineol	99.0	8.0	86.0	13.2	98.6	9.5



esters (ethyl acetate, isobutyl acetate, ethyl butyrate, ethyl 2-methylbutyrate, ethyl isovalerate, butyl acetate, isoamyl acetate, ethyl hexanoate, ethyl lactate, ethyl octanoate, ethyl decanoate, diethyl succinate, and ethyl vanillate); (e) volatile phenols (guaiacol, *m*-cresol, isoeugenol, 4-vinylguaiacol, 4-vinylphenol, vainillin, 4-allyl-2,6-dimethoxy, and acetovanillone); (f) lactones ( $\gamma$ -nonalactone,  $\gamma$ -decalactone, and  $\delta$ -decalactone); and (g) terpene alcohols (linalol, citronellol, nerol, geraniol, and  $\alpha$ -terpineol).

### 3.1. Volatile analysis of the synthetic wine

The average volatile compounds contents of the synthetic wine, which were used to assess the recoveries and repeatability of the extraction methods tested, are displayed in Table 1.

When the LLE-I method was followed, recoveries ranging from 3% to 109% (80% in average) were obtained. The lowest recoveries (<11%) were obtained for acetaldehyde, 4-vinylphenol and 2-butanol, whereas the highest ones corresponded to linalol, phenylacetic acid and 5-hydroxymethylfurfural. In any case, it was seen that overall, this was the methodology that led to the best recovery of volatiles. When the LLE-II method was used, the recovery levels fell within the bracket 2–99%, although the average recovery was roughly three-fold lower (27%), the lowest recoveries (<10%) corresponding to 4-vinyl-phenol, guaiacol, 2-butanol,  $\gamma$ -nonalactone and  $\gamma$ -decalactone, and the highest to hexanoic acid and 5-hydroxymethylfurfural. With regard to the SPE method surveyed, recoveries varying from 1% (2-butanol) to 114% (ethyl vanillate) were obtained with an average recovery of 68%.

The average recovery for the seven groups of volatiles mentioned earlier on achieved by each method is depicted in Fig. 1, from which it can be readily inferred that, overall, the highest recoveries corresponded to acids and terpene alcohols and the lowest to lactones and alcohols. Likewise, it was observed that LLE-I was again the best method in terms of recoveries by groups of volatile compounds. Similar recovery trends have been observed in previously published liquid–liquid extraction work [8]. Considering the LLE-I method it was observed that the highest recoveries were obtained for terpene alcohols (100%) and the lowest for lactones and alcohols (62% and 71%, respectively), whilst in the case of the other liquid–liquid extraction protocol tested (LLE-II), the highest and lowest recoveries (47% and 9%, respectively) corresponded to acids and lactones, in this order. As remarked above, the average recoveries obtained with the LLE-I method was some three-fold higher to that obtained with the LLE-II protocol, which illustrates to perfection the marked different ability of organic solvents to dissolve the wine volatiles and therefore the

need of develop a sensible extraction method to obtain meaningful conclusions when it comes to analyze such compounds. In this regard, it is important to stress that the choice of extraction solvents must be made as a function of the type of sample to be analyzed and the information required. Thus, Caldeira et al. [34] evaluated the effectiveness of seven different extraction solvents (dichloromethane, *n*-hexane, dichloromethane:diethyl ether [3:1 and 1:3], dichloromethane:*n*-hexane [3:1 and 1:3] and diethyl ether:*n*-hexane [1:3]) for the conventional LLE of whiskey volatile compounds and concluded that the highest extraction efficiency was achieved by using dichloromethane as extractant. On the other hand, López and Gómez [35] proposed a mixture dichloromethane:diethyl ether (1:1) for the LLE and analysis of monoterpenes in wine.

As far as the SPE method was concerned, the recoveries by groups of volatiles varied from 38% (alcohols) to 94% (terpene alcohols), which is in agreement with the conclusions reached by López et al. [26], who reported differences in the recoveries between volatile compounds related to their solid–liquid distribution coefficients, which are dependent on the polarity of the molecules. In any case, the overall mean recovery and those corresponding to the different groups of volatiles were intermediate between LLE-I and LLE-II.

Concerning the repeatability of the methods, the coefficients of variation (R.S.D.) corresponding to the LLE-I method only in two cases, specifically for acetaldehyde and vainillin, the R.S.D. values were over 15%. The lowest R.S.D. were obtained for phenylacetic acid, isobutyl acetate and ethyl decanoate. As for the LLE-II method, the lowest R.S.D. was obtained for 5-hydroxymethylfurfural, whereas up to nine compounds showed R.S.D. > 15% (corresponding to different groups of volatiles, specifically two acids, one alcohol, one carbonyl compounds, three esters, one volatile phenols and one lactone). In the case of the SPE method the highest R.S.D. values (>15%) corresponded to two alcohols (isobutanol and furfuryl alcohols) and 4-allyl-2,6-dimethoxy, whilst the lowest corresponded to  $\delta$ -decalactone (Table 1).

Taking into consideration the seven groups of volatile compounds, the SPE method was the best of the three tested in terms of precision and hence the method providing highest repeatability (Fig. 2). The average values of repeatability observed were 7.4%, 12.5% and 6.5% (for LLE-I, LLE-II and SPE, respectively), which agreed with the findings of other methods applied to wines. Thus, Ferreira et al. [36] developed a method based on SPE with R.S.D. values <10% and Ortega-Heras et al. [8] studied three extraction methods, liquid–liquid extraction, static headspace technique and a “stripping with nitrogen” (similar to the dynamic headspace technique), and obtained R.S.D. values of 1–10%, 2–12% and <15%, respectively.

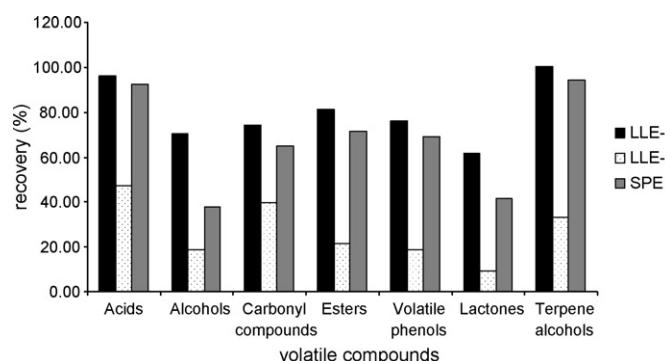


Fig. 1. Comparison of the relative recoveries for different groups of volatile compounds as a function of the extraction method.

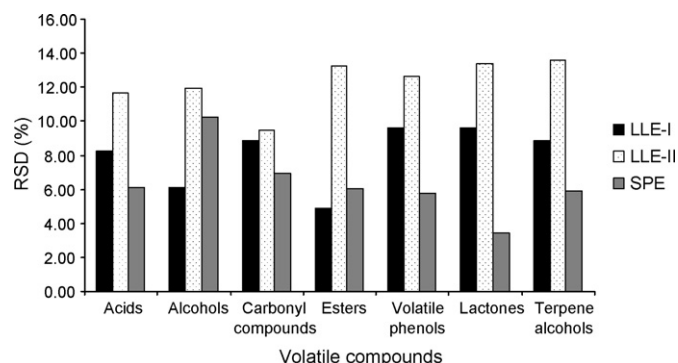


Fig. 2. Comparison of the coefficients of variation (R.S.D.) for different groups of volatile compounds as a function of the extraction method.

Other authors, like Castro et al. [37] obtained repeatability values <14% using rotatory-continuous liquid–liquid and headspace-SPME for the 30 volatile compounds considered, whereas Sieber et al. [38] observed R.S.D. values <5% when analyzing 31 fermentation-derived wine volatiles by HS-SPME-GC-MS. Fariña et al. [39], on their part, noticed repeatability values lower than 5% for volatile phenols using a novel extraction method, called “dispersive liquid–liquid microextraction”.

### 3.2. Volatile analysis of the commercial samples

The volatiles pattern of the commercially available wines surveyed was assessed by applying the three extraction methods, their levels being summarized in Table 2. Although many aroma compounds, such as alcohols, esters and acids, were common to all the samples, some others were more specific. In this sense, it was noticed that the Pedro Ximenez “cream” wine contained

**Table 2**  
Volatile contents (mg/L) in the white young wines studied<sup>a</sup>

	Zalema			Palomino Fino			Colombard		
	LLE-I	LLE-II	SPE	LLE-I	LLE-II	SPE	LLE-I	LLE-II	SPE
Phenylacetic acid	0.2 ± 0.1	0.1 ± 0.1	0.2 ± 0.0	nd	nd	nd	0.5 ± 0.0	0.3 ± 0.0	0.3 ± 0.0
Hexanoic acid	8.6 ± 0.7	8.0 ± 1.0	9.1 ± 0.4	1.4 ± 0.4	1.6 ± 0.7	1.9 ± 0.0	8.3 ± 0.3	7.9 ± 0.3	8.6 ± 0.1
Octanoic acid	15. ± 2.0	15.5 ± 3.3	13.4 ± 1.2	5.2 ± 0.9	5.2 ± 1.5	5.8 ± 0.0	8.5 ± 0.8	9.0 ± 0.8	12.3 ± 0.3
Decanoic acid	1.3 ± 0.0	1.7 ± 0.1	1.4 ± 0.0	0.7 ± 0.0	0.5 ± 0.1	0.6 ± 0.0	0.3 ± 0.0	0.4 ± 0.0	0.4 ± 0.0
∑ Acids	26.0	25.3	24.2	7.3	7.3	8.3	17.7	17.6	21.7
2-Butanol	0.7 ± 0.0	nd <sup>b</sup>	nd	nd	nd	nd	nd	nd	nd
Isobutanol	19.0 ± 0.1	20.9 ± 2.1	19.5 ± 0.1	27.3 ± 0.0	30.4 ± 0.9	28.8 ± 0.0	17.7 ± 0.2	15.4 ± 0.6	17.0 ± 0.1
Isoamyl alcohol	302.6 ± 3.0	240.6 ± 13.0	305.1 ± 1.2	310.5 ± 11.2	325.9 ± 18.1	318.4 ± 4.4	315.5 ± 14.2	326.4 ± 16.1	313.8 ± 4.2
Z-3-Hexenol	0.3 ± 0.1	0.3 ± 0.1	0.4 ± 0.0	0.4 ± 0.0	0.1 ± 0.0	0.4 ± 0.0	0.3 ± 0.0	0.2 ± 0.0	0.2 ± 0.0
Furfuryl alcohol	nd	nd	nd	0.1 ± 0.0	nd	nd	13.6 ± 0.1	13.1 ± 0.1	12.7 ± 0.0
Benzyl alcohol	0.1 ± 0.0	0.1 ± 0.0	0.1 ± 0.0	nd	nd	0.1 ± 0.0	7.9 ± 0.5	14.3 ± 0.8	36.6 ± 0.2
2-Phenylethanol	17.4 ± 0.9	16.7 ± 1.2	17.2 ± 0.3	14.2 ± 1.2	11.8 ± 2.9	15.9 ± 0.9	0.1 ± 0.0	0.1 ± 0.1	0.1 ± 0.0
∑ Alcohols	340.1	278.6	342.2	352.5	368.2	363.7	355.1	369.5	380.5
β-Ionone	nd	nd	nd	nd	nd	nd	nd	nd	nd
Acetaldehyde	1.7 ± 1.1	1.5 ± 0.1	1.6 ± 0.0	nd	nd	nd	0.6 ± 0.0	0.6 ± 0.1	0.0 ± 0.0
5-Methylfurfural	0.1 ± 0.0	0.0 ± 0.0	0.1 ± 0.0	1.4 ± 0.0	nd	1.4 ± 0.0	0.9 ± 0.1	0.4 ± 0.1	0.7 ± 0.0
5-Hydroxymethylfurfural	0.1 ± 0.0	nd	0.1 ± 0.0	0.7 ± 0.9	0.2 ± 2.8	0.1 ± 0.5	0.9 ± 0.1	0.6 ± 0.1	0.8 ± 0.0
∑ Carbonyl compounds	1.9	1.5	1.8	2.1	0.2	1.5	2.4	1.6	1.5
Ethyl acetate	8.3 ± 0.3	6.7 ± 0.6	6.1 ± 0.1	8.0 ± 0.3	8.1 ± 0.4	7.2 ± 0.1	8.9 ± 0.6	7.9 ± 0.8	9.6 ± 0.2
Isosobutyl acetate	0.1 ± 0.0	nd	0.0 ± 0.0	nd	nd	nd	0.0 ± 0.0	nd	nd
Ethyl butyrate	0.3 ± 0.3	0.5 ± 0.3	0.5 ± 0.3	0.6 ± 0.4	0.4 ± 0.5	0.4 ± 0.3	0.5 ± 0.2	0.4 ± 0.3	0.5 ± 0.2
Ethyl 2-methylbutyrate	0.5 ± 0.0	0.5 ± 0.0	0.4 ± 0.0	0.6 ± 0.1	0.9 ± 0.1	0.5 ± 0.1	0.5 ± 0.1	0.3 ± 0.1	0.3 ± 0.1
Ethyl isovalerate	0.2 ± 0.1	nd	0.0 ± 0.0	0.3 ± 0.0	nd	nd	1.8 ± 0.0	nd	nd
Butyl acetate	0.1 ± 0.1	nd	0.0 ± 0.0	0.1 ± 0.3	nd	nd	0.2 ± 0.5	nd	nd
Isoamyl acetate	2.0 ± 0.1	1.5 ± 0.5	1.5 ± 0.1	2.0 ± 0.2	1.6 ± 0.3	1.6 ± 0.1	1.4 ± 0.1	1.5 ± 0.3	1.2 ± 0.1
Ethyl hexanoate	1.5 ± 0.0	1.2 ± 0.1	0.8 ± 0.0	0.7 ± 0.1	0.6 ± 0.1	0.8 ± 0.0	0.9 ± 0.0	0.8 ± 0.1	0.9 ± 0.0
Ethyl lactate	25.0 ± 0.0	25.3 ± 0.4	24.4 ± 0.1	23.0 ± 0.0	20.1 ± 0.2	33.6 ± 0.0	25.1 ± 0.1	22.4 ± 0.2	24.3 ± 0.1
Ethyl octanoate	1.2 ± 0.1	0.8 ± 0.3	0.9 ± 0.1	0.8 ± 0.0	0.7 ± 0.1	0.8 ± 0.0	1.3 ± 0.0	1.2 ± 0.1	0.9 ± 0.0
Ethyl decanoate	1.0 ± 0.0	1.3 ± 0.9	1.0 ± 0.1	0.2 ± 0.1	0.2 ± 0.7	0.3 ± 0.1	nd	nd	nd
Diethyl succinate	6.5 ± 0.1	6.3 ± 0.1	6.0 ± 0.1	3.4 ± 0.1	1.8 ± 0.1	3.1 ± 0.1	nd	nd	nd
Ethyl vanillate	nd	nd	nd	nd	nd	nd	nd	nd	nd
∑ Esters	46.7	44.3	41.7	39.7	34.4	48.3	40.7	34.6	37.8
Guaiacol	nd	nd	nd	nd	nd	nd	nd	nd	nd
m-Cresol	0.0 ± 0.0	nd	nd	nd	nd	nd	nd	nd	nd
4-Vinylguaiacol	nd	nd	nd	nd	nd	nd	nd	nd	nd
4-vinylphenol	0.2 ± 0.0	nd	nd	0.2 ± 0.0	nd	0.1 ± 0.0	0.3 ± 0.0	nd	0.3 ± 0.0
Isoeugenol	0.0 ± 0.0	nd	nd	nd	nd	nd	0.1 ± 0.0	0.1 ± 0.0	0.1 ± 0.0
Vainillin	0.0 ± 0.0	nd	0.0 ± 0.0	nd	nd	nd	nd	nd	nd
4-Allyl-2,6-dimethoxy	0.1 ± 0.1	0.0 ± 0.1	0.0 ± 0.0	0.4 ± 0.1	0.5 ± 0.2	0.4 ± 0.3	nd	nd	nd
Acetovanillone	2.2 ± 0.3	2.1 ± 1.0	2.0 ± 0.5	nd	nd	nd	nd	nd	nd
∑ Volatile phenols	2.5	2.1	2.0	0.6	0.5	0.5	0.4	0.1	0.4
γ-Nonalactone	nd	nd	nd	nd	nd	nd	nd	nd	nd
γ-Decalactone	nd	nd	nd	nd	nd	0.1 ± 0.0	nd	nd	nd
δ-Decalactone	0.1 ± 0.0	nd	0.1 ± 0.0	0.1 ± 0.0	nd	0.9 ± 0.0	0.1 ± 0.0	nd	0.0 ± 0.0
∑ Lactones	0.1	nd	0.1	0.1	nd	0.9	0.1	nd	0.0
Linalol	nd	nd	nd	0.1 ± 0.2	nd	nd	0.7 ± 0.0	nd	nd
Citronellol	nd	nd	nd	0.0 ± 0.0	0.0 ± 0.1	0.0 ± 0.0	0.3 ± 0.0	0.4 ± 0.2	0.3 ± 0.1
Nerol	0.0 ± 0.0	nd	nd	nd	nd	nd	nd	nd	nd
Geraniol	nd	nd	nd	nd	nd	nd	nd	nd	nd
α-Terpineol	nd	nd	nd	nd	nd	nd	nd	nd	nd
∑ Terpene alcohols	0.0	nd	nd	0.1	0.0	0.0	0.4	0.4	0.3

<sup>a</sup> Means ± S.D.

<sup>b</sup> Not detected.

lactones, guaiacol,  $\alpha$ -terpineol and  $\beta$ -ionone and that geraniol was only detected in Syrah wines. On the other hand, ethyl vainillate was not found at detectable levels in the samples analyzed.

The existence or not of significant differences in the levels of volatiles detected as a function of the extraction methods was evaluated by the analysis of variance (ANOVA), after which it was concluded that there were statistically significant differences ( $p < 0.05$ ) between the pairs of methods LLE-I-LLE-II and LLE-II-SPE.

Taking into account the white wines analyzed, it was noticed that the LLE-I method was the more sensitive in all the cases. In this sense, such method led to the detection of 33 volatile compounds in the Zalema wine, whilst with the LLE-II and the SPE methods, only 22 and 28 aroma compounds were detected, respectively. As for the Palomino Fino and Colombard wines, the number of volatiles detected with each extraction method were 26, 19 and 24 and 28, 22 and 24, respectively, for LLE-I, LLE-II and SPE (Table 2).

**Table 3**  
Volatile contents (mg/L) in the red young wines and Pedro Ximenez wines studied<sup>a</sup>

	Syrah			Pedro Ximenez		
	ELL-I	ELL-II	SPE	ELL-I	ELL-II	SPE
Phenylacetic acid	0.0 ± 0.0	nd <sup>b</sup>	nd	0.0 ± 0.0	nd	nd
Hexanoic acid	0.5 ± 0.2	0.4 ± 0.4	0.6 ± 0.0	0.2 ± 0.0	nd	0.2 ± 0.0
Octanoic acid	3.6 ± 0.2	3.6 ± 0.7	3.2 ± 0.1	2.5 ± 0.0	2.7 ± 0.1	2.5 ± 0.1
Decanoic acid	0.0 ± 0.0	0.0 ± 0.0	0.1 ± 0.0	0.0 ± 0.0	0.4 ± 0.0	0.1 ± 0.0
∑ Acids	4.1	4.0	3.9	2.8	3.1	2.8
2-Butanol	0.4 ± 0.0	nd	nd	nd	nd	nd
Isobutanol	40.7 ± 0.2	50.5 ± 0.6	44.7 ± 0.1	11.2 ± 0.6	13.8 ± 0.5	30.8 ± 0.0
Isoamyl alcohol	382.1 ± 10.1	339.3 ± 11.7	380.3 ± 0.6	149.8 ± 3.9	131.0 ± 4.9	149.2 ± 0.2
Z-3-hexenol	0.2 ± 0.0	0.1 ± 0.1	0.2 ± 0.0	0.1 ± 0.0	nd	0.1 ± 0.0
Furfuryl alcohol	0.2 ± 0.0	nd	0.3 ± 0.0	0.4 ± 0.0	nd	nd
Benzyl alcohol	0.2 ± 0.1	0.2 ± 0.1	0.2 ± 0.0	1.1 ± 0.0	1.2 ± 0.1	1.3 ± 0.0
2-Phenylethanol	22.8 ± 0.2	21.7 ± 0.4	23.7 ± 0.2	9.9 ± 0.3	12.0 ± 0.8	12.1 ± 0.3
∑ Alcohols	446.6	411.7	449.4	172.4	158.0	193.4
β-Ionone	nd	nd	nd	4.3 ± 0.0	2.7 ± 0.1	4.0 ± 0.0
Acetaldehyde	2.1 ± 0.1	2.3 ± 0.7	2.2 ± 0.0	3.9 ± 0.5	2.1 ± 0.3	3.0 ± 0.0
5-Methylfurfural	0.5 ± 0.1	0.3 ± 0.3	0.5 ± 0.1	26.5 ± 0.0	21.9 ± 0.1	26.8 ± 0.0
5-Hidroxymethylfurfural	30.7 ± 0.9	22.8 ± 1.1	29.4 ± 0.8	29.8 ± 2.4	18.5 ± 2.7	24.4 ± 0.5
∑ Carbonyl compounds	33.3	25.5	32.1	64.5	45.1	58.2
Ethyl acetate	58.1 ± 1.6	52.1 ± 1.8	53.3 ± 0.4	9.8 ± 1.0	3.3 ± 0.8	9.6 ± 0.5
Isobutyl acetate	0.0 ± 0.0	0.0 ± 0.0	0.0 ± 0.0	0.0 ± 0.0	nd	nd
Ethyl butyrate	0.4 ± 0.1	0.4 ± 0.1	0.4 ± 0.0	0.3 ± 0.0	nd	0.3 ± 0.0
Ethyl 2-methylbutyrate	5.6 ± 0.1	3.9 ± 0.2	5.4 ± 0.1	0.6 ± 0.1	0.1 ± 0.1	0.5 ± 0.0
Ethyl isovalerate	0.1 ± 0.3	nd	nd	0.8 ± 0.0	0.9 ± 0.1	0.9 ± 0.0
Butyl acetate	0.0 ± 0.1	nd	nd	0.5 ± 0.0	nd	0.1 ± 0.0
Isoamyl acetate	0.6 ± 0.0	0.3 ± 0.2	0.5 ± 0.0	0.2 ± 0.0	nd	0.3 ± 0.0
Ethyl hexanoate	0.2 ± 0.0	0.1 ± 0.1	0.1 ± 0.0	0.1 ± 0.0	nd	nd
Ethyl lactate	81.0 ± 2.0	68.6 ± 2.1	87.1 ± 0.1	18.2 ± 1.7	12.0 ± 1.7	12.2 ± 0.3
Ethyl octanoate	0.5 ± 0.1	0.4 ± 0.2	0.3 ± 0.1	0.2 ± 0.0	0.3 ± 0.0	0.1 ± 0.0
Ethyl decanoate	0.7 ± 0.2	8.6 ± 0.1	0.8 ± 0.0	1.0 ± 0.0	5.3 ± 0.0	0.6 ± 0.0
Diethyl succinate	9.9 ± 0.8	8.9 ± 5.5	9.0 ± 0.4	29.5 ± 0.8	13.8 ± 2.7	30.5 ± 0.6
Ethyl vainillate	nd	nd	nd	nd	nd	nd
∑ Esters	157.0	143.4	156.9	61.2	35.7	55.0
Guaiacol	nd	nd	nd	0.2 ± 0.0	0.3 ± 0.0	0.2 ± 0.0
m-Cresol	0.0 ± 0.0	nd	nd	0.2 ± 0.0	nd	0.5 ± 0.0
4-Vinylguaiacol	nd	nd	nd	0.0 ± 0.0	nd	nd
4-Vinylphenol	nd	nd	nd	0.5 ± 0.0	0.3 ± 0.2	0.4 ± 0.0
Isoeugenol	nd	nd	nd	1.1 ± 0.0	0.7 ± 0.1	1.3 ± 0.0
Vainillin	0.2 ± 0.3	nd	0.2 ± 1.1	nd	nd	nd
4-Allyl-2,6-dimethoxy	0.5 ± 0.3	0.5 ± 0.7	0.7 ± 1.8	0.9 ± 0.2	0.8 ± 0.2	1.5 ± 0.1
Acetovanillone	nd	nd	nd	3.9 ± 0.0	0.6 ± 0.0	0.2 ± 0.0
∑ Volatile phenols	0.7	0.5	0.9	6.9	2.7	4.1
γ-Nonalactone	nd	nd	nd	0.1 ± 0.0	nd	0.1 ± 0.0
γ-Decalactone	nd	nd	nd	0.4 ± 0.2	0.4 ± 0.7	0.5 ± 0.2
δ-Decalactone	0.0 ± 0.0	nd	0.0 ± 0.0	0.1 ± 0.0	0.1 ± 0.0	0.1 ± 0.0
∑ Lactones	0.0	nd	0.0	0.6	0.5	0.7
Linalol	0.2 ± 0.0	0.2 ± 0.1	0.2 ± 0.1	0.7 ± 0.0	0.6 ± 0.3	0.6 ± 0.0
Citronellol	nd	nd	nd	nd	nd	nd
Nerol	nd	nd	nd	nd	nd	nd
Geraniol	0.7 ± 0.0	0.6 ± 0.0	0.5 ± 0.0	nd	nd	nd
α-Terpineol	nd	nd	nd	0.3 ± 0.0	0.2 ± 0.0	0.1 ± 0.0
∑ Terpene alcohols	0.9	0.8	0.7	1.0	0.8	0.7

<sup>a</sup> Means ± S.D.

<sup>b</sup> Not detected.

Considering the aroma compounds by groups, the alcohols were the predominant volatiles in white wines (85% of total analyzed volatile components), followed by esters (10% of total analyzed) and acids (4% of total analyzed), the two first groups, produced during the alcoholic fermentation, playing an important role in the flavor of wines [40]. These results are in agreement with previous studies reporting that the alcohol fraction made up 80–90% of the volatile content of wines [41], these compounds being easily recognizable by their strong and pungent smell and taste, related to herbaceous notes [42]. As for the esters, they are regarded as very important in the aroma of young wines and in relation to the fruity flavors of wine [43]. Considering individual compounds, it was noticed that the predominant ones were isoamyl alcohol and ethyl lactate.

Other minor groups of aroma compounds detected were carbonyl compounds, volatile phenols, terpene alcohols and lactones, which represented 0.5–1% of the aromatic content of wines. The volatile phenols were relatively important in the flavor of Zalema wines (0.6% of the total analyzed volatile compounds). Other compounds detected, such as ethylphenols are responsible for animal and smoky odours, whilst vinylphenols are regarded as responsible for heavy pharmaceutical odours [44].

The LLE-I method also proved to be the most sensitive protocol for the extraction of aroma compounds in the Syrah young red wine. As it can be seen in Table 3, LLE-I allowed for the identification of 32 volatile compounds, whereas only 24 and 27 could be detected through the application of the LLE-II and SPE methods, respectively. The predominant aroma compounds were also the alcohols (70% of the total volatiles), followed by esters (24% of the total volatiles) and carbonyl compounds (5% of the total volatiles). Other groups, such as acids, volatile phenols, terpene alcohols and lactones made up less than 1% of the aromatic content of the samples. Considering individual compounds, isoamyl alcohol turned out to be the major volatile, followed by two esters, ethyl lactate and ethyl acetate, which was in agreement with the data reported elsewhere for other red wines [45,46]. The predominant carbonyl compounds identified were 5-hidroxymethylfurfural and acetaldehyde, whereas,  $\beta$ -ionone was not found at detectable levels in the Syrah wine. As for the terpene alcohols, only linalol and geraniol were detected, despite Piñero et al. [47] found linalol, nerol and terpineol in young Syrah wines from grapes grown in Jerez (Spain) using SPE. As far as the acids were concerned, the highest levels corresponded to octanoic and hexanoic acids and the lowest ones to phenylacetic acid.

Regarding the Pedro Ximenez wine, LLE-I was also the most efficient extraction method, allowing for the detection of up to 38 volatile compounds, twelve more than the LLE-II method and 5 more than the SPE one. In this case, the alcohols were again the predominant aroma compounds (60% of the total volatile compounds), followed in this case by carbonyl compounds (19% of the total) and esters (17% of the total volatile content). Other groups like acids and volatile phenols represented less than 1.6% of the aromatic content, whereas the contribution of terpene alcohols and lactones was even lower (less than 0.5% of the volatile content). The major individual aroma compounds were isoamyl alcohol, 5-hidroxymethylfurfural, diethyl succinate and 5-methylfurfural, although the levels of linalol, which has been reported to be the most important aroma compound of these wines [48], were also remarkable.

In conclusion, it was noticed that the method leading to higher recoveries was LLE-I, which also allowed a greater number of aroma compounds to be extracted. Nonetheless, the SPE method exhibited a higher repeatability, which added to its inherent advantages, such as a lower extraction times and solvent consumptions makes

of it another method of choice for the extraction of wine aromas. In any case, LLE-II was the least convenient extraction method for the analysis of the volatiles of the wines surveyed. In this sense, statistically significant differences between the pairs LLE-I-LLE-II and LLE-II-SPE were found.

## Acknowledgement

The authors would like to thank Priska Marrow for his technical assistance with the English version of the manuscript.

## References

- [1] P.X. Etievant, Crit. Rev. Food Sci. Nutr. 36 (1996) 733.
- [2] J. Diez, R. Cela, J.A. Perez-Bustamante, Am. J. Enol. Vitic. 36 (1985).
- [3] C. de la Presa-Owens, R.M. Lamuela-Raventos, S. Buxaderas, M.C. de la Torre, Am. J. Enol. Vitic. 36 (1985).
- [4] J. Villen, F.J. Señorans, G. Reglero, M. Herraiz, J. Agric. Food Chem 43 (1995) 717.
- [5] Y. Zhou, R. Riesen, C.S. Gilpin, J. Agric. Food Chem. 44 (1996) 818.
- [6] R. Schneider, R. Baumes, C. Bayonove, A. Razungles, J. Agric. Food Chem. 46 (1998) 3230.
- [7] V. Lavigne, R. Henry, D. Dubourdieu, Sci. Aliment 18 (1998) 175.
- [8] M. Ortega-Heras, M.L. González-San José, S. Beltrán, Anal. Chim. Acta 458 (2002) 85.
- [9] S. Rocha, F. Rodrigues, P. Coutinho, I. Delgadillo, M. Coimbra, Anal. Chim. Acta 513 (2004) 257.
- [10] S. Cabredo-Pinillos, T. Cedrón-Fernández, M. González-Briongos, L. Puente-Pascual, C. Sáenz-Barrio, Talanta 69 (2006) 1123.
- [11] A. Genovese, A. Gambuti, P. Piombino, L. Moio, Food Chem. 103 (2007) 1228.
- [12] D.R. Webster, C.G. Edwards, S.E. Spayd, J.C. Peterson, B.J. Seymor, Am. J. Enol. Vitic. 44 (1993) 275.
- [13] Ch.S. Cobb, M.M. Bursley, J. Agric. Food Chem. 26 (1978) 197.
- [14] M.E. Mamede, G.M. Pastore, Food Chem. 96 (2006) 586.
- [15] D. Hernanz, F.J. Heredia, R. Beltrán, M.A.F. Recamales, Talanta 50 (1999) 413.
- [16] M.S. Pérez-Coello, M.A. González-Viñas, E. García-Romero, Díaz-Maroto, M.D. Cabezu, Food Control 14 (2003) 301.
- [17] G.P. Blanch, G. Reglero, M. Herraiz, J. Agric. Food Chem. 43 (1995) 1251.
- [18] A. Razungles, E.H. Tarhi, R. Baumes, Z. Gunnata, C. Tapiero, C. Bayonove, Sci. Aliment 14 (1994) 725.
- [19] M.D. Luque, F. Priego-Capote, Talanta 72 (2007) 321.
- [20] C. Cocito, G. Gaetano, C. Delfini, Food Chem. 52 (1995) 311.
- [21] J. Ruiz-Jiménez, M.D. Luque, Anal. Chim. Acta 489 (2003) 1.
- [22] M. Rostagno, M. Palma, C.G. Barroso, J. Chromatogr. A 1012 (2003) 119.
- [23] A. Liazid, M. Palma, J. Brigu, C.G. Barroso, Talanta 71 (2007) 976.
- [24] T.G. Kazi, M.K. Jamali, A. Siddiqui, G.H. Kazi, M.B. Arain, H.I. Afridi, Chemosphere 63 (2006) 411.
- [25] I. Moret, Analyst 120 (1995) 2561.
- [26] R. López, M. Aznar, J. Cacho, V. Ferreira, J. Chromatogr. A 966 (2002) 167.
- [27] V. Ferreira, R. López, J. Cacho, J. Sci. Food Agric. 80 (2000) 1659.
- [28] A.P. Pollnitz, G.P. Jones, M.A. Sefton, J. Chromatogr. A 857 (1999) 239.
- [29] L. Setkova, S. Risticvic, J. Pawliszyn, J. Chromatogr. A 1147 (2007) 213.
- [30] M.C. Díaz-Maroto, E. Sánchez-Palomo, M. Pérez-Coello, J. Agric. Food Chem. 52 (2004) 6857.
- [31] J. Marín, A. Zalacain, C. Miguel, G.L. Alonso, M.R. Salinas, J. Chromatogr. A 1098 (2005) 1.
- [32] B.T. Weldegergis, A.G. Tredoux, A. Crouch, J. Agric. Food Chem. 55 (2007) 8696.
- [33] StatSoft Inc., Statistica 6.0 for Windows Computer Program Manual, Tulsa, OK, 2001.
- [34] M. Caldeira, F. Rodrigues, R. Perestrelo, J.C. Marques, J.S. Cámara, Talanta 74 (2007) 78.
- [35] E.F. López, E.F. Gómez, Chromatographia 52 (2000) 798.
- [36] V. Ferreira, M. Sharman, J. Cacho, J. Dennis, Chromatography A. 731 (1996) 247.
- [37] R. Castro, R. Natera, P. Benitez, C.G. Barroso, Anal. Chim. Acta 513 (2004) 141.
- [38] T.E. Sieber, H.E. Smyth, D.L. Capone, C. Neuwöhner, K. Pardon, G. Skouroumounis, M. Herderich, M. Sefton, A. Pollnitz, Anal. Bional. Chem. 381 (2005) 937.
- [39] L. Fariña, E. Boido, F. Carrau, E. Dellacassa, J. Chromatography A. 1157 (2007) 46.
- [40] E. Valero, L. Moyano, M.C. Millán, M. Medina, J.M. Ortega, Food Chem. 78 (2002) 57.
- [41] L. Usseglio-Tomasset, Química Enológica, Mundi-prensa, Madrid, Spain, 1998.
- [42] M.J. Gómez-Míguez, J.F. Cacho, V. Ferreira, I. Vicario, F.J. Heredia, Food Chem. 100 (2006) 1464.
- [43] A. Rapp, H. Mandery, Experientia 42 (1986) 873.
- [44] R. Castro, R. Natera, M.V. García, C.G. Barroso, J. Chromatogr. A 995 (2003) 11.
- [45] C. Ortega, R. López, J. Cacho, V. Ferreira, Chromatography A. 923 (2001) 205.
- [46] M. Gil, J.M. Cabelles, T. Arroyo, M. Prodanov, Anal. Chim. Acta 563 (2006) 145.
- [47] Z. Piñero, R. Natera, R. Castro, M. Palma, B. Puertas, C.G. Barroso, Anal. Chim. Acta 563 (2006) 165.
- [48] E.M. Campo, R. López, V. Ferreira, Develop. Food Sci. 43 (2006) 213.



# Simultaneous determination of gibberellic acid, indole-3-acetic acid and abscisic acid in wheat extracts by solid-phase extraction and liquid chromatography–electrospray tandem mass spectrometry

Shengjie Hou<sup>a,b</sup>, Jiang Zhu<sup>b</sup>, Mingyu Ding<sup>a,\*</sup>, Guohua Lv<sup>c</sup>

<sup>a</sup> Key Lab of Bioorganic Phosphorus Chemistry & Chemical Biology, Ministry of Education, Department of Chemistry, Tsinghua University, Beijing 100084, China

<sup>b</sup> College of Resources & Environment, Anhui Agricultural University, Hefei 230036, China

<sup>c</sup> Key Laboratory of Water Cycle and Related Land Surface Processes, Institute of Geographic Sciences and Natural Resources Research, Chinese Academy of Sciences, Beijing 100101, China

## ARTICLE INFO

### Article history:

Received 20 February 2008

Received in revised form 7 April 2008

Accepted 12 April 2008

Available online 24 April 2008

### Keywords:

Liquid chromatography–tandem mass spectrometry

Solid-phase extraction

Gibberellic acid

Indole-3-acetic acid

Abscisic acid

## ABSTRACT

A liquid chromatography–tandem mass spectrometry (LC–MS/MS) method was developed for simultaneous determination of three representative phytohormones in plant samples: gibberellic acid (GA<sub>3</sub>), indole-3-acetic acid (IAA) and abscisic acid (ABA). A solid-phase extraction (SPE) pretreatment method was used to concentrate and purify the three phytohormones of different groups from plant samples. The separation was carried out on a C<sub>18</sub> reversed-phase column, using methanol/water containing 0.2% formic acid (50:50, v/v) as the isocratic mobile phase at the flow-rate of 1.0 mL min<sup>-1</sup>, and the three phytohormones were eluted within 7 min. A linear ion trap mass spectrometer equipped with electrospray ionization source was operated in negative ion mode. Selective reaction monitoring (SRM) was employed for quantitative measurement. The SRM transitions monitored were as 345 → 239, 301 for GA<sub>3</sub>, 174 → 130 for IAA and 263 → 153, 219 for ABA. Good linearities were found within the ranges of 5–200 μg mL<sup>-1</sup> for IAA and 0.005–10 μg mL<sup>-1</sup> for ABA and GA<sub>3</sub>. Their detection limits based on a signal-to-noise ratio of three were 0.005 μg mL<sup>-1</sup>, 2.2 μg mL<sup>-1</sup> and 0.003 μg mL<sup>-1</sup> for GA<sub>3</sub>, IAA and ABA, respectively. Good recoveries from 95.5% to 102.4% for the three phytohormones were obtained. The results demonstrated that the SPE–LC–MS/MS method developed is highly effective for analyzing trace amounts of the three phytohormones in plant samples.

© 2008 Elsevier B.V. All rights reserved.

## 1. Introduction

Phytohormones are regulators produced by plants themselves, which control the physiological processes. As a minor component of the metabolome, phytohormones are of particular significance given their role in the regulation of germination, growth, reproduction, and the protective responses of plants against stress. [1] Phytohormones are usually classified into four groups: auxines, gibberellins, cytokinins and inhibitors [2]. Gibberellic acid (GA<sub>3</sub>), indole-3-acetic acid (IAA) and abscisic acid (ABA) are the chief representatives of gibberellins, auxines and inhibitors, respectively. The quantitative analysis of the three phytohormones is often required in agriculture and plant physiology. However, many researches until now have focused on a specific phytohormone or certain group of phytohormones but ignored the others. There is

little information available on the simultaneous determination of several phytohormones of different groups.

It is usually rather difficult to determine phytohormones in plant tissues owing to their presence in trace amounts and to the coexistence of a wide variety of interferents. Therefore, it is very important to develop simple and reliable purification procedures for the accurate determination of the three phytohormones. Common purification procedures such as liquid-phase extraction (LPE) [3], solid-phase extraction (SPE) [4–9], vapor-phase extraction [10] and solid-phase microextraction [11] have been employed for the purification of phytohormones in plants. However, LPE is extremely expensive and adverse to the environment and human health due to the use of large amounts of organic solvents.

Several methods have been used for the analysis of phytohormones. Among them, high performance liquid chromatography (HPLC) coupled to ultraviolet (UV) [5] or fluorescence [12] or coulometric detection [13] has been described and immunoassay [14,15] has also been employed. Mass spectrometry (MS) is the most powerful detector for the determination of phytohormones due to

\* Corresponding author. Tel.: +86 10 62797087; fax: +86 10 62782485.  
E-mail address: [dingmy@mails.tsinghua.edu.cn](mailto:dingmy@mails.tsinghua.edu.cn) (M. Ding).

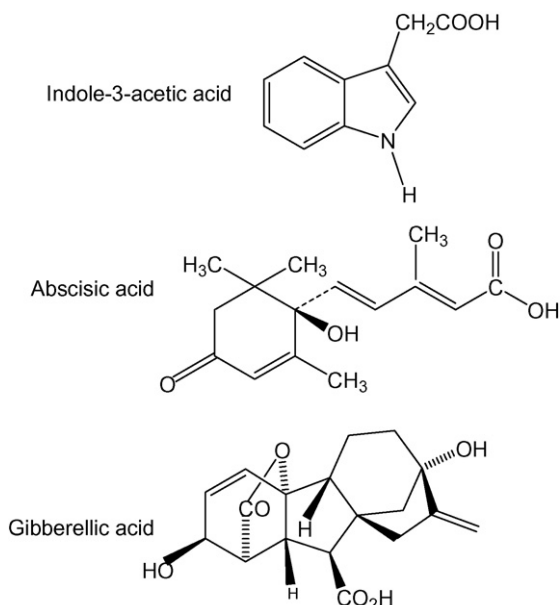


Fig. 1. The structures of GA<sub>3</sub>, IAA and ABA.

its high sensitivity and selectivity. Gas chromatography coupled to mass spectrometry (GC–MS) [6,7,16,17] was also reported. The shortages with GC–MS method were that not only was a prior derivatization required to enhance volatility, but also the high temperatures reached in GC injector and column could decompose the labile phytohormones.

In recent years, liquid chromatography–electrospray ionization tandem mass spectrometry (LC–ESI–MS/MS) has been applied to the determination of IAA [3,8,9,18] and ABA [3,9,18–20] in plant samples, but the determination of GA<sub>3</sub> [9] in LC–ESI–MS/MS has been reported rarely. In this study, the validity of LC–UV to determine the three phytohormones was tested. This detection method was not sensitive and was not able to separate target analytes from co-extractives. In LC–ESI–MS/MS, however, the interference from co-extractives was reduced dramatically by using selected reaction monitoring (SRM). This method was specific and sensitive and did not require chemical derivatization of analytes.

In the present study, the main objectives were to simplify the procedures of extraction and purification and to develop a rapid and sensitive detection method for the determination of the three acidic phytohormones. The conditions of SPE have been optimized. The efficiency of two different extraction solutions for the three phytohormones has also been discussed. In addition, to illustrate the validity of the present method, different plant materials have been used.

## 2. Experimental

### 2.1. Chemicals and reagents

GA<sub>3</sub>, IAA and ABA were purchased from Sigma (St. Louis, MO, USA). The structures of the three phytohormones are shown in Fig. 1. Purified water from a Milli-Q system from Millipore Corp. (Bedford, MA, USA) and analytical reagent grade chemicals were used. Benzoic acid was used as internal standard (ISTD). Stock solutions of the three phytohormones and ISTD (1 g L<sup>-1</sup>) were prepared with 20% methanol in water containing 0.1% formic acid and maintained at 4 °C in a refrigerator. The four stock solutions were then further diluted by 20% methanol in water containing 0.1% formic

acid to yield appropriate working solutions. C<sub>18</sub> SPE cartridges (3 mL, 500 mg) were obtained from Varian (Palo Alto, CA, USA).

### 2.2. Plant materials

Plant samples were obtained by cultivating wheat seeds in circular tray covered with clean papers for 4, 6 and 13 days, respectively. A constant dampness with tap water at 25 °C and a controlled light condition of 16 h light and 8 h darkness were kept. The young wheat plants for 4, 6 and 13 days were at the growth stages of bud, one leaf and two leaves, respectively. The wheat plants at different growth stages were halved into overground tissues and roots for analysis.

### 2.3. Chromatographic and mass procedures

The experiment was performed on a Finnigan LC–MS/MS system (Thermo Electron, San Jose, CA, USA) consisting of a surveyor autosampler, a surveyor MS pump and a Finnigan LTQ linear ion trap mass spectrometer equipped with an ESI source that was operated in negative mode. The data acquisition software used was Xcalibur. The LC separation was carried out by an HiQ Sil C<sub>18</sub> column (250 mm × 4.6 mm i.d., 5 μm). The three phytohormones were eluted isocratically with methanol/water containing 0.2% formic acid (50:50, v/v) at the flow-rate of 1.0 mL min<sup>-1</sup>. The injector volume selected was 25 μL. LC–MS/MS conditions were as follows: ESI spray voltage, 4 kV; sheath gas flow-rate, 70 arb; auxiliary gas flow-rate, 20 arb; capillary voltage, –38 V; capillary temperature, 350 °C and tube lens, 95 V. The SRM mode was used for the determination of the three phytohormones. GA<sub>3</sub>, IAA and ABA were monitored at *m/z* transitions of 345 → 239, 301; 174 → 130 and 263 → 153, 219, respectively. The optimized collision energies for GA<sub>3</sub>, IAA and ABA were 21, 28 and 20 eV, respectively. Selected ion monitoring (SIM) mode was used for the determination of ISTD. ISTD was monitored at *m/z* 121.

### 2.4. Extraction and purification procedures

Plant samples were snipped and ground to fine powder in the presence of liquid nitrogen. Subsequently, 2 g powdered plant materials were extracted at 4 °C for 12 h with either 20 mL deionized water or 20 mL 80% methanol [3,19]. In both cases, before any extraction was performed, 100 μg ISTD was added. The extract was centrifuged at 4 °C at 3000 rpm for 15 min. When water was used as an extractant, the supernatant was passed directly through a C<sub>18</sub> cartridge preconditioned with 3 mL deionized water, followed by 3 mL methanol. When 80% methanol was used as an extractant, the methanol was evaporated in vacuum at room temperature, and then the aqueous residue was adjusted to 20 mL with water before passed through a preconditioned C<sub>18</sub> cartridge. Both cartridges were washed with 1 mL 20% methanol containing 0.1% (v/v) formic acid and the retained phytohormones were eluted with 1 mL 80% methanol.

These SPE conditions were optimized after a deep study, shown in Section 3, the same for optimization of chromatographic conditions and SRM detection.

## 3. Results and discussion

### 3.1. Optimization of LC–ESI–MS/MS conditions

In the study, the full mass spectra of the three phytohormones showed that [M–H]<sup>-</sup> ions were the most intensive at *m/z* 345 for GA<sub>3</sub>, *m/z* 174 for IAA, *m/z* 263 for ABA, and *m/z* 121 for ISTD, so they were chosen as precursor ions for the phytohormones. In the product ions spectra (Fig. 2, 2a for GA<sub>3</sub>, 2b for IAA and 2c for

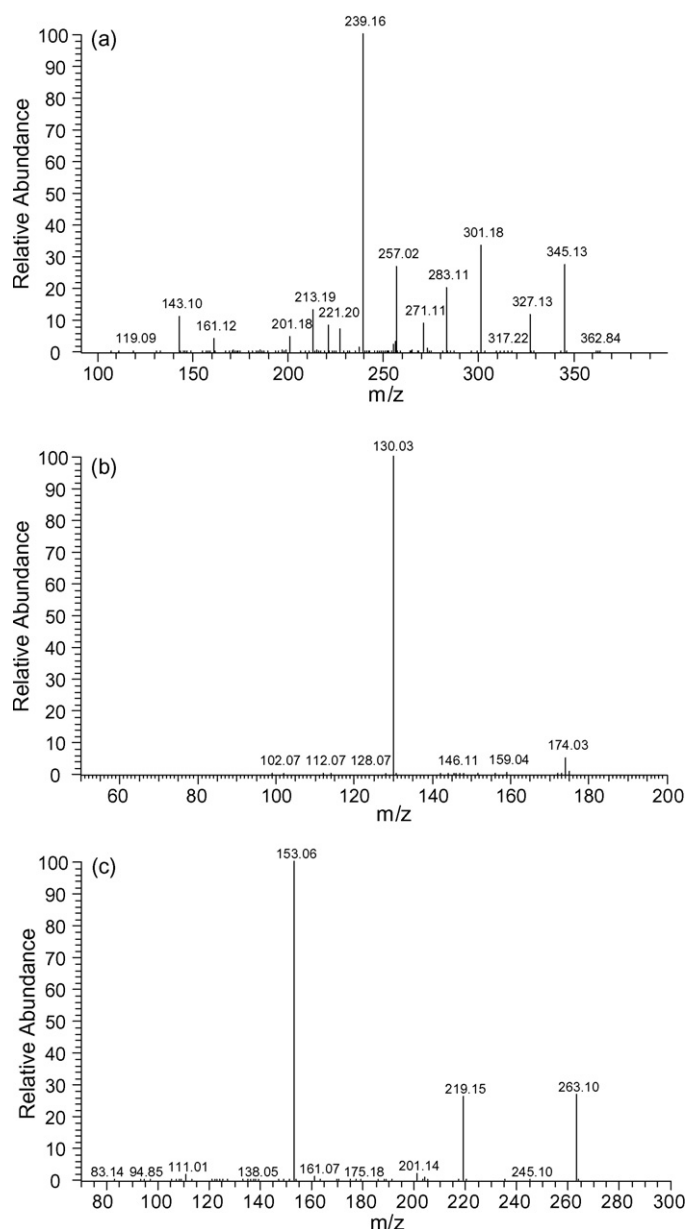


**Fig. 2.** Negative ion MS/MS spectra from LC-ESI-MS/MS analysis of GA<sub>3</sub> (2a), IAA (2b) and ABA (2c).

ABA), [M–H–COO–COO–H<sub>2</sub>O]<sup>–</sup> ion (*m/z* 239) and [M–H–COO]<sup>–</sup> ion (*m/z* 301) for GA<sub>3</sub>, [M–H–COO]<sup>–</sup> ion (*m/z* 130) for IAA and [M–H–C<sub>6</sub>H<sub>6</sub>O<sub>2</sub>]<sup>–</sup> ion (*m/z* 153) and [M–H–COO]<sup>–</sup> ion (*m/z* 219) for ABA were selected in SRM acquisition respectively, because they displayed better intensities.

The three phytohormones were separated using a C<sub>18</sub> column with water/methanol isocratic elution. With the addition of formic acid, chromatographic separation was improved greatly with sharper peak shape and better peak symmetry of the three phytohormones, because formic acid converted the three acidic phytohormones from the anionic forms to the neutral ones. A typical LC-ESI-MS/MS chromatogram of a mixed standard solution containing 50 μg mL<sup>–1</sup> GA<sub>3</sub>, IAA and ABA under SRM conditions is shown in Fig. 3. GA<sub>3</sub>, IAA, ABA and ISTD were eluted at 4.14 ± 0.04 min, 5.21 ± 0.03 min, 6.76 ± 0.05 min and 6.07 ± 0.05 min, respectively. In the GA<sub>3</sub> standard chromatogram, a minor peak occurred at 3.70 min, which could be the GA<sub>3</sub> isomeric

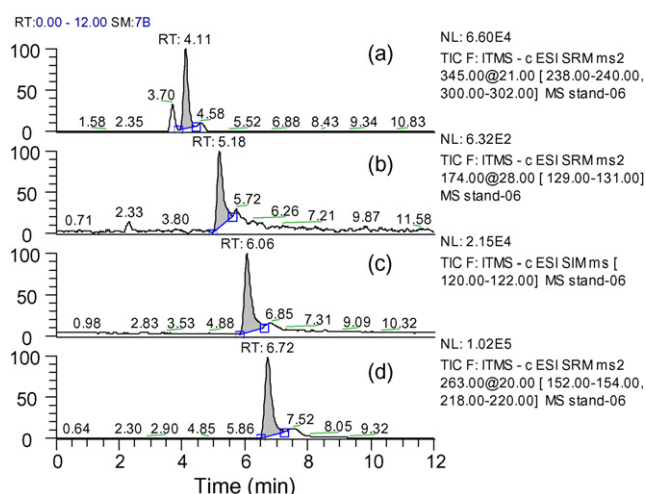


**Fig. 3.** Typical LC-ESI-MS/MS chromatogram of a mixed standard solution containing 50 μg mL<sup>–1</sup> GA<sub>3</sub>, IAA, ABA and ISTD: (3a) GA<sub>3</sub>, 345 → 239, 301 transition; (3b) IAA, 174 → 130 transition; (3c) ISTD, 121; (3d) ABA, 263 → 153, 219 transition.

compound. In addition, benzoic acid instead of labeled isotope was used as internal standard. It is noteworthy that benzoic acid as internal standard not only produced the same effect but made the experiment simpler, compared with the labeled isotope.

### 3.2. Optimization of the procedures of extraction and purification

A series of methanol solutions of different concentrations were tested to determine the suitable medium for loading and washing sample extract on C<sub>18</sub> cartridges. Four mixed standard solutions of the three phytohormones (20 μg mL<sup>–1</sup>) and ISTD (100 μg mL<sup>–1</sup>) were obtained by dissolving their standards into 10%, 20%, 30% and 40% methanol in water containing 0.1% formic acid, respectively. Subsequently, 1 mL of the four mixed standard solutions was loaded onto four preconditioned C<sub>18</sub> cartridges, respectively. The concentration of the acidified methanol containing 0.1% formic acid for washing (1 mL volume) was the same as that for loading. The phytohormones were eluted by 1 mL 80% methanol. For ABA, IAA and ISTD, 30% of methanol solution containing 0.1% formic acid was the highest concentration that allowed for loading and washing with their complete retentions on the cartridge. However, 20% methanol solution containing 0.1% formic acid was required for complete retention of GA<sub>3</sub>, so 20% methanol containing 0.1% formic acid was used for sample loading and washing. In order to elute completely the three phytohormones from C<sub>18</sub> cartridge and eliminate the concomitant interferents as much as possible, a series of methanol solutions of different concentrations in water and the acidified (0.1% formic acid) ones of corresponding concentrations were employed. In our study, 1 mL mixed standard solution of the three phytohormones (20 μg mL<sup>–1</sup>) and ISTD (100 μg mL<sup>–1</sup>) in 20% methanol containing 0.1% formic acid was loaded respectively onto ten preconditioned C<sub>18</sub> cartridges and then washed with 1 mL 20% methanol containing 0.1% formic acid. At last, the eluting operation was carried out using 1 mL of 60%, 70%, 80%, 90% and 100% methanol solutions and the acidified (0.1% formic acid) ones of corresponding concentration, respectively. The results showed that non-acidified methanol solutions had stronger eluting abilities than the acidified (0.1% formic acid) ones, which could be because the acidified (0.1% formic acid) methanol solutions had converted the phytohormones from the anionic forms to the neutral ones. As the phytohormones in the neutral forms tended to retain on C<sub>18</sub> cartridge, the acidified (0.1% formic acid) methanol solutions were excluded in our experiment. Furthermore, 70% methanol was required to elute GA<sub>3</sub> and

**Table 1**  
Calibration curves and other quantitative data for GA<sub>3</sub>, IAA and ABA

Analyte	Calibration curve <sup>a</sup>	Range (μg mL <sup>-1</sup> )	Correlation coefficient	Detection limit (μg mL <sup>-1</sup> )	Precision (R.S.D., %)	
					Retention time	Peak area
GA <sub>3</sub>	Y = 0.0316X + 0.0045	0.005–200	0.9904	0.005	0.73	2.4
IAA	Y = 0.0009X + 0.0044	5.00–200	0.995	2.2	0.96	4.7
ABA	Y = 0.0756X + 0.0087	0.005–200	0.9956	0.003	0.4	2.9

<sup>a</sup> Y: peak area ratio of standard and internal standard; X: concentration (μg mL<sup>-1</sup>).

80% methanol to elute IAA and ABA and ISTD completely. Therefore, 80% methanol was selected as the eluting medium in the experiment.

In order to investigate the efficiency of different extractants, 20 mL water and 20 mL 80% methanol were compared. We affirmed that no significant difference was found between water and 80% methanol (data not shown). So pure water was used as extractant to extract the phytohormones from the wheat samples in the experiment.

### 3.3. Method evaluation

The linearity of each analyte was evaluated by using a series of standard solutions, and each standard solution was measured in triplicate. The calibration curves were constructed based on peak area ratios of the analytes to ISTD versus concentrations of analyte standards. Table 1 is the summary of calibration curves, linear ranges and detection limits of the three phytohormones. Good linearities were found in the ranges of 5–200 μg mL<sup>-1</sup> for IAA and 0.005–10 μg mL<sup>-1</sup> for ABA and GA<sub>3</sub>. The detection limits based on a signal-to-noise ratio of three were 0.005 μg mL<sup>-1</sup>, 2.2 μg mL<sup>-1</sup> and 0.003 μg mL<sup>-1</sup> for GA<sub>3</sub>, IAA and ABA, respectively. The detection limit of IAA was higher than that of ABA or GA<sub>3</sub>.

The precisions of LC–ESI–MS/MS detection were examined by five repeated injections of a mixed standard solution containing 20 μg mL<sup>-1</sup> GA<sub>3</sub>, IAA and ABA. The relative standard deviations (RSDs) of retention times and peak areas were all under 4.7% for GA<sub>3</sub>, IAA and ABA. In order to examine the recovery of the developed method, the standards of the three phytohormones at two different concentration levels were spiked to samples and then extracted by the optimized extraction method. The recoveries are summarized in Table 2. Good recoveries from 95.5% to 102.4% were obtained. The stability of the three phytohormones was investigated by analyzing a wheat sample maintained at 4 °C for 2 days. The three phytohormones were shown to be stable at 4 °C within 2 days.

### 3.4. Quantitative analysis of plant samples

The LC–ESI–MS/MS method developed in our study was successfully applied to analyze GA<sub>3</sub>, IAA and ABA in wheat samples. A typical LC–ESI–MS/MS chromatogram of a wheat sample is shown in Fig. 4. The analytical results of GA<sub>3</sub>, IAA and ABA at the differ-

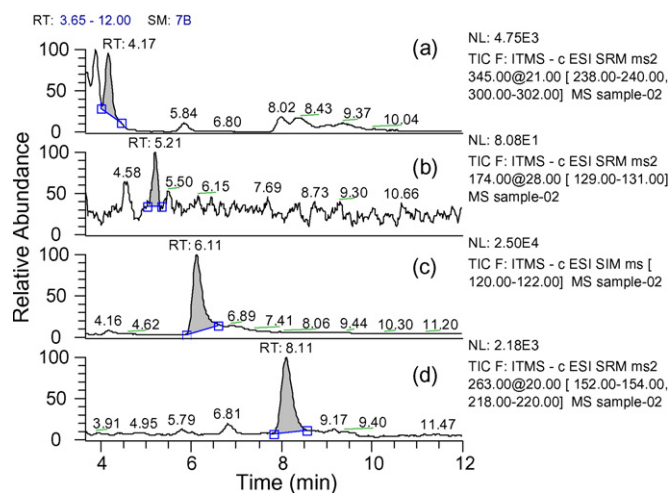


**Fig. 4.** Typical LC–ESI–MS–MS chromatogram of a wheat sample: (4a) GA<sub>3</sub>, 345 → 239, 301 transition; (4b) IAA, 174 → 130 transition; (4c) ISTD, 121; (4d) ABA, 263 → 153, 219 transition.

**Table 3**  
Analytical results of GA<sub>3</sub>, IAA and ABA in wheat samples (n = 3)

Analyte	Mean (R.S.D., %)		
	GA <sub>3</sub> (μg g <sup>-1</sup> )	IAA (μg g <sup>-1</sup> )	ABA (μg g <sup>-1</sup> )
Overground tissue (bud)	1.924a (1.21)	3.124a (2.56)	0.012a (3.37)
Overground tissue (one leaf)	0.817b (3.77)	2.974a (5.67)	0.008b (6.43)
Overground tissue (two leaves)	0.679c (2.44)	3.289b (1.60)	0.009b (3.40)
Roots (bud)	0.733a (2.16)	N.D. <sup>a</sup>	0.010a (4.58)
Roots (one leaf)	0.224b (3.41)	N.D.	0.005b (5.03)
Roots (two leaves)	0.013c (4.45)	N.D.	0.005b (5.29)

Column means followed by the same letters are not significantly different at the 95% confidence level as determined by the Duncan Test.

<sup>a</sup> N.D.: not detected.

ent growth stages of the wheat samples are summarized in Table 3. The results indicated that the developed method was suitable for the determination of the three phytohormones in plant samples. Furthermore, The Duncan Test, a statistical method, was used to analyze the variation of the three phytohormones at the different growth stages of the wheat samples. With the growth of wheat, the content of GA<sub>3</sub> in overground tissues and roots all decreased gradually. The content of ABA in overground tissues and roots decreased from the bud stage to one-leaf stage, but it had no obvious variation from one-leaf stage to two-leaf stage. The content of IAA in overground tissues had no significant difference from the bud stage to one-leaf stage and increased from one-leaf stage to two-leaf stage, but it was not detected in roots.

## 4. Conclusion

In this study, we have developed an LC–ESI–MS/MS method to determine GA<sub>3</sub>, IAA and ABA simultaneously and also simplified the procedures of extracting and purifying plant samples for the

**Table 2**  
Average recoveries of GA<sub>3</sub>, IAA and ABA in wheat samples (n = 3)

Analyte	Added (μg mL <sup>-1</sup> )	Recovery (%) Mean
GA <sub>3</sub>	2	97.3
	5	98.5
IAA	2	97.7
	5	102.4
ABA	0.02	95.5
	0.05	99



analysis. In addition, an SPE method developed in the experiment could remove the interferents effectively and enhance the determination sensitivity. The LC–ESI–MS/MS method has been successfully applied to determine the three phytohormones in wheat samples at different growth stages. The satisfactory results have demonstrated that this method may be suitable for the determination of the three phytohormones in agriculture and plant physiology.

## References

- [1] P.J. Davies, in: P.J. Davies (Ed.), *Plant Hormones: Physiology, Biochemistry and Molecular Biology*, second ed., Kluwer, Dordrecht, Netherlands, 1995, pp. 1–12.
- [2] P. Hernández, M. Dabrio-Ramos, F. Patón, Y. Ballesteros, L. Hernández, *Talanta* 44 (1997) 1783.
- [3] A. Durgbanshi, V. Arbona, O. Pozo, O. Miersch, J.V. Sancho, A. Gomez-Cadenas, *J. Agric. Food Chem.* 53 (2005) 8437.
- [4] R. Zhou, T.M. Squires, S.J. Ambrose, S.R. Abrams, A.R.S. Ross, A.J. Cutler, *J. Chromatogr. A* 1010 (2003) 75.
- [5] P.I. Dobrev, L. Havlíček, M. Vágner, J. Malbeck, M. Kamínek, *J. Chromatogr. A* 1075 (2005) 159.
- [6] J. Rolčík, J. Řečinská, P. Barták, M. Strnad, E. Prinsen, *J. Sep. Sci.* 28 (2005) 1370.
- [7] A. Müller, P. Düchting, E.W. Weiler, *Planta* 216 (2002) 44.
- [8] E. Prinsen, W.V. Dongen, E.L. Esmans, H.A.V. Onckelen, *J. Mass Spectrom.* 32 (1997) 12.
- [9] Z. Ma, L. Ge, A.S.Y. Lee, J.W.H. Yong, S.N. Tan, E.S. Ong, *Anal. Chim. Acta* 610 (2008) 274.
- [10] E.A. Schmelz, J. Engelberth, J.H. Tumlinson, A. Block, H.T. Alborn, *Plant J.* 39 (2004) 790.
- [11] H.T. Liu, Y.F. Li, T.G. Luan, C.Y. Lan, W.S. Shu, *Chromatographia* 66 (2007) 515.
- [12] A. Crozier, K. Loeferski, J.B. Zaerr, B.O. Morris, *Planta* 150 (1980) 366.
- [13] M. Wright, P. Doherty, *J. Plant Growth Reg.* 4 (1985) 91.
- [14] R. Maldiney, B. Leroux, I. Sabbagh, B. Sotta, L. Sossountzov, E. Miginiac, *J. Immunol. Methods* 90 (1986) 151.
- [15] B. Fernandez, M.L. Centeno, I. Feito, R. Sanchez-Tames, A. Rodriguez, *Phytochem. Anal.* 6 (1995) 49.
- [16] A. Champault, *C. R. Acad. Sci. D Nat.* 280 (1975) 591.
- [17] E.A. Schmelz, J. Engelberth, H.T. Alborn, P. O'Donnell, M. Sammons, H. Toshima, J.H. Tumlinson, *Proc. Natl. Acad. Sci. U.S.A.* 100 (2003) 10552.
- [18] J. Cao, S.J. Murch, R. O'Brien, P.K. Saxena, *J. Chromatogr. A* 1134 (2006) 333.
- [19] A. Gómez-Cadenas, O.J. Pozo, P. García-Augustín, J.V. Sancho, *Phytochem. Anal.* 13 (2002) 228.
- [20] M. López-Carbonell, O. Jáuregui, *Plant Physiol. Biochem.* 43 (2005) 407.



## Hydrodistillation–adsorption method for the isolation of water-soluble, non-soluble and high volatile compounds from plant materials

J. Mastelić\*, I. Jerković, I. Blažević, A. Radonić, L. Krstulović

Department of Organic Chemistry, Faculty of Chemistry and Technology, University of Split, N. Tesle 10/V, HR-21000 Split, Croatia

### ARTICLE INFO

#### Article history:

Received 26 November 2007  
Received in revised form 17 April 2008  
Accepted 23 April 2008  
Available online 2 May 2008

#### Keywords:

Acids  
Terpenes and isothiocyanates  
Hydrodistillation–adsorption  
Volatiles isolation  
Water-soluble volatiles

### ABSTRACT

Proposed method of hydrodistillation–adsorption (HDA) on activated carbon and hydrodistillation (HD) with solvent trap were compared for the isolation of water-soluble, non-soluble and high volatile compounds, such as acids, monoterpenes, isothiocyanates and others from carob (*Certonia siliqua* L.), rosemary (*Rosmarinus officinalis* L.) and rocket (*Eruca sativa* L.). Isolated volatiles were analyzed by GC and GC/MS. The main advantages of HDA method over ubiquitous HD method were higher yields of volatile compounds and their simultaneous separation in three fractions that enabled more detail analyses. This method is particularly suitable for the isolation and analysis of the plant volatiles with high amounts of water-soluble compounds. In distinction from previously published adsorption of remaining volatile compounds from distillation water on activated carbon, this method offers simultaneous hydrodistillation and adsorption in the same apparatus.

© 2008 Elsevier B.V. All rights reserved.

### 1. Introduction

The plant volatiles are heterogeneous groups of organic compounds that include monoterpenes, sesquiterpenes, diterpenes and many other nonterpene compounds with different molecular weights and functional groups. Some essential oils contain glucosinolate degradation products, such as isothiocyanates, organic cyanides, epithionitriles, oxazolidinethiones, and thiocyanates. All these classes of compounds exhibit different properties such as volatility, solubility in water and solvents or others that are essential for their isolation and concentration from plant material as well for the separation of their natural compound mixtures to different fractions. Hydrodistillation is one of the most frequently used methods for volatiles isolation. Obtained isolates, called essential oils, according to international definition are distillation products that are not soluble in water and can be easily separated from distillation water. However, some compounds of the essential oils are water-soluble, especially at elevated temperature that can produce losses and smaller oil yields during hydrodistillation. Many other methods are used for volatiles isolation, such as extraction with solvents and supercritical CO<sub>2</sub> extraction [1–5].

The differences in the obtained volatile yields and chemical composition from the same plant are well known due to the use of different isolation methods. Namely, the most volatile compounds

will the most rapidly distill and many of them can be lost by leaking through condenser, while less volatile compounds slowly and partially distill. Furthermore, polar components of some essential oils have high water solubility at boiling temperature and slowly and incompletely distill. After condensation, the part of these compounds remains dissolved in distillation water that recovers in distillation flask, circuit during hydrodistillation and their isolation is not complete. For the oils with large content of water-soluble compounds HD method gives lower yields due to the previous mentioned losses. Therefore, we have developed a method of volatiles isolation by simultaneous hydrodistillation–adsorption (HDA). Several types of sorbents are available (polymeric adsorbents, zeolites, activated carbon, etc.). In this research, for adsorption of water-soluble and high volatile compounds activated carbon was used as adsorbent due to sorption capacity toward many compounds. The principal binding mechanisms include hydrophobic interactions, charge-transfer complexation, hydrogen bonding, cation exchange and another specific interactions [6]. The adsorption characteristics of activated carbon depend on the type of starting material, methods and conditions of preparation [7].

Suitable plant materials selected for this research were carob (*Certonia siliqua* L.), rosemary (*Rosmarinus officinalis* L.) and rocket (*Eruca sativa* L.). Carob belongs to Leguminosae family. It is evergreen tree which is cultivated in many parts of Mediterranean coast and islands. MacLeod and Forcen [8] analyzed volatile components from the carob beans from Spain by simultaneous hydrodistillation–extraction in Likens–Nickerson apparatus and identified water-soluble isobutyric, valeric, isovaleric and butyric

\* Corresponding author. Tel.: +385 21 329 436; fax: +385 21 329 461.  
E-mail address: [josip.mastelic@ktf-split.hr](mailto:josip.mastelic@ktf-split.hr) (J. Mastelić).

acids as the main components (cca. 75%). Rosemary, the second selected sample, belongs to Lamiaceae family. This aromatic plant and its essential oil, isolated from leaves, are very famous and respected on world market and have been researched a lot [9,10]. Rosemary oil contains many volatile and non-polar monoterpene hydrocarbons. Furthermore, the oil contains monoterpene oxygen containing compounds, sesquiterpene hydrocarbons and others. The third sample was rocket, member of Brassicaceae family that contains glucosinolates. It has been reported that 4-methylthiobutyl isothiocyanate (*erucin*), that originates from glucoerucin, was the major glucosinolate degradation product found in the leaves oil of rocket [11].

Previous papers reported isolation of volatiles from aromatic plants using stream of nitrogen and their adsorption on activated carbon column (purge-and-trap method) [12] as well as the adsorption of water-soluble compounds remained in the distillation water on activated carbon [13,14]. The aim of this research was to investigate and compare two isolation methods performed in the same apparatus: hydrodistillation–adsorption (HDA) method and its ability to diminish losses of water-soluble and high volatile compounds and hydrodistillation method with solvent trap (HD).

## 2. Experimental

### 2.1. Plant materials

Ripe carob beans were collected on island Šolta (near Split, Croatia) in September 2007. Carob beans have been de-seeded and grinded in coffee mill to a particle size of cca. 1–2 mm. Rosemary was collected near Split in June 2007. Fresh leaves were used for this research. Rocket was, also, collected near Split in May 2007. Fresh flowers and leaves with green beans were used. The botanical identity of the plant materials was confirmed by a local botanist and the voucher specimens are deposited at Department of Organic Chemistry, Faculty of Chemistry and Technology, Split, Croatia.

### 2.2. Hydrodistillation–adsorption (HDA)

Clevenger type apparatus (Fig. 1) was used for proposed HDA method. Carbon (Kemika, Zagreb, Croatia, granules  $\varnothing = 0.3\text{--}0.5\text{ mm}$ ) was activated in muffle furnace at a temperature of  $800\text{ }^{\circ}\text{C}$  for 2 h in reducing atmosphere. After cooling at room temperature, carbon was added in water and deaerated under vacuum for 10 min. Activated carbon (5 g) was put in a separator (inner apparatus tube) for the adsorption of water-soluble compounds, and in a small column (3 g) situated on the top of condenser for the adsorption of high volatile compounds from gaseous phase.

The height of water layer above carbon column (Fig. 1, a) was 5 cm. Plant material (200 g) and 600 mL water were put in 1000 mL distillation flask. The distillate passed through the water layer: water non-soluble compounds were collected on the water layer (Fig. 1, b), and water-soluble compounds were adsorbed on carbon column (Fig. 1, a). The most volatile compounds from gaseous phase were adsorbed on the carbon column on the top of condenser (Fig. 1, c). After hydrodistillation and adsorption (3 h), the layer of water non-soluble compounds (Fig. 1, b) was dissolved in pentane and carefully separated from the water layer. This procedure was repeated twice and pentane extracts were combined (fraction b). After removing of water, through a pipe on the bottom of apparatus, the extraction of adsorbed compounds was performed in the same apparatus using 50 mL diethyl ether for 8 h. The obtained ether extract was carefully concentrated by distillation to a smaller volume (fraction a). High volatile compounds were extracted from upper column (Fig. 1, c) with ether, and the obtained extract was

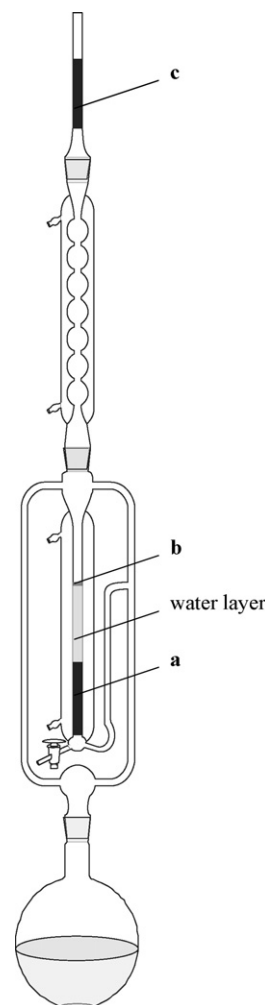


**Fig. 1.** Apparatus for hydrodistillation–adsorption (HDA): **a**, column of activated carbon for the adsorption of water-soluble components; **b**, fraction of water non-soluble compounds; **c**, column of activated carbon for the adsorption of high volatile compounds.

carefully concentrated (fraction c). All the extracts **a**, **b** and **c** were dried over anhydrous  $\text{MgSO}_4$ . HDA method was performed in triplicate for each sample. All the isolates were analyzed by GC and GC–MS.

### 2.3. Hydrodistillation (HD)

Hydrodistillation (HD) of plant material (carob beans, rosemary leaves, rocket flowers and rocket leaves with green beans) was performed in Clevenger type apparatus with solvent trap for 3 h. A mixture (3 mL) of pentane and diethyl ether (1:1, v/v) was used for volatiles trapping. Prior HD, rocket was autolyzed for 24 h on  $27\text{ }^{\circ}\text{C}$  to increase glucosinolate degradation by endogenous myrosinase [15]. All the extracts were dried over anhydrous  $\text{MgSO}_4$ . HD method was performed in triplicate for each sample. All the isolates were analyzed by GC and GC–MS.

### 2.4. Analysis of isolated volatiles

#### 2.4.1. Gas chromatography (GC-FID)

Gas chromatography analysis was performed on a Hewlett-Packard 5890 Series II gas chromatograph equipped with flame ionization detector using HP-20M capillary column (Hewlett

Packard, polyethyleneglycol, 50 m × 0.2 mm i.d., film thickness 0.2 μm). Chromatographic conditions were as follows: helium as carrier gas, flow rate 1.0 mL/min; injector and detector temperatures, 250 and 300 °C. Oven temperature was isothermal at 70 °C for 4 min, then increased to 180 °C, at a rate of 4 °C/min and held isothermal for 15 min. Volume injected 1 μL. Split ratio 1:50.

#### 2.4.2. Gas chromatography–mass spectrometry (GC–MS)

Isolated volatiles were also analyzed by Hewlett Packard GC–MS system (gas chromatograph model 5890 series II with mass selective detector model 5971A). Polar capillary column, HP-20M, was used (Hewlett Packard, polyethyleneglycol, 50 m × 0.2 mm i.d., film thickness 0.2 μm). Oven temperature was programmed as follows: isothermal at 70 °C for 4 min, then increased to 180 °C, at a rate of 4 °C/min and subsequently held isothermal for 15 min. Carrier gas was helium, flow rate 1.0 mL/min; injector temperature: 250 °C; volume injected: 1 μL; split ratio: 1:50. MS conditions: ionization voltage: 70 eV; ion source temperature: 280 °C; mass range: 30–300 mass units, as in previous papers [16,17].

#### 2.4.3. Qualitative and quantitative determinations

The individual peaks were identified by comparison of their retention indices to those of authentic samples, as well as by comparing their mass spectra with the Wiley 275 library (Wiley, New York) and NIST98 (National Institute of Standards and Technology, Gaithersburg) mass spectral database and literature [18].

The percentage composition of compounds (relative quantity) in the essential oil and its fractions were computed from the GC–FID peak areas using the normalization method, without correction factors. Quantitative results were obtained as mean of data derived from duplicate GC–FID analyses.

The yields of oils and fractions were determined by gravimetric method after complete solvent removal, by carefully distillation over Vigreux column at low temperature. The yields of essential oils were calculated as sum of the yields of all three fractions, and chemical composition was calculated as sum of chemical composition of all the fractions. Absolute quantity [mg/kg] for particular compound was calculated from average compound percentage and average masses of each fraction (from triplicate experiments).

### 3. Results and discussion

Volatiles of carob beans, rosemary leaves and rocket flowers and its leaves with green beans were isolated by two methods: hydrodistillation–adsorption (HDA) and hydrodistillation with solvent trap (HD). During the isolation by proposed HDA method the volatiles were separated in three fractions: water-soluble fraction **a**, water non-soluble fraction **b** and fraction **c** of high volatile compounds. Water non-soluble compounds were isolated in the upper layer (above the water), water-soluble compounds and some emulsified compounds from distillation water were adsorbed on carbon column in the separator, and high volatile components were adsorbed on carbon in the upper column, Fig. 1. Activated carbon has not the same adsorption power toward different compounds, but high number of theoretical plates in the column corrects this fault. The identified structures of the main components are shown in Fig. 2, which indicates fractionation (**a**, **b**, **c**) of isolated volatiles according to different water solubility and volatility.

The yields and chemical compositions of volatile compound fractions of carob beans isolated by two methods are given in Table 1. The yield of volatiles obtained by HD method

was 1450.0 mg/kg, and by HDA method 2728.3 mg/kg (88.2% yield increase). The yield of fraction **b** (water non-soluble compounds) was only 148.5 mg/kg with mass ratio 0.0544. Twenty-two compounds were identified in this fraction. The main components were hydrophobic compounds such as hexadecanal (65.89 mg/kg), hexadecanoic acid (18.87 mg/kg), 2-tridecanone (15.17 mg/kg) and 3-dodecyl acetate (15.82 mg/kg). The yield of fraction **a** was 2567.4 mg/kg and of fraction **c** was only 12.4 mg/kg. Fraction **a** was quantitatively the most significant with mass ratio of 0.9410. Only seven water-soluble compounds were identified in this fraction. The main components were acids: 2-methylpropanoic acid (1853.98 mg/kg), hexanoic acid (513.08 mg/kg), butanoic acid (107.95 mg/kg), 2-methylbutanoic acid (48.49 mg/kg) and acetic acid (17.86 mg/kg). Fraction **c** contained eight high volatile compounds with mass ratio of 0.0045. Four of them were identified only in this fraction, Table 1. Volatiles isolated by HD method contained only ten compounds in comparison with 25 volatiles isolated by HDA method. HDA method enabled higher overall yield and simultaneous fractionation and, therefore, more complete analysis. In summary, the main HDA components (**a** + **b** + **c**) of carob beans volatiles were water-soluble acids such as 2-methylpropanoic acid (1853.98 mg/kg), hexanoic acid (514.60 mg/kg) and butanoic acid (107.95 mg/kg). Octanoic, acetic and hexadecanoic acid were identified, but in smaller quantities. The volatiles also contained carbonyl compounds hexadecanal, 2-butenal, 5-methyl-2-hexanone, 2-octanone with small quantity of esters, hydrocarbons and other compounds.

Rosemary leaves contain essential oil with relatively high amount of volatile compounds and small amount of water-soluble compounds. Monoterpene and sesquiterpene hydrocarbons and oxygen containing compounds were identified. The yields and chemical compositions of the isolated oil and its fractions for both methods are given in Table 2. The yield of the volatiles obtained by HD method was 4972.70 mg/kg, and by HDA method was 5546.40 mg/kg (12% yield increase). The yield of fraction **b** (water non-soluble compounds) was 4234.50 mg/kg. Fraction **b** was the main volatile fraction of rosemary leaves with 0.7634 mass ratio in comparison with volatile fraction **b** of carob beans. Twenty-one compounds were identified in this fraction. The main components were 1,8-cineole (2319.20 mg/kg), α-pinene (625.05 mg/kg), camphor (394.15 mg/kg), borneol (165.41 mg/kg), α-terpineol (119.76 mg/kg) and other hydrophobic compounds with smaller contents. Polar compounds of this fraction were also identified in fraction **a** such as 1,8-cineole, camphor, borneol, α-terpineol, terpinene-4-ol, linalool and other polar compounds with small contents. The yield of fraction **a** was 1254.70 mg/kg with mass ratio of 0.2261. Seven compounds were identified. Mass ratio of fraction **c** was 0.0105. High volatile compounds were present. Two compounds (δ-3-carene and myrcene) were identified only in fraction **c**, while others were also identified in fraction **b**. In summary, twenty compounds were identified in rosemary volatiles isolated by HD method and twenty-three compounds in the volatiles isolated by HDA method.

Volatiles from rocket flowers (**I**) and rocket leaves with green beans (**II**) were also isolated by HD and HDA methods. The yields and chemical compositions of the isolated volatiles and their fractions for both methods are given in Table 3. The yield of volatiles obtained from the flowers was: by HD method 152.32 mg/kg, and by HDA method 311.77 mg/kg (104.7% yield increase). Sixteen compounds were identified in the volatiles obtained by HD, and forty-eight by HDA. The yield of volatiles from the leaves with green beans was: by HD method 71.68 mg/kg, and by HDA method 91.70 mg/kg (27.9% yield increase). Twenty-four compounds were

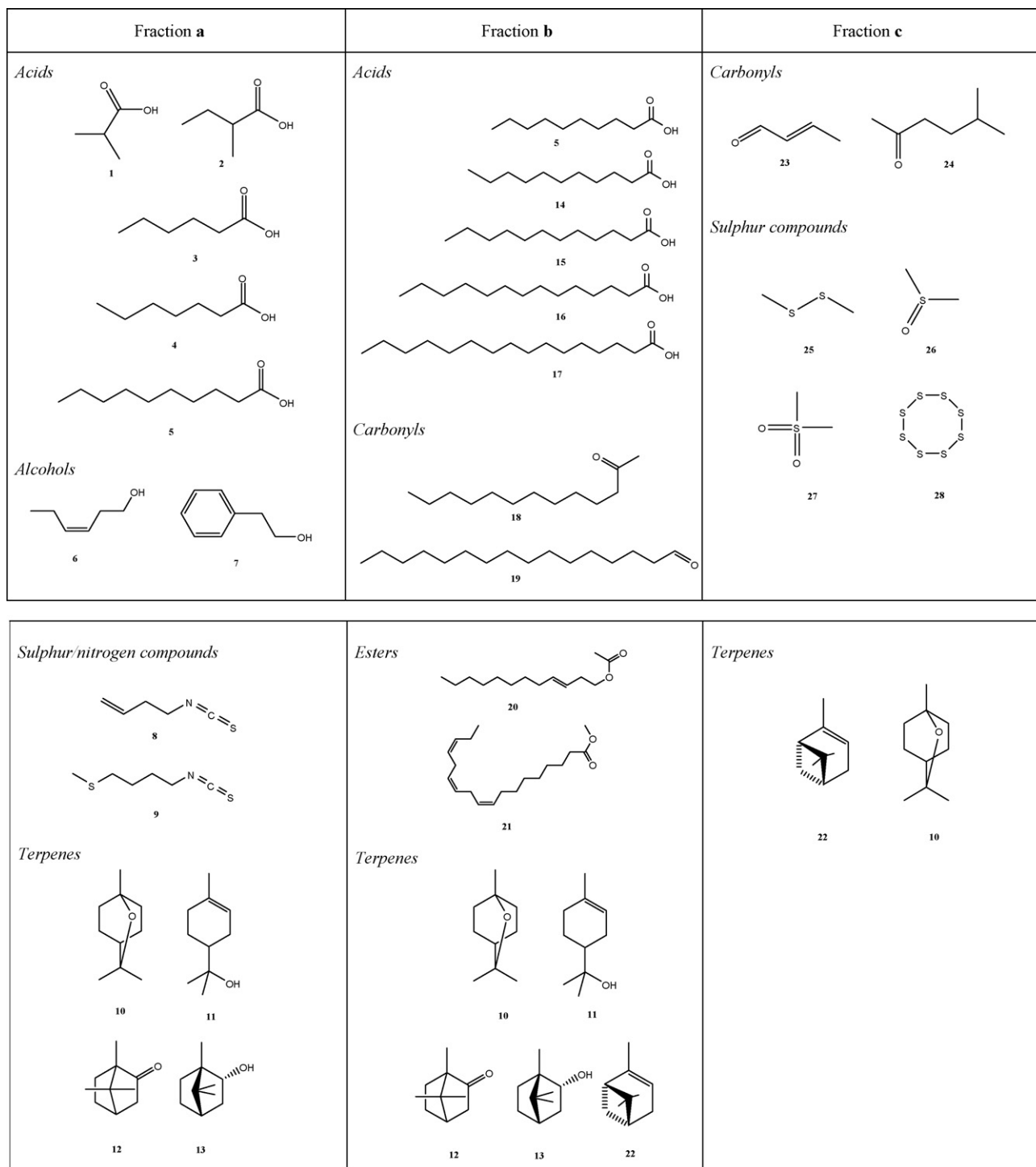


**Fig. 2.** Chemical structures of the main volatile compounds in carob, rosemary and rocket identified in fractions **a**, **b** and **c**. *Compound names:* 2-methylpropanoic acid (**1**); 2-methylbutanoic acid (**2**); hexanoic acid (**3**); heptanoic acid (**4**); decanoic acid (**5**); (Z)-3-hexen-1-ol (**6**); 2-phenylethanol (**7**); 3-butenyl isothiocyanate (**8**); 4-methylthiobutyl isothiocyanate (**9**); 1,8-cineole (**10**);  $\alpha$ -terpineol (**11**); camphor (**12**); borenol (**13**); undecanoic acid (**14**); dodecanoic acid (**15**); tetradecanoic acid (**16**); hexadecanoic acid (**17**); 2-tridecanone (**18**); hexadecanal (**19**); 3-dodecanyl acetate\* (**20**); methyllinolenate (**21**);  $\alpha$ -pinene (**22**); 2-butenal\* (**23**); 5-methyl-2-hexanone (**24**); dimethyl disulfide (**25**); dimethyl sulfoxide (**26**); dimethyl sulfone (**27**); cyclooctasulfur (**28**); \*, correct isomer not identified.

identified in the volatiles obtained by HD and thirty four by HDA. The yield of fraction **b** (water non-soluble compounds) for **I** was 173.55 mg/kg with mass ratio 0.5567 including 21 compounds and for **II** was 31.90 mg/kg with mass ratio 0.3479, including 12 compounds. Depending of the used conditions [19], glucoerucin degradation can produce: 4-methylthiobutylisothiocyanate (*erucin*), 5-methylthiopentanenitrile (*erucin nitrile*) and sulfur.

4-Methylthiobutylisothiocyanate was found mostly in fraction **a** (**I**: 29.52 mg/kg, **II**: 15.51 mg/kg). 5-Methylthiopentanenitrile was detected only in fraction **a** (**II**: 0.31 mg/kg). In addition, water-soluble acids were found in this fraction, such as acetic acid (**I**: 6.73 mg/kg; **II**: 0.70 mg/kg), propionic acid (**I**: 0.14 mg/kg), 2-methylbutanoic acid (**I**: 17.57 mg/kg), pentanoic acid (**I**: 0.14 mg/kg), hexanoic acid (**I**: 2.61 mg/kg; **II**: 0.48 mg/kg), heptanoic acid (**I**:

**Table 1**

Identified constituents, composition and yields of volatile compounds of *Ceratonia siliqua* L. isolated by two methods: hydrodistillation with solvent trap (HD) and hydrodistillation–adsorption (HDA)

Compound	RI	HD [mg/kg]	HDA [mg/kg]			Calculated values (a + b + c)
			a	b	c	
2-Butenal*	1006	–	–	–	2.75	2.75
2-Butenal*	1010	–	–	–	5.49	5.49
5-Methyl-2-hexanone	1139	–	–	–	2.60	2.60
2-Octanone	1340	–	–	–	0.15	0.15
Acetic acid	1380	–	17.86	–	t	17.86
2-Methylpropanoic acid	1469	1077.04	1853.98	t	t	1853.98
2-Nonanon	1545	0.26	–	1.01	0.07	1.08
Butanoic acid	1549	36.35	107.95	–	–	107.95
2-Methylbutanoic acid	1596	30.72	48.49	–	1.34	49.83
Pentanoic acid	1657	0.15	–	0.59	–	0.59
2-Nonanol	1660	2.80	–	0.88	–	0.88
Ethyl butanoate	1672	t	–	0.44	–	0.44
2,6-Dihydro-2H-pyran-2-one	1743	–	4.35	–	–	4.35
Hexanoic acid	1770	290.00	513.08	1.52	–	514.60
2-Dodecanol	1859	–	–	4.28	–	4.28
1-Hexadecene	1867	–	–	3.35	–	3.35
2-Pentadecanone	1957	0.12	–	1.32	–	1.32
2-Tridecanone	1960	–	–	15.17	–	15.17
Octanoic acid	1966	12.56	21.69	–	–	21.69
3-Dodecyl acetate*	1967	–	–	15.82	–	15.82
1-Octadecene	2054	–	–	3.35	–	3.35
Cyclooctadecene	2081	–	–	6.09	–	6.09
2-Nonadecanone	2173	–	–	0.49	–	0.49
Hexadecanal	2197	–	–	65.89	–	65.89
Hexadecanoic acid	>2200	–	–	18.87	–	18.87
Yield [mg/kg]		1450.0	2567.4	148.5	12.4	2728.3
Mass ratio of fractions			0.9410	0.0544	0.0045	

HD, hydrodistillation with solvent trap; HAD, hydrodistillation–adsorption; **a**, fraction of water-soluble compounds; **b**, fraction of water non-soluble compounds; **c**, fraction of high volatile compounds; calculated values – sum [mg/kg] of fractions **a**, **b** and **c**; –, not detected; t, traces <0.01 mg/kg; \*, correct isomer (*E*, *Z*) is not identified; RI, retention index on HP-20M column.

**Table 2**

Identified constituents, composition and yields of volatile compounds of *Rosmarinus officinalis* L. isolated by two methods: hydrodistillation with solvent trap (HD) and hydrodistillation–adsorption (HDA)

Compound	RI	HD [mg/kg]	HDA [mg/kg]			Calculated values (a + b + c)
			a	b	c	
α-Pinene	1034	650.42	–	625.05	31.15	656.20
Camphene	1071	80.28	–	90.85	4.85	95.70
β-Pinene	1107	60.43	–	57.93	4.12	62.05
δ-3-Carene	1141	–	–	–	0.40	0.40
Myrcene	1148	–	–	–	0.78	0.78
1,8-Cineole	1192	2755.57	558.20	2319.20	16.40	2893.80
cis-β-Ocimene	1223	5.20	–	12.37	–	12.37
γ-Terpinene	1237	46.50	–	49.60	–	49.60
p-Cymen	1253	51.65	–	62.21	0.50	62.71
Terpinolene	1263	36.85	–	38.89	–	38.89
Alloocimene	1353	t	–	4.13	–	4.13
Oct-1-en-3-ol	1412	t	–	4.27	–	4.27
Camphor	1482	501.51	282.92	394.15	–	676.07
Pinocarvone	1506	25.89	–	34.75	–	34.75
Isopinocampone	1506	31.10	–	33.90	–	33.90
Linalool	1507	30.95	4.78	60.10	–	64.88
Bornyl acetate	1546	36.15	–	38.92	–	38.92
Terpinene-4-ol	1555	–	13.50	24.78	–	38.28
Trans-caryophyllene	1571	56.82	–	56.74	–	56.74
α-Terpineol	1629	315.28	212.71	119.76	–	332.47
α-Humulene	1638	20.71	–	20.80	–	20.80
Borneol	1657	241.59	175.59	165.41	–	341.00
Caryophyllene oxide	1912	25.80	3.53	20.69	–	3.47
Yield mg/kg		4972.70	1254.70	4234.50	58.20	5546.40
Mass ratio of fractions			0.2261	0.7634	0.0105	

HD, hydrodistillation with solvent trap; HDA, hydrodistillation–adsorption; **a**, fraction of water-soluble compounds; **b**, fraction of water non-soluble compounds; **c**, fraction of high volatile compounds; calculated values – sum [mg/kg] of fractions **a**, **b** and **c**; –, not detected; t, traces <0.01 mg/kg; \*, correct isomer (*E*, *Z*) is not identified; RI, retention index on HP-20M column.

**Table 3**  
Identified constituents, composition and yields of volatile compounds of *Eruca sativa* flowers (**I**) and leaves and green beans (**II**) isolated by two methods HD and HDA

Compound	RI	HD [mg/kg]		HDA [mg/kg]						Calculated values (a + b + c)	
		<b>I</b>	<b>II</b>	<b>a</b>		<b>b</b>		<b>c</b>		<b>I</b>	<b>II</b>
				<b>I</b>	<b>II</b>	<b>I</b>	<b>II</b>	<b>I</b>	<b>II</b>		
α-Pinene	1034	–	0.25	–	–	–	0.10	–	–	–	0.10
Dimethyldisulfide	1059	–	–	–	–	–	–	0.04	0.08	0.04	0.08
Tetrahydrothiophene	1107	–	1.60	0.14	0.35	0.21	–	–	–	0.35	0.35
Heptanal	1157	–	–	–	–	–	–	0.17	–	0.17	–
(E)-2-hexenal	1180	–	2.36	0.69	0.87	–	–	0.20	–	0.89	0.87
Methylisothiocyanate	1228	–	0.25	–	–	–	–	–	–	–	–
(Z)-3-hexenyl formate	1230	–	–	0.41	0.57	–	–	–	–	0.41	0.57
2,4-Hexadiene	1280	t	–	–	–	–	–	0.07	–	0.07	–
(E)-3-hexen-1-ol	1322	–	1.77	1.10	1.18	–	–	0.25	–	1.35	1.18
(Z)-3-hexen-1-ol	1344	–	7.18	20.46	16.26	0.21	–	0.54	0.11	21.21	16.37
Dimethyl trisulfide	1347	–	–	–	–	–	–	0.07	–	0.07	–
(E)-2-hexen-1-ol	1360	–	1.85	–	1.88	–	–	–	–	–	1.88
(Z)-3-hexenyl isobutyrate	1361	–	–	0.20	–	–	–	–	–	0.20	–
Nonanal	1365	–	–	–	–	0.43	–	–	–	0.43	–
Acetic acid	1380	–	–	6.73	0.70	–	–	0.12	–	6.85	0.70
3-Butenyl isothiocyanate	1403	–	–	1.10	0.35	–	–	0.07	–	1.17	0.35
(Z)-3-hexenyl-α-methylbutyrate	1440	–	–	0.14	–	–	–	–	–	0.14	–
Propionic acid	1473	–	–	0.14	–	–	–	–	–	0.14	–
4-Methylpentyl isothiocyanate	1487	–	0.76	0.14	0.22	0.21	0.20	0.06	0.27	0.41	0.69
Dimethylsulfoxide	1522	–	–	1.51	0.39	–	–	1.04	1.57	2.55	1.96
Hexyl isothiocyanate	1536	–	–	–	–	–	–	0.10	–	0.10	–
Methyl decanoate	1552	1.35	–	0.14	–	0.21	–	0.02	–	0.37	–
β-Cyclocitral	1564	–	–	–	–	–	–	0.02	–	0.02	–
Phenylacetaldehyde	1596	–	0.59	–	0.20	–	–	–	–	–	0.20
2-Methylbutanoic acid	1596	0.84	0.74	17.57	–	–	–	–	0.74	17.57	0.74
(Z)-3-hexyl hexanoate	1614	–	–	0.82	–	–	–	–	–	0.82	–
Pentanoic acid	1657	–	–	0.14	–	–	–	–	–	0.14	–
α-Methylbenzyl alcohol	1737	–	–	0.14	–	–	–	–	–	0.14	–
Hexanoic acid	1770	–	0.17	2.61	0.48	–	–	–	–	2.61	0.48
Benzyl alcohol	1797	–	–	0.27	–	–	–	–	–	0.27	–
Dimethylsulfone	1815	–	–	–	–	–	–	0.04	0.05	0.04	0.05
2-Phenylethyl alcohol	1835	–	0.26	2.88	0.14	–	–	–	0.26	2.88	0.40
4-Methylthiobutanenitrile	1851	–	–	0.96	0.35	–	–	–	0.21	0.96	0.56
β-Ionone*	1873	–	0.67	–	1.31	0.86	0.41	–	–	0.86	1.72
Heptanoic acid	1875	1.85	–	7.55	–	–	–	–	–	7.55	–
5-Methylthiopentanenitrile	1892	–	–	–	0.31	–	–	–	–	–	0.31
Nonadecane	1900	0.34	–	–	–	0.86	0.25	–	–	0.86	0.25
Octanoic acid	1966	0.84	0.34	1.24	0.35	0.21	–	0.02	–	1.47	0.35
4-Methylthiobutylisothiocyanate (erucin)	2041	32.18	28.63	29.52	15.51	6.64	1.56	–	–	36.16	17.07
Nonanoic acid	2084	0.67	–	0.69	0.10	–	–	–	–	0.69	0.10
Heneicosane	2100	–	1.94	–	–	0.21	1.53	–	–	0.21	1.53
Methyl hexadecanoate	2182	0.51	0.17	–	–	2.14	0.51	–	–	2.14	0.51
Decanoic acid	2192	56.11	1.60	25.85	1.44	38.57	–	–	–	64.42	1.44
Ethyl hexadecanoate	>2200	–	–	–	–	0.86	–	–	–	0.86	–
Undecanoic acid	>2200	2.70	0.76	1.65	0.46	6.86	–	–	–	8.51	0.46
Dodecanoic acid	>2200	6.57	0.76	1.78	–	14.57	0.31	–	–	16.35	0.31
Tricosane	>2200	–	1.52	–	–	6.21	1.27	–	–	6.21	1.27
Tridecanoic acid	>2200	–	–	–	–	0.64	t	–	–	0.64	t
Tetradecanoic acid	>2200	2.36	1.09	–	–	9.00	1.02	–	–	9.00	1.02
Pentadecanoic acid	>2200	0.51	–	–	–	2.14	–	–	–	2.14	–
Methyl linolenate	>2200	4.04	0.42	0.20	–	9.86	–	–	–	10.06	–
Hexadecanoic acid	>2200	41.45	16.00	0.27	–	72.65	24.74	–	–	72.92	24.74
Cyclooctasulfur	>2200	–	–	0.27	–	–	–	8.08	13.09	8.35	13.09
Total mg/kg			152.32	71.68	127.31	43.42	173.55	31.90	10.91	16.38	311.77
Mass ratio of fractions					0.4083	0.4735	0.5567	0.3479	0.0350	0.1786	

**I**, flowers; **II**, leaves and green beans; HD, hydrodistillation with solvent trap; HDA, hydrodistillation–adsorption; **a**, fraction of water-soluble compounds; **b**, fraction of water non-soluble compounds; **c**, fraction of light volatile compounds; **calculated values** from fractions and their mass ratios; –, not detected; t, traces <0.01 mg/kg; \*correct isomer is not identified; RI, retention index according to HP-20M column.

7.55 mg/kg), octanoic acid (**I**: 1.24 mg/kg; **II**: 0.35 mg/kg) and nonanoic acid (**I**: 0.69 mg/kg; **II**: 0.10 mg/kg). Decanoic acid was found in high amounts in fractions **a** (**I**: 25.85 mg/kg; **II**: 1.44 mg/kg) and **b** (**I**: 38.57 mg/kg). Acids with longer aliphatic chain, undecanoic (**I**: 6.86 mg/kg), dodecanoic (**I**: 14.57 mg/kg; **II**: 0.31 mg/kg), tridecanoic (**I**: 0.64 mg/kg), tetradecanoic (**I**: 9.00 mg/kg; **II**: 1.02 mg/kg), pentadecanoic (**I**: 2.14 mg/kg) and hexadecanoic acid (**I**: 72.65 mg/kg; **II**: 24.74 mg/kg) were found mostly in the fraction **b**. This is in agreement with the volatile analysis of carob beans,

which contain many of these compounds in the same fractions. In fraction **c**, nine compounds were identified, where cyclooctasulfur (**I**: 8.08 mg/kg; **II**: 13.09 mg/kg) was the major compound.

#### 4. Conclusion

Proposed HDA isolation method is particularly suitable for plant samples whose volatiles contain larger amount of water-soluble and high volatile compounds regardless of their functional

group. Mass ratios of the obtained fractions were dependent on their chemical composition, respectively, solubility in water and volatility. This method offers simultaneous hydrodistillation and adsorption that is more practical. Distillation, adsorption, extraction and concentration of volatiles are performed in only one apparatus. The main advantages of HDA method over HD method were the higher yields, fractionation of volatiles in three fractions and elimination of peak overlaps on chromatograms that produced more complete volatile analysis. However, the extraction of adsorbed compounds, performed with diethyl ether for 8 h, prolonged isolation of volatiles.

### Acknowledgements

This work was supported by MZOS, Croatia, project “Essential Oils and Flavours - Biologically Active Compounds and their Modifications” No. 011-098 2929-1329 in the framework of the MZOS “Spectroscopy and Modelling of Bioactive Molecules” No. 0982929. We acknowledge the botanical identification of the plant materials by MSc Mirko Ruščić, Faculty of Philosophy, University of Split.

### References

- [1] E. Guenther, *The Essential Oils*, 1, D. Van Nostrand Company, New York, 1965.
- [2] D.J. Rowe, *Chemistry and Technology of Flavour and Fragrances*, CRC Press, Boca Raton, 2006.
- [3] P. Schreier, *Chromatographic Studies of Biogenesis of Plant Volatiles*, Hüthig, Heidelberg, Basel, New York, 1984.
- [4] S.T. Likens, G.B. Nickerson, *ASBC Proceedings*, 1964, p. 5.
- [5] A. Chaintreu, *Flavour Fragr. J.* 16 (2001) 136.
- [6] E. Matisová, S. Škrabáková, *J. Chromatogr. A* 707 (1995) 145.
- [7] L.H. Wartelle, W.E. Marshall, C.A. Toles, M. Johns, *J. Chromatogr. A* 879 (2000) 169.
- [8] G. MacLeod, M. Forcen, *Phytochem.* 31 (1992) 3113.
- [9] J. Mastelić, D. Kuštrak, *Acta Pharm.* 47 (1997) 139.
- [10] E. Guenther, *The Essential Oils*, 3, D. Van Nostrand Company, New York, 1965.
- [11] M. Miyazawa, T. Maehara, K. Kurose, *Flavour Fragr. J.* 17 (2002) 187.
- [12] K. Grzunov, J. Mastelić, *Arh. Farm.* 32 (1981) 263.
- [13] J. Mastelić, K. Grzunov, *Kem. Ind.* 30 (1982) 249.
- [14] A.E. Edris, B.S. Girgis, H.H.M. Fadel, *Food Chem.* 82 (2003) 195.
- [15] J. Mastelić, I. Blažević, I. Jerković, *Croat. Chem. Acta* 79 (2006) 591.
- [16] I. Jerković, J. Mastelić, Z. Marijanović, Ž. Klein, M. Jelić, *Ultrason. Sonochem.* 14 (2007) 750.
- [17] I. Jerković, J. Mastelić, Z. Marijanović, *Chem. Biodiv.* 3 (2006) 1307.
- [18] R.P. Adams, *Identifications of Essential Oil Components by Gas Chromatography/Mass Spectroscopy*, Allured Publishers, Carol Stream, 1995.
- [19] A.M. Bones, J.T. Rossiter, *Phytochem.* 67 (2006) 1053.





## A new quantitative and low-cost determination method of nitrate in vegetables, based on deconvolution of UV spectra

Pham Hoai Nam<sup>a</sup>, Benitez Alejandra<sup>b</sup>, Hommet Frédéric<sup>c</sup>, Bombe Didier<sup>c</sup>, Schoefs Olivier<sup>a</sup>, Pauss André<sup>a,\*</sup>

<sup>a</sup> Chemical Engineering Department, Université de Technologie de Compiègne, BP 20.529, 60205 Compiègne Cedex, France

<sup>b</sup> Instituto de Ingeniería Química, Facultad de Ingeniería, Julio Herrera Reissig 565, 11300 Montevideo, Uruguay

<sup>c</sup> Centre Technique de la Conservation des Produits Agricoles, 41, avenue Paul Claudel, 80480 Dury les Amiens, France

### ARTICLE INFO

#### Article history:

Received 22 June 2007

Received in revised form 18 March 2008

Accepted 24 April 2008

Available online 2 May 2008

#### Keywords:

Nitrate determination

Vegetables

UV spectrum

PLS

### ABSTRACT

A new UV-spectrophotometric method for the determination of nitrate in vegetables is presented. The method is based on the spectral deconvolution: UV spectrum of a sample is considered as a linear combination of absorption spectra, named reference spectra. The combination of a small number of spectra of reference allows to reconstitute the shape of UV spectrum of an unknown sample. There have been several fresh vegetables (lettuce, curly lettuce, oak-leaf lettuce), as well as frozen spinaches that have been tested. The results obtained were comparable to those obtained with the reference HPLC method (official European reference method for the determination of nitrate in foodstuffs). The nitrate content varied from 377 to 3240 mg kg<sup>-1</sup> of fresh vegetables, and 545 to 1190 mg kg<sup>-1</sup> of frozen spinach. The recovery of added nitrate ranged from 91 to 99%. The results were obtained with a laboratory spectrophotometer and also with a dedicated field-type spectrophotometer. This method does not require almost any consumable, is quantitative and very fast reading with easy and low maintenance.

© 2008 Elsevier B.V. All rights reserved.

### 1. Introduction

Nitrate is monitored in food and agriculture products because it is harmful for human health. It can be reduced to nitrite, which may react with amines to form carcinogenic nitrosamines during digestion in human body. However, the use of nitrogen-containing fertilizers increases the nitrate concentration in the soil and therefore the nitrate content in vegetables. The nitrate concentration in vegetables varies enormously, ranging from 1 to 10,000 mg kg<sup>-1</sup> fresh weight [1] while the maximum allowable nitrate level is between 2000 and 4500 mg kg<sup>-1</sup> for the more concerned vegetables, i.e. lettuce and spinach (Table 1).

HPLC is the official method for foodstuffs, but usually nitrate and nitrite content in vegetables are measured by the Griess method. Nitrite, and nitrate after reduction to nitrite using the Cd–Cu reductor column, is diazotized with sulfanilamide in acid solution to form a diazonium cation, which is coupled with sodium 1-naphthol-4-sulfonate to form an azo dye product measured colorimetrically at 543 nm [3–5]. This method requires a long and demanding pre-treatment of the sample, which makes the pre-treatment quite expensive.

A variety of analytical methods for the determination of nitrate have been developed and applied to the analysis of food and agriculture products, including: high-performance liquid chromatography [6,7], ion chromatography [8–10], liquid chromatography [11], spectrophotometry [12–15], polarography [1], potentiometry with ion selective electrode [16], capillary electrophoresis [17–19], electron paramagnetic resonance [20]. However, these methods are rather expensive and highly time-consuming.

Some quick nitrate tests, Reflectometer Nitratechek [21–23] or RQflex [24,25], are used to control nitrate contents in soil and agriculture products. These methods are relatively cheap but the range of reading is high (Nitratechek: 5–500 mg NO<sub>3</sub><sup>-</sup>/L, RQflex: 3–90 mg NO<sub>3</sub><sup>-</sup>/L), and the precision depends on the matrix. More, Nitratechek only memorizes the last 20 results, while 50 results can be recorded by the RQflex.

On the other hand, the determination of nitrate in wastewater using UV spectroscopy is well documented [26]. In this paper, we developed a UV-spectrophotometric method for the measurement of nitrate content in vegetables by a spectrum deconvolution. The exploitation of UV spectrum is based on two hypotheses: UV spectrum of a sample is a linear combination of absorption spectra named reference spectra, and the combination of a small number of spectra of reference most of the time allows reconstituting the shape of UV spectrum of an unknown sample. Since in fresh vegetables the nitrite level is extremely low in compari-

\* Corresponding author.

E-mail address: [andre.pauss@utc.fr](mailto:andre.pauss@utc.fr) (A. Pauss).

**Table 1**  
Maximum allowed nitrate levels of spinach and lettuce [2]

Product	Maximum nitrate level (mg/kg)	
Fresh spinach	Harvest from 01/11 to 31/03	3000
	Harvest from 01/04 to 31/10	2500
Frozen spinach		2000
Fresh lettuce	Harvest from 01/10 to 31/03	4500
	Harvest from 01/04 to 30/09	3500
"Iceberg" lettuce		2500

son to nitrate [27], the contribution of nitrite was not taken into account.

## 2. Materials and methods

### 2.1. UV-spectrophotometer

The spectrophotometers are an Anthelie UV-vis device (lab-type, resolution of 1 nm, 190–900 nm), and a modified Assistemo-UV device (field-type, resolution of 11 nm, 190–320 nm), both from Secomam (Alès, France). They were controlled by UV-Pro software version 1.25d (Secomam).

### 2.2. Sample preparation

Vegetables (lettuce, curly lettuce, oak-leaf lettuce, frozen spinach) were purchased from a local market. The samples were cut into small pieces of about 1 cm, 1.5 g was weighed (3 g for frozen spinach), and suspended into 500 mL distilled water. After homogenizing in a Waring Blender for 1 min, the suspension was centrifuged (Eppendorf 5810R) at  $1700 \times g$  for 5 min, and filtered through a  $0.45\text{-}\mu\text{m}$  filter (Durapore HV, Millipore). The filtrate is then used for the analytical determinations and UV measurements.

### 2.3. Analytical determinations

Nitrate content of the filtrates was determined by HPLC according to the European method [28] in the CTCPA laboratory. The usual analytical error is about 5%. The residual pigments and unidentified carbon material in the filtrate were measured and expressed as dissolved organic carbon (DOC) (measured with a Total Organic Carbon 1010 analyzer, O-I-Analytical, College Station, TX, USA), with analytical errors of 5–10%.

The UV spectra of the filtrates, measured with a 5 mm quartz cell, and the actual nitrate and DOC contents were then used to create deconvolution models.

### 2.4. Principle of the spectrum deconvolution method

In this work, for each tested vegetables, 10–20 samples were used to create specific deconvolution models, which were validated with other samples. The method of deconvolution is based on a procedure of matrix algebra that each spectrum corresponds to a linear combination of a small number  $p$  of reference spectra [29].

In the model, the coefficients  $a_i$  of the linear combination are calculated by the resolution of a system based on the following relation established for each wavelength with:

$$Se(\lambda) = \sum_{i=1}^p a_i REF_i(\lambda) \pm r$$

$Se(\lambda)$  is the sample absorbance,  $REF_i(\lambda)$  is the absorbance of the reference compound  $i$ ,  $r$  is the error.

The reference spectra can be pure single molecules at different concentrations, or experimental solutions with analytical identi-

fication, or both. In all this work, for each tested vegetable, the UV spectra of a dozen of filtrated suspensions were recorded, and some analytical parameters were analyzed as explained before. We assumed that the UV signal is mainly due to the nitrate molecule and to some undetermined dissolved molecules among chlorophyll pigments (data not shown). We only used nitrate and DOC (determined with TOC measurements after filtration) in the model. That means that all the UV contributors other than nitrate are globalized in one unique DOC value.

Reference spectra are thus different for each vegetable, i.e. common lettuce, curly and oak-leaf lettuces, and spinach. They are not normalized but used to build specific deconvolution models.

A drawback of this reference procedure is that the applicability range is formally given by the values of the selected samples used, even if it could be further extended through additional samples.

In this work, we tested the deconvolution procedures of UV-Pro software (Secomam), and a partial least squares (PLSs) analysis with Matlab software (MathWorks, Natick, MA, USA).

The product of the nitrate coefficient with the concentration of the corresponding reference spectrum gave nitrate concentration.

## 3. Results and discussion

### 3.1. UV absorption of salads

Different types of salads have been analyzed. As shown in Fig. 1, UV spectra were highly reproducible for the same type of lettuce, and that was reproduced several times. All these spectra were recorded with the Anthelie spectrophotometer. But the UV shapes were quite different for the common lettuces as compared to the curly lettuce and the oak-leaf ones. The UV shape of lettuce was mainly due to the a higher nitrate content (see below), that explained the large peak at 206 nm, while the suspensions of curly and oak-leaf lettuces contained less nitrates but more pigments, that were analyzed in global DOC, and provided a higher UV absorption at about 250 nm. First we focused on the common lettuces that are supposed to contain higher amounts of nitrates.

### 3.2. Nitrate content of common lettuces

Ten different common lettuces were purchased from a local market. They were cut in small pieces and all the material was homogenised. Forty samples were constituted at random, then treated as described before. Among those 40 samples, 30 were used

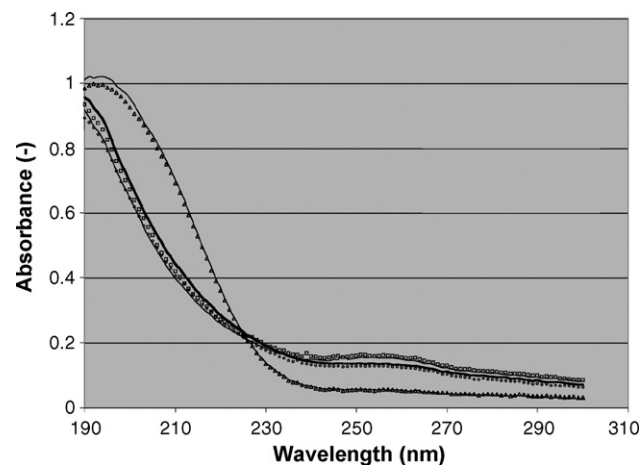


**Fig. 1.** UV spectra of different salads. Solid line and triangles, common lettuce 1 and 2; bold line and circles, curly lettuces 1 and 2; solid line and squares, oak-leaf lettuces 1 and 2.

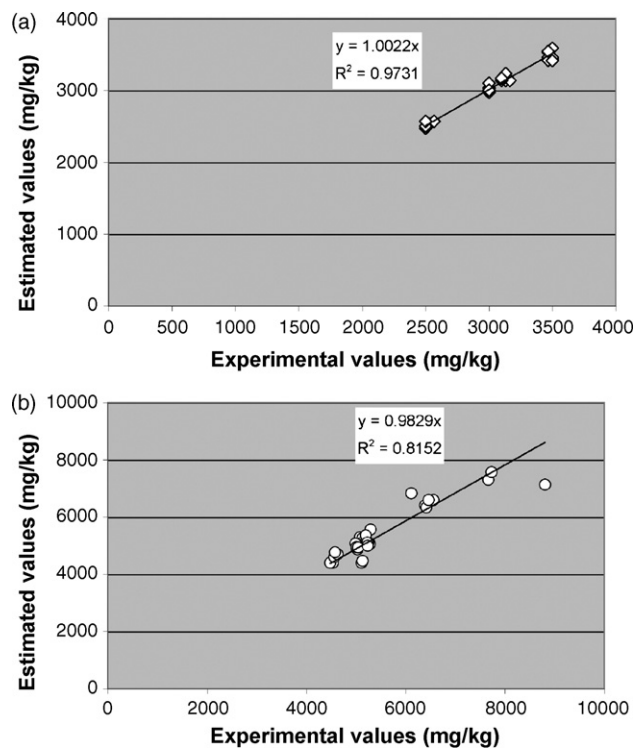


**Fig. 2.** (a) Cross-validation of the nitrate deconvolution model for common lettuces. (b) Cross-validation of the DOC deconvolution model for common lettuces.

to create the model and test a cross-validation, while 10 samples were kept for a later validation. The UV spectra and the experimental analyses of the thirty first samples were used to create a model with two constituents, nitrate and DOC, and the UV-Pro software. This model was then cross-validated, that means that each UV spectrum was deconvoluted and compared to its actual contents, with a particular model created with the other 29 samples. Fig. 2a and b shows that the cross-validation was almost perfect for nitrate and, to a lower extent, for DOC. This cross-validation figures indicate the reliability of the calibration; but also show to which extent the calibration model integrates the individual contribution of each sample.

The last 10 samples were used to formally validate the model. All the validation results are given in Table 2. The average ratio of estimated on actual nitrate content was  $99.9 \pm 2.0\%$ , which is very good considering that the uncertainty of the analytical method is about 4%. In Table 2, the deconvolution error, given by UV-Pro software, indicates the quantitative difference between the UV-

**Table 2**  
Validation results of common lettuces

Sample	Estimated nitrate values		Experimental nitrate values (mg/kg)	Estimated on experimental values (%)
	mg/kg	Deconvolution error (%)		
1	2567	$\pm 0.4$	2533	101
2	3167	$\pm 0.2$	3133	101
3	3000	$\pm 0.1$	3033	99
4	3100	$\pm 0.1$	3000	103
5	3400	$\pm 0.1$	3500	97
6	2500	$\pm 0.2$	2567	97
7	3167	$\pm 0.1$	3100	102
8	2967	$\pm 0.1$	3000	99
9	3000	$\pm 0.1$	3033	99
10	3500	$\pm 0.1$	3500	100

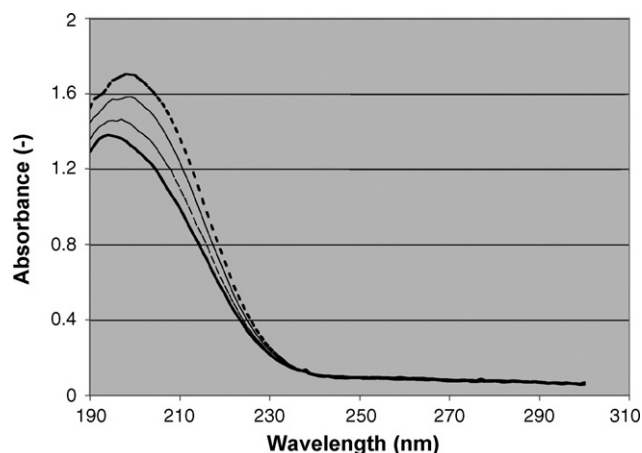


**Fig. 3.** UV spectra of a common lettuce with different amounts of added nitrate. Bold line, common lettuce without added nitrate; --, +900 mg nitrate/kg; solid line, 1500 mg nitrate/kg; bold dotted line, +2100 mg nitrate/kg.

spectra and an equivalent one, rebuilt according to the model with the estimated values. The lower this error the better the result.

It thus appear that the nitrate content of a common lettuce can be easily and rapidly estimated with a simple UV measurement between 2500 and 3500 mg/kg, however after the preparation steps. As said earlier, the current range is given by the samples used for the calibration step; it could be further extended through additional samples.

Known amounts of sodium nitrate were then added to a common lettuce sample to check the correctness of the method. Fig. 3 shows the resulting UV spectra for, respectively, 900, 1500, and 2100 mg of added nitrate per kilogram, to a common lettuce that originally contained 3240 mg nitrate/kg. It can be observed that the wavelength of the maximum peak progressively shifted to about 206 nm, that is characteristic for the nitrate ion. The results of Table 3 show that 91–99% of the expected nitrate contents were recovered, suggesting the correctness of the method.

### 3.3. Nitrate content of curly and oak-leaf lettuces

Since the UV shapes of curly and oak-leaf lettuces were similar, they were considered together. Ten salads of both types were prepared and analyzed as described for the common lettuces. It was found that the curly lettuce actually contained  $880 \pm 208$  mg nitrate/kg (range 547–1160) and  $13,400 \pm 1100$  mg DOC/kg (range 11,588–15,302). The results for oak-leaf lettuce were  $652 \pm 158$  mg nitrate/kg (range 377–983), and  $9900 \pm 710$  mg DOC/kg (range 8963–11,583).

The actual experimental values and the UV spectra were used to create six different models, three models with UV-Pro software and three models with Matlab. For both softwares, a specific model for the curly lettuce was created and then cross-validated, as well

**Table 3**  
Proportioned additions of nitrate to a common lettuce

	Estimated nitrate		Deconvolution error (%)
	mg/kg	% of expected value	
Lettuce without added nitrate	3240	–	$\pm 1.6$
Addition of 900 mg <sub>nitrate</sub> /kg	4110	99.0	$\pm 2.0$
Addition of 1500 mg <sub>nitrate</sub> /kg	4500	94.9	$\pm 3.5$
Addition of 2100 mg <sub>nitrate</sub> /kg	4860	91.0	$\pm 4.9$

**Table 4**

Estimated nitrate contents of curly and oak-leaf lettuces by both different deconvolution methods of UV spectra, in percentage of analytical contents

	UV-Pro software	PLS
Curly lettuces		
Specific deconvolution model	99 ± 3%	100 ± 1%
Global deconvolution model	98 ± 7%	100 ± 3%
Oak-leaf lettuces		
Specific deconvolution model	98 ± 5%	100 ± 1%
Global deconvolution model	101 ± 13%	101 ± 5%

as for the oak-leaf lettuces. Then a global model was built with the 20 lettuces together, and again cross-validated.

The results in Table 4, where the estimated nitrate contents were calculated as percentage of the experimental contents, show that both deconvolution methods provided analogous results. In both cases the deconvolution errors were always lower than 10%, with an average values of about 4.6%. As UV-Pro software appeared as a black box, it was interesting to know if a more usual and documented method could give better or at least equivalent results. PLS algorithm was actually able to deconvolute the UV spectra and to estimate the component contents. However, due to those similar results, and to the user-friendlier interface of UV-Pro, it has been kept for the other experimentations.

Table 4 also indicates that both types of lettuces can be analyzed using specific or global models. This point is crucial because that demonstrates that a global model can be used for different vegetables that exhibit similar UV shapes. It means that it is not necessary to create specific models relative to each vegetables, or even each season or producer. Finally, results in Table 4 also demonstrate that the uncertainties of the estimated value were quite low, and at least in the uncertainty range of the reference methods.

No longer validation step was performed with new curly and oak-leaf salads.

### 3.4. Nitrate content of frozen spinach

Spinach leaves often present large amounts of nitrate that explain why this vegetable is concerned by the EC regulations. Fifteen samples of frozen spinach were defrosted and analyzed as described before. The nitrate content ranged from 545 to 1190 mg nitrate/kg (average value of 962), for a maximum acceptable value of 2000.

Fig. 4 shows the cross-validation between the experimental and the estimated values of nitrate. A good correlation ( $R^2 = 0.935$ ) was also obtained for DOC (data not shown). To validate the method, four sets of about 20 g of frozen spinaches, from two different

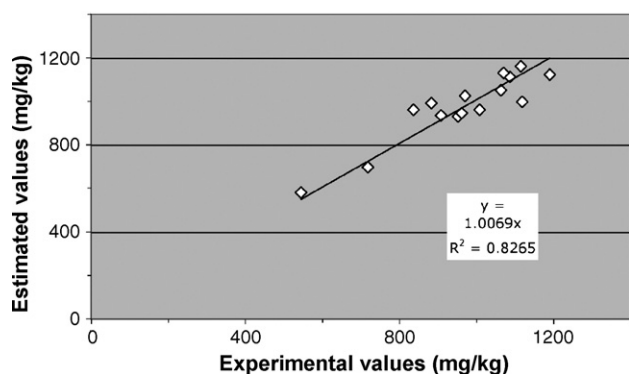


Fig. 4. Correlation between the experimental and the estimated nitrate content of frozen spinach, with the Anthelie spectrophotometer.

**Table 5**

Validation results of frozen spinach

Samples	Estimated nitrate values (mg/kg)	Experimental nitrate values (mg/kg)	Estimated on experimental values (%)
1	981 ± 89	872 ± 70	112.5
2	1422 ± 13	1221 ± 98	116.5
3	1853 ± 50	1768 ± 141	104.8
4	1503 ± 33	1429 ± 114	105.2

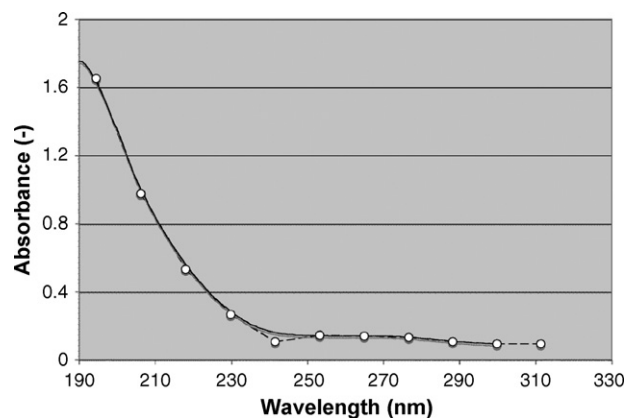


Fig. 5. UV spectra of a suspension of frozen spinach, with the lab-type device (bold line) and the field-type spectrophotometer (dots and dotted line).

trademarks were constituted. For each sets, three samples were analyzed. The results of Table 5 indicate that, as for the lettuces, it was possible to rapidly estimate the nitrate content of spinach, even if the estimated values are weakly overestimated.

All the previous experimentations were achieved with a lab-scale spectrophotometer (Anthelie, Secomam) with contains moving parts for the network and for the UV and the visible lamps. If such a device can be used in a laboratory, its robustness under industrial conditions seems more uncertain. During the spinach campaign for instance, the vegetables are brought to the factory 24 h a day, 7 days a week, and the nitrate content (and obviously other parameters) must be rapidly and exactly determined to accept the spinach cargo into the process. The nitrate analysis must thus be achieved under rather difficult conditions, not actually compatible with a lab-scale device. On the other hand, the Secomam company developed a field-type spectrophotometer for the environmental analysis (called Assistemo). This device contains CCD diodes spaced by 12 nm, whilst the Anthelie spec-

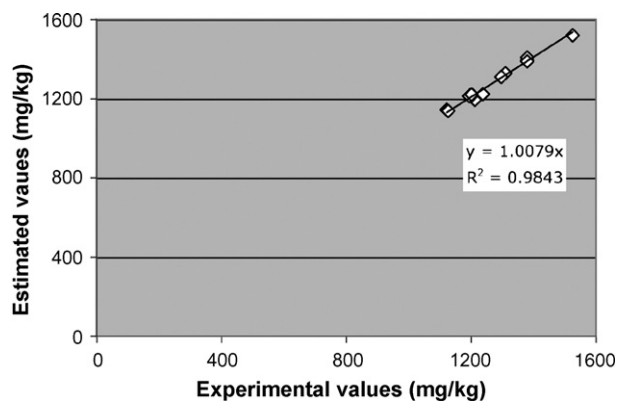


Fig. 6. Correlation between the experimental and the estimated nitrate content of frozen spinach, with the Assistemo-UV spectrophotometer.

trophotometer possesses a resolution range of 1 nm. It was thus decided to evaluate the possibility to downgrade the model created with the Anthelie device. The model was downgraded for the Assistemo device, and 15 new frozen samples of spinach were analyzed and deconvoluted with the modified model. Fig. 5 shows the UV-spectra of frozen spinach for both spectrophotometers. Results of Fig. 6 indicated that, even with this low resolution, nitrate contents can be perfectly estimated by the deconvolution of UV spectra with the Assistemo device. A good correlation ( $R^2 = 0.993$ ) has also been obtained for DOC (data not shown). This device will be tested under real industrial conditions in the near future.

#### 4. Conclusions

In the present work, it was shown that nitrate can be correctly estimated in various vegetables by mathematical deconvolutions of UV-spectra. This method almost does not require any consumable; it is quantitative and very fast reading with easy and low maintenance. Apart the preparation steps, that are common to almost all analytical methods, the nitrate content is given within about 1 min, with low manpower. An interesting point to note is the wide applicability of the models, which allows measuring nitrate in vegetables independently of the variations inside of cargos or other. The large range of measurement and the low uncertainty of the results suggest that this method could be used in replacement of other rapid methods currently used in factories for quality controls.

#### Acknowledgements

The authors like to thank, on one hand, the Région Picardie and the Ministère de l'Education Nationale, de la Recherche et de la Technologie for their financial support through The Pôle Régional Génie des Procédés, and on the other hand, JC Bouvier (INRA, Narbonne, France) for his help in the PLS analysis of the UV spectra.

#### References

- [1] S. Rath, M.I.N. Ximenes, F.G.R. Reyes, *Talanta* 51 (2000) 49.
- [2] European Communities, Regulation No 466/2001 of 8 March 2001 setting maximum levels for certain contaminants in foodstuffs, *Official Journal L 077* (2001), pp. 1–13.
- [3] K. Horita, G.F. Wang, M. Satake, *Microchem. J.* 58 (1998) 162.
- [4] K. Horita, G.F. Wang, M. Satake, *Talanta* 46 (1998) 671.
- [5] M. Cemek, L. Akkaya, Y.O. Birdane, K. Seyrek, S. Bulut, M. Konuk, *J. Food Compos. Anal.* 20 (2007) 236.
- [6] M.J. Dennis, P.E. Key, T. Papworth, M. Pointer, R.C. Massey, *Food Addit. Contam.* 7 (1990) 455.
- [7] C.W. Tsang, C.F. Cheng, *Food Addit. Contam.* 15 (1998) 753.
- [8] P.L. Buldini, S. Cavalli, A. Trifirò, *J. Chromatogr. A* 789 (1997) 529.
- [9] D.C. Siu, A. Henshall, *J. Chromatogr. A* 804 (1998) 157.
- [10] M. Zhou, D. Guo, *Microchem. J.* 65 (2000) 221.
- [11] S.B. Butt, M. Riaz, M.Z. Iqbal, *Talanta* 55 (2001) 789.
- [12] M.I. Karayannis, M.J. Ahmed, C.D. Stalikas, S.M. Tzouwara-Karayanni, *Talanta* 43 (1996) 1009.
- [13] M.A. Ferreira, O. Pinho, I.M.P.L.V.O. Ferreira, M.B.P.P. Oliveira, *Food Chem.* 62 (1998) 359.
- [14] N.A. Zatar, M.A. Abu-Eid, A.F. Eid, *Talanta* 50 (1999) 819.
- [15] S. Rath, R. Andrade, C.O. Viana, S.G. Guadagnin, F.G.R. Reyes, *Food Chem.* 80 (2003) 597.
- [16] R. Pérez-Olmos, R. Herrero, J.L.F.C. Lima, M.C.B.S.M. Montenegro, *Food Chem.* 59 (1997) 305.
- [17] D.L. Massart, M. Jimidar, C. Hartmann, N. Cousement, *J. Chromatogr. A* 706 (1995) 479.
- [18] P.A. Marshall, V.C. Trenerry, *Food Chem.* 57 (1996) 339.
- [19] F.B. Erim, N. Oztekin, M.S. Nutku, *Food Chem.* 76 (2002) 103.
- [20] N.D. Yordanov, E. Novakova, S. Lubenova, *Anal. Chim. Acta* 437 (2001) 131.
- [21] A. Nitsch, E. Varis, *Potato Res.* 34 (1991) 95.
- [22] C. Videla, H. Echeverria, *Ciencia del Suelo* 16 (1998) 131.
- [23] R. Wetselaar, G.D. Smith, J.F. Angus, *Commun. Soil Sci. Plant Anal.* 29 (1998) 729.
- [24] S. Nagarajah, *Aust. J. Grape Wine Res.* 5 (1999) 56.
- [25] M.A. Rodrigues, J. Coutinho, F. Martins, M. Arrobas, *Eur. J. Agron.* 23 (2005) 79.
- [26] M. Karlsson, B. Karlberg, R.J.O. Olsson, *Anal. Chim. Acta* 312 (1995) 107.
- [27] J. Hunt, M.K. Turner, *Food Addit. Contam.* 11 (1994) 327.
- [28] European Communities, Foodstuffs, determination of nitrate and/or nitrite content. Part 2. HPLC/IC method for the determination of nitrite content of vegetables and vegetable products, EN 12014-2, 1997.
- [29] O. Thomas, F. Theraulaz, M. Domeizel, C. Massiani, *Environ. Technol.* 14 (1993) 1187.



## Detection of methyl salicylate using polymer-filled chemicapacitors

Sanjay V. Patel\*, Stephen T. Hobson, Sabina Cemalovic, Todd E. Mlsna

Seacoast Science, Inc., 2151 Las Palmas Drive Suite C, Carlsbad, CA 92011, United States

### ARTICLE INFO

#### Article history:

Received 21 February 2008

Received in revised form 16 April 2008

Accepted 17 April 2008

Available online 24 April 2008

#### Keywords:

Capacitance measurement

Chemical transducers

Methyl salicylate

Microsensors

Sensor array

Man-in-Simulant Test

### ABSTRACT

Methyl salicylate (MeS) is used as a chemical warfare agent simulant to test chemical protective garments and other individual personal protective gear. The accurate and real-time detection of this analyte is advantageous for various testing regimes. This paper reports the results of MeS vapor exposures on polymer-filled capacitance-based sensors at temperatures ranging from 15 °C to 50 °C under dry and humid conditions. Multiple capacitors were arranged in an array on a silicon chip each having a different sorptive polymer. The sensors used parallel-plate electrode geometry to measure the dielectric permittivity changes of each polymer when exposed to water and MeS vapor. Of the four polymers tested against MeS, the optimal polymer displayed near or sub-parts-per-million detection limits at 35 °C (0–80%RH).

© 2008 Elsevier B.V. All rights reserved.

### 1. Introduction

The United States Departments of Homeland Security (DHS) and Defense (DOD) are testing next generation personal protection systems to protect U.S. military personnel from chemical threats. Some of these programs focus on Man-in-Simulant Testing (MIST), where methyl salicylate (MeS) is used to test the effectiveness of chemical suits [1,2]. Currently, the suits are tested with passive absorbent pads to collect samples while soldiers or mannequins wear the suits during MeS exposure [3]. To identify the weaknesses in the system, i.e. chemical break-through sites; small, unobtrusive and light weight sensors are needed to collect real-time data as the suits are used during tests.

A key requirement of this application is that proposed sensors do not interfere with air-flow through the suit or with the wearer's mobility. This significantly restricts the size and power of a viable sensor system. Furthermore, the sensors must operate in high relative humidity and elevated temperature environment proximate to the skin of a warfighter or first responder performing their tasks. Microfabricated sensor arrays have the potential to address this need.

Microsensors using sorbent materials are promising for this niche application since they can operate at ambient temperature and can be miniaturized. Such sensors measure changes in the sorbent material when a vapor or gas is absorbed. Reported tech-

nology platforms include: resistive sensors [4,5] and cantilever stress sensors [6] to measure swelling of polymers; resonating cantilevers [7], surface acoustic wave (SAW) devices [8], and flexural plate wave (FPW) devices [9] to measure mass and viscoelasticity changes; and capacitive sensors [10,11] to measure changes in polymer permittivity. Multi-transducer arrays, systems with multiple different technologies, have also been reported for vapor detection [12].

Presented herein are the results from the exposure of four chemicapacitors, each filled with a different semi-selectively MeS absorbing dielectric polymers. As chemicals sorb into the dielectric, they alter its permittivity and thereby raise or lower the capacitance of the sensor. The four polymers have functional groups of varied polarity, acidity, and dielectric constant (~2–10).

### 2. Experimental

#### 2.1. Sensor structure

The sensor structures used in this study were fabricated using the Multi-User MEMS Process (MUMPs) [13] from MEMSCAP, Inc. (Durham, NC). Fig. 1 shows a top-view photograph and a side-view cross-section diagram of one of these structures. In the present work, two chips were used, each having multiple parallel-plate capacitor structures spaced approximately 300–500 μm apart, on a 2 mm × 5 mm chip [14]. The structures are made from polycrystalline silicon deposited on an insulating silicon nitride layer. Each parallel-plate capacitor is square-shaped, approximately 285 μm on a side, with a 0.75 μm vertical gap between the plates. The top

\* Corresponding author. Tel.: +1 760 268 0083; fax: +1 760 268 0662.  
E-mail address: [sanjay@seacoastscience.com](mailto:sanjay@seacoastscience.com) (S.V. Patel).

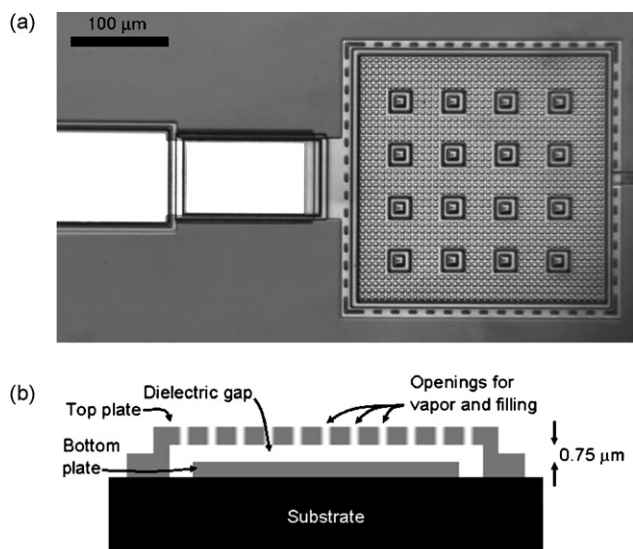


**Fig. 1.** Parallel-plate chemicapacitor element: (a) top-view photograph showing square capacitor and wirebond pad and (b) cross-sectional diagram (not to scale).

plate is perforated forming a waffle pattern, with silicon beams of  $2.5\ \mu\text{m}$  and holes of  $5\ \mu\text{m}$ . The drive circuit [14,15] applies a square wave to the bottom plate, and the top plate is used to sense the capacitance of the structure. The 16 larger squares are support posts, which together with the outer edge of the square (also perforated) keep the top plate from flexing.

## 2.2. Sensitive materials

The dielectric gap between the plates of each capacitor was filled with a dilute polymer solution (<1 wt% in chloroform, toluene, or acetone) injected through holes in the top plate using a piezoelectric-driven ink-jet from MicroFab Technologies, Inc. [16]. The residual solvent was allowed to evaporate, leaving the neat polymer in the capacitor.

The same two chips were used for all of the sensor testing. Each chip contained four chemicapacitors, and each chemicapacitor was coated with one of the four polymers listed in Table 1 [17,18]. All data presented are averaged responses from the same polymer on both chips, and all error bars represent  $\pm 1$  S.D. of the responses for multiple (typically 3–5) chemical exposures. The error bars provide a measure of chip-to-chip repeatability and exposure-to-exposure repeatability.

PEVA and PECH were purchased from Sigma–Aldrich Corp. (St. Louis, MO), PIB from Polysciences, Inc. (Warrington, PA), and ADIOL [19] was received from Dr. McGill at the U.S. Naval Research Laboratories. The values for the dielectric constants were measured on the two chips at  $20\ ^\circ\text{C}$  in dry air, and match well with values found in the

literature [14,20,21]. In comparison, MeS has a reported dielectric constant of 9 at  $20\ ^\circ\text{C}$  and 9.41 at  $30\ ^\circ\text{C}$  [22].

## 2.3. Sensor testing

Sensor chips were wire-bonded in low volume ceramic packages with capacitance measurement circuits [14,23]. The capacitance measurement circuit used in these tests had a range of  $0.01$ – $350\ \text{pF}$  with a resolution of  $0.001\ \text{pF}$ . The circuit uses a square wave to charge each capacitor, which is then discharged to a reference capacitor whose potential is measured. A microprocessor and other related circuitry on a printed circuit board are used to control the timing and applied voltages, and to measure the capacitances. Three modifications were made to the previous circuit [23]; (1) the range of measurements was increased to over  $350\ \text{pF}$ , (2) the measurement circuit operated at  $3.3\ \text{V}$ , reduced from  $5\ \text{V}$ , and (3) the applied voltage was centered to prevent charging across the polymer.

Noise in the system ranged from  $0.001\ \text{pF}$  to  $0.7\ \text{pF}$ , and was dependant on the capacitance being measured, the resolution of the analog to digital converters, and the applied oscillator voltage ( $0.012$ – $3.2\ \text{V}$ ). The highest noise levels occurred at high measured capacitances that were typically encountered at high relative humidity.

A computer controlled gas delivery system, consisting of mass-flow controllers (MKS Instruments, Andover, MA), was used to deliver and dilute the chemical vapors with compressed and dried laboratory air. The sensors were tested under continuous air-flow. The MeS vapors were generated by bubbling air through the liquid in a fritted glass gas-washing bottle (ACE Glass, Inc., Vineland, NJ) that was temperature-controlled in a chilled water bath. Humid air was mixed by adding a stream of air bubbled through deionized water also in a temperature-controlled chilled water bath. Two sensor chips were tested simultaneously in a silcosteel<sup>®</sup> passivated (Restek, Corp., Bellefonte, PA) stainless steel chamber (approximately  $10.8\ \text{cm} \times 2.4\ \text{cm} \times 0.6\ \text{cm}$ , internal wetted volume). To keep the exposed volumes low, only the sensor chips and ceramic packages were exposed to chemicals, while the remaining circuit board was connected using a feed-through to outside of the test chamber. The test chamber was temperature controlled to  $\pm 0.1\ ^\circ\text{C}$ .

Vapor pressures were extrapolated from Antoine coefficients in Lange's Handbook of Chemistry [22] and compared to extrapolations from the NIST Webbook [24]. From these data the vapor pressure of MeS was estimated to be  $0.1\ \text{Torr}$  at  $25\ ^\circ\text{C}$  and  $0.35\ \text{Torr}$  at  $40\ ^\circ\text{C}$ .

## 3. Results and discussion

All four polymers responded to MeS vapor in a monotonic fashion, over the range of temperatures and concentrations tested. Fig. 2 shows the raw response of a PECH- and a PIB-filled chemicapacitor to three concentrations of MeS. PECH-filled chemicapacitors pro-

**Table 1**  
Polymers tested and their nominal capacitance measured at  $20\ ^\circ\text{C}$  in dry air with microcapacitors

Polymer	Functionality and properties	Starting capacitance (pF)	Dielectric constant
Polyisobutylene (PIB); MW = 1350	Low-polarity hydrocarbon; viscous liquid	2.4	2.4
Poly(ethylene-co-vinyl acetate) (40% acetate content) (PEVA)	Low-polarity, solid, semi-crystalline [17]	4.2	4.0
Bis[(E)-1,1,1-trifluoro-2-(trifluoromethyl)pent-4-en-2-ol]siloxane (ADIOL)	Polar; hydrogen-bond acidic; greasy liquid	5.4	5.3
Polyepichlorohydrin (PECH); MW = 700,000	Moderate hydrogen bonding [18]; polar; solid	10.2	9.8

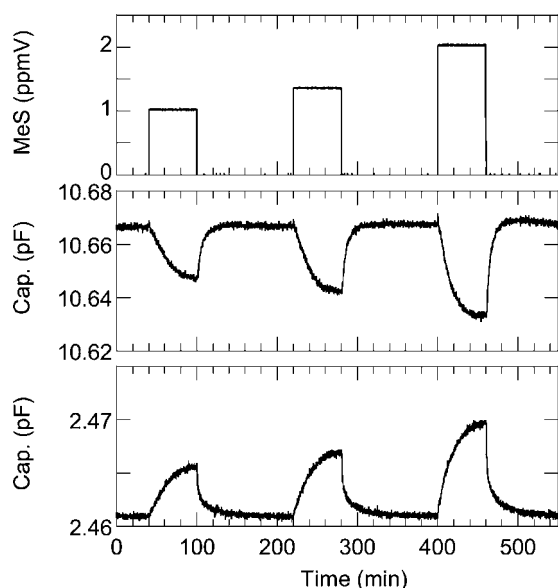


Fig. 2. Sensor responses to MeS in 50% relative humidity at 25 °C. MeS concentrations (top), PECH chemicapacitor (middle), PIB chemicapacitor (bottom).

duced negative capacitance shifts when exposed to MeS, whereas the other polymer-filled chemicapacitors produced positive capacitance changes upon MeS exposure. This discrepancy has been discussed in the literature and is associated with the balance between swelling effects versus the increase in number and density of dipoles in the bulk polymer [10]. If swelling dominates and the analyte has a lower dielectric constant than the polymer, as with PECH, the MeS causes the bulk permittivity to decrease. Other work on parallel-plate chemicapacitors showed that both PIB and PEVA provided decreasing permittivity upon sorption of analytes with low dielectric constants, including some aromatic compounds and alkanes [10,14].

The capacitance and dielectric permittivity of all four polymers increase when exposed to water vapor, but to varying degrees (Table 2). PIB- and PEVA-filled chemicapacitors were the least sensitive, followed by PECH and ADIOL, which was the most sensitive to water vapor. Note that water vapor equilibrated faster than

Table 2

Average capacitance change ( $\Delta C$ ) for a 0–20% relative humidity step at each temperature

	At 35 °C (pF)	At 25 °C (pF)	At 15 °C (pF)
PIB	0.002	0.002	0.002
PEVA	0.024	0.022	0.022
PECH	0.110	0.089	0.076
ADIOL	0.665	0.463	0.338

MeS in the test system. These devices have previously demonstrated response times in the order of 200 ms to 1 s [23]. The measured capacitance of the PECH, PIB and PEVA chemicapacitors all decreased upon heating in both dry air and 50% relative humidity. In contrast, the capacitance of the ADIOL-filled sensors increased in both environments.

Fig. 3 contains graphs of the response of the PECH chemicapacitors at temperatures ranging from 15 °C to 50 °C. At lower temperatures (<30 °C), sub-ppmV (parts-per-million by volume) concentrations of MeS were detectable in both dry and 50% relative humidity. The dashed horizontal line denotes the “noise” floor for the measurements. The lowest detectable concentration increases drastically at higher temperatures consistent with the proposed physisorption-based sensing mechanism [25]. In addition, the slope of the response curves becomes shallower, i.e. the sensitivity decreases as temperature increases. This is primarily due to the vapor–liquid equilibrium favoring the vapor phase at the higher temperatures.

Similarly, PIB- and PEVA-filled chemicapacitors provide sensitivity profiles (Figs. 4 and 5) that exhibit decreased sensitivity at higher temperature; however, their lowest detectable concentrations are better than PECH. ADIOL-filled chemicapacitors were most sensitive to MeS at all temperatures (Fig. 6), although their response speed was significantly slower at 15 °C. Due to the slow equilibration 15 °C ADIOL response data is presented in the inset graphs. This extremely slow equilibration causes the measured response at 15 °C to be much smaller than at 20 °C, behavior that is not observed on the other polymers at 15 °C. PECH and PEVA are solids at this temperature and PEVA is semi-crystalline [17], although PECH is well above its glass transition temperature (−22.5 °C). One possible explanation for this response speed is that ADIOL is approaching its glass transition temperature ( $T_g$ ), drastically slowing the diffu-

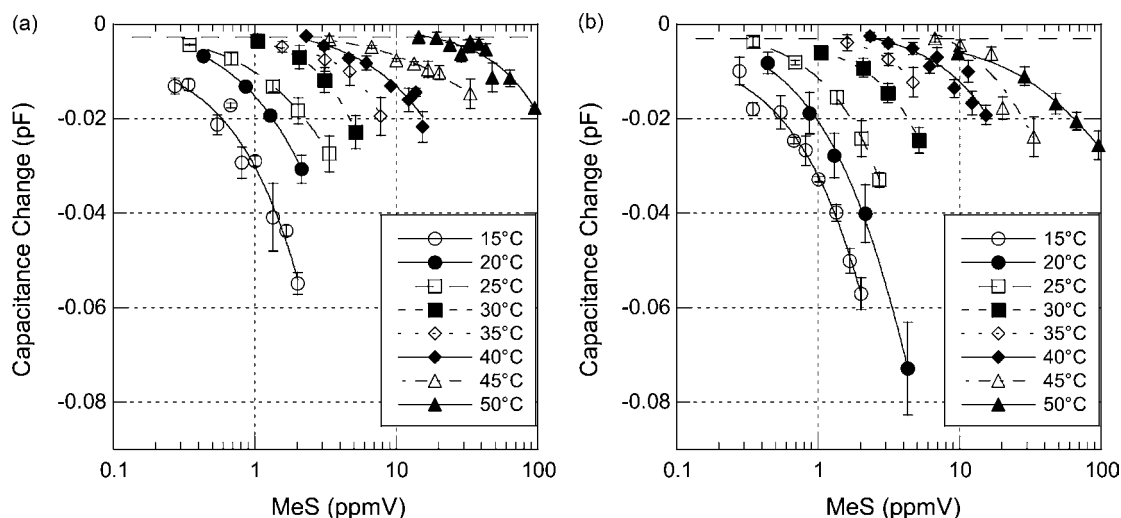


Fig. 3. Isotherms for the PECH-filled chemicapacitors, (a) under 50% relative humidity and (b) in dry air, for MeS concentrations between 300 ppbV and 100 ppmV. The lines are only meant to guide the eye. The dashed horizontal line in each figure represents the peak-to-peak noise. Each point represents the average response and the error bars are  $\pm 1$  S.D. of the responses for multiple (typically 3–5) chemical exposures.



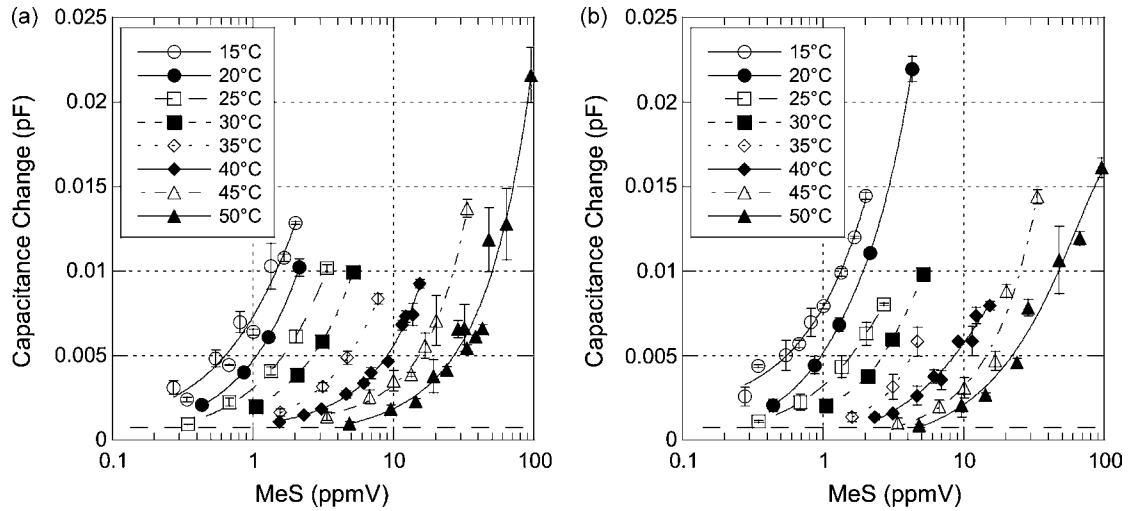


Fig. 4. Isotherms for the PIB-filled chemicapacitors: (a) under 50% relative humidity and (b) in dry air, for MeS concentrations between 300 ppbV and 100 ppmV.

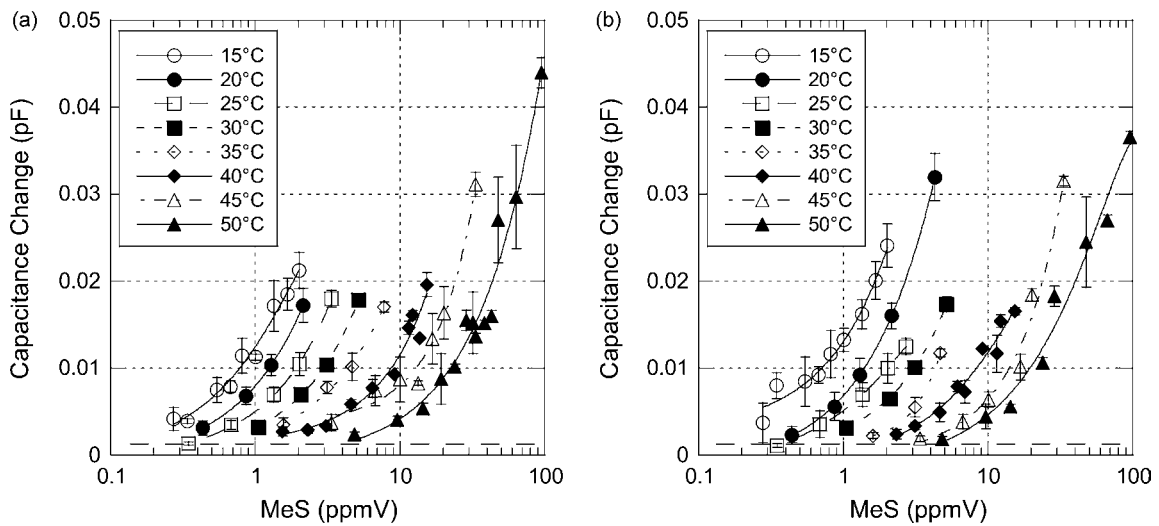


Fig. 5. Isotherms for the PEVA-filled chemicapacitors: (a) under 50% relative humidity and (b) in dry air, for MeS concentrations between 300 ppbV and 100 ppmV.

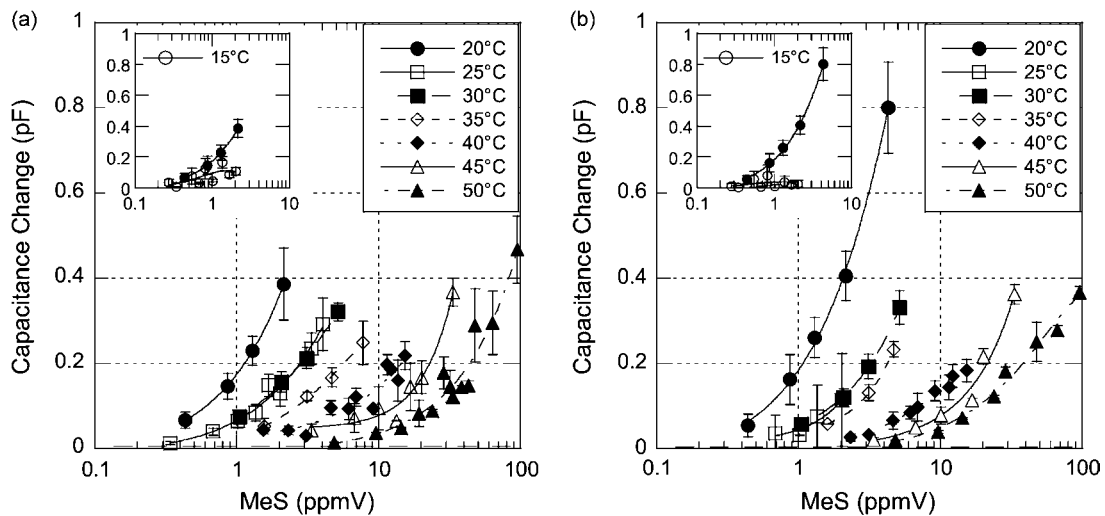
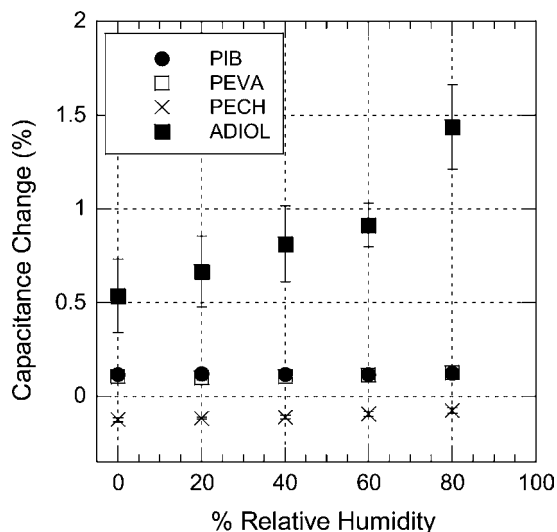


Fig. 6. Isotherms for the ADIOL-filled chemicapacitors: (a) under 50% relative humidity and (b) in dry air, for MeS concentrations between 300 ppbV and 100 ppmV. Inset graphs show the 15°C and 20°C isotherms with the same y-axis scale.



**Fig. 7.** Affect of humidity on response of all four polymer-filled chemicapacitors to 1 ppmV MeS, exposures at 25 °C. Note: PIB and PEVA responses overlap on all exposures.

sion of MeS into the polymer. Another possibility is that at lower temperatures, the ADIOL response is able to accumulate significant amounts of MeS by very strong hydrogen-bonding interactions [26]. Whereas the other polymers equilibrated with MeS in 1 h at 15 °C, ADIOL did not equilibrate even after 3 h except at the highest concentrations. Albeit faster, the ADIOL response was still slow at 20 °C and 25 °C, therefore the equilibrated response after 1 h of exposure is presented in all graphs.

To compare the sensors' sensitivity to MeS under various conditions, sensor responses to 1 ppmV MeS exposures at 15 °C, 25 °C, and 35 °C were measured. 1 ppmV exposures at 25 °C show that PECH, PIB and PEVA are unaffected by the background humidity (Fig. 7). This is true for PIB and PEVA at 15 °C and 35 °C also. In contrast ADIOL's sensitivity to MeS improves at higher relative humidity levels at 25 °C, but does not continue this trend at 35 °C (Fig. 8a). As seen in Fig. 6 at 15 °C the ADIOL response is significantly increased at higher humidity levels when compared to dry conditions. Comparing the behavior of PECH (Fig. 8b) at 15 °C, 25 °C, and 35 °C, one sees a very mild decrease in sensitivity at highest humid-

ity levels, although not nearly as pronounced as the influence of water on the ADIOL response.

One explanation for the observed sensor behavior is that the PECH/water bulk matrix has a higher overall polarity at high humidity, leading to a less soluble matrix than when dry. That is, the water-laden matrix rejects or lessens the amount of MeS absorbed. Furthermore, for PECH the dominant mechanism is swelling, for which the incremental change in dielectric constant is less when preloaded with water vapor and a lower permittivity analyte is added. In either case, the effect is not significant. For ADIOL, the water vapor helps to sorb more MeS, likely because the hydrated polymer chains have an apparent higher polarity increasing the MeS/ADIOL interaction. At higher temperatures the humidity-enhanced sensitivity diminishes for the ADIOL sensors, where less water is sorbed.

Theoretical limits of detection (LOD) are estimated from the lowest concentration exposures (Figs. 3–6) at dry and 50% relative humidity conditions. These values are conservatively estimated using three times the peak-to-peak noise as the figure of merit. Fig. 9 shows the dry and wet LODs estimated at various temperatures for the four polymer-filled chemicapacitors. For ADIOL, in humid conditions, the LOD was ~300 ppbV at 25 °C and ~1 ppmV at 40 °C. This provides a basis for development of a system to be used by chemical suit manufacturers for product testing or potentially even warfighters for real-time use. The trade-off will be size (few cm<sup>3</sup>) versus ppb-level sensitivity that has been achieved with mass spectrometry [27].

#### 4. Summary and conclusions

The capacitive sensing method provides near or sub-ppmV level limits of detection for MeS over the temperature range tested. Of the four polymers tested, ADIOL was most sensitive to MeS; however, the current formulation's response speed decreases at lower temperatures, which may limit its effectiveness. At elevated humidity, the ADIOL coated sensors' response to MeS improved, possibly due to a cosolvency effect [28]. PECH provided some basis for selectivity as its response to MeS was negative; however its response diminishes at higher temperatures. Although their chemical structure is quite different, PIB and PEVA provided little discernable difference in response. Since sensitivity of all of the polymers was temperature-dependent, the sensors must be temperature controlled or the data processed using artificial

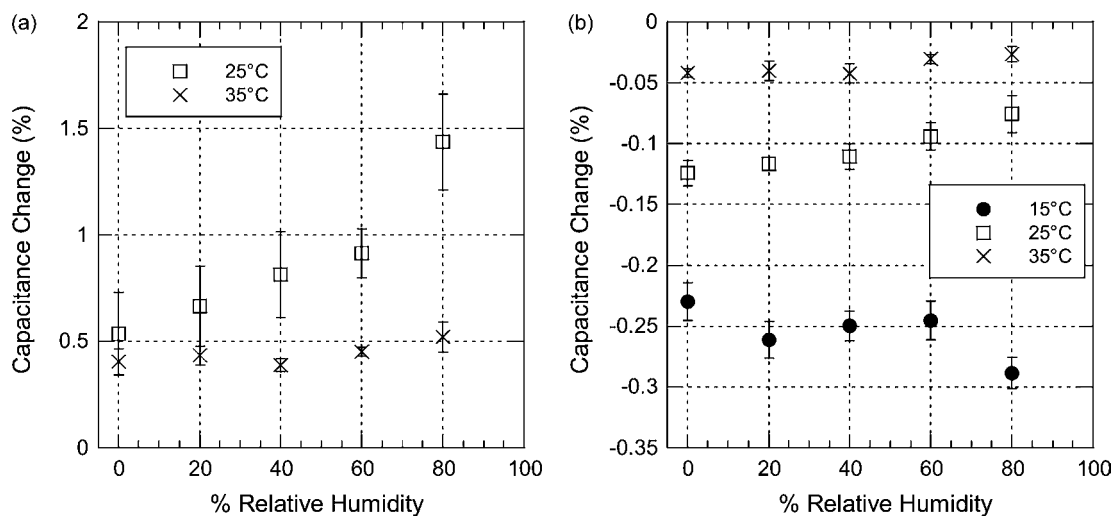


**Fig. 8.** Responses to 1 ppmV MeS exposures from (a) ADIOL chemicapacitors at 25 °C and 35 °C, and (b) PECH chemicapacitors at 15 °C, 25 °C and 35 °C. 15 °C data for ADIOL are not presented in due to slow equilibration.

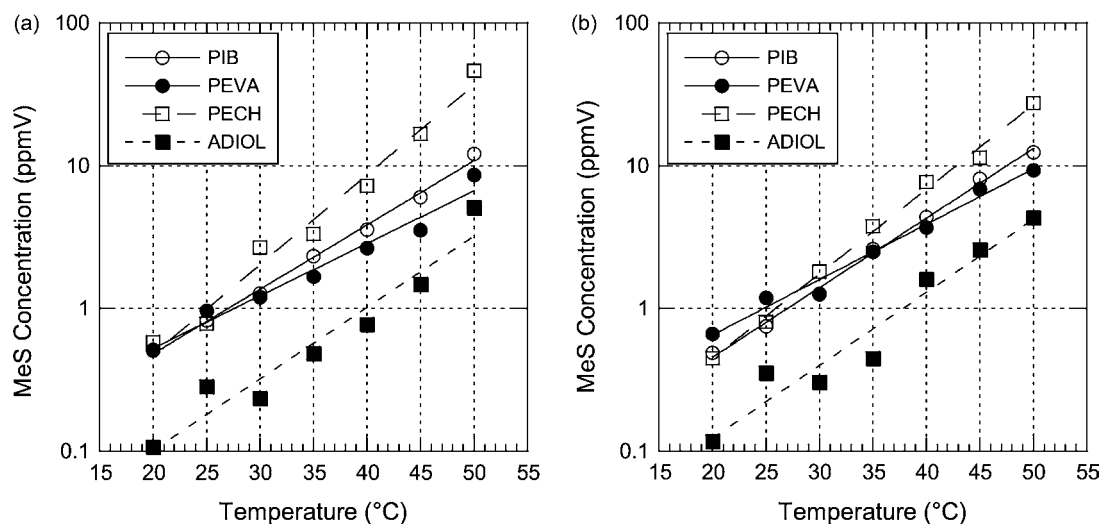


Fig. 9. Calculated limits of detection (LOD) in ppmV at various temperatures in (a) 50% relative humidity and (b) dry air. The lines are only intended to guide the eye.

intelligence algorithms to take into account temperature related changes.

#### Acknowledgements

The authors acknowledge the funding support from the US Army Research Office Program # W911NF-06-C-0009, and the US Department of Homeland Security Program # NBCHC050063. In addition the authors acknowledge the many useful discussions with Dr. Michael von Fahnstock and Dr. Fredrick Cox at Battelle Memorial Laboratories, and Ms. Leticia Mota at TNO Defence, Security and Safety. The authors would also like to thank Dr. R. Andrew McGill and Dr. Eric Houser for the ADIOL sample.

#### References

- [1] National Research Council: Assessment of the U.S. Army Chemical and Biological Defense Command, Report 1, Technical Assessment of the Man-In-Simulant Test (MIST) Program, National Academy Press, Washington, DC, 1997, pp. 30–36.
- [2] R. L. Barker, A review of gaps and limitations in test methods for first responder protective clothing and equipment, final report presented to the National Personal Protection Technology Laboratory at the National Institute for Occupational Safety and Health, January 31, 2005, p. 37.
- [3] P. Gao, W.P. King, R. Shaffer, J. Occup. Environ. Hyg. 4 (2007) 562.
- [4] M.C. Lonergan, E.J. Severin, B.J. Doleman, S.A. Beaver, R.H. Grubbs, N.S. Lewis, Chem. Mater. 8 (1996) 2298.
- [5] M.P. Eastman, R.C. Hughes, G. Yelton, A.J. Ricco, S.V. Patel, M.W. Jenkins, J. Electrochem. Soc. 146 (1999) 3907.
- [6] C.L. Britton, R.L. Jones, P.I. Oden, Z. Hu, R.J. Warmack, S.F. Smith, W.L. Bryan, J.M. Rochelle, Ultramicroscopy 82 (2000) 17.
- [7] M. Maute, S. Raible, F.E. Prins, D.P. Kern, U. Weimar, W. Gopel, Microelectron. Eng. 46 (1999) 439.
- [8] J.W. Grate, B.M. Wise, M.H. Abraham, Anal. Chem. 71 (1999) 4544.
- [9] Q. Cai, J. Park, D. Heldsinger, M.-D. Hsieh, E.T. Zellers, Sens. Actuators B 62 (2000) 121.
- [10] A. Hierlemann, D. Lange, C. Hagleitner, N. Kerness, A. Koll, O. Brand, H. Baltes, Sens. Actuators B 70 (2000) 2.
- [11] M. Kitsara, D. Goustouridis, S. Chatzandroulis, M. Chatzichristidi, I. Raptis, T. Ganetsos, R. Igreja, C.J. Dias, Sens. Actuators B 127 (2007) 186.
- [12] C. Jin, P. Kurzawski, A. Hierlemann, E.T. Zellers, Anal. Chem. 80 (2008) 227.
- [13] J. Carter, A. Cowen, B. Hardy, R. Mahadevan, M. Stonefield, S. Wilcenski, PolyMUMPs Design Handbook, Rev. 11.0, MEMSCAP, Inc. 2005.
- [14] S.V. Patel, T.E. Mlsna, B. Fruhberger, E. Klaassen, S. Cemalovic, D.R. Baselt, Sens. Actuators B 96 (2003) 541.
- [15] D.R. Baselt, B. Fruhberger, E. Klaassen, S. Cemalovic, C.L. Britton Jr., S.V. Patel, T.E. Mlsna, D. McCorkle, B. Warmack, Sens. Actuators B 88 (2003) 120.
- [16] MJ-AB01-030 30  $\mu\text{m}$  dispenser and CT-M3-01 inkjet controller from MicroFab Technologies, Inc., Plano, TX. A 30 or 60  $\mu\text{m}$  diameter nozzle was used to deposit polymer solutions.
- [17] R. Hiss, S. Hobeika, C. Lynn, G. Strobl, Macromolecules 32 (1999) 4390.
- [18] R.A. McGill, M.H. Abraham, J.W. Grate, Chem. Tech. 24 (1994) 27.
- [19] R.A. McGill, E.J. Houser, T.E. Mlsna. Linear and branched chemoselective siloxane polymers and methods for use in analytical and purification applications, U.S. Patent #6,630,560, October 7, 2003.
- [20] F. Rodriguez, Principles of Polymer Systems, 3rd ed., Hemisphere, New York, 1989, pp. 589–603.
- [21] D. McCorkle, R.J. Warmack, S.V. Patel, T. Mlsna, S.R. Hunter, T.L. Ferrell, Sens. Actuators B 107 (2005) 892.
- [22] Lange's Handbook of Chemistry, 14th ed., ed. John A. Dean, McGraw-Hill, New York, 1992, pp. 5–50 and 5–116.
- [23] T.E. Mlsna, S. Cemalovic, M. Warburton, S.T. Hobson, D.A. Mlsna, S.V. Patel, Sens. Actuators B 116 (2006) 192.
- [24] <http://webbook.nist.gov/cgi/cbook.cgi?Name=methyl+salicylate&Units=SI>.
- [25] D.S. Ballantine, R.M. White, S.J. Martin, A.J. Ricco, G.C. Frye, E.T. Zellers, H. Wohltjen, Acoustic Wave Sensors: Theory, Design and Physicochemical Applications, Academic Press, Boston, MA, 1997.
- [26] K. Neimann, R. Neumann, Org. Lett. 2 (2000) 2861.
- [27] I. Cotte-Rodriguez, D.R. Justes, S.C. Nanita, R.J. Noll, C.C. Mulligan, N.L. Sanders, R.G. Cooks, Analyst 131 (2006) 579.
- [28] A.F.M. Barton, CRC Handbook of Solubility Parameters and Other Cohesion Parameters, 2nd ed., CRC Press, Boca Raton, FL, 1983, pp. 390–392.



## Application of a data-processing model to determine the optimal sampling conditions for liquid phase trapping of atmospheric carbonyl compounds

V. Perraud<sup>a,\*</sup>, S. François<sup>a</sup>, H. Wortham<sup>a</sup>, B. Jourdain<sup>b</sup>, S. Houdier<sup>b</sup>, N. Kardos<sup>c</sup>

<sup>a</sup> Laboratoire de Chimie et Environnement, Université de Provence, 3 place Victor Hugo, 13331 Marseille cedex 03, France

<sup>b</sup> Laboratoire de Glaciologie et de Géophysique de l'Environnement, UMR CNRS/UJF 5183, 54 rue Molière, BP 96, 38402 St. Martin d'Hères cedex, France

<sup>c</sup> Laboratoire de Chimie Moléculaire et Environnement, ESIGEC, Campus scientifique Savoie Technolac, Université de Savoie, 73376 Le Bourget du Lac cedex, France

### ARTICLE INFO

#### Article history:

Received 27 November 2007

Received in revised form 4 April 2008

Accepted 16 April 2008

Available online 24 April 2008

#### Keywords:

Air analysis

Data-processing model

Liquid phase sampling technique

2-Diphenylacetyl-1,3-indandione-1-hydrazone

(DIH)

Dansylacetamidooxamine (DNSAOA)

2,4-Dinitrophenylhydrazine (2,4-DNPH)

### ABSTRACT

The reactivity of two fluorescent derivatization reagents, 2-diphenyl-1,3-indandione-1-hydrazone (DIH) and 2-aminoxy-*N*-[3-(5-dimethylamino-naphtalene-1-sulfonamino)-propyl]-acetamide (dansylacetamidooxamine, DNSAOA), was studied towards selected atmospheric carbonyl compounds. The results were compared to those obtained using the 2,4-dinitrophenylhydrazine (2,4-DNPH) UV-vis reagent, a standard well-established technique used to detect atmospheric carbonyl compounds. The experimental rate constants were integrated into a data-processing model developed in the laboratory to simulate the trapping efficiencies of a mist chamber device as a function of temperature, reagent and solvent type among others. The results showed that in an aqueous solution, DNSAOA exhibits a higher reactivity towards carbonyl compounds without the addition of an acidic catalyst than 2,4-DNPH. It was observed that DNSAOA can trap efficiently water-soluble gaseous compounds (for example formaldehyde). However, because of a high initial contamination of the reagent caused by the synthesis procedure used in this work, DNSAOA cannot be used in high concentrations. As a result, very low trapping efficiencies of less reactive water-insoluble gaseous compounds (acetone) using DNSAOA are observed. However, the use of an organic solvent such as acetonitrile improved the trapping efficiencies of the carbonyl compounds. In this case, using DIH as the derivatization reagent (DNSAOA is not soluble in acetonitrile), trapping efficiencies greater than 95% were obtained, similar to 2,4-DNPH. Moreover, fluorescence associated with DIH derivatives (detection limits  $3.33 \times 10^{-8}$  M and  $1.72 \times 10^{-8}$  M for formaldehyde and acetone, respectively) is further advantage of this method for the determination of carbonyl compounds in complex matrix compared to the classical UV-vis detection method (detection limits  $3.20 \times 10^{-8}$  M and  $2.9 \times 10^{-8}$  M for formaldehyde and acetone, respectively).

© 2008 Elsevier B.V. All rights reserved.

### 1. Introduction

The atmospheric chemistry and photochemistry of low molecular mass carbonyl compounds including aldehydes and ketones is well documented. Interest in studying atmospheric chemistry of carbonyl compounds stems from: (1) their importance in atmospheric chemistry, (2) high reactivity, (3) complexity of their mechanism and dynamics, *i.e.* many photochemical reactions occur on multiple potential energy surfaces and generate multiple sets of products, and (4) their potential impact on human health.

During the past two decades, different strategies have been adopted in the analysis of carbonyl compounds in ambient air [1,2].

The most common method uses the 2,4-dinitrophenylhydrazine (2,4-DNPH) derivatization agent coated on a solid sorbent. After trapping, the derivatization products are eluted with an organic solvent and analyzed by liquid chromatography (LC) coupled to an UV-vis detector [3–7]. Unfortunately, interferences mainly induced by oxidant such as ozone [8–10] and NO<sub>x</sub> (NO<sub>x</sub> = NO + NO<sub>2</sub>) [11] were reported. They can be drastically reduced using KI annular denuders as oxidant scavengers but it was reported that this procedure could trap a fraction of the gaseous carbonyl compounds [8,10,12]. Consequently, the sampling procedure based on a gas-liquid scrubber sampling technique seems more reliable because it is free of important oxidizing artefacts [12–15]. With this technique, the role of the derivatization process is not only to stabilize the carbonyl compounds but also to improve the trapping efficiency by avoiding the saturation of the trapping solution by the carbonyl compounds. A calibrated mathematical algorithm

\* Corresponding author. Tel.: +33 491106204; fax: +33 491106377.

E-mail address: [veronique.perraud@univ-provence.fr](mailto:veronique.perraud@univ-provence.fr) (V. Perraud).

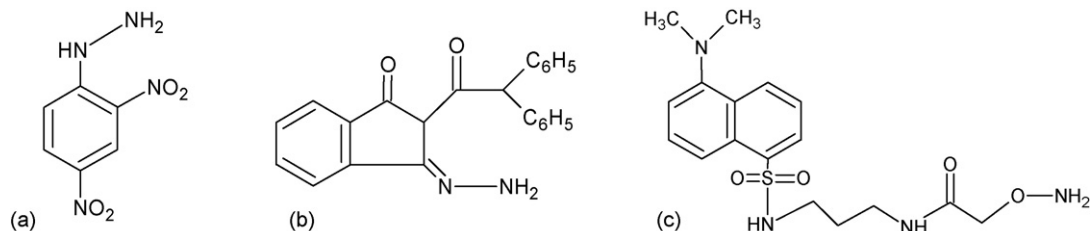


Fig. 1. Chemical structures of (a) 2,4-DNPH, (b) DIH and (c) DNSAOA.

simulating the trapping efficiencies of carbonyl compounds into the liquid phase was developed in a previous work [16]. It was used to determine and compare the trapping efficiencies of two kinds of gas–liquid scrubbers: mist chamber and glass tube. This work highlighted the ability of the mist chamber to concentrate samples and thus to improve the sensibility of the analytical method. Using the data-processing model previously validated, the present work is focused on the determination and the comparison of the performances of various derivatization reagents to trap volatile carbonyl compounds in a mist chamber.

Numerous derivatization reagents were developed for the analysis of carbonyl compounds such as: 2,4-dinitrophenylhydrazine [14,17], dansylhydrazine (DNSH) [1,2,18–21], 2-diphenyl-1,3-indandione-1-hydrazone (DIH) [1,2,21–23], *N*-(5-dimethylamino-1-naphthalenesulphonamido)-3-oxapentane-1,5-dioxyamine (dansyloxyamine, DNSOA) [24], 2-aminoxy-*N*-[3-(5-dimethylamino-naphthalene-1-sulfonamino)-propyl]-acetamide (dansylacetamidooxyamine, DNSAOA) [25], 4-*N,N*-dimethylamino-6-(4'-methoxy-1'-naphthyl)-1,3,5-triazine-2-hydrazone (DMNTH) [26,27]. Because of their fluorescence properties, their solubility in water and/or organic solvents or their kinetic rate reaction towards carbonyl functional group, three of them (2,4-DNPH, DIH and DNSAOA, Fig. 1) seem particularly fit for the analysis of atmospheric carbonyl compounds using an integrative trap such as a mist chamber.

The objective of the present work is to compare the performances of 2,4-DNPH, the most commonly used derivatization reagent, with those of DIH and DNSAOA for the liquid phase sampling of gaseous carbonyl compounds. This work was carried out using formaldehyde and acetone as model molecules because of their different physico-chemical properties (formaldehyde, a water-soluble gaseous compound (*Henry's constant*  $>10^3 \text{ mol L}^{-1} \text{ atm}^{-1}$ ) highly reactive and acetone, a low water-soluble gaseous compound (*Henry's constant*  $\approx 30 \text{ mol L}^{-1} \text{ atm}^{-1}$ ) fairly unreactive). The comparisons were performed using the mathematical algorithm developed and validated by François et al. to simulate the trapping efficiencies of the carbonyl compounds under study in a mist chamber [16]. Laboratory experiments were carried out on DIH and DNSAOA to determine the rate constant of derivatization while those of DNPH were found in literature. The studied parameters were: (1) the solubility of the compounds under study in the trapping solutions ( $K_S$ ), (2) the rate constant ( $k_D$ ) for each derivatization reagent and (3) the influence of the temperature on trapping efficiencies.

## 2. Materials and methods

### 2.1. Derivatization procedure

#### 2.1.1. Carbonyl compound stock solutions

The carbonyl compound stock solutions (formaldehyde and acetone; Riedel de Haën, Seelze, Germany) were prepared weekly by

dissolving a known amount of a pure standard in purified water (from a Milli-Q-RG system; Millipore, Bedford, MA, USA) and in acetonitrile (HPLC grade; SDS Carlo Erba) for DNSAOA and DIH tests, respectively. All stock solutions were stored at  $T = 4^\circ\text{C}$  until use.

#### 2.1.2. DIH trapping solution

The DIH solution was prepared by adding 75 mg of commercial DIH (Aldrich) to 100 mL of acetonitrile with stirring ( $C_{\text{DIH}} = 2 \times 10^{-3} \text{ mol L}^{-1}$ ). This solution was stored at  $T = 4^\circ\text{C}$  until use. Similar to the work of Swarin and Lipari, an acidic catalyst (5  $\mu\text{L}$  of 1 M HCl per 2 mL of reagent solution) was added to the solution to increase the kinetic rate of the derivatization process [22]. The addition was carried out at the beginning of the derivatization tests to avoid the degradation of the reagent observed during the experiment. The estimated lifetime of DIH in an acidic ( $[\text{HCl}] = 2.5 \times 10^{-3} \text{ mol L}^{-1}$ ) liquid organic solution (acetonitrile) is about 5 h.

#### 2.1.3. DNSAOA trapping solution

The DNSAOA was synthesized using a commercial solution of dansyl chloride (Aldrich) as described by Boturyn et al. [28]. Briefly, the reaction products were identified using their physical properties (melting points (Kofler Bank), NMR ( $^1\text{H}$  and  $^{13}\text{C}$ ) and IR spectroscopy). This synthesis led to the formation of a protected molecule where the oxylamino reactive functional group ( $\text{O-NH}_2$ ) was protected by a *t*-butyloxycarbamate group (*t*-BOC). To obtain the reactive hydrochloride form of the reagent ( $\text{O-NH}_3^+$  and  $\text{Cl}^-$ ), *t*-BOC protecting group was removed by acidolysis using gaseous hydrochloric acid [25]. This procedure resulted in the production of a stock solution of the reactive form of DNSAOA in pure water ( $C_{\text{DNSAOA}} = 6.8 \times 10^{-4} \text{ mol L}^{-1}$ ). This solution was stored at  $T = -12^\circ\text{C}$  until used as trapping solution.

#### 2.1.4. Kinetic rate of derivatization

To avoid contamination, all glassware was carefully cleaned by various soaking and rinsing according to the procedure suggested by François et al. [16]. In addition, prior to its use all materials were rinsed with acetonitrile (HPLC grade) and dried under a flow of pure nitrogen. To carry out the derivatization tests, 60  $\mu\text{L}$  of the stock solutions of the carbonyl compounds under study were added to 110  $\mu\text{L}$  of the acidified solution of DIH or to 110  $\mu\text{L}$  of the diluted solution of DNSAOA leading to a DIH and DNSAOA concentrations of  $1.3 \times 10^{-3} \text{ mol L}^{-1}$  and  $4.4 \times 10^{-4} \text{ mol L}^{-1}$ , respectively. The mixtures were stirred at room temperature prior to LC analysis. Under the experimental conditions employed, the molar ratios  $[\text{reagent}]/[\text{R}_2\text{CO}]$  were about 30 for DIH and 10 for DNSAOA.

The rate constant of the reactions of derivatization under study is described according to the following equation:

$$v = -\frac{d[A]}{dt} = k_D[A][\text{reagent}] = k'_D[A] \quad (1)$$

where [reagent] and [A] were, respectively, the concentrations of the derivatization reagent and carbonyl compound under study in the derivatization solution ( $\text{mol L}^{-1}$ ), and where  $k'_D$  was the apparent rate constant ( $\text{min}^{-1}$ ). Assuming that the derivatization reagent was in large excess, the pseudo first-order conditions were applied and the rate constant ( $k_D$ ) were calculated according to the following equation:

$$k_D = \frac{k'_D}{[\text{reagent}]} = \frac{\text{Ln}([A_0]/[A_t])}{t} \frac{1}{[\text{reagent}]} \quad (2)$$

where  $[A_0]$  and  $[A_t]$  were, respectively, the initial and final concentration of the carbonyl compounds under study in the derivatization solution.

### 2.1.5. Analytical procedure

The derivatized carbonyl compounds were analyzed using liquid chromatography equipped with a Krion Instruments (Bio-TEK) System 525 pump, a Rheodyne 7725i injecting valve (Coati, CA, USA) equipped with a 20- $\mu\text{L}$  sample loop, a Varian Star 9075 fluorescent detector equipped with a pulsed xenon lamp and a 8- $\mu\text{L}$  flow cell. Excitation and emission wavelengths were set at 426 and 526 nm for the DIH derivatives and at 330 and 530 nm for the DNSAOA derivatives. Separation was performed on an Alltima (Alltech)  $C_{18}$  column (particles size 5  $\mu\text{m}$ ; column dimension 150 mm  $\times$  4.6 mm) and the liquid flow rate of 1  $\text{mL min}^{-1}$ . An isocratic mixture of acetonitrile and water (48/52) was used in the analysis of the solutions of DNSAOA derivatives while a binary gradient (acetonitrile/water) was used in the solution of DIH derivatives. This gradient was the following: the mixture (76% acetonitrile/24% water) was held for 18 min, then, the linear gradient increased to reach 100% acetonitrile over 12 min ( $2\% \text{ min}^{-1}$ ) and finally, the system was held constant for 8 min. Chromatograms were acquired on a Waters-Millipore Model 745B integrator and on a Jasco-Borwin data-processing system.

### 2.2. Modelization of the trapping efficiencies of mist chamber for gaseous carbonyl compounds using a mathematical algorithm

The collection efficiencies of atmospheric carbonyl compounds using the various derivatization reagents (2,4-DNPH, DIH and DNSAOA) were studied using the theoretical data-processing model developed by François et al. for the mist chamber sampling technique [16]. Briefly, the trapping efficiency versus time ( $\text{TE}_{\text{MCtheo}}(t)$ ) was calculated using the following equation:

$$\text{TE}_{\text{MCtheo}}(t) = \frac{RTV[C_{\text{MCdissolved}}(t) + C_{\text{MCderivate}}(t)]}{P_C d_{\text{gas}} t} \quad (3)$$

where  $V$ ,  $T$  and  $R$  were, respectively, the volume of the trapping solution in the mist chamber (L), the trapping temperature (K) and the ideal gas law constant ( $R = 0.0826 \text{ L atm K}^{-1} \text{ mol}^{-1}$ ), where  $P_C$ ,  $t$  and  $d_{\text{gas}}$  were, respectively, the concentration of the sampled gas (atm), the sampling time (minutes) and the flow rate of the sampled gas phase ( $\text{L min}^{-1}$ ) and finally where  $C_{\text{MCderivate}}$  and  $C_{\text{MCdissolved}}$  were the concentrations ( $\text{mol L}^{-1}$ ) of the compound under study dissolved in the trapping solution which had, respectively, reacted and not yet reacted with the derivative agent. They were calculated as follows:

$$C_{\text{MCdissolved}}(t) = \frac{K_S d P_C d_{\text{gas}}}{XV[d_{\text{gas}} + dRTK_S]} [1 - \exp^{-Xt}] \quad (4)$$

where  $K_S$  was the solubility of the compound under study ( $\text{mol L}^{-1} \text{ atm}^{-1}$ ) and  $d$  was both the spraying flow rate (from the reservoir to the reaction chamber) and the deposition flow rate

**Table 1**

Physical characteristics of the mist chamber device used in the data-processing model simulating trapping efficiencies of gaseous carbonyl compounds

	Description	Values under used
$V$	Volume of the trapping solution	$2.5 \times 10^{-2} \text{ L}$
$T$	Trapping temperature	279 K or 298 K
$P_C$	Concentration of the sampled gas	$10^{-9} \text{ atm}$ (1 ppbv)
$t$	Sampling time	0–300 min
$d_{\text{gas}}$	Flow rate of the sampled gas	$2 \text{ L min}^{-1}$
$d$	Both the spraying flow rate and the deposition flow rate of the mist droplets	$2.5 \times 10^{-3} \text{ L min}^{-1}$

(from the reaction chamber to the reservoir) of the mist droplets formed ( $\text{L min}^{-1}$ ). On the other hand,

$$C_{\text{MCderivate}}(t) = \frac{K_S d P_C d_{\text{gas}}}{XV[d_{\text{gas}} + dRTK_S]} \times [Xk_D C_{\text{rea}} t + k_D C_{\text{rea}} \exp^{-Xt} - k_D C_{\text{rea}}] \quad (5)$$

In Eqs. (4) and (5),  $X$  can be expressed as follow:

$$X = Vk_D C_{\text{rea}} + d - \frac{K_S d^2 RT}{d_{\text{gas}} + dRTK_S} \quad (6)$$

where  $k_D$  was the rate constant for the derivatization reaction ( $\text{L mol}^{-1} \text{ min}^{-1}$ ) and  $C_{\text{rea}}$  the concentration of the derivatization reagent under used for the trapping solution ( $\text{mol L}^{-1}$ ). Tables 1 and 2 resume all the physical characteristics and the constant values used for each simulation.

## 3. Results and discussion

### 3.1. Determination of the rate constant of the derivatization reagents

Derivatization experiments were carried out to determine the derivatization rate constant ( $k_D$ ) of carbonyl compounds (formaldehyde and acetone) with DIH and DNSAOA. Assuming a pseudo first-order kinetic, a linear correlation was obtained for  $\text{Ln}([A_0]/[A_t])$  versus  $t$  according to the following equation:

$$\text{Ln} \left( \frac{[A_0]}{[A_t]} \right) = k'_D * t + \varepsilon \quad (7)$$

where the slope represented the apparent rate constant ( $k'_D$ ). The experimental results were as follows:

- (1) Formaldehyde–DIH in water ( $[\text{DIH}] = 1.3 \times 10^{-3} \text{ M}$ ,  $T = 298 \text{ K}$ ):  $k'_D = 0.61 \text{ min}^{-1}$  ( $r^2 = 0.944$ ).
- (2) Acetone–DIH in water ( $[\text{DIH}] = 1.3 \times 10^{-3} \text{ M}$ ,  $T = 298 \text{ K}$ ):  $k'_D = 0.064 \text{ min}^{-1}$  ( $r^2 = 0.985$ ).
- (3) Acetone–DNSAOA in water ( $[\text{DNSAOA}] = 4.4 \times 10^{-4} \text{ M}$ ,  $T = 298 \text{ K}$ ):  $k'_D = 2.60 \times 10^{-3} \text{ min}^{-1}$  ( $r^2 = 0.980$ ).

The resulting derivatization reaction rate constant ( $k_D$ ) were thus calculated according Eq. (2). The resulting rate constant of DIH and DNSAOA with carbonyl compounds and those collected in literature for 2,4-DNPH are summarized in Table 2.

Whatever the reagent, we observe first that the rate constant of acetone were lower than those of formaldehyde. This observation was consistent with the structure–reactivity theory. Indeed, due to the more electrophilic nature of the carbon in the aldehyde group in comparison to the carbon associated to the ketone group, one can

**Table 2**  
Recapitulative of the derivatization rate constant ( $k_D$ ) observed from literature<sup>a</sup>, from experimental data and from Arrhenius calculations<sup>b</sup>

Temperature	Solvent	Reagent	Carbonyl compounds	$K_{Smin} - K_{Smax}$ [29,30] ( $K_{Smean}$ ) ( $\text{mol L}^{-1} \text{atm}^{-1}$ )	$k_D$ ( $\text{L mol}^{-1} \text{min}^{-1}$ )	Time for 99% of conversion ( $C_{rea}$ , $\text{mol L}^{-1}$ )
Experimental observations						
298 K	Water	2,4-DNPH	Formaldehyde	$3 \times 10^3 - 7 \times 10^3$ ( $5 \times 10^3$ )	390 <sup>a</sup>	118 min ( $10^{-4} \text{ mol L}^{-1}$ ) 17 min ( $6.8 \times 10^{-4} \text{ mol L}^{-1}$ )
			Acetone	22–35 (29)	<1 <sup>a</sup>	>24 h ( $2.36 \times 10^{-3} \text{ mol L}^{-1}$ )
		DNSAOA	Formaldehyde	$3 \times 10^3 - 7 \times 10^3$ ( $5 \times 10^3$ )	2636 <sup>a</sup>	159 min ( $11 \times 10^{-6} \text{ mol L}^{-1}$ ) 2.5 min ( $6.8 \times 10^{-4} \text{ mol L}^{-1}$ )
			Acetaldehyde	9.9–17.0 (13)	3273 <sup>a</sup>	128 min ( $11 \times 10^{-6} \text{ mol L}^{-1}$ ) 2 min ( $6.8 \times 10^{-4} \text{ mol L}^{-1}$ )
			Propionaldehyde	13.0 (–)	2636 <sup>a</sup>	159 min ( $11 \times 10^{-6} \text{ mol L}^{-1}$ ) 2.5 min ( $6.8 \times 10^{-4} \text{ mol L}^{-1}$ )
	Acetonitrile	2,4-DNPH	Formaldehyde	$>3 \times 10^3 - 7 \times 10^3$ ( $>5 \times 10^3$ )	$>390^a$	<6 min ( $2.36 \times 10^{-3} \text{ mol L}^{-1}$ )
			Acetone	828.8–1365.6 [30] ( $1 \times 10^3$ )	65 <sup>a</sup>	30 min ( $2.36 \times 10^{-3} \text{ mol L}^{-1}$ )
		DIH	Formaldehyde	$>3 \times 10^3 - 7 \times 10^3$ ( $>5 \times 10^3$ )	469	5 min ( $2 \times 10^{-3} \text{ mol L}^{-1}$ )
			Acetone	828.8–1365.6 [30] ( $1 \times 10^3$ )	36	64 min ( $2 \times 10^{-3} \text{ mol L}^{-1}$ )
			Acetone	22–35 (29)	6	1146 min ( $6.8 \times 10^{-4} \text{ mol L}^{-1}$ ) 78 min ( $10^{-2} \text{ mol L}^{-1}$ )
Calculation from thermodynamic <sup>b</sup>						
279 K <sup>b</sup>	Water	2,4-DNPH	Formaldehyde	$1.4 \times 10^4 - 3.3 \times 10^4$ ( $2 \times 10^4$ )	103	8 h ( $10^{-4} \text{ mol L}^{-1}$ )
			Acetone	63.8–101.4 (83)	<0.4	>24 h ( $2.36 \times 10^{-3} \text{ mol L}^{-1}$ )
		DNSAOA	Formaldehyde	$1.4 \times 10^4 - 3.3 \times 10^4$ ( $2 \times 10^4$ )	694	10 h ( $11 \times 10^{-6} \text{ mol L}^{-1}$ ) 10 min ( $6.8 \times 10^{-4} \text{ mol L}^{-1}$ )
			Acetone	63.8–101.4 (83)	2	>24 h ( $6.8 \times 10^{-4} \text{ mol L}^{-1}$ ) 230 min ( $10^{-2} \text{ mol L}^{-1}$ )

$K_S$ : solubility of the compound under study ( $\text{mol L}^{-1} \text{atm}^{-1}$ );  $k_D$ : rate constant for the derivatization reaction ( $\text{L mol}^{-1} \text{min}^{-1}$ );  $C_{rea}$ : concentration of the derivatization reagent under used for the trapping solution ( $\text{mol L}^{-1}$ ).

<sup>a</sup>  $k_D$  calculated from apparent rate constant ( $k'_D$ ) found in literature [14,17,25] according to Eq. (2) (Cf. *derivatization procedure* section).

<sup>b</sup>  $K_S$  calculated using Van't Hoff equation (Eq. (7), Cf. *temperature influence* section);  $k_D$  calculated using Arrhenius' law.

expect that the nucleophilic derivatization reaction occurs faster on aldehydes.

The derivatization reaction rate constant ( $k_D$ ) of DIH were 469 and  $36 \text{ L mol}^{-1} \text{min}^{-1}$ , respectively, for formaldehyde and acetone. Using a concentration of DIH of  $2 \times 10^{-3} \text{ mol L}^{-1}$  (corresponding to the upper limit of solubility of the reagent in acetonitrile) the reactions were completed (conversion rate of 99%), respectively, in 5 and 64 min for formaldehyde and acetone. Because we cannot experimentally dissolve the reagent in water (even at very low pH), no kinetic study was obtained.

For DNSAOA in water, Houdier et al. [25] reported apparent rate constant making it possible to calculate derivatization reaction rate constants ( $k_D$ ) according to Eq. (2) (Cf. *derivatization procedure* section). The calculated value were, respectively, 2 636, 3 273 and 2 636  $\text{L mol}^{-1} \text{min}^{-1}$  for formaldehyde, acetaldehyde and propionaldehyde. The experiments were carried out on acetone in the present work to complete the data set reported by Houdier et al. The rate constant calculated from these experiments was  $6 \text{ L mol}^{-1} \text{min}^{-1}$ . The various measured coefficients from literature are grouped in Table 2. Surprisingly, formaldehyde reacts slower than acetaldehyde in spite of its higher electrophilicity. It was reported to be attributed to a solvent effect because aldehydes seem to react with water to form diols ( $\text{R-CHO} + \text{H}_2\text{O} \rightleftharpoons \text{R-HC(OH)}_2$ ). Since the solubility of gaseous formaldehyde is high ( $K_{S\text{water}} > 10^3 \text{ mol L}^{-1} \text{atm}^{-1}$ ), in aqueous solutions, formaldehyde exists predominantly in its *gem*-diol form,  $\text{CH}_2(\text{OH})_2$ . On the contrary, aldehydes and diols exist in comparable concentrations in aqueous solutions for  $\text{C}_2$  and larger aldehydes [31]. Assuming a concentration of DNSAOA of  $6.8 \times 10^{-4} \text{ mol L}^{-1}$ , a quantitative reaction (corresponding to 99% of conversion) was obtained in 2.5, 2, 2.5 and 1 146 min for formaldehyde, acetaldehyde, propionaldehyde and acetone, respectively. However, the reactive form of DNSAOA is only the ionic form of the reagent ( $\text{R-NH}_3^+$ ). Unfortunately, this ion precipitates in acetonitrile, thus no kinetic data were available for this solvent.

### 3.1.1. Comparison with 2,4-DNPH

The literature 2,4-DNPH kinetic data were compared to those experimentally measured for the two fluorescent reagents.

(a) Levart and Veber studied the derivatization reaction between 2,4-DNPH ( $C_{\text{DNPH}} = 2.36 \times 10^{-3} \text{ mol L}^{-1}$ , pH 2) and numerous carbonyl compounds in different binary solution (acetonitrile/water) [17]. They showed that the conversion rates depend mainly on the water content of the trapping solution. Thus, in a mixture acetonitrile/water (95/5), the rate constant of the less reactive compound (assimilated to acetone) was  $65 \text{ L mol}^{-1} \text{min}^{-1}$  while Levart and Veber indicated that no quantitative reaction was obtained in an aqueous solutions of 2,4-DNPH within 24 h [17]. Based on this information, the upper limit of the rate constant of acetone with 2,4-DNPH was estimated to be  $<1 \text{ L mol}^{-1} \text{min}^{-1}$ . Assuming a 2,4-DNPH concentration of  $2.36 \times 10^{-3} \text{ mol L}^{-1}$ , the reaction of acetone goes to completion in about 30 min and more than 24 h for a mixture 95%acetonitrile/5%water and in aqueous solution, respectively. The rate constant measured in the trapping solution 95/5 is quite similar compared to that previously measured for DIH.

(b) On the other hand, Lee and Zhou [14] reported kinetic data for the reactions between 2,4-DNPH and formaldehyde making it possible to calculate the derivatization reaction rate constant ( $k_D$ ) according to Eq. (2) ( $k_D = 390 \text{ L mol}^{-1} \text{min}^{-1}$ ). Assuming a 2,4-DNPH concentration of  $6.8 \times 10^{-4} \text{ mol L}^{-1}$ , this rate constant corresponds to a complete reaction time of about 27 min. This rate constant is 1 order of magnitude lower than that obtained, in the same trapping solution (pure water), with DNSAOA. This underlines the higher efficiency of the aminoxy functional group in comparison to the standard hydrazine function (2,4-DNPH).

### 3.1.2. Temperature influence

The temperature influence on rate constant was studied for a hydroxylamine derivatization reagent chemically close to DNSAOA with acetone by Houdier et al. [24]. The results showed an increase of the rate coefficients ( $6$  and  $15 \text{ L mol}^{-1} \text{min}^{-1}$  at  $T = 285$  and  $298 \text{ K}$ ,

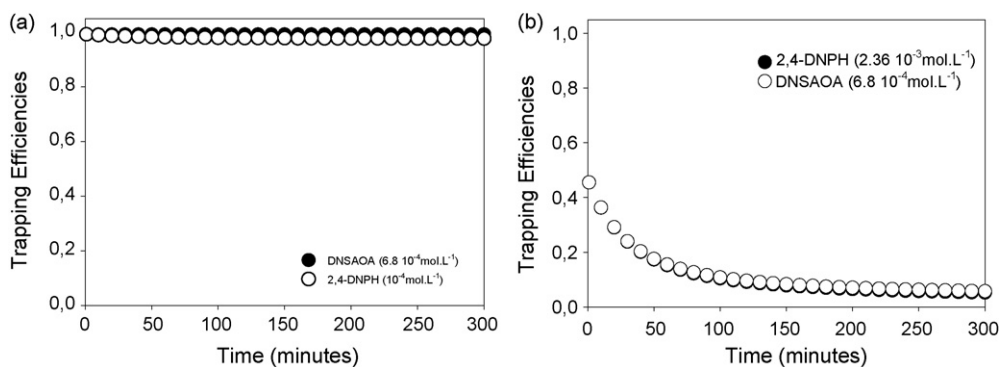


Fig. 2. Comparison of the trapping efficiencies of gaseous formaldehyde (a) and acetone (b) from aqueous solutions at  $T = 298$  K by derivatization with 2,4-DNPH and DNSAOA.

respectively) and are consistent with the Arrhenius thermodynamic theory which forecasts that the coefficient rates increase by a factor ranging between 1.5 and 5 for each increase of 10 degrees. Unfortunately, if an increase of the temperature of the trapping solution improves the kinetic of the derivatization reactions, it decreases the solubility of the carbonyl compounds ( $K_S$ ) and consequently their trapping efficiencies. As a result, a compromise has to be found between these two opposite phenomena in order to optimize the sampling procedure (see next section). To carry out this work, and because of the lack of kinetic data at low temperature, the derivatization rate constants of the carbonyl compounds under study with the three derivatization reagents were calculated at  $T = 279$  K assuming that all the reactions had a similar behaviour towards temperature than that measured experimentally by Houdier et al. [24]. This calculation mode is supported by the fact that all the reactions under study consist in nucleophilic addition catalyzed by acid involving analogous thermodynamic parameters. The results were summarized in Table 2.

### 3.2. Simulation of the trapping efficiencies

The trapping of formaldehyde and acetone were simulated for different experimental trapping conditions (solvent, sampling temperature, and reagent type among others). Because of the restrictive solubility of the reagents, comparisons of the outputs of the model between DNSAOA versus 2,4-DNPH were carried out only in water whereas those between DIH versus 2,4-DNPH were carried out only in acetonitrile. In fact, 2,4-DNPH is soluble and reacts in both water and acetonitrile. Various values of  $K_S$  were reported in literature [29,30] for the carbonyl compounds under study. Because of the low difference between the reported  $K_S$  value, no significant difference were observed in the trapping efficiencies ( $TE_{MC}$ ) using the

data-processing model. As a result, we used the mean value. Table 2 resumes all the  $K_S$  values reported in literature and used in the data-processing model simulating the trapping efficiencies of gaseous carbonyl compounds.

#### 3.2.1. Trapping efficiencies in aqueous trapping solution using DNSAOA and 2,4-DNPH

Assuming a trapping temperature of  $T = 298$  K and concentrations of reagent of  $10^{-4}$  mol.L<sup>-1</sup> and  $6.8 \times 10^{-4}$  mol.L<sup>-1</sup> for 2,4-DNPH and DNSAOA, respectively, the model showed trapping efficiencies of gaseous formaldehyde higher than 95% whatever the reagent used (Fig. 2(a)). Moreover, the trapping efficiencies of this highly soluble molecule were quasi independent of the sampling time because the reaction of derivatization occurred before saturation of the trapping solution by the formaldehyde which had not yet reacted [16].

Under similar experimental conditions employed ( $C_{DNSAOA} = 6.8 \times 10^{-4}$  mol.L<sup>-1</sup>,  $C_{DNPH} = 2.36 \times 10^{-3}$  mol.L<sup>-1</sup>,  $T = 298$  K, trapping solution = pure water) the results obtained with acetone were significantly different than those of formaldehyde (Fig. 2(b)). The trapping efficiencies were quite similar for the two reagents. During the first minutes of the experiment, they were about 45% because of the low solubility of gaseous acetone (Cf. Table 2). Moreover, the trapping efficiency decreased with the sampling time to reach about 10% in about 120 min until 5% in 300 min. This behaviour was the result of the progressive saturation of the trapping solution by the compound under study as the sampling time increase. This saturation was delayed by the phenomenon of derivatization of the trapped compounds but, because of the low derivatization reaction rate this saturation could not be avoided. For 2,4-DNPH experiments, the simulated trapping efficiencies were the maximum trapping efficiencies

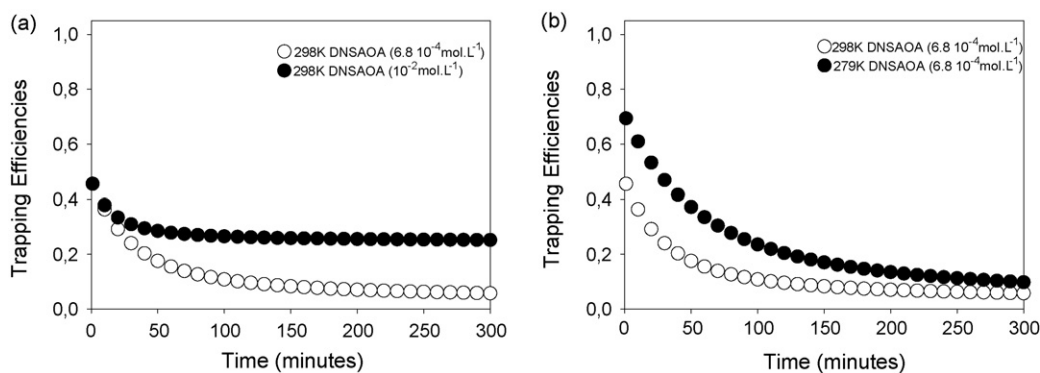


Fig. 3. Influence of different parameters on the trapping efficiencies of gaseous acetone from aqueous solution by derivatization with DNSAOA: (a) influence of the concentration of the reagent, and (b) influence of the temperature of the trapping.



for acetone, as the derivative rate constants input data was the upper limit of the rate constant of acetone with 2,4-DNPH (see Section 3.1). This maximum trapping efficiency was a little bit lower than that obtained for acetone with DNSAOA. Thus, the low rate constant of both DNSAOA and 2,4-DNPH did not allow to use these reagents to trap carbonyl compounds such as acetone in an aqueous trapping solution.

To improve the trapping efficiency it was necessary to increase the derivatization reaction rate by increasing the concentration of derivatization reagent and/or by increasing temperature. The influence of these two parameters was studied using DNSAOA as reagent and by comparing the behaviour of acetone in two experimental conditions ( $T = 298$  or  $279$  K and  $C_{\text{DNSAOA}} = 6.8 \times 10^{-4}$  mol L $^{-1}$  and  $10^{-2}$  mol L $^{-1}$ ). The results were reported in Fig. 3. The increase of the concentration of DNSAOA does not change the trapping efficiency during the first minute of sampling because this value depended only on the solubility of acetone and not on the derivatization reaction. Then, the trapping efficiency increased from about 5% to 29% for the higher concentration of DNSAOA. This behaviour was due to the mechanical effect of an increase of the concentration of the reagent which increased the apparent rate constant and thus limited the saturation of the trapping solution. Consequently, in a general manner, to maximise the trapping efficiency we could increase the concentration of reagent up to saturation of the trapping solution. Nevertheless, according to this work for DNSAOA (see next section), an increase of the concentration of reagent could induce an initial contamination of the trapping solution.

The increase of temperature had two antagonist effects:

(a) According to the following Van't Hoff equation:

$$K_{S279\text{K}} = K_{S298\text{K}} \exp\left(-\frac{\Delta H_{\text{sol}}}{R} \left(\frac{1}{T_{279\text{K}}} - \frac{1}{T_{298\text{K}}}\right)\right) \quad (8)$$

where  $K_{S279\text{K}}$  and  $K_{S298\text{K}}$ , respectively, are the solubility equilibrium coefficient at  $T = 279$  and  $298$  K (mol L $^{-1}$  atm $^{-1}$ ),  $R$  is the ideal gas law constant ( $R = 0.0826$  Latm K $^{-1}$  mol $^{-1}$ ) and  $\Delta H_{\text{sol}}$  is the enthalpy of solubilization which is negative for numerous compounds ( $\Delta H_{\text{sol}}(\text{formaldehyde}) = -5.67 \times 10^4$  J mol $^{-1}$  and  $\Delta H_{\text{sol}}(\text{acetone}) = -3.87 \times 10^4$  J mol $^{-1}$ ), i.e. a temperature increase induces a decrease in the solubility of the carbonyl compound which subsequently decreased the trapping efficiency.

(b) An increase in temperature increased the kinetic rate of derivatization which avoided or at least limit the saturation of the trapping solution and thus increased the trapping efficiency.

The results summarized in Fig. 3 showed that the increased in solubility was the dominant effect because a higher trapping efficiency was obtained at lower temperature. However, these optimizations were not sufficient to trap efficiently low-soluble gaseous compounds such as acetone.

### 3.2.2. Trapping efficiencies in organic trapping solution (acetonitrile) using DIH and 2,4-DNPH

From the kinetic study of Levart and Veber [17] and this work's experimental data, we simulated the trapping efficiencies of both the less-soluble and less-reactive gaseous carbonyl compounds under study (i.e. acetone) at  $T = 298$  K in trapping solutions of 2,4-DNPH and DIH in acetonitrile. To facilitate the comparison between the two reagents, they were used at concentrations in the same order of magnitude ( $C_{\text{DNPH}} = 2.36 \times 10^{-3}$  mol L $^{-1}$  and  $C_{\text{DIH}} = 2 \times 10^{-3}$  mol L $^{-1}$ ). The use of an organic solvent instead of water made it possible to increase both the solubility and the rate constant (Table 2). The combination of these two properties improved significantly the trapping efficiency of acetone using 2,4-DNPH which were about 98% (against 45% in water) during the first minutes of the sampling and which stabilized at 96% (against 5% in water) (Fig. 4). Equivalent results were obtained with an acetonitrile

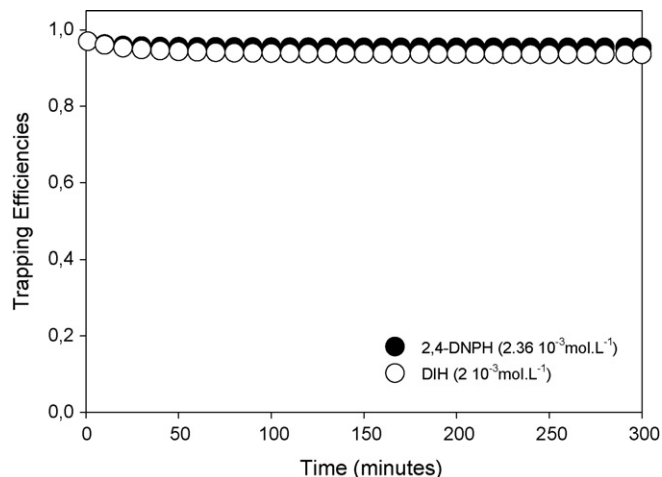


Fig. 4. Comparison of the trapping efficiencies of gaseous acetone from organic solution by derivatization with 2,4-DNPH and DIH ( $T = 298$  K).

trapping solution of DIH (Fig. 4). More in detail, the trapping efficiencies were identical during the first minute of sampling because they depended mainly on the solubility of the compound in acetonitrile. On the other hand, the level of stabilization depended on the apparent rate constant of the reaction of derivatization. As a result, the kinetics of 2,4-DNPH and DIH with acetone were quite similar, the trapping efficiencies were stabilized for approximately the same values. In spite of these results which showed equivalent performance of the two reagents, the 2,4-DNPH was the more convenient because its trapping efficiency could be improved by increasing its concentration while we have already reach the limit of solubility of the DIH ( $2 \times 10^{-3}$  mol L $^{-1}$ ). Thus, the trapping efficiencies corresponded to the maximum values for DIH.

### 3.3. Detection limits and applications

The trapping efficiency is an important parameter to evaluate the performance of a derivatization reagent. Nevertheless, other parameters such as the sensitivity of the detection mode associated to the reagent and the background level influence the detection limits (LOD) and thus, have to be estimated to compare the derivatization reagent. Table 3 summaries the LOD of the derivatized carbonyl compounds with the three reagents under study. Detection limits were defined as three time the relative standard deviation ( $3\sigma$ ) of the analytical blanks. Sample were measured in water, acetonitrile and in a water/acetonitrile (50/50) mixture for, respectively, DNSAOA, DIH and 2,4-DNPH. The lower LOD was observed with DNSAOA (two to three times lower depending both on the carbonyl compound and the derivatization reagent under study). Nevertheless, because of the contamination of DNSAOA stock solution induced by its synthesis procedure, the LOD with this reagent was very sensitive to its concentration (Table 3). To study more in detail the performances of the reagents, the model previously described was used to calculate the concentration, time-dependent, of the compounds under study sampled in the various trapping solution. This concentration corresponded to the sum of the fraction of carbonyl compound in the trap which had already reacted ( $C_{\text{MCDerivate}}$ ) and the fraction which had not yet reacted ( $C_{\text{MCDissolved}}$ ). This work was carried out assuming a gaseous concentration of carbonyl compound of 1 ppbv and a sampling temperature of 298 K. In a general manner, the plot which presents the concentration of trapped carbonyl compound ( $C_{\text{MCDerivate}} + C_{\text{MCDissolved}}$ ) versus time is constituted of two parts corresponding to two different phenomena (Fig. 5). The first part of

**Table 3**  
Detection limits of various carbonyl compounds derivatives

Detection mode	Reagent	Solvent	$C_{\text{rea}}$	Carbonyl compound	Detection limits ( $\text{mol L}^{-1}$ )	References
UV-vis	2,4-DNPH	Water/acetonitrile (50/50)	$2 \times 10^{-4} \text{ mol L}^{-1}$	Formaldehyde Acetone	$3.20 \times 10^{-8}$ $2.90 \times 10^{-8}$	[16]
Fluo	DNSAOA	Water	$11 \times 10^{-6} \text{ mol L}^{-1}$	Formaldehyde	$1.59 \times 10^{-8}$	[25]
			$6.8 \times 10^{-4} \text{ mol L}^{-1}$	Acetone	$9.30 \times 10^{-9}$	
	DIH	Acetonitrile	$2 \times 10^{-3} \text{ mol L}^{-1}$	Formaldehyde	$9.85 \times 10^{-7}$	This work
				Acetone	$5.75 \times 10^{-8}$	
				Formaldehyde	$3.33 \times 10^{-8}$	[23]
				Acetone	$1.72 \times 10^{-8}$	

Detection limits are defined as three time the relative standard deviation ( $3\sigma$ ) of the analytical blanks.

the curve is linear and the slope depends on the kinetics of dissolution of the carbonyl compound under study. In the model, the kinetics of dissolution were not considered and it was assumed that the equilibriums were reached instantaneously. As a result the value of the slope (corresponding to line 1) depends both on the gaseous phase concentrations of carbonyl compounds and the flow rate of the sampled gas. As can be seen in Fig. 5, the plot follows a straight line (dashed line—line 1) up to reach the saturation of the trapping solution. After the saturation, the plot still follows a straight line (full line—line 2) but a lower slope is observed because the trapping phenomenon is limited by the derivatization kinetic.

In this work, both the gaseous concentration of carbonyl compound and the flow rate of the sampled gas were set at 1 ppbv and  $2 \text{ L min}^{-1}$ , respectively. As a result, the slope of the first part of the curve (line 1) will be the same for all carbonyl compounds. On the second part of the curve, the value of the slope (line 2) will be controlled by the reactivity of the carbonyl compound under study.

### 3.3.1. Comparison between DNSAOA and 2,4-DNPH in water

For the trapping experiments of formaldehyde in water using both 2,4-DNPH and DNSAOA as derivatization reagent, the concentration of trapped carbonyl compound ( $C_{\text{MCderivate}} + C_{\text{MCdissolved}}$ ) was linearly time-dependent at least up to 300 min. The obtained equations for the three trapping solutions were as follows:

- aqueous solution of 2,4-DNPH ( $10^{-4} \text{ mol L}^{-1}$ ):  
 $(C_{\text{MCderivate}} + C_{\text{MCdissolved}}) = 9.4 \times 10^{-10} + 3 \times 10^{-9} t$ ,
- aqueous solution of DNSAOA ( $6.8 \times 10^{-4} \text{ mol L}^{-1}$ ):  
 $(C_{\text{MCderivate}} + C_{\text{MCdissolved}}) = 6.5 \times 10^{-13} + 3 \times 10^{-9} t$ ,
- aqueous solution of DNSAOA ( $11 \times 10^{-6} \text{ mol L}^{-1}$ ):  
 $(C_{\text{MCderivate}} + C_{\text{MCdissolved}}) = 1.5 \times 10^{-9} + 3 \times 10^{-9} t$ .

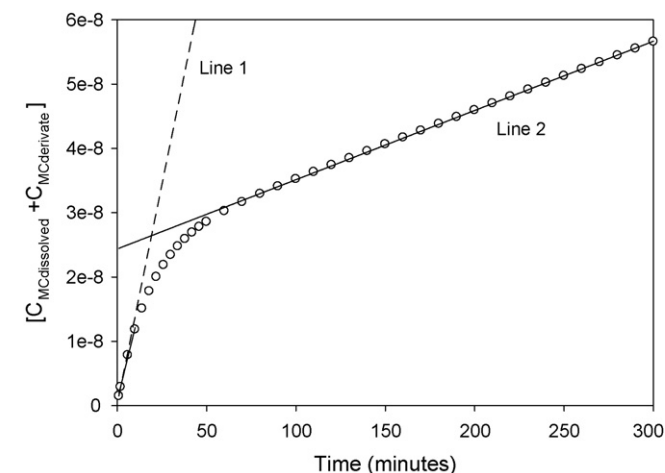


**Fig. 5.** Concentration of acetone trapped in water versus time (experimental conditions:  $T = 298 \text{ K}$ ;  $C_{\text{DNSAOA}} = 6.8 \times 10^{-4} \text{ M}$ ).

- aqueous solution of DNSAOA ( $11 \times 10^{-6} \text{ mol L}^{-1}$ ):  
 $(C_{\text{MCderivate}} + C_{\text{MCdissolved}}) = 1.5 \times 10^{-9} + 3 \times 10^{-9} t$ .

The linear regressions described above were used to compare the concentration of formaldehyde in the various trapping solutions to its LOD. For the analysis of formaldehyde, a sampling time of about 10 and 290 min was required, respectively, to reach the LOD (Table 3) assuming, respectively, a reagent concentration of  $10^{-4} \text{ mol L}^{-1}$  for 2,4-DNPH and  $6.8 \times 10^{-4} \text{ mol L}^{-1}$  for DNSAOA. Thus, under these experimental conditions and in spite of the higher apparent rate constant of DNSAOA, 2,4-DNPH was a better reagent to carry out integrative sampling. The lower efficiency of DNSAOA was mainly due to the high detection limit of formaldehyde with this reagent induced by the high background level (see Table 3). To decrease this background level it was possible to decrease the concentration of DNSAOA as showed. Under these new trapping conditions ( $C_{\text{DNSAOA}} = 11 \times 10^{-6} \text{ mol L}^{-1}$ ), the apparent kinetic rate of derivatization decreased but remained sufficient for an efficient trapping of formaldehyde because the apparent rate constant of DNSAOA was equal to that of 2,4-DNPH at  $10^{-4} \text{ mol L}^{-1}$ . On the other hand, the background level was drastically decreased. As a result, the detection limit was of  $1.59 \times 10^{-8} \text{ mol L}^{-1}$  and the sampling time to reach it was less than 5 min. If the performances of this two derivatization reagents seem equivalent, we note that the use of DNSAOA is associated with a detection by fluorescence which is a more specific detector than the UV-vis associated to 2,4-DNPH. As a result, DNSAOA is a more convenient molecule to study complex matrix.

As discussed previously, both the rate constant and the solubility of gaseous acetone were lower than those of gaseous formaldehyde. As a result, the concentration of trapped acetone ( $C_{\text{MCderivate}} + C_{\text{MCdissolved}}$ ) in water using both 2,4-DNPH and DNSAOA was not linearly time-dependent during the entire sampling time (300 min) (Fig. 5). Saturation of the trapping solution appears rapidly (corresponding to the decrease of the slope). On the other hand, the detection limits of acetone derivatized with both 2,4-DNPH and DNSAOA were in the same order of magnitude than those of formaldehyde. As result, the sampling time required to reach the detection limits were much higher than those of formaldehyde assuming equivalent sampling conditions (concentration of reagent, temperature among others). To reduce these sampling times (and thus to extend the linear time dependence of the curve—part 1) it was possible to increase the reagent concentrations. Nevertheless, this was insufficient for 2,4-DNPH because of its very low rate constant and inefficient for DNSAOA because of the increase of the background level. As a result, these two reagents were unsuitable to carry out an integrative trapping of low-soluble and low-reactive gaseous carbonyl compounds such as acetone. On the other hand, the two reagents could be used to trap soluble and reactive gaseous carbonyl compounds such as formaldehyde with an equivalent efficiency providing that DNSAOA was used at low concentration.

### 3.3.2. Comparison between DIH and 2,4-DNPH in organic solvent

For the trapping experiments of acetone in acetonitrile using both 2,4-DNPH and DIH as derivatization reagent, the concentration of trapped carbonyl compound ( $C_{MCderivate} + C_{MCdissolved}$ ) was linearly time-dependent at least up to 300 min. The obtained equations for the three trapping solutions were as follows:

- (1) acetonitrile solution of 2,4-DNPH ( $2.36 \times 10^{-3} \text{ mol L}^{-1}$ ):  
 $(C_{MCderivate} + C_{MCdissolved}) = 3.4 \times 10^{-10} + 3 \times 10^{-9} t$ ,  
 (2) aqueous solution of DIH ( $2 \times 10^{-3} \text{ mol L}^{-1}$ ):  
 $(C_{MCderivate} + C_{MCdissolved}) = 1.3 \times 10^{-9} + 3 \times 10^{-9} t$ .

The linear regressions described above were used to compare the concentration acetone in the various trapping solutions to its LOD. For the analysis of trapping solution of 2,4-DNPH ( $2.36 \times 10^{-3} \text{ mol L}^{-1}$ ) and DIH ( $2 \times 10^{-3} \text{ mol L}^{-1}$ ) dissolved in acetonitrile, 10 and 5 min sampling times were required to reach the LOD (Table 3). The slight advantage of DIH was the result of the lower detection limit of acetone after derivatization by DIH. It was due to the fluorescence detection mode which was more sensitive and more specific than UV–vis detector used for the analysis of 2,4-dinitrophenylhydrazone (2,4-DNPHone).

## 4. Conclusion

For the trapping and the analysis of gaseous carbonyl compounds in an aqueous matrix, DNSAOA is a good alternative to the classical 2,4-DNPH reagent mainly because of the detection of the reaction products by fluorescence which is more sensitive and specific than the UV–vis detector associated to 2,4-DNPH. Nevertheless, this reagent has to be used at low concentration (about  $10^{-5} \text{ mol L}^{-1}$ ) because it induces a background proportional to its concentration. As a result, the kinetic rates of derivatization are low. Thus, this molecule may be recommended for the non integrative trapping procedure because the reactions of derivatization can occur after sampling. For the integrative trapping procedure such as the mist chamber used in this work, DNSAOA must be hold to the more reactive carbonyl compounds such as formaldehyde in order that the reactions of derivatization occur during sampling.

The use of an organic solvent such as acetonitrile instead of water improves the trapping efficiency because it improves the solubility of the gaseous carbonyls compounds. With this matrix, derivatization reactions with DNSAOA cannot occur and this reagent must be discarded. According to the trapping efficiency and the detection limit, DIH shows quasi equivalent performances than 2,4-DNPH. The main advantage of DIH results from the derivative products by fluorescence which is more specific than the UV–vis detector used with 2,4-DNPH. Thus, the use of DIH is more precisely

recommended for the analysis of gaseous carbonyl compounds dissolved in complexes matrix. Nevertheless, because of the stability of DIH in the trapping solution (acidified acetonitrile), the analysis has to be carried out rapidly (about 1 h) after the sampling step.

## Acknowledgements

This work was supported by ADEME (“Agence De l’Environnement et de la Maitrise de l’Energie”), TERA-Environnement and the Ministry of Research of France through the research program “ACI<sub>capteur</sub>” and a research grant for V. Perraud. All of them are gratefully acknowledged.

## References

- [1] A. Vairavarmurthy, J.M. Roberts, L. Newman, *Atmos. Environ.* 26A (1992) 1965.
- [2] M. Vogel, A. Büldt, U. Karst, *Fresenius J. Anal. Chem.* 366 (2000) 781.
- [3] X. Zhou, K. Mopper, *Environ. Sci. Technol.* 24 (1990) 1482.
- [4] J. Slemr, *Fresenius J. Anal. Chem.* 340 (1991) 672.
- [5] M. Possanzini, V. Di Palo, M. Petricca, R. Fratarcangeli, D. Brocco, *Atmos. Environ.* 30 (1996) 3757.
- [6] D. Grosjean, E. Grosjean, L.F.R. Moreira, *Environ. Sci. Technol.* 36 (2002) 1389.
- [7] E.B. Bakeas, D.I. Argyris, P.A. Siskos, *Chemosphere* 52 (2003) 805.
- [8] D. Helmig, *Atmos. Environ.* 31 (1997) 3635.
- [9] M. Pires, L.R.F. Carvalho, *Anal. Chim. Acta* 367 (1998) 223.
- [10] T.E. Kleindienst, E.W. Corse, F.T. Blanchard, *Environ. Sci. Technol.* 32 (1998) 124.
- [11] U. Karst, N. Binding, K. Cammann, U. Witting, *Fresenius J. Anal. Chem.* 52 (1993) 345.
- [12] R.S. Spaulding, R.W. Talbot, M.J. Charles, *Environ. Sci. Technol.* 36 (2002) 1798.
- [13] R.R. Arnst, S.B. Tejada, *Environ. Sci. Technol.* 23 (1989) 1428.
- [14] Y.N. Lee, X. Zhou, *Environ. Sci. Technol.* 27 (1993) 749.
- [15] C.P. Ferrari, R. Durand-Jolibois, P. Carlier, V. Jacob, A. Roche, P. Foster, P. Freset, *Analisis* 27 (1999) 45.
- [16] S. François, V. Perraud, M. Pflieger, A. Monod, H. Wortham, *Atmos. Environ.* 39 (2005) 6642.
- [17] A. Levart, M. Veber, *Chemosphere* 44 (2001) 701.
- [18] L. Nondek, R.E. Milofsky, B.W. Birks, *Chromatographia* 32 (1991) 33.
- [19] L. Nondek, D.R. Rodier, J.W. Birks, *Environ. Sci. Technol.* 26 (1992) 1174.
- [20] N. Binding, H. Klänig, U. Karst, W. Pötter, P.A. Czeschinski, U. Witting, *Fresenius J. Anal. Chem.* 362 (1998) 270.
- [21] A.H.J. Grömping, K. Cammann, *Chromatographia* 35 (1993) 142.
- [22] S.J. Swarin, F. Lipari, *J. Liq. Chromatogr.* 6 (1983) 425.
- [23] M. Possanzini, V. Di Palo, *Chromatographia* 46 (1997) 235.
- [24] S. Houdier, M. Legrand, D. Boturyn, S. Croze, E. Defrancq, J. Lhomme, *Anal. Chim. Acta* 382 (1999) 253.
- [25] S. Houdier, S. Perrier, E. Defrancq, M. Legrand, *Anal. Chim. Acta* 412 (2000) 221.
- [26] C. Kempter, T.W. Berkhoudt, C. Greve Tolbol, K.N. Egmore, U. Karst, *Anal. Bioanal. Chem.* 372 (2002) 639.
- [27] C. Kempter, W. Pötter, N. Binding, H. Klänig, U. Witting, U. Karst, *Anal. Chim. Acta* 410 (2000) 47.
- [28] D. Boturyn, A. Boudali, J.F. Constant, E. Defrancq, J. Lhomme, *Tetrahedron* 53 (1997) 5485.
- [29] R. Sander, <http://www.mpch-mainz.mpg.de/~sander/res/henry.html>, 1999.
- [30] J.H. Park, Y.K. Lee, J.S. Cha, S.K. Kim, Y.R. Lee, C.S. Lee, P.W. Carr, *Microchem. J.* 80 (2005) 183.
- [31] B.J. Finlayson-Pitts, J.N. Pitts Jr., *Chemistry of the Upper and Lower Atmosphere: Theory, Experiments and Applications*, Academic Press, 2000, p. 303.



# Analysis of nitrosamines in water by automated SPE and isotope dilution GC/HRMS

## Occurrence in the different steps of a drinking water treatment plant, and in chlorinated samples from a reservoir and a sewage treatment plant effluent

Carles Planas<sup>a</sup>, Óscar Palacios<sup>a</sup>, Francesc Ventura<sup>b</sup>, Josep Rivera<sup>a</sup>, Josep Caixach<sup>a,\*</sup>

<sup>a</sup> Mass Spectrometry Laboratory, Department of Ecotechnologies, IIQAB, CSIC, Jordi Girona Salgado 18, 08034 Barcelona, Spain

<sup>b</sup> AGBAR, Aigües de Barcelona S.A., Avinguda Diagonal 211, 08018 Barcelona, Spain

### ARTICLE INFO

#### Article history:

Received 20 December 2007  
Received in revised form 22 April 2008  
Accepted 23 April 2008  
Available online 8 May 2008

#### Keywords:

NDMA  
Automated SPE  
GC/HRMS  
Drinking water

### ABSTRACT

A method based on automated solid-phase extraction (SPE) and isotope dilution gas chromatography/high resolution mass spectrometry (GC/HRMS) has been developed for the analysis of nine nitrosamines in water samples. The combination of automated SPE and GC/HRMS for the analysis of nitrosamines has not been reported previously. The method shows as advantages the selectivity and sensitivity of GC/HRMS analysis and the high efficiency of automated SPE with coconut charcoal EPA 521 cartridges. Low method detection limits (MDLs) were achieved, along with a greater facility of the procedure and less dependence on the operator with regard to the methods based on manual SPE. Quality requirements for isotope dilution-based methods were accomplished for most analysed nitrosamines, regarding to trueness (80–120%), method precision (<15%) and MDLs (0.08–1.7 ng/L).

Nineteen water samples (16 samples from a drinking water treatment plant {DWTP}, 2 chlorinated samples from a sewage treatment plant {STP} effluent, and 1 chlorinated sample from a reservoir) were analysed. Concentrations of nitrosamines in the STP effluent were 309.4 and 730.2 ng/L, being higher when higher doses of chlorine were applied. *N*-Nitrosodimethylamine (NDMA) and *N*-nitrosodiethylamine (NDEA) were the main compounds identified in the STP effluent, and NDEA was detected above 200 ng/L, regulatory level for NDMA in effluents stated in Ontario (Canada). Lower concentrations of nitrosamines were found in the reservoir (20.3 ng/L) and in the DWTP samples (n.d. –28.6 ng/L). NDMA and NDEA were respectively found in the reservoir and in treated and highly chlorinated DWTP samples at concentrations above 10 ng/L (guide value established in different countries). The highest concentrations of nitrosamines were found after chlorination and ozonation processes (ozonated, treated and highly chlorinated water) in DWTP samples.

© 2008 Elsevier B.V. All rights reserved.

### 1. Introduction

Interest in the determination of *N*-nitroso compounds in different matrices was stimulated after the discovery in 1956 that *N*-nitrosodimethylamine (NDMA) produced liver tumors in rats. From about 300 nitrosamines subjected to carcinogenicity tests, 85% of them have been classified as carcinogens for animals. In addition to their presence in cigarette smoke, nitrosamines can originate from the production of pesticides and in several industries (i.e. rubber, metal, cosmetic, tanneries). However, the most important source of nitrosamines for water treatment companies is their formation during disinfection of drinking water [1].

\* Corresponding author. Tel.: +34 93 4006174; fax: +34 93 2045904.  
E-mail address: [jcgeco@iiqab.csic.es](mailto:jcgeco@iiqab.csic.es) (J. Caixach).

Occurrence of nitrosamines in source water, wastewater and finished drinking water is an emerging issue of environmental and public health significance because many nitrosamines are probable human carcinogens [2,3]. NDMA has been detected in drinking water and wastewater after chlorination and chloramination [4]. Dimethylamine and nitrogen compounds (e.g., natural ammonia or nitrogen-containing coagulants used in water treatment) have been identified as precursors of NDMA in drinking water [5,6]. In 1989, NDMA was first detected as a disinfection byproduct in the Province of Ontario (Canada), and in 1999 this compound was found in drinking waters and wastewaters throughout California (USA) [4].

Recommendations about the presence of NDMA and other volatile nitrosamines in drinking water have been recently adopted in different countries [1]. The California Department of Health Services (CDHS) has established a notification level

of 10 ng/L for NDMA, *N*-nitrosodiethylamine (NDEA) and *N*-nitrosodipropylamine (NDPA), and response levels based on a  $10^{-4}$  cancer risk (at which CDHS recommends removing the source from service) of 200, 100 and 500 ng/L for NDMA, NDEA and NDPA, respectively. A provisional guide value of 12 ng/L was proposed for NDMA in the Netherlands in 2004 and a guide value of 10 ng/L for NDMA and *N*-nitrosomorpholine (NMOR) in drinking water was recommended in Germany. Ontario issued in 2003 an interim maximum acceptable concentration for NDMA of 9 ng/L [7]. Recently, the U.S. Environmental Protection Agency (EPA) has added several nitrosamines to the list of non-regulated pollutants [8].

Concerning wastewater, in the early 1990s a regulatory level of 200 ng/L in effluents was established for NDMA by the Ontario Ministry of Environment and Energy [9].

Volatile nitrosamines [NDMA, NDEA, NMOR, NDPA, *N*-nitrosopyrrolidine (NPYR), *N*-nitrosopiperidine (NPIP) and *N*-nitrosodibutylamine (NDBA)] have been detected in wastewater [1,10]. NDMA and NMOR in surface water [1,11] and NDMA, NDEA, NMOR, NPYR, NPIP and *N*-nitrosodiphenylamine (NDPHA) in drinking water [4,12].

Concentration levels of nitrosamines detected were as high as 2.5 mg/L of NDMA and 0.17 mg/L of NDEA in Russian industrial effluents in 1979 [13]. NDMA and NDEA concentrations were 9.040 and 0.132  $\mu\text{g/L}$ , respectively, in German wastewaters in 1980 [14]. More recently, NDMA and the sum of other nitrosamine levels ranged from 160 to 834 ng/L and 4.2–8.0 ng/L, respectively, in chlorinated wastewater effluents from the USA [4] and NDMA and NMOR levels of 8–400 and 56–1390 ng/L were respectively found in wastewater effluents in USA [1]. Concerning surface waters, NDMA was detected at concentration levels of 500–2000 ng/L in German river water samples collected 50 m after purification plant effluent inflows and no nitrosamines were found at longer distances downstream the rivers [11,14]. Much lower levels of nitrosamines (11–29 ng/L of NDMA and 92–114 ng/L of NMOR) were detected in screenings of German and French rivers [1]. Nitrosamine concentrations detected in different countries ranged from <10 to 90 ng/L in drinking water, [1]. However, higher concentrations (180 ng/L of NDMA, 70.5 ng/L of NPYR and 117.8 ng/L of NPIP) were found in distribution drinking water samples collected at increasing distances from the DWTP [4,12].

To date, nitrosamines have been analysed in water samples by gas chromatography with different detection systems, such as a thermal energy analyzer (GC/TEA) [15], nitrogen chemiluminescence detection (NCD), nitrogen–phosphorus detection (NPD) [16], and mass spectrometry. The low molecular weight of nitrosamines makes them susceptible to chemical interferences when analysed by gas chromatography–low resolution mass spectrometry (GC/LRMS) with electron ionization (EI) [16,17]. The lack of selectivity and sensitivity of GC/LRMS in the EI mode can be compensated by using chemical ionization (CI) either with GC/LRMS [4] or gas chromatography–tandem mass spectrometry (GC/MS/MS) [18], and GC/HRMS [9,19]. Liquid chromatography–tandem mass spectrometry (LC/MS/MS) has also been applied to the analysis of nitrosamines in water samples [12], but the sensitivity obtained for most nitrosamines was lower than the one reported by GC/MS/MS or GC/HRMS. Isotopically labeled nitrosamines such as NDMA- $d_6$  and NDPA- $d_{14}$  have been used as internal standards [12,18,19].

Concerning the extraction of nitrosamines from water samples, liquid–liquid extraction (LLE) [20], solid-phase extraction (SPE) with carbonaceous adsorbents such as Ambersorb 572 [9,19,20] and coconut charcoal [18], and solid-phase microextraction (SPME) [16,17] have been used. In spite of the highly variable and low recoveries obtained for NDMA when using LLE and SPE with Ambersorb 572, relative low detection limits were obtained with GC/LRMS analysis (2–5 ng/L) [20]. On the contrary, the methods

based in SPME and GC/LRMS analysis showed a limited sensitivity for nitrosamines, with detection limits of 30–138 ng/L [16].

In 2004, the EPA created a method to measure nitrosamines (EPA Method 521) based on SPE with coconut charcoal cartridges EPA 521 and GC/MS/MS, using large volume injection, an ion trap mass spectrometer and chemical ionization with methanol or acetonitrile [18]. On the other hand, the method from the Ontario Ministry of the Environment is based on SPE with Ambersorb 572 and GC/HRMS analysis [19]. Both methods achieve low detection limits for nitrosamines in water samples (0.26–0.66 and 0.4–0.8 ng/L, respectively).

From all the references found related to methods based on SPE for the analysis of nitrosamines, only one of them used an automatic system for SPE [21].

In this paper, two SPE methods using Ambersorb 572 (manual SPE) and coconut charcoal cartridges EPA 521 with automated SPE, as well as different conditions for GC/HRMS analysis of 9 nitrosamines [NDMA, *N*-nitrosomethylethylamine (NMEA), NDEA, NPYR, NDPA, NMOR, NPIP, NDBA and NDPHA] were evaluated. The method developed is based on isotope dilution with labelled nitrosamines ( $d_6$ -NDMA and  $d_{14}$ -NDPA) used as internal standards. Instrumental and method quality parameters were estimated, and water samples from a DWTP and chlorinated samples from an STP effluent and a reservoir were analysed. The results obtained were compared to the concentration levels of 10 ng/L (guide value for nitrosamines in drinking water established in different countries) [1], and 200 ng/L (regulatory level for NDMA in effluents stated in Ontario) [9].

## 2. Experimental

### 2.1. Chemicals and materials

All reagents were of gas chromatographic (GC) grade. Methanol was purchased from Merck (Darmstadt, Germany) and dichloromethane was obtained from Fluka (Buchs, Switzerland). Sodium thiosulphate was purchased from Merck. High-purity water produced with a Milli-Q Synergy UV system (Millipore, Bedford, MA, USA) was used. Mineral water, contained in glass bottles, was obtained from Font Vella (Sant Hilari Sacalm, Spain). Pre-packed SPE coconut charcoal EPA 521 cartridges (6 mL) from Restek (Bellefonte, PA, USA) and SPE cartridges Isolute  $\text{Na}_2\text{SO}_4$  (2.5 g) from International Sorbent Technology (IST, Mid Glamorgan, UK) were used. The sorbent Ambersorb 572 (Rohm and Haas, Philadelphia, PA, USA) was conditioned at 300 °C during 3 h before use.

A standard solution containing 2000 ng/ $\mu\text{L}$  of the 9 native nitrosamines mentioned in Section 1 (Table 1) in methanol was purchased from Supelco (Bellefonte, PA, USA). Two deuterated standard solutions containing 1000 ng/ $\mu\text{L}$  of NDMA- $d_6$  and NDPA- $d_{14}$  in deuterated dichloromethane ( $\text{CD}_2\text{Cl}_2$ ) were obtained from Cambridge Isotope Laboratories (Andover, MA, USA). Toluene- $d_8$  was acquired from Dr. Ehrenstorfer (Augsburg, Germany).

The following standard solutions were prepared using dichloromethane as diluting solvent: (a) NDMA- $d_6$  and NDPA- $d_{14}$  at 10 ng/ $\mu\text{L}$  as internal standards, (b) the 9 native nitrosamines mentioned above at 10 ng/ $\mu\text{L}$  and (c) toluene- $d_8$  at 1 ng/ $\mu\text{L}$  as a recovery standard.

### 2.2. Sample collection

Sixteen water samples related to the different steps of a DWTP which treatment consists on prechlorination, flocculation, sand filtration, dilution with groundwater (wells), ozonation, granular activated carbon (GAC) filtration and treated water after a final

**Table 1**  
Acquisition data for GC/HRMS analysis of 9 native, 2 labeled nitrosamines and toluene- $d_8$  (recovery standard) by using SIM mode

Compound	Molecular weight	Retention time (min)	$m/z$ of analytes <sup>a</sup>	$m/z$ of perfluorokerosene reference peaks (lock mass) <sup>b</sup>
NDMA- $d_6$	80	9.76	80.086	99.994
NDMA <sup>c</sup>	74	9.88	74.048	
Toluene- $d_8$	100	11.02	98.099	
NMEA <sup>c</sup>	88	13.66	88.064	
NDEA <sup>d</sup>	102	16.66	102.079	
NDPA- $d_{14}$	144	23.15	126.190, 144.199	111.994
NPYR <sup>d</sup>	100	23.28	100.064	
NDPA <sup>d</sup>	130	23.43	113.108, 130.111	
NMOR <sup>d</sup>	116	23.47	116.059	
NPIP <sup>d</sup>	114	24.98	114.079	
NDBA <sup>d</sup>	158	29.91	141.139, 158.142	154.992
NDPHA <sup>d</sup>	198	40.39	168.081, 169.089	

One or two ions were selected for each compound and three acquisition windows (9–20 min, 20.1–27.5 min, 27.6–45 min) were used. Dwell time was 100 ms for the selected ion related to NDMA ( $m/z$  74.048) and 50 ms for the other ions monitored.

<sup>a</sup> Analytes with 2 selected ions were quantified using the sum of 2 ion responses.

<sup>b</sup> One lock mass peak was monitored for each acquisition window.

<sup>c</sup> Quantified using NDMA- $d_6$  as internal standard.

<sup>d</sup> Quantified using NDPA- $d_{14}$  as internal standard.

postchlorination (1–1.2 mg/L of free chlorine residual), as well as highly chlorinated treated water samples (5 mg/L of free chlorine residual) were collected in November and December 2006 ( $n = 8 \times 2$  samples). Sampling was carried out sequentially according to the time needed for each step of the water treatment. Two samples from an STP effluent were collected in June 2006 and chlorinated to 6 and 18 mg/L of free chlorine, respectively. Finally, a sample from a reservoir which supplies water to another DWTP was collected in November 2006 and chlorinated to 5 mg/L of free chlorine. All samples were collected in 1 L amber glass bottles, dechlorinated 24 h after collection with 100 mg of sodium thiosulphate, stored at 4 °C and extracted by SPE within 7 days [22].

### 2.3. Extraction methods

Two methods based on SPE techniques were used for the extraction of nitrosamines from water samples.

#### 2.3.1. Method 1

Based on a manual SPE with the sorbent Ambersorb 572 [9,19,20]. Two milliliters of methanol spiked with 50  $\mu$ L of the internal standard solution and 300 mg of Ambersorb 572 were added to 1 L of sample contained in an amber glass bottle. The sample was stirred with a magnet at 50 rpm during 1 h and then it was filtered through a filter paper to collect the Ambersorb 572. The bottle was rinsed with high-purity water and the suspension was filtered to ensure a complete transfer of the Ambersorb 572 to the filter. The filter paper with the Ambersorb 572 was allowed to air dry for 60 min. The dried Ambersorb 572 was transferred to an amber vial, and 950  $\mu$ L of dichloromethane along with 50  $\mu$ L of the recovery standard solution (toluene- $d_8$  at 1 ng/ $\mu$ L) were added.

#### 2.3.2. Method 2

Based on an automated SPE procedure using coconut charcoal EPA 521 cartridges [18]. Two milliliters of methanol spiked with 25  $\mu$ L of the internal standard solution were added to 500 mL of sample. The sample was homogenised by sonication and extracted using the automated SPE system Power-Prep/SPE (Fluid Management Systems, Waltham, MA, USA). Twenty milliliters each of dichloromethane, methanol and Milli-Q water were passed through an SPE coconut charcoal EPA 521 cartridge (Section 2.1) at a flow rate of 10 mL/min. Next the sample was passed through the cartridge at a flow rate of 10 mL/min, and the sorbent was dried under vacuum for

10 min. Elution was performed with 2  $\times$  6 mL of dichloromethane and the eluate was passed through an SPE cartridge Isolute Na<sub>2</sub>SO<sub>4</sub>. The extract was concentrated to a volume of 500  $\mu$ L on a TurboVap II evaporator (Zymark, Hopkinton, MA, USA), using a water bath near room temperature (20–25 °C) and a gentle stream of nitrogen, and transferred to an amber glass vial. Finally, 25  $\mu$ L of the recovery standard solution were added.

### 2.4. Analysis by GC/HRMS

Analyses were carried out on an AutoSpec Ultima (Micromass, Manchester, UK) double-focusing magnetic mass spectrometer coupled to a GC8000 (Thermo-Finnigan, Manchester, UK) gas chromatograph.

Chromatographic separation was achieved using a Rtx-5Sil MS (30 m, 0.25 mm i.d., 1  $\mu$ m film) from Restek (Bellefonte, PA, USA) fused-silica capillary column along with a Siltek deactivated splitless liner 3 mm i.d. from Restek. A TRB-5A (60 m, 0.25 mm i.d., 0.5  $\mu$ m film) from Teknokroma (Sant Cugat, Spain) fused silica capillary column was also evaluated using a splitless liner 3 mm i.d. from SGE (Ringwood, Australia). Helium was used as carrier gas at a constant head pressure of 80 kPa. Oven temperature was from 35 °C (held for 5 min) to 250 °C (maintained for 10 min) at a rate of 5 °C/min. Injector and interface temperatures were 200 and 280 °C, respectively. Injection mode was splitless for 1 min and injection volume was 1  $\mu$ L.

Mass spectrometry was performed at mass resolving powers of 6000 and 10,000 (5% peak height). The electron ionization mode (EI+) at 35 eV of ionization energy was used. Ion source temperature was 200 °C. Acquisition was carried out in the SIM mode, in three acquisition windows (cycle time between 450 and 520 ms). Table 1 summarizes all acquisition data.

The nitrosamine NDPHA is thermally unstable [12] and the chromatographic peak identified is in fact diphenylamine, which is produced in the injection liner by decomposition of NDPHA. Therefore, the  $m/z$  values listed in the last row of Table 1 ( $m/z$  168.081 and  $m/z$  169.089) are related to diphenylamine.

### 2.5. Identification and quantitation

One perfluorokerosene reference peak (lock mass) was monitored for each acquisition window (see Table 1). For positive identification of nitrosamines, the lock mass intensity must be con-

**Table 2**  
Instrumental detection limits (IDLs) of nitrosamines analysed by GC/HRMS in pg injected

Nitrosamine	Column Rtx-5Sil MS		Column TRB-5A
	Resolving power = 6000	Resolving power = 10,000	Resolving power = 6000
NDMA	0.43	0.91	1.55
NMEA	0.55	0.55	1.00
NDEA	0.07	0.05	0.07
NPYR	0.10	0.05	0.20
NPIP	0.07	0.07	0.06
NMOR	1.38	1.30	1.25
NDPA	0.06	0.01	0.06
NDBA	0.15	0.03	0.10
NDPHA	0.05	0.03	0.20

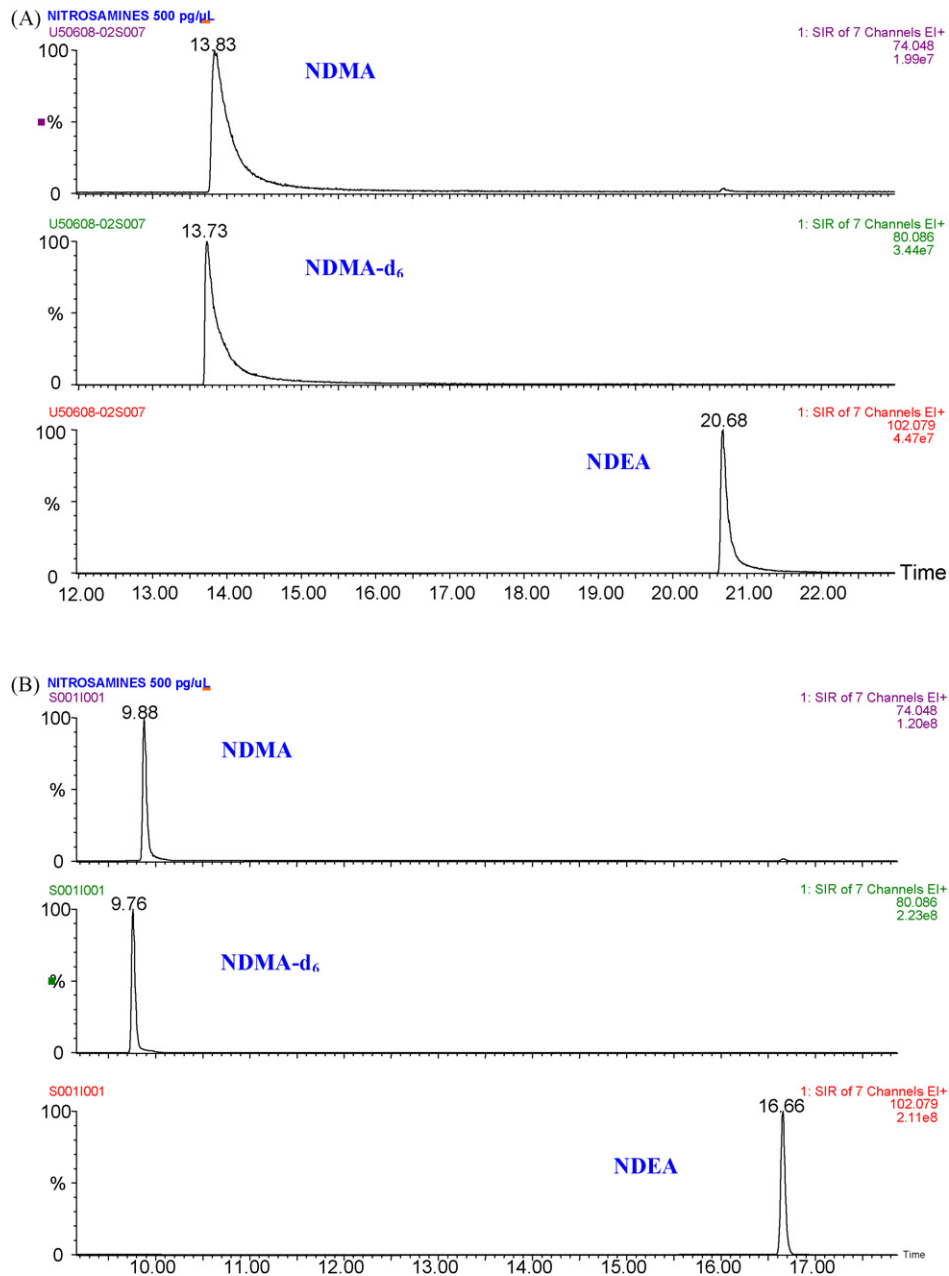


**Fig. 1.** Peak shape of nitrosamines analysed by GC/HRMS at resolving power of 6000 (500 pg/ $\mu$ L of each compound). (A) Column TRB-5A (60 m, 0.25 mm i.d., 0.5  $\mu$ m film). (B) Column Rtx-5Sil MS (30 m, 0.25 mm i.d., 1  $\mu$ m film).

stant in all acquisition windows [19]. Identification of nitrosamines was carried out using the software MassLynx V4.0 (Micromass, Manchester, UK), according to their retention time and the area ratio for the compounds with two selected ions (NDPA, NDBA and NDPHA in Table 1). Tolerances of 0.5% and 20% with regard to the calibration solution were allowed for relative retention times (related to the respective internal standard) and area ratios, respectively [23].

Nitrosamines were quantified using the average response factors related to their respective internal standard (see Table 1), which were calculated daily. For this purpose 5 calibration solutions containing the 9 analytes (nitrosamines) at concentrations from 1 to 500 pg/ $\mu$ L, the two internal standards (NDMA- $d_6$  and NDPA- $d_{14}$ ) at 500 pg/ $\mu$ L and the recovery standard (toluene- $d_8$ ) at 50 pg/ $\mu$ L were analysed daily by GC/HRMS.

### 3. Results and discussion

#### 3.1. Optimisation of GC/HRMS analysis

Standard solutions of native and labelled nitrosamines in dichloromethane (Table 1) containing individual concentrations of 500, 100, 10 and 1 pg/ $\mu$ L were analysed by GC/HRMS using the different chromatographic and spectrometric conditions previously described. Two columns (TRB-5A and Rtx-5Sil MS), and mass resolving powers of 6000 and 10,000 (5% peak height) were evaluated. The column TRB-5A is a typical 5% diphenyl 95% dimethyl polysiloxane and the 5SilMS is a 5% phenyl type with the phenyl rings in the polymer backbone.

The peak shape of nitrosamines analysed by GC/HRMS at a resolving power of 6000 (500 pg/ $\mu$ L of each compound) was improved when the analysis was performed with the column Rtx-5Sil MS (Fig. 1B) with regard to the column TRB-5A (Fig. 1A).

Instrumental limits of detection (IDLs) of nitrosamines were calculated by injecting 1 pg of each compound (10 pg for NMOR) and using a signal-to-noise ratio of 3. IDLs were determined with both columns TRB-5A (resolving power of 6000), and Rtx-5Sil MS (resolving powers of 6000 and 10,000) and results are displayed in Table 2.

Ranges of IDLs for the different nitrosamines were 0.05–1.38 and 0.06–1.55 pg injected with the columns Rtx-5Sil MS and TRB-5A, respectively (resolving power of 6000). Lower IDLs were achieved with the column Rtx-5Sil MS for most nitrosamines, especially for NDMA (0.43 pg versus 1.55 pg injected when using the column TRB-5A). This fact, as well as the better peak shapes (low peak width and tailing) obtained with the column Rtx-5Sil MS, could be mainly explained by the high thermal stability and low bleeding of this column, due to the structure of the stationary phase with the phenyl rings into the polymer backbone [24].

On the other hand, equal or slightly lower IDLs were obtained for most nitrosamines when the GC/HRMS analysis was carried out at a resolving power of 10,000 with regard to a resolving power of 6000, except for NDMA.

According to the results obtained for the different GC/HRMS conditions, the column Rtx-5Sil MS and a resolving power of 6000 were selected for the analysis of nitrosamines in water samples. The better peak shapes and low tailing related to this column and the lower IDL of NDMA at 6000 of resolving power (0.43 pg injected) were the reasons. A better sensitivity for NDMA was preferred to the lower IDLs obtained for other nitrosamines at 10,000 of resolving power, since NDMA is the most commonly regulated nitrosamine in different countries [1].

**Table 3**

Recoveries of nitrosamines (3 replicates) in mineral water (500 ng/L) using the extraction methods 1 and 2

Compound	Recoveries (%)	
	Method 1 (manual SPE with Ambersorb 572)	Method 2 (automated SPE with EPA 521 cartridges)
NDMA	43 $\pm$ 13	88 $\pm$ 6
NMEA	74 $\pm$ 9	91 $\pm$ 7
NDEA	95 $\pm$ 9	88 $\pm$ 7
NPYR	84 $\pm$ 12	93 $\pm$ 9
NDPA	90 $\pm$ 9	87 $\pm$ 10
NMOR	75 $\pm$ 16	90 $\pm$ 6
NPIP	94 $\pm$ 6	91 $\pm$ 11
NDBA	99 $\pm$ 1	73 $\pm$ 6
NDPHA	34 $\pm$ 8	23 $\pm$ 14

#### 3.2. SPE extraction methods

Five hundred milliliters of mineral water spiked with native nitrosamines at 500 ng/L were extracted by triplicate using the methods 1 (manual SPE with Ambersorb 572) and 2 (automated SPE with EPA 521 cartridges) described in Section 2.3. The extracts were analysed by GC/HRMS using the conditions selected in Section 3.1 (column Rtx-5Sil MS and resolving power of 6000). Recoveries of nitrosamines were calculated using their average response factors related to the recovery standard (toluene- $d_8$ ).

The results obtained are shown in Table 3. Comparing both, method 2 showed average recoveries for NDMA, NMEA and NMOR much higher than method 1. On the other hand, method 1 recovered NDBA better whereas the recoveries obtained for the other nitrosamines were similar using both methods. According to the higher recoveries of NDMA and NMOR, method 2 was selected for the analysis of nitrosamines in real water samples, since NDMA is the most commonly regulated nitrosamine, and NDMA and NMOR have been usually detected in industrial and urban effluents from different countries [1].

Average recoveries were above 70% for 8 of the 9 analysed nitrosamines when using the extraction method 2, and for 7 of them the recovery exceeded 80%. Only NDPHA showed a low average recovery (22.5%), probably due to its irreversible adsorption on the coconut charcoal EPA 521 cartridge. This fact could be explained by the large size of the hydrophobic part of the NDPHA molecule (phenyl groups), which causes the high hydrophobicity ( $K_{ow}$ ) and adsorption coefficient ( $K_{oc}$ ) and the low water solubility of NDPHA compared to the other nitrosamines (Table 4) [17,25].

In addition to the high efficiency of the SPE with EPA 521 cartridges, method 2 has the advantage of the automatization, which increases the facility of the procedure and makes it less dependent on the operator when compared to the manual SPE with Ambersorb 572 (method 1).

**Table 4**

Hydrophobicity ( $K_{ow}$ ), adsorption coefficient ( $K_{oc}$ ) and water solubility (mg/L) of nitrosamines

Compound	$K_{ow}$ [17]	$K_{oc}$ [25]	Water solubility (mg/L) [17]
NDMA	0.27	12	1,000,000
NMEA	1.10	4–73	300,000
NDEA	3.02	43	106,000
NPYR	0.65	n.a.	1,000,000
NDPA	2.29	n.a.	13,000
NMOR	0.36	n.a.	861,527.5
NPIP	22.9	n.a.	76,480
NDBA	427	n.a.	1,270
NDPHA	1349	1202	35

n.a.: not available.



**Table 5**  
Instrumental quality parameters of nitrosamines analysed by GC/HRMS (column Rtx-5Sil MS and resolving power of 6000)

Compound	Linear range (pg)	Calibration data	<i>r</i>	IQL <sup>a</sup> (pg)	R.S.D. (%) run-to-run ( <i>n</i> = 5)		R.S.D. (%) day-to-day ( <i>n</i> = 5)
					500 pg injected	10 pg injected	500 pg injected
NDMA	1–500	$y = 0.0012x + 0.0011$	1.000	2.8	1.8	10.7	5.7
NMEA	1–500	$y = 0.0011x - 0.001$	1.000	2.5	3.0	3.3	3.1
NDEA	1–500	$y = 0.0024x + 0.0102$	1.000	0.18	3.2	2.2	8.2
NPYR	1–500	$y = 0.0016x - 0.0013$	1.000	0.26	1.3	2.6	7.2
NDPA	1–500	$y = 0.0019x - 0.0017$	0.999	0.20	1.7	1.9	2.3
NMOR	1–500	$y = 0.001x - 0.001$	0.999	12.8	2.2	7.3	2.4
NPIP	1–500	$y = 0.0028x - 0.0014$	1.000	0.17	2.3	1.7	2.5
NDBA	1–500	$y = 0.0007x + 0.002$	1.000	1.4	1.9	6.4	7.9
NDPHA	1–500	$y = 0.0217x + 0.0997$	1.000	0.28	3.0	4.3	18.8

<sup>a</sup> IQLs: instrumental quantitation limits.

### 3.3. Quality parameters

Instrumental quality parameters calculated for nitrosamines using the conditions specified in the experimental section are shown in Table 5. Linearity was examined over the range 1–500 pg injected (7 data points), which is related to an individual nitrosamine concentration of 1.1–525 ng/L when using the extraction method 2. All analysed nitrosamines showed linear responses in the whole range ( $r \geq 0.999$ ). Relative standard deviation (R.S.D.) values for run-to-run (5 replicate analysis in the same day) were evaluated at the levels of 10 and 500 pg of each compound injected, and R.S.D. values for day-to-day (5 replicate analysis in 5 different days) were calculated at the level of 500 pg. Run-to-run was below 5% for all nitrosamines at the level of 500 pg injected, and it was above 5% for NDMA (10.7%), NMOR (7.3%) and NDBA (6.4%) when injecting 10 pg of each compound. Day-to-day was above 10% only for NDPHA (18.8%), probably due to the thermal unstability of this compound (Zhao et al., 2006). Instrumental quantitation limits (IQLs), calculated by injecting 10 pg of each compound (50 pg for NMOR) and using a signal to noise ratio (S/N) of 10, varied from 0.17 (NPIP) to 12.8 pg (NMOR).

Method quality parameters calculated using the extraction method 2 are summarized in Table 6. Trueness and precision were evaluated by analysing three mineral water samples spiked at the concentration levels of 10 and 500 ng/L, values in the neighborhood of the expected nitrosamine concentrations in WTP and STP effluent samples, respectively. Trueness was in range 80–120% for 8 of the 9 analysed nitrosamines. Only NDPHA showed much lower values for trueness (29.0% and 19.6% at the levels of 500 and 10 ng/L, respectively), due to the low extraction recovery of this compound. Method precision was below 15% for most nitrosamines, and only NMEA showed a value slightly higher at the level of 10 ng/L (16.2%). Method detection limits (MDLs), calculated by analysing

the spiked sample at the level of 10 ng/L and using a signal-to-noise ratio of 3, varied from 0.1 ng/L (NDEA, NPIP and NDBA) to 1.7 ng/L (NMOR).

Most quality requirements for methods based on isotope dilution (high sensitivity, trueness and precision) were accomplished regarding to the studied parameters [26].

### 3.4. Analysis of real water samples

Water samples were analysed by isotope dilution-GC/HRMS at a resolving power of 6000. The SPE was carried out using the method 2 [18]. Additionally, three blanks consisting of 500 mL of mineral water were also analysed along with the real water samples.

The results obtained are shown in Tables 7 and 8. As expected, nitrosamine concentrations were much higher in the chlorinated STP effluents (309.4–730.2 ng/L) than in the DWTP and reservoir samples (n.d. –28.6 ng/L). This fact could be likely explained by the high content in nitrosamine precursors such as secondary amines and nitrogen compounds such as ammonia, nitrite and nitrate [5,6] of the STP effluent. The highest concentrations of nitrosamines were detected in the STP effluent sample containing a higher dose of free chlorine (18 mg/L) with regard to the sample with a lower dose (6 mg/L), as it was expected due to the action of chlorine as oxidizing agent (see Table 7). NDEA (161.1–501.9 ng/L), NDMA (70.8–123.1 ng/L) and NMOR (41.1–44.1 ng/L) were the main nitrosamines found in the STP effluents. NDEA concentration (501.9 ng/L) in the sample containing 18 mg/L of free chlorine exceed the regulatory level of 200 ng/L in effluents stated for NDMA by the Ontario Ministry of Environment and Energy [9].

The sum of nitrosamine concentrations in the reservoir chlorinated water sample (20.3 ng/L) is shown in Table 7 and was

**Table 6**  
Method quality parameters of nitrosamines calculated using the extraction method 2 (automated SPE with EPA 521 cartridges)

Compound	Spiked mineral water (3 replicates) (nitrosamine conc. = 500 ng/L)		Spiked mineral water (3 replicates) (nitrosamine conc. = 10 ng/L)		MDL (ng/L) <sup>c</sup>
	Trueness (%) <sup>a</sup>	Method precision (%) <sup>b</sup>	Trueness (%) <sup>a</sup>	Method precision (%) <sup>b</sup>	
NDMA	97.7	0.4	107.9	11.3	0.8
NMEA	100.6	1.8	96.8	16.2	0.6
NDEA	95.2	5.3	80.8	9.7	0.1
NPYR	102.1	3.3	102.0	8.5	0.2
NDPA	94.0	1.1	97.0	2.7	0.2
NMOR	98.9	3.4	113.7	14.3	1.7
NPIP	94.0	1.1	115.5	11.8	0.1
NDBA	81.5	0.7	116.1	3.6	0.1
NDPHA	29.0	1.4	19.6	1.7	0.2

<sup>a</sup> Trueness, calculated as the average of three calculated concentrations divided by the true concentration.

<sup>b</sup> Method precision, calculated as the relative standard deviation (R.S.D.) of three calculated concentrations.

<sup>c</sup> MDL: method detection limit, calculated as the concentration of analyte which produces a signal equal to three times the standard deviation of noise.

**Table 7**  
Results related to nitrosamine concentrations (ng/L) in chlorinated water samples from a STP effluent and a reservoir which supplies water to a DWTP

Compound	STP effluent 6 mg/L of free chlorine	STP effluent 18 mg/L of free chlorine	Reservoir 5 mg/L of free chlorine
NDMA	70.8	123.1	13.4
NMEA	n.d.	n.d.	n.d.
NDEA	161.1	501.9	4.1
NPYR	8.2	3.5	0.2
NDPA	3.1	11.3	n.d.
NMOR	41.1	44.1	n.d.
NPIP	4.0	3.1	0.2
NDBA	21.1	43.2	2.4
NDPHA	n.d.	n.d.	n.d.
Sum nitrosamines	309.4	730.2	20.3

n.d.: not detected. Concentration < MDL (method detection limit).

similar to the concentration levels of the ozonated, treated and highly chlorinated DWTP samples collected in November 2006 (20.9–28.6 ng/L) displayed in Table 8. The NDMA concentration was higher in the reservoir sample (13.4 ng/L) than in DWTP samples (n.d. – 11.5 ng/L). These results show that chlorination of water from the reservoir has the capability to produce nitrosamines, including NDMA, at concentrations above the guide values of 9–12 ng/L [1,7].

Concerning DWTP samples (Table 8), higher concentrations of nitrosamines were detected in the samples collected in November with regard to the samples from December. These results seem to be in agreement with the characteristics of raw water from the DWTP shown in the footnote of Table 8, as higher nitrosamine concentrations detected in November could be related to the higher chlorine dioxide dose used and organic matter content (Total organic carbon {TOC}, UV adsorption and permanganate oxidability) found in that month.

Nitrosamines were detected at low concentrations or even not detected in the DWTP inputs and DWTP wells from the two series of DWTP samples analysed. Nitrosamine concentrations

increased after chlorination and ozonation processes (maximum concentrations were detected in the ozonated water (28.6 ng/L), treated water (27.7 ng/L) and highly chlorinated water (20.9 ng/L) samples collected in November, and it decreased after GAC filtration (16 ng/L were found in the GAC filtered water sample from November). These facts could be respectively explained by the reaction of chlorine and ozone as oxidizing agents with nitrosamine precursors, and the partial adsorption of nitrosamines onto the GAC filter. Nitrosamines were detected at very low concentrations or even not found in prechlorinated waters, probably due to the short time of action of chlorine (prechlorinated water samples were collected only 7 min and 8 min after DWTP inputs).

Few differences related to nitrosamine concentrations were observed between treated (containing 1–1.2 ppm of free chlorine) and highly chlorinated (5 ppm of free chlorine) water samples from the DWTP. NDMA and NDEA concentrations were slightly higher in the highly chlorinated water, NMOR was only detected in the treated water sample, and NPYR was found at very low concentrations in both samples collected in November. However,

**Table 8**  
Results related to nitrosamine concentrations (ng/L) in water samples from a DWTP collected in November (A) and December 2006 (B)

Compound	Raw water	Prechlorinated water	Sand filtered water	Groundwater wells	Ozonated water	GAC filtered water	Treated water	Highly chlorinated water
(A)								
NDMA	n.d.	n.d.	3.0	1.1	10.1	4.5	5.5	6.5
NMEA	n.d.	n.d.	n.d.	n.d.	n.d.	n.d.	n.d.	n.d.
NDEA	n.d.	n.d.	n.d.	n.d.	n.d.	n.d.	12.9	13.3
NPYR	n.d.	n.d.	n.d.	n.d.	5.4	n.d.	1.4	1.1
NDPA	n.d.	n.d.	n.d.	n.d.	2.6	n.d.	n.d.	n.d.
NMOR	2.8	n.d.	7.9	n.d.	9.2	11.5	7.9	n.d.
NPIP	n.d.	n.d.	n.d.	n.d.	1.3	n.d.	n.d.	n.d.
NDBA	n.d.	n.d.	n.d.	n.d.	n.d.	n.d.	n.d.	n.d.
NDPHA	n.d.	n.d.	n.d.	n.d.	n.d.	n.d.	n.d.	n.d.
Sum nitrosamines	2.8	n.d.	10.9	1.1	28.6	16.0	27.7	20.9
(B)								
NDMA	n.d.	2.6	11.0	n.d.	11.5	n.d.	n.d.	7.3
NMEA	n.d.	n.d.	n.d.	n.d.	n.d.	n.d.	n.d.	n.d.
NDEA	n.d.	n.d.	n.d.	n.d.	n.d.	n.d.	n.d.	n.d.
NPYR	n.d.	n.d.	0.6	n.d.	n.d.	n.d.	n.d.	n.d.
NDPA	n.d.	n.d.	n.d.	n.d.	n.d.	n.d.	n.d.	n.d.
NMOR	7.9	n.d.	6.1	n.d.	n.d.	n.d.	n.d.	n.d.
NPIP	n.d.	n.d.	n.d.	n.d.	n.d.	n.d.	n.d.	n.d.
NDBA	n.d.	n.d.	n.d.	n.d.	n.d.	n.d.	n.d.	n.d.
NDPHA	n.d.	n.d.	n.d.	n.d.	n.d.	n.d.	n.d.	n.d.
Sum nitrosamines	7.9	2.6	17.7	n.d.	11.5	n.d.	n.d.	7.3

n.d.: not detected. Concentration < MDL (method detection limit). Average raw water parameters (November/December): TOC, 5/4.5 mg C/L; UV adsorption, 10.4/8.3 Abs/100 cm; permanganate oxidability, 3.63/3.35 mg O<sub>2</sub>/L; conductivity, 1687/1486 μS/cm; temperature, 14.5/8.7 °C; chlorine dose, 4.5/5 mg Cl<sub>2</sub>/L; chlorine dioxide dose, 2.3/1.5 mg ClO<sub>2</sub>/L; ammonia, 0.23/0.46 mg NH<sub>3</sub>/L; nitrite, 0.35/0.24 mg NO<sub>2</sub>/L.

NDMA was detected in the highly chlorinated water collected in December (7.3 ng/L) but it was not found in the treated water sample.

The most frequently detected nitrosamines in the DWTP samples were NDMA, NMOR, NPYR and NDEA. They were detected in both treated and highly chlorinated water samples but only NDEA was in two samples (treated and highly chlorinated water samples from November) above the guide value of 10 ng/L. The only nitrosamine detected in the DWTP inputs was NMOR.

#### 4. Conclusions

This study has developed a method based on isotope dilution GC/HRMS with previous automated SPE for the analysis of nitrosamines in water samples. The combination of automated SPE and GC/HRMS for the analysis of nitrosamines has not been reported previously. The selectivity and sensibility of GC/HRMS and the high efficiency of automated SPE with coconut charcoal EPA 521 cartridges allow to achieve low MDLs, along with a greater facility of the procedure and less dependence on the operator with regard to the methods based on manual SPE. Quality requirements for isotope dilution-based methods (high sensitivity, accuracy and precision) were accomplished for most analysed nitrosamines, regarding to trueness (80–120%), method precision (<15%) and MDLs (0.08–1.7 ng/L).

Nineteen water samples (16 samples from a DWTP, 2 chlorinated samples from a STP effluent and one chlorinated sample from a reservoir) were analysed. Low nitrosamine concentrations were detected in the reservoir (20.3 ng/L) and the DWTP samples (n.d. –28.6 ng/L) and much higher concentrations were found in the STP effluent (309.4–730.2 ng/L), especially when a higher dose of chlorine (18 mg/L) was applied.

The highest nitrosamine concentrations in DWTP samples were detected after chlorination and ozonation processes (ozonated, treated and highly chlorinated water), especially in the samples collected in November with regard to the samples from December 2006. This fact could be explained by the reaction of ozone and chlorine with nitrosamine precursors as oxidizing agents. The higher nitrosamine levels detected in November could be likely related to the characteristics of raw water that month (higher chlorine dioxide dose and organic matter content compared to the values from December).

NDEA concentration in the STP sample containing 18 mg/L of free chlorine (501.9 ng/L) was above the regulatory level of 200 ng/L in effluents established for NDMA in Ontario (Canada). Moreover, NDMA in the reservoir sample and NDEA in treated and highly chlorinated DWTP samples were found at concentrations above 10 ng/L (guide value for nitrosamines in drinking water established in different countries).

#### Acknowledgements

The authors would like to thank Daniel Almarcha for his help in the extraction of the samples and Jordi Sauló for the optimization of the automated SPE system.

This study was financially supported by the EEORG project from AGBAR-CSIC.

#### References

- [1] Suez Environment, Internal report, 2007.
- [2] International Agency for Research on Cancer (IARC), IARC Monographs on the Evaluation of the Carcinogenic Risk of Chemicals to Humans: Some N-Nitroso Compounds, vol. 17, International Agency for Research on Cancer, Lyon, 1978, p. 365.
- [3] [www.epa.gov/iris/subst/0045.htm](http://www.epa.gov/iris/subst/0045.htm) (accessed June 22, 2007).
- [4] J.W.A. Charrois, M.W. Arend, K.L. Froese, S.E. Hrudey, Environ. Sci. Technol. 38 (2004) 4835.
- [5] C.L. Lv, Y.D. Liu, R. Zhong, Y. Wang, J. Mol. Struct. 802 (2007) 1.
- [6] S.D. Richardson, Anal. Chem. 79 (2007) 4295.
- [7] [www.ene.gov.on.ca/environ/gp/4449e.pdf](http://www.ene.gov.on.ca/environ/gp/4449e.pdf) (accessed June 21, 2007).
- [8] [www.epa.gov/fedrgstr/EPA-WATER/2007/January/Day-04/w22123.htm](http://www.epa.gov/fedrgstr/EPA-WATER/2007/January/Day-04/w22123.htm) (accessed June 21, 2007).
- [9] V.Y. Taguchi, S.W.D. Jenkins, D.T. Wang, J.F.P. Palmantier, E.J. Reiner, Can. J. Appl. Spectrosc. 39 (1994) 87.
- [10] R.C. Cheng, C. Andrews-Tate, C.J. Hwang, Y.C. Guo, J.E. Grebel, I.H. Suffet, Development of low cost method(s) for NDMA analysis: round-robin testing in AWWA WQTC Proceedings wed4.5/1–wed4.5/20, San Antonio, 2004.
- [11] G. Hartmetz, J. Slemrova, Bull. Environ. Contam. Toxicol. 25 (1980) 106.
- [12] Y.Y. Zhao, J. Boyd, S.E. Hrudey, X.F. Li, Environ. Sci. Technol. 40 (2006) 7636.
- [13] A.F. Shushunova, P.E. Shkodich, V.V. Baikovskii, Z.L. Lembik, E.A. Kadulin, Zhurnal Analiticheskoi Khimii 34 (1979) 1855.
- [14] G. Hartmetz, J. Slemrova, Mitteilung der Kommission fuer Wasserforschung 3 (1982) 157.
- [15] M.W. Byun, H.J. Ahn, J.H. Kim, J.W. Lee, H.S. Yook, S.B. Han, J. Chromatogr. A 1054 (2004) 403.
- [16] J.E. Grebel, C.C. Young, I.H. Suffet, J. Chromatogr. A 1117 (2006) 11.
- [17] S. Ventanas, J. Ruiz, Talanta 70 (2006) 1017.
- [18] U.S. Environmental Protection Agency, Method 521, Determination of Nitrosamines in Drinking Water by Solid Phase Extraction and Capillary Column Gas Chromatography with Large Volume Injection and Chemical Ionization Tandem Mass Spectrometry (MS/MS), EPA/600/R-05/054, Cincinnati, 2004.
- [19] Ontario Ministry of Environment, The determination of N-nitrosamines in water by gas chromatography-high resolution mass spectrometry (GC/HRMS), NITROSO-E3388, Toronto, Canada, 2007.
- [20] A. Eaton, M. Briggs, NDMA-Analytical methods options for a new disinfection byproduct, in: In AWWA WQTC Proceedings, Salt Lake City, 2000.
- [21] T. Pérez-Ruiz, C. Martínez-Lozano, V. Tomás, J. Martín, J. Chromatogr. A 1077 (2005) 49.
- [22] U.S. Environmental Protection Agency, Method 1625, Revision B: Semivolatile organic compounds by isotope dilution GC/MS, Fed. Reg. 40 CFR Part 136, 1989.
- [23] Commission Decision 2002/657/CE of 12 August 2002 implementing Council Directive 96/23/CE concerning the performance of analytical methods and the interpretation of results, OJ L 221, 17.8.2002, p. 8.
- [24] <http://www.restek.com> (accessed June 22, 2007).
- [25] <http://www.speclab.com> (accessed June 22, 2007).
- [26] Commission Directive 2002/70/EC of 26 July 2002 establishing requirements for the determination of levels of dioxins and dioxin-like PCBs in feedingstuffs, Off. J. Eur. Commun. L209 (2002) 15.



# A novel electrochemical immunosensor based on colabeled silica nanoparticles for determination of total prostate specific antigen in human serum

Bo Qu, Xia Chu\*, Guoli Shen, Ruqin Yu

State Key Laboratory for Chemo/Biosensing and Chemometrics, College of Chemistry and Chemical Engineering, Hunan University, Changsha 410082, PR China

## ARTICLE INFO

### Article history:

Received 25 January 2008

Received in revised form 2 April 2008

Accepted 12 April 2008

Available online 20 April 2008

### Keywords:

Electrochemical immunosensor

Silica nanoparticles

Silver deposition

Prostate specific antigen

## ABSTRACT

A novel electrochemical immunosensor using functionalized silica nanoparticles (Si NPs) as protein tracer has been developed for the detection of prostate specific antigen (PSA) in human serum. The immunosensor was carried out based on a heterogeneous sandwich procedure. The PSA capture antibody was immobilized on the gold electrode via glutaraldehyde crosslink. After reaction with the antigen in human serum, Si NPs colabeled with detection antibody and alkaline phosphatase (ALP) was sandwiched to form the immunocomplex on the gold electrode. ALP carried by Si NPs convert nonelectroactive substrate into the reducing agent and the latter, in turn, reduce metal ions to form electroactive metallic product on the electrode. Linear sweep voltammetry (LSV) was used to quantify the amount of the deposited silver and give the analytical signal for PSA. The parameters including the concentration of the ALP used to functionalize the Si NPs and the enzyme catalytic reaction time have been studied in detail and optimized. Under the optimum conditions of immunoreaction and electrochemical detection, the electrochemical immunosensor was able to realize a reliable determination of PSA in the range of 1–35 ng/mL with a detection limit of 0.76 ng/mL. For six human serum samples, the results performed with the electrochemical immunosensor were in good agreement with those obtained by chemiluminescent microparticle immunoassay (CMIA), indicating that the electrochemical immunosensor could satisfy the need of practical sample detection.

© 2008 Elsevier B.V. All rights reserved.

## 1. Introduction

Prostate specific antigen (PSA), a 32–33-kDa single-chain glycoprotein, has been extensively studied in the past decades and has shown to be the most reliable tumor marker for the early detection of prostate cancer at organ-confined stage and the monitoring of disease recurrence after treatment [1–3]. Trace levels of PSA are naturally found in the serum, however, prostate cancer tumor growth usually leads to the release of high concentrations of PSA into the circulatory system. A PSA measurement above a cut-off value of 4 ng/mL was first regarded as positive and might indicate the need for a biopsy [4]. Hence, developing rapid, simple and sensitive immunoassay methods for measuring serum PSA concentration has great clinical significance in the diagnosis of prostate cancer.

Currently, most PSA testing takes place at dedicated, centralized laboratories on large, automated high-throughput systems. Therefore, there is a need for a suitable and cost-effective analytical technology to carry out a rapid, simple, and sensitive analysis of PSA. Some methods, such as enzyme-linked immunosorbent

assays (ELISA) [5], fluorescence immunoassay [6], chemiluminescent assay [7], and time-resolved immunofluorometric assay [8,9], have been developed for PSA detection. However, most methods, unfortunately, either are hazardous to the health, time-consuming and labor-intensive, or require highly personnel and sophisticated instrumentation. Electrochemical immunoassays or immunosensors have gained considerable attention in protein detection over the past several decades due to their high sensitivity, rapid analysis time, and relative inexpensive and low reagent consumption. Electrochemical detection systems are easily miniaturized without reducing analytical performance compared to methods mentioned above. These advantages made electrochemical detection powerful in rapid, high-throughput and small volume screening [10].

In recent years, the detection system based on metal deposition has gained considerable attention in the detection of antigen–antibody binding or DNA complementary binding because it possessed the advantages of high sensitivity, simplicity and easy implementation in biomedical application. Some researches have been reported in our group based on the metal deposition–detection system. Yu and co-workers developed an electrochemical immunoassay technique based on the sensitive detection of the enzyme-generated product with a bielelectrode signal transduction system [11] and an electrochemical amplification immunoassay using biocatalytic metal deposition coupled

\* Corresponding author. Tel.: +86 731 8821916; fax: ++86 731 8821916.  
E-mail address: [xiachu@hnu.cn](mailto:xiachu@hnu.cn) (X. Chu).

with anodic stripping voltammetric detection [12]. Shen and co-workers developed an electrochemical stripping metalloimmunoassay based on silver-enhanced gold nanoparticle label [13], in which the immunoreaction was performed in the polystyrene microwells and the electrochemical detection was carried out with a glassy-carbon electrode. In the present work, the immunoreaction and the electrochemical detection were performed on a sensing surface, which made the sensor to be easily miniaturized without reducing analytical performance compared to methods mentioned above. In addition, the use of the Si NPs can further amplify the signal and improve the sensitivity of the immunosensor.

The emergence of nanotechnology is opening a promising field for highly sensitive electrochemical assays of biomarkers. Electrochemical biosensors have shown great promise for diagnosis of trace biomolecules by incorporation with nanoparticles. Cai et al. used the strategy of catalytic precipitation of silver onto electrode surface [14] or Cu@Au alloy nanoparticle as oligonucleotides labels [15] to detect DNA complementary binding. Until now, several kinds of nanoparticles have been used effectively in bioanalysis for their unique properties, including gold nanoparticle [16,17], carbon nanotube [18,19], liposome [20,21], etc. Among them, Si NPs gain more attention because they are biocompatible, easy to be functionalized with bioreagents and quite stable in aqueous environment. Yuan and co-workers [8] used Si NPs in time-resolved fluorescence bioassay for the detection of PSA. Lee [22] prepared surface-enhanced Raman spectroscopic tagging material (SERS dots) composed of metal-embedded silica spheres and organic Raman labels for cellular cancer targeting in living cells. Tan and co-workers [23] developed an ultrasensitive DNA assay to detect gene products using bioconjugated dye-doped silica nanoparticles (Si NPs). However, there are few researches to explore the application of the Si NPs in the field of electrochemical immunoassay.

In this paper, we report the combination of alkaline phosphatase (ALP) and antibody-cofunctionalized Si NPs and biocatalytic deposition of silver for an amplified electrochemical immunoassay of PSA in human serum. The principle of the electrochemical immunosensor is depicted in Scheme 1. We synthesized the functionalized Si NPs carried with ALP and detection antibody through the 1-ethyl-3-(dimethylaminopropyl) carbodiimide hydrochloride (EDC)/*N*-hydroxysuccinimide (NHS) crosslink. After the formation of sandwich type immunocomplex of capture antibody, antigen and functionalized silica NPs on the electrode surface, the ALP carried on the Si NPs converted the ascorbic acid 2-phosphate (AA-P) into ascorbic acid. The later reduced the Ag(I) ions in the solution, leading to the deposition of silver onto the electrode surface. The amount of deposited silver was then determined by linear sweep voltammetry (LSV).

## 2. Experimental

### 2.1. Materials and reagents

A pair of mouse monoclonal antibodies used for the sandwich immunoassay was purchased from T.J. Biotechnologies (Tianjin), Ltd. (China). The mouse anti-human total PSA clone PSA140 was used as the capture antibody, and the mouse anti-human total PSA clone PSA103 was used as the detection antibody. Total PSA was purchased from Beijing Institute of Materia Medica and Biological Products (Beijing, China). Alkaline phosphatase (calf intestinal) was obtained from Promega Corporation (USA). Bovine serum albumin (BSA) was purchased from Beijing Dingguo Biotechnology Development Center (China). AA-P was obtained from Express Technology

Co. Ltd. (Japan). Cyclohexane, *n*-hexanol, Triton X-100 and ammonium hydroxide (25–28 wt%) were obtained from National Reagent Corporation (Shanghai, China). Tetraethyl orthosilicate (TEOS) was purchased from Wulian Chemical Factory (Shanghai, China). 3-Amino-propyltriethoxysilane (APTES) was obtained from Acros (New Jersey, USA). The serum samples of cancer patients were provided by Hunan Provincial Tumor Hospital (Changsha, China). EDC, NHS, trisodium citrate, NaCl, KH<sub>2</sub>PO<sub>4</sub>, Na<sub>2</sub>HPO<sub>4</sub>, and KNO<sub>3</sub> were all purchased from Amresco (Solon, OH). Ultrapure water was obtained through a Nanopure Infinity Ultrapure water system (Barnstead/Thermolyne Corp., Dubuque, IA) with an electrical resistance larger than 18.3 MΩ.

### 2.2. Apparatus

All of the electrochemical experiments were performed with a model CHI660C electrochemical workstation (Shanghai Chenhua Instruments, Shanghai, China) connected to a personal computer. The gold working electrodes (99.99%, 4 mm diameter), platinum wire counter electrode, KCl saturated calomel reference electrode (SCE) and the conventional three-electrode electrochemical cell were all purchased from Shanghai Chenhua Equipments. All potentials were referenced to the SCE reference electrode.

The size and morphology of Si NPs were measured by transmission electron microscopy (TEM, Hitachi 800, Japan). The samples for TEM were prepared by placing a drop of Si NPs aqueous suspension onto the carbon-coated copper grids and then air-dried at room temperature. The TEM images were obtained at an operating voltage of 200 kV.

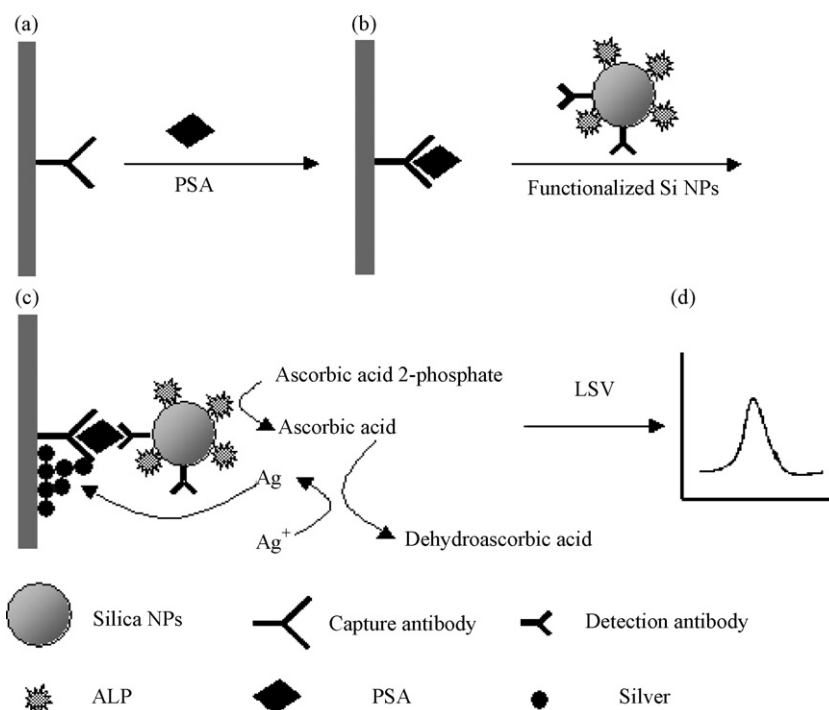
### 2.3. Synthesis of ALP and antibody-cofunctionalized Si NPs

#### 2.3.1. Preparation of Si NPs

The Si NPs were prepared using the microemulsion method. In our experiment, the Si NPs were prepared as follows: 15 mL of Triton X-100 and 15 mL of *n*-hexanol were added to 60 mL of cyclohexane. After the mixture was stirred for about 15 min, 4.5 mL water was added. A transparent and stable reverse microemulsion was obtained after several minutes of stirring, and the stirring continued. After 15 min, 1 mL of NH<sub>4</sub>OH were added and the solution was stirred for another 15 min. Subsequently, 2 mL of TEOS was added to the microemulsion solution and the solution was stirred for 24 h at room temperature. Then, the hydrophilic silica particles were formed. After the reaction was completed, 10 mL of acetone was added, then the nanoparticles were isolated by centrifugation and washed with ethanol and water for several times to remove surfactant. During each washing, the sonicator was used to completely disperse the nanoparticles in ethanol. Surfactant molecules were almost completely removed after the washing process.

#### 2.3.2. Surface modification of Si NPs

An appropriate amount of nanoparticles (1 mg) was dispersed in 2 mL of anhydrous ethanol, and then 0.03 mL of APTES was added. The reaction was allowed to proceed for 1 h under stirring. After centrifuging, the nanoparticles were washed with ethanol and water. The amino-modified nanoparticles were dispersed in 1.5 mL of DMF solution containing 0.15 g glutaric anhydride, and then the mixture was left to stir for 4 h at room temperature. The excess glutaric anhydride was removed by centrifugation and separation, and the nanoparticles were washed with ethanol and water several times. The Si NPs were finally redispersed in 1 mL of 0.1 mol/L PB buffer containing 200 mM EDC, 50 mM NHS, 100 μg/mL PSA detection antibody and 400 U/mL ALP. After stirring for 8 h, an excessive amount of BSA was added and incubated for 1 h. After centrifugation and washing with phosphate buffer and water, the ALP and



**Scheme 1.** Schematic outline of the electrochemical immunosensor. (a) Immobilization of PSA capture antibody on the Au electrode; (b) capture of the analyte PSA in sample solution; (c) association with the functionalized silica NPs, reduction of silver ion by ascorbic acid, and the deposition of metal silver on the electrode surface; (d) linear sweep voltammetry was used for the electrochemical detection of metal silver deposited on the electrode.

antibody-cofunctionalized Si NPs were dispersed in PB buffer containing 3 mg/mL BSA and stored at 4 °C before use.

#### 2.4. Preparation of antibody-modified gold electrode

The gold electrode was polished sequentially with 0.3 and 0.05  $\mu\text{m}$  alumina slurry followed by ultrasonic cleaning in ethanol and double distilled water. Subsequently, the gold electrode was cleaned with piranha solution ( $\text{H}_2\text{SO}_4:\text{H}_2\text{O}_2 = 3:1$ , v/v) and rinsed with water for three times, and then dried under nitrogen gas. The cleaned electrode was immersed in the cysteamine aqueous solution (10 mM) for about 12 h to produce a self-assembled monolayer (SAM). After the electrode was thoroughly rinsed with water to remove adsorbed cysteamine, it was soaked in a glutaraldehyde aqueous solution (2.5%, w/w) for 1 h at 37 °C. Then the electrode was washed with water again. Following that, a 10- $\mu\text{L}$  aliquot of 100  $\mu\text{g}/\text{mL}$  capture antibody was dropped on the electrode and incubated for 1 h at 37 °C. Then the electrode was washed intensively with PB buffer and water. Finally the electrode was incubated for 1 h with 0.3% BSA in 0.03 mM PB buffer to block the unreacted aldehyde.

#### 2.5. Sandwich immunoassay procedure

The capture antibody-modified electrodes were incubated with a series of 10  $\mu\text{L}$  samples containing either purified PSA antigen or serum at various concentrations for 1 h at 37 °C. Then 10  $\mu\text{L}$  solutions containing functionalized Si NPs were dropped on the electrode surface and incubated at 37 °C for 1 h. The resulting electrode was washed with PB buffer and water two times, respectively. Then, the electrodes were incubated with the freshly prepared 50 mM glycine buffer solution (pH 9.08) containing 1 mM  $\text{AgNO}_3$  and 1 mM AA-P at 37 °C for 35 min. After incubation, the electrode was rinsed with ultrapure water.

#### 2.6. Electrochemical determination

Linear sweep voltammetric measurements were performed at a potential range from 0 to 0.8 V (vs. SCE) with a 100 mV/s scanning rate using the three-electrode system. A 0.6 M  $\text{KNO}_3$  solution containing 0.1 M  $\text{HNO}_3$  was used as the supporting electrolyte for electrochemical experiments. The experimental temperature was controlled at room temperature.

### 3. Results and discussion

#### 3.1. Characterization of Si NPs

The uniformity of silica NPs is important to the reproducibility of the electrochemical immunosensors. The size and morphology of these nanoparticles were investigated with transmission electron microscopy (TEM). As shown in Fig. 1, one observes that the nanoparticles have an average size of 36 nm with a standard deviation of 4 nm.

The electrochemical immunoassay was also employed to confirm whether the detection antibody and the ALP were all modified successfully on the surface of the Si NPs. The silica NPs labeled with detection antibody and ALP and the unlabeled silica NPs were used to detect PSA with concentration of 35 ng/mL. The results were shown in Fig. 2. It can be seen that no significant LSV readout was obtained for unlabeled silica NPs, however, about 161  $\mu\text{A}$  stripping peak current was obtained for the silica NPs labeled with detection antibody and ALP. The labeled silica NPs were also used to detect phosphate buffer instead of target protein, and only a little peak current in the LSV measurement was obtained, which may be caused by the nonspecific adsorption of the labeled silica NPs on the electrode surface. These results confirmed that the detection antibody and the ALP were indeed modified successfully on the surface of the Si NPs.

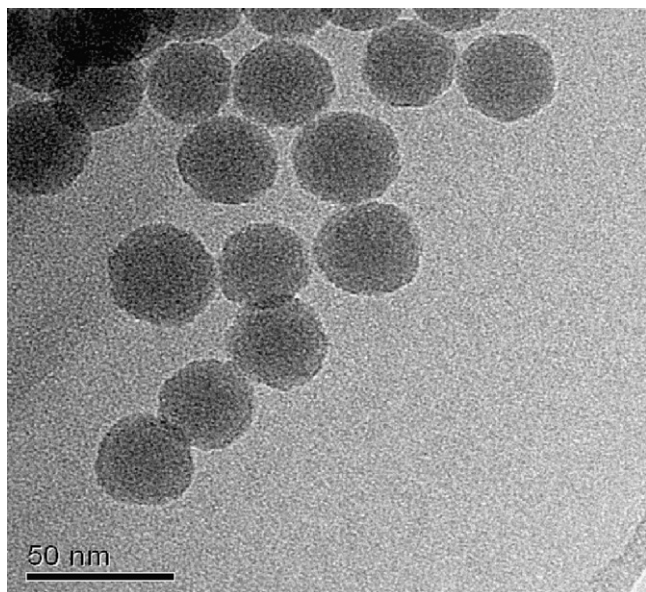


Fig. 1. TEM of silica nanoparticles.

### 3.2. Optimization of the experimental conditions

#### 3.2.1. Effect of the ALP concentration

The amount of biocatalytically deposited metal silver is dependent on the amount of ALP attached on the electrode surface. Apparently, the more the amount of ALP carried on per Si NP, the higher is the sensitivity of the electrochemical immunosensor. So, during the surface modification step, the concentration of PSA detection antibody was fixed at 100  $\mu\text{g}/\text{mL}$  and the concentration of ALP was changed from 100 to 600 U/mL. The number of carboxyl on the Si nanoparticle surface is fixed when the amount of Si nanoparticle is fixed, and the ALP and detection antibody in solution compete to react with the limited carboxyl on the Si nanoparticle surface. The effect of the ALP concentration used to functionalize the Si NPs on the anodic stripping peak current was investigated

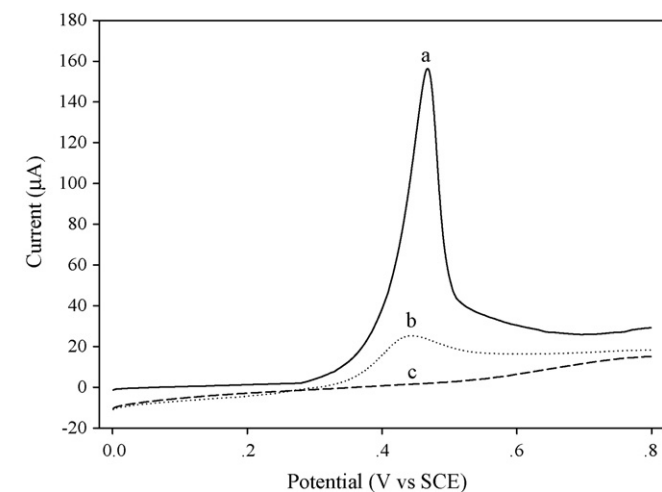


Fig. 2. LSV readouts of enzymatically deposited electrodes in 0.6M  $\text{KNO}_3/0.1\text{M}$   $\text{HNO}_3$  solutions. Curves (a) and (b) were the results of the silica NPs labeled with detection antibody and ALP for the detection of target protein PSA and phosphate buffer, respectively. Curve (c) was the result of the unlabeled silica NPs for the detection of target protein PSA. The concentration of PSA was 35 ng/mL. Scan rate: 100 mV/s.

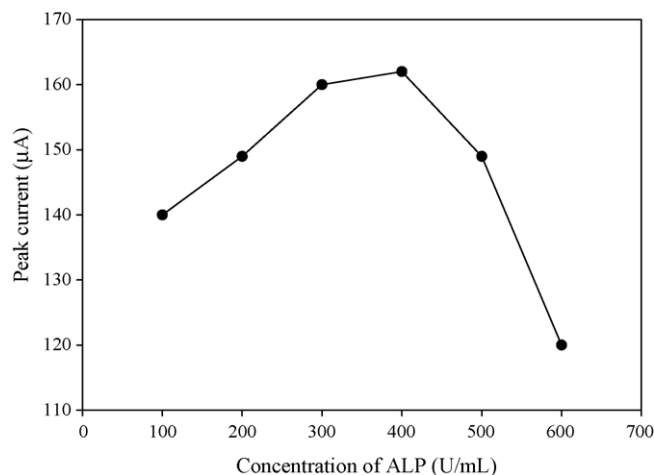


Fig. 3. Effect of the ALP concentration used to functionalize the Si NPs on the anodic stripping peak current.

and the results were shown in Fig. 3. As can be seen from Fig. 3, the anodic stripping peak currents increase substantially when the ALP concentrations change from 100 to 400 U/mL, and then decrease with further increase in ALP concentration up to 600 U/mL. When the ALP concentrations in solution change at the range from 100 to 400 U/mL, the amount of ALP modified on the surface of Si NPs increase with the increase in the ALP concentration, which result in the increase in the stripping peak current of the immunosensor. On the contrary, when the amount of ALP in modified solution is much larger than the amount of the detection antibody, the competition of the detection antibody and ALP induces that the amount of antibody attached on the surface of Si nanoparticle is relatively small, which results in the decrease in the stripping peak currents because the sandwich immunocomplex could not be formed well on the electrode surface. As a result, the optimal ALP concentration for functionalization was selected as 400 U/mL in subsequent studies.

#### 3.2.2. Effect of the biocatalytic deposition time

The effect of the biocatalytic silver deposition time on the stripping peak current was also investigated (Fig. 4). At the beginning, the peak current increased rapidly with deposition time

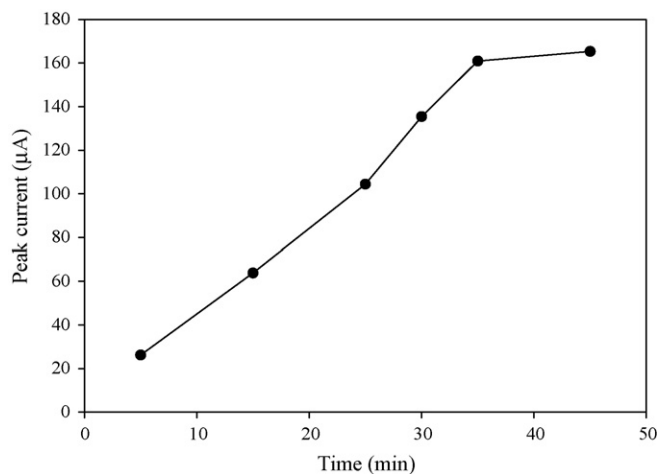
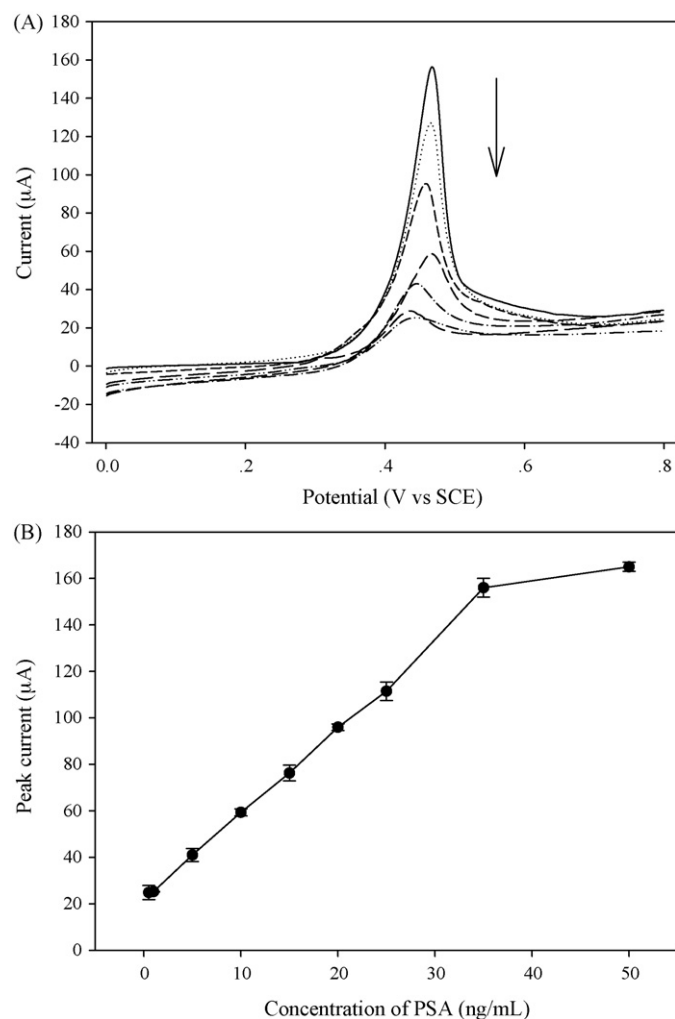


Fig. 4. Effect of the biocatalytic silver deposition time on the anodic stripping peak current.

until 35 min. After 35 min, the currents increased slowly. This phenomenon may be associated with the loss of the enzyme activity with the increase in the deposition time. So, a deposition time of 35 min was selected for the biocatalytic reaction.

### 3.3. Analytical performance of the electrochemical immunosensor

To obtain the calibration curve, a series of different concentrations of target analyte were detected. The operations were performed as mentioned in Section 2. Fig. 5A recorded the LSV responses of the electrochemical immunosensor to the target analyte of different concentrations. One observed that as the concentrations of the target analyte increased, the stripping peak current of the electrochemical immunosensor ascended. Fig. 5B depicted the calibration curve of the electrochemical immunosensor. As can be seen from Fig. 5B that the stripping peak currents of the electrochemical immunosensor and the concentrations of target analyte possessed a linear relationship in the concentration range from 1 to 35 ng/mL. The linear regression equation was  $i$  ( $\mu\text{A}$ ) = 25.48 + 3.28*c* (ng/mL) with a correlation coefficient of 0.9918, where *i* represented stripping peak current and *c* represented the



**Fig. 5.** (A) LSVs of the electrochemical immunosensors in 0.6 M KNO<sub>3</sub>/0.1 M HNO<sub>3</sub> solution with target protein at concentrations of 35, 25, 20, 15, 5, 1 and 0.5 ng/mL (from upper to lower). Scan rate, 100 mV/s. (B) Calibration curve of peak current as a function of target protein concentration using the electrochemical immunosensor. Peak currents are averages of five experiments.

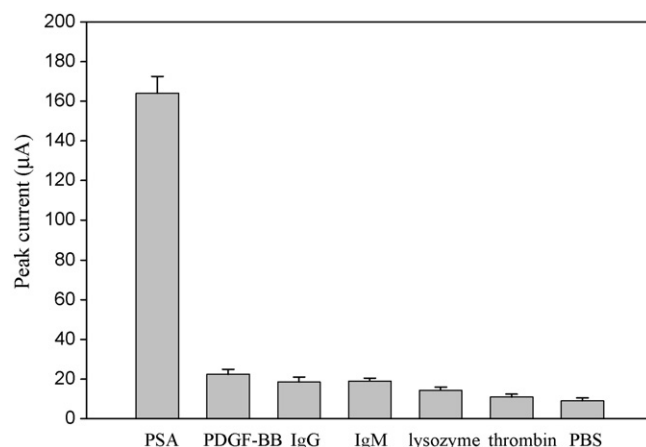


**Fig. 6.** Specificity of the electrochemical immunosensor. The concentrations of PSA, PDGF-BB, IgG, IgM, lysozyme, and thrombin were 30 ng/mL, 100, 300, 100, 15 and 140  $\mu\text{g/mL}$ , respectively. PBS is the phosphate buffer solution. The results were the averages of five experiments.

concentration of target analyte. As calculated by the  $3\sigma$ -rule (where  $\sigma$  is the standard deviation of a blank solution,  $n=5$ ), the detection limit was 0.76 ng/mL, which is lower remarkably than that (2.2 ng/mL) obtained only by enzymatic deposition of metal Ag [12]. When the concentration of the target analyte was higher than 35 ng/mL, saturation was encountered, which was possibly due to the complete binding of antibodies immobilized on the electrode surface.

To estimate the reproducibility of the electrochemical immunosensor, five assays were performed following identical processing steps. Their responses toward 25 ng/mL target analyte gave an average stripping peak current of 105  $\mu\text{A}$  with a relative standard deviation of 5.7%, indicating that the immunosensor could be constructed and used for analysis with excellent reproducibility.

The specificity of the electrochemical immunosensor was also examined using other proteins commonly present in serum. About 100-fold concentrations of IgG, IgM, lysozyme, thrombin, and PDGF-BB were incubated and detected individually with the immunosensor. The stripping peak currents were shown in Fig. 6. It can be seen that no significant LSV readouts are obtained for these interfering proteins. Thus, no significant cross-reactivity was detected for these proteins. It was expected that the developed immunosensor could exhibit a high degree of selectivity for PSA assay.

### 3.4. Detection of human serum samples

In order to investigate the possibility of the developed immunosensor to be applied for clinical analysis, six human serum

**Table 1**

The comparisons of the developed electrochemical immunosensor<sup>a</sup> (EI) with the chemiluminescent microparticle immunoassay (CMIA) method for the detection of PSA in human serum

Serum samples	EI (ng/mL)	CMIA (ng/mL)	Relative deviation (%)
1	2.96 ± 0.22	2.77	6.86
2	5.86 ± 0.38	6.09	-3.78
3	6.62 ± 0.39	6.40	3.44
4	6.74 ± 0.30	6.29	7.15
5	11.50 ± 0.50	11.90	-3.36
6	19.00 ± 0.71	17.93	6.15

<sup>a</sup> The data are given as the average value ± S.D. obtained from five independent experiments ( $n=5$ ).



specimens were obtained from Hunan Provincial Tumor Hospital and tested by the developed electrochemical immunosensor as well as the chemiluminescent microparticle immunoassay (CMIA) as a reference method. The results were shown in Table 1. As can be seen from Table 1, the target analyte concentrations obtained by the presented method were in good agreement with those determined by CMIA and the relative deviations were not more than 7.15%, indicating that it is feasible to apply the developed electrochemical immunosensor to detecting PSA in human serum samples.

#### 4. Conclusions

A kind of uniform, ALP and detection antibody-cofunctionalized Si NPs were synthesized and used for the development of an ultrasensitive electrochemical immunosensor for the detection of human PSA for the first time. A detection limit as low as 0.76 ng/mL was achieved through dual-signal amplification by ALP-functionalized silica NPs and biocatalytic deposition of metal silver. It was demonstrated that the presented method was sensitive, simple, specific and allowed accurate quantification with a low detection limit of 0.76 ng/mL. The cofunctionalization strategy can also be used for a variety of biomolecules based on the well-developed silica surface immobilization chemistry and the corresponding electrochemical immunosensor can be developed for the detection of other proteins. In addition, this work is also useful for other types of sensing using novel nanomaterials to improve existing analytical techniques [24]. The limitation of the non-conductivity of the Si nanoparticle can be improved by using other conductive nanoparticles such as carbon nanotubes and Au nanoparticles. The proposed sensitive approach holds great promise for the extended application in the field of clinical diagnosis, bioaffinity assays and environmental monitoring.

#### Acknowledgment

This work was supported by the National Nature Science Foundation of China with the Grant (No. 20575020).

#### References

- [1] S.H. Landis, T. Murray, S. Bolden, P.A. Wingo, *Cancer J. Clin.* 49 (1999) 8.
- [2] F.-S. César, C.J. McNeil, R. Keith, N. Olle, *Anal. Chem.* 76 (2004) 5649.
- [3] F.-S. César, A.M. Gallardo-Soto, R. Keith, N. Olle, C.J. McNeil, *Electrochem. Commun.* 6 (2004) 138.
- [4] D.A. Healy, C.J. Hayes, P. Leonard, L. McKenna, R. ÓKennedy, *Trends Biotechnol.* 25 (2007) 125.
- [5] B. Acevedo, Y. Perera, M. Ruiz, G. Rojas, J. Benitez, M. Ayala, J. Gavilondo, *Clin. Chim. Acta* 317 (2002) 55.
- [6] F. Yu, B. Persson, S. Löfås, W. Knoll, *Anal. Chem.* 76 (2004) 6765.
- [7] Y. Seto, T. Iba, K. Abe, *Luminescence* 16 (2001) 285.
- [8] Z. Ye, M. Tan, G. Wang, J. Yuan, *Anal. Chem.* 76 (2004) 513.
- [9] T. Soukka, J. Paukkunen, H. Härmä, S. Lönnberg, H. Lindroos, T. Lövgren, *Clin. Chem.* 47 (2001) 1269.
- [10] Y. Tomoyuki, H. Yu, M. Naomi, H. Hitoshi, M. Tomokazu, *Biosens. Bioelectron.* 22 (2007) 3099.
- [11] Z. Chen, J. Jiang, X. Zhang, G. Shen, R. Yu, *Talanta* 71 (2007) 2029.
- [12] Z. Chen, Z. Peng, J. Jiang, X. Zhang, G. Shen, R. Yu, *Sens. Actuator B* 129 (2008) 146.
- [13] X. Chu, X. Fu, K. Chen, G. Shen, R. Yu, *Biosens. Bioelectron.* 20 (2005) 1805.
- [14] H. Cai, Y. Wang, P. He, Y. Fang, *Anal. Chim. Acta* 469 (2002) 165.
- [15] H. Cai, N. Zhu, Y. Jiang, P. He, Y. Fang, *Biosens. Bioelectron.* 18 (2003) 1311.
- [16] J.-M. Nam, S.I. Stoeva, C.A. Mirkin, *J. Am. Chem. Soc.* 126 (2004) 5932.
- [17] S.-B. Zhang, Z.-S. Wu, M.-M. Guo, G.-L. Shen, R.-Q. Yu, *Talanta* 71 (2007) 1530.
- [18] C. Li, M. Curreli, H. Lin, B. Lei, F.N. Ishikawa, R. Datar, R.J. Cote, M.E. Thompson, C. Zhou, *J. Am. Chem. Soc.* 127 (2005) 12484.
- [19] X. Yu, B. Munge, V. Patel, G. Jensen, A. Bhirde, D.G. Joseph, N.K. Sang, J. Gillespie, J.S. Gutkind, F. Papadimitrakopoulos, F.R. James, *J. Am. Chem. Soc.* 128 (2006) 11199.
- [20] S. Viswanathan, L.-C. Wu, M.-R. Huang, Ja.-A. Ho, *Anal. Chem.* 78 (2006) 1115.
- [21] M. Ikonen, L. Murtomäki, K. Kontturi, *J. Electroanal. Chem.* 602 (2007) 189.
- [22] J.-H. Kim, J.-S. Kim, H. Choi, S.-M. Lee, B.-H. Jun, K.-N. Yu, E. Kuk, Y.-K. Kim, D.H. Jeong, M.-H. Cho, Y.-S. Lee, *Anal. Chem.* 78 (2006) 6967.
- [23] X. Zhao, R. Tapecc-Dytioco, W. Tan, *J. Am. Chem. Soc.* 125 (2003) 11474.
- [24] H. Lin, T. Chee-Seng, *Anal. Chim. Acta* 556 (2006) 1.



## Au–TiO<sub>2</sub>/Chit modified sensor for electrochemical detection of trace organophosphates insecticides

Yunhe Qu, Hong Min, Yinyin Wei, Fei Xiao, Guoyue Shi\*, Xiaohua Li, Litong Jin\*

Department of Chemistry, East China Normal University, Zhongshan Road (N), Shanghai 200062, PR China

### ARTICLE INFO

#### Article history:

Received 13 December 2007  
Received in revised form 6 April 2008  
Accepted 12 April 2008  
Available online 30 April 2008

#### Keywords:

Au–TiO<sub>2</sub>  
Parathion  
Detection  
Sensor

### ABSTRACT

In this paper, Au–TiO<sub>2</sub>/Chit modified electrode was prepared with Au–TiO<sub>2</sub> nanocomposite (Au–TiO<sub>2</sub>) and Chitosan (Chit) as a conjunct. The Au–TiO<sub>2</sub> nanocomposite and the films were characterized by electrochemical and spectroscopy methods. A set of experimental conditions was also optimized for the film's fabrication. The electrochemical and electrocatalytic behaviors of Au–TiO<sub>2</sub>/Chit modified electrode to trace organophosphates (OPs) insecticides such as parathion were discussed in this work. By differential pulse voltammetry (DPV) measurement, the current responses of Au–TiO<sub>2</sub>/Chit modified electrode were linear with parathion concentration ranging from 1.0 ng/ml to 7.0 × 10<sup>3</sup> ng/ml with the detection limit of 0.5 ng/ml. In order to evaluate the performance of the detection system, we also examined the real samples successfully in this work. It exhibited a sensitive, rapid and easy-to-use method for the fast determination of trace OPs insecticides.

© 2008 Elsevier B.V. All rights reserved.

### 1. Introduction

OPs are known to be highly neurotoxic and they disrupt the cholinesterase that regulates acetylcholine, a neurotransmitter needed for proper nervous system function [1]. As toxic compounds, the OPs may cause negative effect on the visual system, sensory function, cognitive function, and nervous system which result in severe health problems in both animals and humans. For example, parathion is one kind of OPs that is very toxic with LD<sub>50</sub> of 3 mg/kg in rats, and may be responsible for more death among agricultural field workers than any other pesticides [2]. Thus, OPs insecticides pose major security and environmental risks in present time. The detection of trace OPs is of tremendous importance and there is a necessity for accurate, sensitive, rapid, easy-to-use and portable method to facilitate the detection, quantification and remediation of these OPs present in the natural aquatic system or remain in food.

Currently, several detection techniques such as HPLC, GC/MS, capillary electrophoresis and colorimetry have been developed to measure the OPs insecticides in environment and in food [3–11]. A majority of these methods are time-consuming, expensive, and require trained personnel, which may not be suitable for on-site

use [12]. Electrochemical methods are very attractive for on-site monitoring of OPs, like parathion [13–17]. The electrochemical system possesses high sensitivity, good stability, minimal space and power requirement and low-cost instrumentation [18]. To enhance the sensitivity and stability of the measurements, the electrodes modified with designable molecules have been used in electrochemical determination. The target compounds such as OPs would be adsorbed onto the chemically modified surface which makes the trace detection possible.

In recent years, nanometer-scale materials have been widely used in the fabrication of electrochemical sensors for their large surface area, large pore size, uniform pore structure, and high loading capacity [1,19–25]. These favourable characteristics of the modified materials make the detection of different substrate possible. In the previous articles, the nanocomposite Au–TiO<sub>2</sub> has been applied to the detection of nitric compounds and it has greatly enhanced the sensitivity of the detection system [26–28]. To the best knowledge of the authors, there are little papers which take advantage of Au–TiO<sub>2</sub> nanocomposite modified electrodes to detect the OPs.

In this paper, an Au–TiO<sub>2</sub>/Chit/glass carbon electrode (GCE) was prepared for the fast detection of trace OPs. The film was composed of Au–TiO<sub>2</sub> nanocomposite and Chit as a conjunct. In the nanocomposite, TiO<sub>2</sub> nanoparticles have a strong affinity to the OPs which possess a phosphate group and Au nanoparticles have an excellent conductivity. This modified electrode relies on the two important characteristics to detect ultrace parathion and a lower detection limit that than other methods is achieved [29–31]. The

\* Corresponding authors. Tel.: +86 21 62232627; fax: +86 21 62232627.  
E-mail addresses: [gyshi@chem.ecnu.edu.cn](mailto:gyshi@chem.ecnu.edu.cn), [iamshgy@hotmail.com](mailto:iamshgy@hotmail.com) (G. Shi), [ltjin@chem.ecnu.edu.cn](mailto:ltjin@chem.ecnu.edu.cn) (L. Jin).

nanoparticles were characterized with UV–vis and scan electron microscope (SEM). DPV were employed to optimize the experimental parameters for the detection of pesticides in solution and vegetable samples. The interferences for the determination were also studied in this work. The results illustrate that this method is fast, simple and sensitive, which will have wide application in the fields of foodstuff security and environmental protection.

## 2. Experimental

### 2.1. Chemicals and apparatus

TiO<sub>2</sub> (P-25,  $\Phi = 30$  nm) was purchased from Degussa Company. Parathion, Dichlorvos, Methamidophos and Trichlorfon were purchased from Dr. Ehrenstorfer GmbH Company. Chitosan was purchased from Sinopharm Chemical Regent. All the reagents were used without further purification and the double-distilled water was used in this work.

Au–TiO<sub>2</sub> nanoparticles were characterized by SEM (HITACHI S-4800) and UV–vis spectrophotometer (Cary-50).

All the electrochemical experiments were performed with a CHI 1030 analyzer (CH Instruments). A three-electrode configuration was employed, consisting of a bare glassy carbon electrode ( $d = 3$  mm, Bioanalytical system, Tokyo, Japan) or a Au–TiO<sub>2</sub>/Chit modified electrode serving as working electrode, while a saturated calomel electrode (SCE) and platinum wire served as the reference and counter electrode, respectively. Electrochemical experiments were carried out in a 10.0 ml electrochemical cell at room temperature ( $25^\circ\text{C} \pm 1$ ). All potentials were referred to the SCE reference electrode.

### 2.2. Synthetic of Au–TiO<sub>2</sub> nanocomposite

Nano-TiO<sub>2</sub> solution was prepared by dispersing nano-TiO<sub>2</sub> particles in the double-distilled water and sonicated for 5 min with a concentration about 0.1 mg/ml. The previous solution was stirred with 1.88 ml 0.1 mol/l sodium citrate for 10 min to exchange OH<sup>−</sup> with citrate anions. Then, 0.125 ml of 1% HAuCl<sub>4</sub> were incrementally added (with at least 10 min between additions) along with an excess of 0.07 ml 0.1 mol/l NH<sub>2</sub>OH·HCl. Stirring for about 12 h, the clear solution became purple and  $1.02 \times 10^{-3}$  mol/l Au–TiO<sub>2</sub> nanoparticles were synthesized. The amount of Au was about 0.1 mol of Au per mol of TiO<sub>2</sub>. Nano-Au solution was synthesized by repeating previous procedure without adding TiO<sub>2</sub> particles.

### 2.3. Fabrication of (Au–TiO<sub>2</sub>/Au/TiO<sub>2</sub>)/Chit/GCE

The prepared GCE was immersed into 0.5 mol/l H<sub>2</sub>SO<sub>4</sub> and performed CV until stabilization before used. 10.0  $\mu$ l Au–TiO<sub>2</sub> solution and 2.0  $\mu$ l 1 mg/ml Chit solution were mixed together, and then 8.0  $\mu$ l mixtures were added to the surface of GCE. Finally, the electrode was dried in the air. For contrast, the TiO<sub>2</sub>/Chit electrode and Au/Chit electrode were also prepared in this work.

### 2.4. Electrochemical experiments

DPV measurements were performed to optimize the experimental conditions and determine the OPs compounds at room temperature in the potential range from  $-0.3$  to  $-0.8$  V with the scan rate of 100 mV/s. The supporting electrolyte used in the experiments was thoroughly deoxygenated by bubbling nitrogen (N<sub>2</sub> 99.99%) before each experiment.

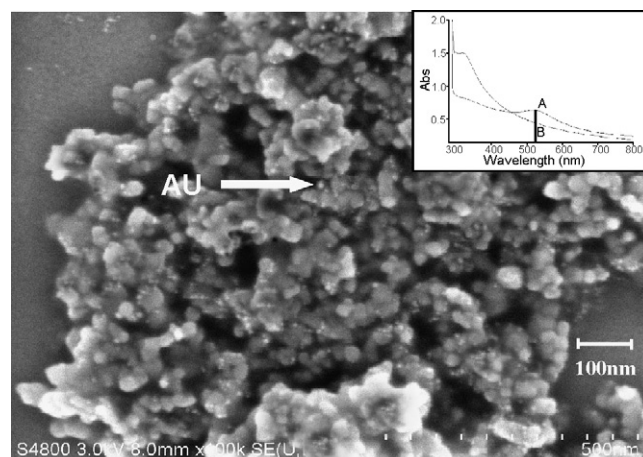


Fig. 1. SEM image of Au–TiO<sub>2</sub> particles and the inset shows UV–vis spectra of nanoparticles. (A) Au–TiO<sub>2</sub> nanoparticles and (B) TiO<sub>2</sub> nanoparticles.

### 2.5. Preparation and determination of real samples

The onion, lettuce and cabbage were purchased from the market and cleaned three times using the double-distilled water. Different concentrations of parathion solution were sprinkled on the surface of different vegetables [32,33]. After about 24 h, all the samples weighing 10–20 g were chopped and meshed before 1 ml of acetone and 9 ml of 0.1 M phosphate buffer (pH 8.0) were added to each sample. All the experiments above maintained on the nitrogen atmosphere and the mixtures were treated in ultrasonic for 15 min. The suspensions were centrifuged (10 min, 2000 rpm) and the supernatants were directly detected by DPV without any extraction or preconcentration step. The content of parathion in the samples can be achieved from the calibration curve.

## 3. Result and discussion

### 3.1. Characterization of Au–TiO<sub>2</sub> by SEM and UV–vis

In pure Au nanoparticles, the collective oscillations of free electrons, known as the surface plasmon, cause an absorption peak ( $\sim 520$  nm) to appear in the visible region [34]. Fig. 1 inset is the UV–vis spectra of nanoparticles of Au–TiO<sub>2</sub> (A) and TiO<sub>2</sub> (B). We find that there is a big absorption peak at 525 nm in curve A and no obvious absorption peak in curve B. Thus, the UV–vis spectra of the nanocomposites confirms that the Au nanoparticles were embedded in the TiO<sub>2</sub> particles.

According to the literatures, the particles size could be calculated in virtue of the following expression:

$$D = (-6.6521 \times 10^{-8})\lambda + (1.9557 \times 10^{-4})\lambda - (9.2352 \times 10^{-2})\lambda + 13.29,$$

$\lambda$  is the wavelength of the UV peak (525 nm). The results show that the particle diameter of the as-prepared Au nanoparticles is about 8.00 nm. Fig. 1 is the SEM image of the Au–TiO<sub>2</sub> nanoparticles which confirms the successfully formation of the nanoparticles. Clearly, Au nanoparticles can be found on the surface of TiO<sub>2</sub> particles and they are dispersed evenly throughout the TiO<sub>2</sub> particles. The Au nanoparticles formed in our work possess an average size of 8–9 nm which is consistent with the diameter that was calculated from the UV–vis spectra. So we confirm that Au–TiO<sub>2</sub> nanocomposite was successfully synthesized in our work.

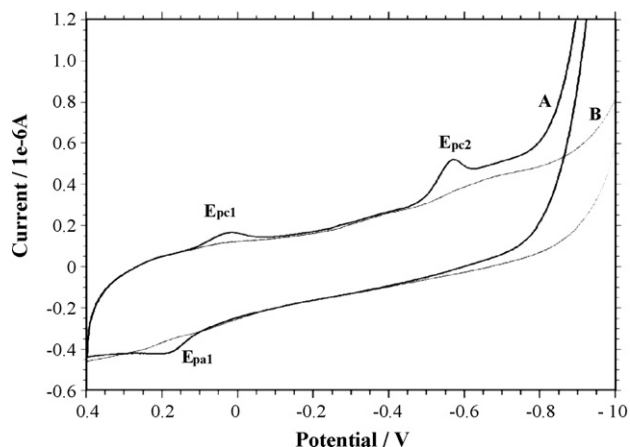


**Fig. 2.** Cyclic voltammograms of Au-TiO<sub>2</sub>/Chit/GCE in a phosphate buffer solution (pH 5.0) with 0.5 µg/ml parathion solution (A) and in the absence of parathion (B).

### 3.2. Electrochemical behavior of parathion

Fig. 2 shows the voltammograms of parathion/Au-TiO<sub>2</sub>/Chit/GCE (A) electrode and Au-TiO<sub>2</sub>/Chit/GCE (B) in a phosphate buffer solution (pH 5.0). A pair of rather well-defined redox peaks ( $E_{pa1}$ , 0.179 V and  $E_{pc1}$ , 0.026 V) and an irreversible reduction peak ( $E_{pc2}$ , -0.573 V) were observed in the potential range from 0.4 to -1.0 V (Fig. 2, curve A). The irreversible reduction peak corresponds to the reduction of the nitro group to the hydroxylamine group (Fig. 3, reaction 1), and the reversible redox peaks are attributed to a two-electrode-transfer process (Fig. 3, reaction 2). The mechanism for this process was widely reported [3]. A control experiment was performed under the same conditions in the absence of parathion; no redox peak was observed (Fig. 2, curve B). So we can conclude that the redox peaks correspond to the reaction of the parathion.

### 3.3. Comparison of different modified electrodes

Fig. 4 shows the current responses to parathion with the electrodes of Au-TiO<sub>2</sub> (a), Au (b), bare (c) and TiO<sub>2</sub> (d). Compared with curves b–d, the curve a of Au-TiO<sub>2</sub> electrode exhibits the biggest current response to the same concentration of parathion and the best linearity. It is because that the nanocomposite has bigger surface area and more active-center. Furthermore, the TiO<sub>2</sub> nanoparticles have a strong affinity to the OPs which possess a phosphate group but the conductivity of the particles is not very well. The better conductivity is due to the Au nanoparticles which play an important role similar to a conducting wire, which was easier for the electron transfer to take place. Curves b and c are the current responses of Au modified electrode and bare electrode, respectively. As can be seen the responses of the two electrodes are similar and much smaller than the nanocomposite modified elec-

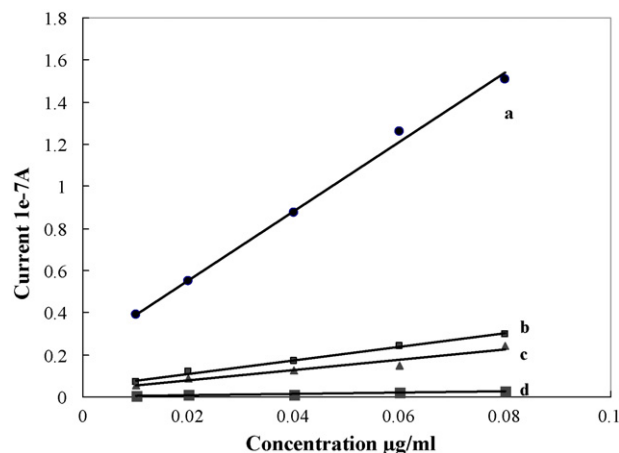


**Fig. 4.** Current responses of electrodes modified with different nanoparticles. (a) Au-TiO<sub>2</sub>, (b) Au, (c) bare and (d) TiO<sub>2</sub>. The concentration of parathion is from 0.2 to 1.0 µg/ml, in the PBS (pH 5.0) DPV scanning potential range, -0.3 to -0.8 V, the scanning rate, 100 mV/s.

trode because either the Au or bare electrode surface do not have a good affinity to the parathion. Curve d is the current response of the TiO<sub>2</sub> modified electrode which has the smallest response to parathion even though TiO<sub>2</sub> has a good affinity to OPs because the TiO<sub>2</sub> nanoparticles baffles the electron transfer from the TiO<sub>2</sub> to the electrode surface. Thus, the Au-TiO<sub>2</sub> nanocomposite that possesses the strong affinity and better conductivity play a really important role in the detection system.

### 3.4. Optimum experimental parameters

We compared the DPV current responses by the electrodes modified with different loadings of nanoparticles in 0.2 µg/ml parathion solution. Theoretically, the nanoparticle films will have more active-centers and larger surface area with the loadings increment. In this work, we found that the electrode modified with 8.0 µl Au-TiO<sub>2</sub> solution ( $1.15 \times 10^{-7}$  mol/cm<sup>2</sup>) resulted in the biggest responses. Deficient loadings modified on the electrode may result in less active-centers and smaller surface area. But we also found the superfluous loadings modified on the electrode were brushed off from the surface and reduced the rate of electron transfer (figure not shown). Furthermore, the excess loadings of Au-TiO<sub>2</sub> may affect the reproducibility and sensitivity of the OPs determination. Therefore, we choose  $1.15 \times 10^{-7}$  mol/cm<sup>2</sup> ( $C_{Au-TiO_2} \times V/S_{GCE}$ ) Au-TiO<sub>2</sub> nanoparticles as the optimum amount in our experiment. We also examined the stability of the optimum sensor (Fig. not shown). The sensor keeps 85% current responses to the same concentration parathion after used 10 days.

Fig. 5 presents the effect of pH on the responses of the parathion. We can see that the irreversible reduction peak potential changes to

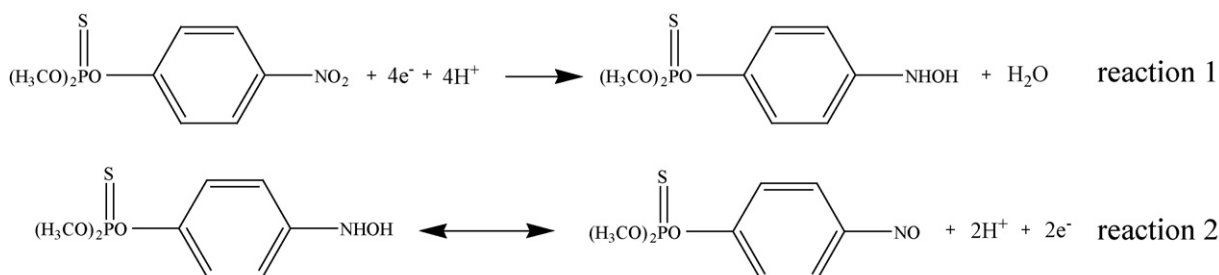


**Fig. 3.** Scheme of the electron-transfer process.

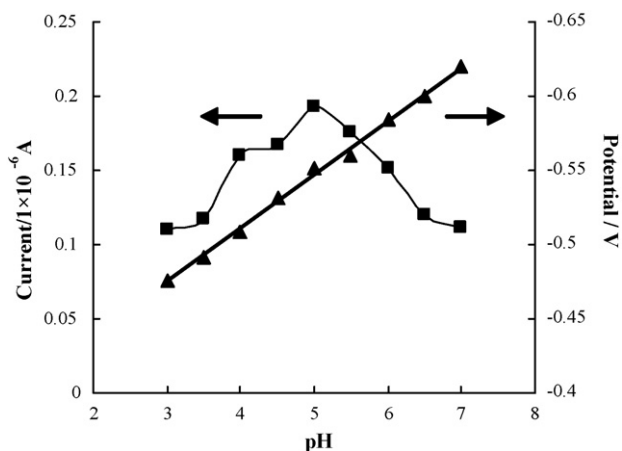


**Fig. 5.** Effects of pH on the electrochemical response of the sensor. The concentration of parathion is 0.2  $\mu\text{g/ml}$ . Electrochemical detection conditions, same as Fig. 4.

more positive potential with the decrease of the pH of the solution, which shows a linear dependence of the reduction peak potential on the pH in the range of 3.0–7.0. A slope of 50.0 mV/pH suggests that the numbers of proton and electron involved in the reaction are equal which is consistent well with the redox mechanism of parathion as shown in Fig. 3 (reaction 1). We can also see that the response current increases with an increase of pH up to 5.0, and then it decreases at higher pH. It indicates that the lower pH value is advantageous to electronation reaction march as the mechanism showed above, but the excessively lower pH such as 3.0 may lead to the analyzing hydrogen side reactions, which may affect the Au-TiO<sub>2</sub> nanoparticles to the parathion adsorption and cause the decrease of electrochemical signal.

### 3.5. The detection of parathion and the analyze of real samples

Under the above optimal parameters, Au-TiO<sub>2</sub>/Chit/GCE was used to detect parathion with DPV in this work. Fig. 6 shows the DPV responses recorded in PBS (pH 5.0) containing different concentration of parathion by the modified electrode. As Fig. 6 shown, there is

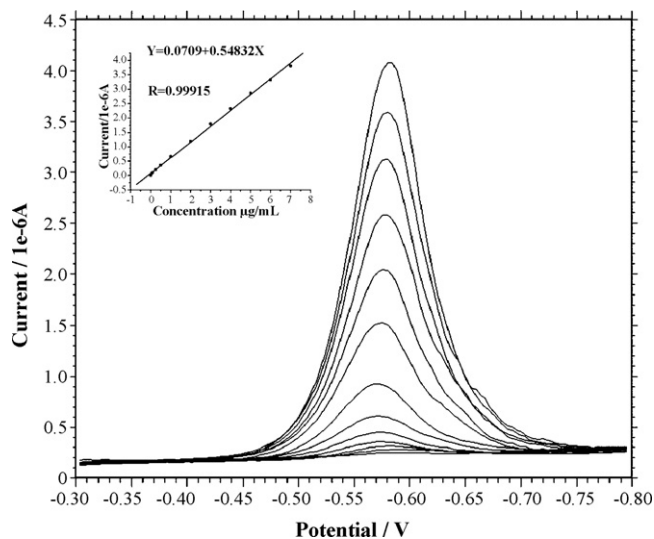


**Fig. 6.** DPV responses of increasing parathion concentration, from bottom to top, 0,  $1.0 \times 10^{-3}$ ,  $5.0 \times 10^{-2}$ , 0.1, 0.25, 0.5, 1.0, 2.0, 3.0, 4.0, 5.0, 6.0, 7.0  $\mu\text{g/ml}$ , respectively. The inset shows the calibration curve. Electrochemical detection conditions, same as Fig. 4.

**Table 1**  
The detection results of real samples

Sample	The amount of parathion sprinkled on the vegetables (ng)	The amount of parathion detected by the modified electrode (ng)
Onion	1000	890
Lettuce	1000	910
Cabbage	1000	880

a well reduction peak at  $-0.575$  V even in 1.0 ng/ml parathion solution and the response currents enhance gradually with the increase of the parathion concentration. It indicates that the parathion can be reduced at the potential of  $-0.575$  V, corresponding to the formation of hydroxylamine with the addition of parathion the reduction current was increased equally with the increase of parathion's concentration [3]. The inset is the calibration curve of the detection system. The current responses are linear with parathion ranging from 1.0 ng/ml to  $7.0 \times 10^3$  ng/ml with the detection limit of 0.5 ng/ml which indicates that Au-TiO<sub>2</sub>/Chit modified electrode displays a better sensitivity to the fast determination of parathion.

To evaluate the performance of the developed modified sensor, the contents of parathion in real samples of onion, lettuce and cabbage were detected by Au-TiO<sub>2</sub>/Chit/GCE. Additionally, a blank sample was prepared from the noncontaminated vegetables and analyzed with the above method. From the data in Table 1, it can be seen that the parathion amount in the vegetable samples were about 10% lower when analyzed by a modified sensor compared to the amount of parathion sprinkled on the vegetables. The lower result can be attributed to the insufficient oxidation of the parathion.

### 3.6. Interferences experiments

The effect of interferences of electroactive nitrophenyl derivatives and oxygen-containing inorganic ions were evaluated during the detection of parathion. The control experiments were performed with 0.4  $\mu\text{g/ml}$  parathion in PBS (pH 5.0) in the absence or presence of 0.4  $\mu\text{g/ml}$  dichlorvos, 0.4  $\mu\text{g/ml}$  methamidophos, 0.4  $\mu\text{g/ml}$  trichlorfon, 0.1 mol/l NO<sub>3</sub><sup>-</sup> or 0.1 mol/l SO<sub>4</sub><sup>2-</sup>, respectively. 95–108% current responses at  $-0.575$  V were remained in the above solutions.

## 4. Conclusion

We have demonstrated an electrochemical approach for the fast determination of OPs with the use of Au-TiO<sub>2</sub>/Chit modified electrode incorporating a three-electrode configuration. The material of nanocomposite Au-TiO<sub>2</sub> exhibits large surface area and good affinity of OPs which help the electrode adsorption and determination of parathion. The sensitivity of the modified electrodes has been investigated by electrochemical methods. The results show that the Au-TiO<sub>2</sub>/Chit modified electrode exhibits high sensitivity for the trace determination of parathion in solution and real samples.

We believe that the nanocomposite Au-TiO<sub>2</sub>/Chit modified sensor on the basis of electrochemical method may have promising application for OPs detection in environmental field.

## Acknowledgements

This work was supported by the National Natural Science Foundation of China (No. 20675032), Science and Technology Commission of Shanghai Municipality (No. 06dz05824), Program for New Century Excellent Talents in University (NCET-07-0293) and Shanghai Rising-Star program (06QH14004).

## References

- [1] Guodong Liu, Yuehe Lin, *Anal. Chem.* 77 (2005) 5894–5901.
- [2] J. Collee, in: D. Greenwood, R. Slack, J. Peutherer (Eds.), *Medical Microbiology*, 15th ed., Churchill Livingstone, London, 1997.
- [3] Joseph Wang, Madhu Prakash Chatrathi, *Anal. Chem.* 73 (2001) 1804–1808.
- [4] T. Ghous, A. Townshend, *Anal. Chim. Acta* 332 (1996) 179–185.
- [5] D.B. Barr, J.R. Barr, V.L. Maggio, *J. Chromatogr. B* 778 (2002) 99–111.
- [6] Elbert Hogendoorn, Piet van Zoonen, *J. Chromatogr. A* 892 (2000) 435–453.
- [7] Guodong Liu, Yuehe Lin, *Electrochem. Commun.* 7 (2005) 339–343.
- [8] Anna.Yu. Kolosova, Jung-hyun Park, Sergey A. Eremin, Sung-Jo Kang, Duck-Hwa Chung, *Agric. Food Chem.* 51 (5) (2003) 1107–1114.
- [9] M.A. Kumar, R.S. Chouhan, M.S. Thakur, B.E. Amita Rani, Bo Mattiasson, N.G. Karanth, *Anal. Chim. Acta* 560 (2006) 30–34.
- [10] Koujiro Futagami, Chie Narazaki, Yasufumi Kataoka, Hideki Shuto, Ryozo Oishi, *J. Chromatogr. B: Biomed. Sci. Appl.* 704 (1997) 369–373.
- [11] A.E. Hiskia, M.E. Atmajidou, D.F. Tsipi, *J. Agric. Food Chem.* 46 (2) (1998) 570–574.
- [12] E. Rainina, E. Efremenco, S. Varfolomeyev, A.L. Simonian, J. Wild, *Biosens. Bioelectron.* 11 (1996) 991.
- [13] P. Mulchandani, W. Chen, A. Mulchandani, *Environ. Sci. Technol.* 35 (12) (2001) 2562–2565.
- [14] V. Sacks, I. Eshkenazi, T. Neufeld, C. Dosoretz, J. Rishpon, *Anal. Chem.* 72 (9) (2000) 2055–2058.
- [15] S. Marx, A. Zaltsman, I. Turyan, D. Mandler, *Anal. Chem.* 76 (1) (2004) 120–126.
- [16] J.-C. Chen, J.-L. Shih, C.-H. Liu, M.-Y. Kuo, J.-M. Zen, *Anal. Chem.* 78 (11) (2006) 3752–3757.
- [17] J. Wang, M.P. Chatrathi, A. Mulchandani, W. Chen, *Anal. Chem.* 73 (8) (2001) 1804–1808.
- [18] Omowunmi A. Sadik, Walker H. Land Jr., Joseph Wang, *Electroanalysis* 15 (2003) 1149–1159.
- [19] Yuehe Lin, Fang Lu, Joseph Wang, *Electroanalysis* 16 (2004) 145–149.
- [20] Chunya Li, Changfa Wang, Chenghang Wang, Shengshui Hu, *Sensors Actuators B* 117 (2006) 166–171.
- [21] Mingming Fang, David M. Kaschak, Anthony C. Sutorik, Thomas E. Mallouk, *J. Am. Chem. Soc.* 119 (1997) 12184–12191.
- [22] Hun Gi Hong, Debra D. Sackett, Thomas E. Mallouk, *Chem. Mater.* 3 (1991) 521–527.
- [23] C.Y. Li, C.F. Wang, Y. Ma, S.S. Hu, *Microchim. Acta* 148 (September (1–2)) (2004) 27–33.
- [24] V.A. Pedrosa, D. Miwa, S.A.S. Machado, L.A. Avaca, *Electroanalysis* 18 (2006) 1590–1597.
- [25] P. Manisankar, G. Selvanathan, C. Vedhi, *Talanta* 68 (2006) 686–692.
- [26] Elizabeth V. Milsom, Jan Novak, Munetaka Oyama, Frank Marken, *Electrochem. Commun.* 9 (2007) 436–442.
- [27] G.N. Chaudhari, A.M. Bende, A.B. Bodade, S.S. Patil, S.V. Manorama, *Talanta* 69 (2006) 187–191.
- [28] P.-G. Su, Wu Ren-Jang, Nieh Fang-Pei, *Talanta* 59 (2003) 667–672.
- [29] Jyh-Myng Zen, Jia-Jen Jou, Annamalai Senthil Kumar, *Anal. Chim. Acta* 396 (1999) 39–44.
- [30] Guangming Huang, Jin Ouyang, Willy R.G. Baeyens, Yiping Yang, Chuanjiang Tao, *Anal. Chim. Acta* 474 (2002) 21–29.
- [31] M.J. Schöning, R. Krause, K. Block, M. Musahmeh, A. Mulchandani, J. Wang, *Sensors Actuators B: Chem.* 95 (2003) 291–296.
- [32] J. Schurek, T. Portolés, J. Hajslova, K. Riddellova, F. Hernández Analytica, *Chim. Acta* 611 (2008) 163–172.
- [33] Anna Yu. Kolosova, Jung-Hyun Park, Sergei A. Eremin, Seon-Ja Park, Sung-Jo Kang, Won-Bo Shim, Hye-Sung Lee, Yong-Tae Lee, Duck-Hwa Chung, *Anal. Chim. Acta* 511 (2004) 323–331.
- [34] Jennifer L. Lyon, David A. Fleming, Matthew B. Stone, Peter Schiffer, Mary Elizabeth Williams, *Nano Lett.* 4 (4) (2004) 719–723.



## Review

# High-speed gas chromatography: The importance of instrumentation optimization and the elimination of extra-column band broadening

Vanessa R. Reid, Robert E. Synovec\*

Department of Chemistry, Box 351700, University of Washington, Seattle, Washington 98195-1700, USA

## ARTICLE INFO

## Article history:

Received 11 April 2008

Accepted 11 May 2008

Available online 21 May 2008

## Keywords:

Gas chromatography

High-speed

Gas chromatographic theory

Optimal linear flow velocity

Instrumentation advancements

Chemical separations

## ABSTRACT

This review provides a summary of chromatographic theory as it applies to high-speed gas chromatography. A novel method for determining the optimal linear flow velocity,  $\bar{u}_{opt}$ , from specific experimental parameters, is discussed. An in-depth theoretical understanding of  $\bar{u}_{opt}$  and its relation to experimental parameters is presented, in the absence of extra-column band broadening, as a means of method evaluation and optimization. Recent developments in high-speed GC are discussed, in the context of the theory presented within this review, to ascertain the influence of extra-column band broadening. The theory presented herein can be used as a means of evaluating the various areas of GC instrumentation (injection, separation, detection, etc.) that need further development to further minimize the effects of extra-column band broadening. The theoretical framework provided in this review, can be, and is, readily used to evaluate high-speed GC results presented in the literature, and thus, the general practitioner may more readily select a specific capillary length and/or internal diameter for a given application. For example, it is theoretically shown, and prior work cited, that demonstrates a peak width of  $\sim 1$  ms is readily achievable in GC, when extra-column band broadening is eliminated.

© 2008 Elsevier B.V. All rights reserved.

## Contents

1. Introduction .....	703
2. Theory .....	705
2.1. Review of separation thermodynamics .....	705
2.2. Band broadening in gas chromatography .....	706
2.3. Deriving $\bar{u}_{opt}$ from experimental parameters .....	706
2.4. Fundamental GC parameters governing theoretical simulations .....	707
3. Chromatographic theory and its implications for the present and future of high-speed gas chromatography .....	708
3.1. Optimizing experimental parameters in the context of chromatographic theory .....	708
3.2. Practical implementation of high-speed GC in the context of theory .....	710
References .....	716

## 1. Introduction

Fundamental gas chromatographic theory and the general practice of gas chromatography (GC) have been developed over the past several decades [1–7]. Much of the theoretical focus has been on the thermodynamic relationships governing chromatographic separations and the origins of band broadening in chromatographic separations. There have been numerous metrics developed

(i.e., separation efficiency ( $N$ ), plate height ( $H$ ), peak capacity ( $n_C$ ), resolution ( $R_S$ ), etc.) to gauge the quality of a particular chromatographic instrument or a specific chromatographic separation [3,8–12]. While these metrics determine whether or not there is room for improvement with respect to the theoretical optimum for a particular instrument or separation, they can also be used to compare one instrumental configuration to another.

In order to design a highly efficient high-speed GC instrument, all the experimental parameters (i.e., column length, capillary inner diameter, stationary phase composition, uniformity and thickness, inlet pressure, oven temperature and temperature programming rate) need to be properly selected and experimentally optimized. In addition, the individual components of the high-speed

\* Corresponding author. Fax: +1 206 685 8665.

E-mail address: [synovec@chem.washington.edu](mailto:synovec@chem.washington.edu) (R.E. Synovec).

### Nomenclature

$B$	longitudinal diffusion ( $\text{cm}^2/\text{s}$ )
$B_o$	column permeability ( $\text{cm}^2$ )
$C_G$	mass transfer in mobile (gas) phase (s)
$C_L$	mass transfer in the stationary (liquid) phase (s)
$d_c$	capillary inner diameter (cm)
$d_f$	stationary phase film thickness (cm)
$D_G$	gas diffusion coefficient ( $\text{cm}^2/\text{s}$ )
$D_{G,o}$	gas phase diffusion coefficient at the column outlet ( $\text{cm}^2/\text{s}$ )
$D_L$	stationary phase diffusion coefficient ( $\text{cm}^2/\text{s}$ )
$F_c$	flow rate at end of column ( $\text{cm}^3/\text{s}$ )
$f$	gas compressibility factor, Giddings
$\Delta G^\circ$	Gibbs free energy (kJ/mol)
$H$	plate height (cm)
$H_{\min}$	minimum plate height (cm)
$\Delta H^\circ$	enthalpy (kJ/mol)
$j$	gas compressibility factor, James–Martin
$K$	analyte (compound) distribution constant
$k$	retention factor
$L$	column length (cm)
$N$	efficiency
$N_{\text{opt}}$	efficiency at average optimal linear flow velocity
$P$	reduced pressure
$P_{\text{@opt}}$	reduced pressure at $\bar{u}_{\text{opt}}$
$P_i$	absolute head pressure (Pa)
$P_o$	pressure at the column outlet (Pa)
$R$	ideal gas constant ( $\text{J K}^{-1} \text{mol}^{-1}$ )
$R_s$	resolution
$\Delta S^\circ$	entropy (kJ/mol)
$T$	separation temperature (K)
$t_M$	mobile phase hold-up time (s)
$t_R$	analyte (compound) retention time (s)
$u$	linear flow velocity ( $\text{cm}/\text{s}$ )
$\bar{u}$	average linear flow velocity ( $\text{cm}/\text{s}$ )
$\bar{u}_{\text{opt}}$	optimum average linear flow velocity ( $\text{cm}/\text{s}$ )
$V_G$	volume of the mobile (gas) phase ( $\text{cm}^3$ )
$V_M$	retention volume of an unretained analyte ( $\text{cm}^3$ )
$V_M^\circ$	retention volume of an unretained analyte corrected for gas compression ( $\text{cm}^3$ )
$V_R^\circ$	retention volume of a retained analyte corrected for gas compression ( $\text{cm}^3$ )
$V_R$	analyte retention volume ( $\text{cm}^3$ )
$V_S$	volume of stationary phase ( $\text{cm}^3$ )
$w_b$	peak width at the base (s)
$w_{b@opt}$	peak width at the base at average optimal linear flow velocity (s)

### Greek letters

$\alpha$	selectivity
$\beta$	phase ratio
$\eta$	gas viscosity (Pa s)

high carrier gas velocities with relatively short capillary columns lengths [15–20]. The optimum linear velocity,  $\bar{u}_{\text{opt}}$ , is the average on-column velocity at which the plate height,  $H$ , has a minimum value, resulting in a maximum of the separation efficiency,  $N$ . The use of a high carrier gas velocity, above  $\bar{u}_{\text{opt}}$ , results in a decrease in the resolution between chromatographic peaks and a reduction in  $N$  [17,21]. One of the most difficult parameters to optimize is the carrier gas velocity since it depends on all the previously mentioned experimental parameters. The dependence of  $\bar{u}_{\text{opt}}$  on specific experimental parameters is unclear based on the current expressions for  $\bar{u}_{\text{opt}}$ . In order to more fully understand how  $\bar{u}_{\text{opt}}$  depends upon the various experimental parameters, specifically column length and inner diameter, a new method for determining  $\bar{u}_{\text{opt}}$  must be derived. A more full understanding of these issues is a key focus of this review. An in depth theoretical understanding of the  $\bar{u}_{\text{opt}}$  and its relation to experimental parameters, in the absence of extra-column band broadening, should provide a more comprehensive method for optimization. Then, experimental data could be readily compared to the theoretical expectations, to ascertain the influence of extra-column band broadening. Ultimately, the process presented in this review should lead researchers toward a better understanding of the true potential and challenges in optimizing high-speed GC instrumentation for general practice.

Thus, one of the primary goals of this review is to provide readers with a summary of chromatographic theory as it applies to high-speed GC. This review is a compilation of previously developed fundamental chromatographic theory combined with a new theoretical approach toward the optimization of current chromatographic systems. This review will also relate these theoretical chromatographic relationships to recently reported high-speed GC developments. Chromatographic theory will also be used as a means for determining which areas of GC instrumentation need further development in order to eliminate, or at least minimize, extra-column band broadening. For more rigorous discussions of the theory behind separation science readers should see texts by Giddings [10], Karger et al. [11], and Purnell [9]. Additionally, a comprehensive study of many of the important theoretical aspects relating to fast capillary GC by Blumberg has been published as a four part series [22–25]. The first part of the series focused on the development of an equation for the plate height, assuming that the gas compressibility is constant, for separations occurring at high pressure drop [22]. The second part of the series involved the derivation of expressions for speed-optimized hold-up time and a comparison of the theoretical hold-up time to the hold-up time of efficiency-optimized columns [23]. In the third part of the series Blumberg examined the difference between speed-optimized carrier gas velocity and speed-optimized flow rate and how they relate to the plate height [24]. The final part of the study determined the effects of stationary phase thickness on column performance [25].

The novel approach utilized to theoretically relate  $\bar{u}_{\text{opt}}$  to key experimental parameters presented in the review herein, cast in the context of column length and inner column diameter, provides a simplified and succinct method for determining  $\bar{u}_{\text{opt}}$ . The theoretically calculated  $\bar{u}_{\text{opt}}$  values can be used as a means of evaluating experimental chromatographic data to ascertain the presence, and impact, of extra-column band broadening. Essentially, a comparison could be made between the theoretically predicted and the experimentally obtained values of  $\bar{u}_{\text{opt}}$ . Another important aspect of the novel approach to determine and evaluate the theoretical  $\bar{u}_{\text{opt}}$  utilized in this review is that there have not been any mathematical assumptions that could lead to a discrepancy between the actual and theoretically predicted values of  $\bar{u}_{\text{opt}}$ . Consequently, any differences between the theoretical and experimental  $\bar{u}_{\text{opt}}$  are likely the result of extra-column band broadening, i.e., non-ideal experimental influences. Finally, the theoretical framework utilized in this

GC instrument need to be designed to eliminate sources of extra-column band broadening [3,10,13,14]. Common sources of extra-column band broadening include, but are not limited to, large injection volumes, non-uniform oven temperatures and/or temperature programs and dead volumes at column connections and/or at the detector [14,15]. Once, the experimental parameters mentioned above have been selected and are implemented, separation efficiency,  $N$ , depends largely on the carrier gas velocity,  $u$ . The most direct route to high-speed GC separations is the use of



review, can be readily used to evaluate high-speed GC results presented in the literature, and thus, the general practitioner may more readily select a specific capillary length and/or internal diameter for a given application.

## 2. Theory

We begin with a brief overview of fundamental gas chromatographic theory including the thermodynamics governing a separation and band broadening theory. This overview also contains an introduction to an in-depth study of the dependence of the optimal linear flow velocity on experimental parameters such as the length and inner diameter of the separation column. A list of the symbols that appear in this review and their definitions are compiled in nomenclature.

### 2.1. Review of separation thermodynamics

The separation of a mixture of compounds in GC depends on their interaction with the stationary phase as they migrate through the column. The magnitude of the separation of the mixture compounds (i.e., analytes) depends on the individual analyte distribution constant,  $K$ , values. Where  $K$  is defined as the following [18]:

$$K = \frac{\text{analyte concentration in the stationary phase}}{\text{analyte concentration in the mobile phase}} \quad (1)$$

A larger distribution constant translates into longer analyte retention on the column. The distribution constant can be calculated by determining the corrected analyte retention volume,  $V_R^\circ$ , the volume of the mobile (gas) phase,  $V_G$ , and the volume of the stationary phase,  $V_S$  [18].

$$K = \frac{V_R^\circ - V_G}{V_S} \quad (2)$$

The volume of the mobile phase,  $V_G$ , is related to the retention volume of an unretained analyte,  $V_M$ , by the following equations [18,26]

$$V_G = V_M^\circ = F_c t_M j \quad (3)$$

$$V_G = V_M j \quad (4)$$

where  $V_M^\circ$  is the retention volume of an unretained analyte corrected for gas compression along the column,  $F_c$  the flow rate at the end of the column at atmospheric temperature and pressure,  $t_M$  the column hold-up time (the elution time of an unretained analyte) and  $j$  is the James–Martin gas compressibility correction factor (this correction factor will be discussed in more detail in Section 2.3). The corrected analyte retention volume,  $V_R^\circ$ , is related to the analyte retention volume,  $V_R$ , and the analyte retention time,  $t_R$ , by the following equations, respectively [18,26].

$$V_R^\circ = V_R j \quad (5)$$

$$V_R^\circ = F_c t_R j \quad (6)$$

The distribution constant,  $K$ , is related to the retention factor,  $k$ , by the factor  $\beta$ . Where  $\beta$  is the ratio of the volume of the mobile phase,  $V_G$ , to the volume of the stationary phase,  $V_S$ , and is represented by the following equation [9,18]

$$\beta = \frac{V_G}{V_S} \quad (7)$$

The relationship between  $K$ ,  $\beta$  and  $k$  can be derived using Eq. (2) by introducing the ratio  $V_G/V_S$  and subsequently factoring out  $\beta$ , as

expressed in Eq. (7), resulting in the following expression [18]

$$K = \frac{V_G}{V_S} \frac{V_R^\circ - V_G}{V_G} = \beta k \quad (8)$$

The relationship in Eq. (8) can be simplified to provide  $k$  by the following

$$k = \frac{V_R^\circ - V_G}{V_G} \quad (9)$$

According to Eq. (9), the retention factor,  $k$ , is the retention volume of the analyte relative to the retention volume of an unretained analyte. Since both  $V_R^\circ$  and  $V_G$  are corrected for the gas compressibility,  $j$ , then  $k$  is also dependent on  $j$ . Substituting Eqs. (4) and (5) into Eq. (9) for  $V_G$  and  $V_R^\circ$ , respectively, removes the dependence of  $k$  on  $j$  and results in the following equation

$$k = \frac{V_R - V_M}{V_M} \quad (10)$$

Further information about the retention of a particular analyte on a specific stationary phase can be obtained using the following relationship between  $K$  and the Gibbs free energy of the evaporation of the analyte from the stationary phase,  $\Delta G^\circ$  [9–11,18,26]

$$\ln K = -\frac{\Delta G^\circ}{RT} \quad (11)$$

where  $R$  is the ideal gas constant and  $T$  is the temperature of the separation. Substituting the right-hand side of Eq. (8) into Eq. (11) results in the following relationship

$$\ln \beta + \ln k = -\frac{\Delta G^\circ}{RT} \quad (12)$$

Additional thermodynamic information can be obtained by substituting the relationship between Gibbs free energy, enthalpy ( $\Delta H^\circ$ ) and entropy ( $\Delta S^\circ$ ) [9–11,26]

$$\Delta G^\circ = \Delta H^\circ - T\Delta S^\circ \quad (13)$$

into Eq. (12), resulting in the following expression:

$$\ln \beta + \ln k = -\frac{\Delta H^\circ - T\Delta S^\circ}{RT} \quad (14)$$

Eq. (14) can be simplified as follows

$$\ln k = -\frac{\Delta H^\circ}{RT} + \frac{\Delta S^\circ}{R} - \ln \beta \quad (15)$$

Typically, the last two terms of Eq. (15) are combined into an “entropy” term,  $\ln(a/\beta)$ , where  $a$  can be defined as [27]

$$a = \exp\left(\frac{\Delta S^\circ}{R}\right) \quad (16)$$

Plots of  $\ln k$  as a function of  $1/T$  (also referred to as van’t Hoff plots) are commonly created as a means of determining thermodynamic information about specific analytes and their interaction with the stationary phase within a particular GC system [9,28]. In these plots, the enthalpy ( $\Delta H/R$ ) and entropy ( $a/\beta$ ) terms can be obtained from the slope and y-intercept, respectively. These plots are usually linear because the enthalpy is essentially constant over the temperature range of interest [26]. The entropy data contained in these plots relates to the selectivity of the stationary phase for a particular analyte. The selectivity,  $\alpha$ , of a specific stationary phase for a particular analyte relative to another analyte is defined as follows [11]:

$$\alpha = \frac{k_1}{k_2} \quad (17)$$

where  $k_1$  is the retention factor of the analyte of interest and  $k_2$  is the retention factor of the other analyte. Larger values of  $\alpha$  translate into a favorable separation of analytes 1 and 2; as  $\alpha$  increases the

chromatographic resolution between analytes 1 and 2 increases, with all else constant (resolution will be discussed in more detail in Section 2.3).

Retention time information has been used to determine thermodynamic properties for various classes of volatile organic compounds [28–33]. Likewise, thermodynamic data determined from retention information (Kovats indices) has been used to predict retention times and peak widths [27]. Van't Hoff plots have also been used to evaluate novel stationary phases [34].

## 2.2. Band broadening in gas chromatography

The quality of a chromatographic separation is governed not only by the selective retention of the compounds in a mixture, but also by the ability to distinguish the individual analytes and interfering compounds. When a sample is injected onto a column and if there is a substantial amount of band broadening (also referred to as zone spreading), the resulting separation may contain peaks that are severely overlapped with one another. Considerable effort has gone into understanding and minimizing the sources of band broadening. There are three main causes of band broadening (neglecting any extra-column band broadening from sources such as injection, detection and dead volumes) in open tubular gas chromatography: (1) longitudinal diffusion, (2) resistance to mass transfer in the mobile phase, and (3) resistance to mass transfer in the stationary phase. The plate height,  $H$ , is a measure of the amount of band broadening that occurs as an analyte travels through the column. An equation describing band broadening for packed columns was proposed by van Deemter et al. [35]. Later, Golay proposed an equation for the band broadening in open tubular capillaries [3]. Gaspar et al. conducted an in-depth theoretical and experimental study of the effects of extra-column band broadening on separation efficiency [36]. In a recent publication [37], a comparison of these three equations came to the conclusion that the equation proposed by Gaspar et al. [36] best describes chromatographic elements that contain an element of extra-column band broadening. In the context of this review,  $H$  is only the on-column band broadening and does not take into account any sources of extra-column band broadening. Where  $H$  can be defined, in general terms, as follows [3,9–11,18,26]:

$$H = \frac{B}{u} + C_G u + C_L u \quad (18)$$

where  $B$  is the term describing the longitudinal diffusion,  $C_G$  and  $C_L$  are the terms describing the resistance to mass transfer in the mobile and stationary phases, respectively, and  $u$  is the linear flow velocity. The plate height is both directly and inversely proportional to  $u$ ; consequently, reducing  $H$  is not as simple as increasing  $u$ . A more thorough version of Eq. (18), the Golay equation [3,18] fully describes the relationship between  $H$  and other experimental parameters

$$H = \frac{2D_G}{\bar{u}} + \frac{1 + 6k + 11k^2}{96(1+k)^2} \frac{d_c^2 \bar{u}}{D_G} + \frac{2kd_f^2 \bar{u}}{3(1+k)^2 D_L} \quad (19)$$

where  $D_G$  is the diffusion coefficient of the analyte in the gas phase,  $\bar{u}$  the average linear flow velocity of the carrier gas,  $k$  the retention factor of the analyte,  $d_c$  the inner diameter (i.d.) of the capillary,  $d_f$  the thickness of the stationary phase and  $D_L$  is the diffusion coefficient of the analyte in the stationary phase. However, Eq. (19) must be corrected for the gas compressibility along the column, as shown [18]

$$H = \frac{2D_{G,\alpha} j f}{\bar{u}} + \frac{1 + 6k + 11k^2}{96(1+k)^2} \frac{d_c^2 \bar{u} f}{D_{G,\alpha} j} + \frac{2kd_f^2 \bar{u}}{3(1+k)^2 D_L} \quad (20)$$

where  $D_{G,\alpha}$  is the diffusion coefficient of the analyte in the gas phase at the outlet of the column and  $j$  and  $f$  are gas compression correction factors. This equation is typically used to calculate theoretical values of  $H$  as a means of comparison and evaluation of experimentally obtained  $H$  values.

## 2.3. Deriving $\bar{u}_{opt}$ from experimental parameters

Experimentally, the optimal average linear flow velocity,  $\bar{u}_{opt}$ , is obtained through a series of chromatographic measurements. Thus, the  $\bar{u}_{opt}$  is determined by creating a Golay plot (a plot of the plate height,  $H$ , vs. average linear flow velocity,  $\bar{u}$ ) where the minimum value of  $H$ ,  $H_{min}$ , occurs at  $\bar{u}_{opt}$  [36]. Creating these plots just for one set of experimental parameters is very time consuming. A set of chromatograms must be obtained using an analyte with a desired retention factor,  $k$ , at various carrier gas velocities (this can be accomplished by varying the inlet pressure,  $P_i$ , while holding all other experimental parameters constant). Values of  $H$  can be obtained from this set of chromatograms by calculating the efficiency,  $N$ , of the separation.

$$N = 16 \left( \frac{t_R}{w_b} \right)^2 = \frac{L}{H} \quad (21)$$

where  $t_R$  is the retention time of the peak and  $w_b$  is the width at the base of the peak [10,18,26].

Obtaining experimental Golay plots is very time consuming, and there could be a large benefit to simulating them. Theoretical  $H$  values can be calculated using the Golay equation (Eq. (20)) [18]. Eq. (20) is the plate height equation that has been corrected for the carrier gas compressibility. The James–Martin gas compressibility factor [38],  $j$ , is defined as

$$j = \frac{3P^2 - 1}{2P^3 - 1} \quad (22)$$

where  $P$  is the ratio of the inlet and outlet pressures ( $P = P_i/P_o$ );  $j$  corrects for the carrier gas compression along the length of the column. The Giddings gas compressibility factor [10,39–41],  $f$ , is defined as

$$f = \frac{9(P^4 - 1)(P^2 - 1)}{8(P^3 - 1)^2} \quad (23)$$

and corrects for additional effects of gas compression on  $H$ .

For the purpose of the calculations reported herein, the Golay equation can be simplified when an analyte has a retention factor equal to zero ( $k = 0$ ). When  $k = 0$ , the following is a simplified version of Eq. (20):

$$H = \frac{2D_{G,\alpha} j f}{\bar{u}} + \frac{d_c^2 \bar{u} f}{96D_{G,\alpha} j} \quad (24)$$

Since the optimal average linear flow velocity,  $\bar{u}_{opt}$ , corresponds to a minimum value of  $H$ , the derivative of Eq. (24) can be set equal to zero and solved for  $\bar{u}_{opt}$  to yield an expression for  $\bar{u}_{opt}$ .

$$\bar{u}_{opt} = \frac{\sqrt{192D_{G,\alpha} j}}{d_c} \quad (25)$$

Additionally, the analyte peak width at the base,  $w_b$ , in units of time, can be expressed as follows:

$$w_b = 4t_R \sqrt{\frac{H}{L}} \quad (26)$$

where  $t_R$  is the retention time of the peak, and  $t_R$  is related to the hold-up time,  $t_M$ , of the separation by the retention factor [18],  $k$ . The relationship between  $t_R$  and  $k$  can be obtained by substituting

Eqs. (3) and (6) into Eq. (9) for  $V_G$  and  $V_R^\circ$ , respectively, resulting in the following equation

$$k = \frac{t_R - t_M}{t_M} \quad (27)$$

Substituting Eq. (27) into Eq. (26) yields the following equation:

$$w_b = 4t_M(1+k)\sqrt{\frac{H}{L}} \quad (28)$$

where  $t_M$  is defined in terms of  $L$  and  $\bar{u}$  ( $t_M = L/\bar{u}$ ). At  $k=0$ , Eq. (28) is simplified to

$$w_b = \frac{4}{\bar{u}}\sqrt{HL} \quad (29)$$

The physical separation between two adjacent compounds (analytes or interferents) is called the resolution,  $R_s$ , of the separation.  $R_s$  is a metric that quantifies the degree of separation of two compounds in a separation and can be expressed in terms of the retention times of two analytes and the width of the second analyte. The  $R_s$  is defined as follows [11]:

$$R_s = \frac{t_2 - t_1}{w_{b2}} \quad (30)$$

where  $t_1$  and  $t_2$  are the retention times of the first and second analytes, respectively, and  $w_{b2}$  is the width at the base of the second (more retained) analyte. The  $R_s$  calculated using Eq. (30) typically underestimates the resolution of a separation because it uses the peak width of the second analyte, which for an isothermal separation, is generally larger for the second analyte than the first analyte. In the case of an ideal temperature programmed separation, where the peak widths are essentially constant, the  $R_s$  calculated using Eq. (30) would be accurate. Some researchers choose to use the average peak width in the denominator of Eq. (30) instead.

Since the equation for  $\bar{u}_{opt}$  (Eq. (25)) does not clearly express the dependence of  $\bar{u}_{opt}$  on the length of the capillary, it would be beneficial to have a method for calculating  $\bar{u}_{opt}$  that shows the relationship between  $\bar{u}_{opt}$ ,  $d_c$ ,  $L$ ,  $w_b$  and  $P$ . Such a method would provide insight into which specific capillary diameter and length combinations could be readily used to optimize a particular separation (herein shown in the context of  $k=0$ ). As we will demonstrate, calculating  $\bar{u}_{opt}$  starting with experimentally relevant parameters will create theoretical simulations with a direct relationship to the parameters of interest, namely  $L$  and  $d_c$ .

The expression relating the average linear flow velocity to experimental parameters is shown below [42]:

$$\bar{u} = \frac{3}{4} \frac{B_0 P_0 (P^2 - 1)^2}{\eta L (P^3 - 1)} \quad (31)$$

where  $\eta$  is the carrier gas viscosity and  $B_0$  is the column permeability. For a capillary column,  $B_0$  is defined as follows:

$$B_0 = \frac{d_c^2}{32} \quad (32)$$

Eq. (32) can be substituted in to Eq. (31) to yield the following expression:

$$\bar{u} = \frac{3}{128} \frac{d_c^2 P_0 (P^2 - 1)^2}{\eta L (P^3 - 1)} \quad (33)$$

This equation can be further simplified by factoring out  $j$  (see Eq. (22) for the definition of  $j$ ), which results in the following equation

$$\bar{u} = \frac{d_c^2 P_0 (P^2 - 1)j}{64\eta L} \quad (34)$$

For a specific set of experimental parameters, and when  $\bar{u} = \bar{u}_{opt}$ , the reduced pressure,  $P$ , can be referred to as  $P_{@opt}$ , i.e., the reduced

pressure at the optimum linear flow velocity, and Eq. (34) can be set equal to Eq. (25), producing the following equality under these conditions:

$$\sqrt{192} \frac{D_{G,o} j}{d_c} = \frac{1}{64} \frac{d_c^2 P_0 (P_{@opt}^2 - 1)j}{\eta L} \quad (35)$$

Solving for  $P_{@opt}$  results in the following equation, noting that  $j$  cancels out:

$$P_{@opt} = \sqrt{64\sqrt{192} \frac{D_{G,o} \eta L}{d_c^3 P_0} + 1} \quad (36)$$

Using Eq. (36), the  $P_{@opt}$  can be calculated for a particular set of experimental parameters (e.g.,  $L$  and  $d_c$  for a typical  $D_{G,o}$ ,  $\eta$  and  $P_0$ ). The  $P_{@opt}$  can be substituted into the  $j$  expression (Eq. (22)), and  $j$  can be determined and subsequently substitution into the  $\bar{u}_{opt}$  expression (Eq. (25)), resulting in the following:

$$\bar{u}_{opt} = \frac{3}{2} \frac{\sqrt{192} D_{G,o}}{d_c} \left( \frac{P_{@opt}^2 - 1}{P_{@opt}^3 - 1} \right) \quad (37)$$

This calculation procedure results in  $\bar{u}_{opt}$  values for each and any set of experimental parameters of interest. The expression in Eq. (36) for  $P_{@opt}$ , and thus implicitly in Eq. (37), provides a clear dependence on both  $L$  and  $d_c$  (where all other experimental parameters,  $P_0$ ,  $D_{G,o}$ , and  $\eta$  are held constant in the calculations presented herein), which translates into a dependence of  $\bar{u}_{opt}$  on both  $L$  and  $d_c$ . The experimental parameters  $P_0$ ,  $D_{G,o}$  and  $\eta$  are held constant for this specific case. It is not, however, necessary that they be held constant for all applications of interest.

The  $\bar{u}_{opt}$  calculated for a specific set of experimental parameters (Eq. (37)) can be substituted into Eq. (24) (with  $k=0$ ) to determine the corresponding value of  $H_{min}$ . A simplified expression for  $H_{min}$  is obtained by substituting Eq. (25) into Eq. (24):

$$H_{min} = \frac{f d_c}{\sqrt{12}} \quad (38)$$

Once both  $\bar{u}_{opt}$  and  $H_{min}$  values have been calculated, other theoretical information about the separation (i.e., hold-up time, efficiency and peak width) can be readily calculated. For example, the efficiency per time is obtained from the following expression:

$$\frac{N_{opt}}{t_M} = \frac{H_{min}}{L t_M} \quad (39)$$

With  $\bar{u} = \bar{u}_{opt}$ , the peak width,  $w_{b@opt}$ , in time units, is readily calculated using Eq. (31):

$$w_{b@opt} = \frac{4}{\bar{u}_{opt}} \sqrt{H_{min} L} \quad (40)$$

Note that  $w_{b@opt}$  obtained from Eq. (40) is the peak width at the base at  $\bar{u}_{opt}$  without any extra-column band broadening. Calculations using Eq. (40) result in the theoretical peak widths that can serve as a means of providing understanding of the demands on designing instruments to minimize extra-column band broadening, and subsequently evaluating experimentally obtained GC data. Peak widths can be calculated for columns of various values of  $L$  and  $d_c$ . This information can then be used to determine which column  $L$  and  $d_c$  combinations should be used to obtain a particular experimental peak width, presuming extra-column band broadening can be minimized.

#### 2.4. Fundamental GC parameters governing theoretical simulations

All simulations were completed via numerical analysis. Simulations were completed for columns of various lengths,  $L$ , and inner diameters,  $d_c$ , holding other parameters constant. All simulations

used  $H_2$  as the carrier gas and, for the sake of brevity, using an analyte retention factor,  $k$ , of 0. An average (i.e., typical) analyte diffusion coefficient,  $D_{G,o}$ , of  $0.6 \text{ cm}^2/\text{s}$  was used. An isothermal temperature of  $150^\circ\text{C}$  was used for the simulation which results in a carrier gas viscosity,  $\eta$ , of  $1.135 \times 10^{-5} \text{ Pa s}$  [43]. The outlet of the column was assumed to be at an ambient pressure of 1 atm (101,325 Pa).

### 3. Chromatographic theory and its implications for the present and future of high-speed gas chromatography

#### 3.1. Optimizing experimental parameters in the context of chromatographic theory

In most cases, a Golay plot is used to determine the optimal linear flow velocity for an experimental setup. In order to create these plots data must be collected at various linear flow velocities while holding all other parameters constant. Golay plots for various capillary lengths and inner diameters have been simulated and are shown in Fig. 1. The optimum linear flow velocities are indicated on the plots. These plots are created by calculating  $H$  for various values of  $\bar{u}$  using Eq. (24). The dotted lines represent linear flow velocities that exceed the pressure limitations of typical commercially available instruments. The capillaries with the smallest inner diameter ( $100 \mu\text{m}$ ) result in  $H_{\text{min}}$  values that are significantly lower than the capillaries with larger inner diameters (250 or  $530 \mu\text{m}$ ). This lower  $H_{\text{min}}$  results in narrower chromatographic peaks. The relationship between  $H_{\text{min}}$  and  $w_b$  (where  $w_b$  is the ideal peak width in the absence of any extra-column band broadening) is expressed in Eq. (29). A plot of  $w_b$  as a function of  $\bar{u}$  is shown in Fig. 2. These plots were simulated using the same parameters and capillary dimensions as shown in Fig. 1. This plot demonstrates the advantage of using a shorter capillary with a small inner diameter (i.e.,  $1 \text{ m} \times 100 \mu\text{m}$ ) in order to obtain narrower chromatographic peaks. The peak obtained with a  $1 \text{ m}$  column with a  $100 \mu\text{m}$   $d_c$  has a  $w_b$  of 5 ms (ideally), while a peak obtained with a  $25 \text{ m}$  column

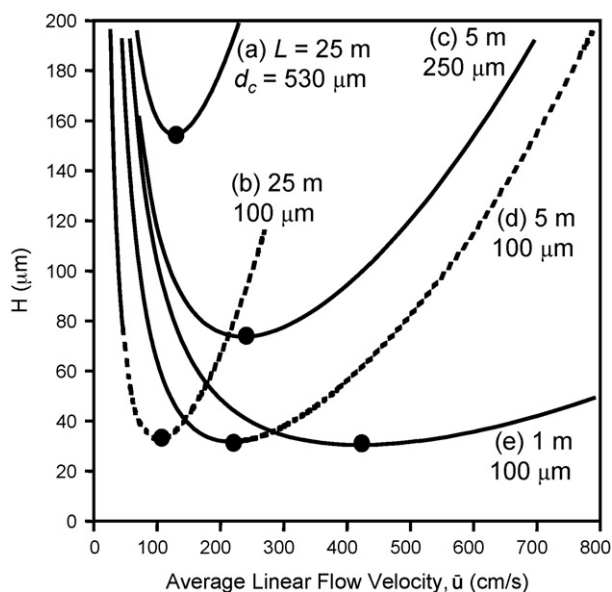


**Fig. 1.** A Golay plot of theoretical  $H$  vs.  $\bar{u}$  for various combinations of column length,  $L$ , and inner diameter,  $d_c$  calculated using Eq. (24). Corresponding  $H_{\text{min}}$ ,  $\bar{u}_{\text{opt}}$  values are represented by (●) on each curve. (a)  $L = 25 \text{ m}$ ,  $d_c = 530 \mu\text{m}$ ; (b)  $L = 25 \text{ m}$ ,  $d_c = 100 \mu\text{m}$ ; (c)  $L = 5 \text{ m}$ ,  $d_c = 250 \mu\text{m}$ ; (d)  $L = 5 \text{ m}$ ,  $d_c = 100 \mu\text{m}$ ; and (e)  $L = 1 \text{ m}$ ,  $d_c = 100 \mu\text{m}$ . Curves were simulated using the following parameters: a typical  $D_{G,o} = 0.6 \text{ cm}^2/\text{s}$ ,  $k = 0$ ,  $H_2$  carrier gas and an oven temperature of  $150^\circ\text{C}$ .

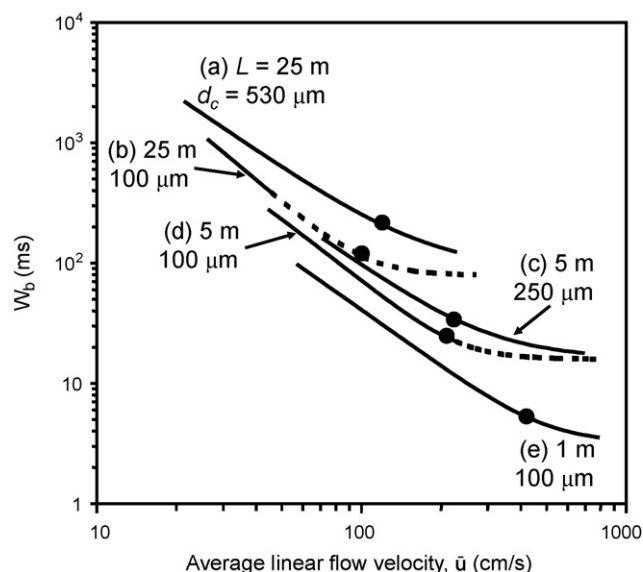


**Fig. 2.** Plots of theoretical  $w_b$  vs.  $\bar{u}$  for various combinations of column length,  $L$ , and inner diameter,  $d_c$  calculated using Eq. (29). The  $w_b$  values at  $\bar{u}_{\text{opt}}$  are represented by (●) on the graph. (a)  $L = 25 \text{ m}$ ,  $d_c = 530 \mu\text{m}$ ; (b)  $L = 25 \text{ m}$ ,  $d_c = 100 \mu\text{m}$ ; (c)  $L = 5 \text{ m}$ ,  $d_c = 250 \mu\text{m}$ ; (d)  $L = 5 \text{ m}$ ,  $d_c = 100 \mu\text{m}$ ; and (e)  $L = 1 \text{ m}$ ,  $d_c = 100 \mu\text{m}$ . Plots were simulated using the same parameters as were used in Fig. 1.

with the same  $d_c$  has a  $w_b$  that is over 100 ms wide. This suggests that there is a significant advantage, in terms of peak width, to using shorter columns with smaller inner diameters. In this particular plot, the length dependence of  $\bar{u}_{\text{opt}}$  is also demonstrated. While the  $H_{\text{min}}$  values are similar for capillaries with the same inner diameter, the  $w_b$  values depend on both the column inner diameter and column length. This suggests that the  $\bar{u}_{\text{opt}}$  values depend not only on the inner diameter of the capillary but also on the capillary length, which is not clearly expressed in Eq. (25).

The traditional approach to determining  $\bar{u}_{\text{opt}}$  requires obtaining experimental Golay plots (or simulating these plots) for each combination of column length and inner diameter. As we demonstrated earlier, this process is simplified by deriving  $\bar{u}_{\text{opt}}$  from the experimental parameters. This new method also makes it possible to compare the  $\bar{u}_{\text{opt}}$  for various column lengths and inner diameters, as well as being able to compare the resulting  $N_{\text{opt}}/t_M$  and  $w_{b@opt}$  values. Application of this new method will serve as a springboard to discuss the most recently reported advances in high-speed GC separation technology. The absolute head pressure,  $P_i$ , necessary to obtain  $\bar{u}_{\text{opt}}$  can be calculated by determining  $P_{@opt}$  using Eq. (36) and solving the relationship between  $P$  and  $P_i$  to obtain  $P_i$  ( $P_{@opt}$  is  $P$  at the optimum linear flow velocity). A plot of  $P_i$  (at  $\bar{u}_{\text{opt}}$ ) vs.  $L$  for various capillary inner diameters is shown in Fig. 3. The absolute head pressure required to achieve the  $\bar{u}_{\text{opt}}$  for smaller  $d_c$  capillaries increases significantly as the length of the column is increased. It is important to note that the electronic pneumatic control (EPC) of a typical commercial GC (i.e., Agilent 6890 GC) is limited to a maximum absolute head pressure of 115 psi (792,700 Pa) [44]. The horizontal line in Fig. 3 represents this pressure limitation. Presuming the equations hold at very high pressures, the pressure required to obtain the  $\bar{u}_{\text{opt}}$  for the  $50 \mu\text{m}$   $d_c$  column at a length of 100 m ( $P_i = 1014 \text{ psi}$ , 6,989,000 Pa) is approximately 10-fold greater than the maximum pressure setting of the instrument. For the sake of discussion, all subsequent plots of simulated data contain only those values that correspond to  $P_i$  values of less than 115 psi (792,700 Pa).

Once values of  $P_{@opt}$  are calculated,  $j$  and  $\bar{u}_{\text{opt}}$  for the same experimental parameters can also be determined. A plot of  $\bar{u}_{\text{opt}}$

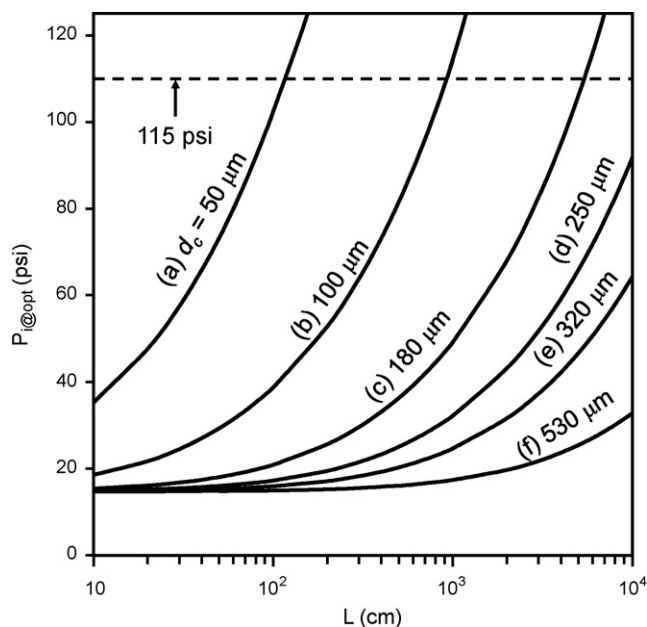


**Fig. 3.** Plot of the inlet pressure,  $P_i$ , at  $\bar{u}_{opt}$  vs. column length,  $L$ , for various column inner diameters,  $d_c$ . Calculated using Eq. (36) and substituting in the following: (a)  $d_c = 50 \mu\text{m}$ , (b)  $d_c = 100 \mu\text{m}$ , (c)  $d_c = 180 \mu\text{m}$ , (d)  $d_c = 250 \mu\text{m}$ , (e)  $d_c = 320 \mu\text{m}$  and (f)  $d_c = 530 \mu\text{m}$ . Plots were simulated using the following parameters:  $k = 0$ ,  $D_{G,o} = 0.6 \text{ cm}^2/\text{s}$ ,  $\eta = 1.135 \times 10^{-5} \text{ Pa s}$ ,  $P_o = 1 \text{ atm}$  (101,325 Pa),  $\text{H}_2$  carrier gas and an oven temperature of  $150^\circ\text{C}$ .

as a function of length for various capillary diameters is shown in Fig. 4. At very short capillary lengths (i.e., 10 cm), the  $\bar{u}_{opt}$  for the two smaller diameter capillaries (50 and  $100 \mu\text{m}$ ) are much larger than the  $\bar{u}_{opt}$  for capillaries with larger diameters (180, 250, 320 and  $530 \mu\text{m}$ ). For example, the  $\bar{u}_{opt}$  for a  $10 \text{ cm} \times 50 \mu\text{m}$  column is  $925 \text{ cm/s}$  which is approximately twice as fast as the  $\bar{u}_{opt}$  for a  $10 \text{ cm} \times 180 \mu\text{m}$  column ( $\bar{u}_{opt} = 450 \text{ cm/s}$ ). As the length of the

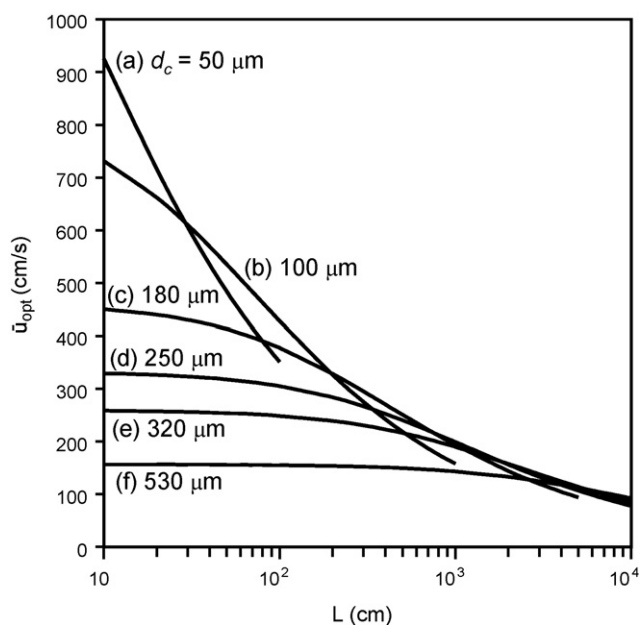


**Fig. 4.** Plot of the average optimum linear flow velocity,  $\bar{u}_{opt}$  vs. column length,  $L$ , for various column inner diameters,  $d_c$ . Calculated using Eq. (37) and substituting in the following: (a)  $d_c = 50 \mu\text{m}$ , (b)  $d_c = 100 \mu\text{m}$ , (c)  $d_c = 180 \mu\text{m}$ , (d)  $d_c = 250 \mu\text{m}$ , (e)  $d_c = 320 \mu\text{m}$  and (f)  $d_c = 530 \mu\text{m}$ . Plots were simulated using the same parameters as Fig. 3.

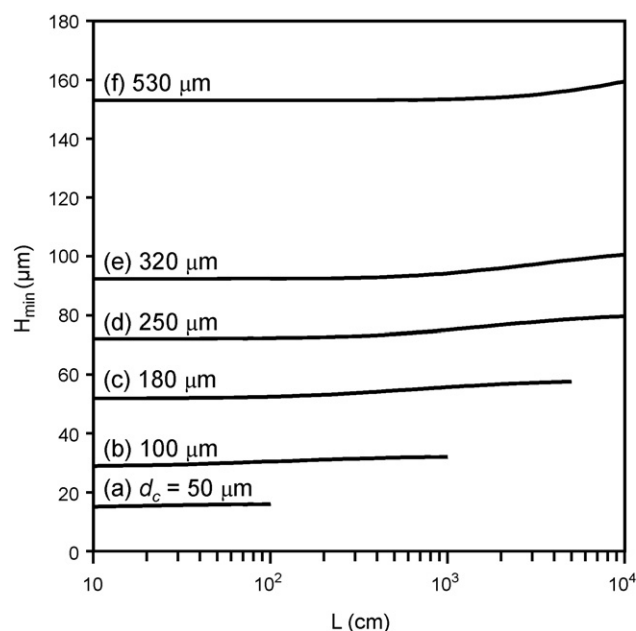


**Fig. 5.** Plot of minimum plate height,  $H_{min}$ , at  $\bar{u}_{opt}$  vs. column length,  $L$ , for various column inner diameters,  $d_c$ . Calculated using Eq. (38) and substituting in the following: (a)  $d_c = 50 \mu\text{m}$ , (b)  $d_c = 100 \mu\text{m}$ , (c)  $d_c = 180 \mu\text{m}$ , (d)  $d_c = 250 \mu\text{m}$ , (e)  $d_c = 320 \mu\text{m}$  and (f)  $d_c = 530 \mu\text{m}$ . Plots were simulated using the same parameters as Fig. 3.

capillary is increased, the values of  $\bar{u}_{opt}$  for the smaller  $d_c$  capillaries decrease more rapidly than for the larger  $d_c$  capillaries. For a length of 5 m, the  $\bar{u}_{opt}$  of a  $100 \mu\text{m}$   $d_c$  column is less than that of the  $320 \mu\text{m}$   $d_c$  column. At 10 m only the  $\bar{u}_{opt}$  for the three largest diameter capillaries (250, 320 and  $530 \mu\text{m}$ ) can be attained using a standard commercial GC within the specified pressure restriction.

Values of  $H_{min}$  can be calculated using Eq. (38), where  $f$  increases from 1.0 to 1.125 as the length of the column is increased. A plot of  $H_{min}$  as a function of  $L$  for various capillary inner diameters is shown in Fig. 5. The plot shows that  $H_{min}$  has a strong dependence on  $d_c$  and is practically independent of  $L$ . The values of  $H_{min}$  increase slightly at large  $L$  ( $L \geq 10 \text{ m}$ ) due to the slight increase of  $f$  from 1.0 to 1.125.

The main focus of high-speed GC is the reduction of analysis time. Reducing the time required for separations makes gas chromatography more applicable for use in rapid chemical analysis situations. One of the most effective ways to reduce analysis time is to reduce the column length. Reducing the length of the column also reduces the efficiency,  $N$ , of the column. A benefit of using a short capillary with a small inner diameter can be shown by calculating the efficiency per unit time ( $N_{opt}/t_M$ ) using Eq. (39). A plot of  $N_{opt}/t_M$  as a function of length for the various capillary diameters is shown in Fig. 6. The plot shows that the  $N_{opt}/t_M$  value is much larger for short capillary columns with small inner diameters. For a 10 cm column with a  $50 \mu\text{m}$   $d_c$ , the  $N_{opt}/t_M$  value is over two orders of magnitude larger than that of a 10 cm column with a  $530 \mu\text{m}$   $d_c$ . Working with these short columns significantly decreases the amount of time required for a separation. As the length of the capillary column is decreased the efficiency of the column is also decreased. However, it is important to put the decrease in efficiency in the context of the analysis time in order to make a fair comparison. Short columns ( $<10 \text{ m}$ ) with small inner diameters ( $<180 \mu\text{m}$ ) provide the most efficiency per unit time when operated at  $\bar{u}_{opt}$ .

Not only do short columns with small inner diameters result in high  $N_{opt}/t_M$  values, the peak widths that are ideally obtained with these columns are also favorable. The width at the base of the peak,  $w_{b@opt}$ , is calculated using Eq. (40). A plot of  $w_{b@opt}$  as a function of length for different capillary diameters is shown in

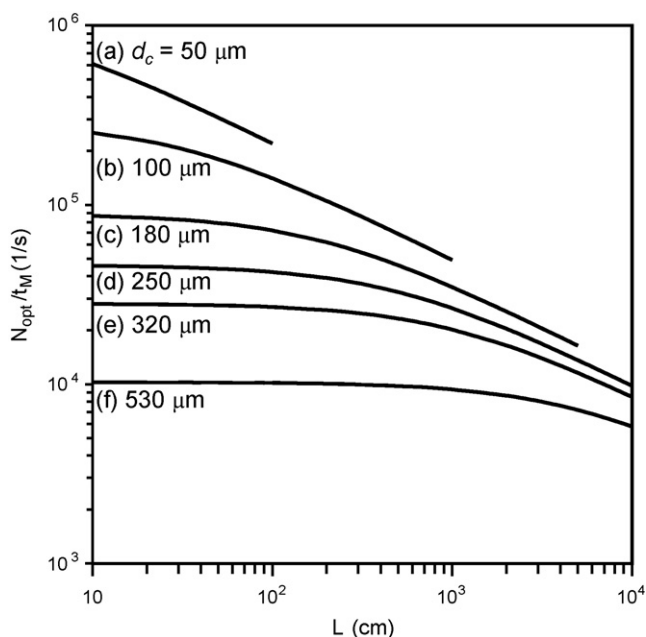


**Fig. 6.** Plot of efficiency per unit time,  $N_{opt}/t_M$ , at  $\bar{u}_{opt}$  vs. column length,  $L$ , for various column inner diameters,  $d_c$ . Calculated using Eq. (39) and substituting in the following: (a)  $d_c = 50 \mu\text{m}$ , (b)  $d_c = 100 \mu\text{m}$ , (c)  $d_c = 180 \mu\text{m}$ , (d)  $d_c = 250 \mu\text{m}$ , (e)  $d_c = 320 \mu\text{m}$  and (f)  $d_c = 530 \mu\text{m}$ . Plots were simulated using the same parameters as Fig. 3.

**Fig. 7.** As the length of the column increases, the  $w_{b@opt}$  values for capillaries with large inner diameters approach a width of 1 s. This particular series of plots can be used as a guideline for which capillary dimensions should be used to obtain a particular peak width, when used in an ideal system in the absence of any extra-column band broadening. For example, if a particular experiment requires 530  $\mu\text{m}$   $d_c$  column and a peak width of 100 ms or less, a capillary with a maximum length of 8 m should be used. Choosing a 530  $\mu\text{m}$

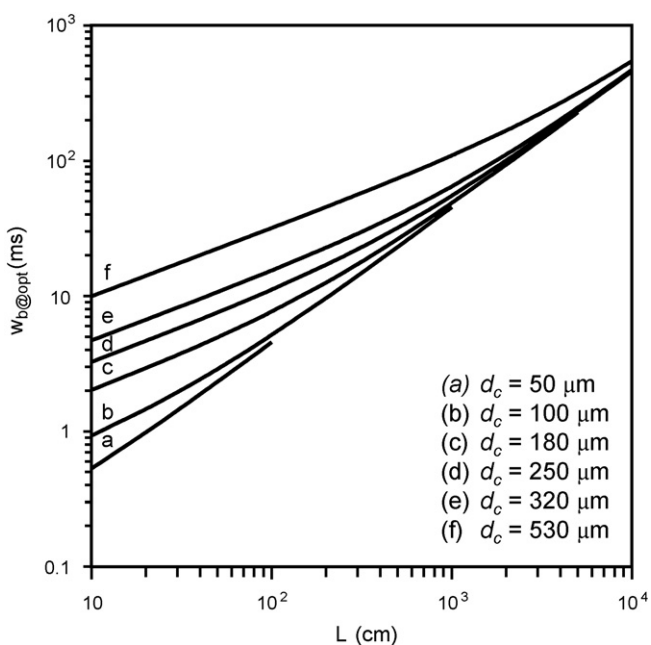


**Fig. 7.** Plot of peak width at the base,  $w_{b@opt}$ , at  $\bar{u}_{opt}$  vs. column length,  $L$ , for various column inner diameters,  $d_c$ . Calculated using Eq. (40) and substituting in the following: (a)  $d_c = 50 \mu\text{m}$ , (b)  $d_c = 100 \mu\text{m}$ , (c)  $d_c = 180 \mu\text{m}$ , (d)  $d_c = 250 \mu\text{m}$ , (e)  $d_c = 320 \mu\text{m}$  and (f)  $d_c = 530 \mu\text{m}$ . Plots were simulated using the same parameters as Fig. 3.

$d_c$  capillary with a length greater than 8 m would result in peak widths, as predicted by theory that are greater than the experimental requirements. Again, all of this assumes that there is no significant extra-column band broadening added to the peak width.

The plot in Fig. 7 can also be used a means of evaluating future developments in the realms of high-speed and micro-fabricated GC. According to Fig. 7, using a short column (i.e., 10 cm) with a small  $d_c$  (i.e., 50 or 100  $\mu\text{m}$ ) it is possible, in principle in the absence of extra-column band broadening, to obtain a peak with a width at the base of less than 1 ms. In order to obtain this narrow of a peak, considerable developments need to be made in both injection and detection technologies. Some of the narrowest injection pulses reported [45] are on the order of 0.5 ms. Columns as short as 10 cm (with an inner diameter of 150  $\mu\text{m}$ ) have been successfully implemented [46], in an application that required a quantitative, high-speed separation of analgin.

### 3.2. Practical implementation of high-speed GC in the context of theory

The theoretical and practical limitations of high-speed gas chromatography have been the subject of numerous publications over the years [5,47–50]. Gaspar [50] made significant advances in the area of high-speed GC theory, coming to the conclusion that high-speed separations are possible using common commercial instruments, however, the experimental parameters must be optimized in the context of the theory. Insight in this regard is provided in this review. Separations to be completed in a few seconds require instrument modification (specifically injector and detector upgrades). A comparison of high-speed and conventional GC of complex fuel samples was conducted using a microbore capillary column (5 m  $\times$  50  $\mu\text{m}$   $\times$  0.05  $\mu\text{m}$  MDN-5S) [51]. The chromatograms from the high-speed separations were completed in 3 min and resulted resolutions that were comparable to those of the 100 min conventional chromatograms obtained with a 25 m  $\times$  250  $\mu\text{m}$   $\times$  0.05  $\mu\text{m}$  MDN-5S column. The comparable resolutions were obtained by applying temperature programs that were optimized for the column dimensions and the carrier gas velocities. In order to obtain a separation of fuel samples in 3 min the column was operated at a velocity of 95 cm/s (which was experimentally determined to be 37 cm/s higher than the optimum velocity). The narrowest resulting peak was approximately 300 ms wide at the

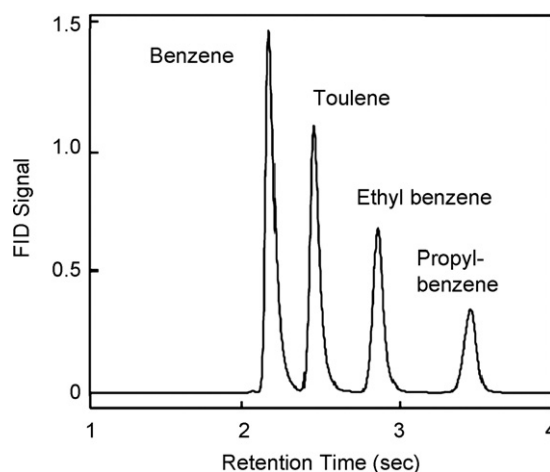


**Fig. 8.** Separation of four alkyl benzenes utilizing a single diaphragm valve injection. The separation was obtained using a 2 m  $\times$  180  $\mu\text{m}$   $\times$  0.20  $\mu\text{m}$  AT-WAX column operated at 100  $^{\circ}\text{C}$  and a column pressure of 20 psi ( $\sim$ 140,000 Pa). Figure reprinted from reference [53] with permission.

base (which is significantly larger than the 22 ms peak width predicted by Eq. (40) and shown in Fig. 7, if the column alone was the major source of band broadening).

Current instrument modifications for high-speed GC typically involve the reduction of injection volumes and dead volumes at the detector. High-speed diaphragm valves equipped with a sample loops have been used to create reproducible injection pulses on the order of 10–20 ms [52–55]. A high-speed separation [53] of four alkyl benzenes using a single diaphragm valve for injection is shown in Fig. 8. The separation was completed in less than 4 s utilizing a 2 m  $\times$  180  $\mu$ m  $\times$  0.25  $\mu$ m DB-1701 separation column, and resulted in peak widths on the order of 250 ms. Using this column in a system without any extra-column band broadening could have resulted in peak widths of approximately 12 ms, as predicted by Eq. (40) and shown in Fig. 7. This suggests that an injection

pulse of 10–20 ms adds a significant amount of extra-column band broadening when using a short column with a small inner diameter. A recently reported injection technique [45], involving the synchronized actuation of two diaphragm valves, resulted in injection pulse widths of less than 1 ms and chromatographic peak widths that approach the peak widths predicted by Golay theory (as shown in Fig. 7). A chromatogram of a seven-compound mixture obtained using synchronized dual-valve injection is shown in Fig. 9A. The resulting chromatographic peak width as a function of the applied pulse width (for two different column lengths) is shown in Fig. 9B. For the longer 1 m  $\times$  100  $\mu$ m column the resulting peak width is constant for pulses widths between 0.5 and 2.5 ms, for the 0.5 m  $\times$  100  $\mu$ m column the resulting peak width begins to increase significantly as the injection pulse is increased above 0.5 ms. This reinforces the importance of a temporally narrow injection pulse

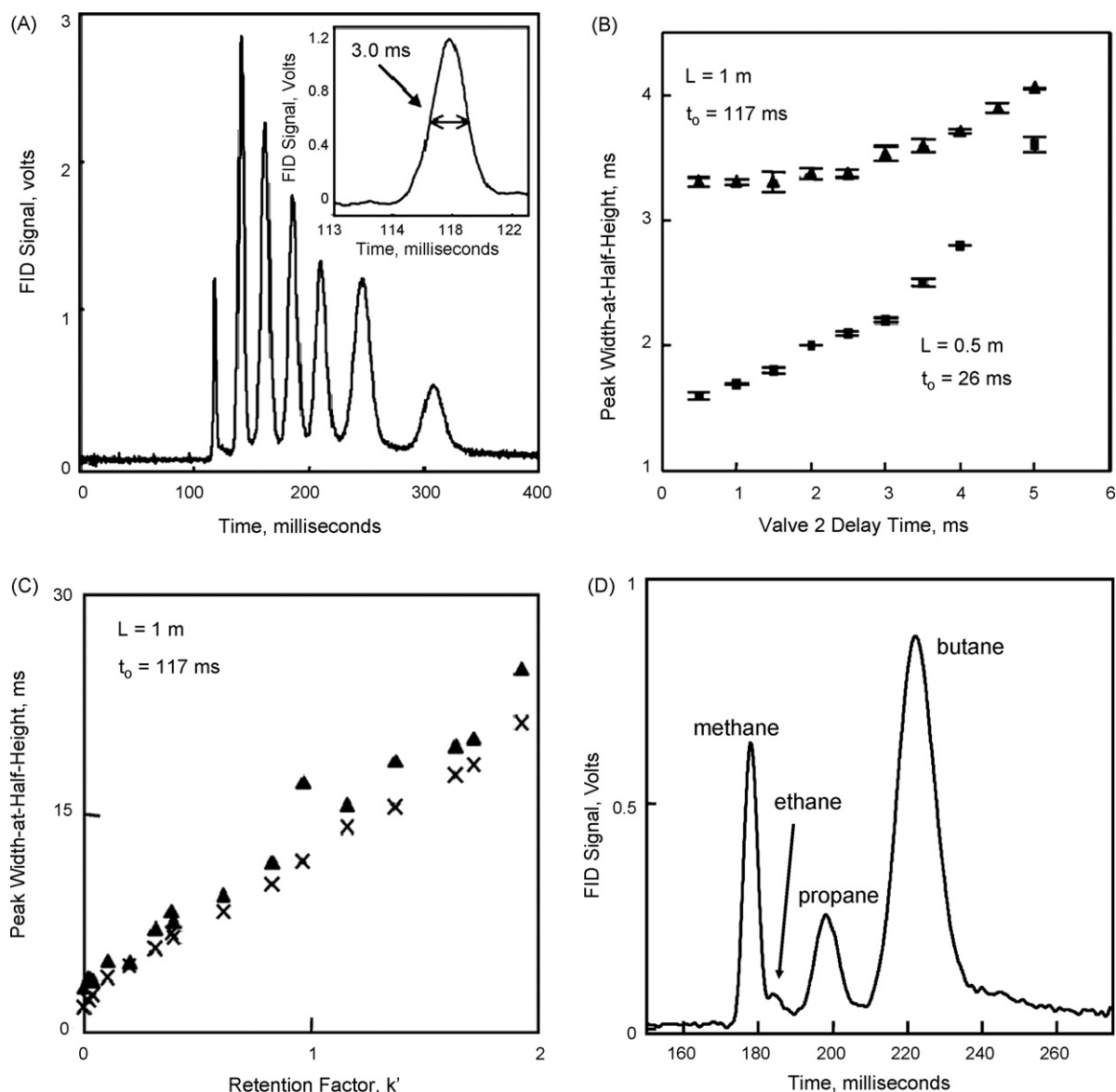


**Fig. 9.** Implementation of synchronized dual valve injection is presented. All data were collected at an oven temperature of 150 °C with H<sub>2</sub> carrier gas at an absolute head pressure of 85 psi (590,000 Pa) unless otherwise noted. (A) Chromatogram of a seven-compound separation obtained using a 2.5 ms injection pulse. Retention order as follows: methane, benzene, octane, chlorobenzene, anisole, *n*-decane and butylbenzene. (B) A plot of peak width as a function of the pulse width injected for 1 and 0.5 m DB-5 columns (both columns have 100  $\mu$ m inner diameters and 0.4  $\mu$ m film thicknesses). (C) A plot of experimental ( $\blacktriangle$ ) and theoretical ( $\times$ ) width at half height values as a function of the analyte retention factor for the 1 m DB-5 column. See cited reference for a complete list of parameters used in the theoretical calculations. (D) Separation of four light alkanes using a 4 ms injection pulse. Separation collected with a 1 m  $\times$  100  $\mu$ m  $\times$  0.4  $\mu$ m DB-5 column at 25 °C and 700 cm/s H<sub>2</sub> (previously unpublished work). Figures in (A), (B) and (C) reprinted from reference [45] with permission, copyright 2008 American Chemical Society.

when using a short chromatographic column in order to avoid introducing any extra-column band broadening. A comparison of actual peak width and the peak width predicted by Golay theory, for a variety of retention factors on the 1 m column, is shown in Fig. 9C. It is important to note that the actual and predicted peak widths are in good agreement. The reported peak widths are also in good agreement with the peak width predicted by Eq. (40) and shown in Fig. 7. In order to detect such narrow peaks the commercial electrometer on the FID was replaced with a high-speed electrometer capable of data collection rates as high as 20 kHz. A discussion of the detection and handling of data this high data collection rates has been addressed by Hinshaw in a three part series [56–58]. Also shown (Fig. 9D) is a previously unpublished separation of four light *n*-alkanes, complete in less than 300 ms that was obtained using the synchronized dual-valve injection technique. Other injection techniques such as cryo-focusing or thermal modulation, have successfully reduced the width of the analyte-containing sample pulse injected onto the column [21,59–61]. An example of a high-speed separation obtained using a cryogenic inlet [61] is shown in Fig. 10. Injections were made onto a  $0.3\text{ m} \times 50\text{ }\mu\text{m} \times 0.17\text{ }\mu\text{m}$  OV-1 column which was interfaced to a time-of-flight mass spectrometer (TOFMS) for detection. The spectrometer was set at its maximum data collection rate of 500 mass spectra/s, this data collection rate was sufficient for the high-speed separation and resulted in plenty of data points (spectra) per peak. The separation of a 10-compound mixture was complete in less than 500 ms and resulted in peak widths on the order of 20 ms. Ideally, the peaks could be approximately 1.5 ms wide (as predicted by Eq. (40) and shown in Fig. 7). Thermal modulation has been used to create injections in the 5–40 ms range [21,59–63]. Due to the cycle time of thermal modulation systems (which is longer relative to the cycle time of a diaphragm valve), diaphragm valve-based instruments are typically used when a repetitive high-speed injection is necessary. Thermal modulation and cryofocusing techniques also incorporate an element of pre-concentration which can decrease (i.e., improve) the limit of detection (LOD) of most systems. Pre-concentration is also an important attribute for most of the portable gas chromatographic instruments [64–71].

A common way to extract selected compounds from a bulk solution is the use of solid-phase microextraction (SPME) [72]. This technique, however, is not frequently coupled to high-speed GC because of the time required for analyte absorption onto the

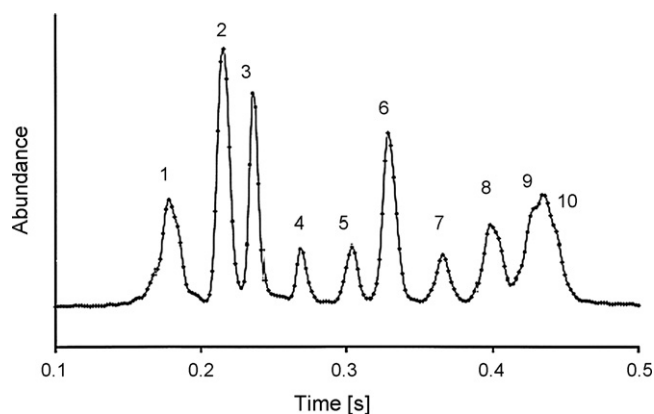


**Fig. 10.** High-speed separations of a 10-compound mixture utilizing a cryogenic focusing inlet and a time-of-flight mass spectrometer (TOFMS) for detection. Separation was performed using a  $0.3\text{ m} \times 50\text{ }\mu\text{m} \times 0.17\text{ }\mu\text{m}$  OV-1 separation column with 450,000 Pa of He carrier gas with a split flow of 400 mL/min. Retention order is as follows: *n*-pentane, 2,3-dimethylbutane, *n*-hexane, benzene, *n*-heptane, methylcyclohexane, toluene, *trans*-1,4-dimethyl cyclohexane, *n*-octane and *cis*-1,4-dimethylcyclohexane. Figure reprinted from reference [61] with permission.

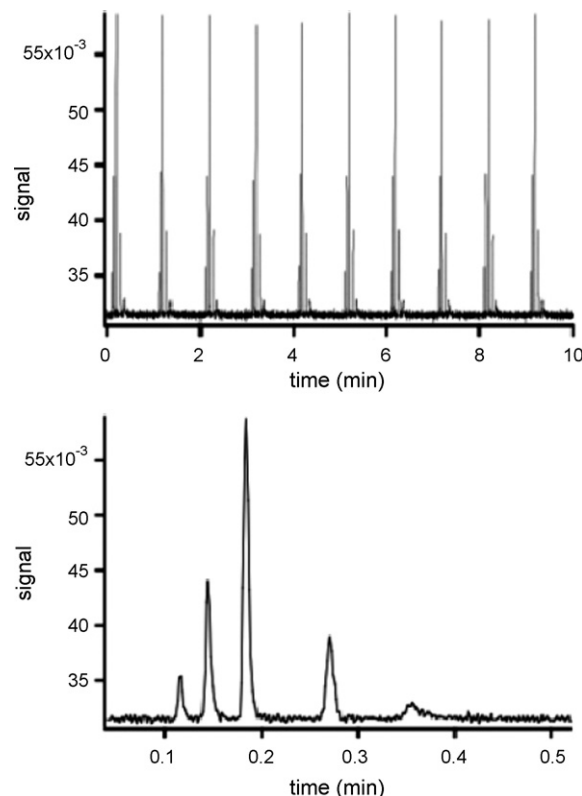


**Fig. 11.** Chromatograms obtained using a microdialysis membrane probe for sample extraction. Analytes extracted from an aqueous solution containing 100 mM of each compound. Chromatograms were collected using a  $3\text{ m} \times 250\text{ }\mu\text{m} \times 0.25\text{ }\mu\text{m}$  DB-1701 column with a carrier gas velocity of 3 mL/min. (Top) 10 replicate injections. (Bottom) Detail of first injection. Retention order is as follows: ethanol, toluene, isobutyl alcohol, *o*-xylene and hexanol. Figure reprinted from reference [76] with permission, copyright 2008 American Chemical Society.

SPME fiber and the subsequent thermal desorption of the analytes from the fiber into the GC inlet is on the order of several minutes [73–75]. One recent report [76] documents the use of a fast microdialysis membrane probe to extract volatile compounds from aqueous solutions; this probe was then coupled to a high-speed GC system for analysis of the extracted compounds. An example of the injection-to-injection reproducibility and a separation of five extracted compounds is shown in Fig. 11. The microdialysis membrane probe was immersed in an aqueous solution containing ethanol, toluene, isobutyl alcohol, *o*-xylene and hexanol each at a concentration of 100 mM. The probe was interfaced to a diaphragm valve for injection directly onto the separation column. The separation of the five compounds used a  $3\text{ m} \times 250\text{ }\mu\text{m} \times 0.25\text{ }\mu\text{m}$  DB-1701 separation column and was completed in less than 30 s. All five compounds (both polar and non-polar) exhibit signals above the LOD, with four of the compounds having high signal-to-noise responses. Utilizing this microdialysis membrane probe, while it addresses an important application need, did result in a trade-off since significant extra-column band broadening occurred. Ideally, the peaks could be approximately 22 ms wide (as opposed to the actual peak width of 1000 ms) as predicted by Eq. (40) and shown in Fig. 7. The membranes were versatile in that they simultaneously extracted both polar and non-polar compounds. Another apparent advantage of these membranes, over SPME fibers, is their rapid response time. The equilibration time for the microdialysis membrane probe is on the order of seconds, with a desorption time of approximately 1 s. These probes have potential applications in the detection of volatile compounds that occur in biological sys-



tems [77–79]. The LOD of these systems could also be improved by coupling the microdialysis membrane probe with various trapping techniques to further concentrate the compounds [80].

The miniaturization of the instrumentation components, most often through micro-fabrication, has significantly reduced the size of dead volumes, which if not intended can be a significant source of extra-column band broadening. Columns have been successfully micro-fabricated from silicon wafers [81–84]. These micro-fabricated columns are typically fairly short (i.e., less than 3 m) and have small cross-sectional channel areas (i.e.,  $100\ \mu\text{m} \times 100\ \mu\text{m}$ ). Stationary phases, resulting in a relatively wide range of chemical selectivity, have been successfully deposited in the micro-fabricated channels via static and dynamic coating processes [81,84]. In one particular case, carbon nanotubes were grown inside the channels [83]. This system also utilized an on-chip resistive heater which allowed the separations to be temperature programmed. Temperature programming rates on the order of  $60\ ^\circ\text{C}/\text{s}$  were reported and resulted in separations of a four compound mixture in less than 1.5 s. The micro-fabricated chip was interfaced with synchronized dual valve injection [45] to study the GC-chip device without introducing significant extra-column band broadening. Connecting micro-fabricated columns to standard injectors and detectors typically results in substantial dead volumes. This problem is being circumvented by the micro-machining of both injection valves [85] and detectors. For example, a micro-FID has been reported [86] with a linear dynamic range of six orders of magnitude and a mass LOD in the sub-nanogram range. Alternative detection techniques such as chemiluminescence, are also being explored [87]; this particular system reported short response times and high sensitivity for a large range of volatile organic compounds. Similar detectors have been used in two-dimensional GC in the detection of sulfur containing compounds in petroleum samples [88–90]. This particular sulfur chemiluminescence detector (SDC) has a significant dead volume, however, the resident time of the compounds in the detector were reported to be approximately 5 ms. The detector electronics were modified so that the detector could be used for high-speed GC  $\times$  GC separations [89]. Overlay plots of SDC and FID signals for the same separation were shown to prove the high-speed electronic modifications eliminated the extra-column band broadening caused by previous models of SCDs. Efforts have also been made toward the development of highly selective detectors as a way to reduce the time of analysis. One such detector is the aromatic selective ionization detector (ArSLID) [91], which has a large dynamic range and results in peak widths that are comparable to a conventional FID.

Multidimensional detection is being introduced to high-speed GC as a way to circumvent the possible loss of peak capacity and/or resolution that can occur in high-speed single dimension separations. A micro-fabricated differential mobility spectrometer (DMS) demonstrates a good mass LOD of approximately 10–90 pg for approximately 30 different volatile organic compounds of various functionalities (aldehydes, ethers, esters and alcohols) [92–95]. A miniature radio-frequency ion mobility spectrometer (RF-IMS) was used as a detector for various volatile organic compounds [93]. This detector was implemented in the detection of insect attractants, which are used for insect management in planted fields. A separation of a mixture of attractants obtained using this RF-IMS detector is shown in Fig. 12. The separations were completed using a 25 m SP-2300 separation column and took approximately 800 s. This mixture contained five different non-pheromone attractants, all of which are resolved and produce distinguishable signals in the two dimensional GC-RF-IMS chromatogram. The advantage of this particular type of DMS detector is its size and response time. The drift region for this detector is  $5\ \text{mm} \times 15\ \text{mm} \times 0.5\ \text{mm}$ . A DMS detector was utilized with a dual-column system as a means of

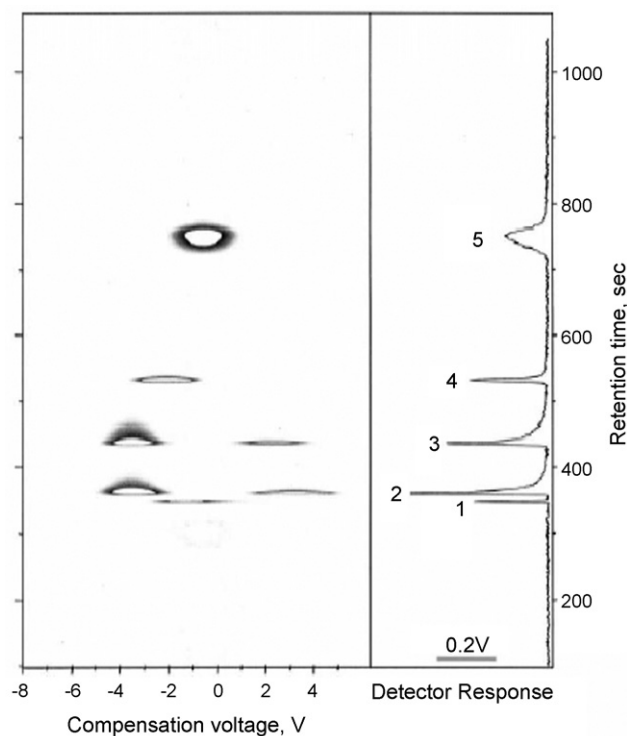


**Fig. 12.** Separation of an insect attractant mixture obtained using GC-RF-IMS is shown. Separation was performed using a 25 m SP-2300 column with a temperature program of  $70\text{--}220\ ^\circ\text{C}$  at  $8\ ^\circ\text{C}/\text{min}$ . Retention order is as follows: *R*(+)-limonene, phenylacetaldehyde, 2-phenylethanol, methyl salicylate and methyl 2-methoxybenzoate. Figure reprinted from reference [93] with permission.

rapid detection of complex headspace samples [96]. This detector was coupled with a micro-fabricated column resulting in minimal extra-column band broadening [82]. The application of chemometrics to high-speed GC samples [97] is another way to compensate for incomplete separation. Chemometrics can be used to classify the samples and to identify characteristics that distinguish the samples, in some cases only minimal separation of the compounds is needed.

As mentioned earlier, there has also been a focus on developing new stationary phases for high-speed GC. It is important that these new materials have optimal mass transfer properties in order to reduce the amount of on-column band broadening as expressed in the  $C_L$  term of the general Golay equation (Eq. (18)). One such phase that has been used is monolayer protected nanoparticles (MPNs) [98–100]. These particles have shown good mass transfer properties [99,100] and have been deposited in a square capillary to demonstrate their nearly “ideal” coating properties [98] (i.e., minimal buildup in the corners of square channels). Scanning electron microscopy (SEM) images of the MPN stationary phase deposited in a ( $1.3\ \text{m} \times 100\ \mu\text{m}$ ) square capillary are shown in Fig. 13. The MPN stationary phase resulted in a film that was 13-nm thick (the average film thickness was determined to be 15 nm) in the middle of the capillary wall (see Fig. 13B) and a thickness of 430 nm in the corners of the capillary (see Fig. 13C). It is important to note that the buildup in the corners only spans approximately  $5\ \mu\text{m}$  of the  $100\ \mu\text{m}$  capillary wall. The separation of a three compound *n*-alkane mixture obtained with the MPN coated square capillary is shown in Fig. 13D. The peak shapes in the 3 s separation are essentially Gaussian, suggesting that the minimal buildup in the capillary corners did not negatively effecting the mass transfer properties of the stationary phase. Studying this column in the absence of any extra-column band broadening could have resulted in peak widths of approx-

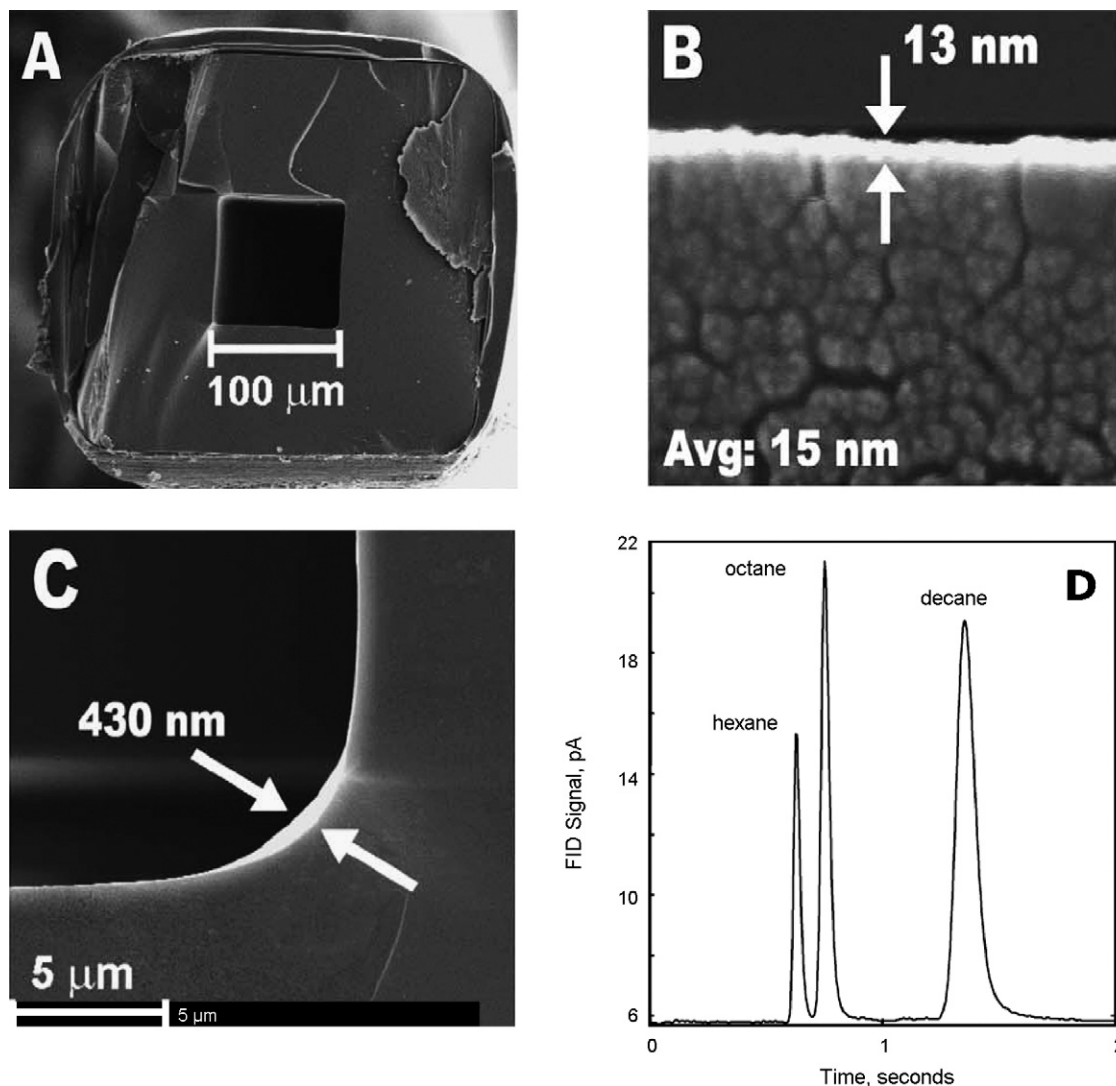


**Fig. 13.** Scanning electron microscopy (SEM) images of, and separations obtained with, a square capillary column coated with a thin film of dodecanethiol MPN stationary phase. (A) SEM image of the MPN stationary phase. (B) SEM image of the stationary phase along the capillary wall. (C) SEM image of the MPN stationary phase in the corner of the square capillary. (D) Separation of a three compound alkane mixture obtained with the  $1.3 \times 100 \mu\text{m}$  square capillary coated with the MPN stationary phase at  $75^\circ\text{C}$  and  $\text{H}_2$  carrier gas at 170,000 Pa. Figures reprinted from reference [98] with permission.

imately 7 ms (as opposed to the actual peak width of 80 ms) as predicted by Eq. (40) and shown in Fig. 7. Note that the higher than ideal peak widths were due to the injection method used.

Other materials such as ionic liquids (ILs) and carbon nanotubes have been reported. Recently developed IL columns have high thermal stability and have been utilized for the separation of a wide range of compounds [34,96]. In one particular application [96], a novel IL column ( $2.8 \text{ m} \times 250 \mu\text{m} \times 0.15 \mu\text{m}$ ) was paired with a commercially available RTX-1 separation column ( $2.8 \text{ m} \times 250 \mu\text{m} \times 0.25 \mu\text{m}$ ) in a dual column ensemble. This particular ensemble was utilized to separate a mixture of 20 compounds, several of which co-elute when the mixture is separated on the individual columns, as shown in Fig. 14. The separations utilizing the commercially available and IL columns are shown in Fig. 14a and b, respectively. The dual column ensemble allowed the flow to be switched between the two columns as a means of tuning the selectivity of the separation. The resulting separation is complete in approximately 200 s and nearly all of the mixture compounds are baseline resolved. Carbon nanotubes are advantageous for micro-fabricated channels because they can be grown directly inside the

channel [83] instead of being deposited inside the already bonded chip like traditional polymeric stationary phases.

Another recent development in high-speed GC has been in the area of temperature programming. High-speed separations present a challenge to temperature program due to the limitations of standard bench top instruments, consequently most high-speed GC work has been isothermal. However, isothermal conditions usually result in separations that do not fully utilize the separation space. The temperature is only optimum for one region of the separation due to the “general elution problem.” By isothermally optimizing the temperature for the first part of the separation the compounds eluting later in the separation are significantly broadened. In turn, choosing to isothermally optimize the temperature for the later eluting peaks usually results in co-eluting peaks in the front of the chromatogram. The dilemma is referred to as the general elution problem; no single isothermal temperature provides optimal resolution for the duration of a separation. The goal of a temperature program is to solve the general elution problem. Temperature programming a separation dynamically reduces the  $k$  of the compounds in order to optimize the resolution per separation time,

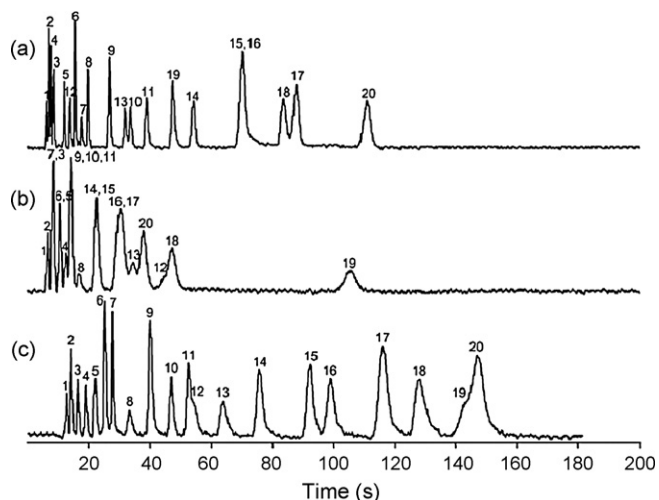


**Fig. 14.** Chromatograms of a 20-compound mixture obtained using (a) commercial  $2.8 \times 250 \mu\text{m} \times 0.25 \mu\text{m}$  RTX-1 column, (b)  $2.8 \times 250 \mu\text{m} \times 0.15 \mu\text{m}$  immobilized ionic liquid column and (c) dual column ensemble. All separations at  $50^\circ\text{C}$  and obtained using  $\text{H}_2$  carrier gas at velocities of  $\sim 54, 53$  and  $54$  cm/s, respectively. Figure reprinted from reference [96] with permission.

while reducing the widths of the resulting peaks [18]. Temperature programming is an effective way to decrease the amount of time required to achieve a desired separation. The development of a temperature-programmable high-speed GC system with a low thermal mass resulted in temperature programming rates of  $30^\circ\text{C/s}$  and required approximately 1.3 min to cool from  $300$  to  $30^\circ\text{C}$  [101]. This particular system utilized an insulated capillary, heating wire, and a temperature sensor wire that are bundled together in a conductive foil. A small fan is used to vent/cool the bundle at the end of the heating cycle. It has always been very challenging to create a reproducible temperature program at a rate high enough to be beneficial to high-speed GC. One promising approach is directly heating the column using resistive heating [64,102,103]. Previous attempts at direct column resistive heating mentioned uneven heating and extra-column band broadening due to inconsistencies in the metal coating of the capillary [62,104]. New commercially available Silcosteel columns make direct resistive heating feasible and result in reproducible temperature programs, with rates on the order of  $240^\circ\text{C/s}$  having been reported [105]. A  $2.3 \text{ m} \times 180 \text{ mm}$  MXT-5 column was used to isothermally separate a mixture of seven *n*-alkanes as shown in Fig. 15a. A voltage was then applied across the column to produce a temperature program. The separation resulting from the application of  $72 \text{ V}$  ( $155^\circ\text{C/s}$ ) is shown in Fig. 15b. The temperature programmed separation has a more optimal use of the separation space and also improves the signal-to-noise ratio of the later eluting compounds. The actual peak width of the first peak in the temperature programmed separation is higher than those predicted by Eq. (40) and shown in Fig. 7. The actual peak width for *n*-hexane in the temperature programmed separation was  $40 \text{ ms}$  while the width predicted by theory (for an unretained compound) is approximately  $14 \text{ ms}$ . Further optimization of the separation conditions (including carrier gas velocity and temperature programming rate) may have resulted in peak widths closer to the values predicted using Eq. (40).

High-speed temperature programming has also been achieved by incorporating resistive heaters onto the chips contained the micro-fabricated columns, as mentioned earlier [83,106]. These heaters, however, only heat the channel from one side which, if not properly engineered, may result in additional band broadening. In one particular case [106], a mixture of *n*-alkanes was separated using temperature programs on the order of  $10^\circ\text{C/s}$ , resulting

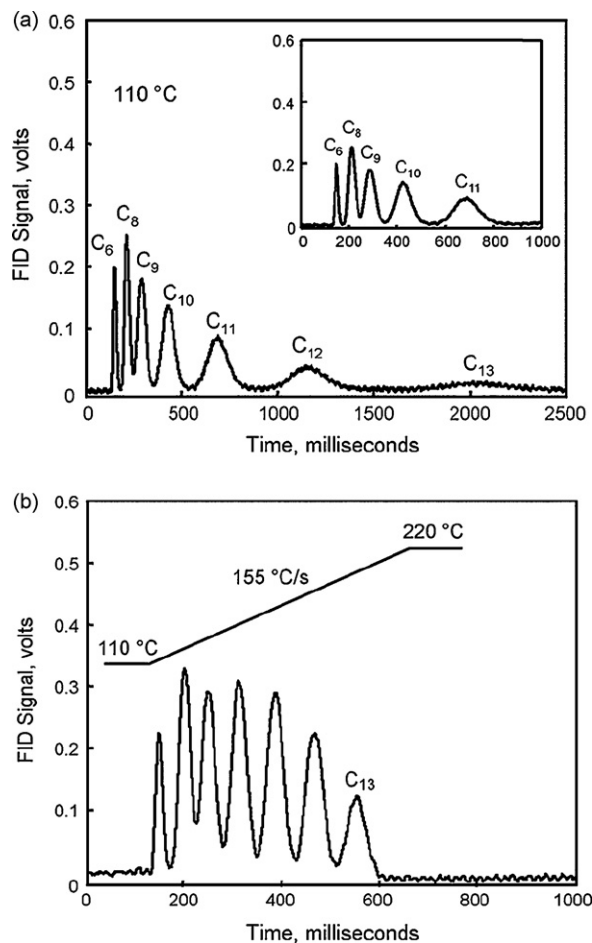


**Fig. 15.** Isothermal and temperature programmed separations of a seven compound *n*-alkane mixture (retention order: *n*-hexane, *n*-octane, *n*-nonane, *n*-decane, *n*-undecane, *n*-dodecane and *n*-tridecane). Separations were obtained using a  $2.3 \text{ m} \times 180 \mu\text{m} \times 0.4 \mu\text{m}$  MXT-5 column and  $\text{H}_2$  carrier gas at an absolute head pressure of  $620,000 \text{ Pa}$ . (a) Isothermal separation at  $110^\circ\text{C}$ . (b) Temperature programmed separation  $110$ – $220^\circ\text{C}$  at  $155^\circ\text{C/s}$ . Figures reprinted from reference [105] with permission.

in a separation of  $\text{C}_5$ – $\text{C}_{16}$  *n*-alkanes. This particular system utilized a  $25 \text{ cm}$  micro-fabricated column with a  $150 \mu\text{m} \times 250 \mu\text{m}$  cross-section and coated with a  $1$ – $2 \mu\text{m}$  thick film of RTX-1. The micro-fabricated chip contained an integrated on-chip heater with temperature and pressure sensors which allowed for programming of both temperature and pressure. Adjusting the temperature programming rate allowed for the separation of a subset of compounds within the large mixture as shown in Fig. 16. Using a shallow temperature program is ideal for separating out the lighter compounds ( $\text{C}_5$ – $\text{C}_9$ ), while the heavier compounds ( $\text{C}_{10}$ – $\text{C}_{16}$ ) require a steeper temperature program. This report also proposed the idea of running multiple micro-fabricated systems in parallel as a means of optimizing the temperature programming, and separation, of larger mixtures. Using these columns in a fully micro-fabricated system has the potential of reducing the amount of extra-column band broadening which could result in peak widths closer to those predicted in Eq. (40) and shown in Fig. 7 (approximately  $4 \text{ ms}$  for a  $25 \text{ cm} \times 100 \mu\text{m}$  column).

Looking toward the future, as the individual components of high-speed GC analyzer systems are optimized, the performance of this analyzer will approach the time frame of a chemical sensor. By using short capillary columns with small inner diameters, the widths of the results chromatographic peaks can be significantly

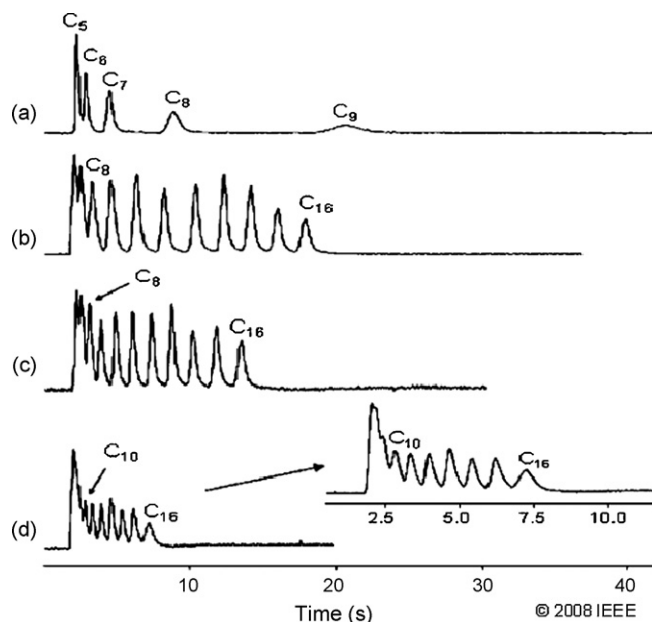


**Fig. 16.** Separations of a gas mixture ( $C_5$ – $C_{16}$ ) obtained using a micro-fabricated column (25 cm with a  $150\ \mu\text{m} \times 250\ \mu\text{m}$  rectangular channel) coated with 1–2  $\mu\text{m}$  of RTX-1 with an on chip heater and air as the carrier gas at 25 cm/s. (a) Isothermal separation at room temperature. (b) Temperature programmed from 25 to 130 °C at 300 °C/min. (c) 25 to 130 °C at 600 °C/min and (d) 50–130 °C at 600 °C/min. Figure reprinted from reference [106] with permission.

reduced (as shown in Fig. 7). With the reduction of injection pulses and detector dead volumes, the amount of extra-column band broadening introduced into the system can be greatly reduced. While synchronized dual valve injection was adequate in experimentally demonstrating that the ideal band broadening can be achieved, it suffers from a poor LOD; hence, future developments in low thermal mass, high-speed thermal modulation injection approaches should be developed. Operating a system with optimized components should result in separations with efficiencies, plate heights and peak widths that are similar to theoretically determined values. The developments of  $\bar{u}_{\text{opt}}$  theory that have been reported herein should provide readers with a starting point for the optimization of experimental parameters, and a means to compare one set of experimental results to another. It is important to note that 10 cm columns with 50  $\mu\text{m}$  inner diameters result in the highest values of efficiency per unit time. Effectively utilizing these separation columns will require further developments of in all areas of GC instrumentation (injection, separation and detection). For example, the smallest reported injection pulses (approximately 0.5 ms [45]) are approximately the same size as the predicted peak width, which leaves no room for on-column band broadening. Even micro-fabricated detectors with low dead volumes introduce a significant amount of band broadening when working with such small capillaries (combination of  $d_c$  and length). These ultra short, narrow  $d_c$  capillaries require new instrumentation developments, which is the impetus for more creative thinking and solutions to the challenges to make the ideal (column limited band broadening) become the reality.

## References

- [1] A.J.P. Martin, R.L.M. Synge, *Biochem. J.* 35 (1941) 1358.
- [2] A.T. James, A.J.P. Martin, *Biochem. J.* 50 (1952) 679.
- [3] M.J.E. Golay, in: V.J. Coates, H.J. Noebels, I.S. Fagerson (Eds.), *Gas Chromatography (1957 Lansing Symposium)*, Academic Press, New York, 1958, p. 36.
- [4] D.H. Desty, A. Goldup, B.H.F. Whyman, *J. Inst. Pet.* 45 (1959) 287.

- [5] D.H. Desty, in: J. Giddings, R. Keller (Eds.), *Advances in Chromatography*, Marcel Dekker, Inc., New York, 1965, p. 214.
- [6] J.C. Giddings, *Anal. Chem.* 34 (1962) 314.
- [7] D.H. Desty, A. Goldup, W.T. Swanton, in: N. Brenner, J.E. Callen, D. Weissnauatuck (Eds.), *Gas Chromatography*, Academic Press, New York, 1962, p. 105.
- [8] J.C. Giddings, *Anal. Chem.* 39 (1967) 1027.
- [9] H. Purnell, *Gas Chromatography*, Wiley, New York, 1962.
- [10] J.C. Giddings, *Unified Separation Science*, Wiley, New York, 1991.
- [11] B.L. Karger, L.R. Snyder, C. Horvath, *An Introduction to Separation Science*, John Wiley & Sons, New York, 1973.
- [12] A.S. Said, *Sep. Sci. Technol.* 13 (1978) 647.
- [13] L.M. Blumberg, M.S. Klee, in: P. Sandra (Ed.), *20th International Symposium of Capillary Chromatography*, Riva del Garda, Italy, 1998.
- [14] J.C. Sternberg, in: J.C. Giddings, R.A. Keller (Eds.), *Advances in Chromatography*, Marcel Dekker, New York, 1966, p. 205.
- [15] R. Sacks, H. Smith, M. Nowak, *Anal. Chem.* 70 (1998) 29A.
- [16] L.S. Ettre, *LC GC N. Am.* 22 (2004) 452.
- [17] C.A. Cramers, G. Janssen, M.M. van Deursen, P.A. Leclercq, *J. Chromatogr. A* 856 (1999) 315.
- [18] M.L. Lee, F.J. Yang, K.D. Bartle, *Open Tubular Column Gas Chromatography*, Wiley, New York, 1984.
- [19] W. Jennings, *Analytical Gas Chromatography*, Academic Press, Inc., Orlando, 1987.
- [20] N.H. Snow, *J. Liquid Chromatogr. Relat. Technol.* 27 (2004) 1317.
- [21] A. Peters, M. Klemp, L. Puig, C. Rankin, R. Sacks, *Analyst* 116 (1991) 1313.
- [22] L.M. Blumberg, *J. High Res. Chromatogr.* 20 (1997) 597.
- [23] L.M. Blumberg, *J. High Res. Chromatogr.* 20 (1997) 679.
- [24] L.M. Blumberg, *J. High Res. Chromatogr.* 22 (1999) 403.
- [25] L.M. Blumberg, *J. High Res. Chromatogr.* 22 (1999) 501.
- [26] J.R. Conder, C.L. Young, *Physicochemical Measurement by Gas Chromatography*, John Wiley & Sons, New York, 1979.
- [27] H. Snijders, H.G. Janssen, C. Cramers, *J. Chromatogr. A* 718 (1995) 339.
- [28] A.I. Canizo, G.N. Eyler, G.P. Barreto, *Chromatographia* 65 (2007) 31.
- [29] K. Heberger, T. Kowalska, *Chromatographia* 44 (1997) 179.
- [30] K. Ciazynska-Halarewicz, T. Kowalska, *J. Chromatogr. Sci.* 40 (2002) 421.
- [31] K. Ciazynska-Halarewicz, T. Kowalska, *Acta Chromatogr.* 13 (2003) 81.
- [32] K. Ciazynska-Halarewicz, T. Kowalska, *J. Chromatogr. Sci.* 41 (2003) 467.
- [33] K. Ciazynska-Halarewicz, T. Kowalska, *J. Chromatogr. Sci.* 45 (2007) 492.
- [34] J.L. Anderson, D.W. Armstrong, *Anal. Chem.* 77 (2005) 6453.
- [35] J.J. van Deemter, F.J. Zuiderweg, A. Klinkenberg, *Chem. Eng. Sci.* 5 (1956) 271.
- [36] G. Gaspar, R. Annino, C. Vidal-Madjar, G. Guiochon, *Anal. Chem.* 50 (1978) 1512.
- [37] V.G. Berezkin, I.V. Malyukova, D.S. Avoce, *J. Chromatogr. A* 872 (2000) 111.
- [38] A.T. James, A.J.P. Martin, *Biochem. J.* 52 (1952) 238.
- [39] J.C. Giddings, *Anal. Chem.* 36 (1964) 741.
- [40] J.C. Giddings, *Anal. Chem.* 35 (1963) 353.
- [41] G.H. Stewart, S.L. Seager, J.C. Giddings, *Anal. Chem.* 30 (1959) 1738.
- [42] G. Guiochon, *Anal. Chem.* 38 (1966) 1020.
- [43] J.V. Hinshaw, L.S. Ettre, *J. High Resolut. Chromatogr.* 20 (1997) 471.
- [44] Agilent Technologies, in [http://www.chem.agilent.com/scripts/cag\\_filexfer.asp?iWHID=40865](http://www.chem.agilent.com/scripts/cag_filexfer.asp?iWHID=40865), 2006.
- [45] G.M. Gross, B.J. Prazen, J.W. Grate, R.E. Synovec, *Anal. Chem.* 76 (2004) 3517.
- [46] V.G. Berezkin, A.B. Lapin, *J. Chromatogr. A* 1075 (2005) 197.
- [47] R. Tijssen, N. van den Hoed, M.E. van Kreveld, *Anal. Chem.* 59 (1987) 1007.
- [48] P. Korytar, H.G. Janssen, E. Matisova, U.A.Th. Brinkman, *Trends Anal. Chem.* 21 (2002) 558.
- [49] M.S. Klee, L.M. Blumberg, *J. Chromatogr. Sci.* 40 (2002) 234.
- [50] G. Gaspar, *J. Chromatogr.* 556 (1991) 331.
- [51] L. Mondello, P.Q. Tranchida, O. Favoino, P. Dugo, G. Dugo, *J. Sep. Sci.* 27 (2004) 1149.
- [52] C.G. Fraga, B.J. Prazen, R.E. Synovec, *Anal. Chem.* 72 (2000) 4154.
- [53] J.L. Hope, K.J. Johnson, M.A. Cavelti, B.J. Prazen, J.W. Grate, R.E. Synovec, *Anal. Chim. Acta* 490 (2003) 223.
- [54] C.A. Bruckner, B.J. Prazen, R.E. Synovec, *Anal. Chem.* 70 (1998) 2796.
- [55] A.E. Sinha, K.J. Johnson, B.J. Prazen, S.B. Lucas, C.G. Fraga, R.E. Synovec, *J. Chromatogr. A* 983 (2003) 195.
- [56] J.V. Hinshaw, *LC GC N. Am.* 19 (2001) 1136.
- [57] J.V. Hinshaw, *LC GC N. Am.* 19 (2001) 1198.
- [58] J.V. Hinshaw, *LC GC N. Am.* 20 (2002) 34.
- [59] A. van Es, J. Janssen, C.A. Cramers, J. Rijks, *J. High Resolut. Chromatogr.* 11 (1988) 852.
- [60] M.A. Klemp, M.L. Akard, R.D. Sacks, *Anal. Chem.* 65 (1993) 2516.
- [61] M.M. van Deursen, J. Beens, H.G. Janssen, P.A. Leclercq, C.A. Cramers, *J. Chromatogr. A* 878 (2000) 205.
- [62] V. Jain, J.B. Phillips, *J. Chromatogr. Sci.* 33 (1995) 55.
- [63] J.B. Phillips, D. Luu, R.-P. Lee, *J. Chromatogr. Sci.* 24 (1986) 369.
- [64] E.B. Overton, K.R. Carney, N. Roques, H.P. Dharmasena, *Field Anal. Chem. Technol.* 20 (2001) 1968.
- [65] U. Lehmann, O. Krusemark, J. Muller, in: A. van den Berg, W. Olthuis, P. Bergveld (Eds.), *Micro Total Analysis Systems 2000, Proceedings of the microTAS Symposium*, fourth ed., Kluwer Academic Publishers, Dordrecht, Netherlands, Enschede, Netherlands, 2000, p. 167.
- [66] G. Frye-Mason, R. Kottenstette, P. Lewis, E. Heller, R. Manginell, D. Adkins, G. Dulleck, D. Martinez, D. Sasaki, C. Mowry, C. Matzke, L. Anderson, in: A.

- van den Berg, W. Olthuis, P. Bergveld (Eds.), *Micro Total Analysis Systems 2000*, Proceedings of the microTAS Symposium, fourth ed., Kluwer Academic Publishers, Dordrecht, Netherlands, Enschede, Netherlands, 2000, p. 229.
- [67] G. Frye-Mason, R. Kottenstette, C. Mowry, C. Morgan, R. Manginell, P. Lewis, C. Matzke, G. Dulleck, L. Anderson, D. Adkins, in: J.M. Ramsey, A. van den Berg (Eds.), *Micro Total Analysis Systems 2001*, Proceedings of the microTAS Symposium, fifth ed., Kluwer Academic Publishers, Dordrecht, Netherlands, Monterey, CA, USA, 2001, p. 658.
- [68] E.S. Kolesar Jr., R.R. Reston, *IEEE T. Compon. Pack. B* 21 (1998) 324.
- [69] C.M. Matzke, R.J. Kottenstette, S.A. Casalnuovo, G.C. Frye-Mason, M.L. Hudson, D.Y. Sasaki, R.P. Manginell, C.C. Wong, in: J.H. Smith (Ed.), *Proceedings of SPIE, SPIE—The International Society for Optical Engineering*, Santa Clara, CA, USA, 1998, p. 262.
- [70] U. Bonne, R. Higashi, C. Cabuz, U.S. Patent 7,000,452, 2006.
- [71] U. Bonne, U.S. Patent 7,104,112, 2006.
- [72] C.L. Arthur, J. Pawliszyn, *Anal. Chem.* 62 (1990) 2145.
- [73] D. Louch, S. Motlagh, J. Pawliszyn, *Anal. Chem.* 64 (1992) 1187.
- [74] A. Saraullo, P.A. Martos, J. Pawliszyn, *Anal. Chem.* 69 (1997) 1992.
- [75] W.H.J. Vaes, C. Hamwijk, E.U. Ramos, H.J.M. Verhaar, J.L.M. Hermens, *Anal. Chem.* 68 (1996) 4458.
- [76] M.A. Jones, A. Kramer, M. Humbert, T. Vanadurongvan, J. Maurer, M.T. Bower, A.J. Borgerding, *Anal. Chem.* 80 (2008) 123.
- [77] X. Zhang, F. Dong, Q. Li, A.J. Borgerding, A.L. Klein, J. Ren, *Appl. Physiol.* 99 (2005) 2246.
- [78] J. Duan, L.B. Esberg, G. Ye, A.J. Borgerding, B.H. Ren, N.S. Aberle, P.N. Epstein, J. Ren, *Comp. Biochem. Physiol., Part A: Mol. Integr. Physiol.* 134A (2003) 607.
- [79] D.L. Robinson, J.A. Lara, L.J. Brunner, R.A. Gonzales, *J. Neurochem.* 75 (2000) 1685.
- [80] R.W. Current, E.I. Kozliak, A.J. Borgerding, *Environ. Sci. Technol.* 35 (2001) 1452.
- [81] G. Lambertus, A. Eistro, K. Sensing, J. Polkay, M. Agah, S. Scheuering, K. Wise, F. Dorman, R. Sacks, *Anal. Chem.* 76 (2004) 2629.
- [82] G.R. Lambertus, C.S. Fix, S.M. Reidy, R.A. Miller, D. Wheeler, E. Nazarov, R. Sacks, *Anal. Chem.* 77 (2005) 7563.
- [83] M. Stadermann, A.D. McBrady, B. Dick, V.R. Reid, A. Noy, R.E. Synovec, O. Bakajin, *Anal. Chem.* 78 (2006) 5639.
- [84] S. Reidy, G. Lambertus, J. Reece, R. Sacks, *Anal. Chem.* 78 (2006) 2623.
- [85] J.A. Dziuban, J. Mroz, M. Szczygielska, M. Malachowski, A. Gorecka-Drzazga, R. Walczak, W. Bula, D. Zalewski, L. Nieradko, J. Lysko, J. Koszur, P. Kowalski, *Sens. Actuators A* 115 (2004) 318.
- [86] C. Deng, X. Yang, N. Li, Y. Huang, X. Zhang, *J. Chromatogr. Sci.* 43 (2005) 355.
- [87] Y. He, Y. Lv, Y. Li, H. Tang, L. Tang, X. Wu, X. Hou, *Anal. Chem.* 79 (2007) 4674.
- [88] R. Hua, Y. Li, W. Liu, J. Zheng, H. Wei, J. Wang, X. Lu, H. Kong, G. Xu, *J. Chromatogr. A* 1019 (2003) 101.
- [89] J. Blomberg, T. Riemersma, M. van Zuijlen, H. Chaabani, *J. Chromatogr. A* 1050 (2004) 77.
- [90] R.X. Hua, J.H. Wang, H.W. Kong, J. Liu, X. Lu, G.W. Xu, *J. Sep. Sci.* 27 (2004) 691.
- [91] M.J. Meyer, G.M. Schieffer, E.K. Moeker, J.J. Brodersen, O.F. Swenson, A.J. Borgerding, *Anal. Chem.* 76 (2004) 1702.
- [92] G.A. Eiceman, E.G. Nazarov, R.A. Miller, E.V. Krylov, A.M. Zapata, *Analyst* 127 (2002) 466.
- [93] G.A. Eiceman, B. Tadjikov, E.V. Krylov, E.G. Nazarov, R.A. Miller, J. Westbrook, P. Funk, *J. Chromatogr. A* 917 (2001) 205.
- [94] G.A. Eiceman, E.V. Krylov, B. Tadjikov, R.G. Ewing, E.G. Nazarov, R.A. Miller, *Analyst* 129 (2004) 297.
- [95] G.A. Eiceman, E.V. Krylov, N.S. Krylov, E.G. Nazarov, R.A. Miller, *Anal. Chem.* 76 (2004) 4937.
- [96] G.R. Lambertus, J.A. Crank, M.E. McGuigan, S. Kendler, D.W. Armstrong, R.D. Sacks, *J. Chromatogr. A* 1135 (2006) 230.
- [97] N.E. Watson, M.M. VanWinderden, K.M. Pierce, B.W. Wright, R.E. Synovec, *J. Chromatogr. A* 1129 (2006) 111.
- [98] G.M. Gross, J.W. Grate, R.E. Synovec, *J. Chromatogr. A* 1029 (2004) 185.
- [99] G.M. Gross, J.W. Grate, R.E. Synovec, *J. Chromatogr. A* 1060 (2004) 225.
- [100] G.M. Gross, D.A. Nelson, J.W. Grate, R.E. Synovec, *Anal. Chem.* 75 (2003) 4558.
- [101] J. Luong, R. Gras, R. Mustacich, H. Cortes, *J. Chromatogr. Sci.* 44 (2006) 253.
- [102] E.B. Overton, K.R. Carney, *Trends Anal. Chem.* 13 (1994) 252.
- [103] E.U. Ehrmann, H.P. Dharmasena, K. Carney, E.B. Overton, *J. Chromatogr. Sci.* 34 (1996) 533.
- [104] J.B. Phillips, V. Jain, *J. Chromatogr. Sci.* 33 (1995) 541.
- [105] V.R. Reid, A.D. McBrady, R.E. Synovec, *J. Chromatogr. A* 1148 (2007) 236.
- [106] M. Agah, G.R. Lambertus, R. Sacks, K. Wise, *J. Microelectromech. Syst.* 15 (2006) 1371.



# New cut angle quartz crystal microbalance with low frequency–temperature coefficients in an aqueous phase

Dazhong Shen\*, Qi Kang, Yu-E Wang, Qiang Hu, Junguo Du

The Key Lab in Molecular and Nano Probes of the Ministry of Education of China, Shandong Normal University, Jinan, 250014, PR China

## ARTICLE INFO

### Article history:

Received 25 February 2008

Received in revised form 6 April 2008

Accepted 12 April 2008

Available online 22 April 2008

### Keywords:

Quartz crystal microbalance

Cut angle

Frequency–temperature coefficient

Polyelectrolyte

Adsorption

## ABSTRACT

In a traditional quartz crystal microbalance (QCM), an AT-cut (cut angle  $\varphi = 35.25^\circ$  in  $yx1$  orientation) quartz wafer is employed because it has low frequency–temperature coefficients ( $dF/dT$ ) at room temperature region. But when a QCM is in contact with a liquid phase, its frequency is also related to the properties of the liquid, which are temperature dependent. The value of  $dF/dT$  is about  $20 \text{ Hz}/^\circ\text{C}$  for a 9 MHz AT-cut QCM with one side facing water. In this work, a group of QCMs in new cut angles were prepared. The influence of the cut angle on the frequency–temperature characteristic, response sensitivities to surface mass loading and viscodensity of liquid were investigated. An intrinsically temperature-compensated QCM sensor that possesses low  $dF/dT$  values in aqueous solution was reported. When a 9 MHz QCM with  $\varphi = 35.65^\circ$  was contacted with water with one side, its  $dF/dT$  value is close to zero at ca.  $25^\circ\text{C}$  and its averaged value of  $|dF/dT|$  is only  $0.6 \text{ Hz}/^\circ\text{C}$  in the temperature range of  $23\text{--}27^\circ\text{C}$ . The frequency responses to surface mass loading and viscodensity of liquid phase are very close among the QCMs with the cut angles in the range of  $35.15\text{--}35.7^\circ$ . The intrinsically temperature-compensated QCM was applied to investigate the alternate adsorption processes of cationic polyelectrolyte and silica nanoparticle.

© 2008 Elsevier B.V. All rights reserved.

## 1. Introduction

Piezoelectric quartz crystal resonators have widely been utilized not only for time keeping devices but also for chemical sensors [1–3]. A quartz crystal microbalance (QCM) is a useful tool to provide the information related to the changes in mass and properties of the interfaces in real time [4–8]. A QCM comprises a thin, vibrating, AT-cut quartz crystal wafer sandwiched between two metal-film electrodes across which an alternating electric field is applied. It was worthy to note that the AT-cut is a quartz crystal disc with a special cut angle ( $\varphi = 35.25^\circ$ ) in  $yx1$  orientation (see Fig. 1). The advantage of the AT-cut quartz crystal resonator is that it possesses low frequency–temperature coefficients ( $dF/dT$ ) in room temperature region, which is helpful for the applications of QCM in gaseous sensors. When a QCM is in contact with a liquid phase, its resonant frequency is related to the surface mass-loading as well as the properties of the liquid [9–12], such as viscosity, density, conductivity and permittivity. Because these liquid properties are temperature dependent, the values of  $dF/dT$  of the QCM in a liquid phase depend mainly on the temperature characteristics of the liquid properties. It was shown that an increase in the viscodensity of the liquid phase results in a decrease in the oscillating frequency of

the QCM in the liquid [9,10]. Because the viscodensity of the liquid was decreased with increasing temperature, an increase in frequency for the QCM was expected. Hence, the value  $dF/dT$  of a QCM in liquid phase is much greater than that in air. As the values of  $dF/dT$  of quartz resonators themselves are related to the cut angle [13,14], it is possible to fabricate an intrinsically temperature-compensated QCM for the applications in liquid phase.

In this contribution, twelve quartz crystal wafers with  $\varphi = 35.15\text{--}35.7^\circ$  were used to fabricate liquid phase QCM sensors. We presented the experimental results for the Y rotational cut QCMs with different cut angles in liquid phases. The point with  $dF/dT = 0$  in liquid was obtained for the QCMs in a special cut angle in a given temperature. The QCM with low frequency–temperature coefficients was expected to increase its signal-to-noise ratio, which, in turn, yields lower detection limit and a higher frequency resolution of the sensor. The intrinsically temperature-compensated QCM sensor was applied to investigate the alternate adsorption processes of cationic polyelectrolyte and  $\text{SiO}_2$  nanoparticle.

## 2. Experiment

### 2.1. Apparatus and reagents

The quartz crystal wafers were prepared by polishing a group of Y rotational cut plates from a quartz crystal. Twelve cut angles were

\* Corresponding author. Fax: +86 531 82615258.  
E-mail address: [dzshen@sdu.edu.cn](mailto:dzshen@sdu.edu.cn) (D. Shen).

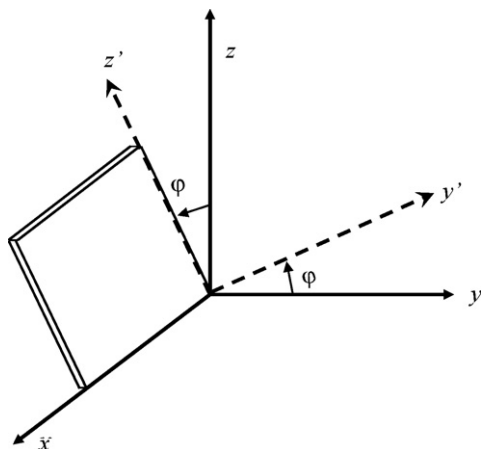


Fig. 1. The  $yxz$  orientation for Y-rotated cut quartz crystal wafer.  $\varphi$  is the cut angle.

used in the range of  $\varphi = 35.15\text{--}35.7^\circ$  with an interval of  $0.05^\circ$ . The cut angle was measured by a DG-3 high precision X-ray crystal orientation instrument (Dandong Qibao Electrical Equipment Plant, China) with precision of  $15''$ . The diameter of the Y-rotated cut quartz crystal wafers was 18 mm. The wafer was polished to 0.1845 mm by a polish machine. Two “key-hole” shaped gold electrodes with a diameter of 8 mm were evaporated in center of the crystal wafer on a chromium adhesion layer. The intrinsic frequency of the resonators was 9000 kHz. The resonant frequencies of the QCMs were measured in a precision impedance analyzer (Agilent 4294A) through 16047E test fixture for axial lead components. A user program written in Visual Basic 6.0 was used to control the impedance analyzer and to acquire and process data. To obtain a better estimation for the resonant frequency of a QCM, an averaged method described in a previous paper was used [15].

3-Mercaptopropionic acid (MPA, 99%) was obtained from Aldrich Chemical Co. Polydiallyldimethylammonium chloride (PDADMAC), with an averaged molecular weight of  $1.2 \times 10^6$  was obtained from Shandong Binzhou Chemical Plant. Silica particle was purchased from Cabot Co. The diameter of the particles was ca. 10 nm. Analytical-reagent grade chemicals and doubly distilled water were used.

### 2.2. Measurement of the frequency–temperature coefficients of the QCMs

To measure the value of  $dF/dT$  of a QCM itself, the QCM and a temperature probe were mounted in a 100 ml sealed flask. The flask was put into a thermostatic water bath. The temperature in water bath was increased at a rate of  $1^\circ\text{C}/\text{min}$ . The resonant frequency of the QCM ( $F$ ) and the temperature ( $T$ ) in flask were recorded as the function of time ( $t$ ) by a computer. The curves of  $T$  versus  $t$  and  $F$  versus  $t$  were regressed by a cubic polynomial model. Based on the two regressed equations, a smoothed curve of  $F$  versus  $T$  was obtained and the value of  $dF/dT$  was calculated. In the temperature experiment of QCM in a liquid phase, a quartz crystal wafer was mounted to a glass detection cell by two O rings with one side exposed to the solution. A thermostatic water jacket was added in the wall of the detection cell. The rough and slanting cell design was used to eliminate the longitudinal wave effect of the QCM [16]. A temperature probe was put in cell close to quartz wafer. Fifty milliliters of cool water (ca.  $8^\circ\text{C}$ ) was added in the cell. The temperature in the cell was increased at a rate of  $1^\circ\text{C}/\text{min}$  by the thermostatic water jacket. Under a mild stir, the curves of  $T$  versus  $t$  and  $F$  versus  $t$  were recorded. The value of  $dF/dT$  was calculated by the approach described above.

### 2.3. Measurement frequency shifts of QCMs in mass deposition process

In the experiment to test the mass effect, a gold layer was added on the electrode surface of the Y-rotated cut QCMs by a vacuum deposition method. To obtain a uniform gold layer, the QCMs were symmetrically mounted on the platform that was rotated at a rate of 15 rpm. After a deposition time of 5 min, the resonant frequencies of the QCMs were measured. Then a new gold layer was deposited on the QCMs and their resonant frequencies were recorded again. Ten stepwise deposition processes were executed and the total frequency decrease was up to ca. 9 kHz.

### 2.4. Monitor the alternate adsorption processes of PDADMAC and $\text{SiO}_2$ nanoparticle

In the alternate adsorption experiment, the gold electrodes of the QCMs with  $\varphi = 35.25^\circ$  and  $35.65^\circ$  were first cleaned by dipping into a hot solution of 30%  $\text{H}_2\text{O}_2/\text{concentrated } \text{H}_2\text{SO}_4$  (50/50, v/v) for 30 s, washed by distilled water, and immersed in a solution of 1 mM MPA in ethanol overnight (15–24 h). Thus, a self-assembled monolayer (SAM) with carboxyl groups was coated on the gold electrodes of the QCM. The SAM-modified QCM was rinsed by ethanol and distilled water. Then the QCM was dried by a stream of nitrogen and mounted in the detection cell. Fifty milliliters of phosphate buffer (pH 7,  $1 \text{ mmol L}^{-1} \text{ Na}^+$ ) was added into the detection cell. After the stability of the baseline, a requisite amount of PDADMAC solution was added in the cell and the frequency shifts of the QCM were recorded with a time interval of 5.6 s. When a stable frequency shift was obtained, the cell was washed by the phosphate buffer. The adsorption of  $\text{SiO}_2$  nanoparticle onto the pre-adsorbed PDADMAC film was started by adding  $\text{SiO}_2$  nanoparticle solution into the cell. After washed by phosphate buffer, PDADMAC was added to the cell again to assemble the second PDADMAC adsorbed layer. Then the cell was washed and  $\text{SiO}_2$  nanoparticle was added into the cell for the second time. The adsorbed amounts were monitored in real time according to the frequency shifts of the QCM.

## 3. Results and discussion

### 3.1. Frequency–temperature coefficients of Y-rotated cut quartz resonators in air

Low frequency–temperature coefficient is useful to improve the detection limit of a QCM sensor. In order to reduce the value of  $dF/dT$  of a QCM sensor in a liquid phase, the quartz resonator that has a given negative  $dF/dT$  value in air may be superior to the classical AT-cut one in which there is  $dF/dT \approx 0$  in air at ca.  $26^\circ\text{C}$ . To explore the possibility of yielding an intrinsically temperature-compensated QCM in aqueous solution, the quartz wafers with different cut angles were prepared. The values of  $dF/dT$  of these QCMs in air were measured and illustrated in Fig. 2. It can be seen that the cut angle is an important parameter to influence the values of  $dF/dT$  of the Y-rotated cut quartz resonators. For example, the  $dF/dT$  values of the quartz resonators at  $25^\circ\text{C}$  were changed from 5 to  $-23 \text{ Hz}/^\circ\text{C}$  when the cut angle was increased from  $35.15^\circ$  to  $35.70^\circ$ . The positive temperature coefficients were obtained for the resonators with  $\varphi < 35.25^\circ$ . Negative  $dF/dT$  values were obtained for the quartz resonators with  $\varphi > 35.25^\circ$ . As the cut angle increases, the  $|dF/dT|$  values increased. In the temperature range of  $15\text{--}35^\circ\text{C}$ , the AT-cut resonator ( $\varphi = 35.25^\circ$ ) has the lowest  $|dF/dT|$  values among the twelve resonators prepared. Consequently, the QCM sensors in gaseous phase by using AT-cut quartz resonator will offer a largest signal-to-noise ratio, which, in turn, yields lowest detection limit.

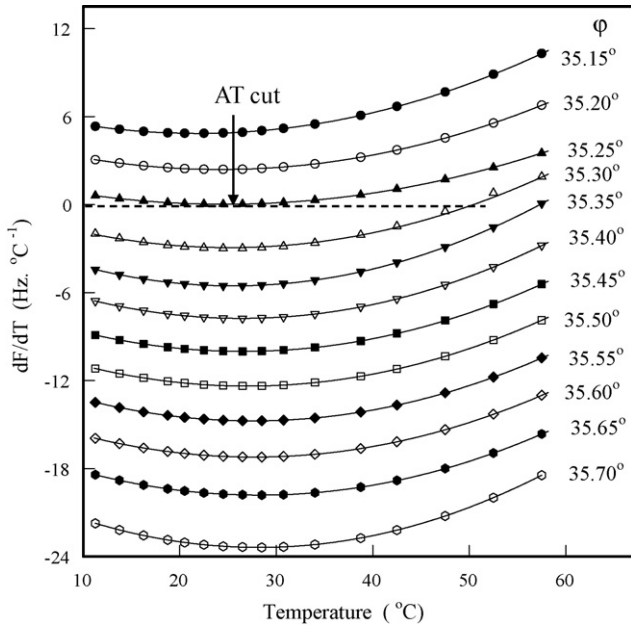


Fig. 2. Influence of the cut angle and temperature on the frequency–temperature coefficients of Y-rotated cut quartz resonators in air.

3.2. Frequency–temperature coefficients of Y-rotated cut QCMs in water

The frequency of a QCM in a liquid phase is related to both the surface mass loading and liquid properties, especially the viscosity ( $\eta$ ) and density ( $\rho$ ) of the liquid [9–12]. As the liquid properties are usually temperature dependent, the frequency–temperature characteristic of a QCM in liquid is different from that in air. The frequency shifts of the twelve Y-rotated cut QCMs in water were measured and illustrated in Fig. 3. With increasing liquid temperature, the frequency shifts of the QCMs with  $\phi < 35.55^\circ$  increase. But the total frequency shifts were decreased as the cut angle increases. A decrease in total frequency shift with increasing liq-

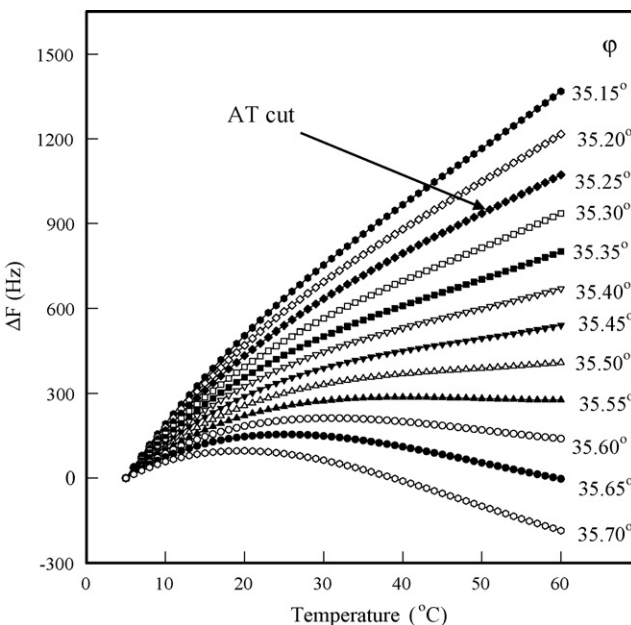


Fig. 3. Influence the cut angle on frequency shifts of Y-rotated cut QCMs with one side facing water during an elevating temperature process.

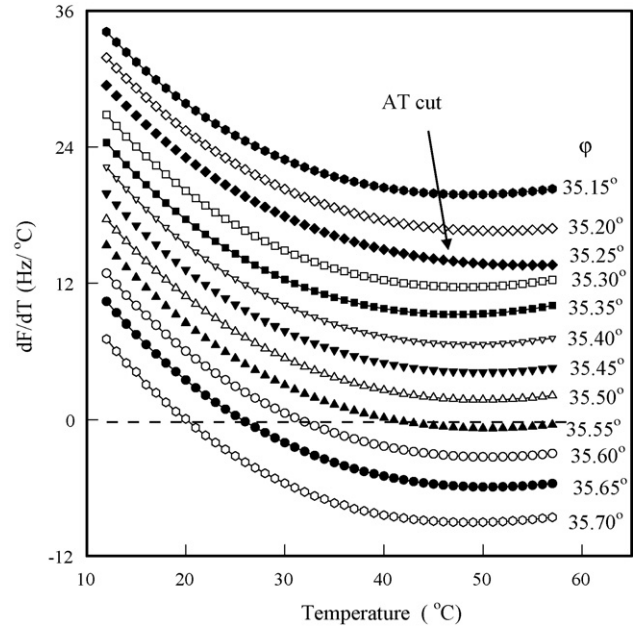


Fig. 4. Influence of the cut angle and temperature on the frequency–temperature coefficients of Y-rotated cut QCMs with one side facing water.

uid temperature was observed in QCMs with  $\phi > 35.55^\circ$ . With the frequency shift used, good reproducibility was obtained of these frequency–temperature curves. For a consideration of the concision in the figure, the error bars were not given in the figure.

Based on the data in Fig. 3, the values of  $dF/dT$  were estimated and shown in Fig. 4. It can be seen that the  $dF/dT$  values of the QCMs in water were much different from those of the resonators in air (see Fig. 2). It is worthy to note that the value of  $dF/dT$  was  $20 \text{ Hz}/^\circ\text{C}$  for the AT-cut QCM in water at  $26^\circ\text{C}$ . The reason is that the values of  $\eta$  and  $\rho$  of water decrease as the liquid temperature increases. According to Kanazawa [9], the frequency of an AT-cut QCM decreases linearly with increasing  $(\rho\eta)^{1/2}$ . Thus, positive  $dF/dT$  values were obtained for the AT-cut QCM in water in despite of the  $dF/dT$  value of the resonator itself is close to zero.

As seen in Fig. 2, the Y-rotated cut QCMs with  $\phi > 35.25^\circ$  have negative  $dF/dT$  values in air. When contacting with water, the Y-rotated cut QCMs with  $\phi > 35.25^\circ$  had smaller  $dF/dT$  values than the most common used AT-cut QCM. The points with  $dF/dT = 0$  in water were available for the QCMs with  $\phi \geq 35.55^\circ$ . As the cut angle was increased further, the point with  $dF/dT = 0$  was shifted to lower temperature. Thus, it is possible to obtain a QCM with low  $dF/dT$  value at a given temperature range by a specially designed cut angle. For example, there is  $dF/dT = 0$  for the QCM with  $\phi = 35.65^\circ$  in water near-by  $25^\circ\text{C}$ , which is especially suited for sensing applications in aqueous solutions. In the temperature range of  $23\text{--}27^\circ\text{C}$ , the averaged value of  $|dF/dT|$  is  $0.6 \text{ Hz}/^\circ\text{C}$  for the QCM with  $\phi = 35.65^\circ$ , which is only 3% of that of the AT-cut QCM. Hence, an approximate 10-fold improvement in detection limit may be achieved by using the QCM with  $\phi = 35.65^\circ$  instead of the AT-cut QCM.

3.3. Mass sensitivity of Y-rotated cut QCMs

According to the Sauerbrey equation [17], the frequency shift ( $\Delta F$ ) and the mass loading ( $\Delta m$ ) is expressed in Eq. (1):

$$\Delta F = \frac{-2f_0^2 \Delta m}{A\sqrt{C_{66}\rho_q}} \quad (1)$$



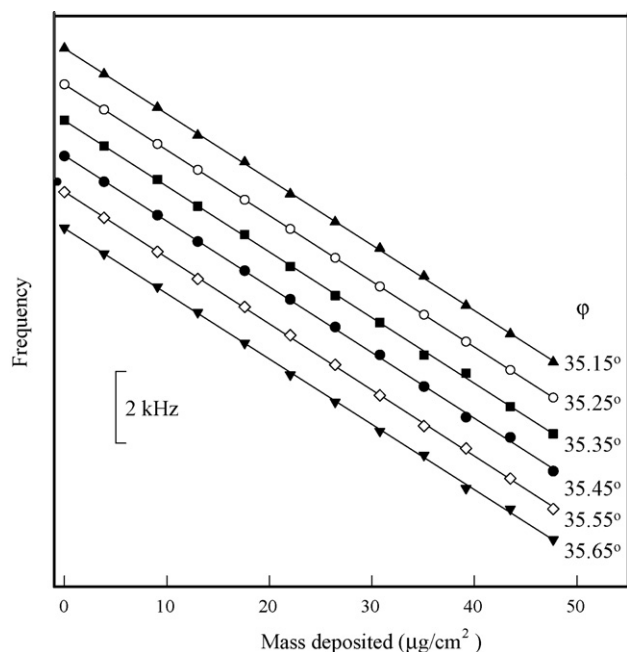


**Fig. 5.** Frequency shifts of cut angle of the rotational QCMs in the vacuum deposition process of gold on the electrodes. The curves were vertically moved for drawing clarity.

where  $f_0$  is the fundamental resonance frequency,  $A$  is the area for mass deposition,  $\rho_q = 2.649 \text{ g/cm}^3$  is the density of quartz crystal, respectively.  $C_{66}^D$  is a component of the elastic stiffness at the constant electric displacement of the Y-rotated cut quartz plate. The relationship between  $C_{66}^D$  and  $\varphi$  is given by [18]:

$$C_{66}^D = C_{66}^D \cos^2 \varphi + C_{44}^D \sin^2 \varphi + 2C_{14}^D \sin \varphi \cos \varphi \quad (2)$$

where  $C_{66}^D = 40.64 \text{ GPa}$ ,  $C_{44}^D = 57.97 \text{ GPa}$ ,  $C_{14}^D = -18.09 \text{ GPa}$  are the elastic stiffness of the quartz crystal [18], respectively.

According to Eq. (2), when  $\varphi$  was increased from  $35.15^\circ$  to  $35.70^\circ$ , the  $C_{66}^D$  value for quartz plates was increased from 29.35 to 29.40 GPa. The relative increase is only 0.17%, which results in a relative decrease of 0.085% in the mass sensitivity in Eq. (1). Hence, the mass sensitivity of the QCMs used will be very closed to that of the AT-cut QCM, which was supported by the experimental results in Fig. 5. In this experiment, a gold layer was deposited on the electrode of the QCM by a vacuum deposition method. The mass deposited was calculated from the frequency shift of the AT-cut QCM by using Eq. (1). It can be seen that the frequency shifts from the Y-rotated cut QCMs with cutting angle deviated slightly from the AT-cut are very close to those from the AT-cut QCM in the deposition process. In other words, the Y-rotated cut QCMs prepared with  $\varphi$  in the range of  $35.15\text{--}35.70^\circ$  have very similar sensitivity to the mass loading change onto their electrode surfaces as the AT-cut QCM. The averaged sensitivity to surface mass of these QCMs was  $-183 \pm 4 \text{ Hz } \mu\text{g}^{-1} \text{ cm}^2$ .

#### 3.4. Response of Y-rotated cut QCMs to viscodensity of the liquid phase

When a QCM was faced a liquid phase with one side, the non-mass effect of this configuration QCMs is mainly the viscodensity of the liquid. Kanazawa and Gordon [9] derived the following equation, which expresses the frequency shift of the QCM in contact

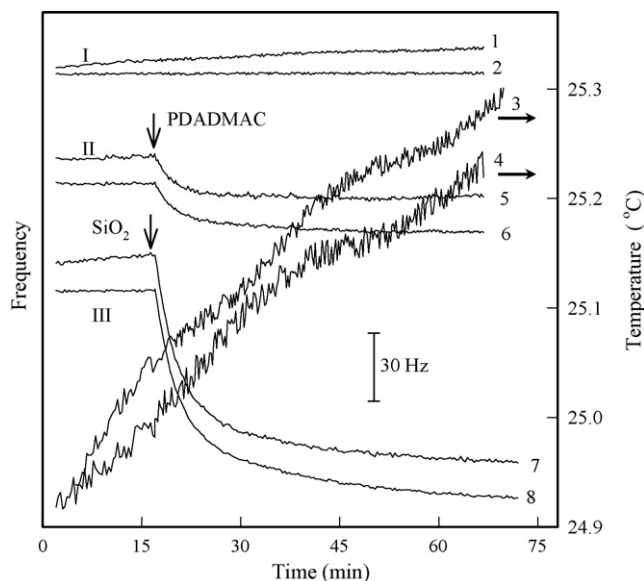


**Fig. 6.** Frequency shifts during the adsorption processes of PDMAAC and nanoparticle of  $\text{SiO}_2$ . (I) Baseline of QCMs with (1)  $\varphi = 35.25^\circ$  and (2)  $\varphi = 35.65^\circ$ ; (3 and 4): temperature drafts in measurement of curves 1 and 2; (II) frequency shifts of QCMs with (5)  $\varphi = 35.25^\circ$  and (6)  $\varphi = 35.65^\circ$  during the adsorption of  $100 \text{ mg L}^{-1}$  PDMAAC on SAM of MPA; (III) frequency shifts of QCMs with (7)  $\varphi = 35.25^\circ$  and (8)  $\varphi = 35.65^\circ$  during the adsorption of  $50 \text{ mg L}^{-1}$   $\text{SiO}_2$  nanoparticle onto the pre-adsorbed PDADMAC layer. Measuring media:  $1 \text{ mmol L}^{-1}$  phosphate buffer of pH 7. The experiments were performed in room temperature of  $25^\circ \text{C}$ . The curves were vertically moved for drawing clarity.

with a Newtonian liquid.

$$\Delta F = -\sqrt{\frac{f_0^3 \eta \rho}{\pi C_{66}^D \rho_q}} \quad (3)$$

As discussed above, the values of  $C_{66}^D$  were very close in these Y-rotated cut QCMs prepared. According to Eq. (3), these QCMs will have similar frequency responses to  $(\rho\eta)^{1/2}$  of the liquid, which is supported by the experimental results. It was revealed that the frequencies of these Y-rotated cut QCM sensors decrease linearly with increasing  $(\rho\eta)^{1/2}$  value. The slopes of the plotting of  $\Delta F$  versus  $(\rho\eta)^{1/2}$  were close in the 12 QCMs. The mean of  $\partial F/\partial(\rho\eta)^{1/2}$  in the 12 QCMs was  $-1.82 \pm 0.06 \times 10^4 \text{ g}^{-1} \text{ cm}^2 \text{ s}^{-1/2}$ , which is a little greater than the expected value of  $-1.73 \times 10^4 \text{ g}^{-1} \text{ cm}^2 \text{ s}^{-1/2}$  in Eq. (3).

#### 3.5. Comparison of the baseline drift of QCM sensors

Usually, the frequency shift is used as the measuring signal of a QCM sensor. Hence, a stable baseline is necessary in the applications of the QCM sensors. Because the frequency of the AT-cut QCM in liquid phase is temperature dependent, it is very important to keep a constant liquid temperature during an experimental measurement. To demonstrate the advantage of the intrinsically temperature-compensated QCM sensor, its baseline was compared with that of the AT-cut QCM. As seen in Fig. 6, the baseline draft of the QCM with  $\varphi = 35.65^\circ$  was much less than that of the AT-cut QCM. In this experiment, the detection cell without a thermostatic water jacket was used. During the measurement of the baselines, a rise in liquid temperature of ca.  $0.4^\circ \text{C}$  was observed due to the mechanical and heat energy from the magnetic mixer. The baseline drafts were 8.3 Hz for AT-cut QCM and only 0.4 Hz for the QCM with  $\varphi = 35.65^\circ$ . The much lower baseline drift in the QCM with  $\varphi = 35.65^\circ$  is a useful characteristic for its practical applications in which the detection cell even without constant temperature device can be used.

**Table 1**  
Regressed parameters for the alternate adsorption processes of PDADMAC and SiO<sub>2</sub> nanoparticle

Surface	Adsorbate	$k_a$ (s <sup>-1</sup> L mg <sup>-1</sup> )	$K$ (L/g)	$\Gamma_\infty$ (mg/m <sup>2</sup> )
SAM of MPA on gold	PDADMAC	0.0643	12.50	2.21
First PDADMAC adsorption layer	SiO <sub>2</sub> nanoparticle	0.0198	37.9	7.56
SiO <sub>2</sub> adsorption layer	PDADMAC	0.0487	7.84	3.55
Second PDADMAC adsorption layer	SiO <sub>2</sub> nanoparticle	0.0165	27.2	15.2

### 3.6. Monitor the alternate adsorption processes of PDADMAC and SiO<sub>2</sub> nanoparticle by intrinsically temperature-compensated QCM sensor

Polyelectrolytes have been found widespread applications in many industrial processes and in numerous products of our daily life [19,20]. An important property of polyelectrolytes is their tendency to adsorb onto solid surfaces [21]. Polyelectrolyte adsorption to charged interfaces is a fundamental problem throughout the natural sciences and in many technological applications. Experimentally, the adsorption behavior of polyelectrolyte systems has been studied quite extensively by various techniques [22–28]. In this work, the interaction between polyelectrolyte and nanoparticle was studied by the QCM sensors. A polyelectrolyte–nanoparticle system was chosen because such systems were applied in many industrial processes such as paper making, paints, coatings and ceramic processing [29–31].

In the alternate adsorption experiments, an SAM film with carboxyl groups was firstly coated on the gold electrodes of the QCM by adsorption of MPA. As shown in Fig. 6, the PDADMAC cation can be adsorbed on the negative charged SAM film of MPA. The frequency shift of the QCM approached to a stable level after an adsorption time of 15 min. After the adsorption, the adsorbed layer was washed by the measuring medium. The adsorption of PDADMAC onto the SAM is strong enough to keep from washing off by the medium. When SiO<sub>2</sub> nanoparticle was added into the detection cell, the frequency of the QCM decreases again, which indicates the adsorption of SiO<sub>2</sub> nanoparticle onto the pre-adsorbed PDADMAC adsorbed layer. The reason is that the surface was positively charged after the adsorption of the PDADMAC layer.

The kinetic of an alternate adsorption process consists of a rapid adsorption process and a slow conformation rearrangement process [19,21]. Hence, in the adsorption process of PDADMAC or SiO<sub>2</sub> nanoparticle, the frequency shifts of the QCM with  $\varphi = 35.65^\circ$  were analyzed by the model in Eq. (4).

$$\Delta F = \Delta F_1 e^{-k_1 t} + \Delta F_2 e^{-k_2 t} - \Delta F_0 \quad (4)$$

where  $\Delta F_0$ ,  $\Delta F_1$  and  $\Delta F_2$  are the regressed parameters,  $t$  is the adsorption time,  $k_1$  and  $k_2$  are the observed rate constants, respectively. The first term in the right of Eq. (4) corresponds to the rapid increase in mass adsorbed in the early adsorption process. The second term denotes a slow increase in mass adsorbed in the later conformation rearrangement process.

For the purpose of comparison, the frequency shifts from an AT-cut QCM were also measured during the alternate adsorption processes. It can be seen that the frequency responses from the two QCM sensors were similar in the early adsorption processes. But in later conformation rearrangement process, the frequency decrease arising from the adsorption was small and it was partly offset by the baseline draft in the AT-cut QCM sensor.

In the early adsorption process, the frequency shifts of the QCM with  $\varphi = 35.65^\circ$  can also be fitted by the model in Eq. (4) without the second term of  $\Delta F_2$  and  $k_2$ . The reason is that the conformation rearrangement of the adsorbed layer is a slow process and the mass change is small, i.e.,  $k_1 \gg k_2$  and  $|\Delta F_1| \gg |\Delta F_2|$ . The contribution of the second term containing  $\Delta F_2$  and  $k_2$  was included in the first

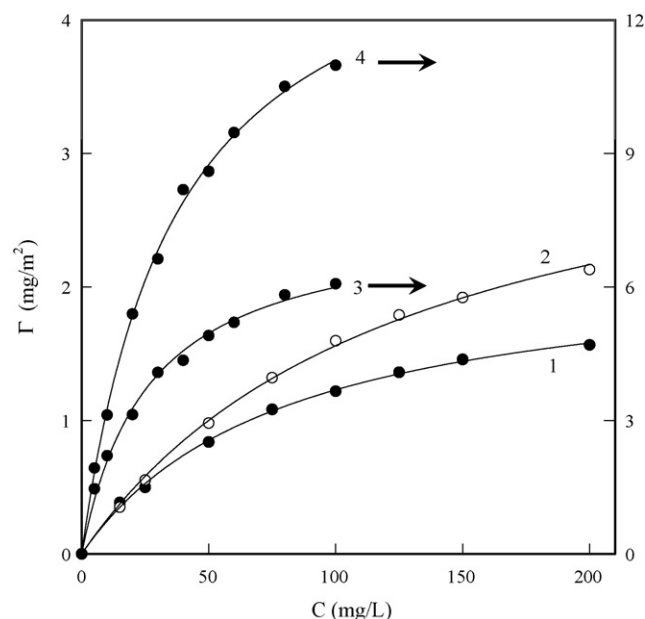


**Fig. 7.** Adsorption isotherms of PDADMAC and SiO<sub>2</sub> nanoparticle in the alternate adsorption. (1) PDADMAC onto SAM of MPA. (2) PDADMAC onto first pre-adsorbed SiO<sub>2</sub> nanoparticle layer. (3) SiO<sub>2</sub> nanoparticle onto the first pre-adsorbed PDADMAC adsorbed layer. (4) SiO<sub>2</sub> nanoparticle onto the second PDADMAC adsorbed layer.

term in the data fitting calculation. It was shown that there was good linearity between  $k_1$  and the concentration of adsorbate ( $C$ ). The slopes of  $k_1$  versus  $C$  were treated as the adsorption rate constants ( $k_a$ ) and listed in Table 1. It was revealed that the adsorption rate constants for the second adsorbed layers are a little less than those of the first ones in the alternate adsorption processes.

According to Sauerbrey equation in Eq. (1), the adsorption isotherms for PDADMAC and SiO<sub>2</sub> nanoparticle were shown in Fig. 7. It was revealed that these adsorption isotherms were well fitted by the Langmuir equation in Eq. (5).

$$\Gamma = \frac{\Gamma_\infty KC}{1 + KC} \quad (5)$$

where  $\Gamma_\infty$  is the saturated adsorbed mass,  $K$  is the adsorption equilibrium constant. According to the adsorption isotherms, the values of  $K$  and  $\Gamma_\infty$  were evaluated and listed in Table 1. It can be seen that the adsorption equilibrium constants of the second adsorbed layers are less than those of the first ones. But the saturated adsorbed masses for the second adsorbed layers of PDADMAC or SiO<sub>2</sub> nanoparticle are greater than those of the first ones. These results suggested that there are conformational differences between the alternately adsorbed layers for cationic polyelectrolyte and silica nanoparticle.

## 4. Conclusions

The experimental results described above demonstrated that the frequency–temperature characteristic of a QCM sensor can be adjusted by the cut angle of the quartz crystal wafers. When a QCM

sensor is in contact with a liquid phase, its frequency–temperature coefficient is related to temperature characteristic of the resonator itself and the properties of the liquid. In a traditional AT-cut QCM of 9 MHz, there is  $dF/dT \approx 0$  in air while  $dF/dT \approx 20 \text{ Hz}/^\circ\text{C}$  in water nearby  $26^\circ\text{C}$ , respectively. But in a 9 MHz QCM with a cut angle of  $35.65^\circ$ , the value of  $dF/dT$  was about  $-20 \text{ Hz}/^\circ\text{C}$  in air while close to zero in water. The intrinsically temperature-compensated sensor was expected to enhance the signal-to-noise ratio, which, in turn, to improve its detection limit in liquid phase. It was shown that the frequency responses to mass and viscodensity are very close among the Y-rotated cut QCMs with the cut angles in the range of  $35.15\text{--}35.7^\circ$ . The applicability of the QCM in new cut angle was demonstrated in monitoring the alternate adsorption processes of polyelectrolyte and nanoparticle.

### Acknowledgements

This work is supported by the National Natural Science Foundation of China (Nos. 20775045, 20527005) and the Natural Science Foundation of Shandong Province (Y2007B03).

### References

- [1] A.R. Hillman, in: A.J. Bard, M. Stratmann (Eds.), *Encyclopaedia of Electrochemistry*, vol. 3, Wiley, New York, 2003, p. 230.
- [2] K.A. Marx, *Biomacromolecules* 4 (2003) 1099.
- [3] S.Z. Yao, *Piezoelectric Chemistry and Biosensors*, Hunan Normal University Press, Changsha, 1997.
- [4] D.A. Buttry, M.D. Word, *Chem. Rev.* 92 (1992) 1355.
- [5] L. Tan, S.Z. Yao, Q.J. Xie, *Talanta* 71 (2007) 827.
- [6] H.O. Fatoyinbo, K.F. Hoettges, S.M. Reddy, M.P. Hughesa, *Biosens. Bioelectron.* 23 (2007) 225.
- [7] S. Tombelli, M. Minunni, A. Santucci, M.M. Spiriti, M. Mascini, *Talanta* 68 (2006) 806.
- [8] H. Wang, D. Li, G.L. Shen, R.Q. Yu, *Talanta* 62 (2004) 199.
- [9] K.K. Kanazawa, J.G. Gordon, *Anal. Chim. Acta* 117 (1985) 99.
- [10] H. Muramatsu, E. Tamiya, I. Karube, *Anal. Chem.* 60 (1988) 2142.
- [11] D.S. Ballantine, R.M. White, S.J. Martin, *Acoustic Wave Sensors, Theory, Design, and Physico-chemical Applications*, Academic Press, San Diego, 1997.
- [12] A.H. Zhou, J.D. Zhang, Q.J. Xie, S.Z. Yao, *Sens. Actuators B* 67 (2000) 68.
- [13] J.J. Caron, R.B. Haskell, J.C. Andle, J.F. Vetelino, *Sens. Actuators B* 35 (1996) 141.
- [14] B. Jakoby, J. Bastemeijer, M.J. Vellekoop, *Sens. Actuators B* 82 (2000) 83.
- [15] Q. Kang, Y. Qi, P. Zhang, D.Z. Shen, *Talanta* 72 (2007) 1474.
- [16] D.Z. Shen, Q. Kang, P. Zhang, C.Y. Guo, J. Lan, *Anal. Chim. Acta* 525 (2004) 205.
- [17] G. Sauerbrey, *Z. Physik.* 155 (1959) 206.
- [18] P.L. Zhang, L.W. Zhong, *Piezoelectric Materials and Elements Physics*, Shandong Science and Technology Press, Jinan, 1997, pp. 323, 112.
- [19] D. Voisin, B. Vincent, *Adv. Colloid Interface Sci.* 106 (2003) 1.
- [20] M. Schonhoff, *Curr. Opin. Colloid Interface Sci.* 8 (2003) 86.
- [21] J. Kotz, S. Kosmella, T. Beitz, *Prog. Polym. Sci.* 26 (2006) 1199.
- [22] S. Schwarz, H.M. Buchhammer, K. Lunkwitz, H.J. Jacobasch, *Colloids Surf. A* 140 (1998) 377.
- [23] D.J.F. Taylor, R.K. Thomas, J.D. Hines, K. Humphreys, J. Penfold, *Langmuir* 18 (2002) 9783.
- [24] J. Kim, G. Kim, P.S. Cremer, *J. Am. Chem. Soc.* 124 (2002) 8751.
- [25] S. Minko, Y. Roiter, *Curr. Opin. Colloid Interface Sci.* 10 (2005) 9.
- [26] M.A. Plunkett, P.M. Claesson, M. Ernstsson, M.W. Rutland, *Langmuir* 19 (2003) 4673.
- [27] S. Schwarz, K.J. Eichhorn, E. Wischerhoff, A. Laschewsky, *Colloids Surf. A* 159 (1999) 491.
- [28] A. Baba, M.K. Park, R.C. Advincula, W. Knoll, *Langmuir* 18 (2002) 4648.
- [29] O. Spalla, *Curr. Opin. Colloid Interface Sci.* 7 (2002) 179.
- [30] T. Sennerfors, D. Solberg, F. Tiberg, *J. Colloid Interface Sci.* 254 (2002) 222.
- [31] S.C. Liufu, H.N. Xiao, Y.P. Li, *J. Colloid Interface Sci.* 285 (2005) 33.



## Reduction of severe bovine serum associated matrix effects on carboxymethylated dextran coated biosensor surfaces

Chen Situ<sup>a,\*</sup>, Alastair R.G. Wylie<sup>b</sup>, Alastair Douglas<sup>b</sup>, Christopher T. Elliott<sup>a</sup>

<sup>a</sup> Institute of Agri-Food and Land Use, Queen's University Belfast, David Keir Building, Stranmillis Road, Belfast BT9 5AG, United Kingdom

<sup>b</sup> AgriFood & Biosciences Institute, Newforge Lane, Belfast BT9 5PX, United Kingdom

### ARTICLE INFO

#### Article history:

Received 29 November 2007

Received in revised form 6 April 2008

Accepted 16 April 2008

Available online 2 May 2008

#### Keywords:

Matrix effect

Biosensor

Bovine serum

Surface plasmon resonance (SPR)

Non-specific binding (NSB)

Carboxymethyl dextran

### ABSTRACT

Surface plasmon resonance (SPR) based biosensor technology has been widely used in life science research for many applications. While the advantages of speed, ruggedness, versatility, sensitivity and reproducibility are often quoted, many researchers have experienced severe problem of non-specific binding (NSB) to chip surfaces when performing analysis of biological samples such as bovine serum. Using the direct measurement of the bovine protein leptin, present in bovine serum samples as a model, a unique buffering system has been developed and optimised which was able to significantly reduce the non-specific interactions of bovine serum components with the carboxymethyl dextran chip (CM5) surface on a Biacore SPR system. The developed NSB buffering system comprised of HBS-EP buffer, containing 0.5 M NaCl, 0.005% CM-dextran, pH 9.0. An average NSB reduction ( $n = 20$ ) of 85.9% and 87.3% was found on an unmodified CM5 surface and a CM5 with bovine leptin immobilised on the chip surface, respectively. A reduction in NSB of up to 94% was observed on both surfaces. The concentration of the constitutive components and pH of the buffer were crucial in achieving this outcome.

© 2008 Elsevier B.V. All rights reserved.

### 1. Introduction

The need for more samples to be tested for an ever-increasing range of complex substances under more defined performance criteria has resulted in an increased demand for sensitive but robust analytical methods capable of high-throughput and with simple sample preparation procedure. Recent advances in bio-analytical sciences have greatly facilitated this need. One of the most frequently exploited techniques is real-time biospecific interaction analysis (BIA) utilising surface plasmon resonance (SPR) technology that is now widely used in many life science research applications [1–4]. The advantage of SPR biosensor method over other technologies is the ability to deliver rapid and reliable analyte detection in real-time, without the use of labels. The applicability of this technology in the fields of animal health monitoring and food analysis has made a valuable addition to the spectrum of analytical tools available.

A number of different commercial SPR platforms exist, but the technology provided by the GE Healthcare Company, Biacore (Biacore AB, Uppsala, Sweden) is a popular choice for method developers in food diagnostics [5,6]. Biosensor analysis based on

carboxymethylated dextran (CM-dextran) surfaces has provided a reliable platform for the rapid determination of a wide range of compounds relevant to food safety and quality, and an equally wide variety of food and related sample types. But while the advantages of speed, ruggedness, versatility, sensitivity and reproducibility are often quoted, many researchers have experienced severe problem of non-specific binding (NSB) in biological samples. It is generally recognized that matrix interference, resulting in interaction between components of biological specimens and the sensor chip surface, is a major technical difficulty in assay development and has, more than any other single factor, limited the success of SPR biosensor system in the study of binding events in complex biological samples such as serum and blood due to an inability to control non-specific adsorption [7].

A number of strategies have been employed to resolve the problem of NSB in real-time BIA applications with various degrees of success. In some cases, worthwhile reductions in NSB have been achieved and workable assays have been developed. For example, Johnsson et al. introduced a simple precipitation step using saturated ammonium sulphate (SAS) to remove proteins of bovine serum and reported the development of a sensitive bioassay for the detection of drug residue (benzimidazole) in bovine serum [8]. However, this technique is not suitable for analysis of proteins since the precipitation step will remove all proteins from the serum sample. No apparent success has been reported in applications where the direct measurement of an analyte present in bovine serum on

\* Corresponding author. Tel.: +44 2890 976546; fax: +44 2890 976513.  
E-mail address: [c.situ@qub.ac.uk](mailto:c.situ@qub.ac.uk) (C. Situ).

carboxymethylated dextran coated biosensor surfaces. Masson et al. claimed that better performance could be obtained for bovine serum assay by replacing the CM-dextran with other biocompatible polymers [9]. High-throughput analysis of serum samples is highly dependent on an ability to assay samples directly and without the need to perform time-consuming and expensive sample preparation prior to analysis.

The present study used the measurement of bovine leptin protein in bovine sera as a model to investigate the possibility of assembling a buffering system to minimise non-specific binding of bovine serum components to the surface of a CM-dextran coated chip (CM5). Leptin, a 146 amino acid peptide hormone (16 kDa) is produced and released from adipocytes [10], and is one of a group of potential protein biomarkers for the detection of anabolic steroid misuse in cattle.

## 2. Experimental

### 2.1. Instrument and reagents

The SPR biosensor instrument (Biacore® Q), carboxymethylated dextran coated sensor chips (CM5 research grade), HBS-EP buffer (10 mM HEPES, 150 mM NaCl, 3.4 mM EDTA, 0.005% P20, pH 7.4), the amine coupling kit containing *N*-hydroxysuccinimide (NHS), *N*-ethyl-*N'*-(3-diethyl-aminopropyl) carbodiimide (EDC), and ethanolamine hydrochloride (pH 8.5) were obtained from Biacore AB (Uppsala, Sweden). Biacore control software (version 3.0.1) was used for instrument operation and data handling. Recombinant bovine leptin (purity >95%) was purchased from Oxford Bio-Innovation Ltd (DSL-OBL, Oxon, UK). Synthetic leptin fragment (<sub>77</sub>SNLDLENLRDLLHLLAA<sub>92</sub>) was supplied by AgriFood and Biosciences Institute (AFBI, Belfast, UK). Anti-leptin antibody was raised in guinea pigs against recombinant ovine leptin (a gift from Professor Arieh Gertler of the Hebrew University of Jerusalem, Israel) and has been used in radioimmunoassay (RIA) for the analysis of both bovine and ovine leptin. Carboxymethyl dextran sodium salts (MW: 75, 500, and 2000 kDa) were purchased from Ssens (Hengelo, The Netherlands). Sodium dihydrogen orthophosphate and di-sodium hydrogen orthophosphate were purchased from BDH Laboratory Supplies (Poole, UK). Carboxymethyl dextran sodium salt and all other chemicals were purchased from Sigma-Aldrich (Poole, UK). Deionised water was obtained using Millipore reverse osmosis and Milli-Q water polishing systems.

Tris-HCl buffer (pH 7.4) was prepared by mixing 44.2 ml 0.1 M solution of tris (hydroxymethyl aminomethane) and 50 ml of 0.1 M HCl, and then diluted to a total of 200 ml with deionised water. Phosphate buffer (pH 7.2) was prepared by mixing 28 ml of 0.2 M solution of sodium dihydrogen orthophosphate and 72 ml of 0.2 M solution of di-sodium hydrogen orthophosphate. Non-specific binding buffer (NSB buffer) was based on HBS-EP (10 mM HEPES, 3 mM EDTA and 0.005% Tween 20) contained 0.5 M NaCl and 0.005% CM-D500, and was adjusted to pH 9.0 using 1 M NaOH.

### 2.2. Methods

#### 2.2.1. Preparation of the SPR sensor chip surface

Modified coupling procedures described previously by Johnsson et al. [11] were used for external immobilisation of recombinant bovine leptin or leptin peptide fragment onto the surface of a CM5 sensor chip. Briefly, the chip surface was activated with 50  $\mu$ l of a mixture of 0.4 M (EDC) and 0.1 M (NHS) (1:1; v/v) for 20 min at ambient temperature on bench. The reactant was removed and 50  $\mu$ l of leptin peptide fragment (1 mg ml<sup>-1</sup> in 10 mM sodium acetate, pH 4.5) or whole bovine leptin (500  $\mu$ g ml<sup>-1</sup> in 10 mM

sodium acetate, pH 4.5) was added and allowed to remain in contact with the chip surface for 2 h (peptide fragment) or overnight (whole leptin) at ambient temperature. Unreacted sites were blocked by the addition of 50  $\mu$ l of 1 M ethanolamine (pH 8.5) for 20 min at room temperature. The reactant was removed and the chip surface was washed with deionised water and then dried under a stream of nitrogen gas. The prepared chip was stored at 4 °C in the presence of desiccant.

#### 2.2.2. R<sub>max</sub> determinations

R<sub>max</sub> is the maximum binding capacity of the surface ligand (peptide) for the anti-peptide antibody, as measured in resonance units (RUs; where 1000 RU  $\approx$  1 ng mm<sup>2</sup> for proteins). R<sub>max</sub> provides useful information about the ability of immobilised ligand and binding partner to interact. R<sub>max</sub> values were obtained by injecting high concentrations of antibody (e.g.  $\times$ 10 dilution) over the chip surface at a low flow rate (5  $\mu$ l min<sup>-1</sup>) for up to 10 min (injection time). The increase in relative response units over this period is denoted as the R<sub>max</sub> value.

#### 2.2.3. Preparation of bovine serum

Bovine serum was prepared by centrifugation (2500 rpm, 15 min) of clotted bovine blood obtained from local cattle. Serum samples were diluted 10-fold with appropriate buffer prior to analysis.

#### 2.2.4. SPR biosensor assay

All experiments were performed on a Biacore® Q and Evaluation software 1.0 was used for data analysis. Freshly diluted bovine serum was mixed with the same volume of diluted antibody and injected over the sensor chip surface for 4 min at a flow of 20  $\mu$ l min<sup>-1</sup>. The surface was regenerated by a 1-min pulse of 50 mM sodium hydroxide at a flow rate of 20  $\mu$ l min<sup>-1</sup>.

The leptin assay was designed as a solution competition (inhibition) assay. The high molecular weight (HMW) interactant (anti-leptin antibody) was added to the bovine serum sample containing the analyte of interest. The analyte itself or an analogue (leptin or peptide fragment) was immobilised on the surface and used to determine the concentration of free HMW interactant in solution. Analyte concentration was measured in terms of inhibition of binding of the HMW interactant (antibody) to the surface. A low response indicated a high analyte concentration (the concentration of free interactant in solution was low due to their binding to the analyte in sample). When the concentration of analyte present was known, i.e. bovine serum spiked with a range of analyte concentrations, a calibration curve could be constructed and used to measure the analyte concentration in unknown samples.

For the study of the non-specific binding of serum components on the CM5 sensor chip surfaces, bovine serum diluted 10-fold with appropriate buffer was injected over the chip surfaces, i.e. blank and leptin immobilised surfaces, with or without the presence of anti-leptin antibody. Two sets of data (i.e. relative response units) were subjected to statistical analysis, as other assay parameters (buffer conditions etc.) remained the same. Preparation of calibration curves was not needed for this task.

## 3. Results and discussion

### 3.1. Preparation of SPR sensor chip surface

The sensor surface immobilised with recombinant bovine leptin displayed an R<sub>max</sub> of 12.6 kRU while the leptin fragment coated surface gave an R<sub>max</sub> of 17.4 kRU. For concentration measurements utilising small molecule coated surfaces (e.g. drug or peptides) to

determine the concentration of free binding partner available (usually an antibody), an  $R_{max}$  in the range of 6–12 kRU has been shown to deliver a suitable degree of assay sensitivity (unpublished data). The use of a selected leptin fragment in this study was due to limitations in the quantity of recombinant bovine leptin available, and previous reported that antibodies raised against a synthetic peptide with similar amino acid sequence could recognise not only the peptide fragment but also the native leptin protein molecule. Such anti-leptin fragment antibodies have been successfully used to measure leptin serum concentrations in cows [12,13].

The choice of immobilisation method has to be considered carefully. Preferably, the ligand should be attached covalently to the surface matrix to facilitate reproducibility of the chip surface but the way in which ligand is immobilised onto the sensor surface is of great importance for generating a uniform binding response. For short peptides or terminal peptide fragments, a well-defined orientation coupling (N- or C-terminal attachment) may be needed to ensure the maximum exposure of the ligand molecule to the injected binding partner. Site-directed immobilisation can be achieved by utilising an existing functional group present in the amino acid (AA) residue or by addition of an AA that contains ionisable side chains, e.g. lysine. Controlled orientation of ligand has been shown to enhance ligand recognition by analytes [14,15].

Other factors that need to be considered in the production of the immobilised surfaces include preconcentration of ligands over the surface matrix, the concentration of ligands used, incubation times, and the ionic strength of the coupling buffer. For immobilisation of ligand onto the CM5 chip surfaces, preconcentration is accomplished by electrostatic attraction between negative charges of the carboxymethyl dextran matrix surface (when  $pH > 3$ ) and positive charges of the ligand at pH values below its  $pI$ . In the present study, the immobilisation of recombinant bovine leptin ( $pI$  8.68) onto CM5 surface was achieved using the standard amine coupling procedure and the ready-to-use coupling buffer from Biacore (10 mM sodium acetate, pH 4.5). For the production of the leptin fragment ( $pI$  4.27) surface, the N-terminal residue of serine ( $pI$  5.7) contains an additional attachment point at the hydroxyl group; it was therefore targeted as the site of immobilisation using also the amino coupling procedure. The use of commercial ready-to-use coupling buffer (pH 4.5) also favours immobilisation of the N-terminus; due to the positive charge of the N-terminal serine residue under this condition, i.e. the pH value of the coupling buffer (4.5) was lower than the  $pI$  of the serine (5.7) but higher than the  $pI$  of the peptide fragment (4.27).

It is the experience of the present researchers that ligand concentrations in the range 0.5–1.0 mg ml<sup>-1</sup> are sufficient for the vast majority of immobilisation procedures when they are performed externally with a longer incubation time (minimum 2 h), while the range 10–200 µg ml<sup>-1</sup> is used as recommended by Biacore, when coupling is performed internally within the biosensor system. For leptin peptide surface, 1 mg ml<sup>-1</sup> was used whilst 0.5 mg ml<sup>-1</sup> was applied to generate the bovine leptin surface. With regard to the ionic strength of the coupling buffer used, a low concentration (10–20 mM) is recommended and is suitable for most applications but higher ionic strength have also been used routinely (e.g. 60 mM sodium borate buffer) in this laboratory.

### 3.2. Preparation of bovine serum

A range of assay buffer factors (dilution, composition, pH and ionic strength) were examined for effects on reduction of NSB and assay performance with respect to the ability to detect leptin in bovine serum samples without the need for sample extraction but at sufficiently high sensitivity.

#### 3.2.1. Sample dilution

Bovine serum samples were analysed at dilutions of 1:2, 1:5, 1:10, 1:20, 1:50, and 1:100 in HBS-EP buffer (Biacore AB, Sweden). The most substantial reduction of NSB was found at 1:100 dilution (3.8 kRU at 1:2 vs 0.4 kRU at 1:100). However, at this dilution, the ability of the assay to detect the presence of bovine serum leptin at the normal range of 1–20 ng ml<sup>-1</sup> was compromised, i.e. the detection limit was of the order of  $1 \times 10^{-2}$  ng ml<sup>-1</sup> using this approach.

#### 3.2.2. Buffer composition

Two different buffering systems were investigated: a Tris–HCl buffer (10 mM, 0.5 M NaCl, pH 7.4) and a commercial HBS-EP buffer. Table 1 shows the effects on binding behaviour of two randomly selected bovine serum samples (10-fold dilution injected over the sensor surface at a flow rate of 20 µl min<sup>-1</sup>) on three different sensor surfaces, i.e. CM5 chips immobilised with leptin fragment (Leptin 16) or, with recombinant bovine leptin, and a blank CM5 surface. A higher NSB was found with the Tris–HCl buffer in all cases compared to HBS-EP buffer. The highest relative response (RU) was observed on the Leptin 16 surface when compared with the other two surfaces (bovine leptin and CM5 blank) for both HBS-EP and Tris–HCl buffer.

Using the CM5 blank surface, consistent responses were found for the two samples tested with the same buffer but significantly different between the two buffering systems, suggesting that the NSB binding behaviour of the serum matrix towards the CM5 dextran surface was affected by buffer composition.

Moreover, the NSB behaviour was significantly altered on the chip surfaces by differential ligand immobilisation, i.e. decreased NSB was observed with recombinant bovine leptin chip on the surface and increased on the Leptin 16 surface. This effect was probably due to the size and structure of the recombinant bovine leptin molecule through a barrier effect at the surface, preventing binding between serum components and the chip matrix while the linear characteristics of leptin fragment (similar to those of dextran), may favour NSB by creating an extended molecular layer. The Leptin 16 surface was therefore selected for further investigation of a potential buffering system that could lead to substantial reduction in NSB. Similar binding behaviour to that observed using Tris–HCl buffer, was found with phosphate buffer (0.1 M, 0.5 M NaCl, pH 7.2) on a CM5 blank chip in a separate experiment. An increased temperature (up to 56 °C) also had no effect on NSB reduction using the HBS-EP system.

#### 3.2.3. Ionic strength

It has been reported that electrostatic interactions between protein molecules are weaker at high ionic strength [16]. In the present study the optimal ionic strength for the Leptin 16 surface as determined by the degree of NSB reduction was found to be 0.5 M NaCl, over the range 0.15–1.0 M, i.e. a 53% drop in NSB (from 1135 to 538 RU) observed at 0.5 M NaCl (Table 2). A different profile was obtained for the CM5 blank surface, i.e. a higher ionic strength (1.0 M) resulted in a lower NSB (from 816 to 309 RU, reduction by

**Table 1**  
Comparative results of binding behaviour of bovine serum prepared in HBS-EP or Tris–HCl buffer on different surfaces

Bovine serum 1	Leptin 16 (RU)	Bovine leptin (RU)	CM5 blank (RU)
HBS-EP pH 7.4	1168	496	816
Tris–HCl pH 7.4	1907	1285	2088
Bovine serum 2			
HBS-EP pH 7.4	1690	600	818
Tris–HCl pH 7.4	2906	1197	2215

**Table 2**

Resonance units measured following injection of bovine serum over CM5 blank and Leptin 16 chips at different concentrations of CM-D500 and ionic strengths (NaCl) (HBS-EP, pH 7.4)

CM5 blank				Leptin 16			
NaCl (M)	RU	CM-D500 (% m/v)	RU	NaCl (M)	RU	CM-D500 (% m/v)	RU
0.15	816	0.01	248	0.15	1135	0.01	784
0.3	502	0.03	250	0.3	725	0.03	790
0.4	417	0.04	238	0.4	703	0.04	849
0.5	365	0.05	253	0.5	538	0.05	848
0.6	340	0.06	241	0.6	565	0.06	881
0.7	337	0.07	242	0.7	615	0.07	990
0.8	330	0.08	239	0.8	613	0.08	1028
0.9	324	0.09	258	0.9	617	0.09	1055
1.0	309	0.1	265	1.0	577	0.1	1181

62%). The data illustrates that different NSB effects will result from varying the ionic strength (NaCl) on modified sensor surfaces, and this is a buffer parameter that should be considered for optimisation during assay development.

### 3.2.4. Optimising ionic strength and CM-D500 concentrations

The addition of a range of CM-dextran with different molecular weights (12–2000 kDa) to HBS-EP (0.15 M NaCl, pH 7.4) was examined. CM-D500 (MW 500 kDa) exhibited the most notable effect on NSB reduction (data not shown). This could be due to similarities between the molecular weight of this dextran and that used on the CM5 sensor chip surface.

Addition of CM-dextran at 0.01–0.1% (m/v) had no significant effect on the CM5 blank chip characteristics. However, an increase in NSB on the Leptin 16 surface was observed as the concentration of CM-D500 increased (Table 2). Further investigation using lower concentrations of CM-D500 in combination with 0.5 M NaCl, showed the greatest degree of NSB reduction (76%; from 1296 to 307 RU) at 0.007% CM-D500. The combination of 0.005% CM-D500 and 0.5 M NaCl (75% reduction of NSB) was chosen in order to assure lower NSB and least addition of dextran.

### 3.2.5. Change of pH value

The degree of NSB reduction was also examined over the pH range 5.3–9.9. A gradual decrease in NSB was observed as pH was increased and was lowest at pH 9.5 (67% reduction). Bovine serum albumin (BSA) is a highly abundant protein and is believed to contribute primarily to the NSB of blood components towards CM-dextran sensor surfaces. The interaction between BSA and the charged dextran can be induced by the primary force of electrostatics, i.e. the negative charges on the CM-dextran and the residual positive charges on the BSA. The isoelectric point for BSA is pH 4.8. At pH 9.5 ( $>pI$ ), BSA acquires a negative charge, i.e. the same as of CM-dextran surface, and hence electrostatic repulsion between the protein and CM-dextran would prevent the formation of complexes. Thompson and McKernan reported no detectable complexes of BSA and dextran sulphate above pH 8.5 [17]. It has been suggested that BSA can partially denature at pH 9 [18]. Moreover, a higher pH ( $>9.5$ ) may lead to a conformational change of the protein and result in an altered binding behaviour towards the sensor chip surface.

The data outlined previously showed the effects of alterations to the composition of the buffering systems used on an individual basis. The combined effects of each of the altered parameters were then examined. It was found that the greatest degree of NSB reduction was obtained using the NSB buffer derived from the HBS-EP buffer but with increased ionic strength (0.5 M NaCl), addition of CM-D500 (0.005% m/v) and a pH of 9.0 (Fig. 1). Reductions of up to 95%, 88%, and 81% reduction of NSB were observed on the blank CM5 chip, the Leptin 16 chip, and bovine leptin chip, respectively. Addition of CM-D500 in the buffer system appeared to act as a 'com-

petitor' to the CM-dextran on chip surface for binding of BSA, most notably at pH 9.0. The synergistic effects of this buffering system were found to be highly effective in minimising the non-specific binding properties of bovine serum components to the CM5 sensor chip surfaces.

During this investigation, it was noted that the degree of NSB measured varied between individual serum samples. The NSB buffer that was developed during the study was further tested against a panel of 20 randomly selected bovine serum samples on a CM5 blank chip and bovine leptin surfaces. An average of 85.9% ( $\pm 4.76$ ) and 87.3% ( $\pm 5.71$ ) of NSB reduction was found on the CM5 blank chip and bovine leptin surface, respectively. Statistical analysis (Paired-samples test,  $t = 0.87$ ) indicated no significant difference between the two means and it was therefore concluded that, using the developed NSB buffering system, a substantial degree of non-specific binding towards the CM5 chip surface had been removed.

Sample matrix effects or sample interference is well known as a major cause of bias in analytical procedures especially when dealing with complex samples such as blood or other biological fluids. The problem is magnified in the case of real-time BIA technology in which the detection principle is based on changes in mass concentration at the surface as molecules bind or dissociate, since any binding to the chip surface (specific or non-specific) is recorded and reflected as part of the total SPR response (RU). In the case of bovine serum, an overwhelming signal of up to 100-fold greater intensity than the signal produced from the analyte may be generated on CM-dextran sensor surfaces. Replacing the CM-dextran with different biocompatible polymers (e.g. CM-hyaluronic acid and alginate) could greatly improve biosensor performance when using serum as a matrix on an optical fiber SPR sensor (7). McArthur et al. also claimed that the electrostatic effects of CM-dextran with different degrees of carboxymethyl substitution on protein adsorption varied towards different proteins and they concluded that elimination

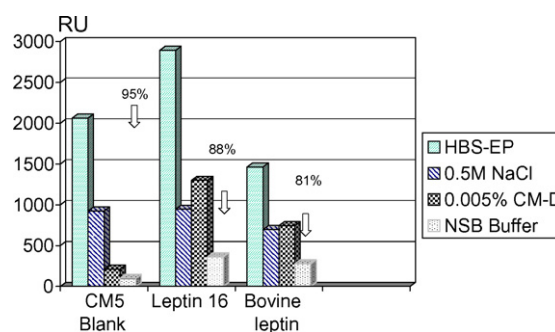


**Fig. 1.** Effect of various conditions on the binding behaviour of bovine serum matrix on different CM5 chip surfaces. HBS-EP: ready-to-use buffer; 0.5 M NaCl: HBS-EP buffer contains 0.5 M NaCl; 0.005% CM-D: HBS-EP buffer contains 0.005% dextran; NSB buffer: HBS-EP buffer contains 0.5 M NaCl, 0.005% CM-dextran and pH 9.0.

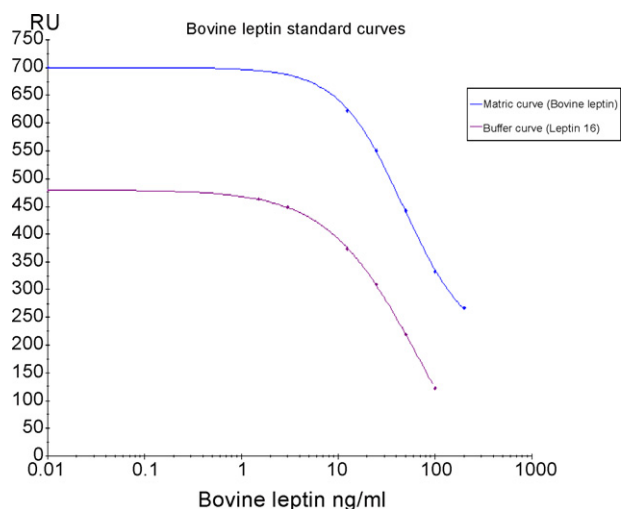


**Fig. 2.** Typical calibration curves constructed in buffer or serum matrix for bovine leptin on Leptin 16 and bovine leptin surfaces.

of adsorption of a broad spectrum of proteins is not straightforward with negatively charged polysaccharide coatings [19].

### 3.3. SPR biosensor assay

In the optimised leptin assay, bovine sera were diluted 10-fold in NSB buffer (10 mM HEPES, 0.5 M NaCl, 0.005% CM-D500, 3.4 mM EDTA, 0.005% P20, pH 9.0) and mixed with an equal volume of diluted antibody solution. At a flow rate of  $20 \mu\text{l min}^{-1}$ , the mixture was injected over the sensor chip surface for 4 min, followed by a 1-min pulse of 50 mM sodium hydroxide to allow surface regeneration. Report points were taken before and after each injection and the biomolecular interaction was recorded as a sensorgram. HBS-EP was used as the running buffer. Typical calibration curves (Fig. 2) were constructed using 10-fold diluted serum on bovine leptin chip and buffer only on Leptin 16 surface. The mid-points ( $\text{IC}_{50}$ ) of the calibration curves were  $38.8 \text{ ng ml}^{-1}$  (matrix curve) and  $26.5 \text{ ng ml}^{-1}$  (buffer curve), indicating slightly decreased assay sensitivity due to matrix. Work is ongoing to improve the sensitivity by screening a panel of anti-leptin antibodies. Serum samples from hormone-treated and non-hormone-treated cattle will be analysed for leptin to determine if this protein is a potential biomarker for growth promoter abuse in cattle.

## 4. Conclusion

Using a leptin SPR assay as the model system, a NSB reduction buffering system has been developed to tackle the significant

problem caused by interference of bovine blood components on carboxymethylated dextran coated sensor chips (CM5) for biotechnological applications using BIACORE biosensors. The current study has shown that up to 94% of the NSB can be eliminated by appropriate use of the buffering system developed in this study. It is believed that this buffering system will have a major impact in reducing the non-specific protein fouling of sensor chip based SPR immunoassays for complex biological solutions, especially when the scope for test sample dilution is limited. Similar effects on NSB reductions in serum samples of other species have currently been observed with the developed buffering system. It may be that for the development of assays for other bovine serum proteins (or other blood based analyse of interest) the parameters determined to give maximum reduction in NSB in the present study may have to be altered in terms of concentration and pH. However the present study should serve as a model for those faced with extreme NSB problems in SRP based analytical systems.

## Acknowledgement

This work was part of the European Commission funded FP6 project: BIOCOP (Contract no. FOOD-CT-2004-06988).

## References

- [1] R.L. Rich, Y.S.N. Day, T.A. Morton, D.G. Myszkka, *Anal. Biochem.* 296 (2001) 197.
- [2] M.A. Cooper, *Curr. Opin. Pharmacol.* 3 (2003) 557.
- [3] I.M. Traynor, S.R.H. Crooks, J. Bowers, C.T. Elliott, *Anal. Chim. Acta* 483 (2003) 18.
- [4] C. Situ, S.R.H. Crooks, A.G. Baxter, J. Ferguson, C.T. Elliott, *Anal. Chim. Acta* 473 (2002) 143.
- [5] M. Caldow, S.L. Stead, J. Day, M. Sharman, C. Situ, C. Elliott, *J. Agric. Food Chem.* 53 (2005) 7367.
- [6] A.A. Bergwerff, F. Van Knapen, *J. AOAC Int.* 89 (2006) 826.
- [7] J.F. Masson, K. Hamersky, S. Beaudoin, K.S. Booksh, *SPIE Proc.* 5261 (2003) 123.
- [8] L. Johnsson, G.A. Baxter, S.R.H. Crooks, D.L. Brandon, C.T. Elliott, *Food Agric. Immunol.* 14 (2002) 209.
- [9] J.F. Masson, T.M. Battaglia, Y.C. Kim, A. Prakash, S. Beaudoin, K.S. Booksh, *Talanta* 64 (2004) 716.
- [10] Y. Zhang, R. Proenca, M. Maffel, L. Leopold, J.M. Friedman, *Nature* 372 (1994) 425.
- [11] B. Johnsson, S. Johnsson, G. Löfås, *Anal. Biochem.* 198 (1991) 268.
- [12] M.P. Richards, T.J. Caperna, T.H. Elsasser, C.M. Ashwell, J.P. McMurtry, *J. Biochem. Biophys. Method* 45 (2000) 147.
- [13] H. Ssuerwein, U. Heintges, M. Hennies, T. Selhorst, A. Daxenberger, *Livest. Prod. Sci.* 87 (2004) 189.
- [14] D.G. Myszkka, P.G. Arulanantham, T. Sana, Z. Wu, T.A. Morton, T.L. Ciardelli, *Protein Sci.* 5 (1996) 2468.
- [15] K. Gregorius, M. Theisen, *Anal. Biochem.* 299 (2001) 84.
- [16] R. Pei, X. Cui, X. Yang, E. Wang, *Talanta* 53 (2000) 481.
- [17] T.E. Thompson, W.M. McKernan, *Biochem. J.* 81 (1961) 12.
- [18] J.L. Boye, I. Allil, A.A. Ismail, *J. Agric. Food Chem.* 44 (1996) 996.
- [19] S.L. McArthur, K.M. McLean, P. Kingshott, H.A.W. St John, R.C. Chatelier, H.J. Griesser, *Colloid Surface B* 17 (2000) 37.





# Design of fluorescent self-assembled multilayers and interfacial sensing for organophosphorus pesticides

Xiangying Sun\*, Kaihao Xia, Bin Liu

College of Material Science and Engineering, The Key Laboratory of Functional Materials for Fujian Higher Education, Huaqiao University, Quanzhou 362021, China

## ARTICLE INFO

### Article history:

Received 11 October 2007

Received in revised form 2 April 2008

Accepted 12 April 2008

Available online 22 April 2008

### Keywords:

Fluorescent sensor

Self-assembled multilayers

Organophosphorus pesticides

Gold nanoparticles

## ABSTRACT

This paper details the fabrication of indole (ID) self-assembled multilayers (SAMs) and fluorescence interfacial sensing for organophosphorus (OP) pesticides. Quartz/APES/AuNP/L-Cys/ID film was constructed on L-cysteine modified Quartz/APES/AuNP surface via electrostatic attraction between ID and L-cysteine. Cyclic voltammetry indicates that ID is immobilized successfully on the gold surface. Fluorescence of the Quartz/APES/AuNP/L-Cys/ID film shows sensitive response toward OPs. The fluorescent sensing conditions of the SAMs are optimized that allow linear fluorescence response for methylparathion and monocrotophos over  $5.97 \times 10^{-7}$  to  $3.51 \times 10^{-6} \text{ g L}^{-1}$  and  $3.98 \times 10^{-6}$  to  $3.47 \times 10^{-5} \text{ g L}^{-1}$ , with detection limit of  $6.1 \times 10^{-8} \text{ g L}^{-1}$  and  $3.28 \times 10^{-6} \text{ g L}^{-1}$ , respectively. Compared to bulk phase detection, interfacial fluorescence sensing based on the SAMs technology shows higher sensitivity by at least 2 order of magnitude.

© 2008 Published by Elsevier B.V.

## 1. Introduction

Since organochlorine pesticides were banned using in agriculture, organophosphorus (OP) derivatives started to find worldwide use in insecticides and pesticides [1]. Organophosphorus compounds are structurally similar to nerve gases and act as neurotoxins by inhibiting the enzyme acetylcholinesterase that is responsible for transmitting nerve impulses across synapses [2–4]. Because of their acute toxicity, rapid detection of OPs in food and ground water has become increasingly demanding for human security and health protection [5]. Traditional analytical methods such as chromatography [6–7] and electrochemical analysis [8] have been devised to detect OPs. These methods have proven to be sensitive and reliable but with significant disadvantages either. For example, they are time-consuming and expensive and can be carried out only by well-trained personnel. Self-assembled multilayers (SAMs) are stable with ordered structure, and easy to be prepared by a simple adsorption from dilute solutions. With the mediation of cysteine, some extremely sensitive fluorescent sensors based on SAMs have been explored in our previous work [9–11]. We report here our attempts in employing molecular SAMs based on gold nanoparticle technology to speed up detection of OPs and further improve analytical sensitivity. Gold nanoparticles were first adsorbed on trialkoxysilane-treated quartz surfaces,

onto which L-cysteine (L-Cys) was assembled to form the SAMs. The SAMs were subsequently assembled with indole (ID) via its electrostatic interaction with L-cysteine. The prepared multilayers Quartz/APES/AuNP/L-Cys/ID were applied for detection of OPs, with capacity of easy regeneration and higher sensitivity.

## 2. Experimental

### 2.1. Reagents

APES was obtained from Shanghai Chemicals Co. Ltd., indole was purchased from China Guoyao Group, and OPs were received from the Environmental Protection and Monitoring Bureau of the Ministry of Agriculture of China.

All chemicals were of analytical grade or above. Aqueous solutions were prepared using ultrapure water from a Millipore Milli-Q water purification system (18 MΩ cm).

### 2.2. Instruments

Electrochemical measurements were carried out on a BAS-100B electrochemical analyzer with a conventional three-electrode system using bare or modified Au as working electrode, platinum wire as counter electrode, and saturated calomel electrode (SCE) as reference electrode. The solutions were bubbled with N<sub>2</sub> for 10 min prior to and during the application of potential.

Corrected fluorescence spectra were recorded on Varian Cary Eclipse fluorescence spectrophotometer with an excitation

\* Corresponding author. Tel.: +86 595 22693548; fax: +86 595 22693999.  
E-mail address: [liumy@hqu.edu.cn](mailto:liumy@hqu.edu.cn) (X. Sun).

wavelength of 470 nm and excitation and emission monochromator slits of 5 nm. The angle between quartz plane and incident excitation light was set at 50° to ensure maximum efficiency of collecting emission light while avoiding reflection light interference.

### 2.3. Preparation of SAMs

#### 2.3.1. Gold colloid preparation

The procedures were essentially the same as those developed by Frens [12]. Glassware was thoroughly cleaned with fresh potassium dichromate solution and rinsed with Milli-Q water prior to use. 0.01 g HAuCl<sub>4</sub> in 100 mL aqueous solution was heated to boiling under vigorous stirring and 2 mL of 2% (v/v) sodium citrate was rapidly added to the vortex of the solution, during which coarse solution color changed from pale yellow to burgundy. The solution was left for boiling for additional 15 min and cooled under stirring to room temperature. Thus prepared gold colloids were stored at 4 °C for further use.

#### 2.3.2. Preparation of AuNP modified quartz wafers

(i) *Pretreatment of quartz wafers.* Quartz plates of 1 cm × 1 cm size were cleaned by polishing for 5 min in the mixture solution of HF/H<sub>2</sub>SO<sub>4</sub>/H<sub>2</sub>O (1:1:3, v/v/v) and extensively washed with distilled water, toluene, acetone, and ultrapure water. Cleaned wafers were then immersed in piranha solution at 80 °C for 1 h to make quartz surface protonated. Thus treated wafers were cleaned by sonication in ethanol, dried with N<sub>2</sub>, and heated in an oven at 80 °C for 30 min.

(ii) *Silanization of quartz wafers.* The above prepared quartz wafers were immersed in 1% (v/v) aqueous solution of APES for 6 h to allow quartz surface functionalized with amino groups. After cleaning with ultrapure water and dried with N<sub>2</sub>, the wafers were ready for next procedure.

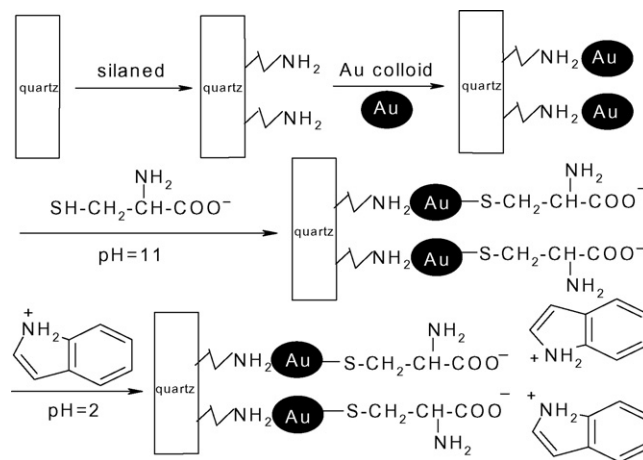
(iii) *Deposition of colloidal gold particles on silanized quartz wafers.* Silanized quartz wafer was dipped in freshly prepared gold colloidal suspension for 12 h. The wafers were then taken out and left to dry in nitrogen for 10 min.

#### 2.3.3. Electrode pretreatment

Gold wafer (3 mm × 4 mm) was first polished, using 1.0, 0.3, and 0.05 μm alumina slurries, respectively, on microcloth pad to a mirror-like finish. After removal of the trace alumina from gold surface, the gold wafer was rinsed with water and briefly cleaned in an ultrasonic bath, and finally cleaned by cycling between -0.5 and +1.5 V (vs SCE) in 1 M H<sub>2</sub>SO<sub>4</sub> at a scan rate of 100 mV s<sup>-1</sup>. Thus treated gold wafer was thoroughly rinsed in ultrapure water before thiol chemisorption.

#### 2.3.4. Fabrication of ID modified SAMs onto the quartz and gold surface

The above fabricated Quartz/APES/AuNP wafer was immersed into 0.01 M L-cysteine solution of pH 11 for 6 h [11], followed by rinsing thoroughly in ultrapure water and dried with N<sub>2</sub>. Under this condition, L-cysteine was adsorbed onto the surface of Quartz/APES/AuNP in the form of -SCH<sub>2</sub>CH(NH<sub>2</sub>)CO<sub>2</sub><sup>-</sup>. Quartz/APES/AuNP/L-Cys/ID was then prepared by immersing Quartz/APES/AuNP/L-Cys into 0.01 M indole ethanol solution of pH 2 for 12 h. In this way indole was electrostatically bound to L-cysteine modified quartz surface. The SAMs composites were stored in dark at 4 °C. Scheme 1 shows the assembling processes on quartz substrate. SAMs on Au wafer were similarly prepared.



Scheme 1. Schematic diagram of indole self-assembling multilayer.

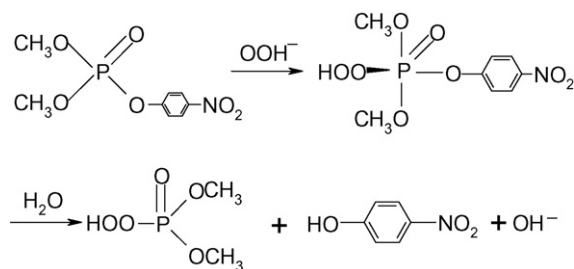


Fig. 1. Reaction producing peroxide phosphate acid.

#### 2.3.5. Fluorescence spectra of ID modified SAMs

The as-prepared Quartz/APES/AuNP/L-Cys/ID wafers were immersed in  $1.5 \times 10^{-4}$  g L<sup>-1</sup> sodium perborate (SPB) solution containing methylparathion for 18 min, indole in SAMs surface thereby being oxidized into indoxyl. The wafer was rinsed thoroughly in ultrapure water and dried with N<sub>2</sub>. The fluorescence emission of the multilayer at 519 nm was found under excitation at 470 nm.

## 3. Results and discussion

### 3.1. Characteristics of indole in solution

#### 3.1.1. Reaction mechanism

Previously it was reported that some amines could be oxidized by OPs in the presence of SPB into fluorescent products [13]. Figs. 1 and 2 show that the reaction proceeds in two steps, the nucleophilic substitution of OPs by OOH<sup>-</sup> (SPB) into peroxide phosphate acid and indole oxidation into indoxyl by the peroxide phosphate acid [14,15].

#### 3.1.2. Fluorescence properties of indoxyl

In bulk aqueous solution SPB and ID are nonfluorescent [16,17]. In the presence methylparathion, the assumed product indoxyl

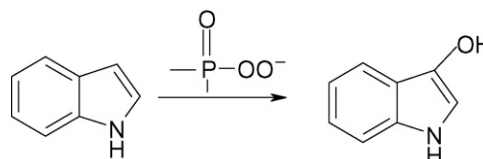


Fig. 2. Oxidation of indole into indoxyl.

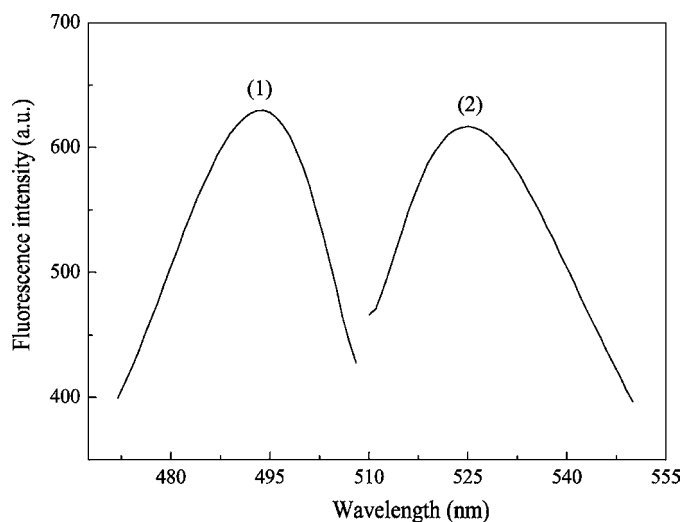


Fig. 3. Fluorescence excitation spectrum (1) and emission spectrum (2) of indoxyl.

emitted fluorescence at 525 nm under 493 nm light excitation (Fig. 3). Fluorescence of methylparathion at 410 nm hence exerts no interference with indoxyl measurement.

Experiments suggested that ethanol content in oxidation reaction medium and reaction time were factors influencing the fluorescence intensity of indoxyl. We chose 5% (v/v) ethanol content and 18 min for reaction time.

### 3.1.3. Detection of methylparathion

Following the aforementioned experimental procedures, varied concentration of methylparathion was added into reaction mixture of SPB and ID in ethanol aqueous solution. As shown in Fig. 4, fluorescence intensity of the reaction system increased with increasing methylparathion concentration. This confirmed the oxidation of indole into indoxyl upon its exposure to methylparathion in solution phase. Inset in Fig. 4 shows that a linear relationship exists between relative fluorescence intensity of indoxyl and methylparathion concentration with a linear correlation coefficient of 0.9907 and a detection limit of  $4.0 \times 10^{-5} \text{ g L}^{-1}$ .

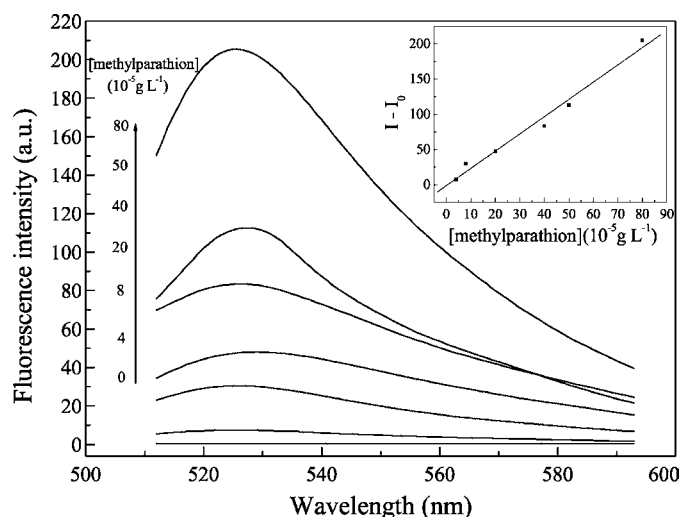


Fig. 4. Fluorescence spectra of indoxyl in bulk phase containing different concentration of methylparathion. Inset shows the linear relationship between methylparathion concentration and relative fluorescence intensity of indoxyl.  $I_0$  and  $I$  represent fluorescence intensity in the absence and presence of methylparathion, respectively.

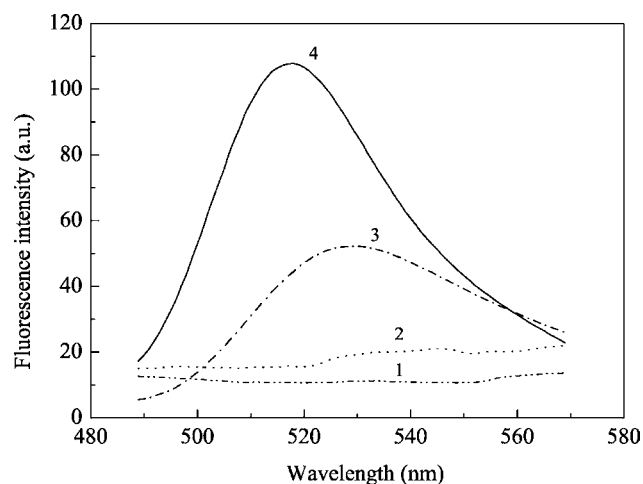


Fig. 5. Surface fluorescence spectra of Quartz/APES/AuNP (1), Quartz/APES/AuNP/L-Cys (2), indoxyl solution of pH 2 (3), and Quartz/APES/AuNP/L-Cys/ID (4).

## 3.2. Characteristics of SAMs

We previously showed that the fluorescence interfacial sensing based on SAMs was more sensitive when compared with those in bulk solution phase detection [9–11]. We therefore examined the detection capacity for OPs with Quartz/APES/AuNP/L-Cys/ID SAMs.

### 3.2.1. Optimal assembling conditions

3.2.1.1. Concentration, immersing time, and pH of indole. It is important to choose conditions for the assembling molecule in constructing self-assembled multilayers. Optimal indole concentration of 0.01 M was chosen for assembling at which the highest fluorescence intensity was obtained. Quartz/APES/AuNP/L-Cys film was immersed in indole solution for varied durations, which suggested an immersing time of 12 h was needed. Indole solution pH of 2 was shown to be the best.

3.2.1.2. Option of concentration, immersing time, and pH of L-cysteine. Indole was assembled onto the self-assembled multilayer films of gold nanoparticles via its electrostatic attraction with L-cysteine. It was therefore critical to choose the suitable pH for L-cysteine solution. Experiments established that L-cysteine SAMs on quartz surface (Quartz/APES/AuNP/L-Cys) could be feasibly formed by dipping Quartz/APES/AuNP in 0.01 M L-cysteine solution of pH 11 for 12 h.

### 3.2.2. Fluorescence properties of SAMs

Fig. 5 shows fluorescence spectra of Quartz/APES/AuNP, Quartz/APES/AuNP/L-Cys, and Quartz/APES/AuNP/L-Cys/ID in the ethanol aqueous solution of SPB and OPs. It is noted that Quartz/APES/AuNP/L-Cys/ID emits indoxyl-characteristic fluorescence, whereas Quartz/APES/AuNP and Quartz/APES/AuNP/L-Cys without indole component are nonfluorescent. This further verifies the assembling of indole molecules on the AuNP modified quartz surface and supports the role of L-cysteine SAMs in ensuring the fluorescence emission of Quartz/APES/AuNP/L-Cys/ID in which the rapid electron transfer between indole and Au surface that leads to fluorescence quenching is blocked. Fluorescence spectrum of Quartz/APES/AuNP/L-Cys/ID immersed in ethanol aqueous solution of SPB and OPs was found peaked at 519 nm which is blue shifted by ca. 5 nm from that of indoxyl in bulk solution. This indicates that the microenvironment of indoxyl on SAMs surface differs from that in the bulk solution [18]. The high stability of the indole modified SAMs ensured the credible detection for OPs.

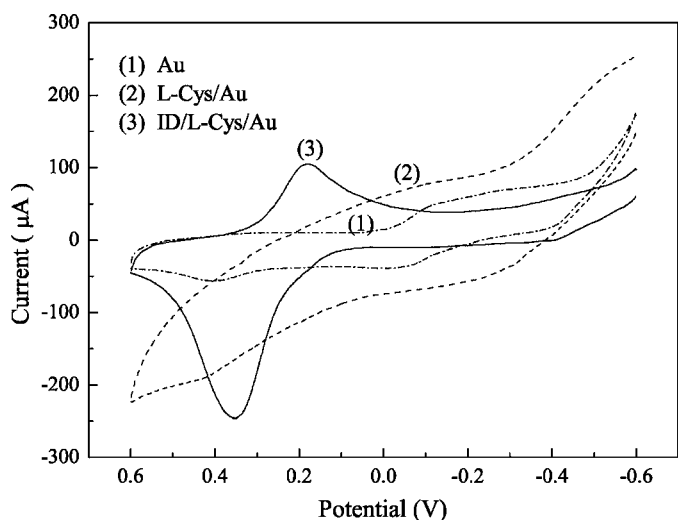


Fig. 6. Cyclic voltammograms of bare Au, L-Cys/Au, and Au/L-Cys/ID electrodes in 0.1 M KCl solution. Scan rate was  $100 \text{ mV s}^{-1}$ .

### 3.2.3. Electrochemical characterization of bare Au, Au/L-Cys, and Au/L-Cys/ID electrodes

We assembled L-cysteine and indole onto bare Au electrode as to monitor indole assembling electrochemically. The assembling of L-cysteine and indole was first investigated by cyclic voltammetry. Fig. 6 shows the cyclic voltammograms of bare Au, Au/L-Cys, and Au/L-Cys/ID electrodes in 0.1 M KCl solution. Compared to those of bare Au electrode and Au/L-Cys electrode, the CV of Au/L-Cys/ID electrode shows a pair of redox peaks at 0.35 and 0.18 V (vs SCE), respectively. It was found that the oxidation peak current increased with increasing indole concentration in solution, suggesting that this peak originated from the oxidation of indole assembled on the surface in form of Au/L-Cys/ID bilayer.

### 3.2.4. Fluorescent sensor for OPs

Under the optimal conditions Quartz/APES/AuNP/L-Cys/ID multilayer emits at 519 nm under the photo-excitation of 470 nm. Figs. 7 and 8 show fluorescence spectra of Quartz/APES/AuNP/L-Cys/ID in the presence of OPs of varied concentration. It was

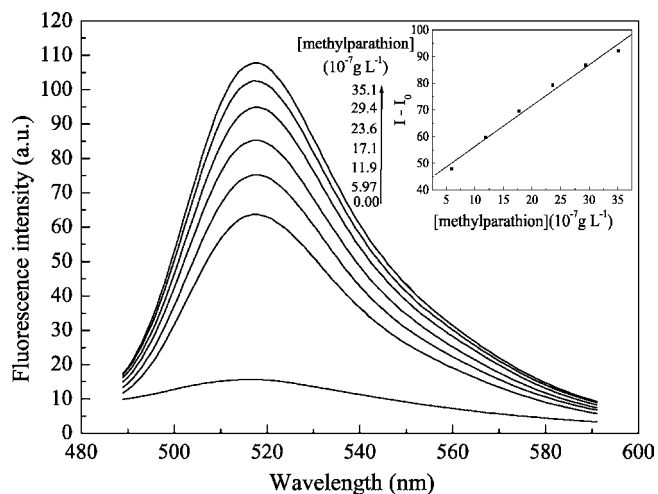


Fig. 7. Fluorescence spectra of Quartz/APES/AuNP/L-Cys/ID in aqueous solutions containing methylparathion of varied concentration. Inset shows the linear relationship between methylparathion concentration and relative fluorescence intensity of SAMs.  $I_0$  and  $I$  represent fluorescence intensity in the absence and presence of methylparathion, respectively.

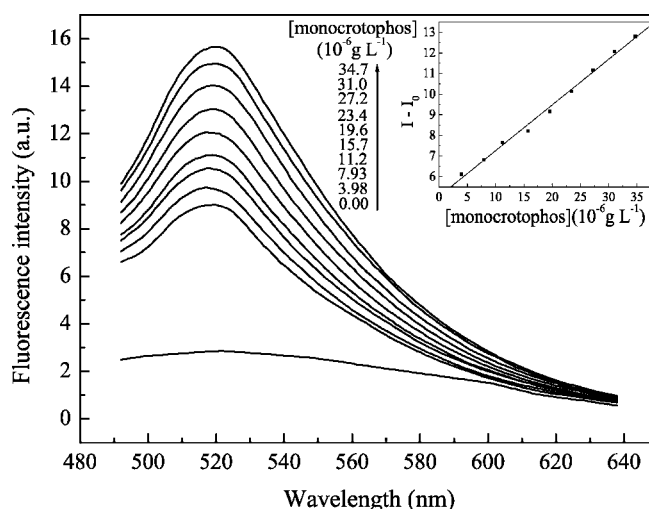


Fig. 8. Fluorescence spectra of Quartz/APES/AuNP/L-Cys/ID in aqueous solutions containing monocrotophos of varied concentration. Inset shows the linear relationship between monocrotophos concentration and relative fluorescence intensity of SAMs.  $I_0$  and  $I$  represent fluorescence intensity in the absence and presence of monocrotophos, respectively.

found that the fluorescence intensity of Quartz/APES/AuNP/L-Cys/ID increased with increasing OPs' concentration. This indicated that ID on the SAMs surface was oxidized into indoxyl when exposed to OPs. Good linear relationships were found between fluorescence intensity of SAMs and methylparathion concentration over  $5.97 \times 10^{-7}$  to  $3.51 \times 10^{-6} \text{ g L}^{-1}$  (Fig. 7 inset) with a detection limit of  $6.10 \times 10^{-8} \text{ g L}^{-1}$ , and over  $3.98 \times 10^{-6}$  to  $3.47 \times 10^{-5} \text{ g L}^{-1}$  for monocrotophos with a detection limit of  $3.28 \times 10^{-6} \text{ g L}^{-1}$  (Fig. 8 inset). Compared with the detection limit in bulk phase of  $10^{-5} \text{ g L}^{-1}$  order of magnitude for methylparathion, the sensitivity of SAMs is obviously higher than that of bulk phase. Again the interfacial fluorescence analysis based on self-assembled multilayers is shown capable of improving sensitivity in microanalysis. Results also indicate that SAMs have good selectivity for pesticides. It only shows response to OPs but not to pyrethroid pesticides under the same concentration. The presence of less than 100 equivalents of  $\text{Ni}^{2+}$  and  $\text{Co}^{2+}$ , and 1000 equivalents of  $\text{K}^+$ ,  $\text{Na}^+$ ,  $\text{Mg}^{2+}$ ,  $\text{Cu}^{2+}$ , and  $\text{Mn}^{2+}$ , respectively, did not lead to interference of the fluorometric detection for OPs by 10% change in the emission intensity. Anions such as  $\text{Cl}^-$  and  $\text{SO}_4^{2-}$  had no influence on the assays. Substantial interference exists in the presence of 20 equivalents of  $\text{Fe}^{3+}$ . The method has been successfully applied to the determination for monocrotophos in natural tea-water matrices with satisfactory recoveries of 102, 103, and 98%, respectively, for  $1.41 \times 10^{-5}$ ,  $1.62 \times 10^{-5}$ , and  $2.47 \times 10^{-5} \text{ g L}^{-1}$  standard monocrotophos.

## 4. Conclusions

Fluorescent assembly of Quartz/APES/AuNP/L-Cys/ID was successfully prepared by chemisorption on the quartz wafer and was shown to be a convenient and supplemental analytical tool for monitoring organophosphorus pesticides in environmental and agricultural samples. The developed SAMs integrated with fluorescence analysis technology were capable of detecting as low as  $10^{-6} \text{ g L}^{-1}$  of monocrotophos and  $10^{-8} \text{ g L}^{-1}$  of methylparathion. Fabrication was shown to be simple and fast with the SAMs being of good stability. The fluorescence detection sensitivity is higher than that in the bulk phase, which ensures the high potentials of applications of this novel methodology in highly sensitive real-sample analysis.

## Acknowledgements

This work was supported by the National Natural Science Foundation of China (grant no. 20575023), Natural Science Foundation of Fujian Province, China (grant no. D0710017), International Cooperative Foundation of Fujian Province (grant no. 200610021), and Overseas Chinese Affairs Office of the State Council of China (grant no. 06QZR10).

## References

- [1] D. Munnecke, J. Agric. Food Chem. 28 (1980) 105.
- [2] S. Zhang, H. Zhao, R. John, Biosens. Bioelectron. 16 (2001) 1119.
- [3] S. Fennouh, V. Casimiri, C. Burstein, Biosens. Bioelectron. 12 (1997) 97.
- [4] C. Cremisini, S. Disario, J. Mela, R. Pilloton, G. Palleschi, Anal. Chim. Acta. 311 (1995) 273.
- [5] J.A. Compton, Military Chemical and Biological Agents, Telford Press, Caldwell, NJ, 1988, p. 135.
- [6] C.E. Mendoza, Thin-layer chromatography, in: K.G. Dumas (Ed.), Pesticide Analysis, Marcel Dekker, New York, 1981, p. 1.
- [7] A.R. Hanks, B.M. Colvin, High-performance liquid chromatography, in: K.G. Dumas (Ed.), Pesticide Analysis, Marcel Dekker, New York, 1981, p. 99.
- [8] I. Palchetti, A. Cagnini, M. Del Carlo, C. Coppi, M. Mascini, A.P.F. Tuner, Anal. Chim. Acta 337 (1997) 315.
- [9] X.-Y. Sun, B. Liu, W.-T. Weng, Y.-B. Jiang, Talanta 62 (2004) 1035.
- [10] X.-Y. Sun, B. Liu, Y.-B. Jiang, Anal. Chim. Acta 515 (2004) 285.
- [11] X.-Y. Sun, W.-T. Weng, Chem. J. Chin. Univ. 26 (2005) 1030.
- [12] G. Frens, Nat. Phys. Sci. 241 (1973) 20.
- [13] J.-H. Yuan, J.-H. Cao, Environ. Chem. 4 (1985) 40.
- [14] Q. Zhang, W.-G. Li, Acta Sci. Circumstantiae 8 (1988) 367.
- [15] Y.-T. Wang, R. Liu, J. Transducer Technol. 16 (2003) 318.
- [16] J.-T. Mei, H.-N. Wang, Chin. J. Anal. Chem. 1 (1997) 82.
- [17] J.-T. Mei, Chem. Anal. Meterage 5 (1996) 28.
- [18] R.R. Naujok, R.V. Duevel, R.M. Corn, Langmuir 9 (1993) 1771.



# A new generation of cyanide ion-selective membranes for flow injection application

## Part III. A simple approach to the determination of toxic metal–cyanide complexes without preliminary separation

Andriana R. Surleva<sup>a</sup>, Milka T. Neshkova<sup>b,\*</sup>

<sup>a</sup> University of Chemical Technology and Metallurgy, Department of Analytical Chemistry, 8 Kl. Ohridski Blvd., 1756 Sofia, Bulgaria

<sup>b</sup> Laboratory of Electrochemical Sensors, Institute of General & Inorganic Chemistry, Bulgarian Academy of Sciences, Acad. G. Bonchev Str., Block 11, 1113 Sofia, Bulgaria

### ARTICLE INFO

#### Article history:

Received 6 January 2008

Received in revised form 21 April 2008

Accepted 23 April 2008

Available online 2 May 2008

#### Keywords:

WAD cyanide determination

Cyanide speciation

$\text{Ag}_{2+\delta}\text{Se}_{1-x}\text{Te}_x$  and  $\text{Ag}_{2+\delta}\text{Se}$  FIP-detectors

Bound cyanide electrochemical release

Ligand exchange

### ABSTRACT

A new flow injection approach to total weak acid-dissociable (WAD) metal–cyanide complexes is proposed, which eliminates the need of a separation step (such as gas diffusion or pervaporation) prior to the detection. The cornerstone of the new methodology is based on the highly selective flow-injection potentiometric detection (FIPD) system that makes use of thin-layer electroplated silver chalcogenide ion-selective membranes of non-trivial composition and surface morphology:  $\text{Ag}_{2+\delta}\text{Se}_{1-x}\text{Te}_x$  and  $\text{Ag}_{2+\delta}\text{Se}$ . An inherent feature of the FIP-detectors is their specific response to the sum of simple  $\text{CN}^- + \text{Zn}(\text{CN})_4^{2-} + \text{Cd}(\text{CN})_4^{2-}$ . For total WAD cyanide determination, ligand exchange (LE) and a newly developed electrochemical pre-treatment procedure for release of the bound cyanide were used. The LE pre-treatment ensures complete recovery only when the sample does not contain  $\text{Hg}(\text{CN})_4^{2-}$ . This limitation is overcome by implementing electrochemical pre-treatment which liberates completely the bound WAD cyanide through cathodic reduction of the complexed metal ions. A complete recovery of toxic WAD cyanide is achieved in the concentration range from  $156 \mu\text{g L}^{-1}$  up to  $13 \text{mg L}^{-1}$ . A three-step protocol for individual and group WAD cyanide speciation is proposed for the first time. The speciation protocol comprises three successive measurements: (i) of non-treated, (ii) LE-exchange pre-treated; (iii) electrochemically pre-treated sample. In the presence of all WAD complexes this procedure provides complete recovery of the total bound cyanide along with its quantitative differentiation into the following groups: (1)  $\text{Hg}(\text{CN})_4^{2-}$ ; (2)  $\text{CN}^- + \text{Cd}(\text{CN})_4^{2-} + \text{Zn}(\text{CN})_4^{2-}$ ; (3)  $\text{Cu}(\text{CN})_4^{3-} + \text{Ni}(\text{CN})_4^{2-} + \text{Ag}(\text{CN})_2^-$ . The presence of a 100-fold excess in total of the following ions:  $\text{CO}_3^{2-}$ ,  $\text{SCN}^-$ ,  $\text{NH}_4^+$ ,  $\text{SO}_4^{2-}$  and  $\text{Cl}^-$  does not interfere. Thus the proposed approach offers a step ahead to meeting the ever increasing demand for cyanide-species-specific methods. The equipment simplicity makes the procedure a good candidate for implementing in portable devices for in-field cyanide monitoring.

© 2008 Elsevier B.V. All rights reserved.

### 1. Introduction

From environmental perspective the most toxicologically significant and hence ecologically important forms are not only the free cyanide ions and soluble HCN but also weak and labile metal–cyanide complexes such as:  $\text{Zn}(\text{CN})_4^{2-}$ ,  $\text{Cd}(\text{CN})_4^{2-}$ ,  $\text{Cu}(\text{CN})_4^{3-}$ ,  $\text{Ni}(\text{CN})_4^{2-}$ ,  $\text{Hg}(\text{CN})_4^{2-}$  and  $\text{Ag}(\text{CN})_2^-$ , generally labeled with the acronym weak acid-dissociable (WAD) complexes, which can easily release  $\text{CN}^-$  in acidic media and hence are also very toxic. That is why the maximum admissible “free cyanide” levels promul-

gated by the Environmental Protection Authorities for regulation and risk assessment comprise the sum of all above-mentioned cyanide species. Accordingly, the imposed need of sample pre-treatment aimed to: (i) convert selectively WAD cyanide species into free cyanide ions, and (ii) separate the latter from the accompanying interferences, is probably the most important and often the most time-consuming part of the whole cyanide analysis, even in the widely accepted lately flow-injection mode. Moreover, it creates serious difficulties for the automation and miniaturization of the cyanide monitoring devices (especially as far as the in-field portable devices are concerned). The successful adoption of on-line gas diffusion [1–7] and, more recently, pervaporation [8,9] flow-injection separation techniques have proved effective substitutes for the very tedious and time-consuming standard WAD cyanide distillation

\* Corresponding author. Tel.: +359 2 872 30 11; fax: +359 2 870 50 24.  
E-mail address: [mneshe@mbox.contact.bg](mailto:mneshe@mbox.contact.bg) (M.T. Neshkova).

method. These new techniques have contributed a lot to speed up gas/liquid separation and have gained wide acceptance. In the particular case of WAD cyanide determination, gas diffusion achieves a dual goal, i.e., partly (depending on pH) releases the bound WAD cyanide as HCN in the acidified donor channel of the gas-diffusion module, and separates the free HCN from the accompanying interferents by its selective transfer across a hydrophobic membrane, into an alkaline receptor channel. For complete recovery of WAD or total cyanide in the FIA mode, however, an additional pre-treatment step such as ligand exchange (LE) cyanide displacement [1,10–12], UV-digestion [9,13–15], focused microwave radiation [16], or other more or less sophisticated techniques [17–19] have been employed.

Ligand exchange displacement using appropriate chelating agents presents the most simple and elegant approach for complete and selective WAD cyanide release. From the numerous ligand exchange reagents examined for effective WAD cyanide displacement, only two reagent mixtures have proved satisfactory for FIA application, because of kinetic restrictions imposing very stringent release reaction conditions. These are the proprietary ligand exchange mixture UNR/PEA A and B used by Milosavljević et al. [10], and the tetraethylenepentamine (TEP)+dithizon mixture [11] with subsequent gas-diffusion separation to enhance the selectivity of the amperometric detection system used. Detailed comparative studies [20,21] have confirmed that the LE approach is more consistent in freeing cyanide from WAD metal complexes than the standard distillation procedure. Thus the U.S. Environmental Protection Agency approved in 1999 a flow-injection method for the determination of WAD cyanide in water and wastewater using on-line ligand exchange/gas-diffusion cyanide separation/amperometric detection (USEPA Method-1677) [22].

Still, cyanide sample pre-treatment and separation remains the “bottleneck” of on-line WAD cyanide monitoring. One reason stems from the fact that both gas-diffusion and pervaporation provide on-line separation in non-equilibrium state. The transfer efficiency of the gaseous species is only 25% of the total amount under favorable conditions, and often as low as 10–15% [3], which inevitably calls for higher sensitivity of the detection system used. A second reason is the lack of highly selective detection system that would make such a separation step unnecessary. The need of selective flow injection detection system becomes even more important in the context of the demand for automated portable devices for in-field cyanide risk assessment.

The present paper proposes an alternative approach to flow-injection WAD cyanide quantification, which allows skipping of the on-line separation step. The cornerstone of the suggested protocol is the recently reported highly selective flow-injection potentiometric detection (FIPD) system which makes use of thin-layer electroplated silver chalcogenide ion-selective membranes of non-trivial composition and surface morphology [23,24].  $\text{Ag}_{2+\delta}\text{Se}_{1-x}\text{Te}_x$  and  $\text{Ag}_{2+\delta}\text{Se}$  cyanide membranes have been chosen for the present investigation. The suitability of both LE and a newly developed electrochemical pre-treatment for complete WAD cyanide recovery without preliminary separation step is evaluated and compared. Further, the possibility for WAD cyanide individual or group speciation is demonstrated, which to the best of our knowledge is made for the first time.

## 2. Experimental

### 2.1. Detector cell and flow injection manifold

The underlying principles of cathodic electrodeposition of thin metal chalcogenide films for use in ion-selective sensor develop-

ment, and the selection of optimum conditions for electrochemical preparation of silver chalcogenide in particular, have been discussed in detail elsewhere [25,26]. In the present study, the thin-layer  $\text{Ag}_{2+\delta}\text{Se}_{1-x}\text{Te}_x$  and  $\text{Ag}_{2+\delta}\text{Se}$ -membranes (around 2- $\mu\text{m}$  thick) were electrodeposited onto Pt-substrate of the flow cell from an electrolytic bath typically comprising:  $2 \times 10^{-3} \text{ M AgNO}_3 + 5 \times 10^{-2} \text{ M Na}_2\text{SeO}_3 + 6.7 \times 10^{-3} \text{ M K}_2\text{TeO}_3$  in 0.5 M  $\text{H}_2\text{SO}_4$  and  $2 \times 10^{-3} \text{ M AgNO}_3 + 5 \times 10^{-2} \text{ M SeO}_2$  in 0.5 M  $\text{H}_2\text{SO}_4$ , respectively. The electrodeposition was carried out in a two-compartment electrolytic cell at controlled potential ( $E_d$ ), chosen within the potential range from +15 to –15 mV vs. a Ag/AgCl/1 M KCl/1 M  $\text{KNO}_3$  double-junction reference electrode as described in [23,24].

The “edge-jet” sandwich-type versatile detector cell was schematically presented elsewhere [26]. The cell design allows for easy dismantling of the sensor part screwed to the detector body to have the active membrane re-deposited, thus preserving the cell parameters unchanged. Pt-substrate of 0.7- $\text{cm}^2$  area, onto which the active membrane (either  $\text{Ag}_{2+\delta}\text{Se}$  or  $\text{Ag}_{2+\delta}\text{Se}_{1-x}\text{Te}_x$ ) was cathodically electrodeposited, was appropriately fixed onto the top of this sensor part. An effective cell volume of approximately 12  $\mu\text{L}$  was kept constant throughout the investigation. The carrier was fed into the cell through an inlet channel drilled into the upper cell block at an angle of 135° vs. the membrane plane and left the cell through an outlet channel connected to a flow-through Ag/AgCl reference electrode.

A single-line manifold as described in [26] was employed throughout this study. PTFE tubing of 0.5-mm i.d., a Reodyne Model 5020 injection valve with loop volume of 110  $\mu\text{L}$  and a 50-cm long dispersion coil (0.5-mm i.d.) were typically used. A home made automated data acquisition system [27] was used for transient signal read-out.

### 2.2. Calibration and pre-treatment procedures

$7 \times 10^{-7} \text{ M CN}^-$  in 0.1 M NaOH was used as a carrier into which replicate samples ( $V = 110 \mu\text{L}$ ) were injected. The flow rate was varied between 3.5 and 5.5  $\text{mL min}^{-1}$ , but 4.5  $\text{mL min}^{-1}$  flow rate was mostly chosen throughout this study. Calibration covering the concentration range of  $5 \times 10^{-6}$  to  $1 \times 10^{-3} \text{ M}$  cyanide was performed daily. Minimum one full calibration run in both concentration directions, with triplicate injections at each concentration, was carried out. In addition, when multi-component samples were analyzed, cyanide standards enclosing the sample concentration were injected in triplicate before and after the sample injection in order to validate/update the calibration graph.

A fairly concentrated ligand exchange reagent solution (either  $10^{-2}$  or  $10^{-3} \text{ M}$ ) of TEP was spiked to the complex cyanide samples so as to cover a range of 1–20 TEP to total cyanide molar ratio. Typically, a calculated volume of the stock TEP solution (20–75  $\mu\text{L}$ ) was added to 5 mL of the sample and the mixture was allowed to react for 10 min under vigorous magnetic stirring. Six replicate samples of 110  $\mu\text{L}$  each were generally injected.

The electrochemical pre-treatment approach to bound WAD cyanide release is based on the cathodic reduction (at constant potential) of the metal part of the complex in the presence of TEP as chelating agent [28]. A two-compartment electrolytic cell with silver amalgamated working electrode of 0.50- $\text{cm}^2$  area and Pt-foil as counter electrode was used. The electrolysis of the sample, containing a 20-fold excess of TEP, was carried out at controlled potential,  $E_d = -1.7 \text{ V}$  vs. Ag/AgCl/1 M KCl/1 M  $\text{KNO}_3$  reference electrode. The deposition potential was determined based on preliminary experiments employing cyclic voltammetry. Fifteen minutes proved enough time to guarantee a complete cyanide release, even at high-sample concentrations.

### 2.3. Reagents

All inorganic reagents used were of analytical reagent-grade. Standard cyanide solutions were prepared daily from 0.3 M KCN stock solution by serial dilution in 0.1 M NaOH. The exact concentration of the stock cyanide solution was determined by potentiometric titration with AgNO<sub>3</sub> standard solution. Ag<sub>2+δ</sub>Se<sub>1-x</sub>Te<sub>x</sub> membrane vs. Ag/AgCl reference electrode was used for end-point detection. When stored in amber glass the concentration of the stock solution remained unchanged for about 20 days. Metal ion solutions with exact concentrations were prepared from Titrisol reagents. Stock solutions of WAD complexes were prepared by mixing stoichiometrically aliquots of the respective metal Titrisol solutions (Merck) and KCN solution (standardized immediately before mixing) and made up to the corresponding volume with NaOH to obtain a final concentration of 0.1 M. Me(CN)<sub>n</sub> standards were obtained by serial dilution of prepared stock complexes with 0.1 M NaOH. Comparatively high concentrations of the corresponding chelating agents: EDTA, CDTA, glycine, dithizone (diphenylthiocarbazone) (all Merck reagent-grade) and TEP (Fluka) were prepared so that sample dilution as a consequence of LE-pretreatment be avoided.

## 3. Results and discussion

### 3.1. FIPDs performance prerequisites

The equations describing the flow-injection response of the FIPDs to cyanide are  $y = 586 - 108 \lg C_{\text{CN}^-}$  ( $2 \times 10^{-6}$  M detection limit) and  $y = 540 - 101 \lg C_{\text{CN}^-}$  ( $4 \times 10^{-6}$  M detection limit) for the Ag<sub>2+δ</sub>Se and Ag<sub>2+δ</sub>Se<sub>1-x</sub>Te<sub>x</sub> membranes, respectively, with upper linearity limit of  $10^{-3}$  M and with almost double Nernstian slope of the electrode function as shown in our previous study [24]. For the purpose of the present investigation the cyanide recovery, in the presence of already accepted chelating agents for the ligand exchange cyanide displacement, and anions, most commonly accompanying cyanide effluents, were studied. Table 1 summarizes the results indicating the maximum admissible interferents against cyanide molar ratio. A constant low cyanide concentration of 0.26 ppm (very close to the maximum contaminant cyanide level generally accepted by most of the Environmental Protection Authorities) was chosen intentionally, since it had been reported that the tolerance to interferents increases with increase in cyanide concentration. Both membranes exhibit perfect selectivity against SCN<sup>-</sup>, S<sub>2</sub>O<sub>3</sub><sup>2-</sup> and Cl<sup>-</sup> (even when present in 100-fold excess) and the differences observed are of no practical importance. However, the tolerance to chelating agents is far lower. As seen from the Table, dithizon should be excluded as potential component of the most recommended ligand exchange reagent TEP+dithizon, while the two types of membranes exhibit different selectivity against TEP. In order to assess the effect of cyanide concentration on the tolerance to TEP, the FI-signals of both membranes to CN<sup>-</sup> and its mixture with TEP at increasing TEP to cyanide molar ratios were registered for a wide cyanide concentration range (from  $5 \times 10^{-6}$  up to  $1 \times 10^{-4}$  M, Fig. 1). Duplicate injections were used everywhere. While identical signals were recorded with the Ag<sub>2+δ</sub>Se<sub>1-x</sub>Te<sub>x</sub> membrane for the whole CN<sup>-</sup> concentration range, the Ag<sub>2+δ</sub>Se-membrane proved appropriate for cyanide concentrations  $\geq 1 \times 10^{-5}$  M. Nonetheless, it is encouraging that TEP does not affect the membrane, which perfectly reproduces its signal to cyanide after TEP injection at low concentration. Moreover, the  $C_{\text{CN}^-}/C_{\text{TEP}}$  maximum admissible ratio increases significantly for  $C_{\text{CN}^-} > 10^{-5}$  M. The signal profiles recorded for CN<sup>-</sup> and its mixture with TEP are practically identical, so no

change in the sample throughput is expected, as reported in [24].

### 3.2. Direct response of the FIPDs to individual WAD complexes

Direct response of both sensor membranes to labile WAD complexes such as Cd(CN)<sub>4</sub><sup>2-</sup> and Zn(CN)<sub>4</sub><sup>2-</sup> has been reported in our recent work [24]. In view of our intention to include direct WAD cyanide measurement as a separate step in a speciation protocol, the study of the direct response of the FIPDs to certain WAD species was extended to cover a broader concentration range and to assess the effect of flow rate, membrane composition and the presence of free cyanide, SCN<sup>-</sup> and chloride ions in the injected sample. As seen from Table 2 the recovery of bound cyanide as cadmium and zinc complexes is satisfactory for both membranes within the whole concentration range examined, and the presence of free CN<sup>-</sup> does not affect the response to the complex, the registered signal measuring the sum of the free and bound cyanide. In view of the obtained very encouraging results, the response to cyanide bound as Cd(CN)<sub>4</sub><sup>2-</sup> and Zn(CN)<sub>4</sub><sup>2-</sup> was further examined in the presence of SCN<sup>-</sup> and chloride, which coexist with cyanide in effluent samples and are recognized as serious interferents when amperometric detection is used. The results are presented in Table 3. The membranes' selectivity against SCN<sup>-</sup> is really impressive and even 500-fold excess of thiocyanate relative to total cyanide content does not affect the correctness of the recovery.

The response to Cu(CN)<sub>4</sub><sup>3-</sup> deserves special mention as the membrane's behavior proved quite different when the complex is present alone or in a mixture with zinc and cadmium cyanides, as will be demonstrated later on. When present alone, the recovery of cyanide in Cu(CN)<sub>4</sub><sup>3-</sup> achieved with both membrane compositions does not surpass 15% for relatively high complex concentrations, while complexed cyanide remains unrecoverable at concentrations below  $5 \times 10^{-5}$  M. Moreover, the presence of free cyanide (even in 4-fold lower concentrations relative to the bound one) completely suppresses recovery of the complexed cyanide and only the free cyanide is detected. Preliminary experiments have shown that, when a mixture of the three complexes is injected, only the cyanide bound as Cd(CN)<sub>4</sub><sup>2-</sup> and Zn(CN)<sub>4</sub><sup>2-</sup> complexes can be detected. We are inclined to ascribe the observed low recovery of the cyanide bound in Cu(CN)<sub>4</sub><sup>3-</sup> to negative steric effects of the latter on the membrane response, moreover that the observed phenomenon developed to complete recovery blockage when either simple cyanide or the above enumerated complexes are present in the sample.

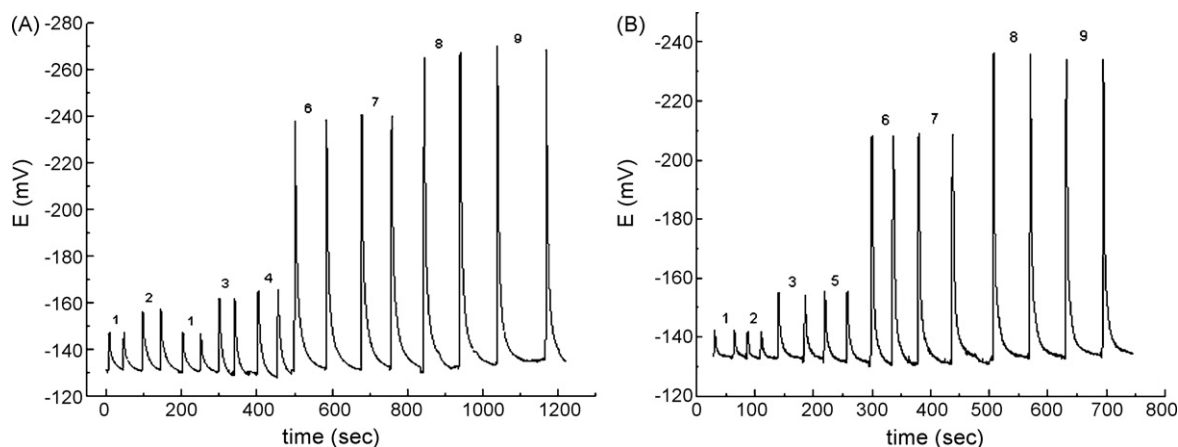
As reported in our previous publication [23], the silver chalcogenide membranes measure the free silver ions when in contact with Ag(CN)<sub>2</sub><sup>-</sup> complex, due to the higher selectivity of the named membranes to Ag<sup>+</sup> ions. The present extended study has shown, however, that the Ag-response of the membranes turns to CN<sup>-</sup> response, when a threshold molar ratio of CN<sup>-</sup> to Ag(CN)<sub>2</sub><sup>-</sup> in the injected sample is reached. This threshold molar ratio proved independent of the Ag(CN)<sub>2</sub><sup>-</sup> concentration and was found to be equal to 25. Actually, this result reflects the dual response of the membranes and is consistent with the respective selectivities towards silver and cyanide ions when present together.

No recovery of the cyanide bound as Ni(CN)<sub>4</sub><sup>2-</sup> or Hg(CN)<sub>4</sub><sup>2-</sup> complexes was observed. However, Hg(CN)<sub>4</sub><sup>2-</sup> suppresses the direct recovery of the total cyanide (as a mixture of CN<sup>-</sup> + Cd(CN)<sub>4</sub><sup>2-</sup> and Zn(CN)<sub>4</sub><sup>2-</sup>), which is due to the secondary response of the membranes to Hg(II) reported earlier [29]. The mercury interference proved concentration dependent. Both Hg(CN)<sub>4</sub><sup>2-</sup> and total bound cyanide concentrations affect their maximum admissible molar ratio, but the effect of mercury proved to be stronger, as seen from Fig. 2. While  $1 \times 10^{-5}$  M total cyanide tolerates the presence



**Table 1**  
Cyanide recovery and admissible molar ratios ( $C_X/C_{CN^-}$ ) in the presence of interferents at constant  $C_{CN^-} = 1 \times 10^{-5}$  M

Interferent	Dithizon		TEP		EDTA		Glycine		SCN <sup>-</sup>	
	Recovery (%)	Ratio	Recovery (%)	Ratio	Recovery (%)	Ratio	Recovery (%)	Ratio	Recovery (%)	Ratio
Membrane										
Ag <sub>2+δ</sub> Se	119	<0.1	106	1	104	5	105	5	103	1000
Ag <sub>2+δ</sub> Se <sub>1-x</sub> Te <sub>x</sub>	164	<0.1	108	10	–	–	–	–	105	100
Interferent										
S <sub>2</sub> O <sub>3</sub> <sup>2-</sup>	Recovery (%)	Ratio	I <sup>-</sup>	Recovery (%)	S <sup>2-</sup>	Recovery (%)	SO <sub>4</sub> <sup>2-</sup>	Recovery (%)	Cl <sup>-</sup>	Recovery (%)
Membrane										
Ag <sub>2+δ</sub> Se	97	100	107	0.1	105	0.05	106	>3 × 10 <sup>4</sup>	102	>10 <sup>5</sup>
Ag <sub>2+δ</sub> Se <sub>1-x</sub> Te <sub>x</sub>	103	100	124	<0.1	99	0.05	104	>3 × 10 <sup>4</sup>	101	>10 <sup>5</sup>

**Fig. 1.** Cyanide flow injection calibration runs using: (A) Ag<sub>2+δ</sub>Se; and (B) Ag<sub>2+δ</sub>Se<sub>1-x</sub>Te<sub>x</sub> membranes, in the presence of tetraethylenepentamine (TEP): (1) 5 × 10<sup>-6</sup> M CN<sup>-</sup>; (2) 5 × 10<sup>-6</sup> M CN<sup>-</sup> + 5 × 10<sup>-6</sup> M TEP; (3) 1 × 10<sup>-5</sup> M CN<sup>-</sup>; (4) 1 × 10<sup>-5</sup> M CN<sup>-</sup> + 1 × 10<sup>-5</sup> M TEP; (5) 1 × 10<sup>-5</sup> M CN<sup>-</sup> + 1 × 10<sup>-4</sup> M TEP; (6) 5 × 10<sup>-5</sup> M CN<sup>-</sup>; (7) 5 × 10<sup>-5</sup> M CN<sup>-</sup> + 5 × 10<sup>-3</sup> M TEP; (8) 1 × 10<sup>-4</sup> M CN<sup>-</sup>; (9) 1 × 10<sup>-4</sup> M CN<sup>-</sup> + 5 × 10<sup>-3</sup> M TEP. Flow rate: 4.5 mL min<sup>-1</sup>; carrier: 7 × 10<sup>-7</sup> M KCN in 0.1 M NaOH; duplicate injections of 110 μL used.

of Hg(CN)<sub>4</sub><sup>2-</sup> at a 20-fold lower concentration, for total cyanide equal to 1 × 10<sup>-4</sup> M, a 30 times lower Hg(CN)<sub>4</sub><sup>2-</sup> concentration is the maximum admissible level.

The above results clearly indicate that the direct determination of CN<sup>-</sup> + Cd(CN)<sub>4</sub><sup>2-</sup> + Zn(CN)<sub>4</sub><sup>2-</sup> WAD cyanide is seriously impeded by the presence of Hg cyanide complexes in the analyte. Therefore, in order to obtain reliable results, preliminary information about the presence of mercury cyanide complex in

the analyte is mandatory. In this context, the problem of calibration, using the most appropriate standards when bound cyanide is to be measured directly, becomes relevant in view of the intended WAD complexes speciation. Therefore, the calibration procedure using simple cyanide ions as standards was compared with the one performed with standards comprising a mixture of CN<sup>-</sup> + Cd(CN)<sub>4</sub><sup>2-</sup> + Zn(CN)<sub>4</sub><sup>2-</sup>. Although the equations describing the two calibration procedures:  $y = (525 \pm 3) - (98 \pm 1) \lg C_{CN^-}$  (for

**Table 2**  
Cyanide recovery dependence on flow rate, membrane composition and type of metal–cyanide complex

Cyanide species		Recovery (%) $N = 3; P = 95\%$							
		Cd(CN) <sub>4</sub> <sup>2-</sup>		Cd(CN) <sub>4</sub> <sup>2-</sup> + CN <sup>-</sup>		Zn(CN) <sub>4</sub> <sup>2-</sup>		Zn(CN) <sub>4</sub> <sup>2-</sup> + CN <sup>-</sup>	
Total CN (mol L <sup>-1</sup> )	V (mL min <sup>-1</sup> )	Ag <sub>2+δ</sub> Se <sup>a</sup>	Ag <sub>2+δ</sub> Se <sub>1-x</sub> Te <sub>x</sub> <sup>a</sup>	Ag <sub>2+δ</sub> Se <sup>a</sup>	Ag <sub>2+δ</sub> Se <sub>1-x</sub> Te <sub>x</sub> <sup>a</sup>	Ag <sub>2+δ</sub> Se <sup>a</sup>	Ag <sub>2+δ</sub> Se <sub>1-x</sub> Te <sub>x</sub> <sup>a</sup>	Ag <sub>2+δ</sub> Se <sup>a</sup>	Ag <sub>2+δ</sub> Se <sub>1-x</sub> Te <sub>x</sub> <sup>a</sup>
8 × 10 <sup>-6b</sup>	3.5	96 ± 5	97 ± 1	95 ± 2	98 ± 3	98 ± 5	96 ± 5	101 ± 5	100 ± 5
	4.5	93 ± 4	94 ± 2	95 ± 3	98 ± 3	98 ± 4	95 ± 2	100 ± 4	101 ± 4
	5.5	94 ± 4	92 ± 3	89 ± 4	93 ± 2	103 ± 6	96 ± 3	98 ± 3	100 ± 3
1 × 10 <sup>-5c</sup>	3.5	96 ± 4	96 ± 4	90 ± 5	97 ± 4	98 ± 5	106 ± 2	95 ± 3	103 ± 5
	4.5	94 ± 4	95 ± 4	97 ± 4	97 ± 2	98 ± 4	103 ± 4	94 ± 3	98 ± 3
	5.5	95 ± 2	95 ± 4	101 ± 3	99 ± 4	99 ± 6	96 ± 4	99 ± 6	101 ± 4
5 × 10 <sup>-5b</sup>	3.5	97 ± 5	94 ± 3	98 ± 2	95 ± 1	100 ± 1	99 ± 1	100 ± 2	101 ± 2
	4.5	94 ± 4	96 ± 1	99 ± 2	96 ± 4	99 ± 3	100 ± 2	99 ± 2	98 ± 2
	5.5	97 ± 3	96 ± 2	96 ± 1	95 ± 2	99 ± 1	101 ± 3	99 ± 2	99 ± 3
1 × 10 <sup>-4c</sup>	3.5	97 ± 3	96 ± 1	95 ± 1	95 ± 2	101 ± 2	100 ± 2	99 ± 2	100 ± 3
	4.5	97 ± 3	94 ± 2	95 ± 3	94 ± 2	100 ± 2	98 ± 2	99 ± 3	99 ± 1
	5.5	98 ± 5	95 ± 3	99 ± 6	94 ± 1	98 ± 1	100 ± 2	99 ± 1	100 ± 2

<sup>a</sup> Membrane type.<sup>b</sup> Cyanide to complex ratio is 1.33.<sup>c</sup> Cyanide to complex ratio is 0.74.

**Table 3**  
WAD cyanide complexes determination in the presence of  $\text{SCN}^-$  and  $\text{Cl}^-$  ions

Recovery (%) ( $N=3$ and $P=95\%$ )				
$C_X/C_{\text{CN}^-}$ (M)	50	100	500	1000
Membrane				
X = $\text{SCN}^-$				
$\text{Ag}_{2+\delta}\text{Se}_{1-x}\text{Te}_x$	$97 \pm 3$	$98 \pm 6$	$99 \pm 2$	$91 \pm 6$
$\text{Ag}_{2+\delta}\text{Se}$	$95 \pm 2$	$103 \pm 2$	$112 \pm 1$	$117 \pm 3$
X = $\text{Cl}^-$				
$\text{Ag}_{2+\delta}\text{Se}_{1-x}\text{Te}_x$	$95 \pm 2$	$104 \pm 2$	$102 \pm 5$	$101 \pm 5$
$\text{Ag}_{2+\delta}\text{Se}$	$99 \pm 4$	$98 \pm 4$	$97 \pm 2$	$98 \pm 5$

Sample composition:  $3.3 \times 10^{-6}$  M  $\text{CN}^- + 8.3 \times 10^{-7}$  M  $\text{Zn}(\text{CN})_4^{2-} + 8.3 \times 10^{-7}$  M  $\text{Cd}(\text{CN})_4^{2-}$ .

simple cyanide) and  $y = (517 \pm 2) - (98 \pm 1) \lg C_{\text{CN}^-}$  (for the mixture), are statistically consistent, i.e.,  $t_{\text{calc.}} = 1.08$  ( $f = 10$ ;  $P = 95\%$ ), the procedure using mixed standards was adopted in order to account for the possible steric and other effects in real samples.

There is no clear understanding up till now of the mechanism of direct FI-response to bound WAD-cyanide. However, the observed differences in the membranes' response to specific WAD-cyanide complex as well as the perfect match of the calibration curves obtained using either free cyanide ions or  $\text{CN}^- + \text{Cd}(\text{CN})_4^{2-} + \text{Zn}(\text{CN})_4^{2-}$  mixture as standards clearly suggest that: (i) the explanation should be sought in the way the silver chalcogenide membranes respond non-destructively to free cyanide ion; (ii) the differences in the energy of Me-CN bond for various WAD complexes, along with possible steric effects should be considered among the response governing parameters. Detailed studies in this context are in progress now.

### 3.3. Ligand exchange approach to total WAD-cyanide determination

The effectiveness of the ligand exchange reagents used so far at displacing cyanide bound as WAD complexes [1,10–12,20–22] has been estimated, after a separation step (such as distillation, steam distillation, and gas diffusion) is applied. However, the separation step itself, which normally involves sample acidification (pH varies from 4.5 up to 0 in the different procedures), contributes substantially to the bound WAD cyanide release, as shown by Sebroski and Ode [11]. Therefore, elimination of the separation step may lead to a considerable change in the cyanide release effectiveness reported by the previous authors. Given that the presently proposed flow-injection ion-selective detection system

measures directly part of the total WAD cyanide, i.e., the sum of  $\text{CN}^- + \text{Cd}(\text{CN})_4^{2-} + \text{Zn}(\text{CN})_4^{2-}$ , the cyanide release problem is reduced to finding appropriate reagents to effectively displace the cyanide from the other WAD complexes:  $\text{Ag}(\text{CN})_2^-$ ,  $\text{Ni}(\text{CN})_4^{2-}$ ,  $\text{Hg}(\text{CN})_4^{2-}$  and  $\text{Cu}(\text{CN})_4^{3-}$ , and to leave unchanged the more stable complexes of Co(II), Fe(III) and Fe(II) ions. That is why our preliminary experiments were focused on the broad spectrum of LE reagents already used, in combination with a separation step, in order to test their displacement effectiveness relative to the above enumerated WAD complexes under the particular experimental conditions of the present investigation, i.e., unchangeable high  $\text{pH} \geq 12$  and direct cyanide determination without preliminary separation. The LE effectiveness was evaluated first for each WAD complex separately on the basis of triplicate injections for each set of experimental parameters (bound cyanide concentration, varied temperature and pre-treatment time). The large group of complexones (EDTA, DTPA and CDTA) first tested in view of the high detector system selectivity towards them, exhibited low WAD cyanide recovery even under rather harsh experimental conditions (temperature of  $60^\circ\text{C}$ ) [30], and therefore dropped off from further investigation. TEP/dithizone LE mixture, claimed as the most effective reagent for release of cyanide from  $\text{Hg}(\text{CN})_4^{2-}$  [11], proved inappropriate as well, because of the interference of dithizone with the sensor's response even when used in concentration as low as  $5 \times 10^{-7}$  M. From all other LE reagents or their mixtures (TEP/EDTA, TEP/DTPA, TEP/glycine and Tiron) under test, only TEP when used at ambient temperature met both requirements, i.e., selectivity to WAD complexes only and effective cyanide displacement from all but  $\text{Hg}(\text{CN})_4^{2-}$  complex. No appropriate LE reagent for the mercury complex can be proposed at this stage. Our observations disagree with the considerably high recovery for  $\text{Hg}(\text{CN})_4^{2-}$  treated with TEP reported by Sebroski and Ode [11]. This is most probably due to the afore-mentioned combined effect of the acidic gas-diffusion separation step [12] with LE displacement, especially at concentrations below 314 ppb, as was the case investigated by the above author. Our efforts, therefore, were aimed to optimize the conditions for FI/LE (TEP) determination of all but  $\text{Hg}(\text{CN})_4^{2-}$  WAD cyanides. The effect of flow rate, when varied from 3 to  $5.5 \text{ mL min}^{-1}$ , on the recovery of each complex separately proved negligible and a recovery close to 100% was observed. In order to avoid unnecessary repetition, the data presented in Table 4 refer to the more tricky case when the injected sample comprises a mixture of complexes, which is further complicated by adding a new component so as to account for the possible adverse effects on total cyanide recovery. For the sake of consistency Table 4 presents also the results obtained by two parallel successive measurements (six replicate injections for each) of one and the same sample, before and after LE pre-treatment: (i) DM in the Table refers to non-treated sample quantification which, according to the previous section, is supposed to measure the sum of  $\text{CN}^- + \text{Cd}(\text{CN})_4^{2-} + \text{Zn}(\text{CN})_4^{2-}$ ; (ii) the results obtained for total WAD cyanide in the sample after LE pre-treatment with TEP are labeled with LEM. As seen from the Table, when TEP is added to the sample mixture in up to 20-fold molar excess it ensures complete total cyanide recovery, when using the ternary  $\text{Ag}_{2+\delta}\text{Se}_{1-x}\text{Te}_x$  for the whole concentration range examined. Complete cyanide displacement is achieved for maximum 15 min even at the highest concentrations. The poor selectivity of the  $\text{Ag}_{2+\delta}\text{Se}$ -membrane towards TEP makes it appropriate for use only at total cyanide content below  $1 \times 10^{-5}$  M, when the lower excess of TEP could ensure complete recovery without interfering with the  $\text{Ag}_{2+\delta}\text{Se}$ -membrane response. The linearity quantification range extends typically from  $156 \mu\text{g L}^{-1}$  up to  $13 \text{ mg L}^{-1}$ . The achieved lower linearity limit by the proposed method seems quite satisfactory when compared with  $50 \mu\text{g L}^{-1}$  calibration limit reported for the Perstorp amperometric analyzer used for the assessment of the

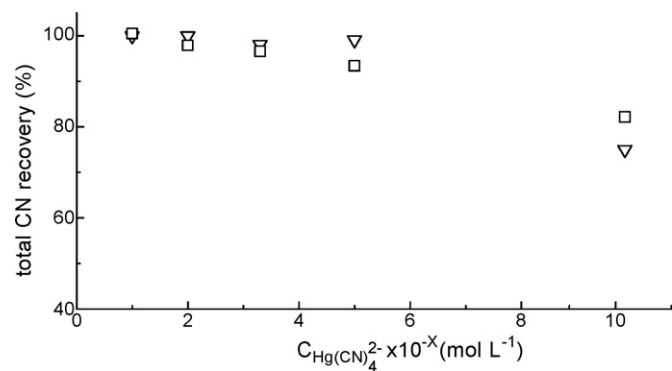


**Fig. 2.**  $\text{CN}^- + \text{Zn}(\text{CN})_4^{2-} + \text{Cd}(\text{CN})_4^{2-}$  total cyanide recovery dependence on  $\text{Hg}(\text{CN})_4^{2-}$  and total cyanide concentrations in the sample. ( $\square$ )  $C_{\text{total CN}^-} = 1 \times 10^{-4}$  M and  $X=6$ ; ( $\triangle$ )  $C_{\text{total CN}^-} = 1 \times 10^{-5}$  M and  $X=7$ .

**Table 4**Successive cyanide recovery in non-treated (DM) and TEP pre-treated ( $C_{TEP}/C_{CN^-} = 20$ ) (LEM) samples comprising various complex mixtures

Total $CN^-$ and component concentrations (mol $L^{-1}$ )	Membrane	Cyanide recovery (%) $N = 6$ and $P = 95\%$		
		Sample composition (A): $CN^- + Cd(CN)_4^{2-} + Zn(CN)_4^{2-} + Ni(CN)_4^{2-}$		
		LEM (100% theor.)	DM (75% theor.)	Calculated (25% theor.)
$8 \times 10^{-6}$ ; $2 \times 10^{-6}$ M $CN^- + 1.5 \times 10^{-6}$ M $Me(CN)_4^{n-4}$	$Ag_{2+\delta}Se_{1-x}Te_x$	$104 \pm 3^a$	$70 \pm 2$	34
	$Ag_{2+\delta}Se$	$108 \pm 3^a$	$72 \pm 2$	36
$1 \times 10^{-5}$ ; $2.5 \times 10^{-6}$ M $CN^- + 1.9 \times 10^{-6}$ M $Me(CN)_4^{n-4}$	$Ag_{2+\delta}Se_{1-x}Te_x$	$107 \pm 3^a$	$71 \pm 1$	36
	$Ag_{2+\delta}Se$	$94 \pm 4^a$	$73 \pm 2$	21
$5 \times 10^{-5}$ ; $1.25 \times 10^{-5}$ M $CN^- + 9.3 \times 10^{-6}$ M $Me(CN)_4^{n-4}$	$Ag_{2+\delta}Se_{1-x}Te_x$	$98 \pm 1$	$72 \pm 4$	26
	$Ag_{2+\delta}Se$	$102 \pm 2$	$73 \pm 6$	29
$1 \times 10^{-4}$ ; $2.5 \times 10^{-5}$ M $CN^- + 1.9 \times 10^{-5}$ M $Me(CN)_4^{n-4}$	$Ag_{2+\delta}Se_{1-x}Te_x$	$98 \pm 2$	$70 \pm 1$	28
	$Ag_{2+\delta}Se$	$98 \pm 2$	$72 \pm 1$	26
		Sample composition (B): $CN^- + Cd(CN)_4^{2-} + Zn(CN)_4^{2-} + Ni(CN)_4^{2-} + Cu(CN)_4^{3-}$		
		LEM (100% theor.)	DM (60% theor.)	Calculated (40% theor.)
$8 \times 10^{-6}$ ; $1.6 \times 10^{-6}$ M $CN^- + 1.6 \times 10^{-6}$ M $Me(CN)_4^{n-4}$	$Ag_{2+\delta}Se_{1-x}Te_x$	$97 \pm 4$	$57 \pm 3$	40
	$Ag_{2+\delta}Se_{1-x}Te_x$	$101 \pm 4$	$55 \pm 2$	46
$5 \times 10^{-5}$ ; $1 \times 10^{-5}$ M $CN^- + 1 \times 10^{-5}$ M $Me(CN)_4^{n-4}$	$Ag_{2+\delta}Se_{1-x}Te_x$	$98 \pm 4$	$56 \pm 2$	42
	$Ag_{2+\delta}Se_{1-x}Te_x$	$101 \pm 5$	$55 \pm 3$	46
		Sample composition (C): $CN^- + Cd(CN)_4^{2-} + Zn(CN)_4^{2-} + Ni(CN)_4^{2-} + Cu(CN)_4^{3-} + Ag(CN)_2^-$		
		LEM (100% theor.)	DM (60% theor.)	Calculated (40% theor.)
$8 \times 10^{-6}$ ; $2.7 \times 10^{-6}$ M $CN^- + 1.2 \times 10^{-6}$ M $Me(CN)_4^{n-4} + 2.5 \times 10^{-7}$ M $Ag(CN)_2^-$	$Ag_{2+\delta}Se_{1-x}Te_x$	$98 \pm 5$	$66 \pm 2$	32
	$Ag_{2+\delta}Se_{1-x}Te_x$	$97 \pm 3$	$63 \pm 2$	34
$5 \times 10^{-5}$ ; $1.5 \times 10^{-5}$ M $CN^- + 8 \times 10^{-6}$ M $Me(CN)_4^{n-4} + 1.5 \times 10^{-6}$ M $Ag(CN)_2^-$	$Ag_{2+\delta}Se_{1-x}Te_x$	$97 \pm 3$	$54 \pm 3$	43
	$Ag_{2+\delta}Se_{1-x}Te_x$	$105 \pm 4$	$55 \pm 4$	50

A—sample contains 25% free cyanide and 25% complexed cyanide in each  $Me(CN)_4^{n-4}$ . B—sample contains 20% free cyanide and 20% complexed cyanide in each  $Me(CN)_4^{n-4}$ . C—sample contains 26% free cyanide and 17% complexed cyanide in each  $Me(CN)_4^{n-4}$  and 6% complexed cyanide in  $Ag(CN)_2^-$ .

<sup>a</sup> Molar ratio of  $C_{TEP}/C_{CN^-} = 1$ .

draft EPA OIA-1677 method [20], with the additional benefit of skipping over the gas-diffusion separation step. The complexity of the sample mixture does not have notable effect on the total (LEM) cyanide determination, even at high concentrations. It exerts a more pronounced effect on the direct cyanide recovery (DM), which possibly accounts for steric complications. Yet, the obtained DM data are reliable enough to be used for WAD group speciation.

The need for cyanide-species-specific methods has long been recognized since different forms of cyanide have different toxicity characteristics and physico-chemical properties. In this context, the total WAD cyanide quantification, too, has its limitations as far as the toxicological risk assessment and the evaluation of cyanide fate and transport in the aquatic environment, and treatment processes are concerned. The procedure of two successive measurements of non-treated and LE-pretreated samples makes it possible to distinguish between the WAD cyanide complexes along with total cyanide determination, in compliance with the above-mentioned toxicological and environmental demands. Depending on the sample composition complexity, one may calculate from the differences between LEM-total and DM-cyanide recoveries the % content of the cyanide donated by the complexes different from the group of  $CN^- + Cd(CN)_4^{2-} + Zn(CN)_4^{2-}$ , as presented in the column "calculated" in Table 4. For sample composition A, it assesses the % of  $Ni(CN)_4^{2-}$ , for sample composition B – the % of the sum of  $Ni(CN)_4^{2-} + Cu(CN)_4^{3-}$ , and for sample C – the sum % content of  $Ni(CN)_4^{2-} + Cu(CN)_4^{3-} + Ag(CN)_2^-$ , respectively. Fig. 3 presents such group speciation for the most complex sample, in the presence of a great excess of  $SCN^-$  and  $Cl^-$ , which have been recognized as serious interferences by other methods.

The combination of a highly selective detection system with LE-cyanide displacement, which makes it possible to skip the complicated separation step, stands on the positive side of the developed protocol for total WAD cyanide determination. Moreover, due to the specific direct membranes' response exhibited to the most labile WAD complexes along with to simple  $CN^-$  group speciation of WAD cyanide became possible. On the negative side stands its applicability only to samples free of  $Hg(CN)_4^{2-}$ .

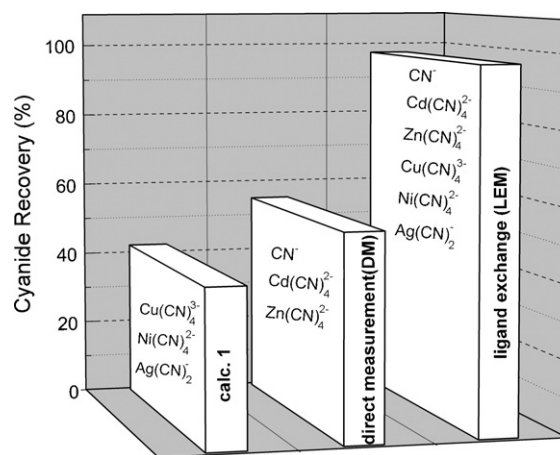


**Fig. 3.** WAD cyanide group speciation in the presence of 100-fold excess of KCl and KSCN. Sample composition: 26% free  $CN^-$ , and 68% cyanide bound as  $Me(CN)_4^{n-4}$  or 17% in each complex (Me = Cd, Zn, Ni and Cu) and 6% cyanide as  $Ag(CN)_2^-$ . Total cyanide concentration is  $5 \times 10^{-5}$  M. Calc.1 is the calculated difference (LEM – DM).

**Table 5**  
Total WAD cyanide recovery using the electrochemical de-complexation pre-treatment approach

Sample composition <sup>a</sup>	Total CN <sup>-</sup> (mol L <sup>-1</sup> )	TEP (mol L <sup>-1</sup> )	E <sub>dep.</sub> , vs. Ag/AgCl (V)	t <sub>dep.</sub> (min)	Recovery (%) (N = 4; P = 95%)
Hg(CN) <sub>4</sub> <sup>2-</sup> + Ni(CN) <sub>4</sub> <sup>2-</sup> + Cu(CN) <sub>4</sub> <sup>3-</sup> + Zn(CN) <sub>4</sub> <sup>2-</sup>	4 × 10 <sup>-5</sup>	8 × 10 <sup>-4</sup>	-1.8	15	100 ± 2
Hg(CN) <sub>4</sub> <sup>2-</sup> + Ni(CN) <sub>4</sub> <sup>2-</sup> + Cu(CN) <sub>4</sub> <sup>3-</sup> + Zn(CN) <sub>4</sub> <sup>2-</sup> + Cd(CN) <sub>4</sub> <sup>2-</sup>	4 × 10 <sup>-5</sup>	8 × 10 <sup>-4</sup>	-1.7	10	101 ± 2
Hg(CN) <sub>4</sub> <sup>2-</sup> + Ni(CN) <sub>4</sub> <sup>2-</sup> + Cu(CN) <sub>4</sub> <sup>3-</sup> + Zn(CN) <sub>4</sub> <sup>2-</sup> + Cd(CN) <sub>4</sub> <sup>2-</sup> + Ag(CN) <sub>2</sub> <sup>-</sup>	4 × 10 <sup>-5</sup>	8 × 10 <sup>-4</sup>	-1.7	15	97 ± 3

<sup>a</sup> Samples contain cyanide complexes in equal molar concentrations.

### 3.4. Electrochemical approach to total WAD cyanide determination

In an attempt to overcome the negative aspect of the proposed LE protocol, an electrochemical approach to complete cyanide liberation from all WAD complexes has been developed quite recently in this laboratory [28]. According to this method cyanide is released from the WAD complexes through cathodic reduction of the metal ions of the cyanide complexes by either potentiostatic or constant current electrolysis. The addition of TEP considerably cuts down the time for cyanide de-complexation in the potentiostatic mode and is crucial under constant current mode for reasons to be discussed elsewhere. Table 5 illustrates the viability of the cathodic potentiostatic cyanide liberation procedure, even at comparatively high total cyanide concentrations, for different synthetic mixtures of WAD complexes containing Hg(CN)<sub>4</sub><sup>2-</sup>. Twenty milliliters of the samples are subjected to cathodic reduction in an ordinary two-compartment electrolytic cell for up to 15 min and the cathodically pre-treated sample is sucked immediately by a pump to feed the injection loop of the single-line FIA system. So the whole procedure for total WAD determination does not take more than 16–18 min. Although the electrochemical pre-treatment in the present investigation was applied off-line, its great advantage is that it can be implemented on-line and such experiments are in progress now. Moreover, the presence of strong cyanide complexes such as Fe(CN)<sub>6</sub><sup>4-</sup> and Fe(CN)<sub>6</sub><sup>3-</sup> do not interfere.

The new electrochemical approach to bound cyanide liberation allows for a more detailed quantitative distinction between the WAD complexes. The speciation protocol developed comprises three successive measurements of one and the same WAD sample: (i) non-treated sample (DM); (ii) LE with TEP pre-treated sample (LEM); (iii) electrochemically pre-treated sample designated as EM.

When the sample contains all WAD complexes, the three measurements (each comprising six replicate injections) identify and quantify the following components:

- (i) DM ⇒ the sum of CN<sup>-</sup> + Cd(CN)<sub>4</sub><sup>2-</sup> + Zn(CN)<sub>4</sub><sup>2-</sup>;
- (ii) LEM ⇒ all WAD complexes, but Hg(CN)<sub>4</sub><sup>2-</sup>;
- (iii) EM ⇒ all WAD complexes.

It is very important to note that the results of these three measurements provide the following additional information:

- (i) The calculated difference (LEM – EM) quantifies only the cyanide bound as Hg(CN)<sub>4</sub><sup>2-</sup>. When the results of the above two measurements coincide, this indicates that the sample is free of mercury complex. Thus, the performance of LEM and EM measurements provides the required preliminary information about the presence of Hg(CN)<sub>4</sub><sup>2-</sup>, as required by the analytical protocol described in the previous section. The possibility to calculate the % content of Hg(CN)<sub>4</sub><sup>2-</sup> is even more important given that there exists a threshold admissible % level above which the results of DM are compromised, as discussed in Section 3.2.

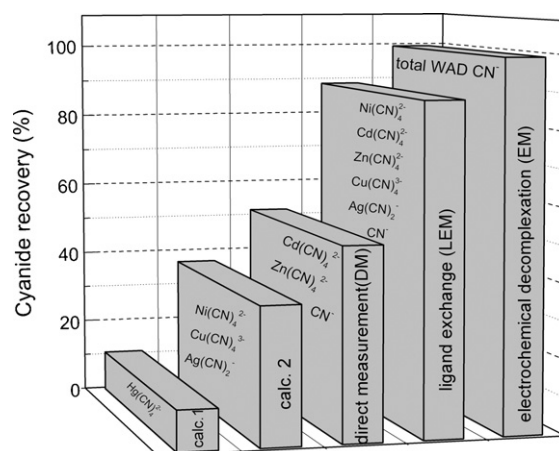


**Fig. 4.** Individual and group speciation following the three-step protocol for a  $5 \times 10^{-5}$  M total WAD cyanide sample comprising: 20% free CN<sup>-</sup>, and 68% cyanide as Me(CN)<sub>4</sub><sup>n-4</sup>, 17% in each complex (Me = Cd, Zn, Ni and Cu), 8% and 4% bound cyanide as Hg(CN)<sub>4</sub><sup>2-</sup> and Ag(CN)<sub>2</sub><sup>-</sup>, respectively. The samples contain also a total of  $7.5 \times 10^{-3}$  M interferent ions: CO<sub>3</sub><sup>2-</sup>, SCN<sup>-</sup>, NH<sub>4</sub><sup>+</sup>, SO<sub>4</sub><sup>2-</sup> and Cl<sup>-</sup> in equimolar concentrations. Calc.1—the calculated difference (EM – LEM); Calc.2—the calculated difference (LEM – DM).

- (ii) The calculated difference between the measurements (LEM – DM) quantifies the sum of Ni(CN)<sub>4</sub><sup>2-</sup> + Cu(CN)<sub>4</sub><sup>3-</sup> + Ag(CN)<sub>2</sub><sup>-</sup>.

Fig. 4 illustrates the results of such speciation protocol for a synthetic sample containing all WAD complexes in the presence of 100-fold excess of anions recognized as possible interferents by the existing methods.

The proposed three-step protocol is easy to perform and provides abundant important environmental and toxicological information covering the same total cyanide concentration interval as specified in Section 3.3.

## 4. Conclusions

The obtained results demonstrate clearly that the combination of a highly selective FI-detection system, ensured by the thin-layer silver chalcogenide FIPDs proposed by this laboratory, with ligand exchange and the newly developed electrochemical pre-treatment procedures for bound cyanide release, provides fast and simple way for total WAD cyanide determination, thus making it possible to skip the preliminary separation step (such as gas diffusion or pervaporation). Consequently, the flow-injection system used is reduced to a single-line one. The proposed alternative protocols are time-efficient, the whole procedure taking no more than 16 min. With the ensured equipment simplicity and the existing potential for further miniaturization and on-line implementation of the electrochemical pre-treatment approach to WAD cyanide release, the new analytical protocol seems a good candidate for developing portable devices for in-field WAD cyanide monitoring. A very important additional feature of the proposed methodology is the possibility for individual

or group speciation of the total WAD cyanide, thus offering a step ahead to meeting the ever increasing demand for cyanide-species-specific methods for environmental risk assessment. To the best of our knowledge, such detailed speciation is reported for the first time.

## References

- [1] Z. Zhu, Z. Fang, *Anal. Chim. Acta* 198 (1987) 25.
- [2] E. Figuerola, A. Florido, M. Aguilar, J. De Pablo, S. Alegret, *Anal. Chim. Acta* 215 (1987) 283.
- [3] Z. Fang, Z. Zhu, S. Zhang, S. Xu, L. Guo, L. Sun, *Anal. Chim. Acta* 214 (1988) 41.
- [4] W. Frenzel, *Fresen. J. Anal. Chem.* 336 (1990) 21.
- [5] W. Frenzel, J. Oleksy-Frenzel, C.Y. Liu, *Anal. Chim. Acta* 233 (1990) 77.
- [6] Y. Liu, R.D. Rocklin, R.J. Joyce, M.J. Doyle, *Anal. Chem.* 62 (1990) 766.
- [7] V. Kubán, *Anal. Chim. Acta* 259 (1992) 45.
- [8] H. Sulistiarti, S.T.J. Cardwell, M.D. Luque de Castro, S.D. Kolev, *Anal. Chim. Acta* 390 (1999) 133.
- [9] B. Vallejo-Pecharrómán, M.D. Luque de Castro, *Analyst* 127 (2002) 267.
- [10] E.B. Milosavljević, L. Solujić, J.L. Hendrix, *Environ. Sci. Technol.* 29 (1995) 426.
- [11] J.R. Sebroski, R.H. Ode, *Environ. Sci. Technol.* 31 (1997) 55.
- [12] E. Miralles, D. Prat, R. Compañó, M. Grandos, *Analyst* 123 (1998) 217.
- [13] L. Solujić, E.B. Milosavljević, M.R. Straka, *Analyst* 124 (1999) 1255.
- [14] H.S. Weinberg, S.J. Cook, *Anal. Chem.* 74 (23) (2002) 6055.
- [15] E. Miralles, R. Compañó, M. Grandos, M.-D. Prat, *Fresen. J. Anal. Chem.* 365 (6) (1999) 516.
- [16] M.C. Quaresma, M.F. de Carvalho, F.A. Meirelles, V.N. Santiago, R.E. Santelli, *Anal. Bioanal. Chem.* 387 (3) (2007) 1017.
- [17] S. Jermark, B. Pranaityte, A. Padarauskas, *J. Chromatogr. A* 1148 (2007) 123.
- [18] T.T. Christison, J.S. Rohrer, *J. Chromatogr. A* 1155 (2007) 31.
- [19] D.E. Barnes, P.J. Wright, S.M. Graham, E.A. Jones-Watson, *Geostandards Newslett.: J. Geostandards Geoanal.* 24 (2000) 183.
- [20] J.D. Evans, L. Thompson, P.J. Clark, S.W. Beckman, *Environ. Sci. Technol.* 37 (2003) 592.
- [21] A. Zheng, D.A. Dzombak, R.G. Luthy, B. Sawyer, W. Lazouskas, P. Tata, M.F. Delaney, L. Zilitinkevitch, J.R. Sebroski, R.S. Swartling, S.M. Drop, J.M. Flaherty, *Environ. Sci. Technol.* 37 (2003) 107.
- [22] U.S. Environmental Protection Agency, Method OIA-1677, Available cyanide by flow injection, ligand exchange, and amperometry, EPA Nr. 821-R-04-001, August, 1999.
- [23] M.T. Neshkova, E.M. Pancheva, V. Pashova, *Sens. Actuator B* 119 (2006) 625.
- [24] A.R. Surleva, V.D. Nikolova, M.T. Neshkova, *Anal. Chim. Acta* 583 (2007) 174.
- [25] M.T. Neshkova, E.M. Pancheva, *Anal. Chim. Acta* 242 (1991) 73.
- [26] M.T. Neshkova, *Anal. Chim. Acta* 273 (1993) 255.
- [27] M.T. Neshkova, I. Gocheva, V. Petrov, *Anal. Chim. Acta* 476 (2003) 55.
- [28] M. Neshkova, A. Surleva, Workshop on Ecomaterials and Processes: Characterization and Metrology, April 14–19, 2007, Plovdiv, Bulgaria, 2007, p. 43 (conference materials).
- [29] M.T. Neshkova, E.M. Pancheva, *Anal. Chim. Acta* 300 (1995) 133.
- [30] D. Ingersoll, W.R. Harris, D.C. Bomberger, D.M. Coulson, Development and Evaluation of Procedures for the Analysis of Simple Cyanides, Total Cyanides and Thiocyanides in Water and Wastewater, U.S. EPA, Washington, DC, 1983 (EPA-600/4-83-054).



## Determination of antioxidant capacities of vegetable oils by ferric-ion spectrophotometric methods

Aleksandra Szydłowska-Czeraniak<sup>a,\*</sup>, Csilla Dianoczki<sup>b</sup>, Katalin Recseg<sup>b</sup>, György Karlovits<sup>c</sup>, Edward Szlyk<sup>a</sup>

<sup>a</sup> Faculty of Chemistry, Nicolaus Copernicus University, ul. Gagarina 7, 87-100 Toruń, Poland

<sup>b</sup> Bunge Europe, Research and Development Center, Kvassay J. ut. 1., Budapest H-1095, Hungary

<sup>c</sup> Bunge Europe Research and Development Center, ul. Niepodległości 42, 88-150 Kruszwica, Poland

### ARTICLE INFO

#### Article history:

Received 19 December 2007

Received in revised form 16 April 2008

Accepted 23 April 2008

Available online 3 May 2008

#### Keywords:

Antioxidant capacity

Vegetable oils

Total phenolic compounds

Principal component analysis

### ABSTRACT

Two ferric-ion-based total antioxidant capacity methods: 1,10-phenanthroline (Phen) and ferric reducing antioxidant power (FRAP) were used for determination of antioxidant capacities (AC) of the acetonic and methanolic extracts of vegetable oils. The obtained mean Phen and FRAP values for acetonic extracts of olive oils, rapeseed, rice and four sunflower oils (39.3–336.5 and 39.5–339.6  $\mu\text{mol Fe}/100\text{ g}$ ) were higher than for methanolic extracts (22.8–307.3 and 23.5–300.1  $\mu\text{mol Fe}/100\text{ g}$ ). However, antioxidant capacities of methanolic extracts of corn oil, blended oils and two sunflower oils with garden green flowers (56.5–312.9 and 53.9–306.5  $\mu\text{mol Fe}/100\text{ g}$  for Phen and FRAP methods, respectively) were higher than for acetonic extracts of these oils (54.2–249.2 and 52.9–244.7  $\mu\text{mol Fe}/100\text{ g}$  for Phen and FRAP methods, respectively). There is a linear and significant correlation between these two analytical methods ( $r=0.9989$  and  $0.9986$  for acetonic and methanolic extracts). Also, total phenolic compounds (TPC) in the studied oils correlated with their antioxidant capacities determined by Phen and FRAP methods ( $r=0.9012$ ,  $0.7818$  and  $0.8947$ ,  $0.7830$  for acetonic and methanolic extracts, respectively). The comparable precision (R.S.D. = 0.8–4.6%, 0.9–4.9% and 0.7–4.0%, 0.6–4.0% for acetonic and methanolic extracts, respectively) and sensitivity ( $\varepsilon=1.27 \times 10^4$ ,  $1.11 \times 10^4$  and  $2.62 \times 10^4\text{ dm}^3\text{ mol}^{-1}\text{ cm}^{-1}$ ) for the proposed Phen and the modified FRAP methods, demonstrate the benefit of the Phen method in the routine analysis of antioxidant capacities of vegetable oils.

© 2008 Elsevier B.V. All rights reserved.

### 1. Introduction

Reactive oxygen species (ROS) in the form of free radicals ( $\text{OH}^\bullet$ ,  $\text{O}_2^{\bullet-}$ ,  $\text{ROO}^\bullet$ ,  $\text{RO}^\bullet$ ,  $\text{H}_2\text{O}_2$ ,  $\text{HOCl}$ ,  $\text{NO}^\bullet$ ,  $\text{ONOO}^-$ ) exist in the oxygen metabolism. ROS are highly reactive chemical species, that can react with any macromolecules such as DNA, lipids and proteins and cause defects in their functions [1]. Such unbalanced oxidative capacity is named oxidative stress which has been implicated in the etiology of many diseases such as: heart disease, autism, cancer, stroke, diabetes, Alzheimer's dementia, Parkinson's disease, arthritis and muscular degeneration [2–7]. However, present day lifestyles, which include consistent exposure to sunlight, radiation, cigarette smoke and medicinal drugs, as well as pollutants in air, water and food dramatically increase the number of ROS. These predispose people to oxidative stress, and drive the processes that lead to metabolic diseases. Therefore, the demand for

the efficient inhibitors of oxidation processes has become essential. It is known, that antioxidants in foods including mono- and polyphenols, sterols, tocopherols, vitamins A and C, urate, thiols, flavonoids, etc. have a major role of protection against diseases, because these compounds scavenge ROS [8]. Furthermore, antioxidant compounds in vegetable oils exhibit an antiradical activity and they are important in the prevention and treatment of the mentioned diseases [9–11].

In the recent years, different methods have been proposed for evaluation of the antioxidant capacity (AC) of vegetable oils. AC of vegetable oils were most often analyzed by the spectrophotometric procedures employing: ABTS (2,2'-azinobis(3-ethylbenzothiaziline-6-sulfonate) [9,12–14], DPPH (2,2'-diphenyl-1-picrylhydrazyl) [9,11,13,15–18], FRAP (ferric reducing antioxidant power) assay [10,14,19,20], the competitive  $\beta$ -carotene or crocin bleaching tests [9,13,17,21,22], phosphomolybdenum [22], thiobarbituric acid-reactive substance (TBARS) and the conjugated diene method [23].

Recently, chemiluminescence (CL) and fluorimetry were used for measurement of the hydrophilic and lipophilic chain-breaking

\* Corresponding author. Tel.: +48 56 611 47 86; fax: +48 56 654 24 77.  
E-mail address: [olasz@umk.pl](mailto:olasz@umk.pl) (A. Szydłowska-Czeraniak).

antioxidant capacity of vegetable oils. The advantages of CL come out from the reduced time of analysis. Usually one run takes a few minutes and the assay can be easily automated [24]. Besides that, the procedure based on photosensitized CL of luminol seems to be also promising. Sacchetti et al. [17] applied the luminol photochemiluminescence (PCL) technique for essential oils antioxidant capacity determination.

Moreover, the total radical-trapping antioxidative potential (TRAP) [9] and the thiobarbituric acid-reactive substances [23] methods were applied for AC determination. Also, the high-throughput fluorescence technique ( $\alpha$ PROX—anti protein oxidation) based on diphenylhexatriene propionic acid (DPHPA) and bovine serum albumin (BSA) equimolar complex was used for determination antioxidant capacities (AC) of pumpkin oils [25]. Among fluorimetric methods, the ORAC assay has found the application for measuring the antioxidant capacity of vegetable oils [26–30]. A noninvasive ORAC method with oxygen probe coated microplates for monitoring antioxidant capacity of vegetable oils was proposed [26]. Ninfali et al. [27,28] and Samaniego Sánchez et al. [13] have used the ORAC test to estimate the antioxidant capacity of virgin olive oils. Moreover, the ORAC method was applied for the determination and comparison of AC of olive oils and rapeseed oils [20]. Besides, ORAC values were obtained for cold-pressed seeds (black caraway, carrot, hemp, cranberry, marionberry, boysenberry, red raspberry, and blueberry) oils [29,30]. However, CL and fluorimetry methods require specialized, expensive equipments. Therefore, spectrophotometric techniques should be modified and employed by the industrial laboratory for AC determination of edible oils.

The red Fe(II)–phenanthroline (Phen) complex is widely applied in classical spectrophotometric method for determination of iron. However, to the best of our knowledge, there was no reference on application of the reaction between ferrous ions and 1,10-phenanthroline for determination of antioxidant capacity of edible oils and the other foodstuffs. Only, Berker et al. [31] used 1,10-phenanthroline method for assay of antioxidant capacities of different antioxidants and their mixtures. Besides that, Phen method was applied for measuring the total antioxidant capacity of plasma, pleural effusion and antioxidant defense system [32,33].

Moreover, in the literature there is a lack of optimal method, or solvent used to extract all antioxidants present in edible oils. Different solvents, acetone [9,16,34,35], methanol [10,11,18–20,27,28,35], ethyl acetate [11,16,18,35], acetonitrile [35], hexane [16] were applied for extraction of antioxidants from vegetable oils.

Therefore, in the presented paper, simple spectrophotometric method for the antioxidant capacities determination of acetic and methanolic extracts of edible oils, based on formation of ferrous–phenanthroline complex was described. The aim of this work was to compare results of AC of vegetable oils obtained by the proposed Phen method and the modified FRAP method for precision, accuracy and sensitivity.

The AC results, total phenolic compounds (TPC) and total tocopherols contents (TTC) were used as descriptors for principal component analysis (PCA) in order to differentiate the analyzed vegetable oils.

## 2. Experimental

### 2.1. Reagents

All reagents were of analytical or HPLC grade. 1,10-phenanthroline (99%), 2,4,6-tris(2-pyridyl)-s-triazine (TPTZ, 99%), Folin-Ciocalteu reagent (FC reagent, 2N), caffeic acid (CA, 98%) and  $\alpha$ -,  $\beta$ -,  $\delta$ - and  $\gamma$ -tocopherols were purchased from

**Table 1**  
Studied oils

Sample	Type of oil	Source
1	Extra virgin olive oil (EVOO1)	Spain
2	Extra virgin olive oil (EVOO2)	Spain
3	Extra virgin olive oil (EVOO3)	Spain
4	Extra virgin olive oil (EVOO4)	Italy
5	Refined olive oil (OO)	Spain
6	Rapeseed oil 1 (RO1)	Poland
7	Rapeseed oil 2 (RO2)	Poland
8	Rice bran oil (RBO)	Germany
9	Corn oil (CO)	Hungary
10	Sunflower oil 1 (SO1)	Romania
11	Sunflower oil 2 (SO2)	Hungary
12	Sunflower oil + garlic (SOG)	Hungary
13	Sunflower oil + paprika (SOP)	Hungary
14	Sunflower oil + garden green flowers (SOF1)	Hungary
15	Sunflower oil + garden green flowers (SOF2)	Hungary
16	Blended vegetable oil: sunflower + olive oils (BO1)	Hungary
17	Blended vegetable oil: sunflower + corn + rapeseed oils (BO2)	Hungary
18	Blended vegetable oil: corn + cereals + nut + some fruits + rice oils (BO3)	Italy

Sigma–Aldrich. Acetic acid, hydrochloric acid, sodium acetate, sodium carbonate, iron(III) chloride hexahydrate ( $\text{FeCl}_3 \cdot 6\text{H}_2\text{O}$ ), iron(II) sulfate heptahydrate ( $\text{FeSO}_4 \cdot 7\text{H}_2\text{O}$ ), methanol (99.8%), acetone (99.5%), hexane (99%), tetrahydrofuran (THF, 99.8%) were obtained from POCH (Gliwice, Poland). Redistilled water was used for the preparation of solutions.

### 2.2. Instruments

The UV–vis spectra of solutions were measured using a Helios  $\alpha$ -UNICAM spectrophotometer in a 1 cm quartz cell. The Agilent 1100 HPLC system with autosampler and fluorescence detector (FLD) were applied for determination of tocopherols content in oils. The pH measurements were made with a pH-meter (Mettler Toledo, SevenGo™). The shaker SHKA 2508 - 1CE (Labo Plus), centrifuge MPW-350 (LABO-MIX) and incubator INP 500 (Mettmert) were used for samples preparation.

### 2.3. Samples

Eighteen commercial edible oils, extra virgin olive oils, refined olive oil, rapeseed, corn, rice, sunflower and blended vegetable oils (Table 1), were manufactured in Spain, Italy, Poland, Germany, Hungary, Romania and were purchased from local markets in the original packing (poly(ethylene terephthalate) (PET) or glass bottles). All oils (ca. 30 g) were transferred into an amber-coloured glass bottles and stored below 10 °C in the dark until analysis.

#### 2.3.1. Oil samples preparation for determination of antioxidant capacity

Acetone and methanol extracts from the studied oils were obtained. The test tubes with oils (1.5000–3.5000 g) and solvent (10 mL) were shaken for 1 h at room temperature in the dark. The extracts were then separated from oils in a freezer (–20 °C, 1 h) and transferred quantitatively into a glass bottles. Each oil sample was extracted in triplicate and extracts were stored in refrigerator, prior to AC analysis.

## 2.4. Antioxidant capacity determination

### 2.4.1. Phenanthroline method

0.6 mL of acetonic or methanolic extracts of an oil sample, 1 mL of 0.2% FeCl<sub>3</sub> solution in acetone (methanol) and 0.5 mL of 0.5% 1,10-phenanthroline solution in acetone (methanol) were placed into a 10-mL volumetric flask and made up to volume with acetone or methanol. The obtained solution was mixed and left at room temperature in a dark. After 20 min, the absorbance of an orange-red solution was measured at 510 nm against a reagent blank (1 mL of FeCl<sub>3</sub> (0.2%) and 0.5 mL of Phen (0.5%) made up to 10 mL with acetone or methanol).

### 2.4.2. FRAP method

The spectrophotometric FRAP method was used for AC determination of oils according to Benzie and Strain [36] with minor modifications. The FRAP reagent contained 2.5 mL of a 10 mmol/L TPTZ solution in 40 mmol/L HCl, 2.5 mL of 20 mmol/L FeCl<sub>3</sub> and 25 mL of 0.1 mol/L acetate buffer (pH 3.6) was prepared freshly and incubated at 37 °C for 10 min. Then, 0.3 mL of acetonic or methanolic extracts of oil samples and 2 mL of FRAP reagent were transferred into a 10-mL volumetric flask and made up to volume with redistilled water. The obtained blue solutions were kept at room temperature for 10 min and centrifuged at 15,000 rpm for 10 min in a lab centrifuge to remove solids. The absorbance was measured at 593 nm against a reagent blank (2 mL of FRAP reagent made up to 10-mL with redistilled water).

### 2.4.3. Calibration curves

Calibration curves were prepared using working solutions of FeSO<sub>4</sub>·7H<sub>2</sub>O between 0.010–0.080 and 0.005–0.040 μmol/mL for Phen and FRAP methods, respectively. Five calibration curves for each method were plotted on the same day. The least-squares method was applied to calculate the lines  $y = 13.1x - 0.015$  and  $y = 10.0x - 0.014$  for acetonic and methanolic solutions of Phen method and  $y = 23.9x + 0.035$  for FRAP method. The correlation coefficients were 0.9988, 0.9997 and 0.9976 for Phen and FRAP methods, respectively. The relative standard deviations (R.S.D.,  $n = 5$ ) of the slopes were 0.2% and 0.8% for Phen method and 0.1% for FRAP method. The within day precision of each method was tested by analyzing five replicate samples containing 0.050 and 0.020 μmol/mL for Phen and FRAP methods, respectively. The obtained values of R.S.D. (1.8% and 2.4% for acetonic and methanolic solutions of Phen method and 2.2% for FRAP method) indicating reasonable repeatability of these methods. The proposed phenanthroline method ( $\epsilon = 1.27 \times 10^4$  and  $1.11 \times 10^4 \text{ dm}^3 \text{ mol}^{-1} \text{ cm}^{-1}$  for acetonic and methanolic solutions) appeared to be less sensitive than FRAP method ( $\epsilon = 2.62 \times 10^4 \text{ dm}^3 \text{ mol}^{-1} \text{ cm}^{-1}$ ). In comparison, Berker's et al. [31] found a similar value of the linear correlation coefficient (0.9997), R.S.D.<sub>slope</sub> (<2%) and molar absorptivity ( $2.14 \times 10^4 \text{ dm}^3 \text{ mol}^{-1} \text{ cm}^{-1}$ ) for the standard antioxidant (Trolox) analysis by Phen method. Moreover, the calculated detection (DL) and quantification limits (QL) (Table 2), confirm linearity concentrations ranges for AC determination by the proposed Phen and FRAP methods.

## 2.5. Determination of total phenols

Total phenols content were determined according to procedure described previously by Haiyan et al. [37], according to which samples of oils were weighed (5.0000 g), dissolved in hexane (15 mL) and extracted with methanol (3 × 5 mL, 2 min). The methanolic extracts were left overnight, washed with hexane (25 mL), 1 mL of extract was transferred into 10 mL calibration flask, 0.5 mL of Folin-Ciocalteu reagent added and shaken (3 min). To the extract, 1 mL of

saturated sodium carbonate solution was added and made up to the mark with redistilled water. After 1 h, solutions were centrifuged at 10,000 rpm (5 min) and absorbances at 725 nm, measured against a reagent blank.

Calibration curves were prepared for working solutions of caffeic acid in the concentration range 0.4–10 μg/mL. Five calibration curves were plotted using the least-squares method resulting in equation  $y = 0.075x + 0.001$ , where  $R^2 = 0.9985$ , R.S.D.<sub>slope</sub> = 0.8% and for  $c = 6 \mu\text{g CA/mL}$ , R.S.D. = 1.1% ( $n = 5$ ).

## 2.6. Determination of tocopherols

Tocopherols content was determined according to Bunge Europe Research and Development Center—in house method. Oil samples dissolved in hexane (0.5000 g in 5 mL) were injected (5–20 μL) on a LiChrospher 100 Diol (125 mm × 4 mm, 5 μm particle size, Agilent Technologies) column and analyzed by an Agilent 1100 HPLC system with autosampler and fluorescence detector. The mobile phase was hexane with tetrahydrofuran (96:4 vol/vol%) and a flow rate of 0.8 mL/min. The excitation and emission wavelengths at 280 and 340 nm were used, respectively. The concentrations were calculated from the calibration curves prepared for α-, β-, γ- and δ-tocopherol isomers.

## 2.7. Statistical analysis

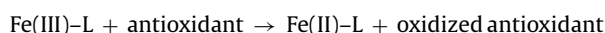
The AC of the studied oils were determined (5 portions of each oil extracts analyzed within 1 day) by the proposed Phen and FRAP methods. The obtained results were presented as: mean ( $c$ ) ± standard deviation (S.D.), within-day precision (R.S.D., %). Both methods of AC determination were compared for precision and accuracy using the Snedecor *F*-test and Student's *t*-test. Moreover, Pearson correlation test was used to determine the correlations between variables: AC results, total phenols content and total tocopherols content for different vegetable oils. Differences of  $p < 0.05$  were considered significant.

Principal component analysis was performed for the results of AC, TPC and TTC of the studied oils using the Statistica (Windows software package) (version 6.0, 2001). PCA score plot was used to determine, whether various oil samples could be grouped into different classes.

## 3. Results and discussion

### 3.1. Determination of antioxidant capacity of edible oil

The relevant chemical reaction of the Phen and FRAP methods should be presented by following equation:



where L is the ferrous-selective chromogenic ligand (1,10-phenanthroline or 2,4,6-tripyridyl-*s*-triazine). These analytical methods were used to determination of antioxidant capacities of vegetables oils and the obtained results were listed in Table 3.

It can be noted, that antioxidant capacity of the oil samples significantly differ from each other. This variability can be explained by the influences of genetic, environmental and technological factors, which would affect the level of antioxidants content. Moreover, the obtained AC results of the studied oils indicated, that acetone was more efficient solvent than methanol for extraction of antioxidants from olive oils, rapeseed, rice and sunflower oils (except SOF1 and SOF2) (Table 3). However, the AC values for acetonic extracts of CO, BO1, BO2 and BO3 oils were lower than for methanolic extracts of these oils. This suggests that the major antioxidants present in corn



**Table 2**  
Analytical parameters for the spectrophotometric determination of antioxidant capacity

Parameter	Phen method		FRAP method
	Acetonic solutions	Methanolic solutions	Aqueous solutions
Concentration range [ $\mu\text{mol/mL}$ ]	0.010–0.080	0.010–0.080	0.005–0.040
$b \pm S_b^a$	$13.1 \pm 0.2$	$10.0 \pm 0.08$	$23.9 \pm 0.6$
$a \pm S_a^a$	$-0.015 \pm 0.009$	$-0.014 \pm 0.002$	$0.035 \pm 0.014$
$S_{y/x}^a$	0.012	0.003	0.017
DL [ $\mu\text{mol/mL}$ ]	0.003	0.0009	0.002
QL [ $\mu\text{mol/mL}$ ]	0.009	0.003	0.007

$b$ : slope;  $a$ : intercept;  $S_b$ ,  $S_a$ : standard deviations of slope and intercept;  $S_{y/x}$ : standard deviation of  $y$ -residuals;  $DL = (3S_{y/x})/b$ ;  $QL = (10S_{y/x})/b$ .

<sup>a</sup>  $n = 5$ .

(CO), sunflower oils with garden green flowers (SOF1 and SOF2) and blended oils (BO1, BO2 and BO3) are more polar than those in olive oils, rapeseed, rice and the other sunflower oils under the experiment conditions. For comparison, acetone was a better extraction solvent than methanol for black peppercorn, rosehip, cinnamon [38] and buckwheat [39].

Moreover, antioxidant capacities of rapeseed (RO1, RO2), two sunflower oils with garden green flowers additives (SOF1, SOF2) and blended oil (BO3) were similar in comparison to the AC of extra virgin olive oils (Table 3). It is noteworthy, that AC values of the rapeseed oil (RO2) were the highest among the analyzed oils. Gorinstein et al. [34] also reported higher total radical-trapping antioxidative potential ( $32.4 \mu\text{mol}/100 \text{g}$ ) of the rapeseed oil than sunflower ( $20.1$  and  $31.9 \mu\text{mol}/100 \text{g}$ ) and grapeseed oils ( $29.0 \mu\text{mol}/100 \text{g}$ ). It can be noted that, olive oil (OO), corn, rice, sunflower oils (except SOF1 and SOF2) and two blended vegetables oils (BO1 and BO2) exhibit similar antioxidant capacities ranged between  $22.8$ – $105.8$  and  $23.5$ – $101.3 \mu\text{mol Fe}/100 \text{g}$  for methanolic extracts determined by Phen and FRAP methods, respectively. Besides, AC results for discussed oils revealed the same level or somewhat higher, when compared to those FRAP values obtained by other authors ( $152$  and  $65.3 \mu\text{mol}/100 \text{g}$  for olive and sunflower oils [14],  $40.0$ ,  $10.8$ ,  $15.3$  and  $10.0 \mu\text{mol}/100 \text{g}$  for canola, sunflower, olive and corn oils, respectively [19],  $20$ – $155 \mu\text{mol}/100 \text{g}$  for six virgin olive oils [10]).

The within-day precisions of the proposed Phen and the modified FRAP methods were tested by analyses of all oils in five replicates. The calculated values of R.S.D. for the proposed Phen method ( $0.8$ – $4.6\%$  and  $0.9$ – $4.9\%$  for acetonic and methanolic extracts, respectively) were comparable to those obtained by FRAP method ( $0.7$ – $4.0\%$  and  $0.6$ – $4.0\%$  for acetonic and methanolic extracts, respectively). These results indicate reasonable repeatability of the proposed Phen and the modified FRAP methods. Therefore, the Phen method can be applicable for antioxidant capacity determination of vegetable oils. In comparison, Sauracalixto and Goñi [14] and Manna et al. [10] found a somewhat higher values of R.S.D. ( $2.6$ – $6.8\%$ ) for AC determination of sunflower oil and olive oils by FRAP method.

Statistical analysis of the results obtained by the proposed Phen and FRAP methods using the  $F$ -test revealed no significant difference between the variances of the applied methods at the probability level  $p = 0.05$ . The calculated  $F$ -values (the variance ratio of FRAP and proposed Phen methods for AC determinations), ranging from  $1.01$  to  $6.24$  and  $1.07$ – $5.88$  for acetonic and methanolic extracts, are below  $F_{\text{theoretical}} = 6.39$  (Table 3). Therefore, the proposed Phen and known FRAP methods do not significantly differ in their precision. However, the experimental  $t$ -values for the studied antioxidant capacities of three methanolic extracts of oil samples EVOO2, EVOO4 and BO1 were higher than the critical value  $t = 2.78$

**Table 3**  
Antioxidant capacities of the studied oils

Sample	Antioxidant capacity								Statistical test			
	Phen method				FRAP method				$F_{\text{AcO}}$	$t_{\text{AcO}}$	$F_{\text{MeOH}}$	$t_{\text{MeOH}}$
	Acetonic extract		Methanolic extract		Acetonic extract		Methanolic extract					
	$c \pm \text{S.D.}^a$ [ $\mu\text{mol Fe}/100 \text{g}$ ]	R.S.D. [%]	$c \pm \text{S.D.}^a$ [ $\mu\text{mol Fe}/100 \text{g}$ ]	R.S.D. [%]	$c \pm \text{S.D.}^a$ [ $\mu\text{mol Fe}/100 \text{g}$ ]	R.S.D. [%]	$c \pm \text{S.D.}^a$ [ $\mu\text{mol Fe}/100 \text{g}$ ]	R.S.D. [%]				
EVOO1	$265.6 \pm 5.2$	2.0	$200.3 \pm 1.9$	0.9	$273.9 \pm 4.2$	1.5	$204.9 \pm 4.4$	2.1	1.57	2.13	5.54	2.37
EVOO2	$135.8 \pm 3.7$	2.7	$77.2 \pm 3.0$	3.9	$142.7 \pm 2.9$	2.1	$88.9 \pm 1.9$	2.2	1.58	2.75	2.37	5.76
EVOO3	$322.5 \pm 7.3$	2.3	$274.4 \pm 5.9$	2.2	$310.7 \pm 7.6$	2.5	$263.3 \pm 3.9$	1.5	1.09	2.35	2.31	2.77
EVOO4	$249.5 \pm 2.2$	0.9	$160.8 \pm 2.4$	1.5	$252.6 \pm 1.9$	0.7	$163.6 \pm 1.0$	0.6	1.34	2.00	5.88	2.96
OO	$55.8 \pm 0.5$	0.8	$42.8 \pm 0.6$	1.3	$54.3 \pm 1.1$	2.0	$42.1 \pm 0.3$	0.7	5.82	2.47	3.44	2.41
RO1	$154.0 \pm 2.6$	1.7	$144.0 \pm 4.0$	2.8	$157.9 \pm 3.5$	2.2	$150.9 \pm 2.7$	1.8	1.78	2.10	2.15	2.61
RO2	$336.5 \pm 3.1$	0.9	$307.3 \pm 3.9$	1.3	$339.6 \pm 4.5$	1.3	$300.1 \pm 6.0$	2.0	2.07	1.71	2.46	2.27
RBO	$66.6 \pm 0.8$	1.2	$61.3 \pm 0.9$	1.5	$68.5 \pm 1.3$	1.9	$62.6 \pm 1.5$	2.4	2.73	2.12	2.68	1.42
CO	$78.4 \pm 1.2$	1.5	$105.8 \pm 1.3$	1.3	$74.1 \pm 3.0$	4.0	$101.3 \pm 3.1$	3.1	6.24	2.63	5.48	2.70
SO1	$60.8 \pm 2.8$	4.6	$32.8 \pm 0.8$	2.5	$62.9 \pm 2.5$	4.0	$30.9 \pm 1.0$	3.4	1.24	1.71	1.56	2.31
SO2	$40.5 \pm 1.4$	3.4	$36.8 \pm 0.9$	2.3	$39.5 \pm 1.2$	3.1	$37.5 \pm 1.3$	3.4	1.27	1.18	2.30	2.32
SOG	$39.3 \pm 1.4$	3.6	$22.8 \pm 0.8$	3.5	$40.6 \pm 0.8$	2.1	$23.5 \pm 0.8$	3.3	2.89	2.65	1.07	1.44
SOP	$89.2 \pm 1.8$	2.0	$67.2 \pm 1.1$	1.6	$87.0 \pm 2.0$	2.3	$70.1 \pm 1.5$	2.1	1.26	1.48	2.02	2.61
SOF1	$249.2 \pm 2.4$	1.0	$312.9 \pm 4.7$	1.5	$244.7 \pm 2.6$	1.1	$306.5 \pm 2.4$	0.8	1.19	2.65	3.76	2.78
SOF2	$117.9 \pm 2.1$	1.8	$186.7 \pm 2.8$	1.5	$120.9 \pm 1.7$	1.4	$192.0 \pm 2.4$	1.2	1.61	2.05	1.45	2.34
BO1	$54.2 \pm 0.7$	1.3	$56.5 \pm 2.8$	4.9	$52.9 \pm 0.7$	1.3	$53.9 \pm 1.8$	3.4	1.01	2.10	2.22	3.84
BO2	$57.6 \pm 0.5$	0.9	$61.4 \pm 1.1$	1.8	$55.9 \pm 0.9$	1.6	$61.4 \pm 2.5$	4.0	2.94	2.78	4.89	0.039
BO3	$112.5 \pm 1.1$	1.0	$131.0 \pm 3.6$	2.7	$109.0 \pm 2.1$	1.9	$126.9 \pm 1.8$	1.4	3.25	2.58	3.83	2.52

S.D.: standard deviation; R.S.D.: relative standard deviation,  $F_{\text{AcO}}(F_{\text{MeOH}}) = s_2^2/s_1^2$ ,  $s_1^2$ ,  $s_2^2$ : variance of AC results for acetonic (AcO) and methanolic (MeOH) extracts obtained by Phen and FRAP methods;  $F_{\text{theoretical}} = 6.39$  ( $p = 0.05$ );  $t_{\text{theoretical}} = 2.78$  ( $p = 0.05$ ).

<sup>a</sup>  $n = 5$ .

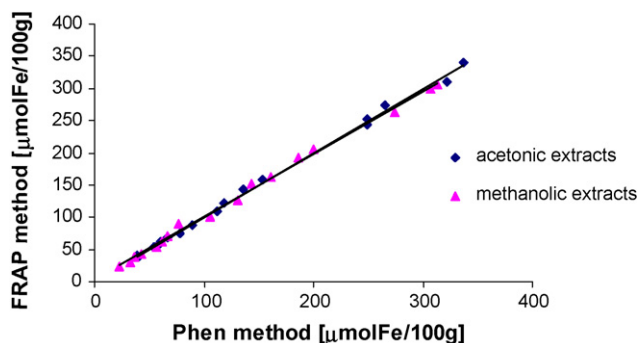


**Fig. 1.** Correlation between the FRAP and the proposed Phen methods for determination of antioxidant capacities of vegetable oils.

( $p=0.05$ ). The results collected in Table 3 indicate, that there are significant differences between the mean AC of two extra virgin olive oil (EVOO2, EVOO4) and blended oil (BO1) assayed by both analytical methods. Comparison of two experimental means of AC ( $n=5$ ) of the studied oils show, that the proposed method in three cases is affected by systematic errors. Although, the results of AC determination for all oils obtained by the two analytical methods do not differ significantly at  $p=0.001$ , because  $t_{\text{calculated}}$  values are below  $t_{\text{theoretical}}=8.61$  (Table 3). Therefore, the proposed Phen method gives accurate results for AC determination of edible oils with the exception of three mentioned above cases.

On the other hand, the regression lines for comparing two analytical methods were used. The correlation plots between the obtained results of AC determination in acetic and methanolic extracts of different oil samples using the proposed Phen and the modified FRAP methods are presented in Fig. 1.

A relatively high correlation coefficients of  $r=0.9989$  and  $0.9986$ , for AC determinations of acetic and methanolic extracts of all studied oils, indicate a good agreement between both methods. Moreover, the slope of the regression lines ( $b=0.9991 \pm 0.0246$  and  $0.9758 \pm 0.0278$  for acetic and methanolic extracts, respectively) were close to the model value of 1. Besides, the confidence limits of the intercepts ( $a=0.2190 \pm 4.1621$ ;  $2.9837 \pm 4.3586$ , for acetic and methanolic extracts, respectively) include the ideal value of 0. Therefore, the comparison between the results obtained by the proposed Phen and the modified FRAP methods suggests that, the two procedures give statistically comparable values of AC of different vegetable oils.

### 3.2. Determination of total phenols content in the studied oils

The total phenols contents in the studied oils are presented in Table 4.

Differences in phenols concentration in vegetable oils, can be related to cultivars, environmental factors, technological process, etc. [10]. It is notable, that TPC in extra virgin olive oils (12.6–34.7 mg CA/100 g), sunflower oils with garden green flowers (9.2 and 17.4 mg CA/100 g), rapeseed oils (4.7–17.5 mg CA/100 g), corn and blended (BO1) oils (5.7 and 5.0 mg CA/100 g) were the highest among all analyzed oils. Besides, sunflower oils (except SOF1 and SOF2) and olive oil, rice and other blended oils (BO2 and BO3) are less rich sources of total phenolic compounds (Table 4). For comparison, the concentrations of total polyphenols in sunflower and olive oils reported by Saura-Calixto and Goñi [14] were on the same level (14.0 and 17.3 mg/100 g). The studied sunflower oils and rapeseed oil (RO1) contain about 10 times higher amounts of TPC in comparison to the reported results (0.17–0.32 and 0.28–0.40 mg/100 g for sunflower and rapeseed oils, respectively) [24,34,40]. However, the average concentrations of phenols

**Table 4**

Total phenolic compounds and tocopherols contents in the studied oils

Sample	Total phenolic content $\pm$ S.D. <sup>a</sup> [mg CA/100 g]	Tocopherol content [mg/kg]				
		$\alpha$ -TE	$\beta$ -TE	$\gamma$ -TE	$\delta$ -TE	Total
EVOO1	23.3 $\pm$ 1.7	130	–	–	–	130
EVOO2	12.6 $\pm$ 0.5	160	–	–	–	160
EVOO3	34.7 $\pm$ 0.9	160	–	–	–	160
EVOO4	21.5 $\pm$ 0.7	190	–	–	–	190
OO	1.9 $\pm$ 0.08	170	–	–	–	170
RO1	4.7 $\pm$ 0.3	240	–	340	10	590
RO2	17.5 $\pm$ 0.3	290	–	370	10	670
RBO	2.6 $\pm$ 0.2	150	20	30	–	200
CO	5.7 $\pm$ 0.4	190	–	630	20	840
SO1	1.4 $\pm$ 0.03	660	–	–	–	660
SO2	3.6 $\pm$ 0.3	610	–	–	–	610
SOG	3.8 $\pm$ 0.1	560	20	–	–	580
SOP	1.9 $\pm$ 0.08	570	20	–	–	590
SOF1	17.4 $\pm$ 0.4	550	20	–	–	570
SOF2	9.2 $\pm$ 0.2	570	20	–	–	590
BO1	5.0 $\pm$ 0.3	470	20	–	–	490
BO2	3.2 $\pm$ 0.2	450	10	160	5	625
BO3	3.6 $\pm$ 0.2	180	20	550	20	770

S.D.: standard deviation.

<sup>a</sup>  $n=5$  (methanolic extract).

in the studied olive oils (1.9–34.7 mg CA/100 g) were similar to results for extra virgin and olive oils (3.4–35.8 mg/100 g [10], 0.4–26.5 mg/100 g [12], 5.5–12.6 mg/100 g [24], 13.9–34.0 mg/100 g [28], 5.7–63.3 mg/100 g [15]). Although, significantly lower TPC in some Spanish olives (0.21–0.46 mg/100 g) was determined by Gorinstein et al. [9].

The values of R.S.D. ranged between 0.9% and 8.2% for total polyphenols determination in all studied oils, indicating reasonable repeatability of the used method. For comparison, R.S.D. values of TPC determination in vegetable oils presented by others were somewhat higher, 7.1–11.6% for rapeseed and sunflower oils [34], 4.1% and 6.4% for olive and sunflower oils [14] and 8.7–11.1% for olive oils [9].

### 3.3. Determination of tocopherol content in the studied oils

Compositions of individual tocopherols in the studied vegetable oils (Table 4) were in good agreement with the values proposed by the Codex Alimentary Standard [41]. Olives and pure sunflower oils contained only  $\alpha$ -tocopherol, whereas  $\gamma$ - and  $\delta$ -tocopherols were determined in the analyzed rapeseed, corn and blended oils (except BO1). Moreover,  $\beta$ -tocopherol was determined in blended oils, rice oil and some sunflower oils (samples with additives). Therefore, the total contents of tocopherols in olive oils (80–190 mg/kg) and in rice oil (200 mg/kg) were significantly lower in comparison to the remaining vegetables oils (490–840 mg/kg). However, the total tocopherols determined in the discussed oils were somewhat lower, when compared to results obtained by Ninfali et al. [28] (124.7–214.2 mg/kg for olives), Pellegrini et al. [12] (138–369 mg/kg for olives), Hay et al. [26] (314, 481 and 1276 mg/kg for olive, canola and sunflower oils, respectively), Koski et al. [40] (96–266 mg/kg for olives and 716–858 mg/kg for rapeseed oils) and Tuberoso et al. [18] (217, 625 and 634 mg/kg for olive, rapeseed and sunflower oils, respectively).

### 3.4. Correlation between antioxidant capacity and total polyphenols and tocopherols in studied oils

Regression analysis was performed to calculate the correlation between the total content of polyphenols and antioxidant capacities of the studied oils.

As can be noted in Fig. 2, the obtained results indicate a significant correlation between TPC in all oils and their AC determined by Phen method ( $r=0.9012$  and  $r=0.7818$ ,  $p<0.000127$  for acetic and methanolic extracts, respectively, Fig. 2A). Similarly, TPC in the studied oils significantly relates to their antioxidant capacities determined by FRAP method ( $r=0.8947$  and  $r=0.7830$ ,  $p<0.000122$  for acetic and methanolic extracts, respectively, Fig. 2B). However, the highest correlation coefficients were observed between TPC in the analyzed oils and AC values for their acetic extracts ( $r=0.9012$  and  $r=0.8947$ ,  $p<0.000001$  for Phen and FRAP methods, respectively). Also, similar correlations between AC values and total phenols in olive oils were reported ( $r=0.8519$ – $0.9448$  [13],  $r=0.8250$ ,  $p<0.001$  [28],  $r=0.9590$ – $0.9979$  [9]).

Moreover, there was no linear correlation between total tocopherol contents in all studied oils (Table 4) and their antioxidant capacity determined by the proposed Phen method ( $r=0.3090$  and  $r=0.0656$  for acetic and methanolic extracts, respectively) and the modified FRAP method ( $r=0.3189$ ,  $0.0831$  for acetic and methanolic extracts, respectively). Probably other, than tocopherols, antioxidants which are present in the studied oils significantly contribute to their antioxidant capacities. For comparison, Tuberoso et al. [18] demonstrate significant correlation between free radical scavenging activity of vegetable oils determined by DPPH method and total tocopherol content ( $r=0.70$  and  $0.75$  for methanolic and ethyl acetate extracts). However, the correlation coefficient obtained by these authors was lower than the one obtained ( $r=0.9006$  and  $0.9032$ ) for the relations between TTC and AC of acetic and methanolic extracts of blended oils determined by Phen method.

### 3.5. Principal component analysis

Principal component analysis was applied to observe any possible clusters within analyzed oils samples. The first two principal components took into account 96.33% (PC1=78.26% and PC2=18.07%, respectively), of the total variation. The scores of the first two principal components, for 18 studied oils are presented in

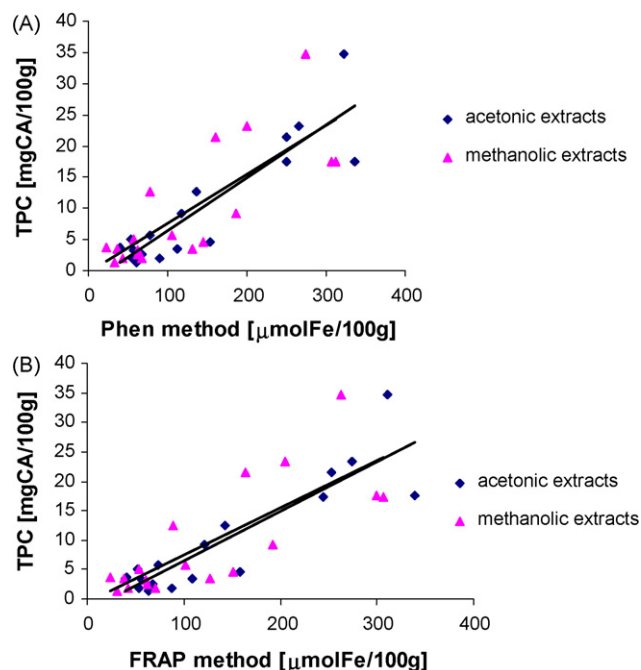


Fig. 2. Correlation between: total phenolic content (TPC) and Phen values (A) and total phenolic content and FRAP values (B).

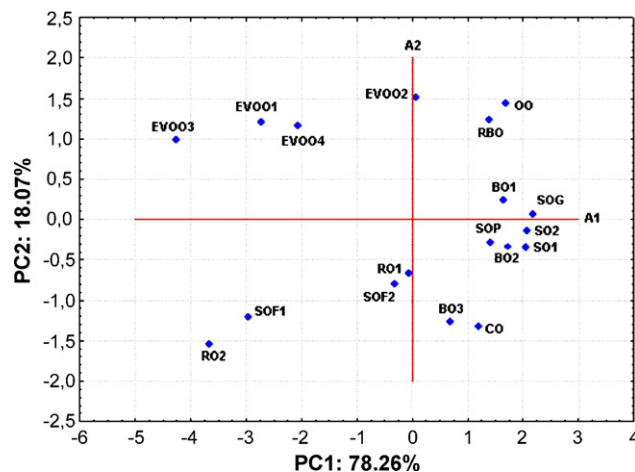


Fig. 3. Principal component analysis plot of antioxidant capacity determination, total phenolic and tocopherols contents in the studied vegetable oils.

Fig. 3. As can be seen, four distinct groups were formed by extra virgin olive oils (1), olive oil and rice oil (2), sunflower oils with two blended oils (BO1 and BO2) (3), rapeseed (RO1), sunflower oil with garden flowers (SOF2), blended (BO3) and corn oil (4), whereas samples of rapeseed oil (RO2) and sunflower oil (SOF1) were clearly separated from these groups. These oils groups generally reveal similar antioxidant capacities. The rapeseed oil (RO2) with the longest distance from other vegetable oils had the highest value of AC (Table 3), whereas the highest concentrations of total tocopherols were determined in corn (CO) and blended oils (BO3) (Table 4). It is noteworthy that, EVOO2 situated between cluster of the other extra virgin olive oils and rice (RBO) and olive oils (OO). Moreover, PCA graph revealed, that the studied oils with high antioxidant capacities were located to the left in the score plot, whereas oils with lower AC were situated at the right in the diagram. Furthermore, oils with low total tocopherols content were situated in the upper side of the scores plot, whereas oils with higher TTC were located under the A1 axis.

## 4. Conclusions

A new ferric-ion spectrophotometric method was developed for determination of antioxidant capacity of vegetable oils. The proposed Phen method is simple, precise and convenient for the determination of antioxidant capacities of vegetable oils. In contrast to FRAP method, the proposed Phen method does not involve the centrifugation of orange-red solutions before spectrophotometric measurements. Besides, the Phen method resulted in determination of AC in the wider concentration range ( $0.010$ – $0.080$   $\mu\text{mol}/\text{mL}$ ) than FRAP method ( $0.005$ – $0.040$   $\mu\text{mol}/\text{mL}$ ). It is noteworthy that, there is the linear and significant correlation between these two different analytical procedures.

The properties of the extracting solvents significantly affected the antioxidant capacity of vegetable oils. Acetone appeared to be better medium than methanol in extraction of antioxidants from olive oils, rapeseed, rice and sunflower oils (without SOF1 and SOF2).

Moreover, the Phen and FRAP results for the analyzed oils significantly correlate with total phenolic content.

The proposed Phen method and acetone were chosen due to preference of the fat industry for a simple procedure of antioxidant capacity determination with clearly low toxicity solvent.

## References

- [1] R. Lichtenthäler, F. Marx, O.M. Kind, *Eur. Food Res. Technol.* 216 (2003) 166.
- [2] J.K. Willcox, S.L. Ash, G.L. Catignani, *Crit. Rev. Food Sci. Nutr.* 44 (2004) 275.
- [3] P.A. Lachance, Z. Nakat, W.-S. Jeong, *Nutrition* 17 (2001) 835.
- [4] I.F.F. Benzie, *Comp. Biochem. Phys. A* 136 (2003) 113.
- [5] C.K.B. Ferrari, E.A.F.S. Torres, *Biomed. Pharmacother.* 57 (2003) 251.
- [6] E.C. Opara, *DM-Dis. Mon.* 52 (2006) 183.
- [7] H.E. Seifried, D.E. Anderson, E.I. Fisher, J.A. Milner, *J. Nutr. Biochem.* 18 (2007) 567.
- [8] O.I. Aruoma, *J. Am. Oil Chem. Soc.* 75 (1998) 199.
- [9] S. Gorinstein, O. Martin-Belloso, E. Katricha, A. Lojek, M. Číž, N. Gligelmo-Miguel, R. Haruenkit, Y.-S. Park, S.-T. Jung, S. Trakhtenberg, *J. Nutr. Biochem.* 14 (2003) 154.
- [10] C. Manna, S. D'Angelo, V. Migliardi, E. Loffredi, O. Mazzoni, P. Morrica, P. Galletti, V. Zappia, *J. Agric. Food Chem.* 50 (2002) 6521.
- [11] A. Valavanidis, C. Nisiotou, Y. Papageorgiou, I. Kremli, N. Satravelas, N. Zinieris, H. Zygalki, *J. Agric. Food Chem.* 52 (2004) 2358.
- [12] N. Pellegrini, F. Visioli, S. Buratti, F. Brighenti, *J. Agric. Food Chem.* 49 (2001) 2532.
- [13] C. Samaniego Sánchez, A.M. Troncoso González, M.C. García-Parrilla, J.J. Quesada Granados, H. López García de la Serrana, M.C. López Martínez, *Anal. Chim. Acta* 593 (2007) 103.
- [14] F. Saura-Calixto, I. Goñi, *Food Chem.* 94 (2006) 442.
- [15] M. Del Carlo, G. Sacchetti, C. Di Mattia, D. Compagnone, D. Mastrocola, L. Liberatore, A. Cichelli, *J. Agric. Food Chem.* 52 (2004) 4072.
- [16] J.C. Espín, C. Soler-Rivas, H.J. Wichers, *J. Agric. Food Chem.* 48 (2000) 648.
- [17] G. Sacchetti, S. Maietti, M. Muzzoli, M. Scaglianti, S. Manfredini, M. Radice, R. Bruni, *Food Chem.* 91 (2005) 621.
- [18] C.I.G. Tuberoso, A. Kowalczyk, E. Sarritzu, P. Cabras, *Food Chem.* 103 (2007) 1494.
- [19] S.Ch.M. Cheung, Y.T. Szeto, I.F.F. Benzie, *Plant Food Hum. Nutr.* 62 (2007) 39.
- [20] A. Szydłowska-Czerniak, Gy. Karlovits, C. Dianoczki, K. Recseg, E. Szlyk, *J. Am. Oil Chem. Soc.* 85 (2008) 141.
- [21] E. Finotti, F. Paoletti, A. Bertone, P. Galassi, G. Quaglia, *Nahrung* 42 (1998) 324.
- [22] G.K. Jayaprakasha, B.S. Jena, P.S. Negi, K.K. Sakariah, *Verlag der Zeitschrift für Naturforschung, Tübingen* 57c (2002) 828.
- [23] J.-L. Mau, E.Y.C. Lai, N.-P. Wang, Ch.-Ch. Chen, Ch.-H. Chang, Ch.-Ch. Chyau, *Food Chem.* 82 (2003) 583.
- [24] K. Papadopoulos, T. Triantis, E. Yannakopoulou, A. Nikokavoura, D. Dimotikali, *Anal. Chim. Acta* 494 (2003) 41.
- [25] G.O. Fruhwirth, F.S. Wagner, A. Hermetter, *Anal. Bioanal. Chem.* 384 (2006) 703.
- [26] K.X. Hay, V.Y. Waisundara, M. Timmins, B. Ou, K. Pappalardo, N. Mchale, D. Huang, *J. Agric. Food Chem.* 54 (2006) 5299.
- [27] P. Ninfali, G. Aluigi, M. Bacchiocca, M. Magnani, *J. Am. Oil Chem. Soc.* 78 (2001) 243.
- [28] P. Ninfali, M. Bacchiocca, E. Biagiotti, M. Servili, G. Montedoro, *J. Am. Oil Chem. Soc.* 79 (2002) 977.
- [29] L.L. Yu, K.K. Zhou, J. Parry, *Food Chem.* 91 (2005) 723.
- [30] J. Parry, L. Su, M. Luther, K. Zhou, M.P. Yurawecz, P. Whittaker, L. Yu, *J. Agric. Food Chem.* 53 (2005) 566.
- [31] K.I. Berker, K. Güçlü, İ. Tor, R. Apak, *Talanta* 72 (2007) 1157.
- [32] X. Liu, J. Zhao, R. Zheng, *Mutat. Res.* 539 (2003) 1.
- [33] R.L. Yang, G. Le, A. Li, J. Zheng, Y. Shi, *Nutrition* 22 (2006) 1185.
- [34] S. Gorinstein, H. Leontowicz, M. Leontowicz, A. Lojek, M. Číž, R. Krzeminski, Z. Zachwieja, Z. Jastrzebski, E. Delgado-Licon, O. Martin-Belloso, S. Trakhtenberg, *Nutr. Res.* 23 (2003) 317.
- [35] Ch.-P. Lee, G.-Ch. Yen, *J. Agric. Food Chem.* 54 (2006) 779.
- [36] I.F.F. Benzie, J.J. Strain, *Anal. Biochem.* 239 (1996) 70.
- [37] Z. Haiyan, D.R. Bedgood Jr., A.G. Bishop, P.D. Prenzler, K. Robards, *Food Chem.* 100 (2007) 1544.
- [38] L. Su, J.-J. Yin, D. Charles, K. Zhou, J. Moore, L.L. Yu, *Food Chem.* 100 (2007) 990.
- [39] T. Sun, Ch.-T. Ho, *Food Chem.* 90 (2005) 743.
- [40] A. Koski, E. Psomiadou, M. Tsimidou, A. Hopia, P. Kefalas, K. Wähälä, M. Heinonen, *Eur. Food Res. Technol.* 214 (2002) 294.
- [41] Codex Standard for Olive Oil, Virgin and Refined, and for Refined Olive-Pomace (Rev. 1-1989) OIL CODEX STAN 33-1981.



# The study of oxidization fluorescence sensor with molecular imprinting polymer and its application for 6-mercaptopurine (6-MP) determination

Li Wang, Zhujun Zhang\*

Department of Chemistry, School of Chemistry and Materials Science, Shaanxi Normal University, Xi'an 710062, PR China

## ARTICLE INFO

### Article history:

Received 25 December 2007  
Received in revised form 7 April 2008  
Accepted 12 April 2008  
Available online 20 April 2008

### Keywords:

6-Mercaptopurine  
Optical fiber sensor  
Molecular imprinted polymer  
Oxidation fluorescence

## ABSTRACT

This paper developed optical fiber sensor based on molecular imprinted polymer as artificial recognition element for the determination of 6-mercaptopurine (6-MP) in human serum. This approach displayed high sensitivity by oxidizing 6-MP to a strong fluorescent compound with  $\text{H}_2\text{O}_2$  in the alkaline media. It offered a relatively nice selectivity for 6-MP detection by molecular imprinted polymer's recognition. The relative standard deviation (R.S.D.) was 5% for a same sensor ( $n=5$ ) when 6-MP concentration was  $1.0 \times 10^{-7} \text{ g mL}^{-1}$  in serum. The developed method was satisfactorily applied to the determination of 6-MP in human serum without any necessity for sample treatment or time-consuming extraction steps prior to the analysis.

© 2008 Elsevier B.V. All rights reserved.

## 1. Introduction

Molecular imprinting is a rapidly developing technique for preparing polymeric materials, which can recognize target molecules by their complementary cavities [1,2]. Molecular imprinting polymer (MIP) has outstanding advantages such as predetermined selectivity, simple and convenient preparation, robustness in organic solvents and acidic or basic reagents, and durability to high temperature. MIP sensors have been developed and applied for the binding of drugs, herbicides, toxins, solvents, vapors and other biologically important molecules such as amino acids and their derivatives, peptides, proteins, nucleotides and nucleotide bases [3–8].

6-Mercaptopurine (6-MP) is an anti-cancer (“antineoplastic” or “cytotoxic”) chemotherapy drug with immunosuppressant properties. It interferes with nucleic acid synthesis by inhibiting purine metabolism and it is used, usually in combination with other drugs, for maintenance therapy of acute lymphoblastic leukemia. Various methodologies had been incorporated into high-performance liquid chromatography to detect 6-MP [9–13]. The chromatographic approach is both selective and sensitive, however, it may require expensive equipment and toxic solvents and often involves

complex sample pretreatments. Therefore, spectroscopic methodologies suitable for routine laboratories are welcomed. However, UV spectrophotometry procedures are subject to low sensitivity. As spectrofluorometry is among the most sensitive spectrophotometry methods of analysis, it has been chosen for developing methods to improve the sensitivity of analysis of 6-MP [14,15]. When they are not combined with sample pretreatment steps, the spectroscopic methodologies may suffer from the effect of the potentially interfering biological background, as well as from other unexpected sample components. Therefore, spectrofluorometry method is only reported for assay of 6-MP in tablets. Molecular imprinting techniques may be able to provide the required selectivity to overcome the problems of spectrofluorometry method, and could be used to assay of 6-MP in complex samples.

Our previous report successfully developed a high throughput chemiluminescence imaging coupled with MIP method for the rapid and selective chiral recognition of dansyl-phenylalanine [16]. Although, 6-MP could not be detected by chemiluminescence imaging, it can be converted to a strong fluorescence compound that can be detected by spectrofluorometry with higher sensitivity.

We present here some results obtained using a fiber-optic fluorescence sensing device analyzing 6-MP-based MIP sensors. The proposed sensors have been successfully applied to the analysis of 6-MP in human serum samples, which confirmed that the current optical fiber sensors based on MIP was a promising procedure for practical analysis.

\* Corresponding author. Tel.: +86 29 8530 8748; fax: +86 29 8530 7774.  
E-mail address: [zzj18@hotmail.com](mailto:zzj18@hotmail.com) (Z. Zhang).

## 2. Experimental

### 2.1. Materials

Trimethylolpropane trimethacrylate (TRIM) was purchased from Sigma (St. Louis, MO, USA). Methacrylic acid (MAA) was purchased from Sinopharm Chemical Co., Ltd. (Beijing, China). 2,2-Azobis(2-methylpropionitrile) (AIBN) was obtained from Shanghai No. 4 Chemical Reagent Factory (Shanghai, China). The standard 6-MP was purchased from the Chinese National Institute for the Control of Pharmaceutical and Biological Product. Stock solution of 6-MP was prepared by dissolving 5 mg 6-MP in 50 mL 0.01 mol L<sup>-1</sup> NaOH solution. The stock solution is stable at 5 °C for at least 2 months. Working standard solutions were obtained by appropriate dilution with 0.01 mol L<sup>-1</sup> NaOH solution.

Other reagents were purchased from Xi'an Chemical Reagent Factory (Xi'an, China). All other reagents used were of analytical reagent grade except for AIBN, which was chemical purity grade. AIBN was recrystallized prior to use.

### 2.2. Apparatus

All fluorescence measurements were carried out on a 970-CRT fluorescence spectrometer (Shanghai, China) with excitation and emission slits both set at 10 nm, respectively. A bifurcated optical fiber was used. The excitation light was carried to the well through one arm of the bifurcated optical fiber and the emission light collected through the other.

### 2.3. Preparation of molecularly imprinted microspheres

To demonstrate the utility of MIP-based sensor, the MIP was prepared using a TRIM/MAA matrix. Polymer was specifically tailored with selectivity by using 6-MP as template. The polymer was synthesized under following conditions: 1 mmol of template molecule and 3.0 mmol of MAA were dissolved in 40 mL of methanol in a glass ampoule by sonication for 5 min. 1.5 mmol of cross-linker (TRIM) and 50 mg of the initiator (AIBN) were then added. The solution was again sonicated for 5 min and saturated with dry nitrogen for 5 min and the tube sealed under nitrogen. Polymerization was started by placing the tube in a water bath at 60 °C for overnight.

The microspheres obtained were collected using a Hermle Labortechnik centrifuge model Z383K (Hermle Labortechnik, Wehingen, Germany) at 5500 rpm for 30 min and dried in vacuum 50 °C for 24 h. The template molecule was removed by several washing steps (3 × 1 h × 45 mL) in methanol containing 10% acetic acid (v/v), followed by the same volume of 0.01 mol L<sup>-1</sup> NaOH, then a final rinsing in acetone. The reference nonimprinted microspheres (NIPs) were prepared and treated in exactly the same way, except that no print molecule was used in the polymerization.

### 2.4. Fluorescence measurements with the fiber-optic device

Thirty microliters of particle suspension (1.5 × 10<sup>-3</sup> g mL<sup>-1</sup>) in methanol/water (1:1, v/v) containing 0.1% PVA was applied to each well of flat-bottom polystyrene microtiter plates (96 wells) dried at 70 °C for 30 min. Added 100 μL test compound solution to the well of microtiter plates coated with MIP microspheres, and the plates were placed 30 min for 6-MP adsorption to the MIP. Subsequently, the plates were rinsed thoroughly with distilled water and ethanol. The 50 μL H<sub>2</sub>O<sub>2</sub> and 50 μL NaOH solutions were added to the well after rinsing. The plates were place in constant temperature box at 80 °C for 40 min make the reaction complete. The fluorescence was quantified using the bifurcated optical fiber and the fluorescence spectrophotometer. The common end of the fiber was put into the

96 well. Two arms of the bifurcated optical fiber were fixed in the detecting chamber of the spectrofluorometer to carry the excitation and emission light. The fluorescence measurements were carried out at the maximum excitation wavelength of 310 nm and the maximum emission wavelength of 397 nm. After each measurement, the optical fiber was washed first with doubly distilled water and then with methanol until the fluorescence intensity reached the original blank value.

## 3. Results and discussion

### 3.1. Conditions optimization

It was reported that 6-MP could be oxidized to a strong fluorescent compound by H<sub>2</sub>O<sub>2</sub> in alkaline solution. In the present work, the oxidized reaction couple to MIP sensor was used to determination 6-MP. Various conditions were optimized.

The effect of H<sub>2</sub>O<sub>2</sub> concentration was investigated in the range from 0.0001 to 1 mol L<sup>-1</sup> at constant concentrations of 6-MP (7.0 × 10<sup>-7</sup> g mL<sup>-1</sup>) and 0.01 mol L<sup>-1</sup> NaOH; reaction temperature, 80 °C and reaction time, 40 min. The results were shown in Fig. 1. The fluorescence intensity increased with raising the concentration of H<sub>2</sub>O<sub>2</sub> up to 0.01 mol L<sup>-1</sup>. When H<sub>2</sub>O<sub>2</sub> concentration above 0.01 mol L<sup>-1</sup>, the fluorescence intensity decreased. Thus 0.01 mol L<sup>-1</sup> H<sub>2</sub>O<sub>2</sub> was used for further work.

The influence of NaOH concentration on the fluorescence intensity was studied at constant concentrations of 6-MP (7.0 × 10<sup>-7</sup> g mL<sup>-1</sup>) and 0.01 mol L<sup>-1</sup> H<sub>2</sub>O<sub>2</sub>; reaction temperature, 80 °C and reaction time, 40 min (Fig. 2). It is noteworthy that 0.01 mol L<sup>-1</sup> NaOH concentration was found to have the best result. Final the 0.01 mol L<sup>-1</sup> NaOH was selected.

The effect of reaction temperature on the fluorescence intensity was studied in the range of 25–80 °C for reaction 40 min at constant concentrations of 6-MP (7.0 × 10<sup>-7</sup> g mL<sup>-1</sup>), 0.01 mol L<sup>-1</sup> H<sub>2</sub>O<sub>2</sub> and 0.01 mol L<sup>-1</sup> NaOH. The results were shown in Fig. 3. The fluorescence intensity increased with raising the reaction temperature. Thus the max temperature of constant temperature box, 80 °C, was selected.

A series of experiments were performed to investigate the best reaction time, because the reaction time had tremendous influence on the extent of reaction. When the reaction temperature was 80 °C and other conditions were unaltered (only the reaction time was changed), the results showed that the fluorescence intensity increased when the reaction time prolonged in 40 min, above 40 min, only a small increase of signal was observed with prolong-

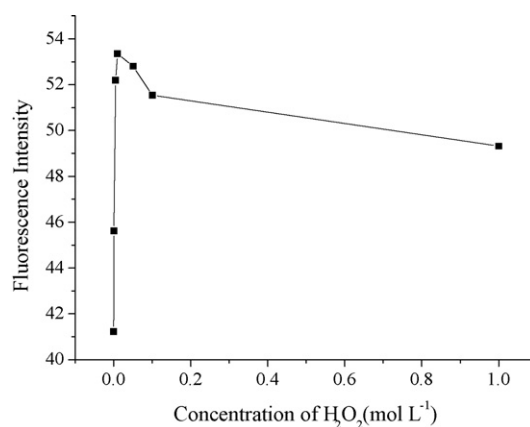


**Fig. 1.** Effect of H<sub>2</sub>O<sub>2</sub> concentration on fluorescence intensity. Detection condition: 6-MP concentration, 7.0 × 10<sup>-7</sup> g mL<sup>-1</sup>; NaOH concentration, 0.01 mol L<sup>-1</sup>; reaction temperature, 80 °C; reaction time, 40 min.

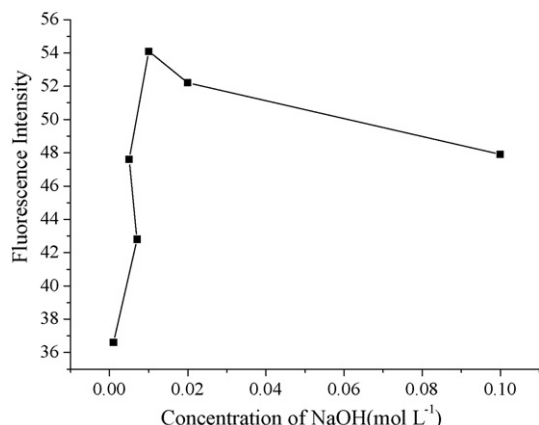


**Fig. 2.** Effect of NaOH concentration on fluorescence intensity. Detection condition: 6-MP concentration,  $7.0 \times 10^{-7}$  g mL $^{-1}$ ; H $_2$ O $_2$  concentration, 0.01 mol L $^{-1}$ ; reaction temperature, 80 °C; reaction time, 40 min.

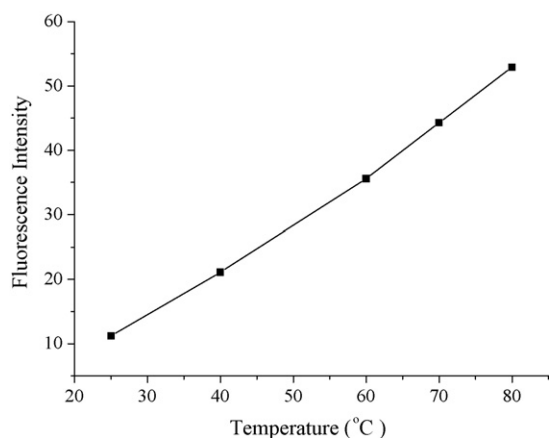


**Fig. 3.** Effect of reaction temperature on fluorescence intensity. Detection condition: 6-MP concentration,  $7.0 \times 10^{-7}$  g mL $^{-1}$ ; H $_2$ O $_2$  concentration, 0.01 mol L $^{-1}$ ; NaOH concentration, 0.01 mol L $^{-1}$ ; reaction time, 40 min.

ing time. Forty minutes was selected as the reaction time in our experiment. These solutions are stable at 25 °C for at least 1 h.

The excitation and emission spectra of 6-MP and its oxidation product were illustrated in Fig. 4. According to these spectra shown in Fig. 4, excitation wavelength of 310 nm and emission wavelength of 397 nm were, respectively selected for the oxidation spectrofluorimetric determination of 6-MP.

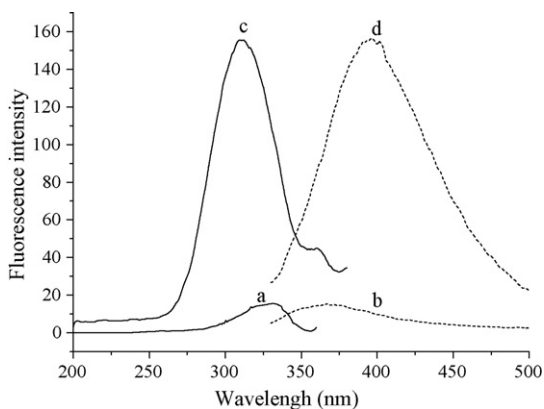


**Fig. 4.** Fluorescence excitation (solid line) and emission spectra (dashed line) for  $6.0 \times 10^{-6}$  g mL $^{-1}$  6-MP (a, b) and its oxidation product (c, d).

**Table 1**

Tolerable concentration ratios with respect to 6-MP for some interfering substances with and without MIP

Interference substances	Concentration ratio (concomitant to 6-MP)	
	With NIP	With MIP
Na $^+$ , Cl $^-$	50	500
Mg $^{2+}$	50	500
Fe $^{3+}$	100	1000
Zn $^{2+}$	500	1000
Vitamin B1	50	500
Vitamin C	50	500
Uric acid	50	500
Urea	100	1000
Glucose	50	500
Ascorbic acid	20	200

MIP microspheres were immobilized at the bottom of polypropylene tubes used 0.1% PVA according to our previous work [16].

### 3.2. Method validation

All quantitative analyses were performed under the optimum conditions.

#### 3.2.1. Linearity, sensitivity and precision

Under the optimum conditions described above, the calibration graph of emission intensity against 6-MP concentration was linear in the range  $1.0 \times 10^{-8}$  g mL $^{-1}$  to  $6.0 \times 10^{-6}$  g mL $^{-1}$  and the detection limit was  $3.0 \times 10^{-9}$  g mL $^{-1}$  (S/N=3). All measurements were carried out using five replicate measurements ( $n=5$ ). The linear calibration response curves can be described by the equation  $I = 63.29C$  ( $10^{-6}$  g mL $^{-1}$ ) + 6.723 ( $r=0.9998$ ) with the sensitivity set at 2, both excitation and emission slit widths set at 10 nm, where  $I$  is S/N,  $C$  is the concentration of 6-MP, and  $r$  is the correlation coefficient. The determination was based on the sensor array (96 microtiter plate). One sensor was used only once, it needs not regeneration. Complete analysis, including sampling and analysis, could be performed in 1 h. The relative standard deviation was less than 7.0% for  $1.0 \times 10^{-7}$  g mL $^{-1}$  6-MP in human serum samples ( $n=5$ ). This level of precision of the proposed method was adequate for the quality analysis of 6-MP.

#### 3.2.2. Interferences study

The interference of some components commonly present in serum was investigated by analyzing a standard solution of  $1.0 \times 10^{-7}$  g mL $^{-1}$  6-MP. The effects of substances including metal ions, amino acids and carbohydrates on the determination were tested by adding the interfering substances to 6-MP solution. The tolerable limit of existed species was taken as a relative error not greater than 5%. At the same time, the interference of these species to 6-MP under the same conditions with NIP was also carried out. The results (Table 1) showed that these substances in human serum in the normal concentration range did not interfere with the determination of 6-MP.

### 3.3. Analytical applications

The above results encourage the use of the proposed method described for the assay of 6-MP in human serum samples.

#### 3.3.1. Determination of 6-MP in serum

Analysis of spiked serum samples was obtained on the optimum conditions. Human serums were obtained from healthy persons. The serum was added to the ultrafiltration tube and centrifuged

**Table 2**  
Recovery for 6-MP in human serum samples

Sample	Added ( $10^{-6}$ g mL $^{-1}$ )	Found ( $10^{-6}$ g mL $^{-1}$ ) <sup>a</sup> ±S.D.	Recovery (%)	R.S.D. (%)
Serum 1	0.30	0.28 ± 0.02	94	2.5
Serum 2	1.00	0.95 ± 0.09	95	2.6
Serum 3	0.050	0.053 ± 0.008	106	3.1

<sup>a</sup> Average of three results.

at 4000 rpm for 30 min. The supernatants were used. A known amount of standard solution added to the 2.5 mL supernatant and the mixture was diluted to 50 mL with doubly distilled water. Fifty microliters spiked sample was added into the 96 well plates and used for 6-MP analysis. The method was validated using the recovery test. The results of the recovery test are showed in Table 2. As can be seen from Table 2, the recoveries of added 6-MP can be quantitative and *t*-test assumed that there is no significant difference between recoveries and 100% at confidence level of 95%.

#### 4. Conclusions

In this paper, we have presented results of fluorescence optical fiber investigation of the oxidation of 6-MP in MIP sensors. MIP has many advantages, including stability under harsh environment, the simplicity of their preparation and can be used as alternatives for enzymes and antibodies in sensors. In this proposed method, the structure of the analyte was changed through the oxidation

reaction, which converts 6-MP to a compound that can be detected with higher sensitivity.

#### Acknowledgement

We gratefully acknowledge Chinese Natural Science Foundation for financial support (project no. 30470886).

#### References

- [1] G. Wulff, A. Sarhan, *Angew. Chem., Int. Ed. Engl.* 34 (1995) 1812.
- [2] J.H.G. Steinke, D.C. Sherrington, I.R. Dunkin, *Adv. Polym. Sci.* 123 (1995) 80.
- [3] S.A. Piletsky, S. Alcock, A.P.F. Turner, *Trends Biotechnol.* 19 (2001) 9.
- [4] Y.F.H. Olivier, D.C. Cullen, S.A. Piletsky, *Anal. Bioanal. Chem.* 382 (2005) 947.
- [5] A.L. Hillberg, K.R. Brain, C.J. Allender, *Adv. Drug. Deliv. Rev.* 57 (2005) 1875.
- [6] S.A. Piletsky, S. Subrahmanyam, A.P.F. Turner, *Sensor Rev.* 21 (2001) 292.
- [7] A. Fernández-González, L. Guardia, R. Badía-Laiño, M.E. Díaz-García, *TrAC, Trends Anal. Chem.* 25 (2006) 949.
- [8] S.A. Piletsky, A.P.F. Turner, *Electroanalysis* 14 (2002) 317.
- [9] C. Stefan, W. Walsh, T. Banka, K. Adeli, Z. Verjee, *Clin. Biochem.* 37 (2004) 764.
- [10] N. Erb, U. Haverland, D.O. Harms, G. Escherich, G. Janka-Schaub, *J. Chromatogr. B* 796 (2003) 87.
- [11] X.-N. Cao, L. Lin, Y.-Y. Zhou, G.-Y. Shi, W. Zhang, K. Yamamoto, L.-T. Jin, *Talanta* 60 (2003) 1063.
- [12] E.C. Van Os, J.A. McKinney, B.J. Zins, D.C. Mays, Z.H. Schriver, W.J. Candborn, J.J. Lipsky, *J. Chromatogr. B* 679 (1996) 147.
- [13] Y. Su, Y.H. Yuen, Y.Q. Chu, E.C. Matthijis, V.D. Poll, M.V. Relling, *J. Chromatogr. B* 732 (1999) 459.
- [14] C. Huang, Z. Pan, *Chin. J. Anal. Lab.* 20 (2001) 58 (in Chinese).
- [15] C. Huang, L. Zhang, Ch. Duanmu, C. Zuo, Z. Pan, *J. Anal. Sci.* 15 (1999) 464 (in Chinese).
- [16] L. Wang, Z. Zhang, L. Huang, *Anal. Bioanal. Chem.* 390 (2008) 1431.





# On-line separation and preconcentration of inorganic arsenic and selenium species in natural water samples with CTAB-modified alkyl silica microcolumn and determination by inductively coupled plasma-optical emission spectrometry

Chaomei Xiong, Man He, Bin Hu\*

Department of Chemistry, Wuhan University, Wuhan 430072, PR China

## ARTICLE INFO

### Article history:

Received 4 January 2008

Received in revised form 10 April 2008

Accepted 12 April 2008

Available online 22 April 2008

### Keywords:

As(III)/As(V)

Se(IV)/Se(VI)

Solid phase extraction (SPE)

ICP-OES

Cetyltrimethylammonium bromide (CTAB)

Natural water

## ABSTRACT

A new, simple, and selective method has been presented for the separation and preconcentration of inorganic arsenic (As(III)/As(V)) and selenium (Se(IV)/Se(VI)) species by a microcolumn on-line coupled with inductively coupled plasma-optical emission spectrometry (ICP-OES). Trace amounts of As(V) and Se(VI) species were separated and preconcentrated from total As and Se at desired pH values by a conical microcolumn packed with cetyltrimethylammonium bromide (CTAB)-modified alkyl silica sorbent in the absence of chelating reagent. The species adsorbed by CTAB-modified alkyl silica sorbent were quantitatively desorbed with 0.10 ml of 1.0 mol l<sup>-1</sup> HNO<sub>3</sub>. Total inorganic arsenic and selenium were similarly extracted after oxidation of As(III) and Se(IV) to As(V) and Se(VI) with KMnO<sub>4</sub> (50.0 μmol l<sup>-1</sup>). The assay of As(III) and Se(IV) were based on subtracting As(V) and Se(VI) from total As and total Se, respectively. All parameters affecting the separation/preconcentration of As(V) and Se(VI) including pH, sample flow rate and volume, eluent solution and volume have been studied. With a sample volume of 3.0 ml, the sample throughput was 24 h<sup>-1</sup> and the enrichment factors for As(V) and Se(VI) were 26.7 and 27.6, respectively. The limits of detection (LODs) were 0.15 μg l<sup>-1</sup> for As(V) and 0.10 μg l<sup>-1</sup> for Se(VI). The relative standard deviations (RSDs) for nine replicate determinations at 5.0 μg l<sup>-1</sup> level of As(V) and Se(VI) were 4.0% and 3.6%, respectively. The calibration graphs of the method for As(V) and Se(VI) were linear in the range of 0.5–1000.0 μg l<sup>-1</sup> with a correlation coefficient of 0.9936 and 0.9992, respectively. The developed method was successfully applied to the speciation analysis of inorganic arsenic and selenium in natural water samples with satisfactory results.

© 2008 Elsevier B.V. All rights reserved.

## 1. Introduction

The different chemical forms of a given element may reveal significant different behavior of mobility and bioavailability [1]. Arsenic is widely known as a toxic element and naturally present in all natural systems in various forms including inorganic arsenic species (As(III)/As(V)) and organic arsenic species (monomethylarsonate (MMA), dimethylarsonate (DMA), arsenobetaine (AsB), arsenocholine (AsC), etc.). It is well documented that inorganic arsenic species, especially arsenite (As(III)), are more toxic than their organic counterparts [2]. Selenium is recognized as both an essential nutrient element and a toxic element to mammalian species, and it is characterized by a very narrow concentration range between essentiality, deficiency and toxicity [3]. Similarly, inorganic forms of selenium are more toxic than organic forms,

and the toxicity of Se(VI) is more severe than Se(IV) for humans and most other mammals [4]. Therefore, it is particularly important to develop analytical methods for the separation and preconcentration of arsenic and selenium in environmental and biological systems [5].

In the majority of environmental matrices, such as natural water, arsenic and selenium are usually present as As(III)/As(V) and Se(IV)/Se(VI) [4,6]. Analytical methods for the separation and preconcentration of arsenic or selenium have been reviewed [4,7,8]. The general methods for the separation and preconcentration of inorganic arsenic and selenium are based on combining a very efficient separation technique with a sensitive detection technique. Various detection techniques, such as atomic fluorescence spectrometry (AFS) [9], atomic absorption spectrometry (AAS) [10], stripping voltammetry [11–13], inductively coupled plasma-optical emission spectrometry (ICP-OES) [14,16–18] and inductively coupled plasma-mass spectrometry (ICP-MS) [8,15] have been applied to accurately determine trace arsenic or selenium and its species in various samples. Of all those detection methods, ICP-OES

\* Corresponding author. Tel.: +86 27 68752126; fax: +86 27 68754067.  
E-mail address: [binhu@whu.edu.cn](mailto:binhu@whu.edu.cn) (B. Hu).

has been considered to be one of the most efficient and robust element-specific techniques due to its high sensitivity, simultaneous multielement determination, simple operation and ease for on-line determination, thus extensively applied in trace element analysis. However, direct application of ICP-OES for the determination of trace elements in environmental and biological systems is limited due to sample matrix or spectral interference. Hence, an effective separation method is often required [16–18].

The separation techniques for the elemental speciation could be generally classified into chromatographic and non-chromatographic techniques. The chromatographic techniques include high performance liquid chromatography [10], capillary electrophoresis [14], size exclusion chromatography (SEC) [15], and ion-chromatography [19]. Non-chromatographic separation techniques include solvent extraction [20], co-precipitation [21], cloud point extraction [22] and solid phase extraction (SPE) [9,23–30]. For a simple elemental speciation, especially for different oxidation state of a given element, non-chromatographic methods are more diffused than the chromatographic techniques. Among these non-chromatographic techniques, SPE has been effectively employed due to some merits including convenience, low cost, time saving, reduced solvent utilization, possible miniaturization and easy automation [31].

There are two operation modes for SPE: batch operation and column operation, while the latter could be divided into off-line and on-line operation modes. In recent years, on-line preconcentration technique has attracted more attention because of its remarkable merits of overcoming the drawback of batch operation to a greater extent and further enhancing preconcentration. Blank values caused by the laboratory environment and reagents can be significantly reduced, and limits of detection (LODs) can be decreased as a result of the inert and closed nature of an on-line system [9].

It should be noted that the investigation of sorbents plays a key role in the development of SPE. Some solid phase sorbents including polytetrafluoroethylene fiber [9], ion-exchange resin [23,24], controlled pore glass [25], non-polar C-18 cartridge [26], Diaion HP-2MG resin [27], modified mesoporous TiO<sub>2</sub> [28], activated carbon [29], and porous graphitic carbon [30] have been employed for the separation and preconcentration of arsenic and/or selenium. Nowadays, much attention has been paid to the investigation of new adsorption materials for elemental speciation in SPE. There are some reports about the application of anionic surfactant or cationic surfactant modified solid phase adsorption materials for the separation and preconcentration of trace elements in various samples [32,33]. These methods were all based on the formation of ion-associated complexes (metal-complexing agent-surfactant) by choosing specific complexing agents. As a cationic surfactant, cetyltrimethylammonium bromide (CTAB) forms ion-associated complexes with complex anions due to its amino group, which can transform into [R<sub>3</sub>R'N]<sup>+</sup>Br<sup>-</sup> in acidic media and be utilized as the counter-ions in the traditional extraction. Thus, it can exchange with anion complexes of metals like conventional anion exchanger. Alkyl silica is a kind of hydrophobic solid phase adsorption material and it is likely for CTAB to be adsorbed onto alkyl silica due to its hydrophobic moieties. Actually no data are published about the use of CTAB-modified alkyl silica as adsorption material for elements analysis.

The aim of this work was to prepare a new kind of sorbent by on-line immobilizing CTAB onto alkyl silica, and to develop a sensitive and simple method for the separation and preconcentration of As(III/V) and Se(IV/VI) based on CTAB-modified alkyl silica sorbent separation/preconcentration on-line coupled with ICP-OES. The retention and elution conditions for separation and preconcentration of inorganic arsenic and selenium species have been

**Table 1**  
Operation parameters of Intrepid XP Radial ICP-OES

RF generator power (W)	1300
Frequency of RF generator (MHz)	27.12
Plasma gas flow rate (l min <sup>-1</sup> )	14
Carrier gas (l min <sup>-1</sup> )	0.6
Auxiliary gas flow rate (l min <sup>-1</sup> )	0.5
Integration times (s)	15
Emission lines (nm)	As, 189.042 Se, 196.090

studied and the optimized experimental conditions were established. The developed method was applied to the separation and preconcentration of inorganic As and Se in natural water samples with satisfactory results.

## 2. Experimental

### 2.1. Apparatus and operating conditions

Intrepid XP Radial ICP-OES (Thermo, Waltham, MA, USA) with a concentric nebulizer and a Cinnabar spray chamber was used for the determination of As and Se species. The instrument operating conditions and wavelengths used are given in Table 1. The pH values were adjusted by a Mettler Toledo 320-S pH meter (Mettler Toledo Instruments Co. Ltd., Shanghai, China) supplied with a combined electrode. A conical microcolumn ( $\Phi$ 0.6 mm  $\times$  5 mm, 50 mm length, 200  $\mu$ l pipet tip, Yuhua Experimental Instrument Factory, Haimen, Jiangsu, China) made of polypropylene material was used as the CTAB-modified alkyl silica sorbent holder. A HL-2 peristaltic pump (Shanghai Qingpu Huxi Instrument Factory, Shanghai, China) was employed to propel the solution.

### 2.2. Standard solution and reagents

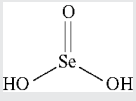
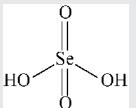
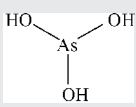
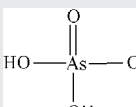
As(III) and As(V) stock solutions (1.0 g l<sup>-1</sup> as As) were prepared from analytical grade sodium arsenite (Shanghai Reagent Co. Ltd., Shanghai, China) and sodium arsenate (Shanghai Reagent Co. Ltd., Shanghai, China), respectively, by dissolving their appropriate amounts in high-purity deionized water (18.2 M $\Omega$  cm) obtained from a Labconco system. Se(IV) and Se(VI) stock solutions (1.0 g l<sup>-1</sup> as Se) were prepared from analytical grade sodium selenite (Wako Pure Chemical Industries, Ltd., Japan) and sodium selenate (Wako Pure Chemical Industries, Ltd., Japan), respectively, by dissolving their appropriate amounts in high-purity deionized water. Working standard solutions were prepared daily by stepwise dilution of their stock solutions with high-purity deionized water. Some characteristics of arsenic and selenium species are summarized in Table 2.

CTAB (99+%) was obtained from Acros Organics, New Jersey, USA. HCl (Shanghai Reagent Co. Ltd., Shanghai, China) and HNO<sub>3</sub> (Shanghai Reagent Co. Ltd., Shanghai, China) were of the highest purity available. 0.1 mol l<sup>-1</sup> sodium acetate-acetic acid buffers were prepared to control pH values.

Alkyl silica (100–150 mesh) (The First Reagent Factory, Shanghai, China) was immersed in ethanol and 1.0 mol l<sup>-1</sup> HNO<sub>3</sub> for 24 h sequentially. It was then filtered, washed with high-purity deionized water until it was neutral, and dried prior to storage for future use.

All laboratory ware made of polyethylene or polypropylene material were thoroughly cleaned by soaking in nitric acid (5%, v/v) for at least 24 h. Prior to use, all acid-washed containers were rinsed with high-purity deionized water.

**Table 2**  
Structure and  $pK_a$  values of inorganic As and Se species [4,23,34]

Species	Molecular formula	$pK_a$	Structure
Selenious acid (Se(IV))	$H_2SeO_3$	$pK_{a1} = 2.46$	
		$pK_{a2} = 7.31$	
Selenic acid (Se(VI))	$H_2SeO_4$	Strong acid	
		$pK_{a2} = 1.92$	
Arsenous acid (As(III))	$H_3AsO_3$	$pK_{a1} = 9.2$	
		$pK_{a2} = 12.1$	
Arsenic acid (As(V))	$H_3AsO_4$	$pK_{a1} = 2.3$	
		$pK_{a2} = 6.8$	
		$pK_{a3} = 11.6$	

### 2.3. On-line preparation of CTAB dynamically modified alkyl silica microcolumn

In this study, CTAB was dynamically coated on alkyl silica sorbent, and the modification procedure is described as follows: a total of 60 mg of alkyl silica sorbent was filled into a 200  $\mu$ l pipet tip plugged with a small portion of cotton at both ends. 1.0 ml 0.5% (m/v) CTAB was passed through the microcolumn at a flow rate of 0.5 ml  $min^{-1}$ . After on-line modification, 1.0 ml of 1.0 mol  $l^{-1}$   $HNO_3$  was passed through the microcolumn to elute the possible impurities. After cleaning with 2 ml of high-purity deionized water, the microcolumn was conditioned to the desired pH value with appropriate HAc-NaAc buffer solution. The on-line modification procedure was repeated after every 15 times usage of the column.

### 2.4. General procedure

Certain volume of sample solution containing the species of interest was divided into three equal parts, which were named sample 1, 2 and 3 and their pH values were adjusted to 2.0, 6.5 and 6.5, respectively. Meanwhile, 50.0  $\mu$ mol  $l^{-1}$   $KMnO_4$  was added into sample 3 for the oxidation of As(III) and Se(IV) into As(V) and Se(VI), respectively.

Three milliliters of sample 1 was pumped through the microcolumn by a peristaltic pump at a flow rate of 1.7 ml  $min^{-1}$ , and then high-purity deionized water was passed through to wash off the residual sample matrix on the column. The retained Se(VI) was eluted with 0.10 ml of 1.0 mol  $l^{-1}$   $HNO_3$  at a flow rate of 1.7 ml  $min^{-1}$ , and the eluate was transferred directly into ICP-OES for Se(VI) determination. Three milliliters of sample 2 (for As(V)) and sample 3 (for total As and total Se) were processed using the same procedure mentioned above. The concentrations of the species were on-line determined by ICP-OES. The concentration of As(III) and Se(IV) in the sample solution were calculated by subtracting As(V) and Se(VI) from total As and Se, respectively.

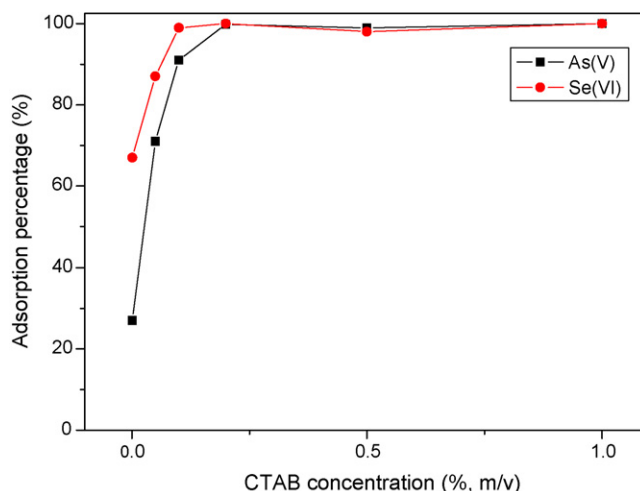


**Fig. 1.** Effect of concentration of CTAB on the adsorption percentage of As(V) and Se(VI) with on-line modification. Conditions: As(V) and Se(VI), 2.0 mg  $l^{-1}$ ; flow rate, 0.5 ml  $min^{-1}$ ; amount of alkyl silica, 60 mg.

Three replicates of high-purity deionized water without any species of interest were used as the blank solutions. The blank values for As(V), Se(VI) and total As and Se were determined after the blank solutions were subjected to the procedures described for samples as in sample 1, 2, and 3. The actual concentrations of the species were obtained after blank subtraction.

The quantitative analysis was performed by the external standard method: the calibration curve for each species was obtained after subjecting a series of standard solutions (0.5, 1.0, 5.0, 10.0, 50.0, 100.0, 500.0, 1000.0  $\mu$ g  $l^{-1}$ ) to the same analytical procedure. The calibration curve was obtained, and the concentrations of analytes in the samples were calculated based on the calibration curve.

### 2.5. Sample preparation

Nine fresh natural water samples (river water, lake water, well water, rain water, pool water, tap water, etc.) were collected and filtered through 0.45  $\mu$ m membrane filters (Tianjin Jinteng Instrument Factory, Tianjin, China) made of polytetrafluoroethylene material. The filtrates were subjected to the analytical procedure described above immediately after filtration to avoid the possible transformation of inorganic As and Se species.

## 3. Results and discussion

### 3.1. On-line optimization of CTAB concentration

Fixing the volume and flow rate of CTAB at 1.0 ml and 0.5 ml  $min^{-1}$ , respectively, the optimum concentration of CTAB loaded onto alkyl silica was estimated. As shown in Fig. 1, As(V) and Se(VI) were adsorbed quantitatively on the CTAB-modified alkyl silica microcolumn when the concentration of CTAB was equal to or higher than 0.2% (m/v). Considering the possible competitive adsorption from other ions, a higher concentration of 0.5% was used in future work.

### 3.2. Effect of pH

Solution pH plays an important role in adsorption and separation of different species on adsorption materials. The effect of pH of the aqueous solutions on the adsorption of As(III)/As(V) and Se(IV)/Se(VI) in the microcolumn of alkyl silica sorbent with

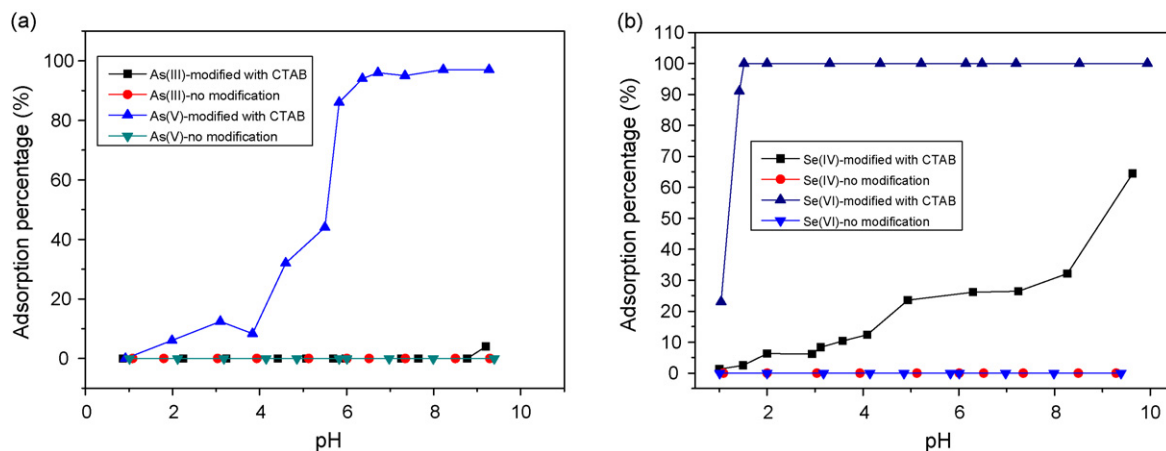
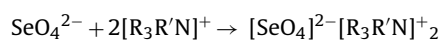
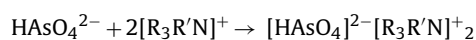


**Fig. 2.** Effect of pH on the adsorption percentage of As(III)/As(V) (a) and Se(IV)/Se(VI) (b) on alkyl silica sorbent with/without CTAB modification. Conditions: As(III/V) and Se(IV/VI),  $1.0 \text{ mg l}^{-1}$ ; sample volume,  $1.0 \text{ ml}$ ;  $\text{HNO}_3$ ,  $1.0 \text{ mol l}^{-1}$ ; eluent volume,  $1.0 \text{ ml}$ ; sample/eluent flow rate,  $1.7 \text{ ml min}^{-1}$ . The errors of the experimental values  $\leq \pm 5.0\%$ .

or without CTAB modification was examined in the pH range of 1.0–10.0. As can be seen in Fig. 2, none of the species had quantitative adsorption on the untreated silica in the studied pH range. On the contrary, the CTAB-modified sorbent showed different adsorption characteristics towards arsenic and selenium species in pH range of 1.0–10.0. As(V) was quantitatively adsorbed by the CTAB-modified sorbent in the pH range of 6.0–10.0, while As(III) was not retained at any pH. Se(VI) could be adsorbed completely in a wide pH range of 1.5–10.0, whereas the percent adsorption of Se(IV) on the modified sorbent was gradually increased with the increase in pH. It should be noted that, in the pH range of 1.0–3.0, only less than 7% of Se(IV) was adsorbed. Thus, Se(VI) and Se(IV) could be separated in the pH range of 1.5–3.0. CTAB is a cationic surfactant, therefore CTAB-modified alkyl silica material could behave as an anion exchange sorbent to selectively adsorb negatively charged ions. The different adsorption behavior of As(III/V) and Se(IV/VI) on CTAB-modified alkyl silica sorbent can be explained by their  $\text{pK}_a$  values (Table 2) and different ionic characters. According to the  $\text{pK}_a$  values of As(III) and As(V), when pH was above 6.0, As(V) exists as negatively charged ions, whereas, As(III) exists mainly as uncharged species in the whole studied pH range [6,23]. Thus, As(V) was adsorbed by CTAB-modified alkyl silica sorbent when  $\text{pH} > 6.0$  and As(III) was not adsorbed in the whole studied pH range. For Se(IV/VI), the  $\text{pK}_{a2}$  of selenic acid is 1.92; thus,  $\text{SeO}_4^{2-}$  is the dominant species when  $\text{pH} > 1.9$ . The  $\text{pK}_{a1}$  and  $\text{pK}_{a2}$  of selenious acid are 2.46 and 7.31, respectively; thus,  $\text{HSeO}_3^-$  was the dominant form when  $\text{pH} > 4$  [34] and barely be adsorbed by the CTAB-modified alkyl silica microcolumn. Whereas, the percent adsorption gradually increased with pH and reached almost 70% at pH 9.5 where the main Se(IV) species was  $\text{SeO}_3^{2-}$ , having the higher ( $-2$ ) negative charge. It seems that the functional groups of CTAB-modified alkyl silica microcolumn are behaving more selective towards the species carrying higher charges. Thus, Se(VI) could be separated from total inorganic Se at high acidic medium. The possible reactions of As(V) and Se(VI) with the CTAB-modified alkyl silica sorbent might be described as follows:



In the subsequent experiments, pH 2.0 and pH 6.5 were selected for the separation of Se(IV) from Se(VI) and As(V) from As(III), respectively.

### 3.3. Effect of sample flow rate

The sample flow rate should be optimized to ensure quantitative adsorption of target species. The influence of the sample flow rate on the adsorption percentage of  $1.0 \text{ mg l}^{-1}$  As(V) and  $1.0 \text{ mg l}^{-1}$  Se(VI) was studied and the results indicated that no obvious difference in the adsorption percentage has been observed when the sample flow rate was varied from  $0.4$  to  $1.7 \text{ ml min}^{-1}$ , suggesting that As(V) and Se(VI) species have a rapid reaction mechanism with CTAB-modified sorbent at desired pH values. In the subsequent experiments, a sample flow rate of  $1.7 \text{ ml min}^{-1}$  was used.

### 3.4. Optimization of elution conditions

#### 3.4.1. Concentration of $\text{HNO}_3$

The influence of  $\text{HNO}_3$  concentration on the recovery of  $1.0 \text{ mg l}^{-1}$  Se(VI) (pH 2.0) and  $1.0 \text{ mg l}^{-1}$  As(V) (pH 6.5) from the microcolumn was studied by keeping the eluent volume equal to the sample volume ( $1.0 \text{ ml}$ ) and the eluent flow rate at  $1.7 \text{ ml min}^{-1}$ . The results indicated that both Se(VI) and As(V) were quantitatively recovered when the concentration of  $\text{HNO}_3$  was varied from  $0.1$  to  $4.0 \text{ mol l}^{-1}$ . In this work,  $1.0 \text{ mol l}^{-1}$   $\text{HNO}_3$  was used for the quantitative recovery of Se(VI) and As(V).

#### 3.4.2. Eluent flow rate

The influence of the eluent flow rate on the recovery of  $1.0 \text{ mg l}^{-1}$  Se(VI) and  $1.0 \text{ mg l}^{-1}$  As(V) was studied by keeping the eluent volume and eluent concentration at  $1.0 \text{ ml}$  and  $1.0 \text{ mol l}^{-1}$ , respectively. The results indicated that any flow rate between  $0.4$  and  $1.7 \text{ ml min}^{-1}$  can be used for elution. In the present study, the flow rate of elution was set at  $1.7 \text{ ml min}^{-1}$  in order to shorten the analysis time.

#### 3.4.3. Eluent volume

Higher enrichment factor requires smaller volume of elution. Therefore, three separate portions ( $0.10 \text{ ml}$  each) of the eluent were passed through the microcolumn and the concentrations of the species in each portion were determined by ICP-OES. The results demonstrated that quantitative recoveries of  $1.0 \text{ mg l}^{-1}$  Se(VI) and  $1.0 \text{ mg l}^{-1}$  As(V) were obtained with the first  $0.10 \text{ ml}$  of eluent. Therefore,  $0.10 \text{ ml}$   $1.0 \text{ mol l}^{-1}$   $\text{HNO}_3$  was used to recover Se(VI) and As(V) in the subsequent experiments.

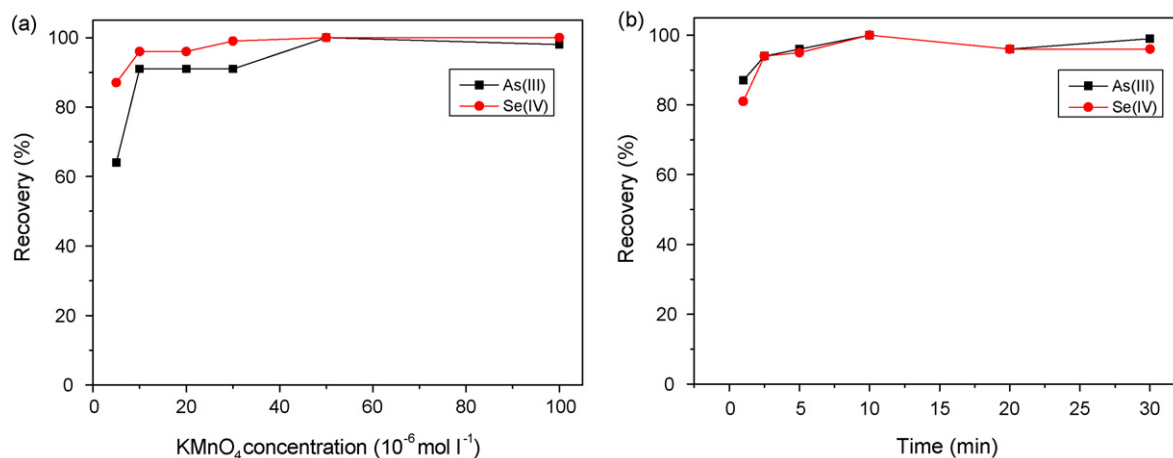
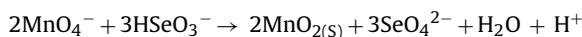
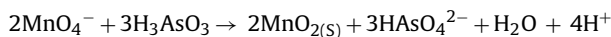


Fig. 3. Optimization of  $\text{KMnO}_4$  concentration (a) and oxidation time (b). Conditions: As(III) and Se(IV),  $1.0 \text{ mg l}^{-1}$ . The errors of the experimental values  $< \pm 5.0\%$ .

### 3.5. Optimization of oxidation conditions

In order to determine the total concentration of inorganic As and Se, an oxidizing agent of  $\text{KMnO}_4$  was added for conversion of As(III) and Se(IV) to As(V) and Se(VI), respectively [6,16]. The oxidation reactions at pH 6.5 are as follows:



The oxidation conditions including  $\text{KMnO}_4$  concentration and oxidation time have been optimized and the results are shown in Fig. 3. As could be seen, although  $10.0 \mu\text{mol l}^{-1}$   $\text{KMnO}_4$  was sufficient for  $>95\%$  adsorption of  $1.0 \text{ mg l}^{-1}$  As(III) and  $1.0 \text{ mg l}^{-1}$  Se(IV),  $50.0 \mu\text{mol l}^{-1}$   $\text{KMnO}_4$  was used in the analysis of real samples.

The oxidation time was studied by fixing the concentration of  $\text{KMnO}_4$  at  $50 \mu\text{mol l}^{-1}$ . As shown in Fig. 3b,  $\text{KMnO}_4$  reacted with As(III) and Se(IV) very rapidly and above 95% adsorption can be obtained even after 2.5 min. To prevent co-precipitation of analytes with  $\text{MnO}_2$  produced during the course of oxidation [6], analysis of real samples after oxidation should be performed according to the desired procedure immediately.

### 3.6. Sample volume

The effect of sample volume on the recovery of As(V) and Se(VI) was studied by passing different volumes (2.0–50.0 ml) of two standard solutions through the microcolumn. The absolute amounts of the As(V) and Se(VI) species were both  $1.0 \mu\text{g}$ , and the pH of the solutions for As(V) and Se(VI) was 6.5 and 2.0, respectively. The results indicated that when the sample volumes of As(V) and Se(VI) were lower than 20.0 and 40.0 ml, respectively, the recoveries of As(V) and Se(VI) were all above 90% and remained constant, whereas a decrease was observed with the continuous increase of sample volume for both As(V) and Se(VI). As described in the previous section, the analytes were quantitatively recovered using a volume of 0.10 ml of  $1.0 \text{ mol l}^{-1}$   $\text{HNO}_3$ , obtaining enrichment factors of 200 for As(V) and 400 for Se(VI). Considering the analysis time, 3.0 ml sample volume was used for the analysis of real samples.

### 3.7. Adsorption capacity

The adsorption capacity was obtained by using breakthrough curve. Under the optimal conditions, the detailed procedure was as follows: 50.0 ml sample solution containing  $10.0 \text{ mg l}^{-1}$  Se(VI)

(pH 2.0) and As(V) (pH 6.5) was passed through the column, and the analyte concentrations in the effluent were determined by ICP-OES, respectively. Based on the method recommended in reference [35], the adsorption capacities evaluated from the breakthrough curve were 5.0 and  $1.7 \text{ mg g}^{-1}$  for Se(VI) (pH 2.0) and As(V) (pH 6.5), respectively, which are comparable with those obtained by Diaion HP-2MG resin [27] and dimercaptosuccinic acid modified mesoporous  $\text{TiO}_2$  [28], respectively.

### 3.8. Coexisting ions interference

Various coexisting ions were added individually to solutions containing  $0.050 \text{ mg l}^{-1}$  As(III/V) and Se(IV/VI), respectively, and their effects on the recovery of analyte species were investigated. Table 3 shows the tolerance concentrations of coexisting ions and it was acceptable when the recoveries of target species were in the range of 90–110%. As can be seen, the developed method was fairly free from interference by coexisting ions commonly found in natural water. It was also found that  $50.0 \text{ mg l}^{-1}$  Mn(VII) (corresponding to  $900.0 \mu\text{mol l}^{-1}$   $\text{MnO}_4^-$ ) did not interfere with the determination of total As and Se.

### 3.9. Sample throughput

The overall time required for preconcentration of 3.0 ml of solution was about 2.5 min, including loading (106 s), washing

Table 3  
Tolerance concentrations of disturbance ions

Ions	Tolerance limit ( $\text{mg l}^{-1}$ ) <sup>a</sup>	Tolerance limit ( $\text{mg l}^{-1}$ ) <sup>b</sup>
$\text{K}^+$ , $\text{Na}^+$	500	500
$\text{Ca}^{2+}$	200	500
$\text{Mg}^{2+}$	30	100
$\text{Ba}^{2+}$	500	1000
$\text{Fe}^{3+}$	500	50
$\text{Zn}^{2+}$ , $\text{Cu}^{2+}$	500	500
$\text{Co}^{2+}$	100	20
$\text{Mn}^{2+}$ , $\text{Al}^{3+}$	50	10
$\text{Ni}^{2+}$	3	5
$\text{CH}_3\text{COO}^-$	2000	5000
$\text{H}_2\text{PO}_4^-$	100	1000
$\text{Cl}^-$	4000	4000
$\text{SO}_4^{2-}$	1700	2000
Citrate <sup>-</sup>	100	200

<sup>a</sup> As(III)/As(V):  $0.050 \text{ mg l}^{-1}$ .

<sup>b</sup> Se(IV)/Se(VI):  $0.050 \text{ mg l}^{-1}$ .

**Table 4**

Comparison of the detection limits of As and Se by different separation/preconcentration approaches prior to ICP-OES/MS determination

Detection method	Separation approach	Detection limit ( $\mu\text{g l}^{-1}$ )		Literature
		As	Se	
FI-ICP-OES	SPE	0.15	0.10	This work
FI-ICP-OES	SPE	0.1		16
HG-ICP-OES	SPE	0.013 <sup>a</sup> , 0.009 <sup>b</sup> , 0.007 <sup>c</sup>		18
ICP-OES	SPE	0.49 <sup>d</sup> , 0.10 <sup>e</sup>		28
HG-CE-ICP-OES	CE		2.3	14
FI-HG-ICP-OES	SPE		0.4	17
FI-HG-ICP-OES	SPE		0.011	25
ICP-MS	SPE		0.007	26
ICP-MS	SPE	0.008		23
ETV-ICP-MS	HF-LPME		0.00056	20
AEC-HG-ICP-DRC-MS	AEC		0.00027	39

HF-LPME, hollow fiber liquid phase microextraction; AEC, anion exchange chromatography.

<sup>a</sup> Sampling time is 60 s.

<sup>b</sup> Sampling time is 120 s.

<sup>c</sup> Sampling time is 180 s.

<sup>d</sup> On-line.

<sup>e</sup> Off-line.

(15 s), eluting (4 s, 0.10 ml), conditioning (20 s) at a flow rate of  $1.7 \text{ ml min}^{-1}$  and conversion operations (5 s). Therefore, the sample throughput was about 24 samples per hour.

### 3.10. Linearity, detection limit, precision and enrichment factor

The analytical performance of the method was evaluated and the results are as follows: after separation/preconcentration by the proposed procedure, the calibration graphs of the method for As(V) (pH 6.5) and Se(VI) (pH 2.0) were  $Y = 27.5X + 0.09$  and  $Y = 26.2X + 0.03$  with a correlation coefficient of 0.9936 and 0.9992, respectively. Both of the calibration graphs were linear in the range of 0.5–1000.0  $\mu\text{g l}^{-1}$ . The relative standard deviation (RSD) of As(V) and Se(VI) were 4.0% and 3.6% ( $C = 5.0 \mu\text{g l}^{-1}$ ,  $n = 9$ ), respectively, and their reproducibilities assessed in focus of between-day variation were less than 6.0% ( $C = 5.0 \mu\text{g l}^{-1}$ ,  $n = 7$ ). Lower detection limits can be achieved using a larger sample volume, even though this prolonged the time of analysis. Using a volume of 3.0 ml of aqueous solution of As(V) or Se(VI), the detection limits ( $3\sigma$ ) were 0.15 and 0.10  $\mu\text{g l}^{-1}$  for As(V) and Se(VI) with on-line concentration factors of 26.7 and 27.6, respectively, obtained by comparing the slope of the calibration graph with and without preconcentration. The quantitation limits ( $10\sigma$ ) were 0.50 and 0.33  $\mu\text{g l}^{-1}$  for As(V) and Se(VI), respectively. Table 4 lists the comparison of the detection limits of As and Se obtained with the present study and the other works reported in literatures. As can be seen, although the detec-

**Table 5**

Recovery values of As(V)/Se(VI) and total arsenic/selenium determined at different concentration ratios, as well as the calculated As(III)/Se(IV) concentrations ( $\mu\text{g l}^{-1}$ , mean  $\pm$  S.D.,  $n = 3$ )

As(III):As(V)	As(V)			As (total)		Calculated As(III)
	Added	Found	Recovery (%)	Found	Recovery (%)	
1:10	100.0	96.1 $\pm$ 5.8	96	103.6 $\pm$ 6.0	94	7.5 $\pm$ 0.2
1:1	10.0	9.0 $\pm$ 0.1	90	18.5 $\pm$ 0.4	93	9.5 $\pm$ 0.3
10:1	10.0	9.3 $\pm$ 0.8	93	107.6 $\pm$ 5.6	98	98.3 $\pm$ 4.8
Se(IV):Se(VI)	Se(VI)			Se (total)		Calculated Se(IV)
	Added	Found	Recovery (%)	Found	Recovery (%)	
1:10	100.0	97.3 $\pm$ 2.8	97	108.0 $\pm$ 4.1	98	10.7 $\pm$ 1.3
1:1	10.0	10.6 $\pm$ 0.3	106	19.9 $\pm$ 0.8	99	9.3 $\pm$ 0.4
10:1	10.0	9.6 $\pm$ 0.2	96	108.0 $\pm$ 7.0	98	98.4 $\pm$ 6.9

**Table 6**

Analytical results of As and Se species in ERM<sup>a</sup> samples (mean  $\pm$  S.D.,  $n = 3$ )

Sample	Element	Found	Certified
GSBZ 50031-94 (203706) <sup>b</sup>	Se(IV)	ND <sup>c</sup>	17.2 $\pm$ 1.8 $\mu\text{g l}^{-1d}$
	Se(VI)	16.6 $\pm$ 0.6 $\mu\text{g l}^{-1}$	
BW3209 (0602) <sup>b</sup>	As(III)	1.06 $\pm$ 0.03 $\mu\text{mol g}^{-1}$	1.01 $\pm$ 0.02 $\mu\text{mol g}^{-1}$
	As(V)	ND	
BW3210 (0602) <sup>b</sup>	As(III)	ND	0.233 $\pm$ 0.004 $\mu\text{mol g}^{-1}$
	As(V)	0.228 $\pm$ 0.010 $\mu\text{mol g}^{-1}$	

<sup>a</sup> Environmental reference material.

<sup>b</sup> National standard of the People's Republic of China.

<sup>c</sup> Not determined.

<sup>d</sup> Total Se.

tion limits of the method are higher than those obtained by ICP-MS [20,23,26,39], they are comparable with those obtained by ICP-OES detection [14,16,17,28], and can be used for the speciation analysis of inorganic arsenic and selenium in environmental water samples.

### 3.11. Regeneration

The regeneration is one of the key factors for evaluating the performance of the sorbent. Under the optimal conditions, a column packed with CTAB-modified alkyl silica sorbent (on-line modification) was subjected to the proposed procedure in a consecutive manner and it is found that the column could be re-used at least 15 times.

### 3.12. Effect of As(III)/As(V) and Se(IV)/Se(VI) ratio

The changes in the redox equilibrium state may occur between As(V) and As(III), Se(VI) and Se(IV) in the air, and thus the contents of species in aqueous solutions may be changed. Therefore, the effect of As(III)/As(V) and Se(IV)/Se(VI) ratio on the analytical results during the separation and preconcentration process has been evaluated. Various synthetic samples with different As(III)/As(V) and Se(IV)/Se(VI) concentration ratio were used and the results are given in Table 5. All species of arsenic and selenium were completely separated and recovered quantitatively with As(III)/As(V) and Se(IV)/Se(VI) ratio varying from 0.1 to 10.0.

### 3.13. Validation and applications

In order to validate the method described, certified reference materials were analyzed for As and Se species concentration (BW3209 (0602), BW3210 (0602) and GSBZ 50031-94 (203706) environmental water samples) (Institute of Reference Materials, SEPA Beijing, P.R. China). Table 6 shows that the determined values are in good agreement with the certified values.

**Table 7**  
Analytical results of inorganic As and Se species in natural water samples ( $\mu\text{g l}^{-1}$ , mean  $\pm$  S.D.,  $n = 3$ )

Sample	Added As		As(V)		As (total)		Calculated As(III)	Added Se		Se(VI)		Se (total)		Calculated Se(IV)
	As(III)	As(V)	Found	Recovery (%)	Found	Recovery (%)		Se(IV)	Se(VI)	Found	Recovery (%)	Found	Recovery (%)	
Yangtze River water <sup>b</sup>	0	0	3.4 $\pm$ 0.3		3.2 $\pm$ 0.3		ND <sup>a</sup>	0	0	1.0 $\pm$ 0.1		1.2 $\pm$ 0.1		0.2 $\pm$ 0.1
	4.0	4.0	7.3 $\pm$ 0.4	99	11.3 $\pm$ 1.4	101	4.0 $\pm$ 0.5	4	4	5.3 $\pm$ 0.2	106	9.6 $\pm$ 0.1	104	4.3 $\pm$ 0.1
Pool water <sup>c</sup>	0	0	4.3 $\pm$ 0.5		4.1 $\pm$ 0.1		ND	0	0	1.8 $\pm$ 0.1		2.4 $\pm$ 0.3		0.6 $\pm$ 0.2
	4.0	4.0	8.4 $\pm$ 0.6	101	12.0 $\pm$ 0.4	99	3.6 $\pm$ 0.3	4	4	6.0 $\pm$ 0.1	103	9.6 $\pm$ 0.4	92	3.6 $\pm$ 0.3
Tap water <sup>d</sup>	0	0	2.4 $\pm$ 0.2		2.3 $\pm$ 0.2		ND	0	0	1.3 $\pm$ 0.1		1.2 $\pm$ 0.2		ND <sup>a</sup>
	4.0	4.0	6.4 $\pm$ 0.8	100	10.9 $\pm$ 1.4	106	4.4 $\pm$ 0.5	4.0	4.0	5.2 $\pm$ 0.6	98	9.0 $\pm$ 0.4	98	3.8 $\pm$ 0.3
East Lake water 1 <sup>e</sup>	0	0	4.5 $\pm$ 0.5		4.6 $\pm$ 0.6		ND	0	0	1.8 $\pm$ 0.1		1.7 $\pm$ 0.2		ND
	4.0	4.0	8.3 $\pm$ 0.6	98	12.0 $\pm$ 0.4	95	3.7 $\pm$ 0.2	4.0	4.0	5.3 $\pm$ 0.1	91	9.8 $\pm$ 0.8	101	4.5 $\pm$ 0.6
Surface water 2 <sup>f</sup>	0	0	4.3 $\pm$ 0.1		5.8 $\pm$ 0.8		1.5 $\pm$ 0.3	0	0	1.7 $\pm$ 0.2		2.1 $\pm$ 0.2		0.4 $\pm$ 0.1
	4.0	4.0	8.6 $\pm$ 0.2	104	13.4 $\pm$ 1.3	97	4.8 $\pm$ 0.6	4.0	4.0	6.0 $\pm$ 0.3	105	9.7 $\pm$ 0.6	96	3.7 $\pm$ 0.3
Well water <sup>g</sup>	0	0	4.0 $\pm$ 0.8		4.6 $\pm$ 0.5		0.6 $\pm$ 0.3	0	0	2.2 $\pm$ 0.2		2.8 $\pm$ 0.1		0.6 $\pm$ 0.1
	4.0	4.0	8.3 $\pm$ 0.3	104	12.8 $\pm$ 0.6	102	4.5 $\pm$ 0.3	4.0	4.0	6.1 $\pm$ 0.3	98	10.3 $\pm$ 0.6	95	4.2 $\pm$ 0.4
Ancient well water <sup>h</sup>	0	0	9.7 $\pm$ 0.9		11.4 $\pm$ 0.3		1.7 $\pm$ 0.4	0	0	ND		ND		ND
	4.0	4.0	13.3 $\pm$ 1.1	97	19.8 $\pm$ 1.0	102	6.5 $\pm$ 0.1	4.0	4.0	3.7 $\pm$ 0.3	93	8.2 $\pm$ 0.5	103	4.5 $\pm$ 0.2
Rain water 1 <sup>i</sup>	0	0	3.6 $\pm$ 0.4		4.4 $\pm$ 0.5		0.8 $\pm$ 0.1	0	0	3.0 $\pm$ 0.4		3.3 $\pm$ 0.3		0.3 $\pm$ 0.1
	4.0	4.0	7.2 $\pm$ 0.4	95	11.9 $\pm$ 1.0	96	4.7 $\pm$ 0.6	4.0	4.0	6.6 $\pm$ 0.6	94	11.6 $\pm$ 1.0	103	5.0 $\pm$ 0.5
Rain water 2 <sup>j</sup>	0	0	3.1 $\pm$ 0.1		3.3 $\pm$ 0.1		0.2 $\pm$ 0.1	0	0	2.3 $\pm$ 0.2		2.8 $\pm$ 0.3		0.5 $\pm$ 0.1
	4.0	4.0	6.6 $\pm$ 0.4	93	12.0 $\pm$ 1.1	106	5.4 $\pm$ 0.7	4.0	4.0	6.8 $\pm$ 0.4	108	10.5 $\pm$ 0.5	97	3.7 $\pm$ 0.1

<sup>a</sup> Not determined.

<sup>b</sup> pH 7.5, Wuhan, China.

<sup>c</sup> pH 7.3, Weiming Pool, Wuhan University, Hubei, China.

<sup>d</sup> pH 7.3, the tap in the laboratory.

<sup>e</sup> pH 7.8, surface water.

<sup>f</sup> pH 7.7, below 1 m of the surface.

<sup>g</sup> pH 7.1, Yiling, Yichang, Hubei, China.

<sup>h</sup> pH 6.2, Zhuodaoquan Temple, Wuhan, Hubei, China.

<sup>i</sup> pH 5.6, collected at the beginning of the raining season in Wuhan, China.

<sup>j</sup> 5.5, collected at the middle of the raining season in Wuhan, China.

The method was also applied to the determination of trace As(V)/Se(VI) and total As/Se in natural water samples such as Yangtze River water, East Lake water, well water, rain water, pool water, tap water. The results are shown in Table 7. It can be seen that the recoveries for the spiked water samples were 93–106% for As species and 91–108% for Se species, respectively.

Based on the regulation set by World Health Organization (WHO) [36] and the US Environmental Protection Agency (USEPA) [37], the maximum permissible concentration of As is  $10.0 \mu\text{g l}^{-1}$  in drinking water. The results listed in Table 7 indicated that the concentrations of As in most natural water samples except for ancient well water were below the WHO and USEPA recommended limit and were safe and fit for consumption. In these natural water samples, As(V) was predominant among the inorganic As species as reported in literatures [16,23]. Higher concentrations of As(V) and As(III) were found in the present study than those in literatures [16,23], probably because of the different geographical area [36]. Surprisingly, high concentrations of As(V) and As(III) were found in ancient well water and the total As was higher than the maximum permissible concentration for drinking water by WHO and USEPA. Fortunately, As(III) was not found in tap water as expected.

Similarly,  $50.0 \mu\text{g l}^{-1}$  is the maximum permissible concentration of Se in drinking water as recommended by the WHO [36]. Table 7 provides evidence that the predominant form of inorganic selenium in natural waters analyzed was Se(VI) and the total concentrations of inorganic selenium were lower than the maximum permissible value recommended by WHO. In these natural water samples, concentrations of Se(VI) and Se(IV) were similar to those reported in literature [20,24,38], whereas much lower values were reported in some other studies [9,29,39], possibly due to the variation of geographical locations where samples were collected [4].

#### 4. Conclusion

In this paper, a new kind of sorbent of CTAB-modified alkyl silica has been prepared by on-line modification and applied for the on-line separation and preconcentration of inorganic arsenic and selenium by ICP-OES in environmental water samples for the first time. A conical pipet tip (200  $\mu\text{l}$ , cheap and easy to obtain) was used as microcolumn for loading the solid phase adsorption material and the operation was very easy. No chelating reagent was used in this experiment, thus, avoiding the possibilities of contamination risks. The proposed method was simple, fast, and selective with on-line detection by ICP-OES and it could be adapted for rugged and routine use by the contract lab population and practitioners in water field who utilize such analyses.

#### Acknowledgments

Financial supports from the Science Fund for Creative Research Groups of NSFC (no. 20621502) and MOE of China (NCET-04-0658) are gratefully acknowledged.

#### References

- [1] A.M. Florea, D. Busselberg, *Biometals* 19 (2006) 419.
- [2] J.C. Ng, *Environ. Chem.* 2 (2005) 146.
- [3] L. Schomburg, U. Schweizer, J. Kohrle, *Cell. Mol. Life Sci.* 61 (2004) 1988.
- [4] B.D. Wake, A.R. Bowie, E.C.V. Butler, P.R. Haddad, *Trac-Tends Anal. Chem.* 23 (2004) 491.
- [5] C.K. Jain, I. Ali, *Water Res.* 34 (2000) 4304.
- [6] V. Lenoble, V. Deluchat, B. Serpaud, J.C. Bollinger, *Talanta* 61 (2003) 267.
- [7] K. Wrobel, K. Wrobel, J.A. Caruso, *Anal. Bioanal. Chem.* 381 (2005) 317.
- [8] C. B'Hymer, J.A. Caruso, *J. Chromatogr. A* 1114 (2006) 1.
- [9] C.Y. Lu, X.P. Yan, Z.P. Zhang, Z.P. Wang, L.W. Liu, *J. Anal. At. Spectrom.* 19 (2004) 277.
- [10] P. Niedzielski, *Anal. Chim. Acta* 551 (2005) 199.
- [11] Y.C. Sun, J. Mierzwa, M.H. Yang, *Talanta* 44 (1997) 1379.
- [12] I. Švancara, K. Vytřas, A. Bobrowsky, K. Kulcher, *Talanta* 58 (2002) 45.
- [13] G. Dugo, L. La Pera, V. Lo Turco, G. Di Bella, *Chemosphere* 61 (2005) 1093.
- [14] B.Y. Deng, J.R. Feng, J. Meng, *Anal. Chim. Acta* 583 (2007) 92.
- [15] V. Gergely, M. Montes-Bayon, P. Fodor, A. Sanz-Medel, *J. Agric. Food Chem.* 54 (2006) 4524.
- [16] K. Jitmanee, M. Oshima, S. Motomizu, *Talanta* 66 (2005) 529.
- [17] J. Stripeikis, M. Tudino, O. Troccoli, R. Wuilloud, R. Olsina, L. Martinez, *Spectrochim. Acta* 56B (2001) 93.
- [18] R.A. Gil, N. Ferrúa, J.A. Salonia, R.A. Olsina, L.D. Martinez, *J. Hazard. Mater.* 143 (2007) 431.
- [19] R.Y. Wang, Y.L. Hsu, L.F. Chang, S.J. Jiang, *Anal. Chim. Acta* 590 (2007) 239.
- [20] L.B. Xia, B. Hu, Z.C. Jiang, Y.L. Wu, R. Chen, L. Li, *J. Anal. At. Spectrom.* 21 (2006) 362.
- [21] L. Zhang, Y. Morita, A. Sakuragawa, A. Isozaki, *Talanta* 72 (2007) 723.
- [22] A.N. Tang, G.S. Ding, X.P. Yan, *Talanta* 67 (2005) 942.
- [23] C.H. Yu, Q.T. Cai, Z.X. Guo, Z.G. Yang, S.B. Khoo, *Spectrochim. Acta* 58B (2003) 1335.
- [24] M. Bueno, M. Potin-Gautier, *J. Chromatogr. A* 963 (2002) 185.
- [25] P.H. Pacheco, R.A. Gil, P. Smichowski, G. Polla, L.D. Martinez, *J. Anal. At. Spectrom.* 22 (2007) 305.
- [26] C.H. Yu, Q.T. Cai, Z.X. Guo, Z.G. Yang, S.B. Khoo, *J. Anal. At. Spectrom.* 19 (2004) 410.
- [27] K.O. Saygi, E. Melek, M. Tuzen, M. Soylak, *Talanta* 71 (2007) 1375.
- [28] C.Z. Huang, B. Hu, Z.C. Jiang, *Spectrochim. Acta* 62B (2007) 454.
- [29] F.A. Bertolino, A.A.J. Torriero, E. Salinas, R. Olsina, L.D. Martinez, J. Raba, *Anal. Chim. Acta* 572 (2006) 32.
- [30] M. Dauthieu, M. Bueno, J. Darrouzes, N. Gilon, M. Potin-Gautier, *J. Chromatogr. A* 1114 (2006) 34.
- [31] K. Wrobel, S. Kannamkumarath, K. Wrobel, J.A. Caruso, *Green Chem.* 5 (2003) 250.
- [32] N. Pourreza, H. Zavvar Mousavi, *Anal. Chim. Acta* 503 (2004) 279.
- [33] J.P. Pancras, B.K. Puri, *Anal. Bioanal. Chem.* 374 (2002) 1306.
- [34] T. Lin, *J. Hazard. Mater.* 149 (2007) 80.
- [35] X.L. Pu, B. Hu, Z.C. Jiang, C.Z. Huang, *Analyst* 130 (2005) 1175.
- [36] <http://www.who.int/>, World Health Organization (WHO).
- [37] <http://www.epa.gov/>, The US Environmental Protection Agency (USEPA).
- [38] N.M. Lawson, R.P. Mason, *Water Res.* 35 (2001) 4039.
- [39] D. Wallschlager, J. London, *J. Anal. At. Spectrom.* 19 (2004) 1119.





## Automated on-line column-switching HPLC–MS/MS method for measuring environmental phenols and parabens in serum

Xiaoyun Ye, Lily J. Tao, Larry L. Needham, Antonia M. Calafat\*

Division of Laboratory Sciences, National Center for Environmental Health, Centers for Disease Control and Prevention, 4770 Buford Highway, Mailstop F53, Atlanta, GA 30341, USA

### ARTICLE INFO

#### Article history:

Received 6 March 2008

Received in revised form 15 April 2008

Accepted 16 April 2008

Available online 24 April 2008

#### Keywords:

Phenols

Parabens

HPLC–MS/MS

Serum

### ABSTRACT

We developed a method using on-line solid phase extraction (SPE) coupled to high performance liquid chromatography–isotope dilution tandem mass spectrometry (HPLC–MS/MS) to measure the serum concentrations of seven environmental phenols and five parabens: bisphenol A; *ortho*-phenylphenol; 2,4-dichlorophenol; 2,5-dichlorophenol; 2,4,5-trichlorophenol; benzophenone-3; triclosan; and methyl-, ethyl-, propyl-, butyl-, and benzyl-parabens. The phenols and parabens present in serum were retained and concentrated on a C18 reversed-phase size-exclusion SPE column, back-eluted from the SPE column while the eluate was diluted through a mixing Tee (analyte peak focusing), separated using a pair of monolithic HPLC columns, and detected by isotope dilution-MS/MS. Sample preparation did not require protein precipitation, only dilution of the serum with 0.1 M formic acid. This method, which combines an on-line SPE with analyte peak focusing feature and the selective atmospheric pressure photoionization MS detection, resulted in limits of detection ranging from 0.1 to 0.5 ng/mL for most of the analytes. The high throughput and adequate sensitivity with yet a relative low serum volume used (100  $\mu$ L) confirm that analytically it is possible to measure simultaneously these phenols and parabens with the precision and accuracy at sub-parts-per-billion levels required for biomonitoring. However, important additional factors, including validated sample collecting, handling, and storing protocols, as well as toxicokinetic data, are required if these measures are used for exposure assessment.

Published by Elsevier B.V.

### 1. Introduction

Humans are exposed to environmental phenols and parabens through industrial pollution, pesticide use, food consumption, and use of personal care and consumer products. Bisphenol A (BPA) is used to manufacture polycarbonate plastic, which can be found in water and infant bottles, and epoxy resins, which can be used in protective coatings on food containers and in dental composites and sealants [1]. Some chlorophenols have been used in the wood preservation industry, as intermediates in the production of pesticides, and as disinfectants or fungicides for industrial and indoor home use [2]. Other phenols, including the sunscreen agent 2-hydroxy-4-methoxybenzophenone (benzophenone-3, BP-3) and the antimicrobial agent 2,4,4'-trichloro-2'-hydroxydiphenyl ether (triclosan), are used extensively in personal care and consumer products [3]. Parabens, esters of *p*-hydroxybenzoic acid, are widely used as antimicrobial preservatives in cosmetics, pharmaceuticals, and in food and beverage processing [4].

The results from human and animal studies have demonstrated that after exposure and absorption, several environmental phenols, such as BPA, BP-3, and triclosan, are mainly metabolized by glucuronidation or sulfatation to facilitate their urinary excretion [5–8]. Therefore, these conjugated and free species can be used as valid biomarkers for exposure assessment in humans [9–11]. Animal studies show that parabens, after being absorbed, are mainly hydrolyzed to *p*-hydroxybenzoic acid, which can be excreted in the urine also as glycine, glucuronide and sulfate conjugates [4]. However, measuring *p*-hydroxybenzoic acid and its conjugates may not be the best approach for assessing human exposure to parabens because *p*-hydroxybenzoic acid is a non-specific biomarker and different parabens can possess rather different estrogenic bioactivities. It has been suggested that the unchanged precursor parabens and their conjugates could be valid biomarkers to assess human exposure to these compounds [12].

Because of their extensive use, human exposure to some phenols and parabens is widespread in the general US population as demonstrated by the high frequency of detection of these compounds in urine [9–13]. Although some of these phenols are toxic in animals, their potential toxic effects in humans are, for the most part, largely unknown. Urinary concentrations of these phenols can be used to

\* Corresponding author. Tel.: +1 770 488 7891; fax: +1 770 488 4371.

E-mail address: [Acalafat@cdc.gov](mailto:Acalafat@cdc.gov) (A.M. Calafat).

estimate the prevalence of exposure to these compounds. However, the presence of phenols and parabens in urine does not indicate that these compounds are detrimental to human health [13]. To answer this question, information on the concentration of the compounds available to interact at the target organ(s) is needed. Assuming that the free form of these compounds is the pharmacologically active species, the concentrations of these free species in blood would be helpful for risk assessment.

Reports exist on the quantification of environmental phenols and parabens in serum using analytical techniques. Gas chromatography–mass spectrometry (GC–MS) had been used to measure alkyl phenols, BPA, and triclosan in human cord blood, plasma, and serum [14–16]. However, GC methods usually require a relatively large amount of sample (1 mL), extensive sample cleanup, and a derivatization step due to the relatively low volatility of these phenols. More recently, high-performance liquid chromatography (HPLC)–tandem mass spectrometry (MS/MS) was used for measuring the concentrations of some of these environmental phenols, such as BPA, in plasma [17] and serum [18]. We report the development and validation of a new on-line SPE–HPLC–MS/MS method to measure simultaneously the serum concentrations of seven environmental phenols and five parabens: BPA; *ortho*-phenylphenol (*O*-PP); 2,4-dichlorophenol (2,4-DCP); 2,5-dichlorophenol (2,5-DCP); 2,4,5-trichlorophenol (2,4,5-TCP); BP-3; triclosan; and methyl-, ethyl-, propyl-, butyl-, and benzyl-parabens.

## 2. Experimental

### 2.1. Analytical standards and reagents

Methanol (MeOH) and water, purchased from Caledon (Ontario, Canada) were analytical or HPLC grade. Formic acid (98%) was purchased from EM Science (Gibbstown, NJ, USA). BPA; *O*-PP; 2,4-DCP; 2,5-DCP; 2,4,5-TCP; triclosan; methyl-, ethyl-, propyl-, butyl-, and benzyl-parabens; 4-methylumbelliferyl glucuronide; 4-methylumbelliferyl sulfate; ammonium acetate (>98%);  $\beta$ -glucuronidase/sulfatase (*Helix pomatia*, H1) were purchased from Sigma–Aldrich Laboratories, Inc. (St. Louis, MO, USA). BP-3 (Eusolex 4360) was provided by EMD Chemicals, Inc. (Hawthorne, NY, USA).  $^{13}\text{C}_{12}$ -BPA;  $^{13}\text{C}_6$ -OPP;  $^{13}\text{C}_6$ -2,4-DCP;  $^{13}\text{C}_6$ -2,5-DCP;  $^{13}\text{C}_6$ -2,4,5-TCP;  $^{13}\text{C}_4$ -4-methylumbelliferone were obtained from Cambridge Isotope Laboratories, Inc. (Andover, MA, USA). D<sub>3</sub>,  $^{13}\text{C}$ -BP-3 was obtained from Los Alamos National Laboratory (Los Alamos, NM, USA).  $^{13}\text{C}_6$ -triclosan was purchased from Wellington laboratories, Inc. (Ontario, Canada). D<sub>4</sub>-methyl paraben was purchased from CDN Isotopes (Quebec, Canada) and D<sub>4</sub>-ethyl-, D<sub>4</sub>-propyl-, D<sub>4</sub>-butyl-parabens were purchased from CanSyn Chem Corp. (Toronto, Canada). 15 commercial human serum samples for method validation were purchased from Interstate Blood Bank, Inc. (Memphis, TN, USA).

### 2.2. Preparation of standards and quality control materials

The initial stock solutions of analytical standards and stable isotope-labeled internal standards were prepared by dissolving measured amounts of the analytes of interest in MeOH. 10 working standard spiking solutions that contained all 12 compounds were generated by serial dilution of the initial stock with MeOH to a final concentration such that a 100- $\mu\text{L}$  spike in 100  $\mu\text{L}$  serum would cover a concentration range from 0.1 to 100 ng/mL for all of the analytes except triclosan (1–1000 ng/mL). The stable isotope-labeled internal standard working solution was prepared by diluting the internal standard stock solutions in MeOH, so that a 50- $\mu\text{L}$  aliquot

in 100  $\mu\text{L}$  serum resulted in a concentration level of 50 ng/mL. All standard stock solutions and spiking solutions were dispensed into glass vials and stored at  $-70^\circ\text{C}$  until used.

Quality control (QC) materials were prepared from calf serum (Gibco, Grand Island, NY, USA). The serum was mixed uniformly and divided into two aliquots for QC low (QCL) and QC high (QCH) concentration pools. The QCL and the QCH pools were enriched with different levels of native target compounds. Initially we added the standard solutions directly into the serum. However, because of the precipitation caused by MeOH, getting homogeneous QC pools was difficult. Therefore, we modified the spiking procedure by first mixing the standard solutions with 3 mL of 0.1 M formic acid then adding serum onto the mixture. We observed no substantial precipitation during the QC preparation using the new procedure and obtained homogeneous QC pools. These pools were mixed thoroughly, sonicated for 15 min, and dispensed in aliquots of 1.5 mL in silanized glass vials (to minimize adsorption of some of the compounds, such as methyl paraben, to the glass). All QC materials were stored at  $-70^\circ\text{C}$  until used.

A mixture of  $^{13}\text{C}_4$ -4-methylumbelliferone, 4-methylumbelliferyl sulfate, and 4-methylumbelliferyl glucuronide was prepared in H<sub>2</sub>O and stored at  $4^\circ\text{C}$  until use. 50  $\mu\text{L}$  of this mixture was added to each sample and used as a deconjugation standard to quantify the extent of the enzymatic reaction. After incubation, 4-methylumbelliferyl sulfate and 4-methylumbelliferyl glucuronide were deconjugated to free 4-methylumbelliferone, and the 4-methylumbelliferone/ $^{13}\text{C}_4$ -4-methylumbelliferone peak area ratio was monitored to check the extent of the deconjugation. The enzyme solution was prepared daily for each run by dissolving 0.04 g of  $\beta$ -glucuronidase/sulfatase (463,000 U/g solid) in 10 mL of 1 M ammonium acetate buffer (pH 5.0).

### 2.3. Sample preparation

To measure both the concentration of free and total species, each unknown sample was prepared in two different ways: one sample was processed without enzyme treatment; the other was treated with  $\beta$ -glucuronidase/sulfatase. Serum was thawed, sonicated, vortex mixed, and divided into aliquots. For a preparation without enzyme treatment to estimate the concentrations of free species, 50  $\mu\text{L}$  of internal standard solution and 100  $\mu\text{L}$  of serum were added into 850  $\mu\text{L}$  of 0.1 M formic acid in 1.5 mL conical bottom autosampler vial. To determine the concentrations of the free plus conjugated species (total) of the compounds, 50  $\mu\text{L}$  of internal standard, 50  $\mu\text{L}$  of 4-methylumbelliferyl glucuronide/4-methylumbelliferyl sulfate/ $^{13}\text{C}_4$ -4-methylumbelliferone mixed standard (0.5  $\mu\text{g}/\text{mL}$ ), and 50  $\mu\text{L}$  of enzyme solution were added to 100  $\mu\text{L}$  of serum in an autosampler vial. After gentle mixing, the sample was incubated at  $37^\circ\text{C}$  for 4 h. After incubation, 750  $\mu\text{L}$  of 0.1 M formic acid was added to the sample. Since some precipitation was observed during incubation, before placing the samples on the HPLC autosampler for the on-line SPE–HPLC–MS/MS analysis, all samples were vortex mixed and centrifuged at  $812 \times g$  for 15 min. The autosampler injector needle was programmed to withdraw the sample 4.5 mm above the bottom of the autosampler vial, so that the precipitate would not be withdrawn into the HPLC system. We prepared analytical standards, QCs, and serum blanks using the same procedure as described above but replaced the serum by the same volume of standard stock solution, QC serum, or calf serum (for blanks).

### 2.4. On-line SPE–HPLC–MS/MS

The on-line SPE–HPLC–MS/MS system was built from several Agilent 1100 modules (Agilent Technologies, Wilmington, DE, USA) coupled with an API 4000 Q Trap<sup>TM</sup> mass spectrometer (Applied

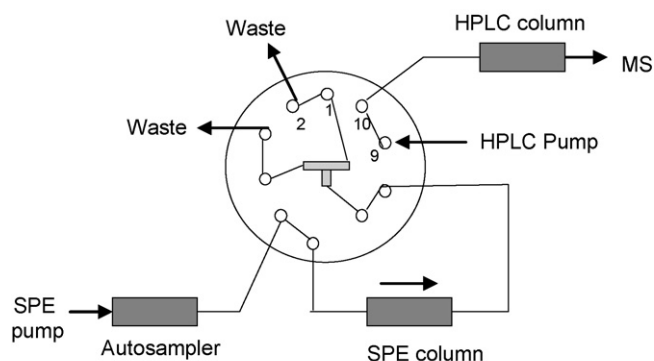
Biosystems, Foster City, CA, USA) equipped with an atmospheric pressure photoionization (APPI) interface. The on-line SPE–HPLC system consisted of two binary pumps with degassers, an autosampler with a 900- $\mu$ L injection loop, a high pressure mixing Tee, and one column compartment with a 10-port switching valve. The mass spectrometer and Agilent modules were programmed and controlled using the Analyst 1.4.1 software (Applied Biosystems), and the on-line SPE–HPLC–MS/MS acquisition method was built in ‘LC sync’ mode (i.e., acquisition was only triggered after the sample injection was completed). The SPE column was a LiChrosphere RP-18 ADS (25 mm  $\times$  4 mm, 25  $\mu$ m particle size, 60 Å pore size, Merck KGaA, Germany), and the HPLC columns were two Chromolith™ Performance RP-18 (100 mm  $\times$  4.6 mm; Merck KGaA, Germany) in tandem.

The on-line SPE–HPLC–MS/MS system used in this study was modified from the one used for measuring urinary concentrations of phenols [19]. We simplified the original set up so that the autosampler valve did not require custom configuration to perform peak focusing (Fig. 1), and advanced programming for the autosampler was not required. The procedure for extracting the environmental phenols and parabens from the serum involved three periods (Table 1). The solvent gradient programs of SPE pump and HPLC pump, and the time schedules of the 10-port switching valve are also listed in Table 1. During the first period (0–3 min), with the 10-port valve at positions 1–2, 700  $\mu$ L of the sample injected was loaded onto the SPE column by the SPE pump with 20% MeOH:80% H<sub>2</sub>O at a flow rate of 1 mL/min. During the second period (3–5 min), the 10-port valve was switched to its alternative positions (1–10), and the analytes retained on SPE column were back-eluted by the HPLC pump, with 50% MeOH:50% H<sub>2</sub>O at a flow rate of 0.5 mL/min. At the same time, the SPE eluate was diluted through a mixing tee with 100% H<sub>2</sub>O at a flow rate of 0.25 mL/min provided by the SPE pump. During the third period, the 10-port valve was switched to its original positions (1–2), and the analytes were transferred to the HPLC column by the HPLC pump using a slow gradient program at a flow of 0.75 mL/min (Table 1). Regeneration of the SPE column by the SPE pump with 100% MeOH and SPE column equilibration with 20% MeOH:80% H<sub>2</sub>O were also performed during this third period.

### 2.5. Mass spectrometry

The mass spectrometer equipped with an APPI interface was used in negative ion mode. The analytes in the sample were ionized by photoionization induced by a continuous beam of ultraviolet radiation in the presence of a dopant (toluene) within the source house. The dopant was provided at a flow rate of 75  $\mu$ L/min by an isocratic pump controlled with the Analyst 1.4.1 software. The APPI settings were curtain gas (N<sub>2</sub>) flow: 20 arbitrary units (au); collision gas (N<sub>2</sub>) flow: 9 au; nebulizer gas (N<sub>2</sub>) flow: 60 au; lamp gas (N<sub>2</sub>) flow: 20 au; nebulizing gas temperature: 500 °C; and ion

(A): Position 1-2 (0-3 min and 5-21 min)



(B): Position 1-10 (3-5 min)

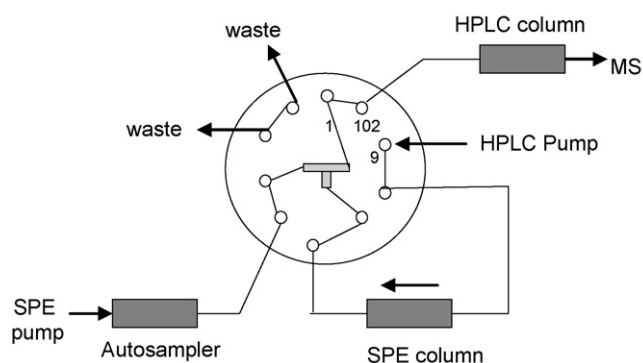


Fig. 1. On-line SPE–HPLC–MS/MS set-up.

transfer voltage: –800 V. Q1 and Q3 were set at unit resolution. Ionization parameters and collision cell parameters were optimized separately for each analyte. The negative fragment ions used for quantification and the retention time for the analytes are listed in Table 2.

## 3. Results and discussion

### 3.1. Pretreatment of serum samples

SPE has gained popularity in the past 20 years as a useful technique for extracting a wide range of analytes from serum and other biological and environmental samples [20,21]. When SPE is used in a stand-alone fashion, the process often involves time-consuming vaporization and reconstitution steps [18,22,23]. By contrast, when SPE is directly coupled to a HPLC–MS system (i.e., online-SPE), these steps are no longer necessary [24–26]. Furthermore, when using

**Table 1**  
Gradient programs of SPE pump and HPLC pump, and the time schedule of the 10-port switching valve

	Period 1: sample loading and SPE washing	Period 2: analytes transfer and peak focusing	Period 3: HPLC separation and SPE regeneration and equilibration
Time (min)	0–3	3–5	5–21
10-Port valve position	1–2	1–10	1–2
SPE gradient A: H <sub>2</sub> O; B: MeOH	20% B (1.0 mL/min)	100% A (0.25 mL/min)	5–10 min: 100% B 10–21 min: 20% B (1.0 mL/min)
HPLC gradient A: H <sub>2</sub> O; B: MeOH	50% B (0.5 mL/min)	50% B (0.5 mL/min)	5–10 min: 50% B–65% B 10–17 min: 65% B–100% B 17–20 min: 100% B 20–21 min: 50% B (0.75 mL/min)

**Table 2**

Analyte retention time (RT), and precursor ion  $\rightarrow$  product ion transitions monitored for quantitation (and confirmation) of native compounds and corresponding isotope-labeled internal standards

Analyte	RT (min)	Precursor ion $\rightarrow$ product ion ( $m/z$ )	
		Native analyte	Internal standard
Bisphenol A	15.4	227 $\rightarrow$ 133 (212)	239 $\rightarrow$ 139
Triclosan	19.3	252 $\rightarrow$ 216	264 $\rightarrow$ 228
Benzophenone-3	18.2	227 $\rightarrow$ 183 (211)	231 $\rightarrow$ 183
<i>Ortho</i> -phenylphenol	16.3	169 $\rightarrow$ 115 (141)	175 $\rightarrow$ 121
2,4-Dichlorophenol	16.2	161 $\rightarrow$ 125 (163 $\rightarrow$ 125)	167 $\rightarrow$ 131
2,5-Dichlorophenol	15.9	161 $\rightarrow$ 125 (163 $\rightarrow$ 125)	167 $\rightarrow$ 131
2,4,5-Trichlorophenol	18.0	195 $\rightarrow$ 159 (197 $\rightarrow$ 161)	201 $\rightarrow$ 165
Methyl paraben	11.5	151 $\rightarrow$ 92 (136)	155 $\rightarrow$ 96
Ethyl paraben	13.3	165 $\rightarrow$ 92 (137)	169 $\rightarrow$ 96
Propyl paraben	15.2	179 $\rightarrow$ 92 (136)	183 $\rightarrow$ 96
Butyl paraben	16.6	193 $\rightarrow$ 92 (136)	197 $\rightarrow$ 96
Benzyl paraben	16.6	227 $\rightarrow$ 92 (136)	197 $\rightarrow$ 96 <sup>a</sup>

<sup>a</sup> D<sub>4</sub>-butyl paraben is used as the internal standard of benzyl paraben.

SPE for serum samples, most approaches require an additional sample pre-treatment step, such as protein precipitation, to prevent proteins from clogging the SPE column [27]. In this study, we used an on-line SPE–HPLC–MS/MS approach to measure the serum concentrations of seven environmental phenols and five parabens. The sample pre-treatment step was simple and only involved dilution of the serum sample with 0.1 M formic acid, followed by centrifugation. Of interest, the addition of formic acid both eliminated the need of a protein precipitation step and improved the retention of some compounds, especially 2,4,5-TCP, on the SPE column. Formic acid has been shown to effectively suppress the interaction of polyfluoroalkyl compounds with serum macromolecules (e.g., proteins) and facilitate binding of these compounds to the SPE sorbent [26].

### 3.2. Peak focusing of the analytes

Our on-line SPE approach not only simplified the sample extraction procedure but also was amenable to provide the peak focusing feature. One of the most common limitations of on-line SPE is compromised HPLC resolution [28]. In our case, elution of the phenols of interest from the SPE column required 0.5 mL/min 50% MeOH:50% water for 2 min. However, a starting HPLC gradient with 50% MeOH content would broaden the chromatographic peaks for the most polar phenols, such as methyl paraben (Fig. 2). However, using a 10-port switching valve and a mixing Tee, we were able to dilute the HPLC flow (0.5 mL/min 50% MeOH) with 100% H<sub>2</sub>O (0.25 mL/min) provided by the SPE pump. As a result, the HPLC resolution was improved greatly as illustrated by the decrease in the peak width of the methyl paraben signal at half height from 0.45 to 0.25 min (Fig. 2).

### 3.3. MS detection

Previously, we used atmospheric pressure chemical ionization (APCI) for measuring the concentrations in urine of 9 phenols [19]. Specifically, due to the dissociation of triclosan into dichlorophenol in  $Q_0$  under the harsh APCI conditions, we used the  $m/z$  161  $\rightarrow$  125 and 163  $\rightarrow$  125 dichlorophenol transitions at the retention time of triclosan for quantification and confirmation of triclosan, respectively [19]. Although the  $m/z$  161  $\rightarrow$  125 transition was more sensitive than the  $m/z$  287  $\rightarrow$  142 (triclosan molecular ion  $\rightarrow$  product ion) transition in the urine matrix [19], the sensitivity of the  $m/z$  161  $\rightarrow$  125 transition was poor in serum due to the more severe ionization suppression from the matrix. Therefore, we chose to use a novel ionization technique, atmospheric

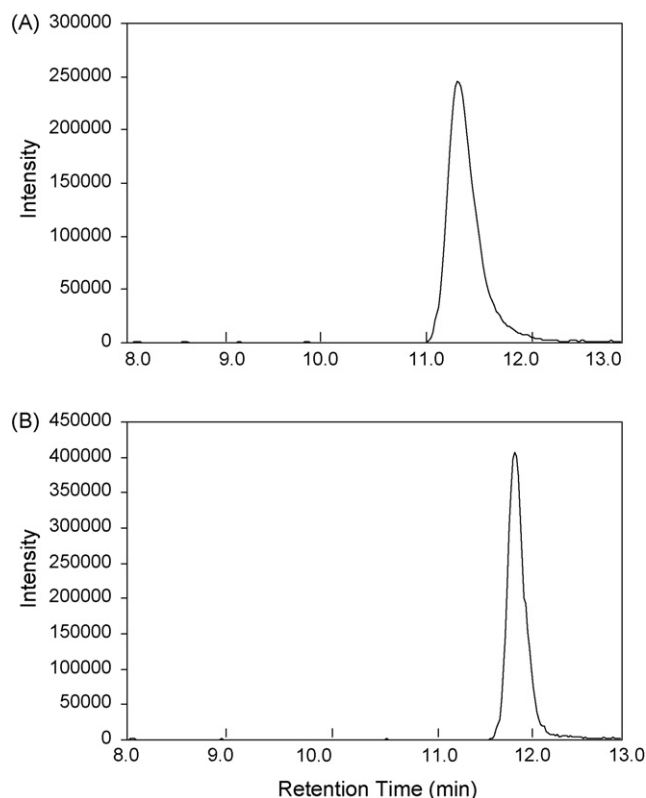


**Fig. 2.** The extracted ion chromatograms (MRM) of methyl paraben: (A) without peak focusing, HPLC–0.75 mL/min 50% MeOH; (B) with peak focusing, HPLC flow (0.5 mL/min 50% MeOH) was diluted with 100% H<sub>2</sub>O (0.25 mL/min) from 3 to 5 min.

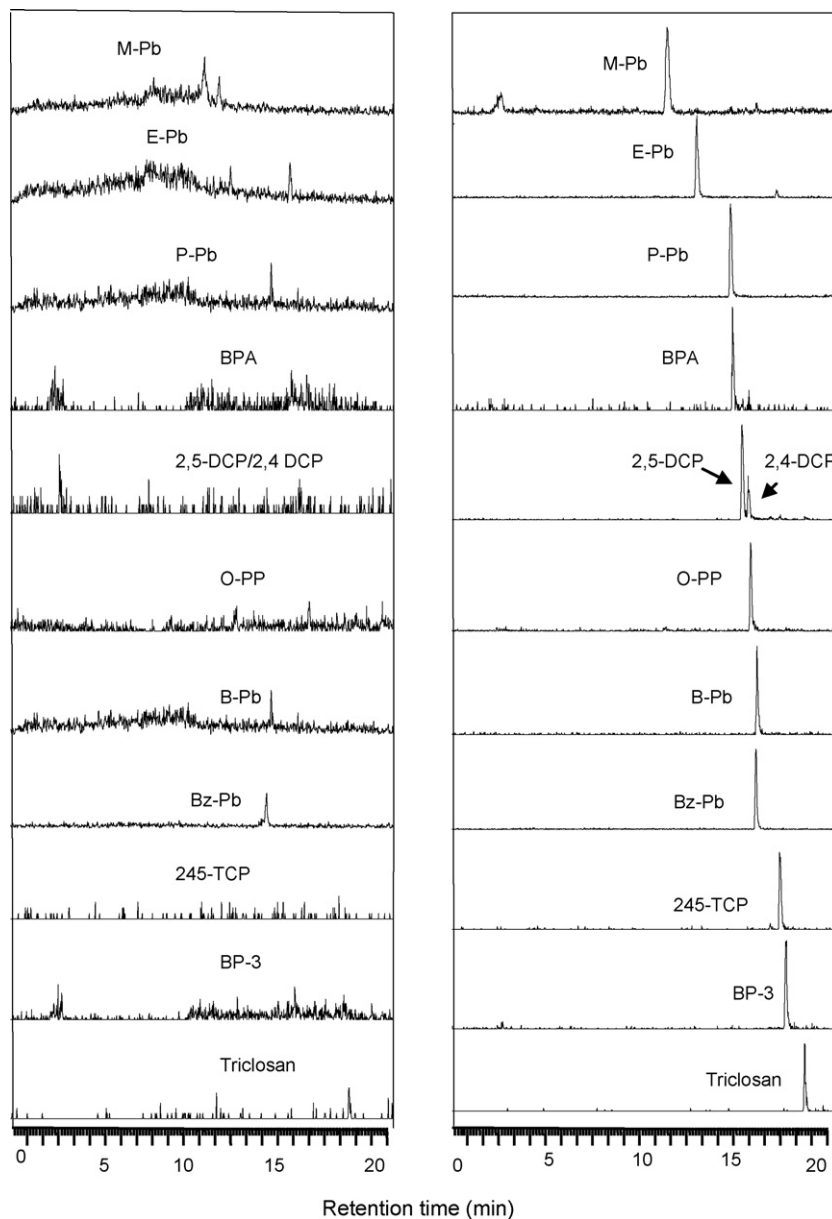
pressure photoionization (APPI), instead of APCI. The full scan mass spectrum of triclosan by APPI gave three ions at  $m/z$  287  $[M-H]^-$ ,  $m/z$  252  $[(M-H)-Cl]^-$ , and  $m/z$  161 (the dichlorophenol ion from the break down of triclosan in  $Q_0$ ). The product ion scan of  $m/z$  252 gave an ion at  $m/z$  216. More importantly, the ion transition  $m/z$  252  $\rightarrow$  216 was about 10 times more sensitive than  $m/z$  287  $\rightarrow$  142 and 161  $\rightarrow$  125. Therefore, for triclosan, we monitored  $m/z$  252  $\rightarrow$  216 (quantitation ion) and 287  $\rightarrow$  142 (confirmation ion). The use of APPI also improved the ionization of *O*-PP and BP-3. For the rest of the analytes, ionization was comparable regardless of the technique used.

### 3.4. Method validation and quality control

Calf serum spiked with standard and isotope-labeled standard solutions was analyzed repeatedly to determine the limit of detection (LOD), accuracy, and precision of the method. The LOD was calculated as  $3S_0$ , where  $S_0$  is the standard deviation as the concentration approaches zero [29].  $S_0$  was determined from five repeated measurements of low-level standards prepared in calf serum. The calculated LODs ranged from 0.1 to 0.5 ng/mL, except for triclosan (1.1 ng/mL) (Table 3). These values reflect the good sensitivity of the method, especially considering the relatively low sample volume (100  $\mu$ L) used and the simplicity of the sample preparation procedure. Typical chromatograms for a reagent blank and a low concentration standard are shown in Fig. 3. The method accuracy was assessed by five replicate analyses of calf serum spiked at four different concentrations and was expressed as the percentage of expected levels (Table 3). The intra-day variability, reflected in the method accuracy, ranged from 82 to 113% for all of the analytes at the four spiking levels (Table 3). We determined the method precision from 40 repeated measurements of QCL and QCH materials

**Table 3**  
Solid-phase extraction (SPE) recoveries, spiked standard concentration recoveries, and limits of detection (LOD)

Analyte	SPE recovery (%)	(Standard concentration) (ng/mL) spiked recovery (%)				LOD (ng/mL)
Bisphenol A	81	(0.5) 113	(1) 115	(5) 115	(10) 108	0.3
Triclosan	25	(5) 100	(10) 110	(25) 111	(50) 100	1.1
Benzophenone-3	96	(1) 87	(5) 106	(10) 106	(25) 101	0.5
<i>Ortho</i> -phenylphenol	76	(0.5) 113	(1) 112	(5) 101	(10) 101	0.1
2,4-Dichlorophenol	88	(0.5) 101	(1) 86	(5) 103	(10) 110	0.1
2,5-Dichlorophenol	82	(1) 101	(5) 105	(10) 111	(50) 106	0.4
2,4,5-Trichlorophenol	101	(2.5) 108	(5) 105	(7.5) 108	(10) 113	1.0
Methyl paraben	83	(0.5) 108	(1) 106	(5) 107	(10) 105	0.1
Ethyl paraben	90	(0.5) 100	(1) 99	(5) 107	(10) 106	0.1
Propyl paraben	89	(0.5) 82	(1) 101	(5) 105	(10) 105	0.2
Butyl paraben	89	(0.5) 103	(1) 99	(5) 105	(10) 106	0.2
Benzyl paraben	88	(0.5) 95	(1) 92	(5) 101	(10) 102	0.1

**Fig. 3.** Typical HPLC–MS/MS extracted ion chromatograms for a serum blank spiked with a low concentration (0.5–1 ng/mL in serum) calibration standard (right) and a serum blank (left). The calculated concentrations of the serum blank were <LOD for all analytes. The y-axis scales of the serum blank were magnified 5–10× times compared to those used for displaying the chromatograms of the spiked serum.

**Table 4**  
Precision of concentration measurements in spiked quality control (QC) samples

Analyte	QC low		QC high	
	Mean (ng/mL)	R.S.D. (%)	Mean (ng/mL)	R.S.D. (%)
Bisphenol A	5.6	9.3	9.5	6.2
Triclosan	4.4	21.5	7.9	17.0
Benzophenone-3	5.7	7.7	9.5	8.7
Ortho-phenylphenol	5.2	8.0	8.8	5.2
2,4-Dichlorophenol	4.1	8.8	6.9	6.0
2,5-Dichlorophenol	5.9	6.8	10.2	8.5
2,4,5-Trichlorophenol	5.6	6.6	9.3	6.0
Methyl paraben	6.7	11.5	13.0	5.0
Ethyl paraben	5.6	7.4	9.5	7.0
Propyl paraben	5.4	7.0	8.9	6.0
Butyl paraben	4.8	9.5	7.0	10.5
Benzyl paraben	5.3	6.8	8.4	7.5

over a period of 2 weeks (Table 4). The R.S.D., which reflect the intra- and inter-day variability of the method, ranged from 5.0 to 21.5%.

Calibration curves were obtained from the standards spiked in water and calf serum. Because the slopes of the calibration curves from water and calf serum were very similar (e.g., for BPA: 0.0204 (water) and 0.0214 (serum), for methyl paraben: 0.0264 (water) and 0.0265 (serum), and for triclosan: 0.00225 (water), and 0.00231 (serum)), only the calibration curve obtained from water was used for quantification. Calibration curves in water showed adequate linearity,  $\leq 100$  ng/mL for all of the analytes except for triclosan ( $\leq 1000$  ng/mL) with correlation coefficients greater than 0.99. Inter-day variation of the calibration curve slopes, measured as the R.S.D., was <10%.

The SPE recoveries of the analytes from serum were calculated on the basis of the following experiment: first, 100  $\mu$ L of serum mixed with a known amount of native analyte standards and 0.1 M formic acid was injected on the SPE column. Right after the native compounds were backflushed from the SPE column and before HPLC separation, 50  $\mu$ L of internal standard solution was injected into the HPLC gradient flow (using a second Agilent 1100 autosampler). Although native compounds and isotope-labeled standards were injected separately, they all eluted from the HPLC column and were detected by MS/MS at about the same time. A response factor (RF<sub>a</sub>) for each analyte was calculated from this experiment as the ratio of peak areas of native compound to its corresponding labeled analog. Second, 100  $\mu$ L of serum spiked with the same amount of native and internal standards was injected on the SPE column, and

50  $\mu$ L of HPLC solvent (50% MeOH) was injected into the HPLC flow. Response factor (RF<sub>b</sub>) was calculated as before. The two experiments differed in that the first (RF<sub>a</sub>), internal standards did not go through the SPE cleanup but the second (RF<sub>b</sub>) did. The SPE recovery was calculated from RF<sub>a</sub>/RF<sub>b</sub> because the internal standard amount used for both experiments was the same and matrix effects were equivalent.

Good SPE recoveries (71–101%) were obtained for all of the analytes except for triclosan (25%) (Table 3). Triclosan was the last compound eluted from the HPLC column. Because the SPE and HPLC columns contain similar sorbents, triclosan was expected to retain strongly on the SPE column; 2 min of backflushing the column with 50% of MeOH may not have been enough time to transfer triclosan completely onto the HPLC column. Even after we extended the backflush time from 2 to 5 min with 50% MeOH, we observed only a slight increase in the SPE recovery of triclosan. However, when we backflushed the SPE column with a higher organic content (70% MeOH) solvent for 3 min, the SPE recovery of triclosan increased to ~80%. Unfortunately, backflushing the SPE column with this higher organic content eluate compromised the separation of the two dichlorophenol isomers. Even with peak focusing before HPLC, the baseline separation of these two isomers could not be accomplished. Nevertheless, although the SPE recovery for triclosan is low, the sensitivity (LOD = 1.1 ng/mL) and accuracy (spiked recoveries are between 100 and 110% at four spiking levels) are still acceptable (Table 3) and may be attributed to the use of the isotope labeled triclosan as internal standard.

### 3.5. Quantification of phenols and parabens in commercial serum samples

We tested the usefulness of this method by analyzing 15 commercially available serum samples collected between 1998 and 2003 from 4 male and 11 female donors. No other demographic information or information regarding potential exposure to the analytes of interest from the donors was available. The mean, median, and range of the concentrations of free and total (free+conjugated) species, and the mean % of the conjugated species of selected analytes are listed in Table 5. Because analytical standards of the conjugated (glucuronidated and sulfated) phenols and parabens were not commercially available, we determined the concentration of these conjugates by subtracting the total concentrations from the respective concentrations of free species. The mean % of the conjugated species of each analyte, calculated as

**Table 5**  
Frequency of detection, mean and median concentrations of free, and total (free plus conjugated) species, range of concentrations, and the mean % of the conjugated species of selected environmental phenols in 15 serum samples<sup>a</sup>

Compound	Frequency of detection (%)	Mean (ng/mL)	Median (ng/mL)	Range (ng/mL)	Mean conjugate (%)
Methyl paraben free	60	1.3	0.2	<LOD-9.8	90
Methyl paraben total	100	42.4	10.9	0.4-301	
Ethyl paraben free	0	<LOD	<LOD	<LOD	100
Ethyl paraben total	53	0.6	0.2	<LOD-5.4	
Propyl paraben free	47	0.4	<LOD	<LOD-2.3	87
Propyl paraben total	80	8.0	1.4	<LOD-67.4	
Triclosan free	0	<LOD	<LOD	<LOD	100
Triclosan total	67	9.3	0.8	<LOD-13.7	
2,5-DCP free	0	<LOD	<LOD	<LOD	100
2,5-DCP total	67	19.5	1.7	<LOD-152	
O-PP free	0	<LOD	<LOD	<LOD	100
O-PP total	22	0.3	0.2	<LOD-0.9	

<sup>a</sup> The limits of detection (LODs) were 0.1 ng/mL (O-PP, and methyl-, ethyl-parabens), 0.2 ng/mL (propyl paraben), 0.4 ng/mL (2,5-DCP), and 1.1 ng/mL (triclosan). Concentrations <LOD were imputed a value of LOD divided by the square root of 2 for the statistical calculations. The calculated mean conjugate % only included the samples with detectable total species concentrations.

the ratio of concentrations of conjugated and total species, only included samples with total concentration values above the LOD.

In the current study, of the 12 analytes examined, 6 were detected infrequently (<10% of samples analyzed). For example, BPA was detected in only one of the 15 commercial samples tested, and the free and total serum concentrations of BPA in this sample were similar (1.5 ng/mL). In one study, the concentrations of BPA in all 19 human blood samples analyzed were <LOD (0.5 ng/mL) [17], but BPA has been detected in blood or serum in several other studies [30–33] using various analytical detection methods, including enzyme-linked immunosorbent assay [34,35] which may overestimate BPA concentrations [18,31,36]. The BPA results presented here must be interpreted with caution because the frequency of detection of BPA was low (6.7%) and we had no information on the procedures for collection, processing, and storage of the samples analyzed, which may be of critical importance to rule out the potential for contamination when measuring concentrations of BPA in the sub-part-per-billion levels in blood or serum [30,37].

By contrast, 6 analytes, namely methyl-, ethyl-, and propylparabens, triclosan, 2,5-DCP, and *O*-PP, were detected frequently in the 15 serum samples analyzed. For these compounds, the mean % of the conjugated species ranged from 87 to 100% (Table 5) suggesting that the conjugated species rather than the free forms of these phenols predominated in serum. This finding was in agreement with the data collected from urine, in which the conjugated species were also found to be dominant [12,38].

#### 4. Conclusions

We developed a sensitive, selective, and precise automated on-line SPE–HPLC–MS/MS method with peak focusing for the simultaneous measurement of seven environmental phenols and five parabens in serum. The method required a small amount of serum (0.1 mL) and minimum sample pretreatment without protein precipitation. This method is rugged, labor and cost effective, and allows for the analysis of large number of samples for epidemiological studies. However, based on a small number of commercial sera analyzed, the analytical sensitivity may not be high enough to allow for the quantitative determination of the analytes detected at the lowest concentrations (e.g., BPA). Because we only tested 15 samples, our findings should be replicated in future studies. More importantly, although analytically it is possible to measure several of these phenols and parabens simultaneously with the precision and accuracy at sub-parts-per-billion levels required for biomonitoring purposes, important additional considerations, such as toxicokinetic data, as well as adequate and validated collection protocols, handling and storage of the samples, including data on the temporal stability of the analytes in serum, are needed to demonstrate the utility of these measures for exposure and risk assessment purposes.

#### Disclaimer

The use of trade names is for identification only and does not constitute endorsement by the US Department of Health and Human Services or the Centers for Disease Control and Prevention. The findings and conclusions in this report are those of the

authors and do not necessarily represent the views of the Centers for Disease Control and Prevention.

#### References

- [1] CERHR, NTP-CERHR Expert Panel Report on the Reproductive and Developmental Toxicity of Bisphenol A, National Toxicology Program, U.S. Department of Health and Human Services, Research Triangle Park, NC, 2007.
- [2] Environmental Health Criteria Monographs (EHCs), Chlorophenols, International Programme on Chemical Safety (IPCS), 1989.
- [3] National Library of Medicine, National Institutes of Health. Household products database. <http://hpd.nlm.nih.gov/index.htm> (accessed June 4, 2007).
- [4] M.G. Soni, I.G. Carabin, G.A. Burdock, Food Chem. Toxicol. 43 (2005) 985.
- [5] W. Volkel, T. Colnot, G.A. Csanady, J.G. Filser, W. Dekant, Chem. Res. Toxicol. 15 (2002) 1281.
- [6] A.M. Kadry, C.S. Okereke, M.S. Abdelrahman, M.A. Friedman, R.A. Davis, J. Appl. Toxicol. 15 (1995) 97.
- [7] T. Moss, D. Howes, F.M. Williams, Food Chem. Toxicol. 38 (2000) 361.
- [8] C.S. Okereke, A.M. Kadry, M.S. Abdelrahman, R.A. Davis, M.A. Friedman, Drug Metab. Dispos. 21 (1993) 788.
- [9] A.M. Calafat, X.Y. Ye, L.Y. Wong, J.A. Reidy, L.L. Needham, Environ. Health Perspect. 116 (2008) 39.
- [10] A.M. Calafat, X. Ye, L.-Y. Wong, J.A. Reidy, L.L. Needham, Environ. Health Perspect. 116 (2008) 303.
- [11] X.Y. Ye, Z. Kuklennyik, L.L. Needham, A.M. Calafat, Anal. Bioanal. Chem. 383 (2005) 638.
- [12] X.Y. Ye, A.M. Bishop, J.A. Reidy, L.L. Needham, A.M. Calafat, Environ. Health Perspect. 114 (2006) 1843.
- [13] CDC, Third National Report on Human Exposure to Environmental Chemicals, Centers for Disease Control and Prevention, National Center for Environmental Health, Division of Laboratory Sciences, Atlanta, GA, 2005.
- [14] B.L.L. Tan, M.A. Mohd, Talanta 61 (2003) 385.
- [15] Y. Yoshimura, J.W. Brock, T. Makino, H. Nakazawa, Anal. Chim. Acta 458 (2002) 331.
- [16] M. Allmyr, M.S. McLachlan, G. Sandborgh-Englund, M. Adolfsson-Erici, Anal. Chem. 78 (2006) 6542.
- [17] W. Volkel, N. Bittner, W. Dekant, Drug Metabol. Dispos. 33 (2005) 1748.
- [18] T. Tominaga, T. Negishi, H. Hirooka, A. Miyachi, A. Inoue, I. Hayasaka, Y. Yoshikawa, Toxicology 226 (2006) 208.
- [19] X.Y. Ye, Z. Kuklennyik, L.L. Needham, A.M. Calafat, Anal. Chem. 77 (2005) 5407.
- [20] N.C. Maragou, E.N. Lampi, N.S. Thomaidis, M.A. Koupparis, J. Chromatogr. A 1129 (2006) 165.
- [21] S. Moors, M. Blaszkewicz, H.M. Bolt, G.H. Degen, Mol. Nutr. Food Res. 51 (2007) 787.
- [22] K. Inoue, Y. Yoshimura, T. Makino, H. Nakazawa, Analyst 125 (2000) 1959.
- [23] K. Inoue, K. Kato, Y. Yoshimura, T. Makino, H. Nakazawa, J. Chromatogr. B 749 (2000) 17.
- [24] K. Inoue, M. Kawaguchi, F. Okada, N. Takai, Y. Yoshimura, M. Horie, S. Izumi, T. Makino, H. Nakazawa, Anal. Chim. Acta 486 (2003) 41.
- [25] X.Y. Ye, Z. Kuklennyik, L.L. Needham, A.M. Calafat, J. Chromatogr. B 831 (2006) 110.
- [26] Z. Kuklennyik, L.L. Needham, A.M. Calafat, Anal. Chem. 77 (2005) 6085.
- [27] S.P.J. Van Leeuwen, J. De Boer, J. Chromatogr. A 1153 (2007) 172.
- [28] R. Wissiack, E. Rosenberg, M. Grasserbauer, J. Chromatogr. A 896 (2000) 159.
- [29] J.K. Taylor, Quality Assurance of Chemical Measurements, Lewis Publishers, Chelsea, MI, 1987.
- [30] V. Padmanabhan, V.K. Siefert, S. Ransom, T. Johnson, J. Pinkerton, L. Anderson, L. Tao, K. Kannan, J. Perinatol. 28 (2008) 258.
- [31] W. Dekant, W. Volkel, Toxicol. Appl. Pharm. 228 (2007) 114.
- [32] A.C. Dirtu, L. Roosens, T. Geens, A. Gheorghe, H. Neels, A. Covaci, Anal. Bioanal. Chem. 391 (2008) 1175.
- [33] L.N. Vandenberg, R. Hauser, M. Marcus, N. Olea, W.V. Welshons, Reprod. Toxicol. 24 (2007) 139.
- [34] Y. Ikezuki, O. Tsutsumi, Y. Takai, Y. Kamei, Y. Taketani, Hum. Reprod. 17 (2002) 2839.
- [35] M. Sugiura-Ogasawara, Y. Ozaki, S.I. Sonta, T. Makino, K. Suzumori, Hum. Reprod. 20 (2005) 2325.
- [36] K. Inoue, M. Wada, T. Higuchi, S. Oshio, T. Umeda, Y. Yoshimura, H. Nakazawa, J. Chromatogr. B 773 (2002) 97.
- [37] J. Sajiki, K. Takahashi, J. Yonekubo, J. Chromatogr. B 736 (1999) 255.
- [38] X.Y. Ye, A.M. Bishop, J.A. Reidy, L.L. Needham, A.M. Calafat, J. Expos. Sci. Environ. Epidemiol. 17 (2007) 567.



# Flow injection–hydride generation atomic absorption spectrometric determination of selenium, arsenic and bismuth

Yanlin Zhang, Samuel B. Adeloju\*

NanoScience and Sensor Technology Research Group, School of Applied Sciences and Engineering,  
Monash University Gippsland Campus, Churchill, Victoria 3842, Australia

## ARTICLE INFO

### Article history:

Received 19 August 2007  
Received in revised form 28 March 2008  
Accepted 28 March 2008  
Available online 16 April 2008

### Keywords:

Flow injection  
Hydride generation atomic absorption spectrometry  
Selenium  
Arsenic  
Bismuth

## ABSTRACT

A simple and robust flow injection system which permits low sample and reagent consumption is described for rapid and reliable hydride generation atomic absorption spectrometric determination of selenium, arsenic and bismuth. The system, which composed of one peristaltic pump and one four channel solenoid valve, used water as the carrier streams for both sample and  $\text{NaBH}_4$  solution. Rapid off-line pre-reduction of the analytes was achieved by using hydroxylamine hydrochloride for selenium and a mixture of potassium iodide and ascorbic acid for arsenic and bismuth. Transition metal interference was eliminated with the addition of thiourea and EDTA into the  $\text{NaBH}_4$  solution and significant sensitivity enhancement was observed for selenium in the presence of thiourea in the reductant solution. Under optimised conditions, the method achieved detection limits of  $0.2 \text{ ng mL}^{-1}$  for Se,  $0.5 \text{ ng mL}^{-1}$  for As and  $0.3 \text{ ng mL}^{-1}$  for Bi. The method was very reproducible, achieving relative standard deviations of 6.3% for Se, 3.6% for As and 4.7% for Bi, and has a sample throughput of  $360 \text{ h}^{-1}$ . Successful application of the method to the quantification of selenium, arsenic and bismuth in a certified reference river sediment sample is reported.

© 2008 Elsevier B.V. All rights reserved.

## 1. Introduction

Hydride generation atomic absorption spectrometry (HGAAS) is one of the widely used methods for the determination of hydride-forming elements, particularly at ultra-trace concentrations because of its high sensitivity, tolerance for inorganic and organic interference, relatively low cost, and high sample throughput [1]. To improve sample throughput, various versions of flow injection manifolds have been proposed and applied to the analysis of metalloid elements by HGAAS [2–9]. However, many of these manifolds employed complex hardware configurations, which include the use of more than one pump and/or valve, as well as three or more pumping channels [4–7]. For these reasons, the control and operation of these systems are often complex. Furthermore, the sample throughput achieved with many of these flow injection manifolds is usually under  $90 \text{ h}^{-1}$  [3–5], except in some cases where sample throughputs up to  $180 \text{ h}^{-1}$  have been reported [8]. Yet it is still possible, with adequate FIA system design, which utilizes minimum hardware and simple configuration, to achieve substantially higher sample throughput with minimum sample and reagent consumption.

Most of the existing FI systems also commonly used acid as the carrier stream for the sample, and the reductant ( $\text{NaBH}_4$  or  $\text{KBH}_4$ ) solution is usually aspirated continuously. This approach is therefore somewhat expensive and wasteful due to the high cost of the reductants, and the use of significant volume of acid may require treatment prior to disposal.

The work reported to date has also revealed that various reducing agents and modes of addition have been proposed for the pre-reduction of higher oxidation states of metalloid elements, and consequently achieving different reaction rates [4,10–15]. Some of these pre-reduction methods are slow, but are still commonly employed. For example, the pre-reduction of Se(VI) is often performed by heating the sample in HCl and this can take 20–90 min [10]. To automate and simplify the analysis of such samples, in-line pre-reduction has also been reported [8,16–23], including the use of microwave-assisted system [18,19]. These approaches often require complex hardware configurations and the sample throughput is often very low due to the time-requirement for the pre-reduction. Therefore, there is still a need for the development of a fast and simple pre-reduction approach which will require minimum use of hardware.

Although it has been reported that thiourea (TU) can enhance the sensitivity obtained for Se by HGAAS [24], there are also evidence that the presence of TU depresses Se signal [25–27].

\* Corresponding author. Tel.: +61 3 9902 6450; fax: +61 3 9902 6738.  
E-mail address: [Sam.Adeloju@sci.monash.edu.au](mailto:Sam.Adeloju@sci.monash.edu.au) (S.B. Adeloju).



In particular, Se signal depression was observed when TU was added into the sample solution in batch mode and it was suggested the reduction of Se(IV) to elemental Se was responsible for this effect [25]. It has further been reported that the mode of addition of TU also plays an important role in the observed depression of Se signal. These observations therefore suggest that special care must be taken when using TU as a pre-reduction or masking agent for HGAAS determination of Se.

Another common problem in the HGAAS determination of metalloids elements is the interference by transition metal ions and this is often eliminated or minimized by use of masking agents. Two of the most effective and commonly used masking agents for control of such interferences in the determination of arsenic, antimony, bismuth, tin and germanium are L-cysteine (Cys) and TU. However, it is much more difficult to find suitable masking agents for selenium [26]. Potential masking agents, such as thiocyanate, triethanolamine and cupferon, often give low recoveries for selenium and other elements, while many other masking agents, such as EDTA, tartaric acid and 2,3-dimercaptopropan-1-ol, have limited complexing capacity in strongly acidic media [13]. The use of EDTA, diethylenetriamine pentacetic acid (DPTA) and tartrate in alkaline reduction medium with  $\text{NaBH}_4$  followed by acidification have been found to improve the tolerance limits for Co(II), Ni(II), Fe(III) and Cr(III) significantly [29,30], but their effects on other metals were not considered. It has also been reported [28] that the use of combination of TU and KI was effective for improving the tolerance limit of most transition metals, but the effectiveness for Fe(III) was limited. In another study 1,10-phenanthroline was used as a masking agent to control the interferences of Cu and Ni on HGAAS determination of Se [4]. However, when we employed this reagent, significant foaming was observed and this resulted in the suppression of the stripping of the hydride. In general, there are many discrepancies in the literature about the effectiveness of various masking agents in eliminating or reducing the interference of transition metals on HGAAS determination of metalloid elements. For example, Li and Guo [14] reported that TU can effectively eliminate the interference of a number of metals on Se determination without significant loss of sensitivity, yet Liu and co-workers [27] observed noticeable loss of sensitivity in Se signal when TU was used as a pre-reductant. It was obvious from many of these studies that the effectiveness of masking agents in removing interference from transition metals is not only dependent on their properties and concentrations, but also on the mode of addition [26]. There is therefore still a need for the identification or development of more simple, effective and reliable masking methods for overcoming transition metal interferences in HGAAS measurements.

This paper proposes a simple and robust flow injection manifold for hydride generation based on the use of only one peristaltic pump with two channels, one sampling valve, and a U-tube gas-liquid phase separator. The use of a multi-channel solenoid, instead of a rotary valve, which is easier to control and quicker to activate or deactivate is considered for achieving high sampling frequency. Also, the use of water as the carrier streams for both sample and the reductant will be considered as a means of reducing reagent and sample consumption. Fast off-line pre-reduction will be considered for improving the overall speed of analysis. The elimination of transition metal interferences in the FI-HGAAS measurement of Se, As and Bi will be investigated with the addition of thiourea and EDTA into  $\text{NaBH}_4$  solution. Also the effect of TU on Se signal during HGAAS measurement will be investigated. The application of the method to the quantification of selenium, arsenic and bismuth in sediment samples will also be considered.

**Table 1**  
Parameters employed for HGAAS measurements

Element	Wavelength (nm)	Current (mA)	Bandpass width (nm)	Atomisation temperature ( $^{\circ}\text{C}$ )
Se	196.0	16	0.7	950
As	193.7	18	0.7	950
Bi	223.1	16	0.7	850

## 2. Experimental

### 2.1. Instruments and reagents

A PerkinElmer model 3030 (Perkin Elmer Pty. Ltd., Rowville, Victoria, Australia) atomic absorption spectrometer was used with selenium, arsenic and bismuth hollow cathode lamps (Varian Australia Pty. Ltd., Mulgrave, Victoria, Australia) for HGAAS measurements. The parameters used for the AAS measurements are listed in Table 1. A T-shaped quartz tube was used as the atomizer. The inner diameter of the tube was 8 mm and the length was 150 mm. The branch of the tube had an inner diameter of 6 mm and a length of 7 cm. The tube was heated electrically and its temperature was adjusted with the aid of an adjustable transformer. A PerkinElmer 56 recorder was used for recording the peak sequence.

A flow injection system assembled in our laboratory for this study is shown in Fig. 1. The system composed of a solenoid pinch valve, a Miniplus 3 peristaltic pump (Gilson, Villiers Le Bel, France), a U-tube gas-liquid phase separator (GLS). The valve was made in our laboratory and had four channels in two groups, with two channels in each group. One group is normally open while the other is normally closed. The normally open channels were employed for delivery of carrier streams and the normally closed channels were used when opened for loading sample and reductant. A 7951 multi-functional digit LCD programmable time delay relay (Trumeter Company Inc., Deerfield Beach, Florida, USA) was used to activate and control the valve. A pump speed of 48 rpm was used with a Tygon pump tubing (Elkay Products Inc., Massachusetts, USA) of 2.5 mm ID for the sample channel and 0.42 mm ID for the reductant channel, generating flow rates of 11.0 and 2.0  $\text{mL min}^{-1}$ , respectively. The carrier gas flow rates were 302, 305 and 305  $\text{mL min}^{-1}$  for Se, As and Bi, respectively.

Individual standard solutions ( $1000 \mu\text{g mL}^{-1}$ ) of selenium, arsenic and bismuth were purchased from BDH Chemicals Pty. Ltd. (Kilsyth, Victoria, Australia). Appropriate dilution was made with Milli-Q water as required. All other reagents were of analytical

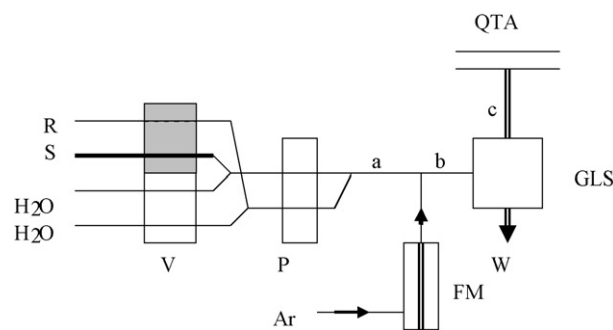


**Fig. 1.** Manifold of the flow injection hydride generation system. V: solenoid valve, P: peristaltic pump, FM: gas flow meter, GLS: gas-liquid phase separator, QTA: quartz tube atomizer, R:  $\text{NaBH}_4$ , S: sample, Ar: argon gas, W: waste.  $a = 15, 20, 20 \text{ cm}$  for Se, As and Bi, respectively;  $b = 10 \text{ cm}$  for all analytes;  $c = 30 \text{ cm}$  for all analytes.

reagent grade purity. Milli-Q water was used throughout the experiment for dilution and rinsing. A 20% hydroxylamine hydrochloride (BDH Chemicals Pty. Ltd., Kilsyth, Victoria, Australia) was prepared and stored in the fridge at 4 °C for one week. A solution mixture which contained 10% potassium iodide (BDH Chemicals Pty. Ltd., Kilsyth, Victoria, Australia) and 10% ascorbic acid (BDH Chemicals Pty. Ltd., Kilsyth, Victoria, Australia) was prepared freshly each time before use. To prepare the NaBH<sub>4</sub> solution, a mixture containing TU and EDTA was made and then neutralised with 10% NaOH to pH 11 before adding appropriate amount of solid NaBH<sub>4</sub> (Sigma–Aldrich Pty. Ltd., Castle Hill, NSW, Australia) which was subsequently dissolved in the mixture. The final TU and EDTA concentrations were 1 and 2%, respectively, and the concentrations of NaBH<sub>4</sub> for Se, As and Bi were 0.2, 0.5–1, and 0.2%, respectively. A river sediment reference material AGAL-10, which was collected from the Hawkesbury River in New South Wales, Australia and provided by Australian Government Analytical Laboratories, was used for the validation of the FI–HGAAS method developed in this study.

### 2.2. Pretreatment of sediment samples

Sediment sample was dried at 70 °C in an oven, homogenized and passed through a 63 μm Nylon sieve. 1 g of the sample was then digested with 10 mL aqua regia in a 50 mL Pyrex conical flask or beaker by heating on a hot plate to about 1 mL. Then 5 mL concentrated HCl was added and again heated to about 1 mL. Finally, another 5 mL concentrated HCl was added and heated for 15 min. The sample was then filtered through filter paper and collected into a 50 mL volumetric flask and then made up to volume with Milli-Q water. For Se determination, 5 mL of the sample solution was transferred into a 10 mL volumetric flask, followed by the addition of 1 mL of hydroxylamine hydrochloride solution (20%) and 2 mL 2M HCl and dilution to volume with Milli-Q water. For As and Bi determinations, 5 mL of the sample solution was transferred into a 10 mL volumetric flask, followed with the addition of 1 mL of a mixture of KI (10%) and ascorbic acid (10%) solution, 2 mL of 2 M HCl and the solution was then diluted to volume with Milli-Q water. Quantification of Se, As and Bi was also achieved by the standard calibration method.

### 2.3. Measurement procedures

The recycle operation mode of the time delay relay (TDR) was used for controlling the valve. In this mode, the valve was activated for a chosen time interval for sample and reagent loading, followed by deactivation of the valve for sample and reagent injection into the carrier streams, and the activation/deactivation of the valve were recycled by the TDR automatically. Prior to energising the TDR, water was aspirated through the open channels. Once the TDR was initialised, the two open channels of the valve were closed, while the closed channels were opened to aspirate the sample and reductant solutions into the system. Then the latter channels were closed, while the former were opened again and the sample and reductant bands were propelled into the system by the water flow and merged downstream of the pump allowing hydride generation reaction to occur. The generated hydride was carried into the GLS with an argon flow and the gaseous phase was delivered into the atomizer, where the hydride molecules were atomised and the atomic absorption signal (peak height) was recorded. Se, As and Bi concentrations in samples were quantified by standard calibration. The optimisation of the loading volumes for sample and reductant solutions was achieved by varying the active time interval of the valve.

## 3. Results and discussion

### 3.1. System design

The reproducible introduction of a fixed sample volume into a continuously flowing carrier stream is a fundamental aspect of flow injection analysis. Rotary PTFE injection valves which are prone to wearing are commonly used in most commercial purpose-built manifolds. However, applications of solenoid valves in FI systems have also been reported [31–34]. Generally, the configurations of most of these systems are complex. To simplify the design, the FI system proposed in this study used only one pinch valve in conjunction with a peristaltic pump for sample and reagent injection. The use of the valve has resulted in a simple hardware configuration and avoids the risk of wearing and leakage. Furthermore, the control of the action of the valve is extremely simple and, hence, the construction cost is very low. To optimise the performance of the FI system, the influence of key primary and secondary parameters was investigated.

### 3.2. Optimisation of primary parameters

Prior to optimisation of secondary parameters, the influence of primary parameters, such as pump speed, pump tubing sizes, and sample injection volume, on the performance of the FI system was investigated. It was found that the sensitivity obtained for Se, As and Bi increased with corresponding increase in pump speed. Consequently, a maximum speed of 48 rpm was used for the FI–HGAAS measurements. Also, the sensitivity increased with increasing pump tubing ID used for the sample channel. A tubing ID of 2.5 mm gave optimum responses for all elements, and was used for other investigations. For the reagent channel, tubing size between 0.42 and 1.0 mm ID gave the optimum sensitivity and beyond this range the sensitivity decreased. A pump tubing of 0.42 mm ID was therefore used for reagent delivery in all other investigations. In addition to the pump speed and tubing size, the lengths of the reaction coils *a* and *b* (Fig. 1) and the size of the gas phase delivery tube *c* also had noticeable influence on the performance of the FI system. Optimum sensitivities were obtained for Se, As and Bi measurements when the lengths of reaction coil *a* (1.2 mm ID) were 15, 20 and 20 cm, respectively. In contrast, the variation of the length of *b* (1.5 mm ID) within 10–20 cm had no significant effect on the sensitivity and, hence, a 10 cm length was used. For tube *c*, it was found that 4–6 mm ID and a length of 20–35 cm gave the best sensitivities for Se, As and Bi.

The sensitivity was also improved with an increase in sample loading time, and a maximum sensitivity was achieved when a loading time of 3.5 s, which corresponds to 0.64 mL and 0.12 mL of sample and reductant solutions, respectively, was used. The use of longer sampling time requires increased cleaning time. For this reason, a sample loading time of 3.5 s was employed. To ensure recovery of the baseline with a carryover of less than 1%, an injection (cleaning) step time of 6.5 s was required. To ensure adequate cleaning, a 10 s cleaning time was used for each operation cycle.

### 3.3. Optimisation of secondary parameters

#### 3.3.1. Sample acidity and NaBH<sub>4</sub> concentration

Two of the major factors influencing the rate and efficiency of hydride generation reaction are sample acidity and NaBH<sub>4</sub> concentration. Fig. 2 shows the influence of acid and NaBH<sub>4</sub> concentrations on the sensitivities of Se, As and Bi. Evidently, optimum sensitivities were obtained for the three elements in presence of 0.5–1.0 M HCl. However, the optimum NaBH<sub>4</sub> concentrations are different for the three elements. For selenium, the optimum sensitivity was

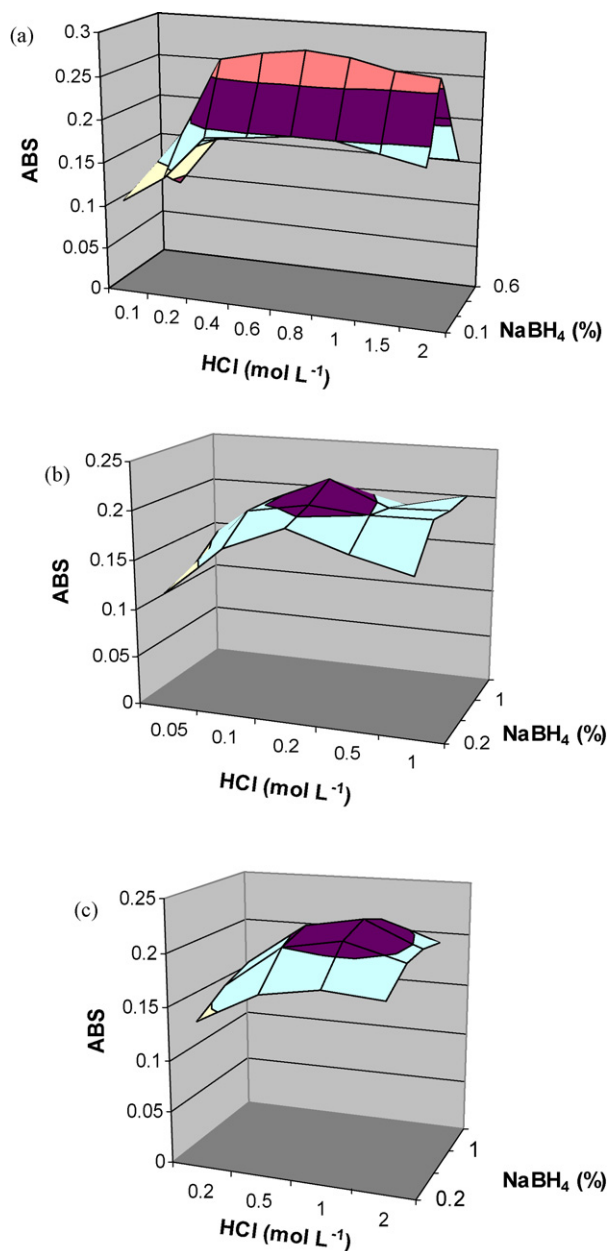


**Fig. 2.** Influence of HCl and  $\text{NaBH}_4$  concentrations on the sensitivities of (a) Se, (b) As and (c) Bi measurements by FI-HGAAS.

achieved with a  $\text{NaBH}_4$  concentration of 0.2%, whereas it must be above 0.5% for arsenic, and 0.2–1.0% gave similar sensitivity for bismuth.

### 3.3.2. Carrier gas flow rate and atomisation temperature

The sensitivities obtained for Se, As and Bi measurements increased with increasing argon gas flow rate up to the optimum for each element and then decreased beyond this value. The optimum argon gas flow rates for Se, As and Bi were 356, 360 and 360  $\text{mL min}^{-1}$ , respectively. These flow rates were subsequently used for all further investigations.

The sensitivity was also susceptible to change in atomisation temperature and optimum sensitivities were obtained for Se and As with an atomisation temperature of 950 °C, while for bismuth optimum sensitivity was obtained at 850 °C.

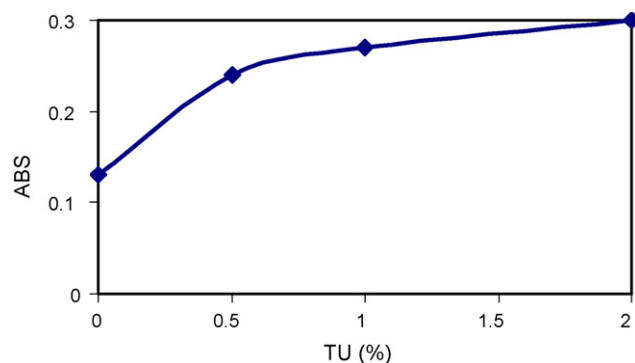


**Fig. 3.** Catalytic effect of thiourea on the sensitivity of Se measurement by FI-HGAAS. [Se] was 20  $\text{ng mL}^{-1}$ .

### 3.4. Pre-reduction of high oxidation states of Se, As and Bi

Pre-reduction of metalloid elements in higher oxidation states, such as Se(VI), As(V) and Bi(V), is necessary to achieve adequate hydride generation efficiency, and fast simple pre-reduction method is often favoured. The key requirement is to choose a method which uses an effective reagent for off-line reduction and, thus, avoids tedious reduction process or use of complex system. In this study we have chosen hydroxylamine hydrochloride, and a mixture of KI and ascorbic acid as pre-reductants. It was found that off-line addition of hydroxylamine hydrochloride to sample solution rapidly reduced Se(VI) to Se(IV) at room temperature. Liu and co-workers [27] have also indicated that this reagent can be used to reduce both Se(VI) and As(V) to their lower oxidation states. However, we were unable to achieve fast reduction of As(V) in this study, possibly due to the different medium used for the reaction. Instead, we found that As(V) and Bi(V) were easily reduced to As(III) and Bi(III) with a mixture of KI and ascorbic acid at room temperature. Due to the reported interference of  $\text{I}^-$  on Se [13,35,36], the pre-reduction of Se(VI) and As(V) was performed in separate sample aliquots. By using these methods with the simple FI system, sample throughput of up to 360  $\text{h}^{-1}$  was achieved and the overall determination speed was more superior than for previously reported methods.

### 3.5. Enhancement of Se signal with thiourea

Different modes of addition of TU to solutions reportedly have different effect on the sensitivity of Se signal obtained by HGAAS. For example, it was reported that batch addition of TU to sample solution caused remarkable attenuation of sensitivity, whereas only a slight increase in sensitivity was observed when on-line addition of TU was employed [26,28]. In our study, we found that the addition of adequate amount of TU to the  $\text{NaBH}_4$  solution in a batch mode significantly increased the sensitivity. As shown in Fig. 3, the sensitivity was increased by 150% with the addition of 2% TU in the  $\text{NaBH}_4$  solution.

The signal enhancement effect of thiols on the hydride generation (HG) reaction of metalloids has been reviewed by Kumar and Riyazuddin [37]. It was proposed that a compound formed between  $\text{NaBH}_4$  and the SH group of thiols is a more potent reducing agent than  $\text{NaBH}_4$  and it is responsible for the enhancement of the hydride generation process [38]. Qiu and co-workers [21] used thiourea (TU) as the pre-reductant for Se(VI) by on-line addition and high temperature reaction. They found that HG efficiency of Se(VI) improved considerably and was even higher than obtained for the same amount of Se(IV) by using a conventional HG system. The possible mechanism of the pre-reduction was discussed from

**Table 2**  
Reduction of transition metal interferences in Se measurement with TU and EDTA

Interfering ions (mg L <sup>-1</sup> )	Masking agents		
	None <sup>a</sup>	TU (0.8%) <sup>a</sup>	TU + EDTA (0.8% + 2%) <sup>a</sup>
None	0.13	0.270	0.270
Fe(III), 500	0.096	0.250	0.270
Co(II), 10	0.13	0.265	0.270
Ni(II), 10	0.11	0.210	0.263
Cu(II), 1	0.043	0.082	0.268
Pb(II), 1	0.092	0.090	0.260
Fe(III) + Cu(II), 500 + 1	0.037	0.055	0.266

<sup>a</sup> Data in columns 2–4 are absorbance values for 20 ng mL<sup>-1</sup> Se.

the perspectives of thermodynamics and the chemical isomerism of TU. They indicated that the reaction time of TU and Se also affects the sensitivity [21].

From the above data, it can be suggested that both the addition mode and concentration of TU influenced the sensitivity of Se. When added to the sample solution in the batch mode, loss of sensitivity can be caused by the long reaction time which allows the reduction of Se(IV) into elemental state. On the other hand, by using on-line addition, the reaction time can be easily regulated and optimised to ensure adequate reduction of Se(VI) to Se(IV) and avoid the occurrence of further reduction. Consequently, on-line addition of TU results in more pronounced sensitivity for Se. Yet, when added into the NaBH<sub>4</sub> solution in batch mode, a compound may be formed between TU and NaBH<sub>4</sub> which enhances the sensitivity of Se measurement. Similar effect was not observed for As and is not significant for Bi measurement. This may highlight the different reactivity of the different elements in the hydride formation reactions.

### 3.6. Elimination of interferences from transition metals

To minimise or remove interferences from the HGAAS measurements of the three metalloid elements, TU and EDTA were used as masking agents by addition into the NaBH<sub>4</sub> solution. The inclusion in the reductant not only avoided the depression of Se signal by TU, but also ensured the solubility and effectiveness of EDTA. The results in Tables 2–4 indicate that TU alone cannot completely remove interferences of common transition metal ions on Se measurements and it is also not effective for eliminating interference from As measurements. In contrast, the addition of TU alone was more effective for the removal of interferences from Bi measurements. This may reflect on the dynamic advantage of H<sub>3</sub>Bi formation. When TU and EDTA were used together, the tolerant limits of the interfering ions were significantly improved, especially for Fe(III) ions. It is worth noting that the concentrations of the interfering metals considered in this study were above the levels usually encountered in environmental samples and therefore the tolerant limits demonstrated here are high enough for real samples. Some other metals, especially groups IA–IIIA, IIIB–VB, as well as some

**Table 3**  
Reduction of transition metal interferences in As measurement with TU and EDTA

Interfering ions (mg L <sup>-1</sup> )	Masking agents		
	None <sup>a</sup>	TU (0.8%) <sup>a</sup>	TU + EDTA (0.8% + 2%) <sup>a</sup>
None	0.202	0.203	0.203
Fe(III), 500	0.102	0.105	0.202
Co(II), 10	0.201	0.202	0.203
Ni(II), 10	0.194	0.192	0.203
Cu(II), 10	0.160	0.175	0.192
Pb(II), 10	0.130	0.130	0.180
Fe(III) + Cu(II), 500 + 1	0.090	0.120	0.190

<sup>a</sup> Data in columns 2–4 are absorbance values for 20 ng mL<sup>-1</sup> As.

**Table 4**  
Reduction of transition metal interferences in Bi measurement with TU and EDTA

Interfering ions (mg L <sup>-1</sup> )	Masking agents		
	None <sup>a</sup>	TU (0.8%) <sup>a</sup>	TU + EDTA (0.8% + 2%) <sup>a</sup>
None	0.195	0.194	0.196
Fe(III), 500	0.205	0.195	0.195
Co(II), 10	0.200	0.200	0.201
Ni(II), 10	0.160	0.205	0.204
Cu(II), 10	0.082	0.205	0.203
Pb(II), 10	0.162	0.190	0.198
Fe(III) + Cu(II), 500 + 1	0.078	0.190	0.196

<sup>a</sup> Data in columns 2–4 are absorbance values for 20 ng mL<sup>-1</sup> Bi.

VIB and VIIB elements that are usually present in environmental samples did not cause noticeable interference.

The results of these studies have clearly demonstrated that the effectiveness of TU and EDTA as masking agents is very dependent on the mode of addition to sample solutions. Addition to acidic medium deteriorates the masking ability of EDTA [30] and causes the depression of Se signal [26–28]. On the other hand, the addition of masking agents to NaBH<sub>4</sub> in alkaline sample solution followed by acidification achieved improved masking ability [31,32]. It was proposed that the kinetic difference could play an important role. For example, if the dissociation of the metal complex formed with the masking agents in alkaline medium does not occur as fast as the decomposition of tetrahydroborate when mixed with acid, the formation of metal or metal borides should be insignificant [31]. In the present study, improved solubility of EDTA in the NaBH<sub>4</sub> solution is an important factor for its effectiveness as a masking agent. Overall, the tolerances for interfering transition metals achieved in this study are comparable to those reported previously in some studies [8,9,14,28]. Better tolerances have also been reported by using different reagents and methods [4,26,27,29–31]. However, the tolerances obtained in this study are sufficient to ensure reliable determination of the three metalloid elements in most environmental samples.

### 3.7. Carrier stream and background correction

The intermittent injection of NaBH<sub>4</sub> resulted in slight improvement of Se sensitivity, but this observation was dependent on the concentration of NaBH<sub>4</sub> solution. Evidently, higher NaBH<sub>4</sub> concentration resulted in more improved sensitivity. At the same time, the baseline recovery was faster by this approach than by using continuous NaBH<sub>4</sub> input. Also better precision was obtained by replacing the acid with water as the sample carrier stream, as shown in Fig. 4 (1). The lower sensitivity obtained by using continuous input of the reductant may be caused by the dilution of the hydride with the hydrogen evolved from the excess NaBH<sub>4</sub>, and the baseline shift with acid as the sample carrier stream may also be caused by the extra hydrogen evolved compared to when water was used as the carrier stream. Similar observations were made for As and Bi. Therefore, water was used as the carrier streams both for sample and reductant solutions. Also intermittent injection of NaBH<sub>4</sub> solution was used.

Under optimised conditions, stable baseline was obtained for HGAAS measurement of the three metalloid elements. Fig. 4 (2) shows a comparison of the results obtained for Se by using atomic absorption (AA) and background correction (BGC) modes. The results demonstrate that AA mode gave better performance than BGC mode. This is further reflected by the calibration equation which is  $y = 0.0198x + 0.0009$  with  $R^2 = 0.9998$  for AA mode compared to  $y = 0.0168x + 0.0002$  with  $R^2 = 0.9997$  for BGC mode. Consequently, atomic absorption mode, without background correction, was used for all measurements.

**Table 5**  
Analytical performance of the FI-HGAAS system

Parameter	Se	As	Bi
Sample consumption per assay (mL)	0.64	0.64	0.64
Sampling frequency ( $\text{h}^{-1}$ )	360	360	360
Regression equation	$y = 0.0198x + 0.0009$	$y = 0.0121x + 0.0075$	$y = 0.0132x + 0.0018$
Correlation coefficient	0.9985	0.9983	0.9982
Detection limit ( $\text{ng mL}^{-1}$ )	0.2	0.5	0.3
R.S.D. (%)	6.3	3.6	4.7

**Table 6**  
Concentrations and recovery efficiencies for Se, As and Bi in a river sediment sample

Element	Measured value ( $n = 6, \mu\text{g g}^{-1}$ )	R.S.D. (% , $n = 6$ )	Certified value ( $\mu\text{g g}^{-1}$ )	Recovery (%)
Se	$11.2 \pm 0.5$	6.3	$11.8 \pm 3.2$	$94.9 \pm 4.2$
As	$17.5 \pm 0.6$	4.6	$16.8 \pm 3.2$	$104.2 \pm 3.6$
Bi	$10.2 \pm 0.3$	3.7	NA <sup>a</sup>	
Bi	10.0 (Added)		20.0 (Found) <sup>b</sup>	98.0 <sup>b</sup>

<sup>a</sup> Not available.<sup>b</sup> Standard addition result.

### 3.8. Method performance and analytical application

Table 5 shows that, under the optimised conditions, excellent performances were achieved by the FI-HGAAS method for the three metalloid elements. The achieved sensitivities, linear concentra-

tion ranges and detection limits are all adequate for their reliable determination in environmental samples.

The FI-HGAAS method was successfully applied to the determination of Se, As and Bi in the river sediment reference material (AGAL-10). The results in Table 6 show that the concentrations obtained for Se and As are in a very good agreement with the certified values and the recovery of Bi (98% by recovery study) was also satisfactory.

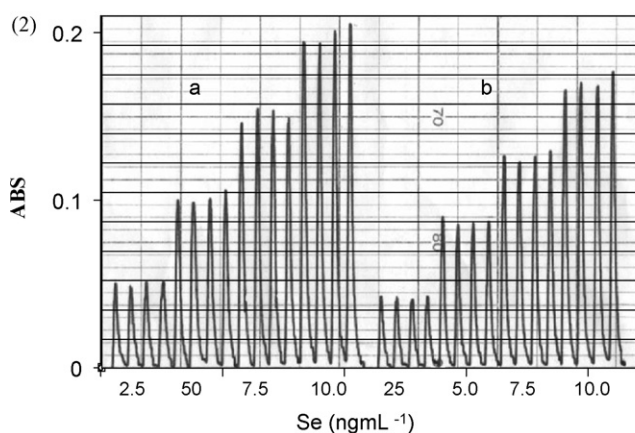
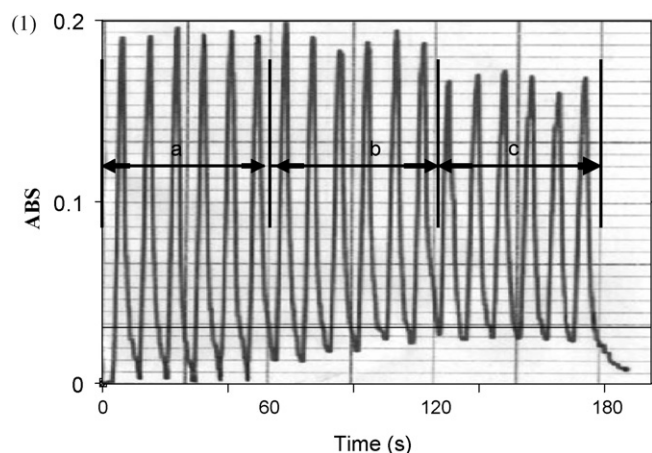


**Fig. 4.** Peak sequences of (1) Se measurement with different carrier streams: (a) sample and reductant carrier streams are water, (b) sample carrier stream is HCl and reductant carrier stream is water, and (c) sample carrier stream is HCl and reductant injected continuously and (2) Se measurement in (a) atomic absorption mode, and (b) background correction mode—sample and reagent carrier streams are water.

## 4. Conclusions

A simple FI system, which comprised one peristaltic pump and one solenoid valve, has been successfully employed for rapid hydride generation atomic absorption spectrometric determination of selenium, arsenic and bismuth. Under optimised conditions, the system achieved a very high sample throughput of  $360 \text{ h}^{-1}$ , and sample and reagent consumption was very low. The use of water as carrier streams for both the sample and reagent gave stable baseline and better sensitivity for the samples. Rapid off-line pre-reduction steps for Se(VI) were achieved with hydroxylamine hydrochloride, and for As(V) and Bi(V) with a mixture of KI and ascorbic acid. In addition, significant enhancement of Se signal was observed with the addition of TU. Furthermore, the interferences from transition metal ions were easily eliminated by using TU and EDTA as masking agents added to the reductant solution. The FI-HGAAS method was successfully applied to the quantification of Se, As and Bi in a river sediment reference material. The recovery efficiency for the three elements ranged from 95 to 104%.

## References

- [1] X. Yan, Z. Ni, *Anal. Chim. Acta* 291 (1994) 89.
- [2] Z. Fang, G. Tao, S. Xu, X. Liu, J. Wang, *Microchem. J.* 53 (1996) 42.
- [3] E.H. Hansen, J.E.T. Andersen, *Lab. Autom. Inform. Manag.* 34 (1999) 91.
- [4] C.C.Y. Chan, R.S. Sadana, *Anal. Chim. Acta* 270 (1992) 231.
- [5] N.V. Semenova, L.O. Leal, R. Forteza, V. Cerdà, *Anal. Chim. Acta* 455 (2002) 277.
- [6] T. Näykkö, P. Perämäki, J. Kujala, A. Mikkonen, *Anal. Chim. Acta* 439 (2001) 229.
- [7] P. Carrero, A. Malavé, J.L. Burguera, M. Burguera, C. Rondón, *Anal. Chim. Acta* 438 (2001) 195.
- [8] S. Nielsen, E.H. Hansen, *Anal. Chim. Acta* 343 (1997) 5.
- [9] N.M.M. Coelho, A. Cósme da Silva, C. Moraes da Silva, *Anal. Chim. Acta* 460 (2002) 227.
- [10] R. Bye, W.Z. Lund, *Fresenius' Z. Anal. Chem.* 332 (1988) 242.
- [11] Q. Wang, J. Liang, J. Qiu, B. Huang, *J. Anal. At. Spectrom.* 19 (2004) 715.
- [12] Z. Liu, H. Sun, S. Shen, L. Li, H. Shi, *Anal. Chim. Acta* 550 (2005) 151.
- [13] M. Thompson, B. Pahlavanpour, S.J. Walton, G.F. Kirkbright, *Analyst* 103 (1978) 705.
- [14] Z. Li, Y. Guo, *Talanta* 65 (2005) 1318.

- [15] I.B. Karadjova, L. Lampugnani, M. Onor, A. D'Ulivo, D.L. Tsalev, *Spectrochim. Acta Part B* 60 (2005) 816.
- [16] M.G.C. Fernandez, M.A. Palacios, C. Camara, *Anal. Chim. Acta* 283 (1993) 386.
- [17] J. Stripeikis, P. Costa, M. Tudino, O. Troccoli, *Anal. Chim. Acta* 408 (2000) 191.
- [18] J.L. Burguera, P. Carrero, M. Burguera, C. Rondon, M.R. Brunetto, M. Gallignani, *Spectrochim. Acta Part B* 51 (1996) 1837.
- [19] M. Gallignani, M. Valero, M.R. Brunetto, J.L. Burguera, M. Burguera, Y. Petit de Peña, *Talanta* 52 (2000) 1015.
- [20] J. Qiu, Q. Wang, Y. Ma, L. Yang, B. Huang, *Spectrochim. Acta Part B* 61 (2006) 803.
- [21] D.L. Tsalev, M. Sperling, B. Welz, *Talanta* 51 (2000) 1059.
- [22] K.J. Lamble, S.J. Hill, *Anal. Chim. Acta* 334 (1996) 261.
- [23] A.A. Menegário, M.F. Giné, *Spectrochim. Acta Part B* 55 (2000) 355.
- [24] J. Dedina, D.L. Tsalev, *Hydride Generation Atomic Absorption Spectrometry*, Wiley, Chichester, 1995, p. 314.
- [25] H. Uggerud, W. Lund, *J. Anal. At. Spectrom.* 10 (1995) 405.
- [26] A. D'Ulivo, L. Gianfranceschi, L. Lampugnani, R. Zamboni, *Spectrochim. Acta Part B* 57 (2002) 2081.
- [27] Z. Liu, H. Sun, S. Shen, L. Li, H. Shi, *Anal. Chim. Acta* 550 (2005) 151.
- [28] K. Marcucci, R. Zamboni, A. D'Ulivo, *Spectrochim. Acta Part B* 56 (2001) 393.
- [29] T. Wickstrøm, W. Lund, R. Bye, *J. Anal. At. Spectrom.* 10 (1995) 803.
- [30] T. Wickstrøm, W. Lund, R. Bye, *Analyst* 120 (1995) 2695.
- [31] S.L.C. Ferreira, V.A. Lemos, R.E. Santelli, E. Ganzarolli, A.J. Curtius, *Microchem. J.* 68 (2001) 41.
- [32] E.N. Fernandes, B.F. Reis, *Anal. Chim. Acta* 557 (2006) 380.
- [33] A.F. Lavorante, C.K. Pires, B.F. Reis, *J. Pharm. Biomed. Anal.* 42 (2006) 423.
- [34] S.M. Oliveira, T.I.M.S. Lopes, I.V. Tóth, A.O.S.S. Rangel, *Anal. Chim. Acta* 600 (2007) 29.
- [35] J. Agterdenbos, J.T. van Elteren, D. Bax, J.P. Ter Heege, *Spectrochim. Acta Part B* 41 (1986) 303.
- [36] A. D'Ulivo, K. Marcucci, E. Bramanti, L. Lampugnani, R. Zamboni, *Spectrochim. Acta Part B* 55 (2000) 1325.
- [37] A.R. Kumar, P. Riyazuddin, *Anal. Sci.* 21 (2005) 1401.
- [38] I.D. Brindle, X. Le, *Anal. Chim. Acta* 229 (1990) 239.



# Sensitive determination of biogenic amines by capillary electrophoresis with a new fluorogenic reagent 3-(4-fluorobenzoyl)-2-quinolinecarboxaldehyde

Niu Zhang, Hong Wang, Zi-Xing Zhang, Ying-Hua Deng, Hua-Shan Zhang\*

Department of Chemistry, Wuhan University, Wuhan 430075, PR China

## ARTICLE INFO

### Article history:

Received 29 January 2008

Received in revised form 2 April 2008

Accepted 12 April 2008

Available online 20 April 2008

### Keywords:

Biogenic amines

Derivatization

Food samples

3-(4-Fluorobenzoyl)-2-quinolinecarboxaldehyde (FBQCA)

Micellar electrokinetic capillary chromatography laser-induced fluorescence

## ABSTRACT

An effective approach was proposed to the derivatization of seven biogenic amines using 3-(4-fluorobenzoyl)-2-quinolinecarboxaldehyde (FBQCA) as a fluorogenic reagent. The sensitive determinations of these derivatives were achieved by micellar electrokinetic capillary chromatography (MEKC) with laser-induced fluorescence (LIF) detection. The derivatization and electrophoretic conditions have been optimized. A running buffer was composed of mixtures of 25 mM pH 9.5 boric acid, 25 mM SDS, and 27% ACN. At 25 °C and 22.5 kV, the baseline separation of the derivatives was accomplished in 13 min. The detection limit ( $S/N=3$ ) was found as low as 0.4 nM. The proposed method was validated by the linearity of two orders magnitude and correlation coefficient in the range 0.9969–0.9998. Also, the procedure was successfully applied to the determination of biogenic amines in soy sauce, fish and wine samples.

© 2008 Published by Elsevier B.V.

## 1. Introduction

The ubiquitous biogenic amines, classified as organic bases with small molecular weight [1], are closely related to various living organisms, cells, foods, and beverages. Especially, the biologically active amines have received considerable interest owing to their significant functions both in biological systems such as nerve and metabolism, and in cell processes including cell proliferation and differentiation, as well as synthesizing nucleic acids and proteins, stabilizing membrane and signal transduction [2–10]. Regardless of the importance of intracellular biogenic amines, it should be envisaged that biological activity may convert to toxicity upon consumption of large amounts of these amines. For example, some symptoms involving headaches, nausea, hypo- or hypertension, and cardiac palpitations, have been reported as a result of excessive uptake of biogenic amines [11]. Furthermore, it is evidenced that high level polyamine causes some cancer diseases [12–16]. Thus, simultaneous determination of the important biogenic amines is increasingly urgent for clinical and food analysis.

Of methods developed for the determination of biogenic amines, such as GC [17,18], HPLC [19–23] and CE [24–29], CE is the most

important one affording high resolution, strong separation efficiency, low sample volume, and short analysis time [30]. In many cases, however, poor response of analytes to the employed detection system prevents somewhat the wide application of CE. So a good way to overcome this drawback is to use the covalent labeling with chromophore or fluorophore, leading to great improvement in detection sensitivity and detection limit by use of UV–vis and LIF detection with CE. Relative to the UV–vis absorption, the laser-induced fluorescence (LIF) detection provides lower detection limits of at least 2–3 orders of magnitude [31,32], and therefore, CE-LIF is expected as the most used analysis method for detecting the low-concentration biogenic amines.

To date, some derivatizing reagents have become available, such as fluorescein isothiocyanate (FITC) [33,34], 6-aminoquinoyl-*N*-hydroxysuccinimidyl carbamate (AccQ) [25], 6-oxy-(*N*-succinimidyl acetate)-9-(2'-methoxy-carbonyl)fluorescein (SAMF) [27], 5-(4,6-dichloro-*s*-triazin-2-ylamino) fluorescein (DTAF) [35,36], *O*-phthalaldehyde (OPA) [28,30], naphthalene-2,3-dicarboxaldehyde (NDA) [37,38], 3-(2-furoyl)-quinoline-2-carboxaldehyde (FQCA) [26], and so on. However, DTAF and its conjugated forms have low stability upon exposure in water for a long period of time [39]. Normally, more than 5 h are needed for the derivatization between FITC and amines, so it is a time consuming process. In addition, unexpected hydrolysis of some reagents often occurs in aqueous environment, which does not afford a clean background.

\* Corresponding author. Tel.: +86 27 87218924; fax: +86 27 68754067.  
E-mail address: [hshzhang@whu.edu.cn](mailto:hshzhang@whu.edu.cn) (H.-S. Zhang).

For these competition reactions, use of high concentration labeling reagent is required, typically at mM level. More importantly, a preferable methodology for the labeling is to introduce fluorogenic reagents since the detected fluorescence of solutions may be swamped by the background signal from the excess fluorescent reagents or hydrolysis products. Although the fluorogenic reagents 4-Fluor-7-nitro-1,2,3-benzaxadiazole (NBD-F), OPA, NDA and FQCA are known so far for amine labeling, only the FQCA derivatives show the excitation wavelength which closely matches the 488 nm line of the argon ion laser [26].

A new fluorogenic reagent, 3-(4-fluorobenzoyl)-2-quinolinecarboxaldehyde (FBQCA) with little background and satisfied selectivity, was synthesized in our laboratory. The excitation maximum of the formed fluorescent derivatives was centered at 480 nm, corresponding to the commercial argon ion laser. Previously, we have used FBQCA for the determination of aliphatic amines with HPLC [40]. Herein, the feasibility of FBQCA as a derivatizing reagent in CE has been further evaluated by the simultaneous detection of biogenic amines in different food samples. The derivatization and separation conditions were optimized carefully, followed by the baseline separation of seven biogenic amine derivatives within 13 min. The current investigation indicates that this simple, sensitive and background-free method applies to determination of biogenic amines with CE-LIF.

## 2. Experimental

### 2.1. Chemicals and reagents

The biogenic amine standards (Histamine (His), tyramine (Tyr), 2-phenylethylamine (Phe), putrescine (Put), cadaverine (Cad), spermine (Spm), spermidine (Spd)), potassium cyanide (KCN) and sodium dodecyl sulfate (SDS) were purchased from Sigma (St. Louis, MO, USA). Stock solutions of each amine were prepared in water to make 0.1 M and stored at 4 °C. FBQCA was synthesized in our laboratory and a 10 mM stock solution was prepared in methanol. 0.2 M KCN stock solution was prepared with water and stored at 4 °C. A working cyanide solution was obtained from an aliquot of the stock solution diluted to a final concentration of 10 mM by borate buffer.

Borate buffer was obtained by mixing 0.2 M H<sub>3</sub>BO<sub>3</sub>–KCl solution with 0.2 M Na<sub>2</sub>CO<sub>3</sub> solution to the required pH value. The running buffer was prepared by boric acid, SDS, and acetonitrile into deionized water and pH of the solution was adjusted by using 1 M NaOH before diluting to final volume.

All other reagents were of analytical grade and obtained from Shanghai Chemical (Shanghai, China). All aqueous solutions were prepared with deionized water purified by a Millipore-Q system (Millipore, Bedford, MA, USA). Soy sauce, fish, and red wine samples were purchased from local supermarket.

### 2.2. Apparatus

CE experiments were performed on a Beckman P/ACE MDQ capillary electrophoresis system (Beckman, Fullerton, CA, USA) with an LIF detector. An argon ion laser (3 mW) was used as excitation source (488 nm) and the electropherograms were recorded at 520 nm emission wavelength. All separations were performed in an uncoated fused-silica capillary (Yongnian, Optic Fiber, Hebei, PR China) 60.2 cm in length (effective length of 50 cm) and 75 μm I.D.

### 2.3. Electrophoretic procedure

Prior to use, each new capillary was conditioned by rinsing with water, 1 M HCl, H<sub>2</sub>O, 1 M NaOH, and H<sub>2</sub>O for 20 min in order. The instrument was programmed to rinse the capillary with 0.1 M NaOH

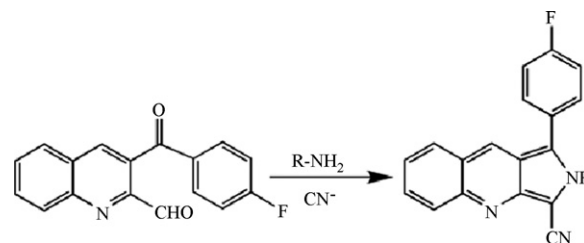


Fig. 1. The reaction of FBQCA with biogenic amines.

for 5 min, H<sub>2</sub>O for 5 min, and then running buffer for 10 min daily. Between runs, the capillary was swilled out with 0.1 M NaOH followed H<sub>2</sub>O and running buffer for 3 min each. And all the rinse programs above were performed at 25 °C. Sample solutions were introduced into the capillary tubes from the anodic side by pressure of 0.5 psi for 5 s and the injection volume was approximately 25 nL. Analyses were performed at 25 °C using a liquid coolant in a sealed cartridge with a running voltage of 22.5 kV and the current obtained was 29.5 μA. For biogenic amines separation, the running buffer consisted of 25 mM SDS, 25 mM boric acid (modified with 1 M NaOH to pH 9.5), and 27% (v/v) ACN. Before use, the running buffer was filtered using a 0.22 μm nylon membrane filter and degassed in an ultrasonic for 5 min.

### 2.4. Derivatization procedure

The structural formula of FBQCA and its reaction with biogenic amines is shown in Fig. 1. Derivatization procedure was performed according to the literature [40]. With some modification, 20 μL of 10 mM FBQCA, which corresponds to at least 10-fold molar excess for the total biogenic amines, was added into a 1-mL vial containing an appropriate volume of mixed biogenic amines solution. And then, 30 μL of working cyanide solution was added. In order to ensure dissolution of biogenic amine derivatives and homogeneous derivatization reaction process, 30 μL methanol was added. After that, the vial was capped and vortexed. The mixture was incubated at 50 °C for 20 min in the dark. Before analysis, the reaction mixture was diluted to the mark with the running buffer in order to maintain a background electrolyte compatible with that in the separation capillary. A blank solution of the same volume was prepared using the same protocol.

### 2.5. Sample preparation

Sample preparation was performed as described by Lapa-Guimarães et al. [41]. Five grams of fish fillet was homogenized in 10 mL of 6% trichloroacetic acid (TCA). After centrifugation, the supernatants were filtered with filter paper. The procedure was repeated a second time and the solutions were then collected and diluted to 50 mL with water.

As the similar method reported previously [34], soy sauce samples were treated via liquid extraction procedure. Simply to say, suitable amount of soy sauce samples were filtered through a filter paper. A 3 mL sample was diluted with Millipore water to 6 mL. Then 3 mL of this diluted sample was transferred into a capped test tube where 1 mL of 5 M NaOH was added. The solution was saturated by the addition of anhydrous Na<sub>2</sub>CO<sub>3</sub>, and extracted twice with 3 mL of water-saturated *n*-butanol. Two portions of extraction solution were combined together, 3 mL of which was transferred to another test tube. After the solution was then extract three times with 2 mL of 0.1 M HCl, 3 mL of the acid phase was filtered through a 0.45 μm membrane and dried under vacuum at room temperature. The dried residue was dissolved in borate buffer. To ensure the



concentration of analyte in the calibration range, the above small aliquot of fish and soy sauce were neutralized with 1 M sodium hydroxide, and subsequently diluted with water.

Red wine samples were diluted in water and filtered through a 0.45  $\mu\text{m}$  membrane. These procedures were performed just prior to use in the experiment, then 20  $\mu\text{L}$  of the solution obtained was taken for the derivatization with FBQCA under the same conditions as used for the standards.

### 3. Results and discussion

#### 3.1. Optimization of separation conditions

The optimized conditions were carefully studied to accomplish the best separation of biogenic amine derivatives labeled with FBQCA. These derivatives have poor solubility in water and bear relatively few charges, so they are very difficult to separate in capillary zone electrophoresis mode. Owing to the suitability of micellar electrokinetic capillary chromatography (MEKC) for the uncharged analytes [42], this approach has been adopted in our experiment. Normally, SDS is the most popular surfactant used in MEKC; but here the use of only SDS and borate buffer did not lead to the desired separation of seven biogenic amine derivatives. In MEKC, addition of organic modifiers has been demonstrated to improve the resolution of highly hydrophobic compounds, because they are able to increase hydrophobicity of the mobile phase and change the distribution of analytes between micellar pseudophase and mobile phase. Herein, a number of different CE parameters were optimized to decrease the migration time and increase the resolution and efficiency.

##### 3.1.1. Choice of capillary size

Generally, what size of the capillary should be chosen depends upon the separation mode and objects. First, the Beckman P/ACE MDQ capillary cartridge assembly is provided with two different length (corresponding total capillary length 60.2 and 57 cm) coolant tubing by manufacturer. Capillary length is determined by the length of coolant tubing from the Cartridge Tubing Kit. In order to achieve better separation efficiency, 60.2 cm in length was used. Besides, the derivatives from the reaction of FBQCA and biogenic amines belong to free solution and own relatively few charges. Usually, 50 and 75  $\mu\text{m}$  I.D. capillary columns are mostly used for free solutions electrophoresis. Although smaller I.D. capillaries offer more heat dissipation, the shorter pathlength is detrimental to LIF detection sensitivity. In this study, the longer pathlength, 75  $\mu\text{m}$  I.D. capillary was selected to lower detection limits.

##### 3.1.2. Optimization of acetonitrile concentration

Highly hydrophobic analytes are most likely to be separated using the small amount of organic modifier [43]. Various concentrations of organic modifiers (methanol and ACN) were investigated. The result showed that both methanol and acetonitrile could improve the separation. As is shown in Fig. 2a, when the concentration of methanol reached 35% (v/v), the analysis time was tedious. In comparison, however, the addition of acetonitrile could provide better resolution for seven derivatives (Fig. 2b). As illustrated in Fig. 3a, the desired separations were achieved with 27% ACN, which have good resolution as well as short analysis time.

##### 3.1.3. Optimization of the SDS concentration

The concentration of SDS also played a critical role in the separation. To evaluate the influence of SDS concentration on the resolution, different concentrations were used (Fig. 3b) in the presence of 25 mM boric acid and 27% ACN in buffer (pH 9.5). When the concentration of SDS was lower than 20 mM, two pairs (Put/Cad

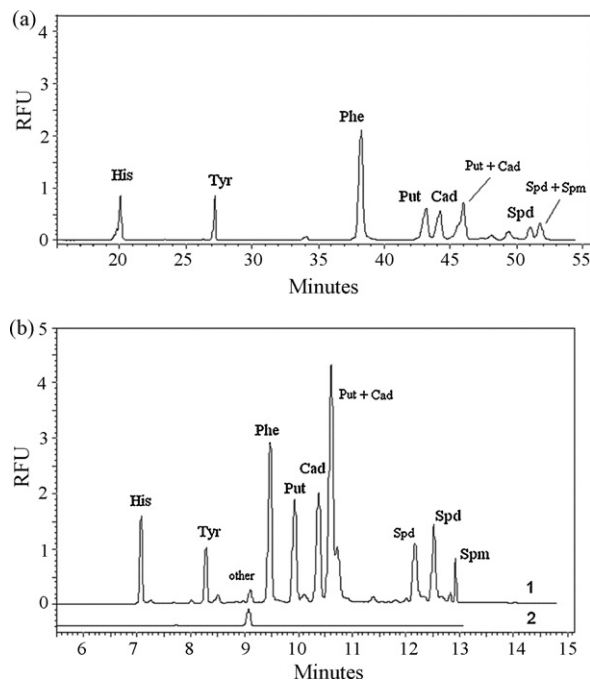


**Fig. 2.** Optimization of the separation of FBQCA labeled seven biogenic amines with different running buffer. The origin of each peak is identified on the figure. The peaks identified in bold were used for quantification. (a) Running buffer: 35% (v/v) methanol, 25 mM boric acid, 25 mM SDS, pH 9.5; separation voltage: 22.5 kV; capillary temperature: 25 °C; injection 5 s at 34.5 mbar. (b) 27% ACN, 25 mM boric acid, 25 mM SDS, pH 9.5; curve 1 for real standard amines and curve 2 for the blank; other conditions as in (a).

and the double of Cad) could not be baseline separated. Also, Spd and Spm showed broad peaks. Increasing SDS concentration caused longer separation time. This effect contributed to the higher Joule heating that is due to the increased conductivity of the buffer [44]. When SDS concentration was more than 35 mM, all peaks were shifted to longer migration time, and even were lost in resolution. The best SDS concentration for the separation of biogenic amines was 25 mM.

##### 3.1.4. Effect of buffer concentration, pH and running voltage

Effect of boric acid concentration on the separation was examined in the range of 10–40 mM. When boric acid concentration was lower than 15 mM, the double derivative peaks of Cad could not be resolved completely. When the buffer concentration increased, the resolution of derivatives was improved. However, higher concentrations resulted in longer migration time. Then, 25 mM concentration of boric acid was chosen as the optimized concentration.

Another factor affecting the resolution and selectivity is the pH of running buffer. The results showed that very little changes of migration time take place in the range of pH 9.3–9.7. At pH 9.0, FBQCA-Spd and FBQCA-Spm showed broad peaks. When the pH of buffer was above 9.7, a longer migration time was consumed. Therefore, pH 9.5 was adopted for further studies.

The running voltage was investigated between 20 and 27 kV. At 25 kV or higher, the whole analysis time was less than 11 min, but Put and the former peak of Cad overlapped partly. It was known that higher potentials favored faster migration, while the separation resolution was lowered. As a result, a voltage of 22.5 kV was preferred to obtain the full resolution and short analysis time. A typical electropherogram of a standard solution was shown in Fig. 2b. The baseline separation of the derivatives of seven biogenic amines was completed in 13 min.

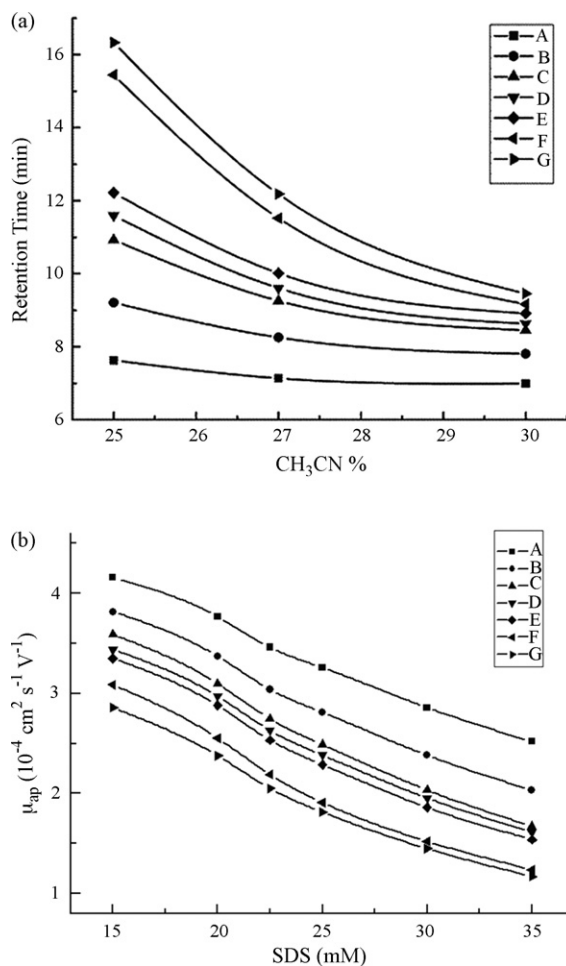


**Fig. 3.** Effect of (a) different ACN content; (b) concentration of SDS on the migration time and mobility of amine derivatives, respectively. (A) His; (B) Tyr; (C) Phe; (D) Cad; (E) Put; (F) Spd; (G) Spm.

### 3.2. Optimization of derivatization conditions

FBQCA is non-fluorescent itself, but it reacts with amines to form highly fluorescent isoindole derivatives in the presence of cyanide. Curve in Fig. 2b presents the electropherogram of a reagent blank. The blank generated one peak with a migration time of 9.1 min. Excess FBQCA did not interfere with the determination of analytes due to weak self-fluorescence.

Generally, reagent concentration is a paramount factor for the derivatization yield. Excess derivatization reagents were used for the quantitative analysis of biogenic amines. The biogenic polyamines, especially Cad, have double derivative peaks. For this issue, different amounts of FBQCA were studied with a fixed value of Cad. Fig. 4 shows the variation of Cad peak intensities as the FBQCA-to-Cad molar ratio was changed from 5:1 to 75:1. The peak height increased to a constant value with increasing reagent concentration. Despite the additionally excessive reagent, double peaks were still observed, which was similar to other polyamines [27,29,36,45]. This phenomenon could be partly attributed to the steric factor hindering their complete substitution or altering the reactivity of the amines involved. It was clear that both derivative peaks could be used for quantification, but here we used the former derivative to avoid interference from other derivative peaks. For Put and Spd, although small peaks that correspond to di- or mono- FBQCA-amine occurred, there was a dominant peak. Spm had a weak derivative peak also. Of many conditions responsible for various derivatiza-

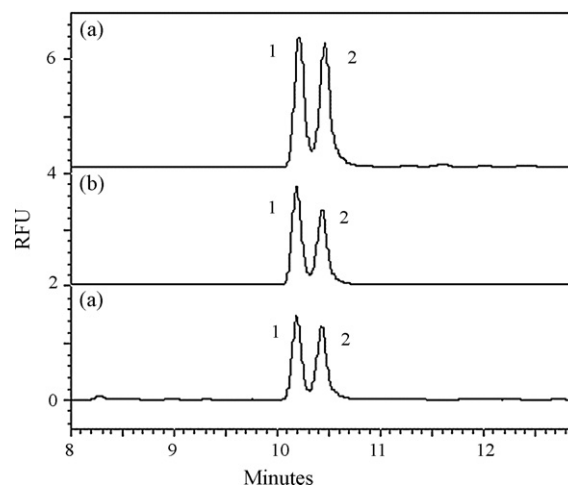


**Fig. 4.** Electropherograms of the different molar ratios of FBQCA/Cad. Peaks 1 and 2 are derivative peaks of Cad. FBQCA/Cad molar ratio: (a) 5:1; (b) 25:1; (c) 75:1.

tion phenomena, the key factor is the steric hindrance and reaction activity of FBQCA bearing different amino groups.

The effect of FBQCA concentration was tested in the range from  $2 \times 10^{-5}$  to  $5 \times 10^{-4}$  M. When the reagent concentration was lower than  $1 \times 10^{-4}$  M, the major derivative peaks of polyamines did not produce. CE-LIF analysis showed that the peak areas of derivatives were maximum and stable when the concentration of Cl-BQCA was  $2 \times 10^{-4}$  M. With the increase of reagent concentration, the peak areas did not obviously increase. Then,  $2 \times 10^{-4}$  M was used in the following experiments.

Furthermore, the influence of KCN concentration on the derivatization was investigated from  $2 \times 10^{-5}$  to  $6 \times 10^{-4}$  M. When KCN concentration was  $1 \times 10^{-4}$  M or lower, major derivative peaks disappeared. When it was above  $3 \times 10^{-4}$  M, the fluorescence intensity had no obvious change. Accordingly, a  $3 \times 10^{-4}$  M concentration of KCN was chosen for further experiment.

The labeling reaction must be carried out in weak alkaline solutions. Amino groups of the biogenic amines would undergo deprotonation in alkaline medium, and they are prone to the reaction with CN<sup>-</sup> ion. Effect of the pH value of borate buffer on the fluorescence intensity was examined in the range of pH 8.8–10.0. It was found that peak areas of the derivatives reached the largest at pH 9.6, which was chosen as the optimal alkalinity for derivatization.

Reaction temperature also significantly affects the derivatization yield. The derivatization reactions of FBQCA with amino compounds need heating. In this paper, the effect of different temperatures on the peak areas was performed by changing the temperature from 30 to 70 °C (Fig. 5). It was found that the largest peak area appeared at 50 °C. Especially for Spd and Spm, temperature higher than 60 °C led to a worse yield. This was in part ascribed to the instability of biogenic amines at high temperature. In this experiment, 50 °C was selected. Additionally, the study of reaction time showed that peak area reached the maximum in 20 min that was selected as the optimal time for further experiments.

### 3.3. Validation of the method

Calibration curves were constructed by derivatizing amine standards at different concentration under the selected derivatization, separation, and detection conditions. Good linearity has been obtained by plotting peak area versus analyte concentration, with correlation coefficients larger than 0.997. The detection limits (LOD)

**Table 1**  
Characteristic parameters of the calibration graphs and analytical figures of merit of the determination of FBQCA derivatives

Amine	$t_M$ (min)	Linear range ( $\mu\text{M}$ )	Regression equation <sup>a</sup>	$r^2$	LOD (nM) <sup>b</sup>
His	7.06 ± 0.02	0.01–2	$y = 3.73 \times 10^5 x - 3412$	0.9989	1.5
Tyr	8.21 ± 0.03	0.01–2	$y = 2.83 \times 10^5 x + 2663$	0.9988	1.2
2-Phe	9.40 ± 0.04	0.005–1	$y = 1.70 \times 10^6 x + 10306$	0.9998	0.4
Put	9.81 ± 0.05	0.01–2	$y = 7.54 \times 10^5 x - 6164$	0.9994	1.5
Cad	10.24 ± 0.05	0.01–2	$y = 4.80 \times 10^5 x + 10944$	0.9980	1.4
Spd	12.21 ± 0.10	0.01–2	$y = 5.85 \times 10^5 x - 1430$	0.9996	1.4
Spm	12.92 ± 0.15	0.05–10	$y = 3.96 \times 10^4 x - 371$	0.9969	12

<sup>a</sup>  $x$ , concentration of amine ( $\mu\text{M}$ );  $y$ , peak area of amine derivatives in electropherogram. Number of data point for calibration curves is 7 and three repetition per point.

<sup>b</sup>  $S/N=3$ .

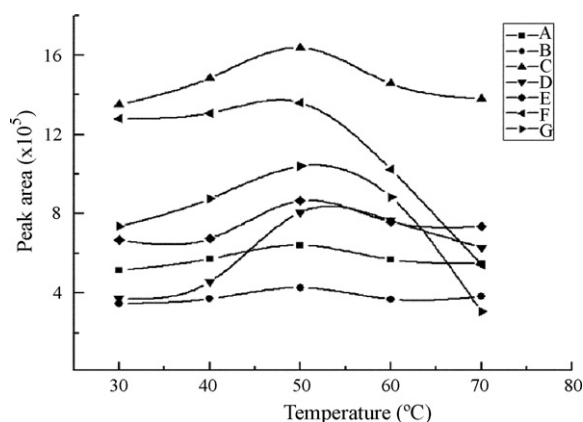


**Fig. 5.** Effect of reaction temperature on peak area of derivatized biogenic amines. Meanings for the inserted text are identical to those illustrated in Fig. 3. Other conditions as described in Fig. 2b.

shown in Table 1 were defined as the concentration ranging from 0.4 nM for Phe to 10 nM for Spm ( $S/N=3$ ).

The analytical reproducibility of the present method was evaluated in terms of relative standard deviations (%R.S.D.) of the migration time and peak areas. Three concentration levels of amines were tested. The intra-day precisions of the relative migration time were below 2.7% and the inter-day precisions were below 4.0%. They both were calculated as R.S.D. for five measurements. The intra-day and inter-day precisions of the relative peak areas were calculated in the same way, showing values lower than 4.8 and 5.9%, respectively. The accuracy of the proposed method was also evaluated. As shown in Table 2, the concentrations calculated were close to the real ones.

Comparison of the present method with other derivatization-based CE methods for the determination of biogenic amines is summarized in Table 3. The MEKC-LIF method shows highly sensitive by using FBQCA due to very weak self-fluorescence, which offers a non-fluorescent background. Besides, the FBQCA derivatives display an absorption maximum closely matching a commercial argon ion laser line (488 nm), leading to increased sensitivity with a relatively inexpensive detection system. In contrast,

**Table 2**  
Precision and accuracy of the method expressed for the determination of FBQCA-derivatized biogenic amines at three levels

Amine	Concentration evaluated (nM)	Concentration detected <sup>a</sup> (nM)	Precision (R.S.D.%) <sup>b</sup>			
			Inter-day ( $n=5$ )		Inter-day ( $n=5$ )	
			MT	PA	MT	PA
His	50	53.4	0.9	4.8	1.5	5.9
	100	94.0	0.9	3.2	0.7	3.2
	500	502	0.3	3.1	0.3	3.5
Tyr	50	49	1.4	4.0	1.7	4.4
	100	97	1.2	2.9	1.1	2.1
	500	506	0.2	2.3	0.7	2.4
Phe	25	25.8	1.8	3.7	2.6	4.4
	50	56	1.2	2.3	2.0	3.1
	250	240	0.2	2.7	0.9	4.2
Put	50	55.8	1.5	2.4	2.8	2.4
	100	99.7	1.6	1.5	1.1	3.9
	500	490	0.3	3.0	1.0	2.6
Cad	50	47.3	1.6	3.6	3.2	2.4
	100	95	1.7	1.4	1.8	2.3
	500	567	0.4	2.7	0.9	3.3
Spd	50	47	2.5	4.2	3.7	3.8
	100	88	1.4	2.4	1.5	1.5
	500	504	0.4	2.7	1.2	4.0
Spm	250	263	2.7	4.5	4.0	4.5
	500	477	2.0	2.2	2.1	3.7
	2500	2289	1.3	3.0	2.1	2.6

<sup>a</sup> Average of four determinations.

<sup>b</sup> MT, migration time; PA, peak area. Intra-day precisions were calculated by injecting of the standard solution over a day. Inter-day precisions were accessed by injecting the standard solution for continuous 5 days.

**Table 3**  
Experimental presentation of various derivatizing reagents for biogenic amines derivatization used in CE

Reagents	CE mode	Optical properties	Reaction conditions	Analytes	Separation time (min)	LODs	Reference
AccQ	MEKC-LIF	Ex: 254 nm, Em: 395 nm	Borate buffer, 55 °C, 10 min	Cad, His, Put, Spd, Spm, Tryp, Tyr	25	1–40 μM	[25]
FITC	MEKC-LIF	Ex: 488 nm, Em: 516 nm	20 mM borate buffer, pH 10.0, r.t. 5–12 h	1,6-Diaminohexane, Phe, Cad, His, Put, Spd, Spm, Tryp, Tyr	20	0.72–35 nM	[46]
FITC	MEKC-FL	Ex: 488 nm, Em: 519 nm	20 mM borate buffer, pH 10.0, r.t. 5–12 h	His, Tyr, Phe, Tryp, Put, Cad, Spd, Spm	15	~10 nM	[34]
NBD-F	CZE-FL	Ex: 400–490 nm, Em: 515 nm	5 mM borate buffer, pH 7.2, 65 °C, 15 min	Diaminopropane, diaminohexane, Cad, His, Put, Spd, Spm	3	21–51 nM	[29]
DTAF	MEKC-LIF CZE-LIF	Ex: 488 nm, Em: 520 nm	0.5 M carbonate buffer, pH 9.5, 35–40 °C, 1 h	Cad, Put, Spm	20	120–410 nM	[36]
NDA	CZE-FL	Ex: 400–490 nm, Em: 515 nm	20 mM borate buffer, pH 9.1, r.t. 15 min	Histidine, Cad, His, Put	3	3.8–5.5 nM	[37]
FQ	MEKC-LIF	Ex: 488 nM, Em: 560 nM	40 °C, 40 min	Phe, Cad, His Put, Spd, Spm, Tryp, Tyr	28	0.5–10 nM	[26]
OPA	MEKC-FL	Ex: 340 nM, Em: 450 nM	20 mM phosphate-borate buffer, pH 10.0	Cad, His, Spd, Tyr	30	1.0–5 μM	[47]
OPA	CEC-UV	Abs: 340 nM	10 mM borate buffer, pH 10.0, r.t. 5 min	5-HT, Cad, His, Put, Tyr	15	50–100 μM	[48]
OPA	MEKC-LIF	Ex: 350 nM, Em: 450 nM	100 mM MBCD, 1 mM EDTA, pH 10.7, 5 °C	Phe, Cad, His, Put, Spd, Spm, Tryp, Tyr	25	0.25 μM	[28]
FBQCA	MEKC-LIF	Ex: 488 nM, Em: 520 nM	Borate buffer, PH 9.6, 50 °C, 20 min	His, Tyr, Phe, Put, Cad, Spd, Spm	13	0.4–12 nM	This work

the maximum excitation of AccQ derivatives at shorter wavelengths makes the reagent unsuitable for use in the analysis of biological samples (many species present in biological samples have excitation maxima in the ultraviolet region), which may not afford higher sensitivity. The detection limits of most reagents were higher than FBQCA, except FQCA; however, it has a longer derivatization and separation time. Moreover, the current method has a shorter separation time relative to others. For these overall properties (reaction conditions, separation time, and detection limits), such proposed method provides more advantages for determination of low concentration of biogenic amines.

#### 3.4. Detection of biogenic amines in samples

The accumulation of biogenic amines in fish samples over time at different storage temperatures was detected using our proposed method. Trace of Fig. 6 shows the electropherograms obtained from live fish and dead fish that was allowed to age for 2 days at 15 °C. Identification was performed according to standard addition method by spiking with standard amine solutions and matching the migration time (Fig. 6a). Each sample was analyzed five reduplicate times. Amine concentrations of the samples are listed in Table 4. With the exception of Spd, their levels progressively increased during storage, especially for Put and Cad. Putrescine and cadaverine are notorious in food poisoning because they not only potentiate the toxicity of histamine [49–53] but also react with nitrites to form

carcinogenic nitrosamines [54]. These diamines give off unpleasant decaying odors at very low concentration. Therefore, the concentration is more valuable as the spoilage indicator for these two amines other than histamine [55]. As expected, the levels of these fish spoilage markers increased with storage time as well as stor-

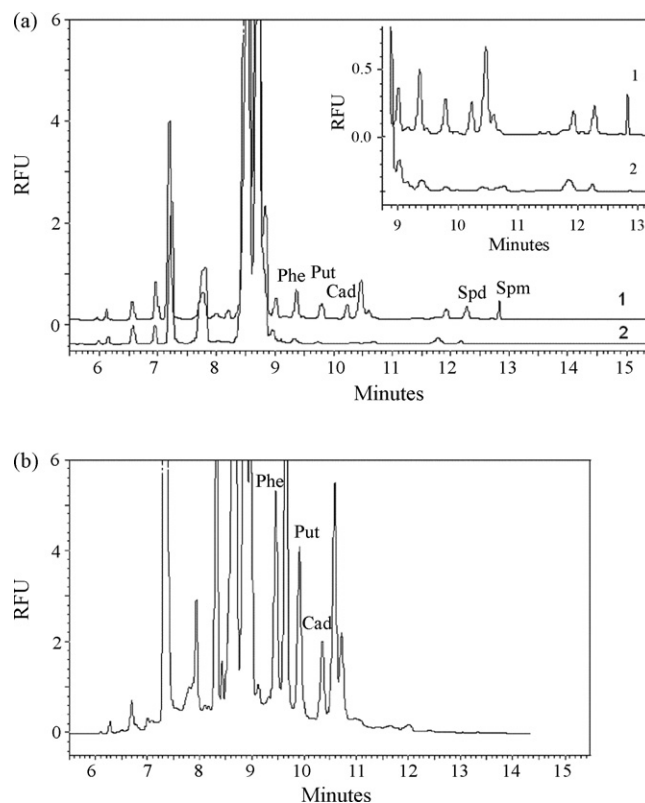


**Fig. 6.** Electropherograms obtained from fish samples: (a) curve 1 for live fish spiked with standard amines, and curve 2 for live fish; (b) dead fish at 15 °C for 2 days. Other conditions as described in Fig. 2b.

**Table 4**  
Biogenic amine content of samples analyzed ( $n=5$ )

Analyte	<sup>a</sup> Fish ( $\mu\text{g g}^{-1}$ )	<sup>b</sup> Fish ( $\mu\text{g g}^{-1}$ )	Soy sauce ( $\mu\text{g mL}^{-1}$ )	Red wine ( $\mu\text{g mL}^{-1}$ )
Phe	0.425	18.4	3.58	0.363
Put	0.801	43.6	2.87	1.06
Cad	0.812	47.6	0.710	0.172
Spd	0.719	0.812	0.967	nd
Spm	nd	nd	nd	nd

<sup>a</sup> Live fish. His and Tyr were not detected. nd: not detectable.

<sup>b</sup> Fish dead for 2 days at 15 °C.

age temperature. Further store duration would increase the amount undoubtedly [56]. The regulatory action level for most fish is >10 mg histamine/100 g of flesh [57] as indices of spoilage. However, histamine and tyramine in the tested samples could not be identified due to the interfering signals. The reaction between neutral amino acids and FBQCA gave products that migrate at about the same time as the FBQCA-His and Tyr peaks. Other biogenic amines were interference free. Due to this reason, the method is unsuitable for the quantification of the global level of biogenic amines in red wine, but numerous interference peaks largely can be removed from the desired amines by pretreating the samples [58].

The reliability of the proposed method was further evaluated by applying it to soy sauce and red wine. Four amines in soy sauce were identified, which have ever been identified by other methods [46,55]. Three amines in red wine samples were detected and the concentrations reported here are lower than those in other red wines [59]. The results obtained from the analysis of food samples are shown in Table 4.

#### 4. Conclusion

The proposed MEKC-LIF method using FBQCA as a fluorescent reagent, has been demonstrated an effective procedure for the simultaneous separation and determination of seven biogenic amines in food samples. The derivatives are highly fluorescent and can be detected in low concentration. Besides the versatility and simplicity, this MEKC-LIF method primarily provides good sensitivity and short separation period (13 min). The detection limits of 0.4 nM are lower than other CE methods. In addition, the present method only offers very weak fluorescence interference from background signals. This investigation indicates that the MEKC-LIF strategy is suitable for the sensitive determination of bioactive amino compounds with small amounts.

#### Acknowledgments

The research presented in this manuscript was supported by the National Natural Science Foundation of China (Nos. 20575047, 30770550 and 20775058, Beijing, China).

#### References

- [1] T. Davidek, J. Davidek (Eds.), *Biogenic Amines in Natural Toxic Compounds of Foods*, CRC Press, Boca Raton, FL, 1995, p. 108.
- [2] M.Y. Khuhawar, G.A. Qureshi, *J. Chromatogr. B* 764 (2001) 385.
- [3] H.M. Wallace, *Eur. J. Clin. Invest.* 30 (2000) 1.
- [4] R.L. Zhang, C.L. Cooper, Y.F. Ma, *Anal. Chem.* 65 (1993) 704.
- [5] T.A. Smith, *Annu. Rev. Plant Physiol. Plant Mol. Biol.* 36 (1985) 117.
- [6] F.A.J. Muskiet, B. Dorhout, G.A. van den Berg, J. Hessels, *J. Chromatogr. B* 667 (1995) 189.
- [7] V. Milovic, W.F. Caspary, J. Stein, *Digestion* 59 (1998) 60.
- [8] A. Toninello, M. Salvi, B. Mondovi, *Curr. Med. Chem.* 11 (2004) 2349.
- [9] A.A. Ouameur, H.A. Tajmir-Riahi, *J. Biol. Chem.* 279 (2004) 42041.
- [10] Y.H. Qiu, C. Cheng, L. Dai, Y.P. Peng, *J. Neuroimmunol.* 167 (2005) 45.
- [11] S. Bardocz, *Trends Food Sci. Technol.* 6 (1995) 341.
- [12] V. Quemener, Y. Blanchard, L. Chamailard, R. Havouis, B. Cipolla, J.P. Moulinoux, *Anticancer Res.* 14 (1994) 443.
- [13] D.H. Russell, C.C. Levy, S.C. Schimpff, I.A. Hawk, *Cancer Res.* 31 (1971) 1555.
- [14] L.M. Nairn, G.S. Lindsay, P.M. Woster, H.M. Wallace, *J. Cell. Physiol.* 182 (2000) 209.
- [15] E.W. Gerner, F.L. Meyskens, *Nat. Rev. Cancer* 4 (2004) 781.
- [16] S. Heimbecher, Y.C. Lee, S.E. Tabibi, S.H. Yalkowsky, *J. Chromatogr. B* 691 (1997) 173.
- [17] R.L.H. Clements, A. Holt, E.S. Gordon, K.G. Todd, G.B. Baker, *J. Pharmacol. Toxicol. Methods* 50 (2004) 35.
- [18] M.H. Choi, K.R. Kim, B.C. Chung, *J. Chromatogr. A* 897 (2000) 295.
- [19] I. Molnar-Perl, *J. Chromatogr. A* 987 (2003) 291.
- [20] M.C. Vidal-Carou, F. Lahoz-Portoles, S. Bover-Cid, A. Marine-Font, *J. Chromatogr. A* 998 (2003) 235.
- [21] J. Kirschaum, K. Rebscher, H. Brückner, *J. Chromatogr. A* 881 (2000) 517.
- [22] O. Busto, M. Miracle, J. Guasch, F. Borrull, *J. Chromatogr. A* 757 (1997) 311.
- [23] Z. nLoukou, A. Zotou, *J. Chromatogr. A* 996 (2003) 103.
- [24] S. Oguri, *J. Chromatogr. B* 747 (2000) 1.
- [25] A. Kovacs, L. Simon-Sarkadi, K. Ganzler, *J. Chromatogr. A* 836 (1999) 305.
- [26] X. Liu, L.X. Yang, Y.T. Lu, *J. Chromatogr. A* 998 (2003) 213.
- [27] L.W. Cao, H. Wang, M. Ma, H.Sh. Zhang, *Electrophoresis* 27 (2006) 827.
- [28] K.B. Male, J.H.T. Luong, *J. Chromatogr. A* 926 (2001) 309.
- [29] L.Y. Zhang, X.C. Tang, M.X. Sun, *J. Chromatogr. B* 820 (2005) 211.
- [30] J. Lange, K. Thomas, C. Wittmann, *J. Chromatogr. B* 779 (2002) 229.
- [31] K.W. Ro, K. Lim, H. Kim, J.H. Hahn, *Electrophoresis* 23 (2002) 1129.
- [32] B.G. Belenkii, V.E. Kurochkin, R.A. Kozulin, V.M. Zolotarev, *J. Opt. Technol.* 69 (2002) 191.
- [33] N.P. Beard, C.X. Zhang, A.J. DeMello, *Electrophoresis* 24 (2003) 732.
- [34] I. Rodriguez, H.K. Lee, S.F.Y. Li, *J. Chromatogr. A* 745 (1996) 255.
- [35] M. Molina, M. Silva, *Electrophoresis* 23 (2002) 1096.
- [36] M. Molina, M. Silva, *Electrophoresis* 23 (2002) 2333.
- [37] L.Y. Zhang, M.X. Sun, *J. Chromatogr. A* 1040 (2004) 133.
- [38] L.Y. Zhang, Y.M. Liu, Z.L. Wang, J.K. Cheng, *Anal. Chim. Acta* 508 (2004) 141.
- [39] N.P. Beard, J.B. Edell, A.J. deMello, *Electrophoresis* 25 (2004) 2363.
- [40] N. Zhang, Y.Z. Zhao, H.S. Zhang, H. Wang, *J. Sep. Sci.* 31 (2008) 38.
- [41] J. Lapa-Guimarães, J. Pickova, *J. Chromatogr. A* 1045 (2004) 223.
- [42] S. Terabe, *Anal. Chem.* 76 (2004) 240A.
- [43] K.D. Altria, B.J. Clark, M.A. Kelly, *J. High Resolut. Chromatogr.* 22 (1999) 55.
- [44] S. Michaelsen, P. Moller, H. Sorensen, *J. Chromatogr. A* 680 (1994) 299.
- [45] R.E. Paproski, K.I. Roy, C.A. Lucy, *J. Chromatogr. A* 946 (2002) 265.
- [46] I. Rodriguez, H.K. Lee, S.F.Y. Li, *Electrophoresis* 20 (1999) 1862.
- [47] S. Oguri, S. Watanabe, S. Abe, *J. Chromatogr. A* 790 (1997) 177.
- [48] S. Oguri, Y. Yoneya, M. Mizunuma, Y. Fujiki, *Anal. Chem.* 74 (2002) 3463.
- [49] L.F. Bjeldanes, D.E. Schutz, M.M. Morris, *Food Cosmet. Toxicol.* 16 (1978) 157.
- [50] J.L. Parrot, M. Gabe, A. Herrault, *C. R. Soc. Biol. (Paris)* 141 (1947) 486.
- [51] J.L. Parrot, *C. R. Soc. Biol. (Paris)* 142 (1948) 631.
- [52] H.Y.P. Jung, L.F. Bjeldanes, *Food Cosmet. Toxicol.* 17 (1979) 629.
- [53] S.L. Taylor, E.R. Lieber, *Food Cosmet. Toxicol.* 17 (1979) 237.
- [54] A.R. Shalaby, *Food Res. Int.* 29 (1996) 675.
- [55] R. Stute, K. Petridis, H. Steinhart, G. Biernoth, *Eur. Food Res. Technol.* 215 (2002) 101.
- [56] K.B. Male, P. Bouvrette, J.H.T. Luong, B.F. Gibbs, *J. Food Sci.* 61 (1996) 1012.
- [57] I.M. Mackil, L. Pirie, A.H. Ritchie, H. Yamanaka, *Food Chem.* 60 (1997) 291.
- [58] S. Moret, L.S. Conte, *J. Chromatogr. A* 729 (1996) 363.
- [59] N. Garcia-Villar, J. Saurina, S. Hernandez-Cassou, *Electrophoresis* 27 (2006) 474.



## Simultaneous determination of flavonoids in chrysanthemum by capillary zone electrophoresis with running buffer modifiers

Shan Zhang, Shuqing Dong, Langzhu Chi, Pingang He, Qingjiang Wang\*, Yuzhi Fang\*

Department of Chemistry, East China Normal University, Shanghai 200062, China

### ARTICLE INFO

#### Article history:

Received 10 January 2008

Received in revised form 27 March 2008

Accepted 12 April 2008

Available online 20 April 2008

#### Keywords:

Capillary zone electrophoresis

Amperometric detection

Flavonoids

Chrysanthemum

### ABSTRACT

Despite the separation efficiency of capillary electrophoresis (CE) is much higher than other chromatographic methods, it is sometimes difficult to perfectly separate the complex ingredients in biological samples. One possible and simple way to develop the separation effect in CE is to add some modifiers in the running buffer. In this paper, the suitable running buffer modifiers were explored to simultaneously separate and detect six typical flavonoids (apigenin, luteolin, kaempferol, quercetin, (+)-catechin and (–)-epicatechin) which are the main active ingredients in chrysanthemum by capillary zone electrophoresis with amperometric detection (CZE-AD). It was found that when  $\beta$ -cyclodextrin ( $\beta$ -CD) and the mixture of methanol and ethanol were used as running buffer modifiers, a baseline separation of the six analytes could be accomplished in less than 20 min and the detection limits were as low as  $10^{-7}$  or  $10^{-8}$  g ml $^{-1}$ . Other factors affecting the CZE separation, such as working potential, pH value and ionic strength of running buffer, separation voltage and sample injection time were extensively investigated. Under the optimum conditions, a successful practical application on the determination of chrysanthemum samples confirmed the validity and practicability of this method.

© 2008 Elsevier B.V. All rights reserved.

### 1. Introduction

Among so many kinds of separation techniques such as thin-layer chromatography (TLC), high performance liquid chromatography (HPLC), gas chromatography (GC), capillary electrophoresis (CE) and so on, CE is a very economical technique and it has the advantages of remarkable separation efficiency, rapid analysis, and minimum consumption of samples and solvents [1]. In CE, many modes have been developed, such as CZE [2], MEKC [3], CGE [4] and CEC [5], etc. However, CE is sometimes still very difficult to perfectly separate some complicated system. To solve this problem, the addition of modifier is an effective solution.

There are many effective means of achieving the separation of complex systems under the addition of modifiers, such as chiral crown ether, protein, surfactant like bile salt or sodium dodecyl sulfate (SDS), cyclodextrins (CDs) and their derivatives, ionic liquid (IL), etc [6–9]. Among those additives, CDs and their derivatives as modifiers are the most common strategies employed. As for flavonoids, Shi and co-workers have studied the determination of flavonoids in *hippophae rhamnoides* by CZE using dimethyl- $\beta$ -cyclodextrin as modifier [10], and the group of Smith has investigated the enan-

tiomeric assay for the flavonoids medicarpin and vestitone using hydroxypropyl- $\beta$ -cyclodextrin and hydroxypropyl- $\gamma$ -cyclodextrin as additives [11]. The use of organic or aqueous organic medium may also extend the applicability of CZE to a wider range of compounds. It was found that adding more than one kind of selectors to the buffer can improve separation efficiency. However, there were few reports about the detection of flavonoids by simultaneously employing chiral selector and organic solvents as modifiers [11,12], and nonetheless further studying their proper adding locations.

Swinney and Bornhop [13] had a review on detection techniques of CE. The main detection methods coupled with CE, such as UV absorbance detection, fluorescence detection, mass spectroscopy (MS), electrochemiluminescence detection as well as amperometric detection (AD) etc. have been reported [14–17]. Because amperometric detection has the advantage of lower cost, free derivatization, better selectivity as well as higher sensitivity [18], it is a good choice to be coupled with CE.

Chrysanthemum is a herbaceous perennial plant possessing antimicrobial, antibacterial, antifungal, antiviral and anti-inflammatory activities [19,20]. Flavonoids, pentacyclic triterpenes and essential oils are the main bioactive constituents of chrysanthemum [21], among which the flavonoids play an important role in human body. Many researches about the separation of its flavonoid ingredients have been reported. Wang and Huang [22] had compared the determination of flavonoids in chrysanthemum by HPLC

\* Corresponding authors. Tel.: +86 21 6223 3510; fax: +86 21 6223 3508.

E-mail addresses: [qjwang@chem.ecnu.edu.cn](mailto:qjwang@chem.ecnu.edu.cn) (Q. Wang), [yuzhi@online.sh.cn](mailto:yuzhi@online.sh.cn) (Y. Fang).

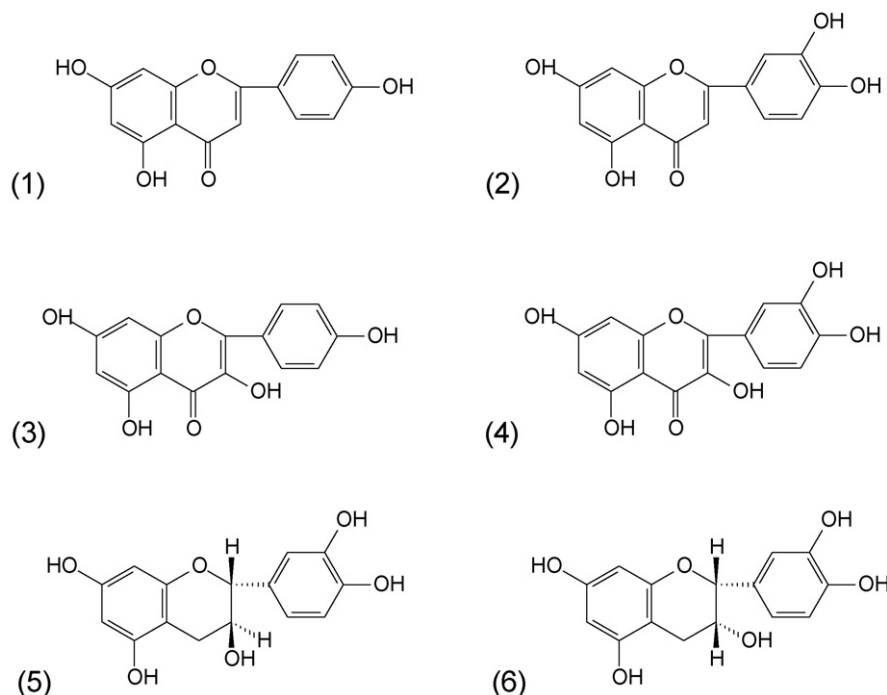


Fig. 1. The molecular structures of (1) apigenin, (2) luteolin, (3) kaempferol, (4) quercetin, (5) (+)-catechin, (6) (–)-epicatechin.

and CE, but the results of that CE do not seem to be very satisfying because of the incomplete separation of luteolin and quercetin, and many other papers included apigenin, luteolin, kaempferol and quercetin [23], or focused on enantioseparation of catechin and epicatechin [24], yet not including all those together because these ingredients are not easy to separate under the common CE conditions.

In this paper, we developed a CZE-AD method with the addition of  $\beta$ -CD and the mixture of methanol and ethanol as modifiers to separate and determine six flavonoids whose structures were shown in Fig. 1, including two flavones (1 and 2), two flavonols (3 and 4) and two flavan-3-ols (5 and 6) in chrysanthemum. These six analytes could achieve good baseline separation employing three kinds of modifiers together in our research and the limits of detection were as low as  $10^{-7}$  or  $10^{-8}$  g ml $^{-1}$ . These results proved that the method was a simple and economical means for the analysis of flavonoids comparing with other methods. This method can be used for real applications in practical samples.

## 2. Experimental

### 2.1. Apparatus

The self-constructed CZE-AD system was as described in our previous work [18]: electrophoresis was driven by a high-voltage power supply ( $\pm 30$  kV, Shanghai Institute of Nuclear Research, Shanghai, China). Separation part of the system, which included a fused silica capillary (70 cm  $\times$  25  $\mu$ m i.d.  $\times$  360  $\mu$ m o.d., Polymicro Technologies, Phoenix, AZ, USA), a three-dimensional manipulator as well as a three-electrode system, were housed in a plexiglas box equipped with an interlock in case of accidental shock. Amperometric detection was performed by a potentiostat (CH-2 amperometric detector, Jiangsu Electrochemical Analytical Instrumental Factory, China), and the electropherograms were recorded by a chart recorder (EB2P00, Shanghai Dahua Instrument Factory,

China). Electrochemical experiments were carried out by a CHI 830b electrochemical analyzer (CHI Instruments, Austin, TX, USA). All solutions were degassed in an ultrasonic cleaner (Branson Soest, NL). The three-electrode system consisted of a carbon disk working electrode (300  $\mu$ m o.d.), a saturated calomel reference electrode (SCE) and a platinum wire counter electrode.

### 2.2. Reagents

Apigenin, luteolin, kaempferol, quercetin, (+)-catechin, and (–)-epicatechin were purchased from Shanghai Institute for Drug Control (Shanghai, China) without further purification. Sodium tetraborate, phosphate,  $\beta$ -cyclodextrin, methanol, ethanol and all the other chemicals were obtained from Shanghai First Reagent Factory (Shanghai, China), and they were all of analytical reagent grade. Chrysanthemum herbs were purchased from a local supermarket.

Accurately weighed six kinds of standard analytes were dissolved by ethanol to a concentration of 1 mg ml $^{-1}$  stock solution for each. Before CZE experiment, they were diluted by BGE with/without additives. All solutions were filtered through 0.22  $\mu$ m polypropylene acrodisc syringe filter (Xinya Purification Instrument Factory, Shanghai, China) and degassed by agitation in ultrasonic bath for 5 min.

### 2.3. Procedure

Prior to CZE experiments, the three-electrode system was fixed in the corresponding holes of the electrochemical cell and the carbon disk working electrode was positioned straightly opposite to the capillary outlet as close as possible by a three-dimension manipulator. Before each run in CZE experiments, the capillary was sequentially rinsed with 0.1 mol l $^{-1}$  hydrochloric acid, doubly distilled water, 0.1 mol l $^{-1}$  sodium hydroxide, 3 min for each and then with corresponding running buffer till the inside current of the capillary remained stable. This was crucial to get a reproducible electroosmotic flow (EOF).

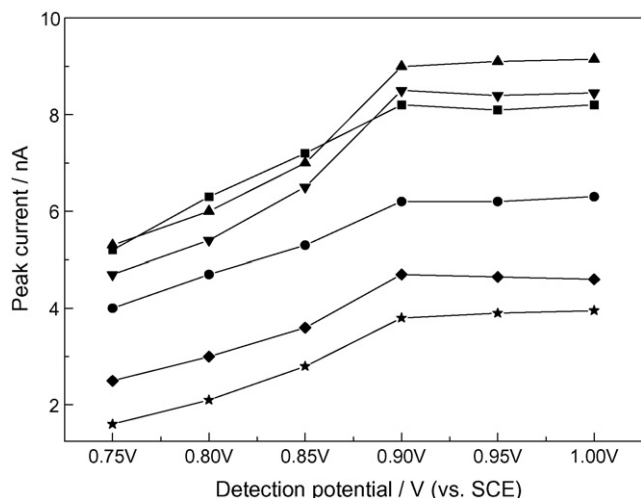


**Fig. 2.** Hydrodynamic voltammograms of apigenin ( $\nabla$ ), luteolin ( $\blacklozenge$ ), kaempferol ( $\blacktriangle$ ), quercetin ( $\ast$ ), (+)-catechin ( $\blacksquare$ ) and (-)-epicatechin ( $\bullet$ ). Conditions: fused silica capillary: 70 cm  $\times$  25  $\mu$ m i.d.  $\times$  360  $\mu$ m o.d.; working electrode: 300  $\mu$ m diameter carbon disc electrode; running buffer: 36 mM borate-phosphate (pH 8.8); separation voltage: 18 kV; electrokinetic injection: 10 s (at 18 kV); room temperature.

#### 2.4. Sample preparation

Chrysanthemum herbs were dried to constant weight, then cut into pieces and ground into powders. Accurately 1.00 g powder was weighed and extracted with 25 ml methanol for 60 min in an ultrasonic cleaner. The extraction process was repeated for three times, and the gathered extraction was then concentrated to dryness by a rotary evaporator. The residual was dissolved in 10 ml methanol, filtered through a cellulose filter and thereafter stored at 4 °C.

The stock solution was diluted with borate-phosphate buffer with/without organic solvent to desired concentrations, filtered with 0.22  $\mu$ m polypropylene acrodisc syringe filter and then sonicated before CZE-AD experiments.

### 3. Results and discussion

#### 3.1. Effect of the detection potential

Since flavonoids can be electrochemically oxidized at a relatively moderate potential, amperometric detection was used in this work. Fig. 2 shows the hydrodynamic voltammograms (HDVs) of the six analytes, which were obtained by monitoring the current responses after CZE separations within the applied potential ranging from +0.75 to +1.0 V. It was found that the current responses of these analytes increased with the applied potential increasing. However, the noise was too high when the applied potential was more than +0.90 V. In order to obtain the best signal-to-noise ratio, +0.90 V was selected as the most suitable detection potential in this experiment.

#### 3.2. Effect of buffer pH and concentration

A key factor in CZE-AD is the pH value. The effect of buffer pH was studied for a mixture of these six compounds by varying the borate-phosphate electrolyte from pH 7.0–11.0 in the concentrations ranging from 6 to 42 mM. The results showed that the background buffer with pH between 8.4 and 9.0, especially pH 8.8 with a concentration of 12 mM was most appropriate for the separation of kaempferol and apigenin. However, as shown in Fig. 3A, the comparatively best pH value and concentration was only resolvable for kaempferol and apigenin, while (+)-catechin and (-)-epicatechin as well as luteolin and quercetin both showed considerable overlap

despite the varying of buffer pH and concentration. Thus, a simple buffer is insufficient for the separation.

#### 3.3. Modification of buffer conditions

For a better separation of the six analytes,  $\beta$ -CD, which was proved to be with the best characteristics to obtain inclusion complexes with flavonoids [25], was used as an additive in running buffer. Fig. 3B shows the electropherogram in the presence of  $\beta$ -CD in running buffer, in which five peaks appeared. In the concentration test of  $\beta$ -CD ranging from 2.5 to 5.0 mM with an interval of 0.5, 3.0 mM  $\beta$ -CD was chosen as the optimum condition. With this modified buffer, it was easy to distinguish the peaks of (+)-catechin and (-)-epicatechin. Besides this, the addition of  $\beta$ -CD also showed a tiny improvement for the separation of luteolin and quercetin.

#### 3.4. Effects of organic solvent additives

In order to get the last overlapped pair, luteolin and quercetin resolved, some organic solvents were added to the sample or running buffer as EOF modifiers, because organic solvent modifiers are very useful to modulate separation selectivity [26]. In the process of further optimisation of the separation condition, methanol, ethanol and acetonitrile were tried out in series. Different proportions of organic additives were added to investigate their effects on the results of separation. Fig. 3C showed that the peaks of luteolin and quercetin were partially separated, and all peaks were sharpened with the addition of organic modifier. The best result was achieved by diluting the stock solution with 50% borate-phosphate, 25% methanol and 25% ethanol (v/v/v).

#### 3.5. Further optimization of the concentration of running buffer

With the help of chiral selector  $\beta$ -CD and organic modifier methanol and ethanol, six analytes were separated, but as is shown in Fig. 3C, the resolution was far from satisfaction. Finally, in order to enable a baseline separation of all six analytes, it was better to further optimize the concentration of running buffer, because the increase of ionic strength of running buffer can result in the decrease of EOF in capillary and improve the resolution. Among the range from 6 to 42 mM, 36 mM was finally chosen as the proper condition. Though the increase of the buffer concentration made the current responses decrease to some extent, the migration time of analytes increases accordingly, which led to a perfect baseline separation. Fig. 3D illustrates that all the six compounds could be baseline-separated in less than 20 min.

#### 3.6. Effect of separation voltage and sampling time

The separation efficiency of CZE was investigated within the separation voltage range from 12 to 20 kV. The migration time of the analytes was significantly shortened and their corresponding current peaks were sharpened when the separation voltage was increased. However, if the separation voltage was too high, more Joule heat was produced because of the higher current inside the capillary, which caused peak broadening and reduced separation efficiency. Therefore, 18 kV was selected as the optimum separation voltage in this experiment.

Samples were injected into the capillary in an electrokinetic mode. The effect of sampling time was investigated by selecting different injection time (8, 10, 12, 14 and 16 s at a voltage of 18 kV). It was found that the peak current increased as the injection time prolonged. However, the current peaks of the analytes were obviously broadened and overlapped when the injection time was more than



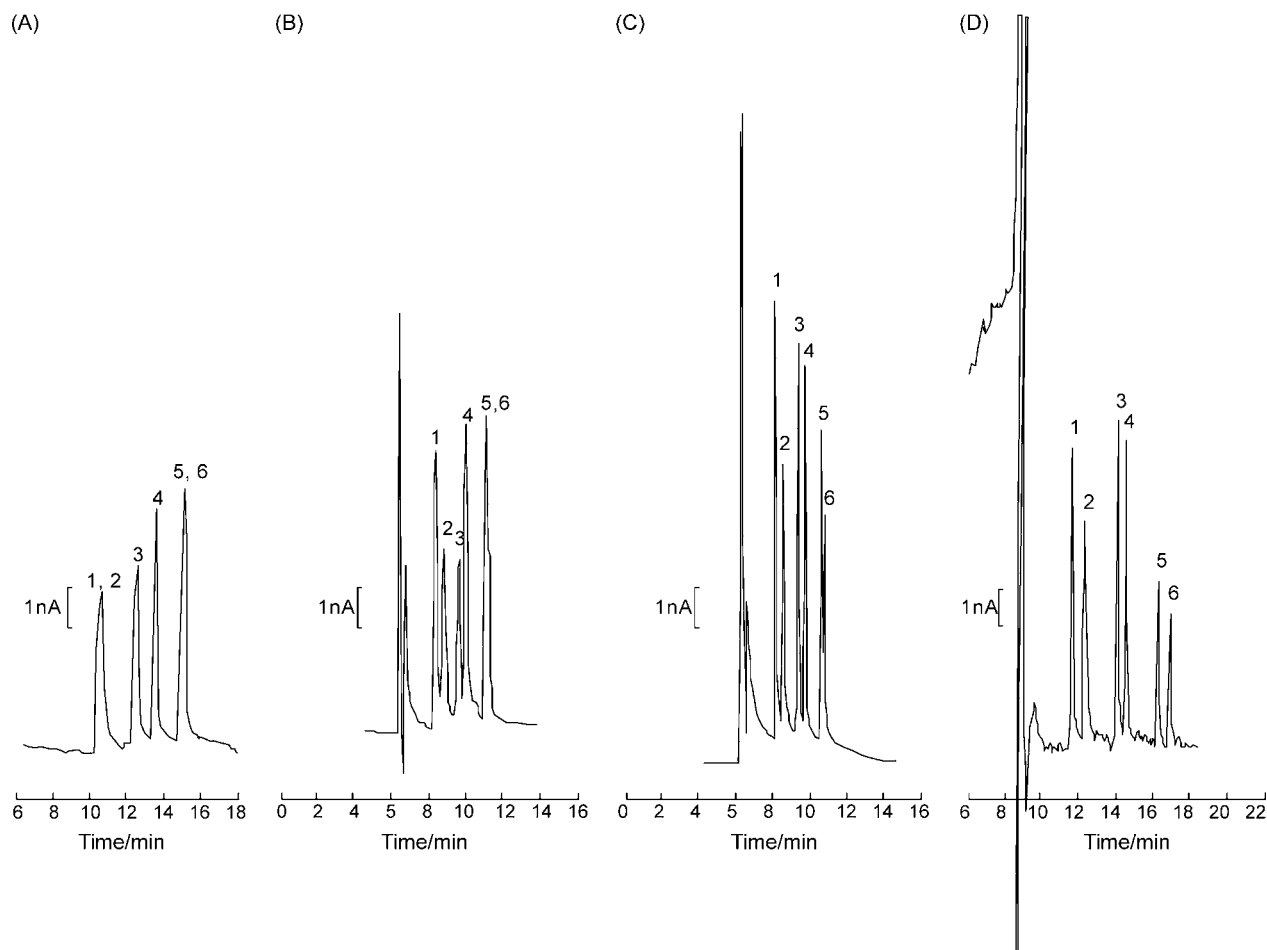


**Fig. 3.** From (A) to (D), electropherograms of solutions containing: (1) apigenin, (2) luteolin, (3) kaempferol, (4) quercetin, (5) (+)-catechin and (6) (–)-epicatechin with the concentration of  $5 \times 10^{-5} \text{ g ml}^{-1}$  each, under the detection potential +0.90 V (vs. SCE), and separation voltage 18 kV. (A) pH 8.8, 12 mM borate-phosphate electrolyte as BGE; (B) (A) in the presence of 3.0 mM  $\beta$ -CD as BGE; (C) on the basis of (B), diluting the stock solution with 50% borate-phosphate, 25% methanol and 25% ethanol (v/v/v); (D) all other conditions are the same as (C), except that the concentration of borate-phosphate buffer were changed to 36 mM.

12 s. So 10 s was selected as the injection time in this experiment and satisfactory results were obtained under this condition.

### 3.7. Analysis performance

According to the experiments above, the optimum conditions of CZE-AD for determining the six analytes were detection potential +0.90 V (versus SCE), separation voltage 18 kV, electrokinetic injection time 10 s (voltage 18 kV), 36 mM borate-phosphate buffer (pH 8.8) in addition with 3.0 mM  $\beta$ -CD and the injection sample diluted with 25% methanol and 25% ethanol (v/v). Fig. 3D shows the electropherogram of a standard solution of the six analytes with the concentrations of  $5 \times 10^{-5} \text{ g ml}^{-1}$  each under the optimum conditions at the carbon disk electrode. It is clear that a very good baseline separation is achieved for the six analytes within 20 min.

### 3.8. Linearity, detection limits and reproducibility

To determine the linearity for apigenin, luteolin, kaempferol, quercetin, (+)-catechin and (–)-epicatechin in CZE-AD, a series of mixed standard solutions of the analytes were tested. From Table 1, the linear ranges, regression equations, correlation coefficients, detection limits and the RSDs of peak current values are listed. Good linear relationships of the six analytes were obtained in the concentration ranging from  $5.0 \times 10^{-7}$  to  $1.2 \times 10^{-5} \text{ g ml}^{-1}$ . The detection limits were calculated according to the  $3sb/m$  criterion [27], where  $m$  is the slope of the calibration curve and  $sb$  is the standard deviation. The LODs of apigenin, luteolin, kaempferol, quercetin, (+)-catechin and (–)-epicatechin were as low as  $7.3 \times 10^{-8}$ ,  $2.1 \times 10^{-7}$ ,  $3.7 \times 10^{-8}$ ,  $2.8 \times 10^{-7}$ ,  $7.0 \times 10^{-8}$  and  $1.3 \times 10^{-7} \text{ g ml}^{-1}$ , respectively. After the analysis was repeated five

**Table 1**

The regression equations and the detection limits of apigenin, luteolin, kaempferol, quercetin, (+)-catechin and (–)-epicatechin

Analyte	Concentration range ( $\text{g ml}^{-1}$ )	Regression equation $I/\text{nA}$ , $C$ ( $\text{g ml}^{-1}$ )	Correlation coefficient	Detection limit ( $\text{g ml}^{-1}$ )	RSD (%) of concentration
Apigenin	$5 \times 10^{-7}$ – $1.2 \times 10^{-5}$	$I = 1.12 \times 10^6 C + 0.123$	0.9981	$7.3 \times 10^{-8}$	2.70
Luteolin	$5 \times 10^{-7}$ – $1.2 \times 10^{-5}$	$I = 6.28 \times 10^5 C + 0.149$	0.9990	$2.1 \times 10^{-7}$	4.36
Kaempferol	$5 \times 10^{-7}$ – $1.2 \times 10^{-5}$	$I = 1.26 \times 10^6 C + 0.277$	0.9979	$3.7 \times 10^{-8}$	1.57
Quercetin	$5 \times 10^{-7}$ – $1.2 \times 10^{-5}$	$I = 5.33 \times 10^5 C + 0.103$	0.9980	$2.8 \times 10^{-7}$	4.89
(+)-Catechin	$5 \times 10^{-7}$ – $1.2 \times 10^{-5}$	$I = 1.12 \times 10^6 C - 0.085$	0.9982	$7.0 \times 10^{-8}$	2.60
(–)-Epicatechin	$5 \times 10^{-7}$ – $1.2 \times 10^{-5}$	$I = 8.32 \times 10^5 C - 0.157$	0.9991	$1.3 \times 10^{-7}$	3.51

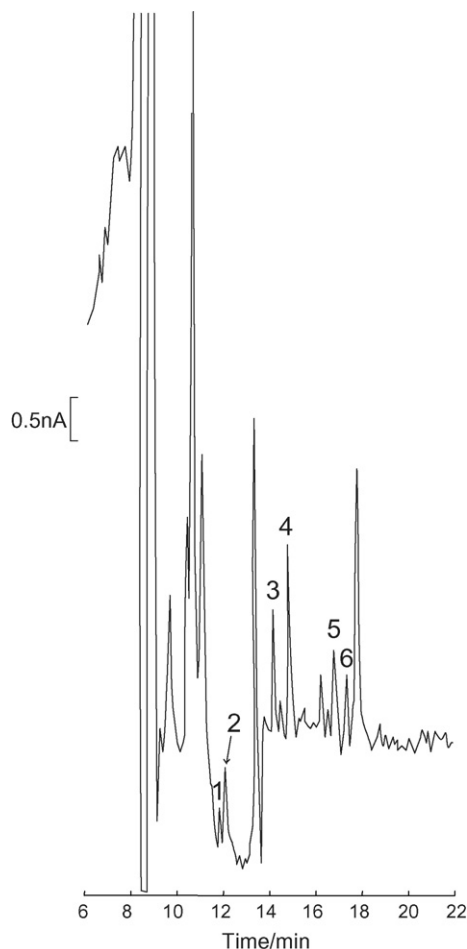


**Fig. 4.** Electropherogram of  $5 \text{ mg l}^{-1}$  chrysanthemum herb extraction under the optimal CZE-AD conditions mentioned above: (1) (+)-catechin, (2) (-)-epicatechin, (3) kaempferol, (4) apigenin, (5) luteolin and (6) quercetin.

times under the same conditions, the peak signals only decreased slightly, and the RSDs were all less than 5%, which demonstrated that this method was of good repeatability.

### 3.9. Sample analysis

Sample determinations were carried out under the optimal conditions according to the procedures stated above. The determination of the six flavonoids in chrysanthemum extracts was performed by standard addition method. Typical electropherogram of the sample is shown in Fig. 4. The contents of the six analytes were calculated as  $3.4 \times 10^{-6}$ ,  $7.9 \times 10^{-6}$ ,  $7.3 \times 10^{-6}$ ,  $1.6 \times 10^{-5}$ ,  $7.2 \times 10^{-6}$  and  $7.4 \times 10^{-6} \text{ g g}^{-1}$  for (+)-catechin, (-)-epicatechin, kaempferol, apigenin, luteolin and quercetin, respectively. Recovery tests were performed by adding 3–5 folds of these substances, and the recoveries of all six analytes were 91.2%, 94.3%, 105.8%,

108.6%, 98.3% and 96.1% respectively, which indicated that this method was accurate and practical.

## 4. Conclusions

Capillary electrophoresis is a helpful tool for investigating the flavonoids profile in chrysanthemum. In this paper, apigenin, luteolin, kaempferol, quercetin, (+)-catechin and (-)-epicatechin were separated and determined by CZE-AD with the help of modifiers. Besides the optimization of some basic affecting factors of CZE-AD, the addition of  $\beta$ -CD and organic additives in the system all helped to obtain the final results. The results showed that this method is of high separation efficiency, short analysis time, and convenience of analysis.

## Acknowledgements

This work is financially supported by the National Nature Science Foundation of China (No. 20575022) and Natural Science Research Foundation from Shanghai Science and Technology Committee (No. 04ZR14041).

## References

- [1] S.F. Wang, J.Y. Zhang, X.G. Chen, Z.D. Hu, *Chromatographia* 59 (2004) 507.
- [2] N.G. Vanifatova, B.Ya. Spivakov, J. Mattusch, U. Franck, R. Wennrich, *Talanta* 66 (2005) 605.
- [3] M.G. Cornelius, H.H. Schmeiser, *Electrophoresis* 28 (2007) 3901.
- [4] S.Q. Luo, J.M. Feng, H.-m. Pang, *J. Chromatogr. A* 1051 (2004) 131.
- [5] F. Qin, C.H. Xie, S. Feng, J.J. Ou, L. Kong, M.L. Ye, H.F. Zou, *Electrophoresis* 27 (2006) 1050.
- [6] L.L. Zhou, Z.H. Lin, R.A. Reamer, B. Mao, Z.H. Ge, *Electrophoresis* 28 (2007) 2658.
- [7] S. Fanali, *J. Chromatogr. A* 875 (2000) 89.
- [8] J.M. Herrero-Martinez, F.Z. Oumada, M. Roses, E. Bosch, C. Rafols, *J. Sep. Sci.* 30 (2007) 2493.
- [9] P. Laamanen, S. Busi, M. Lahtinen, R. Matilainen, *J. Chromatogr. A* 1095 (2005) 164.
- [10] M.E. Yue, T.F. Jiang, Y.P. Shi, *Talanta* 62 (2004) 695.
- [11] D.J. Allen, J.C. Gray, N.L. Paiva, J.T. Smith, *Electrophoresis* 21 (2000) 2051.
- [12] F.N. Fonseca, M.J. Kato, L. Oliveira Jr., N.P. Neto, M.F.M. Tavares, *J. Microcolumn Separations* 13 (2001) 227.
- [13] K. Swinney, D.J. Bornhop, *Electrophoresis* 21 (2000) 1239.
- [14] H. Curiel, W. Vanderaerden, H. Velez, J. Hoogmartens, A.V. Schepdael, *J. Pharm. Biomed. Anal.* 44 (2007) 49.
- [15] J. Jiang, C.A. Lucy, *Talanta* 72 (2007) 113.
- [16] L.A. Gennaro, O. Salas-Solano, S. Ma, *Anal. Biochem.* 355 (2006) 249.
- [17] S.C. Liu, Y.J. Liu, J. Li, M.L. Guo, W. Pan, S.Z. Yao, *Talanta* 69 (2006) 154.
- [18] S.Q. Dong, S. Zhang, X. Cheng, P.G. He, Q.J. Wang, Y.Z. Fang, *J. Chromatogr. A* 1161 (2007) 327.
- [19] S.Y. Zhu, Y. Yang, H.D. Yu, Y. Ying, G.L. Zou, *J. Ethnopharmacol.* 96 (2005) 151.
- [20] C.Q. Hu, K. Chen, Q. Shi, R.E. Kilkuskie, Y.C. Cheng, K.H. Lee, *J. Nat. Prod.* 57 (1994) 42.
- [21] J. Zhang, Y.B. Li, D.W. Qian, S.H. Qian, J.A. Duan, A.W. Ding, *Lishizhen Med. Materia Medica Res.* 17 (2006) 1941.
- [22] S.P. Wang, K.J. Huang, *J. Chromatogr. A* 1032 (2004) 273.
- [23] Q.C. Chu, L. Fu, Y.Q. Guan, J.N. Ye, *J. Agric. Food Chem.* 52 (2004) 7828.
- [24] M. Kofink, M. Papagiannopoulos, R. Galensa, *Eur. Food Res. Technol.* 225 (2007) 569.
- [25] M.C. Bergonzi, A.R. Bilia, L. Di Bari, G. Mazzi, F.F. Vincieri, *Bioorg. Med. Chem. Lett.* 17 (2007) 5774.
- [26] Y.Z. Yang, R.I. Boysen, M.T.W. Hearn, *J. Chromatogr. A* 1043 (2004) 81.
- [27] M. Chicharro, A. Sánchez, A. Zapardiel, M.D. Rubianes, G. Rivas, *Anal. Chim. Acta* 523 (2004) 185.



## Short communication

# Application of bamboo charcoal as solid-phase extraction adsorbent for the determination of atrazine and simazine in environmental water samples by high-performance liquid chromatography-ultraviolet detector

Ru-Song Zhao\*, Jin-Peng Yuan, Ting Jiang, Jun-Bo Shi, Chuan-Ge Cheng

Key laboratory for applied technology of sophisticated analytical instruments of Shandong province, Analysis and Test Center, Shandong Academy of Sciences, Jinan, Shandong 250014, China

## ARTICLE INFO

## Article history:

Received 25 January 2008

Received in revised form 31 March 2008

Accepted 12 April 2008

Available online 22 April 2008

## Keywords:

Atrazine

Simazine

Bamboo charcoal

Solid-phase extraction

High-performance liquid chromatography

## ABSTRACT

In this article, a new method for the determination of triazine herbicides atrazine and simazine in environment aqueous samples was developed. It was based on solid-phase extraction (SPE) using bamboo charcoal as adsorbent and high-performance liquid chromatography-ultraviolet detector (HPLC-UV) for the enrichment and determination of atrazine and simazine at trace level. Related important factors influencing the extraction efficiency, such as the kind of eluent and its volume, flow rate of the sample, pH of the sample, and volume of the sample, were investigated and optimized in detail. Under the optimal conditions, the experimental results showed that excellent linearity was obtained over the range of 0.5–30  $\mu\text{g L}^{-1}$  with correlation coefficients 0.9991 and 0.9982, for atrazine and simazine, respectively; and the relative standard deviations of two analytes were 8.3, 8.7%, respectively. The proposed method was successfully applied to the analysis of tap water and well water samples. And satisfactory spiked recoveries were obtained in the range of 75.2–107.1%. The above results indicated that the developed method was an excellent alternative for the routine analysis in environmental field.

© 2008 Elsevier B.V. All rights reserved.

## 1. Introduction

Triazine herbicides, such as atrazine and simazine, provide great benefits for weed control in agricultural domain over past years, however, their residues have attracted great concern worldwide because of widespread use. And they are also in the list of chemical pollutants that need to be more heavily monitored due to their toxicity, persistence, cumulation in the environment and their effects on the environment and health [1,2]. At the same time, according to the European Union Directive, individual pesticide in drinking water must not exceed 0.1  $\mu\text{g L}^{-1}$  for individual compound and some of its degradation products, and 0.5  $\mu\text{g L}^{-1}$  for the sum of all compounds [3]. Therefore, it is necessary to develop cheap, simple, rapid and sensitive methods for monitoring their residues in the environment.

The most widely used methods for the determination of triazine herbicides are chromatographic techniques including gas chromatography [4,5] and high-performance liquid chromatography [6], however, generally, without enrichment procedure their instrumental sensitivity and selectivity are insufficient for direct

determination of these compounds at trace or ultratrace level in environmental samples. Therefore, a sample enrichment step prior to chromatographic analysis is very necessary. The commonly used sample preparation methods for chromatographic determination include liquid–liquid extraction (LLE), solid-phase extraction (SPE), ultrasonic extraction (USE) and so on. Among the above mentioned sample pretreatment methods, solid-phase extraction is the most common technique for environmental water sample pretreatment because it offers a number of important benefits in comparison with laborious classical LLE, such as reduced solvent usage and exposure, low disposal costs and short extraction times for sample preparation [7]. Recently, cell sorption as a novel and successful mode of SPE has appeared [8–10]. For the SPE procedure, the choice of adsorbent is the most important factor for obtaining higher enrichment efficiency of analytes. And various different types of hydrophobic materials, such as C8, C18, PS-DVB polymer, polytetrafluoroethylene and carbon nanotubes, have been used as adsorbents for the enrichment of triazine herbicides and other environmental pollutants in water samples [2,11–14]. In addition, one problem should be pointed out that some of them are expensive. Therefore, searching cheap and suitable adsorbents for the SPE of target analytes is necessary.

Bamboo charcoal has attracted great attention in recent years because of its special microporous structure and biological

\* Corresponding author. Tel.: +86 531 82605340; fax: +86 531 82964889.  
E-mail address: [zhaors1976@126.com](mailto:zhaors1976@126.com) (R.-S. Zhao).

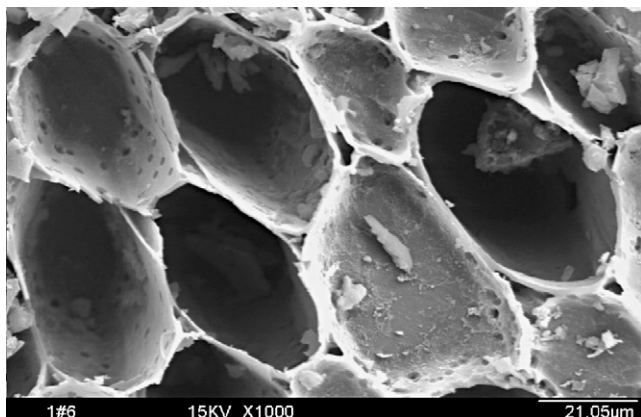


Fig. 1. The picture of bamboo charcoal under Electron Probe X-ray Microanalyzer.

characteristics [15]. Bamboo charcoal burnt at temperatures over 800 degrees centigrade exhibits properties vastly different from the bamboo plant, including a high density and porous structure [16]. Compared with wood charcoal, bamboo charcoal has about 4 times more cavities, 3 times more mineral content and 4 times better absorption rate. In terms of surface area, bamboo charcoal ( $300\text{ m}^2\text{ g}^{-1}$ ) is 10 times greater than wood charcoal ( $30\text{ m}^2\text{ g}^{-1}$ ) [16], and is larger than multiwalled carbon nanotubes (less than  $200\text{ m}^2\text{ g}^{-1}$ ) [17]. Bamboo charcoal is a kind of cheap material (1 US\$/500 g), which was much lower than other adsorbents such as PS-DVB polymer, carbon nanotubes and so on. The low price, extremely large surface area and the unique microporous structure make bamboo charcoal a promising adsorbent material for the enrichment of pollutants at trace level or ultratrace level in the environment (The picture of bamboo charcoal under Electron Probe X-ray Microanalyzer is given in Fig. 1.) To our knowledge, up to now, no report about solid-phase extraction using bamboo charcoal as adsorbent for the enrichment and determination of triazine herbicides has appeared.

The goal of this study is to exploit the adsorptive potential of bamboo charcoal as solid-phase extraction adsorbent for the enrichment of atrazine and simazine at trace level. Related important factors influencing the extraction efficiency, such as the kind of eluent and its volume, flow rate of the sample, pH of the sample, and volume of the sample, were investigated and optimized in detail. At the same time, the proposed enrichment procedure was used for the determination of atrazine and simazine at trace level in environmental water samples.

## 2. Experimental

### 2.1. Reagents and materials

HPLC-grade methanol and acetonitrile were purchased from Tedia company Inc. (Fairfield, OH, USA). Acetone was chromatographic grade, and purchased from Fuchen chemical reagent factory (Tianjin, China). Atrazine were purchased from Dr. Ehrenstorfer (Augsburg, Germany) (purity 99.5%). Standard stock solution of atrazine was prepared by dissolving appropriate amount into methanol. Simazine standard with a concentration of  $100\text{ mg L}^{-1}$  was purchased from Institute of Environmental Protection and Monitoring, Department of Agriculture (Beijing, China). These solutions were further diluted into  $10.0\text{ mg L}^{-1}$  with methanol and stored at  $4^\circ\text{C}$ . Fresh working solutions were prepared daily by appropriate dilution of the stock solution with purified water.

Bamboo Charcoal (Quzhou Minxin charcoal company, Zhejiang, China) as an indoor air fresher was purchased from a local

market. The picture of bamboo charcoal under Electron Probe X-ray Microanalyzer is given in Fig. 1. Before use to develop SPE method, it was triturated and sieved through a 80 mesh sieve and dried at  $80^\circ\text{C}$  for 2 h. Through the observation of JXA-733 Electron Probe X-ray Microanalyzer, bamboo charcoals with an average length of  $3\text{--}15\ \mu\text{m}$  was obtained. Bamboo charcoal includes 81.21% carbon element, 2.52% hydrogen element, and 16.27% other components.

### 2.2. Apparatus

The high-performance liquid chromatography-ultraviolet detector (HPLC-UV) equipment used was an Agilent 1100 HPLC system including a ultraviolet detection, a quaternary pump, a column thermostat and an automatic sample injector with a  $100\ \mu\text{L}$  loop. A personal computer equipped with an Agilent ChemStation program for HPLC was used to process chromatographic data. A reversed-phase VP-ODS C18 column ( $250\text{ mm} \times 4.6\text{ mm}$  i.d., particle size  $5\ \mu\text{m}$ ) (Shimadzu, Japan) was used for analysis of two triazine herbicides at  $25^\circ\text{C}$ . The mobile phase was obtained with acetonitrile/water (70/30, v/v), and the flow rate, the injection volume and detection wavelength was  $0.5\text{ mL min}^{-1}$ ,  $100\ \mu\text{L}$  and  $223\text{ nm}$ , respectively.

Preparation of bamboo charcoal packed cartridge was performed by modifying an Agilent AccuBond SPE ENV PS DVB cartridge ( $1000\text{ mg}$ ,  $6\text{ mL}$ , polypropylene), which was obtained from Agilent Technologies, USA. After the PS-DVB packing was removed,  $1.0\text{ g}$  bamboo charcoal, which had been pretreated, was packed in the SPE cartridge. The polypropylene upper frit was reset at the upper end of the cartridge to hold the bamboo charcoal packing in place. Then the outlet tip of the cartridge was connected to a SHB-III vacuum pump (Great wall scientific and trade Co. Ltd., Zhengzhou, Henan), and the inlet end of cartridge was connected to PTFE suction tube whose other end was inserted into sample solution. In order to reduce the interferences of organic contaminants, the entire SPE assembly needed to be washed with  $50\text{ mL}$  methanol and enough purified water before the first use.

### 2.3. Solid-phase extraction

The cartridge packed with bamboo charcoal was pretreated by washing with  $2\text{ mL}$  acetonitrile and  $10\text{ mL}$  purified water prior to each SPE procedure. Then  $100\text{ mL}$  purified water sample spiked with two compounds was passed through the pre-conditioned cartridge at the optimum flow rate. After the sample solution had passed through, the cartridge was washed with  $10\text{ mL}$  purified water to remove co-adsorbed matrix materials from the cartridge. Then the bamboo charcoal column was dried by negative pressure for  $10\text{ min}$ . Subsequently the analytes retained on the SPE cartridge were eluted with  $10\text{ mL}$  acetonitrile. In order to simplify the SPE procedure, further concentration of extract was not performed. Finally, the extract was then analyzed by HPLC-UV with an injection of  $100\ \mu\text{L}$ .

### 2.4. Water samples

In this experiment, two real world environmental water samples, tap water and well water, were used for evaluating the feasibility of the developed method. Tap water was collected from our lab. Well water sample was collected from Baotuquan of Jinan, Shandong Province. Before the environmental water samples were used, they were filtered through  $0.45\ \mu\text{m}$  micropore membranes and stored in brown glass bottoms at  $4^\circ\text{C}$ , respectively.

### 3. Results and discussion

#### 3.1. Optimization of enrichment conditions

To evaluate the enrichment potential of bamboo charcoal as solid-phase adsorbent for atrazine and simazine, related important factors influencing the extraction efficiency, such as the kind of eluent and its volume, flow rate of the sample, pH of the sample, and volume of the sample, were optimized and investigated in detail.

##### 3.1.1. Selection of kind and volume of eluent

Firstly, to ensure the targeted compounds be eluted completely, a suitable eluent should be selected. In this experiment, three solvents differing in polarity, HPLC-methanol, acetonitrile and chromatographic grade acetone were tested. Trials results indicated that acetonitrile had the best gas chromatographic behavior and can provide the best elution performance. Therefore, in the following experiments, acetonitrile was used as the eluent. The volume of the eluent is another factor that should be considered. A series experiments was designed and investigated through changing the volume of eluent acetonitrile from 2 to 12 mL. In the operation process of solid-phase extraction, another 10 mL acetonitrile and 10 mL purified water were employed passing through bamboo charcoal packed cartridge before next SPE extraction in order to get rid of possible residue of analytes. The experimental results obtained are shown in Fig. 2. From Fig. 2, the recoveries of two analytes increased with the increase of the volumes of acetonitrile between 2 and 8 mL. When the volume of acetonitrile was more than 8 mL, the recovery of simazine remained constant. And the recovery of atrazine reached its maximal value when the volume of acetonitrile was more than 10 mL. Therefore, in all subsequent experiments, 10 mL acetonitrile was used as the eluent.

##### 3.1.2. Selection of pH

Secondly, pH value of working solution or sample solution play a critical role in the SPE procedure, because the pH value of solution determined the existing state of analytes, and thus influenced the extraction efficiency of the targeted compounds. In order to investigate this effect, in this experiment, different pH value of working solution ranging from 3 to 11 was studied. The experimental results are shown in Fig. 3. From Fig. 3, it is clear that at the pH 5–9, the recoveries of two compounds can reach 94.8–105%. And the recov-

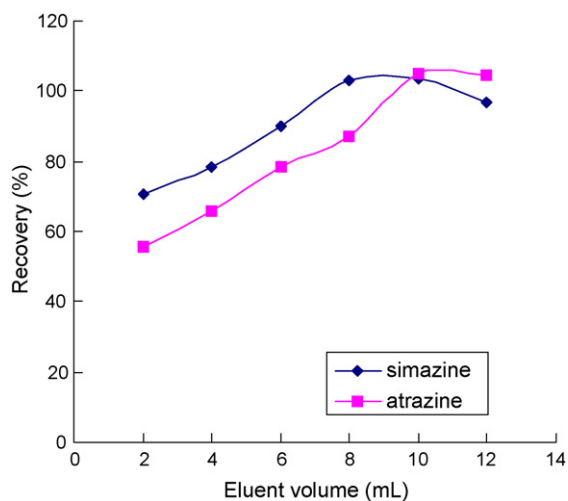


Fig. 2. Influence of the volume of the eluent on the recoveries of simazine and atrazine. Conditions: volume of the sample, 100 mL; concentration for two compounds,  $5 \mu\text{g L}^{-1}$ ; pH of the sample, 7; flow rate of the sample,  $2.5 \text{ mL min}^{-1}$ .

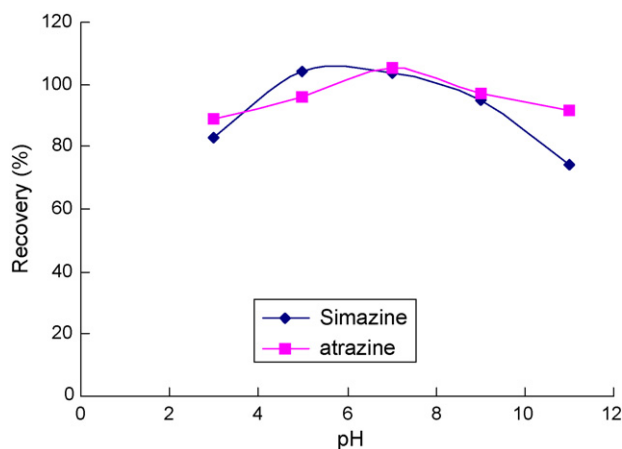


Fig. 3. Influence of pH of the sample on the recoveries of simazine and atrazine. Conditions: volume of the sample, 100 mL; concentration for three compounds,  $5 \mu\text{g L}^{-1}$ ; volume of acetonitrile, 10 mL; flow rate of the sample,  $2.5 \text{ mL min}^{-1}$ .

eries at  $\text{pH} < 5$  or  $\text{pH} > 9$  were lower than those at the  $\text{pH} 5\text{--}9$ . At the  $\text{pH} 7$ , the best extraction efficiency for two compounds can be obtained. This was accordant with the results obtained in the previous report [2]. Possible reason for this is that atrazine and simazine may hydrolyze in strong acidic and basic aqueous environments or ionized [2].

##### 3.1.3. Effect of sample flow rate

Flow rate of working solution also is an important factor that should be considered, which affects the enrichment efficiency. In this experiment, the flow rate was investigated in the range of  $1.0\text{--}2.5 \text{ mL min}^{-1}$ . The experimental results showed that flow rate of working solution had no obvious influence on the recoveries of simazine and atrazine. Therefore, in the following experiments,  $2.5 \text{ mL min}^{-1}$  was selected for saving sample pretreatment time.

##### 3.1.4. Effect of sample volume

In order to obtain reliable and reproducible analytical results and a high enrichment factor, breakthrough volume is another important parameter that should be considered for solid-phase extraction. In this experiment, the influence of sample volume on the recoveries of two compounds was investigated in the range of  $100\text{--}1000 \text{ mL}$ .

For this purpose, 100, 250, 500, 750, 1000 mL of sample solution containing  $5.0 \mu\text{g L}^{-1}$  simazine and atrazine, respectively, were passed through the bamboo charcoal solid-phase extraction cartridge with optimal flow rate. It was found that quantitative recoveries ( $>89\%$ ) were obtained for sample volume up to 500 mL for the targeted compounds. When the volume of sample was more than 500 mL, the recoveries of two compounds decreased slightly. In order to save time volume of sample 100 mL was adopted in further experiments.

#### 3.2. Analytical performance

Under the above optimum conditions, some characteristics of the present method were investigated. Linear range, limit of detection and precision were obtained. Extended standard method was used for quantitative determination of atrazine and simazine. Linearity was observed over the range  $0.5\text{--}30 \mu\text{g L}^{-1}$  for two herbicides. Correlation coefficients ( $R$ ) were 0.9991 and 0.9982 for simazine and atrazine, respectively. The limits of detection (LODs), based on a signal-to-noise ratio ( $S/N$ ) of 3, were 0.1 and  $0.1 \mu\text{g L}^{-1}$ ,

**Table 1**  
Results of determination and recoveries of real water samples spiked with two target analytes

Water samples	Compounds	Blank	Spiked levels ( $\mu\text{g L}^{-1}$ )	Found ( $\mu\text{g L}^{-1}$ )	Recovery (%)
Tap water	Simazine	–	1.0	$0.752 \pm 0.082$	75.2
		–	5.0	$4.815 \pm 0.327$	96.3
	Atrazine	–	1.0	$1.071 \pm 0.160$	107.1
		–	5.0	$4.480 \pm 0.248$	89.6
Well water	Simazine	–	1.0	$0.800 \pm 0.007$	80.0
		–	5.0	$4.370 \pm 0.332$	87.4
	Atrazine	–	1.0	$1.063 \pm 0.147$	106.3
		–	5.0	$4.285 \pm 0.418$	85.7

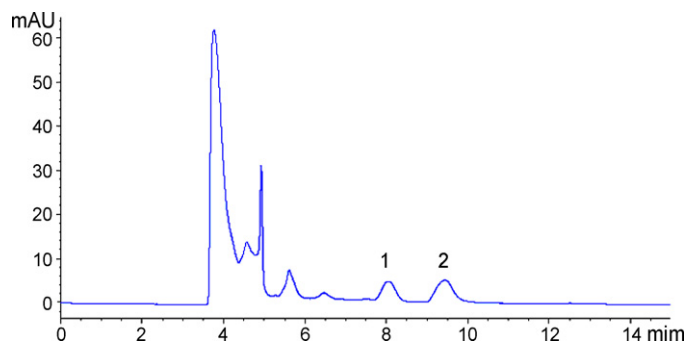


**Fig. 4.** Typical chromatogram of well water sample spiked with  $5 \mu\text{g L}^{-1}$  simazine and atrazine: (1) Simazine (2) Atrazine. *Conditions:* volume of the sample, 100 mL; concentration for two compounds,  $5 \mu\text{g L}^{-1}$ ; pH of the sample, 7; flow rate of the sample,  $2.5 \text{ mL min}^{-1}$ ; volume of acetonitrile, 10 mL.

for two compounds. The sensitivity of the method can be further improved if more than 100 mL sample was used. To assess the precision of the measurement, the repeatability of the method was determined by performing 5 times using aqueous standard solutions with  $1.0 \mu\text{g L}^{-1}$  atrazine and simazine. The RSD% was were 8.3 and 8.7% for atrazine and simazine, respectively.

### 3.3. Real environmental water samples analysis

In order to evaluate the proposed method, two aqueous samples including tap water and well water were analyzed, and the recoveries were determined at 1.0 and  $5.0 \mu\text{g L}^{-1}$  simazine and atrazine spiked level, respectively. The results are listed in Table 1. The results indicate that the contents of simazine and atrazine in the samples were under the detection limits. The recoveries of simazine and atrazine were in the range of 75.2–107.1, and 80.0–106.3%, respectively. Fig. 4 showed the typical chromatogram of well water sample collected from Baotuquan.

## 4. Conclusion

In this paper, a cheap, simple and reliable method was developed for the enrichment and determination of two triazine herbicides

atrazine and simazine in environmental water samples based on using bamboo charcoal as solid-phase extraction adsorbents. Bamboo charcoal exhibited excellent merits as solid-phase extraction adsorbent in the enrichment procedure of two herbicides. The developed sample pretreatment procedure offered many obvious advantages such as cheapness, simplicity, rapidness, easy to operate, sensitiveness and good repeatability. All of these proved that bamboo charcoal was a good adsorbent for the preconcentration of atrazine and simazine at trace level from environmental water samples. In a word, it can be concluded that the bamboo charcoal has great potential for the enrichment and determination of more other herbicides in environmental water samples.

## Acknowledgements

This work is jointly supported by research encouragement foundation of excellent midlife-youth scientists of Shandong province (2006BS08026, 2006BS08013), Upgrade Foundation of Scientific Instruments of Shandong Province and Shandong Academy of Sciences.

## References

- [1] F. Hern'andea, C. Hidalgo, J.V. Sancho, F. L'opez, Anal. Chem. 70 (1998) 3322.
- [2] Q. Zhou, J. Xiao, W. Wang, G. Liu, Q. Shi, J. Wang, Talanta 68 (2006) 1309.
- [3] Official Journal of European Communities Council Directive 98/83/EC.
- [4] J.J.B. Nevado, C.G. Cabanillas, M.J.V. Llerena, V.R. Robledo, Microchem. J. 87 (2007) 62.
- [5] D. Nagaraju, S.D. Huang, J. Chromatogr. A 1161 (2007) 89.
- [6] J. You, H. Zhang, H. Zhang, A. Yu, T. Xiao, Y. Wang, D. Song, J. Chromatogr. B 856 (2007) 278.
- [7] K. Pyzyska, Anal. Sci. 23 (2007) 631.
- [8] A.-M. Zou, M.-L. Chen, X.-W. Chen, J.-H. Wang, Anal. Chim. Acta 598 (2007) 74.
- [9] A.-M. Zou, X.-W. Chen, M.-L. Chen, J.-H. Wang, J. Anal. At. Spectrom. 23 (2008) 412.
- [10] A.-M. Zou, M.-L. Chen, Y. Shu, M. Yang, J.-H. Wang, J. Anal. At. Spectrom. 22 (2007) 392.
- [11] Y. Cai, G. Jiang, J. Liu, Q. Zhou, Anal. Chim. Acta 494 (2003) 149.
- [12] K. Holadova, J. Hajslova, Int. J. Environ. Anal. Chem. 59 (1995) 43.
- [13] M.L. Davi, M. Liboni, M.G. Malfatto, Int. J. Environ. Anal. Chem. 74 (1999) 155.
- [14] Y. Cai, G. Jiang, J. Liu, Q. Zhou, Anal. Sci. 19 (2003) 1491.
- [15] X.F. Wang, H.P. Zhan, X.Y. Xiao, H.Q. Chen, Funct. Mater. 6 (2005) 746.
- [16] <http://www.blacktonature.com/abtrbc.shtml>.
- [17] Y. Cai, G. Jiang, J. Liu, Q. Zhou, Anal. Chem. 75 (2003) 2517.